

Targeted Tropomyosin Receptor Kinase Radiotracers for
Positron Emission Tomography Imaging

By

Vadim Bernard-Gauthier

A thesis submitted in partial fulfillment of the requirements for the degree of

Doctor of Philosophy

in

Cancer Sciences

Department of Oncology
University of Alberta

© Vadim Bernard-Gauthier, 2017

Abstract

Tropomyosin receptor kinases TrkA/B/C family supports neuronal growth, survival and differentiation during development, adult life and ageing. Downregulation of TrkA/B/C is a prominent hallmark of numerous neurological disorders including Alzheimer disease (AD). Abnormally expressed or overexpressed full length or fusion TrkA/B/C proteins which bear oncogenic potential and were shown to drive tumorigenesis in a variety of neurogenic and non-neurogenic human cancers are currently the focus of intensive clinical research. The study, both in oncology and neurology, of the spatiotemporal alterations in TrkA/B/C expression and density or the determination of target engagement of emerging antineoplastic kinase inhibitor drugs with those receptors in normal and diseased tissue is crucially needed but has however remained largely unexplored due to the lack of suitable non-destructive analytic tools. Here, we aim to develop and provide multi-species validation of carbon-11- and fluorine-18-labeled positron emission tomography (PET) radiotracers based on purposely designed small molecule kinase catalytic domain-binding inhibitors of TrkA/B/C.

We first demonstrate that pan-Trk selective inhibitor scaffolds which target both the active DFG-in and inactive DFG-out kinase conformations can be rationally modified to yield suitable compounds for translation into PET radiotracers. In particular, the carbon-11 isotopologue of the preclinical 4-aza-2oxindole lead GW441756 is characterized as the first brain penetrant Trk radiotracer based on rodent PET experiments *in vivo*. Using human neuroblastoma tissue, it is also shown that type-I pan-Trk-selective radiotracers, including [¹¹C]GW441756, enable tumor visualization selectivity, based on TrkB status *in vitro*.

Subsequently, we show that impediments associated with the development of orthosteric tracers for intracellular *in vivo* neuroimaging of protein kinases can be addressed via thorough structure-activity relationship (SAR) screening such as generating a lead suitable for human

use. From the screening of an imidazo[1,2-*b*]pyridazine-based pan-Trk inhibitors library, followed by the *in vivo* assessment of multiple radiotracers from this series, we provide the detailed evaluation of [¹¹C]-(*R*)-IPMICF16 as the first TrkB/C-targeted lead radiotracer with suitable properties for neuroimaging in human. The evaluation presented includes PET imaging studies in four species from mice to first-in-human as well as Trk kinase inhibitor target engagement confirmation using the phase II clinical inhibitor entrectinib in mice. Relying on extensive human kinome analyses, we also show that (*R*)-IPMICF16 constitutes both the most potent and most selective TrkB/C inhibitor known to date. We furthermore demonstrate that this lead efficiently enables the discrimination of AD versus healthy control brains based on hippocampal binding in human *in vitro*.

We present additional efforts in our exploration of Trk radiotracers with the development of an ¹⁸F-labeled quinazoline-based pan-Trk lead which displays suitable properties for *in vivo* translation and favorable Trk activities, including towards clinically relevant Trk oncogenic drivers such as TrkA-TPM3. Finally, current work in the second generation optimization of our [¹¹C]-(*R*)-IPMICF16 clinical lead is described. Of interest, it is shown that a state-of-art copper-mediated ¹⁸F-fluorination technique can be used to secure the inactivated ¹⁸F-arene moiety of our new lead tracer, [¹⁸F]-(*R*)-IPMICF17.

The Trk-targeted probes delineated here represent a novel class of molecular imaging radiotracers for the non-invasive and in-depth interrogation study of signal transduction at the interface of oncology and neurology. Globally, the results presented entail the further exploration of Trk radiotracers as a novel tool for the study and diagnosis of human neurodegenerative diseases and patients identification in the context of personalized oncology.

Keywords: Tropomyosin receptor kinases, Trk, positron emission tomography, PET, neuroimaging, tyrosine kinase inhibitor, carbon-11, fluorine-18, oncogenic driver, Alzheimer's disease, *NTRK*.

Preface

This thesis is an original work by Vadim Bernard-Gauthier and is based on research conducted between September 2013 and December 2016 at the McConnell Brain Imaging Centre of the Montreal Neurological Institute (McGill University, Department of Experimental Medicine) and Medical Isotope and Cyclotron Facility (University of Alberta, Department of Oncology) within the laboratory of Prof. R. Schirrmacher. Important portions of the research presented were also conducted in collaboration with different research groups. All articles and portions of articles included (published, submitted and in preparation) are first or last authored contributions by the author of the present thesis. Chapter 1 (Introduction) comprises portions from four published review articles. The body text (Chapter 2-6) is organized based on an article thesis format. Chapters 2 to 6 each reproduces an article as published or submitted for publication including corresponding experimental sections and supporting information (as published or submitted as of March 1st 2017). Chapters 2 to 6 are organized chronologically based on publication or submission dates. Chapter 7 (Conclusion) presents selected data included in a manuscript in preparation. The first page of each chapter details the respective contributions of all co-authors as well as the complete reference of the published work (or working title and planned journal for publication in the case of Chapter 7). The title page of each chapter also details affiliations for all co-authors as published or submitted in the corresponding article. When applicable, relevant considerations regarding research ethics can be found in the corresponding experimental section as published or submitted in the original articles.

Our imagination is stretched to the utmost,
not, as in fiction, to imagine things which are not really there,
but just to comprehend those things which *are* there.

RICHARD FEYNMAN,
The Character of Physical Law

Acknowledgements

First and foremost I wish to thank Professor Ralf Schirmacher for accepting me in his research group and allowing me to conduct my work in the finest imaginable research environment. Thank you for trusting my ideas and guiding the impetus behind my determination to move things forward. Also, thank you for allowing so many resources, financial and professional, to have fueled such a high risk endeavor – especially at the very beginning of the project where none of us really grasped the extent of what could emerge from it. Your open-mindedness, humility and conviction that science comes before personal interests have not only shaped the project we built but also built the scientist I am today. Thank you.

The insights gained during this project, especially regarding the applications of our work in human would have been unattainable without the key contribution of numerous collaborators. In particular, I wish to thank Prof. Pedro Rosa-Neto and Arturo Aliaga from the Douglas Mental Health University Institute at McGill University, for allowing me, from the very beginning, to learn and perform autoradiography experiments and for supporting numerous crucial experiments with human tissue. I wish to thank the entire research group of Prof. Peter Scott at the University of Michigan without whom the translational validation of multiple radiotracers presented in this thesis would not have been possible. Those include Dr. Andrew V. Mossine, Dr. Xia Shao, Carole A. Quesada, Phillip Sherman and of course Prof. Peter Scott himself. I also wish to thank Dr. Peter Bartenstein, Dr. Simon Lindner and Lena Vomacka from Ludwig-Maximilians University of Munich as well as Prof. Björn Wängler of Heidelberg University for collectively enabling the *in vivo* human evaluation of our clinical lead and for their remarkable professionalism. Other important people which were instrumental in the effective conduct of this project include, Prof. Alexey Kostikov (Montreal Neurological Institute), Dr. Anne Mahringer and Prof. Gert Fricker (Heidelberg University), Dr. Alexander Thiel (Lady Davis Institute), Dr. Jean-Paul Soucy (Montreal Neurological Institute), Prof. David R. Kaplan (University of Toronto), Dr.

Garrett M. Brodeur (The Children's Hospital of Philadelphia) and Dr. Hervé Sartelet (CHU Sainte-Justine). I wish to thank Antonio Aliaga, Dr. Justin J. Bailey and Dr. Melinda Wuest for their help with the preclinical imaging experiments, data collection and image reconstruction. I am also grateful to the multiple undergraduate and graduate students with whom I was fortunate to work with in the Schirmacher group; especially, I think here of my good friends Mehdi Boudjemeline and Sheldon Berke. I am also deeply grateful to Dr. Esther Schirmacher for the time spent at meticulously reviewing my work and manuscripts and providing significant and enlightening comments.

Also, I wish to acknowledge the important support from the different members of the Chemistry Departments at the Université de Montreal and the University of Alberta: Dr. Alexandra Furtos from the Centre for Mass Spectral Analysis (UdeM), Dr. Michel Simard from the X-ray diffraction laboratory (UdeM), Dr. Angelina Morales-Izquierdo Mass Spectrometry Laboratory (UofA), Dr. Mark Miskolzie from the Nuclear Magnetic Resonance Laboratory (UofA) and Dr. Robert McDonald the X-ray Crystallography Laboratory (UofA). I want to thank Dr. Gassan Massarweh, Robert Hopewell, Dean Jolly and Miriam M. Kovacevic from the Cyclotron Laboratory at the Montreal Neurological Institute as well as Dave Clendening and Blake Lazurko from the Edmonton PET Centre for radionuclide production. I am grateful to Prof. Frank Wuest for allowing me to work in his laboratory at the Cross Cancer Institute and for his time and suggestions as part of my thesis committee. I also wish to thank Prof. Carlos Velasquez-Martinez for his support as a member of my thesis committee.

J'aimerais finalement remercier ma famille et mes amis proches. En particulier, je me demande comment j'aurais pu traverser ces dernières années sans le support, la force calme et l'amour de ma fiancée. Marilyn, mon amour, je te l'ai dit déjà et je te le redirai encore, cette thèse est autant la mienne que la tienne.

Table of Contents

| | |
|---|----|
| Chapter 1. Introduction | 1 |
| 1.1 Overview of radiopharmaceutical development | 2 |
| 1.2 Trk family of neurotrophin receptors..... | 5 |
| 1.2.1 Trk signaling and role in neurobiology | 5 |
| 1.2.2 Trk structure and normal expression | 9 |
| 1.2.3 Trk in human diseases | 13 |
| 1.2.3.1 Role of Trk in neurological diseases and ageing | 13 |
| 1.2.3.2 Role of Trk in cancer | 13 |
| 1.2.3.3 Role of Trk in pain | 16 |
| 1.2.4 Structural biology considerations: Trk protein-small molecule interactions | 17 |
| 1.2.4.1 Small molecule neurotrophin mimics | 17 |
| 1.2.4.2 Trk kinase domains: structures, molecular basis for inhibition and selectivity | 20 |
| 1.2.5 Clinical trials with Trk inhibitors: current state | 29 |
| 1.3 Positron emission tomography imaging and radiotracer design | 36 |
| 1.3.1 Principle and instrumentation | 36 |
| 1.3.2 Development of small molecule PET radiotracers for neuroimaging | 39 |
| 1.3.3 Enzyme neuroimaging and oncological imaging using small molecule PET radioligands | 42 |
| 1.4 PET radiochemistry | 45 |
| 1.4.1 Overview of carbon-11 radiochemistry | 45 |
| 1.4.2 Overview of fluorine-18 radiochemistry | 47 |
| 1.6 Conclusion and objectives..... | 52 |
| 1.7 References | 53 |

| | |
|--|-----|
| Chapter 2. Article 5 | 82 |
| 2.1 Abstract | 83 |
| 2.2 Introduction..... | 83 |
| 2.3 Results and discussion..... | 85 |
| 2.3.1 Design of compounds..... | 85 |
| 2.3.2 Chemical syntheses | 88 |
| 2.3.3 Biological evaluations and in silico studies..... | 90 |
| 2.3.4 Radiosynthesis of [¹⁸ F] 2.10 | 94 |
| 2.4 Conclusion..... | 95 |
| 2.5 Supporting Information of Article 5 | 96 |
| 2.6 References | 135 |
| | |
| Chapter 3. Article 6 | 141 |
| 3.1 Abstract | 142 |
| 3.2 Introduction..... | 143 |
| 3.3 Results and discussion..... | 147 |
| 3.3.1 Synthesis and photoisomerization of (Z)- 3.9 | 147 |
| 3.3.2 In vitro binding assays | 149 |
| 3.3.3 Molecular docking study of compound 3.9 | 150 |
| 3.3.4 Radiolabeling of [¹¹ C] 3.9 | 151 |
| 3.3.5 In vitro metabolism of [¹¹ C] 3.9 | 153 |
| 3.3.6 In vitro autoradiography of [¹¹ C] 3.9 | 154 |
| 3.3.7 In vivo PET imaging of [¹¹ C] 3.9 in rats..... | 156 |
| 3.3.8 Design, syntheses and structure-activity-relationship (SAR) of 4-aza-2-oxindole derivatives towards ¹⁸ F-labeling | 157 |
| 3.3.9 Radiolabeling of [¹⁸ F] 3.10 | 162 |

| | |
|---|-----|
| 3.3.10 In vitro autoradiography of [¹⁸ F] 3.10 | 163 |
| 3.3.11 Preliminary in vivo PET imaging of [¹⁸ F] 3.10 in rats | 164 |
| 3.4 Conclusion..... | 165 |
| 3.5 Material and methods..... | 167 |
| 3.6 Supporting Information of Article 6 | 183 |
| 3.7 References | 195 |
| | |
| Chapter 4. Article 7 | 203 |
| 4.1 Abstract | 204 |
| 4.2 Introduction..... | 205 |
| 4.3 Results and discussion..... | 208 |
| 4.3.1 Amide moiety design for radiolabeling and chemistry | 210 |
| 4.3.2 In vitro binding studies..... | 214 |
| 4.3.3 Radiosyntheses and plasma stability | 217 |
| 4.3.4 In vitro autoradiography..... | 219 |
| 4.4 Conclusion..... | 220 |
| 4.5 Supporting Information of Article 7 | 222 |
| 4.6 References | 263 |
| | |
| Chapter 5. Article 8 | 269 |
| 5.1 Abstract | 270 |
| 5.2 Introduction..... | 271 |
| 5.3 Results | 273 |
| 5.3.1 Chemistry, biochemical evaluations and radiochemistry | 273 |
| 5.3.2 In vivo PET imaging of [¹¹ C]-(R)-IPMICF16 in the rodent brain demonstrates rapid and specific TrkB/C binding | 275 |

| | |
|--|-----|
| 5.3.3 [¹¹ C]-(R)-IPMICF16 accumulates in the non-human primate brain in accordance to TrkB/C expression | 280 |
| 5.3.4 [¹¹ C]-(R)-IPMICF16 binds TrkB/C in human post-mortem brain tissue and parallels decreased TrkB hippocampal density in AD brain tissue in vitro..... | 282 |
| 5.3.5 Imaging TrkB/C in the human brain using [¹¹ C]-(R)-IPMICF16 | 284 |
| 5.4 Discussion | 285 |
| 5.5 Conclusion..... | 287 |
| 5.6 Material and methods..... | 289 |
| 5.7 Supporting Information of Article 8 | 296 |
| 5.8 References | 346 |
| | |
| Chapter 6. Article 9 | 353 |
| 6.1 Abstract | 354 |
| 6.2 Introduction..... | 355 |
| 6.3 Results and discussion..... | 357 |
| 6.3.1 Compound optimization and in silico study | 357 |
| 6.3.2 Biological evaluation | 359 |
| 6.3.3 Development of (R)-[¹⁸ F]6.9 | 360 |
| 6.4 Conclusion..... | 363 |
| 6.5 Supporting Information of Article 9 | 365 |
| 6.6 References | 379 |
| | |
| Chapter 7. Conclusion and perspective | 382 |
| 7.1 Current and future work..... | 383 |
| 7.1.1 Development of [¹⁸ F]-(R)-IPMICF17 | 383 |
| 7.1.2 Proposed SAR for optimizing brain penetration of the IPMICF series | 392 |
| 7.1.3 Progress in the GW2580 series..... | 393 |

| | |
|---|------------|
| 7.1.4 Proposed work to improve the GW441756 series..... | 394 |
| 7.1.5 Proposed work with other scaffolds..... | 395 |
| 7.1.6 Current and proposed in vitro/in vivo experiments | 396 |
| 7.2 Conclusion and significance..... | 397 |
| 7.3 Material and methods..... | 399 |
| 7.4 References | 414 |
| Complete Bibliography | 419 |
| Annex 1. Additional Experimental Data (Crystallographic Data for Compounds 2.25 and (E)-2.29 from Supporting Information Section 7 - Chapter 2)..... | 456 |
| Annex 2. Additional Experimental Data (Crystallographic Data for Compounds 3.12 and (Z)-3.9 from Supporting Information Section 3 - Chapter 3)..... | 477 |
| Annex 3. Additional Experimental Data (NMR Spectrum and Crystallographic Data for Compound 4.22 from Supporting Information Section 5 and 6 - Chapter 4) | 498 |
| Annex 4. Additional Experimental Data (Chiral SFC/MS Analyses of Intermediates (±)-5.12, (R)-5.12 and (S)-5.12, Crystallographic Data for Compound (R_S-R)-5.9. and NMR Spectrum from Supporting Information Section 4, 5 and 8 - Chapter 5) | 549 |
| Annex 5. Additional Experimental Data (NMR Spectrum from Supporting Information Section 5 - Chapter 6)..... | 578 |
| Annex 6. Additional Experimental Data (NMR Spectrum and Crystallographic Data for Compound (2S,4S)-7.6 - Chapter 7)..... | 587 |

List of Tables

Chapter 1

Table 1.1. Properties of non-metal radionuclides commonly used in PET, corresponding half-lives, nuclear reactions, targets, products and decay products 37

Table 1.2. Physicochemical Properties, Weighting, and Parameter Ranges for CNS MPO and CNS PET MPO^a 41

Chapter 2

Table 2.1. *In Vitro* Activity of Fluorinated Diaminopyrimidine Inhibitors **2.10-2.12**, **2.20** and **2.9** 91

Table S2.1. Selectivity of compound **2.10** tested on a panel of 342 protein kinases at Reaction Biology Corporation. The results are expressed as the percentage of kinase activity measured at (...) 113

Table S2.2. Selectivity of compound **2.12** tested on a panel of 342 protein kinases at Reaction Biology Corporation. The results are expressed as the percentage of kinase activity measured at (...). 122

Chapter 3

Table 3.1. Potency and Physico-Chemical Data for 4-Aza-2-Oxindole Trk Inhibitors 160

Chapter 4

Table 4.1. SAR and *In Vitro* Enzymatic Activities and Physicochemical Data for Imidazo[1,2-*b*]pyridazines Trk Inhibitors 212

Table 4.2. Kinase Profiling of **4.16** and **4.27** 217

Table S4.1. Data for off-Trk inhibitory activity of compound **4.16** (0.1 μ M) 258

Table S4.2. Data for off-Trk inhibitory activity of compound **4.27** (0.1 μ M) 259

Table S4.3. PSL Data [¹⁸F]-(\pm)-**IPMICF6** Autoradiography 261

Table S4.4. PSL Data for [¹⁸F]-(\pm)-**IPMICF10** Autoradiography 261

Chapter 5

Table S5.1. Characteristics of TrkA/B/C inhibitors in recent and current clinical trials for cancer treatment (updated August 2016, <https://clinicaltrials.gov/>)..... 298

Table S5.2. SAR and *in vitro* enzymatic activities and physicochemical data for imidazo[1,2-*b*]pyridazines Trk inhibitors 300

Table S5.3. Demographic characteristics and autoradiography data for brain tissue from healthy controls and Alzheimer's disease patients 301

Table S5.4. Selectivity of (*R*)-IPMICF16 tested on a panel of 369 protein kinases at Reaction Biology Corporation (expressed as the percentage of kinase activity measured at 0.2 μ M of (*R*) IPMICF16 (...)) 322

Chapter 6

Table 6.1. In Vitro enzymatic activities and physico-chemical Data for Compounds (*S*)-**6.6**, (*R*)-**6.6** and (*R*)-**6.9**..... 359

Table 6.2 Kinase Profiling of (*R*)-**6.6** and (*R*)-**6.9** 360

Chapter 7

Table 7.1. SAR and *In Vitro* Enzymatic Activities and Physicochemical Data for Novel Imidazo[1,2-*b*]pyridazines Trk Inhibitors 388

List of Schemes

Chapter 1

- Scheme 1.1.** Representative examples of electrophilic ^{18}F -radiofluorination and the synthesis of 6- ^{18}F fluoro-L-DOPA. Comparison of electrophilic fluorodestannylation and silver-mediated radiosynthetic (...) 48
- Scheme 1.2.** General substrate scope for (A) $\text{S}_{\text{N}}\text{Ar}$ and (B) $\text{S}_{\text{N}}2$ ^{18}F -radiofluorination reactions and representative radiosynthesis of ^{18}F fluorodeoxyglucose (^{18}F FDG)..... 49
- Scheme 1.3.** Comparative radiosynthesis of ^{18}F flumazenil (^{18}F FMZ) by diaryliodonium salts and $\text{S}_{\text{N}}\text{A}$ 50
- Scheme 1.4.** Spirocyclic iodonium ylides approach and representative radiosynthesis of ^{18}F FPEB..... 50
- Scheme 1.5.** Comparison of representative conditions and application of the Cu-mediated ^{18}F -fluorination of arylboronate esters and acids. 51

Chapter 2

- Scheme 2.1.** Chemical synthesis of intermediate **2.20**. Reagents and conditions: (a) MOMCl, DIPEA, CH_2Cl_2 , 0°C – rt, 30 min, then rt, 20 h; (b) 3,4-dihydro-2*H*-pyran, PPTS cat., CH_2Cl_2 , rt, 12 h (...) 87
- Scheme 2.2.** Chemical synthesis of 2,4-diaminopyrimidines compounds **2.10-2.12**. Reagents and conditions: (a) K_2CO_3 , benzyl halide derivative, DMSO, EtOH, rt, 12 h. 88
- Scheme 2.3.** Chemical synthesis of intermediate **2.24**. Reagents and conditions: (a) K_2CO_3 , 2-fluoroethyl 4-methylbenzenesulfonate (**S2.5**), DMF, rt, 10 h; (b) LiAlH_4 , THF, 0°C – rt, 2-4 h; (c) cyanuric (...). 89
- Scheme 2.4.** Reagents and conditions: (a) Benzyl halide, K_2CO_3 , DMF, $70^\circ\text{C}/3$ h or rt/12 h rt; (b) 3-morpholinopropionitrile, DMSO, $60-75^\circ\text{C}$, 40 min; (c) aniline.HCl, *i*-PrOH, 40°C , 30 min; (d) guanidine.HCl (...). 89
- Scheme 2.5.** Radiosynthesis of ^{18}F **2.10**. Reagents and conditions: (a) ^{18}F **S2.8**, Cs_2CO_3 , TBAI, DMSO/EtO₂ (2:1), 100°C , 10 min. 94
- Scheme S2.1.** Radiosynthesis of ^{18}F **S2.8** and ^{18}F **2.10**. 133

Chapter 3

- Scheme 3.1.** Synthesis of (*Z*)-**3.9** and (*E*)-**3.9**. Reagents and conditions: (a) NaH, dimethyl malonate, DMSO, rt, 30 min then 100°C , 1 h (97 %). (b) LiCl, H_2O , DMSO, rt - 100°C , 18h (98 %) (...) 148

Scheme 3.2. Syntheses of 3-((1-methyl-1*H*-indol-3-yl)methylene)-1*H*-pyrrolo[3,2-*b*]pyridin-2(3*H*)-one. Reagents and conditions: (a) indole-3-carboxaldehyde fragment, AcOH, HCl_{conc}, 40°C (...) 159

Scheme 3.3. Synthesis and photoisomerization of (*Z*)-[¹⁸F]**3.7b**. (A) Reagents and conditions: (a) **3.22b**, AcOH, HCl_{conc}, 40°C, 12 h (44 %). (b) KOH(s), [¹⁸F]FETos, DMF, 90°C, 10 min (...) 162

Scheme S3.1. Mechanistic rationale for the synthesis of (*Z*)-**3.9** from intermediate **3.15**. The formation of (*Z*)-**3.9** proceeds via the sterically less congested β-hydroxyketone transition states TS₁ (...) 184

Chapter 4

Scheme 4.1. Reagents and conditions: (A) (a) *N*-*boc*-ethanolamine, NaH, DMF, rt, 12 h (50%). (b) TFA, CH₂Cl₂, rt, 1 h, then HCl (1M in diethyl ether) (98%). (B) (c) Boc₂O, Et₃N, THF, 0°C - rt, 16 h (...) 214

Scheme 4.2. Reagents and conditions: (a) 3-Aminocyclobutanol hydrochloride, HATU, DIPEA, DMF, rt, 12 h (99%). (b) TsCl, Et₃N, CH₂Cl₂, rt, 48 h (70%). (c) Kryptofix-222/K⁺/[¹⁸F]F⁻, DMF, 120°C (...) 218

Scheme 4.3. Reagents and conditions: (a) TBDPSCI, imid., DMF, rt, 16 h (80%). (b) **9**, HATU, DIPEA, DMF, rt, 12 h (99%). (c) TBAF, THF, rt, 2 h (89%). (d) TsCl, Et₃N, CH₂Cl₂, rt, 96 h (64%). (...) 219

Scheme S4.1. Syntheses of amides **4.11-4.27**. Reagents and conditions: (a) 2-(3-Fluorophenyl)pyrrolidine, KF, DMSO, 100°C, 22 h (77%). (b) ammonia solution (7.0 M in methanol) (...) 224

Chapter 6

Scheme 6.1. Synthesis of (*R*)-2-(1-(6,7-dimethoxyquinazolin-4-yl)pyrrolidin-3-yl)-*N*-(4-(2-fluoroethyl)phenyl)acetamide (*R*)-**6.9**. Reagents and conditions: (a) 4-(2-Fluoroethyl)aniline, HBTU (...) 361

Scheme 6.2. Synthesis of the mesylate precursor **6.16**. Reagents and conditions: (a) TBDPSCI, imid., DMF, rt, 16 h (80%); (*R*)-(1-*Boc*-pyrrolidin-3-yl)-acetic acid, HBTU, DIPEA, DMF, rt, 16 h (78%) (...) 363

Scheme 6.3. Radiosynthesis of (*R*)-[¹⁸F]**6.9** ([¹⁸F]-(*R*)-QMICF). Reagents and conditions: (a) Kryptofix-222/K⁺/[¹⁸F]F⁻, MeCN, 80°C, 20 min (...) 363

Chapter 7

Scheme 7.1. Synthesis of novel imidazo[1,2-*b*]pyridazine inhibitors. Reagents and conditions: (a) TBSCl, imidazole, DMF, rt, 3 h; (b) Boc₂O, MeCN, Et₃N, DMAP, (83%, 2 steps); (c) 3-Fluorophenyl (...) 385

Scheme 7.2. Synthesis of non-fluorinated inhibitor 7.17. Reagents and conditions: (a) 2-Phenylpyrrolidine, KF, DMSO, 110°C, 16 h (94%); (b) MeNH₂, rt, 16 h (62 %). 387

Scheme 7.3. Synthesis of boronic ester precursor 7.19 and radiosynthesis of [¹⁸F]-(*R*)-IPMICF17. Reagents and conditions: (a) 4-Aminophenylboronic acid pinacol ester, HBTU, DIPEA (...) 391

List of Figures

Chapter 1

| | |
|--|----|
| Figure 1.1. Overview of PET radiopharmaceutical development..... | 3 |
| Figure 1.2. Overview of synaptic functions mediated by neurotrophins/Trk receptors (NTs: neurotrophins; PLC γ : phospholipase γ pathway; MAPK: mitogen-activated protein kinase; MYO6 (...))..... | 7 |
| Figure 1.3. (A) Sequence of human TrkA. Residues from the extracellular domain are shown in cyan. Residues from the transmembranar domain are shown in pale blue. Residues from the kinase (...) | 10 |
| Figure 1.4. Expression of Trk in the rodent CNS. (A) Sagittal depiction of the mouse brain (caudate/ putamen/ basal forebrain outlined). Analogous sections corresponding to (B,C,E) <i>NTRK1</i> (...) | 12 |
| Figure 1.5. (A) Representation of TrkA isoforms including deletions and mutations. (B) Schematic overview of known NTRK1-3 fusions with corresponding tumor types. Known gene partner (...) | 15 |
| Figure 1.6. (A) Carton/stick and (B) surface rendering of the coil-coiled structure of a representative tropomyosin polypeptide (PDB ID: 1MV4) | 16 |
| Figure 1.7. Extracellular Trk receptor domains and binding interfaces with neurotrophins – potential druggable sites; (A,B) Two views of the NGF-TrkA-d5 complex (PDB ID: 2IFG). (C) Interaction (...) | 18 |
| Figure 1.8. Representative Trk extracellular-binding small molecules and peptide-based probes | 20 |
| Figure 1.9. Trk kinase domain. (A) Overlap of TrkA, TrkB and TrkC kinase domain (inactive conformations, PDB ID: 4FOI, 4ASZ, 3V5Q). (B,C) Views of the conformational differences between (...) | 21 |
| Figure 1.10. Representative examples of early Trk-TKI inhibitors (pre-2011). The hinge binder fragments are shown in blue..... | 22 |
| Figure 1.11. (A) Apo-TrkA DFG-out (PDB: 4FOI) with key structural features depicted in bronze. (B) Superposition of the Phe565/Phe521 residues of glycine-rich loops of TrkB (shades of green) (...) | 24 |
| Figure 1.12. Representative examples of Trk-TKI inhibitors (2011-present). The hinge binder fragments are shown in blue (when applicable). | 25 |

| | |
|---|----|
| Figure 1.13. (A) Co-crystal structure of TrkA (gray) with a urea-based type III inhibitor 1.31 (salmon). The juxtamembrane domain (JM) sequence is shown in orange and the DFG motif in yellow (...) | 27 |
| Figure 1.14. Trk-TKI under evaluation in clinical trials for the treatment of cancer | 31 |
| Figure 1.15. (A) Cyclotron (adapted from http://www.iba-radiopharmasolutions.com/products/cyclotrons - accessed Jan 2017). (B) Plan view diagram of the path of ions in a classical (...) | 36 |
| Figure 1.16. Principle of positron emission tomography. | 39 |
| Figure 1.17. (A) Representation of bound and unbound drug concentration equilibrium across BBB (B) Relation between unbound brain-to-plasma ratio ($K_{p,uu}$) and transport across the BBB (adapted (...)) | 40 |
| Figure 1.18. (A,B) CNS PET radiotracers in clinical research based on target classes (adapted CNS Radiotracer Table http://www.nimh.nih.gov/researchpriorities/therapeutics/cns-radiotracer-table.shtml (...)) | 42 |
| Figure 1.19. Overview of carbon-11 radiochemistry | 46 |

Chapter 2

| | |
|--|-----|
| Figure 2.1. Chemical structures of selected Trk receptor ligands and radioligands | 85 |
| Figure 2.2. (A) Binding interactions of GW2580 (2.9) to TrkB based on the co-crystal structure of 2.9 -TrkB (PDB code: 4AT5). Hydrogen bonds between the ligand and the hinge region, DFG motif (...) | 86 |
| Figure 2.3. Predicted binding poses of 2.10 (purple) and 2.11 (cyan) bound to TrkB (PDB code: 4AT5) showing (A) the hinge binding interactions and (B) the interaction with Asp710 from the DFG (...) | 92 |
| Figure 2.4. Selectivity profile of compound (A) 2.10 and (B) 2.12 tested on a panel of 342 kinases. The kinome dendrogram represents the percent of inhibition at 1.0 μ M of inhibitors. The (...) | 93 |
| Figure S2.1. Dose-response curves for the in vitro kinase assays with 2.9 , 2.10 , 2.11 and 2.12 versus (A) CSF-1R, (B) TrkA, (C) TrkB and (D) TrkC. The inhibitors were tested at ten different concentrations (...) | 130 |
| Figure S2.2. Different angles presenting the overlay between the ortho-fluoro diaminopyrimidine derivative 2.11 (cyan) and 2.9 (green) docking poses in the hydrophobic back pocket of CSF-1R (...) | 131 |
| Figure S2.3. (A) Conformation of GW2580 in complex with TrkB (the same conformation has been observed with (GW2580-CSF-1R). The tail benzyloxy group is nearly perpendicular to the central (...) | 131 |

Chapter 3

- Figure 3.1.** Chemical structures of selected Trk receptor ligands and radioligands 145
- Figure 3.2.** Comparison of the predicted binding poses for (Z)-**3.9** bound to (A) TrkC (PDB code: 3V5Q) with a DFG-out binding mode and to (B,C) TrkB (PDB code: 4AT3) and with a DFG-in (...) 150
- Figure 3.3.** Synthesis of precursor (E)-**3.16** and radiosyntheses of (Z)-[¹¹C]**3.9** and (E)-[¹¹C]**3.9**. (A) Reagents and conditions: (a) Indole-3-carboxaldehyde, AcOH, HCl_{conc}, 40°C, 12 h. (B) Optimization (...) 152
- Figure 3.4.** *In silico* top predicted CYP-mediate sites of metabolism for (Z)-**3.9** and (E)-**3.9** and corresponding metabolites confirmed by RLM assays. 154
- Figure 3.5.** (A) Representative *in vitro* autoradiography in four representative coronal sections of rat brain. (*Upper row*) Autoradiography images showing the binding of [¹¹C]**3.9** alone. (*Middle row*) (...) 155
- Figure 3.6.** PET studies in Sprague Dawley rats. Time-radioactivity curves (TACs) illustrate the accumulation of [¹¹C]**3.9** in (A) the whole brain and (B) the lungs as function of time for baseline studies (...) 156
- Figure 3.7.** Design rationale and docking modes for 4-aza-oxindole-based Trk inhibitors. (A) Potential binding site interaction between TrkB and inhibitor (Z)-**3.9** based on docking studies. (B,C) (...) 158
- Figure 3.8.** (A) Representative *in vitro* autoradiograms and cresyl violet staining from coronal sections of rat brain showing the binding of [¹⁸F]**3.10** and competition experiments with **3.9** (10 μM). (...) 163
- Figure 3.9.** Preliminary metabolism and PET studies with [¹⁸F]**3.10** in sprague dawley in rats. Time-activity curves for (A) brain regions (*n* =3) at baseline, (B) for selected organs (*n* =1) and (C) (...) 165
- Figure S3.1.** Assessment of the conformational equilibrium leading to the formation of (E)-**3.9** from (Z)-**3.9**. (A) Photoisomerization of a mixture (Z)-**3.9** > (E)-**3.9** in H₂O (pH 6) monitored by UV-vis (...) 185
- Figure S3.2.** The structure of (*left*) the crystalized MeOH•(Z)-**3.9**, (*center*) the low-energy calculated structure of (Z)-**3.9** and (*right*) the low-energy calculated structure of (E)-**3.9** (FITTED) (...) 186
- Figure S3.3.** Top predicted binding mode of (E)-**3.9** within the active site of TrkA from FITTED docking (PDB code: 4AOJ) 186
- Figure S3.4.** Comparison of the modeled binding of (Z)-**3.9** with (A) TrkB (PDB code: 4AT3) and (B) TrkA (PDB code: 4AOJ) both in DFG-in conformation. Minor differences include the replacement (...) 187

| | |
|--|-----|
| Figure S3.5. Plausible mechanistic explanation for the formation of (Z)-[¹¹ C] 3.9 from (E)- 3.16 . (A) ¹¹ C-methylation plausibly proceeds through the more stable 3-2'-s- <i>trans</i> -azatriene enolate intermediate (...) | 188 |
| Figure S3.6. UV-visible spectra changes upon treatment 3.9 (E/Z mixture) with NaOH _(aq) under aqueous condition (identical condition to Figure S3.5) does not lead to a bathochromic shift. | 188 |
| Figure S3.7. In silico predicted sites of metabolism using IMPACT (In-silico Metabolism Prediction by Activated Cytochromes and Transition States) with transitions states modeling exemplified (...) | 189 |
| Figure S3.8. HPLC chromatograms over 90 min for the RLM assay with (E/Z)- 3.9 . | 190 |
| Figure S3.9. ¹ H-NMR spectra at different time points during the course of the ambient light-induced photoisomerization of (Z)- 3.10 leading to the formation of (E)- 3.10 . | 190 |
| Figure S3.10. (A-C) LC-MS/MS analysis of the 3.10 E/Z mixture. | 191 |
| Figure S3.11. Dose-response curves for the [γ - ³³ P]ATP-based enzymatic in vitro assays with 3.16 , 3.10 and 3.18a-e versus (A) TrkA, (B) TrkB and (C) TrkC. The inhibitors were tested at ten different (...) | 191 |
| Figure S3.12. In vitro autoradiography of four representative sections from four human neuroblastoma tumor. (A) Autoradiography images showing the binding of [¹⁸ F] 3.10 alone and in co-incubation (...) | 192 |
| Figure S3.13. HPLC chromatograms over 60 min for the RLM assay with (E/Z)- 3.10 . | 192 |

Chapter 4

| | |
|---|-----|
| Figure 4.1. Structure of Trk agonistic radioligands, tyrosine kinase inhibitor (TKIs) radioligands and fluorophenyl- and difluorophenyl pyrrolidine-containing Trk TKIs. | 206 |
| Figure 4.2. Predicted binding poses for (R)- 4.27 bound to TrkA/B in DFG-in conformation. (A) Docking of (R)- 4.27 to the ATP binding site of TrkA (PDB 4PMT). (B) Surface model of (R)- 4.27 docked (...) | 209 |
| Figure 4.3. Single-crystal X-Ray structure of (R)- 4.22 ; ellipsoids drawn at 30% probability. | 215 |
| Figure 4.4. Representative <i>in vitro</i> autoradiograms from coronal sections of rat brain showing the binding of [¹⁸ F] 4.16 and competition experiments with 4.16 (1 μ M) (successive sections between (...) | 220 |
| Figure S4.1. Comparison of the predicted binding poses for (R)- 4.16 bound to TrkA/B/C in DFG-in (A-C) and DFG-out (D-F) conformations. (A) Docking of (R)- 4.16 (<i>trans</i> -substituted cyclobutyl (...) | 244 |
| Figure S4.2. (A) Docking of <i>trans</i> -(S)- 4.16 to the ATP binding site of TrkB (PDB 4AT3). (B) Surface model of <i>trans</i> -(S)- 4.16 docked to TrkB. (C) Superposition of TrkA (blue, PDB 4PMT) and (...) | 245 |

| | |
|---|-----|
| Figure S4.3. Typical semi-preparative HPLC chromatogram of the radiofluorination of the tolylate precursor 4.36 leading to the formation of [¹⁸ F]-(\pm)- IPMICF6 (HPLC Method A). (In this instance(...)) | 249 |
| Figure S4.4. Representative HPLC-QC chromatogram of the collected [¹⁸ F]-(\pm)- IPMICF6 co-injected with the non-radioactive standard 4.16 (HPLC Method A) | 249 |
| Figure S4.5. HPLC analysis of human plasma at 60 min after [¹⁸ F]-(\pm)- IPMICF6 incubation at 37°C (HPLC Method B) | 250 |
| Figure S4.6. Typical semi-preparative HPLC chromatogram of the radiofluorination of the tolylate precursor 4.41 leading to the formation of [¹⁸ F]-(\pm)- IPMICF10 (HPLC Method C). | 250 |
| Figure S4.7. Representative HPLC-QC chromatogram of the collected [¹⁸ F]-(\pm)- IPMICF10 co-injected with the non-radioactive standard 4.27 (HPLC Method C) | 251 |
| Figure S4.8. HPLC analysis of human plasma at 60 min after [¹⁸ F]-(\pm)- IPMICF10 incubation at 37°C (HPLC Method C). | 251 |
| Figure S4.9. HPLC-QC chromatogram of the collected/formulated [¹⁸ F]-(\pm)- IPMICF6 (HPLC Method F) (McConnell Brain Imaging Center Site) | 252 |
| Figure S4.10. HPLC-QC chromatogram of the collected/formulated [¹⁸ F]-(\pm)- IPMICF10 (HPLC Method F). (McConnell Brain Imaging Center Site) | 252 |
| Figure S4.11. Dose-response curve for inhibitor 4.9 (left; <i>n</i> = 1) and 4.10 (right; <i>n</i> = 1) versus TrkA, TrkB and TrkC. | 253 |
| Figure S4.12. Dose-response curve for inhibitor 4.11 (left; <i>n</i> = 1) and 4.12 (right; <i>n</i> = 1) versus TrkA, TrkB and TrkC. | 254 |
| Figure S4.13. Dose-response curve for inhibitor 4.13 (left; <i>n</i> = 3) and 4.14 (right; <i>n</i> = 3) versus TrkA, TrkB and TrkC (error bars represent standard deviation from the mean). | 254 |
| Figure S4.14. Dose-response curve for inhibitor 4.15 (left; <i>n</i> = 3) and 4.16 (right; <i>n</i> = 3) versus TrkA, TrkB and TrkC (error bars represent standard deviation from the mean). | 254 |
| Figure S4.15. Dose-response curve for inhibitor 4.17 (left; <i>n</i> = 1) and 4.18 (right; <i>n</i> = 1) versus TrkA, TrkB and TrkC. | 255 |
| Figure S4.16. Dose-response curve for inhibitor 4.19 (left; <i>n</i> = 1) and 4.20 (right; <i>n</i> = 1) versus TrkA, TrkB and TrkC. | 255 |
| Figure S4.17. Dose-response curve for inhibitor 4.21 (left; <i>n</i> = 1) and 4.22 (right; <i>n</i> = 1) versus TrkA, TrkB and TrkC. | 255 |
| Figure S4.18. Dose-response curve for inhibitor 4.23 (left; <i>n</i> = 1) and 4.24 (right; <i>n</i> = 1) versus TrkA, TrkB and TrkC. | 256 |
| Figure S4.19. Dose-response curve for inhibitor 4.25 (left; <i>n</i> = 3) and 4.26 (right; <i>n</i> = 3) versus TrkA, TrkB and TrkC (error bars represent standard deviation from the mean). | 256 |

| | |
|--|-----|
| Figure S4.20. Dose-response curve for inhibitor 4.27 (left; $n = 3$) and staurosporine (control, right; $n = 1$) versus TrkA, TrkB and TrkC (error bars represent standard deviation from the mean)..... | 256 |
| Figure S4.21. Inhibition of TrkB kinase versus TrkB selectivity with regard to TrkA. The potencies are expressed as $-\log_{10}(IC_{50})$. Inhibitors 4.16 and 4.27 were selected based on TrkB potency (...). | 257 |
| Figure S4.22. (A) Representative <i>in vitro</i> autoradiograms from coronal sections of rat brain showing the binding of [^{18}F] 4.27 (A, right) and competition experiments with GNF-5837 (10 μ M) (A, left) (...) | 260 |

Chapter 5

| | |
|--|-----|
| Figure 5.1. Binding mode, potency/affinity and kinome selectivity profiling of (<i>R</i>)-IPMICF16. (a) View of the predicted type-I binding mode of (<i>R</i>)-IPMICF16 with TrkA (grey ribbons, PDB: 4PMT) (...) | 273 |
| Figure 5.2. Preclinical <i>in vivo</i> PET imaging of [^{11}C](\pm)-IPMICF16, [^{11}C](<i>R</i>)-IPMICF16 and [^{11}C]GW441756 in FVB and <i>Mdr1a/b</i> ^(-/-) <i>Bcrp1</i> ^(-/-) mice, [^{11}C](<i>R</i>)-IPMICF16 <i>in vivo</i> stability and blocking (...) | 276 |
| Figure 5.3. <i>In vivo</i> PET imaging of [^{11}C](<i>R</i>)-IPMICF16, [^{11}C](\pm)-IPMICF16 and [^{11}C]GW441756 in the rhesus monkey brain. CB, cerebellum; CC, corpus callosum; Ctx, cortex; TH, thalamus. (a) (...) | 281 |
| Figure 5.4. Regional quantification for the <i>in vitro</i> human brain tissue autoradiography experiments with [^{11}C](<i>R</i>)-IPMICF16. Quantification for the hippocampus ($n = 11-12$) (a,b), inferior (...) | 282 |
| Figure 5.5. <i>In vivo</i> PET imaging of [^{11}C](<i>R</i>)-IPMICF16 in the human brain. Top row: V_T images (RE plot) of the human subject illustrating the distribution of TrkB/C. The highest values are observed (...) | 284 |
| Figure S5.1. Trk tyrosine kinase inhibitor radiotracers, selected clinical Trk inhibitors and synthesis of [^{11}C](<i>R</i>)-IPMICF16. The key (<i>R</i>)-2-(3-fluorophenyl)pyrrolidine ((<i>R</i>)- 5.11) intermediate (...) | 302 |
| Figure S5.2. The racemic series. The decision to convert inhibitors 5.1-5.4 into radiotracers ensues from favorable CNS drug-like and radiotracer-like attributes evidenced by multiparameter (...) | 303 |
| Figure S5.3. Structure (left) and dose-response curve (right) for inhibitor (<i>S</i>)-IPMICF16 ($n = 1$) versus TrkA, TrkB and TrkC ($[\gamma\text{-}^{33}P]$ ATP-based enzymatic assay performed by Reaction Biology)..... | 304 |
| Figure S5.4. Preclinical rodents <i>in vivo</i> PET imaging data for representative IPMICF radiotracers. (a) TACs showing tracer uptakes (whole brain) for [^{18}F](\pm)-IPMICF6, [^{18}F](\pm)-IPMICF10 (...) | 305 |

| | |
|---|-----|
| Figure S5.5. [¹¹ C]-(\pm)-IPMICF16 biodistribution in mice. Selected biodistribution data presenting the accumulation of [¹¹ C]-(\pm)-IPMICF16 in liver, kidneys, blood (heart), lung in comparison to brain (...) | 306 |
| Figure S5.6. Calcein-AM and BODIPY-Prazosin cellular assays and Lineweaver Burk plot to study interactions with P-gp and BCRP. Calcein-AM assays were conducted in human P-gp overexpressing (...) | 307 |
| Figure S5.7. Rhesus monkey regional brain TACs from radiotracers screening. TACs showing tracers binding and regional distribution in baseline conditions in the NHP brain for (a) [¹⁸ F]-(\pm)-IPMICF6 (...) | 308 |
| Figure S5.8. Comparative regional SUV ratio (SUVR, summed 0-60 min) for [¹¹ C]-(<i>R</i>)-IPMICF16, [¹¹ C]-(\pm)-IPMICF16 and [¹¹ C]GW441756. | 309 |
| Figure S5.9. [¹¹ C]-(<i>R</i>)-IPMICF16 binding is highly specific and TrkB/C-selective in the human brain <i>in vitro</i> . Representative <i>in vitro</i> autoradiograms. Sections of human brains showing the binding (...) | 310 |
| Figure S5.10. Analysis of [¹¹ C]-(<i>R</i>)-IPMICF16 in the human brain. (a) Time activity curves of the human [¹¹ C]-(<i>R</i>)-IPMICF16 study 0-60 min p.i.. For illustrative purposes the SUV scale was truncated (...) | 311 |
| Figure S5.11. Unbound fraction in the plasma (Fu _p) based on 3 measurements made 6, 18, and 20 min post injection. | 312 |
| Figure S5.12. Image derived input function (IDIF) of whole blood (blue) obtained from images with TrueX reconstruction and rescaling based on a bi-exponential fit to manual blood sample data (...) | 313 |
| Figure S5.13. ORTEP view of the C ₁₄ H ₂₁ ClF ₃ NOS compound with the numbering scheme adopted ((<i>R</i> _S - <i>R</i>)-5.9). | 320 |
| Figure S5.14. Representative semi-preparative HPLC chromatograms for the radiosynthesis [¹¹ C]-(<i>R</i>)-IPMICF16 (UV yellow, Rad blue). | 332 |
| Figure S5.15. Representative HPLC-QC chromatograms of the collected [¹¹ C]-(<i>R</i>)-IPMICF16 co-injected with the non-radioactive standard IPMICF16 (5.3) (UV yellow, Rad blue). | 333 |
| Figure S5.16. Representative semi-preparative HPLC chromatograms for the radiosynthesis [¹¹ C]-(\pm)-IPMICF22 (UV yellow, Rad blue). | 334 |
| Figure S5.17. Representative HPLC-QC chromatograms of the collected [¹¹ C]-(\pm)-IPMICF16 co-injected with the non-radioactive standard IPMICF22 (5.4) (UV yellow, Rad blue) | 334 |
| Figure S5.18. Representative semi-preparative HPLC chromatograms for the radiosynthesis [¹⁸ F]-(\pm)-IPMICF6 (Rad above, UV below). | 336 |

| | |
|---|-----|
| Figure S5.19. Representative HPLC-QC chromatograms of the collected [¹⁸ F]-(\pm)-IPMICF6 co-injected with the non-radioactive standard IPMICF6 (5.1) (UV above, Rad below)..... | 336 |
| Figure S5.20. Representative semi-preparative HPLC chromatograms for the radiosynthesis [¹⁸ F]-(\pm)-IPMICF10 (Rad above, UV below)..... | 337 |
| Figure S5.21. Representative HPLC-QC chromatograms of the collected [¹⁸ F]-(\pm)-IPMICF10 co-injected with the non-radioactive standard IPMICF10 (5.2) (UV above, Rad below)..... | 338 |
| Figure S5.22. Representative semi-preparative HPLC chromatogram for the radiosynthesis [¹¹ C]-(<i>R</i>)-IPMICF16 (UV above, Rad below)..... | 339 |
| Figure S5.23. Representative HPLC-QC chromatograms of the collected [¹¹ C]-(<i>R</i>)-IPMICF16 co-injected with the non-radioactive standard IPMICF16 (5.3) (UV above, Rad below)..... | 339 |
| Figure S5.24. Representative semi-preparative HPLC chromatograms for the radiosynthesis [¹¹ C]-(\pm)-IPMICF22 (UV above, Rad below)..... | 340 |
| Figure S5.25. Representative HPLC-QC chromatograms of the collected [¹¹ C]-(\pm)-IPMICF22 co-injected with the non-radioactive standard IPMICF22 (5.4) (UV above, Rad below)..... | 340 |
| Figure S5.26. Representative semi-preparative HPLC chromatograms for the radiosynthesis [¹¹ C]GW441756 (UV above, Rad below). | 341 |
| Figure S5.27. Representative HPLC-QC chromatograms of the collected [¹¹ C]GW441756 co-injected with the non-radioactive standard GW441756 (5.5) (UV above, Rad below)..... | 342 |
| Figure S5.28. Representative HPLC-QC chromatogram of the collected [¹¹ C]-(<i>R</i>)-IPMICF16 used for in vitro autoradiography experiments..... | 343 |

Chapter 6

| | |
|---|-----|
| Figure 6.1. Chemical structures and characteristics of (A) pan-Trk anticancer inhibitors under clinical investigation, (B) quinazoline-based EGFR/HER2 radiolabeled inhibitors validated in clinical (...) | 356 |
| Figure 6.2. Comparison of the predicted binding poses for (<i>R</i>)- 6.6 (yellow) and (<i>S</i>)- 6.6 (cyan) bound to TrkB in the DFG-out conformation (PDB code: 4AT5) at (A) the hinge and at (B) the DFG (...) | 358 |
| Figure 6.3. Results from Calcein-AM uptake assay demonstrate low interaction of (<i>R</i>)- 6.9 with P-gp in the range of 1-10 μ M (the intracellular fluorescence in the absence of test compounds was (...)) | 362 |
| Figure S6.1. Dose-response curves for inhibitors (<i>R</i>)- 6.6 , (<i>S</i>)- 6.6 against TrkA, TrkB and TrkC. | 374 |

Chapter 7

- Figure 7.1.** [^{11}C]-(*R*)-IPMICF16: first round of lead optimization. 384
- Figure 7.2.** Dose-response curve for inhibitor (*R*)-IPMICF17 versus TrkA, TrkB, TrkC, ($[\text{ATP}] = K_{\text{m ATP}}, n = 3$, error bars represent standard deviation from the mean). ($[\gamma\text{-}^{33}\text{P}]\text{ATP}$ -based enzymatic (...))..... 390
- Figure 7.3.** Structural optimization of the IPMICF series. (A) First and second generation IPMICF radiotracers. (B) Putative structural modification for optimization. (C) Macrocyclic IPMICF (...))..... 392
- Figure 7.4.** Predicted binding poses for representative macrocyclic Trk inhibitor lead bound to TrkA in DFG-in conformation (PDB 4PMT). (A) Docking of the inhibitor to the ATP binding site of TrkA (...)) 393
- Figure 7.5.** Novel radiosynthesis of [^{18}F]7.27 394
- Figure 7.6.** Conformational stabilisation via bioisosteric modifications of GW441756. (A) Photoisomerization of [^{11}C]GW441756. (B) Potential structural modification to address the photoisomerization (...))..... 395
- Figure 7.7.** Predicted binding poses for compound 7.32 bound to TrkA in DFG-in conformation (PDB 4AT3). (A) Docking of the inhibitor to the ATP binding site of TrkA. (B) Surface model of the (...))..... 396

List of Abbreviations

| | |
|------------|--|
| β^+ | positron |
| β^- | electron |
| $A\beta$ | beta-amyloid |
| Ac | acetyl |
| AD | Alzheimer's disease |
| ADME | absorption, distribution, metabolism, and excretion |
| ALK | anaplastic lymphoma kinase |
| AM | acetoxymethyl |
| AML | acute myeloid leukemia |
| AMPA | α -amino-3-hydroxy-5-methyl-4-isoxazolepropionic acid |
| aq. | Aqueous |
| ATP | adenosine triphosphate |
| Ar | aryl |
| BBB | blood-brain barrier |
| BCRP | breast cancer resistance protein |
| BDNF | brain-derived neurotrophic factor |
| B_{max} | total density (concentration) of receptor |
| Boc | tert-butoxycarbonyl |
| Bq | becquerel |
| br. | broad |
| BW | body weight |
| CDK | cyclin-dependent kinase |
| $CHCl_3$ | chloroform |
| CH_2Cl_2 | dichloromethane |
| Ci | curie |

| | |
|------------------------|---------------------------------------|
| CNS | central nervous system |
| Cm | centimeter |
| conc. | Concentrated |
| CP | caudate putamen |
| CSR-1R | colony-stimulating factor-1 receptor |
| CRC | colorectal cancer |
| CYP | cytochrome p450 |
| <i>d</i> | deuterium |
| DCM | dichloromethane |
| DFG | Asp-Phe-Gly sequence |
| DHF | dihydroxyflavone |
| DIPEA | N,N-diisopropylethylamine |
| DLT | dose-limiting toxicity |
| DMF | dimethylformamide |
| DMSO | dimethyl sulfoxide |
| ECD | extracellular domain |
| EC₅₀ | half maximal effective concentration |
| EDG | electron-donating group |
| EOB | end of bombardment |
| ERK | extracellular signal-regulated kinase |
| Et₃N | triethylamine |
| EtOAc | ethyl acetate |
| EtOH | ethanol |
| eV | electron-volt |
| EWG | electron-withdrawing group |
| FDA | food and drug administration |
| FETos | 2-fluoroethyl tosylate |

| | |
|------------------------------------|---|
| FISH | fluorescence <i>in situ</i> hybridization |
| FL | full length |
| FLT-3 | fms like tyrosine kinase 3 |
| <i>f_{u,b}</i> | unbound fraction in brain |
| <i>f_{u,p}</i> | unbound fraction in plasma |
| GPCR | G protein-coupled receptor |
| h | hour(s) |
| H⁻ | hydride |
| HATU | (1-[bis(dimethylamino)methylene]-1H-1,2,3-triazolo[4,5-b]pyridinium 3-oxid hexafluorophosphate) |
| HBTU | (2-(1 <i>H</i> -benzotriazol-1-yl)-1,1,3,3-tetramethyluronium hexafluorophosphate) |
| HCl | hydrochloric acid |
| HD | Huntington's disease |
| HPLC | High-performance liquid chromatography |
| HRMS | High resolution mass spectrometry |
| Hz | hertz |
| IC₅₀ | half maximal inhibitory concentration |
| IDIF | image-derived input function |
| Ig | immunoglobulin domain |
| IHC | immunohistochemistry |
| i-PrOH | propan-2-ol |
| J | coupling constant |
| JM | juxtamembrane domain |
| K₂₂₂ | kryptofix-222 |
| K₂CO₃ | potassium carbonate |
| KF | potassium fluoride |
| K_i | inhibitory constant |

| | |
|-------------------------------------|---------------------------------------|
| KID | kinase insert domain |
| KOH | potassium hydroxide |
| LG | leaving group |
| LiAlH₄ | lithium aluminum hydride |
| LiHMDS | Lithium bis(trimethylsilyl)amide |
| LogD | logarithm of distribution coefficient |
| LogP | logarithm of partition coefficient |
| LRR | leucine-rich repeat |
| M | molar, mol/L |
| MAPK | mitogen-activated protein kinase |
| MDCKII | Madin-Darby canine kidney cell |
| Me | methyl |
| MeCN | acetonitrile |
| MeCP2 | methyl CpG binding protein 2 |
| MeOH | methanol |
| min | minute(s) |
| MOMCl | chloromethyl methyl ether |
| MPO | multiparameter optimization |
| MW | molecular weight |
| MW_{FC} | fluorine-corrected molecular weight |
| mTOR | mammalian target of rapamycin |
| <i>n</i> | neutron |
| NaH | sodium hydride |
| NaHCO₃ | sodium bicarbonate |
| Na₂SO₄ | sodium sulfate |
| NGF | nerve growth factor |

| | |
|-------------------------------|-----------------------------------|
| NGS | next generation sequencing |
| NMR | nuclear magnetic resonance |
| NSCLC | non-small cell lung carcinoma |
| NT-3 | neurotrophin 3 |
| NT-4/5 | neurotrophin 4/5 |
| NTRK1 | neurotrophin receptor kinase 1 |
| NTRK2 | neurotrophin receptor kinase 2 |
| NTRK3 | neurotrophin receptor kinase 3 |
| <i>p</i> | proton |
| PBS | phosphate buffered saline |
| PD | Parkinson's disease |
| PDB | protein data bank |
| Pd/C | palladium on carbon |
| PET | positron emission tomography |
| PG | protecting group |
| PI3K | phosphatidylinositide 3-kinases |
| PK/PD | pharmacokinetics/pharmacodynamics |
| PLCγ | phospholipase C γ |
| Ph | phenyl |
| PMB | 4-methoxybenzyl |
| PNS | peripheral nervous system |
| Ppm | parts per million |
| RB | rotatable bonds |
| RCY | radiochemical yield |
| RLM | rat liver microsome |
| ROI | region of interest |

| | |
|-----------------------|--|
| Rt | room temperature |
| RTK | receptor tyrosine kinase |
| SAR | structure-activity relationship |
| sat. | saturated |
| S_N2 | aromatic nucleophilic substitution |
| SPECT | single-photon emission computed tomography |
| SUV | Standardized Uptake Value |
| TAC | time-activity curve |
| TBAF | tetramethylammonium fluoride |
| TBAOH | tetramethylammonium hydroxide |
| TBDPSCI | tert-butyl(chloro)diphenylsilane |
| TBSCI | tert-butyldimethylsilyl chloride |
| TBI | traumatic brain injury |
| temp | temperature |
| TFA | trifluoroacetic acid |
| THF | tetrahydrofuran |
| THP | tetrahydropyran |
| TK | tyrosine kinase |
| TKI | tyrosine kinase inhibitor |
| TLC | thin layer chromatography |
| TM | transmembranar domain |
| TMP3 | tropomyosin alpha-3 chain |
| TMS | tetramethylsilane |
| TNF | tumor necrosis factor |
| TPSA | topological polar surface area |
| TrkA | tropomyosinreceptor kinase A |

| | |
|----------------------|-------------------------------|
| TrkB | tropomyosin receptor kinase B |
| TrkC | tropomyosin receptor kinase C |
| Ts | <i>p</i> -toluenesulfonyl |
| VOI | volume of interest |
| V_T | volume of distribution |
| xs. | Excess |

Introduction

Portions of this chapter have been published in the following review articles:

Article 1

Bernard-Gauthier, V.*; Bailey, J. J.*; Berke, S.; Schirmacher, R. Recent Advances in the Development and Application of Radiolabeled Kinase Inhibitors for PET Imaging. *Molecules*, **2015**, *20*, 22000-22027. * equal contribution (*Invited review*)

Author contributions: **V.B.G.**, J.J.B. and R.S. managed the project; **V.B.G.**, J.J.B. and S.B. conducted literature research; **V.B.G.** wrote the paper; **V.B.G.**, J.J.B. and R.S. reviewed/corrected paper.

Article 2

Bernard-Gauthier, V.; Schirmacher, R. Evaluation of WO2015042088 A1 - a novel urea-based scaffold for TrkA inhibition. *Expert Opin. Ther. Patents*, **2016**, *26*, 291-295. (*Invited review*)

Author contributions: **V.B.G.** managed the project, conducted literature research and wrote the paper; **V.B.G.** and R.S. reviewed/corrected paper.

Article 3

Bailey, J. J.; Schirmacher, R.; Farrell, K.; **Bernard-Gauthier, V.** Tropomyosin receptor kinase inhibitors: an updated patent review 2010-2016 Part 1. *Expert Opin. Ther. Patents*. **2017**, *ahead of print*, <http://dx.doi.org/10.1080/13543776.2017.1297796>. (*Invited review*)

Author contributions: **V.B.G.** managed the project; **V.B.G.**, J.J.B. and K.F. conducted literature research; **V.B.G.** and J.J.B. wrote the paper; **V.B.G.**, J.J.B. and R.S. reviewed/corrected paper.

Article 4

Bailey, J. J.; Schirmacher, R.; Farrell, K.; **Bernard-Gauthier, V.** Tropomyosin receptor kinase inhibitors: an updated patent review 2010-2016 Part 2. *Expert Opin. Ther. Patents*. **2017**, *ahead of print*, <http://dx.doi.org/10.1080/13543776.2017.1297797>. (*Invited review*)

Author contributions: **V.B.G.** managed the project; **V.B.G.**, J.J.B. and K.F. conducted literature research; **V.B.G.** and J.J.B. wrote the paper; **V.B.G.**, J.J.B. and R.S. reviewed/corrected paper.

1.1 Overview of radiopharmaceutical development

Throughout the last decades, the use of radiotracers in medical research has provided unique insights and supported fundamental advances in neurology, oncology and cardiology.¹⁻³ In nuclear medicine, the study of radiopharmaceuticals suitably labeled with gamma- (γ) or positron-emitting (β^+) isotopes offers a powerful way to achieve three-dimensional distribution imaging through the use of single photon computed tomography (SPECT) and positron emission tomography (PET). In particular, PET enables quantitative dynamic imaging with both high spatial resolution (~ 2 mm) and remarkable sensitivity ($\sim 10^{-12}$ mol \cdot L $^{-1}$) via the detection of coincidental annihilation high-energy photons originating from β^+ decay. Beyond sensitivity and resolution, another advantage of PET relates to the diverse nature of chemically appropriate β^+ -emitting radioisotopes available which can be incorporated into biologically relevant molecules. Most notably, the use of carbon-11 ($t_{1/2} = 20.38$ min) and fluorine-18 ($t_{1/2} = 109.8$ min) offers the possibility of investigating exact isotopologues or minor structural derivatives of bioactive organic compounds or prospective pharmaceuticals. PET tracers often provide specific data relating to enzyme functions, diseases pathophysiology or expression levels of specific receptors or other relevant biomarkers – data which would otherwise be impossible to collect non-invasively with other currently available techniques. In the context of neuroimaging, which constitutes a central theme of the current thesis, PET is uniquely positioned to delineate proof-of-mechanism of emerging drugs, clarify dosing protocols via occupancy studies or assess brain penetration of peripherally administered drug candidates and has therefore played an increasing role in drug development and discovery.⁴⁻⁶ Importantly, despite those major progresses, the development of PET radiotracers remains altogether a time-consuming, high cost, iterative and empirical process which faces substantial attrition rates, like drug development itself. Those limitations are best illustrated in the light of the fact that only a few dozen protein targets have

been successfully visualized using PET neuroimaging so far in human,⁷ such coverage representing less than 0.01% of the brain proteome.⁸⁻⁹

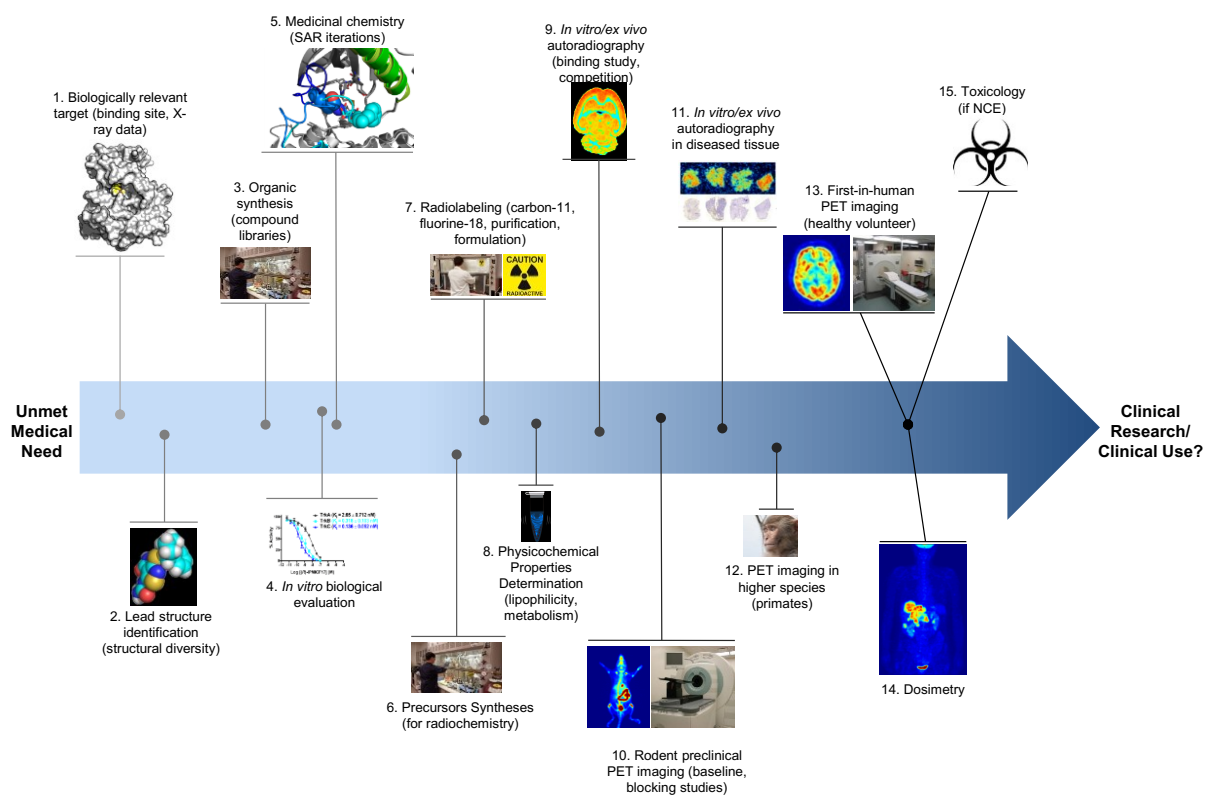


Figure 1.1. Overview of PET radiopharmaceutical development.

Figure 1.1 provides an overview of the radiopharmaceutical development process from the identification of medically relevant target to the resulting clinical application.¹⁰ In broad terms, the underlying challenge behind the development of PET radiotracers resides in the fact that only a minute mass of material has to distribute and reach a target tissue or region *in vivo*, then engage this target whilst generating minimal non-target signal. Crucially, this has to be achieved while surviving metabolism.¹¹ Such stringent criteria preclude most compounds to serve as suitable candidates for radiotracer development and require careful selection parameters and often extensive structure-activity relationship (SAR) screenings prior to *in vivo* imaging experiments. Upstream of imaging considerations, the planning of radiochemical routes

Chapter 1

to access lead tracers and the synthesis of the corresponding precursors as well as relevant cross validations using cellular or tissue autoradiography techniques should be well-thought-out. In this thesis, each step from the identification of an unmet clinical need to first-in-human imaging will be detailed and discussed. A description of our molecular target is provided below.

1.2 Trk family of neurotrophin receptors

1.2.1 Trk signaling and role in neurobiology. Tropomyosin receptor kinases A, B and C (TrkA, TrkB and TrkC – also referred to as tropomyosin-related kinases) are single-pass type I transmembrane tyrosine kinases encoded by the *NTRK1*, *NTRK2* and *NTRK3* genes, respectively, which are predominantly found in various subsets of neurons.¹²⁻¹³ Those receptors are 3 homologous members of the kinome which, in human, encompasses 518 related proteins.¹⁴ TrkA, TrkB, and TrkC, are most responsive to their respective primary neurotrophic ligands: nerve growth factor (NGF),¹⁵⁻¹⁶ brain-derived neurotrophic factor (BDNF)¹⁷ and neurotrophin-3 (NT-3).¹⁷⁻¹⁸ Neurotrophin-4 (NT-4) has also been characterized and shown to primarily interact with TrkB.¹⁹ Extracellular recognition of neurotrophins, which occur as noncovalent dimers,²⁰⁻²¹ by their cognate Trk receptors induce dimerization and trans-autophosphorylation of tyrosine residues in the receptor's cytosolic catalytic domain.¹³ The ensuing activation of downstream signal transduction pathways, mitogen-activated protein kinase (MAPK/Erk), phosphatidylinositol 3-kinase (PI3K) and phospholipase C γ (PLC γ), mediates neuronal survival and differentiation in developing and mature neural circuits and significantly affects the functional properties of neurons in both the central nervous system (CNS) and the periphery.²²⁻²³ The cytoplasmic domains of Trk receptors each include 5 tyrosine residues which upon phosphorylation provide docking sites for several effector/adaptor proteins. Briefly, phosphorylation at the juxtamembrane tyrosine Tyr490/515 (TrkA/B) activates PI3K via translocation and activation of Akt promoting survival.²⁴ PI3K signaling also enhances RNA translation supporting neuronal development and dendritic arborisation via the mammalian target of rapamycin (mTOR) (**Figure 1.2**).²⁵⁻²⁷ Differently, phosphorylation at the tyrosine residue close to C-terminal region triggers phospholipase C γ (PLC γ) activation leading to the intracellular release of Ca²⁺. Calcium release in turn increases presynaptic neurotransmitter release as well as activation of Ca²⁺-calmodulin-regulated protein kinase (CaMKII) and protein kinase C (PKC) resulting in a rise in AMPA receptor expression.²⁸⁻²⁹ Postsynaptic Trk activation

can also directly modulate glutamate receptors activity and increase actin polymerization.²⁹⁻³⁰ In addition, mitogen-activated protein kinase (MAPK) pathway activation results in pre- and postsynaptic pro-survival gene transcription while favoring neurotransmitter release via synapsin phosphorylation (**Figure 1.2**).^{29, 31-33} Thereupon, Trk receptors play pivotal roles in synaptogenesis, plasticity and neuron survival during embryogenesis as well as for the maintenance of the mammalian nervous system.²⁹

In addition to full-length Trk receptors (herein referred as Trk), truncated spliced variants such as TrkB.T1 (gp95^{TrkB}) and TrkB.T2 which lack kinase domain activity but act as dominant negative regulators are also found extensively within the nervous system.³⁴ All neurotrophins also non-selectively interact with another structurally unrelated receptor, the *low affinity* neurotrophin receptor (p75^{NTR}), member of the tumor necrosis factor receptor superfamily (TNF receptors).³⁵ The p75^{NTR} receptor has been mostly characterized for its involvement in neuronal apoptosis signaling but was also shown to act as a co-receptor with Trk, enhancing neurotrophin affinity while conferring increased selectivity.³⁶⁻³⁸ As discussed in some detail below, dysregulation of Trk expression and signalling can potentiate many aberrant physiological processes that negatively impact human health. Substantial evidence has emerged over the last decade that implicates irregular Trk signalling in a multitude of neurodegenerative diseases including Alzheimer's (AD), Huntington's (HD), and Parkinson's (PD) diseases for example.³⁹ Neurotrophins and Trk signalling, particularly through TrkA, also play significant roles in peripherally derived ailments such as atopic dermatitis, psoriasis, nociceptive pain, and Chagas disease.⁴⁰ Pathological over-expression and activation of Trk in non-neural tissues are involved in many cancers.⁴¹⁻⁴³ Perhaps most significantly, *NTRK1/2/3* gene rearrangements leading to oncogenic Trk proteins expressing intact Trk kinase domains have been identified increasingly in recent years for multiple tumor histologies suggesting that Trk oncogenic fusions may be a wide spread but low frequency occurrence in human cancer.⁴⁴

Albeit less studied, most signaling pathways relevant to full-length Trk receptors, initially studied in rat adrenal pheochromocytoma (PC12) then later in diverse primary neuron cultures (Figure 1.2), are anticipated to be relevant in the context of Trk fusion proteins as well.⁴⁴⁻⁴⁷

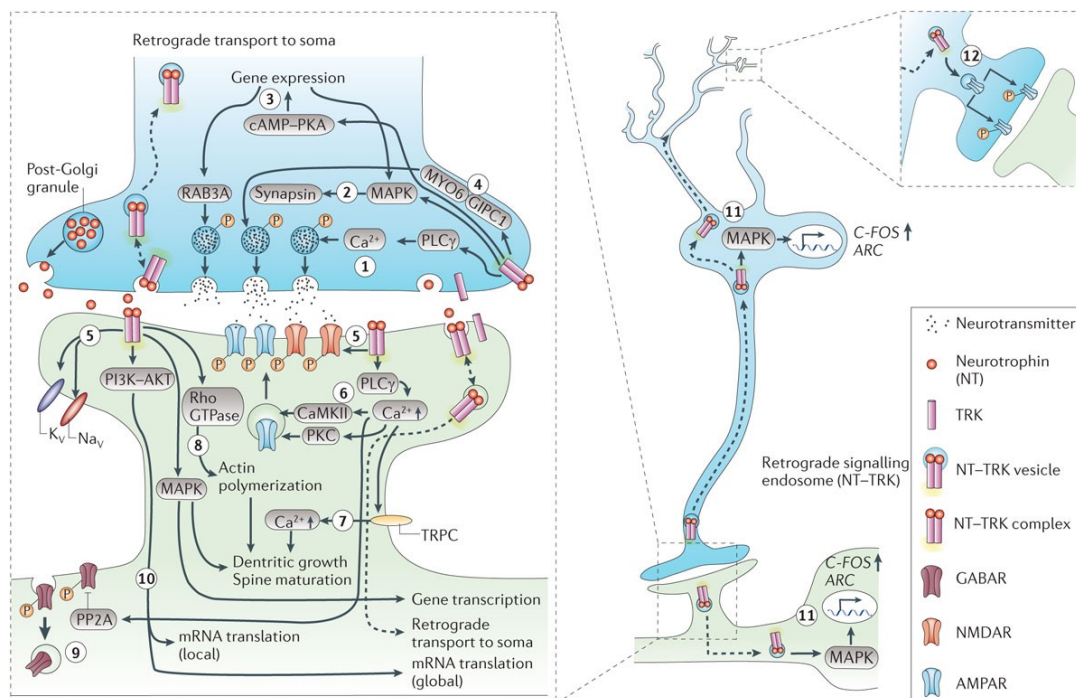


Figure 1.2. Overview of synaptic functions mediated by neurotrophins/Trk receptors (NTs: neurotrophins; PLC γ : phospholipase C γ pathway; MAPK: mitogen-activated protein kinase; MYO6: motor myosin VI; NMDAR: N-methyl-D-aspartate -type glutamate receptor; CaMKII: calmodulin-dependent kinase II; PKC: protein kinase C; AMPAR: α -amino-3-hydroxy-5-methyl-4-isoxazolepropionic acid-type glutamate receptor; TRPC: transient receptor potential cation channels; PP2A: protein phosphatase 2A; GABAARs: γ -aminobutyric acid (GABA) receptors; (PI3K)-AKT: phosphoinositide 3-kinase-protein kinase B; ARC: activity-regulated cytoskeleton-associated protein; cAMP: cyclic AMP). (adapted from Park *et al.*²⁹)

The study of the relevance of Trk kinase signalling is profoundly intertwined in the very history of oncology and neuroscience.⁴⁸ The discovery and initial characterization of NGF, the prototypical neurotropic factor, was detailed in a series of seminal contributions at the turn of 1960 led by Levi-Montalcini resulting in the isolation of the protein.⁴⁹⁻⁵² Those findings were immediately followed by the demonstration of the remarkable growth promoting nature of NGF and the concurrent dramatic effect leading to the near obliteration of the sympathetic nervous

system *in vivo* in mice upon treatment with anti-NGF serum.⁵³⁻⁵⁴ Not only was NGF the first “growth factor” described, which at the time was a profound conceptual discovery,⁵⁵⁻⁵⁶ the “immunosympathectomy” experiments described with the anti-NGF serum also represent the first phenotypic knockout using antibodies⁵⁷ – both discoveries ultimately having a profound impact beyond developmental neurobiology, most notably in oncology. Extensive work in the ensuing decades led to the full description of the additional neurotrophins BDNF⁵⁸⁻⁵⁹ and NT-3⁶⁰⁻⁶¹ (and later on NT-4⁶²). However, the identity of the receptor family responsible for the trophic action of those factors remained elusive for over three decades. In parallel, increasing work in the 1980s, pioneered by Barbacid and colleagues, led to the characterization of various oncogenes in some cases containing activable tyrosine kinase (TK) sequences.⁶³⁻⁶⁴ One the first identified such transforming gene was *trk*, which was originally described from transfection studies of a human colon carcinoma and shown to contained a nonmuscle tropomyosin gene fused with a novel transmembrane and kinase domain sequence (hence the nomenclature *trk* – in reference to Tropomyosin-Receptor-Kinase).⁶⁴⁻⁶⁶ Further studies showed that the transcription of the human *trk* proto-oncogene was tightly regulated during mouse embryonic development and restricted to specific regions of the peripheral nervous system (PNS).⁶⁷ Other proto-oncogenic receptors from the same family, namely *trkB* and *trkC* were also identified in neurons, engendering the expectation of a specific and crucial role for those receptors in neuronal development while the nature of the possible ligands of those receptors was indefinite.⁶⁸ The recognition that the receptor responsible for the trophic activity of NGF contained a phosphokinase domain came in 1991.⁶⁹ The same year, two groups showed that NGF was indeed the obscure TrkA (trk proto-oncoprotein) ligand,^{15, 70-71} providing remarkable – and somewhat unexpected at the time – demonstration of the bridge which exists between oncology and neurobiology with regard to Trk receptors.⁷²

Among the large body of evidence including cellular and *in vitro* studies gathered through decades of detailing the influences of Trk in the mammalian nervous system, perhaps

the most striking indication of the centrality of Trk signaling comes from the study of Trk receptor knockout mice.⁷³⁻⁷⁴ Knockout mice for all Trk receptors have been studied and showed to exhibit dramatic phenotypes (also true in the case of *NGF*, *BDNF* and *NT-3* knockouts). For example, TrkA null mice have reduced response to painful stimuli and show massive neuronal loss in sympathetic nervous system ganglia.⁷⁵ Those animals display limited changes in the CNS but die within 3 weeks of birth. In contrast, neuronal losses in *TrkB*^{-/-} mice are comparatively limited except in CNS motor neurons but animals fail to feed and die within the first hours following birth.⁷⁶ Finally, TrkC knockouts ultimately present proprioceptive defects and die before 1 month of age despite appearing relatively normal at birth compared to other Trk deficient mice.⁷⁷ Collectively, those data unveil the complex and crucial nature of Trk in neuronal processes and brain function.

1.2.2 Trk structure and normal expression. From a structural standpoint, all Trk receptors share a common architecture which includes a highly organized and N-glycosylated N-terminal ectodomain (ECD) connected to a transmembrane region (TM) followed by an archetypal C-terminal cytoplasmic kinase domain (KD) (**Figure 1.3**).⁷⁸⁻⁸⁰ On both sides, the TM domain is flanked by sequences of residues, about 30 on the N-terminal ectodomain region and 60 on the cytoplasmic C-terminal side respectively, which lack determined secondary structures and allow for overall receptor flexibility and regulation.⁸¹⁻⁸³ Crystallographic data of the distinct regions of Trk receptors (ECD, TM and KD) have been reported and have provided a mechanistic rationalization for receptors functionality.^{36, 78-79, 81, 84} The extracellular domains of TrkA/B/C display three leucine-rich repeats entrapped between two cysteine clusters (domains D1-D3) which are joined towards the membrane to two successive immunoglobulin domains, Ig-1 and Ig-2 (D4, D5, **Figure 1.3**). Only the crystal structure of the full ECD TrkA domain has been described, that is in complex with dimeric NGF in a 2:2 ligand receptor cluster.⁷⁸ Those data, alongside reports of 2:2 TrkA-D5/NGF and TrkB-D5/NT-4 complexes as well as the individual unliganded TrkA-D5, TrkB-D5 and TrkC-D5 crystallized segments have provided direct

evidence that the D5 (Ig-2) subdomains are primarily responsible for neurotrophin interaction and specific recognition (*vide infra*, and **Figure 1.7**).⁸⁵⁻⁸⁷

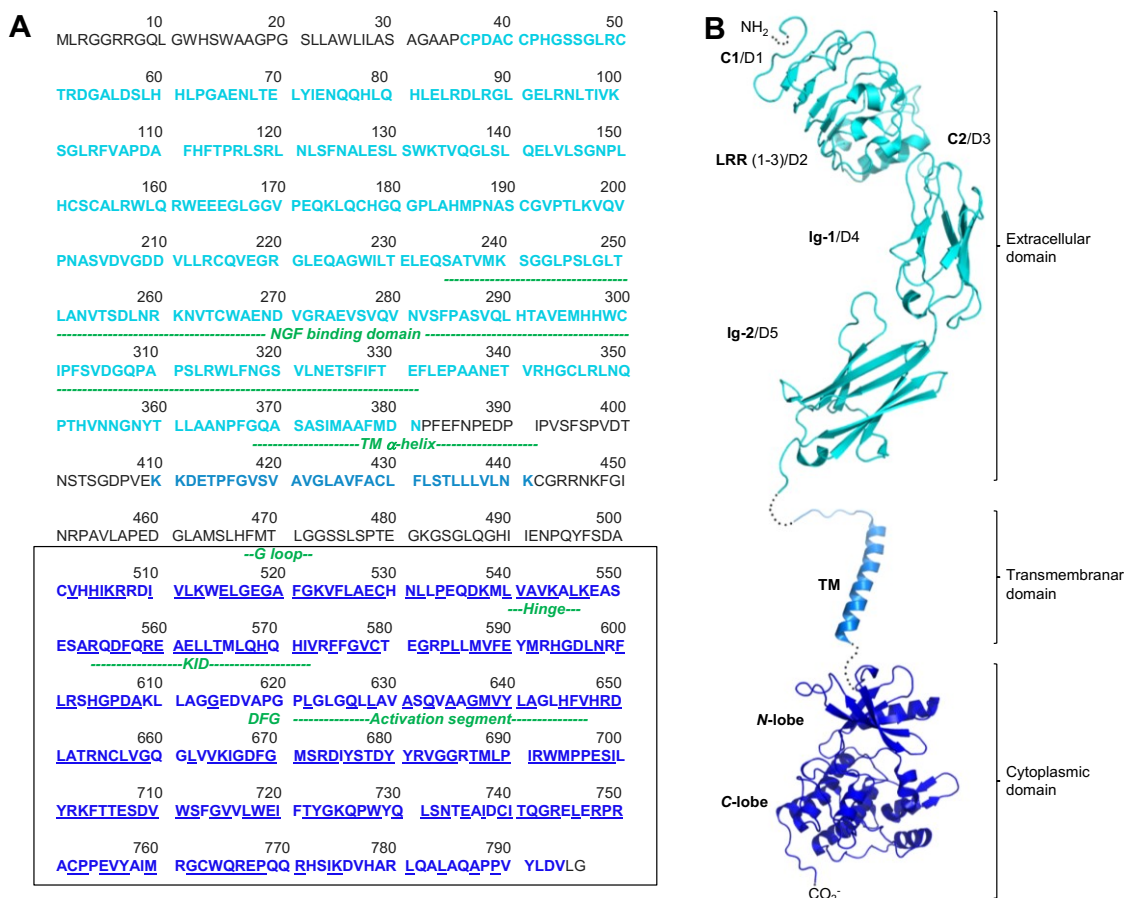


Figure 1.3. (A) Sequence of human TrkA. Residues from the extracellular domain are shown in cyan. Residues from the transmembranar domain are shown in pale blue. Residues from the kinase domain are shown in dark blue. The residues corresponding to the kinase domain are framed. Key structural elements are shown above the sequence (green). Identical residues are underlined (kinase domain only). (B) Structure overview of the full TrkA receptor (D1-D5: domain 1-5; C1/3: cysteine cluster 1/3; LRR: leucine-rich repeat; Ig-1/2: immunoglobulin domain 1/2, TM: transmembranar domain).

The sequence homology found in the Trk ECDs, although important, is comparatively small relative to the kinase domains. Comparison of the crucial D5 unit for example reveals 41-44% pairwise sequence identity between TrkA/B/C. In contrast, the corresponding intracellular kinase domains are not only architecturally conserved but also bear a particularly high degree of sequence homology within the Trk family; TrkA, TrkB, and TrkC share between 71.9% to 78.3% sequence homology, with TrkB and TrkC being the closest homologues (**Figure 1.3A**). The

catalytic domain consists of an archetypal bi-lobed catalytic core structure where ATP binds in a deep cleft located between the N- and C-terminal lobes (**Figure 1.3B**, see also **Figure 1.9**), forming key hydrogen bonds between the adenine ring and the hinge segment that connects the two lobes.⁷⁹ The apo crystal structures of TrkA and TrkB have been reported.⁷⁹ Otherwise, all available X-ray data involving the Trk kinase domains are co-crystal inhibitor-bound structures gathered in the development small molecules tyrosine kinase inhibitors (TKIs) programs. Details regarding the kinase domain plasticity in this context will be provided in the section describing the development of Trk TKIs as a drug class (section 1.2.4.2).

Multiple lines of evidence have confirmed the expected regional CNS TrkA/B/C expression deduced via early cellular analyses and phenotypic observations made with knockouts for example. In key studies, using iodinated human recombinant NGF ¹²⁵I-rhNGF, Altar and colleagues⁸⁸⁻⁸⁹ quantified regionally limited high affinity binding sites (e.g. TrkA) in the rat brain (**Figure 1.4A-E**). This work and previous *in situ* hybridization experiments⁹⁰ confirmed the highly restricted nature of TrkA expression in the mammalian CNS which is found almost exclusively in cholinergic neurons of the basal forebrain and caudate-putamen. Highest specific binding levels of ¹²⁵I-rhNGF corresponding to TrkA binding sites were not only discrete but also low in density in the rat brain with B_{max} values ≤ 13 fmol/mg of protein. Similar regional binding experiments, combining hybridization and radiolabelled neurotrophins binding, were also conducted for TrkB and TrkC with rodent and human brains (**Figure 1.4F-L**).⁹¹⁻⁹³ Those experiments confirmed that, in comparison to TrkA, TrkB expression is extensive and near-ubiquitous in mammalian CNS. Comparative binding experiments using ¹²⁵I-BDNF, ¹²⁵I-NT-3 and ¹²⁵I-NT-4 showed binding distribution matching TrkB/C hybridization. However, only the high affinity binding site of ¹²⁵I-NT-3 (which mainly interact with TrkC but display also interact to a lesser extent with TrkB) were quantified in the rat brain and showed to exceed by over 3-fold

that of ^{125}I -rhNGF in the highest ^{125}I -rhNGF binding regions and by much higher proportions in other regions.

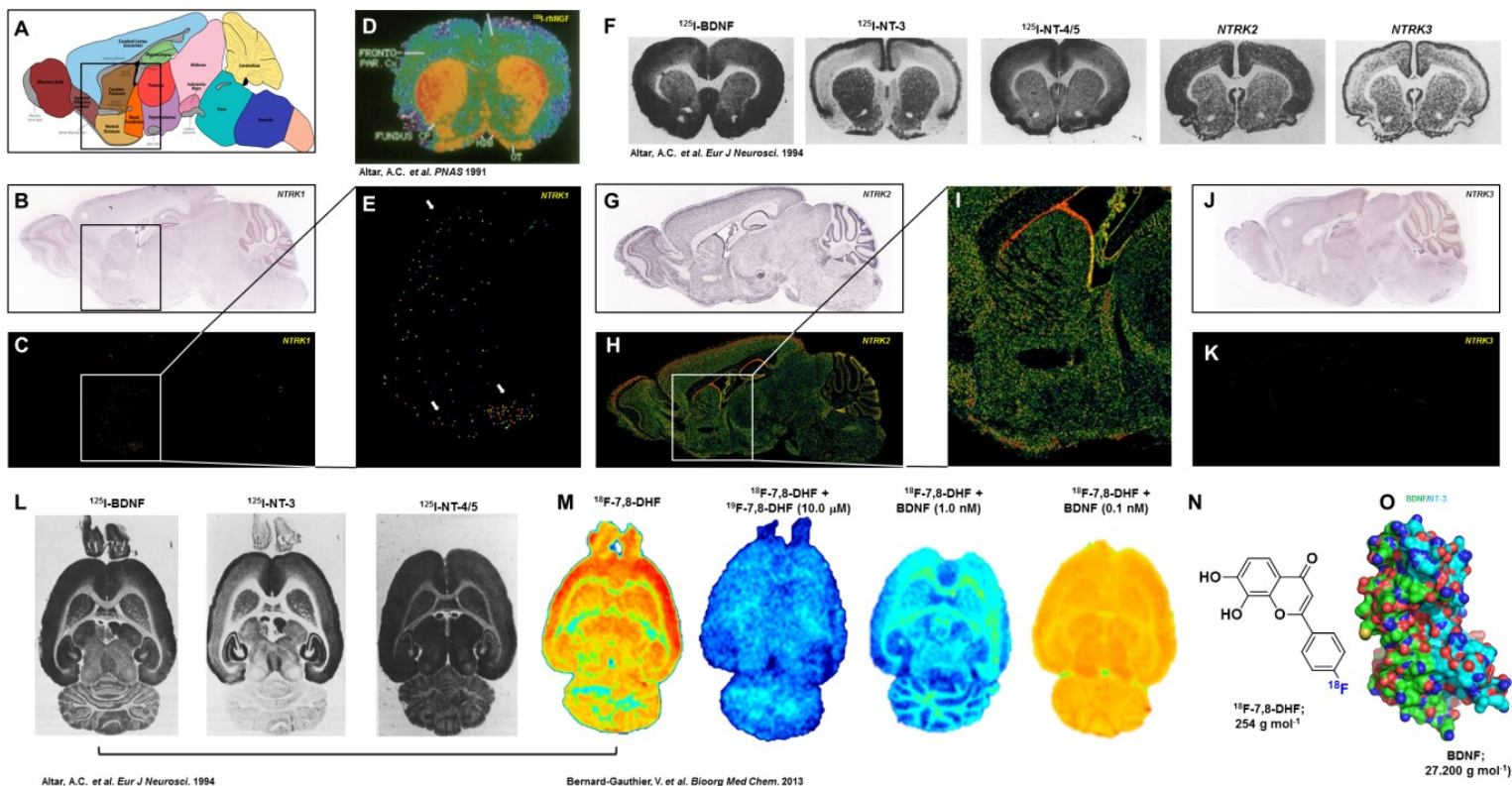


Figure 1.4. Expression of Trk in the rodent CNS. (A) Sagittal depiction of the mouse brain (caudate/putamen/ basal forebrain outlined). Analogous sections corresponding to (B,C,E) *NTRK1*, (G,H,I) *NTRK2* and (J,K) *NTRK3* transcripts analyzed by *in situ* hybridization in the Allen Brain Atlas project. Images are taken from the Allen Brain Atlas (<http://mouse.brain-map.org>). Image credit: Allen Institute for Brain Science. (D) Quantitative map of displaceable ^{125}I -rhNGF binding in rat brain. (F,L) Representative autoradiographs and *in situ* hybridization data for labeled neurotrophins and *NTRK* (rat brain). (M) Representative autoradiograms illustrating the distribution of ^{18}F -7,8-DHF in baseline, self-block and BDNF competition experiments (rat brain). (N) Chemical structure of ^{18}F -7,8-DHF and (O) surface rendering of BDNF/NT-3 (PDB ID: 1BND) (adapted from refs.^{88, 93-94}).

Hybridization data also showed that probes targeting the ECD and KD of TrkB had widespread but non-overlapping distributions. While full-length TrkB receptors targeted by KD-binding probes were found exclusively expressed in neuronal populations and virtually absent from white matter, truncated variants were found extensively in non-neural cells when using the

ECD-binding probe *in addition to* the neuronal populations seen with the KD riboprobe (indication of truncated TrkB binding). Considering that sufficient target density is one of the central requirements for the development of a PET radiotracer, the expectation that catalytically-competent full-length TrkB receptors display a relative high capacity and distribution in most neurons of the mammalian CNS is noteworthy. In the pursuit of the first TrkB-targeted PET radiotracer, we have shown previously that the TrkB binding topology observed in the rat brain *in vitro* could be recapitulated using the small molecule BDNF mimic radioligand ^{18}F -7,8-DHF as a surrogate for the large dimeric ^{125}I -BDNF probe (**Figure 1.4L-O**).⁹⁴ However, ^{18}F -7,8-DHF and ECD-binding tracers in the context of TrkB especially, intrinsically fail to differentiate between full-length and truncated populations of receptors – which would be crucial.

1.2.3 *Trk in human diseases*

1.2.3.1 Role of Trk in neurological diseases. The many roles of Trk dysregulation in the context of neurological disorders and neurodegenerative diseases have been reviewed extensively.^{39, 95} Briefly, changes in expression level or dysfunctional Trk signalling have been linked to a plethora of neurological conditions, chief among which is AD (see discussion in **Chapter 5** for a more detailed overview in the context of AD).⁹⁶⁻¹⁰⁰ Other conditions and diseases associated with changes in TrkA/B/C function include PD,¹⁰¹⁻¹⁰² HD,¹⁰³⁻¹⁰⁴ Rett's syndrome,¹⁰⁵⁻¹⁰⁶ Down's syndrome,¹⁰⁷⁻¹⁰⁸ amyotrophic lateral sclerosis,¹⁰⁹ epilepsy,¹¹⁰⁻¹¹¹ ischemic brain injuries¹¹²⁻¹¹³ and anxiety disorders.¹¹⁴

1.2.3.2 Role of Trk in cancer. Accumulating *in vivo* preclinical evidence and *in vitro* human data have indicated the involvement of neurotrophin-mediated autocrine/paracrine signaling of Trk proto-oncoproteins in the aggressiveness and metastatic potential of different human neoplasms. Examples of cancers where full-length Trk receptors signaling or overexpression were shown to play pro-tumorigenic roles include breast (TrkA/TrkB),¹¹⁵⁻¹¹⁶ prostate cancers (TrkA/TrkB),¹¹⁷ adrenal cancer (TrkA),¹¹⁸ esophageal cancer (TrkA),¹¹⁸ ovarian cancer (TrkA),

pancreatic cancer (TrkA/TrkB),^{42, 118} colorectal cancers (TrkA/TrkB),⁴³ as well as neuroblastoma.⁴¹ As further discussed in **Chapter 3**, the case of neuroblastoma is of particular interest since TrkA/C and TrkB expressions have been associated with drastically opposite clinical outcomes, leading to good and poor prognoses respectively.¹¹⁹⁻¹²⁰ In addition, TrkB and TrkC signaling has recently been implicated in the growth of brain tumor-initiating cells.¹²¹

The centrality of *NTRK* fusions in human cancer has become evident with recent analyses. Those realisations have been fueled by the rise of next-generation sequencing (NGS) techniques, which revealed that oncogenic *NTRK1/2/3* gene fusions are recurrent occurrences in human cancer, well beyond the initially described *TPM3-NTRK1* mutation in colorectal cancer^{65, 122} and *ETV6-NTRK3* identified in congenital mesoblastic nephroma and secretory breast cancer.¹²³⁻¹²⁵ The diversity and incidence of *NTRK1/2/3* oncogenic fusions, which are now recognized in approximately twenty cancer types, have been reviewed recently (**Figure 1.5B**).^{44, 126-127} *NTRK* gene fusions are rare occurrences in common neoplasms, such as NSCLC, and are displayed in high frequency in a number of rare cancers such as MASC.^{44, 128} Importantly, *NTRK* fusions were also reported in up to 40% cases of non-brainstem pediatric high-grade glioma.¹²⁹ The chimeric products resulting from those chromosomal rearrangements can either be membrane bound or cytoplasmic proteins. Most such identified transforming fusions bear an unrelated gene 5'-partner dimerization/multimerization domains in the place of the cognate extracellular/TM Trk domains constitutively triggering sustained activation of kinase signaling.¹³⁰ **Figure 1.6** illustrates the structure of such coil-coiled domain in the context of tropomyosin partners.¹³¹ The rapid unfoldment of the relevance of *NTRK* fusions in human cancer has engendered increasing interest in the development of drugs with Trk inhibitory capacity and the study of those oncogenic drivers *in vivo* (*vide infra*).

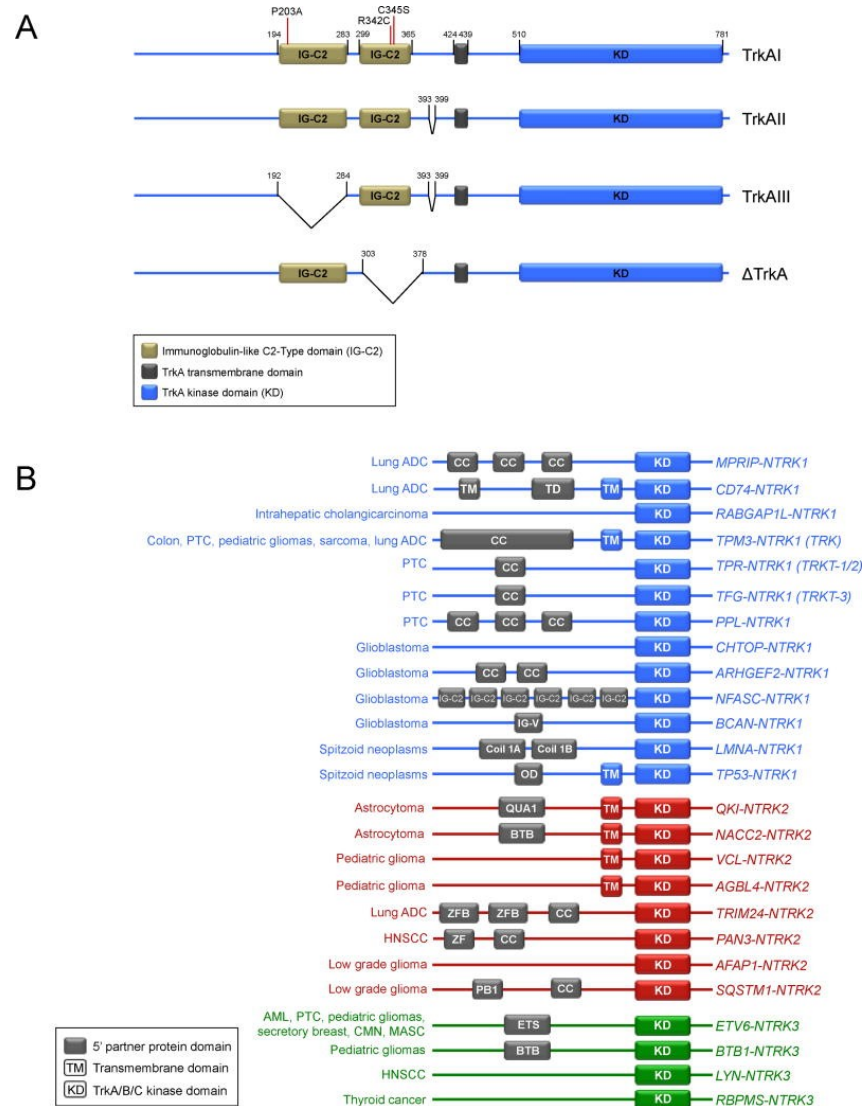


Figure 1.5. (A) Representation of TrkA isoforms including deletions and mutations. (B) Schematic overview of known NTRK1-3 fusions with corresponding tumor types. Known gene partner are shown (ADC: adenocarcinoma; PTC: papillary thyroid cancer; AML: acute myeloid leukemia; CMN: congenital mesoblastic nephroma; MASC: mammary analogue secretory carcinoma; HNSCC: head and neck squamous cell cancer; CCD: coiled-coil domain; TD: trimerization domain; IG-C2: Immunoglobulin-like C2-type domain; IG-V: Immunoglobulin-like V domain; OD: oligomerization domain; ZF QUA1: Quaking 1 domain; BTB: bric-a-brac, tramtrack, and broad complex domain; ETS: E26 transformation-specific domain (adapted from ref⁴⁴).

Other mechanisms of Trk oncogenic activation were also characterized such as the NGF-unresponsive TrkA splice variant (TrkAIII) in neuroblastoma¹³² and activating TrkA deletion (Δ TrkA) in acute myeloid leukemia (AML) both leading to the loss of multiple glycosylation sites

(Figure 1.5A).¹³³⁻¹³⁵ All those alterations are associated with the loss of some level of ECD integrity which supports the view that the ectodomain of TrkA/B/C plays a crucial regulatory role by preventing spontaneous receptor dimerization.¹³⁶

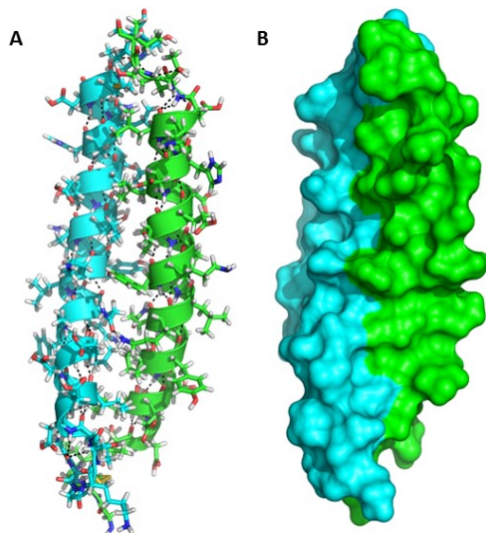


Figure 1.6. (A) Cartoon/stick and (B) surface rendering of the coil-coiled structure of a representative tropomyosin polypeptide (PDB ID: 1MV4, see ref¹³⁷)

1.2.3.3 Role of Trk in pain. The TrkA/NGF pathway plays a central role in nociceptive and neuropathic pain and as such represents a promising target for the development of a novel potential NSAID/non-narcotic analgesic drug class.¹³⁸⁻¹³⁹ Diverse early reports provided support to the clinical relevance of TrkA regarding pain beyond preclinical validation.¹⁴⁰⁻¹⁴¹ For example, defects in TrkA have been characterized as the causative factors in hereditary neuropathies¹⁴²⁻¹⁴³ while local hyperalgesia has been described following NGF injection.¹⁴⁴

Ultimately, the increasing recognition of the pleiotropic pathogenicity of Trk has provided a strong enticement for the development of novel targeted therapeutic and diagnostic tools – including, as discussed in the next chapters, imaging probes. The next section examines the different chemical strategies developed to target Trk pharmacologically including Trk TKIs which constitute the foundation of our radiotracer development efforts.

1.2.4 Structural biology considerations: Trk protein-small molecule interactions.

1.2.4.1 *Small molecule neurotrophin mimetics.* With the appreciation of the relevance of Trk in brain disorders came almost immediately the obvious, yet challenging question, of whether or not small molecule neurotrophin mimetics could be developed.¹⁴⁵ The study of nonprotein Trk ECD-binding compounds largely predates the advent of Trk-targeted TKIs described below but has had very limited success due to the inherent poor druggability of the ectodomains compared to the kinase domains of TrkA/B/C. Initial hopes in the treatment of Trk-related neurodegeneration were placed in neurotrophins themselves. Yet, those expectations rapidly eroded after the successive failure of neurotrophins in clinical trials for AD,¹⁴⁶ amyotrophic lateral sclerosis¹⁴⁷ and neuropathies^{95, 148-152} which altogether shed light on the suboptimal drug-like properties of those proteins, when exogenously administered.¹⁵³ Strategies to develop smaller yet selective and highly potent peptidic probes have largely relied on the mimicry of key neurotrophin regions responsible for the multidomain-based interaction with TrkA/B/C (**Figure 1.7**).^{85, 154-157} While peptides and peptidomimetic constructs targeting TrkA or TrkB and displaying a range of Trk-agonistic activities have been relatively well explored,¹⁵⁸⁻¹⁶¹ examples of peptidic Trk antagonists have been comparatively more limited (**Figure 1.8**).¹⁶²⁻¹⁶³ In an attempt to further address the limited brain permeation, high proteolytic degradation and overall poor half-life *in vivo* of neurotrophin which also affect peptide derivatives,¹⁶⁴ library-based and virtual compound screening has been used to identify Trk-targeting small molecule compounds with limited success. Gambogic amide (**1.7**, **Figure 1.8**), a xanthonoid derivative, was the first TrkA isoform-selective agonist described. Other compounds identified, mostly with claims of selective agonistic activities towards one of the Trk receptors, include the symmetric triamide **1.1** (LM22A-4),¹⁶⁵ 7,8-dihydroxyflavone (7,8-DHF)¹⁶⁶ and imidazole-containing bioisosteric derivatives thereof,¹⁶⁷⁻¹⁶⁸ compound **1.4** (MT2)¹⁶⁹ and deoxygedunin.¹⁷⁰ The entire repertoire of small molecule Trk ECD-binding compounds also comprises the antagonist ANA-12,¹⁷¹ dimeric

TrkC antagonists¹⁷²⁻¹⁷⁵ and the non-selective compounds amitriptyline¹⁷⁶ and N-acetylserotonin (Figure 1.8).¹⁷⁷

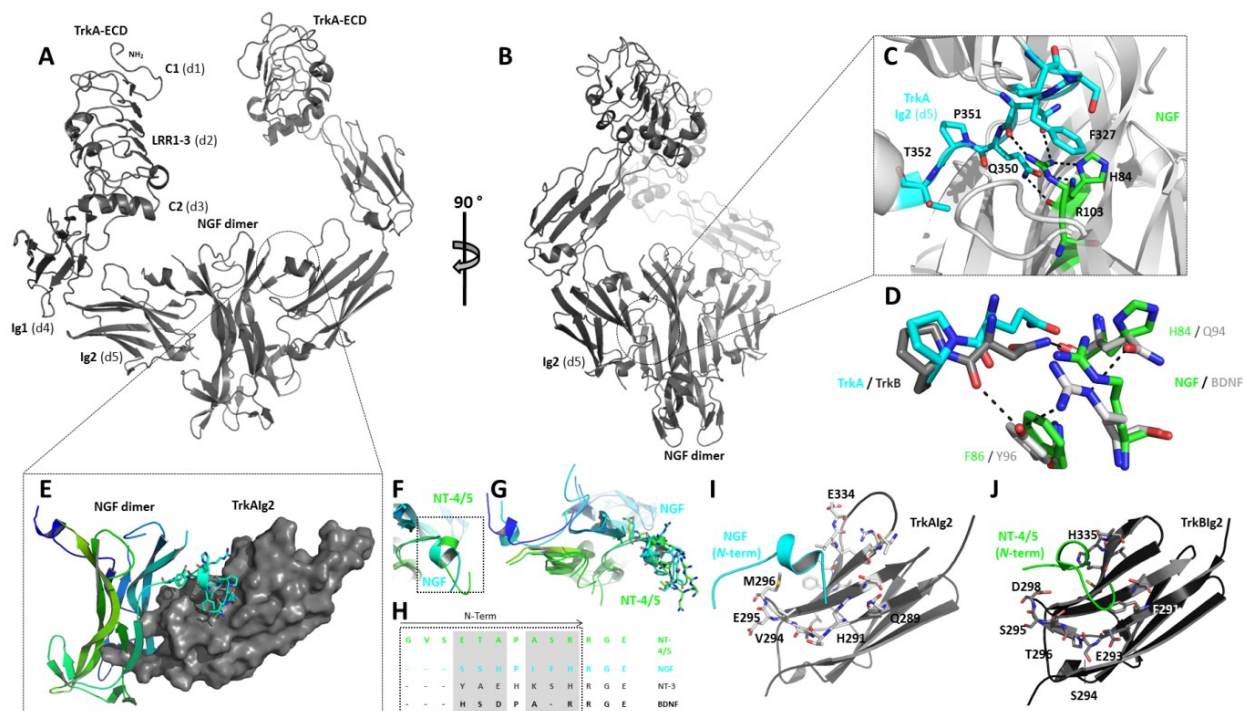


Figure 1.7. Extracellular Trk receptor domains and binding interfaces with neurotrophins – potential druggable sites; (A,B) Two views of the NGF-TrkA-d5 complex (PDB ID: 2IFG). (C) Interaction at the *conserved* patch surrounding R103 of NGF with TrkA. (D) Superposition of selected residues of TrkA/NGF and TrkB/BDNF at the *conserved* patch. (E) Overview of one of the NGF N terminus-TrkAlg2 interaction patch (TrkAlg2 is represented as a grey surface and the N terminus region of NGF is cyan sticks/ribbon). (F,G) Superposition of the NGF (PDB ID: 1WWW) and NT-4/5 (PDB ID: 1HCF) N terminus residues. (H) Sequence alignments of the N terminus region (neurotrophins). (I,J) View of the non-conserved residues the Ig2 domains of TrkA (I) and TrkB (J) (specificity patch) in contact with the N terminus of NGF and NT-4/5.

In each case, original compounds characterization has been conducted in TrkA- or TrkB-expressing cell lines with the demonstration of TrkA/B dimerization/autophosphorylation and activation/blocade modulations downstream of TrkA/B in those complex biological systems only. In most instances, original reports were also accompanied by phenotypic experiments in neurodegenerative disease mice models showing favorable and diverse neuroprotective effects

when compounds were administered *in vivo*.^{167, 178-179} Yet, most of those compounds display poor drug-like properties and undesirable physico-chemical properties for brain penetration and bioavailability (*vide infra*).¹⁸⁰⁻¹⁸¹ Importantly, cross-validations beyond original publication have been scarce. One exception is 7,8-DHF, which has attracted significant attention and has been studied repeatedly since its original characterization.¹⁸²⁻¹⁸³ However, those experiments only looked at the phenotypical and cellular outcomes following large systemic administration and prolonged dosing regimens in rodents *in vivo*. We (*unpublished data*) and others¹⁸⁴ have attempted revising the original biochemical findings in neuron systems of a number of those compounds, including 7,8-DHF, LM22A-4, ANA-12, N-acetylserotonin and amitriptyline as well as additional synthetic derivatives but failed to observe any effect on TrkB phosphorylation or downstream signaling with any of those compounds in concentrations and conditions matching original reports. Intriguingly and as mentioned before, we also previously used the ¹⁸F-isotopologue of a fluorinated derivative initially validated in the original description of 7,8-DHF for *in vitro* autoradiography experiments in rat brains and observed a specific and BDNF-competitive binding profile reminiscent of ¹²⁵I-BDNF binding topology (**Figure 1.4M,N**).⁹⁴ As of today, we have not been able to reconcile the lack of reproducibility of the basic biochemical effects of 7,8-DHF derivatives and the apparent TrkB-specific signal obtained in autoradiography experimentations. It remains that radiotracers derived from 7,8-DHF are not suitable for *in vivo* PET imaging due to rapid metabolism as expected.¹⁸⁵ Globally, the lack of reproducibility of the most basic biochemical data compounded with the absence of structural crystallographic information to support structural derivatization – often required for tracer development – have provided little incentive to use this compound class for CNS radiotracer development despite the advantage of an extracellular binding site versus an intracellular one. Other strategies to target Trk ectodomains pharmacologically include the use of monoclonal antibodies¹⁸⁶⁻¹⁸⁸ and aptamers¹⁸⁹ – all of which are poorly suitable for CNS imaging. Differently, the development of a probe which would target the cytoplasmic kinase domains appears more

suitable given that, ECD-binding probes even if successful would in the end fail to differentiate catalytically-incompetent truncated from full-length receptors and would be unable to engage targets which lack cognate ectodomains such as the many *NTRK* fusion proteins which are a prime clinical interest.

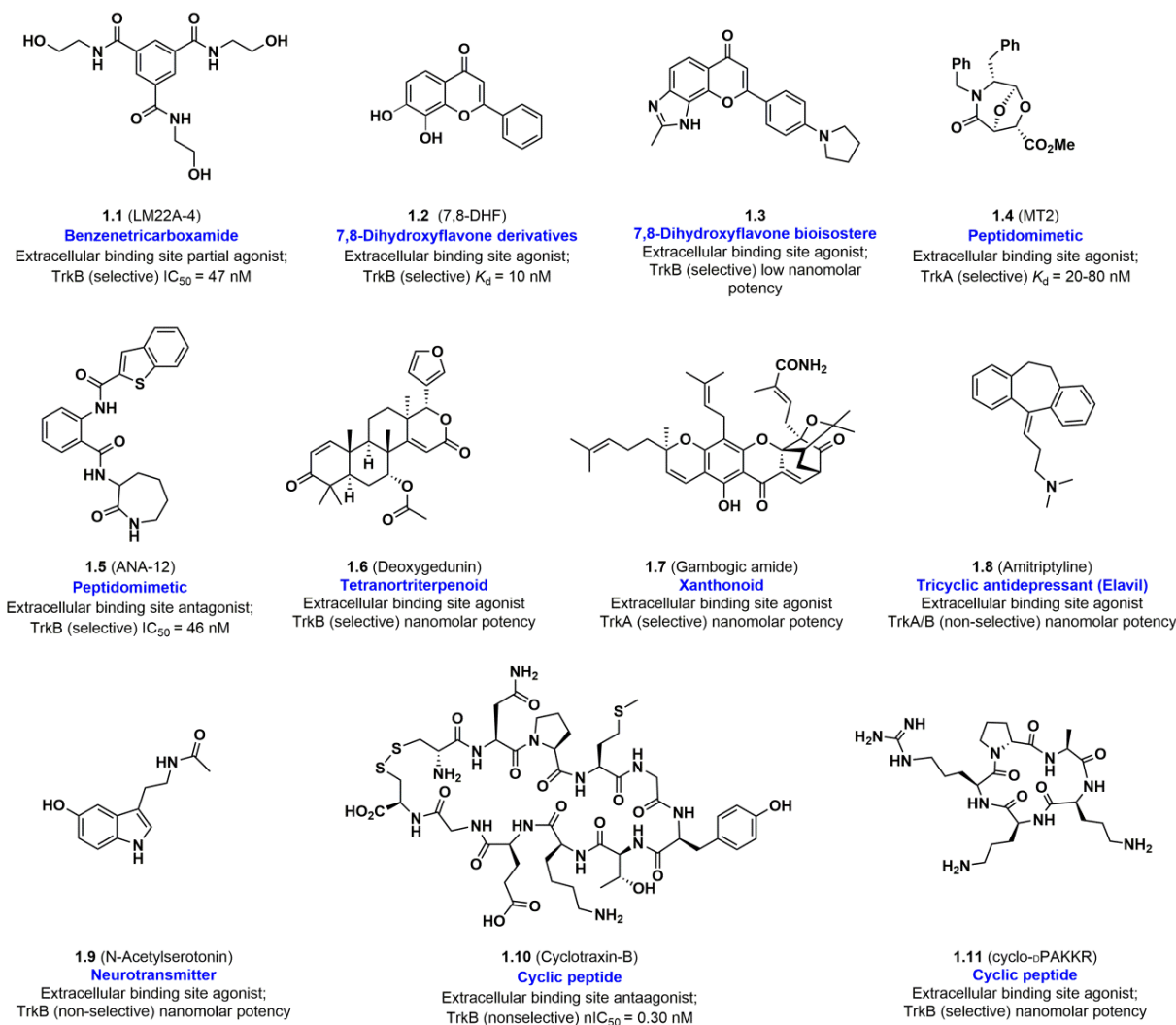


Figure 1.8. Representative Trk extracellular-binding small molecules and peptide-based probes.

1.2.4.2 *Trk* kinase domains: structures, molecular basis for inhibition and selectivity. In comparison to extracellular binding compounds, inhibitors targeting the cytoplasmic Trk kinase domains tend to be well characterized both functionally and structurally and have been reported

alongside detailed crystallographic data. From a structural standpoint, Trk TKIs also embody a significantly more diverse compound class relative to small molecule neurotrophin mimics or antagonists and bear potential for rational design, both crucial aspects for eventual PET radiotracer development.¹⁹⁰⁻¹⁹¹ Most of the data which pertain to Trk TKIs has been described in patent literature while reports in primary literature have, for the most part, only begun to emerge in recent years (and more significantly so in the course of this project). In the following section, we take a closer look at Trk TKIs and emphasise basic structural aspect of Trk kinase domains through the presentation of a brief overview of the Trk TKI compound class. For in depth-analyses of Trk TKIs, please refer to **Article 2-4**¹⁹²⁻¹⁹⁴ and prior comprehensive reviews.¹⁹⁵⁻¹⁹⁶

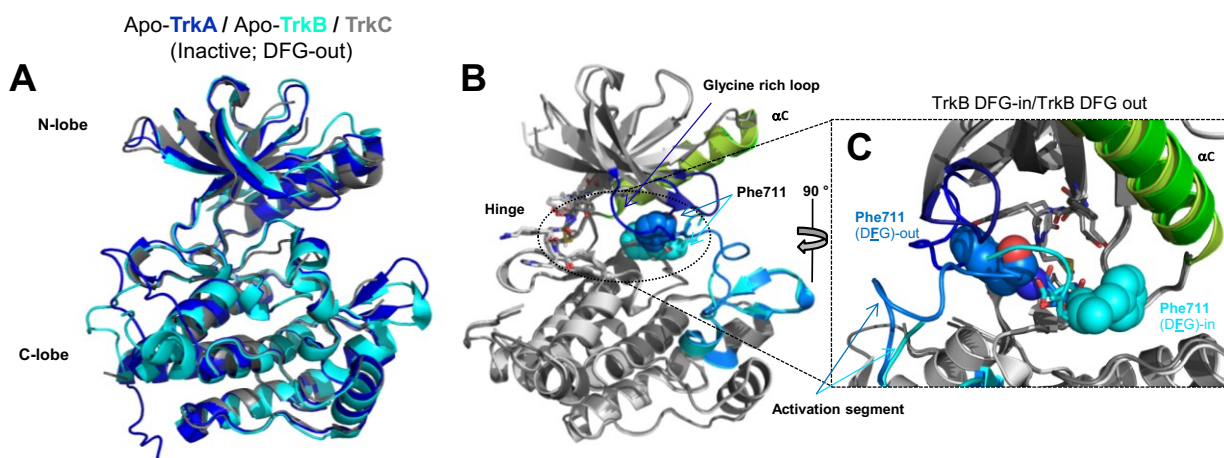


Figure 1.9. Trk kinase domain. (A) Overlap of TrkA, TrkB and TrkC kinase domain (inactive conformations, PDB ID: 4F0I, 4ASZ, 3V5Q). (B,C) Views of the conformational differences between DFG-in and DFG-out TrkB. The Phe residues of the DFG triad are shown in spheres (PDB ID: 4AT3, 4AT5).

Figure 1.9A illustrates the overlap of TrkA, TrkB and TrkC kinase domain. Most Trk inhibitors described, except recent TrkA-selective allosteric examples, display pan-Trk activity due to kinase domain homology. Fundamentally, the primary function of kinases is to catalyze the transfer of a terminal phosphate from ATP to a protein substrate as part of a signalling cascade as described before for Trk. The proximal activation loop, marked by a conserved Asp-

Phe-Gly (DFG) sequence, regulates the activity of the enzyme (**Figure 1.9B, C**, see also **Figure 11A**). This loop is fully ordered in the inactivated state of Trk and occupies the active site, preventing ATP from binding.¹⁹⁷ This conformation is referred to as the DFG-out conformation and positions the Phe of the DFG motif in a hydrophobic pocket behind the gatekeeper Phe in the active site (**Figure 1.9B, C**). A conformational change wherein the DFG residues rotate out of the active site, known as the DFG-in conformation, allows ATP to bind to the kinase and subsequently transfer its terminal phosphate group.

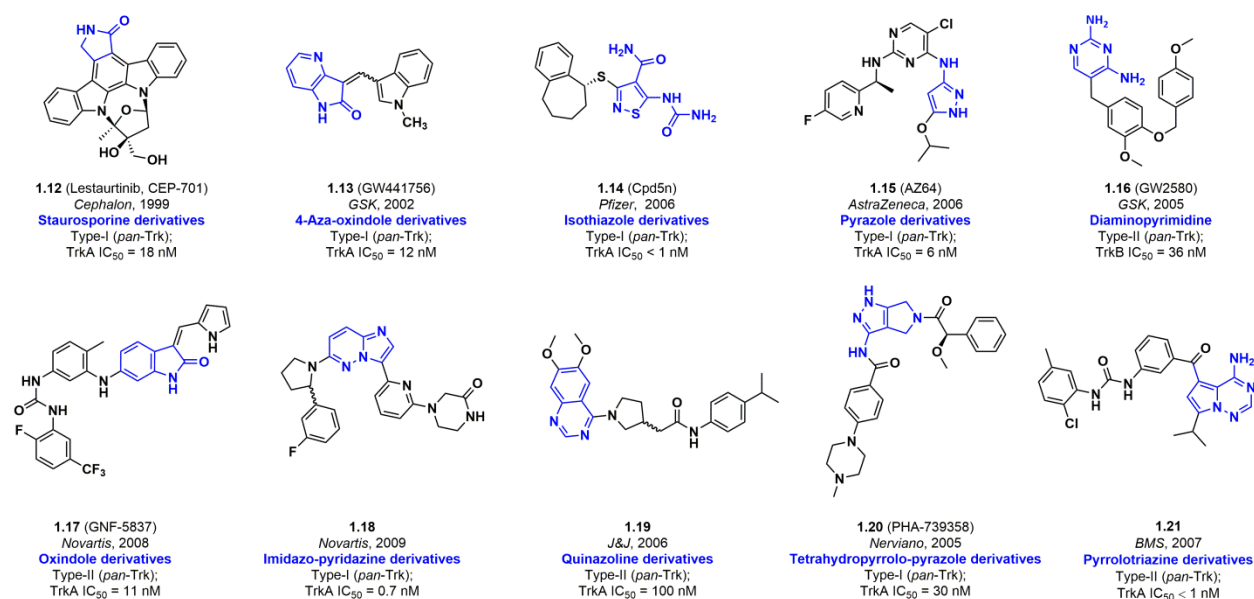


Figure 1.10. Representative examples of early Trk-TKI inhibitors (pre-2011). The hinge binder fragments are shown in blue.

A significant portion of the Trk inhibitors developed to date, including most early Trk inhibitors developed (pre-2010, see **Figure 1.10**), have been type I inhibitors which recognize the active DFG-in conformation of the kinase. This inhibitor class engages the ATP-binding site through hydrogen bonds with the hinge residues and backbone and through hydrophobic interactions in the small adjacent pocket created by the activation loop (**Figure 1.11F**). This type I binding mode was first illustrated in Trk by AstraZeneca in 2012 with the co-crystal structure of their diamino-substituted pyridine inhibitor AZ-64 (**Figure 1.10**) bound to TrkA,¹⁹⁸

and was later accompanied by additional type I inhibitor-Trk complexes such as the thiazole carboxamide inhibitor Cpd5n (**Figure 1.10**) bound to TrkB as disclosed by Sanofi,¹⁹⁹ and Merck's imidazopyridazine inhibitor **1.33** bound to TrkA (**Figure 1.11F**, **Figure 1.12**).²⁰⁰ Other early type I inhibitors described include the promiscuous inhibitor lestaurtinib²⁰¹ and 4-azaxindole inhibitor GW441756 (**Figure 1.10**, see **Chapter 3**).^{196, 202-203} Inhibitors bearing 6,5-bicyclic nitrogen-containing hinge binder such as imidazo[1,2-*b*]pyridazine, triazolo[4,3-*b*]pyridazine, triazolo[4,3-*a*]pyridine and pyrazolo[1,5-*a*]pyrimidine have in fact emerged as privileged structure for type I Trk inhibitor in the last five years (see **Chapter 4** and **5**).^{193-194, 204-205} More recent such examples of type I Trk inhibitor include macrocycles wherein a phenylpyrrolidine moiety is tethered via an alkyl chain to the 3 position of the pyrazolo[1,5-*a*]pyrimidine core such as compound **1.23** (**Figure 1.12**, see discussion in **Chapter 7**).²⁰⁶

Type II inhibitors bind to and stabilize the inactive DFG-out conformation of the kinase. These inhibitors not only engage the ATP-binding site through the hinge, but are able to exploit an additional site, the allosteric pocket, which is made accessible via the rotation of the DFG motif to its 'out' conformation which opens up the adjacent hydrophobic pocket (**Figure 1.11D**, **E**). Type II inhibitors are characteristically elongated in structure, which is a requisite to engage both the ATP-binding site and the distal allosteric pocket (see for the case of Trk **Figure 1.10** and **Figure 1.12**). Planar aromatic systems are common to the hydrophobic pocket and allosteric pocket pharmacophore, and are typically joined by a polar entity, such as a urea, that may engage in hydrogen bonding interactions with the DFG motif and the opposing α C helix. The first co-crystal structure of a type II inhibitor/Trk complex was disclosed by GNF/Novartis in 2012 with a derivative of the ureayl inhibitor GNF-5837 (**Figure 1.10**) complexed with TrkC.²⁰⁷ Subsequent co-crystal structures include, but are not limited to, the inhibitors EX429 and GW2580 bound to TrkB (disclosed by Sanofi) (**Figure 1.10**, see **Chapter 2**),^{199, 208} and the

phenyltriazole acetamide which binding mode is shown in **Figure 1.11D, E** (derivative from **1.28, Figure 1.12**), from Merck in complex with TrkA.²⁰⁹

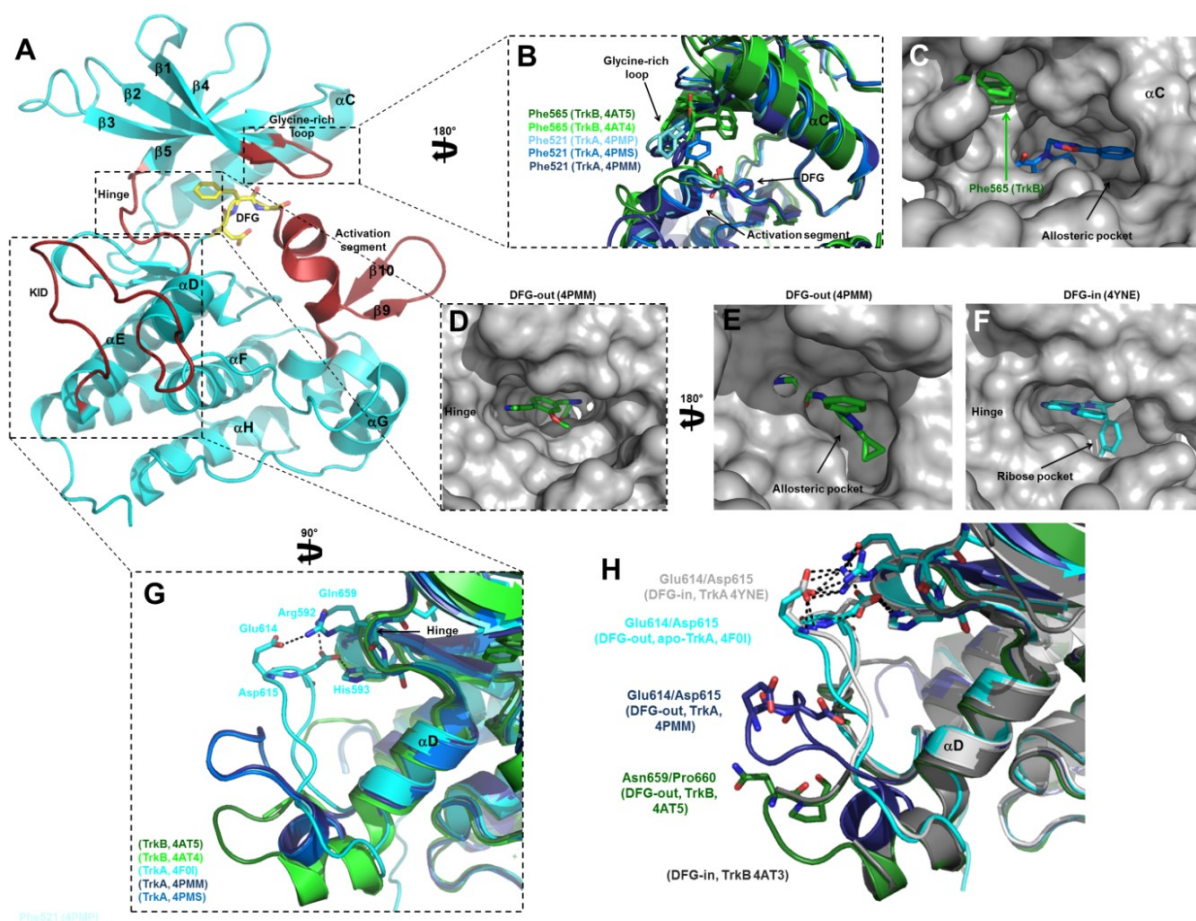


Figure 1.11. (A) Apo-TrkA DFG-out (PDB: 4FOI) with key structural features depicted in bronze. (B) Superposition of the Phe565/Phe521 residues of glycine-rich loops of TrkB (shades of green)/TrkA (shades of blue) in the DFG-out conformation. (C) Superposition of TrkA-type II inhibitor complex (PDB: 4PMS, surface rendering) with Phe565 residues of TrkB (PDB: 4AT5, 4AT4). (D, E) Two views of representative DFG-out (derivative of **1.28**) kinase binding a pan-Trk inhibitor. (F) View of representative DFG-in binding pan-Trk inhibitor (**1.33**). (G) Comparison of the position of the TrkA (shades of blue) and TrkB (shades of greens) KID in DFG-out conformation. (H) Comparison of the position of the TrkA (shades of blue) and TrkB (shades of greens) KID in DFG-out conformation with TrkA (pale gray) and TrkB (dark gray) KID in DFG-in conformation.

Interestingly, Trk's documented basic conformational plasticity is not the rule among kinases as few kinases have been observed to readily adopt both classic DFG-in and DFG-out conformations.²¹⁰⁻²¹¹ Type III inhibitors also bind the kinase through the extended hydrophobic

pocket and contiguous allosteric site but do not interact with the ATP-binding site and are typically non-competitive with ATP binding.²¹² This binding mode has been identified for a very small number of kinase targets.²¹³⁻²¹⁴ A recent report by Merck has provided robust biochemical and crystallographic data describing a unique juxtamembrane domain (JM)-dependant subclass of type III inhibitors of Trk – including the structural rationalization for allosteric TrkA inhibitors (*vide infra*).^{82, 215}

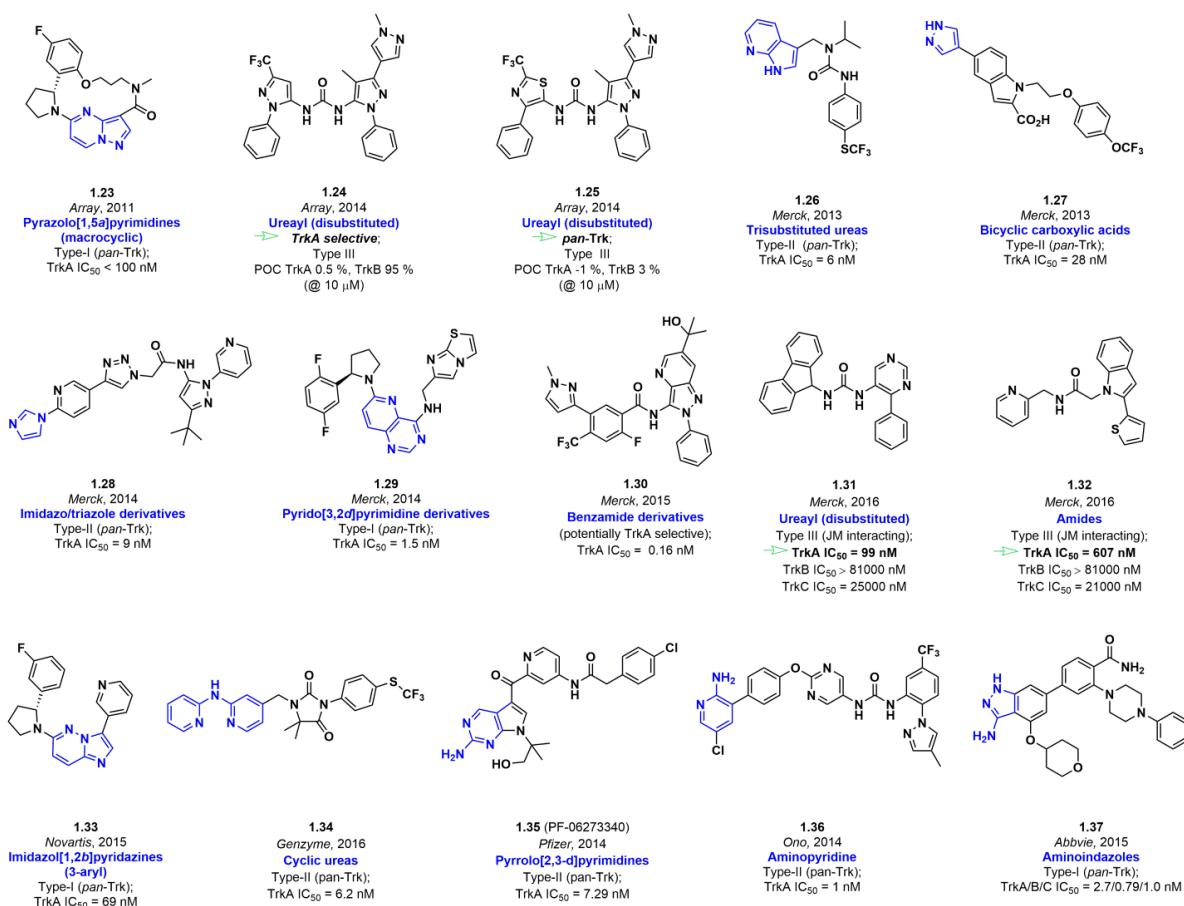


Figure 1.12. Representative examples of Trk-TKI inhibitors (2011-present). The hinge binder fragments are shown in blue (when applicable).

Regarding potential therapy using Trk TKIs, achieving selectivity within the Trk family is desirable to limit potentially avoidable adverse side effects. When considering potential CNS PET applications, Trk family selectivity may be less crucial if TrkB is targeted owing to the higher global expression this receptor compared to TrkA/C. For the same reason however, the

prospect of imaging TrkA in the CNS would require a probe with remarkable selectivity over TrkB/C. Altogether, intra-Trk family selectivity has been particularly challenging to achieve with Trk due to the high degree of homology between Trk isoforms especially around the ATP binding site which share 95% and 100% residue identity between TrkA/TrkB and TrkB/TrkC respectively. Therefore, type I and II Trk inhibitors display relatively marginal differences in their ability to inhibit TrkA, TrkB and TrkC (typically within ~10-fold). One important exception to this observation is the preferential TrkB/C inhibitor developed and described in **Chapter 5** of the present thesis. The residues within the ATP-binding site, adjacent hydrophobic pocket, and distal allosteric site of the three isoforms of Trk are highly conserved and may not be sufficient to support an isoform-specific inhibitor but may explain more modest potency differences within the Trk family for type I and type II inhibitors.¹⁹⁹ Flanking the binding site, there are two regions with structural differences between Trk isoforms that could facilitate partial selective recognition, one being the glycine-rich loop which forms a lid over the active site (**Figure 1.11A**). The residues of this loop are fully conserved between Trk isoforms, although comparison of multiple TrkA/B crystal structures reveal that the Phe side chain on the end of the loop is orientated away from the allosteric site of TrkA whereas it is positioned toward the allosteric site of TrkB (**Figure 1.11B, C**). This subtle arrangement of the Phe side chain restricts the gap between the hydrophobic pocket and the allosteric site. The second site is the kinase insert domain (KID) which was proposed by Sanofi in a 2012 publication¹⁹⁹ as a possible region to achieve Trk isoform selectivity based on differences observed between TrkA/B crystal structures. The KID is an extension from the C-terminal lobe which is positioned below the hinge region (**Figure 1.11G**) and differs in length and sequence between Trk isoforms. Comparison of the inactive form of apo-TrkA/B crystal structures reveals the KID extending to and engaging the hinge in TrkA and adopting a compressed conformation well below the hinge in TrkB (**Figure 1.11G**). Crystal structures included for DFG-out TrkA and DFG-in/out TrkB bound to an inhibitor reveal the same compressed KID for TrkB while the KID of TrkA no longer engages the hinge and

instead adopts a conformation halfway between the fully extended and fully compressed conformations. However, more recent crystal structures of inhibitor-bound TrkA in the DFG-in conformation²⁰⁰ expose a KID-hinge interaction similar to the apo-TrkA crystal structure (**Figure 1.11H**). While such disparities in the KID conformation may arise from artifacts derived from crystal packing, the structural differences of these loops and their propensity to interact with the hinge appear to be more complex than previously thought. Yet, neither the glycine-rich loop nor the KID appear sufficient to explain TrkA isoform recognition from recent small molecule inhibitors.

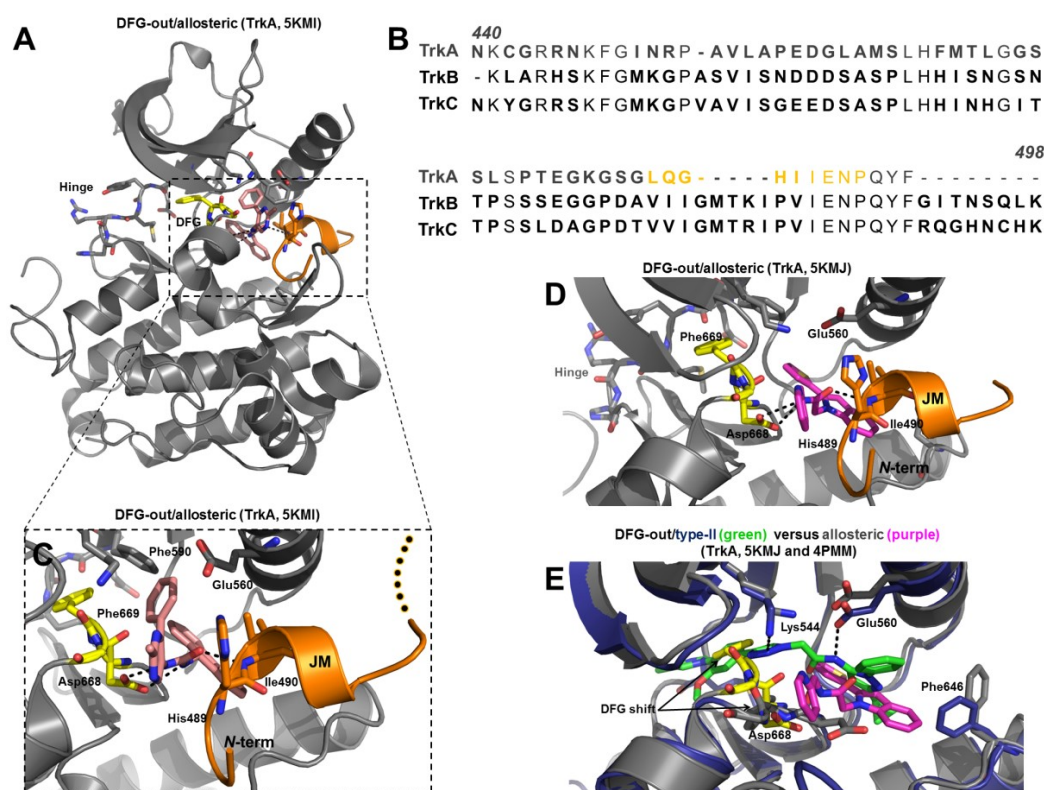


Figure 1.13. (A) Co-crystal structure of TrkA (gray) with a urea-based type III inhibitor **1.31** (salmon). The juxtamembrane domain (JM) sequence is shown in orange and the DFG motif in yellow. (B) Sequence alignment of human TrkA, TrkB and TrkC juxtamembrane domains. TrkA-specific residues are bold. Contact residues from the N-terminal sequence in orange correspond to residues in orange in the cartoon rendering. (D) View of the co-crystal structure of TrkA (gray) with an amide-based type III inhibitor **1.32** (purple). (C) Expanded view of inhibitor binding from (A). (K) Superposition of the co-crystal structure of TrkA (gray) and bound amide-based type III inhibitor (cyan) with the co-crystal structure of an amide-based type II to inhibitor (green, derivative of **1.28**) bound to TrkA (blue), highlighting the shifted DFG motif (yellow and grey sticks).

Urea-based TrkA-selective inhibitors, claiming > 200-1000-fold TrkA selectivity over TrkB/C, were first described by Array (**1.24**, **1.25**, **Figure 1.12**).²¹⁶⁻²¹⁷ The binding mode of those compounds has remained elusive until Merck recently showed that hits such as **1.31** and **1.32** (**Figure 1.12**) at the origin of a number of their recent Trk inhibitor series act as non-conventional type III inhibitors (**Figure 1A, C, D, E**). Representative amide- and urea-based inhibitors, lacking conventional hinge binder motifs (similar to Array's ureas), make bidentate hydrogen-bond interactions with Asp668 side chain (DFG) while engaging different residues from the juxtamembrane domain (JM) which sequence is largely not conserved between Trk family members (36% identity between TrkA and TrkB, and 40% identity between TrkA and TrkC – residues 440-497 of TrkA) (**Figure 1.13B**). The involvement of the JM domain includes residues in the vicinity of Ile490 backbone which interact via hydrogen bond with the carbonyl of both urea and amide inhibitors. Close inspection of those crystal structures shows that the accommodation of large lipophilic substituents such as the fluorene moiety shown in **Figure 13A, C** is possible due to the side chain rearrangement of residues from the α C loop as well as a drastic displacement of the DFG triad, well beyond its observed position when TrkA (or TrkB/C) is bound to type II DFG-out inhibitors (**Figure 13E**). Supported by biochemical assay using various JM truncated variants of the intracellular TrkA domain and crystallographic data, this study also shows that while interaction with non-conserved JM residues seems to enable type III allosteric binding and trigger TrkA selectivity in selected examples, interaction at more conserved amino acid portion from the JM domain is also possible but lead to pan-Trk allosteric inhibitors. This suggests that allosteric JM domain-interacting type III Trk inhibitors may either be TrkA-selective or display pan-Trk activity. While type III inhibitors have not been used as scaffolds for the development of radiotracers in the present thesis due to the recent advent of their characterization, the development of such inhibitors undoubtedly represent a definite advance not only in the field of Trk TKIs but also in the broader context of kinase pharmacology.

1.2.5 Clinical trials with Trk inhibitors: current state. Based on robust preclinical data regarding the role of Trk in neuroblastoma especially,²¹⁸⁻²²¹ an early clinical trial using the multitargeted pan-Trk inhibitor lestaurtinib (formerly CEP-701, compound **1.12**, **Figure 1.10**) was conducted within the context of refractory neuroblastoma.²²² At that point, the lack of Trk selectivity of lestaurtinib combined with the unspecified Trk expression status from responsive versus unresponsive patient groups emerged as conspicuous limitations which prevented unambiguous validation of the anti-Trk approach in the clinical setting.²²³ The characterization of Trk chimeric protein, combined with the discovery of novel pan-Trk inhibitors with favorable kinome selectivity profiles constitute the mainstay of current clinical trials. Nearly a dozen distinct Trk kinase inhibitors are currently investigated in several recruiting or active phase I and II trials for cancer treatment (**Figure 1.14**). In contrast to the early lestaurtinib trial, all inhibitors currently under investigation except one (milciclib) are included in genomically-driven trials focused around *NTRK* fusion-positive patient subpopulations. Milciclib (Tiziana Life Sciences) is a dual Trk/CDK inhibitor which has been previously investigated in patients with advanced malignancies in phase I.²²⁴ Milciclib has progressed to phase II evaluations based on promising phase I results. Yet, as for lestaurtinib, no data on Trk expression has been provided in the phase I report. The authors have however described reversible dose-limiting neurological toxicities (e.g. grade 2-4 ataxia and grade 2-3 tremors) which may be attributed to CNS Trk engagement at higher doses.

The other ten Trk inhibitors currently under evaluation can be divided into either a multitargeted or a selective inhibitor category. The ostensible proof-of-concept of the clinical relevance of Trk inhibition for human cancer has been provided consecutively by the early disclosure of phase I study results from the investigation of the multitargeted inhibitor entrectinib (Ignyta)²²⁵⁻²²⁶ and the Trk-selective inhibitor LOXO-101 (formerly ARRY-470, Loxo Oncology)²²⁷ for *NTRK* fusion-positive solid cancers. Interestingly, two years prior to those reports, a

study which compared the inhibitory activities of LOXO-101 (then identified as ARRY-470 – first structural disclosure) with lestaurtinib and the anaplastic lymphoma kinase (ALK) inhibitor crizotinib (also displaying moderate pan-Trk activity), described the off-label use of crizotinib in a lung cancer patient presenting with a *NTRK1* fusion-expressing tumor.²²⁸ In spite of the modest clinical activity observed then, likely due in part to the suboptimal Trk activity of crizotinib, it is reasonable to assume that this result catalyzed the increasing interest in clinical Trk inhibitors for cancers harboring *NTRK* oncogenic drivers. Favorable results from two early phase trials with entrectinib were first reported at the 2015 ASCO Annual Meeting.²²⁵⁻²²⁶ Entrectinib was initially described and optimized as part of an ALK inhibitor program from the Nerviano pipeline.²²⁹ The compound was later shown to display stronger pan-Trk inhibition compared to ALK as well as ROS1 activity – all relevant molecular targets in the context of fusion oncogenic drivers – and showed promising preclinical activities.²³⁰⁻²³¹ Further kinase profiling revealed ≥ 10-fold selectivity for all targets tested except JAK2 and ACK1. The ALKA-372-001 and STARTRK-1 trials are evaluating the safety and dose escalation responses of entrectinib in adult patients with advanced solid tumors presenting oncogenic alterations (fusion, amplification and SNP for *NTRK1/2/3*, *ROS1* and *ALK*) and have enrolled 119 patients so far. Most subjects in those trials are NSCLC patients presenting ALK alterations. Antitumor response in the phase II-eligible patient population has been reported. Within those 25 patients treated at or above the recommended phase II dose (RP2D), 100% objective response rate was achieved in patients with *NTRK*-rearranged tumors (3/3)^{128, 232-233} For a NSCLC case study, the patient showed complete and durable response of brain metastasis upon treatment, which is in line with appropriate CNS penetration initially described in preclinical investigations and the fact that entrectinib was purposely designed in order to permeate the BBB.²²⁹⁻²³⁰ So far in early studies, entrectinib has been demonstrated to be safe and well-tolerated under RP2D. Three occurrences of dose-limiting toxicities (DLTs) were described at higher dose. Pediatric patients presenting with recurrent or refractory solid tumors (including neuroblastoma) and primary CNS

tumors are currently being recruited for a new trial based on the aforementioned CNS-related results.²³¹ An important corollary of the deep molecular profiling dimension of those studies has been the rapid characterization of the first resistance mechanisms from phase I case study patients. Russo *et al.*²³⁴ described the emergence and detailed biochemical characterization of p.G595R (solvent front) and p.G667C (activation loop) TrkA mutations following 4 months of treatment in the CRC case study. While the pG595R mutation completely abrogated the activity of entrectinib, p.G667C only partially affected its inhibitory effect (as for LOXO-101). Those residues are conserved outside the Trk family and have been previously linked with secondary resistance for other TKIs. The investigation of entrectinib is currently pursued in the ongoing STARTRK-2 trial (phase II).

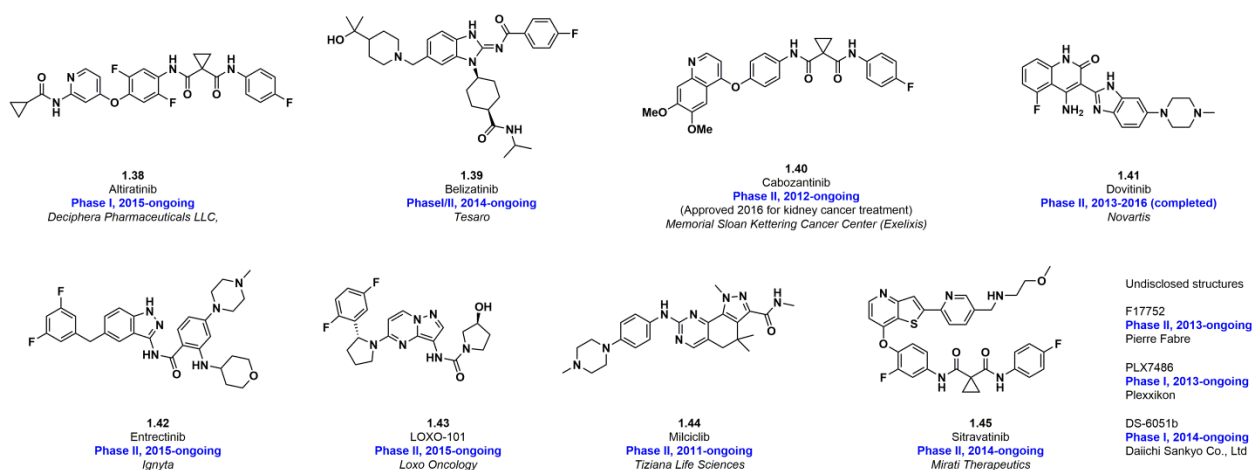


Figure 1.14. Trk-TKI under evaluation in clinical trials for the treatment of cancer.

In parallel, summaries from the evaluation of LOXO-101 from a phase I trial have also been provided.^{227, 235} LOXO-101 is a type I low nanomolar pan-Trk inhibitor with >1000-fold selectivity over all off-targets tested so far and was initially described in an Array Biopharma patent application (selectivity in a 226 kinases panel and an 82-non-kinase targets screen). With respect to Trk-selectivity, LOXO-101 stands alone amongst all clinical Trk inhibitors currently under investigation. The clinical efficacy and safety of this inhibitor has been tested in

seven *NTRK*-positive patients so far, identified from a larger 43 patient group enrolled in the phase I trial. Tumor regression was observed in all six patients evaluable.²³⁶⁻²³⁷ Treatment with LOXO-101 was overall well-tolerated. LOXO-101, contrary to entrectinib, was selected based on its modest CNS exposure in order to contain potential toxicities associated with the inhibition of Trk signaling in the brain and balance possible CNS efficacy. Early data indicate potential utility for CNS tumors as the NSCLC case report also mentioned brain metastasis regression upon treatment in addition to modest primary tumor reduction. Overall, patients lacking *NTRK* fusions did not experience a response to LOXO-101. Accordingly, the NAVIGATE phase II basket trial is currently enrolling patients with *NTRK*-fusion positive cancer. No LOXO-101 responders have been reported to have experienced secondary resistance upon prolonged treatment as of yet. However, the potency of this inhibitor has already been shown to be dramatically affected by point mutations *in vitro* as previously described in the context of entrectinib. With this perspective, Loxo Oncology is already developing a second generation Trk inhibitor, LOXO-195 (undisclosed structure) which is claimed to retain activity against all resistance mutations characterized so far for Trk. This inhibitor is expected to enter phase I in 2017.

The additional pan-Trk inhibitors with claimed kinome selectivity currently under investigation are the dual Trk/ROS1 inhibitor DS-6051a (Daiichi Sankyo) and the dual Trk/ALK inhibitor belizatinib (formerly TSR-011, Amgen/Tesaro). Both compounds have demonstrated promising preclinical and *in vitro* activities.²³⁸⁻²³⁹ Belizatinib is developed as a second generation ALK inhibitor, affording better retention of potency upon point mutations during secondary resistance compared to crizotinib. Early phase I/IIa trial results for patients with *ALK*-driven tumors have been described.²⁴⁰ Although 11 patients with *NTRK*-positive molecular drivers have reportedly been enrolled, no data on this patient subpopulation is currently available. Similarly, no data has arisen so far from clinical studies of DS-6051a. The multitarget ALK/ROS1/Trk

inhibitor F17752 is in a solid tumor study in France with a particular focus on targeting gene rearrangements and patients who are resistant to a prior ALK inhibitor, although no data from the trial is yet available. The remaining five clinical leads are multitargeted inhibitors which show some level of anti-Trk activities. Some of the corresponding trials aim at diversifying or repurposing otherwise clinically approved (e.g. cabozantinib) or heavily investigated (e.g. dovitinib) inhibitors initially developed for other kinase targets which are or have been included in several trials unrelated to Trk. Altiratinib, PLX7486 and sitravatinib are inhibitors undergoing a first time clinical setting investigation and the corresponding trials capitalize on a basket design to gain insights on potentially useful indications for those novel multitargeted agents. No data from those clinical trials is available at the moment. Apart from antineoplastic applications, Trk inhibitors are currently screened as putative therapeutics for the treatment of chronic pain.¹⁹³⁻¹⁹⁴

The most important caution in the clinical development of Trk inhibitors remains the prospect of potential CNS neurotoxicity – hence the importance of developing a PET tracer for neuroimaging. Until details from larger trials are available, it would be prudent not to interpret the safety profiles described in case studies from phase I trials at or under RP2D with LOXO-101 and entrectinib as supporting the overall safety of Trk inhibitors. In fact, preclinical and clinical evidence of the risks associated with CNS exposure upon treatment with Trk inhibitors have been accumulating on many fronts. In preclinical studies with a series of selective pan-Trk inhibitors (from which LOXO-101 emerged), Array characterized reversible ataxia profiles in rats with therapeutic indices correlated to the brain-to-plasma ratios of individual inhibitors. Ataxia scores were shown to increase moving from peripherally restricted to CNS-penetrating inhibitors and ultimately abrogated upon treatment with TrkA selective inhibitors. Array also described hyperphagia and weight gain in rats following treatment with CNS-penetrating selective pan-Trk inhibitors – behaviour not seen with TrkA-selective compounds. Similar phenotypes were also

observed in preclinical work involving humanized TrkB agonist antibody, TAM-163, although the authors described drastic species dependent variations.¹⁸⁶ Neurotoxicity was also demonstrated during the early development of the brain penetrating CDK2/Trk inhibitor milciclib.²⁴¹ CNS side effects, reversible upon treatment cessation, included cases of ataxia (Grade 2-4) and tremors (Grade 2-3) and were likely associated with a sustained CNS Trk signaling blockade. The selective dual Tie-2/Trk inhibitor CE-245677 (Pfizer) was also discontinued in a phase I trial for the treatment of solid tumors due to Trk-related CNS side effects.^{195, 242} In order to address risks associated with unnecessary brain penetration in the treatment of peripheral indications, Pfizer's strategy has been to purposely target P-glycoprotein (P-gp) interaction at the BBB (see section 1.3.2). Recent reports from entrectinib trials also described one case of Grade 3 cognitive impairment above RP2D (reversible following treatment interruption) while paresthesia and peripheral sensory neuropathy was observed in 28% and 9% of patients respectively (at RP2D). As such, potential side effects from CNS exposure will require careful examination in the ongoing phase II trials both for cancer and pain treatment. It is of interest that the data emerging from the development of entrectinib delineate the effort towards achieving robust brain penetration while progress from all other companies emphasize the need to avoid or limit CNS penetration in the light of possible CNS adverse effects as discussed above. For example, the indication of the potential of LOXO-101 in the treatment of brain metastases has been described in spite of low brain penetration. Loxo Oncology has provided detailed preclinical modeling suggesting that intermittent or pulsatile CNS Trk inhibition with LOXO-101 may achieve sufficient CNS exposure for anti-tumor efficacy while preventing neurotoxicity associated with continued CNS inhibition. As the study of brain exposure for TKIs is gaining momentum for the treatment of neurooncological malignancies²⁴³, it may be important to recognize that systematic BBB permeation assessment is also crucially needed for some kinase targets such as Trk which play key biological roles in the CNS. Globally, there is an urgent need to implement efficient preclinical screening for brain penetration as a systematic and basic tool in compound selection

and more importantly, tools to enable patient identification, stratification, staging and pharmacokinetics/pharmacodynamics (PK/PD) studies. Moving forward, the development of an efficient, non-invasive and targeted approach to assess Trk kinase target engagement and support drug development process would be crucial.

1.3 Positron emission tomography imaging and radiotracer design

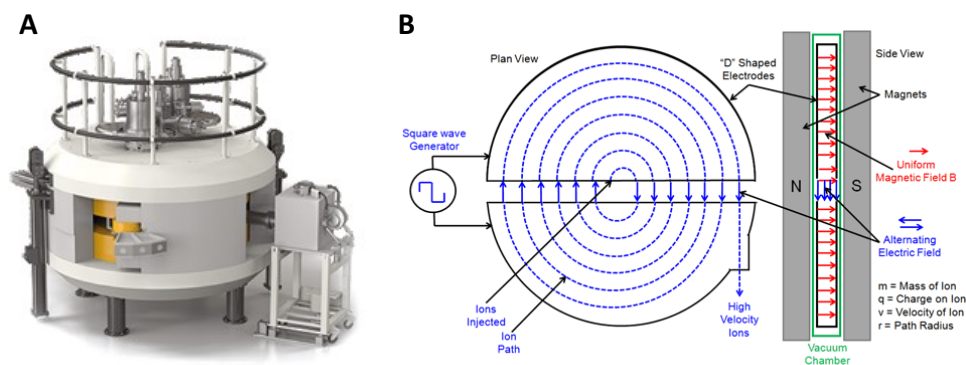


Figure 1.15. (A) Cyclotron (adapted from <http://www.iba-radiopharmasolutions.com/products/cyclotrons> - accessed Jan 2017). (B) Plan view diagram of the path of ions in a classical cyclotron (adapted from <http://www.mpoweruk.com/figs/cyclotron.htm> - accessed Jan 2017).

1.3.1 Principle and instrumentation. The development of PET radiotracers begins with radionuclide production which, in the case of carbon-11 and fluorine-18 as discussed here, is a daily task required to be closely coordinated with the radiotracer synthesis, purification, formulation and use owing to the short half-life of those isotopes.²⁴⁴ Production of those radioisotopes is performed using a cyclotron which accelerates ions, in many cases hydride ions (H^-), in a spiral path before focussing them into a target material to enable a desired nuclear reaction to occur (**Figure 1.15**). Hydride ions are initially produced in a central ion chamber placed in a magnetic field and are accelerated under high vacuum by the charge oscillation of two semi-circular chambers called “dees”. After reaching maximum energy close to the limit of the dees, negatively charged ions are extracted by interacting with a carbon stripper foil, liberating a proton beam which, for example, can be directed at an $[^{18}O]H_2O$ enriched target to generate fluorine-18 via the $^{18}O(p,n)^{18}F$ nuclear reaction. **Table 1.1** lists selected properties of the primary non-metallic radioisotopes used in PET.²⁴⁵

Table 1.1. Properties of non-metal radionuclides commonly used in PET, corresponding half-lives, nuclear reactions, targets, products and decay products

| Radionuclide (β + decay, %; E_{\max} (β +)) | Half-life, $t_{1/2}$ (min) | Nuclear reaction | Target | Product | Decay product |
|---|-------------------------------|--|--|--|-----------------|
| ^{11}C (100 %, 961 KeV) | 20,4 | $^{14}\text{N}(p,\alpha)^{11}\text{C}$ | N_2 (+ O_2) N_2 (+ H_2) | $[^{11}\text{C}]\text{CO}_2$ $[^{11}\text{C}]\text{CH}_4$ | ^{11}B |
| ^{13}N (100 %, 1190 KeV) | 9,97 | $^{16}\text{O}(p,\alpha)^{13}\text{N}$ | H_2O $\text{H}_2\text{O} +$ EtOH | $[^{13}\text{N}]\text{NO}_x$ $[^{13}\text{N}]\text{NH}_3$ | ^{13}C |
| ^{15}O (100 %, 1732 KeV) | 2,04 | $^{15}\text{N}(d,n)^{15}\text{O}$ | N_2 (+ O_2) | $[^{15}\text{O}]\text{O}_2$ | ^{15}N |
| ^{18}F (97 %, 634 KeV) | 110 | $^{20}\text{Ne}(d,\alpha)^{18}\text{F}$ $^{18}\text{O}(p,n)^{18}\text{F}$ | Ne (+ F_2) $[^{18}\text{O}]\text{H}_2\text{O}$ | $[^{18}\text{F}]\text{F}_2$ $^{18}\text{F}^-$ | ^{18}O |

The central challenges of radiotracer production truly begin with the radioisotope use, when the chemistry and isolation steps required for the radiosynthesis of a given radiotracer has to be deployed in a short period of time under stringent conditions. Owing to the short half-lives of neutron-deficient isotopes used in PET, a three isotope-half-life rule is normally accepted as the maximum timeframe from the end of bombardment (EOB) to the completed formulation of a radiotracer. The labeling of small molecules with carbon-11 or fluorine-18 normally operates under large excess of unlabeled precursor (typically in micromolar amounts) relative to the radioactive synthon (e.g. picomole to low nanomole of $^{11}\text{CH}_3\text{I}$, $^{18}\text{F}^-$, etc. *vide infra*). While enabling reactions to occur in short period of time relative to macroscopic scale conditions, in some cases such stoichiometry also comes at the cost of high susceptibility to impurity – even so only present in minute amounts. The handling of such small quantity of reagent requires the use of purposely small reaction vessels and equipment and also implies that exceptional caution has to be taken in manipulation and transfer steps in order to minimize possible loss of material. Radiotracers for clinical use are produced in automated synthesis modules allowing the manipulation of large amounts of radioactivity, minimum radiation exposure for the operators and, ideally, high reproducibility.²⁴⁶ In a research environment, radiotracers are often initially developed using manual procedures with smaller radioactivity quantities, which enables some

flexibility and optimization. Manual radiosyntheses may also be required in cases where multiple steps are needed to obtain a tracer which may not be suitable for automation.²⁴⁷ For practical reasons, it is however preferable to aim for the radioisotope to be incorporated efficiently in a single step from a suitable precursor. In this regard, the availability and choice of optimal chemical routes and techniques is crucial (*vide infra*). In all cases, purification and characterization of radiotracers are generally performed using high performance liquid chromatography (HPLC) equipped with a radioactivity detector. The assessment of the identity of the radiotracer is performed using HPLC, thin-layer chromatography and gas chromatography employing suitable detectors. Production of radiopharmaceuticals for human use follows current good manufacturing practice (cGMP) and faces quality control with similar constraints as for pharmaceuticals in general. For both preclinical and clinical work, tracers are normally formulated as injectable sterile isotonic saline solutions (with up to 10% v/v ethanolic content).

An important aspect to consider in the process of radiotracer synthesis is the specific activity (S_A) which is defined as the amount of radioactivity by unit of mass of radiotracer ($S_A = A_i/\sum n_i$, where A_i is the activity of the radiopharmaceutical expressed as GBq and $\sum n_i$ the sum of the entire isotopic forms of the radiopharmaceutical in μmol). Maximum theoretical S_A for carbon-11 and fluorine-18 are 3.4×10^5 and 6.3×10^4 GBq $\cdot\mu\text{mol}^{-1}$ respectively but values much lower are obtained with labeled tracers due to unavoidable isotopic dilution which occurs during radioisotope production and radiosynthesis. Routinely obtained S_A ranges around 100-10,000-fold under maximum theoretical values which is sufficient to visualize most targets, including CNS ones.^{245, 248}

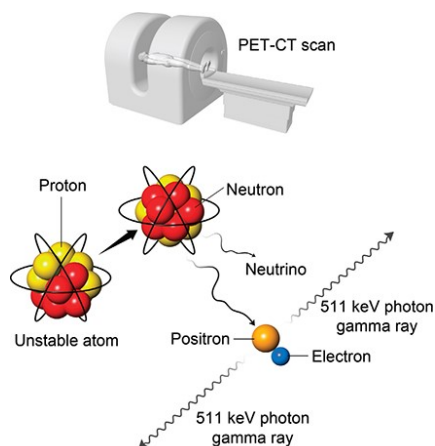


Figure 1.16. Principle of positron emission tomography.

In PET, the reconstruction of the spatiotemporal localization of radiotracers is possible following the detection of a large amount of coincidental 511 keV γ -ray photons which originate from the annihilation of β^+ , emitted by PET radionuclides upon decay, with surrounding electrons (**Figure 1.16**). Before annihilating with an electron, an emitted β^+ travels in the surrounding tissue (typically 1 mm - 2 cm) while losing kinetic energy in a process known as thermalization. The distance traveled by a β^+ prior to annihilation (e.g. the positron range) is a key determinant of spatial resolution and is specific for each nuclide (**Table 1.1**).²⁴⁹ In the next sections we will examine some key principles for radiotracer design in the context of PET neuroimaging and enzyme targets more specifically.

1.3.2 Development of small molecule PET radiotracers for neuroimaging. In the relative short period of time (60-120 min) from the injection into a living subject, which can coincide or not with the beginning of the imaging procedure depending on the nature of the tracer, to the end of the PET scan, radiotracers will generally undergo extensive distribution and complex chemical transformations. With the imaging technique being naturally insensitive to the chemical nature of positron-emitting species detected, it is important to ensure that the signal obtained corresponds to the bioactive radiotracer and measures which metabolite may be

present. It is uncommon, yet highly desirable, to discover a tracer which will remain metabolically untouched or will undergo only inconsequential metabolism following injection *in vivo*.¹¹ A minimum criterion is that radiometabolites should be minimal, well-characterized and excluded from the tissue or region of interest in ways not to confound quantitative measurements. In the context of CNS imaging, where most probes are expected to reach the brain through passive diffusion, a radiotracer can still be useful despite metabolism if radiometabolites are more polar and hence restricted to the periphery – which is frequently the case from phase I oxidative metabolism (Figure 1.17B).¹¹ Although site-of-metabolism prediction can often be derived accurately using *in silico* tools,²⁵⁰⁻²⁵¹ obtaining reliable data on rates of metabolism at subpharmacological doses prior to *in vivo* assessment in different species is more challenging and constitutes a central limitation to radiotracer success.¹¹

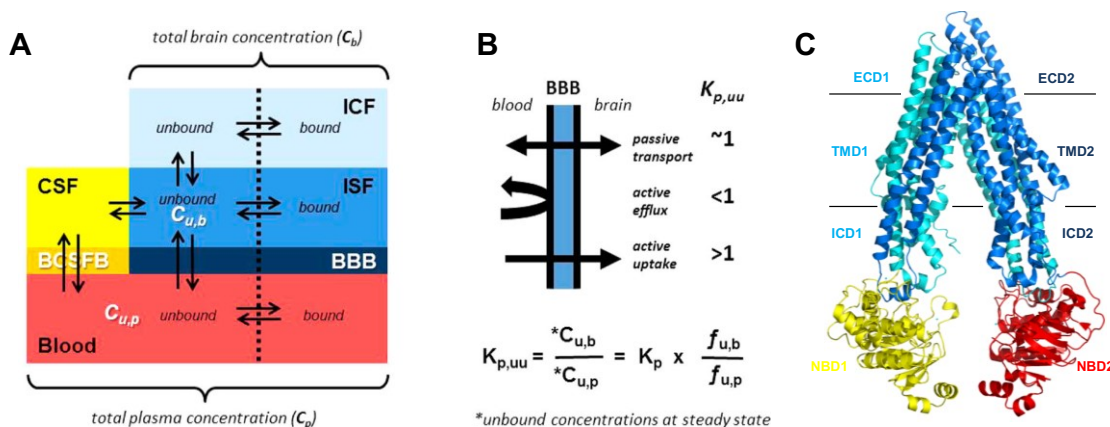


Figure 1.17. (A) Representation of bound and unbound drug concentration equilibrium across BBB; nterstitial fluid (ISF), intracellular fluid (ICF), and cerebrospinal fluid (CSF). (B) Relation between unbound brain-to-plasma ratio ($K_{p,uu}$) and transport across the BBB (adapted from ref.²⁵²). (C) Crystal structure of the mouse P-gp (ECD1/2: extracellular domains 1/2; TMD1/2: transmembranar domains 1/2; ICD1/2: intracellular domains 1/2, PDB ID: 3G5U²⁵³).

Meta-analyses documenting desired physico-chemical properties to favor brain permeation while limiting non-specific binding (NSB), including studies aimed at PET tracers specifically, have recently provided guidelines to “de-risk” CNS drugs and neuroimaging tracers development.^{252, 254-256} Most of those parameters outline optimal properties for diffusion through

the highly restricted blood-brain barrier (**Figure 1.17**). Ranges for CNS multiparameter optimization (MPO) are presented in **Table 1.2**.

Table 1.2. Physicochemical Properties, Weighting, and Parameter Ranges for CNS MPO and CNS PET MPO

| Properties | Weight ^a | CNS MPO ^b | | CNS PET MPO ^c | |
|-----------------|---------------------|---------------------------------|---------------------------------|---------------------------------|---------------------------------|
| | | More desirable range (T0 = 1.0) | Less desirable range (T0 = 0.0) | More desirable range (T0 = 1.0) | Less desirable range (T0 = 0.0) |
| ClogP | 1.0 | ClogP ≤ 3 | ClogP > 5 | ClogP ≤ 2.8 | ClogP ≥ 4.0 |
| ClogD | 1.0 | ClogD ≤ 2 | ClogD > 4 | ClogD ≤ 1.7 | ClogD > 2.8 |
| MW | 1.0 | MW ≤ 360 | MW > 500 | MW ≤ 305.3 | MW > 350.5 |
| TPSA | 1.0 | 40 < TPSA ≤ 90; | TPSA ≤ 20; TPSA > 120 | 44.8 < TPSA ≤ 63.3 | TPSA ≤ 32.3; TPSA > 86.2 |
| HBD | 1.0 | HBD ≤ 0.5 | HBD > 3.5 | HBD ≤ 1 | HBD > 2 |
| pK _a | 1.0 | pK _a ≤ 8 | pK _a > 10 | pK _a ≤ 7.2 | pK _a > 9.5 |

^a Scores > 3 are desirable for CNS PET tracers. ^b Adapted from Ref.²⁵⁵ ^c Adapted from Ref.²⁵⁴.

Although those parameters have been delineated in the context of CNS exposure, they also undeniably apply to peripheral imaging in case of intracellular target requiring passive permeability and a ligand-receptor type interaction for tracer accumulation. From an ADME standpoint, CNS tracers should also have low liability for efflux transporters and non-negligible unbound fraction in plasma ($f_{u,p} > 0.15$) and brain ($f_{u,b} > 0.05$). High-throughput *in vitro* assays aimed at determining those properties are readily accessible in industry but often not available in academia, where most radiotracer research and development is conducted. In average, when fulfilling basic CNS MPO properties adequately, compounds however in turn tend to display also favorable ADME properties.²⁵⁴

One of the most important and least predictable aspect of CNS tracer development is efflux active transport.²⁵⁷ P-gp, which belong to the ATP-binding cassette transporter family, has been the most characterized efflux transporter (**Figure 1.17C**) and shown to be heavily expressed at the luminal face of endothelial cells from the BBB where it acts as a pump extruding a wide variety of compound classes outside the brain compartment.²⁵⁸⁻²⁵⁹ With efflux

pumps also expressed in tumor cells, the question of minimizing efflux liability is also of central importance for oncological tracers. Finally, in terms of pharmacology, PET tracer should display high affinity in relation with expression density such as $K_d/B_{max} > 10$ and excellent target selectivity (again, depending on the expression level of off target proteins).¹¹ The criteria of selectivity is of paramount importance if aiming at imaging a specific target from the human kinome owing to the non-negligible homology amongst kinases and the sizable diversity of this protein family (2.2% of the human genome).¹⁴ The requirements listed here and the limitations associated with radiolabeling techniques discussed below largely narrow the number compounds which may be suitable to serve as PET tracers and implies that extensive SAR and iterative trial and errors rounds tend to be norms for radiotracer development.

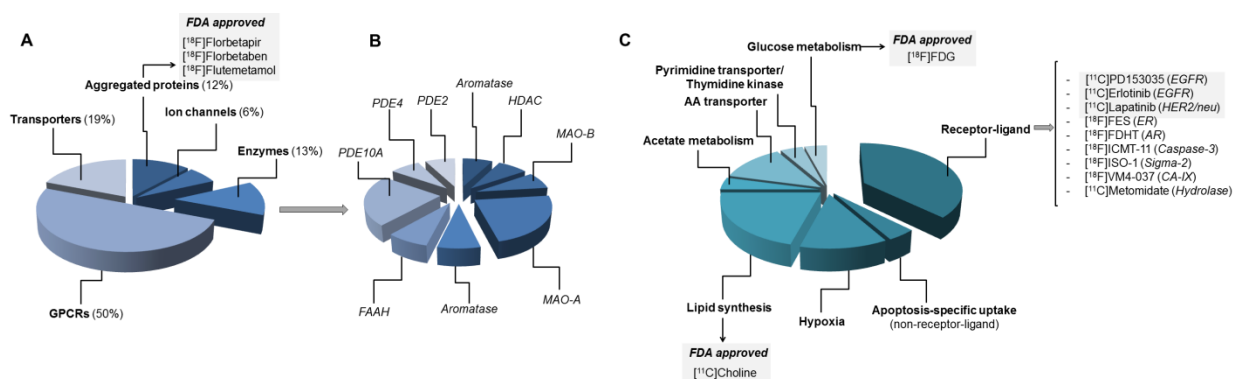


Figure 1.18. (A,B) CNS PET radiotracers in clinical research based on target classes (adapted CNS Radiotracer Table <http://www.nimh.nih.gov/researchpriorities/therapeutics/cns-radiotracer-table.shtml> - accessed Jan 2017). (C) Small molecule oncology PET radiotracers in clinical research based on tumor uptake mechanisms (adapted from Ref.²⁶⁰).

1.3.3 Enzyme neuroimaging and oncological imaging using small molecule PET radioligands. Neuroimaging clinical PET tracers (agonists, antagonists or binders) have historically targeted G protein-coupled receptors (GPCR), ion channels, transporters and more recently abnormally conformed proteins (Figure 1.18).⁷ In comparison, the use of high affinity enzyme radiolabeled inhibitors has been relatively unexplored (< 13% of CNS human radiotracers; Figure 1.18A).²⁶¹ Few notable exceptions include radiotracers for

phosphodiesterases (PDE), monoamine oxidases (MAO), and most recently histone deacetylases (HDAC) (**Figure 1.18B**).²⁶¹⁻²⁶² As opposed to conventional neurotransmitter receptors, most enzymes tend to display relatively low densities and intracellular binding sites, which constitute additional burdens in terms of PET tracer development and may explain the historical penchant not to aim at enzymes PET imaging to the profit of “lower risk” targets.^{261, 263} Since progresses in radiotracer development also inevitably follow progresses in drug development, the very history of CNS drug development certainly constitutes a key reason to explain the relegation of enzymes, including kinases, as high affinity tracer targets to the profit of better characterized neuroreceptors in previous decades.²⁶⁴ To our knowledge, before our contribution, there has not been a single neuroimaging human study with radiotracer targeting endogenous kinases despite increasing preclinical work in recent years.²⁶⁵⁻²⁷⁰

In the context of oncological clinical PET imaging (including neurooncology), tracer retention tends to rely on various mechanisms beyond high affinity receptor-ligand interaction. There has been, for example, extensive work relating to probing enzyme *activity*, with the use most notably of [¹⁸F]-fluorodeoxyglucose ([¹⁸F]FDG) and to a lesser extent, tracers such as [¹⁸F]-fluoro-3'-deoxy-3'-L-fluorothymidine ([¹⁸F]FLT) and [¹¹C]choline among others (**Figure 1.18C**).²⁶⁰ A number of more recently developed clinical oncology tracers rely on receptor-ligand interaction for tumor accumulation. Prominent targets covered include hydrolases, caspases and kinases (**Figure 1.18C**).²⁷⁰⁻²⁷¹ Importantly, in recent years, radiolabeled kinase inhibitors have been used to identify cancer patients most likely to respond kinase inhibitor therapy non-invasively.²⁷²⁻²⁷³ So far, only isotopologues of approved inhibitors or advanced leads have reached a clinical evaluation stage. While the radiolabeling of approved compounds enjoys the obvious advantages of a facilitated clinical translation, such a strategy presents some shortcomings efflux liabilities and limited kinome selectivity.²⁷⁰ In the next section, we present a

Chapter 1

brief overview of carbon-11 and fluorine-18 radiochemistry and positioned the labelling techniques used in this thesis in the broader context of both fields.

1.4 PET radiochemistry

The practice of organic radiochemistry largely differs from the practice of nonradioactive *macroscopic* organic chemistry. One major difference relates to the notion of yield for example. While achieving high radiochemical yields (RCYs) is always desirable, it is however not always necessary. In many cases, it may be possible to deliver sufficient amounts of radiotracer for *in vivo* imaging experiments, even for clinical imaging, despite low RCYs – yields which in organic chemistry would be deemed inadequate (e.g. < 5% RCY). The overall efficiency of a radiosynthesis depends on a number of factors which have often precedence over the RCY (for example; the reaction time, the reaction conditions, the nature of the side product generated and the ease of separation and purification). RCYs are either reported as decay corrected or non-decay corrected. Non-decay corrected RCYs contain information relative to the temporal dimension of a synthesis and provide, arguably, a more accurate descriptor of the efficiency of a radiosynthetic sequence – which is highly time-sensitive due to the short half-life of the radioisotope involved.²⁴⁵ High radiochemical and chemical purities (ideally > 98%) are also key parameters alongside the RCY during synthesis optimization. It is important to bear in mind that the choice of a radiosynthetic sequence and radiolabelling position may also ultimately impact *in vivo* imaging results. For example, depending on metabolism, the same compound labeled at different positions may give drastically opposite *in vivo* results.^{11, 274} When selecting a radiochemistry approach, all the abovementioned aspects have to be weighted.

1.4.1 Overview of carbon-11 radiochemistry. Carbon-11 ($t_{1/2} = 20.38$ min) offers diverse synthetic possibilities with regard to labeling bioactive drug-like small molecules owing to the ubiquitous presence of carbon in those compounds. Carbon-11 radiochemistry is however limited by the availability of ^{11}C -labeled synthons and the straightforwardness and reliability with which these can be produced (**Figure 1.19**).²⁴⁵ The carbon-11 half-life also poses a formidable challenge in terms of synthesis, requiring ideally reactions to occur in a matter of seconds or

minutes from cyclotron-produced material. The most used precursor building blocks in carbon-11 radiochemistry are $[^{11}\text{C}]\text{CO}_2$ and $[^{11}\text{C}]\text{CH}_4$ (Table 1.1 and Figure 1.19) which can be further converted into reactive species to perform a range of radiochemical transformations.

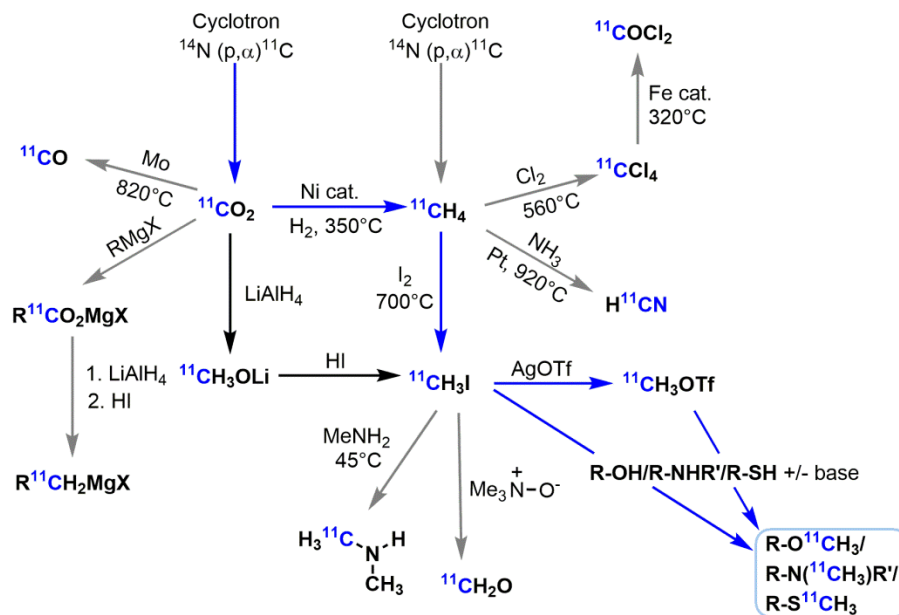


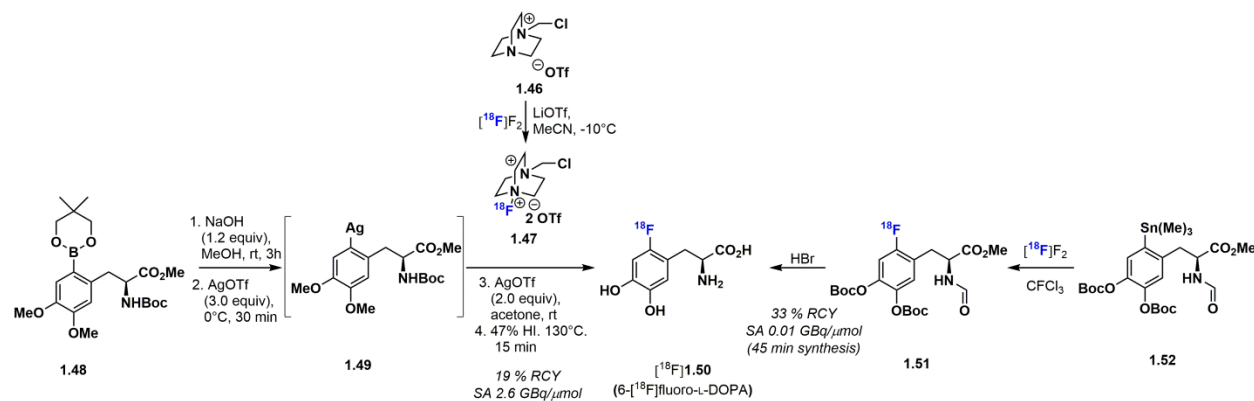
Figure 1.19. Overview of carbon-11 radiochemistry.

Methylation reactions using either $[^{11}\text{C}]\text{CH}_3\text{I}$ or $[^{11}\text{C}]\text{CH}_3\text{OTf}$, which can be produced efficiently following automated protocols, account for the vast majority and the radiochemistry performed with carbon-11. The synthesis of $[^{11}\text{C}]\text{CH}_3\text{I}$ via the LiAlH_4 reduction followed by iodination with hydroiodic acid (the so-called “wet method”) has been used for over three decades.²⁷⁵ A widely used alternative to produce $[^{11}\text{C}]\text{CH}_3\text{I}$ which also procures higher S_A involves the conversion of $[^{11}\text{C}]\text{CO}_2$ to $[^{11}\text{C}]\text{CH}_4$ and the solid-gas iodination of $[^{11}\text{C}]\text{CH}_4$ at elevated temperature (“dry method”) (Figure 1.19).²⁷⁶ Highly reactive $[^{11}\text{C}]\text{CH}_3\text{OTf}$ may be preferable in some cases and can be readily obtained by passing $[^{11}\text{C}]\text{CH}_3\text{I}$ over a silver triflate column at around 200°C.²⁷⁷ Substitution reactions involving $[^{11}\text{C}]\text{CH}_3\text{I}$ and $[^{11}\text{C}]\text{CH}_3\text{OTf}$ with suitable nor-methyl O-, N- and S-nucleophilic precursors is generally straightforward and rapid (< 5 min). Collectively, carbon-11 methylation reactions have been used to synthesized a plethora methylated research and

clinical tracers and also constitute the privileged carbon-11 approach throughout this thesis.²⁷⁸ $[^{11}\text{C}]\text{CH}_3\text{I}$ is also suitable for palladium-mediated cross-coupling reactions.^{245, 279} The use of $[^{11}\text{C}]\text{CO}_2$ itself for Grignard reaction²⁸⁰ and more recently the emergence of efficient carboxylation (carbon-fixation) and carbonylation (following conversion into $[^{11}\text{C}]\text{CO}$) synthetic methods have enable the synthesis of various ^{11}C -labeled functional groups including ureas, carbamates, oxazolidinones, carboxylic acids, esters, and amides.²⁸¹⁻²⁸² Other less commonly used ^{11}C -based synthons included $[^{11}\text{C}]\text{CH}_2\text{O}$,²⁸³ $[^{11}\text{C}]\text{dimethylamine}$,²⁸⁴ $[^{11}\text{C}]\text{HCN}$ ²⁸⁵ and $[^{11}\text{C}]\text{COCl}_2$.²⁸⁶

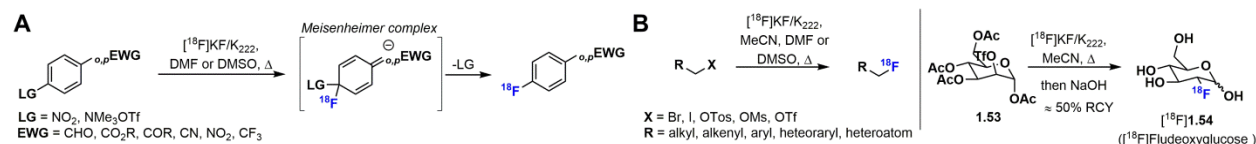
1.4.2 Overview of fluorine-18 radiochemistry. Fluorine-18, with its longer half-life ($t_{1/2} = 109.8$ min) and near-optimal nuclear properties relative to other available positron emitters, is the most widely used PET isotope. A disadvantage of using fluorine-18 relates to the limited pool of suitable fluoroorganic compounds available. This often requires additional work to be conducted in the biological validation process if a fluorine substituent has to be added in a position amenable for labeling from a bioactive non-fluorinated lead. Radiotracers labeled with fluorine-18 can be obtained following electrophilic or nucleophilic reactions.²⁸⁷⁻²⁸⁸ Although now mostly abandoned as a result of headways made in nucleophilic ^{18}F -fluorination, electrophilic ^{18}F -fluorinations have been instrumental in the development of a large number of radiotracers. For example, the first synthesis of $[^{18}\text{F}]\text{FDG}$ employed an electrophilic reaction with $[^{18}\text{F}]\text{acetyl hypofluorite}$ obtained from elemental fluorine ($[^{18}\text{F}]\text{F}_2$; **Table 1.1**).²⁸⁹ Radiofluorination using highly reactive $[^{18}\text{F}]\text{F}_2$ gas directly is possible but often leads to mixtures of products of low S_A due to the carrier-added production method required for the synthesis of this synthon.²⁴⁵ Those limitations have led to the development of alternative approaches to achieve regioselectivity such as the use of fluorodemetalation of electron-rich aryl stannanes using $[^{18}\text{F}]\text{F}_2$ or the reaction of boronic ester precursors in the presence of silver triflate with more versatile

electrophilic N- ^{18}F -fluorinated reagents²⁹⁰ has illustrated by the synthesis 6- ^{18}F fluoro-L-DOPA in **Scheme 1.1**.^{287, 291}



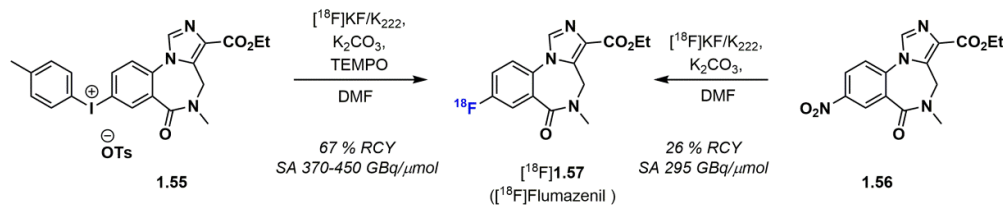
Scheme 1.1. Representative examples of electrophilic ^{18}F -radiofluorination and the synthesis of 6- ^{18}F fluoro-L-DOPA. Comparison of electrophilic fluorodestannylation and silver-mediated radiosynthetic approaches.

Otherwise, nucleophilic fluorination is the primary labeling technique in ^{18}F -radiochemistry. Cyclotron-produced aqueous $^{18}\text{F}\text{F}^-$ (**Table 1.1**), which is largely inert, requires a few processing steps before being useful in nucleophilic reactions. Typically, this is achieved via the trapping of $^{18}\text{F}\text{F}^-$ onto an ion-exchange cartridge, followed by elution with an acetonitrile/water mixture containing potassium carbonate and a phase-transfer reagent such as kryptofix-222 (K_{222}). The $^{18}\text{F}\text{K}/\text{K}_{222}$ solution hence obtained is then azeotropically dried which minimises the water content and the residue obtained is ultimately redissolved in a polar aprotic solvent which generates an activated nucleophilic “naked” $^{18}\text{F}\text{F}^-$ with sufficient reactivity to performed well in various nucleophilic reactions. Nucleophilic aromatic substitutions ($\text{S}_{\text{N}}\text{Ar}$) using activated aryl precursors and $\text{S}_{\text{N}}2$ nucleophilic substitutions with alkyl precursors bearing suitable leaving groups are by far the most usual practices encountered in ^{18}F -radiochemistry to date and account, to all intents and purposes, for the synthesis of all ^{18}F -labeled tracers in clinical use (**Scheme 1.2**).



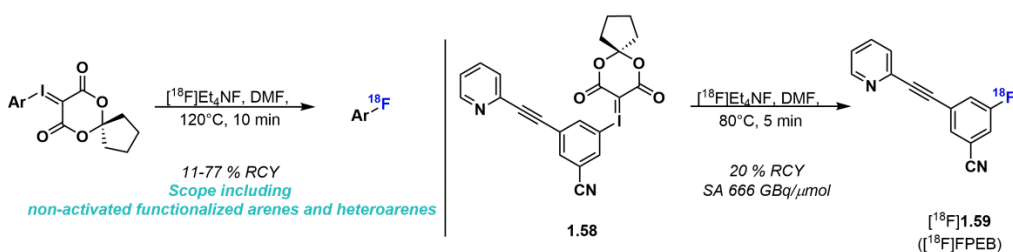
Scheme 1.2. General substrate scope for (A) S_NAr and (B) S_N2 ¹⁸F-radiofluorination reactions and representative radiosynthesis of [¹⁸F]fluorodeoxyglucose ([¹⁸F]FDG).

Under normal circumstances, ¹⁸F-fluoroalkyl radiotracers or prosthetic groups can be obtained readily from alkyl halides or alkyl sulfonates. [¹⁸F]FDG for example is routinely obtained via S_N2 from O-acetyl-2-triflate-β-mannose (**Scheme 1.2B**).²⁹²⁻²⁹³ Obtaining high yields in this context is frequent but special caution has to be taken to avoid competing elimination of the ¹⁸F-fluoroalkyl species or the precursors under some reaction conditions. As for most reactions using [¹⁸F]F⁻, adjacent reactive functional groups such as alcohols, amines and acids have to be protected prior the radiofluorination. A radiosynthetic approach relying on the S_NAr reaction requires the use of an aryl precursor bearing a strong electron-withdrawing group in either *para* or *ortho* to the fluorination position (**Scheme 1.2A**). Nitro and trimethylammonium triflate leaving groups are readily displaced with [¹⁸F]KF/K₂₂₂ and lead to ¹⁸F-labeled tracers in good RCYs with substrates containing suitable electron-withdrawing substitutions (*p*-NO₂ > *p*-CF₃ ≈ *p*-CN > *p*-CHO > *p*-Ac > *m*-NO₂).²⁸⁷ Apart from rare exceptions, the S_NAr is however only productive at high temperatures which may not be suitable for every precursors. ¹⁸F-fluoropyridine labeled at C-2 and C-4 positions can also be obtained by S_NAr.²⁹⁴ Despite the undeniable utility and the robustness of the S_NAr reaction, the limitations imposed by the activated nature and electronic arrangement of functional precursors imply that only a very narrow set of aryl and heteroaryl motifs can be obtained efficiently following this route. The use of both the aliphatic and aromatic nucleophilic substitutions approaches are described in this thesis.



Scheme 1.3. Comparative radiosynthesis of $[^{18}\text{F}]$ flumazenil ($[^{18}\text{F}]$ FMZ) by diaryliodonium salts and $\text{S}_{\text{N}}\text{Ar}$.

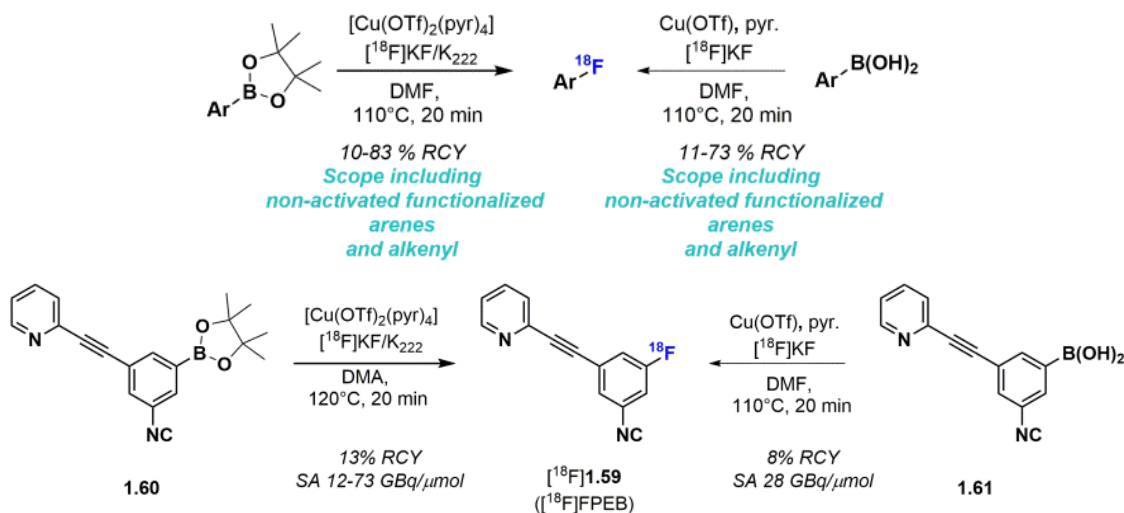
For decades, besides the use of diaryliodonium salts which tend to generate various amounts of undesired radioactive side products, there have been limited general alternatives for the radiofluorination of electron-neutral and electron-rich aryls and heteroaryls (which account for a much larger portion of bioactive drug-like compounds compared to electron-deficient structures alone) (**Scheme 1.3**).^{287, 295-296} However, the last five years have seen the emergence of a promising new set of techniques to synthesize such compounds.^{288, 297-301} Two of the most encouraging approaches are the use of spiroiodine(III)-based precursors and the radiochemical adaptation of the Cu-mediated radiofluorination of arylboronate esters and acids initially described in non-radioactive chemistry.³⁰² Spirocyclic hypervalent iodine(III)-mediated radiofluorination has been pioneered by the groups of Coenen³⁰³ and Vasdev²⁹⁷ and shown to provide remarkable regioselectivity along with functional group tolerability and high efficiency with both electron-rich and sterically hindered arenes (**Scheme 1.4**). This technique has also been demonstrated recently to be suitable for the production of clinical radiopharmaceuticals.³⁰⁴



Scheme 1.4. Spirocyclic iodonium ylides approach and representative radiosynthesis of $[^{18}\text{F}]$ FPFB.

Concurrently, Cu-mediated radiofluorination using either boronic esters or acids have been developed and shown to provide an expedient route towards a wide range of ^{18}F -

fluoroaryl fragments, more or less irrespectively of specific electronic considerations (**Scheme 1.5**).^{288, 305-307} Being versatile and operationally simple, this approach, in comparison to most other novel ¹⁸F-aryl labeling techniques, is emerging as a practical and realistic radiolabeling method for routine ¹⁸F-tracer production. In particular, the fact that this approach uses boronic acids and esters which are easily accessible motifs from a synthetic standpoint offers a true advantage relative to most other techniques. We have explored the utility of this labeling technique for the last radiotracer described in this thesis.



Scheme 1.5. Comparison of representative conditions and application of the Cu-mediated ¹⁸F-fluorination of arylboronate esters and acids.

1.5 Conclusion and objectives

Non-invasive molecular tools to quantify TrkA/B/C expression in preclinical/clinical neurology, oncology and drug development would be highly desirable but are, at the moment, critically lacking. Moreover, there is currently only sparse data with regard to the broader possibility of achieving CNS kinase imaging and the specific steps required to achieve such goal. The level of structural flexibility of Trk TKIs provides, we conjectured, an appropriate framework for the development of the first Trk-targeted PET radiotracers. Therefore, we hypothesize that a suitable TrkA/B/C radioligand for *in vivo* PET imaging applications could be developed using a broad TKIs-based radiotracer platform through a rational design strategy. The overarching goal of the present thesis is to identify structural and biological guidelines necessary for successful kinase neuroimaging, from compound design to human use, using TrkA/B/C as a pharmacologically relevant target. In this sense, the primary objectives of the thesis were to explore and refine a diverse set of highly potent Trk TKIs leads and perform small library syntheses revolving around key CNS PET selection parameters. Another key objective relates to the design and syntheses of suitable precursors for radiolabeling and the implementation of appropriate and efficient radiosynthetic strategies for radioisotope incorporation using fluorine-18 or carbon-11 sources. Owing to the diverse potential applications of Trk radiotracers, we envisioned that the molecular probes developed should be assessed using a wide variety of *in vitro* and *in vivo* techniques and various experimental approaches when applicable including: *in vitro* autoradiography experiments (rat/mice brain, TrkB-expressing human neuroblastoma sections, human brain), metabolic studies (plasma, whole blood, microsomal assay), plasma binding studies and *in vivo* PET imaging using different species (including: Sprague Dawley rat, BALB/c mice, FVB/ Mdr1a/b^(-/-) Bcrp1^(-/-) mice, primates).

1.6 References

1. Politis, M.; Piccini, P., Positron emission tomography imaging in neurological disorders. *J Neurol* **2012**, *259* (9), 1769-80.
2. Farwell, M. D.; Pryma, D. A.; Mankoff, D. A., PET/CT Imaging in Cancer: Current Applications and Future Directions. *Cancer* **2014**, *120* (22), 3433-3445.
3. Dobrucki, L. W.; Sinusas, A. J., PET and SPECT in cardiovascular molecular imaging. *Nat Rev Cardiol* **2010**, *7* (1), 38-47.
4. Matthews, P. M.; Rabiner, E. A.; Passchier, J.; Gunn, R. N., Positron emission tomography molecular imaging for drug development. *Br J Clin Pharmacol* **2012**, *73* (2), 175-86.
5. Marik, J.; Bohorquez, S. M.; Williams, S. P.; van Bruggen, N., New imaging paradigms in drug development: the PET imaging approach. *Drug Discov Today Technol* **2011**, *8* (2-4), e63-9.
6. Rudin, M.; Weissleder, R., Molecular imaging in drug discovery and development. *Nature Reviews Drug Discovery* **2003**, *2* (2), 123-131.
7. Van de Bittner, G. C.; Ricq, E. L.; Hooker, J. M., A Philosophy for CNS Radiotracer Design. *Accounts Chem Res* **2014**, *47* (10), 3127-3134.
8. Sharma, K.; Schmitt, S.; Bergner, C. G.; Tyanova, S.; Kannaiyan, N.; Manrique-Hoyos, N.; Kongi, K.; Cantuti, L.; Hanisch, U. K.; Philips, M. A.; Rossner, M. J.; Mann, M.; Simons, M., Cell type- and brain region-resolved mouse brain proteome. *Nat Neurosci* **2015**, *18* (12), 1819-31.
9. Martins-de-Souza, D.; Carvalho, P. C.; Schmitt, A.; Junqueira, M.; Nogueira, F. C.; Turck, C. W.; Domont, G. B., Deciphering the human brain proteome: characterization of the anterior temporal lobe and corpus callosum as part of the Chromosome 15-centric Human Proteome Project. *J Proteome Res* **2014**, *13* (1), 147-57.
10. Lever, S. Z.; Fan, K. H.; Lever, J. R., Tactics for preclinical validation of receptor-binding radiotracers. *Nucl Med Biol* **2017**, *44*, 4-30.
11. Pike, V. W., PET radiotracers: crossing the blood-brain barrier and surviving metabolism. *Trends Pharmacol Sci* **2009**, *30* (8), 431-40.
12. Deinhardt K, C. M., Trk Receptors. *Handb Exp Pharmacol*. **2014**, *220*, 103-119.
13. Chao, M. V., Neurotrophins and their receptors: a convergence point for many signalling pathways. *Nat Rev Neurosci* **2003**, *4* (4), 299-309.
14. Manning, G.; Whyte, D. B.; Martinez, R.; Hunter, T.; Sudarsanam, S., The protein kinase complement of the human genome. *Science* **2002**, *298* (5600), 1912-34.

15. Klein, R.; Jing, S. Q.; Nanduri, V.; O'Rourke, E.; Barbacid, M., The Trk Protooncogene Encodes a Receptor for Nerve Growth-Factor. *Cell* **1991**, 65 (1), 189-197.
16. Kaplan, D. R.; Martin-Zanca, D.; Parada, L. F., Tyrosine phosphorylation and tyrosine kinase activity of the trk proto-oncogene product induced by NGF. *Nature* **1991**, 350 (6314), 158-60.
17. Klein, R.; Nanduri, V.; Jing, S. Q.; Lamballe, F.; Tapley, P.; Bryant, S.; Cordoncardo, C.; Jones, K. R.; Reichardt, L. F.; Barbacid, M., The Trkb Tyrosine Protein-Kinase Is a Receptor for Brain-Derived Neurotrophic Factor and Neurotrophin-3. *Cell* **1991**, 66 (2), 395-403.
18. Lamballe, F.; Klein, R.; Barbacid, M., Trkc, a New Member of the Trk Family of Tyrosine Protein-Kinases, Is a Receptor for Neurotrophin-3. *Cell* **1991**, 66 (5), 967-979.
19. Klein, R.; Lamballe, F.; Bryant, S.; Barbacid, M., The Trkb Tyrosine Protein-Kinase Is a Receptor for Neurotrophin-4. *Neuron* **1992**, 8 (5), 947-956.
20. Bothwell, M. A.; Shooter, E. M., Dissociation equilibrium constant of beta nerve growth factor. *J Biol Chem* **1977**, 252 (23), 8532-6.
21. Radziejewski, C.; Robinson, R. C.; DiStefano, P. S.; Taylor, J. W., Dimeric structure and conformational stability of brain-derived neurotrophic factor and neurotrophin-3. *Biochemistry* **1992**, 31 (18), 4431-6.
22. Huang, E. J.; Reichardt, L. F., Trk receptors: roles in neuronal signal transduction. *Annu Rev Biochem* **2003**, 72, 609-42.
23. Reichardt, L. F., Neurotrophin-regulated signalling pathways. *Philos Trans R Soc Lond B Biol Sci* **2006**, 361 (1473), 1545-64.
24. Hetman, M.; Cavanaugh, J. E.; Kimelman, D.; Xia, Z., Role of glycogen synthase kinase-3beta in neuronal apoptosis induced by trophic withdrawal. *J Neurosci* **2000**, 20 (7), 2567-74.
25. Schrott, G. M.; Nigh, E. A.; Chen, W. G.; Hu, L.; Greenberg, M. E., BDNF regulates the translation of a select group of mRNAs by a mammalian target of rapamycin-phosphatidylinositol 3-kinase-dependent pathway during neuronal development. *J Neurosci* **2004**, 24 (33), 7366-77.
26. Takei, N.; Inamura, N.; Kawamura, M.; Namba, H.; Hara, K.; Yonezawa, K.; Nawa, H., Brain-derived neurotrophic factor induces mammalian target of rapamycin-dependent local activation of translation machinery and protein synthesis in neuronal dendrites. *J Neurosci* **2004**, 24 (44), 9760-9.
27. Kumar, V.; Zhang, M. X.; Swank, M. W.; Kunz, J.; Wu, G. Y., Regulation of dendritic morphogenesis by Ras-PI3K-Akt-mTOR and Ras-MAPK signaling pathways. *J Neurosci* **2005**, 25 (49), 11288-99.

28. Caldeira, M. V.; Melo, C. V.; Pereira, D. B.; Carvalho, R.; Correia, S. S.; Backos, D. S.; Carvalho, A. L.; Esteban, J. A.; Duarte, C. B., Brain-derived neurotrophic factor regulates the expression and synaptic delivery of alpha-amino-3-hydroxy-5-methyl-4-isoxazole propionic acid receptor subunits in hippocampal neurons. *J Biol Chem* **2007**, *282* (17), 12619-28.
29. Park, H.; Poo, M. M., Neurotrophin regulation of neural circuit development and function. *Nature Reviews Neuroscience* **2013**, *14* (1), 7-23.
30. Rex, C. S.; Lin, C. Y.; Kramar, E. A.; Chen, L. Y.; Gall, C. M.; Lynch, G., Brain-derived neurotrophic factor promotes long-term potentiation-related cytoskeletal changes in adult hippocampus. *J Neurosci* **2007**, *27* (11), 3017-29.
31. Alonso, M.; Medina, J. H.; Pozzo-Miller, L., ERK1/2 activation is necessary for BDNF to increase dendritic spine density in hippocampal CA1 pyramidal neurons. *Learn Memory* **2004**, *11* (2), 172-178.
32. Jovanovic, J. N.; Czernik, A. J.; Fienberg, A. A.; Greengard, P.; Sihra, T. S., Synapsins as mediators of BDNF-enhanced neurotransmitter release. *Nature Neuroscience* **2000**, *3* (4), 323-329.
33. Riccio, A.; Pierchala, B. A.; Ciarallo, C. L.; Ginty, D. D., An NGF-TrkA-mediated retrograde signal to transcription factor CREB in sympathetic neurons. *Science* **1997**, *277* (5329), 1097-100.
34. Eide, F. F.; Vining, E. R.; Eide, B. L.; Zang, K. L.; Wang, X. Y.; Reichardt, L. F., Naturally occurring truncated trkB receptors have dominant inhibitory effects on brain-derived neurotrophic factor signaling. *Journal of Neuroscience* **1996**, *16* (10), 3123-3129.
35. Dechant, G.; Barde, Y. A., The neurotrophin receptor p75(NTR): novel functions and implications for diseases of the nervous system. *Nature Neuroscience* **2002**, *5* (11), 1131-1136.
36. Esposito, D.; Patel, P.; Stephens, R. M.; Perez, P.; Chao, M. V.; Kaplan, D. R.; Hempstead, B. L., The cytoplasmic and transmembrane domains of the p75 and Trk a receptors regulate high affinity binding to nerve growth factor. *Journal of Biological Chemistry* **2001**, *276* (35), 32687-32695.
37. Hempstead, B. L.; Martin-Zanca, D.; Kaplan, D. R.; Parada, L. F.; Chao, M. V., High-affinity NGF binding requires coexpression of the trk proto-oncogene and the low-affinity NGF receptor. *Nature* **1991**, *350* (6320), 678-83.
38. Bibel, M.; Hoppe, E.; Barde, Y. A., Biochemical and functional interactions between the neurotrophin receptors trk and p75NTR. *EMBO J* **1999**, *18* (3), 616-22.

39. Gupta, V. K.; You, Y. Y.; Gupta, V. B.; Klistorner, A.; Graham, S. L., TrkB Receptor Signalling: Implications in Neurodegenerative, Psychiatric and Proliferative Disorders. *Int J Mol Sci* **2013**, *14* (5), 10122-10142.
40. Hefti, F. F.; Rosenthal, A.; Walicke, P. A.; Wyatt, S.; Vergara, G.; Shelton, D. L.; Davies, A. M., Novel class of pain drugs based on antagonism of NGF. *Trends Pharmacol Sci* **2006**, *27* (2), 85-91.
41. Brodeur, G. M.; Minturn, J. E.; Ho, R.; Simpson, A. M.; Iyer, R.; Varela, C. R.; Light, J. E.; Kolla, V.; Evans, A. E., Trk receptor expression and inhibition in neuroblastomas. *Clin Cancer Res* **2009**, *15* (10), 3244-50.
42. Sclabas, G. M.; Fujioka, S.; Schmidt, C.; Li, Z.; Frederick, W. A.; Yang, W.; Yokoi, K.; Evans, D. B.; Abbruzzese, J. L.; Hess, K. R.; Zhang, W.; Fidler, I. J.; Chiao, P. J., Overexpression of tropomyosin-related kinase B in metastatic human pancreatic cancer cells. *Clin Cancer Res* **2005**, *11* (2 Pt 1), 440-9.
43. Yu, Y.; Zhang, S.; Wang, X.; Yang, Z.; Ou, G., Overexpression of TrkB promotes the progression of colon cancer. *APMIS* **2010**, *118* (3), 188-95.
44. Vaishnavi, A.; Le, A. T.; Doebele, R. C., TRKING Down an Old Oncogene in a New Era of Targeted Therapy. *Cancer Discovery* **2015**, *5* (1), 25-34.
45. Ranzi, V.; Meakin, S. O.; Miranda, C.; Mondellini, P.; Pierotti, M. A.; Greco, A., The signaling adapters fibroblast growth factor receptor substrate 2 and 3 are activated by the thyroid TRK oncoproteins. *Endocrinology* **2003**, *144* (3), 922-8.
46. Roccato, E.; Miranda, C.; Ranzi, V.; Gishizki, M.; Pierotti, M. A.; Greco, A., Biological activity of the thyroid TRK-T3 oncogene requires signalling through Shc. *Br J Cancer* **2002**, *87* (6), 645-53.
47. Miranda, C.; Greco, A.; Miele, C.; Pierotti, M. A.; Van Obberghen, E., IRS-1 and IRS-2 are recruited by TrkA receptor and oncogenic TRK-T1. *J Cell Physiol* **2001**, *186* (1), 35-46.
48. Nakagawara, A., Trk receptor tyrosine kinases: A bridge between cancer and neural development. *Cancer Letters* **2001**, *169* (2), 107-114.
49. Levi-Montalcini, R.; Cohen, S., In Vitro and in Vivo Effects of a Nerve Growth-Stimulating Agent Isolated from Snake Venom. *Proc Natl Acad Sci U S A* **1956**, *42* (9), 695-9.
50. Cohen, S.; Levi-Montalcini, R., A Nerve Growth-Stimulating Factor Isolated from Snake Venom. *Proc Natl Acad Sci U S A* **1956**, *42* (9), 571-4.
51. Cohen, S.; Levi-Montalcini, R.; Hamburger, V., A Nerve Growth-Stimulating Factor Isolated from Sarcom as 37 and 180. *Proc Natl Acad Sci U S A* **1954**, *40* (10), 1014-8.

52. Cohen, S., Purification of a Nerve-Growth Promoting Protein from the Mouse Salivary Gland and Its Neuro-Cytotoxic Antiserum. *Proc Natl Acad Sci U S A* **1960**, 46 (3), 302-11.
53. Levi-Montalcini, R.; Booker, B., Destruction of the Sympathetic Ganglia in Mammals by an Antiserum to a Nerve-Growth Protein. *Proc Natl Acad Sci U S A* **1960**, 46 (3), 384-91.
54. Levi-Montalcini, R.; Booker, B., Excessive Growth of the Sympathetic Ganglia Evoked by a Protein Isolated from Mouse Salivary Glands. *Proc Natl Acad Sci U S A* **1960**, 46 (3), 373-84.
55. Iversen, L. L., Rita Levi-Montalcini: Neuroscientist par excellence. *P Natl Acad Sci USA* **2013**, 110 (13), 4862-4863.
56. Zeliadt, N., Rita Levi-Montalcini: NGF, the prototypical growth factor. *P Natl Acad Sci USA* **2013**, 110 (13), 4873-4876.
57. Cattaneo, A., Immunosympathectomy as the first phenotypic knockout with antibodies. *P Natl Acad Sci USA* **2013**, 110 (13), 4877-4885.
58. Barde, Y. A.; Edgar, D.; Thoenen, H., Purification of a new neurotrophic factor from mammalian brain. *EMBO J* **1982**, 1 (5), 549-53.
59. Leibrock, J.; Lottspeich, F.; Hohn, A.; Hofer, M.; Hengerer, B.; Masiakowski, P.; Thoenen, H.; Barde, Y. A., Molecular cloning and expression of brain-derived neurotrophic factor. *Nature* **1989**, 341 (6238), 149-52.
60. Hohn, A.; Leibrock, J.; Bailey, K.; Barde, Y. A., Identification and characterization of a novel member of the nerve growth factor/brain-derived neurotrophic factor family. *Nature* **1990**, 344 (6264), 339-41.
61. Jones, K. R.; Reichardt, L. F., Molecular-Cloning of a Human Gene That Is a Member of the Nerve Growth-Factor Family. *P Natl Acad Sci USA* **1990**, 87 (20), 8060-8064.
62. Berkemeier, L. R.; Winslow, J. W.; Kaplan, D. R.; Nikolics, K.; Goeddel, D. V.; Rosenthal, A., Neurotrophin-5: a novel neurotrophic factor that activates trk and trkB. *Neuron* **1991**, 7 (5), 857-66.
63. Downward, J.; Parker, P.; Waterfield, M. D., Autophosphorylation Sites on the Epidermal Growth-Factor Receptor. *Nature* **1984**, 311 (5985), 483-485.
64. Pulciani, S.; Santos, E.; Lauver, A. V.; Long, L. K.; Aaronson, S. A.; Barbacid, M., Oncogenes in Solid Human-Tumors. *Nature* **1982**, 300 (5892), 539-542.
65. Martin-Zanca, D.; Hughes, S. H.; Barbacid, M., A human oncogene formed by the fusion of truncated tropomyosin and protein tyrosine kinase sequences. *Nature* **1986**, 319 (6056), 743-8.
66. Coulier, F.; Martinzanca, D.; Ernst, M.; Barbacid, M., Mechanism of Activation of the Human Trk Oncogene. *Molecular and Cellular Biology* **1989**, 9 (1), 15-23.

67. Martinzanca, D.; Barbacid, M.; Parada, L. F., Expression of the Trk Protooncogene Is Restricted to the Sensory Cranial and Spinal Ganglia of Neural Crest Origin in Mouse Development. *Gene Dev* **1990**, *4* (5), 683-694.
68. Klein, R.; Parada, L. F.; Coulier, F.; Barbacid, M., Trkb, a Novel Tyrosine Protein-Kinase Receptor Expressed during Mouse Neural Development. *Embo Journal* **1989**, *8* (12), 3701-3709.
69. Meakin, S. O.; Shooter, E. M., Molecular Investigations on the High-Affinity Nerve Growth-Factor Receptor. *Neuron* **1991**, *6* (1), 153-163.
70. Kaplan, D. R.; Hempstead, B. L.; Martin-Zanca, D.; Chao, M. V.; Parada, L. F., The trk proto-oncogene product: a signal transducing receptor for nerve growth factor. *Science* **1991**, *252* (5005), 554-8.
71. Kaplan, D. R.; Hempstead, B. L.; Martinzanca, D.; Chao, M. V.; Parada, L. F., The Trk Protooncogene Product - a Signal Transducing Receptor for Nerve Growth-Factor. *Science* **1991**, *252* (5005), 554-558.
72. Ragsdale, C.; Woodgett, J., Neurobiology. trking neurotrophic receptors. *Nature* **1991**, *350* (6320), 660-1.
73. Conover, J. C.; Yancopoulos, G. D., Neurotrophin regulation of the developing nervous system: analyses of knockout mice. *Rev Neurosci* **1997**, *8* (1), 13-27.
74. Snider, W. D., Functions of the Neurotrophins during Nervous-System Development - What the Knockouts Are Teaching Us. *Cell* **1994**, *77* (5), 627-638.
75. Smeyne, R. J.; Klein, R.; Schnapp, A.; Long, L. K.; Bryant, S.; Lewin, A.; Lira, S. A.; Barbacid, M., Severe sensory and sympathetic neuropathies in mice carrying a disrupted Trk/NGF receptor gene. *Nature* **1994**, *368* (6468), 246-9.
76. Klein, R.; Smeyne, R. J.; Wurst, W.; Long, L. K.; Auerbach, B. A.; Joyner, A. L.; Barbacid, M., Targeted disruption of the trkB neurotrophin receptor gene results in nervous system lesions and neonatal death. *Cell* **1993**, *75* (1), 113-22.
77. Klein, R.; Silos-Santiago, I.; Smeyne, R. J.; Lira, S. A.; Brambilla, R.; Bryant, S.; Zhang, L.; Snider, W. D.; Barbacid, M., Disruption of the neurotrophin-3 receptor gene trkC eliminates la muscle afferents and results in abnormal movements. *Nature* **1994**, *368* (6468), 249-51.
78. Wehrman, T.; He, X.; Raab, B.; Dukipatti, A.; Blau, H.; Garcia, K. C., Structural and mechanistic insights into nerve growth factor interactions with the TrkA and p75 receptors. *Neuron* **2007**, *53* (1), 25-38.

79. Bertrand, T.; Kothe, M.; Liu, J.; Dupuy, A.; Rak, A.; Berne, P. F.; Davis, S.; Gladysheva, T.; Valtre, C.; Crenne, J. Y.; Mathieu, M., The crystal structures of TrkA and TrkB suggest key regions for achieving selective inhibition. *J Mol Biol* **2012**, *423* (3), 439-53.
80. Watson, F. L.; Porcionatto, M. A.; Bhattacharyya, A.; Stiles, C. D.; Segal, R. A., TrkA glycosylation regulates receptor localization and activity. *J Neurobiol* **1999**, *39* (2), 323-36.
81. Barker, P. A., High affinity not in the vicinity? *Neuron* **2007**, *53* (1), 1-4.
82. Su, H. P.; Rickert, K.; Burlein, C.; Narayan, K.; Bukhtiyarova, M.; Hurzy, D. M.; Stump, C. A.; Zhang, X.; Reid, J.; Krasowska-Zoladek, A.; Tummala, S.; Shipman, J. M.; Kornienko, M.; Lemaire, P. A.; Krosky, D.; Heller, A.; Achab, A.; Chamberlin, C.; Saradjian, P.; Sauvagnat, B.; Yang, X.; Ziebell, M. R.; Nickbarg, E.; Sanders, J. M.; Bilodeau, M. T.; Carroll, S. S.; Lumb, K. J.; Soisson, S. M.; Henze, D. A.; Cooke, A. J., Structural characterization of nonactive site, TrkA-selective kinase inhibitors. *Proc Natl Acad Sci U S A* **2017**, *114* (3), E297-E306.
83. Peng, X.; Greene, L. A.; Kaplan, D. R.; Stephens, R. M., Deletion of a conserved juxtamembrane sequence in Trk abolishes NGF-promoted neuritogenesis. *Neuron* **1995**, *15* (2), 395-406.
84. Gong, Y.; Cao, P.; Yu, H. J.; Jiang, T., Crystal structure of the neurotrophin-3 and p75NTR symmetrical complex. *Nature* **2008**, *454* (7205), 789-93.
85. Banfield, M. J.; Naylor, R. L.; Robertson, A. G.; Allen, S. J.; Dawbarn, D.; Brady, R. L., Specificity in Trk receptor:neurotrophin interactions: the crystal structure of TrkB-d5 in complex with neurotrophin-4/5. *Structure* **2001**, *9* (12), 1191-9.
86. Ultsch, M. H.; Wiesmann, C.; Simmons, L. C.; Henrich, J.; Yang, M.; Reilly, D.; Bass, S. H.; de Vos, A. M., Crystal structures of the neurotrophin-binding domain of TrkA, TrkB and TrkC. *J Mol Biol* **1999**, *290* (1), 149-59.
87. Wiesmann, C.; Ultsch, M. H.; Bass, S. H.; de Vos, A. M., Crystal structure of nerve growth factor in complex with the ligand-binding domain of the TrkA receptor. *Nature* **1999**, *401* (6749), 184-8.
88. Altar, C. A.; Burton, L. E.; Bennett, G. L.; Dugich-Djordjevic, M., Recombinant human nerve growth factor is biologically active and labels novel high-affinity binding sites in rat brain. *Proc Natl Acad Sci U S A* **1991**, *88* (1), 281-5.
89. Altar, C. A.; Dugich-Djordjevic, M.; Armanini, M.; Bakhit, C., Medial-to-lateral gradient of neostriatal NGF receptors: relationship to cholinergic neurons and NGF-like immunoreactivity. *J Neurosci* **1991**, *11* (3), 828-36.

90. Merlio, J. P.; Ernfors, P.; Jaber, M.; Persson, H., Molecular cloning of rat trkC and distribution of cells expressing messenger RNAs for members of the trk family in the rat central nervous system. *Neuroscience* **1992**, *51* (3), 513-32.
91. Anderson, K. D.; Alderson, R. F.; Altar, C. A.; DiStefano, P. S.; Corcoran, T. L.; Lindsay, R. M.; Wiegand, S. J., Differential distribution of exogenous BDNF, NGF, and NT-3 in the brain corresponds to the relative abundance and distribution of high-affinity and low-affinity neurotrophin receptors. *J Comp Neurol* **1995**, *357* (2), 296-317.
92. Altar, C. A.; Criden, M. R.; Lindsay, R. M.; DiStefano, P. S., Characterization and topography of high-affinity ¹²⁵I-neurotrophin-3 binding to mammalian brain. *J Neurosci* **1993**, *13* (2), 733-43.
93. Altar, C. A.; Siuciak, J. A.; Wright, P.; Ip, N. Y.; Lindsay, R. M.; Wiegand, S. J., In-Situ Hybridization of Trkb and Trkc Receptor Messenger-Rna in Rat Forebrain and Association with High-Affinity Binding of [¹²⁵I] Bdnf, [¹²⁵I] Nt-4/5 and [¹²⁵I] Nt-3. *European Journal of Neuroscience* **1994**, *6* (9), 1389-1405.
94. Bernard-Gauthier, V.; Boudjemeline, M.; Rosa-Neto, P.; Thiel, A.; Schirmacher, R., Towards tropomyosin-related kinase B (TrkB) receptor ligands for brain imaging with PET: radiosynthesis and evaluation of 2-(4-[(¹⁸F]fluorophenyl)-7,8-dihydroxy-4H-chromen-4-one and 2-(4-[(N-methyl-(¹¹C)-dimethylamino)phenyl]-7,8-dihydroxy-4H-chromen-4-one. *Bioorg Med Chem* **2013**, *21* (24), 7816-29.
95. Longo, F. M.; Massa, S. M., Small-molecule modulation of neurotrophin receptors: a strategy for the treatment of neurological disease. *Nat Rev Drug Discov* **2013**, *12* (7), 507-25.
96. Allen, S. J.; Wilcock, G. K.; Dawbarn, D., Profound and selective loss of catalytic TrkB immunoreactivity in Alzheimer's disease. *Biochem Bioph Res Co* **1999**, *264* (3), 648-651.
97. Ginsberg, S. D.; Che, S. L.; Wu, J.; Counts, S. E.; Mufson, E. J., Down regulation of trk but not p75(NTR) gene expression in single cholinergic basal forebrain neurons mark the progression of Alzheimer's disease. *Journal of Neurochemistry* **2006**, *97* (2), 475-487.
98. Savaskan, E.; Muller-Spahn, F.; Olivieri, G.; Bruttel, S.; Otten, U.; Rosenberg, C.; Hulette, C.; Hock, C., Alterations in trk A, trk B and trk C receptor immunoreactivities in parietal cortex and cerebellum in Alzheimer's disease. *Eur Neurol* **2000**, *44* (3), 172-80.
99. Cozza, A.; Melissari, E.; Iacopetti, P.; Mariotti, V.; Tedde, A.; Nacmias, B.; Conte, A.; Sorbi, S.; Pellegrini, S., SNPs in neurotrophin system genes and Alzheimer's disease in an Italian population. *J Alzheimers Dis* **2008**, *15* (1), 61-70.

100. Vepsalainen, S.; Castren, E.; Helisalmi, S.; Iivonen, S.; Mannermaa, A.; Lehtovirta, M.; Hanninen, T.; Soininen, H.; Hiltunen, M., Genetic analysis of BDNF and TrkB gene polymorphisms in Alzheimer's disease. *J Neurol* **2005**, *252* (4), 423-428.
101. Baydyuk, M.; Nguyen, M. T.; Xu, B., Chronic deprivation of TrkB signaling leads to selective late-onset nigrostriatal dopaminergic degeneration. *Exp Neurol* **2011**, *228* (1), 118-25.
102. Haque, N. S.; Hlavin, M. L.; Fawcett, J. W.; Dunnett, S. B., The neurotrophin NT4/5, but not NT3, enhances the efficacy of nigral grafts in a rat model of Parkinson's disease. *Brain Res* **1996**, *712* (1), 45-52.
103. Gines, S.; Bosch, M.; Marco, S.; Gavaldà, N.; Diaz-Hernandez, M.; Lucas, J. J.; Canals, J. M.; Alberch, J., Reduced expression of the TrkB receptor in Huntington's disease mouse models and in human brain. *European Journal of Neuroscience* **2006**, *23* (3), 649-658.
104. Gauthier, L. R.; Charrin, B. C.; Borrell-Pages, M.; Dompierre, J. P.; Rangone, H.; Cordelieres, F. P.; De Mey, J.; MacDonald, M. E.; Lessmann, V.; Humbert, S.; Saudou, F., Huntingtin controls neurotrophic support and survival of neurons by enhancing BDNF vesicular transport along microtubules. *Cell* **2004**, *118* (1), 127-38.
105. Abuhatzira, L.; Makedonski, K.; Kaufman, Y.; Razin, A.; Shemer, R., MeCP2 deficiency in the brain decreases BDNF levels by REST/CoREST-mediated repression and increases TRKB production. *Epigenetics* **2007**, *2* (4), 214-22.
106. Chen, W. G.; Chang, Q.; Lin, Y.; Meissner, A.; West, A. E.; Griffith, E. C.; Jaenisch, R.; Greenberg, M. E., Derepression of BDNF transcription involves calcium-dependent phosphorylation of MeCP2. *Science* **2003**, *302* (5646), 885-9.
107. Cooper, J. D.; Salehi, A.; Delcroix, J. D.; Howe, C. L.; Belichenko, P. V.; Chua-Couzens, J.; Kilbridge, J. F.; Carlson, E. J.; Epstein, C. J.; Mobley, W. C., Failed retrograde transport of NGF in a mouse model of Down's syndrome: reversal of cholinergic neurodegenerative phenotypes following NGF infusion. *Proc Natl Acad Sci U S A* **2001**, *98* (18), 10439-44.
108. Dorsey, S. G.; Renn, C. L.; Carim-Todd, L.; Barrick, C. A.; Bambrick, L.; Krueger, B. K.; Ward, C. W.; Tessarollo, L., In vivo restoration of physiological levels of truncated TrkB.T1 receptor rescues neuronal cell death in a trisomic mouse model. *Neuron* **2006**, *51* (1), 21-8.
109. Nishio, T.; Sunohara, N.; Furukawa, S., Neurotrophin switching in spinal motoneurons of amyotrophic lateral sclerosis. *neuroreports* **1998**, *9*, 1661-1665.
110. He, X. P.; Kotloski, R.; Nef, S.; Luikart, B. W.; Parada, L. F.; McNamara, J. O., Conditional deletion of TrkB but not BDNF prevents epileptogenesis in the kindling model. *Neuron* **2004**, *43* (1), 31-42.

111. Binder, D. K.; Routbort, M. J.; Ryan, T. E.; Yancopoulos, G. D.; McNamara, J. O., Selective inhibition of kindling development by intraventricular administration of TrkB receptor body. *J Neurosci* **1999**, *19* (4), 1424-36.
112. Gomes, J. R.; Costa, J. T.; Melo, C. V.; Felizzi, F.; Monteiro, P.; Pinto, M. J.; Inacio, A. R.; Wieloch, T.; Almeida, R. D.; Graos, M.; Duarte, C. B., Excitotoxicity downregulates TrkB.FL signaling and upregulates the neuroprotective truncated TrkB receptors in cultured hippocampal and striatal neurons. *J Neurosci* **2012**, *32* (13), 4610-22.
113. Vidaurre, O. G.; Gascon, S.; Deogracias, R.; Sobrado, M.; Cuadrado, E.; Montaner, J.; Rodriguez-Pena, A.; Diaz-Guerra, M., Imbalance of neurotrophin receptor isoforms TrkB-FL/TrkB-T1 induces neuronal death in excitotoxicity. *Cell Death Dis* **2012**, *3*, e256.
114. Martinowich, K.; Manji, H.; Lu, B., New insights into BDNF function in depression and anxiety. *Nat Neurosci* **2007**, *10* (9), 1089-93.
115. Laurent, D.; Eric, A.; Ikram El, Y.-B.; Xuefen Le, B.; Victor, N.; Hubert, H., Nerve Growth Factor Receptors and Signaling in Breast Cancer. *Curr. Cancer Drug Targets* **2004**, *4* (6), 463-470.
116. Kim, M. S.; Lee, W. S.; Jeong, J.; Kim, S. J.; Jin, W., Induction of metastatic potential by TrkB via activation of IL6/JAK2/STAT3 and PI3K/AKT signaling in breast cancer. *Oncotarget* **2015**, *6* (37), 40158-71.
117. Weeraratna, A. T.; Dalrymple, S. L.; Lamb, J. C.; Denmeade, S. R.; Miknyoczki, S.; Dionne, C. A.; Isaacs, J. T., Pan-trk Inhibition Decreases Metastasis and Enhances Host Survival in Experimental Models as a Result of Its Selective Induction of Apoptosis of Prostate Cancer Cells. *Clin. Cancer Res.* **2001**, *7* (8), 2237-2245.
118. Narayanan, R.; Yepuru, M.; Coss, C. C.; Wu, Z.; Bauler, M. N.; Barrett, C. M.; Mohler, M. L.; Wang, Y.; Kim, J.; Snyder, L. M.; He, Y.; Levy, N.; Miller, D. D.; Dalton, J. T., Discovery and preclinical characterization of novel small molecule TRK and ROS1 tyrosine kinase inhibitors for the treatment of cancer and inflammation. *PLoS One* **2013**, *8* (12), e83380.
119. Nakagawara, A.; Arima-Nakagawara, M.; Scavarda, N. J.; Azar, C. G.; Cantor, A. B.; Brodeur, G. M., Association between High Levels of Expression of the TRK Gene and Favorable Outcome in Human Neuroblastoma. *N. Engl. J. Med.* **1993**, *328* (12), 847-854.
120. Schramm, A.; Schulte, J. H.; Astrahantseff, K.; Apostolov, O.; Limpt, V. v.; Sieverts, H.; Kuhfittig-Kulle, S.; Pfeiffer, P.; Versteeg, R.; Eggert, A., Biological effects of TrkA and TrkB receptor signaling in neuroblastoma. *Cancer Lett.* **2005**, *228* (1-2), 143-153.
121. Lawn, S.; Krishna, N.; Pisklakova, A.; Qu, X.; Fenstermacher, D. A.; Fournier, M.; Vrionis, F. D.; Tran, N.; Chan, J. A.; Kenchappa, R. S.; Forsyth, P. A., Neurotrophin signaling

via TrkB and TrkC receptors promotes the growth of brain tumor-initiating cells. *J Biol Chem* **2015**, 290 (6), 3814-24.

122. Ardini, E.; Bosotti, R.; Borgia, A. L.; De Ponti, C.; Somaschini, A.; Cammarota, R.; Amboldi, N.; Radrizzani, L.; Milani, A.; Magnaghi, P.; Ballinari, D.; Casero, D.; Gasparri, F.; Banfi, P.; Avanzi, N.; Saccardo, M. B.; Alzani, R.; Bandiera, T.; Felder, E.; Donati, D.; Pesenti, E.; Sartore-Bianchi, A.; Gambacorta, M.; Pierotti, M. A.; Siena, S.; Veronese, S.; Galvani, A.; Isacchi, A., The TPM3-NTRK1 rearrangement is a recurring event in colorectal carcinoma and is associated with tumor sensitivity to TRKA kinase inhibition. *Mol Oncol* **2014**, 8 (8), 1495-507.

123. Morrison, K. B.; Tognon, C. E.; Garnett, M. J.; Deal, C.; Sorensen, P. H. B., ETV6-NTRK3 transformation requires insulin-like growth factor 1 receptor signaling and is associated with constitutive IRS-1 tyrosine phosphorylation. *Oncogene* **2002**, 21 (37), 5684-5695.

124. Rubin, B. P.; Chen, C.-J.; Morgan, T. W.; Xiao, S.; Grier, H. E.; Kozakewich, H. P.; Perez-Atayde, A. R.; Fletcher, J. A., Congenital Mesoblastic Nephroma t(12;15) Is Associated with ETV6-NTRK3 Gene Fusion: Cytogenetic and Molecular Relationship to Congenital (Infantile) Fibrosarcoma. *The American Journal of Pathology* **1998**, 153 (5), 1451-1458.

125. Euhus, D. M.; Timmons, C. F.; Tomlinson, G. E., ETV6-NTRK3—Trk-ing the primary event in human secretory breast cancer. *Cancer Cell* **2002**, 2 (5), 347-348.

126. Passiglia, F.; Caparica, R.; Giovannetti, E.; Giallombardo, M.; Listi, A.; Diana, P.; Cirrincione, G.; Caglevic, C.; Raez, L. E.; Russo, A.; Rolfo, C., The potential of neurotrophic tyrosine kinase (NTRK) inhibitors for treating lung cancer. *Expert Opin Investig Drugs* **2016**, 25 (4), 385-92.

127. Khotskaya, Y. B.; Holla, V. R.; Farago, A. F.; Mills Shaw, K. R.; Meric-Bernstam, F.; Hong, D. S., Targeting TRK family proteins in cancer. *Pharmacol Ther* **2017**.

128. Drilon, A.; Li, G.; Dogan, S.; Gounder, M.; Shen, R.; Arcila, M.; Wang, L.; Hyman, D. M.; Hechtman, J.; Wei, G.; Cam, N. R.; Christiansen, J.; Luo, D.; Maneval, E. C.; Bauer, T.; Patel, M.; Liu, S. V.; Ou, S. H. I.; Farago, A.; Shaw, A.; Shoemaker, R. F.; Lim, J.; Hornby, Z.; Multani, P.; Ladanyi, M.; Berger, M.; Katabi, N.; Ghossein, R.; Ho, A. L., What hides behind the MASC: clinical response and acquired resistance to entrectinib after ETV6-NTRK3 identification in a mammary analogue secretory carcinoma (MASC). *Ann. Oncol.* **2016**, 27 (5), 920-926.

129. Wu, G.; Diaz, A. K.; Paugh, B. S.; Rankin, S. L.; Ju, B.; Li, Y.; Zhu, X.; Qu, C.; Chen, X.; Zhang, J.; Easton, J.; Edmonson, M.; Ma, X.; Lu, C.; Nagahawatte, P.; Hedlund, E.; Rusch, M.; Pounds, S.; Lin, T.; Onar-Thomas, A.; Huether, R.; Kriwacki, R.; Parker, M.; Gupta, P.; Becksfort, J.; Wei, L.; Mulder, H. L.; Boggs, K.; Vadodaria, B.; Yergeau, D.; Russell, J. C.; Ochoa, K.; Fulton, R. S.; Fulton, L. L.; Jones, C.; Boop, F. A.; Broniscer, A.; Wetmore, C.;

- Gajjar, A.; Ding, L.; Mardis, E. R.; Wilson, R. K.; Taylor, M. R.; Downing, J. R.; Ellison, D. W.; Zhang, J.; Baker, S. J.; St. Jude Children's Research Hospital-Washington University Pediatric Cancer Genome, P., The genomic landscape of diffuse intrinsic pontine glioma and pediatric non-brainstem high-grade glioma. *Nat Genet* **2014**, *46* (5), 444-50.
130. Mertens, F.; Johansson, B.; Fioretos, T.; Mitelman, F., The emerging complexity of gene fusions in cancer. *Nature Reviews Cancer* **2015**, *15* (6), 371-381.
131. Medves, S.; Demoulin, J. B., Tyrosine kinase gene fusions in cancer: translating mechanisms into targeted therapies. *J Cell Mol Med* **2012**, *16* (2), 237-48.
132. Tacconelli, A.; Farina, A. R.; Cappabianca, L.; DeSantis, G.; Tessitore, A.; Vetuschi, A.; Sferra, R.; Rucci, N.; Argenti, B.; Screpanti, I.; Gulino, A.; Mackay, A. R., TrkA alternative splicing: A regulated tumor-promoting switch in human neuroblastoma. *Cancer Cell* **2004**, *6* (4), 347-360.
133. Reuther, G. W.; Lambert, Q. T.; Caligiuri, M. A.; Der, C. J., Identification and Characterization of an Activating TrkA Deletion Mutation in Acute Myeloid Leukemia. *Mol. Cell. Biol.* **2000**, *20* (23), 8655-8666.
134. Arevalo, J. C.; Conde, B.; Hempstead, B. I.; Chao, M. V.; Martin-Zanca, D.; Perez, P., A novel mutation within the extracellular domain of TrkA causes constitutive receptor activation. *Oncogene* **2001**, *20* (10), 1229-34.
135. Coulier, F.; Kumar, R.; Ernst, M.; Klein, R.; Martin-Zanca, D.; Barbacid, M., Human trk oncogenes activated by point mutation, in-frame deletion, and duplication of the tyrosine kinase domain. *Mol Cell Biol* **1990**, *10* (8), 4202-10.
136. Arevalo, J. C.; Conde, B.; Hempstead, B. L.; Chao, M. V.; Martin-Zanca, D.; Perez, P., TrkA immunoglobulin-like ligand binding domains inhibit spontaneous activation of the receptor. *Mol Cell Biol* **2000**, *20* (16), 5908-16.
137. Greenfield, N. J.; Swapna, G. V.; Huang, Y.; Palm, T.; Graboski, S.; Montelione, G. T.; Hitchcock-DeGregori, S. E., The structure of the carboxyl terminus of striated alpha-tropomyosin in solution reveals an unusual parallel arrangement of interacting alpha-helices. *Biochemistry* **2003**, *42* (3), 614-9.
138. Watson, J. J.; Allen, S. J.; Dawbarn, D., Targeting Nerve Growth Factor in Pain. *Biodrugs* **2008**, *22* (6), 349-359.
139. McKelvey, L.; Shorten, G. D.; O'Keefe, G. W., Nerve growth factor-mediated regulation of pain signalling and proposed new intervention strategies in clinical pain management. *J. Neurochem.* **2013**, *124* (3), 276-289.

140. McMahon, S. B.; Bennett, D. L.; Priestley, J. V.; Shelton, D. L., The biological effects of endogenous nerve growth factor on adult sensory neurons revealed by a trkA-IgG fusion molecule. *Nat Med* **1995**, *1* (8), 774-80.
141. McNamee, K. E.; Burleigh, A.; Gompels, L. L.; Feldmann, M.; Allen, S. J.; Williams, R. O.; Dawbarn, D.; Vincent, T. L.; Inglis, J. J., Treatment of murine osteoarthritis with TrkAd5 reveals a pivotal role for nerve growth factor in non-inflammatory joint pain. *Pain* **2010**, *149* (2), 386-92.
142. Indo, Y.; Tsuruta, M.; Hayashida, Y.; Karim, M. A.; Ohta, K.; Kawano, T.; Mitsubuchi, H.; Tonoki, H.; Awaya, Y.; Matsuda, I., Mutations in the TRKA/NGF receptor gene in patients with congenital insensitivity to pain with anhidrosis. *Nat Genet* **1996**, *13* (4), 485-8.
143. Yis, U.; Mademan, I.; Kavukcu, S.; Baets, J., A novel NTRK1 mutation in a patient with congenital insensitivity to pain with anhidrosis. *Acta Neurol Belg* **2015**, *115* (3), 509-11.
144. Petty, B. G.; Cornblath, D. R.; Adornato, B. T.; Chaudhry, V.; Flexner, C.; Wachsman, M.; Sinicropi, D.; Burton, L. E.; Peroutka, S. J., The effect of systemically administered recombinant human nerve growth factor in healthy human subjects. *Ann Neurol* **1994**, *36* (2), 244-6.
145. LeSauter, L.; Wei, L.; Gibbs, B. F.; Saragovi, H. U., Small peptide mimics of nerve growth factor bind TrkA receptors and affect biological responses. *J Biol Chem* **1995**, *270* (12), 6564-9.
146. Eriksson Jonhagen, M.; Nordberg, A.; Amberla, K.; Backman, L.; Ebendal, T.; Meyerson, B.; Olson, L.; Seiger, Shigeta, M.; Theodorsson, E.; Viitanen, M.; Winblad, B.; Wahlund, L. O., Intracerebroventricular infusion of nerve growth factor in three patients with Alzheimer's disease. *Dement Geriatr Cogn Disord* **1998**, *9* (5), 246-57.
147. A controlled trial of recombinant methionyl human BDNF in ALS: The BDNF Study Group (Phase III). *Neurology* **1999**, *52* (7), 1427-33.
148. Apfel, S. C.; Schwartz, S.; Adornato, B. T.; Freeman, R.; Biton, V.; Rendell, M.; Vinik, A.; Giuliani, M.; Stevens, J. C.; Barbano, R.; Dyck, P. J., Efficacy and safety of recombinant human nerve growth factor in patients with diabetic polyneuropathy: A randomized controlled trial. rhNGF Clinical Investigator Group. *JAMA* **2000**, *284* (17), 2215-21.
149. Schifitto, G.; Yiannoutsos, C.; Simpson, D. M.; Adornato, B. T.; Singer, E. J.; Hollander, H.; Marra, C. M.; Rubin, M.; Cohen, B. A.; Tucker, T.; Koralnik, I. J.; Katzenstein, D.; Haidich, B.; Smith, M. E.; Shriver, S.; Millar, L.; Clifford, D. B.; McArthur, J. C.; Team, A. C. T. G., Long-term treatment with recombinant nerve growth factor for HIV-associated sensory neuropathy. *Neurology* **2001**, *57* (7), 1313-6.

150. McArthur, J. C.; Yiannoutsos, C.; Simpson, D. M.; Adornato, B. T.; Singer, E. J.; Hollander, H.; Marra, C.; Rubin, M.; Cohen, B. A.; Tucker, T.; Navia, B. A.; Schifitto, G.; Katzenstein, D.; Rask, C.; Zaborski, L.; Smith, M. E.; Shriver, S.; Millar, L.; Clifford, D. B.; Karalnik, I. J., A phase II trial of nerve growth factor for sensory neuropathy associated with HIV infection. AIDS Clinical Trials Group Team 291. *Neurology* **2000**, *54* (5), 1080-8.
151. Wellmer, A.; Misra, V. P.; Sharief, M. K.; Kopelman, P. G.; Anand, P., A double-blind placebo-controlled clinical trial of recombinant human brain-derived neurotrophic factor (rhBDNF) in diabetic polyneuropathy. *J Peripher Nerv Syst* **2001**, *6* (4), 204-10.
152. Thoenen, H.; Sendtner, M., Neurotrophins: from enthusiastic expectations through sobering experiences to rational therapeutic approaches. *Nat Neurosci* **2002**, *5 Suppl*, 1046-50.
153. Poduslo, J. F.; Curran, G. L., Permeability at the blood-brain and blood-nerve barriers of the neurotrophic factors: NGF, CNTF, NT-3, BDNF. *Brain Res Mol Brain Res* **1996**, *36* (2), 280-6.
154. Robinson, R. C.; Radziejewski, C.; Spraggon, G.; Greenwald, J.; Kostura, M. R.; Burtnick, L. D.; Stuart, D. I.; Choe, S.; Jones, E. Y., The structures of the neurotrophin 4 homodimer and the brain-derived neurotrophic factor/neurotrophin 4 heterodimer reveal a common Trk-binding site. *Protein Sci* **1999**, *8* (12), 2589-97.
155. Robinson, R. C.; Radziejewski, C.; Stuart, D. I.; Jones, E. Y., Structure of the brain-derived neurotrophic factor/neurotrophin 3 heterodimer. *Biochemistry* **1995**, *34* (13), 4139-46.
156. McDonald, N. Q.; Lapatto, R.; Murray-Rust, J.; Gunning, J.; Wlodawer, A.; Blundell, T. L., New protein fold revealed by a 2.3-Å resolution crystal structure of nerve growth factor. *Nature* **1991**, *354* (6352), 411-4.
157. Urfer, R.; Tsoulfas, P.; O'Connell, L.; Shelton, D. L.; Parada, L. F.; Presta, L. G., An immunoglobulin-like domain determines the specificity of neurotrophin receptors. *EMBO J* **1995**, *14* (12), 2795-805.
158. Xiao, J.; Hughes, R. A.; Lim, J. Y.; Wong, A. W.; Ivanusic, J. J.; Ferner, A. H.; Kilpatrick, T. J.; Murray, S. S., A small peptide mimetic of brain-derived neurotrophic factor promotes peripheral myelination. *J Neurochem* **2013**, *125* (3), 386-98.
159. Maliartchouk, S.; Feng, Y.; Ivanisevic, L.; Debeir, T.; Cuello, A. C.; Burgess, K.; Saragovi, H. U., A designed peptidomimetic agonistic ligand of TrkA nerve growth factor receptors. *Mol Pharmacol* **2000**, *57* (2), 385-91.
160. Beglova, N.; Maliartchouk, S.; Ekiel, I.; Zaccaro, M. C.; Saragovi, H. U.; Gehring, K., Design and solution structure of functional peptide mimetics of nerve growth factor. *J Med Chem* **2000**, *43* (19), 3530-40.

161. Travaglia, A.; Pietropaolo, A.; Di Martino, R.; Nicoletti, V. G.; La Mendola, D.; Calissano, P.; Rizzarelli, E., A small linear peptide encompassing the NGF N-terminus partly mimics the biological activities of the entire neurotrophin in PC12 cells. *ACS Chem Neurosci* **2015**, *6* (8), 1379-92.
162. Cazorla, M.; Jouvenceau, A.; Rose, C.; Guilloux, J. P.; Pilon, C.; Dranovsky, A.; Premont, J., Cyclotraxin-B, the first highly potent and selective TrkB inhibitor, has anxiolytic properties in mice. *PLoS One* **2010**, *5* (3), e9777.
163. Constandil, L.; Goich, M.; Hernandez, A.; Bourgeais, L.; Cazorla, M.; Hamon, M.; Villanueva, L.; Pelissier, T., Cyclotraxin-B, a new TrkB antagonist, and glial blockade by propentofylline, equally prevent and reverse cold allodynia induced by BDNF or partial infraorbital nerve constriction in mice. *J Pain* **2012**, *13* (6), 579-89.
164. Otvos, L., Jr.; Wade, J. D., Current challenges in peptide-based drug discovery. *Front Chem* **2014**, *2*, 62.
165. Massa, S. M.; Yang, T.; Xie, Y.; Shi, J.; Bilgen, M.; Joyce, J. N.; Nehama, D.; Rajadas, J.; Longo, F. M., Small molecule BDNF mimetics activate TrkB signaling and prevent neuronal degeneration in rodents. *J Clin Invest* **2010**, *120* (5), 1774-85.
166. Jang, S. W.; Liu, X.; Yepes, M.; Shepherd, K. R.; Miller, G. W.; Liu, Y.; Wilson, W. D.; Xiao, G.; Bianchi, B.; Sun, Y. E.; Ye, K., A selective TrkB agonist with potent neurotrophic activities by 7,8-dihydroxyflavone. *Proc Natl Acad Sci U S A* **2010**, *107* (6), 2687-92.
167. Liu, X.; Chan, C. B.; Jang, S. W.; Pradoldej, S.; Huang, J.; He, K.; Phun, L. H.; France, S.; Xiao, G.; Jia, Y.; Luo, H. R.; Ye, K., A synthetic 7,8-dihydroxyflavone derivative promotes neurogenesis and exhibits potent antidepressant effect. *J Med Chem* **2010**, *53* (23), 8274-86.
168. Liu, X.; Chan, C. B.; Qi, Q.; Xiao, G.; Luo, H. R.; He, X.; Ye, K., Optimization of a small tropomyosin-related kinase B (TrkB) agonist 7,8-dihydroxyflavone active in mouse models of depression. *J Med Chem* **2012**, *55* (19), 8524-37.
169. Scarpi, D.; Cirelli, D.; Matrone, C.; Castronovo, G.; Rosini, P.; Occhiato, E. G.; Romano, F.; Bartali, L.; Clemente, A. M.; Bottegoni, G.; Cavalli, A.; De Chiara, G.; Bonini, P.; Calissano, P.; Palamara, A. T.; Garaci, E.; Torcia, M. G.; Guarna, A.; Cozzolino, F., Low molecular weight, non-peptidic agonists of TrkA receptor with NGF-mimetic activity. *Cell Death Dis* **2012**, *3*, e339.
170. Jang, S. W.; Liu, X.; Chan, C. B.; France, S. A.; Sayeed, I.; Tang, W.; Lin, X.; Xiao, G.; Andero, R.; Chang, Q.; Ressler, K. J.; Ye, K., Deoxygedunin, a natural product with potent neurotrophic activity in mice. *PLoS One* **2010**, *5* (7), e11528.

171. Cazorla, M.; Premont, J.; Mann, A.; Girard, N.; Kellendonk, C.; Rognan, D., Identification of a low-molecular weight TrkB antagonist with anxiolytic and antidepressant activity in mice. *J Clin Invest* **2011**, *121* (5), 1846-57.
172. Zhang, A. J.; Khare, S.; Gokulan, K.; Linthicum, D. S.; Burgess, K., Dimeric beta-turn peptidomimetics as ligands for the neurotrophin receptor TrkC. *Bioorg Med Chem Lett* **2001**, *11* (2), 207-10.
173. Pattarawarapan, M.; Zaccaro, M. C.; Saragovi, U. H.; Burgess, K., New templates for syntheses of ring-fused, C-10 beta-turn peptidomimetics leading to the first reported small-molecule mimic of neurotrophin-3. *Journal of Medicinal Chemistry* **2002**, *45* (20), 4387-4390.
174. Brahimi, F.; Malakhov, A.; Lee, H. B.; Pattarawarapan, M.; Ivanisevic, L.; Burgess, K.; Saragovi, H. U., A peptidomimetic of NT-3 acts as a TrkC antagonist. *Peptides* **2009**, *30* (10), 1833-9.
175. Ko, E.; Kamkaew, A.; Burgess, K., Small Molecule Ligands For Active Targeting Of TrkC-expressing Tumor Cells. *ACS Med Chem Lett* **2012**, *3* (12), 1008-1012.
176. Jang, S. W.; Liu, X.; Chan, C. B.; Weinshenker, D.; Hall, R. A.; Xiao, G.; Ye, K., Amitriptyline is a TrkA and TrkB receptor agonist that promotes TrkA/TrkB heterodimerization and has potent neurotrophic activity. *Chem Biol* **2009**, *16* (6), 644-56.
177. Jang, S. W.; Liu, X.; Pradoldej, S.; Tosini, G.; Chang, Q.; Iuvone, P. M.; Ye, K., N-acetylserotonin activates TrkB receptor in a circadian rhythm. *Proc Natl Acad Sci U S A* **2010**, *107* (8), 3876-81.
178. Massa, S. M.; Yang, T.; Xie, Y. M.; Shi, J.; Bilgen, M.; Joyce, J. N.; Nehama, D.; Rajadas, J.; Longo, F. M., Small molecule BDNF mimetics activate TrkB signaling and prevent neuronal degeneration in rodents. *Journal of Clinical Investigation* **2010**, *120* (5), 1774-1785.
179. Cazorla, M.; Premont, J.; Mann, A.; Girard, N.; Kellendonk, C.; Rognan, D., Identification of a low-molecular weight TrkB antagonist with anxiolytic and antidepressant activity in mice. *Journal of Clinical Investigation* **2011**, *121* (5), 1846-1857.
180. Manach, C.; Williamson, G.; Morand, C.; Scalbert, A.; Remesy, C., Bioavailability and bioefficacy of polyphenols in humans. I. Review of 97 bioavailability studies. *Am J Clin Nutr* **2005**, *81* (1 Suppl), 230S-242S.
181. Dahlin, J. L.; Nissink, J. W.; Strasser, J. M.; Francis, S.; Higgins, L.; Zhou, H.; Zhang, Z.; Walters, M. A., PAINS in the assay: chemical mechanisms of assay interference and promiscuous enzymatic inhibition observed during a sulfhydryl-scavenging HTS. *J Med Chem* **2015**, *58* (5), 2091-113.

182. Liu, C.; Chan, C. B.; Ye, K., 7,8-dihydroxyflavone, a small molecular TrkB agonist, is useful for treating various BDNF-implicated human disorders. *Transl Neurodegener* **2016**, *5*, 2.
183. Du, X.; Hill, R. A., 7,8-Dihydroxyflavone as a pro-neurotrophic treatment for neurodevelopmental disorders. *Neurochem Int* **2015**, *89*, 170-80.
184. Todd, D.; Gowers, I.; Dowler, S. J.; Wall, M. D.; McAllister, G.; Fischer, D. F.; Dijkstra, S.; Fratantoni, S. A.; van de Bospoort, R.; Veenman-Koepke, J.; Flynn, G.; Arjomand, J.; Dominguez, C.; Munoz-Sanjuan, I.; Wityak, J.; Bard, J. A., A monoclonal antibody TrkB receptor agonist as a potential therapeutic for Huntington's disease. *PLoS One* **2014**, *9* (2), e87923.
185. Shia, C. S.; Tsai, S. Y.; Kuo, S. C.; Hou, Y. C.; Chao, P. D., Metabolism and pharmacokinetics of 3,3',4',7-tetrahydroxyflavone (fisetin), 5-hydroxyflavone, and 7-hydroxyflavone and antihemolysis effects of fisetin and its serum metabolites. *J Agric Food Chem* **2009**, *57* (1), 83-9.
186. Perreault, M.; Feng, G.; Will, S.; Gareski, T.; Kubasiak, D.; Marquette, K.; Vugmeyster, Y.; Unger, T. J.; Jones, J.; Qadri, A.; Hahm, S.; Sun, Y.; Rohde, C. M.; Zwijnenberg, R.; Paulsen, J.; Gimeno, R. E., Activation of TrkB with TAM-163 Results in Opposite Effects on Body Weight in Rodents and Non-Human Primates. *PLoS One* **2013**, *8* (5), e62616.
187. Tsao, D.; Thomsen, H. K.; Chou, J.; Stratton, J.; Hagen, M.; Loo, C.; Garcia, C.; Sloane, D. L.; Rosenthal, A.; Lin, J. C., TrkB agonists ameliorate obesity and associated metabolic conditions in mice. *Endocrinology* **2008**, *149* (3), 1038-48.
188. Qian, M. D.; Zhang, J.; Tan, X. Y.; Wood, A.; Gill, D.; Cho, S., Novel agonist monoclonal antibodies activate TrkB receptors and demonstrate potent neurotrophic activities. *J Neurosci* **2006**, *26* (37), 9394-403.
189. Huang, Y. Z.; Hernandez, F. J.; Gu, B.; Stockdale, K. R.; Nanapaneni, K.; Scheetz, T. E.; Behlke, M. A.; Peek, A. S.; Bair, T.; Giangrande, P. H.; McNamara, J. O., 2nd, RNA aptamer-based functional ligands of the neurotrophin receptor, TrkB. *Mol Pharmacol* **2012**, *82* (4), 623-35.
190. Liu, Y.; Gray, N. S., Rational design of inhibitors that bind to inactive kinase conformations. *Nat Chem Biol* **2006**, *2* (7), 358-64.
191. Muller, S.; Chaikuad, A.; Gray, N. S.; Knapp, S., The ins and outs of selective kinase inhibitor development. *Nat Chem Biol* **2015**, *11* (11), 818-21.
192. Bernard-Gauthier, V.; Schirmacher, R., Evaluation of WO2015042088 A1 - a novel urea-based scaffold for TrkA inhibition. *Expert Opin Ther Pat* **2016**, *26* (2), 291-5.

193. Bailey, J. J. S., R.; Farrell, K.; Bernard-Gauthier, V. , Tropomyosin receptor kinase inhibitors: an updated patent review 2010-2016 Part 1. . *Expert Opin. Ther. Patents*. **2017**, *Accepted*.
194. Bailey, J. J. S., R.; Farrell, K.; Bernard-Gauthier, V. , Tropomyosin receptor kinase inhibitors: an updated patent review 2010-2016 Part 2. . *Expert Opin. Ther. Patents*. **2017**, *Accepted*.
195. McCarthy, C.; Walker, E., Tropomyosin receptor kinase inhibitors: a patent update 2009 – 2013. *Expert Opin. Ther. Pat.* **2014**, *24* (7), 731-744.
196. Wang, T.; Yu, D.; Lamb, M. L., Trk kinase inhibitors as new treatments for cancer and pain. *Expert Opin Ther Pat* **2009**, *19* (3), 305-19.
197. Huse, M.; Kuriyan, J., The Conformational Plasticity of Protein Kinases. *Cell* **2002**, *109* (3), 275-282.
198. Wang, T.; Lamb, M. L.; Block, M. H.; Davies, A. M.; Han, Y.; Hoffmann, E.; Ioannidis, S.; Josey, J. A.; Liu, Z.-Y.; Lyne, P. D.; MacIntyre, T.; Mohr, P. J.; Omer, C. A.; Sjögren, T.; Thress, K.; Wang, B.; Wang, H.; Yu, D.; Zhang, H.-J., Discovery of Disubstituted Imidazo[4,5-b]pyridines and Purines as Potent TrkA Inhibitors. *ACS Med. Chem. Lett.* **2012**, *3* (9), 705-709.
199. Bertrand, T.; Kothe, M.; Liu, J.; Dupuy, A.; Rak, A.; Berne, P. F.; Davis, S.; Gladysheva, T.; Valtre, C.; Crenne, J. Y.; Mathieu, M., The Crystal Structures of TrkA and TrkB Suggest Key Regions for Achieving Selective Inhibition. *Journal of Molecular Biology* **2012**, *423* (3), 439-453.
200. Choi, H.-S.; Rucker, P. V.; Wang, Z.; Fan, Y.; Albaugh, P.; Chopiuk, G.; Gessier, F.; Sun, F.; Adrian, F.; Liu, G.; Hood, T.; Li, N.; Jia, Y.; Che, J.; McCormack, S.; Li, A.; Li, J.; Steffy, A.; Culazzo, A.; Tompkins, C.; Phung, V.; Kreuzsch, A.; Lu, M.; Hu, B.; Chaudhary, A.; Prasad, M.; Tuntland, T.; Liu, B.; Harris, J.; Seidel, H. M.; Loren, J.; Molteni, V., (R)-2-Phenylpyrrolidine Substituted Imidazopyridazines: A New Class of Potent and Selective Pan-TRK Inhibitors. *ACS Med. Chem. Lett.* **2015**, *6* (5), 562-567.
201. George, D. J.; Dionne, C. A.; Jani, J.; Angeles, T.; Murakata, C.; Lamb, J.; Isaacs, J. T., Sustained in vivo regression of Dunning H rat prostate cancers treated with combinations of androgen ablation and Trk tyrosine kinase inhibitors, CEP-751 (KT-6587) or CEP-701 (KT-5555). *Cancer Res* **1999**, *59* (10), 2395-401.
202. Wood, E. R.; Kuyper, L.; Petrov, K. G.; Hunter, R. N.; Harris, P. A.; Lackey, K., Discovery and in vitro evaluation of potent TrkA kinase inhibitors: oxindole and aza-oxindoles. *Bioorg Med Chem Lett* **2004**, *14* (4), 953-957.
203. Bernard-Gauthier, V.; Aliaga, A.; Aliaga, A.; Boudjemeline, M.; Hopewell, R.; Kostikov, A.; Rosa-Neto, P.; Thiel, A.; Schirmacher, R., Syntheses and Evaluation of Carbon-11-and

Fluorine-18-Radiolabeled pan-Tropomyosin Receptor Kinase (Trk) Inhibitors: Exploration of the 4-Aza-2-oxindole Scaffold as Trk PET Imaging Agents. *Acs Chemical Neuroscience* **2015**, 6 (2), 260-276.

204. Green, A.; Li, Y.; Stachel, S. TrkA kinase inhibitors, compositions and methods thereof. WO2012125667, 2012.

205. Bernard-Gauthier, V.; Bailey, J. J.; Aliaga, A.; Kostikov, A.; Rosa-Neto, P.; Wuest, M.; Brodeur, G. M.; Bedell, B. J.; Wuest, F.; Schirmacher, R., Development of subnanomolar radiofluorinated (2-pyrrolidin-1-yl)imidazo[1,2-b]pyridazine pan-Trk inhibitors as candidate PET imaging probes. *Medchemcomm* **2015**, 6 (12), 2184-2193.

206. Andrews, S. W.; Condroski, K. R.; Haas, J.; Jiang, Y.; Kolakowski, G. R.; Seo, J.; Yang, H. W.; Zhao, Q. Macrocyclic compounds as inhibitors of trk kinase. WO2011146336 A1, 2011.

207. Albaugh, P.; Fan, Y.; Mi, Y.; Sun, F.; Adrian, F.; Li, N.; Jia, Y.; Sarkisova, Y.; Kreuzsch, A.; Hood, T.; Lu, M.; Liu, G.; Huang, S.; Liu, Z.; Loren, J.; Tuntland, T.; Karanewsky, D. S.; Seidel, H. M.; Molteni, V., Discovery of GNF-5837, a Selective TRK Inhibitor with Efficacy in Rodent Cancer Tumor Models. *ACS Med. Chem. Lett.* **2012**, 3 (2), 140-145.

208. Bernard-Gauthier, V.; Schirmacher, R., 5-(4-((4-[F-18]fluorobenzyl)oxy)-3-methoxybenzyl)pyrimidine-2,4-diamine: A selective dual inhibitor for potential PET imaging of Trk/CSF-1R. *Bioorg Med Chem Lett* **2014**, 24 (20), 4784-4790.

209. Stachel, S. J.; Sanders, J. M.; Henze, D. A.; Rudd, M. T.; Su, H.-P.; Li, Y.; Nanda, K. K.; Egbertson, M. S.; Manley, P. J.; Jones, K. L. G.; Brnardic, E. J.; Green, A.; Grobler, J. A.; Hanney, B.; Leitl, M.; Lai, M.-T.; Munshi, V.; Murphy, D.; Rickert, K.; Riley, D.; Krasowska-Zoladek, A.; Daley, C.; Zuck, P.; Kane, S. A.; Bilodeau, M. T., Maximizing Diversity from a Kinase Screen: Identification of Novel and Selective pan-Trk Inhibitors for Chronic Pain. *J. Med. Chem.* **2014**, 57 (13), 5800-5816.

210. Zuccotto, F.; Ardini, E.; Casale, E.; Angiolini, M., Through the "Gatekeeper Door": Exploiting the Active Kinase Conformation. *J. Med. Chem.* **2010**, 53 (7), 2681-2694.

211. Hari, Sanjay B.; Merritt, Ethan A.; Maly, Dustin J., Sequence Determinants of a Specific Inactive Protein Kinase Conformation. *Chem. Biol.* **2013**, 20 (6), 806-815.

212. Garuti, L.; Roberti, M.; Bottegoni, G., Non-ATP Competitive Protein Kinase Inhibitors. *Curr. Med. Chem.* **2010**, 17 (25), 2804-2821.

213. Wu, P.; Clausen, M. H.; Nielsen, T. E., Allosteric small-molecule kinase inhibitors. *Pharmacol. Ther.* **2015**, 156, 59-68.

214. Jia, Y.; Yun, C. H.; Park, E.; Ercan, D.; Manuia, M.; Juarez, J.; Xu, C.; Rhee, K.; Chen, T.; Zhang, H.; Palakurthi, S.; Jang, J.; Lelais, G.; DiDonato, M.; Bursulaya, B.; Michellys, P. Y.;

- Epple, R.; Marsilje, T. H.; McNeill, M.; Lu, W.; Harris, J.; Bender, S.; Wong, K. K.; Janne, P. A.; Eck, M. J., Overcoming EGFR(T790M) and EGFR(C797S) resistance with mutant-selective allosteric inhibitors. *Nature* **2016**, *534* (7605), 129-32.
215. Furuya, N.; Momose, T.; Katsuno, K.; Fushimi, N.; Muranaka, H.; Handa, C.; Ozawa, T.; Kinoshita, T., The juxtamembrane region of TrkA kinase is critical for inhibitor selectivity. *Bioorg Med Chem Lett* **2017**.
216. Brandhuber, B. J.; Jiang, Y.; Kolakowski, G. R.; Winski, S. L. Pyrazolyl urea, thiourea, guanidine and cyanoguanidine compounds as trka kinase inhibitors. WO2014078417 A1, 2014.
217. Andrews, S. W.; Blake, J. F.; Brandhuber, B. J.; Kercher, T.; Winski, S. L. N-(monocyclic aryl),N'-pyrazolyl-urea, thiourea, guanidine and cyanoguanidine compounds as trka kinase inhibitors. WO2014078325 A1, 2014.
218. Shabbir, M.; Stuart, R., Lestaurtinib, a multitargeted tyrosinse kinase inhibitor: from bench to bedside. *Expert Opinion on Investigational Drugs* **2010**, *19* (3), 427-436.
219. Evans, A. E.; Kisselbach, K. D.; Yamashiro, D. J.; Ikegaki, N.; Camoratto, A. M.; Dionne, C. A.; Brodeur, G. M., Antitumor Activity of CEP-751 (KT-6587) on Human Neuroblastoma and Medulloblastoma Xenografts. *Clin. Cancer Res.* **1999**, *5* (11), 3594-3602.
220. Evans, A. E.; Kisselbach, K. D.; Liu, X.; Eggert, A.; Ikegaki, N.; Camoratto, A. M.; Dionne, C.; Brodeur, G. M., Effect of CEP-751 (KT-6587) on neuroblastoma xenografts expressing TrkB. *Med. Pediatr. Oncol.* **2001**, *36* (1), 181-184.
221. Iyer, R.; Evans, A. E.; Qi, X.; Ho, R.; Minturn, J. E.; Zhao, H.; Balamuth, N.; Maris, J. M.; Brodeur, G. M., Lestaurtinib Enhances the Antitumor Efficacy of Chemotherapy in Murine Xenograft Models of Neuroblastoma. *Clin. Cancer Res.* **2010**, *16* (5), 1478-1485.
222. Minturn, J. E.; Evans, A. E.; Villablanca, J. G.; Yanik, G. A.; Park, J. R.; Shusterman, S.; Groshen, S.; Hellriegel, E. T.; Bensen-Kennedy, D.; Matthay, K. K.; Brodeur, G. M.; Maris, J. M., Phase I trial of lestaurtinib for children with refractory neuroblastoma: a new approaches to neuroblastoma therapy consortium study. *Cancer Chemother. Pharmacol.* **2011**, *68* (4), 1057-1065.
223. Wang, T.; Yu, D.; Lamb, M. L., Trk kinase inhibitors as new treatments for cancer and pain. *Expert Opin. Ther. Pat.* **2009**, *19* (3), 305-319.
224. Weiss, G. J.; Hidalgo, M.; Borad, M. J.; Laheru, D.; Tibes, R.; Ramanathan, R. K.; Blydorn, L.; Jameson, G.; Jimeno, A.; Isaacs, J. D.; Scaburri, A.; Pacciarini, M. A.; Fiorentini, F.; Ciomei, M.; Von Hoff, D. D., Phase I study of the safety, tolerability and pharmacokinetics of PHA-848125AC, a dual tropomyosin receptor kinase A and cyclin-dependent kinase inhibitor, in patients with advanced solid malignancies. *Invest. New Drugs* **2012**, *30* (6), 2334-2343.

225. De Braud, F.; Niger, M.; Damian, S.; Bardazza, B.; Martinetti, A.; Pelosi, G.; Marrapese, G.; Palmeri, L.; Cerea, G.; Valtorta, E.; Veronese, S.; Sartore-Bianchi, A.; Ardini, E.; Isachi, A.; Martignoni, M.; Galvani, A.; Luo, D.; Yeh, L.; Senderowicz, A.; Siena, S., Alka-372–001: first-in-human, phase I study of entrectinib—an oral pan-trk, ROS1, and ALK inhibitor—in patients with advanced solid tumors with relevant molecular alterations. *J. Clin. Oncol.* **2015**, *33*, suppl; abstr 2517.
226. Patel, M. R.; Bauer, T. M.; Liu, S. V.; Drilon, A. E.; Wheler, J. J.; Shaw, A. T.; Farago, A. F.; Ou, S.-H. I.; Luo, D.; Yeh, L.; Hornby, Z.; Senderowicz, A. M.; Lim, J., STARTRK-1: Phase 1/2a study of entrectinib, an oral Pan-Trk, ROS1, and ALK inhibitor, in patients with advanced solid tumors with relevant molecular alterations. *J. Clin. Oncol.* **2015**, *33*, suppl; abstr 2596.
227. Burris, H. A.; Brose, M. S.; Shaw, A. T.; Bauer, T. M.; Farago, A. F.; Doebele, R. C.; Smith, S.; Fernandes, M.; Cruickshank, S.; Low, J. A., A first-in-human study of LOXO-101, a highly selective inhibitor of the tropomyosin receptor kinase (TRK) family. *J. Clin. Oncol.* **2015**, *33*, suppl TPS2624.
228. Vaishnavi, A.; Capelletti, M.; Le, A. T.; Kako, S.; Butaney, M.; Ercan, D.; Mahale, S.; Davies, K. D.; Aisner, D. L.; Pilling, A. B.; Berge, E. M.; Kim, J.; Sasaki, H.; Park, S.-i.; Kryukov, G.; Garraway, L. A.; Hammerman, P. S.; Haas, J.; Andrews, S. W.; Lipson, D.; Stephens, P. J.; Miller, V. A.; Varella-Garcia, M.; Janne, P. A.; Doebele, R. C., Oncogenic and drug-sensitive NTRK1 rearrangements in lung cancer. *Nat. Med.* **2013**, *19* (11), 1469-1472.
229. Menichincheri, M.; Ardini, E.; Magnaghi, P.; Avanzi, N.; Banfi, P.; Bossi, R.; Buffa, L.; Canevari, G.; Ceriani, L.; Colombo, M.; Corti, L.; Donati, D.; Fasolini, M.; Felder, E.; Fiorelli, C.; Fiorentini, F.; Galvani, A.; Isacchi, A.; Borgia, A. L.; Marchionni, C.; Nesi, M.; Orrenius, C.; Panzeri, A.; Pesenti, E.; Rusconi, L.; Saccardo, M. B.; Vanotti, E.; Perrone, E.; Orsini, P., Discovery of Entrectinib: A New 3-Aminoindazole As a Potent Anaplastic Lymphoma Kinase (ALK), c-ros Oncogene 1 Kinase (ROS1), and Pan-Tropomyosin Receptor Kinases (Pan-TRKs) inhibitor. *J. Med. Chem.* **2016**, *59* (7), 3392-3408.
230. Ardini, E.; Menichincheri, M.; Banfi, P.; Bosotti, R.; De Ponti, C.; Pulci, R.; Ballinari, D.; Ciomei, M.; Texido, G.; Degrassi, A.; Avanzi, N.; Amboldi, N.; Saccardo, M. B.; Casero, D.; Orsini, P.; Bandiera, T.; Mologni, L.; Anderson, D.; Wei, G.; Harris, J.; Vernier, J.-M.; Li, G.; Felder, E.; Donati, D.; Isacchi, A.; Pesenti, E.; Magnaghi, P.; Galvani, A., Entrectinib, a Pan-TRK, ROS1 and ALK Inhibitor with Activity in Multiple Molecularly Defined Cancer Indications. *Mol. Cancer Ther.* **2016**, *15* (4), 628-629.
231. Iyer, R.; Wehrmann, L.; Golden, R. L.; Naraparaju, K.; Croucher, J. L.; MacFarland, S. P.; Guan, P.; Kolla, V.; Wei, G.; Cam, N.; Li, G.; Hornby, Z.; Brodeur, G. M., Entrectinib is a

potent inhibitor of Trk-driven neuroblastomas in a xenograft mouse model. *Cancer Lett.* **2016**, 372 (2), 179-186.

232. Sartore-Bianchi, A.; Ardini, E.; Bosotti, R.; Amatu, A.; Valtorta, E.; Somaschini, A.; Radrizzani, L.; Palmeri, L.; Banfi, P.; Bonazzina, E.; Misale, S.; Marrapese, G.; Leone, A.; Alzani, R.; Luo, D.; Hornby, Z.; Lim, J.; Veronese, S.; Vanzulli, A.; Bardelli, A.; Martignoni, M.; Davite, C.; Galvani, A.; Isacchi, A.; Siena, S., Sensitivity to Entrectinib Associated With a Novel LMNA-NTRK1 Gene Fusion in Metastatic Colorectal Cancer. *J. Natl. Cancer Inst.* **2016**, 108 (1).

233. Farago, A. F.; Le, L. P.; Zheng, Z.; Muzikansky, A.; Drilon, A.; Patel, M.; Bauer, T. M.; Liu, S. V.; Ou, S.-H. I.; Jackman, D.; Costa, D. B.; Multani, P. S.; Li, G. G.; Hornby, Z.; Chow-Maneval, E.; Luo, D.; Lim, J. E.; Iafrate, A. J.; Shaw, A. T., Durable Clinical Response to Entrectinib in NTRK1-Rearranged Non-Small Cell Lung Cancer. *J. Thorac. Oncol.* **2015**, 10 (12), 1670-1674.

234. Russo, M.; Misale, S.; Wei, G.; Siravegna, G.; Crisafulli, G.; Lazzari, L.; Corti, G.; Rospo, G.; Novara, L.; Mussolin, B.; Bartolini, A.; Cam, N.; Patel, R.; Yan, S.; Shoemaker, R.; Wild, R.; Di Nicolantonio, F.; Bianchi, A. S.; Li, G.; Siena, S.; Bardelli, A., Acquired Resistance to the TRK Inhibitor Entrectinib in Colorectal Cancer. *Cancer Discov.* **2016**, 6 (1), 36-44.

235. Hong, D. S.; Brose, M. S.; Doebele, R. C.; Shaw, A. T.; Dowlati, A.; Bauer, T. M.; Farago, A. F.; Estrada-Bernal, A.; Lee, A. T.; Cox, M. C.; Nanda, N.; Low, J. A.; Burris, H. A., Abstract PR13: Clinical safety and activity from a phase 1 study of LOXO-101, a selective TRKA/B/C inhibitor, in solid-tumor patients with NTRK gene fusions. *Mol. Cancer Ther.* **2015**, 14 (12 Supplement 2), PR13-PR13.

236. Doebele, R. C.; Davis, L. E.; Vaishnavi, A.; Le, A. T.; Estrada-Bernal, A.; Keysar, S.; Jimeno, A.; Varella-Garcia, M.; Aisner, D. L.; Li, Y.; Stephens, P. J.; Morosini, D.; Tuch, B. B.; Fernandes, M.; Nanda, N.; Low, J. A., An Oncogenic NTRK Fusion in a Patient with Soft-Tissue Sarcoma with Response to the Tropomyosin-Related Kinase Inhibitor LOXO-101. *Cancer Discov.* **2015**, 5 (10), 1049-1057.

237. Nagasubramanian, R.; Wei, J.; Gordon, P.; Rastatter, J. C.; Cox, M. C.; Pappo, A., Infantile Fibrosarcoma With NTRK3–ETV6 Fusion Successfully Treated With the Tropomyosin-Related Kinase Inhibitor LOXO-101. *Pediatr. Blood Cancer* **2016**, 63 (8), 1468-1470.

238. Yeh, I.; Tee, M. K.; Botton, T.; Hunter Shain, A.; Sparatta, A. J.; Gagnon, A.; Vemula, S. S.; Garrido, M. C.; Nakamaru, K.; Isoyama, T.; McCalmont, T. H.; LeBoit, P. E.; Bastian, B. C., NTRK3 kinase fusions in Spitz tumours. *The Journal of Pathology* **2016**, doi: 10.1002/path.4775.

239. Lewis, R. T.; Bode, C. M.; Choquette, D. M.; Potashman, M.; Romero, K.; Stellwagen, J. C.; Teffera, Y.; Moore, E.; Whittington, D. A.; Chen, H.; Epstein, L. F.; Emkey, R.; Andrews, P. S.; Yu, V. L.; Saffran, D. C.; Xu, M.; Drew, A.; Merkel, P.; Szilvassy, S.; Brake, R. L., The Discovery and Optimization of a Novel Class of Potent, Selective, and Orally Bioavailable Anaplastic Lymphoma Kinase (ALK) Inhibitors with Potential Utility for the Treatment of Cancer. *J. Med. Chem.* **2012**, *55* (14), 6523-6540.
240. Arkenau, H.-T.; Sachdev, J. C.; Mita, M. M.; Dziadziuszko, R.; Lin, C.-C.; Yang, J. C.; Infante, J. R.; Anthony, S. P.; Voskoboynik, M.; Su, W.-C.; Castro, J. D.; Natale, R. B.; Zhang, Z.-Y.; Hughes, L.; Bobilev, D.; Weiss, G. J., Phase (Ph) 1/2a study of TSR-011, a potent inhibitor of ALK and TRK, in advanced solid tumors including crizotinib-resistant ALK positive non-small cell lung cancer. *J. Clin. Oncol.* **2015**, *33*, suppl; abstr 8063.
241. Weiss, G. J.; Hidalgo, M.; Borad, M. J.; Laheru, D.; Tibes, R.; Ramanathan, R. K.; Blydorn, L.; Jameson, G.; Jimeno, A.; Isaacs, J. D.; Scaburri, A.; Pacciarini, M. A.; Fiorentini, F.; Ciomei, M.; Von Hoff, D. D., Phase I study of the safety, tolerability and pharmacokinetics of PHA-848125AC, a dual tropomyosin receptor kinase A and cyclin-dependent kinase inhibitor, in patients with advanced solid malignancies. *Invest. New Drugs* **2012**, *30* (6), 2334-2343.
242. Skerratt, S. E.; Andrews, M.; Bagal, S. K.; Bilsland, J.; Brown, D.; Bungay, P. J.; Cole, S.; Gibson, K. R.; Jones, R.; Morao, I.; Nedderman, A.; Omoto, K.; Robinson, C.; Ryckmans, T.; Skinner, K.; Stupple, P.; Waldron, G., The Discovery of a Potent, Selective, and Peripherally Restricted Pan-Trk Inhibitor (PF-06273340) for the Treatment of Pain. *Journal of Medicinal Chemistry* **2016**, *59* (22), 10084-10099.
243. Heffron, T. P., Small Molecule Kinase Inhibitors for the Treatment of Brain Cancer. *J. Med. Chem.* **2016**.
244. Qaim, S. M., Cyclotron production of medical radionuclides. In *Handbook of Nuclear Chemistry, 2nd ed.*; Vertes, A., Nagy, S., Klencsar, Z., Lovas, R. G., Rösch, F., Eds.; Springer: Dordrecht, The Netherlands **2011**, 1903-1933.
245. Miller, P. W.; Long, N. J.; Vilar, R.; Gee, A. D., Synthesis of ¹¹C, ¹⁸F, ¹⁵O, and ¹³N radiolabels for positron emission tomography. *Angew Chem Int Ed Engl* **2008**, *47* (47), 8998-9033.
246. Piel, M.; Vernaleken, I.; Rosch, F., Positron emission tomography in CNS drug discovery and drug monitoring. *J Med Chem* **2014**, *57* (22), 9232-58.
247. Liang, S. H.; Vasdev, N., Total Radiosynthesis: Thinking outside "the box". *Aust J Chem* **2015**, *68* (9), 1319-1328.

248. Ametamey, S. M.; Honer, M.; Schubiger, P. A., Molecular imaging with PET. *Chem Rev* **2008**, *108* (5), 1501-16.
249. Levin, C. S., Primer on molecular imaging technology. *Eur J Nucl Med Mol Imaging* **2005**, *32 Suppl 2*, S325-45.
250. Campagna-Slater, V.; Pottel, J.; Therrien, E.; Cantin, L. D.; Moitessier, N., Development of a Computational Tool to Rival Experts in the Prediction of Sites of Metabolism of Xenobiotics by P450s. *Journal of Chemical Information and Modeling* **2012**, *52* (9), 2471-2483.
251. Zaretzki, J.; Boehm, K. M.; Swamidass, S. J., Improved Prediction of CYP-Mediated Metabolism with Chemical Fingerprints. *J Chem Inf Model* **2015**, *55* (5), 972-82.
252. Rankovic, Z., CNS Drug Design: Balancing Physicochemical Properties for Optimal Brain Exposure. *Journal of Medicinal Chemistry* **2015**, *58* (6), 2584-2608.
253. Aller, S. G.; Yu, J.; Ward, A.; Weng, Y.; Chittaboina, S.; Zhuo, R.; Harrell, P. M.; Trinh, Y. T.; Zhang, Q.; Urbatsch, I. L.; Chang, G., Structure of P-glycoprotein reveals a molecular basis for poly-specific drug binding. *Science* **2009**, *323* (5922), 1718-22.
254. Zhang, L.; Villalobos, A.; Beck, E. M.; Bocan, T.; Chappie, T. A.; Chen, L.; Grimwood, S.; Heck, S. D.; Helal, C. J.; Hou, X.; Humphrey, J. M.; Lu, J.; Skaddan, M. B.; McCarthy, T. J.; Verhoest, P. R.; Wager, T. T.; Zasadny, K., Design and selection parameters to accelerate the discovery of novel central nervous system positron emission tomography (PET) ligands and their application in the development of a novel phosphodiesterase 2A PET ligand. *J Med Chem* **2013**, *56* (11), 4568-79.
255. Wager, T. T.; Hou, X. J.; Verhoest, P. R.; Villalobos, A., Moving beyond Rules: The Development of a Central Nervous System Multiparameter Optimization (CNS MPO) Approach To Enable Alignment of Druglike Properties. *Acs Chemical Neuroscience* **2010**, *1* (6), 435-449.
256. Wager, T. T.; Hou, X.; Verhoest, P. R.; Villalobos, A., Central Nervous System Multiparameter Optimization Desirability: Application in Drug Discovery. *ACS Chem Neurosci* **2016**, *7* (6), 767-75.
257. Di, L.; Rong, H. J.; Feng, B., Demystifying Brain Penetration in Central Nervous System Drug Discovery. *Journal of Medicinal Chemistry* **2013**, *56* (1), 2-12.
258. Cordon-Cardo, C.; O'Brien, J. P.; Casals, D.; Rittman-Grauer, L.; Biedler, J. L.; Melamed, M. R.; Bertino, J. R., Multidrug-resistance gene (P-glycoprotein) is expressed by endothelial cells at blood-brain barrier sites. *Proc Natl Acad Sci U S A* **1989**, *86* (2), 695-8.
259. Hitchcock, S. A., Structural modifications that alter the P-glycoprotein efflux properties of compounds. *J Med Chem* **2012**, *55* (11), 4877-95.

260. Alam, I. S.; Arshad, M. A.; Nguyen, Q. D.; Aboagye, E. O., Radiopharmaceuticals as probes to characterize tumour tissue. *Eur J Nucl Med Mol Imaging* **2015**, *42* (4), 537-61.
261. Holland, J. P.; Cumming, P.; Vasdev, N., PET radiopharmaceuticals for probing enzymes in the brain. *Am J Nucl Med Mol Imaging* **2013**, *3* (3), 194-216.
262. Wey, H. Y.; Gilbert, T. M.; Zurcher, N. R.; She, A.; Bhanot, A.; Taillon, B. D.; Schroeder, F. A.; Wang, C. G.; Haggarty, S. J.; Hooker, J. M., Insights into neuroepigenetics through human histone deacetylase PET imaging. *Sci Transl Med* **2016**, *8* (351).
263. Hicks, J. W.; VanBrocklin, H. F.; Wilson, A. A.; Houle, S.; Vasdev, N., Radiolabeled small molecule protein kinase inhibitors for imaging with PET or SPECT. *Molecules* **2010**, *15* (11), 8260-78.
264. Santos, R.; Ursu, O.; Gaulton, A.; Bento, A. P.; Donadi, R. S.; Bologa, C. G.; Karlsson, A.; Al-Lazikani, B.; Hersey, A.; Oprea, T. I.; Overington, J. P., A comprehensive map of molecular drug targets. *Nat Rev Drug Discov* **2017**, *16* (1), 19-34.
265. Gao, M.; Wang, M.; Zheng, Q. H., Synthesis of carbon-11-labeled isonicotinamides as new potential PET agents for imaging of GSK-3 enzyme in Alzheimer's disease. *Bioorg Med Chem Lett* **2017**, *27* (4), 740-743.
266. Li, L.; Shao, X.; Cole, E. L.; Ohnmacht, S. A.; Ferrari, V.; Hong, Y. T.; Williamson, D. J.; Fryer, T. D.; Quesada, C. A.; Sherman, P.; Riss, P. J.; Scott, P. J.; Aigbirhio, F. I., Synthesis and Initial in Vivo Studies with [(11)C]SB-216763: The First Radiolabeled Brain Penetrative Inhibitor of GSK-3. *ACS Med Chem Lett* **2015**, *6* (5), 548-52.
267. Cole, E. L.; Shao, X.; Sherman, P.; Quesada, C.; Fawaz, M. V.; Desmond, T. J.; Scott, P. J., Synthesis and evaluation of [(11)C]PyrATP-1, a novel radiotracer for PET imaging of glycogen synthase kinase-3beta (GSK-3beta). *Nucl Med Biol* **2014**, *41* (6), 507-12.
268. Kumata, K.; Yui, J.; Xie, L.; Zhang, Y.; Nengaki, N.; Fujinaga, M.; Yamasaki, T.; Shimoda, Y.; Zhang, M. R., Radiosynthesis and preliminary PET evaluation of glycogen synthase kinase 3beta (GSK-3beta) inhibitors containing [(11)C]methylsulfanyl, [(11)C]methylsulfinyl or [(11)C]methylsulfonyl groups. *Bioorg Med Chem Lett* **2015**, *25* (16), 3230-3.
269. Liang, S.; Chen, J. S.; Normandin, M.; Collier, T.; Perlis, R.; Holson, E.; Haggarty, S.; El Fakhri, G.; Kurumbail, R.; Vasdev, N., Discovery of [C-11]PF-367 for neuroimaging of glycogen synthase kinase 3. *Journal of Nuclear Medicine* **2015**, *56* (3).
270. Bernard-Gauthier, V.; Bailey, J. J.; Berke, S.; Schirrmacher, R., Recent Advances in the Development and Application of Radiolabeled Kinase Inhibitors for PET Imaging. *Molecules* **2015**, *20* (12), 22000-22027.

271. Slobbe, P.; Poot, A. J.; Windhorst, A. D.; van Dongen, G. A., PET imaging with small-molecule tyrosine kinase inhibitors: TKI-PET. *Drug Discov Today* **2012**, *17* (21-22), 1175-87.
272. Memon, A. A.; Weber, B.; Winterdahl, M.; Jakobsen, S.; Meldgaard, P.; Madsen, H. H. T.; Keiding, S.; Nexø, E.; Sørensen, B. S., PET imaging of patients with non-small cell lung cancer employing an EGF receptor targeting drug as tracer. *Brit J Cancer* **2011**, *105* (12), 1850-1855.
273. Meng, X.; Loo, B. W., Jr.; Ma, L.; Murphy, J. D.; Sun, X.; Yu, J., Molecular imaging with ¹¹¹C-PD153035 PET/CT predicts survival in non-small cell lung cancer treated with EGFR-TKI: a pilot study. *J Nucl Med* **2011**, *52* (10), 1573-9.
274. Osman, S.; Lundkvist, C.; Pike, V. W.; Halldin, C.; McCarron, J. A.; Swahn, C. G.; Ginovart, N.; Luthra, S. K.; Bench, C. J.; Grasby, P. M.; Wikstrom, H.; Barf, T.; Cliffe, I. A.; Fletcher, A.; Farde, L., Characterization of the radioactive metabolites of the 5-HT_{1A} receptor radioligand, [O-methyl-¹¹C]WAY-100635, in monkey and human plasma by HPLC: comparison of the behaviour of an identified radioactive metabolite with parent radioligand in monkey using PET. *Nucl Med Biol* **1996**, *23* (5), 627-34.
275. Langstrom, B.; Antoni, G.; Gullberg, P.; Halldin, C.; Malmberg, P.; Nagren, K.; Rimland, A.; Svard, H., Synthesis of L- and D-[methyl-¹¹C]methionine. *J Nucl Med* **1987**, *28* (6), 1037-40.
276. Link, J. M.; Krohn, K. A.; Clark, J. C., Production of [¹¹C]CH₃I by single pass reaction of [¹¹C]CH₄ with I₂. *Nucl Med Biol* **1997**, *24* (1), 93-7.
277. Jewett, D. M., A simple synthesis of [¹¹C]methyl triflate. *Int J Rad Appl Instrum A* **1992**, *43* (11), 1383-5.
278. Wuest, F.; Berndt, M.; Kniess, T., Carbon-11 labeling chemistry based upon [¹¹C]methyl iodide. *Ernst Schering Res Found Workshop* **2007**, (62), 183-213.
279. Doi, H., Pd-mediated rapid cross-couplings using [(¹¹C)methyl iodide: groundbreaking labeling methods in (¹¹C) radiochemistry. *J Labelled Comp Radiopharm* **2015**, *58* (3), 73-85.
280. Hwang, D. R.; Simpson, N. R.; Montoya, J.; Man, J. J.; Laruelle, M., An improved one-pot procedure for the preparation of [¹¹C-carbonyl]-WAY100635. *Nucl Med Biol* **1999**, *26* (7), 815-9.
281. Rotstein, B. H.; Liang, S. H.; Placzek, M. S.; Hooker, J. M.; Gee, A. D.; Dolle, F.; Wilson, A. A.; Vasdev, N., (¹¹C)[double bond, length as m-dash]O bonds made easily for positron emission tomography radiopharmaceuticals. *Chem Soc Rev* **2016**, *45* (17), 4708-26.
282. Rotstein, B. H.; Liang, S. H.; Holland, J. P.; Collier, T. L.; Hooker, J. M.; Wilson, A. A.; Vasdev, N., ¹¹CO₂ fixation: a renaissance in PET radiochemistry. *Chem Commun (Camb)* **2013**, *49* (50), 5621-9.

283. Neelamegam, R.; Hellenbrand, T.; Schroeder, F. A.; Wang, C.; Hooker, J. M., Imaging evaluation of 5HT_{2C} agonists, [(11)C]WAY-163909 and [(11)C]vabicaserin, formed by Pictet-Spengler cyclization. *J Med Chem* **2014**, *57* (4), 1488-94.
284. Jacobson, O.; Mishani, E., [11C]-dimethylamine as a labeling agent for PET biomarkers. *Appl Radiat Isot* **2008**, *66* (2), 188-93.
285. Iwata, R.; Ido, T.; Takahashi, T.; Nakanishi, H.; Iida, S., Optimization of [11C]HCN production and no-carrier-added [1-11C]amino acid synthesis. *Int J Rad Appl Instrum A* **1987**, *38* (2), 97-102.
286. Nishijima, K.; Kuge, Y.; Seki, K.; Ohkura, K.; Motoki, N.; Nagatsu, K.; Tanaka, A.; Tsukamoto, E.; Tamaki, N., A simplified and improved synthesis of [11C]phosgene with iron and iron (III) oxide. *Nucl Med Biol* **2002**, *29* (3), 345-50.
287. Preshlock, S.; Tredwell, M.; Gouverneur, V., (18)F-Labeling of Arenes and Heteroarenes for Applications in Positron Emission Tomography. *Chem Rev* **2016**, *116* (2), 719-66.
288. Tredwell, M.; Preshlock, S. M.; Taylor, N. J.; Gruber, S.; Huiban, M.; Passchier, J.; Mercier, J.; Genicot, C.; Gouverneur, V., A general copper-mediated nucleophilic 18F fluorination of arenes. *Angew Chem Int Ed Engl* **2014**, *53* (30), 7751-5.
289. Ehrenkauf, R. E.; Potocki, J. F.; Jewett, D. M., Simple synthesis of F-18-labeled 2-fluoro-2-deoxy-D-glucose: concise communication. *J Nucl Med* **1984**, *25* (3), 333-7.
290. Teare, H.; Robins, E. G.; Kirjavainen, A.; Forsback, S.; Sandford, G.; Solin, O.; Luthra, S. K.; Gouverneur, V., Radiosynthesis and evaluation of [18F]Selectfluor bis(triflate). *Angew Chem Int Ed Engl* **2010**, *49* (38), 6821-4.
291. Stenhagen, I. S.; Kirjavainen, A. K.; Forsback, S. J.; Jorgensen, C. G.; Robins, E. G.; Luthra, S. K.; Solin, O.; Gouverneur, V., [18F]fluorination of an arylboronic ester using [18F]selectfluor bis(triflate): application to 6-[18F]fluoro-L-DOPA. *Chem Commun (Camb)* **2013**, *49* (14), 1386-8.
292. Hamacher, K.; Coenen, H. H.; Stocklin, G., Efficient stereospecific synthesis of no-carrier-added 2-[18F]-fluoro-2-deoxy-D-glucose using aminopolyether supported nucleophilic substitution. *J Nucl Med* **1986**, *27* (2), 235-8.
293. Beuthien-Baumann, B.; Hamacher, K.; Oberdorfer, F.; Steinbach, J., Preparation of fluorine-18 labelled sugars and derivatives and their application as tracer for positron-emission-tomography. *Carbohydr Res* **2000**, *327* (1-2), 107-18.
294. Dolle, F., Fluorine-18-labelled fluoropyridines: advances in radiopharmaceutical design. *Curr Pharm Des* **2005**, *11* (25), 3221-35.

295. Moon, B. S.; Kil, H. S.; Park, J. H.; Kim, J. S.; Park, J.; Chi, D. Y.; Lee, B. C.; Kim, S. E., Facile aromatic radiofluorination of [¹⁸F]flumazenil from diaryliodonium salts with evaluation of their stability and selectivity. *Org Biomol Chem* **2011**, *9* (24), 8346-55.
296. Massaweh, G.; Schirmacher, E.; la Fougere, C.; Kovacevic, M.; Wangler, C.; Jolly, D.; Gravel, P.; Reader, A. J.; Thiel, A.; Schirmacher, R., Improved work-up procedure for the production of [(18)F]flumazenil and first results of its use with a high-resolution research tomograph in human stroke. *Nucl Med Biol* **2009**, *36* (7), 721-7.
297. Rotstein, B. H.; Stephenson, N. A.; Vasdev, N.; Liang, S. H., Spirocyclic hypervalent iodine(III)-mediated radiofluorination of non-activated and hindered aromatics. *Nat Commun* **2014**, *5*.
298. Lee, E.; Hooker, J. M.; Ritter, T., Nickel-Mediated Oxidative Fluorination for PET with Aqueous [F-18] Fluoride. *J Am Chem Soc* **2012**, *134* (42), 17456-17458.
299. Eumann, C. N. N.; Hooker, J. M.; Ritter, T., Concerted nucleophilic aromatic substitution with F-19(-) and F-18(-). *Nature* **2016**, *534* (7607), 369-373.
300. Ren, H.; Wey, H. Y.; Strebl, M.; Neelamegam, R.; Ritter, T.; Hooker, J. M., Synthesis and Imaging Validation of [F-18]MDL100907 Enabled by Ni-Mediated Fluorination. *Acs Chemical Neuroscience* **2014**, *5* (7), 611-615.
301. Lee, E.; Kamlet, A. S.; Powers, D. C.; Neumann, C. N.; Boursalian, G. B.; Furuya, T.; Choi, D. C.; Hooker, J. M.; Ritter, T., A fluoride-derived electrophilic late-stage fluorination reagent for PET imaging. *Science* **2011**, *334* (6056), 639-42.
302. Ye, Y.; Schimler, S. D.; Hanley, P. S.; Sanford, M. S., Cu(OTf)₂-mediated fluorination of aryltrifluoroborates with potassium fluoride. *J Am Chem Soc* **2013**, *135* (44), 16292-5.
303. Cardinale, J. E., J.; Humpert, S.; Coenen, H. H. , Iodonium ylides for one-step, no-carrier-added radiofluorination of electron rich arenes, exemplified with 4-([(18)F]fluorophenoxy)-phenylmethyl)-piperidine NET and SERT ligands. *RSC Adv.* **2014**, *4*, 17293–17299.
304. Stephenson, N. A.; Holland, J. P.; Kassenbrock, A.; Yokell, D. L.; Livni, E.; Liang, S. H.; Vasdev, N., Iodonium ylide-mediated radiofluorination of 18F-FPEB and validation for human use. *J Nucl Med* **2015**, *56* (3), 489-92.
305. Zischler, J.; Kolks, N.; Modemann, D.; Neumaier, B.; Zlatopolskiy, B. D., Alcohol-Enhanced Cu-Mediated Radiofluorination. *Chemistry* **2016**.
306. Zlatopolskiy, B. D.; Zischler, J.; Krapf, P.; Zarrad, F.; Urusova, E. A.; Kordys, E.; Endepols, H.; Neumaier, B., Copper-mediated aromatic radiofluorination revisited: efficient production of PET tracers on a preparative scale. *Chemistry* **2015**, *21* (15), 5972-9.

307. Mossine, A. V.; Brooks, A. F.; Makaravage, K. J.; Miller, J. M.; Ichiishi, N.; Sanford, M. S.; Scott, P. J., Synthesis of [^{18}F]Arenes via the Copper-Mediated [^{18}F]Fluorination of Boronic Acids. *Org Lett* **2015**, *17* (23), 5780-3.

Article 5

*A version of this chapter has been published as: Bernard-Gauthier, V. & Schirmacher, R. 5-(4-((4-[¹⁸F]fluorobenzyl)oxy)-3-methoxybenzyl)pyrimidine-2,4-diamine: A Selective Dual Inhibitor for Potential PET Imaging of Trk/CSF-1R. *Bioorg. Med. Chem. Lett.* **2014**, *24*, 4784-4790.*

Author contributions: V.B.G. and R.S. design research; V.B.G. performed all research, data analysis and interpretation; V.B.G. wrote the paper; V.B.G. and R.S. reviewed/corrected paper.

5-(4-((4-[¹⁸F]Fluorobenzyl)oxy)-3-methoxybenzyl)pyrimidine-2,4-diamine: A Selective Dual Inhibitor for Potential PET Imaging of Trk/CSF-1R

Vadim Bernard-Gauthier^{1,2} & Ralf Schirmacher^{2,3}*

¹Experimental Medicine, Department of Medicine, McGill University, 1110 Pine Avenue West, Montreal, QC, H3A 1A3. ²Department of Oncology, University of Alberta, 11560 University Avenue, Edmonton, AB, Canada, T6G 1Z2. ³McConnell Brain Imaging Centre, Montreal Neurological Institute, McGill University, 3801 University Street, Montreal, QC, Canada, H3A 2B4. *Corresponding author

2.1 Abstract

The tropomyosin receptor kinases (TrkA/B/C) and colony-stimulating factor-1 receptor (CSF-1R) represent highly pursued oncological therapeutic targets. The 2,4-diaminopyrimidine inhibitor GW2580 (**2.9**) has been previously reported as a highly selective low nanomolar TrkB/TrkC/CSF-1R inhibitor. In this study, fluorinated derivatives of **2.9** were designed, synthesized and evaluated in enzymatic assays. The highly potent inhibitor **2.10** was identified, which retained the selectivity profile of the non-fluorinated lead compound **2.9**, and the radiosynthesis of [¹⁸F]**2.10** was developed. The results obtained from the biological evaluation of **2.10** and the radiosynthesis of [¹⁸F]**2.10** support further investigation of this tracer as a potential PET imaging probe for TrkB/TrkC and CSF-1R.

2.2 Introduction

In recent years, the growing understanding of the underlying role of protein tyrosine kinases in the abnormal signal transduction in cancer has sustained the development of numerous targeted small molecule tyrosine kinase inhibitors (TKIs) for cancer treatment.¹⁻³ TKIs stand as one of the fastest growing anticancer drug classes with 16 FDA-approved inhibitors within the last twelve years and hundreds more currently in development.⁴ Despite those clinical

successes, the low response rates of those TKIs reaching the market forces the development of efficient tools to facilitate drug development and ultimately identify patients which are most likely to respond to treatment.⁵ The current use of invasive approaches such as tumor biopsy only provide partial information on specific target expression/mutation status. In this context, the advent of radiolabeled TKIs for positron emission tomography (PET) may potentially offer fundamental insights useful for drug development and individualized medicine as far as target expression, binding kinetics, potential toxicity and treatment efficacy is concerned.⁵⁻¹⁰

Trk receptors critically support the development and maintenance of the nervous system¹¹⁻¹³ but their over-expression in various neural and non-neural neoplasms such as breast,¹⁴ pancreatic,¹⁵⁻¹⁶ lung¹⁷ and neuroendocrine tumors¹⁸⁻²¹ also confers aggressive phenotypes to tumor cells and correlates with poor prognosis.²² In the last decade, many studies have focused on the development of Trk ligands, especially ATP-competitive inhibitors for the treatment of cancer (**Figure 2.1**).²³⁻²⁵ Currently, the inhibition of Trk receptors is investigated in six clinical trials and numerous pre-clinical studies.²⁶⁻²⁷

Comprehensive kinase inhibitor analysis recently demonstrated that the orally bioactive diaminopyrimidine colony-stimulating factor-1 receptor (CSF-1R) inhibitor GW2580 (**2.9**)²⁸ strongly inhibits Trk receptors – especially TrkB (K_d ; CSF-1R = 2.2 nM, TrkA = 630 nM, TrkB = 36 nM, TrkC = 120 nM).²⁹⁻³¹ Notably, GW2580 exhibits one of the most specific kinase inhibition profiles among known kinase inhibitors (no supplementary inhibition of other kinases with $K_d < 3\mu\text{M}$) which, when considering PET imaging, represents an advantageous target selectivity.³² Therefore, we hypothesized that the high selectivity of **2.9** could constitute a promising basis for the development of PET-TKI probes with potential imaging applications for CSF-1R, since CSF-1R also represents a useful PET imaging target. CSF-1R regulates mononuclear phagocyte differentiation and proliferation and as such plays a central role in multiple macrophage-mediated pathological conditions.³³⁻³⁴ In particular, infiltration of tumor-associated macrophages

(TAMs) within tumor microenvironments relying upon CSF-1R for survival and differentiation, is associated with poor prognosis in numerous cancers.³⁵⁻³⁶ Thus, translation of **2.9** into a dual Trk/CSF-1R PET probe could be highly useful in many cases where cancer cells overexpress Trk receptors while abundant CSF-1R is found within the stromal cells due to high TAMs infiltration.³⁷⁻³⁹

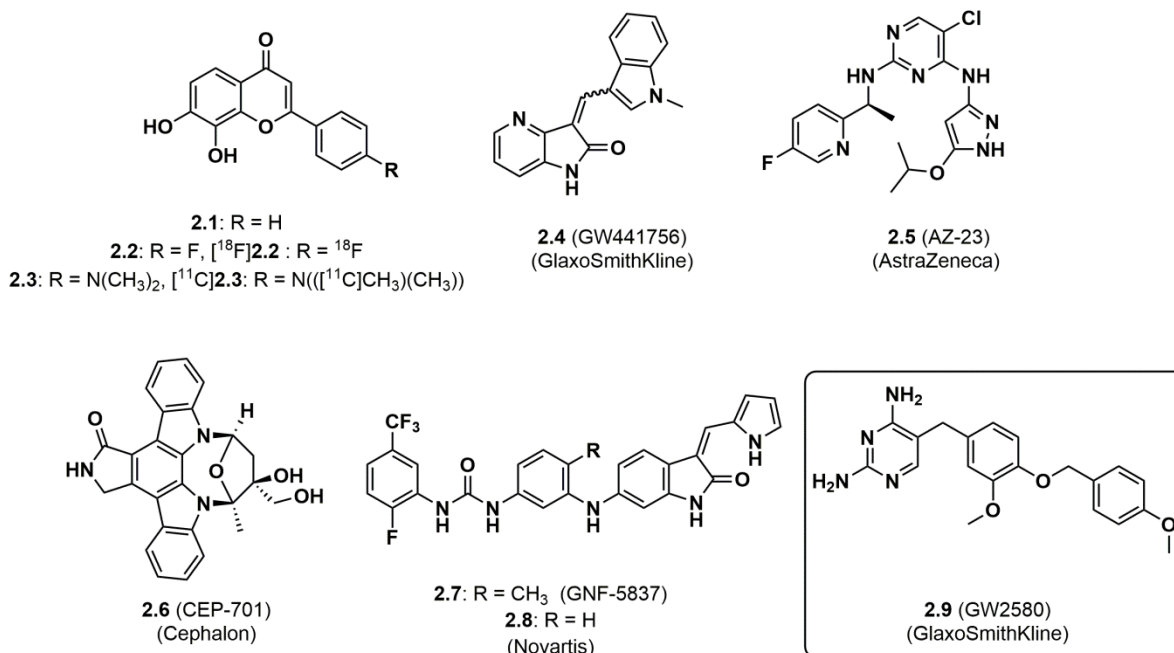


Figure 2.1. Chemical structures of selected Trk receptor ligands and radioligands.

2.3 Results and Discussion

2.3.1 Design of compounds. The structure of GW2580 possesses two aromatic methoxy moieties potentially amenable for carbon-11 ($t_{1/2} = 20$ min) labeling (**Figure 2.1**). However, fluorine-18 displays better nuclear properties ($t_{1/2} = 109$ min; 97% β^+ ; $E_{\max}(\beta^+) = 0.64$ MeV) which allow for a more flexible radiosynthesis and lead to high quality PET images. It is also documented that the introduction of fluorine into bioactive molecules may positively influence physicochemical properties and oxidative/hydrolytic metabolic stabilities.⁴⁰ This study thus describes the design, synthesis and biological evaluation of a small series of fluorinated analogs

of GW2580. The derivatives were selected in order to be accessible as ^{18}F -isotopologues. A new potent fluorinated Trk(B/C)/CSF-1R inhibitor **2.10** was identified, which was consequently labeled with fluorine-18. In addition, exhaustive selectivity profiling over a panel of 342 kinases established that **2.10** maintains the remarkable selectivity of the non-fluorinated lead compound **2.9**.

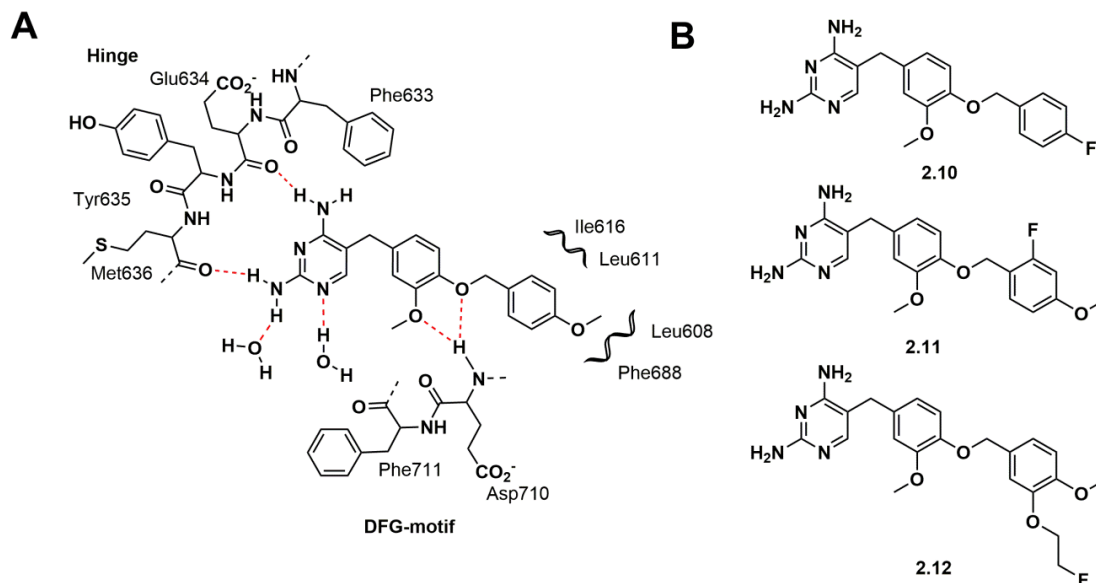
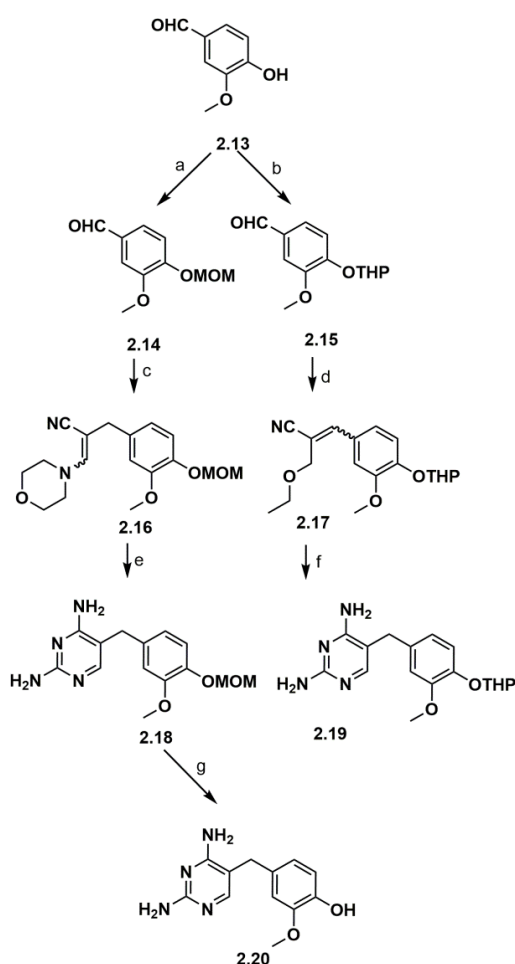


Figure 2.2. (A) Binding interactions of GW2580 (**2.9**) to TrkB based on the co-crystal structure of **2.9**-TrkB (PDB code: 4AT5). Hydrogen bonds between the ligand and the hinge region, DFG motif and adjacent water molecules are indicated with red dash lines. (B) Derivatization of the *para*-methoxybenzyl ring for the introduction of fluorine substituents accessible with common radiofluorination methods.

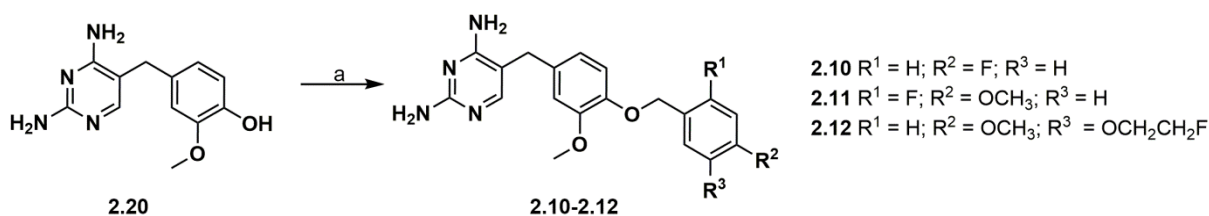
Three fluorinated derivatives of inhibitor **2.9** were rationally designed based on the available co-crystal structure of TrkB with GW2580 (PDB code: 4AT5)⁴¹ and developed with the objectives of maintaining the potency/selectivity profile of the lead while being amenable towards ^{18}F -labeling. Our rationale consisted of introducing structural modifications on the *para*-methoxybenzyl (PMB) ring occupying the selectivity hydrophobic pocket formed by residues Ile616, Leu611, Leu608 and Leu688. The diaminopyrimidine fragment in contact with the hinge region and the 1-(benzyloxy)-2-methoxybenzene central ring interacting with Asp710 from the

DFG motif (**Figure 2.2**) were left untouched. Inspection of the hydrophobic back pocket revealed that the *ortho*- and *para*-position of the tail fragment can probably only accommodate small structural modifications. The orientation from one side of the PMB ring left the *meta*-position solvent exposed thus suggesting that this position might be compatible with bulkier alterations. Therefore, fluoroaryl-derivatives **2.10** and **2.11** (*ortho* and *para*-activated position for labeling – *vide supra*) and the 2-fluoroethoxy-derivative **2.12** (**Figure 2.1B**) were synthesized and evaluated.

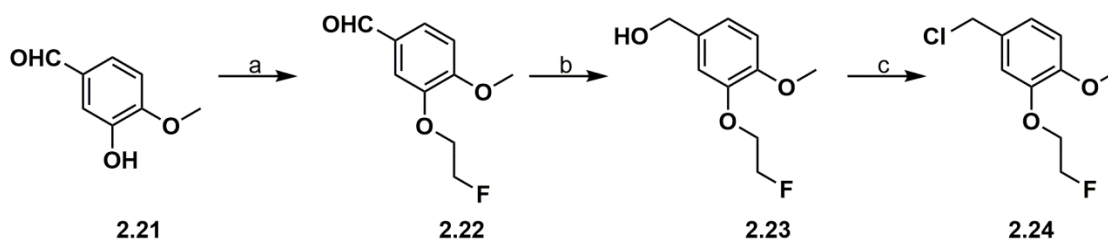


Scheme 2.1. Chemical synthesis of intermediate **2.20**. Reagents and conditions: (a) MOMCl, DIPEA, CH₂Cl₂, 0°C – rt, 30 min, then rt, 20 h; (b) 3,4-dihydro-2H-pyran, PPTS cat., CH₂Cl₂, rt, 12 h; (c) 3-morpholinopropionitrile, NaOMe, DMSO, 75°C, 1 h; (d) 3-ethoxypropionitrile, NaOEt, DMSO, 75°C, 1 h; (e) i. aniline.HCl, EtOH, reflux, 1 h; ii. guanidine.HCl, NaOEt, EtOH, reflux, 12 h; (f) guanidine.HCl, NaOEt, EtOH, reflux, 16 h (g) HCl conc., MeOH, rt, 5 h.

2.3.2 Chemical syntheses. First, we synthesized inhibitor **2.9** following the patent procedure reported by Shewchuk *et al.*⁴² to provide its first complete characterization (See **Supporting Information**). Two different synthetic approaches were used to obtain compounds **2.10-2.12**. The first method relied on the alkylation of the common 5-phenol-2,4-diaminopyrimidine intermediate **2.20** (**Scheme 2.1**). We envisioned that this fragment could also be used as nonradioactive precursor for the synthesis of [¹⁸F]**2.10** and [¹⁸F]**2.11** via simple alkylation employing ¹⁸F-fluorobenzyl halides.⁴³⁻⁴⁵ Our initial strategy towards **2.20** involved the direct catalytic hydrogenolysis of **2.9**. Disappointingly, this approach only delivered very low yields of **2.20** under the different conditions tested. Alternatively, the synthesis of **2.20** was envisioned via the deprotection of either the O-MOM- or O-THP-protected 2,4-diaminopyrimidine intermediates **2.18** and **2.19**. Those compounds were synthesized via condensation/cyclization using the protected vanillin **2.14** and **2.15** with either the 3-morpholinopropionitrile/aniline exchange strategy⁴⁶ or with 3-ethoxypropionitrile⁴⁷ followed by treatment with guanidine (**Scheme 2.1**). Overall, the cyclization with the β -morpholinopropionitrile intermediate proved far more useful than the synthesis of **2.19**. MOM deprotection of **2.18** afforded the phenol intermediate **2.20** in 28% overall yield from vanillin. Attempts to combine the use of the more labile THP protecting group with the 3-morpholinopropionitrile/aniline exchange strategy failed to yield **2.19** or **2.20**, presumably due to acid promoted aminolysis of the THP fragment in the presence of aniline hydrochloride.

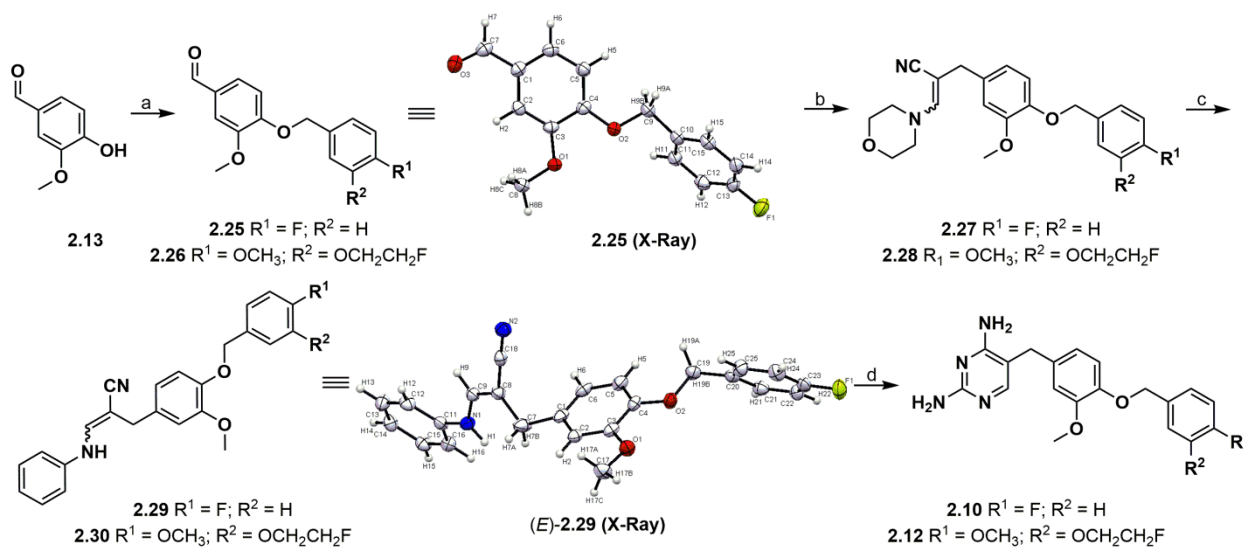


Scheme 2.2. Chemical synthesis of 2,4-diaminopyrimidines compounds **2.10-2.12**. Reagents and conditions: (a) K₂CO₃, benzyl halide derivative, DMSO, EtOH, rt, 12 h.



Scheme 2.3. Chemical synthesis of intermediate **2.24**. Reagents and conditions: (a) K_2CO_3 , 2-fluoroethyl 4-methylbenzenesulfonate (**S2.5**), DMF, rt, 10 h; (b) $LiAlH_4$, THF, $0^\circ C - rt$, 2-4 h; (c) cyanuric chloride, DMSO, rt, 5 min.

Alkylation of **2.20** with suitable benzyl halides afforded **2.10-2.12** in good yields (**Schemes 2 and 3**). Yet, the high polarity imparted by the common diaminopyrimidine moiety shared by **2.20** and **2.10-2.12** often led to the isolation of poorly separable residual starting material/alkylated product mixtures. We thus adapted a linear synthesis similar to the approach used to obtain **2.9** which is exemplified by the synthesis of **2.10** and **2.12** as depicted in **Scheme 2.4** (Intermediate **2.29** was recrystallized as a mixture of the *E* and *Z* geometric isomer. Only (*E*)-**2.29** was fully identified and illustrated in **Scheme 2.4**).



Scheme 2.4. Reagents and conditions: (a) Benzyl halide, K_2CO_3 , DMF, $70^\circ C/3$ h or $rt/12$ h rt ; (b) 3-morpholinopropionitrile, DMSO, $60-75^\circ C$, 40 min; (c) aniline.HCl, *i*-PrOH, $40^\circ C$, 30 min; (d) guanidine.HCl, NaOEt, EtOH, reflux, 16 h. Single-Crystal X-Ray structure of **2.25** and (*E*)-**2.29**; ellipsoids drawn at 70% probability.

2.3.3 Biological evaluations and in silico studies. The synthesized compounds were then evaluated for their inhibitory activity against TrkA, TrkB, TrkC and CSF-1R in comparison to GW2580 (**2.9**). The resulting IC₅₀s along with relevant physico-chemical properties are summarized in **Table 2.1** (dose-response curves are presented in **Scheme S1, Supporting Information**). Under assayed conditions, lead inhibitor **2.9** was shown to display moderate intra Trk isoform selectivity compared to K_d values reported with binding assays.²⁹⁻³¹ Fluorine-for-methoxy substitution had a negligible impact on the potency towards TrkB (IC₅₀ = 119 ± 38.7 nM for **2.10** versus IC₅₀ = 132 ± 12.0 nM for **9**). This highly potent fluorinated TrkB inhibitor **2.10** also displayed similar potencies for TrkC (135 ± 5.66 nM) and CSF-1R (169 ± 27.6 nM) and slightly improved selectivity towards TrkA. Therefore, **2.10** has a suitable affinity for PET imaging. Fluorinated compound **2.10** also showed a reduced surface polar area (TSPA) and increased cLogD/cLogP compared to **2.9** in a range which is favorable considering ideal physico-chemical properties for PET radiotracers.^{32, 48} Inhibitor **2.12** was 2- to 4.5-fold less potent towards Trk receptors and 28-fold less potent for CSF-1R as compared to **2.9**. Interestingly, replacement of one hydrogen for a fluorine atom in *ortho*-position in **2.11** had a dramatic negative impact on the potency for all four targets despite being the smallest structural modification of all tested derivatives (>100-fold decrease in potency). As expected, derivative **2.20**, lacking the tail benzyloxy fragment did not display kinase inhibition (**Table 2.1**).

In order to rationalize the unexpected potency leap between **2.9/2.10** and **2.11**, a molecular modeling study was performed using the X-ray co-crystal structure of TrkB-GW2580 complex (PDB ID: 4AT5) and CSF-1R co-crystal complex (PDB ID: 3LCO) with FITTED (FORECASTER platform).⁴⁹⁻⁵¹ The binding modes of compounds **2.10** and **2.11** in the ATP-binding cavity of TrkB (DFG-out), which as expected overlaid significantly with the resolved crystal structure of **2.9**, are depicted in **Figure 3A,B**. While key hydrogen bonds and hydrophobic interactions at the hinge and within the DFG motif do not differ between inhibitors, discrepancies occur at the

hydrophobic back pocket regarding the spatial orientation of the tail benzyl moiety. The fluorobenzyl ring in **2.10** displays the same perpendicular orientation relative to the central methoxybenzyl ring as the PMB ring in **2.9**.

Table 2.1. *In Vitro* Activity of Fluorinated Diaminopyrimidine Inhibitors **2.10-2.12**, **2.20** and **2.9**

| cpd | MW | clogD ^a | ClogP ^a | TPSA (Å ²) ^a | <i>In vitro</i> IC ₅₀ (nM) ^b | | | | IC ₅₀ TrkB/IC ₅₀ TrkC; IC ₅₀ TrkB/IC ₅₀ CSF-1R |
|-------------|-------|--------------------|--------------------|--|--|------------------------------------|--------------------------------------|--------------------------------------|---|
| | | | | | TrkA | TrkB | TrkC | CSF-1R | |
| 2.9 | 366.4 | 1.89 | 2.30 | 105.51 | 338 ± 29.0 (630) ^c | 119 ± 38.7 (36) ^c | 69.1 ± 0.99 (120) ^c | 33.0 ± 10.8 (2.2) ^c | 2.84;3.61 |
| 2.10 | 354.4 | 2.35 | 2.80 | 96.28 | 663 ± 19.8 | 132 ± 12.0 | 135 ± 5.66 | 169 ± 27.6 | 5.02;0.78 |
| 2.11 | 384.4 | - | 2.75 | 105.53 | ni ^d | >10000 | >10000 | 5060 ± 226 | - |
| 2.12 | 428.5 | - | 2.55 | 114.77 | 674 ± 79.2 | 409 ± 3.54 | 309 ± 31.2 | 939 ± 115 | 1.65;0.44 |
| 2.20 | 246.3 | - | 0.70 | 107.29 | ni ^d | ni ^d | ni ^d | ni ^d | - |

^a Values were computed with the program Pallas 3.7 for Windows (CompuDrug; San Francisco, CA). cLogD at pH = 7.4. ^b All data given in nM and are an average of duplicate measurements. ^c K_D values in nM from Ref. 30. ^d ni = no inhibition (at 10⁻⁵ M).

This conformation is also favoured considering the lowest energy conformation in this motif and presumably allows for the optimal interaction with the hydrophobic pocket residues. In contrast, the *ortho*-fluoro PMB fragment in **2.11** is distorted from this conformation (**Figure 2.3C**). The *ortho*-hydrogen atoms (position 2- and 6-) in **2.9** are positioned in close proximity (2.8 Å) to the oxygen atom from the carbonyl groups from both sides, namely residues Asp710

and Val617 – which is inferior to the sum of the van der Waals radii of fluorine and oxygen (2.99 Å).

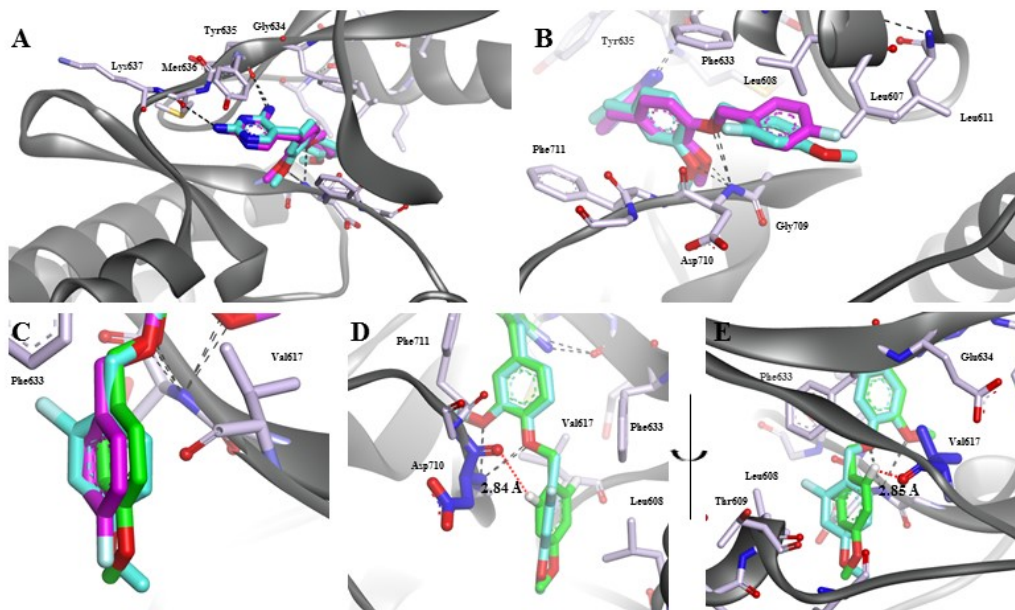


Figure 2.3. Predicted binding poses of **2.10** (purple) and **2.11** (cyan) bound to TrkB (PDB code: 4AT5) showing (A) the hinge binding interactions and (B) the interaction with Asp710 from the DFG motif (hydrogen bonds are depicted with black dash lines). (C) Superposition of the docking pose of **2.10** and **2.11** with the crystal structure of GW2580-TrkB illustrating the disruption in the orientation of the benzyloxy moiety in **2.11** compared to GW2580 and **2.10**. (D-E) Opposite angles presenting the overlay between the *ortho*-fluoro diaminopyrimidine derivative **2.11** docking pose and the distances between the *ortho*-hydrogen of GW2580 (green) and the oxygen from the carbonyl group of the residues Asp710 and Val617 (highlighted in blue; distances are depicted with red lines).

Those unfavorable electrostatic interactions, exacerbated in **2.11** as compared to **2.9** when considering the longer C-F bond compared to C-H, results in the distorted and seemingly disfavored orientation of the tail group of **2.11** (Figure 2.3D,E) – similar interactions occur with CSF-1R (Figure S2.2, Supporting Information). Moreover, even in this conformation, the fluorine substituent is potentially forced to lie in the vicinity of Asp710 only, due to the overlapping proximity of the side chain from Val617 if oriented towards the back of the hydrophobic cavity. In addition, conformational factors involving intermolecular hydrogen bonding of the solvated ligand, reminiscent of the intramolecular interactions observed in *ortho*-

fluorobenzyl alcohol structures⁵² and *ortho*-fluoro arylamides⁵³⁻⁵⁴, may also contribute to the poor relative potency of **2.11** through the stabilisation of suboptimal conformations for binding (Figure S2.3, Supporting Information).

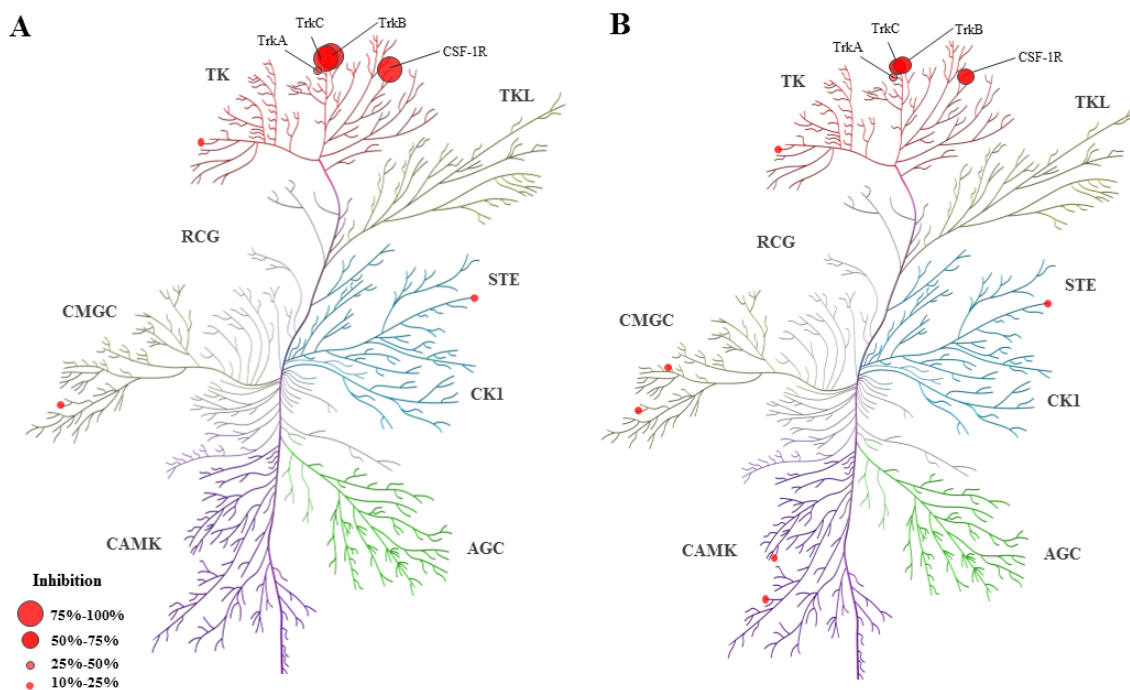
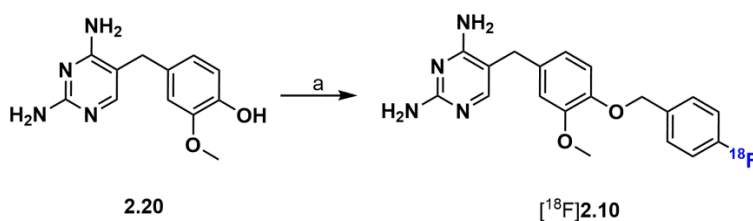


Figure 2.4. Selectivity profile of compound (A) **2.10** and (B) **2.12** tested on a panel of 342 kinases. The kinome dendrogram represents the percent of inhibition at 1.0 μ M of inhibitors. The measurements were performed using a [γ -³³P]ATP-based enzymatic assay performed by Reaction Biology Corporation and the dendrogram was obtained from Kinase Mapper (Reaction Biology).

Apart from its high affinity, the selection of GW2580 as a lead in our radiotracer development program was motivated by its exceptional selectivity. The observed profound impact of small structural modifications on the selected panel of four kinases tested prompted us to conduct comprehensive kinase selectivity profiling of our fluorinated inhibitors. Compound **2.10**, as well as the less potent derivative **2.12**, were tested in enzymatic assays on a panel of 342 kinases (Reaction Biology Corporation, full wild type kinase panel, Figure 2.4, Supporting

Information). In the presence of 1.0 μM of **2.10**, only TrkB, TrkC and CSF-1R were strongly inhibited – remaining activity inferior to 25% compared to DMSO control (**Figure 2.4A**). Compound **2.10** also showed moderate TrkA inhibition ($55.7 \pm 1.4\%$ remaining activity) and negligible inhibition of only few other kinases (CDK6, HGK/MAP4K4, TXK). A similar kinase profile was obtained for **2.12** with few more off-target minor inhibitions (**Figure 2.4B**, 10-25% inhibition: CDK6, CK1g3, DAPK2, ERK5/MAPK7, HGK/MAP4K4, SNARK/NUAK2, TXK). Those results confirmed the retention of the high selectivity of **2.10** towards TrkB/TrkC/CSF-1R relative to the non-fluorinated lead and encourage its further development into a radiolabeled probe.



Scheme 2.5. Radiosynthesis of $[^{18}\text{F}]\mathbf{2.10}$. Reagents and conditions: (a) $[^{18}\text{F}]\mathbf{S2.8}$, Cs_2CO_3 , TBAI, DMSO/EtO₂ (2:1), 100°C, 10 min.

2.3.4 Radiosynthesis of $[^{18}\text{F}]\mathbf{2.10}$. In preliminary radiolabeling experiments, $[^{18}\text{F}]\mathbf{2.10}$ was prepared via the alkylation of precursor **2.20** with $[^{18}\text{F}]\text{fluorobenzyl bromide}$ ($[^{18}\text{F}]\mathbf{S2.8}$, **Scheme 2.5**, **Supporting Information**). Alkylation leading to $[^{18}\text{F}]\mathbf{2.10}$ was performed in radiochemical yield (RCY) of 13% (HPLC incorporation yield, non-decay corrected) in the presence of Cs_2CO_3 and tetrabutylammonium iodide (TBAI) at 100°C for 10 min. $[^{18}\text{F}]\mathbf{S2.8}$ was obtained following an on-cartridge procedure adapted from Lemaire *et al.*⁴⁵ starting with 4-formyl-*N,N,N*-trimethylanilinium triflate (**S2.5**). The radiosynthesis of $[^{18}\text{F}]\mathbf{S2.8}$ was typically accomplished in 25-30% RCY (non-decay corrected) as a crude mixture (>85% $[^{18}\text{F}]\mathbf{S2.8}$ containing residual 4- $[^{18}\text{F}]\text{fluorobenzaldehyde}$ – $[^{18}\text{F}]\mathbf{S2.6}$, **Supporting Information**) which was used directly in the alkylation step. The multi-step approach used, carried out manually, despite being sufficient for evaluation purposes, will be difficult to implement into an automated synthesis unit for routine

production. Therefore, an alternative and more straightforward route to [^{18}F]**2.10** will be developed, such as a diaryliodonium salt strategy.⁵⁵⁻⁵⁶

2.4 Conclusion

In conclusion, starting from the known inhibitor **2.9** a potent and highly selective fluorinated TrkB/TrkC/CSF-1R inhibitor, **2.10**, was designed and labeled with fluorine-18. The remarkable selectivity profile of **2.10** was confirmed by exhaustive kinase profiling. Those initial results, together with our preliminary radiosynthesis study, warrant further evaluation of [^{18}F]**2.10** as a uniquely selective tool to assess TrkB, TrkC and CSF-1R level in vivo with PET. Imaging studies in Trk-positive tumor bearing nude mice, especially TrkB-overexpressing neuroblastoma xenograft models, will be reported in due course.

Supporting Information.

Supporting information available. Syntheses of **2.9** and 2-fluoroethyl 4-methylbenzenesulfonate, [^{18}F]**2.31**, supplementary **Figures S2.1-S2.3** and **Scheme S2.1**, kinase profiling data for inhibitors **2.10** and **2.12** and crystallographic data for compounds **2.25** and (*E*)-**2.29**.

Author Information.

*To whom the correspondence should be addressed. Prof. R. Schirmmacher. Fax: (+1) 514-396-1857; e-mail: ralf.schirmmacher@mcgill.ca

Acknowledgement.

We thank Mehdi Boudjemeline for his support with the collection of the NMR data. We thank Marilyn Grand'Maison for the valuable help for the preparation of figures. This work was financially supported by Canada Foundation for Innovation (CFI) project no. 203639 to R.S.

2.5 Supporting Information of Article 5

5-(4-((4-[¹⁸F]fluorobenzyl)oxy)-3-methoxybenzyl)pyrimidine-2,4-diamine: A Selective Dual Inhibitor for Potential PET Imaging of Trk/CSF-1R

Vadim Bernard-Gauthier^{1,2} & Ralf Schirmacher^{2,3}*

¹Experimental Medicine, Department of Medicine, McGill University, 1110 Pine Avenue West, Montreal, QC, H3A 1A3. ²Department of Oncology, University of Alberta, 11560 University Avenue, Edmonton, AB, Canada, T6G 1Z2. ³McConnell Brain Imaging Centre, Montreal Neurological Institute, McGill University, 3801 University Street, Montreal, QC, Canada, H3A 2B4. *Corresponding author

CONTENT OF SUPPORTING INFORMATION

1. CHEMISTRY
2. BIOLOGICAL EVALUATION
3. DOCKING SIMULATION.
4. COMPUTATION OF PHYSICO-CHEMICAL PROPERTIES
5. FIGURES (**Figure S2.1-S2.3**)
6. RADIOCHEMISTRY
7. CRYSTALLOGRAPHY DATA FOR COMPOUNDS **2.25** AND **2.29**.

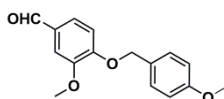
1. CHEMISTRY

1.1 Material and Methods.

General. All moisture sensitive reactions were carried out in oven-dried flasks under nitrogen atmosphere with dry solvents. Reagents and solvents were purchased at the highest commercial quality from Sigma-Aldrich, Acros or Alfa-Aesar, and were used without further purification unless specified otherwise. 4-Formyl-*N,N,N*-trimethylanilinium triflate (**S2.5**) was purchased from ABX Advanced Biochemical Compounds. Organic solutions were concentrated under reduced pressure on a Heidolph rotary evaporator. In general, reactions were magnetically stirred and monitored by TLC performed on pre-coated glass-backed TLC plates (Analtech, 250 microns) and chromatographic purification of products was accomplished using flash chromatography on Alfa-Aesar silica gel (230-450 mesh). TLC visualization was performed by fluorescence quenching, KMnO_4 or ninhydrin. ^1H NMR and ^{13}C NMR spectra were recorded on a 300 Varian Mercury spectrometer in CDCl_3 or d_6 -DMSO and peak positions are given in parts per million using TMS as internal standard. ^{19}F NMR spectra were recorded on a 200 Varian Mercury in CDCl_3 or d_6 -DMSO and peak positions are given in parts per million using CFCl_3 as internal standard. Peaks are reported as: s = singlet, d = doublet, t = triplet, q = quartet, p = quintet, m = multiplet, b = broad; coupling constant(s) in Hz; integration. High Resolution Mass Spectra (HRMS) were obtained from the Regional Center for Mass Spectrometry of The Chemistry Department of the Université de Montréal (LC-MSD-TOF Agilent). No-carrier-added (n.c.a) aqueous [^{18}F]fluoride was prepared by the $^{18}\text{O}(\text{p},\text{n})^{18}\text{F}$ nuclear reaction on an enriched [^{18}O]water (98 %) target.

The synthesis of compounds **S2.1-S2.3**, **S2.4** and **2.9** were adapted from reported procedures.^{42, 57-58}

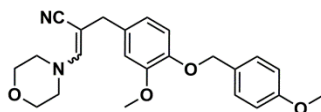
1.2 Chemical synthesis of GW2580 (2.9) and intermediates.



1.2.1. 3-Methoxy-4-((4-methoxybenzyl)oxy)benzaldehyde (S2.1). To a heterogeneous mixture of 4-hydroxy-3-methoxybenzaldehyde (3.0 g, 19.7 mmol, 1 equiv.) and K_2CO_3 (6.53 g, 47.3 mmol, 2.4 equiv.) in DMF (55 mL) at room temperature was added dropwise 4-

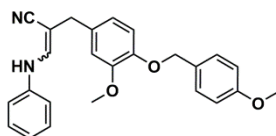
methoxybenzyl chloride (3.18 g, 20.9 mmol, 1.06 equiv.). The mixture was heated at 70°C for 3 h, cooled and concentrated under reduced pressure. The crude residue was taken in diethyl ether (200 mL) and the organic layer was washed with water (200 mL). The aqueous phase was subsequently extracted with diethyl ether (100 ml) and CH₂Cl₂ (2 X 100 mL). The combined organic phases were washed water (100 mL), brine (100 mL), dried over Na₂SO₄ and concentrated *in vacuo*. The crude residue was triturated from CHCl₃/hexane and washed with cold hexane to afford 4.94 g of the title compound as a white solid (92%).

¹H NMR (300 MHz, CDCl₃) δ 9.83 (s, 1H), 7.42 – 7.35 (m, 4H), 7.00 (d, *J* = 8.1 Hz, 1H), 6.91 (dd, *J*₂ = 8.7 Hz, *J*₁ = 2.1 Hz, 1H), 5.16 (s, 2H), 3.93 (s, 3H), 3.80 (s, 3H) ppm. ¹³C NMR (75 MHz, CDCl₃) δ 190.9, 159.6, 153.7, 150.0, 130.2, 129.0, 127.9, 126.6, 114.1, 112.3, 109.2, 70.7, 56.0, 55.2 ppm. HRMS (ESI) calcd for C₁₆H₁₆O₄ (M+H)⁺ 273.11214, found 273.1132.



1.2.2. 2-(3-Methoxy-4-((4-methoxybenzyl)oxy)benzyl)-3-morpholinoacrylonitrile (S2.2). The aldehyde **S2.1** (1.09 g, 4 mmol, 1 equiv.) and 3-morpholinopropionitrile (617 mg, 4.4 mmol, 1.1 equiv.) were stirred in DMSO (4 mL) at 65°C. Upon homogenisation, the reaction mixture was cooled to 40°C and sodium methoxide (2.66 mL from 0.5M in MeOH, 1.33 mmol, 0.3 equiv.) was added. The mixture was stirred at 75°C for 15-25 minutes and cooled to room temperature. CH₂Cl₂ (40 mL) and brine (40 mL) were added and the two layers were separated. The organic phase was dried over Na₂SO₄ and concentrated *in vacuo*. The crude reddish oil obtained was purified by flash chromatography (50% EtOAc/hexane) and afforded 1.19 g of the title compound as a yellow oil (76%).

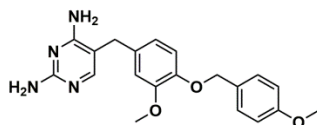
¹H NMR (300 MHz, CDCl₃) δ 7.35 (d, *J* = 8.4 Hz, 2H), 6.89 (d, *J* = 8.4 Hz, 2H), 6.87 - 6.68 (m, 3H), 6.20 (s, 1H) (olefinic proton), 5.05 (s, 1H) (olefinic proton), 3.87 (s, 3H), 3.80 (s, 3H), 3.70 (t, *J* = 5.1 Hz, 4H), 3.46 (t, *J* = 5.1 Hz, 4H), 3.30 (s, 2H) ppm. ¹³C NMR (75 MHz, CDCl₃) δ 159.3, 149.7, 148.8, 147.0, 132.5, 129.2, 129.0, 120.3, 114.2, 114.0, 113.9, 112.2, 75.4, 70.9, 66.3, 56.0, 55.3, 49.5, 38.9 ppm. HRMS (ESI) calcd for C₂₃H₂₇N₂O₄ (M+H)⁺ 395.19653, found 395.19671.



1.2.3. 2-(3-Methoxy-4-((4-methoxybenzyl)oxy)benzyl)-3-(phenylamino)acrylonitrile (S2.3).

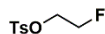
To a solution of 2-(3-methoxy-4-((4-methoxybenzyl)oxy)benzyl)-3-morpholinoacrylonitrile (1.45 g, 3.67 mmol, 1 equiv.) in isopropanol (5.0 mL) was added aniline hydrochloride (0.49 g, 3.75 mmol, 1.02 equiv.). The reaction mixture was stirred at reflux for 20 minutes, combined with 2.0 mL of water and cooled in an ice bath for 30 minutes. The resulting precipitate was filtered off, washed with water and air dried. The crude residue was recrystallized from methanol/ethanol to afford 1.12 g of the pure title product as crystalline beige needles (76%).

^1H NMR (300 MHz, $\text{DMSO-}d_6$) δ 9.08 (d, J = 12.9 Hz, 1H), 7.64 (d, J = 12.9 Hz, 1H), 7.34 (d, J = 8.7 Hz, 2H), 7.28 – 7.15 (m, 4H), 6.98 – 6.87 (m, 5H), 6.74 (dd, J_2 = 6.9 Hz, J_1 = 1.2 Hz, 1H), 4.94 (s, 2H), 3.73 (s, 3H), 3.72 (s, 3H), 3.54 (s, 2H) ppm. ^{13}C NMR (75 MHz, $\text{DMSO-}d_6$) δ 159.4, 149.5, 146.9, 141.9, 141.0, 131.7, 129.8, 129.5, 123.3, 131.9, 120.4, 115.6, 114.2, 112.9, 110.0, 82.9, 70.2, 55.9, 55.5, 31.5 ppm. HRMS (ESI) calcd for $\text{C}_{25}\text{H}_{24}\text{N}_2\text{O}_3$ ($\text{M}+\text{H}$) $^+$ 401.18597, found 401.18447.

**1.2.4. 5-(3-Methoxy-4-((4-methoxybenzyl)oxy)benzyl)pyrimidine-2,4-diamine (2.9).**

2-(3-methoxy-4-((4-methoxybenzyl)oxy)benzyl)-3-(phenylamino)acrylonitrile (300 mg, 0.75 mmol, 1 equiv.) was suspended in EtOH (5 mL) and guanidinium chloride (108 mg, 1.13 mmol, 1.5 equiv.) was added. The reaction mixture was stirred at room temperature while sodium ethoxide (77 mg, 1.13 mmol, 1.5 equiv.) was added. The reaction mixture was stirred at reflux for 12 h. The mixture was cooled at 5°C and aqueous sodium hydroxide (2 mL, 2N solution) was added. The mixture was allowed to precipitate at 5°C for 15 minutes and filtered. The precipitate was successively washed with a mixture of cold ethanol/water (1:1), EtOAc and hexane and dried *in vacuo* to afford 212 mg of the title compound as a white amorphous solid (77%).

^1H NMR (300 MHz, $\text{DMSO-}d_6$) δ 7.45 (s, 1H), 7.32 (d, J = 8.7 Hz, 2H), 6.91 (d, J = 8.7 Hz, 2H), 6.89 (d, J = 8.1 Hz, 1H), 6.85 (d, J = 1.8 Hz, 1H), 6.65 (dd, J_2 = 8.4 Hz, J_1 = 1.5 Hz, 1H), 6.06 (s, 2H), 5.66 (s, 2H), 4.91 (s, 2H), 3.73 (s, 3H), 3.69 (s, 3H), 3.49 (s, 2H) ppm. ^{13}C NMR (75 MHz, $\text{DMSO-}d_6$) δ 162.7, 162.6, 159.4, 156.0, 149.4, 146.5, 133.4, 130.0, 129.8, 129.6, 120.6, 115.6, 114.2, 113.2, 106.5, 70.2, 22.9, 55.5, 32.7 ppm. HRMS (ESI) calcd for $\text{C}_{20}\text{H}_{22}\text{N}_4\text{O}_3$ ($\text{M}+\text{H}$) $^+$ 367.17647, found 367.1753.



1.2.5. 2-Fluoroethyl 4-methylbenzenesulfonate (S2.5). To a solution of 2-fluoroethanol (5.0 g, 78.1 mmol, 1 equiv.) in pyridine (25 mL) was added 4-methylbenzene-1-sulfonyl chloride (17.9 g, 93.7 mmol, 1.2 equiv.) in five portions over 30 min. The reaction mixture was stirred at room temperature for 24 h and the volume was reduced *in vacuo*. The residue was taken in 1N aqueous HCl (50 mL) and extracted with CHCl₃ (4 X 50 mL). The combined organic phases were dried over Na₂SO₄ and concentrated *in vacuo*. The crude product was purified by flash chromatography (30% EtOAc/hexane) to afford 10.6 g of the title compound as a colorless solid (92%).

¹H NMR (300 MHz, CDCl₃) δ 7.80 (d, *J* = 8.1 Hz, 2H), 7.36 (d, *J* = 8.1 Hz, 2H), 4.56 (dt, *J*₂ = 47.1 Hz, *J*₁ = 1.5 Hz, 2H), 4.25 (dt, *J*₂ = 27.3 Hz, *J*₁ = 3.9 Hz, 2H), 2.45 (s, 3H) ppm. ¹³C NMR (75 MHz, CDCl₃) δ 145.2, 132.6, 129.9, 128.0, 80.5 (d, *J* = 172.7 Hz), 68.5 (d, *J* = 20.8 Hz), 21.7 ppm. ¹⁹F NMR (188 MHz, DMSO-*d*₆) δ -224.66 ppm. HRMS (ESI) calcd for C₉H₁₂FO₃S (M+H)⁺ 219.04857, found 219.04849.

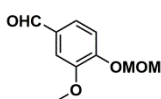
1.3 Chemical synthesis.

1.3.1. General procedure for the synthesis of 2,4-diaminopyrimidine derivatives from 4-((2,4-diaminopyrimidin-5-yl)methyl)-2-methoxyphenol (20). Syntheses of 2.10, 2.11, 2.12. To a solution of 4-((2,4-diaminopyrimidin-5-yl)methyl)-2-methoxyphenol and K₂CO₃ (2 equiv.) in DMSO (3 mL/mmol) was added dropwise a solution of substituted benzyl chloride (1.5 equiv.) in EtOH (3 mL/mmol). The reaction mixture was stirred for 12 h at room temperature, then concentrated *in vacuo*, diluted in EtOAc (10mL) and directly eluted on a silica plug (0 – 10 % MeOH/EtOAc) to give the pure corresponding 2,4-diaminopyrimidine derivatives.

1.3.2. General procedure for the synthesis of 2,4-diaminopyrimidine derivatives from 3-morpholinoacrylonitrile intermediates. Syntheses of 2.18, 2.29, 2.30, 2.10 and 2.12. Step 1: The morpholinoacrylonitrile intermediate was dissolved in *i*-PrOH (0.1M) at 40°C and anilinium chloride (1.05 equiv.) was added in one portion. The reaction mixture was stirred at reflux for 20 – 30 min and cooled at room temperature. Water was added (40% of *i*-PrOH volume) and the reaction mixture was cooled in an ice bath for 30 minutes. The resulting precipitate was filtered, washed with water and air dried. The crude phenylamino-acrylonitrile residue was recrystallized from methanol/ethanol and used in the next. If no precipitate formed, the reaction mixture was

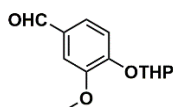
dilute with water, extracted with EtOAc, dried over Na₂SO₄ and concentrated *in vacuo* and the crude phenylamino-acrylonitrile residue was directly used in the next without further purification.

Step 2: The crude phenylamino-acrylonitrile was suspended in EtOH (0.15 M) at room temperature and guanidinium chloride (1.5 equiv.) was added in one portion. Sodium ethoxide (1.5 equiv.) was added and the reaction mixture was stirred at reflux overnight. The mixture then was cooled at 5°C and aqueous sodium hydroxide (2N solution, 40% of EtOH volume) was added. The mixture was allowed to precipitate at 5°C for 15 minutes and filtered. The precipitate was successively washed with a mixture of cold EtOH/water (1:1), EtOAc and hexane and dried *in vacuo* to give the pure corresponding 2,4-diaminopyrimidine derivative.



1.3.4. 3-Methoxy-4-(methoxymethoxy)benzaldehyde (2.14). To an ice cold mixture of 4-hydroxy-3-methoxybenzaldehyde (3.04 g, 20 mmol, 1 equiv.) and *N,N*-diisopropylethylamine (2.83 g, 22 mmol, 1.1 equiv.) in CH₂Cl₂ (50 mL) was added chloromethyl methyl ether (1.76 g, 22 mmol, 1.1 equiv.). Following addition, the reaction mixture was allowed to warm at room temperature and stirred at this temperature for 20 h. Water was added to the mixture and the aqueous phase was extracted with CH₂Cl₂. The combined organic phases were dried over Na₂SO₄ and concentrated *in vacuo*. The crude product was purified by flash chromatography (20% EtOAc/hexane) to afford 3.60 g of the title compound as a pale yellow oil (92%). R_f 0.24 (20% EtOAc/hexane).

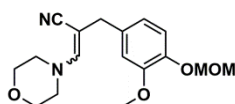
¹H NMR (300 MHz, CDCl₃) δ 9.84 (s, 1H), 7.41 – 7.38 (m, 2H), 7.25 (d, *J* = 9.0 Hz, 1H), 5.30 (s, 2H), 3.92 (s, 3H), 3.49 (s, 3H) ppm. ¹³C NMR (75 MHz, CDCl₃) δ 191.0, 151.9, 150.0, 131.0, 126.4, 114.6, 109.4, 94.5, 56.5, 56.0 ppm. HRMS (ESI) calcd for C₁₀H₁₃O₄ (M+H)⁺ 197.08084, found 197.0809.



1.3.5. 3-Methoxy-4-((tetrahydro-2H-pyran-2-yl)oxy)benzaldehyde (2.15). To a mixture of 4-hydroxy-3-methoxybenzaldehyde (4.56 g, 30 mmol, 1 equiv.) and pyridinium *p*-toluenesulfonate (754 mg, 3.0 mmol, 0.1 equiv.) in CH₂Cl₂ (200 mL) was added 3,4-dihydro-2H-pyran (3.83 mL, 45 mmol, 1.5 equiv.). The reaction mixture was stirred at room temperature for 24 h and water

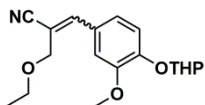
was added. The aqueous phase was extracted with CH_2Cl_2 and the combined organic phases were dried over Na_2SO_4 and concentrated *in vacuo*. The crude product was purified by flash chromatography (50% EtOAc/hexane) to afford 4.39 g of the title compound as a colorless oil (62%). R_f 0.74 (50% EtOAc/hexane).

^1H NMR (300 MHz, CDCl_3) δ 9.82 (s, 1H), 7.39 (s, 1H), 7.38 (dd, $J_2 = 46.6$ Hz, $J_1 = 1.8$ Hz, 1H), 7.21 (d, $J = 8.7$ Hz, 1H), 5.51 (t, $J = 3.0$ Hz, 1H), 3.88 (s, 3H), 3.86 – 3.82 (m, 1H), 3.64 - 3.55 (m, 1H), 2.11 - 1.79 (m, 3H), 1.74 -1.56 (m, 3H) ppm. ^{13}C NMR (75 MHz, CDCl_3) δ 191.0, 151.9, 150.3, 130.8, 126.3, 115.5, 109.8, 96.8, 62.1, 56.0, 30.0, 25.0, 18.5 ppm. HRMS (ESI) calcd for $\text{C}_{13}\text{H}_{16}\text{NaO}_4$ ($\text{M}+\text{Na}$) $^+$ 259.09408, found 259.09361.



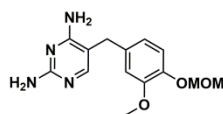
1.3.6. 2-(3-Methoxy-4-(methoxymethoxy)benzyl)-3-morpholinoacrylonitrile (2.16). To a solution of 3-methoxy-4-(methoxymethoxy)benzaldehyde (3.50 g, 17.84 mmol, 1 equiv.) in DMSO (15 mL) was added NaOMe (10.7 mL from 0.5M MeOH solution, 5.35 mmol, 0.3 equiv.). The reaction mixture was heated at 70°C for 1 h and quenched by addition of brine (50 mL) and extracted with CH_2Cl_2 (3 X 50 mL). The organic phase was dried over Na_2SO_4 and concentrated *in vacuo* and the crude residue was purified by flash chromatography (30% EtOAc/hexane) to afford 4.24 g of the title compound as a yellow gum (75%). R_f 0.20 (30% EtOAc/hexane).

^1H NMR (300 MHz, CDCl_3) δ 7.07 (d, $J = 8.4$ Hz, 1H), 6.77 (d, $J = 2.1$ Hz, 1H), 6.73 (dd, $J_2 = 8.1$ Hz, $J_1 = 2.1$ Hz, 1H), 6.22 (s, 1H), 5.19 (s, 2H), 3.87 (s, 3H), 3.69 (t, $J = 4.5$ Hz, 4H), 3.50 (s, 3H), 3.46 (t, $J = 4.5$ Hz, 4H), 3.31 (s, 2H) ppm. ^{13}C NMR (75 MHz, CDCl_3) δ 149, 7, 148.8, 145.2, 133.8, 120.4, 120.1, 116.5, 112.1, 95.5, 75.3, 66.3, 56.2, 55.9, 49.5, 39.0 ppm. HRMS (ESI) calcd for $\text{C}_{17}\text{H}_{23}\text{N}_2\text{O}_4$ ($\text{M}+\text{H}$) $^+$ 319.16523, found 319.16543.



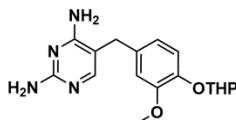
1.3.7. 2-(Ethoxymethyl)-3-(3-methoxy-4-((tetrahydro-2H-pyran-2-yl)oxy)phenyl)acrylonitrile (2.17). To a solution of 3-methoxy-4-((tetrahydro-2H-pyran-2-yl)oxy)benzaldehyde (118.0mg, 0.5mmol, 1.0 equiv.) in DMSO (5 mL) was added 3-ethoxypropanenitrile (0.06 mL, 0.525 mmol, 1.05 equiv.). The reaction was stirred 10 minutes at 40°C and to the reaction mixture was added sodium ethoxide (7.0 mg, 0.1, 0.2 equiv.) and

finally heated at 75°C until completion as monitored by TLC. The reaction was cooled to room temperature and poured into 20 mL of ice-cold water. The aqueous phase was extracted with dichloromethane. The combined organic phases were dried over Na₂SO₄ and concentrated *in vacuo*. The crude residue was purified by flash chromatography (25% EtOAc/hexane) and afforded 119.03 g of the title compound as a wide powder (75%). R_f 0.52 (25% EtOAc/hexane). ¹H NMR (300 MHz, CDCl₃) δ 7.40 (m, 2H), 7.23 (d, *J* = 8.7 Hz, 1H), 7.05 (bs, 1H), 5.46 (t, *J* = 3.3 Hz, 1H), 4.18 (d, *J* = 1.2 Hz, 2H), 3.90 (s, 3H), 3.64-3.50 (m, 4H), 2.09-1.57 (m, 6H), 1.25 (t, *J* = 6.9 Hz, 3H) ppm. ¹³C NMR (75 MHz, CDCl₃) δ 149.9, 148.4, 144.6, 127.1, 123.7, 118.4, 116.5, 111.4, 97.0, 96.8, 71.9, 66.1, 62.1, 56.0, 30.1, 25.1, 18.6, 15.0 ppm. HRMS (ESI) calcd for C₁₈H₂₃NNaO₄ (M+Na)⁺ 340.15193, found 340.15099.



1.3.8. 5-(3-Methoxy-4-(methoxymethoxy)benzyl)pyrimidine-2,4-diamine (2.18). The general procedure 1.3.2 for the cyclization of 3-morpholinoacrylonitriles with guanidine was followed starting with 1.59 g (5 mmol) of 2-(3-methoxy-4-(methoxymethoxy)benzyl)-3-morpholinoacrylonitrile (**2.16**). The title compound (980 mg, 67%) was obtained as white needles. R_f 0.30 (10% MeOH/EtOAc).

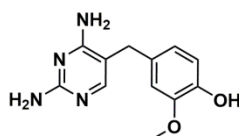
¹H NMR (300 MHz, DMSO-*d*₆) δ 7.47 (s, 1H), 6.93 (d, *J* = 8.4 Hz, 1H), 6.89 (s, 1H), 6.66 (d, *J* = 8.1 Hz, 1H), 6.07 (bs, 2H), 5.70 (bs, 2H), 5.06 (s, 2H), 3.71 (s, 3H), 3.51 (s, 2H), 3.35 (s, 3H) ppm. ¹³C NMR (75 MHz, DMSO-*d*₆) δ 162.6(3), 162.6(2), 156.0, 150.1, 144.4, 135.1, 120.6, 117.6, 113.4, 106.4, 95.5, 56.0, 55.9, 32.8 ppm. HRMS (ESI) calcd for C₁₄H₁₉N₄O₃ (M+H)⁺ 291.14517, found 291.14559.



1.3.9. 5-(3-Methoxy-4-((tetrahydro-2H-pyran-2-yl)oxy)benzyl)pyrimidine-2,4-diamine (2.19). To a solution of 2-(ethoxymethyl)-3-(3-methoxy-4-((tetrahydro-2H-pyran-2-yl)oxy)phenyl)acrylonitrile (1.59 g, 5 mmol, 1 equiv.) in EtOH (50 mL) was added solution of guanidinium chloride (2.89 g, 25 mmol, 5 equiv.) and NaOEt (1.70 g, 25 mmol, 5 equiv.) in EtOH

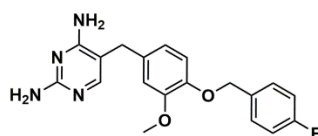
(10 mL). The reaction mixture was refluxed for 16 h and then concentrated *in vacuo*. The crude residue was purified on a silica plug (0 – 10 % MeOH/1% Et₃N/EtOAc) to afford 206 mg of the title compound as a white amorphous solid (12%). $R_f = 0.20$ (10% MeOH/EtOAc). R_f 0.10 (10% MeOH/EtOAc).

¹H NMR (300 MHz, DMSO-*d*₆) δ 7.47 (s, 1H), 6.94 (d, *J* = 8.4 Hz, 1H), 6.88 (d, *J* = 1.8 Hz, 1H), 6.65 (dd, *J*₂ = 8.1 Hz, *J*₁ = 1.8 Hz, 2H), 6.05 (bs, 2H), 5.67 (bs, 2H), 5.28 (d, *J* = 3.3 Hz, 1H), 3.85 – 3.78 (m, 1H), 3.71 (s, 3H), 3.51 (s, 2H), 3.49 – 3.45 (m, 1H), 1.85 – 1.49 (m, 6H) ppm. ¹³C NMR (75 MHz, DMSO-*d*₆) δ 162.7, 162.6, 156.1, 150.2, 144.2, 134.9, 120.7, 118.3, 113.6, 106.4, 97.3, 61.8, 56.1, 32.7, 30.4, 25.2, 19.0 ppm. HRMS (ESI) calcd for C₁₇H₂₂N₄O₃ (M+H)⁺ 331.17647, found 331.17652.



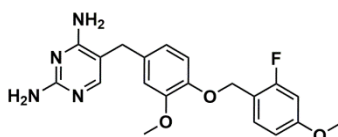
1.3.10. 4-((2,4-Diaminopyrimidin-5-yl)methyl)-2-methoxyphenol (2.20). 37% HCl (0.25 mL/mmol of compound) was added to an ice-cold solution of the 5-(3-methoxy-4-(methoxymethoxy)benzyl)pyrimidine-2,4-diamine (**2.18**) (290 mg, 1 mmol) in MeOH (0.1M). The reaction mixture was stirred at room temperature for 3 – 5 h and the volatiles were removed *in vacuo*. The residue was diluted in water (2 mL/mmol) followed by adjustment of the pH to neutrality by addition of aqueous sodium hydroxide (2N). The mixture was kept at 5°C for 15 min, filtered and the crude residue was diluted with EtOAc and purified on a silica plug (0 – 10 % MeOH/EtOAc) to give the pure corresponding phenol derivative. The title compound (140 mg, 61%) was obtained as a white amorphous solid. R_f 0.10 (50% MeOH/EtOAc).

¹H NMR (300 MHz, DMSO-*d*₆) δ 8.72 (bs, 1H), 7.42 (s, 1H), 6.79 (s, 1H), 6.65 (d, *J* = 8.1 Hz, 1H), 6.55 (d, *J* = 7.8 Hz, 1H), 6.08 (bs, 2H), 5.72 (bs, 2H), 3.70 (s, 3H), 3.46 (s, 2H) ppm. ¹³C NMR (75 MHz, DMSO-*d*₆) δ 162.7, 162.3, 155.4, 147.8, 145.1, 131.1, 120.9, 115.7, 113.3, 106.8, 56.0, 32.7 ppm. HRMS (ESI) calcd for C₁₂H₁₄N₄O₂ (M+H)⁺ 247.11895, found 247.11805.



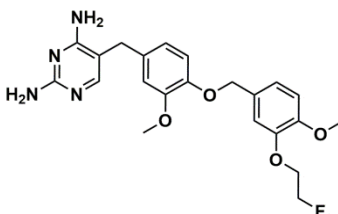
1.3.11. 5-(4-((4-Fluorobenzyl)oxy)-3-methoxybenzyl)pyrimidine-2,4-diamine (2.10). The general procedure 1.3.1 for the synthesis of 2,4-diaminopyrimidines was followed starting with 76 mg (0.3 mmol) of 4-((2,4-diaminopyrimidin-5-yl)methyl)-2-methoxyphenol. The title compound (81 mg, 76%) was obtained as a white amorphous solid. Alternatively, the general procedure 4.1.2 afforded **2.10** in 31% yield from intermediate **27**. R_f 0.10 (40% MeOH/EtOAc).

^1H NMR (300 MHz, $\text{DMSO-}d_6$) δ 7.47 – 7.43 (m, 3H), 7.22 – 7.16 (m, 2H), 6.92 – 6.87 (m, 2H), 6.66 (d, J = 7.8 Hz, 1H), 6.05 (bs, 2H), 5.68 (bs, 2H), 4.98 (s, 2H), 3.71 (s, 3H), 3.50 (s, 2H) ppm. ^{13}C NMR (75 MHz, $\text{DMSO-}d_6$) δ 162.7, 162.6, 158.6 (d, J = 292.5 Hz), 156.1, 149.4, 146.3, 134.0 (d, J = 2.3 Hz), 133.6, 130.4 (d, J = 8.3 Hz), 120.6, 115.6 (d, J = 21.2 Hz), 114.3, 113.3, 106.4, 69.8, 55.9, 32.7 ppm. ^{19}F NMR (188 MHz, $\text{DMSO-}d_6$) δ -114.6 ppm. HRMS (ESI) calcd for $\text{C}_{19}\text{H}_{19}\text{FN}_4\text{O}_2$ ($\text{M}+\text{H}$) $^+$ 355.15648, found 355.15579.



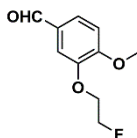
1.3.12. 5-(4-((2-Fluoro-4-methoxybenzyl)oxy)-3-methoxybenzyl)pyrimidine-2,4-diamine (2.11). The general procedure 1.3.1 for the synthesis of 2,4-diaminopyrimidines was followed starting with 49 mg (0.2 mmol) of 4-((2,4-diaminopyrimidin-5-yl)methyl)-2-methoxyphenol. The title compound (50 mg, 64%) was obtained as a white amorphous solid. R_f 0.10 (40% MeOH/EtOAc).

^1H NMR (300 MHz, $\text{DMSO-}d_6$) δ 7.63 (s, 1H), 7.41 (d, J = 8.7 Hz, 1H), 7.24 – 7.17 (m, 4H), 6.99 (d, J = 8.1 Hz, 1H), 6.89 – 6.77 (m, 4H), 4.96 (s, 2H), 3.76 (s, 3H), 3.70 (s, 3H), 3.55 (s, 2H) ppm. ^{13}C NMR (75 MHz, $\text{DMSO-}d_6$) δ 163.4, 161.3, 131.2, 160.1, 149.5, 146.8, 132.4 (d, J = 6.0 Hz), 129.8, 120.4, 116.1.6 (d, J = 15.0 Hz), 115.6, 114.3, 113.0, 110.7 (d, J = 2.6 Hz), 101.9 (d, J = 25.2 Hz), 64.5, 56.1, 55.9, 31.5 ppm. ^{19}F NMR (188 MHz, $\text{DMSO-}d_6$) δ -116.2 ppm. HRMS (ESI) calcd for $\text{C}_{20}\text{H}_{21}\text{FN}_4\text{O}_3$ ($\text{M}+\text{H}$) $^+$ 385.16705, found 385.19782.



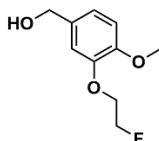
1.3.13. 5-(4-((3-(2-Fluoroethoxy)-4-methoxybenzyl)oxy)-3-methoxybenzyl)pyrimidine-2,4-diamine (2.12). The general procedure 1.3.1 for the synthesis of 2,4-diaminopyrimidines was followed starting with 49 mg (0.2 mmol) of 4-((2,4-diaminopyrimidin-5-yl)methyl)-2-methoxyphenol. The title compound (50 mg, 64%) was obtained as a white amorphous solid. Alternatively, the general procedure 4.1.2 afforded **2.10** in 47% yield from intermediate **26**. R_f 0.10 (40% MeOH/EtOAc).

^1H NMR (300 MHz, $\text{DMSO-}d_6$) δ 7.44 (s, 1H), 7.03 (s, 1H), 6.95 – 6.85 (m, 4H), 6.53 (dd, $J_2 = 8.4$ Hz, $J_1 = 0.9$ Hz, 1H), 6.04 (bs, 2H), 5.67 (bs, 2H), 4.90 (s, 2H), 4.71 (dt, $J_2 = 48.0$ Hz, $J_1 = 3.3$ Hz, 2H), 4.17 (dt, $J_2 = 30.0$ Hz, $J_1 = 3.9$ Hz, 2H), 3.74 (s, 3H), 3.70 (s, 3H), 3.49 (s, 2H) ppm. ^{13}C NMR (75 MHz, $\text{DMSO-}d_6$) δ 162.7, 162.6, 156.0, 149.4, 149.2, 147.8, 146.5, 133.5, 130.0, 121.6, 120.6, 114.4, 114.0, 113.3, 113.3, 106.5, 82.7 (d, $J = 172.5$ Hz), 70.5, 68.3 (d, $J = 18.9$ Hz), 56.0, 55.9, 32.7 ppm. ^{19}F NMR (188 MHz, $\text{DMSO-}d_6$) δ -221.7 ppm. HRMS (ESI) calcd for $\text{C}_{22}\text{H}_{25}\text{FN}_4\text{O}_4$ ($\text{M}+\text{H}$) $^+$ 429.19326, found 429.19206.



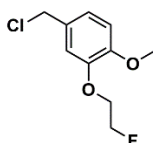
1.3.14. 3-(2-Fluoroethoxy)-4-methoxybenzaldehyde (2.22). To a solution of 3-hydroxy-4-methoxybenzaldehyde (761 mg, 5 mmol, 1 equiv.) in DMF (10 mL) was added K_2CO_3 (1.04 g, 7.5 mmol, 1.5 equiv.) followed by dropwise addition of a solution of 2-fluoroethyl 4-methylbenzenesulfonate (2.18 g, 10 mmol, 2 equiv.) in DMF (5 mL). The reaction mixture was stirred at room temperature for 10 h and water (50 mL) was added. The phases were separated and the aqueous layer was extracted with diethyl ether (3 X 50 mL). The combined organic phases were washed with brine, dried over Na_2SO_4 and concentrated *in vacuo*. The crude product was purified by flash chromatography (20% EtOAc/hexane) to afford 865 mg of the title compound as colorless oil (62%). R_f 0.44 (20% EtOAc/hexane).

^1H NMR (300 MHz, CDCl_3) δ 9.83 (s, 1H), 7.48 (dd, $J_2 = 8.1$ Hz, $J_1 = 1.8$ Hz, 1H), 7.40 (d, $J = 1.8$ Hz, 1H), 6.99 (d, $J = 8.4$ Hz, 1H), 4.80 (dt, $J_2 = 47.4$ Hz, $J_1 = 3.9$ Hz, 2H), 4.32 (dt, $J_2 = 27.6$ Hz, $J_1 = 3.9$ Hz, 2H), 3.94 (s, 3H) ppm. ^{13}C NMR (75 MHz, CDCl_3) δ 190.6, 155.0, 148.4, 111.0, 110.9, 81.6 (d, $J = 170.3$ Hz), 38.1 (d, $J = 20.4$ Hz), 56.2 ppm. ^{19}F NMR (188 MHz, CDCl_3) δ -223.52 ppm. HRMS (ESI) calcd for $\text{C}_{10}\text{H}_{12}\text{FO}_3$ ($\text{M}+\text{H}$) $^+$ 199.0765, found 199.07735.



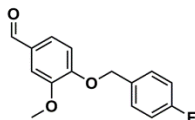
1.3.15. (3-(2-Fluoroethoxy)-4-methoxyphenyl)methanol (2.23). To a solution of 3-(2-fluoroethoxy)-4-methoxybenzaldehyde (396 mg, 2 mmol, 1 equiv.) in THF (10 mL) was added LiAlH_4 (76 mg, 2 mmol, 1 equiv.) in one portion. The reaction mixture was stirred at room temperature for 2 h then quenched with water and passed through a celite pad. The celite was washed with cyclohexane and the filtrates were dried over Na_2SO_4 and concentrated *in vacuo*. The title compound (349 mg, 87%) was obtained as a colorless oil. R_f 0.10 (30% EtOAc/hexane).

^1H NMR (300 MHz, CDCl_3) δ 6.92 – 6.80 (m, 3H), 4.75 (dt, $J_2 = 47.4$ Hz, $J_1 = 4.2$ Hz, 2H), 4.56 (s, 2H), 4.24 (dt, $J_2 = 27.9$ Hz, $J_1 = 4.2$ Hz, 2H), 3.84 (s, 3H) ppm. ^{13}C NMR (75 MHz, CDCl_3) δ 149.2, 147.9, 133.6, 120.6, 113.3, 11.8, 81.9 (d, $J = 169.5$ Hz), 68.4 (d, $J = 20.6$ Hz), 65.0, 56.0 ppm. HRMS (ESI) calcd for $\text{C}_{10}\text{H}_{13}\text{FNaO}_3$ ($\text{M}+\text{Na}$) $^+$ 223.07409, found 223.07464.



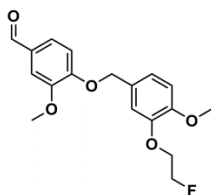
1.3.16. 4-(Chloromethyl)-2-(2-fluoroethoxy)-1-methoxybenzene (2.24). (3-(2-fluoroethoxy)-4-methoxyphenyl)methanol (1.30 g, 6.5 mmol 1 equiv.) was dissolved in DMSO (7 mL) and cyanuric chloride (659 mg, 3.58 mmol, 0.55 equiv.) was added in small quantities over 5 min to the stirred solution at room temperature. Once the addition was completed, the reaction mixture was stirred for an additional 5 min and then diluted with Et_2O (70 mL). The organic phase was washed with water (5 X 50 mL), dried over Na_2SO_4 and concentrated *in vacuo*. The crude residue was eluted through a silica plug with Et_2O and the volatile were removed to give 1.22 g of the title compound as a low-melting point beige solid (86%). R_f 0.68 (30% EtOAc/hexane).

^1H NMR (300 MHz, CDCl_3) δ 6.99 – 6.95 (m, 2H), 6.84 (d, $J = 8.1$ Hz, 1H), 4.78 (dt, $J_2 = 47.4$ Hz, $J_1 = 4.2$ Hz, 2H), 4.54 (s, 2H), 4.28 (dt, $J_2 = 27.6$ Hz, $J_1 = 4.5$ Hz, 2H), 3.86 (s, 3H) ppm. ^{13}C NMR (75 MHz, CDCl_3) δ 149.9, 147.9, 130.0, 122.3, 114.6, 111.7, 81.9 (d, $J = 169.8$ Hz), 68.5 (d, $J = 20.6$ Hz), 56.0, 46.5 ppm. HRMS (ESI) calcd for $\text{C}_{10}\text{H}_{13}[^{35}\text{Cl}]\text{FO}_2$ ($\text{M}+\text{H}$) $^+$ 219.05826, found 219.05747.



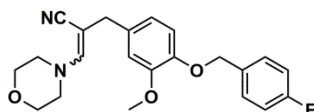
1.3.17. 4-((4-fluorobenzyl)oxy)-3-methoxybenzaldehyde (2.25). To a heterogeneous mixture of 4-hydroxy-3-methoxybenzaldehyde (1.52 g, 10.0 mmol, 1.0 equiv.) and K_2CO_3 (3.45g, 25 mmol, 2.5 equiv.) in DMF (25 mL) at room temperature was added dropwise a solution of 4-(chloromethyl)-2-(2-fluoroethoxy)-1-methoxybenzene (918 mg, 4.2 mmol, 1.05 equiv.) in DMF (2 mL). The reaction mixture was stirred at 70°C for 3h. The reaction mixture was then concentrated under reduced pressure and diluted with EtOAc (100 mL). The organic phase was washed with water (2 X 50 mL) and brine (1 X 50 mL), dried over Na_2SO_4 and evaporated *in vacuo*. The crude residue was recrystallized from CH_2Cl_2 /hexane to afford of the title compound quantitatively as white crystals. R_f 0.45 (20% EtOAc/hexane).

1H NMR (300 MHz, $DMSO-d_6$) δ 9.83 (s, 1H), 7.54-7.50 (m, 3H), 7.40 (d, $J = 1.8$ Hz, 1H), 7.26-7.19 (m, 3H), 5.18 (s, 2H), 3.82 (s, 3H) ppm. ^{13}C NMR (75 MHz, $DMSO-d_6$) δ 191.8, 162.4 (d, $J = 242.5$ Hz), 133.0 (d, $J = 3.1$ Hz), 130.7 (d, $J = 8.3$ Hz), 130.3, 126.3, 115.8 (d, $J = 21.3$ Hz), 113.1, 110.2, 69.7, 56.0 ppm. ^{19}F NMR (188 MHz, $DMSO-d_6$) δ -114.1 ppm. HRMS (ESI) calcd for $C_{15}H_{14}FO_3$ (M+H) $^+$ 261.09215, found 261.09316.



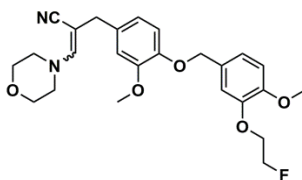
1.3.18. 4-((3-(2-fluoroethoxy)-4-methoxybenzyl)oxy)-3-methoxybenzaldehyde (2.26). To a heterogeneous mixture of 4-hydroxy-3-methoxybenzaldehyde (609 mg, 4 mmol, 1 equiv.) and K_2CO_3 (1.11 g, 8 mmol, 2 equiv.) in DMF (15 mL) at room temperature was added dropwise a solution of 4-(chloromethyl)-2-(2-fluoroethoxy)-1-methoxybenzene (918 mg, 4.2 mmol, 1.05 equiv.) in DMF (2 mL). The mixture was stirred at room temperature for 12 h. The reaction mixture was then concentrated under reduced pressure and diluted with EtOAc (100 mL). The organic phase was washed with water (2 X 50 mL) and brine (1 X 50 mL), dried over Na_2SO_4 and evaporated *in vacuo*. The crude residue was recrystallized from CH_2Cl_2 /hexane to afford 1.11 g of the title compound as white needles (83%). R_f 0.40 (30% EtOAc/hexane).

^1H NMR (300 MHz, $\text{DMSO-}d_6$) δ 9.82 (s, 1H), 7.52 (dd, $J_2 = 8.1$ Hz, $J_1 = 1.8$ Hz, 1H), 7.38 (d, $J = 1.8$ Hz, 1H), 7.26 (d, $J = 8.4$ Hz, 1H), 7.08 (d, $J = 1.8$ Hz, 1H), 7.01 (d, $J = 1.8$ Hz, 1H), 6.99 (s, 1H), 5.09 (s, 2H), 4.72 (dt, $J_2 = 49.2$ Hz, $J_1 = 3.9$ Hz, 2H), 4.19 (dt, $J_2 = 30.3$ Hz, $J_1 = 3.9$ Hz, 2H), 3.81 (s, 3H), 3.76 (s, 3H) ppm. ^{13}C NMR (75 MHz, $\text{DMSO-}d_6$) δ 191.8, 153.6, 149.8, 149.4, 147.8, 130.1, 128.9, 126.3, 122.0, 114.3, 113.1, 112.4, 110.1, 82.5 (d, $J = 165.5$ Hz), 70.5, 68.3 (d, $J = 19.0$ Hz), 55.9 ppm. ^{19}F NMR (188 MHz, $\text{DMSO-}d_6$) δ -221.8 ppm HRMS (ESI) calcd for $\text{C}_{18}\text{H}_{19}\text{FO}_5$ ($\text{M}+\text{Na}$) $^+$ 357.11087, found 357.10946.



1.3.19. 2-(4-((4-fluorobenzyl)oxy)-3-methoxybenzyl)-3-morpholinoacrylonitrile (2.27). To a solution of 4-((4-fluorobenzyl)oxy)-3-methoxybenzaldehyde (775.8 mg, 3 mmol, 1 equiv.) in DMSO (3 mL) was added 3-morpholinopropionitrile (0.43 mL, 3.15 mmol, 1.05 equiv.) and the mixture was stirred for 10 min at 65°C. The reaction mixture was cooled to 40°C and sodium ethoxide (41.0 mg, 0.6 mmol, 0.2 equiv.) was added and the reaction was heated at 75°C for 30 min. The reaction was cooled to room temperature and poured into brine solution (50 mL). The aqueous solution was extracted with dichloromethane. The combined organic phases were dried over Na_2SO_4 and concentrated *in vacuo*. The crude residue was purified by flash chromatography (50% EtOAc/hexane) and afforded 1.043 g of the title compound as a red oil (91%). R_f 0.49 (50% EtOAc/hexane).

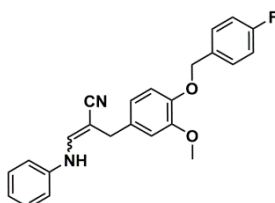
^1H NMR (300 MHz, CDCl_3) δ 7.39 (dd, $J_2 = 8.7$ Hz, $J_1 = 1.8$ Hz, 2H), 7.06-7.02 (m, 2H), 6.83-6.59 (m, 2H), 6.21 (s, 1H), 5.06 (s, 2H), 3.87 (s, 3H), 3.68 (t, $J = 4.5$ Hz, 4H), 3.45 (t, $J = 4.5$ Hz, 4H), 3.30 (s, 2H) ppm. ^{13}C NMR (75 MHz, CDCl_3) δ 162.4 (d, $J = 244.3$ Hz), 149.1, 148.8, 146.8, 133.0, 131.9, 129.3 (d, $J = 3.5$ Hz), 120.03, 119.5, 115.4 (d, $J = 21.3$ Hz), 114.3, 112.2, 75.3, 70.5, 66.4, 56.0, 49.5, 38.9 ppm. ^{19}F NMR (188 MHz, CDCl_3) δ -114.543 (-114.446 *minor isomer*) ppm HRMS (ESI) calcd for $\text{C}_{22}\text{H}_{23}\text{FN}_2\text{O}_3$ ($\text{M}+\text{H}$) $^+$ 383.17655, found 383.17772.



1.3.20. 2-(4-((3-(2-fluoroethoxy)-4-methoxybenzyl)oxy)-3-methoxybenzyl)-3-morpholinoacrylonitrile (2.28). 4-((3-(2-Fluoroethoxy)-4-methoxybenzyl)oxy)-3-

methoxybenzaldehyde (669 g, 2 mmol, 1 equiv.) and 3-morpholinopropionitrile (294 mg, 2.1 mmol, 1.05 equiv.) were stirred in DMSO (2 mL) at 65°C. Upon homogenisation, the reaction mixture was cooled to 40°C and sodium ethoxide (27 mg, 0.4 mmol, 0.2 equiv.) was added. The mixture was stirred at 75°C for 30 minutes and cooled to room temperature. CH₂Cl₂ (40 mL) and brine (40 mL) were added and the two layers were separated. The organic phase was dried over Na₂SO₄ and concentrated *in vacuo*. The crude reddish oil obtained was purified by flash chromatography (50% EtOAc/hexane) and afforded 876 mg of the title compound as a yellow oil (96%). R_f 0.43 (50% EtOAc/hexane).

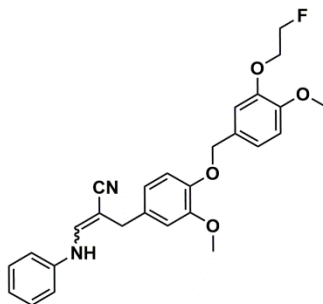
¹H NMR (300 MHz, CDCl₃) δ 7.00 (s, 1H), 6.98 (d, *J* = 4.8 Hz, 1H), 6.87 – 6.80 (m, 2H), 6.75 (s, 1H), 6.68 (dt, *J*₂ = 8.1 Hz, *J*₁ = 2.1 Hz, 2H), 6.59 (s, 1H), 6.21 (s, 1H, *minor isomer*), 5.02 (s, 2H), 4.75 (dt, *J*₂ = 47.4 Hz, *J*₁ = 3.9 Hz, 2H), 4.25 (dt, *J*₂ = 27.9 Hz, *J*₁ = 4.2 Hz, 2H), 3.86 (s, 3H, *minor isomer*), 3.85 (s, 3H), 3.84 (s, 3H), 3.68 (t, *J* = 4.8 Hz, 2H), 3.54 (t, *J* = 4.5 Hz, 2H), 3.53 (s, 2H), 3.44 (t, *J* = 5.7 Hz, 2H), 3.23 (t, *J* = 4.8 Hz, 2H) ppm. ¹³C NMR (75 MHz, CDCl₃) δ 149.9, 149.5, 149.1, 147.8, 146.8, 132.7, 129.7, 121.2, 119.5, 114.6, 113.7, 112.2, 111.8, 111.4, 81.8 (d, *J* = 169.4 Hz), 76.8, 71.1, 68.4 (d, *J* = 22.7 Hz), 66.4, 56.0, 55.9, 50.3, 33.4 ppm. ¹⁹F NMR (188 MHz, DMSO-*d*₆) δ -223.6 ppm HRMS (ESI) calcd for C₂₅H₂₉FN₂O₅ (M+H)⁺ 457.21333, found 457.21494.



1.3.21. 2-(4-((4-fluorobenzyl)oxy)-3-methoxybenzyl)-3-(phenylamino)acrylonitrile (2.29).

The general procedure 1.3.2 for the cyclization of 3-morpholinoacrylonitriles with guanidine was followed. Recrystallization afforded the title compound quantitatively as white needles (mixed *E/Z*). R_f 0.83 (50% EtOAc/hexane).

¹H NMR (300 MHz, DMSO-*d*₆) δ 9.07 (d, *J* = 12.9 Hz, 1H), 7.62 (d, *J* = 20.7 Hz, 1H), 7.46 (dd, *J* = 8.4 Hz, *J* = 5.7 Hz, 2H), 7.28-7.15 (m, 3H), 6.99-6.83 (m, 5H), 6.76 (d, *J* = 1.8 Hz, 1H), 5.01 (s, 2H), 3.73 (s, 3H), 3.31 (s, 2H) ppm. ¹³C NMR (75 MHz, DMSO-*d*₆) δ 162.1 (d, *J* = 241.9 Hz), 149.5, 146.7, 141.9, 140.9, 132.0, 130.3, 130.1 (d, *J* = 49.5 Hz), 129.6, 123.2, 121.9, 120.4, 115.6 (d, *J* = 12.6 Hz), 115.4, 114.3, 112.9, 82.8, 69.7, 55.9, 31.5 ppm. ¹⁹F NMR (188 MHz, DMSO-*d*₆) δ -114.6 ppm.



1.3.22. 2-(4-((3-(2-fluoroethoxy)-4-methoxybenzyl)oxy)-3-methoxybenzyl)-3-(phenylamino)acrylonitrile (2.30). The general procedure 1.3.2 for the cyclization of 3-morpholinoacrylonitriles with guanidine was followed and afforded the crude title compound (876 mg, 96%) as yellow oil. This compound was used in the second step (cyclization) without further characterization. R_f 0.43 (50% EtOAc/hexane).

2. BIOLOGICAL EVALUATION

2.1. [γ - ^{33}P]ATP-Based Enzymatic Assay on TrkA, TrkB, TrkC and CSF-1R.

Compounds **2.9**, **2.10**, **2.11**, **2.12** and **2.20** were tested in a [γ - ^{33}P]ATP based enzymatic assay by Reaction Biology Corporation (Malvern, PA). Briefly, the compounds were tested in a 10-concentration IC_{50} curve with 3-fold serial dilution starting at 10 μM . The reactions were performed with 10 μM ATP and initially profiled against 4 tyrosine kinases (Tropomyosin receptor kinase A (TrkA), tropomyosin receptor kinase B (TrkB), tropomyosin receptor kinase C (TrkC) and colony stimulating factor 1 receptor (CSF-1R)).

2.2. Selectivity Profiling.

Compounds **2.10** and **2.12** were subsequently investigated for general kinase selectivity (tested against 342 wild type kinase at Reaction Biology Corporation) using “HotSpot” assay platform. Briefly, kinase/substrate pairs along with required cofactors were prepared in reaction buffer. The selected compounds were delivered into the reaction. [γ - ^{33}P]ATP (10 μM) was delivered into the reaction mixture to initiate the reactions, and the reactions continued for 120 min at room temperature, followed by spotting of the reactions onto P81 ion exchange filter paper (Whatman). Unbound phosphate was removed by extensive washing of filters in 0.75% phosphoric acid. After subtraction of background derived from control reactions containing inactive enzyme, kinase activity data were expressed as the percent remaining kinase activity in

test samples compared to vehicle (DMSO) reactions.³¹ The kinase dendrogram was generated with Kinase Mapper – Reaction Biology (reactionbiology.com/webapps/mapper/kinase/launch.jnlp).

Table S2.1. Selectivity of compound **2.10** tested on a panel of 342 protein kinases at Reaction Biology Corporation. The results are expressed as the percentage of kinase activity measured at 1 μ M of GW2580F01 compared to a 100% DMSO control (duplicate).

| Kinase: | GW2580F01 (%) | | Compound IC50 (M): | | |
|--------------------|---------------|--------|--------------------|------------------------|-----------------------|
| | Data 1 | Data 2 | Staurosporine | Alternate Control cpd. | Alternate compound ID |
| ABL1 | 104.40 | 99.63 | 4.93E-08 | | |
| ABL2/ARG | 106.38 | 113.03 | 2.07E-08 | | |
| ACK1 | 99.46 | 95.33 | 4.81E-08 | | |
| AKT1 | 96.04 | 100.40 | 6.89E-09 | | |
| AKT2 | 108.30 | 99.89 | 1.60E-08 | | |
| AKT3 | 104.27 | 100.97 | 3.61E-09 | | |
| ALK | 120.26 | 103.74 | 2.37E-09 | | |
| ALK1/ACVRL1 | 108.03 | 106.14 | ND | 1.01E-08 | LDN193189 |
| ALK2/ACVR1 | 95.53 | 93.37 | ND | 6.37E-09 | LDN193189 |
| ALK3/BMPR1A | 123.29 | 115.82 | ND | 4.57E-09 | LDN193189 |
| ALK4/ACVR1B | 114.23 | 111.20 | ND | 3.44E-07 | LDN193189 |
| ALK5/TGFB1 | 111.60 | 100.45 | ND | 3.90E-07 | LDN193189 |
| ALK6/BMPR1B | 102.08 | 104.60 | ND | 1.06E-08 | LDN193189 |
| ARAF | 91.97 | 91.07 | ND | 4.91E-09 | GW5074 |
| ARK5/NUAK1 | 98.18 | 103.01 | 1.18E-09 | | |
| ASK1/MAP3K5 | 100.77 | 96.19 | 1.66E-08 | | |
| Aurora A | 108.65 | 92.33 | 2.31E-09 | | |
| Aurora B | 97.19 | 93.01 | 2.92E-08 | | |
| Aurora C | 93.19 | 102.57 | 2.48E-09 | | |
| AXL | 104.06 | 99.85 | 5.34E-09 | | |
| BLK | 104.32 | 101.63 | 1.75E-09 | | |
| BMPR2 | 102.61 | 109.28 | 4.18E-07 | | |
| BMX/ETK | 96.21 | 93.28 | 5.61E-09 | | |
| BRAF | 98.34 | 92.27 | ND | 8.80E-09 | GW5074 |
| BRK | 99.07 | 95.53 | 8.34E-08 | | |
| BRSK1 | 100.00 | 99.42 | 3.92E-10 | | |
| BRSK2 | 100.21 | 95.39 | 1.89E-09 | | |
| BTK | 95.73 | 94.42 | 2.46E-08 | | |

Table S2.1. (Continued)

| | | | | | |
|-----------------------------|--------|--------|-----------|----------|--------|
| c-Kit | 97.65 | 95.27 | 7.85E-08 | | |
| c-MER | 106.21 | 104.73 | 1.44E-08 | | |
| c-MET | 106.18 | 98.73 | 1.63E-07 | | |
| c-Src | 104.54 | 95.78 | 2.29E-09 | | |
| CAMK1a | 100.10 | 100.23 | 2.58E-09 | | |
| CAMK1b | 104.72 | 103.96 | 9.45E-09 | | |
| CAMK1d | 113.77 | 112.09 | 5.69E-10 | | |
| CAMK1g | 98.65 | 93.67 | 8.11E-09 | | |
| CAMK2a | 99.69 | 98.90 | 1.31E-10 | | |
| CAMK2b | 103.54 | 92.45 | 8.07E-11 | | |
| CAMK2d | 104.26 | 101.38 | <7.63E-11 | | |
| CAMK2g | 103.75 | 95.86 | 8.52E-10 | | |
| CAMK4 | 108.80 | 96.27 | 3.28E-07 | | |
| CAMKK1 | 108.62 | 112.91 | 2.30E-08 | | |
| CAMKK2 | 102.41 | 102.54 | 1.03E-07 | | |
| CDC7/DBF4 | 113.38 | 95.68 | 3.51E-08 | | |
| CDK1/cyclin A | 114.25 | 103.12 | 4.44E-09 | | |
| CDK1/cyclin B | 106.25 | 97.25 | 2.17E-09 | | |
| CDK1/cyclin E | 99.48 | 98.95 | 2.29E-09 | | |
| CDK16/cyclin Y (PCTAIRE) | 104.85 | 109.26 | 1.37E-08 | | |
| CDK2/cyclin A | 94.64 | 96.95 | 1.02E-09 | | |
| CDK2/Cyclin A1 | 105.45 | 97.74 | 4.32E-09 | | |
| CDK2/cyclin E | 94.50 | 88.07 | 5.60E-10 | | |
| CDK3/cyclin E | 109.35 | 99.29 | 6.94E-09 | | |
| CDK4/cyclin D1 | 104.63 | 106.75 | 1.10E-08 | | |
| CDK4/cyclin D3 | 97.51 | 99.12 | 3.56E-08 | | |
| CDK5/p25 | 109.96 | 97.33 | 2.87E-09 | | |
| CDK5/p35 | 98.12 | 99.88 | 2.44E-09 | | |
| CDK6/cyclin D1 | 83.02 | 87.91 | 5.94E-09 | | |
| CDK6/cyclin D3 | 98.98 | 98.92 | 9.51E-08 | | |
| CDK7/cyclin H | 100.19 | 93.65 | 1.05E-06 | | |
| CDK9/cyclin K | 97.46 | 99.29 | 2.75E-08 | | |
| CDK9/cyclin T1 | 116.58 | 107.76 | 1.31E-08 | | |
| CHK1 | 99.09 | 101.84 | 1.44E-09 | | |
| CHK2 | 103.85 | 94.33 | 5.02E-09 | | |
| CK1a1 | 98.71 | 98.65 | 8.10E-06 | | |
| CK1d | 90.59 | 97.68 | ND | 3.70E-07 | D4476 |
| CK1epsilon | 97.78 | 99.31 | ND | 2.44E-07 | D4476 |
| CK1g1 | 93.08 | 97.56 | 6.72E-06 | | |
| CK1g2 | 113.80 | 96.73 | 2.76E-06 | | |
| CK1g3 | 73.74 | 94.01 | 2.61E-06 | | |
| CK2a | 123.64 | 111.04 | ND | 1.20E-07 | GW5074 |
| CK2a2 | 129.57 | 121.16 | 6.57E-07 | | |
| CLK1 | 95.63 | 104.93 | 2.05E-08 | | |
| CLK2 | 101.45 | 96.52 | 1.05E-08 | | |

Table S2.1. (Continued)

| | | | | | |
|--------------|--------|--------|-----------|----------|------------|
| CLK3 | 124.22 | 101.47 | 1.46E-06 | | |
| CLK4 | 112.30 | 106.56 | 4.75E-08 | | |
| COT1/MAP3K8 | 95.39 | 93.95 | ND | 9.52E-06 | Ro-31-8220 |
| CSK | 107.60 | 98.98 | 7.58E-09 | | |
| CTK/MATK | 112.12 | 102.16 | 2.78E-06 | | |
| DAPK1 | 106.58 | 102.24 | 1.03E-08 | | |
| DAPK2 | 100.12 | 102.45 | 8.10E-09 | | |
| DCAMKL1 | 90.36 | 102.10 | 7.83E-07 | | |
| DCAMKL2 | 101.37 | 108.73 | 8.32E-08 | | |
| DDR1 | 97.12 | 97.62 | 3.43E-09 | | |
| DDR2 | 104.85 | 103.70 | 2.21E-08 | | |
| DLK/MAP3K12 | 91.76 | 83.50 | 3.33E-08 | | |
| DMPK | 99.62 | 98.04 | 5.35E-08 | | |
| DMPK2 | 100.59 | 98.91 | 6.50E-10 | | |
| DRAK1/STK17A | 94.60 | 90.24 | 1.61E-08 | | |
| DYRK1/DYRK1A | 99.38 | 100.69 | 3.62E-09 | | |
| DYRK1B | 98.70 | 93.28 | 1.20E-09 | | |
| DYRK2 | 109.43 | 100.52 | 3.21E-07 | | |
| DYRK3 | 107.40 | 98.24 | 7.13E-08 | | |
| DYRK4 | 111.47 | 100.74 | ND | 3.02E-06 | GW5074 |
| EGFR | 102.40 | 101.16 | 1.13E-07 | | |
| EPHA1 | 94.46 | 100.62 | 9.30E-08 | | |
| EPHA2 | 99.52 | 95.62 | 4.61E-08 | | |
| EPHA3 | 100.50 | 96.41 | 2.31E-08 | | |
| EPHA4 | 101.66 | 101.62 | 1.28E-08 | | |
| EPHA5 | 101.86 | 101.25 | 2.46E-08 | | |
| EPHA6 | 105.52 | 97.70 | 1.40E-08 | | |
| EPHA7 | 101.72 | 95.69 | 3.57E-08 | | |
| EPHA8 | 100.98 | 93.43 | 2.01E-07 | | |
| EPHB1 | 93.39 | 99.52 | 5.74E-08 | | |
| EPHB2 | 102.71 | 99.61 | 7.46E-08 | | |
| EPHB3 | 88.93 | 100.30 | 9.81E-07 | | |
| EPHB4 | 105.62 | 95.05 | 1.97E-07 | | |
| ERBB2/HER2 | 97.37 | 102.21 | 7.18E-08 | | |
| ERBB4/HER4 | 96.03 | 90.60 | 4.10E-07 | | |
| ERK1 | 98.33 | 103.11 | >2.00E-05 | | |
| ERK2/MAPK1 | 91.55 | 92.05 | 9.10E-06 | | |
| ERK5/MAPK7 | 93.28 | 93.76 | 1.24E-05 | | |
| ERK7/MAPK15 | 111.84 | 105.81 | 1.04E-08 | | |
| FAK/PTK2 | 99.88 | 96.94 | 9.06E-09 | | |
| FER | 96.92 | 95.14 | 3.67E-10 | | |
| FES/FPS | 104.76 | 100.30 | 2.93E-09 | | |
| FGFR1 | 106.67 | 101.51 | 6.29E-09 | | |
| FGFR2 | 110.40 | 94.10 | 2.95E-09 | | |
| FGFR3 | 104.46 | 96.33 | 1.79E-08 | | |

Table S2.1. (Continued)

| | | | | | |
|--------------------|--------|--------|-----------------|-----------------|-------------------|
| FGFR4 | 104.24 | 87.85 | 2.75E-07 | | |
| FGR | 109.41 | 99.78 | 1.02E-09 | | |
| FLT1/VEGFR1 | 107.33 | 97.28 | 6.94E-09 | | |
| FLT3 | 102.43 | 92.67 | 5.05E-10 | | |
| FLT4/VEGFR3 | 98.49 | 96.13 | 3.06E-09 | | |
| FMS | 20.56 | 21.10 | 1.08E-09 | | |
| FRK/PTK5 | 94.88 | 93.38 | 8.04E-09 | | |
| FYN | 110.39 | 103.61 | 1.71E-09 | | |
| GCK/MAP4K2 | 104.20 | 95.89 | 5.21E-10 | | |
| GLK/MAP4K3 | 98.50 | 102.94 | 1.36E-10 | | |
| GRK1 | 96.34 | 104.18 | 9.64E-08 | | |
| GRK2 | 92.41 | 96.61 | 8.17E-07 | | |
| GRK3 | 90.01 | 102.47 | 1.05E-06 | | |
| GRK4 | 101.41 | 97.86 | 9.69E-08 | | |
| GRK5 | 98.31 | 101.21 | 4.80E-08 | | |
| GRK6 | 101.11 | 101.78 | 2.20E-08 | | |
| GRK7 | 101.66 | 104.07 | 4.27E-09 | | |
| GSK3a | 99.71 | 103.05 | 6.13E-09 | | |
| GSK3b | 108.27 | 100.69 | 5.64E-09 | | |
| Haspin | 95.73 | 101.86 | 2.57E-08 | | |
| HCK | 107.16 | 103.66 | 2.10E-09 | | |
| HGK/MAP4K4 | 81.05 | 84.94 | 4.40E-10 | | |
| HIPK1 | 102.16 | 102.40 | ND | 2.61E-07 | Ro-31-8220 |
| HIPK2 | 106.80 | 99.79 | 1.23E-06 | | |
| HIPK3 | 109.96 | 105.88 | 1.32E-06 | | |
| HIPK4 | 98.96 | 109.37 | 5.56E-07 | | |
| HPK1/MAP4K1 | 107.19 | 99.60 | ND | 2.06E-08 | Ro-31-8220 |
| IGF1R | 99.38 | 102.34 | 3.88E-08 | | |
| IKKa/CHUK | 103.35 | 102.06 | 1.11E-07 | | |
| IKKb/IKBKB | 111.26 | 100.42 | 4.19E-07 | | |
| IKKe/IKBKE | 105.16 | 101.62 | 2.81E-10 | | |
| IR | 98.83 | 89.28 | 1.63E-08 | | |
| IRAK1 | 105.68 | 98.72 | 7.36E-08 | | |
| IRAK4 | 107.50 | 100.01 | 3.52E-09 | | |
| IRR/INSRR | 99.71 | 87.59 | 1.17E-08 | | |
| ITK | 99.13 | 103.12 | 2.75E-08 | | |
| JAK1 | 91.98 | 96.00 | 3.37E-10 | | |
| JAK2 | 102.88 | 101.24 | 4.37E-10 | | |
| JAK3 | 105.16 | 93.52 | 8.71E-11 | | |
| JNK1 | 101.33 | 101.03 | 2.25E-06 | | |
| JNK2 | 100.38 | 96.37 | 5.79E-06 | | |
| JNK3 | 89.57 | 89.56 | ND | 4.13E-07 | JNKi VIII |
| KDR/VEGFR2 | 107.72 | 100.52 | 1.56E-08 | | |
| KHS/MAP4K5 | 100.28 | 96.46 | 2.18E-10 | | |

Table S2.1. (Continued)

| | | | | | |
|----------------|--------|--------|-----------|--|--|
| LATS1 | 97.38 | 102.04 | 1.05E-08 | | |
| LATS2 | 99.70 | 97.94 | 3.07E-09 | | |
| LCK | 96.26 | 87.12 | 1.11E-09 | | |
| LCK2/ICK | 103.06 | 107.29 | 1.26E-07 | | |
| LIMK1 | 107.56 | 99.12 | 6.84E-09 | | |
| LIMK2 | 103.71 | 100.97 | 2.19E-07 | | |
| LKB1 | 101.02 | 100.57 | 7.12E-08 | | |
| LOK/STK10 | 97.54 | 96.17 | 7.44E-09 | | |
| LRRK2 | 100.94 | 93.42 | 1.06E-08 | | |
| LYN | 103.45 | 96.35 | 1.01E-09 | | |
| LYN B | 103.15 | 93.74 | 2.56E-09 | | |
| MAPKAPK2 | 105.59 | 97.97 | 2.58E-07 | | |
| MAPKAPK3 | 107.33 | 97.06 | 4.53E-06 | | |
| MAPKAPK5/PRAK | 95.47 | 95.22 | 4.17E-07 | | |
| MARK1 | 101.64 | 102.29 | <7.63E-11 | | |
| MARK2/PAR-1Ba | 97.38 | 99.14 | 1.46E-10 | | |
| MARK3 | 103.26 | 103.65 | 2.51E-10 | | |
| MARK4 | 100.04 | 84.85 | 1.11E-10 | | |
| MEK1 | 110.98 | 103.07 | 2.60E-08 | | |
| MEK2 | 104.61 | 97.47 | 4.28E-08 | | |
| MEK3 | 108.12 | 106.56 | 5.06E-08 | | |
| MEKK1 | 97.48 | 94.30 | 6.46E-07 | | |
| MEKK2 | 100.17 | 97.94 | 1.28E-08 | | |
| MEKK3 | 110.51 | 114.68 | 2.44E-08 | | |
| MELK | 96.55 | 93.91 | 5.16E-10 | | |
| MINK/MINK1 | 96.76 | 86.95 | 7.89E-10 | | |
| MKK4 | 117.73 | 96.76 | 3.39E-06 | | |
| MKK6 | 107.80 | 107.85 | 2.66E-08 | | |
| MLCK/MYLK | 98.56 | 93.80 | 3.14E-08 | | |
| MLCK2/MYLK2 | 108.83 | 97.96 | 2.13E-08 | | |
| MLK1/MAP3K9 | 100.97 | 107.60 | 3.85E-10 | | |
| MLK2/MAP3K10 | 100.15 | 102.01 | 2.47E-09 | | |
| MLK3/MAP3K11 | 99.00 | 104.00 | 7.57E-09 | | |
| MNK1 | 107.42 | 107.60 | 5.84E-08 | | |
| MNK2 | 100.82 | 104.78 | 2.82E-08 | | |
| MRCKa/CDC42BPA | 91.64 | 90.19 | 1.05E-08 | | |
| MRCKb/CDC42BPB | 109.35 | 101.05 | 6.34E-09 | | |
| MSK1/RPS6KA5 | 108.76 | 107.00 | 7.02E-10 | | |
| MSK2/RPS6KA4 | 97.27 | 99.13 | 2.70E-09 | | |
| MSSK1/STK23 | 103.90 | 103.96 | 1.97E-06 | | |
| MST1/STK4 | 96.04 | 91.36 | 5.77E-10 | | |
| MST2/STK3 | 104.92 | 104.71 | 4.75E-09 | | |
| MST3/STK24 | 103.00 | 101.81 | 1.59E-09 | | |
| MST4 | 110.52 | 109.19 | 4.28E-09 | | |

Table S2.1. (Continued)

| | | | | | |
|-----------------|--------|--------|----------|----------|---------------|
| MUSK | 95.32 | 102.28 | 1.66E-07 | | |
| MYLK3 | 97.29 | 94.65 | 1.83E-07 | | |
| MYO3b | 102.18 | 99.07 | 8.57E-09 | | |
| NEK1 | 113.02 | 98.72 | 2.15E-08 | | |
| NEK11 | 97.37 | 87.16 | 8.97E-07 | | |
| NEK2 | 106.62 | 103.70 | 6.31E-07 | | |
| NEK3 | 114.36 | 102.92 | 1.38E-05 | | |
| NEK4 | 116.60 | 112.83 | 1.59E-07 | | |
| NEK5 | 121.48 | 107.20 | 7.58E-08 | | |
| NEK6 | 95.39 | 96.98 | ND | 5.28E-06 | PKR Inhibitor |
| NEK7 | 102.16 | 95.99 | ND | 3.50E-06 | PKR Inhibitor |
| NEK9 | 109.17 | 99.86 | 1.25E-07 | | |
| NLK | 101.40 | 107.75 | 1.46E-07 | | |
| OSR1/OXSR1 | 98.98 | 94.72 | 8.92E-08 | | |
| P38a/MAPK14 | 98.11 | 96.00 | ND | 6.07E-09 | SB202190 |
| P38b/MAPK11 | 93.52 | 96.66 | ND | 1.76E-08 | SB202190 |
| P38d/MAPK13 | 128.48 | 110.26 | 2.60E-07 | | |
| P38g | 95.77 | 92.37 | 2.57E-07 | | |
| p70S6K/RPS6KB1 | 105.40 | 97.63 | 3.07E-10 | | |
| p70S6Kb/RPS6KB2 | 104.27 | 96.79 | 2.89E-09 | | |
| PAK1 | 104.80 | 105.52 | 7.43E-09 | | |
| PAK2 | 99.86 | 100.43 | 1.88E-09 | | |
| PAK3 | 102.16 | 100.46 | 3.68E-10 | | |
| PAK4 | 93.22 | 94.40 | 2.04E-08 | | |
| PAK5 | 110.23 | 105.65 | 4.08E-09 | | |
| PAK6 | 103.81 | 91.22 | 7.00E-08 | | |
| PASK | 104.36 | 102.47 | 9.81E-09 | | |
| PBK/TOPK | 98.53 | 102.64 | 1.67E-07 | | |
| PDGFRa | 91.25 | 92.58 | 9.02E-10 | | |
| PDGFRb | 103.33 | 99.12 | 1.86E-09 | | |
| PDK1/PDPK1 | 91.92 | 99.29 | 5.23E-10 | | |
| PHKg1 | 96.26 | 102.89 | 1.28E-09 | | |
| PHKg2 | 104.26 | 104.73 | 5.60E-10 | | |
| PIM1 | 104.42 | 99.51 | 4.27E-09 | | |
| PIM2 | 93.27 | 99.46 | 2.90E-08 | | |
| PIM3 | 104.42 | 103.75 | 1.03E-10 | | |
| PKA | 97.79 | 100.22 | 1.49E-09 | | |
| PKAcb | 105.77 | 98.85 | 2.36E-09 | | |
| PKAcg | 92.01 | 101.88 | 9.59E-09 | | |
| PKCa | 99.89 | 99.02 | 1.82E-09 | | |
| PKCb1 | 108.68 | 103.26 | 3.94E-09 | | |
| PKCb2 | 97.86 | 81.22 | 8.42E-10 | | |
| PKCd | 112.35 | 112.23 | 2.16E-10 | | |
| PKCepsilon | 171.23 | 167.23 | 2.09E-10 | | |

Table S2.1. (Continued)

| | | | | | |
|-------------|--------|--------|----------|----------|--------|
| PKCeta | 99.06 | 99.91 | 6.04E-10 | | |
| PKCg | 98.29 | 107.57 | 1.73E-09 | | |
| PKCiota | 104.84 | 103.19 | 2.16E-08 | | |
| PKCmu/PRKD1 | 105.34 | 96.05 | 5.77E-10 | | |
| PKCnu/PRKD3 | 94.16 | 70.34 | 7.53E-10 | | |
| PKCtheta | 106.68 | 110.19 | 3.74E-09 | | |
| PKCzeta | 106.18 | 105.47 | 7.42E-08 | | |
| PKD2/PRKD2 | 108.90 | 98.83 | 1.39E-09 | | |
| PKG1a | 94.31 | 89.97 | 1.35E-09 | | |
| PKG1b | 96.94 | 100.13 | 2.73E-09 | | |
| PKG2/PRKG2 | 100.77 | 102.46 | 1.74E-08 | | |
| PKN1/PRK1 | 104.33 | 104.24 | 1.17E-10 | | |
| PKN2/PRK2 | 112.71 | 107.68 | 2.79E-10 | | |
| PKN3/PRK3 | 96.88 | 102.91 | 1.35E-08 | | |
| PLK1 | 93.28 | 96.80 | 1.35E-07 | | |
| PLK2 | 107.93 | 102.49 | 3.41E-07 | | |
| PLK3 | 103.06 | 92.57 | 2.78E-07 | | |
| PLK4/SAK | 117.54 | 110.57 | 2.34E-08 | | |
| PRKX | 100.39 | 111.22 | 2.99E-09 | | |
| PYK2 | 104.57 | 93.40 | 8.18E-09 | | |
| RAF1 | 104.12 | 98.06 | ND | 1.93E-09 | GW5074 |
| RET | 106.82 | 100.72 | 3.05E-09 | | |
| RIPK2 | 104.49 | 104.67 | 8.38E-07 | | |
| RIPK3 | 98.33 | 103.84 | ND | 6.78E-07 | GW5074 |
| RIPK5 | 103.22 | 87.03 | 4.20E-08 | | |
| ROCK1 | 92.39 | 94.95 | 1.11E-09 | | |
| ROCK2 | 96.59 | 96.95 | 5.35E-10 | | |
| RON/MST1R | 107.91 | 101.32 | 2.07E-07 | | |
| ROS/ROS1 | 105.12 | 93.76 | 1.10E-10 | | |
| RSK1 | 110.29 | 107.61 | 2.84E-10 | | |
| RSK2 | 98.87 | 99.61 | 1.61E-10 | | |
| RSK3 | 92.39 | 98.73 | 2.25E-10 | | |
| RSK4 | 108.03 | 101.72 | 1.51E-10 | | |
| SGK1 | 99.22 | 106.13 | 1.40E-08 | | |
| SGK2 | 105.24 | 93.77 | 3.09E-08 | | |
| SGK3/SGKL | 105.24 | 94.65 | 1.08E-07 | | |
| SIK1 | 100.36 | 95.94 | 4.37E-10 | | |
| SIK2 | 109.78 | 101.26 | 3.80E-10 | | |
| SIK3 | 109.31 | 104.73 | 1.70E-09 | | |
| SLK/STK2 | 113.12 | 102.87 | 2.06E-08 | | |
| SNARK/NUAK2 | 99.33 | 104.62 | 2.87E-08 | | |
| SRMS | 94.50 | 95.85 | 9.03E-06 | | |
| SRPK1 | 107.85 | 103.03 | 3.26E-08 | | |
| SRPK2 | 109.83 | 102.84 | 2.95E-07 | | |

Table S2.1. (Continued)

| | | | | | |
|--------------|--------|--------|-----------|----------|----------------|
| SSTK/TSSK6 | 99.79 | 97.77 | 1.91E-07 | | |
| STK16 | 102.48 | 99.88 | 3.15E-07 | | |
| STK22D/TSSK1 | 98.54 | 79.39 | 8.14E-11 | | |
| STK25/YSK1 | 97.93 | 100.44 | 2.31E-09 | | |
| STK32B/YANK2 | 94.44 | 93.93 | 1.67E-07 | | |
| STK32C/YANK3 | 109.30 | 108.48 | 2.76E-07 | | |
| STK33 | 101.17 | 92.68 | 3.06E-08 | | |
| STK38/NDR1 | 98.24 | 101.41 | 1.19E-08 | | |
| STK38L/NDR2 | 101.88 | 98.07 | 1.29E-09 | | |
| STK39/STLK3 | 107.08 | 92.29 | 3.89E-08 | | |
| SYK | 102.43 | 102.14 | 7.20E-10 | | |
| TAK1 | 108.04 | 105.31 | 5.08E-08 | | |
| TAOK1 | 98.35 | 97.48 | 1.33E-09 | | |
| TAOK2/TAO1 | 104.36 | 101.54 | 4.74E-09 | | |
| TAOK3/JIK | 125.79 | 97.83 | 8.74E-10 | | |
| TBK1 | 112.85 | 104.31 | 1.30E-09 | | |
| TEC | 104.29 | 101.16 | 4.12E-08 | | |
| TESK1 | 97.77 | 93.05 | 4.53E-07 | | |
| TGFBR2 | 89.17 | 87.98 | ND | 4.65E-06 | GW5074 |
| TIE2/TEK | 105.98 | 100.01 | 7.56E-08 | | |
| TLK1 | 117.95 | 97.28 | 3.08E-08 | | |
| TLK2 | 106.58 | 104.65 | 2.38E-09 | | |
| TNIK | 100.80 | 101.97 | 5.19E-10 | | |
| TNK1 | 100.08 | 102.79 | 5.54E-09 | | |
| TRKA | 55.66 | 57.67 | 1.51E-09 | | |
| TRKB | 26.24 | 19.48 | <7.63E-11 | | |
| TRKC | 18.10 | 16.69 | 3.60E-10 | | |
| TSSK2 | 106.35 | 103.07 | 7.41E-09 | | |
| TSSK3/STK22C | 91.46 | 92.87 | 9.14E-09 | | |
| TTBK1 | 100.01 | 97.56 | >2.00E-05 | | |
| TTBK2 | 100.85 | 103.00 | >2.00E-05 | | |
| TXK | 74.48 | 76.05 | 2.71E-08 | | |
| TYK1/LTK | 105.19 | 101.70 | 2.53E-08 | | |
| TYK2 | 102.29 | 94.63 | 3.83E-10 | | |
| TYRO3/SKY | 108.89 | 99.97 | 4.12E-09 | | |
| ULK1 | 97.07 | 100.37 | 9.49E-09 | | |
| ULK2 | 108.81 | 124.29 | 4.01E-09 | | |
| ULK3 | 104.98 | 86.73 | 2.94E-09 | | |
| VRK1 | 101.98 | 110.64 | ND | 3.67E-07 | Ro-31-8220 |
| VRK2 | 123.01 | 119.53 | ND | 1.89E-05 | Ro-31-8220 |
| WEE1 | 110.77 | 104.34 | ND | 1.68E-07 | Wee1 inhibitor |
| WNK1 | 106.19 | 100.62 | >2.00E-05 | | |
| WNK2 | 97.44 | 95.79 | 1.16E-06 | | |
| WNK3 | 99.80 | 98.28 | ND | 1.99E-06 | Wee1 inhibitor |

Table S2.1. (Continued)

| | | | | | |
|-------------------|--------|--------|-----------------|-----------------|---------------|
| YES/YES1 | 108.29 | 100.53 | 1.76E-09 | | |
| ZAK/MLTK | 97.16 | 87.24 | ND | 7.76E-07 | GW5074 |
| ZAP70 | 104.64 | 98.41 | 9.00E-09 | | |
| ZIPK/DAPK3 | 103.86 | 101.23 | 5.41E-09 | | |

Table S2.2. Selectivity of compound **2.12** tested on a panel of 342 protein kinases at Reaction Biology Corporation. The results are expressed as the percentage of kinase activity measured at 1 μ M of GW2580F01 compared to a 100% DMSO control (duplicate).

| Kinase: | GW2580F03 (%) | | Compound IC50 (M): | | |
|---------------------|---------------|--------|--------------------|------------------------|-----------------------|
| | Data 1 | Data 2 | Staurosporine | Alternate Control cpd. | Alternate compound ID |
| | | | | | |
| ABL1 | 104.34 | 101.75 | 4.93E-08 | | |
| ABL2/ARG | 104.15 | 113.96 | 2.07E-08 | | |
| ACK1 | 96.88 | 87.83 | 4.81E-08 | | |
| AKT1 | 109.85 | 103.15 | 6.89E-09 | | |
| AKT2 | 108.87 | 100.48 | 1.60E-08 | | |
| AKT3 | 103.18 | 103.36 | 3.61E-09 | | |
| ALK | 107.77 | 97.69 | 2.37E-09 | | |
| ALK1/ACVRL1 | 103.48 | 106.02 | ND | 1.01E-08 | LDN193189 |
| ALK2/ACVR1 | 100.01 | 102.12 | ND | 6.37E-09 | LDN193189 |
| ALK3/BMPR1A | 109.45 | 116.29 | ND | 4.57E-09 | LDN193189 |
| ALK4/ACVR1B | 114.97 | 115.37 | ND | 3.44E-07 | LDN193189 |
| ALK5/TGFBFR1 | 101.35 | 100.30 | ND | 3.90E-07 | LDN193189 |
| ALK6/BMPR1B | 103.36 | 109.32 | ND | 1.06E-08 | LDN193189 |
| ARAF | 96.34 | 88.15 | ND | 4.91E-09 | GW5074 |
| ARK5/NUAK1 | 117.72 | 103.64 | 1.18E-09 | | |
| ASK1/MAP3K5 | 93.96 | 94.59 | 1.66E-08 | | |
| Aurora A | 101.77 | 95.57 | 2.31E-09 | | |
| Aurora B | 99.99 | 99.24 | 2.92E-08 | | |
| Aurora C | 94.04 | 100.11 | 2.48E-09 | | |
| AXL | 98.61 | 98.95 | 5.34E-09 | | |
| BLK | 104.95 | 97.39 | 1.75E-09 | | |
| BMPR2 | 105.54 | 110.41 | 4.18E-07 | | |
| BMX/ETK | 98.39 | 98.47 | 5.61E-09 | | |
| BRAF | 98.40 | 93.87 | ND | 8.80E-09 | GW5074 |
| BRK | 105.60 | 99.69 | 8.34E-08 | | |
| BRSK1 | 98.28 | 96.61 | 3.92E-10 | | |
| BRSK2 | 99.97 | 94.24 | 1.89E-09 | | |
| BTK | 99.67 | 97.48 | 2.46E-08 | | |
| c-Kit | 98.86 | 99.17 | 7.85E-08 | | |
| c-MER | 103.77 | 104.33 | 1.44E-08 | | |
| c-MET | 106.18 | 99.57 | 1.63E-07 | | |
| c-Src | 103.97 | 97.61 | 2.29E-09 | | |
| CAMK1a | 95.52 | 101.96 | 2.58E-09 | | |
| CAMK1b | 108.36 | 105.13 | 9.45E-09 | | |
| CAMK1d | 118.36 | 107.22 | 5.69E-10 | | |

Table S2.2. (Continued)

| | | | | | |
|-------------------------------------|--------|--------|---------------------|-----------------|-------------------|
| | | | | | |
| CAMK1g | 102.22 | 95.24 | 8.11E-09 | | |
| CAMK2a | 99.13 | 99.68 | 1.31E-10 | | |
| CAMK2b | 102.47 | 100.50 | 8.07E-11 | | |
| CAMK2d | 104.44 | 95.32 | <7.63E-11 | | |
| CAMK2g | 103.50 | 98.42 | 8.52E-10 | | |
| CAMK4 | 107.54 | 100.04 | 3.28E-07 | | |
| CAMKK1 | 104.58 | 101.59 | 2.30E-08 | | |
| CAMKK2 | 102.29 | 114.54 | 1.03E-07 | | |
| CDC7/DBF4 | 102.18 | 89.95 | 3.51E-08 | | |
| CDK1/cyclin A | 113.74 | 107.21 | 4.44E-09 | | |
| CDK1/cyclin B | 100.09 | 91.12 | 2.17E-09 | | |
| CDK1/cyclin E | 99.58 | 98.81 | 2.29E-09 | | |
| CDK16/cyclin Y (PCTAIRE) | 98.45 | 102.93 | 1.37E-08 | | |
| CDK2/cyclin A | 100.38 | 97.48 | 1.02E-09 | | |
| CDK2/Cyclin A1 | 102.17 | 98.96 | 4.32E-09 | | |
| CDK2/cyclin E | 95.63 | 91.64 | 5.60E-10 | | |
| CDK3/cyclin E | 116.32 | 97.13 | 6.94E-09 | | |
| CDK4/cyclin D1 | 102.88 | 101.72 | 1.10E-08 | | |
| CDK4/cyclin D3 | 96.80 | 94.56 | 3.56E-08 | | |
| CDK5/p25 | 103.54 | 94.97 | 2.87E-09 | | |
| CDK5/p35 | 103.41 | 102.48 | 2.44E-09 | | |
| CDK6/cyclin D1 | 81.21 | 93.69 | 5.94E-09 | | |
| CDK6/cyclin D3 | 98.04 | 95.70 | 9.51E-08 | | |
| CDK7/cyclin H | 99.07 | 98.32 | 1.05E-06 | | |
| CDK9/cyclin K | 96.86 | 102.23 | 2.75E-08 | | |
| CDK9/cyclin T1 | 112.78 | 103.02 | 1.31E-08 | | |
| CHK1 | 104.26 | 108.76 | 1.44E-09 | | |
| CHK2 | 99.22 | 98.92 | 5.02E-09 | | |
| CK1a1 | 103.08 | 96.66 | 8.10E-06 | | |
| CK1d | 94.07 | 102.98 | ND | 3.70E-07 | D4476 |
| CK1epsilon | 100.09 | 93.49 | ND | 2.44E-07 | D4476 |
| CK1g1 | 89.54 | 93.99 | 6.72E-06 | | |
| CK1g2 | 106.76 | 96.44 | 2.76E-06 | | |
| CK1g3 | 71.06 | 62.92 | 2.61E-06 | | |
| CK2a | 116.85 | 95.46 | ND | 1.20E-07 | GW5074 |
| CK2a2 | 117.96 | 116.52 | 6.57E-07 | | |
| CLK1 | 99.60 | 103.91 | 2.05E-08 | | |
| CLK2 | 100.97 | 100.57 | 1.05E-08 | | |
| CLK3 | 104.54 | 99.62 | 1.46E-06 | | |
| CLK4 | 105.01 | 98.15 | 4.75E-08 | | |
| COT1/MAP3K8 | 102.00 | 96.71 | ND | 9.52E-06 | Ro-31-8220 |
| CSK | 108.82 | 106.04 | 7.58E-09 | | |
| CTK/MATK | 112.87 | 108.32 | 2.78E-06 | | |

Table S2.2. (Continued)

| | | | | | |
|--------------|--------|--------|-----------|----------|--------|
| DAPK1 | 111.06 | 100.60 | 1.03E-08 | | |
| DAPK2 | 71.12 | 99.37 | 8.10E-09 | | |
| DCAMKL1 | 97.11 | 101.12 | 7.83E-07 | | |
| DCAMKL2 | 91.51 | 94.55 | 8.32E-08 | | |
| DDR1 | 101.45 | 96.23 | 3.43E-09 | | |
| DDR2 | 100.46 | 100.92 | 2.21E-08 | | |
| DLK/MAP3K12 | 84.44 | 82.79 | 3.33E-08 | | |
| DMPK | 97.44 | 97.62 | 5.35E-08 | | |
| DMPK2 | 104.18 | 95.05 | 6.50E-10 | | |
| DRAK1/STK17A | 83.32 | 97.08 | 1.61E-08 | | |
| DYRK1/DYRK1A | 105.59 | 94.70 | 3.62E-09 | | |
| DYRK1B | 99.56 | 91.29 | 1.20E-09 | | |
| DYRK2 | 105.39 | 110.94 | 3.21E-07 | | |
| DYRK3 | 99.29 | 91.41 | 7.13E-08 | | |
| DYRK4 | 105.67 | 103.42 | ND | 3.02E-06 | GW5074 |
| EGFR | 102.01 | 101.51 | 1.13E-07 | | |
| EPHA1 | 91.93 | 100.28 | 9.30E-08 | | |
| EPHA2 | 101.72 | 96.08 | 4.61E-08 | | |
| EPHA3 | 97.87 | 97.44 | 2.31E-08 | | |
| EPHA4 | 102.73 | 95.07 | 1.28E-08 | | |
| EPHA5 | 99.48 | 99.52 | 2.46E-08 | | |
| EPHA6 | 104.03 | 102.62 | 1.40E-08 | | |
| EPHA7 | 104.02 | 101.09 | 3.57E-08 | | |
| EPHA8 | 106.35 | 93.92 | 2.01E-07 | | |
| EPHB1 | 97.07 | 87.94 | 5.74E-08 | | |
| EPHB2 | 102.67 | 103.94 | 7.46E-08 | | |
| EPHB3 | 98.90 | 101.57 | 9.81E-07 | | |
| EPHB4 | 106.00 | 98.37 | 1.97E-07 | | |
| ERBB2/HER2 | 98.26 | 101.08 | 7.18E-08 | | |
| ERBB4/HER4 | 94.56 | 92.09 | 4.10E-07 | | |
| ERK1 | 97.50 | 102.58 | >2.00E-05 | | |
| ERK2/MAPK1 | 86.07 | 92.53 | 9.10E-06 | | |
| ERK5/MAPK7 | 88.86 | 86.71 | 1.24E-05 | | |
| ERK7/MAPK15 | 108.24 | 105.59 | 1.04E-08 | | |
| FAK/PTK2 | 104.82 | 95.78 | 9.06E-09 | | |
| FER | 95.13 | 94.74 | 3.67E-10 | | |
| FES/FPS | 107.15 | 98.11 | 2.93E-09 | | |
| FGFR1 | 99.41 | 99.21 | 6.29E-09 | | |
| FGFR2 | 125.01 | 103.58 | 2.95E-09 | | |
| FGFR3 | 108.57 | 95.97 | 1.79E-08 | | |
| FGFR4 | 107.09 | 99.69 | 2.75E-07 | | |
| FGR | 118.58 | 100.00 | 1.02E-09 | | |
| FLT1/VEGFR1 | 101.90 | 101.92 | 6.94E-09 | | |
| FLT3 | 100.51 | 89.54 | 5.05E-10 | | |
| FLT4/VEGFR3 | 96.36 | 100.80 | 3.06E-09 | | |
| FMS | 38.92 | 38.35 | 1.08E-09 | | |

Table S2.2. (Continued)

| | | | | | |
|-------------|--------|--------|----------|----------|------------|
| FRK/PTK5 | 95.50 | 90.00 | 8.04E-09 | | |
| FYN | 107.92 | 100.85 | 1.71E-09 | | |
| GCK/MAP4K2 | 105.54 | 98.62 | 5.21E-10 | | |
| GLK/MAP4K3 | 98.78 | 100.16 | 1.36E-10 | | |
| GRK1 | 101.28 | 100.70 | 9.64E-08 | | |
| GRK2 | 98.81 | 96.80 | 8.17E-07 | | |
| GRK3 | 101.36 | 103.38 | 1.05E-06 | | |
| GRK4 | 99.66 | 94.81 | 9.69E-08 | | |
| GRK5 | 100.55 | 98.98 | 4.80E-08 | | |
| GRK6 | 92.50 | 99.61 | 2.20E-08 | | |
| GRK7 | 99.07 | 106.90 | 4.27E-09 | | |
| GSK3a | 98.07 | 99.51 | 6.13E-09 | | |
| GSK3b | 108.74 | 100.50 | 5.64E-09 | | |
| Haspin | 99.36 | 100.04 | 2.57E-08 | | |
| HCK | 111.44 | 103.29 | 2.10E-09 | | |
| HGK/MAP4K4 | 84.69 | 83.18 | 4.40E-10 | | |
| HIPK1 | 94.91 | 102.67 | ND | 2.61E-07 | Ro-31-8220 |
| HIPK2 | 105.40 | 102.15 | 1.23E-06 | | |
| HIPK3 | 102.73 | 98.40 | 1.32E-06 | | |
| HIPK4 | 97.28 | 109.96 | 5.56E-07 | | |
| HPK1/MAP4K1 | 102.48 | 106.62 | ND | 2.06E-08 | Ro-31-8220 |
| IGF1R | 99.29 | 92.11 | 3.88E-08 | | |
| IKKa/CHUK | 95.61 | 98.19 | 1.11E-07 | | |
| IKKb/IKBKB | 111.07 | 101.32 | 4.19E-07 | | |
| IKKe/IKBKE | 107.00 | 99.69 | 2.81E-10 | | |
| IR | 95.29 | 91.39 | 1.63E-08 | | |
| IRAK1 | 109.99 | 101.54 | 7.36E-08 | | |
| IRAK4 | 101.05 | 95.27 | 3.52E-09 | | |
| IRR/INSRR | 97.41 | 90.79 | 1.17E-08 | | |
| ITK | 105.08 | 102.89 | 2.75E-08 | | |
| JAK1 | 93.11 | 97.23 | 3.37E-10 | | |
| JAK2 | 101.35 | 100.56 | 4.37E-10 | | |
| JAK3 | 102.51 | 95.53 | 8.71E-11 | | |
| JNK1 | 103.86 | 105.44 | 2.25E-06 | | |
| JNK2 | 104.67 | 98.60 | 5.79E-06 | | |
| JNK3 | 97.20 | 92.02 | ND | 4.13E-07 | JNKi VIII |
| KDR/VEGFR2 | 102.91 | 98.25 | 1.56E-08 | | |
| KHS/MAP4K5 | 110.21 | 91.82 | 2.18E-10 | | |
| LATS1 | 101.22 | 99.90 | 1.05E-08 | | |
| LATS2 | 99.61 | 101.28 | 3.07E-09 | | |
| LCK | 95.62 | 89.69 | 1.11E-09 | | |
| LCK2/ICK | 97.79 | 100.70 | 1.26E-07 | | |
| LIMK1 | 109.34 | 97.02 | 6.84E-09 | | |
| LIMK2 | 103.77 | 102.63 | 2.19E-07 | | |
| LKB1 | 100.87 | 95.17 | 7.12E-08 | | |
| LOK/STK10 | 98.54 | 99.79 | 7.44E-09 | | |

Table S2.2. (Continued)

| | | | | | |
|----------------|--------|--------|-----------|----------|---------------|
| LRRK2 | 101.55 | 94.31 | 1.06E-08 | | |
| LYN | 107.42 | 93.28 | 1.01E-09 | | |
| LYN B | 99.65 | 90.17 | 2.56E-09 | | |
| MAPKAPK2 | 100.99 | 98.96 | 2.58E-07 | | |
| MAPKAPK3 | 101.78 | 93.52 | 4.53E-06 | | |
| MAPKAPK5/PRAK | 96.06 | 102.15 | 4.17E-07 | | |
| MARK1 | 107.10 | 98.65 | <7.63E-11 | | |
| MARK2/PAR-1Ba | 99.74 | 98.19 | 1.46E-10 | | |
| MARK3 | 101.78 | 103.57 | 2.51E-10 | | |
| MARK4 | 97.84 | 94.80 | 1.11E-10 | | |
| MEK1 | 110.46 | 98.30 | 2.60E-08 | | |
| MEK2 | 103.70 | 96.92 | 4.28E-08 | | |
| MEK3 | 106.17 | 99.62 | 5.06E-08 | | |
| MEKK1 | 98.59 | 95.73 | 6.46E-07 | | |
| MEKK2 | 100.23 | 101.98 | 1.28E-08 | | |
| MEKK3 | 114.65 | 113.93 | 2.44E-08 | | |
| MELK | 95.50 | 95.34 | 5.16E-10 | | |
| MINK/MINK1 | 97.26 | 83.63 | 7.89E-10 | | |
| MKK4 | 104.77 | 97.65 | 3.39E-06 | | |
| MKK6 | 108.61 | 112.49 | 2.66E-08 | | |
| MLCK/MYLK | 101.91 | 102.86 | 3.14E-08 | | |
| MLCK2/MYLK2 | 106.34 | 103.32 | 2.13E-08 | | |
| MLK1/MAP3K9 | 104.03 | 103.69 | 3.85E-10 | | |
| MLK2/MAP3K10 | 102.98 | 96.25 | 2.47E-09 | | |
| MLK3/MAP3K11 | 102.72 | 103.41 | 7.57E-09 | | |
| MNK1 | 107.44 | 104.71 | 5.84E-08 | | |
| MNK2 | 106.01 | 102.35 | 2.82E-08 | | |
| MRCKa/CDC42BPA | 95.27 | 93.39 | 1.05E-08 | | |
| MRCKb/CDC42BPB | 106.00 | 98.58 | 6.34E-09 | | |
| MSK1/RPS6KA5 | 106.15 | 102.05 | 7.02E-10 | | |
| MSK2/RPS6KA4 | 102.88 | 102.26 | 2.70E-09 | | |
| MSSK1/STK23 | 101.73 | 98.41 | 1.97E-06 | | |
| MST1/STK4 | 102.19 | 94.44 | 5.77E-10 | | |
| MST2/STK3 | 104.81 | 102.99 | 4.75E-09 | | |
| MST3/STK24 | 104.01 | 104.90 | 1.59E-09 | | |
| MST4 | 118.72 | 103.17 | 4.28E-09 | | |
| MUSK | 93.66 | 105.22 | 1.66E-07 | | |
| MYLK3 | 112.35 | 99.81 | 1.83E-07 | | |
| MYO3b | 106.30 | 100.52 | 8.57E-09 | | |
| NEK1 | 109.04 | 106.10 | 2.15E-08 | | |
| NEK11 | 105.46 | 99.31 | 8.97E-07 | | |
| NEK2 | 101.73 | 94.02 | 6.31E-07 | | |
| NEK3 | 102.63 | 92.31 | 1.38E-05 | | |
| NEK4 | 118.85 | 110.95 | 1.59E-07 | | |
| NEK5 | 103.69 | 103.41 | 7.58E-08 | | |
| NEK6 | 99.96 | 101.85 | ND | 5.28E-06 | PKR Inhibitor |

Table S2.2. (Continued)

| | | | | | |
|-----------------|--------|--------|----------|----------|---------------|
| NEK7 | 101.06 | 102.28 | ND | 3.50E-06 | PKR Inhibitor |
| NEK9 | 103.26 | 109.32 | 1.25E-07 | | |
| NLK | 99.58 | 102.96 | 1.46E-07 | | |
| OSR1/OXSR1 | 99.18 | 94.78 | 8.92E-08 | | |
| P38a/MAPK14 | 96.39 | 96.99 | ND | 6.07E-09 | SB202190 |
| P38b/MAPK11 | 100.00 | 98.21 | ND | 1.76E-08 | SB202190 |
| P38d/MAPK13 | 121.86 | 117.48 | 2.60E-07 | | |
| P38g | 94.43 | 96.49 | 2.57E-07 | | |
| p70S6K/RPS6KB1 | 100.26 | 96.79 | 3.07E-10 | | |
| p70S6Kb/RPS6KB2 | 90.11 | 92.69 | 2.89E-09 | | |
| PAK1 | 106.76 | 100.53 | 7.43E-09 | | |
| PAK2 | 102.38 | 103.61 | 1.88E-09 | | |
| PAK3 | 98.21 | 101.48 | 3.68E-10 | | |
| PAK4 | 98.28 | 94.26 | 2.04E-08 | | |
| PAK5 | 110.70 | 101.44 | 4.08E-09 | | |
| PAK6 | 102.56 | 96.77 | 7.00E-08 | | |
| PASK | 106.92 | 104.17 | 9.81E-09 | | |
| PBK/TOPK | 100.09 | 99.72 | 1.67E-07 | | |
| PDGFRa | 101.60 | 93.74 | 9.02E-10 | | |
| PDGFRb | 106.40 | 98.78 | 1.86E-09 | | |
| PDK1/PDPK1 | 100.95 | 99.01 | 5.23E-10 | | |
| PHKg1 | 99.03 | 97.10 | 1.28E-09 | | |
| PHKg2 | 107.95 | 96.23 | 5.60E-10 | | |
| PIM1 | 101.08 | 100.09 | 4.27E-09 | | |
| PIM2 | 93.35 | 96.15 | 2.90E-08 | | |
| PIM3 | 103.79 | 97.82 | 1.03E-10 | | |
| PKA | 106.62 | 102.74 | 1.49E-09 | | |
| PKAcb | 80.13 | 100.88 | 2.36E-09 | | |
| PKAcb | 108.01 | 96.17 | 9.59E-09 | | |
| PKCa | 96.62 | 92.08 | 1.82E-09 | | |
| PKCb1 | 108.03 | 101.23 | 3.94E-09 | | |
| PKCb2 | 100.38 | 93.29 | 8.42E-10 | | |
| PKCd | 107.71 | 106.50 | 2.16E-10 | | |
| PKCepsilon | 119.57 | 106.62 | 2.09E-10 | | |
| PKCeta | 108.34 | 102.44 | 6.04E-10 | | |
| PKCg | 97.98 | 102.33 | 1.73E-09 | | |
| PKCiota | 104.30 | 101.21 | 2.16E-08 | | |
| PKCmu/PRKD1 | 106.50 | 104.43 | 5.77E-10 | | |
| PKCnu/PRKD3 | 102.66 | 102.65 | 7.53E-10 | | |
| PKCtheta | 96.73 | 99.76 | 3.74E-09 | | |
| PKCzeta | 103.38 | 108.05 | 7.42E-08 | | |
| PKD2/PRKD2 | 104.75 | 92.97 | 1.39E-09 | | |
| PKG1a | 88.25 | 102.91 | 1.35E-09 | | |
| PKG1b | 97.50 | 115.45 | 2.73E-09 | | |
| PKG2/PRKG2 | 97.76 | 99.05 | 1.74E-08 | | |
| PKN1/PRK1 | 109.04 | 103.62 | 1.17E-10 | | |

Table S2.2. (Continued)

| | | | | | |
|---------------------|--------|--------|-----------------|-----------------|---------------|
| PKN2/PRK2 | 108.61 | 101.01 | 2.79E-10 | | |
| PKN3/PRK3 | 97.53 | 95.99 | 1.35E-08 | | |
| PLK1 | 105.46 | 102.74 | 1.35E-07 | | |
| PLK2 | 106.08 | 108.88 | 3.41E-07 | | |
| PLK3 | 104.53 | 104.20 | 2.78E-07 | | |
| PLK4/SAK | 113.08 | 111.56 | 2.34E-08 | | |
| PRKX | 105.40 | 98.50 | 2.99E-09 | | |
| PYK2 | 102.73 | 94.15 | 8.18E-09 | | |
| RAF1 | 102.21 | 112.51 | ND | 1.93E-09 | GW5074 |
| RET | 103.21 | 103.24 | 3.05E-09 | | |
| RIPK2 | 108.24 | 102.66 | 8.38E-07 | | |
| RIPK3 | 103.55 | 104.69 | ND | 6.78E-07 | GW5074 |
| RIPK5 | 100.27 | 100.27 | 4.20E-08 | | |
| ROCK1 | 91.88 | 93.26 | 1.11E-09 | | |
| ROCK2 | 103.10 | 97.95 | 5.35E-10 | | |
| RON/MST1R | 101.73 | 105.64 | 2.07E-07 | | |
| ROS/ROS1 | 104.65 | 91.18 | 1.10E-10 | | |
| RSK1 | 105.19 | 100.69 | 2.84E-10 | | |
| RSK2 | 105.80 | 104.92 | 1.61E-10 | | |
| RSK3 | 94.11 | 97.66 | 2.25E-10 | | |
| RSK4 | 104.10 | 102.76 | 1.51E-10 | | |
| SGK1 | 101.66 | 96.79 | 1.40E-08 | | |
| SGK2 | 103.29 | 106.10 | 3.09E-08 | | |
| SGK3/SGKL | 103.21 | 102.87 | 1.08E-07 | | |
| SIK1 | 102.63 | 96.76 | 4.37E-10 | | |
| SIK2 | 104.67 | 98.99 | 3.80E-10 | | |
| SIK3 | 108.18 | 106.17 | 1.70E-09 | | |
| SLK/STK2 | 101.15 | 95.52 | 2.06E-08 | | |
| SNARK/NUAK2 | 89.46 | 85.69 | 2.87E-08 | | |
| SRMS | 98.33 | 98.36 | 9.03E-06 | | |
| SRPK1 | 104.69 | 98.20 | 3.26E-08 | | |
| SRPK2 | 95.88 | 98.36 | 2.95E-07 | | |
| SSTK/TSSK6 | 105.76 | 97.63 | 1.91E-07 | | |
| STK16 | 99.72 | 95.46 | 3.15E-07 | | |
| STK22D/TSSK1 | 124.06 | 92.98 | 8.14E-11 | | |
| STK25/YSK1 | 93.24 | 102.75 | 2.31E-09 | | |
| STK32B/YANK2 | 94.92 | 96.55 | 1.67E-07 | | |
| STK32C/YANK3 | 112.82 | 112.00 | 2.76E-07 | | |
| STK33 | 99.74 | 94.62 | 3.06E-08 | | |
| STK38/NDR1 | 111.99 | 97.59 | 1.19E-08 | | |
| STK38L/NDR2 | 102.29 | 101.30 | 1.29E-09 | | |
| STK39/STLK3 | 105.74 | 81.06 | 3.89E-08 | | |
| SYK | 102.60 | 103.50 | 7.20E-10 | | |
| TAK1 | 109.67 | 102.38 | 5.08E-08 | | |
| TAOK1 | 100.13 | 96.14 | 1.33E-09 | | |
| TAOK2/TAO1 | 102.77 | 104.65 | 4.74E-09 | | |

Table S2.2. (Continued)

| | | | | | |
|---------------------|--------|--------|---------------------|-----------------|-----------------------|
| TAOK3/JIK | 122.19 | 110.64 | 8.74E-10 | | |
| TBK1 | 109.28 | 101.38 | 1.30E-09 | | |
| TEC | 102.65 | 104.39 | 4.12E-08 | | |
| TESK1 | 97.61 | 96.82 | 4.53E-07 | | |
| TGFBR2 | 90.28 | 100.70 | ND | 4.65E-06 | GW5074 |
| TIE2/TEK | 107.53 | 98.79 | 7.56E-08 | | |
| TLK1 | 101.91 | 95.67 | 3.08E-08 | | |
| TLK2 | 114.32 | 96.57 | 2.38E-09 | | |
| TNIK | 115.26 | 98.31 | 5.19E-10 | | |
| TNK1 | 101.09 | 97.77 | 5.54E-09 | | |
| TRKA | 64.62 | 62.65 | 1.51E-09 | | |
| TRKB | 48.35 | 41.48 | <7.63E-11 | | |
| TRKC | 37.22 | 33.61 | 3.60E-10 | | |
| TSSK2 | 102.00 | 99.79 | 7.41E-09 | | |
| TSSK3/STK22C | 92.70 | 91.21 | 9.14E-09 | | |
| TTBK1 | 99.75 | 99.77 | >2.00E-05 | | |
| TTBK2 | 97.50 | 96.94 | >2.00E-05 | | |
| TXK | 79.12 | 90.90 | 2.71E-08 | | |
| TYK1/LTK | 105.21 | 104.22 | 2.53E-08 | | |
| TYK2 | 101.39 | 92.68 | 3.83E-10 | | |
| TYRO3/SKY | 102.92 | 98.39 | 4.12E-09 | | |
| ULK1 | 99.10 | 101.47 | 9.49E-09 | | |
| ULK2 | 112.10 | 116.65 | 4.01E-09 | | |
| ULK3 | 98.83 | 98.65 | 2.94E-09 | | |
| VRK1 | 102.06 | 107.14 | ND | 3.67E-07 | Ro-31-8220 |
| VRK2 | 113.02 | 123.01 | ND | 1.89E-05 | Ro-31-8220 |
| WEE1 | 114.55 | 101.48 | ND | 1.68E-07 | Wee1 inhibitor |
| WNK1 | 99.48 | 101.11 | >2.00E-05 | | |
| WNK2 | 97.05 | 97.96 | 1.16E-06 | | |
| WNK3 | 96.93 | 94.00 | ND | 1.99E-06 | Wee1 inhibitor |
| YES/YES1 | 106.61 | 99.46 | 1.76E-09 | | |
| ZAK/MLTK | 97.94 | 97.03 | ND | 7.76E-07 | GW5074 |
| ZAP70 | 106.59 | 99.30 | 9.00E-09 | | |
| ZIPK/DAPK3 | 107.69 | 101.01 | 5.41E-09 | | |

3. DOCKING SIMULATION

Molecular docking simulations of structures **2.10**, **2.11** and **2.12** were performed using the X-ray co-crystal structure of TrkB-GW2580 complex (PDB ID: 4AT5) and CSF-1R co-crystal (PDB ID: 3LCO) using FITTED 3.5 program (FORECASTER platform).⁴⁹⁻⁵¹ Docking structures with TrkB were prepared using Discovery Studio 3.5 Visualizer. The validity of FITTED was assessed by comparing the ligand GW2580 (**2.9**) bound to the crystal structure with the docked ligand predicted by FITTED (self-docking, RMSD = 0.24).

4. COMPUTATION OF PHYSICO-CHEMICAL PROPERTIES

cLogP, cLogD and TSPA values were computed with the program Pallas 3.0 for Windows (CompuDrug; San Francisco, CA).

5. FIGURES (Figure S2.1-S2.3)

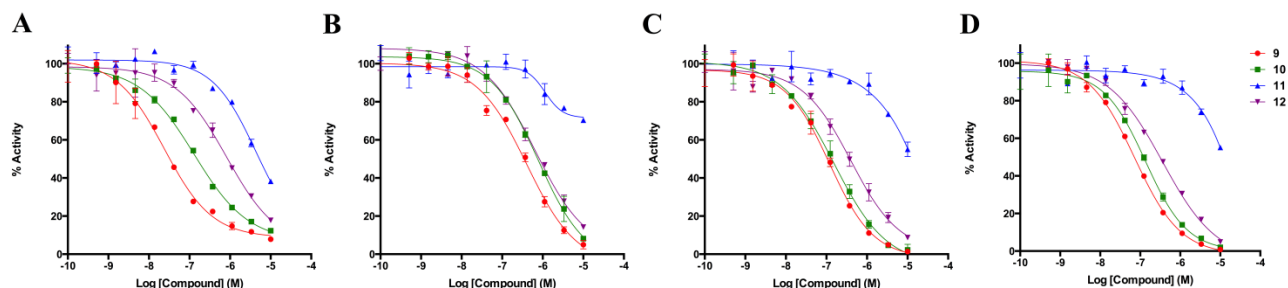


Figure S2.1. Dose-response curves for the in vitro kinase assays with **2.9**, **2.10**, **2.11** and **2.12** versus (A) CSF-1R, (B) TrkA, (C) TrkB and (D) TrkC. The inhibitors were tested at ten different concentrations using serial dilution and error bars represent standard deviation from the mean.

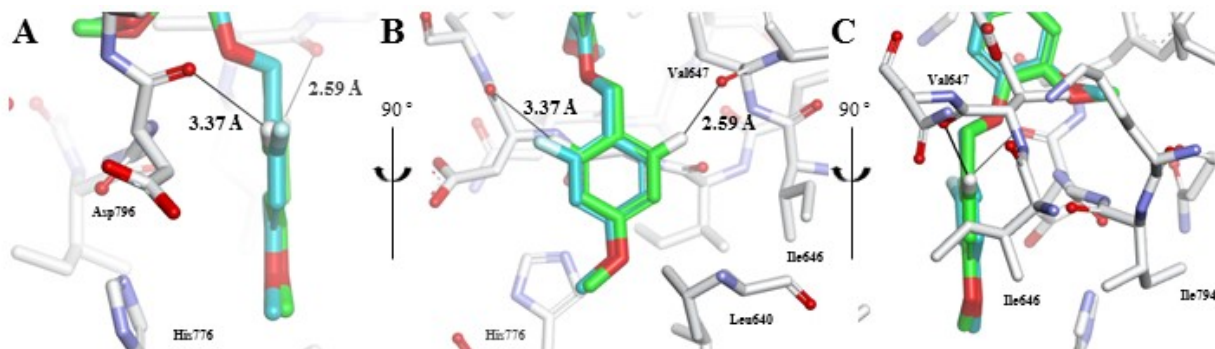


Figure S2.2. Different angles presenting the overlay between the ortho-fluoro diaminopyrimidine derivative **2.11** (cyan) and **2.9** (green) docking poses in the hydrophobic back pocket of CSF-1R (PDB code: 3LCO). The ortho-hydrogen of **2.9** (2- and 6-) are depicted in white. The fluorine atom is in pale blue. Distances are depicted with black lines.

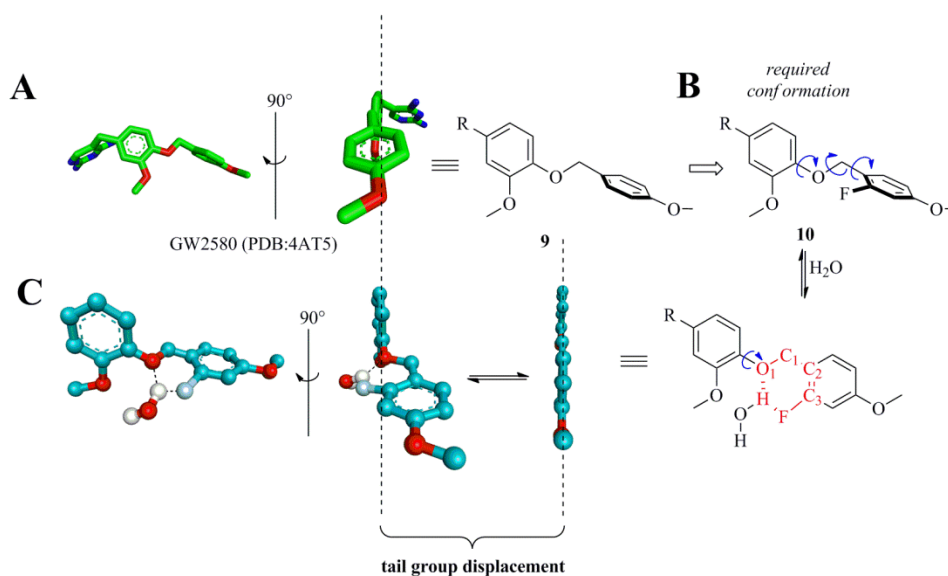
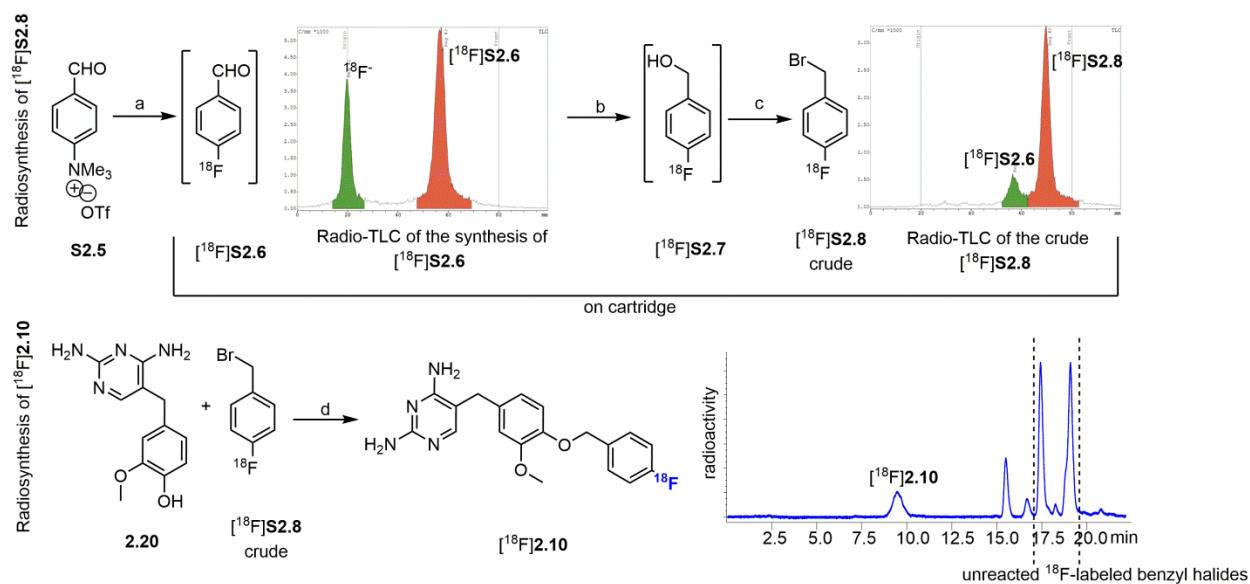


Figure S2.3. (A) Conformation of GW2580 in complex with TrkB (the same conformation has been observed with (GW2580-CSF-1R)). The tail benzyloxy group is nearly perpendicular to the central methoxybenzyl moiety in accordance to the lowest-energy conformation for this motif. (B) Analogous required perpendicular conformation for **2.10** (rotatable bonds in blue). (C) Putative intermolecular hydrogen bonding involving a water molecule bonded to O_1 and the *ortho*-fluorine substituent. Such interaction may stabilize a rigid six-membered ring form by $-O_1-C_1-C_2-C_3-F-H-$ and result in the stabilisation of **2.10** in conformations suboptimal for binding.

6. RADIOCHEMISTRY

Radiosynthesis of [¹⁸F]S2.8 and [¹⁸F]2.10. [¹⁸F]Fluoride was produced using an IBA cyclotron (Cyclon 18/9) by the ¹⁸O(p,n)¹⁸F nuclear reaction on an enriched [¹⁸O]water target and passed through a Sep-Pak Light QMA cartridge (Waters) as an aqueous solution in ¹⁸O-enriched water. The cartridge was then dried by airflow, and the ¹⁸F activity was eluted with 1.0 mL (from a 10.0 mL stock solution) of a Kryptofix 222/K₂CO₃ solution (22.6 mg of Kryptofix 222 and 4.2 mg of K₂CO₃ in acetonitrile/water (95/5)) in a 5.0 mL conical vial with a stirring bar. The solvent was removed at 100°C under reduced pressure, agitation and a stream of argon gas. The residue was azeotropically dried with 1.0 mL of anhydrous acetonitrile twice at 100°C under a stream of argon gas and dissolved in 300 µL of DMSO solution containing 3.0 mg of **S2.5** and the reaction mixture was heated at 140°C for 5 min. Radiolabeling was assessed by radio-TLC as depicted in Scheme S1, RCY of 60-70% after 5 min – determine by radio-TLC (hexane/ethyl acetate (1:1)). The ensuing on-cartridge synthesis of [¹⁸F]**S2.8** was adapted from a procedure reported by Lemaire *et al.*⁴⁵ After labeling, the reaction solution containing [¹⁸F]**S2.6** and ¹⁸F-fluoride was diluted with water (20 mL) and passed through a pre-conditioned Sep-Pak C18 Plus Cartridge. Direct reduction of [¹⁸F]**S2.6** to the benzyl alcohol [¹⁸F]**S2.7** was carried out on the cartridge by eluting 4.0 mL of a freshly prepared sodium borohydride (NaBH₄ aq) solution (125 mg NaBH₄) dropwise over 1.5 min. For the halogenation step, hydrogen bromide (HBr, 48%, 4.0 mL) was eluted dropwise through the cartridge containing [¹⁸F]**S2.7** under gentle heating (50°C approx.) with an air drier. The elution of HBr was carried out in two portions: first 2.5 mL in 1 min followed by constant gentle heating for 4 min and then, 1.5 mL of the remaining acid was passed through the cartridge over 1 min. Then, sodium formate buffer (5.0 mL, pH 4) and water (4.0 mL) were passed through the cartridge dropwise. The cartridge was dried with a stream of nitrogen and eluted with diethyl ether (Et₂O) via a Sep-Pak Dry Sodium Sulfate (Plus Long Cartridge) and the purity of the collected crude [¹⁸F]**S2.8** was assessed by radio-TLC (80-85% with residual [¹⁸F]**S2.6**). Overall, this procedure delivers the crude [¹⁸F]**S2.7** in 25-30% RCY (non decay-corrected) from [¹⁸F]F⁻/H₂O in 50 min.



Scheme S2.1. Radiosynthesis of [¹⁸F]S2.8 and [¹⁸F]2.10.

The crude [¹⁸F]S2.8 (in 100 μ L Et₂O) was transferred in 5.0 mL conical vial containing precursor **2.20** (3.0 mg), Cs₂CO₃ (10 mg), TBAI (10 mg) and DMSO (200 μ L). The vial was sealed and allowed to react at 100°C for 10 min. Alkylation of **2.20** with [¹⁸F]S2.8 was assessed by analytical HPLC with an Agilent 1200 system (Agilent Technologies, Santa Clara, CA, USA; running on Agilent ChemStation software) equipped with a Raytest Gabi Star radioactivity detector (Raytest Isotopenmessgeräte GmbH, Straubenhardt, Germany) and a Phenomenex aeris peptide 3.6u XB-C18 column (250*4.60 mm). Method: H₂O (A)/MeCN (B) gradient ($t = 0$ min: 85% A; $t = 10$ min A = 85%; $t = 20$ min A = 5%; $t = 25$ min A = 5%;) at 1.0 mL/min ($t_r = 8.80$ min – calibrated delay between uv and radio-detector: 0.5 min) . RCY for the formation of [¹⁸F]2.10 was 13% (non decay-corrected, HPLC determination).

7. CRYSTALLOGRAPHIC DATA FOR COMPOUNDS 2.25 AND (E)-2.29

Data from this subsection can be found in **Annex 1**.

2.6 References

1. Zhang, J.; Yang, P. L.; Gray, N. S., Targeting cancer with small molecule kinase inhibitors. *Nat Rev Cancer* **2009**, *9* (1), 28-39.
2. Levitzki, A., Tyrosine kinase inhibitors: views of selectivity, sensitivity, and clinical performance. *Annu Rev Pharmacol Toxicol* **2013**, *53*, 161-85.
3. Hartmann, J. T.; Haap, M.; Kopp, H. G.; Lipp, H. P., Tyrosine kinase inhibitors - a review on pharmacology, metabolism and side effects. *Curr Drug Metab* **2009**, *10* (5), 470-81.
4. O'Brien, Z.; Moghaddam, M. F., Small molecule kinase inhibitors approved by the FDA from 2000 to 2011: a systematic review of preclinical ADME data. *Expert Opin Drug Met* **2013**, *9* (12), 1597-1612.
5. Slobbe, P.; Poot, A. J.; Windhorst, A. D.; van Dongen, G. A., PET imaging with small-molecule tyrosine kinase inhibitors: TKI-PET. *Drug Discov Today* **2012**, *17* (21-22), 1175-87.
6. Petrulli, J. R.; Sullivan, J. M.; Zheng, M. Q.; Bennett, D. C.; Charest, J.; Huang, Y.; Morris, E. D.; Contessa, J. N., Quantitative analysis of [11C]-erlotinib PET demonstrates specific binding for activating mutations of the EGFR kinase domain. *Neoplasia* **2013**, *15* (12), 1347-53.
7. Meng, X.; Loo, B. W., Jr.; Ma, L.; Murphy, J. D.; Sun, X.; Yu, J., Molecular imaging with 11C-PD153035 PET/CT predicts survival in non-small cell lung cancer treated with EGFR-TKI: a pilot study. *J Nucl Med* **2011**, *52* (10), 1573-9.
8. Memon, A. A.; Jakobsen, S.; Dagnaes-Hansen, F.; Sorensen, B. S.; Keiding, S.; Nexø, E., Positron emission tomography (PET) imaging with [11C]-labeled erlotinib: a micro-PET study on mice with lung tumor xenografts. *Cancer Res* **2009**, *69* (3), 873-8.
9. van Dongen, G. A.; Poot, A. J.; Vugts, D. J., PET imaging with radiolabeled antibodies and tyrosine kinase inhibitors: immuno-PET and TKI-PET. *Tumour Biol* **2012**, *33* (3), 607-15.
10. Hicks, J. W.; VanBrocklin, H. F.; Wilson, A. A.; Houle, S.; Vasdev, N., Radiolabeled small molecule protein kinase inhibitors for imaging with PET or SPECT. *Molecules* **2010**, *15* (11), 8260-78.
11. Chao, M. V., Neurotrophins and their receptors: a convergence point for many signalling pathways. *Nat Rev Neurosci* **2003**, *4* (4), 299-309.
12. Huang, E. J.; Reichardt, L. F., Neurotrophins: roles in neuronal development and function. *Annu Rev Neurosci* **2001**, *24*, 677-736.
13. Muragaki, Y.; Timothy, N.; Leight, S.; Hempstead, B. L.; Chao, M. V.; Trojanowski, J. Q.; Lee, V. M., Expression of trk receptors in the developing and adult human central and peripheral nervous system. *J Comp Neurol* **1995**, *356* (3), 387-97.

14. Lagadec, C.; Meignan, S.; Adriaenssens, E.; Foveau, B.; Vanhecke, E.; Romon, R.; Toillon, R. A.; Oxombre, B.; Hondermarck, H.; Le Bourhis, X., TrkA overexpression enhances growth and metastasis of breast cancer cells. *Oncogene* **2009**, *28* (18), 1960-70.
15. Zhu, Z.; Kleeff, J.; Kayed, H.; Wang, L.; Korc, M.; Buchler, M. W.; Friess, H., Nerve growth factor and enhancement of proliferation, invasion, and tumorigenicity of pancreatic cancer cells. *Mol Carcinog* **2002**, *35* (3), 138-47.
16. Sclabas, G. M.; Fujioka, S.; Schmidt, C.; Li, Z.; Frederick, W. A.; Yang, W.; Yokoi, K.; Evans, D. B.; Abbruzzese, J. L.; Hess, K. R.; Zhang, W.; Fidler, I. J.; Chiao, P. J., Overexpression of tropomyosin-related kinase B in metastatic human pancreatic cancer cells. *Clin Cancer Res* **2005**, *11* (2 Pt 1), 440-9.
17. Okamura, K.; Harada, T.; Wang, S.; Ijichi, K.; Furuyama, K.; Koga, T.; Okamoto, T.; Takayama, K.; Yano, T.; Nakanishi, Y., Expression of TrkB and BDNF is associated with poor prognosis in non-small cell lung cancer. *Lung Cancer* **2012**, *78* (1), 100-6.
18. Nakagawara, A.; Azar, C. G.; Scavarda, N. J.; Brodeur, G. M., Expression and function of TRK-B and BDNF in human neuroblastomas. *Mol Cell Biol* **1994**, *14* (1), 759-67.
19. Matsumoto, K.; Wada, R. K.; Yamashiro, J. M.; Kaplan, D. R.; Thiele, C. J., Expression of brain-derived neurotrophic factor and p145TrkB affects survival, differentiation, and invasiveness of human neuroblastoma cells. *Cancer Res* **1995**, *55* (8), 1798-806.
20. Brodeur, G. M.; Minturn, J. E.; Ho, R.; Simpson, A. M.; Iyer, R.; Varela, C. R.; Light, J. E.; Kolla, V.; Evans, A. E., Trk receptor expression and inhibition in neuroblastomas. *Clin Cancer Res* **2009**, *15* (10), 3244-50.
21. Schramm, A.; Schulte, J. H.; Astrahantseff, K.; Apostolov, O.; Limpt, V.; Sieverts, H.; Kuhfittig-Kulle, S.; Pfeiffer, P.; Versteeg, R.; Eggert, A., Biological effects of TrkA and TrkB receptor signaling in neuroblastoma. *Cancer Lett* **2005**, *228* (1-2), 143-53.
22. Thiele, C. J.; Li, Z.; McKee, A. E., On Trk--the TrkB signal transduction pathway is an increasingly important target in cancer biology. *Clin Cancer Res* **2009**, *15* (19), 5962-7.
23. Jang, S. W.; Liu, X.; Yepes, M.; Shepherd, K. R.; Miller, G. W.; Liu, Y.; Wilson, W. D.; Xiao, G.; Blanchi, B.; Sun, Y. E.; Ye, K., A selective TrkB agonist with potent neurotrophic activities by 7,8-dihydroxyflavone. *Proc Natl Acad Sci U S A* **2010**, *107* (6), 2687-92.
24. Bernard-Gauthier, V.; Boudjemeline, M.; Rosa-Neto, P.; Thiel, A.; Schirmacher, R., Towards tropomyosin-related kinase B (TrkB) receptor ligands for brain imaging with PET: radiosynthesis and evaluation of 2-(4-[(18)F]fluorophenyl)-7,8-dihydroxy-4H-chromen-4-one and 2-(4-[(N-methyl-(11)C]-dimethylamino)phenyl)-7,8-dihydroxy-4H-chromen-4-one. *Bioorg Med Chem* **2013**, *21* (24), 7816-29.

25. Wang, T.; Yu, D.; Lamb, M. L., Trk kinase inhibitors as new treatments for cancer and pain. *Expert Opin Ther Pat* **2009**, *19* (3), 305-19.
26. Marshall, J. L.; Kindler, H.; Deeken, J.; Bhargava, P.; Vogelzang, N. J.; Rizvi, N.; Luhtala, T.; Boylan, S.; Dordal, M.; Robertson, P.; Hawkins, M. J.; Ratain, M. J., Phase I trial of orally administered CEP-701, a novel neurotrophin receptor-linked tyrosine kinase inhibitor. *Invest New Drugs* **2005**, *23* (1), 31-7.
27. Albaugh, P.; Fan, Y.; Mi, Y.; Sun, F.; Adrian, F.; Li, N.; Jia, Y.; Sarkisova, Y.; Kreusch, A.; Hood, T.; Lu, M.; Liu, G.; Huang, S.; Liu, Z.; Loren, J.; Tuntland, T.; Karanewsky, D. S.; Seidel, H. M.; Molteni, V., Discovery of GNF-5837, a Selective TRK Inhibitor with Efficacy in Rodent Cancer Tumor Models. *ACS Med Chem Lett* **2012**, *3* (2), 140-5.
28. Conway, J. G.; McDonald, B.; Parham, J.; Keith, B.; Rusnak, D. W.; Shaw, E.; Jansen, M.; Lin, P.; Payne, A.; Crosby, R. M.; Johnson, J. H.; Frick, L.; Lin, M. H.; Depee, S.; Tadepalli, S.; Votta, B.; James, I.; Fuller, K.; Chambers, T. J.; Kull, F. C.; Chamberlain, S. D.; Hutchins, J. T., Inhibition of colony-stimulating-factor-1 signaling in vivo with the orally bioavailable cFMS kinase inhibitor GW2580. *Proc Natl Acad Sci U S A* **2005**, *102* (44), 16078-83.
29. Davis, M. I.; Hunt, J. P.; Herrgard, S.; Ciceri, P.; Wodicka, L. M.; Pallares, G.; Hocker, M.; Treiber, D. K.; Zarrinkar, P. P., Comprehensive analysis of kinase inhibitor selectivity. *Nat Biotechnol* **2011**, *29* (11), 1046-51.
30. Karaman, M. W.; Herrgard, S.; Treiber, D. K.; Gallant, P.; Atteridge, C. E.; Campbell, B. T.; Chan, K. W.; Ciceri, P.; Davis, M. I.; Edeen, P. T.; Faraoni, R.; Floyd, M.; Hunt, J. P.; Lockhart, D. J.; Milanov, Z. V.; Morrison, M. J.; Pallares, G.; Patel, H. K.; Pritchard, S.; Wodicka, L. M.; Zarrinkar, P. P., A quantitative analysis of kinase inhibitor selectivity. *Nat Biotechnol* **2008**, *26* (1), 127-32.
31. Anastassiadis, T.; Deacon, S. W.; Devarajan, K.; Ma, H.; Peterson, J. R., Comprehensive assay of kinase catalytic activity reveals features of kinase inhibitor selectivity. *Nat Biotechnol* **2011**, *29* (11), 1039-45.
32. Pike, V. W., PET radiotracers: crossing the blood-brain barrier and surviving metabolism. *Trends Pharmacol Sci* **2009**, *30* (8), 431-40.
33. Chitu, V.; Stanley, E. R., Colony-stimulating factor-1 in immunity and inflammation. *Curr Opin Immunol* **2006**, *18* (1), 39-48.
34. Pixley, F. J.; Stanley, E. R., CSF-1 regulation of the wandering macrophage: complexity in action. *Trends Cell Biol* **2004**, *14* (11), 628-38.
35. Lewis, C. E.; Pollard, J. W., Distinct role of macrophages in different tumor microenvironments. *Cancer Research* **2006**, *66* (2), 605-612.

36. Murdoch, C.; Giannoudis, A.; Lewis, C. E., Mechanisms regulating the recruitment of macrophages into hypoxic areas of tumors and other ischemic tissues. *Blood* **2004**, *104* (8), 2224-34.
37. Pyonteck, S. M.; Gadea, B. B.; Wang, H. W.; Gocheva, V.; Hunter, K. E.; Tang, L. H.; Joyce, J. A., Deficiency of the macrophage growth factor CSF-1 disrupts pancreatic neuroendocrine tumor development. *Oncogene* **2012**, *31* (11), 1459-1467.
38. Abraham, D.; Zins, K.; Sioud, M.; Lucas, T.; Schafer, R.; Stanley, E. R.; Aharinejad, S., Stromal cell-derived CSF-1 blockade prolongs xenograft survival of CSF-1-negative neuroblastoma. *International Journal of Cancer* **2010**, *126* (6), 1339-1352.
39. Ide, H.; Seligson, D. B.; Memarzadeh, S.; Xin, L.; Horvath, S.; Dubey, P.; Flick, M. B.; Kacinski, B. M.; Palotie, A.; Witte, O. N., Expression of colony-stimulating factor 1 receptor during prostate development and prostate cancer progression. *Proc Natl Acad Sci U S A* **2002**, *99* (22), 14404-9.
40. Purser, S.; Moore, P. R.; Swallow, S.; Gouverneur, V., Fluorine in medicinal chemistry. *Chem Soc Rev* **2008**, *37* (2), 320-30.
41. Bertrand, T.; Kothe, M.; Liu, J.; Dupuy, A.; Rak, A.; Berne, P. F.; Davis, S.; Gladysheva, T.; Valtre, C.; Crenne, J. Y.; Mathieu, M., The crystal structures of TrkA and TrkB suggest key regions for achieving selective inhibition. *J Mol Biol* **2012**, *423* (3), 439-53.
42. Shewchuk, L. M. H., A. M.; Holmes, W. D. , U.S. Pat. Appl. US 2.004.002.145 **2004**.
43. Garg, S.; Thopate, S. R.; Minton, R. C.; Black, K. W.; Lynch, A. J.; Garg, P. K., 3-Amino-4-(2-((4-[¹⁸F]fluorobenzyl)methylamino)methylphenylsulfanyl)benzonitrile, an F-18 fluorobenzyl analogue of DASB: synthesis, in vitro binding, and in vivo biodistribution studies. *Bioconjug Chem* **2007**, *18* (5), 1612-8.
44. Donohue, S. R.; Halldin, C.; Schou, M.; Hong, J.; Phebus, L.; Chernet, E.; Hitchcock, S. A.; Gardinier, K. M.; Ruley, K. M.; Krushinski, J. H.; Schaus, J.; Pike, V. W., Radiolabeling of a high potency cannabinoid subtype-1 receptor ligand, N-(4-fluoro-benzyl)-4-(3-(piperidin-1-yl)-indole-1-sulfonyl)benzamide (PipISB), with carbon-11 or fluorine-18. *J Labelled Compd Rad* **2008**, *51* (3-4), 146-152.
45. Lemaire, C.; Libert, L.; Plenevaux, A.; Aerts, J.; Franci, X.; Luxen, A., Fast and reliable method for the preparation of ortho- and para-[F-18]fluorobenzyl halide derivatives: Key intermediates for the preparation of no-carrier-added PET aromatic radiopharmaceuticals. *J Fluorine Chem* **2012**, *138*, 48-55.
46. Otzen, T.; Wempe, E. G.; Kunz, B.; Bartels, R.; Lehwerk-Yvetot, G.; Hansel, W.; Schaper, K. J.; Seydel, J. K., Folate-synthesizing enzyme system as target for development of

inhibitors and inhibitor combinations against *Candida albicans*-synthesis and biological activity of new 2,4-diaminopyrimidines and 4'-substituted 4-aminodiphenyl sulfones. *J Med Chem* **2004**, *47* (1), 240-53.

47. Pez, D.; Leal, I.; Zuccotto, F.; Boussard, C.; Brun, R.; Croft, S. L.; Yardley, V.; Perez, L. M. R.; Pacanowska, D. G.; Gilbert, I. H., 2,4-diaminopyrimidines as inhibitors of leishmanial and trypanosomal dihydrofolate reductase. *Bioorgan Med Chem* **2003**, *11* (22), 4693-4711.

48. Zhang, L.; Villalobos, A.; Beck, E. M.; Bocan, T.; Chappie, T. A.; Chen, L.; Grimwood, S.; Heck, S. D.; Helal, C. J.; Hou, X.; Humphrey, J. M.; Lu, J.; Skaddan, M. B.; McCarthy, T. J.; Verhoest, P. R.; Wager, T. T.; Zasadny, K., Design and selection parameters to accelerate the discovery of novel central nervous system positron emission tomography (PET) ligands and their application in the development of a novel phosphodiesterase 2A PET ligand. *J Med Chem* **2013**, *56* (11), 4568-79.

49. Englebienne, P.; Moitessier, N., Docking ligands into flexible and solvated macromolecules. 5. Force-field-based prediction of binding affinities of ligands to proteins. *J Chem Inf Model* **2009**, *49* (11), 2564-71.

50. Therrien, E.; Englebienne, P.; Arrowsmith, A. G.; Mendoza-Sanchez, R.; Corbeil, C. R.; Weill, N.; Campagna-Slater, V.; Moitessier, N., Integrating Medicinal Chemistry, Organic/Combinatorial Chemistry, and Computational Chemistry for the Discovery of Selective Estrogen Receptor Modulators with FORECASTER, a Novel Platform for Drug Discovery. *Journal of Chemical Information and Modeling* **2012**, *52* (1), 210-224.

51. Corbeil, C. R.; Englebienne, P.; Yannopoulos, C. G.; Chan, L.; Das, S. K.; Bilimoria, D.; L'Heureux, L.; Moitessier, N., Docking ligands into flexible and solvated macromolecules. 2. Development and application of fitted 1.5 to the virtual screening of potential HCV polymerase inhibitors. *J Chem Inf Model* **2008**, *48* (4), 902-9.

52. Cantacuzene, D.; Kirk, K. L.; McCulloh, D. H.; Creveling, C. R., Effect of fluorine substitution on the agonist specificity of norepinephrine. *Science* **1979**, *204* (4398), 1217-9.

53. Galan, J. F.; Brown, J.; Wildin, J. L.; Liu, Z.; Liu, D.; Moyna, G.; Pophristic, V., Intramolecular hydrogen bonding in ortho-substituted arylamide oligomers: a computational and experimental study of ortho-fluoro- and ortho-chloro-N-methylbenzamides. *J Phys Chem B* **2009**, *113* (38), 12809-15.

54. Schneider, H. J., Hydrogen bonds with fluorine. Studies in solution, in gas phase and by computations, conflicting conclusions from crystallographic analyses. *Chemical Science* **2012**, *3* (5), 1381-1394.

55. Pike, V. W. A., F. I. , Reactions of cyclotron-produced [18F]fluoride with diaryliodonium salts—a novel single-step route to no-carrier-added [18F]fluoroarenes *J. Chem. Soc. Chem. Commun.* **1995**, 21, 2215.
56. Wang, B.; Qin, L.; Neumann, K. D.; Uppaluri, S.; Cerny, R. L.; DiMugno, S. G., Improved arene fluorination methodology for I(III) salts. *Org Lett* **2010**, 12 (15), 3352-5.
57. Kopka, K.; Faust, A.; Keul, P.; Wagner, S.; Breyholz, H. J.; Holtke, C.; Schober, O.; Schafers, M.; Levkau, B., 5-Pyrrolidinylsulfonyl isatins as a potential tool for the molecular imaging of caspases in apoptosis. *Journal of Medicinal Chemistry* **2006**, 49 (23), 6704-6715.
58. Hugenberg, V.; Riemann, B.; Hermann, S.; Schober, O.; Schafers, M.; Szardenings, K.; Lebedev, A.; Gangadharmath, U.; Kolb, H.; Walsh, J.; Zhang, W.; Kopka, K.; Wagner, S., Inverse 1,2,3-triazole-1-yl-ethyl substituted hydroxamates as highly potent matrix metalloproteinase inhibitors: (radio)synthesis, in vitro and first in vivo evaluation. *J Med Chem* **2013**, 56 (17), 6858-70.

Article 6

*A version of this Chapter has been published as: **Bernard-Gauthier, V.**; Aliaga, A.; Aliaga, A.; Boudjemeline, M.; Hopewell, R.; Kostikov, A.; Rosa-Neto, P.; Thiel, A.; Schirmacher, R. Syntheses and Evaluation of Carbon-11- and Fluorine-18-Radiolabeled pan-Tropomyosin Receptor Kinases (Trk) Inhibitors: Exploration of the 4-aza-2-Oxindole Scaffold as Trk PET Imaging Agents *ACS Chem. Neurosci.* **2015**, 6, 260-267.*

*Author contributions: **V.B.G.** managed the study, designed all experiments, conducted chemical syntheses and characterizations studies, conducted *in silico* analyses, radiochemistry experiments, metabolism experiments, contributed to autoradiography studies and PET imaging experiments, analyzed and interpreted all data and wrote the paper; A.(Arturo)A. performed autoradiography experiments and analyzed autoradiography data; A.(Antonio)A. performed PET imaging experiments and PET imaging data; M.B. contributed to chemical synthesis under the supervision of **V.B.G.**; R.H. and A.K. contributed to radiochemistry; P.R.-N., A.T. and R.S. contributed new reagents and analytic tools; the manuscript was approved by all co-authors; R.S. supervised the research and corrected manuscript.*

Syntheses and Evaluation of Carbon-11- and Fluorine-18-Radiolabeled pan-Tropomyosin Receptor Kinases (Trk) Inhibitors: Exploration of the 4-aza-2-Oxindole Scaffold as Trk PET Imaging Agents

Vadim Bernard-Gauthier^{1,2*}, Arturo Aliaga³, Antonio Aliaga⁴, Mehdi Boudjemeline⁴, Robert Hopewell⁴, Alexey Kostikov⁴, Pedro Rosa-Neto³, Alexander Thiel⁵, Ralf Schirmacher^{2,4*}

¹Experimental Medicine, Department of Medicine, McGill University, 1110 Pine Avenue West, Montreal, QC, H3A 1A3. ²Department of Oncology, University of Alberta, 11560 University Avenue, Edmonton, AB, Canada, T6G 1Z2. ³Translational Neuroimaging Laboratory, McGill Centre for Studies in Aging, Douglas Mental Health University Institute, 6875 Boulevard LaSalle, QC, Canada, H4H 1R3. ⁴McConnell Brain Imaging Centre, Montreal Neurological Institute, McGill University, 3801 University Street, Montreal, QC, Canada, H3A 2B4. ⁵Department of Neurology and Neurosurgery, McGill University, Jewish General Hospital, 3755 Cote St. Catherine Rd., Montreal, QC, Canada, H2T 1E2. * Corresponding authors.

3.1 Abstract

Tropomyosin receptor kinases (TrkA/B/C) are critically involved in the development of the nervous system, in neurological disorders as well as in multiple neoplasms of both neural and non-neural origins. The development of Trk radiopharmaceuticals would offer unique opportunities towards a more complete understanding of this emerging therapeutic target. To that end, we first developed [¹¹C]GW441756 ([¹¹C]**3.9**), a high affinity photoisomerizable pan-Trk inhibitor as a lead radiotracer for our PET program. Efficient carbon-11 radiolabeling afforded [¹¹C]**3.9** in high radiochemical yields (isolated RCY, 25.9 ± 5.7 %). In vitro autoradiographic studies in rat brain and TrkB-expressing human neuroblastoma cryosections confirmed that [¹¹C]**3.9** specifically binds to Trk receptors in vitro. MicroPET studies revealed that binding of [¹¹C]**3.9** in the rodent brain is mostly nonspecific despite initial high brain uptake (SUV_{max} = 2.0). Modeling studies of the 4-aza-2-oxindole scaffold led to the successful identification of a small series of high affinity fluorinated and methoxy derivatized pan-Trk inhibitors based on our lead

compound **3.9**. Out of this series, the fluorinated compound **3.10** was selected for initial evaluation and radiolabeled with fluorine-18 (isolated RCY, 2.5 ± 0.6 %). Compound [^{18}F]**3.10** demonstrated excellent Trk selectivity in a panel of cancer relevant kinase targets and a promising *in vitro* profile in tumors and brain sections but high oxidative metabolic susceptibility leading to nonspecific brain distribution *in vivo*. The information gained in this study will guide further exploration of the 4-aza-2-oxindole scaffold as a lead for Trk PET ligands development.

3.2 Introduction

Tropomyosin receptor kinases (Trk) encompass the three highly homologous receptors TrkA, TrkB and TrkC which are transphosphorylated and activated upon preferential and high affinity binding with dimeric neurotrophins. Nerve growth factor (NGF) binds TrkA, brain-derived neurotrophic factor (BDNF) and neurotrophin-4/5 binds TrkB, while neurotrophin-3 (NT-3) preferentially binds TrkC ($K_d \approx 1.7\text{-}2.3 \times 10^{-11}$ M).¹ All Trk proteins share an analogous sequence and common general arrangement, which includes an intracellular kinase domain connected via a transmembrane region to five consecutive extracellular domains.² The downstream signaling ensuing from the extracellular activation of those receptor tyrosine kinases (RTKs) with their cognate ligands supports pivotal functions in the development and maintenance of the mammalian nervous system such as synaptogenesis, neuronal differentiation and synaptic plasticity.³⁻⁶ Each neurotrophin also interacts with a common low affinity receptor, p75^{NTR} – a member of the tumor necrosis factor family ($K_d \approx 10^{-9}$ M).⁷ TrkA expression, along with its cognate ligand, is extensive in restricted neuronal populations such as cholinergic neurons of the basal forebrain (BFCNs) and striatum as well as in sensory and sympathetic ganglia.⁸⁻⁹ TrkB and TrkC receptors are, for their part, widely co-expressed throughout the mammalian central (CNS) and peripheral nervous system (PNS).¹⁰⁻¹¹ Outside of neural lineages, cell-type specific expression of the different Trk receptors is also found in many organs such as diverse components of the lung.¹²

Within the CNS, alterations in expression and abnormal function of NGF/TrkA and BDNF/TrkB systems have been extensively investigated and linked to various neurological diseases and conditions.¹³⁻¹⁴ For example, the observation that the NGF/TrkA system crucially supports survival and differentiation in BFCNs combined with the significant cholinergic dysfunction observed in early Alzheimer's disease (AD) points towards the underlying implication of NGF/TrkA in the onset and progression of AD.¹⁵⁻¹⁶ Indeed, substantial down-regulation of Trk genes has been characterized within BFCNs of the nucleus basalis (NB) in mild cognitive impairment (MCI) and more significantly, in mild to moderate AD compared to no cognitive impairment (NCI) cases.¹⁷⁻¹⁸ Furthermore, TrkA receptor densities in cholinergic NB neurons are diminished in MCI and AD in contrast with NCI.¹⁹ In early-stage AD, TrkA protein levels are also reduced in cortical regions – where TrkA is naturally expressed in lower concentrations compared to the basal forebrain and caudate putamen (CP).²⁰ Analogously, the decline in cortical TrkB receptor and BDNF levels are also found in AD patients.²¹ In fact, dysregulation of the BDNF/TrkB system is found in a variety of neurodegenerative/psychiatric diseases and neuropathological conditions such as Parkinson's disease (PD), Rett syndrome, Huntington's disease (HD), schizophrenia and traumatic brain injury (TBI).²²⁻²⁵ Moreover, accumulating evidence supports the critical involvement of Trk in malignant transformations, chemotaxis, anoikis resistance, metastasis and survival signaling in various neural and non-neural human cancers including pancreatic, lung, prostate and neuroendocrine tumors.²⁶⁻³⁰

Therefore, Trk receptors have been actively pursued as therapeutic targets for both neurological and oncological diseases.³¹⁻³² The development of non-invasive *in vivo* imaging probes allowing the assessment and quantitation of Trk levels would provide an invaluable tool to evaluate Trk-related neurological and oncological conditions. Such a research tool would offer a deeper understanding of the expression and functions of those receptors within the normal as well as pathological nervous system. It would provide a molecular instrument for the

assessment of receptor occupancy and therapeutic effects during current drug development efforts. Among available imaging techniques, positron emission tomography (PET) is particularly well suited to address these objectives owing to its high sensitivity and dynamic measurement.

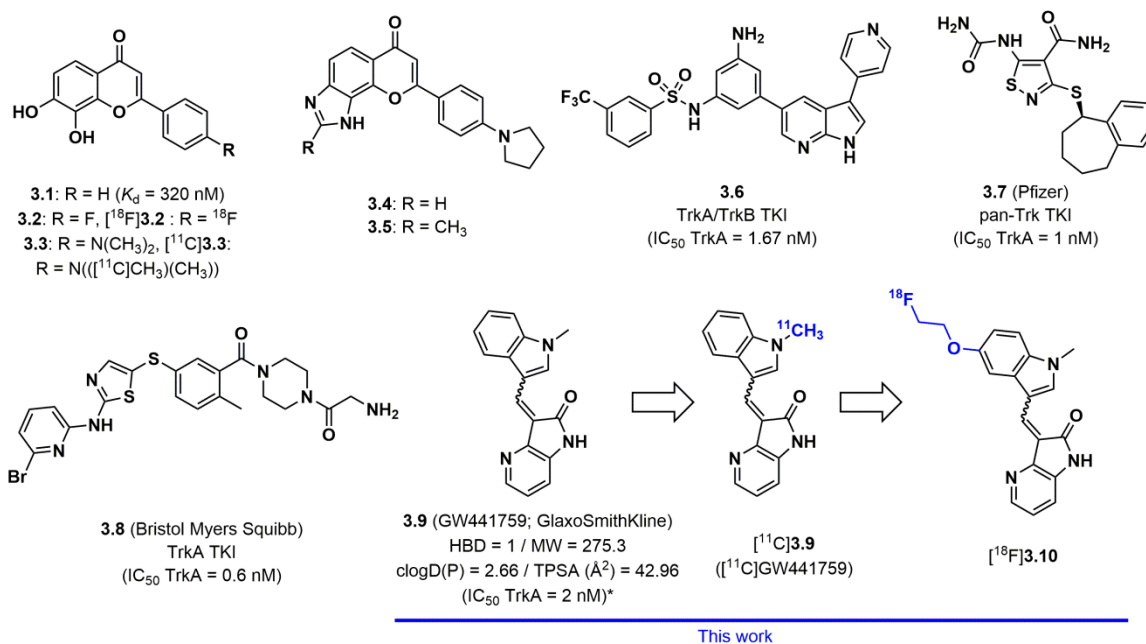


Figure 3.1. Chemical structures of Trk agonists, tyrosine kinase inhibitors and Trk radioligands.*From Ref. 47.

Small molecules (MW < 500 Da) binding Trk receptors have been explored from two distinct perspectives. First, from a neurological standpoint, efforts have mainly been directed at compounds exerting their effect upon binding the extracellular domain (ECD) of Trk receptors.³¹ This approach has relied on either random screening or neurotrophin mimicry and typically targets challenging druggable sites corresponding to clefts in protein-protein interfaces from individual Trk/neurotrophin heterodimers.³³⁻³⁵ One of the rare examples of successful non-peptidic EDC-binding Trk probes of this type is the TrkB-selective agonist 7,8-dihydroxyflavone (**3.1**, $K_d \approx 320$ nM; **Figure 3.1**) and its derivatives.³⁶⁻³⁸ From an oncological perspective, applications have focused on the intracellular well-characterized kinase domain, which has led to the identification of numerous and structurally diverse potent tyrosine kinase inhibitors (TKI).³²

Some examples of Trk-TKI include 3,5-disubstituted 7-azaindoles **3.6** (TrkA IC_{50} = 1.67 nM),³⁹ isothiazole **3.7** (TrkA IC_{50} = 1 nM)⁴⁰ and 2-amino-5-(thioaryl)thiazole **3.8** (TrkA IC_{50} = 0.6 nM)⁴¹ (**Figure 3.1**). As a result of important kinase homology sequences of the different Trk isoforms, Trk-TKI, including the aforementioned inhibitors, generally present limited intra-Trk selectivity profiles – but often display excellent selectivity over non-Trk kinase targets.⁴²

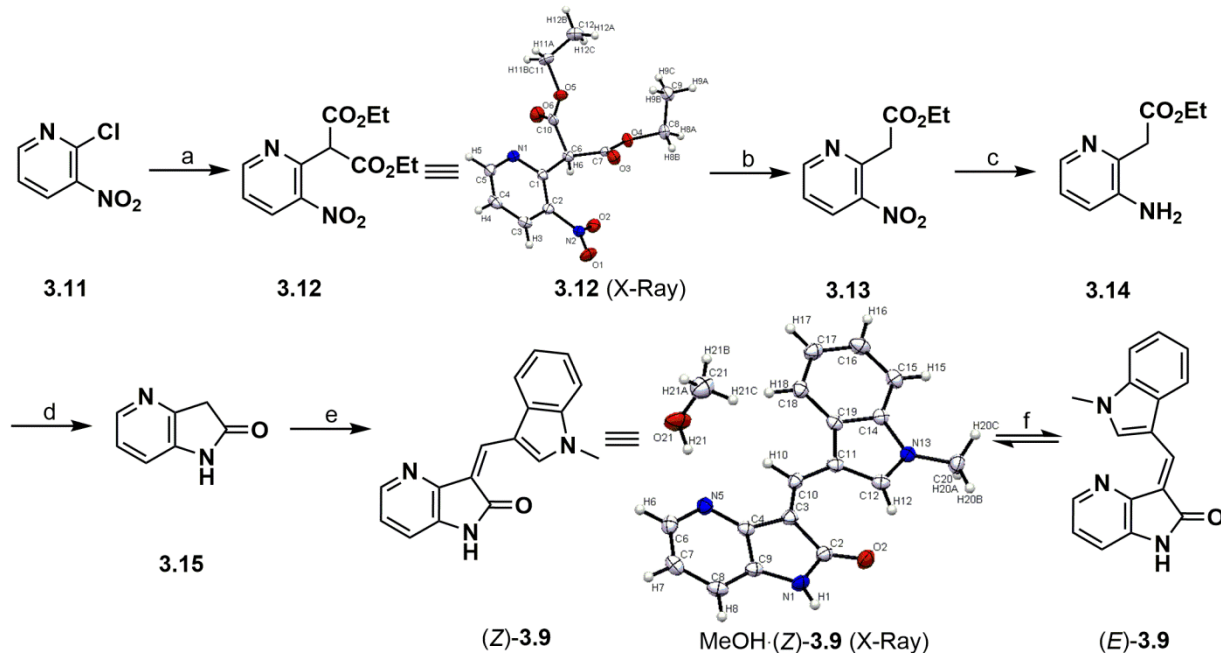
Our group has recently reported the radiosyntheses of the first radiotracers aimed at Trk PET imaging.⁴³ The probes evaluated, 4'-[¹⁸F]-7,8-DHF ([¹⁸F]**3.2**) and 4'-([N-methyl-¹¹C]-dimethylamino-7,8-DHF ([¹¹C]**3.3**) (**Figure 3.1**), are derivatives of 7,8-dihydroxyflavone (**1**). Despite promising *in vitro* autoradiographic profiles paralleling [¹²⁵I]-BDNF assays⁴⁴ and showing BDNF-competitive binding, the tracers were subject to rapid hepatic *in vivo* metabolism caused by the catechol moiety and were consequentially found unsuitable for PET brain imaging. While bioisosteric modifications of those EDC-binding tracers are currently underway, we aimed at accessing Trk receptors via the intracellular kinase domain with radiolabeled TKIs. As the ultimate goal of this project is the development of PET tracer candidates for both peripheral tumor and central nervous system imaging, our probe identification efforts were focused on TKIs with narrowed physicochemical properties such as : 1) blood-brain barrier (BBB) permeation and neuroreceptor imaging binding potential (ideally $BP = B_{max}/K_d > 10$), 2) molecular weight (MW) ≤ 305 , 3) calculated distribution coefficient ($cLogD_{7.4}$) in the range of 2.0-3.5), 4) topological polar surface area (TSPA) of 30-80Å² and 5) hydrogen bond donor (HBD) ≤ 1 .⁴⁵⁻⁴⁶ Based on those and other crucial considerations such as radiolabeling compatibility, we selected 3-((1-methyl-1*H*-indol-3-yl)methylene)-1*H*-pyrrolo[3,2-*b*]pyridin-2(3*H*)-one (GW441756, **3.9**)⁴⁷ from an initial screening of over one hundred reported Trk-TKIs. 4-Aza-2-oxindole **3.9** displays favourable physicochemical properties for BBB permeation (**Figure 3.1**) and high TrkA affinity (IC_{50} = 2 nM) leading to theoretical binding potentials up to $BP > 6.6$ in TrkA-rich brain regions (B_{max} = 13.2 fmol mg⁻¹tissue in rat CP).⁴⁸ Also, **3.9** displays >100 fold selectivity over off-

target tested kinases⁴¹ and importantly, can be readily converted into a radiolabeled *N*-[¹¹C]-methyl isotopologue for *in vivo* PET imaging.

In the present study, the development of the 4-aza-2-oxindole Trk-binding tracer [¹¹C]**3.9** is described, including the syntheses of (*Z*)-**3.9** along with the desmethyl precursor (*E*)-**3.16**, their intrinsic isomerization properties and a molecular modeling investigation. Results from biological evaluations are provided including the *in vitro* enzymatic activity of **3.9** for all Trk receptors (TrkA, TrkB and TrkC), rat brain and human neuroblastoma *in vitro* autoradiography studies of [¹¹C]**3.9**, metabolic studies as well as microPET imaging experiments, demonstrating that [¹¹C]**3.9** readily crosses the BBB but binds non-specifically in the rat brain. Furthermore, a series of novel highly potent 4-aza-2-oxindole-based Trk inhibitors amenable for ¹¹C- or ¹⁸F-radiochemistry are described. This effort led to the synthesis of [¹⁸F]**3.10** which demonstrates promising *in vitro* profile. The tracer [¹¹C]**3.9** is the first brain penetrating Trk radioligands described and suggest that 4-aza-2-oxindoles represent a potentially versatile scaffold for further development of PET Trk probes.

3.3 Results and discussion

3.3.1 Synthesis and photoisomerization of (Z)-3.9. Inhibitor **3.9** belongs to the family of 3-arylideneindolin-2-one RTK inhibitors with anti-oncogenic properties.⁴⁹⁻⁵² Typically the arylidene fragment in these structures is incorporated via base-catalyzed or acid-promoted aldehyde condensation with a suitable indolin-2-one intermediate. In the present case, we synthesized the required precursor 4-aza-indoline-2-one (**3.15**) in four steps and 48% overall yield from 2-chloro-3-nitropyridine (**3.11**) as previously described but without detailed instructions and characterization (**Scheme 3.1**).⁴⁷ Intermediate **3.12** was also characterized by single molecule X-ray crystallography.



Scheme 3.1. Synthesis of (Z)-3.9 and (E)-3.9. Reagents and conditions: (a) NaH, dimethyl malonate, DMSO, rt, 30 min then 100°C, 1 h (97 %). (b) LiCl, H₂O, DMSO, rt - 100°C, 18h (98 %). (c) H₂ (1 atm), Pd/C, MeOH, rt, 6 h (98 %). (d) HCl_{aq} (2.0N), Et₂O, rt, 12 h, 52% (52 %). (e) 1-Methylindole-3-carboxaldehyde, AcOH, HCl_{conc}, 40°C, 12 h (65 %). (f) H₂O/MeCN (1:1), visible light (ambient conditions). Single-Crystal X-Ray structure of 3.12 and MeOH·(Z)-3.9; ellipsoids drawn at 70% probability.

The exocyclic olefin can adopt a strict *Z* conformation, *E* conformation or exists as a *Z/E* mixture, depending on the nature of the arylidene fragment in 3-substituted indolin-2-ones.⁴⁴ Increased inhibitory activities for various kinases have previously been reported for compounds preferentially adopting the *Z* conformation.^{50, 52-53} Initial synthesis of 3.9 by Wood *et al.*⁴⁷ described the isolation of a crude 8:1 mixture of non-specified isomeric composition. In our experiments, the condensation of 3.15 with 1-methylindole-3-carboxaldehyde in glacial acetic acid and concentrated HCl at 40°C gave 3.9 as a single isomer in 65% yield after flash chromatography (**Scheme 3.1**). This compound was identified as the *Z* isomer based on the characteristic ¹H NMR downfield chemical shift (9.48 ppm) corresponding to the H-2' proton in proximity to the carbonyl group.^{49, 53} This assignment was unambiguously confirmed by single molecule X-ray crystallography elucidation of the planar (Z)-3.9 MeOH adduct (**Scheme 3.1**).

Mechanistically, the preferential formation of the *Z* isomer under the reaction conditions used can be rationalized considering the least sterically hindered transition state of the stabilized β -hydroxyketone intermediate which ultimately dictates the orientation of the arylidene moieties relative to the 4-azaoxindole core (**Scheme S3.1, Supporting Information**). Despite the isolation of the pure crystalline (*Z*)-**3.9**, we observed under various conditions rapid photoisomerization leading to the formation of a mixed-isomers photostationary state (PSS) of equimolar *E/Z* composition (**Figure S3.1, Supporting Information**). The *N*-desmethyl radiolabeling precursor **3.16** for ^{11}C -radiomethylation was then synthesized in good yields following the procedure used for preparing (*Z*)-**3.9** (**Figure 3.3A**). Interestingly, this product was obtained as the pure *E* isomer based on the H-2' proton ^1H NMR peak found 10.02 ppm (**Figure S3.2, Supporting Information**). This structural assignment is in agreement with previous NMR characterization of 3-substituted 4-azaindolin-2-ones derivatives.⁴⁹ We hypothesized that the isolation of (*E*)-**3.15** was the consequence of a base-promoted isomerization during the workup procedure. Despite the fact that it should be expected that the inhibitory activity of **3.9** arises from the interaction of the *Z* isomer with the ATP binding pocket (*vide infra*), we anticipated that the radiomethylation of (*E*)-**3.16** would release [^{11}C]**3.9** as a \approx 1:1 *E/Z* mixture owing to the rapid photoisomerization irrespective of the isomeric composition of the precursor.

3.3.2 In vitro binding assays. Our focus on **3.9** as a potential radiotracer originated from the early work by Wood *et al.* which demonstrated that **3.9** displays a 2 nM IC_{50} for TrkA inhibition and >100-fold selectivity for TrkA over a panel of receptor tyrosine kinases (C-FMS, ITK, VEGFR2), non-receptor tyrosine kinases (SRC), mitogen-activated kinases (CDK1, CDK2, JNK3, p38, ERK) and histidine kinases (PDHK4).⁴⁷ Yet, all Trk inhibitors characterized to date only display at best marginal intra-Trk selectivity as the three Trk isoforms share between 71.9% and 78.3% of their kinase domain and between 95% to 100% residue identity when considering only the 40 amino acids that are potentially involved in ligand binding from the DFG-in ATP

binding site.⁵⁴ Therefore, we sought to evaluate the ability of MeOH•(Z)-**3.9** to inhibit the entire human Trk receptor family –TrkA, TrkB and TrkC. Hence, the compound MeOH•(Z)-**3.9** was tested in a radiolabeled ATP-based *in vitro* enzymatic assay and was shown to inhibit TrkA with an IC₅₀ of 29.6 nM, but 4- and 6-fold more potent against TrkB and TrkC respectively (IC₅₀ TrkB = 6.7 nM and IC₅₀ TrkC = 4.6 nM) (**Figure 3.2D**). Although the specific isomeric composition responsible for the observed *in vitro* inhibition could not be determined, our previous photoisomerization study suggests that it was derived from a near equimolar *E/Z* mixture (in dilute solutions).

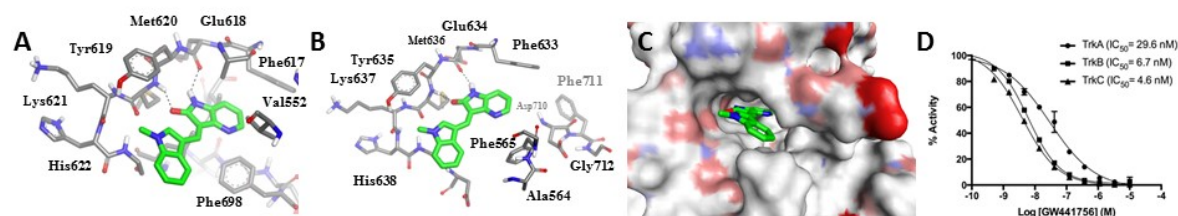


Figure 3.2. Comparison of the predicted binding poses for (Z)-**3.9** bound to (A) TrkC (PDB code: 3V5Q) with a DFG-out binding mode and to (B,C) TrkB (PDB code: 4AT3) and with a DFG-in binding mode. The lactam moiety of (Z)-**3.9** forms H-bonding interactions between with Glu634 and Met636 from TrkB and Glu618 and Met620 from TrkC. The coloring of the protein surface emphasizes positive/neutral/negative atom charge (red, white, blue). (D) Dose-response curves and comparison of IC₅₀ values for the *in vitro* kinase assays with **3.9** (GW441756) versus TrkA, TrkB and TrkC. The inhibitor (**3.9**) was tested at ten different concentrations using serial dilution, experiments were carried out in duplicates in the presence of 1 μ M of ATP and error bars represent standard deviation from the mean.

3.3.3 Molecular docking study of compound 3.9. In order to gain insight into the putative binding modes of **3.9** and indications for potential positions for eventual structural modifications, a docking study was performed using the FITTED program.⁵⁵⁻⁵⁷ Assessment of the differences in the binding poses of (Z)-**3.9** and (E)-**3.9** as well as the influence of the activation state of the kinase domain on binding were first conducted. Accordingly, we selected the available crystal structures of (1) the activated (DFG-in) TrkB kinase domain (PDB code: 4AT3) and (2) the inactivated (DFG-out) TrkC kinase domain (PDB code: 3V5Q). Docking of (Z)-**3.9** on both proteins converged on analogous binding poses anchoring the ligand via H-bonding interactions

between the lactam proton with Glu634 or Glu618 and the carbonyl oxygen atom with Met636 or Met620 in TrkB and TrkC respectively (**Figure 3.2A-C**). Edge-to-face stacking interactions are also present between the pyridine ring and the gatekeeper Phe633 (TrkB) and Phe617 (TrkC). This binding mode does not involve interactions with the DFG motif and is overall consistent with most available 3-arylideneindolin-2-one -based ligands co-crystallized with various kinases (DFG-in)⁵⁸⁻⁶¹ as well as TrkC (DFG-out).⁴² On the other hand, attempts of docking (*E*)-**3.9** did not convincingly generate adequate binding modes with TrkB and TrkC, presumably due to unfavorable protein contact between the 1-methylindole and Phe565 in TrkB (DFG-in) and Phe698 in TrkC (DFG-out) (**Figure 3.2A,B**). An alternative binding mode, which brings the 1-methylindole fragment into the vicinity of Phe589, could be obtained from the docking of (*E*)-**3.9** with TrkA (PDB code: 4AOJ) (**Figure S3.3, Supporting Information**), but this binding mode within the ATP binding site has only been rarely encountered in co-crystal structures and is associated with low affinity ligands.⁶²

As expected, the binding pose of (*Z*)-**3.9** with TrkA corroborates the previously modeled TrkB- and TrkC-(*Z*)-**3.9** interactions (**Figure S3.4B**). The docking information also exposed small discrepancies in non-covalent interactions between TrkA and TrkB/TrkC that may account for the moderate selectivity of **3.9** for the latter (See Supporting Information, **Figure S4**). Taken together, those results support the hypothesis that Trk inhibition of **3.9** involves the binding of the *Z* geometric isomer within the ATP binding site and provide reasonable details to explain the observed differences in IC₅₀S.

3.3.4 Radiolabeling of [¹¹C]3.9. Radiolabeling of (*E*)-**3.16** was performed by reacting the precursor with [¹¹C]methyl iodide ([¹¹C]CH₃I) – obtained from reduction/iodination of cyclotron-produced [¹¹C]CO₂ – in either DMF or acetone in the presence of a suitable base (**Figure 3A,B**). Optimization reactions were carried out in duplicates at room temperature for 5 min. Initial radiomethylation attempts with minute amounts of aqueous NaOH in acetone only yielded (*E*)-

[^{11}C]3.9 with $5.0 \pm 0.3\%$ radiochemical yield (RCY, HPLC-based and non-decay corrected, n.d.c.). However, the labeling was found to be highly efficient in the presence of either Cs_2CO_3 in DMF or solid KOH suspended in acetone. Under those conditions, (*E*)-[^{11}C]3.9 was obtained in $48 \pm 13.0\%$ and $49 \pm 2.5\%$ RCYs (HPLC-based and non-decay corrected) respectively.

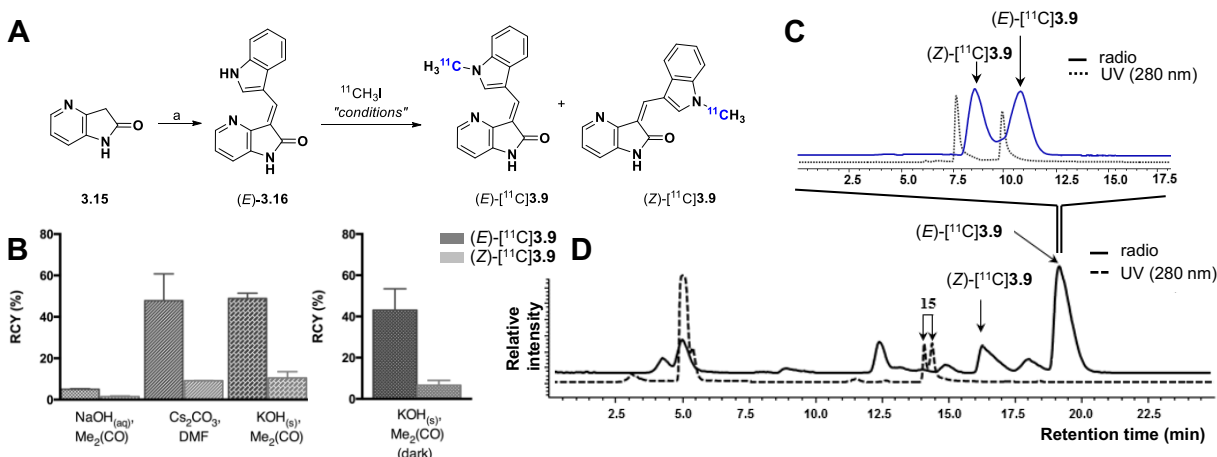


Figure 3.3. Synthesis of precursor (*E*)-3.16 and radiosyntheses of (*Z*)-[^{11}C]3.9 and (*E*)-[^{11}C]3.9. (A) Reagents and conditions: (a) Indole-3-carboxaldehyde, AcOH, HCl_{conc} , 40°C , 12 h. (B) Optimization for the radiosynthesis of (*Z*)-[^{11}C]3.9 and (*E*)-[^{11}C]3.9; the RCYs are calculated by radio-HPLC and reported as the $\text{RCY} \pm \text{SD}$ (%) (n.d.c.) from two independent experiments. Reagents and conditions: 1.0 mg of precursor (*E*)-3.15 in 250 μL of solvent; (*left*) i. $\text{NaOH}_{(\text{aq})}$ (4.0N, 5.0 μL); ii. Cs_2CO_3 (10 mg); iii. $\text{KOH}_{(\text{s})}$ (10 mg). (*right*) i. $\text{KOH}_{(\text{s})}$ (10 mg), no light. (C) HPLC radiodetection QC of the collected (*E*)-[^{11}C]3.9 peak at time of microPET injection showing racemization (HPLC method D). The dash line correspond to the UV trace of (*Z*)-3.9 and (*E*)-3.9 (0.7 min calibrated delay between UV and radioactivity detector). (D) HPLC separation of (*Z*)-[^{11}C]3.9 and (*E*)-[^{11}C]3.9 from (*E*)-3.15 (HPLC method B).

Radiomethylation in the presence of stronger bases such as NaH or *t*-BuOK in THF only resulted in radioactive side-product formation. Reactions leading to the formation of (*E*)-[^{11}C]3.9 also afforded non-negligible and consistent amounts of (*Z*)-[^{11}C]3.9 corresponding to 0.23 ± 0.06 of the *E* isomer (HPLC-based and non-decay corrected **Figure 3.3B,D**). Considering the low $\text{p}K_{\text{a}}$ of the N-H indole moiety in (*E*)-3.16 ($\text{p}K_{\text{a}} < 12$),⁶³ we hypothesize that the radiomethylation quantitatively proceeds via the highly conjugated potassium (caesium) enolate azatriene intermediate (**Figure S3.5A, Supporting Information**). Thus, the isomeric ratio of the ^{11}C -labeled end products likely reflects the proportion of 3-8'-*s-cis* and 3-8'-*s-trans* intermediates, and not the isomeric composition of the precursor. Moreover, the formation of (*Z*)-[^{11}C]3.9 was

not the result of a light-induced isomerization of the (*E*)-[¹¹C]**3.9** product, as the labeling reactions performed in light-protected conical vials with the identical KOH/acetone conditions resulted in similar RCYs and *Z*:*E* ratios (**Figure 3.3B**). Moreover, the quantitative formation of a strongly conjugated anionic intermediate was confirmed by the UV-visible absorbance spectra of (*E*)-**3.16** which undergoes a characteristic and rapid bathochromic shift of around 50 nm in the presence of NaOH under labeling conditions in water (**Figures S3.5, S3.6, Supporting Information**).⁶³

Therefore, the tracer [¹¹C]**3.9** could easily be obtained as a *E*:*Z* (1:1) mixture as anticipated. Reverse-phase HPLC purification and collection of the *E* isomer peak afforded (*E*)-[¹¹C]**3.9** in 26 ± 5.7% (*n* = 8) RCY n.d.c. (based on starting activity of [¹¹C]CH₃I) which, within the time required for sterile medium formulation for imaging studies (*t* ~ 5 min), reached a PSS composed of approximately equimolar quantities of both *Z* and *E* isomers as expected (Figure 3C). The formulated tracer was obtained in >98% radiochemical purity and specific activities ranging from 29.6-59.2 GBq/μmol at the end of synthesis in a procedure of approximately 60 min from bombardment and was stable for over 60 min at room temperature.

3.3.5 In vitro metabolism of [¹¹C]3.9**.** Tracer [¹¹C]**3.9** (mixed isomers) was highly stable in rat plasma *in vitro*. No significant decomposition was observed by reverse phase radio-HPLC upon incubation for 60 min at 37°C (>99% [¹¹C]**3.9** unchanged). In addition, *in silico* predictions of the phase I cytochrome P450 (CYP) mediated sites of metabolism (SoM) were carried out using IMPACTS.⁶⁴ This study provided the top two predicted sites of oxidation (**Figure 3.4**) and transition states modeling (**Figure S3.7, Supporting Information**) for a set of five CYP isoenzymes responsible for 90% of xenobiotics metabolism in human (CYP1A2, CYP2C9, CYP2D6, CYP3A4, CYP2C19).⁶⁵⁻⁶⁶

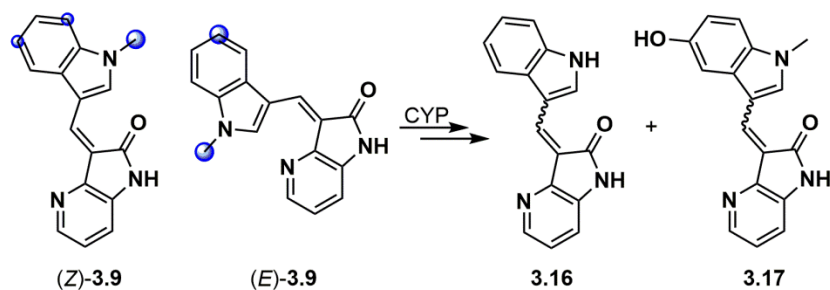


Figure 3.4. *In silico* top predicted CYP-mediate sites of metabolism for (Z)-3.9 and (E)-3.9 and corresponding metabolites confirmed by RLM assays.

1-Methylindole carbon (C'-1) was identified as the main SoM over the entire set of CYP evaluated for both (Z)-3.9 and (E)-3.9. Aromatic hydroxylations at C-5' and C-7' were also predicted. *In vitro* microsomal assays with rat liver microsome (RLM) and the non-radioactive inhibitor 3.9 (*E/Z* mixture) were consistent with the computational predictions and confirmed that phase I metabolism preferentially led to the slow formation of desmethyl metabolite 3.16 (over 90 min). HPLC analysis at various time points also revealed the formation of a minor and more polar metabolite consistent with a hydroxylated metabolite (Peak A, **Figure S3.8**).

3.3.6 *In vitro* autoradiography of [¹¹C]3.9. Binding of [¹¹C]3.9 in the brain was assessed using *in vitro* autoradiography with rat brain slices ($n = 3$) over successive coronal sections ($n = 10$). Nonspecific binding was evaluated by co-incubation with excess of the corresponding non-radioactive ligand. **Figures 3.5A** illustrates representative autoradiograms of brain slices after incubation with [¹¹C]3.9 and blocking experiments along with the histological staining of the immediately adjacent sections. The radiotracer displays widespread displaceable binding to essentially all areas of the forebrain, midbrain and hindbrain including the neocortex, striatum, thalamus, hippocampus and cerebellum with the exception of white matter. The extensive binding distribution of [¹¹C]3.9 is in agreement with the near ubiquitous expression of TrkB and TrkC in the mammal brain as assessed by mRNA *in situ* hybridization and [¹²⁵I]BDNF, [¹²⁵I]NT-4/5 and [¹²⁵I]NT-3 binding studies.⁴⁴ Binding in the whole brain was uniformly reduced by $69.2 \pm$

1.5% ($n = 30$ sections) upon co-incubation with excess of **3.9** ($10 \mu\text{M}$, **Figure 3.5B**). Moreover, the lack of preferential binding in the caudate putamen suggests that [^{11}C]**3.9** does not preferentially bind to TrkA. This result is in line with the IC_{50} values obtained which showed moderate selectivity for TrkB/C (*vide supra*). The binding to TrkB and TrkC is also supported by the superior receptor densities of those isoforms compared to TrkA in virtually all brain regions including the caudate putamen – $B_{\text{max}} ([^{125}\text{I}]\text{NT-3}) = 26 \text{ fmol mg}^{-1} \text{ tissue}$ versus $B_{\text{max}} ([^{125}\text{I}]\text{NGF}) \leq 13.2 \text{ fmol mg}^{-1} \text{ tissue}$.⁶⁷ It is likely that non-displaceable binding during blocking experiments ensued in part from off-Trk but kinase-specific interactions.

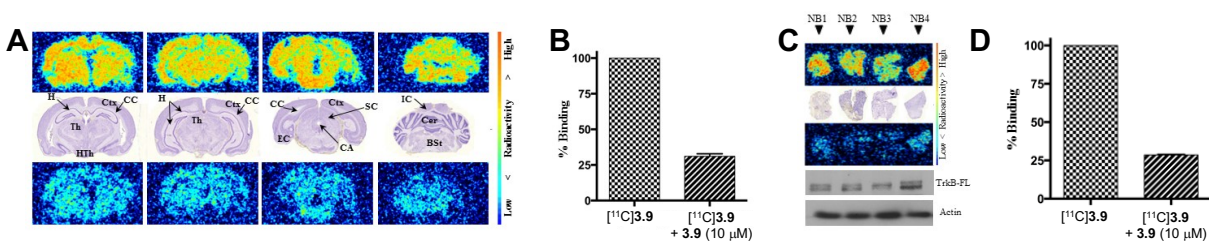


Figure 3.5. (A) Representative in vitro autoradiography in four representative coronal sections of rat brain. (*Upper row*) Autoradiography images showing the binding of [^{11}C]**3.9** alone. (*Middle row*) Cresyl violet staining of the corresponding coronal sections. BSt = brain stem; CA = cerebral aqueduct; CC = corpus callosum; Cer = cerebellum; Ctx = cortex; EC = entorhinal cortex; H = hippocampus; HTh = hypothalamus; IC = inferior colliculus, SC = superior colliculus; Th = Thalamus. (*Lower row*) Autoradiography images showing the binding of [^{11}C]**3.9** in co-incubation with unlabeled **3.9** ($10 \mu\text{M}$). (B) Quantitative results of blocking experiments with brain sections. (C) In vitro autoradiography of four representative sections from four human neuroblastoma tumor. Autoradiography images showing the binding of [^{11}C]**3.9** alone, cresyl violet staining of the corresponding sections and binding of [^{11}C]**3.9** in co-incubation with unlabeled **3.9** ($10 \mu\text{M}$). Western blots analysis of the TrkB (FL: full length) protein levels. Actin was used as loading control. (D) Quantitative results of blocking experiments from human neuroblastoma tumor cryosections. Value expressed as mean \pm SD (from the average of 10 sections from three rat brain and (from four tumors with 2 sections analyzed each).

Owing to the critical role of Trk receptors in various neoplasms,²⁶⁻³⁰ we sought to investigate the potential of [^{11}C]**3.9** for tumor imaging. In neuroendocrine tumors and neuroblastomas in particular, heterogeneous expression of Trk is strongly predictive of clinical outcomes, TrkB and BDNF being highly expressed in aggressive tumors with poor prognoses.^{30,}

⁶⁸⁻⁶⁹ **Figure 3.5C** shows representative autoradiograms of four human neuroblastoma samples

after incubation with [^{11}C]3.9 in identical conditions as previously used for brain samples along with the corresponding histological staining. Binding of [^{11}C]3.9 was highly heterogeneous and significantly reduced upon co-incubation with 3.9 ($\Delta = -71.3 \pm 0.3 \%$, $n = 4$; **Figure 3.5C,D**). To confirm TrkB expression in the tumor samples, western blot analysis was performed with homogenate of each tumor.

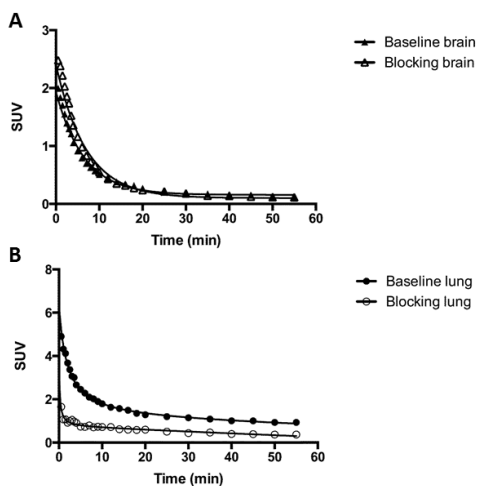


Figure 3.6. PET studies in Sprague Dawley rats. Time-radioactivity curves (TACs) illustrate the accumulation of [^{11}C]3.9 in (A) the whole brain and (B) the lungs as function of time for baseline studies and for pretreatment studies with 3.9 (1 mg/kg, i.v. 15 min prior to [^{11}C]3.9 injection). SUV, standardized uptake value.

3.3.7 *In vivo* PET imaging of [^{11}C]3.9 in rats. Using microPET imaging, [^{11}C]3.9 was preliminary evaluated in Sprague Dawley rats to determine brain permeation and *in vivo* distribution. In a brain scan at baseline, the tracer rapidly crossed the BBB, peaked at a maximum of 2.0 SUV (standardized uptake value) in the whole brain within 30 sec, then decreased rapidly over the remaining 60 min of scanning as depicted by the time-activity curve in **Figure 3.6A**. Regional brain distribution was uniform as could be expected from the near ubiquitous Trk expression in the CNS. A second imaging experiment conducted to assess the specific binding of [^{11}C]3.9 where unlabeled inhibitor 3.9 was administered 15 min prior to tracer injection (1 mg/kg, i.v.) demonstrated that the uptake of [^{11}C]3.9 in the rat brain was essentially

non-specific. The somewhat higher brain uptake in the pretreatment study may imply saturation of peripheral receptors while the similarly fast kinetics in baseline/blocking studies show that brain clearance overwhelms Trk-specific binding in the brain during the time of scanning. In another experiment, a thoracic/abdominal PET scan revealed hepatobiliary clearance of the tracer as well as an important uptake of radioactivity in the lungs in agreement with high pulmonary Trk-receptor concentrations (**Figure 3.6B**).⁷⁰⁻⁷¹ Pretreatment with unlabeled **3.9** (1 mg/kg, i.v. 15 min prior to [¹¹C]**3.9** injection) resulted in a marked reduction of the radioactivity uptake in the lungs compared to baseline – from 4.9 SUV to 1.6 SUV at 1 min and from 0.4 SUV to 0.1 SUV at 55 min. Blocking also resulted in a more pronounced renal radioactivity uptake. Those observations support the additional evaluation of [¹¹C]**3.9** in non-rodent species due to known drug pharmacokinetics inter-species differences, as well as a derivatization into a radiolabeled tracer with a longer physical half-life (e.g. fluorine-18).

3.3.8 Design, syntheses and structure-activity-relationship (SAR) of 4-aza-2-oxindole derivatives towards ¹⁸F-labeling. On the basis of our previous results with [¹¹C]**3.9**, the possibilities of potential derivatives of ¹⁸F-labeled analogues of **3.9** were explored. The selected structural alterations were chosen based on molecular modeling information from the interaction of **3.9** with TrkB/C (**Figure 3.2A-C**; **Figure 3.7A**) and their accessibility as carbon-11 and fluorine-18 isotopologues. The solvent exposed phenyl moiety from the indole core of **3.9** appeared to provide derivatization opportunities and was therefore explored. In particular, introduction of methoxy or 2-fluoroethoxy fragments (selected for radiolabeling purposes) at positions C4' and C5' seemed to potentially allow additional interactions either directly or via water-mediated contacts with Asp624 (TrkC) or Asp640 (TrkB) as exemplified with docking simulations (**Figure 3.7B,C**). The 2-fluoroethoxy substitution at C6' position appeared more problematic owing to the close proximity of Arg598, Lys643 and Lys627 in TrkA, TrkB and TrkC respectively.

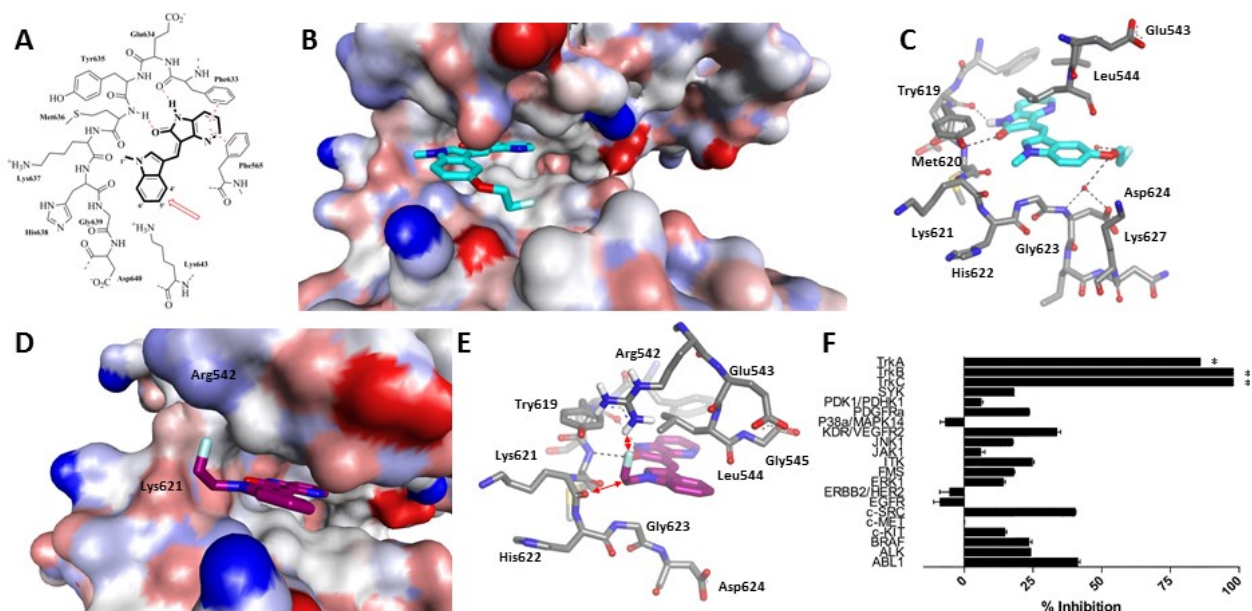
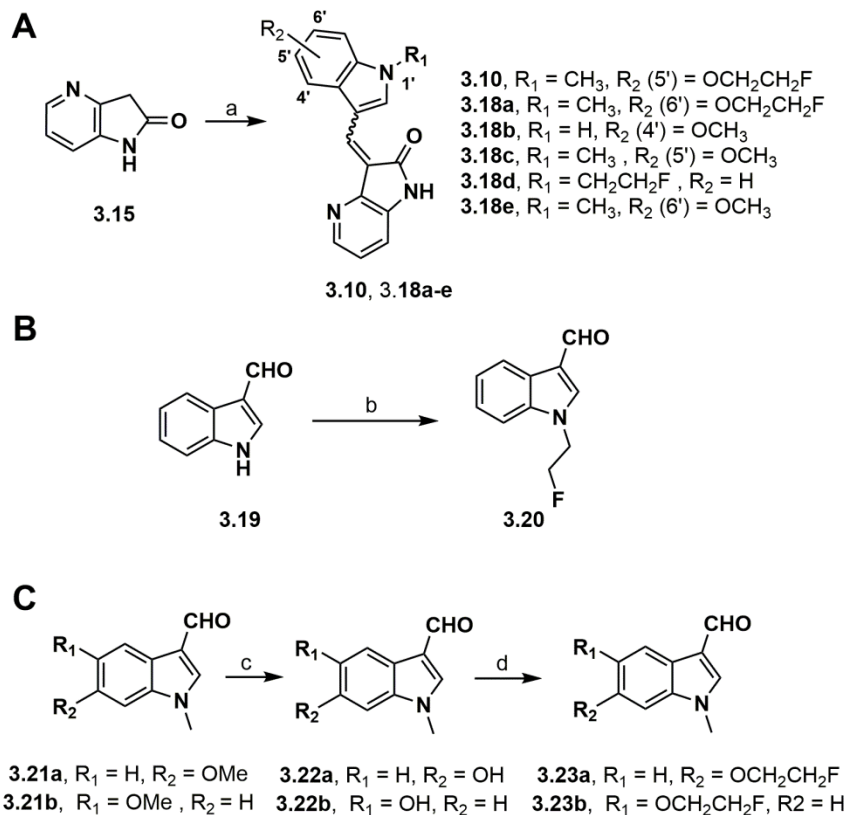


Figure 3.7. Design rationale and docking modes for 4-aza-oxindole-based Trk inhibitors. (A) Potential binding site interaction between TrkB and inhibitor (*Z*)-**3.9** based on docking studies. (B,C) Overviews of the predicted binding pose of fluorinated (*Z*)-**3.10** in the ATP-binding site of TrkC (PDB code: 3V5Q). (D,E) Overviews of the predicted binding pose of (*Z*)-**3.18d** in the ATP-binding site of TrkC. The coloring of the protein surface emphasizes positive/neutral/negative atom charge (red, white, blue). (F) Inhibitory activity of **3.10** on 18 kinases at 500 nM ($n = 2$). *Derived from IC_{50} curves.

Despite being the most straightforward modification, the introduction of a 2-fluoroethyl moiety at the *N*-1' position of the indole fragment seemed disfavored compared to **3.9** due to repulsive interactions with the proximal backbone of the hinge forcing a gauche conformation bringing the fluorine substituent into close proximity with residues from the glycine rich loop for all TrkA/B/C receptors (**Figure 3.7D,E**). Still, to corroborate our binding model, the *N*-fluoroethyl derivative was included in the small series of synthesized derivatives (**Scheme 3.2, Table 3.1**). The synthesis of compounds **3.10** and **3.18a-e** relied on the same approach as for **3.9** using suitable indole-3-carboxaldehyde building blocks (**Scheme 3.2A**). The intermediates **3.22a,b** were prepared from the C5'/C6'-OMe precursors via BBr_3 -promoted deprotection in high yields and compounds **3.20** and **3.23a,b** were obtained via alkylation with 2-fluoroethyl 4-methylbenzenesulfonate (**Scheme 3.2B,C; Supporting Information**).



Scheme 3.2. Syntheses of 3-((1-methyl-1H-indol-3-yl)methylene)-1H-pyrrolo[3,2-b]pyridin-2(3H)-one. Reagents and conditions: (a) indole-3-carboxaldehyde fragment, AcOH, HCl_{conc}, 40°C, 12 h (43 – 72 %). (b) NaH, 2-fluoroethyl 4-methylbenzenesulfonate, THF, 0°C – rt, 12 h (96 %). (c) BBr₃, CH₂Cl₂, 0°C – rt, 3 h (94 – 100 %). (d) K₂CO₃, 2-fluoroethyl 4-methylbenzenesulfonate, DMF, 70°C, 12 h (72 – 80 %).

The synthesized derivatives, as well as the previously used desmethyl compound **3.16**, were tested for TrkA/B/C receptor binding. **Table 3.1** lists IC₅₀ values, isolated isomeric compositions, selected isomerization studies as well as physico-chemical properties. Compounds having an *N*-alkylated indole position were isolated as *Z* isomers while the non-alkylated compound **3.18b** bearing an highly acidic indole proton was, as shown with **3.16** previously, obtained as the *E* configurational isomer (*vide supra*). Configuration assignment was based on our previous X-ray structure determination in combination with the characteristic H¹-NMR signal from *E* and *Z* isomers as described earlier (see also **Figure S3.9-3.10, Supporting Information**).

Table 3.1. Potency and Physico-Chemical Data for 4-Aza-2-Oxindole Trk Inhibitors

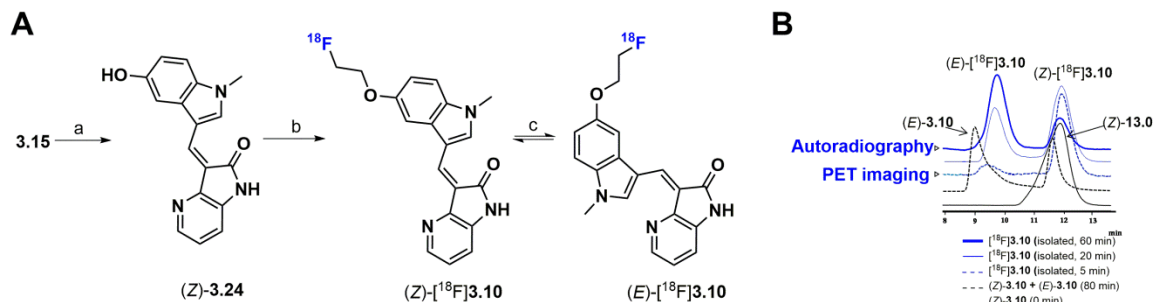
| Cpd | clogP ^a | TPSA (Å ²) ^a | % of Z isomer ^b | IC ₅₀ (nM) ^c | | | B _{max} /IC ₅₀ | B _{max} /IC ₅₀ | TrkC selectivity (over TrkA) |
|--------------|--------------------|--|--------------------------------------|------------------------------------|------|------|------------------------------------|------------------------------------|---------------------------------------|
| | | | | TrkA | TrkB | TrkC | (TrkA) ^d | (TrkB/C) ^d | |
| 3.9 | 2.66 | 42.96 | 100/56/nt ^e | 29.6 | 6.7 | 4.6 | 0.5 | 3.9 | 6.4 |
| 3.16 | 2.48 | 57.78 | <1/nt ^f /nt ^e | 103 | 34.0 | 10.9 | 0.1 | 0.8 | 9.4 |
| 3.10 | 2.87 | 56.15 | >99/95/40 | 28.3 | 4.1 | 3.4 | 0.5 | 6.3 | 8.3 |
| 3.18a | 2.87 | 56.15 | 100/nt ^f /nt ^e | 62.1 | 10.1 | 9.1 | 0.2 | 2.9 | 6.8 |
| 3.18b | 2.39 | 70.80 | 0/nt ^f /nt ^e | 15.1 | 1.4 | 2.0 | 0.9 | 18.6 | 7.6 |
| 3.18c | 2.48 | 59.90 | 100/97/24 | 16.3 | 1.7 | 2.1 | 0.8 | 12.4 | 7.8 |
| 3.18d | 2.69 | 46.92 | 100/nt ^f /nt ^e | 660 | 108 | 45.9 | 0.02 | 0.6 | 14.4 |
| 3.18e | 2.48 | 59.90 | 100/nt ^f /nt ^e | 71.9 | 6.3 | 4.7 | 0.2 | 5.5 | 15.3 |

^aValues were computed with the program Pallas 3.7 for Windows (CompuDrug; San Francisco, CA). ^bThe % of Z isomer was calculated based on the ratio of the diagnostic ¹H NMR H-2' peak at isolation (*t* = 0 min) in *d*₆-DMSO and after ambient light incubation in *d*₆-DMSO/D₂O (5:1) after *t* = 120 min and *t* = 2 days. Values are presented as % of Z at *t* = 0 min/*t* = 120 min/*t* = 2 days. ^cValues from enzymatic assays. ^dCalculated with *B*_{max} value for the caudate putamen and from the whole brain from Ref. 48 and the IC₅₀s from TrkB. ^ent = not tested.

NMR-based photoisomerism analysis for selected inhibitors confirmed that visible light exposition results in PSS formation of different isomeric compositions (**Table 3.1**). To our satisfaction and in agreement with modeling studies, all substitutions were well tolerated except for the *N*-fluoroethyl inhibitor **3.18d** which was characterized by a marked decrease in potencies compared to the lead (IC₅₀ = 660 nM for TrkA, IC₅₀ = 108 nM for TrkB and IC₅₀ = 45.9 nM for TrkC). The presence of an OMe or fluoroethoxy group at position C5' and C6' had a negligible

to modestly favourable impact on potency compared to **3.9**, except in the case of the C6'-fluoroethoxy inhibitor **3.18a** as expected ($IC_{50} = 62.1$ nM for TrkA, $IC_{50} = 10.1$ nM for TrkB and $IC_{50} = 9.1$ nM for TrkC). Replacement of the *N*-methyl fragment by an NH group negatively affected potency for all Trk receptors (especially TrkB) for compound **3.16** but increased the potency when combined with the 4'-OMe substitution in **3.18b**, suggesting that the loss of van der Waals interactions at the *N*-1' position may be compensated by additional hydrogen bonding permitted through the oxygen of the C4' substituent. It is also important to bear in mind that small discrepancies in potency may ensue from different fractions of *Z*-isomer in the PSS of those inhibitors which could not be characterized in detail for the enzymatic assay. All inhibitors displayed modest 6 to 15-fold inter-Trk selectivity (TrkC \approx TrkB $>$ TrkA). Considering those results, compound **3.10** was selected for radiotracer development as the most favorable fluorinated derivative in the series ($cLogP = 2.87$; $TPSA = 56.16 \text{ \AA}^2$; $IC_{50} = 28.3$ nM for TrkA, $IC_{50} = 4.1$ nM for TrkB and $IC_{50} = 3.4$ nM for TrkC; $B_{max}/IC_{50} = 6.3$ for TrkB/C; see [Table 3.1](#)).

Prior to its conversion into a potential PET tracer, a more detail description of the selectivity profile of **3.10** was sought ([Figure 3.7F](#)). The compound was therefore tested for inhibitory activity at 500 nM concentration with a panel of 18 cancer-related kinases with an additional focus on kinase targets expressed at high concentration in neurons and various components of the mammalian CNS under non-pathological conditions.⁷²⁻⁷⁶ Kinases tested were focused on closely related tyrosine kinases (TK) but also encompassed kinases from other major branches (TLK, CMGC and AGC). Inhibitor **3.10** demonstrated excellent specificity and >120-fold greater potency for TrkB/C and >15-fold greater potency for TrkA compared to all other tested kinases (ABL1, ALK, BRAF, c-KIT, c-MET, c-SRC, EGFR, ERBB2/HER2, ERK1, FMS, ITK, JAK1, JNK1, KDR/VEGFR2, P38a/MAPK14, PDGFRa, PDK1/PDHK1, SYK; tested at Reaction Biology Corporation).



Scheme 3.3. Synthesis and photoisomerization of (Z)-[¹⁸F]3.7b. (A) Reagents and conditions: (a) **3.22b**, AcOH, HCl_{conc}, 40°C, 12 h (44 %). (b) KOH(s), [¹⁸F]FETos, DMF, 90°C, 10 min (2.5 ± 0.6 % RCY, *n* = 4, non-decay corrected isolated yield from ¹⁸F/¹⁸H₂O). (c) ambient light. (B) HPLC radiodetection QC of the collected (Z)-[¹⁸F]3.10 (*t_R* = 12.3 min) peak at 20 and 80 min post isolation showing racemization leading to the formation of (E)-[¹⁸F]3.10 (*t_R* = 9.8 min) (blue lines) and UV chromatogram of the corresponding (Z)-3.10 (*t_R* = 11.5 min) and isomerized sample (*E* isomer, *t_R* = 9.0 min) (black lines).

3.3.9 Radiolabeling of [¹⁸F]3.10. The radiolabeling of [¹⁸F]3.10 was achieved using a two-step procedure involving the synthesis of 2-[¹⁸F]fluoroethyl tosylate ([¹⁸F]FETos)⁷⁷ followed by the fluoroalkylation of precursor (Z)-3.24 under basic conditions (**Scheme 3.3**). The phenolic precursor (Z)-3.24 was obtained and characterized as previously described for analogous structures (*vide supra*). Azeotropic drying of anionic fluorine-18 and radiosynthesis of [¹⁸F]FETos were carried out on a modified PET tracer module (Scintomics GRP) with in-house manifold setup and afforded [¹⁸F]FETos in 27.0 ± 2.0 % RCY (*n* = 4, non-decay corrected isolated yield from ¹⁸F/¹⁸H₂O) after reverse-phase HPLC purification. This intermediate was aliquoted and used in a manual procedure for the alkylation of (Z)-3.24 (typically 0.74 GBq; ~ 20 mCi). Following a second HPLC purification, [¹⁸F]3.10 was obtained in sufficient yields for preliminary biological evaluation (2.5 ± 0.6% n.d.c. RCY, end of bombardment) over a 60 min procedure in > 98% radiochemical purity and 122 – 180 GBq/μmol specific activities. A photoisomerization study of [¹⁸F]3.10 demonstrated a slower isomerization kinetic as compared to [¹¹C]3.9 (**Scheme 3.3B**). In spite of the slower rate of photoconversion, the tracer ultimately reached a PSS composed of a ~ 2:1 (*E/Z*) mixture when unshielded from light over 60 min, as compared to the fast-reached 1:1 mixture observed for [¹¹C]3.9. The lower rate of isomerization,

which turned out to be advantageous in providing the tracer in > 90% of the putative potent Z isomer for preliminary PET imaging studies (after final formulation, the tracer was immediately injected into the animal to minimize photoconversion), was ascribed to the electron donating nature of the alkyloxy substituent in **3.10** which may disfavor electron delocalization from the *N*-1' position of the indole core as compared to **3.9**.

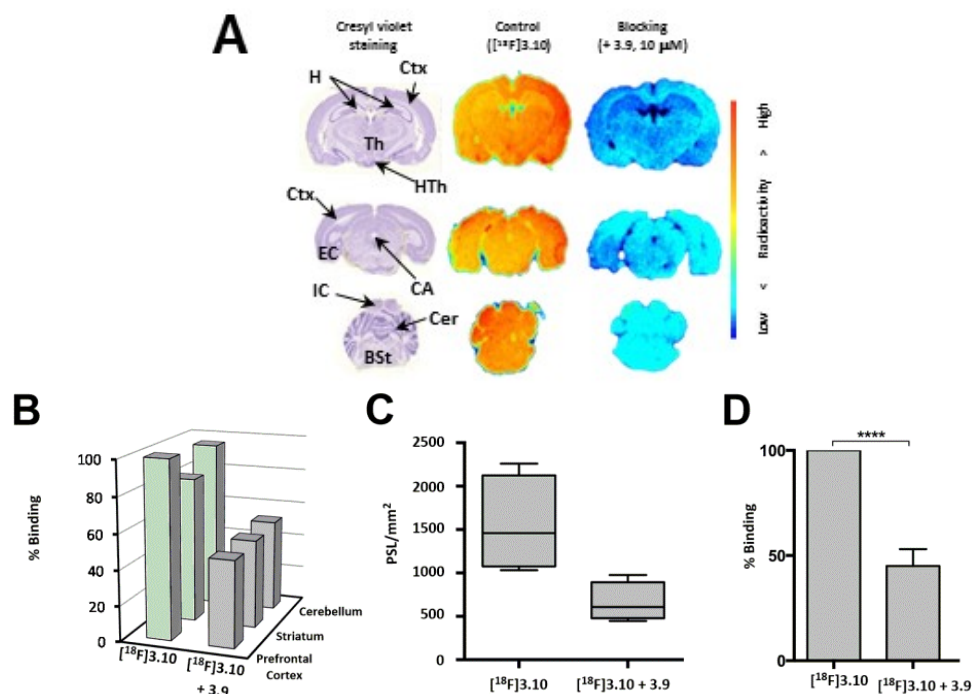


Figure 3.8. (A) Representative in vitro autoradiograms and cresyl violet staining from coronal sections of rat brain showing the binding of $[^{18}\text{F}]\mathbf{3.10}$ and competition experiments with **3.9** (10 μM). Autoradiograms have the same absolute intensity range. BSt = brain stem; CA = cerebral aqueduct; Cer = cerebellum; Ctx = cortex; EC = entorhinal cortex; H = hippocampus; HTh = hypothalamus; IC = inferior colliculus; Th = Thalamus. (B) Quantitative results of competition experiments for selected regions of interest (ROI's) relative to control for prefrontal cortex. (C,D) Quantitative results of baseline and blocking experiments with neuroblastoma. Human neuroblastoma tumor cryosections ($n = 4$). PSL/mm² = photo-stimulated luminescence events per square millimetre. Value expressed as mean \pm SD ($n = 4$). **** $p < 0.0001$.

3.3.10 In vitro autoradiography of $[^{18}\text{F}]\mathbf{3.10}$. In an analogous study as previously detailed for $[^{11}\text{C}]\mathbf{3.9}$, the distribution of $[^{18}\text{F}]\mathbf{3.10}$ in rat brain and human neuroblastoma was assessed (Figure 3.8). Binding of $[^{18}\text{F}]\mathbf{3.10}$ in the rat brain was rather ubiquitous, similar to our previous results with $[^{11}\text{C}]\mathbf{3.9}$. Yet, a more detailed analysis of selected regions of interest (prefrontal

cortex, striatum and cerebellum) revealed small regional differences. Binding to the prefrontal cortex and the cerebellum (TrkB/C-rich regions) was more pronounced than what was found for the striatum (TrkA-rich region), which is in line with the Trk isoform selectivity of **3.10** and the regional concentration of the different Trk receptors. In the presence of an excess of unlabeled **3.9**, binding of [¹⁸F]**3.10** was significantly reduced in all evaluated regions ($\Delta = -52\%$ for prefrontal cortex, $\Delta = -39\%$ for striatum and $\Delta = -45\%$ for cerebellum, **Figure 3.8A,B**). Binding to neuroblastoma cryosections was heterogeneous (**Figure 3.8C**) and also significantly reduced by pre-treatment with excess **3.9** ($\Delta = -55.0 \pm 8.0\%$, $n = 4$; **Figure 3.8D**, see also **Figures S3.12, Supporting Information**).

3.3.11 Preliminary in vivo PET imaging of [¹⁸F]3.10 in rats. The evaluation of the *in vivo* distribution of [¹⁸F]**3.10** was assessed with PET in rats (tracer at injection was > 90% (Z)-[¹⁸F]**3.10**, **Figure 3.9A, B**). Similar to the results obtained with [¹¹C]**3.9**, the regional brain distribution of [¹⁸F]**3.10** was uniform. Yet, a major difference regarding phase I metabolism arose when comparing [¹⁸F]**3.10** to [¹¹C]**3.9**. Whereas the non-fluorinated inhibitor **3.9** was found stable in RLM assays, the fluoroethoxy-linked inhibitor **3.10** was highly susceptible towards CYP450 metabolism at the 2-fluoroethoxy C-1 position. Rapid formation of **3.24** detected by HPLC was observed. This ultimately led to the formation of more polar metabolites – presumably further desmethylated/hydroxylated products (**Figure 3.9D**). Those results were paralleled by *in silico* predictions (O-dealkylation >> N-dealkylation > C-hydroxylation). The immediate consequence of this oxidative metabolism for [¹⁸F]**3.10** is the sustained formation of ¹⁸F-labeled brain penetrating metabolites stemming from the release and further *in vivo* reduction/oxidation of 2-[¹⁸F]fluoroacetaldehyde (**3.26**, **Figure 3.4D**).⁷⁸ Moreover, pretreatment with **9** (1 mg/kg, i.v., 15 min prior to tracer injection) did not alter brain pharmacokinetics or maximal radioactivity uptake significantly. This is consistent with the brain distribution being dominated by radiometabolites which are inactive towards Trk. This suggests that further

structural derivatization is needed to arrive at a fluorinated 3-indolydene 4-aza-2-oxindole scaffold suitable for Trk PET radioligands. For example, a fluoroalkyl chain without phenolic oxygen might be required in order to avoid unwanted elimination of the radionuclide bearing moiety.

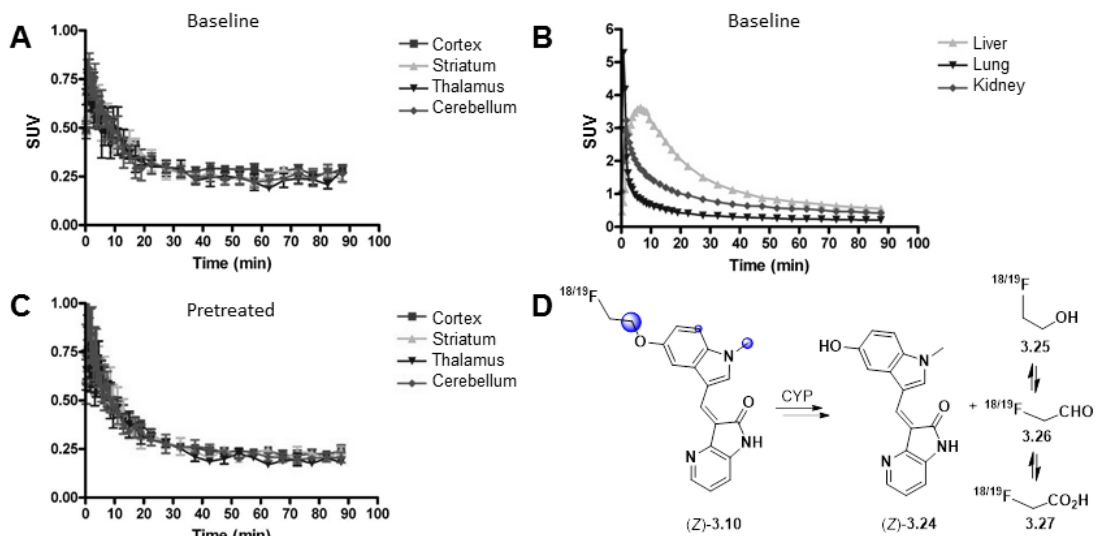


Figure 3.9. Preliminary metabolism and PET studies with [^{18}F]3.10 in sprague dawley in rats. Time–activity curves for (A) brain regions ($n = 3$) at baseline, (B) for selected organs ($n = 1$) and (C) brain regions ($n = 3$) for pretreatment studies with 3.9 (1 mg/kg, i.v. 15 min prior to [^{18}F]3.10 injection, $n = 3$). SUV, standardized uptake value. (D) *In silico* top predicted CYP-mediate sites of metabolism for (*E/Z*)-3.10 confirmed by RLM assays.

3.4 Conclusion

In summary, we have explored the 3-indolydene 4-aza-2-oxindole scaffold for the potential development of pan-Trk PET ligands. We presented the radiosynthesis of 3-((^{11}C)-1-methyl-1*H*-indol-3-yl)methylene)-1*H*-pyrrolo[3,2-*b*]pyridin-2(3*H*)-one (^{11}C]GW441756, [^{11}C]3.9) along with the synthesis, photoisomerism characterization and biological evaluation of the corresponding nonradioactive highly potent inhibitor. Promising *in vitro* and *in vivo* profiles of [^{11}C]3.9 led to the radiosynthesis of [^{18}F]3.10 selected from a small series of novel highly potent pan-Trk inhibitors. [^{18}F]3.10 displayed excellent Trk selectivity in a panel of brain and cancer

relevant kinases and Trk-specific binding *in vitro* in rat brain and human neuroblastoma cryosections. PET imaging studies in rodents provided valuable biodistribution information. Radioligand [¹¹C]**3.9** exhibited higher brain uptake and metabolic stability towards CYP450 compared to [¹⁸F]**3.10**. In both cases, albeit for distinct reasons, the radioactivity in the brain was nonspecifically distributed. Currently, the major drawback of those tracers as a potential class of Trk-targeted PET ligands remains their propensity towards photoisomerization even though we could show that small structural modifications may have a significant impact on the rate of formation and isomer ratios in the PSS (compound **3.9** vs **3.10**). Hence, structural optimization is underway to generate an isomerically and metabolically stable counterpart to the 3-indolydene 4-aza-2-oxindole scaffold. Collectively, this work constitutes the first promising basis for future developments of Trk radioligands for *in vivo* PET imaging.

3.5 Material and methods

General. All moisture sensitive reactions were carried out in oven-dried flasks under nitrogen atmosphere with dry solvents. Reagents and solvents were purchased at the highest commercial quality from Fisher, Sigma-Aldrich or Alfa-Aesar, and were used without further purification unless specified otherwise. Organic solutions were concentrated under reduced pressure on a Heidolph rotary evaporator. In general, reactions were magnetically stirred and monitored by TLC performed on pre-coated glass-backed TLC plates (Analtech, 250 microns) and chromatographic purification of products was accomplished using flash chromatography on Alfa-Aesar silica gel (230-450 mesh). TLC visualization was performed by fluorescence quenching, KMnO_4 or ninhydrin. ^1H NMR and ^{13}C NMR spectra were recorded on a 300 Varian Mercury spectrometer in CDCl_3 or d_6 -DMSO and peak positions are given in parts per million using TMS as internal standard. Peaks are reported as: s = singlet, d = doublet, t = triplet, q = quartet, p = quintet, m = multiplet, b = broad; coupling constant(s) in Hz; integration. High Resolution Mass Spectra (HRMS) and LC-MS/MS analysis were obtained from the Regional Center for Mass Spectrometry of The Chemistry Department of the Université de Montréal (LC-MSD-TOF Agilent). Radio TLCs were monitored using Mini Gita (Raytest).

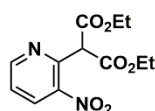
$[^{11}\text{C}]\text{MeI}$ for radiolabeling was prepared by reducing cyclotron-produced $[^{11}\text{C}]\text{carbon dioxide}$ ($[^{11}\text{C}]\text{CO}_2$) (IBA cyclotron (Cyclon 18/9); prepared by the $^{14}\text{N}(p,\alpha)^{11}\text{C}$ reaction with 0,5% O_2). Lithium aluminum hydride (LiAlH_4) in THF reduced the $[^{11}\text{C}]\text{CO}_2$ to $[^{11}\text{C}]\text{methanolate}$, followed by iodination with 57% hydroiodic acid. Gamma counting was performed using a CRC-25PET Dose Calibrator (Capintec, Ramsey, NJ, USA). No-carrier-added (n.c.a) aqueous $[^{18}\text{F}]\text{fluoride}$ was prepared by the $^{18}\text{O}(p,n)^{18}\text{F}$ nuclear reaction on an enriched $[^{18}\text{O}]\text{water}$ (98 %) target.

HPLC Methods. Analytical and radio-preparative HPLC were performed on an Agilent 1200 system (Agilent Technologies, Santa Clara, CA, USA; running on Agilent ChemStation software) equipped with a Raytest Gabi Star radioactivity detector (Raytest Isotopenmessgeräte GmbH, Straubenhardt, Germany) and a Phenomenex aeris peptide 3.6u XB-C18 column (250*4.60 mm).

Method A: elution at 0.8 ml min^{-1} with a mixture of H_2O (A) and MeCN (B) isocratic at 40% A and 60% B ($t_{r(Z)-3.9} = 4.48 \text{ min}$, $t_{r(E)-3.9} = 5.28 \text{ min}$). Method B: elution at 0.6 ml min^{-1} with a mixture of H_2O (A) and MeCN (B) starting at 80% A from 0 to 1 min, decreasing from 80% A to 50% A from 1 to 3 min, remaining at 50% A from 3 to 20 min ($t_{r(Z)-3.9} = 15.59 \text{ min}$, $t_{r(E)-3.9} = 18.49 \text{ min}$). Method C: elution at 0.4 ml min^{-1} with a mixture of H_2O (A) and MeCN (B) starting at 80%

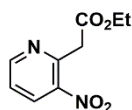
A at 0 min and decreasing to 50% A from 0 to 3 min, remaining at 50% A from 3 to 30 min ($t_{r(Z)-3.9} = 21.24$ min, $t_{r(E)-3.9} = 25.17$ min). Method D: elution at 0.4 ml min^{-1} with a mixture of H_2O (A) and MeCN (B) isocratic at 50% A and 50% B ($t_{r(Z)-3.9} = 7.87$ min, $t_{r(E)-3.9} = 10.17$ min). Method E: (Phenomenex partisil 5u OSD(3) column (250×4.60 mm) elution at 1.0 ml min^{-1} with a mixture of H_2O (A) and MeCN (B) isocratic at 30% A and 70% B ($t_{r(Z)-3.9} = 4.99$ min, $t_{r(E)-3.9} = 5.54$ min). Method F: (Phenomenex partisil 5u OSD(3) column (250×4.60 mm) elution at 1.0 ml min^{-1} with a mixture of H_2O (A) and MeCN (B) isocratic at 50% A and 50% B ($t_{r(Z)-3.10} = 11.5$ min, $t_{r(E)-3.10} = 9.0$ min).

Chemical Synthesis.



Diethyl (3-nitropyridin-2-yl)-malonate (3.12). To a solution of sodium hydride (60% dispersion in oil, 0.6 g, 25 mmol, 2.3 equiv.) in DMSO (25 mL) was added dimethyl malonate (3.8 mL, 25 mmol, 2.3 equiv.) dropwise over 20 min and the mixture was stirred for an additional 30 min at room temperature. 2-chloro-3-nitropyridine (1.74 g, 11 mmol, 1 equiv.) was added to the reaction and the reaction was heated at 100°C for 1h. The reaction was cooled to room temperature and poured into aqueous ammonium chloride (saturated solution, 45 mL). The aqueous solution was extracted with ethyl acetate. The combined organic phases were dried over Na_2SO_4 and concentrated *in vacuo*. The crude residue was purified by flash chromatography (30% EtOAc/hexane) and afforded 3.0 g of the title compound as a orange oil (97%). R_f 0.40 (30% EtOAc/hexane).

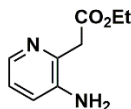
^1H NMR (300 MHz, CDCl_3) δ 8.81 (d, $J = 4.5$ Hz, 1H), 8.48 (d, $J = 8.4$ Hz, 1H), 7.52 (dd, $J = 8.4$ Hz, $J = 4.8$ Hz, 1H), 5.51 (s, 1H), 4.28 (q, $J = 7.2$ Hz, 4H), 1.27 (t, $J = 7.2$ Hz, 6H) ppm. ^{13}C NMR (300 MHz, CDCl_3) δ 166.4, 153.0, 149.0, 144.8, 133.2, 123.8, 62.1, 59.3, 13.9 ppm. HRMS (APCI) calcd for $\text{C}_{12}\text{H}_{14}\text{N}_2\text{O}_6$ ($\text{M}+\text{H}$) $^+$ 283.09246, found 283.09175.



Ethyl 2-(3-nitropyridin-2-yl)-acetate (3.13). A suspension of diethyl (3-nitropyridin-2-yl)-malonate (5.6 g, 20 mmol, 1 equiv.) in DMSO (65 mL) and water (0.37 mL, 20 mmol, 1 equiv.)

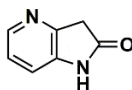
was added lithium chloride (2.1 g, 50 mmol, 2.5 equiv.) at room temperature. The reaction was heated to 100°C overnight and more lithium chloride (1 g, 24 mmol) was added to the reaction. The reaction was heated for another 6 h and cooled to room temperature. The reaction mixture was poured into brine (100 mL) and the aqueous phase was extracted ethyl acetate. The organic layers were combined and dried over Na₂SO₄ and concentrated in *vacuo*. The crude residue was purified by flash chromatography (10-50% EtOAc/hexane) and afforded 4.1g of the title compound as a red oil (98%). R_f 0.62 (50% EtOAc/hexane).

¹H NMR (300 MHz, CDCl₃) δ 8.77 (d, *J* = 4.5 Hz, 1H), 8.41 (d, *J* = 8.4 Hz, 1H), 7.47 (dd, *J* = 8.4 Hz, *J* = 4.5 Hz, 1H), 4.31 (s, 2H), 4.17 (q, *J* = 7.2 Hz, 2H), 1.24 (t, *J* = 7.2 Hz, 3H) ppm. ¹³C NMR (300 MHz, CDCl₃) δ 169.1, 153.0, 150.0, 132.9, 123.2, 109.9, 61.4, 43.2, 14.0 ppm. HRMS (APCI) calcd for C₉H₁₁N₂O₄ (M+H)⁺ 211.07133, found 211.07186.



Ethyl 2-(3-amino-pyridin-2-yl)-acetate (3.14). To a solution of ethyl 2-(3-nitro-pyridin-2-yl)-acetate (2.7 g, 13 mmol, 1 equiv.) in ethanol (20 mL) was added Pd/C (10%, 0.2 g) slowly. The reaction was placed under an atmosphere of hydrogen and stirred at room temperature for 6 h. The reaction was filtered through celite and the filtrate was concentrated in *vacuo* (98%). R_f 0.28 (50% EtOAc/hexane).

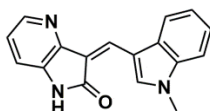
¹H NMR (300 MHz, DMSO) δ 7.94 (d, *J* = 5.4 Hz, 1H), 7.70 (d, *J* = 8.7 Hz, 1H), 7.59 (dd, *J* = 8.7 Hz, *J* = 5.4 Hz, 1H), 6.51 (s, 2H), 4.17 (s, 2H), 4.09 (q, *J* = 6.9 Hz, 2H), 1.17 (t, *J* = 6.9 Hz, 3H) ppm. ¹³C NMR (300 MHz, CDCl₃) δ 168.1, 147.2, 131.9, 128.7, 128.0, 126.4, 61.5, 34.1, 14.4 ppm. HRMS (APCI) calcd for C₉H₁₃N₂O₂ (M+H)⁺ 181.09715, found 181.09642.



1H-pyrrolo[3,2-*b*]pyridin-2(3H)-one (4-aza-2-oxindole) (3.15). To a solution of ethyl 2-(3-amino-pyridin-2-yl)-acetate (2.4 g, 13 mmol, 1 equiv.) in diethyl ether (100 mL) at room temperature was added a hydrochloric acid solution (2M, 50 mL) and the reaction was stirred for 12 hours. The diethyl ether was removed *in vacuo* and the aqueous phase was brought to pH 7 and was concentrated in *vacuo*. The crude residue was purified by flash chromatography (5%

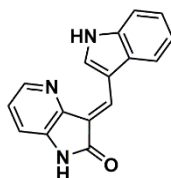
MeOH/AcOEt) and afforded 0.92 g of the title compound as a beige solid (52%). R_f 0.28 (5% MeOH/EtOAc).

^1H NMR (300 MHz, DMSO- d_6) δ 10.50 (s, 1H), 8.03 (dd, $J = 4.7$ Hz, $J = 1.8$ Hz, 1H), 7.15-7.08 (m, 2H), 3.55 (s, 2H) ppm. ^{13}C NMR (300 MHz, DMSO- d_6) δ 174.7, 149.0, 141.9, 138.9, 122.8, 115.4 ppm. HRMS (ESI) calcd for $\text{C}_7\text{H}_7\text{N}_2\text{O}$ (M+H) $^+$ 135.05529, found 135.05499.



(3Z)-3-[(1-methyl-1H-indol-3-yl)methylene]-1,3-dihydro-2H-pyrrolo[3,2-b]pyridin-2-one ((Z)-3.9). 1-Methylindole-3-carboxaldehyde (0.318 g, 2 mmol, 1 equiv), 4-aza-2-oxindole (0.268 g, 2 mmol, 1 equiv.), acetic acid (20 mL) and concentrated HCl (5mL) were combined at room temperature and then warmed to 40°C for 12 h. The mixture was concentrated in *vacuo* and the crude was added to a NaHCO_3 solution (sat.) and extracted several times with ethyl acetate. The organic layers were combined and dried over Na_2SO_4 and concentrated in *vacuo*. The crude residue was purified by flash chromatography (5% MeOH/AcOEt) and afforded 340 mg of a red solid (65%) and then recrystallized from MeOH/EtOAc. R_f 0.79 (5% MeOH/EtOAc).

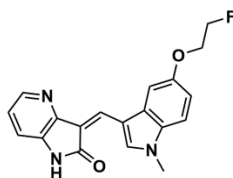
^1H NMR (300 MHz, DMSO) δ 10.66 (s, 1H), 9.48 (s, 1H), 8.33 (s, 1H), 8.12 (dd, $J = 4.8$ Hz, $J = 1.5$ Hz, 1H), 7.97 (dd, $J = 6.6$ Hz, $J = 1.8$ Hz, 1H), 7.60 (dd, $J = 6.6$ Hz, $J = 1.8$ Hz, 1H), 7.31 (m, 2H), 7.15 (dd, $J = 7.8$ Hz, $J = 1.5$ Hz, 1H), 7.08 (dd, $J = 7.8$ Hz, $J = 4.8$ Hz, 1H), 3.95 (s, 3H) ppm. ^{13}C NMR (300 MHz, CDCl_3) δ 167.2, 145.4, 141.6, 139.0, 137.2, 134.2, 129.0, 128.9, 123.4, 122.3, 121.7, 118.3, 117.4, 115.2, 111.5, 110.8, 34.1 ppm. HRMS (ESI) calcd for $\text{C}_7\text{H}_7\text{N}_2\text{O}$ (M+H) $^+$ 276.11314, found 276.11266.



(3E)-3-[(1H-indol-3-yl)methylene]-1,3-dihydro-2H-pyrrolo[3,2-b]pyridin-2-one (3.16). Indole-3-carboxaldehyde (0.318 g, 2 mmol, 1 equiv), 4-aza-2-oxindole (0.268 g, 2 mmol, 1 equiv.), acetic acid (20 mL) and concentrated HCl (5mL) were combined at room temperature and then warmed to 40°C for 12h. The mixture was concentrated in *vacuo* and the crude was

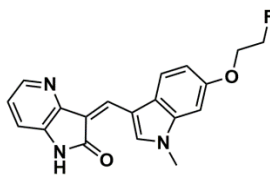
added to a NaHCO₃ solution (sat.) and extracted several times with ethyl acetate. The organic layers were combined and dried over Na₂SO₄ and concentrated in *vacuo*. The crude residue was purified by flash chromatography (100% AcOEt) and afforded 350 mg of a yellow solid (75%). R_f 0.66 (100% EtOAc).

¹H NMR (300 MHz, DMSO) δ 12.26 (s, 1H), 10.53 (s, 1H), 10.02 (s, 1H), 8.28 (d, *J* = 4,17 Hz, 1H), 8.06 (s, 1H), 7.92 (m, 1H), 7.55 (m, 1H), 7.26-7.13 (m, 4H) ppm. ¹³C NMR (300 MHz, CDCl₃) δ 168.9, 144.1, 141.5, 136.9, 136.8, 136.6, 130.5, 128.4, 123.3, 121.9, 118.3, 117.7, 115.4, 113.1, 112.2, 109.9 ppm. HRMS (ESI) calcd for C₇H₇N₂O (M+H)⁺ 262.09749, found 262.09742.



(Z)-3-((5-(2-fluoroethoxy)-1-methyl-1H-indol-3-yl)methylene)-1,3-dihydro-2H-pyrrolo[3,2-b]pyridine-2-one ((Z)-3.10). The general procedure used for the synthesis of (Z)-9 was followed using 5-(2-fluoroethoxy)-1-methyl-1H-indole-3-carbaldehyde (0.123 g, 0.55 mmol) as starting material. The crude residue was purified by flash chromatography (100% AcOEt) and afforded 81.0 mg of a red solid (43%). R_f 0.42 (80% EtOAc/Hexane).

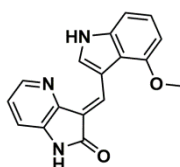
¹H NMR (300 MHz, DMSO-*d*₆) δ 10.64 (s, 1H), 9.45 (s, 1H), 8.33 (s, 1H), 8.11 (dd, *J* = 4.8 Hz, *J* = 1.5 Hz, 1H), 7.52 (s, 1H), 7.51 (d, *J* = 6.3 Hz, 1H), 7.14 (dd, *J* = 7.8 Hz, *J* = 1.5 Hz, 1H), 7.08 (dd, *J* = 7.65 Hz, *J* = 4.8 Hz, 1H), 6.96 (dd, *J* = 8.85 Hz, *J* = 2.4 Hz, 1H), 4.77 (td, *J* = 47.7 Hz, *J* = 3.9 Hz, 2H), 4.37 (td, *J* = 30.6 Hz, *J* = 3.9 Hz, 2H), 3.92 (s, 3H) ppm. ¹³C NMR (75 MHz, DMSO-*d*₆) δ 167.3, 155.0, 145.6, 141.5, 139.3, 134.1, 132.4, 129.9, 129.4, 121.5, 116.7, 115.1, 113.8, 112.5, 110.9, 101.3, 82.0 (*J* = 165.6 Hz), 67.7 (*J* = 18.9 Hz), 34.2 ppm. HRMS (ESI) calcd for C₁₉H₁₇FN₃O₂ (M+H)⁺ 338.12993, found 338.13073.



(Z)-3-((6-(2-fluoroethoxy)-1-methyl-1H-indol-3-yl)methylene)-1,3-dihydro-2H-pyrrolo[3,2-b]pyridine-2-one ((Z)-3.18a). The general procedure used for the synthesis of (Z)-9 was

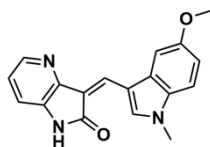
followed using 6-(2-fluoroethoxy)-1-methyl-1*H*-indole-3-carbaldehyde (0.133 g, 0.6 mmol) as starting material. The crude residue was purified by flash chromatography (100% AcOEt) and afforded 106.5 mg of a red solid (53%). R_f 0.42 (80% EtOAc/Hexane).

^1H NMR (300 MHz, DMSO- d_6) δ 10.64 (s, 1H), 9.37 (s, 1H), 8.27 (s, 1H), 8.11 (d, J = 4.8 Hz, 1H), 7.85 (d, J = 8.7 Hz, 1H), 7.21 (d, J = 1.2 Hz, 1H), 7.16-7.06 (m, 2H), 6.95 (dd, J = 8.7 Hz, J = 1.8 Hz, 1H), 4.77 (td, J = 48 Hz, J = 3.3 Hz, 2H), 4.37 (td, J = 30.3 Hz, J = 3.6 Hz, 2H), 3.90 (s, 3H) ppm. ^{13}C NMR (75 MHz, DMSO- d_6) δ 167.1, 156.0, 145.4, 141.6, 138.4, 138.1, 134.2, 129.0, 123.1, 121.6, 119.2, 117.4, 115.2, 112.1, 110.9, 96.2, 82.0 (J = 165.6 Hz), 68.0 (J = 18.9 Hz), 34.1 ppm. HRMS (ESI) calcd for $\text{C}_{19}\text{H}_{17}\text{FN}_3\text{O}_2$ ($\text{M}+\text{H}$) $^+$ 338.12993, found 338.13069.



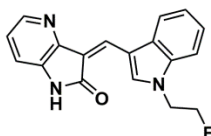
(E)-3-((4-methoxy-1*H*-indol-3-yl)methylene)-1,3-dihydro-2*H*-pyrrolo[3,2-*b*]pyridine-2-one ((E)-3.18b). The general procedure used for the synthesis of (*Z*)-**9** was followed using 4-methoxy-1*H*-indole-3-carboxaldehyde (0.100 g, 0.57 mmol) as starting material. The crude residue was purified by flash chromatography (100% AcOEt) and afforded 120.0 mg of a red solid (72%). R_f 0.48 (80% EtOAc/Hexane).

^1H NMR (300 MHz, DMSO- d_6) δ 12.21 (s, 1H), 10.50 (s, 1H), 10.09 (s, 1H), 8.68 (s, 1H), 8.26 (d, J = 4.8 Hz, 1H), 7.20-7.11 (m, 4H), 6.77 (d, J = 6.9 Hz, 1H), 3.97 (s, 3H) ppm. ^{13}C NMR (75 MHz, DMSO- d_6) δ 169.0, 154.9, 144.1, 141.2, 138.4, 136.7, 136.2, 134.9, 124.2, 121.7, 117.3, 116.8, 115.2, 113.2, 106.2, 103.0, 55.8 ppm. HRMS (ESI) calcd for $\text{C}_{17}\text{H}_{14}\text{N}_3\text{O}_2$ ($\text{M}+\text{H}$) $^+$ 292.10805, found 292.10858.



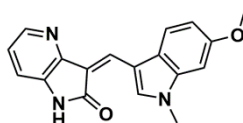
(Z)-3-((5-methoxy-1-methyl-1*H*-indol-3-yl)methylene)-1,3-dihydro-2*H*-pyrrolo[3,2-*b*]pyridine-2-one ((Z)-3.18c). The general procedure used for the synthesis of (*Z*)-**9** was followed using 5-methoxy-1-methyl-1*H*-indole-3-carbaldehyde (0.151 g, 0.8 mmol) as starting material. The crude residue was purified by flash chromatography (3% MeOH/DCM) and afforded 149.7 mg of a red solid (61%). R_f 0.25 (3% MeOH/DCM).

^1H NMR (300 MHz, $\text{DMSO-}d_6$) δ 10.63 (s, 1H), 9.44 (s, 1H), 8.32 (s, 1H), 8.11 (d, $J = 4.5$ Hz, 1H), 7.50 (d, $J = 9$ Hz, 1H), 7.45 (d, $J = 2.4$ Hz, 1H), 7.15-7.06 (m, 2 H), 6.92 (dd, $J = 8.7$ Hz, $J = 2.1$ Hz, 1H), 3.91 (s, 3H), 3.87 (s, 3H) ppm. ^{13}C NMR (75 MHz, $\text{DMSO-}d_6$) δ 167.3, 156.2, 145.6, 141.5, 139.3, 134.0, 132.2, 129.9, 129.4, 121.4, 116.6, 115.1, 113.3, 112.4, 110.8, 100.3, 55.9, 34.2 ppm. HRMS (ESI) calcd for $\text{C}_{18}\text{H}_{16}\text{N}_3\text{O}_2$ ($\text{M}+\text{H}$) $^+$ 306.1237, found 306.12434.



(Z)-3-((1-(2-fluoroethyl)-1H-indol-3-yl)methylene)-1,3-dihydro-2H-pyrrolo[3,2-b]pyridin-2-one ((Z)-3.18d). The general procedure used for the synthesis of (Z)-9 was followed using 1-(2-fluoroethyl)-1H-indole-3-carbaldehyde (0.153 g, 0.55 mmol) as starting material. The crude residue was purified by flash chromatography (4% MeOH/DCM) afforded 159.0 mg of a red solid (64%). R_f 0.46 (4% MeOH/DCM).

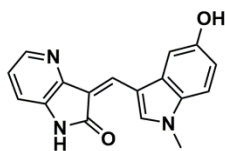
^1H NMR (300 MHz, $\text{DMSO-}d_6$) δ 10.67 (s, 1H), 9.56 (s, 1H), 8.34 (s, 1H), 8.13 (dd, $J = 4.5$ Hz, $J = 0.6$ Hz, 1H), 8.00-7.97 (m, 1H), 7.71-7.67 (m, 1H), 7.35-7.27 (m, 2H), 7.18-7.09 (m, 2H), 4.82 (td, $J = 39.6$ Hz, $J = 4.2$ Hz, 2H), 4.69 (td, $J = 20.7$ Hz, $J = 4.5$ Hz, 2H) ppm. ^{13}C NMR (75 MHz, $\text{DMSO-}d_6$) δ 167.2, 145.3, 141.7, 138.4, 136.6, 134.4, 129.0, 128.7, 123.5, 122.4, 121.9, 118.4, 118.1, 115.3, 111.7, 111.2, 82.0 ($J = 167.2$ Hz), 47.5 ($J = 19.6$ Hz) ppm. HRMS (ESI) calcd for $\text{C}_{18}\text{H}_{15}\text{FN}_3\text{O}$ ($\text{M}+\text{H}$) $^+$ 308.11937, found 308.12011.



(Z)-3-((6-methoxy-1-methyl-1H-indol-3-yl)methylene)-1,3-dihydro-2H-pyrrolo[3,2-b]pyridine-2-one ((Z)-3.18e). The general procedure used for the synthesis of (Z)-9 was followed using 6-methoxy-1-methyl-1H-indole-3-carbaldehyde (0.100 g, 0.53 mmol) as starting material. The crude residue was purified by flash chromatography (3% MeOH/DCM) afforded 97.0 mg of a red solid (60%). R_f 0.37 (3% MeOH/DCM).

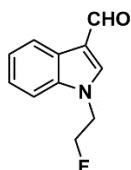
^1H NMR (300 MHz, $\text{DMSO-}d_6$) δ 10.64 (s, 1H), 9.36 (s, 1H), 8.26 (s, 1H), 8.11 (dd, $J = 4.5$ Hz, $J = 1.0$ Hz, 1H), 8.83 (d, $J = 8.7$ Hz, 1H), 7.15-7.06 (m, 3H), 6.91 (dd, $J = 8.7$ Hz, $J = 1.8$ Hz, 1H), 3.91 (s, 3H), 3.83 (s, 3H) ppm. ^{13}C NMR (75 MHz, $\text{DMSO-}d_6$) δ 167.1, 157.3, 145.5, 141.6,

138.2, 138.1, 134.1, 129.1, 122.8, 121.6, 119.1, 117.3, 115.2, 111.9, 110.9, 95.1, 55.9, 34.1 ppm. HRMS (ESI) calcd for $C_{18}H_{16}N_3O_2$ (M+H)⁺ 306.1237, found 306.12424.



(Z)-3-((5-hydroxy-1-methyl-1H-indol-3-yl)methylene)-1,3-dihydro-2H-pyrrolo[3,2-b]pyridine-2-one ((Z)-3.24). The general procedure used for the synthesis of (Z)-9 was followed using 5-hydroxy-1-methyl-1H-indole-3-carbaldehyde (0.125 g, 0.72 mmol) as starting material. The crude residue was purified by flash chromatography (5% MeOH/DCM) afforded 92.0 mg of a red solid (44%). R_f 0.41 (5% MeOH/DCM).

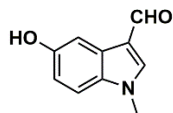
1H NMR (300 MHz, DMSO- d_6) δ 10.61 (s, 1H), 9.36 (s, 1H), 9.26 (s, 1H), 8.18 (s, 1H), 8.10 (dd, $J = 4.8$ Hz, $J = 1.2$ Hz, 1H), 7.41 (d, $J = 8.7$ Hz, 1H), 7.20 (d, $J = 2.1$ Hz, 1H), 6.92 (dd, $J = 8.7$ Hz, $J = 2.1$ Hz, 1H), 7.15-7.04 (m, 3H), 6.81 (dd, $J = 8.7$ Hz, $J = 1.8$ Hz, 1H), 3.89 (s, 3H) ppm. ^{13}C NMR (75 MHz, DMSO- d_6) δ 167.3, 153.9, 145.6, 141.6, 139.1, 133.9, 131.6, 130.3, 129.0, 121.3, 116.1, 115.1, 113.2, 112.3, 110.3, 102.4, 34.2 ppm. HRMS (ESI) calcd for $C_{17}H_{14}N_3O_2$ (M+H)⁺ 292.10805, found 292.10861.



1-(2-fluoroethyl)-1H-indole-3-carbaldehyde (3.20). To a solution of 1H-indole-3-carbaldehyde (300 mg, 2.07 mmol, 1 equiv), in THF (5 mL) was added sodium hydride (60% dispersion in oil, 83 mg, 2.07 mmol, 1 equiv.) and stirred at 0°C during 10 minutes. 2-Fluoroethyl 4-methylbenzenesulfonate (904 mg, 4.14 mmol, 2 equiv) was added dropwise and the reaction mixture was warmed at room temperature for 12 hours. Water was added and the aqueous layers was extracted with ethyl acetate 3 times. The combined organics layers was dried with Na_2SO_4 and concentrated in *vacuo*. The crude residue was purified by flash chromatography (0-3% MeOH/DCM) and afforded 379 mg of an orange solid (96%). R_f 0.80 (3% MeOH/DCM).

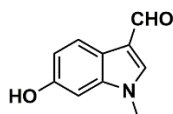
1H NMR (300 MHz, $CDCl_3$) δ 10.00 (s, 1H), 8.32 (m, 1H), 7.76 (s, 1H), 7.34-7.32 (m, 3H), 4.76 (td, $J = 46.8$ Hz, $J = 4.5$ Hz, 2H), 4.45 (td, $J = 26.4$ Hz, $J = 4.8$ Hz, 2H) ppm. ^{13}C NMR (75 MHz,

CDCl_3) δ 184.6, 138.7, 137.0, 125.3, 124.2, 123.0, 122.3, 118.7, 109.6, 81.0 ($J = 172.05$ Hz), 47.2 ($J = 21$ Hz) ppm. HRMS (ESI) calcd for $\text{C}_{11}\text{H}_{11}\text{FNO}$ ($\text{M}+\text{H}$) $^+$ 192.08192, found 192.08208.



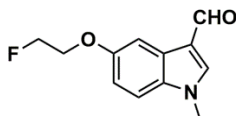
5-Hydroxy-1-methyl-1H-indole-3-carbaldehyde (3.22b). To a solution of 5-methoxy-1-methyl-1H-indole-3-carbaldehyde (1.0 g, 5.29 mmol, 1 equiv.) in DCM (30 mL) was added BBr_3 (1M in DCM, 26.4 mL, 26.42 mmol, 5 equiv.) at 0°C with stirring for 10 min. The reaction mixture was slowly warmed up to room temperature and stirred during 3h. The temperature was then lowered at 0°C , MeOH (100 mL) was slowly added and the pH of the mixture was adjusted to 8 by adding saturated solution of NaHCO_3 . The organic solvents were removed under reduce pressure and the remaining aqueous mixture was extracted with ethyl acetate five times. The organic layers were combined, dried over Na_2SO_4 , filtered and evaporated under reduced pressure. To the crude residue was added DCM and the precipitate was filtered off. The solid was air dried to give the title compound as 870 mg of purple powder (94%). R_f 0.28 (5% MeOH/DCM).

^1H NMR (300 MHz, $\text{DMSO}-d_6$) δ 9.77 (s, 1H), 9.10 (s, 1H), 8.06 (s, 1H), 7.48 (d, $J = 2.4$ Hz, 1H), 7.31 (d, $J = 8.7$ Hz, 1H), 6.77 (dd, $J = 8.7$ Hz, $J = 2.4$ Hz, 1H), 3.79 (s, 3H) ppm. ^{13}C NMR (300 MHz, $\text{DMSO}-d_6$) δ 184.2, 154.1, 141.5, 132.4, 126.1, 116.8, 113.5, 111.7, 105.9, 33.8 ppm. HRMS (ESI) calcd for $\text{C}_{10}\text{H}_{10}\text{NO}_2$ ($\text{M}+\text{H}$) $^+$ 176.0706, found 176.07042.



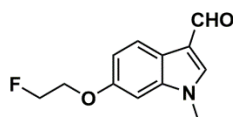
6-Hydroxy-1-methyl-1H-indole-3-carbaldehyde (3.22a). The general procedure used for the synthesis of 5-hydroxy-1-methyl-1H-indole-3-carbaldehyde was followed using 6-methoxy-1-methyl-1H-indole-3-carbaldehyde (200 mg, 1.06 mmol) as starting material (quantitative). R_f 0.54 (5% MeOH/DCM).

^1H NMR (300 MHz, $\text{DMSO}-d_6$) δ 9.76 (s, 1H), 9.40 (s, 1H), 8.03 (s, 1H), 7.84 (d, $J = 8.7$ Hz, 1H), 7.03 (d, $J = 1.2$ Hz, 1H), 6.75 (dd, $J = 8.7$ Hz, $J = 1.2$ Hz, 1H), 3.75 (s, 3H) ppm. ^{13}C NMR (300 MHz, $\text{DMSO}-d_6$) δ 184.3, 155.2, 141.0, 139.5, 122.0, 117.8, 117.6, 112.8, 96.5, 33.6 ppm. HRMS (ESI) calcd for $\text{C}_{10}\text{H}_{10}\text{NO}_2$ ($\text{M}+\text{H}$) $^+$ 176.0706, found 176.06982.



5-(2-fluoroethoxy)-1-methyl-1H-indole-3-carbaldehyde (3.23b). To a solution of 5-hydroxy-1-methyl-1H-indole-3-carbaldehyde (195.5 mg, 1.12 mmol, 1 equiv), in DMF (15 mL) was added potassium carbonate (308 mg, 2.23 mmol, 2 equiv.). The reaction mixture was stirred at room temperature during 10 minutes. 2-Fluoroethyl 4-methylbenzenesulfonate (489 mg, 2.24 mmol, 2 equiv) was added dropwise and the reaction mixture was warmed at 70°C for 12 hours. Water was added after the reaction was cooled to room temperature and the aqueous layer was extracted with ethyl acetate 3 times. The combined organics layers were dried with Na₂SO₄ and concentrated *in vacuo*. The crude residue was purified by flash chromatography (0-5% MeOH/DCM) and afforded 169 mg of a yellow solid (72%). R_f 0.55 (80% EtOAc/Hexane).

¹H NMR (300 MHz, CDCl₃) δ 9.91 (s, 1H), 7.77 (d, *J* = 2.4 Hz, 1H), 7.61 (s, 1H), 7.24 (d, *J* = 8.4 Hz, 1H), 7.02 (dd, *J* = 8.4 Hz, *J* = 2.4 Hz, 1H), 4.78 (td, *J* = 47.4 Hz, *J* = 4.2 Hz, 2H), 4.30 (td, *J* = 28.5 Hz, *J* = 4.2 Hz, 2H), 3.82 (s, 3H) ppm. ¹³C NMR (75 MHz, CDCl₃) δ 184.3, 155.4, 139.4, 135.8, 133.0, 125.8, 115.0, 110.8, 104.3, 82.0 (*J* = 169.3 Hz), 67.7 (*J* = 20.0 Hz), 33.8 ppm. HRMS (ESI) calcd for C₁₂H₁₃FNO₂ (M+H)⁺ 222.09248, found 222.09156.



6-(2-fluoroethoxy)-1-methyl-1H-indole-3-carbaldehyde (3.23a). The general procedure used for the synthesis of 5-(2-fluoroethoxy)-1-methyl-1H-indole-3-carbaldehyde was followed using 5-hydroxy-1-methyl-1H-indole-3-carbaldehyde (185.0 mg, 1.05 mmol) as starting material and afforded 169 mg of a yellow solid (80%). R_f 0.63 (3% MeOH/DCM).

¹H NMR (300 MHz, CDCl₃) δ 9.88 (s, 1H), 8.15 (d, *J* = 8.7 Hz, 1H), 7.53 (s, 1H), 6.96 (dd, *J* = 8.7 Hz, *J* = 2.1 Hz, 1H), 6.79 (d, *J* = 2.1 Hz, 1H), 4.77 (td, *J* = 47.4 Hz, *J* = 3.9 Hz, 2H), 4.30 (td, *J* = 27.9 Hz, *J* = 4.2 Hz, 2H), 3.75 (s, 3H) ppm. ¹³C NMR (75 MHz, CDCl₃) δ 184.2, 156.3, 139.0, 138.7, 122.8, 119.6, 118.1, 112.2, 95.1, 82.0 (*J* = 169.6 Hz), 67.7 (*J* = 20.2 Hz), 33.6 ppm. HRMS (ESI) calcd for C₁₂H₁₃FNO₂ (M+H)⁺ 222.09248, found 222.09264.

[γ-³³P]ATP-Based Enzymatic Assay. Compound MeOH•(Z)-3.9 was tested in a [γ-³³P]ATP based enzymatic assay by Reaction Biology Corporation (Malvern, PA). Briefly, the compound

was tested in a 10-concentration IC_{50} curve with 3-fold serial dilution starting at 10 μ M. The reactions were performed with 1 μ M ATP and profiled against 3 tyrosine kinases (Tropomyosin receptor kinase A (TrkA), tropomyosin receptor kinase B (TrkB), tropomyosin receptor kinase C (TrkC)). IC_{50} values less than 5.08E-10 M or higher than 1.00E-05 is estimated based on the best curve fitting available ($n = 2$). The same procedure was followed for the evaluation of inhibitors **3.16**, **3.10** and **3.18a-e** ($n = 1$). Compound **3.10** was tested for inhibitory activity at 500 nM on a panel of 18 selected kinases (SYK, PDK1/PDHK1, PDGFRa, P38a/MAPK14, KDR/VEGFR2, JNK1, JAK1, ITK, FMS, ERK1, ERBB2/HER2, EGFR, c-SRC, c-MET, c-KIT, BRAF, ALK, ABL1) under similar conditions ($n = 2$).

Docking Simulation and Computational Prediction of Sites of Metabolism. Molecular docking simulations of (Z)-**3.9**, (E)-**3.9**, (Z)-**3.10** and (E)-**3.10** were performed using the X-ray co-crystal structure of TrkB-cpdn5 complex (PDB code: 4AT3), TrkA-AZ-23 complex (PDB code: 4AOJ) and TrkC-GNF-5837 (PDB code: 3V5Q) using FITTED 3.5 program (FORECASTER platform).⁵⁵⁻⁵⁷ Docking structures and figures were prepared using Discovery Studio 3.5 Visualizer. The simulations for the SoM were performed using IMPACTS (FORECASTER platform) which predicts the top 2 SoM combining docking to metabolic enzymes, transition state modeling, and rule-based substrate reactivity prediction.⁶⁴ (PDB ID for enzymes: CYP1A2: 2HI4; CYP2C9: 1R9O, 1OG2, 1OG5; CYP2D6: 3QM4; CYP3A4: 1TQN, 1W0E, 1W0F, 1W0G, 2J0D, 2V0M, 3NXU; CYP2C19: 4GQS).

Radiosynthesis of (E/Z)-[¹¹C]3.9**.** Precursor (E)-**3.15** (1.0 mg, 4 μ mol) was placed in a 4.0 mL conical vial containing KOH (half a pellet crushed) and dissolved in acetone (250 μ L). [¹¹C]MeI (~ 0.37 Gbq (10 mCi) for reaction optimization and ~ 7.4 Gbq (200 mCi) for isolation) was transported by a stream of nitrogen into the reaction vial for 5 minutes and the reaction mixture was purified by analytical HPLC using either HPLC Method B or C (0.037-0.37 GBq (1-10 mCi) HPLC injections). Eluates were monitored for radioactivity and for UV absorbance at 280 nm and the peak corresponding to (E)-[¹¹C]**3.9** was collected ($25.9 \pm 5.7\%$ ($n = 8$) RCYs n.d.c. (based on trapped [¹¹C]CH₃I), 29.6-59.2 GBq/ μ mol (0.8-1.6 Ci/ μ mol)). When used for PET animal studies, the collected [¹¹C]**3.9** (isomerised upon light exposure – from (E)-[¹¹C]**3.9** peak collection yielding a 1:1 E/Z mixture) was passed through a preconditioned (10 mL EtOH

followed by 10 mL water) Sep-Pak C18 Light Cartridge, eluted with 0.5-1.0 mL EtOH and diluted with sterile saline prior to injection.

Radiosynthesis of (E/Z)-[¹⁸F]3.10. The azeotropic drying of ¹⁸F⁻ and the radiosynthesis of [¹⁸F]-FETos⁶⁰ were carried out using a modified PET tracer radiosynthesis module (Scintomics GRP, Germany) with a home-made manifold setup operated with Scintomics software. The module was equipped with a radioactivity detector and a Knauer UV detector.

Reaction of [¹⁸F]fluoride with Ethylene di(p-toluenesulfonate). The [¹⁸F]F⁻/H₂O⁻ (~ 11.1-18.5 GBq – 300-500 mCi) was passed through a Sep-Pak Light QMA cartridge (Waters) as an aqueous solution in ¹⁸O-enriched water and the ¹⁸F activity was eluted with 1.0 mL of a Kryptofix 222/K₂CO₃ solution (Kryptofix2.2.2. - 10-12 mg, dissolved in 150 μL of 0.125M K₂CO₃ + 1.3 mL MeCN) in a 5.0 mL conical vial with a stirring bar. The solvent was removed at 100°C under reduced pressure, agitation and a stream of argon gas. The residue was azeotropically dried with 0.5 mL of anhydrous acetonitrile twice at 100°C. Following azeotropic drying, the reaction vial was charged with ethylene di(p-toluenesulfonate) (8-10 mg, in 1.0 mL MeCN) and the mixture was allowed to react for 10 min at 90°C. The crude [¹⁸F]FETos was then diluted with HPLC eluent (1.5 mL, 40% MeCN, 60% H₂O) and injected on HPLC. Preparative radio-HPLC for the isolation of [¹⁸F]FETos was performed using a Waters uBondapak C18 10μm, 125A, column (7.8x300 mm) with an isocratic eluent (40% MeCN/ 60% H₂O) at 4.0 ml min⁻¹. The [¹⁸F]FETos labeling precursor was obtained in 27.0 ± 2.0 % RCY, *n* = 4, non-decay corrected isolated yield from ¹⁸F⁻/H₂O. An aliquot of the product fraction corresponding to [¹⁸F]FETos (~ 1.85 GBq – 50 mCi) was collected and diluted with 50 mL H₂O and passed through a preconditioned (10 mL EtOH followed by 10 mL water) Sep-Pak C18 Plus Cartridge and then eluted with 0.5-1.0 mL DMF, aliquoted and directly used in the second step.

Radiosynthesis of (E/Z)-[¹⁸F]10. The radiosynthesis of (Z)-[¹⁸F]3.10 using [¹⁸F]FETos ([¹⁸F]) was carried out manually. [¹⁸F]FETos from the previous step (~ 0.74 GBq – 20 mCi, in 300 μL DMF) was directly transferred to a 4.0 mL reaction conical vial containing precursor (Z)-3.24 (1.0 mg, 3.4 μmol), KOH (half a pellet crushed). The conical vial was sealed and allowed to react at 90°C for 10 min. The reaction mixture was subsequently quenched with HPLC mobile phase (1 mL, 50% MeCN, 50% H₂O) and cooled at room temperature in an ice bath (2 min). An aliquot of the reaction mixture (~ 0.2-0.3 GBq – 6-8 mCi) was purified by analytical reverse-phase HPLC, HPLC Method F. The eluates were monitored for radioactivity and for UV absorbance (280 nm)

and the peak corresponding to (Z)-[¹⁸F]3.10 (~ 0.74 GBq – 2 mCi) was collected. When used for autoradiography, animal PET and for photoisomerization studies, the collected (Z)-[¹⁸F]3.10 was passed through a preconditioned (10 mL EtOH followed by 10 mL water) Sep-Pak C18 Light Cartridge, eluted with 0.5-1.0 mL EtOH and diluted with sterile saline. The tracer was obtained in 2.5 ± 0.6 % RCY ($n = 4$, non-decay corrected isolated yield from ¹⁸F-/H₂O) and >98% radiochemical purity with SA in the range of 122.0-181.3 GBq/μmol (3.3-4.9 Ci/μmol) at the end of synthesis (60-70 min from end of bombardment). The ethanolic solution containing (E/Z)-[¹⁸F]3.10 was used for the photoisomerization studies of the tracer with the Method F. The photoisomerization was previously evaluated for the non-radioactive compound 3.10 ($t_{r(Z)-10} = 11.5$ min, $t_{r(E)-10} = 9.0$ min) – 0.7 min calibrated delay between the UV and radiodetector. The determination of SA was achieved by the comparison of the 280 nm UV absorbance peak (integration) of the carrier product with standard calibration curves of the corresponding non-radioactive standards. The peak corresponding to (Z)-3.10 from non-isomerized solutions kept in light-protected conical vials was used to obtain the calibration curve. Radiochemical purity was determined by HPLC injection of samples from the final ethanolic solutions as the sum of the E- and Z-isomers.

In Vitro Metabolism of [¹¹C]3.9 and non-radioactive 3.9 and 3.10.

Plasma Stability. Compound [¹¹C]3.9 (radiochemical purity > 99%) was incubated in rat plasma (500 μL) at 37°C and ice-cold acetonitrile (250 μL, after 5, 10, 30, 60 min) was added for protein precipitation at different time points followed by centrifugation. The amount of intact [¹¹C]3.9 was determined by HPLC analysis of the supernatant.

Rat liver microsomal assay. In a shaking water bath at 37°C, 3.9 (or 3.10, 10.0 μM) was incubated in a final volume of 500 μL of 100 mM phosphate buffer (pH = 7.4) containing pooled rat microsomes (RLM) (0.25 mg/mL protein) together with NADPH regenerating system (Solution A : 1.3 mM NADP⁺, 3.3 mM glucose-6-phosphate, 3.3 mM MgCl₂; Solution B : 0.4 U/mL glucose-6-phosphate dehydrogenase). Reactions were initiated by successive addition of microsomes in a pre-incubated mixture (5 min) of NADPH regenerating system and 3.9. 50 μL aliquots of incubations samples were protein precipitated at 0, 5, 15, 60 and 90 min with 150 μL of ice-cold acetonitrile and centrifuged. The supernatants were analyzed by HPLC. Two control experiments were carried out: first incubation without NADPH regenerating system (no enzymatic activity) and second, incubation without the test compound (baseline).

Computational physicochemical properties. CLogP, cLogD (at pH = 7.4) and TPSA values were computed with the program Pallas 3.0 for Windows (CompuDrug; San Francisco, CA).

Western blot analysis. Neuroblastoma tissue samples were homogenized in ice-cold RIPA buffer (Tris 50mM, NaCl 150 mM, SDS 0.1 %, Sodium Deoxycholate 0.5 %, Triton X 100 0.1%, 1mM PMSF, Roche Complete Protease inhibitor tablet), disrupted mechanically and centrifuged. Protein concentrations of each sample were determined by Bradford method. Next, 10µg of samples were then separated by SDS-PAGE electrophoresis in Tris-glycine buffer under denaturing conditions and transferred to nitrocellulose membrane (Bio-Rad, Hercules, CA, USA) in Tris-glycine buffer (25 mM Tris, 250 mM glycine, 0.1% SDS; pH 8.3) with 20% methanol. Membranes were blocked with either 2% BSA for phospho-TrkB (TrkBY515; Abcam, Cambridge, MA, USA; ab51187, 1:100) or 5% nonfat milk for TrkB (the polyclonal antibody against TrkB (RTB) has been previously described⁵⁵ in Tris-buffered saline-Tween 20 (TBS-Tween; 25 mM Tris base, 125 mM NaCl, 0.1% Tween 20) for 1h at room temperature. Membranes were then incubated overnight at 4°C in 2% BSA or 5% nonfat milk in Tris-buffered saline with primary antibodies. Membranes were rinsed three times for 10 min with TBS-Tween then incubated for 1h at room temperature with a horseradish peroxidase-conjugated secondary antibody against the primary antibody host species (anti-rabbit from Sigma, St Louis, MO, USA). The membranes were washed three times for 10 min in TBS-Tween. Proteins were detected by enhanced chemiluminescence (ECL reagents; Amersham, Little Chalfont, UK). Monoclonal anti-Actin (Fischer, 1:2000) was used as a loading control of each sample.

Autoradiography. Three rats were decapitated, the brains rapidly removed, frozen in 2-methylbutane (-40°C), and stored at -80°C. Brain sections (20 µm thick) were thaw mounted onto Superfrost Plus slides (Thermo Scientific) and stored at -80°C. Cryogenized human neuroblastoma tumors (Dr. Hervé Sartelet from Sainte-Justine Hospital courteously provided human neuroblastoma samples) were also mounted onto Superfrost Plus slides (Thermo Scientific) and stored at -80°C. After a pre-incubation in PBS buffer (30 mmol/L; pH 7.4 containing 137 mmol/L NaCl, 27 mmol/L) for 10 minutes at room temperature, rat and tumor sections were incubated 60 minutes (room temperature) in buffer containing [¹¹C]9 (344 µCi in 1050 mL buffer total) and 3 h (room temperature) for [¹⁸F]3.10 (518 µCi in 750 mL buffer total). Compound 9 (10 µM) was used to determine the specific binding of [¹¹C]3.9 and [¹⁸F]3.10. After

three washes in incubation buffer (5 minutes, 4°C) and a rapid rinse with ice-cold water (15 seconds), the sections were dried in a stream of air (room temperature). Sections were then dried further in a vacuum container with formaldehyde powder for mild fixation. Specific binding was calculated as the difference of total and nonspecific binding. Labeled sections were placed on phosphor-imaging plates (BAS 2025; Fuji, Japan), with industrial tritium activity standards (Amersham Biosciences, Piscataway, NJ, USA). On exposure, the plates were scanned with a plate reader (spatial resolution of 50 μm ; BAS 5000; Fuji). A correction factor of 3 was applied for the specific binding of the binding of the (Z)-[^{18}F]3.10 isomer in competition with 3.25 to account for the $\approx 2:1$ (E/Z) isomer composition of the tracer during the assay.

[^{11}C]3.9 and [^{18}F]3.10 PET Biodistribution Studies in Rat . MicroPET measurements were performed on a Siemens MicroPET R4 scanner (Siemens-CTI, Knoxville, TN, USA) which has a spatial resolution at the centre of the field of view of 1.84 mm full-width at half-maximum (FWHM) in the axial direction and 1.66 mm FWHM in the radial and tangential directions. The animals were prepared for imaging while under isoflurane (Abbott Laboratories), anesthesia delivered through a nose cone at a concentration of 2.0% volume and 2 L/min oxygen flow; a butterfly cannula (butterfly-25 Short; Venisystems) was placed in the tail vein and the radiotracer was administered as a 0.2 ml bolus injection. Respiration rate, heart rate and body temperature were monitored throughout the scan (Biopac systems MP150, Goleta, CA, USA). A 10 min ^{57}Co -transmission scan was acquired to correct for attenuation. Total acquisition time was 90 min. All images were reconstructed using the filtered back projection after applying normalization, scatter corrected for attenuation and radioactivity decay. PET imaging studies were performed in 8 (4 for each tracer) Sprague Dawley rats during 2% isoflurane anaesthesia. Between 300-500 μCi [^{11}C]3.9 or [^{18}F]3.10 were injected into the tail vein at the beginning of each scan. Dynamic scans with 27 frames (8x30s, 6x60s, 5x120s, 8x300s) for [^{11}C]3.9 and 33 frames (8x30s, 6x60s, 5x120s, 14x300s) for [^{18}F]3.10 were acquired over 60 minutes and 90 minutes respectively. PET images were reconstructed in a 128x128x62 matrix with a voxel size of 0.6mm x 0.6mm x 1.2 mm using a filtered back projection algorithm with a Hanning filter. For analysis of the [^{11}C]3.9 studies, decay corrected brain PET images of radioactivity concentrations [Bq/cc] were analyzed using VINCI 4.07 (Max-Planck-Institute for neurological research, Cologne, <http://www.nf.mpg.de/vinci3/>). Sum images of all 27 frames were used to place 3D elliptical volumes of interest (VOI) on brain, lung and liver. These VOIS were then used to generate time activity curves from the dynamic scans. Regional radioactivity

concentrations [Bq/cc] were converted to standard uptake values relative to bodyweight (SUV_{BW}) and injected dose. For analysis of the [^{18}F]**3.10** studies The PET images were analyzed using minctools (<http://www.bic.mni.mcgill.ca/ServicesSoftware/HomePage>). The time-activity curves (TAC) based on regions of interest (ROI) defined on the rat template were calculated for the following brain regions; cortex, stratum, thalamus, and cerebellum.⁷⁹ Uptake of [^{18}F]**3.10** in the tissues were expressed as standard uptake value (%SUV) calculated as average tissue concentration (MBq/cc) divided by the ratio of injected dose (MBq) over subject mass (grams, with the assumption cc = 1g) multiplied by 100%.⁸⁰

Animal Experiments. The MicroPET imaging protocol was approved by the Animal Care Committee of McGill University (Montreal, Canada).

Supporting information. Supplementary **Figures S3.1-S3.13** and **Scheme S3.1**, chemical synthesis of 2-fluoroethyl 4-methylbenzenesulfonate and crystallographic data for compounds **3.12** and (Z)-**3.9**.

Author Information.

* To whom the correspondence should be addressed. Prof. R. Schirmacher. Fax: (+1) 514-396-1857; e-mail: schirma@ualberta.ca

Acknowledgement. We thank Dr. Esther Schirmacher for reading the manuscript and providing useful comments. We are thankful to Dr. Hervé Sartelet who courteously provided human neuroblastoma samples for autoradiography experiments. We thank Marilyn Grand'Maison for the valuable help for the preparation of figures and histological staining. We thank Antonio Aliaga for small animal PET imaging and Arturo Aliaga for autoradiography experiments. We are also grateful to Dean Jolly and Miriam M. Kovacevic for radioisotope production. We thank Ming-Kai Ho for the digitalization of the histological staining sections. We thank Dr. Perrine Gaub for western blot analysis. This work was financially supported by Canada Foundation for Innovation (CFI) project no. 203639 to R.S.

3.6 Supporting Information of Article 6

Syntheses and Evaluation of Carbon-11- and Fluorine-18-Radiolabeled pan-Tropomyosin Receptor Kinases (Trk) Inhibitors: Exploration of the 4-aza-2-Oxindole Scaffold as Trk PET Imaging Agents

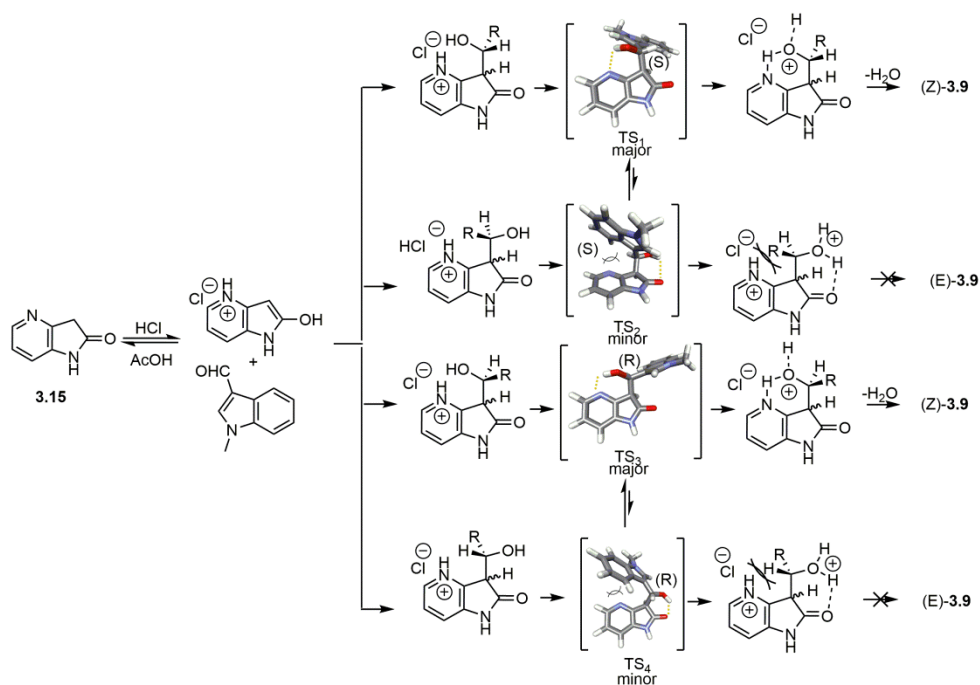
Vadim Bernard-Gauthier^{1,2}, Arturo Aliaga³, Antonio Aliaga⁴, Mehdi Boudjemeline⁴, Robert Hopewell⁴, Alexey Kostikov⁴, Pedro Rosa-Neto³, Alexander Thiel⁵, Ralf Schirmacher^{2,4*}*

¹Experimental Medicine, Department of Medicine, McGill University, 1110 Pine Avenue West, Montreal, QC, H3A 1A3. ²Department of Oncology, University of Alberta, 11560 University Avenue, Edmonton, AB, Canada, T6G 1Z2. ³Translational Neuroimaging Laboratory, McGill Centre for Studies in Aging, Douglas Mental Health University Institute, 6875 Boulevard LaSalle, QC, Canada, H4H 1R3. ⁴McConnell Brain Imaging Centre, Montreal Neurological Institute, McGill University, 3801 University Street, Montreal, QC, Canada, H3A 2B4. ⁵Department of Neurology and Neurosurgery, McGill University, Jewish General Hospital, 3755 Cote St. Catherine Rd., Montreal, QC, Canada, H2T 1E2. * Corresponding authors.

CONTENT OF SUPPORTING INFORMATION

1. SUPPORTING INFORMATION **Scheme S3.1** AND **Figures S3.1-S3.13**
2. CHEMICAL SYNTHESIS OF 2-FLUOROETHYL 4-METHYLBENZENESULFONATE
3. CRYSTALLOGRAPHIC DATA FOR COMPOUNDS **3.12** AND **(Z)-3.9**

1. SUPPORTING INFORMATION Scheme S3.1 AND Figures S3.1-S3.13



Scheme S3.1. Mechanistic rationale for the synthesis of (Z)-**3.9** from intermediate **3.15**. The formation of (Z)-**3.9** proceeds via the sterically less congested β -hydroxyketone transition states TS_1 and TS_3 which are in equilibrium with the sterically demanding states TS_2 and TS_4 respectively. The final position of the 1-methylindole moiety relative to the aza-oxindole fragment is dictated by their orientations in the depicted transition states.

We explored the isomerization of (*Z*)-**3.9** as it is expected to influence the potencies and kinase inhibition profile. We observed that (*Z*)-**3.9** isomerises within < 0.5 h under ambient condition upon incubation in mixtures of polar organic solvent and water (pH 6.0). The kinetics of isomerisation were assessed by reverse-phase HPLC. The 2 isomers were well resolved and their identity confirmed by LC-MS/MS. This rapid isomerization presumably ensues from the low rotational energy barrier of the highly conjugated (indolylmethylene)indolin-2-one system. As expected, the isomerization was prevented in the absence of light and significantly slower in slightly basic DMSO/phosphate buffer media (pH 7.4). Moreover, the photoisomerization of (*Z*)-**3.9** was followed by observing the UV-visible spectra at 294 K with ambient light exposure (Figure 2A). The large absorption band centered in the visible region at 438 nm, corresponding to $n-\pi^*$ transition, progressively decreased until it reached the PSS over one hour. The absorbance of the $\pi-\pi^*$ transition bands at 285 nm also decreased until reaching the PSS. The composition of the PSS was determined with the integration of the ^1H NMR spectra low field region corresponding to the N-H lactam, H-2' and vinyl protons. This *Z*:*E* ratio in DMSO- d_6 /D $_2$ O mixture was 56:44.

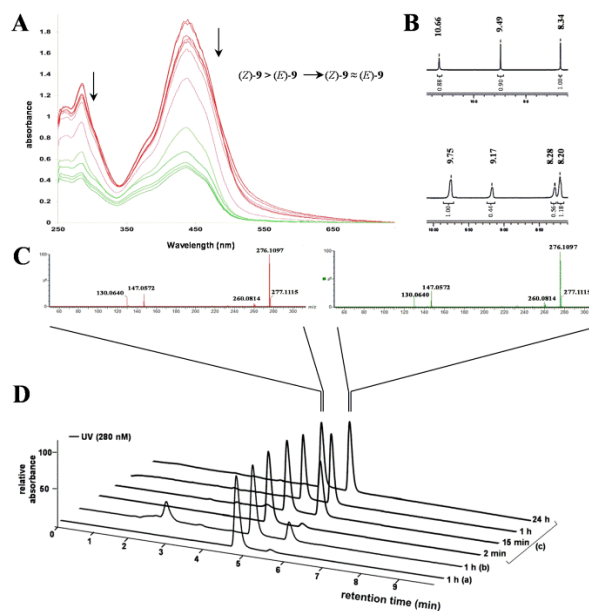


Figure S3.1. Assessment of the conformational equilibrium leading to the formation of (*E*)-**3.9** from (*Z*)-**3.9**. (A) Photoisomerization of a mixture (*Z*)-**3.9** > (*E*)-**3.9** in H $_2$ O (pH 6) monitored by UV-vis spectroscopy over 60 min at 295 K (5 min intervals). (B) Downfield sections of the NMR spectra of (*Z*)-**9** in d_6 -DMSO and after 1h in D $_2$ O/ d_6 -DMSO (1:1). (C) LC-MS/MS analysis of (*Z*)-**3.9** and (*E*)-**3.9**. (D) Representative chromatograms (HPLC method A) from 1.0 mM solutions of (*Z*)-**3.9** at 280 nm incubated (a) in MeCN/H $_2$ O (1:1) in absence of light (1h), (b) in DMSO/phosphate buffer (pH 7.4) (1:9) under ambient light (1h) and (c) in MeCN/H $_2$ O (1:1) under ambient light.

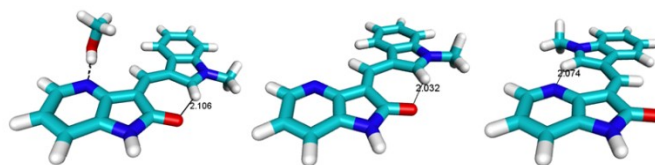


Figure S3.2. The structure of (*left*) the crystalized MeOH·(*Z*)-**3.9**, (*center*) the low-energy calculated structure of (*Z*)-**3.9** and (*right*) the low-energy calculated structure of (*E*)-**3.9** (FITTED). Black dash line represents H-bonding and black lines represent inter-atomic distances (Å). Proximity between the H-2' proton and the carbonyl in the *Z* isomer leads to H-2' deshielding. It is expected and observed that equivalent deshielding associated with the physical proximity between the H-2' proton and the nitrogen doublet should lead to even more pronounced. The same rationale applies to precursor **3.16**.

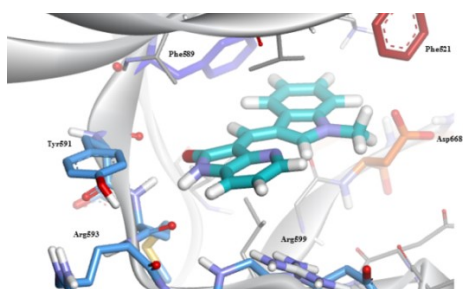


Figure S3.3. Top predicted binding mode of (*E*)-**3.9** within the active site of TrkA from FITTED docking (PDB code: 4AOJ).

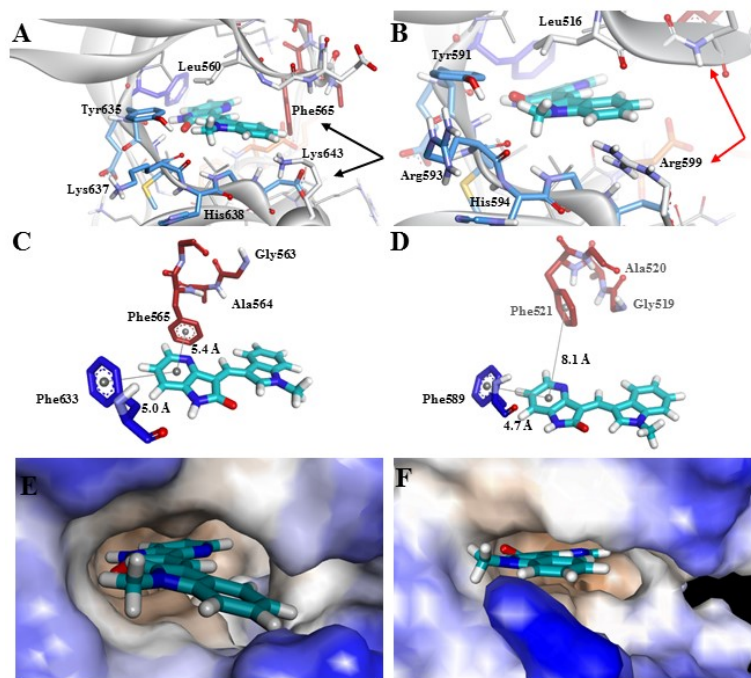


Figure S3.4. Comparison of the modeled binding of (Z)-3.9 with (A) TrkB (PDB code: 4AT3) and (B) TrkA (PDB code: 4AOJ) both in DFG-in conformation. Minor differences include the replacement of residues Lys637 and Lys643 in TrkB by Arg593 and Arg599 respectively in TrkA as well as the organization of the β -strand-1 and the glycine-rich loop (arrows). The major difference in the orientation of Phe565 (TrkB) (C) or Phe521 (TrkA) (D) from the glycine-rich loop is highlight. The ensuing differences in the ligand-protein interactions are reflected with the receptors presented in the solvent-accessible surface area (hydrophobicity); TrkB (E) and TrkA (F). Residue sequence in proximity to the ligand only differ by the replacement of TrkA Arg593 and Arg599 by two lysines residues in TrkB and TrkC. Side chains of TrkA Arg593 and the corresponding Lys637 and Lys621 in TrkB and TrkC respectively are remotely oriented vis-à-vis the ligand and most likely do influence the binding of (Z)-9 nor the orientation of the hinge. Otherwise, the charged amino acid side chains of Arg599 (TrkA), Lys643 (TrkB) and Lys627 (TrkC) lies in the in proximity of the solvent exposed face of the 1-methylindole moiety (Figure S4A,B.). Therefore, the bulkier arginine side chain may engage in unfavorable electrostatic contact with (Z)-9 compared to the lysine residues. Additionally, the pyridine ring in (Z)-3.9 is firmly sandwiched between Phe633 (R_{cen} 5.0 Å) and Phe565 (R_{cen} 5.4 Å) from the glycine-rich loop in TrkB whereas no corresponding hydrophobic interaction is possible between the ligand and the Phe521 (R_{cen} 8.1 Å) from the glycine-rich loop in TrkA owing to the more compact organization of the loop in TrkA – leaving the vinyl and pyridine moieties solvent exposed (Figure 4SC-E.). This difference in the ordering of the glycine-rich loop was also characterize in the structures of apo-TrkA (PDB code: 4F0I) and apo-TrkB (PDB code: 4ASZ).

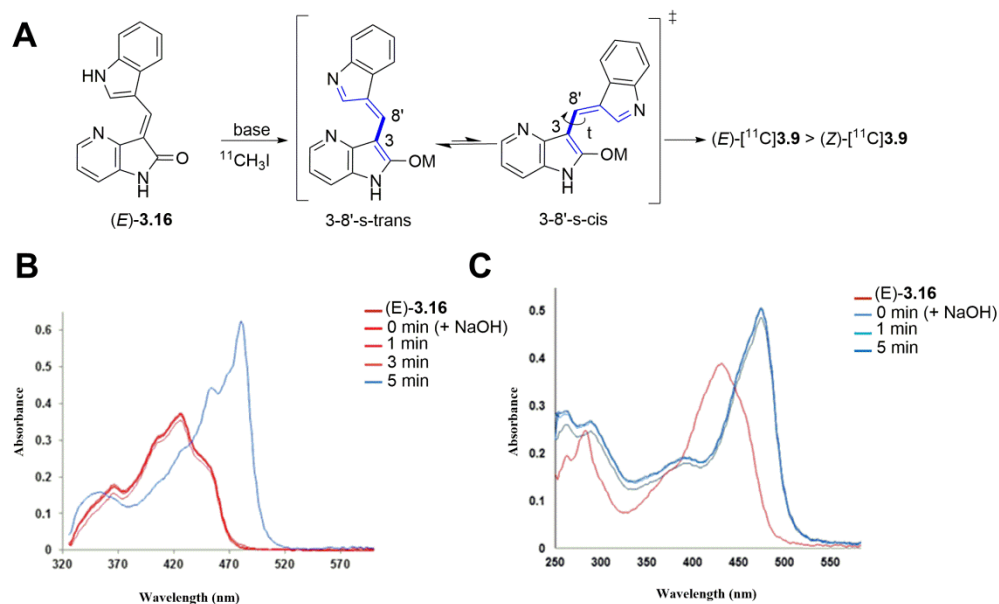


Figure S3.5. Plausible mechanistic explanation for the formation of (Z)-[^{11}C]3.9 from (E)-3.16. (A) ^{11}C -methylation plausibly proceeds through the more stable 3-2'-s-*trans*-azatriene enolate intermediate leading to the preferential formation of (E)-[^{11}C]3.9 with minor (Z)-[^{11}C]3.9 (M = Na, K, Cs). The formation of the proposed 3-8'-s-*trans*-azatriene and 3-8'-s-*cis*-azatriene anionic states is supported by the bathochromic shift observed in the UV-visible spectra of 3.16 upon addition of $\text{NaOH}_{(\text{aq})}$ in (B) acetone or (C) aqueous condition.

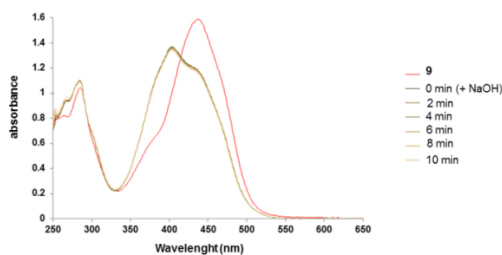


Figure S3.6. UV-visible spectra changes upon treatment 3.9 (E/Z mixture) with $\text{NaOH}_{(\text{aq})}$ under aqueous condition (identical condition to Figure S3.5) does not lead to a bathochromic shift.

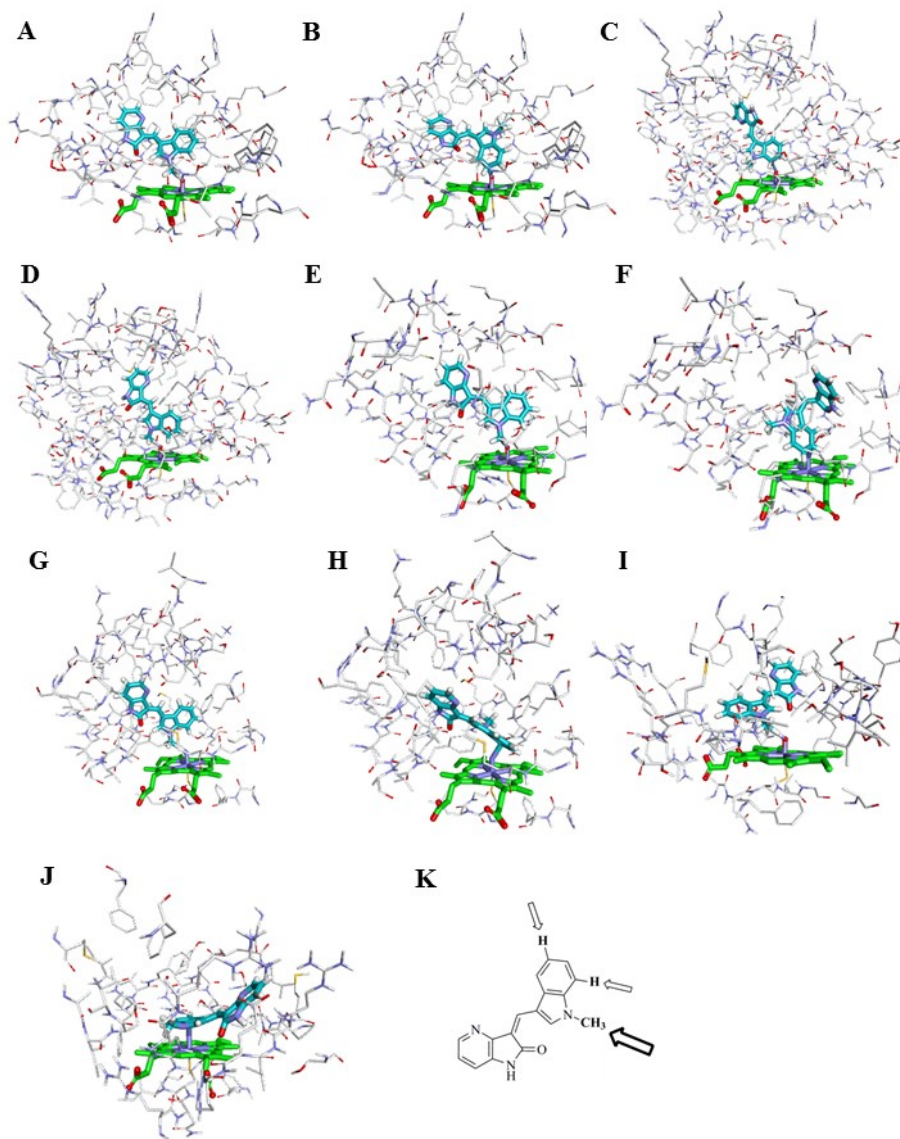


Figure S3.7. In silico predicted sites of metabolism using IMPACT (In-silico Metabolism Prediction by Activated Cytochromes and Transition States) with transition states modeling exemplified for (Z)-3.9 (See experimental section for details).

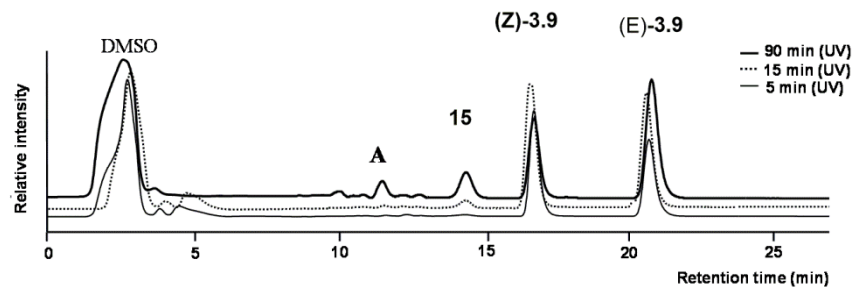


Figure S3.8. HPLC chromatograms over 90 min for the RLM assay with (E/Z)-3.9.

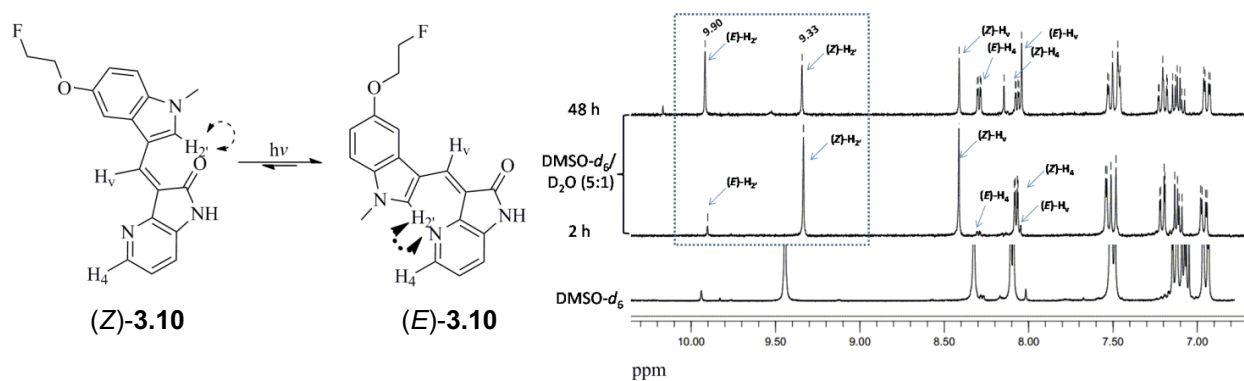


Figure S3.9. $^1\text{H-NMR}$ spectra at different time points during the course of the ambient light-induced photoisomerization of (Z)-3.10 leading to the formation of (E)-3.10.

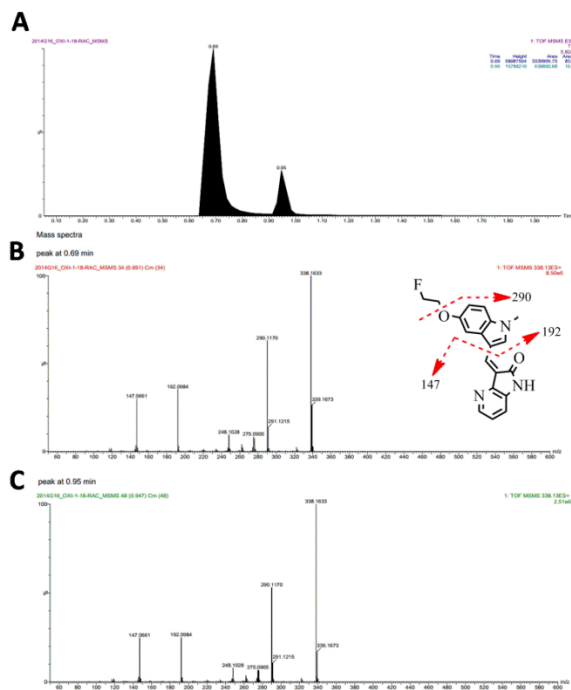


Figure S3.10. (A-C) LC-MS/MS analysis of the **3.10** *E/Z* mixture.

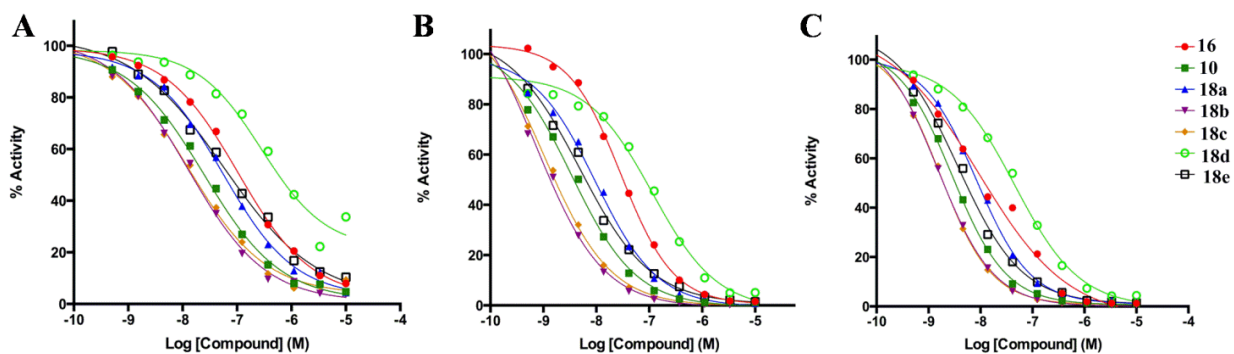


Figure S3.11. Dose-response curves for the $[\gamma\text{-}^{33}\text{P}]\text{ATP}$ -based enzymatic *in vitro* assays with **3.16**, **3.10** and **3.18a-e** versus (A) TrkA, (B) TrkB and (C) TrkC. The inhibitors were tested at ten different concentrations using serial dilution.

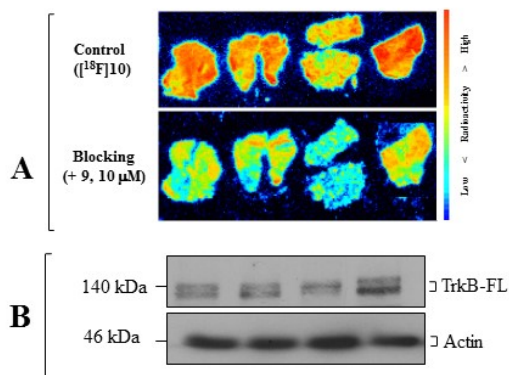


Figure S3.12. In vitro autoradiography of four representative sections from four human neuroblastoma tumor. (A) Autoradiography images showing the binding of [¹⁸F]3.10 alone and in co-incubation with inhibitors 3 (10 μM). (B) Western blots analysis of the TrkB (FL: full length) protein levels. Actin was used as loading control.

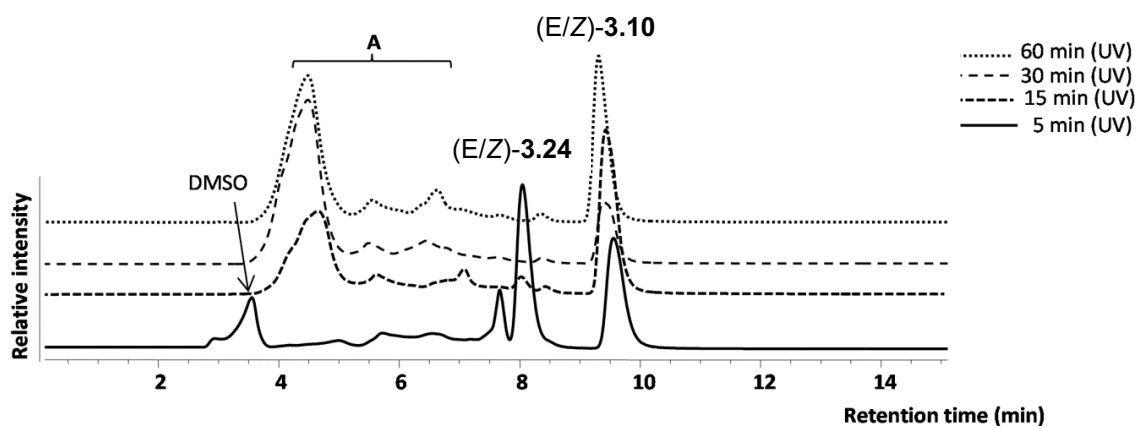


Figure S3.13. HPLC chromatograms over 60 min for the RLM assay with (E/Z)-3.10.

2. CHEMICAL SYNTHESIS OF 2-FLUOROETHYL 4-METHYLBENZENESULFONATE

2-Fluoroethyl 4-methylbenzenesulfonate.⁸¹ To a solution of 2-fluoroethanol (5.0 g, 78.1 mmol, 1 equiv.) in pyridine (25 mL) was added 4-methylbenzene-1-sulfonyl chloride (17.9 g, 93.7 mmol, 1.2 equiv.) in five portions over 30 min. The reaction mixture was stirred at room temperature for 24 h and the volume was reduced *in vacuo*. The residue was taken in 1N aqueous HCl (50 mL) and extracted with CHCl₃ (4 X 50 mL). The combined organic phases were dried over Na₂SO₄ and concentrated *in vacuo*. The crude product was purified by flash chromatography (30% EtOAc/hexane) to afford 10.6 g of the title compound as a colorless solid (92%). ¹H NMR (300 MHz, CDCl₃) δ 7.80 (d, *J* = 8.1 Hz, 2H), 7.36 (d, *J* = 8.1 Hz, 2H), 4.56 (dt, *J*₂ = 47.1 Hz, *J*₁ = 1.5 Hz, 2H), 4.25 (dt, *J*₂ = 27.3 Hz, *J*₁ = 3.9 Hz, 2H), 2.45 (s, 3H) ppm. ¹³C NMR (75 MHz, CDCl₃) δ 145.2, 132.6, 129.9, 128.0, 80.5 (d, *J* = 172.7 Hz), 68.5 (d, *J* = 20.8 Hz), 21.7 ppm. ¹⁹F NMR (188 MHz, DMSO-*d*₆) δ -224.66 ppm. HRMS (ESI) calcd for C₉H₁₂FO₃S (M+H)⁺ 219.04857, found 219.04849.

3. CRYSTALLOGRAPHIC DATA FOR COMPOUNDS 3.12 AND (Z)-3.9

Data form this subsection can be found in **Annex 2**.

3.7 References

1. Pattarawarapan, M.; Burgess, K., Molecular basis of neurotrophin-receptor interactions. *J Med Chem* **2003**, *46* (25), 5277-91.
2. Schneider, R.; Schweiger, M., A novel modular mosaic of cell adhesion motifs in the extracellular domains of the neurogenic trk and trkB tyrosine kinase receptors. *Oncogene* **1991**, *6* (10), 1807-11.
3. Huang, E. J.; Reichardt, L. F., Neurotrophins: roles in neuronal development and function. *Annu Rev Neurosci* **2001**, *24*, 677-736.
4. Huang, E. J.; Reichardt, L. F., Trk receptors: roles in neuronal signal transduction. *Annu Rev Biochem* **2003**, *72*, 609-42.
5. Chao, M. V., Neurotrophins and their receptors: a convergence point for many signalling pathways. *Nat Rev Neurosci* **2003**, *4* (4), 299-309.
6. Snider, W. D., Functions of the Neurotrophins during Nervous-System Development - What the Knockouts Are Teaching Us. *Cell* **1994**, *77* (5), 627-638.
7. Chao, M. V.; Hempstead, B. L., p75 and Trk: a two-receptor system. *Trends Neurosci* **1995**, *18* (7), 321-6.
8. Kaplan, D. R.; Martin-Zanca, D.; Parada, L. F., Tyrosine phosphorylation and tyrosine kinase activity of the trk proto-oncogene product induced by NGF. *Nature* **1991**, *350* (6314), 158-60.
9. Holtzman, D. M.; Kilbridge, J.; Li, Y. W.; Cunningham, E. T.; Lenn, N. J.; Clary, D. O.; Reichardt, L. F.; Mobley, W. C., Trka Expression in the Cns - Evidence for the Existence of Several Novel Ngf-Responsive Cns Neurons. *Journal of Neuroscience* **1995**, *15* (2), 1567-1576.
10. Muragaki, Y.; Timothy, N.; Leight, S.; Hempstead, B. L.; Chao, M. V.; Trojanowski, J. Q.; Lee, V. M., Expression of trk receptors in the developing and adult human central and peripheral nervous system. *J Comp Neurol* **1995**, *356* (3), 387-97.
11. Tessarollo, L.; Tsoulfas, P.; Martinzanca, D.; Gilbert, D. J.; Jenkins, N. A.; Copeland, N. G.; Parada, L. F., Trkc, a Receptor for Neurotrophin-3, Is Widely Expressed in the Developing Nervous-System and in Nonneuronal Tissues. *Development* **1993**, *118* (2), 463-475.
12. Shibayama, E.; Koizumi, H., Cellular localization of the Trk neurotrophin receptor family in human non-neuronal tissues. *Am J Pathol* **1996**, *148* (6), 1807-18.
13. Gupta, V. K.; You, Y. Y.; Gupta, V. B.; Klistorner, A.; Graham, S. L., TrkB Receptor Signalling: Implications in Neurodegenerative, Psychiatric and Proliferative Disorders. *Int J Mol Sci* **2013**, *14* (5), 10122-10142.

14. Cattaneo, A.; Calissano, P., Nerve Growth Factor and Alzheimer's Disease: New Facts for an Old Hypothesis. *Molecular Neurobiology* **2012**, *46* (3), 588-604.
15. Sanchez-Ortiz, E.; Yui, D. S.; Song, D. L.; Li, Y.; Rubenstein, J. L.; Reichardt, L. F.; Parada, L. F., TrkA Gene Ablation in Basal Forebrain Results in Dysfunction of the Cholinergic Circuitry. *Journal of Neuroscience* **2012**, *32* (12), 4065-4079.
16. Scott, S. A.; Mufson, E. J.; Weingartner, J. A.; Skau, K. A.; Crutcher, K. A., Nerve Growth-Factor in Alzheimers-Disease - Increased Levels Throughout the Brain Coupled with Declines in Nucleus Basalis. *Journal of Neuroscience* **1995**, *15* (9), 6213-6221.
17. Ginsberg, S. D.; Che, S. L.; Wu, J.; Counts, S. E.; Mufson, E. J., Down regulation of trk but not p75(NTR) gene expression in single cholinergic basal forebrain neurons mark the progression of Alzheimer's disease. *Journal of Neurochemistry* **2006**, *97* (2), 475-487.
18. Mufson, E. J.; Li, J. M.; Sobreviela, T.; Kordower, J. H., Decreased trkA gene expression within basal forebrain neurons in Alzheimer's disease. *Neuroreport* **1996**, *8* (1), 25-29.
19. Mufson, E. J.; Counts, S. E.; Fahnstock, M.; Ginsberg, S. D., Cholinergic molecular substrates of mild cognitive impairment in the elderly. *Curr Alzheimer Res* **2007**, *4* (4), 340-350.
20. Counts, S. E.; Nadeem, M.; Wu, J.; Ginsberg, S. D.; Saragovi, H. U.; Mufson, E. J., Reduction of cortical TrkA but not p75(NTR) protein in early-stage Alzheimer's disease. *Ann Neurol* **2004**, *56* (4), 520-531.
21. Ferrer, I.; Marin, C.; Rey, M. J.; Ribalta, T.; Goutan, E.; Blanco, R.; Tolosa, E.; Marti, E., BDNF and full-length and truncated TrkB expression in Alzheimer disease. Implications in therapeutic strategies. *J Neuropath Exp Neur* **1999**, *58* (7), 729-739.
22. Fumagalli, F.; Racagni, G.; Riva, M. A., Shedding light into the role of BDNF in the pharmacotherapy of Parkinson's disease. *Pharmacogenomics J* **2006**, *6* (2), 95-104.
23. Zuccato, C.; Marullo, M.; Conforti, P.; MacDonald, M. E.; Tartari, M.; Cattaneo, E., Systematic assessment of BDNF and its receptor levels in human cortices affected by Huntington's disease. *Brain Pathol* **2008**, *18* (2), 225-238.
24. Pillai, A., Brain-derived neurotrophic factor/TrkB signaling in the pathogenesis and novel pharmacotherapy of schizophrenia. *Neurosignals* **2008**, *16* (2-3), 183-193.
25. Griesbach, G. S.; Hovda, D. A.; Gomez-Pinilla, F., Exercise-induced improvement in cognitive performance after traumatic brain injury in rats is dependent on BDNF activation. *Brain Research* **2009**, *1288*, 105-115.
26. Sclabas, G. M.; Fujioka, S.; Schmidt, C.; Li, Z.; Frederick, W. A.; Yang, W.; Yokoi, K.; Evans, D. B.; Abbruzzese, J. L.; Hess, K. R.; Zhang, W.; Fidler, I. J.; Chiao, P. J.,

Overexpression of tropomyosin-related kinase B in metastatic human pancreatic cancer cells. *Clin Cancer Res* **2005**, *11* (2 Pt 1), 440-9.

27. Okamura, K.; Harada, T.; Wang, S.; Ijichi, K.; Furuyama, K.; Koga, T.; Okamoto, T.; Takayama, K.; Yano, T.; Nakanishi, Y., Expression of TrkB and BDNF is associated with poor prognosis in non-small cell lung cancer. *Lung Cancer* **2012**, *78* (1), 100-6.
28. Hisaoka, M.; Sheng, W. Q.; Tanaka, A.; Hashimoto, H., Gene expression of TrkC (NTRK3) in human soft tissue tumours. *Journal of Pathology* **2002**, *197* (5), 661-667.
29. Geiger, T. R.; Peeper, D. S., The neurotrophic receptor TrkB in anoikis resistance and metastasis: A prespective. *Cancer Research* **2005**, *65* (16), 7033-7036.
30. Nakagawara, A.; Azar, C. G.; Scavarda, N. J.; Brodeur, G. M., Expression and function of TRK-B and BDNF in human neuroblastomas. *Mol Cell Biol* **1994**, *14* (1), 759-67.
31. Longo, F. M.; Massa, S. M., Small-molecule modulation of neurotrophin receptors: a strategy for the treatment of neurological disease. *Nat Rev Drug Discov* **2013**, *12* (7), 507-25.
32. Wang, T.; Yu, D.; Lamb, M. L., Trk kinase inhibitors as new treatments for cancer and pain. *Expert Opin Ther Pat* **2009**, *19* (3), 305-19.
33. Cazorla, M.; Premont, J.; Mann, A.; Girard, N.; Kellendonk, C.; Rognan, D., Identification of a low-molecular weight TrkB antagonist with anxiolytic and antidepressant activity in mice. *Journal of Clinical Investigation* **2011**, *121* (5), 1846-1857.
34. Massa, S. M.; Yang, T.; Xie, Y. M.; Shi, J.; Bilgen, M.; Joyce, J. N.; Nehama, D.; Rajadas, J.; Longo, F. M., Small molecule BDNF mimetics activate TrkB signaling and prevent neuronal degeneration in rodents. *Journal of Clinical Investigation* **2010**, *120* (5), 1774-1785.
35. Pattarawarapan, M.; Zaccaro, M. C.; Saragovi, U. H.; Burgess, K., New templates for syntheses of ring-fused, C-10 beta-turn peptidomimetics leading to the first reported small-molecule mimic of neurotrophin-3. *Journal of Medicinal Chemistry* **2002**, *45* (20), 4387-4390.
36. Jang, S. W.; Liu, X.; Yepes, M.; Shepherd, K. R.; Miller, G. W.; Liu, Y.; Wilson, W. D.; Xiao, G.; Bianchi, B.; Sun, Y. E.; Ye, K., A selective TrkB agonist with potent neurotrophic activities by 7,8-dihydroxyflavone. *Proc Natl Acad Sci U S A* **2010**, *107* (6), 2687-92.
37. Liu, X.; Chan, C. B.; Jang, S. W.; Pradoldej, S.; Huang, J.; He, K.; Phun, L. H.; France, S.; Xiao, G.; Jia, Y.; Luo, H. R.; Ye, K., A synthetic 7,8-dihydroxyflavone derivative promotes neurogenesis and exhibits potent antidepressant effect. *J Med Chem* **2010**, *53* (23), 8274-86.
38. Liu, X.; Chan, C. B.; Qi, Q.; Xiao, G.; Luo, H. R.; He, X.; Ye, K., Optimization of a small tropomyosin-related kinase B (TrkB) agonist 7,8-dihydroxyflavone active in mouse models of depression. *J Med Chem* **2012**, *55* (19), 8524-37.

39. Hong, S.; Kim, J.; Seo, J. H.; Jung, K. H.; Hong, S. S.; Hong, S., Design, Synthesis, and Evaluation of 3,5-Disubstituted 7-Azaindoles as Trk Inhibitors with Anticancer and Antiangiogenic Activities. *Journal of Medicinal Chemistry* **2012**, *55* (11), 5337-5349.
40. Lippa, B.; Morris, J.; Corbett, M.; Kwan, T. A.; Noe, M. C.; Snow, S. L.; Gant, T. G.; Mangiaracina, M.; Coffey, H. A.; Foster, B.; Knauth, E. A.; Wessel, M. D., Discovery of novel isothiazole inhibitors of the TrkA kinase: Structure-activity relationship, computer modeling, optimization, and identification of highly potent antagonists. *Bioorg Med Chem Lett* **2006**, *16* (13), 3444-3448.
41. Kim, S. H.; Tokarski, J. S.; Leavitt, K. J.; Fink, B. E.; Salvati, M. E.; Moquin, R.; Obermeier, M. T.; Trainor, G. L.; Vite, G. G.; Stadnick, L. K.; Lippy, J. S.; You, D.; Lorenzi, M. V.; Chen, P., Identification of 2-amino-5-(thioaryl)thiazoles as inhibitors of nerve growth factor receptor TrkA. *Bioorg Med Chem Lett* **2008**, *18* (2), 634-9.
42. Albaugh, P.; Fan, Y.; Mi, Y.; Sun, F.; Adrian, F.; Li, N.; Jia, Y.; Sarkisova, Y.; Kreusch, A.; Hood, T.; Lu, M.; Liu, G.; Huang, S.; Liu, Z.; Loren, J.; Tuntland, T.; Karanewsky, D. S.; Seidel, H. M.; Molteni, V., Discovery of GNF-5837, a Selective TRK Inhibitor with Efficacy in Rodent Cancer Tumor Models. *ACS Med Chem Lett* **2012**, *3* (2), 140-5.
43. Bernard-Gauthier, V.; Boudjemeline, M.; Rosa-Neto, P.; Thiel, A.; Schirmacher, R., Towards tropomyosin-related kinase B (TrkB) receptor ligands for brain imaging with PET: radiosynthesis and evaluation of 2-(4-[(18)F]fluorophenyl)-7,8-dihydroxy-4H-chromen-4-one and 2-(4-[(N-methyl-(11)C]-dimethylamino)phenyl)-7,8-dihydroxy-4H-chromen-4-one. *Bioorg Med Chem* **2013**, *21* (24), 7816-29.
44. Altar, C. A.; Siuciak, J. A.; Wright, P.; Ip, N. Y.; Lindsay, R. M.; Wiegand, S. J., In-Situ Hybridization of Trkb and Trkc Receptor Messenger-Rna in Rat Forebrain and Association with High-Affinity Binding of [I-125] Bdnf, [I-125] Nt-4/5 and [I-125] Nt-3. *European Journal of Neuroscience* **1994**, *6* (9), 1389-1405.
45. Zhang, L.; Villalobos, A.; Beck, E. M.; Bocan, T.; Chappie, T. A.; Chen, L.; Grimwood, S.; Heck, S. D.; Helal, C. J.; Hou, X.; Humphrey, J. M.; Lu, J.; Skaddan, M. B.; McCarthy, T. J.; Verhoest, P. R.; Wager, T. T.; Zasadny, K., Design and selection parameters to accelerate the discovery of novel central nervous system positron emission tomography (PET) ligands and their application in the development of a novel phosphodiesterase 2A PET ligand. *J Med Chem* **2013**, *56* (11), 4568-79.
46. Pike, V. W., PET radiotracers: crossing the blood-brain barrier and surviving metabolism. *Trends Pharmacol Sci* **2009**, *30* (8), 431-40.

47. Wood, E. R.; Kuyper, L.; Petrov, K. G.; Hunter, R. N.; Harris, P. A.; Lackey, K., Discovery and in vitro evaluation of potent TrkA kinase inhibitors: oxindole and aza-oxindoles. *Bioorg Med Chem Lett* **2004**, *14* (4), 953-957.
48. Altar, C. A.; Criden, M. R.; Lindsay, R. M.; DiStefano, P. S., Characterization and topography of high-affinity ¹²⁵I-neurotrophin-3 binding to mammalian brain. *J Neurosci* **1993**, *13* (2), 733-43.
49. Zou, H. B.; Zhang, L.; Ouyang, J. F.; Giulianotti, M. A.; Yu, Y. P., Synthesis and biological evaluation of 2-indolinone derivatives as potential antitumor agents. *Eur J Med Chem* **2011**, *46* (12), 5970-5977.
50. Liu, J. J.; Dermatakis, A.; Lukacs, C.; Konzelmann, F.; Chen, Y.; Kammlott, U.; Depinto, W.; Yang, H.; Yin, X. F.; Chen, Y. S.; Schutt, A.; Simcox, M. E.; Luk, K. C., 3,5,6-trisubstituted naphthostyryls as CDK2 inhibitors. *Bioorg Med Chem Lett* **2003**, *13* (15), 2465-2468.
51. Laufer, R.; Forrest, B.; Li, S. W.; Liu, Y.; Sampson, P.; Edwards, L.; Lang, Y. H.; Awrey, D. E.; Mao, G. D.; Plotnikova, O.; Leung, G.; Hodgson, R.; Beletskaya, I.; Mason, J. M.; Luo, X. Y.; Wei, X.; Yao, Y.; Feher, M.; Ban, F. Q.; Kiarash, R.; Green, E.; Mak, T. W.; Pan, G. H.; Pauls, H. W., The Discovery of PLK4 Inhibitors: (E)-3-((1H-Indazol-6-yl)methylene)indolin-2-ones as Novel Antiproliferative Agents. *Journal of Medicinal Chemistry* **2013**, *56* (15), 6069-6087.
52. Prakash, C. R., Theivendren, P., Raja, S., Indolin-2-ones in clinical trials as potential kinase inhibitors: a review. *Pharmacology & Pharmacy* **2012**, *3*, 62-71.
53. Sun, L.; Tran, N.; Tang, F.; App, H.; Hirth, P.; McMahan, G.; Tang, C., Synthesis and biological evaluations of 3-substituted indolin-2-ones: A novel class of tyrosine kinase inhibitors that exhibit selectivity toward particular receptor tyrosine kinases. *Journal of Medicinal Chemistry* **1998**, *41* (14), 2588-2603.
54. Bertrand, T.; Kothe, M.; Liu, J.; Dupuy, A.; Rak, A.; Berne, P. F.; Davis, S.; Gladysheva, T.; Valtre, C.; Crenne, J. Y.; Mathieu, M., The crystal structures of TrkA and TrkB suggest key regions for achieving selective inhibition. *J Mol Biol* **2012**, *423* (3), 439-53.
55. Englebienne, P.; Moitessier, N., Docking ligands into flexible and solvated macromolecules. 5. Force-field-based prediction of binding affinities of ligands to proteins. *J Chem Inf Model* **2009**, *49* (11), 2564-71.
56. Therrien, E.; Englebienne, P.; Arrowsmith, A. G.; Mendoza-Sanchez, R.; Corbeil, C. R.; Weill, N.; Campagna-Slater, V.; Moitessier, N., Integrating Medicinal Chemistry, Organic/Combinatorial Chemistry, and Computational Chemistry for the Discovery of Selective

Estrogen Receptor Modulators with FORECASTER, a Novel Platform for Drug Discovery. *Journal of Chemical Information and Modeling* **2012**, 52 (1), 210-224.

57. Corbeil, C. R.; Englebienne, P.; Yannopoulos, C. G.; Chan, L.; Das, S. K.; Bilimoria, D.; L'Heureux, L.; Moitessier, N., Docking ligands into flexible and solvated macromolecules. 2. Development and application of fitted 1.5 to the virtual screening of potential HCV polymerase inhibitors. *J Chem Inf Model* **2008**, 48 (4), 902-9.

58. Mologni, L.; Rostagno, R.; Brussolo, S.; Knowles, P. P.; Kjaer, S.; Murray-Rust, J.; Rosso, E.; Zambon, A.; Scapozza, L.; McDonald, N. Q.; Lucchini, V.; Gambacorti-Passerini, C., Synthesis, structure-activity relationship and crystallographic studies of 3-substituted indolin-2-one RET inhibitors. *Bioorgan Med Chem* **2010**, 18 (4), 1482-1496.

59. Bramson, H. N.; Corona, J.; Davis, S. T.; Dickerson, S. H.; Edelstein, M.; Frye, S. V.; Gampe, R. T.; Harris, P. A.; Hassell, A.; Holmes, W. D.; Hunter, R. N.; Lackey, K. E.; Lovejoy, B.; Luzzio, M. J.; Montana, V.; Rocque, W. J.; Rusnak, D.; Shewchuk, L.; Veal, J. M.; Walker, D. H.; Kuyper, L. F., Oxindole-based inhibitors of cyclin-dependent kinase 2 (CDK2): Design, synthesis, enzymatic activities, and X-ray crystallographic analysis. *Journal of Medicinal Chemistry* **2001**, 44 (25), 4339-4358.

60. Gajiwala, K. S.; Wu, J. C.; Christensen, J.; Deshmukh, G. D.; Diehl, W.; DiNitto, J. P.; English, J. M.; Greig, M. J.; He, Y. A.; Jacques, S. L.; Lunney, E. A.; McTigue, M.; Molina, D.; Quenzer, T.; Wells, P. A.; Yu, X.; Zhang, Y.; Zou, A. H.; Emmett, M. R.; Marshall, A. G.; Zhang, H. M.; Demetri, G. D., KIT kinase mutants show unique mechanisms of drug resistance to imatinib and sunitinib in gastrointestinal stromal tumor patients. *P Natl Acad Sci USA* **2009**, 106 (5), 1542-1547.

61. Mohammadi, M.; McMahon, G.; Sun, L.; Tang, C.; Hirth, P.; Yeh, B. K.; Hubbard, S. R.; Schlessinger, J., Structures of the tyrosine kinase domain of fibroblast growth factor receptor in complex with inhibitors. *Science* **1997**, 276 (5314), 955-960.

62. Mashhoon, N.; DeMaggio, A. J.; Tereshko, V.; Bergmeier, S. C.; Egli, R.; Hoekstra, M. F.; Kuret, J., Crystal structure of a conformation-selective casein kinase-1 inhibitor. *Journal of Biological Chemistry* **2000**, 275 (26), 20052-20060.

63. Sarkisyan, K. S.; Yampolsky, I. V.; Solntsev, K. M.; Lukyanov, S. A.; Lukyanov, K. A.; Mishin, A. S., Tryptophan-based chromophore in fluorescent proteins can be anionic. *Sci Rep-Uk* **2012**, 2.

64. Campagna-Slater, V.; Pottel, J.; Therrien, E.; Cantin, L. D.; Moitessier, N., Development of a Computational Tool to Rival Experts in the Prediction of Sites of Metabolism of Xenobiotics by P450s. *Journal of Chemical Information and Modeling* **2012**, 52 (9), 2471-2483.

65. Martignoni, M.; Groothuis, G. M. M.; de Kanter, R., Species differences between mouse, rat, dog, monkey and human CYP-mediated drug metabolism, inhibition and induction. *Expert Opin Drug Met* **2006**, 2 (6), 875-894.
66. Wilkinson, G. R., Drug therapy - Drug metabolism and variability among patients in drug response. *New Engl J Med* **2005**, 352 (21), 2211-2221.
67. Altar, C. A.; Burton, L. E.; Bennett, G. L.; Dugich-Djordjevic, M., Recombinant human nerve growth factor is biologically active and labels novel high-affinity binding sites in rat brain. *Proc Natl Acad Sci U S A* **1991**, 88 (1), 281-5.
68. Matsumoto, K.; Wada, R. K.; Yamashiro, J. M.; Kaplan, D. R.; Thiele, C. J., Expression of brain-derived neurotrophic factor and p145TrkB affects survival, differentiation, and invasiveness of human neuroblastoma cells. *Cancer Res* **1995**, 55 (8), 1798-806.
69. Brodeur, G. M.; Minturn, J. E.; Ho, R.; Simpson, A. M.; Iyer, R.; Varela, C. R.; Light, J. E.; Kolla, V.; Evans, A. E., Trk receptor expression and inhibition in neuroblastomas. *Clin Cancer Res* **2009**, 15 (10), 3244-50.
70. Ricci, A.; Felici, L.; Mariotta, S.; Mannino, F.; Schmid, G.; Terzano, C.; Cardillo, G.; Amenta, F.; Bronzetti, E., Neurotrophin and neurotrophin receptor protein expression in the human lung. *Am J Resp Cell Mol* **2004**, 30 (1), 12-19.
71. Garcia-Suarez, O.; Perez-Pinera, P.; Laura, R.; Germana, A.; Esteban, I.; Cabo, R.; Silos-Santiago, I.; Cobo, J. L.; Vega, J. A., TrkB is necessary for the normal development of the lung. *Resp Physiol Neurobi* **2009**, 167 (3), 281-291.
72. Raab, S.; Plate, K. H., Different networks, common growth factors: shared growth factors and receptors of the vascular and the nervous system. *Acta Neuropathol* **2007**, 113 (6), 607-626.
73. Coffey, E. T., Nuclear and cytosolic JNK signalling in neurons. *Nature Reviews Neuroscience* **2014**, 15 (5), 285-299.
74. Ingraham, C. A.; Cox, M. E.; Ward, D. C.; Fults, D. W.; Maness, P. F., C-Src and Other Proto-Oncogenes Implicated in Neuronal Differentiation. *Mol Chem Neuropathol* **1989**, 10 (1), 1-14.
75. Iwahara, T.; Fujimoto, J.; Wen, D. Z.; Cupples, R.; Bucay, N.; Arakawa, T.; Mori, S.; Ratzkin, B.; Yamamoto, T., Molecular characterization of ALK, a receptor tyrosine kinase expressed specifically in the nervous system. *Oncogene* **1997**, 14 (4), 439-449.
76. Achim, C. L.; Katyal, S.; Wiley, C. A.; Shiratori, M.; Wang, G.; Oshika, E.; Petersen, B. E.; Li, J. M.; Michalopoulos, G. K., Expression of HGF and cMet in the developing and adult brain. *Dev Brain Res* **1997**, 102 (2), 299-303.

77. Block, D., Coenen, H.H., Stöcklin, G. , The n.c.a. nucleophilic ¹⁸F-fluorination of 1,N-disubstituted alkanes as fluoralkylation agents. . *J. Labelled Compd. Radiopharm* **1987**, *24*, 1029-1042.
78. Zoghbi, S. S.; Shetty, H. U.; Ichise, M.; Fujita, M.; Imaizumi, M.; Liow, J. S.; Shah, J.; Musachio, J. L.; Pike, V. W.; Innis, R. B., PET imaging of the dopamine transporter with ¹⁸F-FECNT: a polar radiometabolite confounds brain radioligand measurements. *J Nucl Med* **2006**, *47* (3), 520-7.
79. Parent, M.; Bedard, M. A.; Aliaga, A.; Soucy, J. P.; St-Pierre, E. L.; Cyr, M.; Kostikov, A.; Schirmacher, E.; Massarweh, G.; Rosa-Neto, P., PET imaging of cholinergic deficits in rats using [¹⁸F]fluoroethoxybenzovesamicol ([¹⁸F]FEOBV). *Neuroimage* **2012**, *62* (1), 555-561.
80. Aliaga, A.; Rousseau, J. A.; Cadorette, J.; Croteau, E.; van Lier, J. E.; Lecomte, R.; Benard, F., A small animal positron emission tomography study of the effect of chemotherapy and hormonal therapy on the uptake of 2-deoxy-2-[¹⁸F]fluoro-D-glucose in murine models of breast cancer. *Mol Imaging Biol* **2007**, *9* (3), 144-150.
81. Kopka, K.; Faust, A.; Keul, P.; Wagner, S.; Breyholz, H. J.; Holtke, C.; Schober, O.; Schafers, M.; Levkau, B., 5-Pyrrolidinylsulfonyl isatins as a potential tool for the molecular imaging of caspases in apoptosis. *Journal of Medicinal Chemistry* **2006**, *49* (23), 6704-6715.

Article 7

*A version of this chapter has been published as: Bernard-Gauthier, V.; Bailey, J. J.; Aliaga, A.; Kostikov, A.; Rosa-Neto, P.; Wuest, M.; Brodeur, G. M.; Bedell, B. J.; Wuest, F.; Schirmacher, R. Development of Subnanomolar Radiofluorinated (2-Pyrrolidin-1-yl)imidazo[1,2-*b*]pyridazine pan-Trk Inhibitors as Candidate PET Imaging Probes. *MedChemComm*, **2015**, *6*, 2184-2193. This article was selected for the [2015 MedChemComm Hot Articles](#) and the [Neurodegenerative diseases](#) collections.*

*Author contributions: V.B.G. managed the study, designed all experiments, conducted all chemical syntheses (except compounds **4.29** and **4.30**) and characterizations, conducted all *in silico* analyses, radiochemistry experiments, contributed to autoradiography studies, analyzed and interpreted all data and wrote the paper; J.J.B. synthesized compounds **4.29** and **4.30**; A.A. performed autoradiography experiments and analyzed autoradiography data. A.K. contributed to radiochemistry (for autoradiography experiments); A.K., P.R.-N., M.W., G.M.B., B.J.B., F.W. and R.S. contributed new reagents and analytic tools; the manuscript was approved by all co-authors; R.S. supervised the research and corrected manuscript.*

Development of Subnanomolar Radiofluorinated (2-Pyrrolidin-1-yl)imidazo[1,2-b]pyridazine Pan-Trk Inhibitors as Candidate PET Imaging Probes

Vadim Bernard-Gauthier^{1}, Justin J. Bailey¹, Arturo Aliaga², Alexey Kostikov³, Pedro Rosa-Neto², Melinda Wuest¹, Garrett M. Brodeur⁴, Barry J. Bedell^{5,6}, Frank Wuest¹ and Ralf Schirmacher^{1*}*

¹Department of Oncology, University of Alberta, 11560 University Avenue, Edmonton, AB, T6G 1Z2, Canada. ²Translational Neuroimaging Laboratory, McGill Centre for Studies in Aging, Douglas Mental Health University Institute, 6875 Boulevard LaSalle, Montreal, QC, H4H 1R3, Canada. ³McConnell Brain Imaging Centre, Montreal Neurological Institute, McGill University, 3801 University Street, Montreal, QC, H3A 2B4, Canada. ⁴Oncology Research, The Children's Hospital of Philadelphia, 3501 Civic Center Blvd., Philadelphia, PA, 19104-4302, USA. ⁵Biospective Inc., 6100 Avenue Royalmount, Montreal, QC H4P 2R2, Canada. ⁶Research Institute of the McGill University Health Centre, 1001 boulevard Decarie, Montreal, QC H4A 3J1, Canada. *Corresponding authors

4.1 Abstract

Dysregulation of tropomyosin receptor kinases (TrkA/B/C) expression and signalling is recognized as a hallmark of numerous neurodegenerative diseases including Parkinson's, Huntington's and Alzheimer's disease. TrkA/B/C is known to drive tumorigenesis and metastatic potential in a wide range of neurogenic and nonneurogenic human cancers. The development of suitable positron emission tomography (PET) radioligands would allow an *in vivo* exploration of this versatile potential therapeutic target. Herein, the rational remodeling of the amide moiety of a 6-(2-(3-fluorophenyl)pyrrolidin-1-yl)imidazo[1,2-b]pyridazine-3-amide lead structure to accommodate efficient fluorine-18 labeling led to the identification of a series of fluorinated Trk inhibitors with picomolar IC₅₀. The ensuing representative radiolabeled inhibitors [¹⁸F]**4.16** ([¹⁸F]-(±)-IPMICF6) and [¹⁸F]**4.27** ([¹⁸F]-(±)-IPMICF10) constitute novel lead radioligands with about 2- to 3- orders of magnitude increased TrkB/C potencies compared to previous lead tracers and display favorable selectivity profiles and physicochemical parameters for translation into *in vivo* PET imaging agents.

4.2 Introduction

The tropomyosin receptor kinase (Trk) family consists of three structurally analogous tyrosine kinases with pivotal significance in the embryonic development and post-natal maintenance of the mammalian nervous system. Upon extracellular binding of cognate specific neurotrophins and subsequent kinase domain autophosphorylation of the full length receptors, the Trk/neurotrophin protein interplay activates key signal transduction pathways including Ras/MAPK, PI3K and PLC γ which spatiotemporally support growth, survival and differentiation within distinct neuronal populations.¹⁻³ Nerve growth factor (NGF) specifically interacts with TrkA, while brain derived neurotrophic factor (BDNF) and neurotrophin-3 (NT-3) selectively bind TrkB and TrkC respectively ($K_d \approx 1.7- 2.3 \times 10^{-11}$ M).⁴ NT-3 was also shown to activate TrkA and TrkB, albeit with lower efficiency.⁴ TrkA receptor expression in the central nervous system (CNS) is mostly circumscribed to cholinergic neurons of the basal forebrain (BFCNs) and dorsal root ganglion (DRG).⁵⁻⁷ TrkA density is reduced in BFCNs and cholinergic projections in the cerebral cortex at early Alzheimer's disease (AD) stages underlining the involvement of TrkA in the cognitive decline characteristic of the early onset of AD.⁸⁻¹⁰ In the periphery, TrkA activation is involved in nociception and is a validated target for chronic pain.¹¹⁻¹² In contrast to TrkA, TrkB/C have comparatively high expression levels in the CNS with topographies encompassing most brain regions including cortex, striatum, thalamus and cerebellum.^{6, 13-14} In rodents, the *NTRK2* (TrkB) family gene expression includes the full length TrkB.tk+ (herein referred to as TrkB) and the truncated splice variants TrkB.T1 and TrkB.T2 which lack the intracellular kinase domain.¹⁵⁻¹⁶ TrkB.T1 has been characterized and shown to be abundantly expressed in the CNS.¹⁷ Specific biological functions of TrkB.T1 remain elusive but include negative regulation of TrkB.tk+ signalling and BDNF sequestration and translocation.¹⁸ The expression ratio of TrkB.tk+/TrkB.T1 are highly regulated in the embryonic and early postnatal nervous system development. In adult life, mounting evidences support TrkB isoform dysregulation and aberrant

TrkB/BDNF signalling as a hallmark of neurodegenerative and psychiatric diseases/ conditions including AD, Parkinson's disease (PD), Huntington's disease (HD), schizophrenia and traumatic brain injury (TBI).¹⁹⁻²³

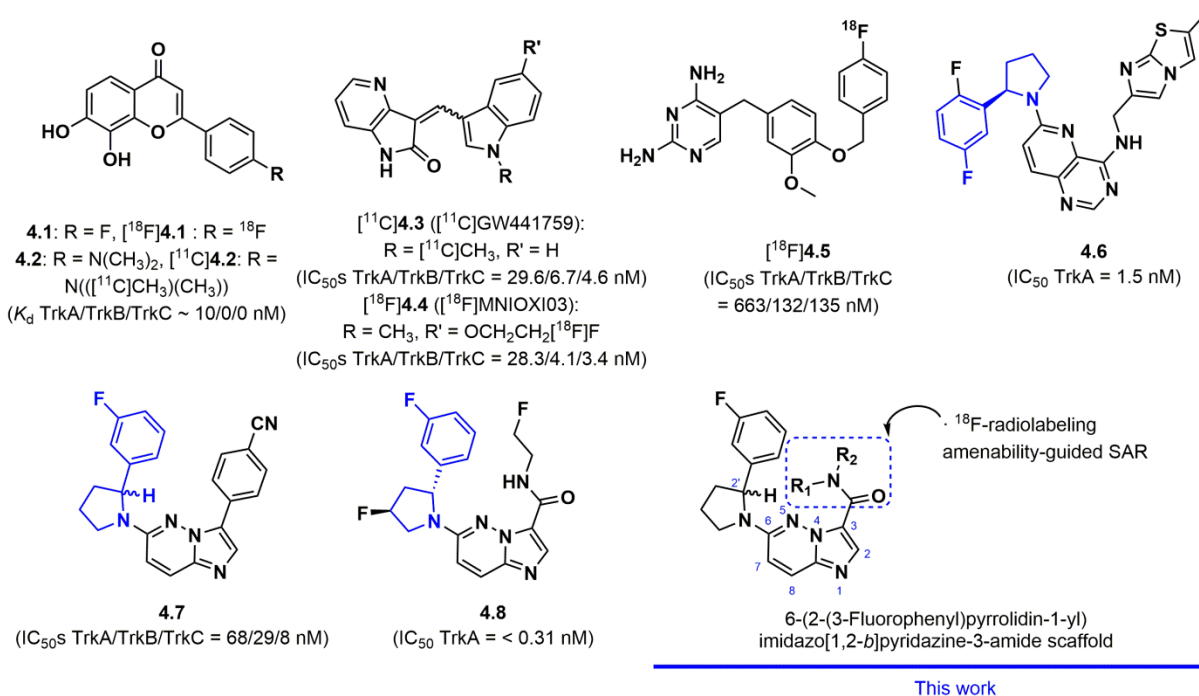


Figure 4.1. Structure of Trk agonistic radioligands, tyrosine kinase inhibitor (TKIs) radioligands and fluorophenyl- and difluorophenyl pyrrolidine-containing Trk TKIs.

Though historically explored in the context of neurology, Trk involvement in tumorigenesis and aggressiveness of human cancers is also well recognized.²⁴⁻²⁶ Indeed, the prototypical *NTRK1* (TrkA) gene was initially identified from a colon carcinoma leading to a constitutively activated fused tropomyosin-TrkA protein.²⁷ Besides rearranged/mutated *NTRK* gene products, compelling evidence shows that overexpression of the intact Trk proto-oncoproteins, especially TrkB, is associated with aggressive tumor growth and treatment resistance in a set of neurogenic and nonneurogenic neoplasms including neuroblastoma and pancreatic cancer.²⁸⁻²⁹ During the last decade, considerable medicinal chemistry effort, mostly

focused towards intracellular binding kinase inhibitors, has led to the identification of diverse and highly potent selective pan-Trk tyrosine kinase inhibitors (TKIs) as putative cancer therapeutics.³⁰⁻³⁴

In order to non-invasively assess and monitor TrkA/B/C levels in the brain and in cancer, our group has sought to develop ¹¹C- and ¹⁸F-labeled Trk-targeted positron emission tomography (PET) radiotracers suitable for *in vivo* imaging. We have previously described both extracellular and intracellular binding PET radioligands, the first of which being the TrkB selective 7,8-dihydroxyflavone-based probes [¹⁸F]4.1 and [¹¹C]4.2 (**Figure 4.1**).³⁵ These radioligands, based on one of the rare efficacious small molecules to bind the extracellular Trk proteins described thus far suffered extensive metabolism *in vivo* and did not permeate the blood brain barrier (BBB) despite favorable *in vitro* profiling. More recently, we reported on the development of low nanomolar pan-Trk inhibitor [¹¹C]GW441759 and an analogous fluorinated derivative [¹⁸F]4.4.³⁶ Preclinical imaging in rodents confirmed [¹¹C]GW441759 as the first brain penetrating Trk PET radiotracer but blocking studies failed to demonstrate specific brain binding at the tested dose. Both [¹¹C]GW441759 and [¹⁸F]4.4 also successfully imaged Trk in rat brain sections and human neuroblastoma tumor samples expressing TrkB *in vitro*. In addition, the radiosynthetic methodology to access the fluorinated demethoxy derivative of the Trk inhibitor GW2580 ([¹⁸F]4.5), was described.³⁷ Despite its unique selectivity, [¹⁸F]4.5 only displays moderate potencies towards Trk (IC₅₀s = 135–663 nM) and lacks necessary physicochemical properties to be suitable for brain PET imaging (**Figure 4.1**). Those radioligands are currently being evaluated for peripheral neuroblastoma tumor imaging by our group. As far as Trk neuroimaging is concerned, it would be desirable to concentrate efforts on compounds exhibiting subnanomolar affinities for Trk in combination with desired properties for PET ligand development (including $B_{\max}/K_d > 10$, $\text{clogD}_{7.4}$ in the range of 2.0 – 3.5, topological polar surface area (TSPA) < 80 Å², hydrogen bond donor (HBD) ≤ 1).³⁸ Amenability to fluorine-18 labeling ($t_{1/2}$

= 109.8 min; 97% β^+ ; $E_{\max}(\beta^+) = 0.64$ MeV) would also be favorable due to the better nuclear properties, including longer half-life which allow for longer synthesis time and shipping, as compared to carbon-11.

In recent years, diverse scaffolds including heterocycle cores such as imidazo[1,2-*b*]pyridazine, pyrido[3,2-*d*]pyrimidine and pyrazolo[1,5-*a*]pyrimidine related through conserved fluorinated 2-phenylpyrrolidines fragments have emerged as Trk selective inhibitor pharmacophores (**4.6–4.8**, **Figure 4.1**).³⁹⁻⁴⁶ (*R*)-2-Phenylpyrrolidine is the preferred enantiomeric building block. However in most cases where pure (*S*)-2-phenylpyrrolidine containing derivatives were characterized, nanomolar Trk inhibitions were still achieved.⁴⁰ Moreover, *N*-(2-fluoroethyl)acetamide inhibitor (*R*)-**4.8** and related compounds showed unprecedented picomolar potencies towards TrkA.⁴⁰ Very recently, a derivative of **4.7** was also shown to achieve tumor regression in a KM12 rat tumor model.⁴⁵ We hypothesized that a scaffold derived from compound **4.8**, which provides a favorable alignment of the required physicochemical parameters for PET radioligand development and was shown to tolerate numerous 3-carboxamide structural alterations, would be valuable in the exploration of new Trk radioligands bearing purposely designed ¹⁸F-radiolabeled amide substituents. Herein, we present the design, syntheses and first *in vitro* evaluation of novel ¹⁸F-labeled Trk PET 6-(2-(3-fluorophenyl)pyrrolidin-1-yl)imidazo[1,2-*b*]pyridazine-3-amide radioligand candidates.

4.3 Results and discussion

A priority of this work was to explore and identify the optimal fluorinated 3-carboxamide building blocks integrated into the (2-pyrrolidin-1-yl)imidazo[1,2-*b*]pyridazine lead structure to yield Trk inhibitors of highest possible affinity. As another important premise, the identified compounds should be easily labeled in one step with [¹⁸F]fluoride to facilitate applicability. Since both (*R*)- and (*S*)-substituted pyrrolidines were previously shown to be highly potent and the

racemic building block is readily available, we selected the racemic 2-(3-fluorophenyl)pyrrolidine motif with the core structure of lead 8 as a starting point in our structure activity relationship (SAR) study (it was decided that at a later stage, once the SAR study delineating the amide motif would be completed, selected radiolabeled inhibitors could then more easily be obtained in pure enantiomeric forms for comparison with the corresponding racemates. This decision was also motivated by the current worldwide sparteine shortage – the only described synthesis of the putatively preferred compound (*R*)-2-(3-fluorophenyl)pyrrolidine proceeding via a key sparteine-mediated lithiation stage).

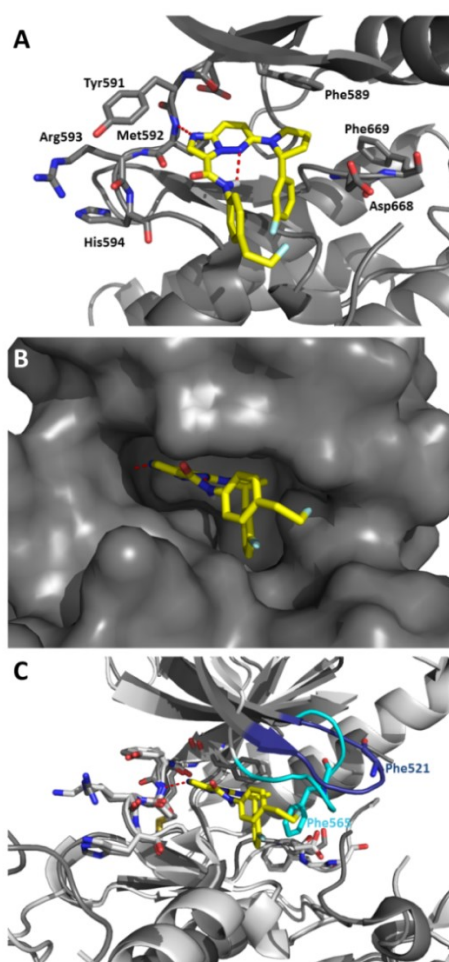


Figure 4.2. Predicted binding poses for (*R*)-4.27 bound to TrkA/B in DFG-in conformation. (A) Docking of (*R*)-4.27 to the ATP binding site of TrkA (PDB 4PMT). (B) Surface model of (*R*)-4.27 docked to TrkA (PDB 4PMT). (C) Superposition of TrkB (pale gray, DFG-in, PDB 4AT3) and the docking of (*R*)-4.27 with TrkA (dark gray, PDB 4PMT). The TrkA (blue) and TrkB (cyan) glycine-rich loops are highlighted.

Following procedures previously described,⁴⁴ this approach allowed the preparation of a sufficient amount of the key 3-carboxylic acid intermediate **4.9** for further derivatization (**Table 4.1**, see **Scheme S4.1**; **Supporting Information**).

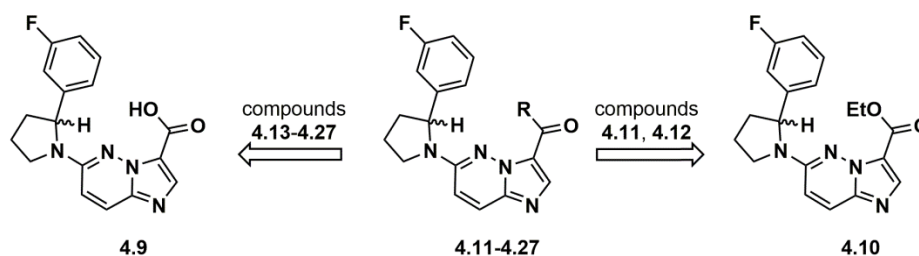
4.3.1 Amide moiety design for radiolabeling and chemistry. It was noted that despite the excellent potency attained with the *N*-(2-fluoroethyl)-amide substituent in **4.8** as reported in patent literature, the synthesis of the ¹⁸F-labeled counterpart of this motif would require a multistep approach using 2-[¹⁸F]-fluoroethylamine which in turn would ultimately limit the later use of the resulting radioligand in a clinical setting.⁴⁷⁻⁴⁸ Initial SAR efforts therefore focussed on introducing small aliphatic fluorinated chains attainable as ¹⁸F-isotopologues via simple S_N2-type radiofluorination but which would not undergo intramolecular five-exo-tet cyclisation to the oxazoline upon prior functionalization with a leaving group or during the radiolabeling. In this context structurally analogous fluorocyclobutyl moieties were selected. Previous reports also suggest that ¹⁸F-labeled fluorocyclobutyl-containing PET probes may be metabolically more robust than their linear equivalents.⁴⁹ Hence, compounds **4.15** and **16** along with the linear *N*-fluoroalkyl amides **4.13** and **4.14** were synthesized in good yield via HATU coupling between **4.9** and the corresponding amines (**Table 4.1**). In order to assess the impact of the amide proton towards Trk binding, the 3-azetidine amide **4.17** was synthesized as the closest cyclized structural analog to **4.13**. Direct amidation of the ester intermediate **4.10** also efficiently provided the simpler derivatives **4.11** and **4.12**. Using docking simulations, congruent binding poses to TrkA/B/C were initially obtained in both the inactive (DFG-out) and active (DFG-in) conformations for **4.16** (*R* and *S*; **Figure S4.1** and **S4.2**; **Supporting Information**). Choi *et al.*⁴⁵ recently described X-ray cocrystal structures of (*R*)-enantiomer derivatives of **4.7** bound to TrkA and TrkC in DFG-in and DFG-out conformations and suggested that the favoured binding mode likely depends upon the substituent pattern of the imidazo[1,2-*b*]pyridazine core. The binding modes of **4.16** and derivatives thereof obtained in our *in silico* experiments corroborate those X-

ray results with regard to the binding with the active Trk kinases. In this conformation, the N₁ from the imidazo[1,2-*b*]pyridazine interacts via H-bonding with the backbone nitrogen of Met592/636 (TrkA/TrkB) from the hinge and provides excellent overlap of the fluorophenyl ring to the ribose binding pocket including π -stacking with the proximal Phe521/565 (no DFG-in TrkC crystal structure is publicly available).⁵⁰ In this model, the amide substituent is pointing towards the solvent region and rotation of the C₃-C(carbonyl) can lead to the amide carbonyl or NH directed at the hinge (**Figure S4.1, Supporting Information**). The predicted binding pose of the representative compound **4.27** (*vide infra*) is shown in **Figure 4.2**. With the carbonyl pointing outward, additional water-mediated H-bonds to residue Met592/636 may occur while a strong intramolecular H-bond is possible between the amide proton and N₅. It is likely that the binding of this preorganized rigidified low energy conformation to Trk in the DFG-in mode explains in part the increased potencies observed between inhibitors such as **4.8** versus **4.7** due to a lower entropic penalty. This binding conformation is also consistent with the disclosure of highly potent related macrocyclized Trk inhibitors.⁵¹ In agreement with the plausible binding mode elucidated, the synthesis of potential inhibitors incorporating larger amide substituents was undertaken. Compounds bearing a 4,4-difluorocyclohexyl group and a *N*-2-(2-fluoroethoxy)ethyl chain were synthesized. The amine **4.30** required for the synthesis of **4.19** was obtained in two steps from 2-fluoroethyl 4-methylbenzenesulfonate **4.28** (**Scheme 4.1A**).

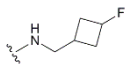
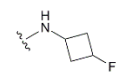
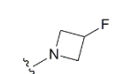
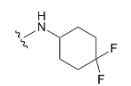
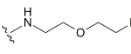
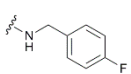
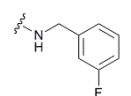
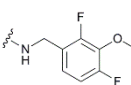
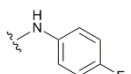
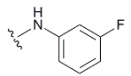
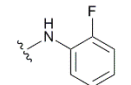
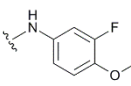
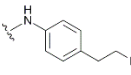
Fluorobenzyl- (**4.20–4.22**) and fluorophenylamide (**4.23–4.27**) compounds were also obtained. The required aniline **4.34** for the synthesis of **4.27** was prepared via a protection/DAST fluorination/deprotection sequence (**Scheme 4.1B**). It was anticipated that compounds **4.20–4.26** would be accessible for radiolabeling using direct radiofluorination of non-activated arenes bearing iodonium ylides leaving groups if required.⁵²⁻⁵³ Compound **4.27** was designed to be readily accessible using conventional S_N2 radiofluorination. Compounds **4.22** and **4.26** also bear alternative anisol moieties suitable for carbon-11 labelling using

[¹¹C]CH₃I. The suggested low energy intramolecular H-bonded U-shaped conformation was illustrated by single crystal X-ray diffraction of the representative compound (*R*)-**4.22** (obtained from the racemate; **Figure 4.3**).

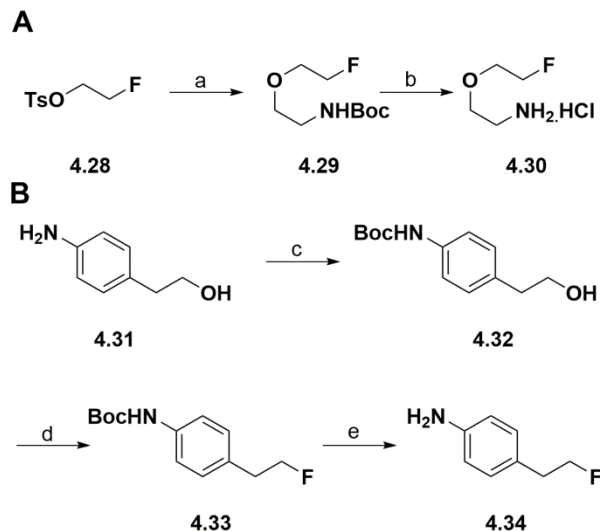
Table 4.1. SAR and *In Vitro* Enzymatic Activities and Physicochemical Data for Imidazo[1,2-*b*]pyridazines Trk Inhibitors



| Cpd | R | clog P | TPSA (Å ²) | IC ₅₀ (nM) ^a | | | IC ₅₀ _{TrkA} /IC ₅₀ _{TrkB} ; IC ₅₀ _{TrkA} /IC ₅₀ _{TrkC} | B _{max} / IC ₅₀ (caudate putamen/ cortex; TrkA) ^b | B _{max} / IC ₅₀ (whole brain average; TrkB/C) ^b |
|-------------------------|---|--------|------------------------|------------------------------------|---------------|---------------|--|--|---|
| | | | | TrkA | TrkB | TrkC | | | |
| 4.10 | | 2.39 | 59.73 | 17.7 | 2.36 | 1.37 | 7.5; 12.9 | 0.8/0.1 | 11.0 |
| 4.9 | | 1.66 | 70.73 | >10 000 | 3250 | 1880 | - ^c | - ^c | - ^c |
| 4.11 | | 1.16 | 76.52 | 12.9 | 1.31 | 0.943 | 9.8; 13.7 | 1.1/0.2 | 19.8 |
| 4.12 | | 1.51 | 62.53 | 7.66 | 0.565 | 0.374 | 13.6; 20.5 | 1.8/0.3 | 46.0 |
| 4.13^d | | 1.70 | 62.53 | 1.11 ± 0.13 | 0.037 ± 0.013 | 0.080 ± 0.030 | 30.0; 13.8 | 8.9/1.8 | 703 |
| 4.14^d | | 2.15 | 62.53 | 2.48 ± 0.96 | 0.105 ± 0.043 | 0.115 ± 0.034 | 23.6; 21.6 | 4.0/0.8 | 248 |

| | | | | | | | | | |
|-------------------------|---|------|-------|-------------|---------------|---------------|------------|----------|------|
| 4.15^d |  | 2.28 | 62.53 | 2.69 ± 0.24 | 0.120 ± 0.021 | 0.163 ± 0.011 | 22.4; 16.5 | 3.7/0.7 | 217 |
| 4.16^d |  | 2.08 | 62.53 | 1.91 ± 0.41 | 0.076 ± 0.035 | 0.076 ± 0.035 | 25.1; 25.1 | 5.2/1.0 | 342 |
| 4.17 |  | 1.93 | 53.74 | 140 | 22.8 | 13.8 | 6.1; 10.1 | 0.1/0.01 | 1.1 |
| 4.18 |  | 3.06 | 62.53 | 1.50 | 0.132 | 0.154 | 11.4; 9.7 | 9.1/1.3 | 197 |
| 4.19 |  | 1.45 | 71.76 | 4.31 | 0.926 | 0.440 | 4.7; 9.8 | 3.2/0.5 | 28.1 |
| 4.20 |  | 2.88 | 62.53 | 3.53 | 1.09 | 0.580 | 3.2; 6.1 | 3.9/0.6 | 23.8 |
| 4.21 |  | 2.88 | 62.53 | 2.76 | 0.509 | 0.299 | 5.4; 9.2 | 4.9/0.7 | 51.1 |
| 4.22 |  | 2.91 | 71.76 | 11.2 | 1.96 | 0.950 | 5.7; 11.8 | 1.2/0.2 | 13.3 |
| 4.23 |  | 3.17 | 62.53 | 5.00 | 0.584 | 0.408 | 8.6; 12.3 | 2.7/0.4 | 44.5 |
| 4.24 |  | 3.1 | 71.76 | 4.80 | 0.456 | 0.233 | 10.5; 20.6 | 2.8/0.4 | 57.0 |
| 4.25^d |  | 3.17 | 62.53 | 2.06 ± 0.17 | 0.131 ± 0.047 | 0.214 ± 0.093 | 15.7; 9.6 | 4.8/1.0 | 199 |
| 4.26^d |  | 3.17 | 62.53 | 1.94 ± 0.90 | 0.080 ± 0.012 | 0.095 ± 0.013 | 24.3; 20.4 | 5.1/1.0 | 325 |
| 4.27^d |  | 3.61 | 62.53 | 2.10 ± 0.34 | 0.099 ± 0.008 | 0.127 ± 0.005 | 21.2; 16.5 | 4.7/1.0 | 262 |

^a[γ -³³P]ATP-based enzymatic assay performed by Reaction Biology. ^bCalculated with B_{\max} value for the caudate putamen for TrkA and from the whole brain for TrkB from Ref. 56 and the IC_{50} s from TrkA and TrkB respectively. ^cNot determined. ^dValues accompanied by standard deviation were averaged from three independent experiments.



Scheme 4.1. *Reagents and conditions:* (A) (a) *N*-boc-ethanolamine, NaH, DMF, rt, 12 h (50%). (b) TFA, CH₂Cl₂, rt, 1 h, then HCl (1M in diethyl ether) (98%). (B) (c) Boc₂O, Et₃N, THF, 0°C - rt, 16 h (85%). (d) DAST, CH₂Cl₂, -78°C, 30 min then 0°C, 6 h (86%). (e) TFA, CH₂Cl₂, 0°C - rt, 5 h (93%).

4.3.2 *In vitro* binding studies. The inhibitory activity of compounds **4.9–4.27** was obtained using a [γ -³³P]ATP-based enzymatic assay (the assay was performed in using the same conditions than previously used in ref. 36). The TrkA/B/C assay data is summarized in **Table 4.1**. The most potent inhibitor for all Trk proteins was derivative **4.13** containing the 2-fluoroethyl amide lateral chain with an IC₅₀ of 1.11 nM for TrkA, 0.037 nM for TrkB and 0.080 nM for TrkC. To our satisfaction, replacement of the linear chain of **4.13** with the fluorocyclobutyl found in **4.16** did not significantly alter the excellent potencies observed (1.05 to 2.05-fold reduction). Elongation of the amide chains in **4.14** and **4.15** by one additional carbon only slightly affected the potencies. Compound **4.12** displayed subnanomolar and low nanomolar potencies for TrkB/C and TrkA respectively while being ~2-fold more potent than the primary amide **4.11** for all Trks. While the ester **4.10** displayed significantly lower, yet still low nanomolar potencies, the presence of a carboxylate in **4.9** was highly detrimental to the affinity. As predicted above, the removal of the amide proton in **4.17** had a negative effect despite this inhibitor being the closest analog of **4.13** with respect to all other structural elements (616-fold decreased potency for

TrkB). As expected, good tolerance of the sterically demanding gem-difluorocyclohexane (compound **4.18**), extended linear chain (compound **4.19**) and aryl-containing derivatives (compounds **4.20–4.27**) was also observed. The best potencies in the aryl-containing derivatives were attained by fluorophenyl – compared to fluorobenzylamides. Inhibitors **4.13** and **4.16** were found to match the Trk activity of staurosporine – to our knowledge, the most potent Trk inhibitor currently available (**Figure S4.20, Supporting Information**). All compounds also show favorable clogP and TPSA values for translation into PET tracers (**Table 4.1**).

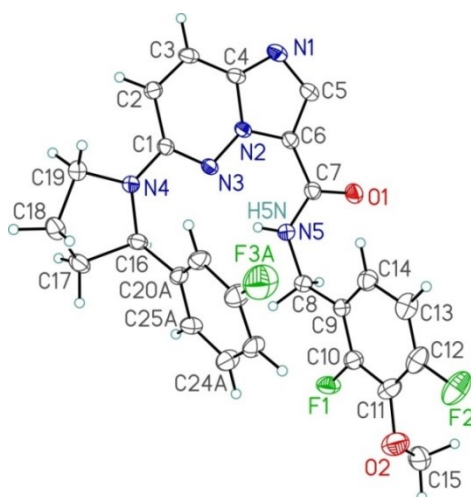


Figure 4.3. Single-crystal X-Ray structure of (*R*)-**4.22**; ellipsoids drawn at 30% probability.

Overall, we identified a total of 8 inhibitors (**4.13–4.16**, **4.18**, **4.25–4.27**) displaying approximately 200 pM potencies or lower for TrkB/C and low nanomolar potencies for TrkA with radiotracer-favorable properties. These most potent derivatives, except for **4.18**, were also found to display the best selectivity profile in the assayed conditions (TrkB/C versus TrkA, **Figure S4.21, Supporting Information**, the use of the IC₅₀s obtained for TrkA/B/C comparison and selectivity is based on the hypothesis that KmATP for TrkA, TrkB and TrkC do not differ significantly due to their conserved sequence at the ATP binding site). Due to the extensive sequence conservation in the 40 residues likely to be involved in binding at the ATP site (DFG-

in) between TrkA and TrkB (95%) and TrkB and TrkC (100%), it is largely accepted that Trk isoform selectivity for ATP competitive inhibitors will be challenging to attain.^{30-31, 54} The observed moderate selectivity here may be related to the organization of the glycine-rich loops (**Figure 4.2C**) or the difference in conformational restriction of the hinge in TrkA versus TrkB as previously suggested.⁵⁴

While the development of a pan-Trk PET radioligand would be highly valuable, selectively imaging TrkB/C independently of TrkA and vice versa would be even more desirable. In imaging studies, the specific PET signal is contingent on both the receptor density (B_{\max}) and affinity of the tracer for the specific target.⁵⁵ Hence, for Trk neuroimaging, visualizing TrkB/C selectively will likely be facilitated by the drastic differences in B_{\max} and topographies of Trks in the brain. Binding studies with [¹²⁵I]-neurotrophins along with in situ hybridization experiments have shown that TrkB/C densities largely exceed that of TrkA.^{7, 14, 56} While TrkB/C are largely co-expressed in all brain regions with an average $B_{\max} > 26$ nM, TrkA expression is mostly restricted to the striatum with a $B_{\max} < 9$ nM. Therefore, the (TrkB/C)/TrkA B_{\max} ratios for all brain regions range from 3 in the striatum to $\gg 10$ in most other brain regions. It should then be expected that, even in the absence of selectivity, the binding of a PET radiolabeled Trk inhibitor should mostly reflect the TrkB/C distribution. This implies that selective visualization of TrkA in the brain would require a highly selective probe to overcome those B_{\max} differences. With our most potent and selective compounds (**4.13–4.16**, **4.18**, **4.25–4.27**), using IC_{50} values as a substitute for K_d , this translates into substantial whole brain average binding potentials for TrkB/C and significantly lower values for TrkA (striatum; **Table 4.1**).

Compounds **4.16** and **4.27** were selected for initial evaluation based on their potencies and expected labeling in one step. The selectivity profile of the two inhibitors was first performed in the presence of 0.1 μ M of compounds on a panel of 20 kinases (**Table 4.2**). This initial off-Trk kinase coverage included targets from different kinase groups with an emphasis on kinases

expressed in the nervous system and neoplasms. Only ERBB2/HER2 and EGFR were significantly affected by co-incubation of **4.16** with remaining activities of 50% and 67% respectively. Those interactions were less pronounced in the presence of **4.27**. Other minor reductions in inhibitory activity were observed with **4.16** towards FLT3 and PDHK1 (15% reduction) and **27** with PDHK1 (20% reduction). Overall both compounds were found to be ≥ 1000 -fold selective for TrkB/C for all tested kinases.

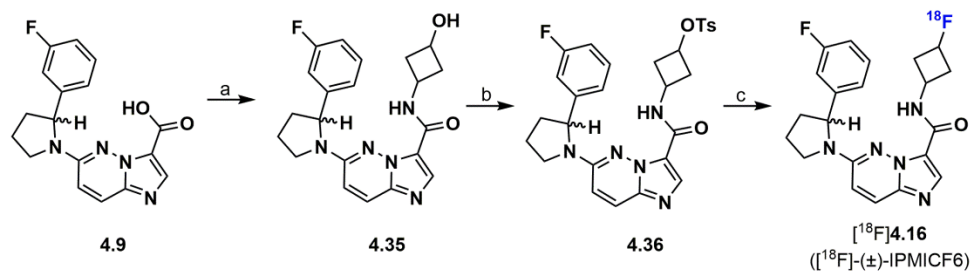
Table 4.2. Kinase Profiling of **4.16** and **4.27**

| Kinase Target | Inhibitory activity of 4.16 (% remaining at 0.1 μ M \pm SD) ^a | Inhibitory activity of 4.27 (% remaining at 0.1 μ M \pm SD) ^a |
|----------------|--|--|
| CSF-1R | 102.53 \pm 0.91 | 104.90 \pm 3.63 |
| VEGRR-2 | 110.00 \pm 0.54 | 95.05 \pm 0.79 |
| ITK | 93.38 \pm 0.22 | 97.63 \pm 0.80 |
| FLT3 | 85.07 \pm 0.11 | 95.09 \pm 1.39 |
| ERK1/MAPK3 | 103.41 \pm 0.08 | 101.28 \pm 0.40 |
| ABL1 | 95.64 \pm 0.46 | 91.34 \pm 0.64 |
| c-Src | 97.01 \pm 0.52 | 103.11 \pm 0.40 |
| EGFR | 66.65 \pm 2.02 | 93.12 \pm 4.80 |
| c-MET | 94.81 \pm 1.41 | 97.05 \pm 1.78 |
| P38A/MAPK14 | 98.46 \pm 1.58 | 99.54 \pm 0.07 |
| ALK | 95.20 \pm 0.92 | 89.00 \pm 0.57 |
| ERBB2/HER2 | 49.61 \pm 0.55 | 79.63 \pm 0.13 |
| JNK1 | 99.44 \pm 0.08 | 100.24 \pm 62 |
| PDHK1 | 85.47 \pm 0.13 | 78.90 \pm 0.26 |
| PDGFR α | 99.81 \pm 1.14 | 99.52 \pm 0.05 |
| JAK1 | 90.67 \pm 0.42 | 99.69 \pm 1.43 |
| SYK | 105.04 \pm 0.28 | 103.93 \pm 0.59 |
| RET | 90.21 \pm 1.10 | 105.87 \pm 0.06 |
| BRAF | 100.30 \pm 1.48 | 94.07 \pm 1.97 |
| c-KIT | 104.76 \pm 0.57 | 100.86 \pm 0.48 |
| TrkA | 2.95 \pm 0.46^b | 3.37 \pm 0.65 |
| TrkB | 0.44 \pm 0.29^b | 0.56 \pm 0.18 |
| TrkC | 0.39 \pm 0.52^b | 0.58 \pm 0.40 |

^a[γ -³³P]ATP-based enzymatic assay performed by Reaction Biology. Values relative to DMSO controls; duplicate experiments. ^bDerived from dose-response curves at 1.11×10^{-07} M (triplicates).

4.3.3 Radiosyntheses and plasma stability. Radiosyntheses of [¹⁸F]**4.16** (named [¹⁸F]IPMICF6) and [¹⁸F]**4.27** (named [¹⁸F]IPMICF10) proceeded from the corresponding tosylate

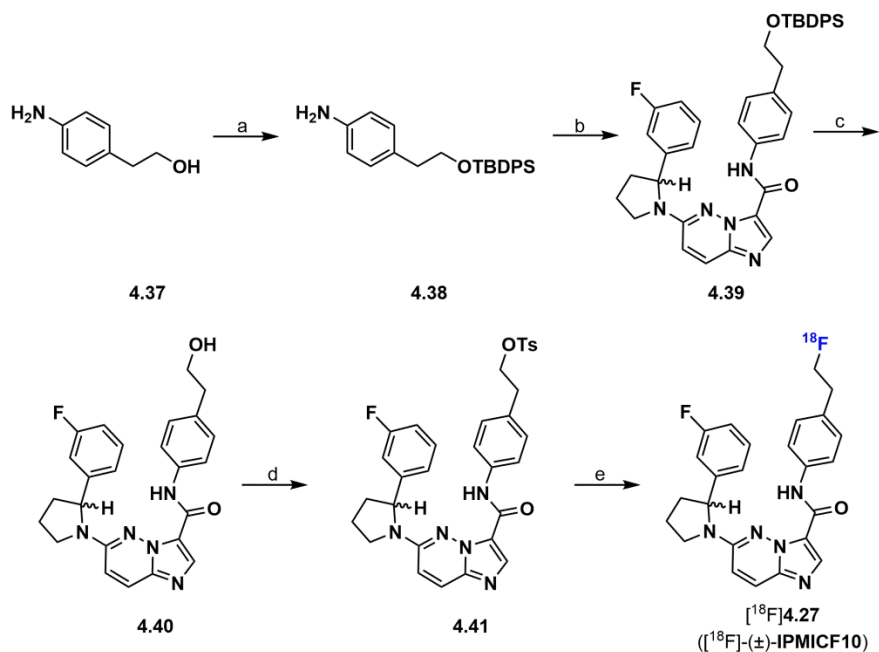
precursors. Precursor **4.36** was obtained in 70% yield from the intermediate **35** which was synthesized near-quantitatively from the coupling of **4.9** with 3-aminocyclobutanol·HCl (**Scheme 4.2**). Synthesis of the tosylate **4.41** was obtained in 45% overall yield and 4 steps from 2-(4-aminophenyl)ethanol (**37**, **Scheme 4.3**). Initial ^{18}F -fluoride incorporation was optimized manually using standard conditions. The radiosynthesis of ^{18}F **4.16** proceeded efficiently at 120 °C for 10 min in anhydrous dimethylformamide (DMF) with ^{18}F fluoride as a Kryptofix-222/ $\text{K}^+/\text{[}^{18}\text{F}\text{]}^-$ complex while the ideal conditions to obtain ^{18}F **4.27** required a lower temperature due to the apparent degradation of the tosylate precursor. Following semi-preparative reverse-phase high performance liquid chromatography (HPLC), the radiochemical yields (RCYs) obtained under those optimal reaction conditions were $24.8 \pm 2.6\%$ ($n = 3$) and $18.3 \pm 3.7\%$ ($n = 3$) for ^{18}F **4.16** and ^{18}F **27** respectively (non-decay-corrected (n.d.c.) based on injected HPLC activity).



Scheme 4.2. Reagents and conditions: (a) 3-Aminocyclobutanol hydrochloride, HATU, DIPEA, DMF, rt, 12 h (99%). (b) TsCl, Et₃N, CH₂Cl₂, rt, 48 h (70%). (c) Kryptofix-222/ $\text{K}^+/\text{[}^{18}\text{F}\text{]}^-$, DMF, 120 °C, 10 min, $24.8 \pm 2.6\%$ RCY (n.d.c.), ($n = 3$).

For *in vitro* autoradiography experiments, the radiofluorination was successfully implemented on a Scintomics automated radiosynthesis module using similar procedures as manually developed. Radioligands ^{18}F **4.16** and ^{18}F **4.27** were then respectively obtained in 3% and 8% isolated RCYs (n.d.c.), >98.5% radiochemical purities (RCP), specific activity (SA) of 163–244 GBq μmol^{-1} at the end of synthesis (EOS) in a total synthesis time of 75 min or under (see ESI†). Both tracers were shown to be highly stable in human plasma *in vitro* at 37 °C with

only minute amounts of ^{18}F -fluoride (<5%) emerging at 60 min post-incubation (**Figure S4.5,S4.8**).



Scheme 4.3. Reagents and conditions: (a) TBDPSCI, imid., DMF, rt, 16 h (80%). (b) **9**, HATU, DIPEA, DMF, rt, 12 h (99%). (c) TBAF, THF, rt, 2 h (89%). (d) TsCl, Et₃N, CH₂Cl₂, rt, 96 h (64%). (e) Kryptofix-222/K⁺/[^{18}F]F⁻, MeCN, 100°C, 20 min, 18.4 ± 3.7 % RCY (n.d.c.), (*n* = 3).

4.3.4 In vitro autoradiography. In addition, the autoradiograms generated from the incubation of [^{18}F]**4.16** with coronal rat brain sections conclusively matched the high affinity binding sites of [^{125}I]BDNF, [^{125}I]NT3 and [^{125}I]NT4/5 and the topographies of TrkB and TrkC mRNA hybridization (including cortex, striatum, thalamus and cerebellum; **Figure 4.4**).¹⁴ In those assays, moderate but significant specific binding was confirmed with co-incubation of non-labeled **4.16** (1.0 μM; Δ ~ -30%) and similar blocking results were also obtained with the incubation of [^{18}F]**27** in the presence of the selective Trk inhibitor GNF-5837 (**Figure S4.22, Supporting Information**). The analogous blocking obtained with the racemic **4.16** and the structurally unrelated oxindole-based DFG-out inhibitor GNF-5837 is indicative that both the (*R*)- and (*S*)-enantiomers binds Trk receptors *in vitro*.

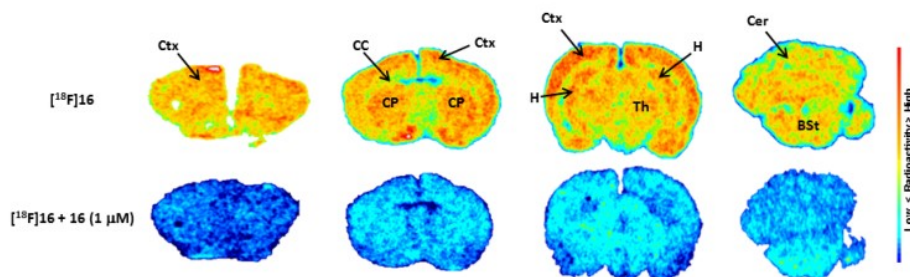


Figure 4.4. Representative *in vitro* autoradiograms from coronal sections of rat brain showing the binding of [^{18}F]4.16 and competition experiments with 4.16 (1 μM) (successive sections between baseline and blocking; anterior: left, posterior: right). BSt = brain stem; CC = corpus callosum; Cer = cerebellum; CP = caudate putamen; Ctx = cortex; H = hippocampus; Th = Thalamus.

4.4 Conclusion

In this study we report the design, synthesis and evaluation of a series of novel fluorinated 6-(2-(3-fluorophenyl)pyrrolidin-1-yl)imidazo[1,2-*b*]pyridazine-based Trk inhibitors with the aim of identifying suitable candidates for translation into PET imaging agents for brain and tumor imaging. Compounds 4.16 and 4.27 were selected from a group of 8 identified structures which displayed around or < 200 pM potency against TrkB/C and were shown to be at least 1000-fold selective in a kinase panel. The rationally designed amide side chains of 4.16 and 4.27 allowed for their straightforward ^{18}F -radiolabeling. *In vitro* autoradiography using [^{18}F]4.16 and [^{18}F]4.27 on coronal rat brain sections confirmed specific binding to TrkB/C-rich brain regions. The selected representative probes from this series, [^{18}F]4.16 ([^{18}F]IPMICF6) and [^{18}F]4.27 ([^{18}F]IPMICF10), constitute novel potential PET tracers with 2 to 3 orders of magnitude potency improvement compared with our previous leads [^{11}C]GW441759 and [^{18}F]4.5, while possessing various other key properties suitable for conversion into PET tracers. While the radioligands developed in this work were evaluated as isomeric mixtures, further structural refinement is currently ongoing in order to deliver pure pyrrolidine motifs as it is to be expected that those different enantiomers will also display distinct affinities and potentially distinctive *in*

in vivo imaging profiles. Comparative *in vivo* imaging studies of [^{18}F]4.16, [^{18}F]4.27 and other radiotracers derived from this work will be reported in due course.

Acknowledgement

We thank Dr. Esther Schirmacher for reading the manuscript and providing useful comments. We are thankful to Angelina Morales-Izquierdo for the mass spectrometry analysis. We thank Marilyn Grand'Maison for the valuable help for the preparation of figures. We are also grateful to Dave Clendening and Blake Lazurko from the Edmonton PET Centre and Robert Hopewell, Miriam Kovacevic and Dean Jolly from the Montreal Neurological Institute for radionuclide production. We thank Bob McDonald and Michael Ferguson for the X-ray crystallographic service. This work was financially supported by Canada Foundation for Innovation (CFI) project no. 203639 to R.S.

4.5 Supporting Information of Article 7

Development of subnanomolar radiofluorinated (2-pyrrolidin-1-yl)imidazo[1,2-b]pyridazine pan-Trk inhibitors as candidate PET imaging probes

Vadim Bernard-Gauthier^{1}, Justin J. Bailey¹, Arturo Aliaga², Alexey Kostikov³, Pedro Rosa-Neto², Melinda Wuest¹, Garrett M. Brodeur⁴, Barry J. Bedell^{5,6}, Frank Wuest¹ and Ralf Schirmmayer^{1*}*

¹Department of Oncology, University of Alberta, 11560 University Avenue, Edmonton, AB, T6G 1Z2, Canada. ²Translational Neuroimaging Laboratory, McGill Centre for Studies in Aging, Douglas Mental Health University Institute, 6875 Boulevard LaSalle, Montreal, QC, H4H 1R3, Canada. ³McConnell Brain Imaging Centre, Montreal Neurological Institute, McGill University, 3801 University Street, Montreal, QC, H3A 2B4, Canada. ⁴Oncology Research, The Children's Hospital of Philadelphia, 3501 Civic Center Blvd., Philadelphia, PA, 19104-4302, USA. ⁵Biospective Inc., 6100 Avenue Royalmount, Montreal, QC H4P 2R2, Canada. ⁶Research Institute of the McGill University Health Centre, 1001 boulevard Decarie, Montreal, QC H4A 3J1, Canada. *Corresponding authors

CONTENT OF SUPPORTING INFORMATION

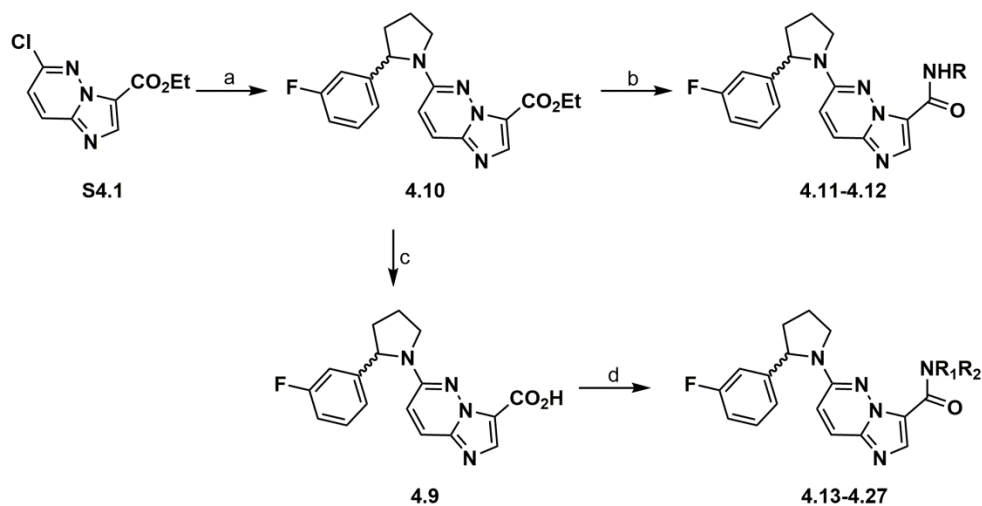
1. ORGANIC SYNTHESSES (**Scheme S4.1**)
2. DOCKING STUDIES (**Figure S4.1-S4.2**)
3. RADIOCHEMISTRY (**Figures S4.3-S4.10**)
4. BIOLOGICAL STUDIES (**Figure S4.11-S4.22; Table S4.1-S4.4**)
5. NMR SPECTRA
6. CRYSTALLOGRAPHIC DATA FOR COMPOUND **4.22**

1. ORGANIC SYNTHESSES

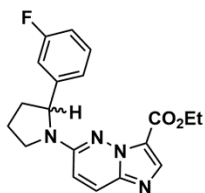
1.1 Material and Methods

General Procedures. All moisture sensitive reactions were carried out in oven-dried flasks under nitrogen atmosphere with dry solvents. Reagents and solvents were purchased at the highest commercial quality from Fisher, Sigma-Aldrich, Alfa-Aesar, Synthonix or Oakwood Products and were used without further purification unless specified otherwise. GNF-5837 ($\geq 98\%$) was purchased from EMD Millipore. 2-Fluoroethyl 4-methylbenzenesulfonate (**32**) was synthesized as previously described. Organic solutions were concentrated under reduced pressure on a Heidolph rotary evaporator. In general, reactions were magnetically stirred and monitored by TLC performed on pre-coated glass-backed TLC plates (Analtech, 250 microns) and chromatographic purification of products was accomplished using flash chromatography on Alfa-Aesar silica gel (230-450 mesh). TLC visualization was performed by fluorescence quenching, KMnO_4 or ninhydrin. ^1H NMR and ^{13}C NMR spectra were recorded on a Agilent/Varian DD2 MR two channel 400 MHz spectrometer, a Agilent/Varian VNMRS two-channel 500 MHz spectrometer or a Agilent/Varian Inova four-channel 500 MHz spectrometer in CDCl_3 or d_6 -DMSO and peak positions are given in parts per million using TMS as internal standard. Peaks are reported as: s = singlet, d = doublet, t = triplet, q = quartet, p = quintet, m = multiplet, b = broad; coupling constant(s) in Hz; integration. High Resolution Mass Spectra (HRMS) analysis was obtained from the Mass Spectrometry Facility of the Chemistry Department of the University of Alberta (Agilent Technologies 6220 oaTOF). Compounds tested in vitro were $>95\%$ pure (HPLC). Crystallographic analyses were performed by the X-Ray crystallography laboratory at the Chemistry Department of the University of Alberta.

1.2 Chemical Synthesis.



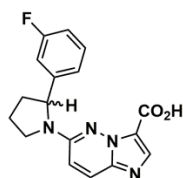
Scheme S4.1. Syntheses of amides 4.11-4.27. Reagents and conditions: (a) 2-(3-Fluorophenyl)pyrrolidine, KF, DMSO, 100°C, 22 h (77%). (b) ammonia solution (7.0 M in methanol) or methylamine solution (33 wt. % in absolute ethanol), rt, 15 h (96-100%). (c) EtOH, H₂O, KOH, rt, 3 h (72%). (d) amine, HATU, DIPEA, DMF, rt, 12-14 h (43-100%).



Ethyl 6-(2-(3-fluorophenyl)pyrrolidin-1-yl)imidazo[1,2-b]pyridazine-3-carboxylate (4.10). To a solution of ethyl 6-chloroimidazo[1,2-b]pyridazine-3-carboxylate (1.13 g, 5.0 mmol) in DMSO (6.0 mL) was added KF (872 mg, 15 mmol). This reaction mixture was heated at 100°C and 2-(3-fluorophenyl)pyrrolidine (991 mg, 6.0 mmol) was added. After stirring the reaction mixture at this temperature for 12 h, additional portions of 2-(3-fluorophenyl)pyrrolidine (165 mg, 1.0 mmol) and KF (58 mg, 1.0 mmol) were successively added. Third portions of 2-(3-fluorophenyl)pyrrolidine (165 mg, 1.0 mmol) and KF (58 mg, 1.0 mmol) were added 5 h after the second addition step and the reaction mixture was stirred at 100°C for an additional 5 h. The heterogeneous mixture was cooled at room temperature, poured into water and extracted with EtOAc. The combined organic layers were washed with brine, dried over Na₂SO₄ and concentrated in *vacuo*. The crude residue was purified by flash chromatography (gradient

1/19/80 Et₃N/hexane/EtOAc – 1/99; Et₃N /EtOAc) and afforded the title compound (1.37 g, 77%) as a pale yellow solid. *R_f* 0.15 (1:1:98 Et₃N/MeOH/ CH₂Cl₂).

¹H NMR (498 MHz, CDCl₃) δ 8.10 (s, 1H), 7.60 - 7.55 (m, *J* = 9.9 Hz, 1H), 7.29 - 7.22 (m, 1H), 7.01 (d, *J* = 7.5 Hz, 1H), 6.95 - 6.88 (m, 2H), 6.49 - 6.43 (m, *J* = 9.9 Hz, 1H), 5.01 - 4.94 (m, 1H), 4.38 (q, *J* = 7.1 Hz, 2H), 3.96 (s, 1H), 3.80 (s, 1H), 2.51 - 2.42 (m, 1H), 2.08 - 1.96 (m, 3H), 1.38 (t, *J* = 7.1 Hz, 3H); ¹³C NMR (125 MHz, CDCl₃) δ 163.11 (d, *J* = 247.0 Hz, 1C), 159.24, 152.87, 146.01 (d, *J* = 6.5 Hz, 1C), 139.35, 138.86, 130.37 (br d, *J* = 8.0 Hz, 1C), 125.75, 121.32 (d, *J* = 2.6 Hz, 1C), 119.54, 114.19 (br d, *J* = 21.2 Hz, 1C), 112.76 (br d, *J* = 22.2 Hz, 1C), 111.82, 61.91, 60.25, 48.58, 35.97, 22.84, 14.43; HRMS: Calcd *m/z* for C₁₉H₂₀FN₄O₂ [M+H]⁺ : 355.1565, Found: 355.1566.



6-(2-(3-Fluorophenyl)pyrrolidin-1-yl)imidazo[1,2-*b*]pyridazine-3-carboxylic acid (4.9). To a solution of ethyl 6-(2-(3-fluorophenyl)pyrrolidin-1-yl)imidazo[1,2-*b*]pyridazine-3-carboxylate (1.06 g, 3 mmol) in ethanol (20 mL) and water (1 mL) was added KOH (842 mg, 15 mmol). The reaction mixture was stirred at room temperature for 3 h and evaporated to dryness. The residue was diluted with water (10 mL) and the pH was adjusted to 5-6 using concentrated hydrochloric acid. The aqueous phase was extracted with CH₂Cl₂ (2 X 25 mL) and EtOAc (2 X 25 mL). The combined organic layers were washed with brine, dried over Na₂SO₄ and concentrated in *vacuo* to afford the title compound (701 mg, 72%) as a white yellow solid. *R_f* 0.10 (1:1:98 Et₃N/MeOH/ CH₂Cl₂).

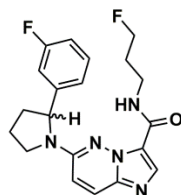
¹H NMR (498 MHz, DMSO-*d*₆) δ 7.98 (s, 1H), 7.86 (d, *J* = 9.9 Hz, 1H), 7.37 - 7.27 (m, 1H), 7.16 - 7.06 (m, 2H), 7.06 - 6.97 (m, 1H), 7.02 (br t, *J* = 8.4 Hz, 1H), 5.14 (dd, *J* = 2.8, 8.1 Hz, 1H), 3.93 - 3.85 (m, 1H), 3.63 (br d, *J* = 10.4 Hz, 1H), 2.47 - 2.35 (m, 1H), 2.03 - 1.93 (m, 2H), 1.93 - 1.83 (m, 1H); ¹³C NMR (125 MHz, DMSO-*d*₆) δ 162.75 (d, *J* = 243.6 Hz, 1C), 159.70, 152.73, 147.11 (d, *J* = 6.5 Hz, 1C), 138.98, 138.43, 130.89 (br d, *J* = 8.5 Hz, 1C), 126.50, 122.35 (br d, *J* = 2.1 Hz, 1C), 119.67, 114.15 (d, *J* = 20.9 Hz, 1C), 113.36 (br d, *J* = 21.9 Hz, 1C), 113.06, 61.46, 48.74, 35.63, 23.05; HRMS: Calcd *m/z* for C₁₇H₁₅FN₄NaO₂ [M+Na]⁺ : 349.1074, Found: 349.1071.

General procedure A: Coupling of carboxylic acid 4.10 with amines. DIPEA (44 μ L, 0.25 mmol, 2.5 equiv) was added to a solution of 6-(2-(3-fluorophenyl)pyrrolidin-1-yl)imidazo[1,2-*b*]pyridazine-3-carboxylic acid (33 mg, 0.10 mmol, 1 equiv) in DMF (1 mL). Solutions of HATU (38 mg, 0.10 mmol, 1 equiv) and the appropriate amine (0.12 mmol, 1.2 equiv; free amine or hydrochloric salt) in DMF (0.5 mL) were successively added dropwise. The reaction mixture was stirred at room temperature for 12 – 14 h. After completion, the reaction mixture was diluted with EtOAc (100 mL), washed with water (25 mL) and brine (25 mL). The organic phase was dried over Na_2SO_4 and concentrated in *vacuo*. The crude residue was purified by flash chromatography (gradient 1/99; MeOH/ CH_2Cl_2 – 3/97; MeOH/ CH_2Cl_2).



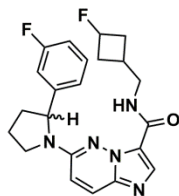
***N*-(2-Fluoroethyl)-6-(2-(3-fluorophenyl)pyrrolidin-1-yl)imidazo[1,2-*b*]pyridazine-3-carboxamide (4.13).** The general procedure A was used with 2-fluoroethylamine hydrochloride. The title compound was obtained as a pale yellow solid (37 mg, quantitative). R_f 0.27 (1:1:98 $\text{Et}_3\text{N}/\text{MeOH}/\text{CH}_2\text{Cl}_2$).

^1H NMR (498 MHz, CDCl_3) δ 8.91 (br s, 1H), 8.21 (br s, 1H), 7.72 (br d, $J = 9.8$ Hz, 1H), 7.35 - 7.29 (m, 1H), 7.01 (d, $J = 7.8$ Hz, 1H), 6.97 (dt, $J = 1.9, 8.4$ Hz, 1H), 6.92 (d, $J = 9.7$ Hz, 1H), 6.59 (br d, $J = 7.6$ Hz, 1H), 5.07 (br d, $J = 8.0$ Hz, 1H), 4.58 (td, $J = 4.1, 47.3$ Hz, 2H), 3.95 - 3.80 (m, 2H), 3.73 - 3.66 (m, 1H), 3.57 (br s, 1H), 2.57 - 2.47 (m, 1H), 2.17 - 2.01 (m, 3H); ^{13}C NMR (125 MHz, CDCl_3) δ 163.16 (d, $J = 247.2$ Hz, 1C), 159.38, 151.87, 145.27 (d, $J = 6.2$ Hz, 1C), 136.32 (br s, 1C), 135.42, 130.55 (d, $J = 8.3$ Hz, 1C), 126.96, 121.10, 121.02 (br d, $J = 2.8$ Hz, 1C), 114.41 (br d, $J = 21.2$ Hz, 1C), 112.49 (br d, $J = 21.9$ Hz, 1C), 110.70, 83.17 (d, $J = 166.2$ Hz, 1C), 62.02, 48.61, 39.14 (d, $J = 19.4$ Hz, 1C), 35.80, 22.84; HRMS: Calcd m/z for $\text{C}_{19}\text{H}_{19}\text{F}_2\text{N}_5\text{NaO}$ $[\text{M}+\text{Na}]^+$: 394.1450, Found: 394.1453.



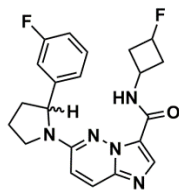
6-(2-(3-Fluorophenyl)pyrrolidin-1-yl)-N-(3-fluoropropyl)imidazo[1,2-*b*]pyridazine-3-carboxamide (4.14). The general procedure A was used with 2-fluoropropylamine hydrochloride. The title compound was obtained as a beige solid (36 mg, 92 %). R_f 0.27 (1:1:98 Et₃N/MeOH/ CH₂Cl₂).

¹H NMR (498 MHz, CDCl₃) δ 8.47 (br s, 1H), 8.17 (s, 1H), 7.72 (br d, J = 9.8 Hz, 1H), 7.33 (dt, J = 5.8, 7.9 Hz, 1H), 7.01 (d, J = 7.7 Hz, 1H), 6.96 (dt, J = 2.1, 8.4 Hz, 1H), 6.93 - 6.84 (m, 3H), 6.70 - 6.55 (m, 1H), 5.14 - 5.01 (m, 1H), 4.64 - 4.42 (m, 2H), 3.94 - 3.85 (m, 1H), 3.72 - 3.63 (m, 1H), 3.59 - 3.49 (m, 1H), 3.39 (br s, 1H), 2.57 - 2.48 (m, 1H), 2.16 - 2.08 (m, 2H), 2.07 - 2.01 (m, 1H), 2.01 - 1.81 (m, 2H); ¹³C NMR (125MHz, CDCl₃) δ = 163.17 (d, J = 247.2 Hz, 1C), 159.44, 151.90, 145.23 (d, J = 6.2 Hz, 1C), 137.10, 130.68 (br d, J = 8.0 Hz, 1C), 126.97, 122.43, 120.94, 120.92, 114.37 (d, J = 21.2 Hz, 1C), 112.30 (d, J = 22.2 Hz, 1C), 110.50, 81.97 (d, J = 164.4 Hz, 1C), 62.07, 48.69, 35.73, 35.28 (d, J = 5.2 Hz, 1C), 30.59 (d, J = 19.4 Hz, 1C), 22.91; HRMS: Calcd m/z for C₂₀H₂₁F₂N₅NaO [M+Na]⁺ : 408.1606, Found: 408.1608.



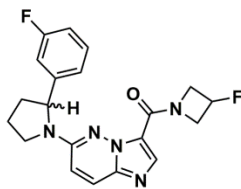
N-((3-Fluorocyclobutyl)methyl)-6-(2-(3-fluorophenyl)pyrrolidin-1-yl)imidazo[1,2-*b*]pyridazine-3-carboxamide (4.15). The general procedure A was used with (3-fluorocyclobutyl)methanamine hydrochloride. The title compound was obtained as a white solid (37 mg, 90 %). R_f 0.25 (1:1:98 Et₃N/MeOH/ CH₂Cl₂).

¹H NMR (498 MHz, CDCl₃) δ 8.47 (br s, 1H), 8.18 (s, 1H), 7.72 (br d, J = 9.7 Hz, 1H), 7.33 (dt, J = 5.9, 8.0 Hz, 1H), 7.06 - 6.96 (m, 2H), 6.90 (td, J = 1.9, 9.7 Hz, 1H), 6.60 (br d, J = 8.6 Hz, 1H), 5.25 - 5.08 (m, 1H), 5.05 (br d, J = 7.3 Hz, 1H), 3.92 - 3.82 (m, 1H), 3.73 - 3.61 (m, J = 8.1 Hz, 1H), 3.53 - 3.42 (m, 1H), 3.34 (br s, 1H), 2.44 - 2.44 (m, 1H), 2.59 - 2.42 (m, 2H), 2.41 - 2.28 (m, 2H), 2.20 - 2.20 (m, 1H), 2.28 - 2.04 (m, 4H); ¹³C NMR (125 MHz, CDCl₃) δ 163.19 (d, J = 247.5 Hz, 1C), 159.47, 152.00, 145.08 (d, J = 6.2 Hz, 1C), 137.78, 137.22, 130.65 (br d, J = 8.3 Hz, 1C), 127.02, 122.38, 120.92 (d, J = 2.6 Hz, 1C), 114.48 (br d, J = 21.2 Hz, 1C), 112.42 (d, J = 21.9 Hz, 1C), 110.53, 87.30 (br d, J = 206.5 Hz, 1C), 62.10, 48.62, 43.31, 35.79, 33.88 (d, J = 4.4 Hz, 1C), 33.71 (d, J = 4.6 Hz, 1C), 27.62 (br d, J = 11.9 Hz, 1C), 22.81; HRMS: Calcd m/z for C₂₂H₂₃F₂N₅NaO [M+Na]⁺ : 434.1763, Found: 434.1767.



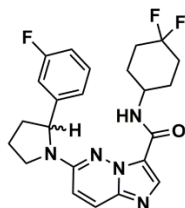
N-(3-Fluorocyclobutyl)-6-(2-(3-fluorophenyl)pyrrolidin-1-yl)imidazo[1,2-*b*]pyridazine-3-carboxamide (4.16). The general procedure A was used with 3-fluorocyclobutanamine hydrochloride (*cis-trans*). The title compound was obtained as a white solid (35 mg, 88 %). R_f 0.25 (1/1/98; Et₃N/MeOH/ CH₂Cl₂). The NMR characterization was achieved on the inseparable diastereoisomeric mixture. Whenever distinguishable, chemical shifts given are for one isomer with those of the second one listed in square brackets.

¹H NMR (498 MHz, CDCl₃) δ 8.77 (d, J = 34.6 Hz, 1H), 8.18 (s, 1H), 7.69 (br d, J = 9.9 Hz, 1H), 7.41 - 7.29 (m, 1H), 7.08 - 6.94 (m, 2H), 6.93 - 6.85 (m, 1H), 6.55 (br d, J = 8.6 Hz, 1H), 5.19 (d, J = 56.8 Hz, 0.5H), 5.09 (br t, J = 7.0 Hz, 1H), [4.86 (q, J = 6.6, 55.7 Hz, 0.5H)], 4.74 - 4.62 (m, 0.5H), [4.21 (br sxt, J = 7.8 Hz, 0.5H)], 3.95 - 3.84 (m, 1H), 3.76 - 3.65 (m, 1H), 3.01 - 2.90 (m, 1H), 2.76 - 2.60 (m, 1H), 2.59 - 2.50 (m, 1H), 2.42 - 1.94 (m, 5H); ¹³C NMR (125 MHz, CDCl₃) δ 163.19 (d, J = 247.8 Hz, 1C), 158.89, [158.57], 152.09, [152.06], 144.73, 137.84, 137.31, 130.81 (d, J = 8.3 Hz, 1C), [130.67 (br d, J = 8.0 Hz, 1C)], 127.03, [127.00], 122.31, [122.14], 121.23 (br d, J = 2.6 Hz, 1C), [121.10 (br d, J = 2.6 Hz, 1C)], 114.54 (br d, J = 21.2 Hz, 1C), 112.62 (d, J = 4.9 Hz, 1C), [112.47 (br d, J = 4.9 Hz, 1C)], 110.71, [110.62], 86.84 (br d, J = 200.3 Hz, 1C), [81.67 (br d, J = 210.6 Hz, 1C)], 61.84, 48.53, [48.46], 40.57 (d, J = 8.3 Hz, 1C), 39.97 (d, J = 20.1 Hz, 1C), [39.83 (d, J = 21.2 Hz, 1C)], 38.55 (d, J = 3.4 Hz, 1C), [38.37 (br d, J = 3.6 Hz, 1C)], 35.84, [35.80], [34.35 (br d, J = 23.0 Hz, 1C)], 22.74, [22.70]; HRMS: Calcd for C₂₁H₂₁F₂N₅NaO [M+Na]⁺ : 420.1606, Found: 420.1610.



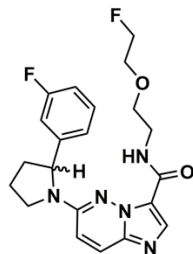
(3-Fluoroazetididin-1-yl)(6-(2-(3-fluorophenyl)pyrrolidin-1-yl)imidazo[1,2-*b*]pyridazin-3-yl)methanone (4.17). The general procedure A was used with 3-fluoroazetididine hydrochloride. The title compound was obtained as a white solid (36 mg, 95 %). R_f 0.27 (1:1:98 Et₃N/MeOH/ CH₂Cl₂).

^1H NMR (498 MHz, CDCl_3) δ 7.81 (s, 1H), 7.60 (d, $J = 9.9$ Hz, 1H), 7.27 (br s, 1H), 7.01 (br d, $J = 7.7$ Hz, 1H), 6.92 (br d, $J = 9.0$ Hz, 2H), 6.51 (br d, $J = 9.9$ Hz, 1H), 5.23 (br d, $J = 59.7$ Hz, 1H), 5.02 (d, $J = 7.0$ Hz, 1H), 4.50 - 4.17 (m, 4H), 4.00 - 3.89 (m, 1H), 3.78 - 3.69 (m, 1H), 2.53 - 2.38 (m, 1H), 2.11 - 1.94 (m, 3H); ^{13}C NMR (125 MHz, CDCl_3) δ 163.12 (d, $J = 247.0$ Hz, 1C), 161.37, 152.73, 138.07, 135.43, 130.44, 130.38, 125.96, 121.56, 121.22 (d, $J = 2.6$ Hz, 1C), 114.19 (d, $J = 21.2$ Hz, 1C), 112.68 (br d, $J = 22.2$ Hz, 1C), 111.30, 82.43 (br d, $J = 204.7$ Hz, 1C), 61.92, 48.71, 38.58, 36.43, 35.78, 22.84; HRMS: Calcd m/z for $\text{C}_{20}\text{H}_{20}\text{F}_2\text{N}_5\text{O}$ $[\text{M}+\text{H}]^+$: 384.1630, Found: 384.1632.



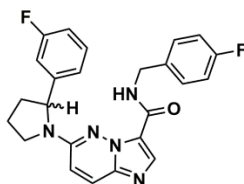
N-(4,4-Difluorocyclohexyl)-6-(2-(3-fluorophenyl)pyrrolidin-1-yl)imidazo[1,2-b]pyridazine-3-carboxamide (4.18). The general procedure A was used with 4,4-difluorocyclohexanamine hydrochloride. The title compound was obtained as a white solid (30 mg, 68 %). R_f 0.22 (1:1:98 $\text{Et}_3\text{N}/\text{MeOH}/\text{CH}_2\text{Cl}_2$).

^1H NMR (498 MHz, CDCl_3) δ 8.55 (br s, 1H), 8.19 (s, 1H), 7.70 (br d, $J = 9.9$ Hz, 1H), 7.34 (dt, $J = 5.9, 7.9$ Hz, 1H), 7.01 (d, $J = 7.7$ Hz, 1H), 6.97 (dt, $J = 2.0, 8.2$ Hz, 1H), 6.87 (br d, $J = 9.5$ Hz, 1H), 6.55 (br d, $J = 8.6$ Hz, 1H), 5.06 (br d, $J = 7.7$ Hz, 1H), 4.18 - 4.07 (m, 1H), 3.90 - 3.81 (m, 1H), 3.67 (dt, $J = 7.1, 9.6$ Hz, 1H), 2.52 (s, 1H), 2.23 - 1.81 (m, 9H), 1.68 - 1.51 (m, 2H), 1.45 - 1.29 (m, 1H); ^{13}C NMR (125 MHz, CDCl_3) δ 163.19 (d, $J = 247.5$ Hz, 1C), 158.69, 152.10, 144.69, 137.86, 137.28, 130.73 (br d, $J = 8.3$ Hz, 1C), 127.03, 122.34, 121.23 (d, $J = 2.8$ Hz, 1C), 114.49 (br d, $J = 21.2$ Hz, 1C), 112.53 (br d, $J = 22.2$ Hz, 1C), 110.63, 61.82, 48.51, 45.54, 38.59, 35.80, 32.43 (br t, $J = 24.8$ Hz, 1C), 32.36 (br t, $J = 24.6$ Hz, 1C), 28.92 (br dd, $J = 9.3, 30.7$ Hz, 1C), 22.69; HRMS: Calcd m/z for $\text{C}_{23}\text{H}_{25}\text{F}_3\text{N}_5\text{O}$ $[\text{M}+\text{H}]^+$: 444.2006, Found: 444.2009.



***N*-(2-(2-Fluoroethoxy)ethyl)-6-(2-(3-fluorophenyl)pyrrolidin-1-yl)imidazo[1,2-*b*]pyridazine-3-carboxamide (4.19)**. The general procedure A was used with 2-(2-fluoroethoxy)ethanamine hydrochloride. The title compound was obtained as a white solid (41 mg, 98 %). R_f 0.23 (1:1:98 Et₃N/MeOH/ CH₂Cl₂).

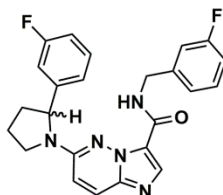
¹H NMR (498 MHz, CDCl₃) δ 8.88 (br s, 1H), 8.16 (s, 1H), 7.68 (br d, J = 9.9 Hz, 1H), 7.28 - 7.28 (m, 1H), 7.29 (dt, J = 5.9, 8.1 Hz, 1H), 7.03 (d, J = 7.7 Hz, 1H), 6.99 - 6.89 (m, 2H), 6.56 (br d, J = 8.4 Hz, 1H), 5.07 (br d, J = 7.3 Hz, 1H), 4.74 - 4.72 (m, 1H), 4.66 - 4.51 (m, 2H), 3.95 - 3.89 (m, 1H), 3.88 - 3.81 (m, 1H), 3.80 - 3.71 (m, 2H), 3.71 - 3.57 (m, 3H), 3.46 (br s, 1H), 2.56 - 2.45 (m, 1H), 2.15 - 1.96 (m, 3H); ¹³C NMR (125 MHz, CDCl₃) δ 163.12 (d, J = 247.0 Hz, 1C), 159.31, 151.78, 145.54 (d, J = 6.5 Hz, 1C), 137.74, 137.11, 130.48 (br d, J = 8.0 Hz, 1C), 126.81, 122.39, 121.09 (d, J = 3.1 Hz, 1C), 114.30 (br d, J = 21.2 Hz, 1C), 112.56 (br d, J = 22.2 Hz, 1C), 110.60, 82.89 (d, J = 169.8 Hz, 1C), 70.70, 70.26 (d, J = 19.6 Hz, 1C), 61.90, 48.62, 38.46, 35.71, 22.83; HRMS: Calcd m/z for C₂₁H₂₃F₂N₅NaO₂ [M+Na]⁺ : 438.1712, Found: 438.1714.



***N*-(4-Fluorobenzyl)-6-(2-(3-fluorophenyl)pyrrolidin-1-yl)imidazo[1,2-*b*]pyridazine-3-carboxamide (4.20)**. The general procedure A was used with (4-fluorophenyl)methanamine. The title compound was obtained as a white solid (41 mg, 95 %). R_f 0.20 (1:1:98 Et₃N/MeOH/ CH₂Cl₂).

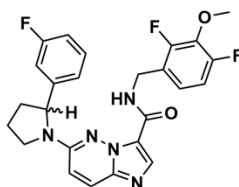
¹H NMR (400 MHz, CDCl₃) δ 8.74 (br s, 1H), 8.17 (s, 1H), 7.68 (br d, J = 9.8 Hz, 1H), 7.34 - 7.24 (m, 2H), 7.20 (dt, J = 5.9, 7.8 Hz, 1H), 7.06 - 6.97 (m, 2H), 6.87 (dd, J = 2.3, 8.4 Hz, 1H), 6.83 (d, J = 7.9 Hz, 1H), 6.73 (br d, J = 9.7 Hz, 1H), 6.55 (d, J = 8.5 Hz, 1H), 4.94 - 4.86 (m, 1H), 4.62 (dd, J = 6.2, 14.8 Hz, 1H), 4.33 (br dd, J = 5.9, 19.8 Hz, 1H), 3.58 (br s, 1H), 3.46 - 3.30 (m, 1H), 2.48 - 2.35 (m, 1H), 2.05 - 1.89 (m, 3H); ¹³C NMR (101 MHz, CDCl₃) δ 163.31 - 163.28 (m, 1C), 163.31 - 163.28 (m, 1C), 163.80 (d, J = 97.0 Hz, 1C), 161.35 (d, J = 95.0 Hz, 1C), 159.17, 151.78, 145.01 (d, J = 6.2 Hz, 1C), 137.22, 134.43 (d, J = 3.3 Hz, 1C), 130.55 (br d, J = 8.3 Hz, 1C), 129.31 (br d, J = 8.3 Hz, 1C), 126.97, 122.17, 120.78 (br d, J = 2.5 Hz, 1C), 115.37 (br d, J = 21.6 Hz, 1C), 114.36 (d, J = 21.1 Hz, 1C), 112.24 (br d, J = 22.0 Hz, 1C),

110.59, 61.96, 48.48, 42.21, 35.67, 22.67; HRMS: Calcd m/z for $C_{24}H_{21}F_2N_5NaO$ $[M+Na]^+$: 456.1606, Found: 456.1615.



***N*-(3-Fluorobenzyl)-6-(2-(3-fluorophenyl)pyrrolidin-1-yl)imidazo[1,2-*b*]pyridazine-3-carboxamide (4.21).** The general procedure A was used with (3-fluorophenyl)methanamine. The title compound was obtained as a white solid (41 mg, 95 %). R_f 0.20 (1:1:98 Et₃N/MeOH/CH₂Cl₂).

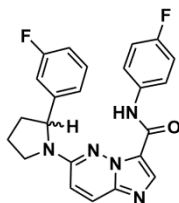
¹H NMR (498 MHz, CDCl₃) δ 8.77 (br s, 1H), 8.22 (s, 1H), 7.73 (br d, J = 9.7 Hz, 1H), 7.32 (dt, J = 6.1, 7.8 Hz, 1H), 7.22 (br q, J = 7.7 Hz, 1H), 7.12 (br d, J = 7.5 Hz, 1H), 7.03 (br d, J = 9.5 Hz, 1H), 6.99 (dt, J = 2.2, 8.4 Hz, 1H), 6.93 - 6.81 (m, 2H), 6.75 (br d, J = 9.5 Hz, 1H), 6.60 (br d, J = 6.6 Hz, 1H), 4.99 - 4.92 (m, 1H), 4.69 (dd, J = 6.2, 15.2 Hz, 1H), 4.42 (br s, 1H), 3.66 (br s, 1H), 3.54 - 3.40 (m, 1H), 2.45 (br qd, J = 8.5, 11.8 Hz, 1H), 2.02 (dt, J = 4.8, 7.9 Hz, 3H); ¹³C NMR (125 MHz, CDCl₃) δ 163.09 (br d, J = 247.2 Hz, 1C), 163.03 (d, J = 246.2 Hz, 1C), 159.26, 151.83, 145.02 (d, J = 6.2 Hz, 1C), 141.34 (d, J = 6.7 Hz, 1C), 137.82, 137.41, 130.57 (br d, J = 8.3 Hz, 1C), 130.13 (d, J = 8.3 Hz, 1C), 127.06, 122.18, 120.77, 114.30 (d, J = 21.2 Hz, 1C), 114.13 (br d, J = 20.9 Hz, 1C), 112.32, 112.14, 110.56, 62.04, 48.61, 42.36, 35.67, 22.75; HRMS: Calcd m/z for $C_{24}H_{22}F_2N_5O$ $[M+H]^+$: 434.1787, Found: 434.1794.



***N*-(2,4-Difluoro-3-methoxybenzyl)-6-(2-(3-fluorophenyl)pyrrolidin-1-yl)imidazo[1,2-*b*]pyridazine-3-carboxamide (4.22).** The general procedure A was used with (2,4-difluoro-3-methoxyphenyl)methanamine. The title compound was obtained as a white solid (22 mg, 46 %). R_f 0.20 (1:1:98 Et₃N/MeOH/CH₂Cl₂).

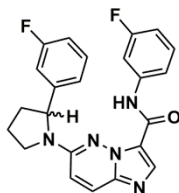
¹H NMR (498 MHz, CDCl₃) δ 8.85 (br s, 1H), 8.22 (s, 1H), 7.75 (br d, J = 9.6 Hz, 1H), 7.33 - 7.25 (m, 1H), 7.06 - 7.00 (m, 1H), 6.96 - 6.84 (m, 4H), 6.61 (br d, J = 9.2 Hz, 1H), 5.02 (dd, J = 1.2, 8.7

Hz, 1H), 4.69 - 4.62 (m, 1H), 4.54 - 4.43 (m, 1H), 4.06 - 4.03 (m, 3H), 3.84 - 3.76 (m, 1H), 3.64 - 3.56 (m, 1H), 2.56 - 2.47 (m, 1H), 2.13 - 2.02 (m, 3H); ^{13}C NMR (125 MHz, CDCl_3) δ = 163.17 (d, $J=247.4$ Hz, 1C), 159.37, 155.15 (br d, $J = 252.1$ Hz, 1C), 151.86, 148.25 (d, $J = 181.2$ Hz, 1C), 145.13, 145.08, 137.84, 137.51, 130.61 (br d, $J=8.2$ Hz, 1C), 127.15, 122.80 (d, $J = 10.1$ Hz, 1C), 122.20, 120.86 (br d, $J = 2.3$ Hz, 1C), 114.45 (d, $J = 21.1$ Hz, 1C), 112.30 (d, $J = 21.9$ Hz, 1C), 111.82 (br d, $J = 19.3$ Hz, 1C), 111.79 (br d, $J = 19.3$ Hz, 1C), 110.57, 62.10, 62.02 - 61.92 (m, 1C), 48.57, 36.60, 35.82, 22.84; HRMS: Calcd m/z for $\text{C}_{25}\text{H}_{23}\text{F}_3\text{N}_5\text{NaO}_2$ $[\text{M}+\text{Na}]^+$: 504.1618, Found: 504.1623.



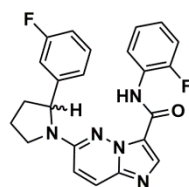
***N*-(4-Fluorophenyl)-6-(2-(3-fluorophenyl)pyrrolidin-1-yl)imidazo[1,2-*b*]pyridazine-3-carboxamide (4.23).** The general procedure A was used with 4-fluoroaniline. The title compound was obtained as a white solid (18 mg, 43 %). R_f 0.20 (1:1:98 $\text{Et}_3\text{N}/\text{MeOH}/\text{CH}_2\text{Cl}_2$).

^1H NMR (498 MHz, CDCl_3) δ 10.50 (br s, 1H), 8.31 (br s, 1H), 7.73 (d, $J = 9.9$ Hz, 1H), 7.49 (br s, 2H), 7.33 - 7.28 (m, 1H), 7.05 (t, $J = 8.7$ Hz, 2H), 7.02 - 6.96 (m, 2H), 6.92 (td, $J = 2.0, 9.5$ Hz, 1H), 6.58 (br d, $J = 8.1$ Hz, 1H), 5.12 (br d, $J = 8.1$ Hz, 1H), 4.02 - 3.96 (m, 1H), 3.83 - 3.76 (m, 1H), 2.62 - 2.53 (m, 1H), 2.25 - 2.10 (m, 3H); ^{13}C NMR (125 MHz, CDCl_3) δ 163.24 (d, $J = 247.8$ Hz, 1C), 159.37 (d, $J = 243.4$ Hz, 1C), 157.15, 152.12, 144.68, 130.70 (br d, $J = 8.3$ Hz, 1C), 127.17, 122.14, 122.10 (br s, 1C), 121.13, 121.11, 115.65 (br d, $J = 22.7$ Hz, 1C), 114.64 (d, $J=21.4$ Hz, 1C), 112.59 (d, $J = 22.2$ Hz, 1C), 110.91, 62.08, 48.66, 35.86, 22.79; HRMS: Calcd m/z for $\text{C}_{23}\text{H}_{20}\text{F}_2\text{N}_5\text{O}$ $[\text{M}+\text{H}]^+$: 420.1630, Found: 420.1635.



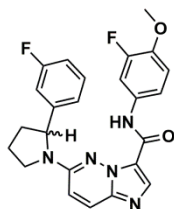
***N*-(3-Fluorophenyl)-6-(2-(3-fluorophenyl)pyrrolidin-1-yl)imidazo[1,2-*b*]pyridazine-3-carboxamide (4.24).** The general procedure A was used with 3-fluoroaniline. The title compound was obtained as a white solid (21 mg, 50 %). R_f 0.20 (1:1:98 $\text{Et}_3\text{N}/\text{MeOH}/\text{CH}_2\text{Cl}_2$).

^1H NMR (498 MHz, CDCl_3) δ 10.64 (br s, 1H), 8.29 (s, 1H), 7.69 (br d, $J = 9.7$ Hz, 1H), 7.57 (br d, $J = 6.8$ Hz, 1H), 7.33 (br dt, $J = 6.0, 7.9$ Hz, 1H), 7.26 (dt, $J = 6.6, 8.1$ Hz, 1H), 7.18 - 7.06 (m, 1H), 7.03 (d, $J = 7.9$ Hz, 1H), 7.01 - 6.99 (m, 1H), 6.99 (dt, $J = 2.0, 8.4$ Hz, 1H), 6.93 (br td, $J = 2.1, 9.6$ Hz, 1H), 6.81 (ddt, $J = 0.7, 2.6, 8.3$ Hz, 1H), 6.55 (br d, $J = 9.3$ Hz, 1H), 5.12 (br d, $J = 7.9$ Hz, 1H), 4.03 - 3.95 (m, 1H), 3.85 - 3.75 (m, 1H), 2.66 - 2.55 (m, 1H), 2.16 (br s, 3H); ^{13}C NMR (125 MHz, CDCl_3) δ 163.25 (d, $J = 247.8$ Hz, 1C), 163.00 (d, $J = 244.7$ Hz, 1C), 157.16, 152.14, 144.67 (br d, $J = 7.7$ Hz, 1C), 139.50 (br d, $J = 11.1$ Hz, 1C), 138.17, 130.76 (br d, $J = 8.3$ Hz, 1C), 130.01 (br d, $J = 9.3$ Hz, 1C), 127.10, 122.22, 121.15 (d, $J = 2.8$ Hz, 1C), 115.41, 114.69 (br d, $J = 21.2$ Hz, 1C), 112.60 (br d, $J = 22.2$ Hz, 1C), 111.13, 110.82 (br d, $J = 21.4$ Hz, 1C), 107.74 (br d, $J = 26.6$ Hz, 1C), 62.12, 48.66, 35.88, 22.75; HRMS: Calcd m/z for $\text{C}_{23}\text{H}_{20}\text{F}_2\text{N}_5\text{O}$ $[\text{M}+\text{H}]^+$: 420.1630, Found: 420.1638.



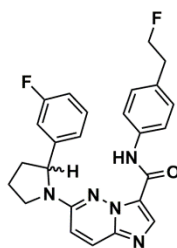
***N*-(2-Fluorophenyl)-6-(2-(3-fluorophenyl)pyrrolidin-1-yl)imidazo[1,2-*b*]pyridazine-3-carboxamide (4.25).** The general procedure A was used with 2-fluoroaniline. The title compound was obtained as a white solid (41 mg, quantitative). R_f 0.19 (1:1:98 $\text{Et}_3\text{N}/\text{MeOH}/\text{CH}_2\text{Cl}_2$).

^1H NMR (498 MHz, CDCl_3) δ 10.73 (br s, 1H), 8.58 (t, $J = 7.9$ Hz, 1H), 8.35 (s, 1H), 8.79 - 8.09 (m, 1H), 7.69 (d, $J = 9.9$ Hz, 1H), 7.31 - 7.25 (m, 1H), 7.24 - 7.19 (m, 1H), 7.19 - 7.09 (m, 3H), 7.04 - 6.99 (m, 1H), 6.96 (dt, $J = 2.3, 8.4$ Hz, 1H), 6.91 (td, $J = 1.8, 9.5$ Hz, 1H), 6.51 (d, $J = 9.9$ Hz, 1H), 5.07 (dd, $J = 1.7, 8.0$ Hz, 1H), 4.09 - 4.01 (m, 1H), 3.89 - 3.81 (m, 1H), 2.62 - 2.52 (m, 1H), 2.19 - 2.04 (m, 3H); ^{13}C NMR (125 MHz, CDCl_3) δ 163.22 (d, $J = 247.8$ Hz, 1C), 157.32, 152.31, 152.87 (d, $J = 242.8$ Hz, 1C), 145.19 (d, $J = 5.9$ Hz, 1C), 138.41, 138.19, 130.65 (br d, $J = 8.5$ Hz, 1C), 126.89, 126.66, 124.67 (d, $J = 3.1$ Hz, 1C), 124.24 (br d, $J = 8.0$ Hz, 1C), 122.88, 122.51, 121.08 (d, $J = 3.1$ Hz, 1C), 114.74 (d, $J = 19.1$ Hz, 1C), 114.55 (d, $J = 21.2$ Hz, 1C), 112.54 (br d, $J = 22.2$ Hz, 1C), 111.39, 62.30, 48.58 (d, $J = 9.8$ Hz, 1C), 36.04, 22.78; HRMS: Calcd m/z for $\text{C}_{23}\text{H}_{20}\text{F}_2\text{N}_5\text{O}$ $[\text{M}+\text{H}]^+$: 420.1630, Found: 420.1636.



***N*-(3-Fluoro-4-methoxyphenyl)-6-(2-(3-fluorophenyl)pyrrolidin-1-yl)imidazo[1,2-*b*]pyridazine-3-carboxamide (4.26).** The general procedure A was used with 3-fluoro-4-methoxyaniline. The title compound was obtained as a white solid (45 mg, quantitative). R_f 0.20 (1:1:98 Et₃N/MeOH/ CH₂Cl₂).

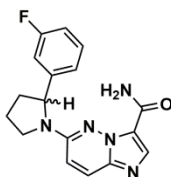
¹H NMR (498 MHz, CDCl₃) δ 10.45 (br s, 1H), 8.27 (s, 1H), 7.69 (br d, J = 9.9 Hz, 1H), 7.48 (br s, 1H), 7.31 (dt, J = 6.0, 7.9 Hz, 1H), 7.10 (br d, J = 4.4 Hz, 1H), 7.01 (td, J = 0.7, 7.7 Hz, 1H), 6.98 (dt, J = 2.6, 8.5 Hz, 2H), 6.95 - 6.84 (m, 2H), 6.55 (br d, J = 8.2 Hz, 1H), 5.11 (br d, J = 7.9 Hz, 1H), 3.97 (br s, 1H), 3.89 (s, 3H), 3.78 (br d, J = 19.4 Hz, 1H), 2.65 - 2.54 (m, 1H), 2.24 - 2.11 (m, 3H); ¹³C NMR (125 MHz, CDCl₃) δ 165.22, 163.23 (d, J = 247.8 Hz, 1C), 157.01, 152.08, 151.09, 149.10 - 149.10 (m, 1C), 150.10 (br d, J = 247.8 Hz, 1C), 144.47 (br d, J = 63.7 Hz, 1C), 131.41 (br d, J = 7.5 Hz, 1C), 131.37 - 131.29 (m, 1C), 131.37 - 131.29 (m, 1C), 130.73 (br d, J = 8.5 Hz, 1C), 127.04, 122.29, 121.13 (br d, J = 2.6 Hz, 1C), 114.64 (br d, J = 21.4 Hz, 1C), 113.73, 112.58 (br d, J = 21.9 Hz, 1C), 110.97, 62.09, 56.60, 48.64, 35.87, 22.77; HRMS: Calcd m/z for C₂₄H₂₂F₂N₅O₂ [M+H]⁺ : 450.1736, Found: 450.1746.



***N*-(4-(2-Fluoroethyl)phenyl)-6-(2-(3-fluorophenyl)pyrrolidin-1-yl)imidazo[1,2-*b*]pyridazine-3-carboxamide (4.27).** The general procedure A was used with 4-(2-fluoroethyl)aniline. The title compound was obtained as a white solid (28 mg, 62 %). R_f 0.22 (1:1:98 Et₃N/MeOH/ CH₂Cl₂).

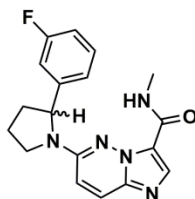
¹H NMR (498 MHz, CDCl₃) δ 10.54 (br s, 1H), 8.28 (s, 1H), 7.65 (d, J = 9.9 Hz, 1H), 7.57 - 7.42 (m, 2H), 7.33 - 7.28 (m, 1H), 7.22 (d, J = 8.2 Hz, 2H), 7.02 - 6.95 (m, 2H), 6.91 (td, J = 1.9, 9.6 Hz, 1H), 6.51 (br d, J = 9.2 Hz, 1H), 5.09 (br d, J = 8.1 Hz, 1H), 4.65 (td, J = 6.4, 47.1 Hz, 2H), 4.01 - 3.94 (m, 1H), 3.80 - 3.71 (m, 1H), 3.01 (td, J = 6.4, 23.4 Hz, 2H), 2.60 (s, 1H), 2.22 - 2.09 (m, 3H); ¹³C NMR (125 MHz, CDCl₃) δ 163.22 (d, J = 247.5 Hz, 1C), 157.08, 152.05, 144.85,

144.80, 137.89, 136.57, 133.03, 132.98, 130.67 (br d, $J = 8.3$ Hz, 1C), 129.54, 126.96, 121.15 (br d, $J = 2.6$ Hz, 1C), 120.53, 114.60 (br d, $J = 21.2$ Hz, 1C), 112.60 (br d, $J = 21.9$ Hz, 1C), 110.96, 84.10 (d, $J = 168.8$ Hz, 1C), 62.08, 48.63, 36.39 (d, $J = 20.4$ Hz, 1C), 35.87, 22.73; HRMS: Calcd m/z for $C_{25}H_{24}F_2N_5O$ $[M+H]^+$: 448.1943, Found: 448.1948.



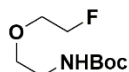
6-(2-(3-Fluorophenyl)pyrrolidin-1-yl)imidazo[1,2-*b*]pyridazine-3-carboxamide (4.11). Ethyl 6-(2-(3-fluorophenyl)pyrrolidin-1-yl)imidazo[1,2-*b*]pyridazine-3-carboxylate (89 mg, 0.25 mmol) was dissolved in an ammonia solution (7.0 M in methanol, 5 mL). The reaction mixture was stirred at room temperature for 15 h then concentrated and dried in *vacuo* to afford the title compound (78 mg, 96 %) as a white solid. R_f 0.10 (1:99 MeOH/ CH_2Cl_2).

1H NMR (498 MHz, $DMSO-d_6$) δ 8.04 - 7.87 (m, 2H), 7.87 - 7.72 (m, 1H), 7.71 - 7.58 (m, 1H), 7.39 - 7.29 (m, 1H), 7.14 - 6.96 (m, 3H), 6.84 (br s, 1H), 5.17 - 5.05 (m, 1H), 3.93 (br s, 1H), 3.61 (br d, $J = 9.6$ Hz, 1H), 2.47 - 2.40 (m, 1H), 2.04 - 1.90 (m, 2H), 1.81 (br s, 1H); ^{13}C NMR (126 MHz, $DMSO-d_6$) δ 162.41 (d, $J = 244.1$ Hz, 1C), 159.44, 151.75, 146.33 (d, $J = 6.4$ Hz, 1C), 137.43, 135.99, 130.64 (br d, $J = 8.2$ Hz, 1C), 126.65, 122.07, 121.58 (br d, $J = 2.1$ Hz, 1C), 113.74 (br d, $J = 20.9$ Hz, 1C), 112.18 (br d, $J = 21.4$ Hz, 1C), 111.84, 61.23, 48.28, 35.24, 22.50; HRMS: Calcd m/z for $C_{17}H_{16}FN_5O$ $[M+H]^+$: 326.1412, Found: 326.1418.



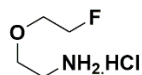
6-(2-(3-Fluorophenyl)pyrrolidin-1-yl)-*N*-methylimidazo[1,2-*b*]pyridazine-3-carboxamide (4.12). Ethyl 6-(2-(3-fluorophenyl)pyrrolidin-1-yl)imidazo[1,2-*b*]pyridazine-3-carboxylate (89 mg, 0.25 mmol) was dissolved in a methylamine solution (33 wt. % in absolute ethanol, 5 mL). The reaction mixture was stirred at room temperature for 15 h then concentrated and dried in *vacuo* to afford the title compound (85 mg, quantitative) as a tan solid. R_f 0.10 (1:99 MeOH/ CH_2Cl_2).

^1H NMR (498 MHz, DMSO- d_6) δ 8.18 - 7.98 (m, 1H), 7.95 (br d, J = 9.9 Hz, 1H), 7.87 (s, 1H), 7.37 (dt, J = 6.1, 8.0 Hz, 1H), 7.17 - 7.09 (m, 2H), 7.07 - 7.01 (m, 1H), 7.01 - 6.86 (m, 1H), 5.16 (dd, J = 2.7, 8.3 Hz, 1H), 4.00 - 3.93 (m, 1H), 3.68 - 3.60 (m, 1H), 2.82 - 2.61 (m, 3H), 2.47 - 2.39 (m, 1H), 2.06 - 1.94 (m, 2H), 1.89 - 1.79 (m, 1H); ^{13}C NMR (125 MHz, DMSO- d_6) δ 162.88 (br d, J = 243.9 Hz, 1C), 159.05, 152.10, 146.94 (br d, J = 6.2 Hz, 1C), 137.70, 135.99, 131.12 (d, J = 8.0 Hz, 1C), 127.17, 122.18, 121.86, 114.11 (br d, J = 20.6 Hz, 1C), 112.72 (br d, J = 20.1 Hz, 1C), 112.36, 61.68, 48.88, 35.66, 25.63, 23.09; HRMS: Calcd m/z for $\text{C}_{18}\text{H}_{18}\text{FN}_5\text{NaO}$ $[\text{M}+\text{Na}]^+$: 362.1388, Found: 362.1391.



tert-Butyl (2-(2-fluoroethoxy)ethyl)carbamate (4.29). To a solution of *N*-Boc-ethanolamine (0.75 g, 4.71 mmol, 1.03) and 2-fluoroethyl tosylate (1.00 g, 4.58 mmol) in DMF (10 mL) was added NaH (60% disp. in oil, 0.19 g, 4.75 mmol) in portions. After 12 hours, the reaction mixture was diluted with EtOAc and water was slowly added. The aqueous layer was extracted with EtOAc and the combined organic phases were washed with brine, dried over Na_2SO_4 , and concentrated in vacuo to yield a crude yellow oil. Purification by flash chromatography (gradient 9/1; hexane/EtOAc – 6/4; hexane/EtOAc) yielded 0.47 g of the title compound as clear oil (50%). R_f 0.27 (6:4 hexanes/EtOAc).

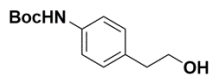
^1H NMR (498 MHz, CDCl_3) δ 4.94 (br s, 1H), 4.62 - 4.47 (m, 2H), 3.75 - 3.65 (m, 2H), 3.57 (t, J = 5.2 Hz, 2H), 3.33 (br q, J = 5.1 Hz, 2H), 1.44 (s, 9H); ^{13}C NMR (125 MHz, CDCl_3) δ 155.95, 82.95 (d, J = 169.0 Hz, 1C), 79.21, 70.43, 70.08 (d, J = 19.6 Hz, 1C), 28.38; HRMS: Calcd m/z for $\text{C}_9\text{H}_{18}\text{FNNaO}_3$ $[\text{M}+\text{Na}]^+$: 230.1163, Found: 230.1164.



2-(2-Fluoroethoxy)ethanamine hydrochloride (4.30). To a solution of *tert*-butyl (2-(2-fluoroethoxy)ethyl)carbamate (0.42 g, 2.03 mmol) in dichloromethane (2 mL) was added TFA (2 mL). After 1 hour, the reaction mixture was concentrated under reduced pressure to a crude brown oil. The crude product precipitated as the amine hydrochloride salt upon addition of a 1 M solution of HCl in diethyl ether (4 mL), filtered and obtained as a white powder (0.28 g, 98% yield).

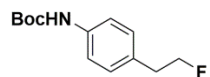
^1H NMR (498 MHz, CDCl_3) δ 8.40 - 8.13 (m, 3H), 4.72 - 4.56 (m, 2H), 3.87 (t, J = 4.8 Hz, 2H), 3.81 (td, J = 3.8, 30.0 Hz, 2H), 3.34 - 3.24 (m, 2H); ^{13}C NMR (125 MHz, CDCl_3) δ 83.14 (d, J =

168.0 Hz, 1C), 70.29 (d, $J = 19.4$ Hz, 1C), 66.77, 39.59; HRMS: Calcd m/z for $C_4H_{11}FNO$ $[M^*]^+$: 108.0819, Found: 108.0822.



tert-Butyl (4-(2-hydroxyethyl)phenyl)carbamate (4.32). To a solution of 2-(4-aminophenyl)ethanol (1.0 g, 7.3 mmol) in THF (20 mL) at 0°C was added Et_3N (1.01 mL, 7.3 mmol) followed by Boc_2O in 3 portions (1.59 g, 7.3 mmol). The reaction mixture was left to warm to room temperature and stirred overnight. The mixture was diluted with EtOAc and washed with water. The aqueous phase was further extracted with EtOAc and the combined organic phases were washed with brine, dried over Na_2SO_4 , filtered and concentrated in *vacuo*. The crude product was purified by flash chromatography (20% EtOAc/ CH_2Cl_2) to afford 1.47 g of the title compound as a white solid (85%). R_f 0.35 (1:4 EtOAc/ CH_2Cl_2).

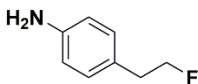
1H NMR (400 MHz, $CDCl_3$) δ 7.30 (d, $J = 8.4$ Hz, 2H), 7.15 (d, $J = 7.4$ Hz, 2H), 6.47 (br s, 1H), 3.82 (t, $J = 6.6$ Hz, 2H), 2.81 (t, $J = 6.6$ Hz, 2H), 1.51 (s, 9H), 1.49 (s, 1H); ^{13}C NMR (101 MHz, $CDCl_3$) δ 152.83, 136.78, 133.07, 129.50, 118.93, 80.47, 63.70, 38.49, 28.34; HRMS: Calcd m/z for $C_{13}H_{23}N_2O_3$ $[M+NH_4]^+$: 255.1703, Found: 255.1700.



tert-Butyl (4-(2-fluoroethyl)phenyl)carbamate (4.33). To a solution of *tert*-butyl (4-(2-hydroxyethyl)phenyl)carbamate (949 mg, 4 mmol) in CH_2Cl_2 (25 mL, plastic vessel) at -78°C under nitrogen was added DAST (1.06 mL, 8 mmol) dropwise. After 30 min, the reaction mixture was left to warm to 0°C and stirred at this temperature for 6 h. Unreacted DAST was carefully quenched by water under vigorous stirring followed by addition of saturated K_2CO_3 aqueous solution. The phases were separated and the aqueous layer extracted three times with CH_2Cl_2 . The combined organic layers were washed with brine, dried over Na_2SO_4 , filtered and concentrated in *vacuo*. The crude product was purified by flash chromatography (10% EtOAc/ CH_2Cl_2) to afford 824 mg of the title compound as a pale yellow crystalline solid (86%). R_f 0.90 (1:9 EtOAc/ CH_2Cl_2).

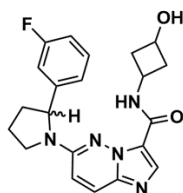
1H NMR (498 MHz, $CDCl_3$) δ 7.32 (br d, $J = 8.2$ Hz, 2H), 7.17 (d, $J = 7.9$ Hz, 2H), 6.46 (br s, 1H), 4.60 (td, $J = 6.6, 47.1$ Hz, 2H), 2.98 (td, $J = 6.6, 22.9$ Hz, 2H), 1.54 (s, 9H); ^{13}C NMR (125 MHz, $CDCl_3$) δ 152.77, 136.98, 131.67 (br d, $J = 6.7$ Hz, 1C), 129.48, 129.35, 118.79, 84.15 (br

d, $J = 169.0$ Hz, 1C), 80.49, 38.54, 36.25 (br d, $J = 20.4$ Hz, 1C), 28.35; HRMS: Calcd m/z for $C_{13}H_{18}FNNa_2O_2$ $[M+Na]^+$: 262.1214, Found: 262.1213.



4-(2-Fluoroethyl)aniline (4.34). To an ice cold solution of *tert*-Butyl (4-(2-fluoroethyl)phenyl)carbamate (600 mg, 2.5 mmol) in CH_2Cl_2 (10 mL) was added TFA (1.15 mL, 15 mmol). The reaction mixture was left to warm to room temperature and stirred for 5 h. The volatiles were removed in *vacuo* and the residue was dissolved in EtOAc and washed with aqueous saturated $NaHCO_3$. The organic layer was washed with brine, dried over Na_2SO_4 , filtered and concentrated under reduced pressure. The crude product was purified by flash chromatography (30% EtOAc/hexanes) to afford 325 mg of the title compound as a pale yellow oil (93%). R_f 0.31 (3:7 EtOAc/hexanes).

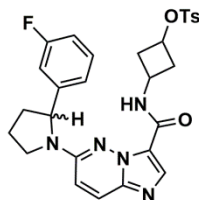
1H NMR (400 MHz, $CDCl_3$) δ 7.05 - 7.00 (m, 2H), 6.67 - 6.63 (m, 2H), 4.57 (td, $J = 6.8, 47.2$ Hz, 2H), 3.75 - 3.28 (m, 2H), 2.91 (td, $J = 6.8, 22.2$ Hz, 2H); ^{13}C NMR (101 MHz, $CDCl_3$) δ 145.03, 129.80, 126.80 (d, $J = 7.3$ Hz, 1C), 115.30, 84.50 (br d, $J = 169.0$ Hz, 1C), 36.08 (d, $J = 20.1$ Hz, 1C); HRMS: Calcd m/z for $C_8H_{11}FN$ $[M+H]^+$: 140.0870, Found: 140.0871.



6-(2-(3-Fluorophenyl)pyrrolidin-1-yl)-*N*-(3-hydroxycyclobutyl)imidazo[1,2-*b*]pyridazine-3-carboxamide (4.35). To a solution of 6-(2-(3-fluorophenyl)pyrrolidin-1-yl)imidazo[1,2-*b*]pyridazine-3-carboxylic acid (90 mg, 0.28 mmol) in DMF (4 mL) was added DIPEA (0.12 mL, 0.7 mmol) and HATU (107 mg, 0.28 mmol). The reaction mixture was stirred at room temperature for 5 min and 3-aminocyclobutanol hydrochloride (42 mg, 0.34 mmol) was added in one portion. The reaction mixture was stirred overnight and then diluted with EtOAc and poured into water. The aqueous phase was extracted three times with EtOAc and the combined organic phases were washed with brine, dried over Na_2SO_4 , filtered and concentrated under reduced pressure. The crude product was purified by flash chromatography (5% MeOH/ CH_2Cl_2) to afford 110 mg of the title compound as a beige solid (99%). R_f 0.15 (5:95 MeOH/ CH_2Cl_2). The NMR characterization was achieved on the inseparable diastereoisomeric mixture. Whenever

distinguishable, chemical shifts given are for one isomer with those of the second one listed in square brackets.

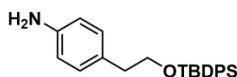
^1H NMR (500 MHz, CDCl_3) δ 8.84 (br s, 1H), 8.22 (d, $J = 3.7$ Hz, 1H), 7.74 (br d, $J = 9.9$ Hz, 1H), 7.39 - 7.32 (m, 1H), 7.09 - 6.97 (m, 2H), 6.97 - 6.91 (m, 1H), 6.63 - 6.49 (m, 1H), 5.10 (br d, $J = 7.3$ Hz, 1H), 4.71 - 4.52 (m, 1H), 4.21 - 4.12 (m, 1H), 3.98 - 3.90 (m, 1H), 3.79 - 3.72 (m, 1H), 3.20 (dq, $J = 4.2, 7.5$ Hz, 1H), [2.97 - 2.91 (m, 1H)], 2.61 - 2.53 (m, 1H), 2.52 - 2.42 (m, 1H), 2.42 - 2.28 (m, 1H), 2.28 - 2.04 (m, 3H), 2.00 - 1.91 (m, 1H), 1.85 (br d, $J = 9.2$ Hz, 1H); ^{13}C NMR (126 MHz, CDCl_3) δ 163.24 (br d, $J = 247.5$ Hz, 1C), [163.21 (br d, $J = 247.5$ Hz, 1C)], 158.93, [158.70], 152.14, [152.07], 144.84, 137.79, 137.20 (br d, $J = 7.3$ Hz, 1C), 130.76 (d, $J = 8.5$ Hz, 1C), [130.71 (d, $J = 8.5$ Hz, 1C)], 127.05, [127.01], 122.47 (br s, 1C), [122.36 (br s, 1C)], 121.21 (d, $J = 2.8$ Hz, 1C), [121.14 (d, $J = 2.8$ Hz, 1C)], 114.57 (br d, $J = 21.3$ Hz, 1C), [114.59 (br dd, $J = 3.4, 21.2$ Hz, 1C)], 112.63 (br d, $J = 22.3$ Hz, 1C), [112.65 (br d, $J = 21.8$ Hz, 1C)], 110.69, [110.65], 65.28, 61.92, [61.42], 55.75, 48.59, [48.47], 41.78, [41.63], 40.50, [40.38], 35.88, [35.75], 22.77, [22.76]; HRMS: Calcd m/z for $\text{C}_{21}\text{H}_{22}\text{FN}_5\text{NaO}_2$ $[\text{M}+\text{Na}]^+$: 418.1650, Found: 418.1650.



3-(6-(2-(3-Fluorophenyl)pyrrolidin-1-yl)imidazo[1,2-b]pyridazine-3-

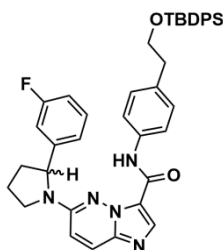
carboxamido)cyclobutyl 4-methylbenzenesulfonate (4.36). To an ice cold solution of 6-(2-(3-Fluorophenyl)pyrrolidin-1-yl)-*N*-(3-hydroxycyclobutyl)imidazo[1,2-b]pyridazine-3-carboxamide (156 mg, 0.40 mmol) in CH_2Cl_2 (15 mL) was successively added Et_3N (84 μL , 0.60 mmol) and 4-toluenesulfonyl chloride (81 mg, 0.42 mmol). The reaction was left to warm to room temperature and allowed to stir for 2 days. The reaction mixture was then diluted with CH_2Cl_2 and poured into water. The layers were separated and the aqueous phase was extracted three times with CH_2Cl_2 . The combined organic extracts were washed with brine, dried over Na_2SO_4 , filtered and concentrated under reduced pressure. The crude product was purified by flash chromatography (5% $\text{MeOH}/\text{CH}_2\text{Cl}_2$) to afford 149 mg of the title compound as a tan solid (70 %). R_f 0.46 (5:95 $\text{MeOH}/\text{CH}_2\text{Cl}_2$). The NMR characterization was achieved on the inseparable diastereoisomeric mixture. Whenever distinguishable, chemical shifts given are for one isomer with those of the second one listed in square brackets.

^1H NMR (498 MHz, CDCl_3) δ 8.76 (br s, 1H), 8.14 (br s, 1H), 7.81 - 7.74 (m, 2H), 7.70 - 7.64 (m, 1H), 7.39 - 7.29 (m, 3H), 7.07 - 7.00 (m, 1H), 6.99 - 6.94 (m, 1H), 6.90 - 6.84 (m, 1H), 6.54 (br s, 1H), 5.09 - 5.04 (m, 1H), 4.56 - 4.49 (m, 1H), 4.23 - 4.15 (m, 1H), 3.87 (br d, $J = 8.6$ Hz, 1H), 3.73 - 3.64 (m, 1H), [3.39 - 3.24 (m, 1H)], 2.87 - 2.79 (m, 1H), 2.74 (br s, 1H), [2.62 - 2.50 (m, 2H)], 2.44 (d, $J = 4.7$ Hz, 3H), 2.39 - 2.07 (m, 5H); ^{13}C NMR (126 MHz, CDCl_3) δ 163.20 (br d, $J = 247.5$ Hz, 1C), [163.23 (br d, $J = 247.5$ Hz, 1C), 144.78 (br d, $J = 6.0$ Hz, 1C), 144.66 (br d, $J = 6.0$ Hz, 1C), 131.01 (d, $J = 8.0$ Hz, 1C), 130.76 (d, $J = 8.0$ Hz, 1C), 129.98, 129.93, 127.92, 127.77, 121.27 (br d, $J = 2.5$ Hz, 1C), 121.11 (d, $J = 2.5$ Hz, 1C), 114.64 (br d, $J = 21.3$ Hz, 1C), 114.60 (br d, $J = 21.1$ Hz, 1C), 112.57 (br d, $J = 22.1$ Hz, 1C), 112.51 (br d, $J = 22.1$ Hz, 1C), 37.75, 35.89, 22.77, 21.69; HRMS: Calcd m/z for $\text{C}_{28}\text{H}_{29}\text{FN}_5\text{O}_4\text{S}$ $[\text{M}+\text{H}]^+$: 550.1919, Found: 550.1926.



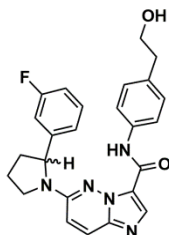
4-(2-((*tert*-butyldiphenylsilyl)oxy)ethyl)aniline (4.38). A solution of TBDPSCI (1.32 g, 4.8 mmol) in DMF (5 mL) was added to a mixture of 2-(4-aminophenyl)ethanol (660 mg, 4.8 mmol) and imidazole (654 mg, 9.6 mmol) in DMF (20 mL) at room temperature. The reaction mixture was stirred overnight and water was added. The mixture was extracted with EtOAc and the combined organic phases were washed with brine, dried over Na_2SO_4 , filtered and concentrated under reduced pressure. The crude product was purified by flash chromatography (30% EtOAc/hexane) to afford 1.44 g of the title compound as a yellow oil (80 %). R_f 0.48 (30% EtOAc/hexane).

^1H NMR (498 MHz, CDCl_3) δ = 7.68 (d, $J = 7.0$ Hz, 4H), 7.49 - 7.38 (m, 6H), 6.99 (d, $J = 8.3$ Hz, 2H), 6.64 (d, $J = 7.8$ Hz, 2H), 3.85 (t, $J = 7.1$ Hz, 2H), 3.57 (br s, 2H), 2.82 (t, $J = 7.1$ Hz, 2H), 1.10 (s, 9H); ^{13}C NMR (125 MHz, CDCl_3) δ = 144.56, 135.64, 134.00, 130.03, 129.54, 129.09, 127.62, 115.13, 65.62, 38.52, 26.92, 19.22; HRMS: Calcd m/z for $\text{C}_{24}\text{H}_{30}\text{NOSi}$ $[\text{M}+\text{H}]^+$: 376.2091, Found: 376.2091.



***N*-(4-(2-((*tert*-butyldiphenylsilyl)oxy)ethyl)phenyl)-6-(2-(3-fluorophenyl)pyrrolidin-1-yl)imidazo[1,2-*b*]pyridazine-3-carboxamide (4.39).** To a solution of 6-(2-(3-fluorophenyl)pyrrolidin-1-yl)imidazo[1,2-*b*]pyridazine-3-carboxylic acid (**38**) (90 mg, 0.28 mmol) in DMF (3 mL) was added DIPEA (0.12 mL, 0.7 mmol) and HATU (107 mg, 0.28 mmol). The reaction mixture was stirred at room temperature for 5 min and a solution of **38** (128 mg, 0.34 mmol) in DMF (1 mL) was added in one portion. The reaction mixture was stirred overnight and then diluted with EtOAc and poured into water. The aqueous phase was extracted three times with EtOAc and the combined organic phases were washed with brine, dried over Na₂SO₄, filtered and concentrated under reduced pressure. The crude product was purified by flash chromatography (1% MeOH/CH₂Cl₂) to afford 191 mg of the title compound as a beige solid (99%). *R*_f 0.24 (1:99 MeOH/CH₂Cl₂).

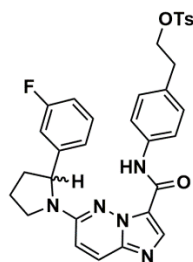
¹H NMR (498 MHz, CDCl₃) δ = 10.64 - 10.46 (m, 1H), 8.31 (s, 1H), 7.71 (br d, *J* = 10.0 Hz, 1H), 7.66 - 7.57 (m, 4H), 7.25 - 7.23 (m, 1H), 7.53 - 7.13 (m, 11H), 7.04 - 6.87 (m, 3H), 6.60 - 6.49 (m, 1H), 5.11 (br d, *J* = 7.6 Hz, 1H), 4.00 (br t, *J* = 7.0 Hz, 1H), 3.90 - 3.76 (m, 3H), 2.87 (t, *J* = 6.8 Hz, 2H), 2.63 - 2.51 (m, 1H), 2.25 - 2.05 (m, 3H), 1.07 (s, 9H); ¹³C NMR (125 MHz, CDCl₃) δ = 163.24 (d, *J* = 247.5 Hz, 1C), 157.06, 152.10, 144.84 (br s, 1C), 144.80 (br s, 1C), 136.09, 135.58, 135.51, 135.18, 133.81, 130.73, 129.80, 129.57, 127.63, 127.09, 122.62, 121.16, 120.29, 114.62 (br d, *J* = 21.2 Hz, 1C), 112.60 (br d, *J* = 22.2 Hz, 1C), 110.90, 65.17, 62.05, 48.65, 38.78, 35.88, 26.87, 22.75, 19.20; HRMS: Calcd *m/z* for C₄₁H₄₂FN₅NaO₂Si [M+Na]⁺ : 706.2984, Found: 706.2999.



6-(2-(3-fluorophenyl)pyrrolidin-1-yl)-*N*-(4-(2-hydroxyethyl)phenyl)imidazo[1,2-*b*]pyridazine-3-carboxamide (4.40). To a solution of *N*-(4-(2-((*tert*-butyldiphenylsilyl)oxy)ethyl)phenyl)-6-(2-(3-fluorophenyl)pyrrolidin-1-yl)imidazo[1,2-*b*]pyridazine-3-carboxamide (180 mg, 0.26 mmol) in THF (8 mL) was added TBAF (1.0 M in THF, 0.39 mL, 0.39 mmol) and the reaction mixture was stirred at room temperature for 2 h then diluted with water and extracted with EtOAc. The combined organic phases were washed with brine, dried over Na₂SO₄, filtered and concentrated under reduced pressure. The crude product was purified

by flash chromatography (10% MeOH/CH₂Cl₂) to afford 103 mg of the title compound as a beige solid (89%). *R_f* 0.42 (10:90 MeOH/CH₂Cl₂).

¹H NMR (498 MHz, CDCl₃) δ = 10.56 (br s, 1H), 8.28 (s, 1H), 7.68 (br d, *J* = 9.7 Hz, 1H), 7.57 - 7.39 (m, 2H), 7.32 (dt, *J* = 6.0, 7.8 Hz, 1H), 7.21 (d, *J* = 8.4 Hz, 2H), 7.03 (d, *J* = 7.7 Hz, 1H), 6.99 (dt, *J* = 2.2, 8.4 Hz, 1H), 6.96 - 6.91 (m, 1H), 6.54 (br d, *J* = 9.4 Hz, 1H), 5.11 (br d, *J* = 7.8 Hz, 1H), 4.05 - 3.95 (m, 1H), 3.89 (t, *J* = 6.5 Hz, 2H), 3.84 - 3.75 (m, 1H), 2.87 (t, *J* = 6.5 Hz, 2H), 2.65 - 2.52 (m, 1H), 2.27 - 2.07 (m, 3H), 1.98 - 1.73 (m, 1H); ¹³C NMR (125 MHz, CDCl₃) δ = 163.25 (d, *J* = 247.5 Hz, 1C), 157.09, 152.10, 144.79, 137.97, 136.31, 134.55, 130.70 (d, *J* = 8.0 Hz, 1C), 129.59, 127.01, 122.49, 121.16, 121.14, 120.53, 114.63 (d, *J* = 20.6 Hz, 1C), 112.65 (br d, *J* = 21.9 Hz, 1C), 110.96, 63.62, 62.11, 48.66, 38.72, 35.90, 22.76; HRMS: Calcd *m/z* for C₂₅H₂₅FN₅O₂ [M+H]⁺ : 446.1987, Found: 446.1994.



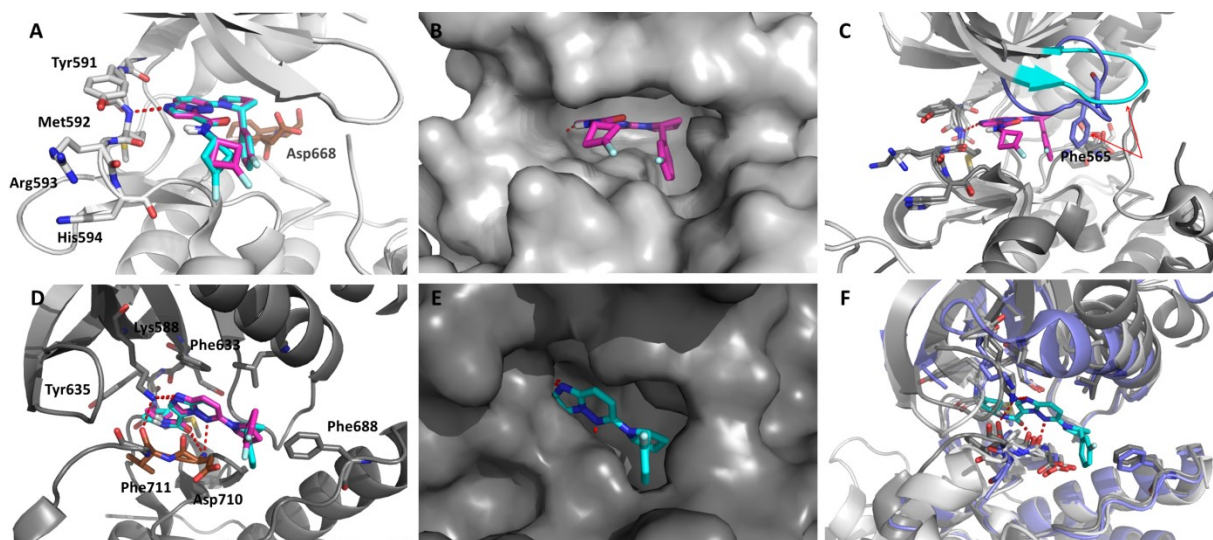
4-(6-(2-(3-fluorophenyl)pyrrolidin-1-yl)imidazo[1,2-*b*]pyridazine-3-carboxamido)phenethyl 4-methylbenzenesulfonate (4.41). To an ice cold solution of 6-(2-(3-fluorophenyl)pyrrolidin-1-yl)-N-(4-(2-hydroxyethyl)phenyl)imidazo[1,2-*b*]pyridazine-3-carboxamide (100 mg, 0.22 mmol) in CH₂Cl₂ (5 mL) was successively added Et₃N (46 μL, 0.33 mmol) and 4-toluenesulfonyl chloride (50 mg, 0.26 mmol). The reaction was left to warm at room temperature and allowed to stir for 4 days. The reaction mixture was then diluted with CH₂Cl₂ and poured into water. The layers were separated and the aqueous phase was extracted three times with CH₂Cl₂. The combined organic extracts were washed with brine, dried over Na₂SO₄, filtered and concentrated under reduced pressure. The crude product was purified by flash chromatography (5% MeOH/CH₂Cl₂) to afford 84 mg of the title compound as a tan solid (64 %). *R_f* 0.52 (10:90 MeOH/CH₂Cl₂).

¹H NMR (498 MHz, CDCl₃) δ = 10.59 (br s, 1H), 8.32 (s, 1H), 7.77 - 7.70 (m, 3H), 7.53 - 7.41 (m, 2H), 7.36 - 7.29 (m, 3H), 7.13 (d, *J* = 8.3 Hz, 2H), 7.05 - 6.96 (m, 2H), 6.95 - 6.90 (m, 1H), 6.61 - 6.54 (m, 1H), 5.16 - 5.09 (m, 1H), 4.23 (t, *J* = 7.0 Hz, 2H), 4.06 - 3.99 (m, 1H), 3.87 - 3.79 (m, 1H), 2.97 (t, *J* = 6.9 Hz, 2H), 2.63 - 2.53 (m, 1H), 2.45 (s, 3H), 2.25 - 2.13 (m, 3H); ¹³C NMR (125 MHz, CDCl₃) δ = 163.23 (d, *J* = 247.8 Hz, 1C), 157.11, 156.02, 152.14, 144.78, 136.81,

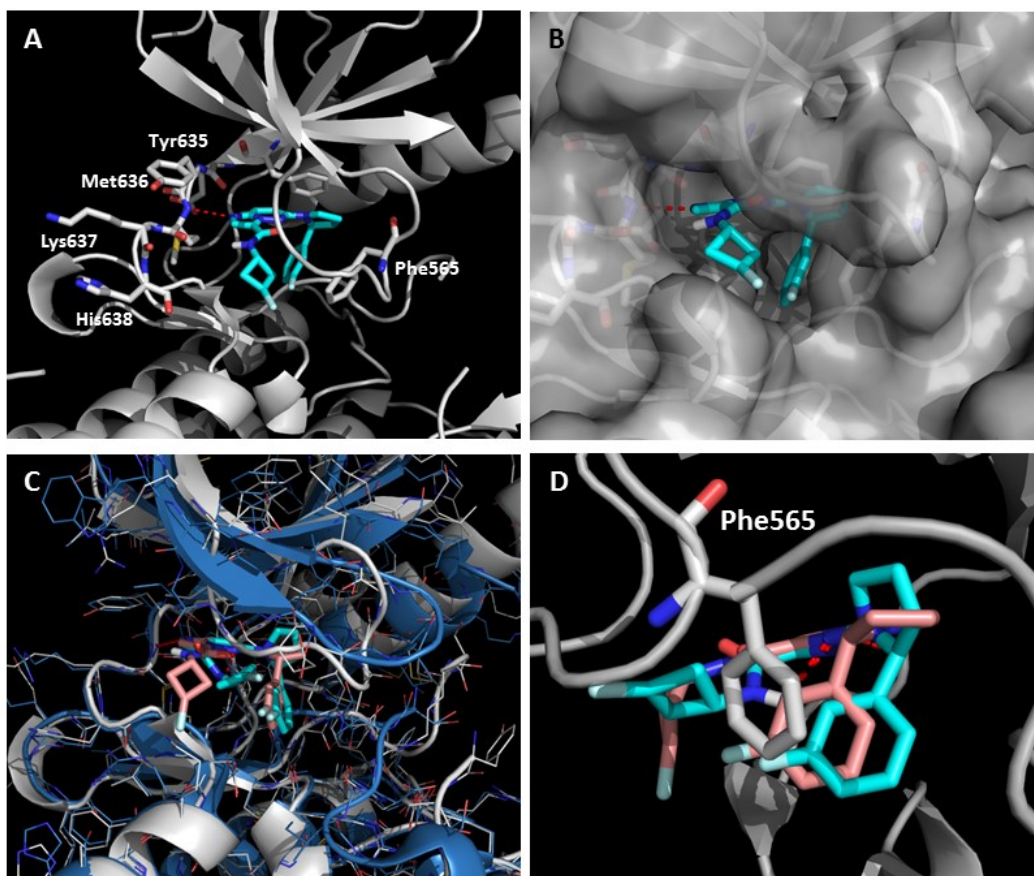
132.91, 132.09, 130.73 (br d, $J = 8.3$ Hz, 1C), 129.83, 129.52, 127.82, 127.14, 122.48, 121.16 (br d, $J = 2.8$ Hz, 1C), 120.57 (br s, 1C), 120.54, 114.64 (br d, $J = 20.9$ Hz, 1C), 112.60 (d, $J = 22.2$ Hz, 1C), 110.98, 70.64, 62.11, 48.69, 35.89, 34.84, 22.78, 21.64; HRMS: Calcd m/z for $C_{32}H_{30}FN_5NaO_4S [M+Na]^+$: 622.1895, Found: 622.1903.

2. DOCKING STUDIES

Molecular docking simulations of compounds **4.9-4.27** were performed using the X-ray co-crystal structure of TrkA complex (PDB 4PMT), TrkA complex (PDB 4PMM), TrkB-cpd5n complex (PDB 4AT3), TrkB-EX429 complex (PDB 4AT4) and TrkC-GNF-5837 (PDB 3V5Q) using FITTED 3.5 program (FORECASTER platform).⁵⁷⁻⁵⁹ Docking structures and figures were prepared using PyMOL.



Figures S4.1. Comparison of the predicted binding poses for (*R*)-**4.16** bound to TrkA/B/C in DFG-in (A-C) and DFG-out (D-F) conformations. (A) Docking of (*R*)-**4.16** (*trans*-substituted cyclobutyl: cyan; *cis*-substituted cyclobutyl: purple) to the ATP binding site of TrkA (PDB 4PMT). The DFG motif highlighted in brown. (B) Surface model of *cis*-(*R*)-**4.16** docked to TrkA (*trans*-(*R*)-**4.16** omitted for simplicity). (C) Superposition of TrkB (dark gray, DFG-in, PDB 4AT3) and the docking of *trans*-(*R*)-**4.16** with TrkA. The TrkA (cyan) and TrkB (blue) glycine-rich loops are highlighted. (D) Docking of *cis*-(*R*)-**4.16** (purple) and *trans*-(*R*)-**4.16** (cyan) to the ATP binding site of TrkB (PDB 4AT4). (E) Surface model of *trans*-(*R*)-**4.16** docked to TrkB (*cis*-(*R*)-**4.16** omitted for simplicity). (C) Superposition of TrkA (pale gray, PDB 4PMM), TrkB (blue, PDB 4AT4) and TrkC (blue, PDB 3V5Q) and the docking of *trans*-(*R*)-**4.16** with TrkB.



Figures S4.2. (A) Docking of *trans*-(S)-4.16 to the ATP binding site of TrkB (PDB 4AT3). (B) Surface model of *trans*-(S)-4.16 docked to TrkB. (C) Superposition of TrkA (blue, PDB 4PMT) and TrkB (pale gray, PDB 4AT3) and the docking of *trans*-(S)-4.16 (cyan) and *trans*-(R)-4.16 (light pink) to TrkB. (D) The key Pi-interaction between the 3-fluorophenyl moiety positioned in the ribose binding pocket and the Phe565 from the glycine-rich loop is conserved due to the rotation of the C₆ – N-pyrrolidine bond and concomitant rearrangement of the pyrrolidine ring.

3. RADIOCHEMISTRY

Radiochemistry. The manual radiosyntheses of [^{18}F]-(\pm)-**IPMICF6** ([^{18}F]**4.16**) and [^{18}F]-(\pm)-**IPMICF10** ([^{18}F]**4.27**) were performed and optimized in the radiochemistry laboratory of the Edmonton PET Center Site (ACSI 19/9 MeV cyclotron). For in vitro autoradiography experiments, the radiotracers [^{18}F]-(\pm)-**IPMICF6** and [^{18}F]-(\pm)-**IPMICF10** were produced at the cyclotron laboratory (IBA Cyclon 18/9 MeV cyclotron) of the McConnell Brain Imaging Center Site (Montreal Neurological Institute, McGill University) using radiosynthesis module Scintomics GRP (Germany). No-carrier-added (n.c.a) aqueous [^{18}F]Fluoride was produced by a $^{18}\text{O}(\text{p},\text{n})^{18}\text{F}$ nuclear reaction on an enriched [^{18}O]water target.

3.1 Edmonton PET Center Site.

HPLC Methods. Semi preparative, radio-preparative high performance liquid chromatography (HPLC) purifications and quality control analyses were performed using a Phenomenex LUNA® C18 column (100 Å, 250 × 10 mm, 10 μm) using a Gilson 322 Pump module fitted with a 171 Diode Array and a radio detector. Method A: elution at 3.0 ml min⁻¹ with a mixture of H₂O (A) and MeCN (B) isocratic at 40% A and 60% B ($t_{r[\text{18F}]\text{-}(\pm)\text{-IPMICF6(16)}} = 10.81$ min). Method B: elution at 3.0 ml min⁻¹ with a mixture of H₂O (A) and MeCN (B) isocratic at 43% A and 57% B ($t_{r[\text{18F}]\text{-}(\pm)\text{-IPMICF6(16)}} = 12.40$ min). Method C: elution at 3.0 ml min⁻¹ with a mixture of H₂O (A) and MeCN (B) isocratic at 32% A and 68% B ($t_{r[\text{18F}]\text{-}(\pm)\text{-IPMICF10(27)}} = 13.20$ min).

*Radiosynthesis of [^{18}F]-(\pm)-**IPMICF6**.* No-carrier-added (n.c.a) aqueous [^{18}F]fluoride was passed through a Sep-Pak Light QMA cartridge (Waters) (typically 1-2 GBq in 2.0 mL water). The cartridge was dried by airflow, and the ^{18}F activity was eluted with 1.0 mL of a Kryptofix 2.2.2/K₂CO₃ solution (from a 10.0 mL stock solution of 22.6 mg of Kryptofix 222 and 4.2 mg of K₂CO₃ in acetonitrile/water (95/5)) to a 10.0 mL conical vial. The solvent was removed at 100°C under atmospheric pressure and a stream of nitrogen gas. The residue was azeotropically dried with a total of 6.0 mL of anhydrous acetonitrile at 100°C to afford the *dried* K2.2.2/K[^{18}F]F complex residue which was dissolved in a solution of the tosylate precursor **4.36** (2.5 mg) in DMF (300 μL) and heated at 120°C for 10 min. The reaction mixture was cooled to room temperature and diluted with 600 μL of a mixture of MeCN/H₂O (1:1) and purified by semi-preparative HPLC (HPLC Method A or B). The eluates were monitored for radioactivity and for UV absorbance (254 nm) and the peak corresponding to [^{18}F]-(\pm)-**IPMICF6** was collected and diluted with 15 mL of water followed by trapping on a preconditioned (10 mL EtOH followed by

10 mL water) Sep-Pak C18 Ligth. The cartridge was eluted with 0.6 mL EtOH. The identity of [^{18}F]-(\pm)-**IPMICF6** was further confirmed by co-injection with nonradioactive **16**. The tracer was obtained in 24.8 ± 2.6 % RCY ($n = 3$, non-decay corrected isolated yield from injected activity) and >99% radiochemical purities. (< 50 min procedure from end of bombardment).

*Radiosynthesis of [^{18}F]-(\pm)-**IPMICF10**.* The $\text{K}_2.2.2/\text{K}[^{18}\text{F}]\text{F}$ complex residue from the drying step (1-2 GBq) was dissolve in a solution of the tosylate precursor **4.41** (2.5 mg) in MeCN (250 μL) and heated at 100°C for 20 min. The reaction mixture was cooled to room temperature and diluted with a 600 μL of a mixture of MeCN/ H_2O (1:1) and purified by semi-preparative HPLC (HPLC Method C). The eluates were monitored for radioactivity and for UV absorbance (254 nm) and the peak corresponding to [^{18}F]-(\pm)-**IPMICF10** was collected and diluted with 15 mL of water followed by trapping on a preconditioned (10 mL EtOH followed by 10 mL water) Sep-Pak C18 Ligth. The cartridge was eluted with 0.6 mL EtOH. The identity of [^{18}F]-(\pm)-**IPMICF10** was further confirmed by co-injection with nonradioactive **27**. The tracer was obtained in 18.4 ± 3.7 % RCY ($n = 3$, non-decay corrected isolated yield from injected activity) and >99% radiochemical purities. (< 60 min procedure from end of bombardment).

3.2 McConnell Brain Imaging Center Site.

HPLC Methods. Semi preparative, radio-preparative high performance liquid chromatography (HPLC) purifications were performed using a Phenomenex LUNA® C18 column (100 Å, 250 × 10 mm, 10 μm). Method D: elution at 3.0 ml min⁻¹ with a mixture of H_2O (A) and MeCN (B) isocratic at 43% A and 57% B ($t_{r[\text{F}^{18}\text{F}-(\pm)\text{IPMICF6}(\text{16})]} = 12.60$ min). Method E: elution at 3.0 ml min⁻¹ with a mixture of H_2O (A) and MeCN (B) isocratic at 32% A and 68% B ($t_{r[\text{F}^{18}\text{F}-(\pm)\text{IPMICF10}(\text{27})]} = 14.30$ min). Quality control analysis was performed on an Agilent 1200 system (Agilent Technologies, Santa Clara, CA, USA; running on Agilent ChemStation software) equipped with a Raytest Gabi Star radioactivity detector (Raytest Isotopenmessgeräte GmbH, Straubenhardt, Germany) using a Phenomenex Partisil ODS-3 (250 × 4.6 mm, 5 μm) column. Method F: elution at 1.0 ml min⁻¹ with a mixture of H_2O (A) and MeCN (B) isocratic at 30% A and 70% B ($t_{r[\text{F}^{18}\text{F}-(\pm)\text{IPMICF6}(\text{16})]} = 7.39$ min; $t_{r[\text{F}^{18}\text{F}-(\pm)\text{IPMICF10}(\text{27})]} = 9.73$ min).

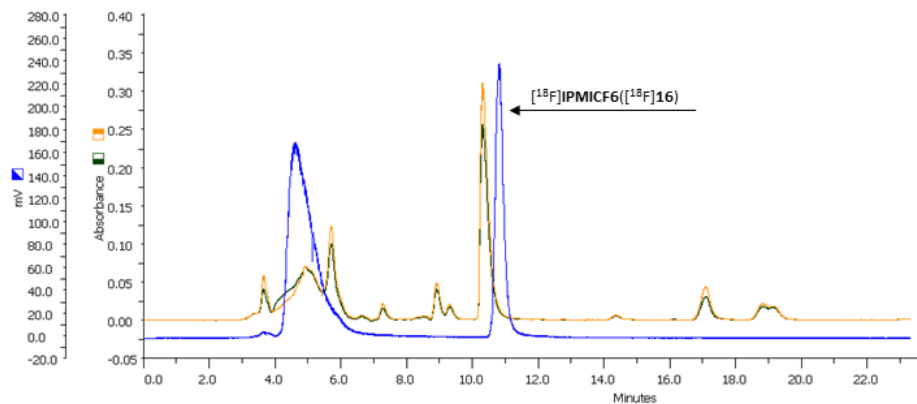
*Radiosynthesis of [^{18}F]-(\pm)-**IPMICF6**.* The azeotropic drying of $^{18}\text{F}^-$ and the radiosyntheses were carried out using a radiosynthesis module Scintomics GRP (Germany) with a home-made manifold setup operated with Scintomics software. The module was equipped with a radioactivity detector and a Knauer UV detector. The [^{18}F] $\text{F}^-/\text{H}_2\text{O}$ (32.2 GBq – 870 mCi) was passed through a Sep-Pak Light QMA cartridge (Waters) as an aqueous solution in ^{18}O -

enriched water and the ^{18}F activity was eluted with 1.5 mL of a Kryptofix2.2.2./ K_2CO_3 solution (Kryptofix2.2.2. - 10-12 mg, dissolved in 150 μL of 0.125M K_2CO_3 + 1.3 mL MeCN) to a disposable plastic reactor. The solvent was removed at 100°C under reduced pressure and a stream of argon gas. The residue was azeotropically dried with 0.5 mL of anhydrous acetonitrile twice at 100°C. Following azeotropic drying, the reaction vial was charged with tosylate precursor **4.36** (2.5 mg, in 0.5 mL DMF) and the mixture was allowed to react for 10 min at 120°C. The crude mixture was then diluted with HPLC eluent (1.5 mL, 57% MeCN, 43% H_2O) and injected on HPLC. The pure ^{18}F -(±)-**IPMICF6** was obtained in 7.9 % RCY (EOS, non-decay corrected isolated yield from $^{18}\text{F}/\text{H}_2\text{O}$; HPLC method D), > 99% radiochemical purity and specific activity of 163 GBq/ μmol (4414 Ci/mmol). An aliquot of the product fraction corresponding to ^{18}F -(±)-**IPMICF6** was collected and diluted with 15 mL H_2O and passed through a preconditioned (10 mL EtOH followed by 10 mL water) Sep-Pak C18 Plus Cartridge and then eluted with 0.5 mL EtOH and used directly in the autoradiography experiments. Quality control, of the isolated ^{18}F -(±)-**IPMICF6** was performed using HPLC method F.

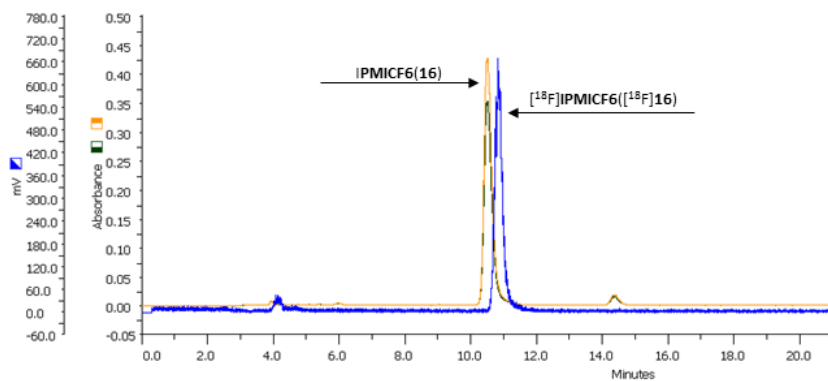
*Radiosynthesis of ^{18}F -(±)-**IPMICF10**.* The radiotracer was synthesized in a similar procedure using the precursor **4.41** (2.5 mg, in 0.5 mL MeCN). The reaction was carried out for 20 min at 95°C and led to the isolation of ^{18}F -(±)-**IPMICF10** in 3.4 % RCY (EOS, non-decay corrected isolated yield from $^{18}\text{F}/\text{H}_2\text{O}$; HPLC method D), > 98.5% radiochemical purity and specific activity of 242 GBq/ μmol (6549 Ci/mmol). Quality control, of the isolated ^{18}F -(±)-**IPMICF10** was performed using HPLC method F.

3.3 Plasma Stability.

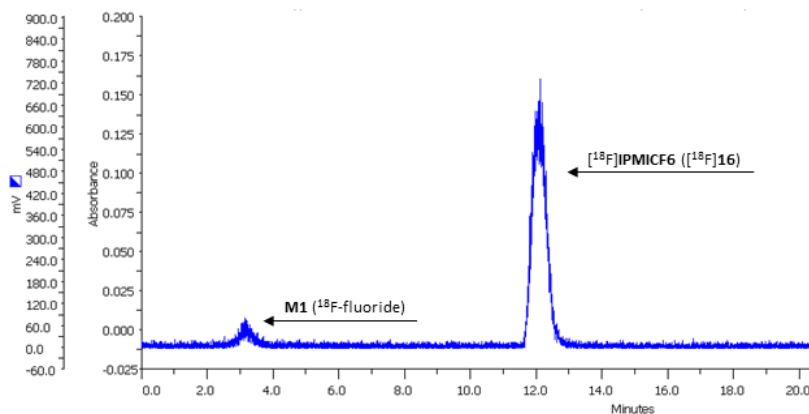
Compound ^{18}F -(±)-**IPMICF6** and ^{18}F -(±)-**IPMICF10** (radiochemical purity > 99%) were incubated in human plasma (500 μL) at 37°C and ice-cold acetonitrile (250 μL , after 60 min) was added for protein precipitation at different time points followed by centrifugation. The amount of intact ^{18}F -(±)-**IPMICF6** and ^{18}F -(±)-**IPMICF10** was determined by HPLC analysis of the supernatant.



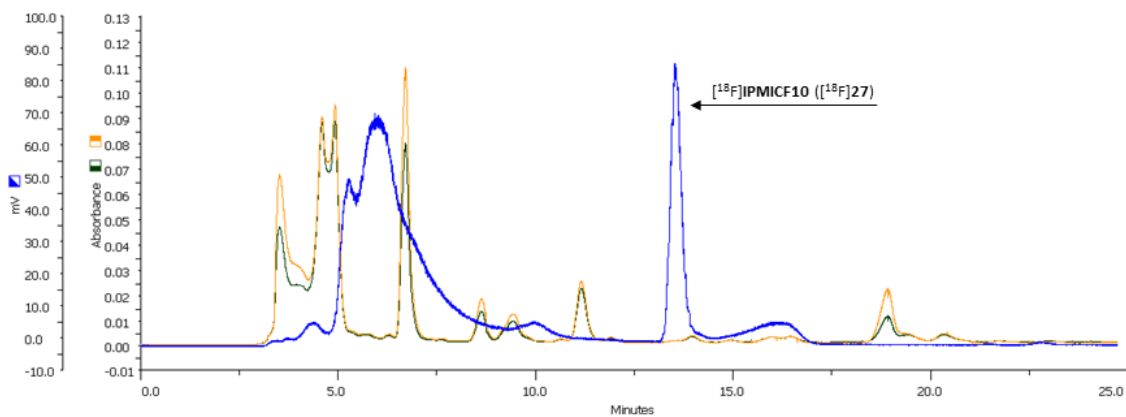
Figures S4.3. Typical semi-preparative HPLC chromatogram of the radiofluorination of the tosylate precursor **4.36** leading to the formation of [^{18}F]-(\pm)-**IPMICF6** (HPLC Method A). (In this instance, the UV peak at $t = 10.5$ min in this chromatogram is expected to be an elimination products from the tosylate precursor which was observed when the reaction mixture was injected on HPLC >15 min after quenching. It illustrates the fact that the precursor readily degrades after quenching and that isolation as to be performed immediately after the reaction mixture is diluted with HPLC eluent.)



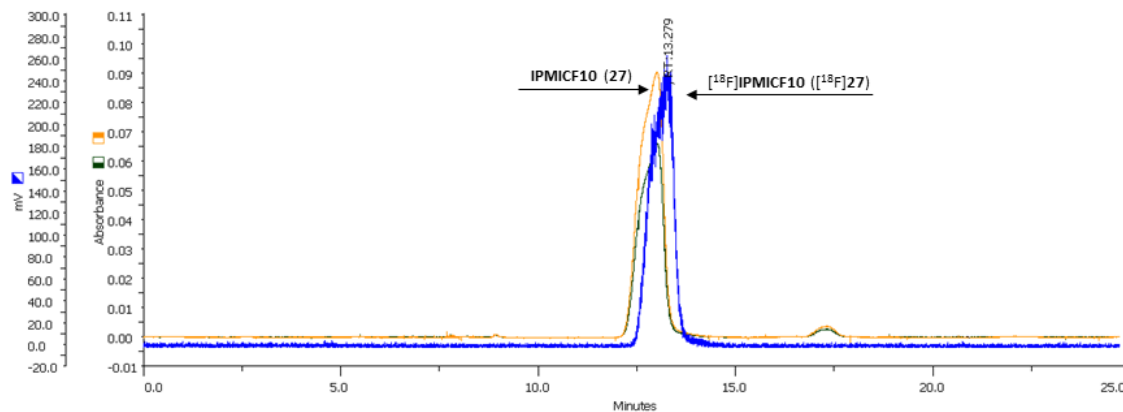
Figures S4.4. Representative HPLC-QC chromatogram of the collected [^{18}F]-(\pm)-**IPMICF6** co-injected with the non-radioactive standard **4.16** (HPLC Method A).



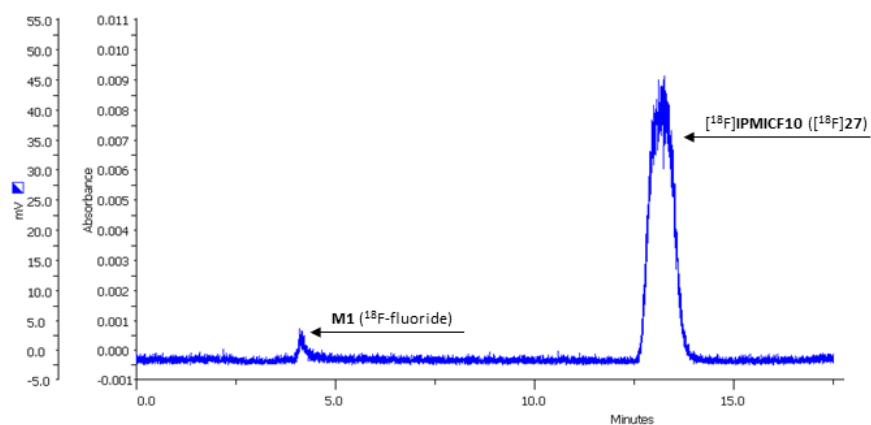
Figures S4.5. HPLC analysis of human plasma at 60 min after [¹⁸F]-(\pm)-IPMICF6 incubation at 37°C (HPLC Method B).



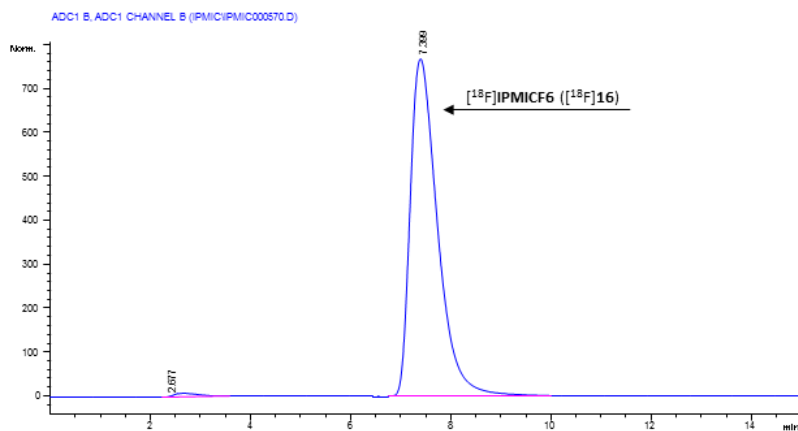
Figures S4.6. Typical semi-preparative HPLC chromatogram of the radiofluorination of the tolylate precursor **4.41** leading to the formation of [¹⁸F]-(\pm)-IPMICF10 (HPLC Method C).



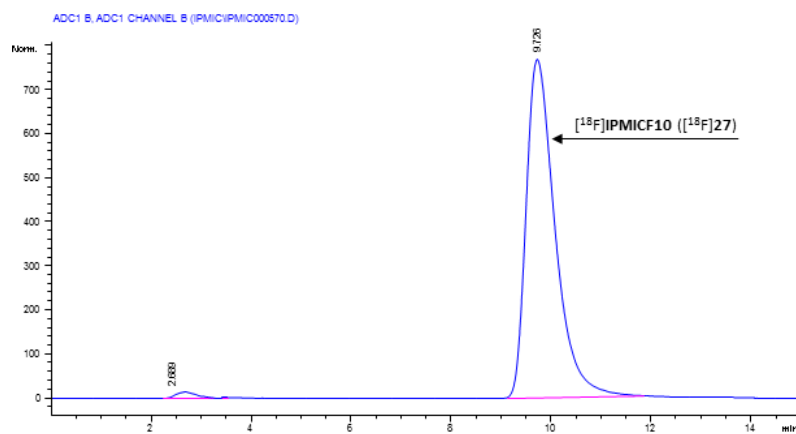
Figures S4.7. Representative HPLC-QC chromatogram of the collected [^{18}F]-(\pm)-IPMICF10 co-injected with the non-radioactive standard 4.27 (HPLC Method C).



Figures S4.8. HPLC analysis of human plasma at 60 min after [^{18}F]-(\pm)-IPMICF10 incubation at 37°C (HPLC Method C).



Figures S4.9. HPLC-QC chromatogram of the collected/formulated [¹⁸F]-(\pm)-IPMICF6 (HPLC Method F) (McConnell Brain Imaging Center Site)



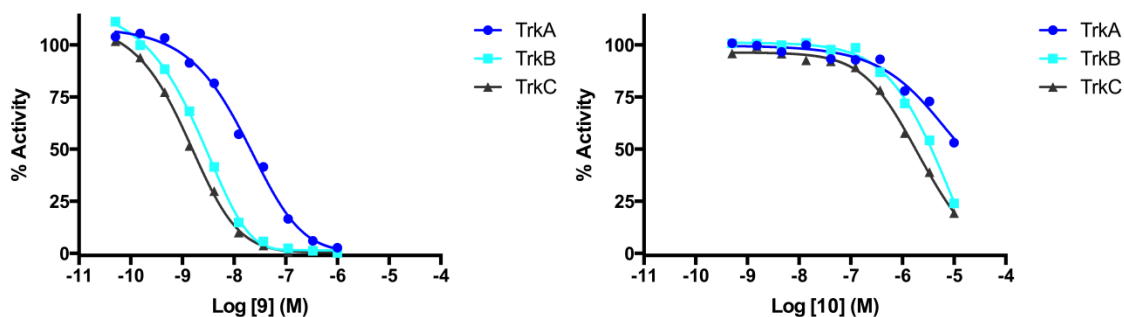
Figures S4.10. HPLC-QC chromatogram of the collected/formulated [¹⁸F]-(\pm)-IPMICF10 (HPLC Method F). (McConnell Brain Imaging Center Site)

4. BIOLOGICAL EVALUATION

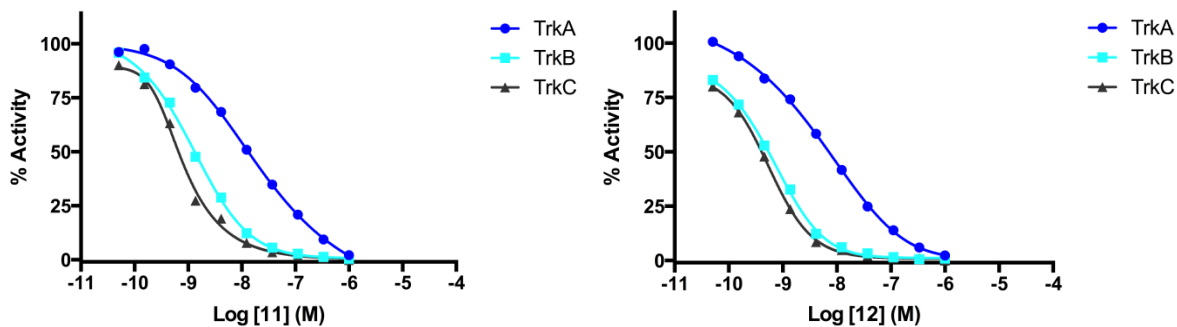
4.1 [γ - ^{33}P]ATP-Based Enzymatic Assay.

Compounds **4.9-4.27** were tested in a [γ - ^{33}P]ATP based enzymatic assay by Reaction Biology Corporation (Malvern, PA). Briefly, the compound was tested in a 10-concentration IC_{50} curve with 3-fold serial dilution starting at 1 or 10 μM (when required, additional dilutions were made). The reactions were initially performed with 1 μM ATP and profiled against 3 tyrosine kinases (tropomyosin receptor kinase A (TrkA), tropomyosin receptor kinase B (TrkB), tropomyosin receptor kinase C (TrkC)) in singlicate with staurosporine as a control. Additional measurements were carried out for selected compounds (triplicates for inhibitors **4.13-4.16** and **4.25-4.27**). Compounds **4.16** and **4.27** were subsequently investigated for off-Trk kinase activity (Reaction Biology Corporation). Compounds **4.16** and **4.27** were tested for inhibitory activity at (0.1 μM) on a panel of 20 selected kinases (SYK, RET, PDK1/PDHK1, PDGFR α , P38a/MAPK14, KDR/VEGFR2, JNK1, JAK1, ITK, FMS, FLT3, ERK1, ERBB2/HER2, EGFR, c-SRC, c-MET, c-KIT, BRAF, ALK, ABL1) under similar conditions as previously described ($n = 2$) (**Table S4.1, S4.2**).

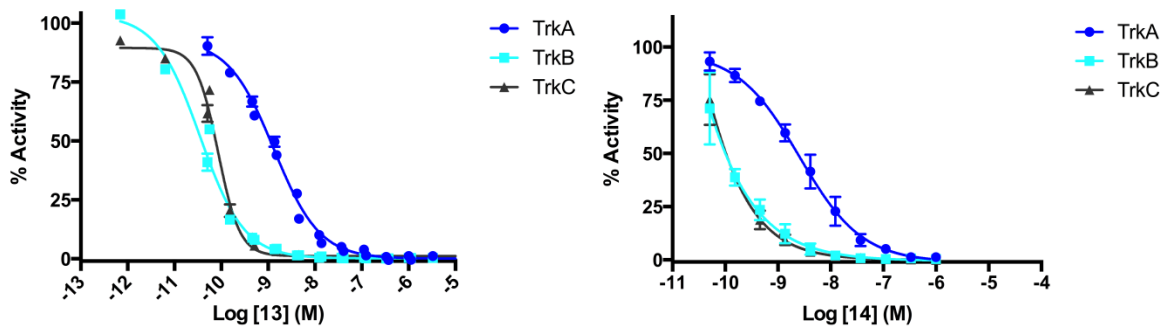
4.2 Dose Response Curves for Compounds 4.9-4.27



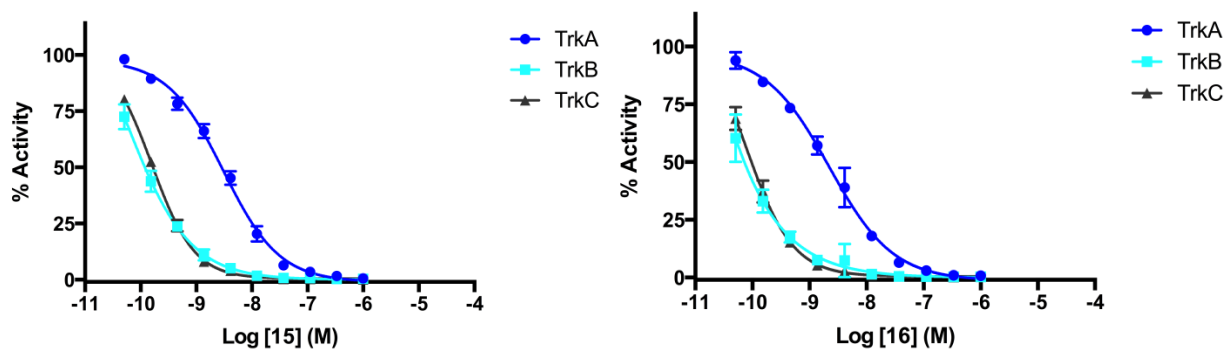
Figures S4.11. Dose-response curve for inhibitor **4.9** (left; $n = 1$) and **4.10** (right; $n = 1$) versus TrkA, TrkB and TrkC.



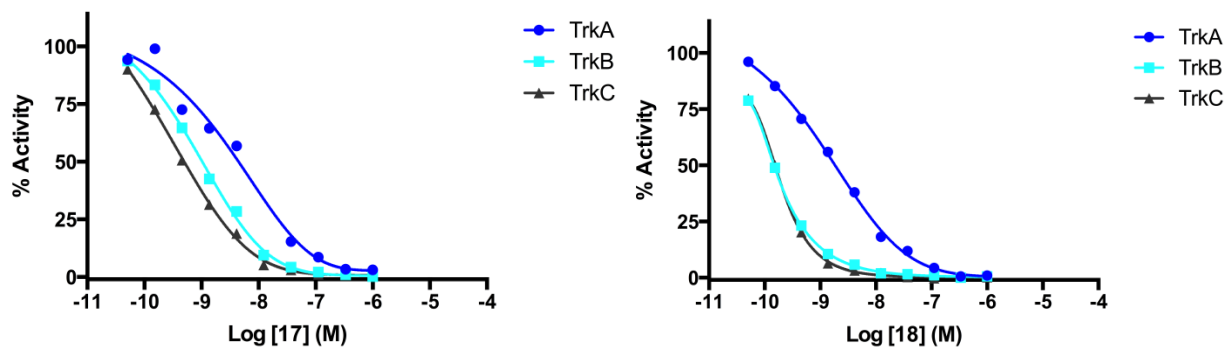
Figures S4.12. Dose-response curve for inhibitor 4.11 (left; $n = 1$) and 4.12 (right; $n = 1$) versus TrkA, TrkB and TrkC.



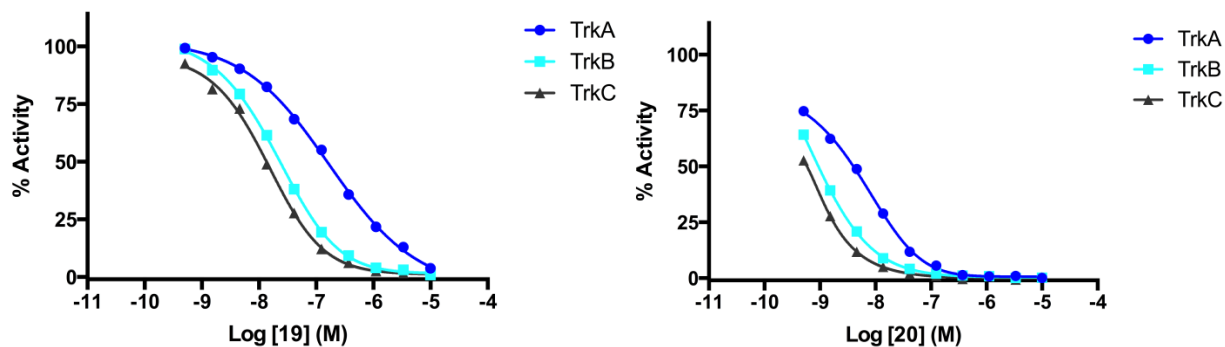
Figures S4.13. Dose-response curve for inhibitor 4.13 (left; $n = 3$) and 4.14 (right; $n = 3$) versus TrkA, TrkB and TrkC (error bars represent standard deviation from the mean).



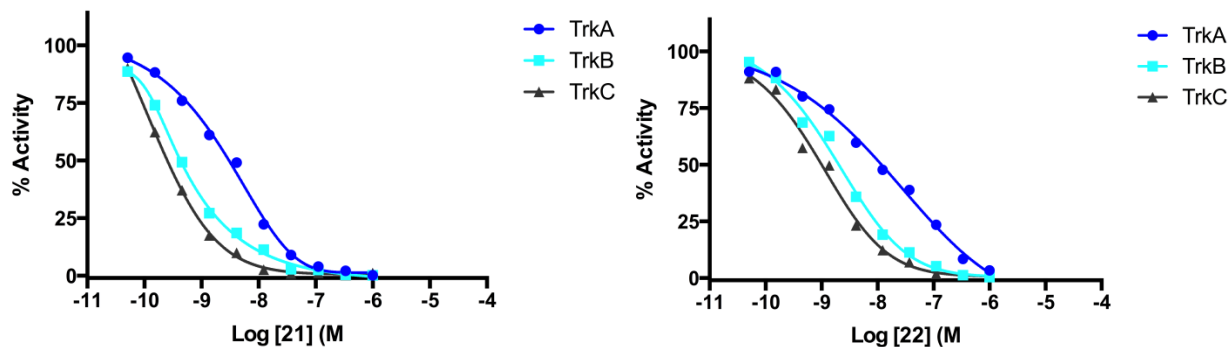
Figures S4.14. Dose-response curve for inhibitor 4.15 (left; $n = 3$) and 4.16 (right; $n = 3$) versus TrkA, TrkB and TrkC (error bars represent standard deviation from the mean).



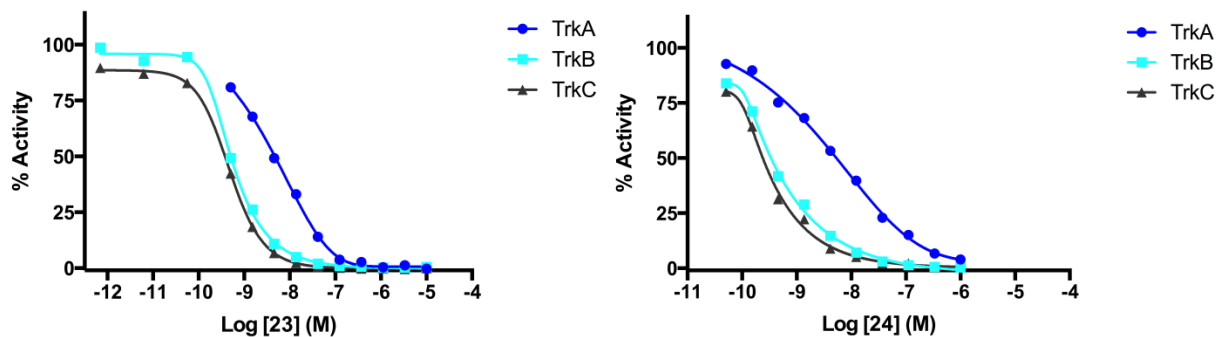
Figures S4.15. Dose-response curve for inhibitor **4.17** (left; $n = 1$) and **4.18** (right; $n = 1$) versus TrkA, TrkB and TrkC.



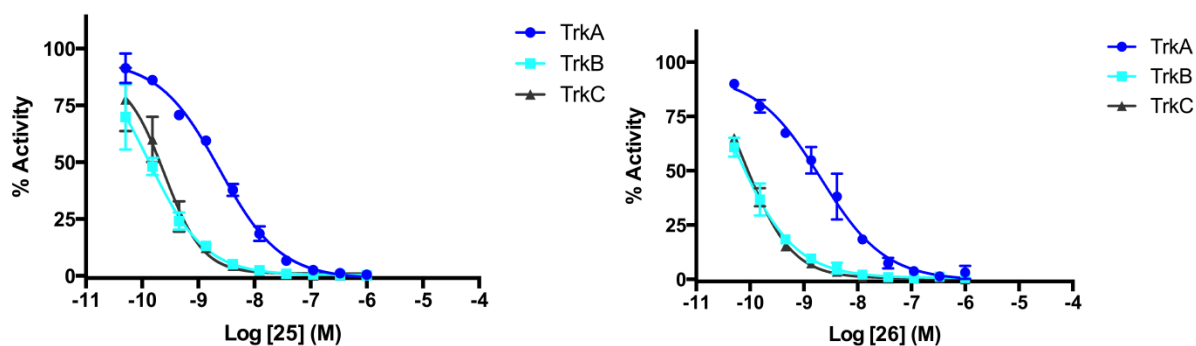
Figures S4.16. Dose-response curve for inhibitor **4.19** (left; $n = 1$) and **4.20** (right; $n = 1$) versus TrkA, TrkB and TrkC.



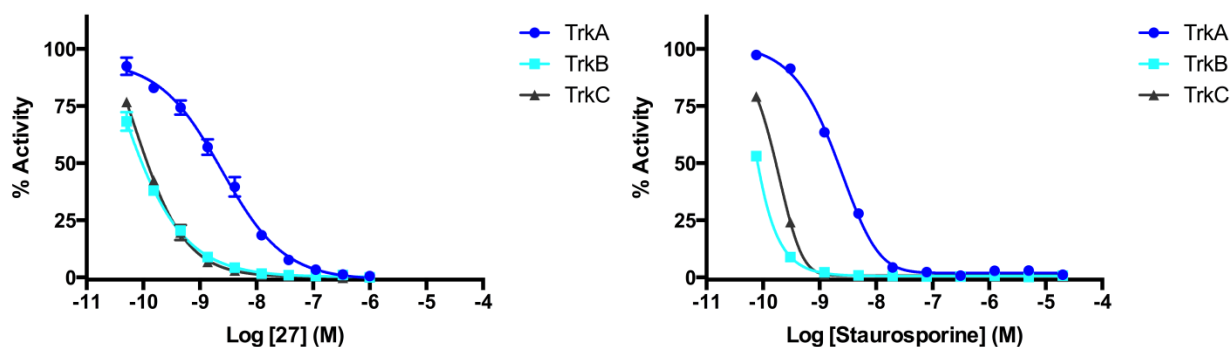
Figures S4.17. Dose-response curve for inhibitor **4.21** (left; $n = 1$) and **4.22** (right; $n = 1$) versus TrkA, TrkB and TrkC.



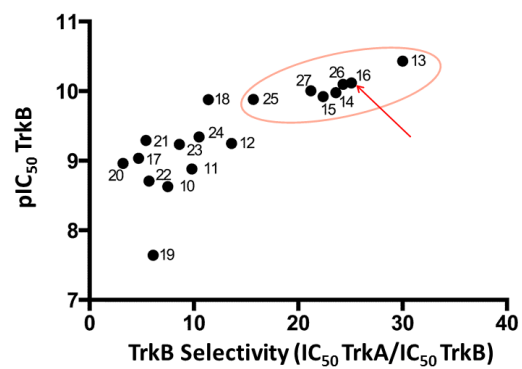
Figures S4.18. Dose-response curve for inhibitor **4.23** (left; $n = 1$) and **4.24** (right; $n = 1$) versus TrkA, TrkB and TrkC.



Figures S4.19. Dose-response curve for inhibitor **4.25** (left; $n = 3$) and **4.26** (right; $n = 3$) versus TrkA, TrkB and TrkC (error bars represent standard deviation from the mean).



Figures S4.20. Dose-response curve for inhibitor **4.27** (left; $n = 3$) and staurosporine (control, right; $n = 1$) versus TrkA, TrkB and TrkC (error bars represent standard deviation from the mean).



Figures S4.21. Inhibition of TrkB kinase versus TrkB selectivity with regard to TrkA. The potencies are expressed as $-\log_{10}(IC_{50})$. Inhibitors **4.16** and **4.27** were selected based on TrkB potency, selectivity and radiolabeling amenability.

4.3 Selectivity Profiling.

Table S4.1. Data for off-Trk inhibitory activity of compound **4.16** (0.1 μ M)

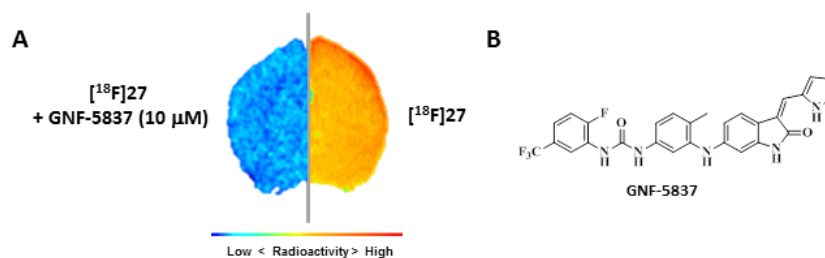
| Kinases | % Enzyme Activity (relative to DMSO controls) | | IC50 (M) Staurosporine* | IC50 (M) Alternate Control cpd*. | Alternate compound ID |
|--------------------|---|--------|----------------------------|---|--------------------------|
| | IPMICF6 | | | | |
| | Data 1 | Data 2 | | | |
| ABL1 | 95.96 | 95.31 | 1.85E-08 | | |
| ALK | 94.54 | 92.85 | 8.60E-10 | | |
| BRAF | 101.34 | 99.25 | ND | 2.37E-08 | GW5074 |
| c-Kit | 105.16 | 104.36 | 4.46E-08 | | |
| c-MET | 95.81 | 93.81 | 4.36E-08 | | |
| c-Src | 97.38 | 96.64 | 2.34E-09 | | |
| EGFR | 68.08 | 65.22 | 3.12E-08 | | |
| ERBB2/HER2 | 49.99 | 49.22 | 1.97E-08 | | |
| ERK1 | 103.46 | 103.35 | 3.93E-06 | | |
| FLT3 | 85.14 | 84.99 | 1.08E-09 | | |
| FMS | 103.17 | 101.89 | 6.24E-10 | | |
| ITK | 93.59 | 93.22 | 7.75E-09 | | |
| JAK1 | 90.97 | 90.37 | 2.96E-10 | | |
| JNK1 | 99.49 | 99.38 | 1.67E-07 | | |
| KDR/VEGFR2 | 110.38 | 109.61 | 4.00E-09 | | |
| P38a/MAPK14 | 99.59 | 97.36 | ND | 2.09E-08 | SB202190 |
| PDGFRa | 100.61 | 99.00 | 2.07E-10 | | |
| PDK1/PDHK1 | 85.56 | 85.37 | ND | 1.88E-05 | GW5074 |
| RET | 90.98 | 89.43 | 9.79E-10 | | |
| SYK | 105.23 | 104.84 | 7.74E-10 | | |

Table S4.2. Data for off-Trk inhibitory activity of compound 4.27 (0.1 μ M)

| Kinase: | % Enzyme Activity (relative to DMSO controls) | | Compound IC50* (M): | | |
|--------------------|---|--------|---------------------|---------------------------|-----------------------------|
| | IPMICF10 | | Staurosporine | Alternate Control cpd. | Alternate compound ID |
| | Data 1 | Data 2 | | | |
| ABL1 | 91.79 | 90.89 | 3.51E-08 | | |
| ALK | 89.40 | 88.60 | 8.92E-10 | | |
| BRAF | 95.46 | 92.68 | | 2.98E-08 | GW5074 |
| c-Kit | 101.20 | 100.52 | 5.74E-08 | | |
| c-MET | 98.31 | 95.79 | 2.60E-08 | | |
| c-Src | 103.39 | 102.83 | 1.61E-09 | | |
| EGFR | 96.51 | 89.72 | 2.08E-08 | | |
| ERBB2/HER2 | 79.72 | 79.54 | 1.64E-08 | | |
| ERK1 | 101.56 | 100.99 | 1.21E-06 | | |
| FLT3 | 96.07 | 94.11 | 9.65E-10 | | |
| FMS | 107.46 | 102.33 | 9.87E-11 | | |
| ITK | 98.19 | 97.06 | 4.16E-09 | | |
| JAK1 | 100.70 | 98.68 | 1.32E-10 | | |
| JNK1 | 100.68 | 99.80 | 1.41E-07 | | |
| KDR/VEGFR2 | 95.60 | 94.49 | 1.26E-09 | | |
| P38a/MAPK14 | 99.59 | 99.49 | | 2.09E-08 | SB202190 |
| PDGFRa | 99.55 | 99.48 | 7.30E-12 | | |
| PDK1/PDHK1 | 79.08 | 78.71 | | 1.37E-04 | GW5074 |
| RET | 105.91 | 105.83 | 1.44E-09 | | |
| SYK | 104.34 | 103.51 | 7.96E-10 | | |

4.4 Autoradiography.

A rat was decapitated, the brains rapidly removed, frozen in 2-methylbutane (-40°C), and stored at -80°C . Brain sections ($20\ \mu\text{m}$ thick) were thawed and mounted onto Superfrost Plus slides (Thermo Scientific) and stored at -80°C . After pre-incubation in PBS buffer (30 mmol/L; pH 7.4 containing 137 mmol/L NaCl, 27 mmol/L) for 10 minutes at room temperature, rat and tumor sections were incubated 2 h 30 (room temperature) in buffer containing [^{18}F]-(\pm)-**IPMICF6** (67 μCi in 200 mL buffer total) and 2 h 30 (room temperature) for [^{18}F]-(\pm)-**IPMICF10** (279 μCi in 200 mL buffer total). Compound **4.16** (**IPMICF6**; 1.0 μM) and GNF-5839 (10 μM) were used to determine the specific binding of [^{18}F]-(\pm)-**IPMICF6** and [^{18}F]-(\pm)-**IPMICF10** respectively. After three washes in incubation buffer (5 minutes, 4°C) and a rapid rinse with ice-cold water (15 seconds), the sections were dried in a stream of air (room temperature). Sections were then dried further in a vacuum container with formaldehyde powder for mild fixation. Labeled sections were placed on phosphor-imaging plates (BAS 2025; Fuji, Japan), with industrial tritium activity standards (Amersham Biosciences, Piscataway, NJ, USA). On exposure, the plates were scanned with a plate reader (spatial resolution of $50\ \mu\text{m}$; BAS 5000; Fuji or Typhoon Trio + Variable Mode Imager).



Figures S4.22. (A) Representative in vitro autoradiograms from coronal sections of rat brain showing the binding of [^{18}F]4.27 (A, right) and competition experiments with **GNF-5837** (10 μM) (A, left). (B) Structure of GNF-5837.

Table S4.3. PSL Data [^{18}F]-(\pm)-**IPMICF6** Autoradiography ^{18}F -IPMICF6 MEAN

| The area of brain Rat | NORMAL | CRTL NS- SPECIFIC IPMICF6 1.0 μM | %CHANGE IN RAT IPMICF6 |
|--------------------------|----------|---|------------------------------|
| Prefrontal cortex | 2611,793 | 1913,229 | 26,75 |
| Posterior cortex | 2702,114 | 1950,547 | 27,81 |
| Hippocampus | 2586,560 | 1904,214 | 26,38 |
| Cerebellum | 2457,055 | 1860,967 | 24,26 |

Table S4.4. PSL Data for [^{18}F]-(\pm)-**IPMICF10** Autoradiography ^{18}F -IPMICF10 MEAN

| The area of brain Rat | NORMAL RAT | CRTL NS- SPECIFIC GNF-5837 10 μM | %CHANGE IN RAT GNF-5837 |
|--------------------------|---------------|---|-------------------------------|
| Anterior cortex | 54801,107 | 39985,001 | 27,04 |
| Posterior cortex | 55746,791 | 40286,937 | 27,73 |
| Hippocampus | 54356,573 | 39561,146 | 27,22 |
| Cerebellum | 57319,550 | 41240,174 | 28,05 |

5. NMR SPECTRA

Data form this subsection can be found in **Annex 3**.

6. CRYSTALLOGRAPHIC DATA FOR COMPOUND 4.22

Data form this subsection can be found in **Annex 3**.

4.6 References

1. Huang, E. J.; Reichardt, L. F., Neurotrophins: roles in neuronal development and function. *Annu Rev Neurosci* **2001**, *24*, 677-736.
2. Huang, E. J.; Reichardt, L. F., Trk receptors: roles in neuronal signal transduction. *Annu Rev Biochem* **2003**, *72*, 609-42.
3. Chao, M. V., Neurotrophins and their receptors: a convergence point for many signalling pathways. *Nat Rev Neurosci* **2003**, *4* (4), 299-309.
4. Pattarawarapan, M.; Burgess, K., Molecular basis of neurotrophin-receptor interactions. *J Med Chem* **2003**, *46* (25), 5277-91.
5. Holtzman, D. M.; Kilbridge, J.; Li, Y. W.; Cunningham, E. T.; Lenn, N. J.; Clary, D. O.; Reichardt, L. F.; Mobley, W. C., TrkA Expression in the Cns - Evidence for the Existence of Several Novel Ngf-Responsive Cns Neurons. *Journal of Neuroscience* **1995**, *15* (2), 1567-1576.
6. Muragaki, Y.; Timothy, N.; Leight, S.; Hempstead, B. L.; Chao, M. V.; Trojanowski, J. Q.; Lee, V. M., Expression of trk receptors in the developing and adult human central and peripheral nervous system. *J Comp Neurol* **1995**, *356* (3), 387-97.
7. Altar, C. A.; Burton, L. E.; Bennett, G. L.; Dugich-Djordjevic, M., Recombinant human nerve growth factor is biologically active and labels novel high-affinity binding sites in rat brain. *Proc Natl Acad Sci U S A* **1991**, *88* (1), 281-5.
8. Ginsberg, S. D.; Che, S. L.; Wu, J.; Counts, S. E.; Mufson, E. J., Down regulation of trk but not p75(NTR) gene expression in single cholinergic basal forebrain neurons mark the progression of Alzheimer's disease. *Journal of Neurochemistry* **2006**, *97* (2), 475-487.
9. Mufson, E. J.; Li, J. M.; Sobreviela, T.; Kordower, J. H., Decreased trkA gene expression within basal forebrain neurons in Alzheimer's disease. *Neuroreport* **1996**, *8* (1), 25-29.
10. Counts, S. E.; Nadeem, M.; Wu, J.; Ginsberg, S. D.; Saragovi, H. U.; Mufson, E. J., Reduction of cortical TrkA but not p75(NTR) protein in early-stage Alzheimer's disease. *Ann Neurol* **2004**, *56* (4), 520-531.
11. Ghilardi, J. R.; Freeman, K. T.; Jimenez-Andrade, J. M.; Mantyh, W. G.; Bloom, A. P.; Kuskowski, M. A.; Mantyh, P. W., Administration of a tropomyosin receptor kinase inhibitor attenuates sarcoma-induced nerve sprouting, neuroma formation and bone cancer pain. *Mol Pain* **2010**, *6*.
12. Mantyh, P. W.; Koltzenburg, M.; Mendell, L. M.; Tive, L.; Shelton, D. L., Antagonism of Nerve Growth Factor-TrkA Signaling and the Relief of Pain. *Anesthesiology* **2011**, *115* (1), 189-204.

13. Tessarollo, L.; Tsoulfas, P.; Martinzanca, D.; Gilbert, D. J.; Jenkins, N. A.; Copeland, N. G.; Parada, L. F., Trkc, a Receptor for Neurotrophin-3, Is Widely Expressed in the Developing Nervous-System and in Nonneuronal Tissues. *Development* **1993**, *118* (2), 463-475.
14. Altar, C. A.; Siuciak, J. A.; Wright, P.; Ip, N. Y.; Lindsay, R. M.; Wiegand, S. J., In-Situ Hybridization of Trkb and Trkc Receptor Messenger-Rna in Rat Forebrain and Association with High-Affinity Binding of [I-125] Bdnf, [I-125] Nt-4/5 and [I-125] Nt-3. *European Journal of Neuroscience* **1994**, *6* (9), 1389-1405.
15. Klein, R.; Conway, D.; Parada, L. F.; Barbacid, M., The Trkb Tyrosine Protein-Kinase Gene Codes for a 2nd Neurogenic Receptor That Lacks the Catalytic Kinase Domain. *Cell* **1990**, *61* (4), 647-656.
16. Middlemas, D. S.; Lindberg, R. A.; Hunter, T., Trkb, a Neural Receptor Protein-Tyrosine Kinase - Evidence for a Full-Length and 2 Truncated Receptors. *Molecular and Cellular Biology* **1991**, *11* (1), 143-153.
17. Silhol, M.; Bonnichon, V.; Rage, F.; Tapia-Arancibia, L., Age-related changes in brain-derived neurotrophic factor and tyrosine kinase receptor isoforms in the hippocampus and hypothalamus in male rats. *Neuroscience* **2005**, *132* (3), 613-624.
18. Fenner, B. M., Truncated TrkB: Beyond a dominant negative receptor. *Cytokine Growth F R* **2012**, *23* (1-2), 15-24.
19. Zhang, F.; Kang, Z. L.; Li, W.; Xiao, Z. C.; Zhou, X. F., Roles of brain-derived neurotrophic factor/tropomyosin-related kinase B (BDNF/TrkB) signalling in Alzheimer's disease. *J Clin Neurosci* **2012**, *19* (7), 946-949.
20. Fumagalli, F.; Racagni, G.; Riva, M. A., Shedding light into the role of BDNF in the pharmacotherapy of Parkinson's disease. *Pharmacogenomics J* **2006**, *6* (2), 95-104.
21. Gines, S.; Bosch, M.; Marco, S.; Gavaldà, N.; Diaz-Hernandez, M.; Lucas, J. J.; Canals, J. M.; Alberch, J., Reduced expression of the TrkB receptor in Huntington's disease mouse models and in human brain. *European Journal of Neuroscience* **2006**, *23* (3), 649-658.
22. Pillai, A., Brain-derived neurotropic factor/TrkB signaling in the pathogenesis and novel pharmacotherapy of schizophrenia. *Neurosignals* **2008**, *16* (2-3), 183-193.
23. Griesbach, G. S.; Hovda, D. A.; Gomez-Pinilla, F., Exercise-induced improvement in cognitive performance after traumatic brain injury in rats is dependent on BDNF activation. *Brain Research* **2009**, *1288*, 105-115.
24. Thiele, C. J.; Li, Z.; McKee, A. E., On Trk--the TrkB signal transduction pathway is an increasingly important target in cancer biology. *Clin Cancer Res* **2009**, *15* (19), 5962-7.

25. Nakagawara, A.; Azar, C. G.; Scavarda, N. J.; Brodeur, G. M., Expression and Function of Trk-B and Bdnf in Human Neuroblastomas. *Molecular and Cellular Biology* **1994**, *14* (1), 759-767.
26. Nakagawara, A., Trk receptor tyrosine kinases: A bridge between cancer and neural development. *Cancer Letters* **2001**, *169* (2), 107-114.
27. Martin-Zanca, D.; Hughes, S. H.; Barbacid, M., A human oncogene formed by the fusion of truncated tropomyosin and protein tyrosine kinase sequences. *Nature* **1986**, *319* (6056), 743-8.
28. Brodeur, G. M.; Minturn, J. E.; Ho, R.; Simpson, A. M.; Iyer, R.; Varela, C. R.; Light, J. E.; Kolla, V.; Evans, A. E., Trk receptor expression and inhibition in neuroblastomas. *Clin Cancer Res* **2009**, *15* (10), 3244-50.
29. Sclabas, G. M.; Fujioka, S.; Schmidt, C.; Li, Z.; Frederick, W. A.; Yang, W.; Yokoi, K.; Evans, D. B.; Abbruzzese, J. L.; Hess, K. R.; Zhang, W.; Fidler, I. J.; Chiao, P. J., Overexpression of tropomyosin-related kinase B in metastatic human pancreatic cancer cells. *Clin Cancer Res* **2005**, *11* (2 Pt 1), 440-9.
30. Wang, T.; Yu, D.; Lamb, M. L., Trk kinase inhibitors as new treatments for cancer and pain. *Expert Opin Ther Pat* **2009**, *19* (3), 305-19.
31. McCarthy, C.; Walker, E., Tropomyosin receptor kinase inhibitors: a patent update 2009-2013. *Expert Opinion on Therapeutic Patents* **2014**, *24* (7), 731-744.
32. Albaugh, P.; Fan, Y.; Mi, Y.; Sun, F.; Adrian, F.; Li, N.; Jia, Y.; Sarkisova, Y.; Kreusch, A.; Hood, T.; Lu, M.; Liu, G.; Huang, S.; Liu, Z.; Loren, J.; Tuntland, T.; Karanewsky, D. S.; Seidel, H. M.; Molteni, V., Discovery of GNF-5837, a Selective TRK Inhibitor with Efficacy in Rodent Cancer Tumor Models. *ACS Med Chem Lett* **2012**, *3* (2), 140-5.
33. Croucher, J. L.; Iyer, R.; Li, N. X.; Molteni, V.; Loren, J.; Gordon, W. P.; Tuntland, T.; Liu, B.; Brodeur, G. M., TrkB inhibition by GNF-4256 slows growth and enhances chemotherapeutic efficacy in neuroblastoma xenografts. *Cancer Chemoth Pharm* **2015**, *75* (1), 131-141.
34. Evans, A. E.; Kisselbach, K. D.; Liu, X.; Eggert, A.; Ikegaki, N.; Camoratto, A. M.; Dionne, C.; Brodeur, G. M., Effect of CEP-751 (KT-6587) on neuroblastoma xenografts expressing TrkB. *Med Pediatr Oncol* **2001**, *36* (1), 181-184.
35. Bernard-Gauthier, V.; Boudjemeline, M.; Rosa-Neto, P.; Thiel, A.; Schirmacher, R., Towards tropomyosin-related kinase B (TrkB) receptor ligands for brain imaging with PET: radiosynthesis and evaluation of 2-(4-[(¹⁸F]fluorophenyl)-7,8-dihydroxy-4H-chromen-4-one and 2-(4-[(N-methyl-(¹¹C)-dimethylamino)phenyl]-7,8-dihydroxy-4H-chromen-4-one. *Bioorg Med Chem* **2013**, *21* (24), 7816-29.

36. Bernard-Gauthier, V.; Aliaga, A.; Aliaga, A.; Boudjemeline, M.; Hopewell, R.; Kostikov, A.; Rosa-Neto, P.; Thiel, A.; Schirrmacher, R., Syntheses and Evaluation of Carbon-11-and Fluorine-18-Radiolabeled pan-Tropomyosin Receptor Kinase (Trk) Inhibitors: Exploration of the 4-Aza-2-oxindole Scaffold as Trk PET Imaging Agents. *Acs Chemical Neuroscience* **2015**, 6 (2), 260-276.
37. Bernard-Gauthier, V.; Schirrmacher, R., 5-(4-((4-[F-18]fluorobenzyl)oxy)-3-methoxybenzyl)pyrimidine-2,4-diamine: A selective dual inhibitor for potential PET imaging of Trk/CSF-1R. *Bioorg Med Chem Lett* **2014**, 24 (20), 4784-4790.
38. Zhang, L.; Villalobos, A.; Beck, E. M.; Bocan, T.; Chappie, T. A.; Chen, L.; Grimwood, S.; Heck, S. D.; Helal, C. J.; Hou, X.; Humphrey, J. M.; Lu, J.; Skaddan, M. B.; McCarthy, T. J.; Verhoest, P. R.; Wager, T. T.; Zasadny, K., Design and selection parameters to accelerate the discovery of novel central nervous system positron emission tomography (PET) ligands and their application in the development of a novel phosphodiesterase 2A PET ligand. *J Med Chem* **2013**, 56 (11), 4568-79.
39. S. W. Andrews, J. H., Y. Jiang and G. Zhang, G. , WO/2010/033941; International application No. PCT/US2009/057726;. **2010**, (March 25).
40. P. A. Albaugh, G. C., Y. Fan, B. T. Flatt, J. Loren, V. Molteni and J. M. Smith, WO/2012/034091 A1; International application No. PCT/US2011/051108. **2011**, September 9.
41. J. Haas, S. W. A., Y. Jiang and G. Zhang, WO/2010/048314 A1; International application No. PCT/US2009/061519. **2010**, April 29.
42. S. Allen, S. S. A., K. R. Condroski, J.; Haas, L. Huang, L.; Jiang, T. Kercher and J. Seo, WO/2011/006074 A1; International application No. PCT/US2010/041538. **2011**, January 11.
43. P. K. Sasmal, S. A., A. Tehim, V. Pradkar, P. Dattatreya and N. J. Mavinahalli, WO/2013/088256 A1; International application No. PCT/IB2012/003013. **2013**, June 20.
44. Y. Fan, J. L., V. Molteni, P. A. Albaugh, G. Chopiuk, J. M. Smith and B. T. Flatt, US/2012/0065184 A1; International application No. PCT/US2012/026377. **2012**, August 30.
45. Choi, H. S.; Rucker, P. V.; Wang, Z. C.; Fan, Y.; Albaugh, P.; Chopiuk, G.; Gessier, F.; Sun, F. X.; Adrian, F.; Liu, G. X.; Hood, T.; Li, N. X.; Jia, Y.; Che, J. W.; McCormack, S.; Li, A.; Li, J.; Steffy, A.; Culazzo, A.; Tompkins, C.; Phung, V.; Kreuzsch, A.; Lu, M.; Hu, B.; Chaudhary, A.; Prashad, M.; Tuntland, T.; Liu, B.; Harris, J.; Seidel, H. M.; Loren, J.; Molteni, V., (R)-2-Phenylpyrrolidine Substituted Imidazopyridazines: A New Class of Potent and Selective Pan-IRK Inhibitors. *Acs Medicinal Chemistry Letters* **2015**, 6 (5), 562-567.
46. Stachel, S. J.; Sanders, J. M.; Henze, D. A.; Rudd, M. T.; Su, H. P.; Li, Y. W.; Nanda, K. K.; Egbertson, M. S.; Manley, P. J.; Jones, K. L. G.; Brnardic, E. J.; Green, A.; Grobler, J. A.;

- Hanney, B.; Leitl, M.; Lai, M. T.; Munshi, V.; Murphy, D.; Rickert, K.; Riley, D.; Krasowska-Zoladek, A.; Daley, C.; Zuck, P.; Kane, S. A.; Bilodeau, M. T., Maximizing Diversity from a Kinase Screen: Identification of Novel and Selective pan-Trk Inhibitors for Chronic Pain. *Journal of Medicinal Chemistry* **2014**, *57* (13), 5800-5816.
47. Gilissen, C.; Bormans, G.; de Groot, T.; Verbruggen, A., Synthesis of N-(2-[F-18]fluoroethyl)-N'-methylthiourea: a hydrogen peroxide scavenger. *J Labelled Compd Rad* **1998**, *41* (6), 491-502.
48. Glaser, M.; Arstad, E.; Gaeta, A.; Nairne, J.; Trigg, W.; Robins, E. G., Copper-mediated reduction of 2-[18F]fluoroethyl azide to 2-[18F]fluoroethylamine. *J Labelled Compd Rad* **2012**, *55* (9), 326-331.
49. Franck, D.; Kniess, T.; Steinbach, J.; Zitzmann-Kolbe, S.; Friebe, M.; Dinkelborg, L. M.; Graham, K., Investigations into the synthesis, radiofluorination and conjugation of a new [F-18]fluorocyclobutyl prosthetic group and its in vitro stability using a tyrosine model system. *Bioorgan Med Chem* **2013**, *21* (3), 643-652.
50. Bertrand, T.; Kothe, M.; Liu, J.; Dupuy, A.; Rak, A.; Berne, P. F.; Davis, S.; Gladysheva, T.; Valtre, C.; Crenne, J. Y.; Mathieu, M., The Crystal Structures of TrkA and TrkB Suggest Key Regions for Achieving Selective Inhibition. *Journal of Molecular Biology* **2012**, *423* (3), 439-453.
51. S. W. Andrews, K. R. C., J. Haas, Y. Jiang, G. R. Kolakowski, J. Seo, H. Yang and Q. Zhao, WO/2011/146336 A1; International Application No. PCT/IB2012/003012. **2013**, June 20.
52. Cardinale, J.; Ermert, J.; Humpert, S.; Coenen, H. H., Iodonium ylides for one-step, no-carrier-added radiofluorination of electron rich arenes, exemplified with 4-([F-18] fluorophenoxy)-phenylmethyl) piperidine NET and SERT ligands. *Rsc Adv* **2014**, *4* (33), 17293-17299.
53. Rotstein, B. H.; Stephenson, N. A.; Vasdev, N.; Liang, S. H., Spirocyclic hypervalent iodine(III)-mediated radiofluorination of non-activated and hindered aromatics. *Nat Commun* **2014**, *5*.
54. Bertrand, T.; Kothe, M.; Liu, J.; Dupuy, A.; Rak, A.; Berne, P. F.; Davis, S.; Gladysheva, T.; Valtre, C.; Crenne, J. Y.; Mathieu, M., The crystal structures of TrkA and TrkB suggest key regions for achieving selective inhibition. *J Mol Biol* **2012**, *423* (3), 439-53.
55. Paterson, L. M.; Kornum, B. R.; Nutt, D. J.; Pike, V. W.; Knudsen, G. M., 5-HT radioligands for human brain imaging with PET and SPECT. *Med Res Rev* **2013**, *33* (1), 54-111.
56. Altar, C. A.; Criden, M. R.; Lindsay, R. M.; DiStefano, P. S., Characterization and topography of high-affinity 125I-neurotrophin-3 binding to mammalian brain. *J Neurosci* **1993**, *13* (2), 733-43.

57. Englebienne, P.; Moitessier, N., Docking ligands into flexible and solvated macromolecules. 5. Force-field-based prediction of binding affinities of ligands to proteins. *J Chem Inf Model* **2009**, *49* (11), 2564-71.
58. Corbeil, C. R.; Englebienne, P.; Yannopoulos, C. G.; Chan, L.; Das, S. K.; Bilimoria, D.; L'Heureux, L.; Moitessier, N., Docking ligands into flexible and solvated macromolecules. 2. Development and application of fitted 1.5 to the virtual screening of potential HCV polymerase inhibitors. *J Chem Inf Model* **2008**, *48* (4), 902-9.
59. Therrien, E.; Englebienne, P.; Arrowsmith, A. G.; Mendoza-Sanchez, R.; Corbeil, C. R.; Weill, N.; Campagna-Slater, V.; Moitessier, N., Integrating Medicinal Chemistry, Organic/Combinatorial Chemistry, and Computational Chemistry for the Discovery of Selective Estrogen Receptor Modulators with FORECASTER, a Novel Platform for Drug Discovery. *Journal of Chemical Information and Modeling* **2012**, *52* (1), 210-224.

Article 8

A version of this chapter has been submitted to: Journal of the American Chemical Society, JACS

Bernard-Gauthier, V.; Bailey, J.J.; Mossine, A.V.; Lindner, S.; Vomacka, L.; Aliaga, A.; Shao, X.; Quesada, C.A.; Sherman, P.; Mahringer, A.; Kostikov, A.; Grand'Maison, M.; Rosa-Neto, P.; Soucy, J.-P.; Thiel, A.; Kaplan, D.R.; Fricker, G.; Wängler, B.; Bartenstein, P.; Schirmacher, R.; Scott, P.J.H. Shedding Light on Selective Neurotrophin Receptors *in vivo*: a First-in-Class Radioligand Candidate for Trk PET Neuroimaging

Author contributions: **V.B.G.** design and managed the study, conducted all chemical syntheses and characterizations studies, conducted *in silico* analyses, developed radiosyntheses and contributed to radiochemistry experiments (rodents PET studies and autoradiography studies), contributed to metabolism experiments, developed and performed autoradiography studies, interpreted all data and wrote the paper; J.J.B. contributed to radiochemistry (for rodents PET studies); A.V.M., X.S., C.A.Q., P.S., P.J.H.S. contributed to radiochemistry, PET experiments and data analysis (for non-human primate PET studies); S.L. contributed to radiochemistry (for human PET study); L.V. contributed to data analysis (for human PET study); A.A. performed autoradiography experiments and analyzed autoradiography data; A.M. performed and analysed P-gp/BCRP cellular assays; A.K. contributed to radiochemistry (for autoradiography studies); M.G.'M. contributed to data analysis and manuscript preparation; P.R.N., J.-P.S., A.T., D.R.K., G.F., B.W., P.B., R.S. and P.J.H.S. contributed new reagents and analytic tools; the manuscript was discussed and approved by all co-authors; R.S. supervised the research and corrected manuscript.

Shedding Light on Trk Neurotrophin Receptors with PET Neuroimaging

Vadim Bernard-Gauthier^{a,1*}, Justin J. Bailey^a, Andrew V. Mossine^b, Simon Lindner^c, Lena Vomacka^c, Arturo Aliaga^d, Xia Shao^b, Carole A. Quesada^b, Phillip Sherman^b, Anne Mahringer^e, Alexey Kostikov^f, Marilyn Grand'Maison^g, Pedro Rosa-Neto^d, Jean-Paul Soucy^h, Alexander Thiel^{f,i}, David R. Kaplan^{j,k}, Gert Fricker^e, Björn Wängler^l, Peter Bartenstein^c, Ralf Schirmacher^{a,1,2*}, Peter J. H. Scott^{b,m,2}

^aDepartment of Oncology, Division of Oncological Imaging, University of Alberta, Edmonton, AB, T6G 2R3, Canada. ^bDivision of Nuclear Medicine, Department of Radiology, The University of Michigan Medical School, Ann Arbor, MI, 48109, United States. ^cDepartment of Nuclear Medicine, Ludwig-Maximilians-University of Munich, Marchioninistr. 15, Munich, 81377, Germany. ^dTranslational Neuroimaging Laboratory, McGill Centre for Studies in Aging, Douglas Mental Health University Institute, 6875 Boulevard LaSalle, Montreal, QC, H4H 1R3, Canada. ^eInstitute of Pharmacy and Molecular Biotechnology, University of Heidelberg, Heidelberg 69120, Germany. ^fMcConnell Brain Imaging Centre, Montreal Neurological Institute, McGill University, 3801 University Street, Montreal, QC, H3A 2B4, Canada. ^gBiospective Inc., 6100 Avenue Royalmount, Montreal, QC H4P 2R2, Canada. ^hDepartment of Neurology and Neurosurgery, Montreal Neurological Institute, McGill University, 3801 University Street, Montreal, QC, H3A 2B4, Canada. ⁱJewish General Hospital, Lady Davis Institute, Montreal, QC, HT3 1E2, Canada. ^jProgram in Neurosciences and Mental Health, Hospital for Sick Children, Toronto, ON, M5G 0A4, Canada. ^kDepartment of Molecular Genetics, University of Toronto, ON, M5S1A8, Canada. ^lMolecular Imaging and Radiochemistry, Department of Clinical Radiology and Nuclear Medicine, Medical Faculty Mannheim of Heidelberg University, Theodor-Kutzer-Ufer 1-3, Mannheim 68167, Germany. ^mThe Interdepartmental Program in Medicinal Chemistry, University of Michigan, Ann Arbor, MI 48109, United States. ¹Corresponding authors. ²P.J.H.S. and R.S. contributed equally to this work.

5.1 Abstract

The proto-oncogenes *NTRK1/2/3* encode the tropomyosin receptor kinases TrkA/B/C which play pivotal roles in neurobiology and cancer. Although the centrality of Trk in neurology has long been documented, the precise understanding and implications of the spatiotemporal fluctuations of Trk expression in the human brain remain poorly understood. The lack of non-invasive techniques to determine Trk densities in the living brain impedes quantitative characterisation of Trk alterations in healthy and diseased states as well as the determination of antineoplastic inhibitor central nervous system (CNS) Trk occupancy. We describe herein the discovery of [¹¹C]-(*R*)-IPMICF16, a first-in-class positron emission tomography (PET) TrkB/C-targeting radiolabeled kinase inhibitor lead. Molecular imaging characterisation in four species is

provided including first-in-human. It is demonstrated that [^{11}C]-(*R*)-IPMICF16 readily crosses the blood-brain barrier (BBB) in rodents and selectively binds to TrkB/C receptors *in vivo*, as evidenced by entrectinib blocking studies. Notably, the brain disposition of [^{11}C]-(*R*)-IPMICF16 was found to be translatable to rhesus-monkeys and human. TrkB/C-specific binding in human brain tissue is observed *in vitro*, with specific reduction in the hippocampus of Alzheimer's disease (AD) versus healthy brains. These results illustrate for the first time the use of a kinome-wide selective radioactive probe for endogenous kinase PET neuroimaging in human.

5.2 Introduction

Specific interaction between the full-length catalytic tropomyosin receptor kinases TrkA/B/C (encoded by *NTRK1-3* respectively) and their cognate neurotrophin ligands (nerve growth factor (NGF), brain-derived neurotrophic factor (BDNF) and neurotrophin-3 (NT-3), respectively) crucially supports differentiation, growth and survival within distinct neuronal populations of the mammalian central (CNS) and peripheral nervous systems (PNS) as well as non-neural tissues during development and adult life.¹⁻³ Reduced expression or impaired signaling of Trk tyrosine kinase (TK) receptors in the CNS is found in an extensive spectrum of disorders and pathologies including ischemic brain injury, schizophrenia, Rett syndrome, depression and various neurodegenerative diseases.²⁻¹⁴ In addition to their central roles in neurobiology, all three members of the Trk family are proto-oncoproteins with well-defined oncogenic potential in human, both in neural and non-neural neoplasms.¹⁵⁻¹⁹ So far, the validation of Trk changes during aging and neurodegenerative diseases has solely originated from studies relying on immunohistochemical (IHC) detection and *in situ* hybridization (ISH) of post-mortem tissue^{11-13, 20-24} while preclinical assessment of brain exposure for anticancer Trk inhibitors (**Figure S5.1a** and **Table S5.1, Supporting Information**) has been circumscribed to the use of destructive methods²⁵⁻²⁶ due to the absence of a non-invasive approach to assess and quantify Trk levels *in vivo*.

Quantitative neuroimaging of proteins in humans using positron emission tomography (PET) is a robust *in vivo* approach which relies on short-lived radiolabeled small molecules.²⁷ Most clinical CNS radiotracers validated to date target G protein-coupled receptors (GPCR), ion channels, transporters and abnormally conformed proteins²⁸ (see also CNS Radiotracer Table <http://www.nimh.nih.gov/researchpriorities/therapeutics/cns-radiotracer-table.shtml>, accessed Oct 20, 2016). Clinical neuroimaging of CNS endogenous kinases has not yet been achieved despite key realisations in a few other enzyme classes.²⁸⁻³⁰ Given the importance of Trk (especially TrkB/C, which are most abundant in the CNS), we sought to develop a radiolabeled targeted kinase inhibitor for PET imaging to enable the visualisation and quantification of TrkB/C receptor density in healthy and diseased brains. An important advantage of the selection of a radiolabeled TKI rather than an extracellular binding compound resides in the intrinsic capacity of such probes to dissect pro-survival neuronal full-length TrkB/C receptors from catalytically-incompetent truncated isoforms (most notably TrkB.T1) largely present in glia.³¹⁻³²

Herein, we describe our radiotracer development effort in the assessment of [¹¹C]-(*R*)-**5.3** (referred herein as [¹¹C]-(*R*)-IPMICF16) as a first-in-class brain penetrating TrkB/C-targeted lead for PET neuroimaging. The work presented includes the radiotracer structure-activity relationship (SAR) characterization and comparative analysis leading to [¹¹C]-(*R*)-IPMICF16, the enantioselective synthesis of (*R*)-IPMICF16 and precursor thereof, as well as the entire *in vivo* imaging translational work in four species from early evaluation in rats and mice, preclinical non-human primates as well as first-in-human clinical PET imaging. We concomitantly provide proof-of-principle of *in vivo* TrkB/C target engagement in the living brain for [¹¹C]-(*R*)-IPMICF16 and TrkB/C receptor occupancy with pharmacological pre-dosing of the phase II clinical lead entrectinib using imaging experiments in mice. We also demonstrate that the radiotracer displays high TrkB/C-specific binding in human brain tissue and observes a distinct regional binding pattern in AD versus healthy control (HC) *in vitro*.

5.3 Results

5.3.1 Chemistry, biochemical evaluations and radiochemistry. Optimal compound triage for the development of neuroimaging PET radioligands entails the alignment of favorable physicochemical properties (molecular weight (MW) < 500 Da, topological polar surface area (TPSA) $\leq 80 \text{ \AA}^2$, hydrogen bond donor (HBD) ≤ 1 , $2 \leq \text{clogD} < 4$, $3 \leq \text{clogP} < 5$, $\text{pK}_a \leq 8$, rotatable bonds (RBs) < 5, flexibility for radiolabeling with carbon-11 ($t_{1/2} = 20.3 \text{ min}$) or fluorine-18 ($t_{1/2} = 109.8 \text{ min}$)) and pharmacological parameters (low nano or picomolar affinity, $B_{\text{max}}/K_D > 10$, > 30-100-fold target selectivity).^{28, 33-35}

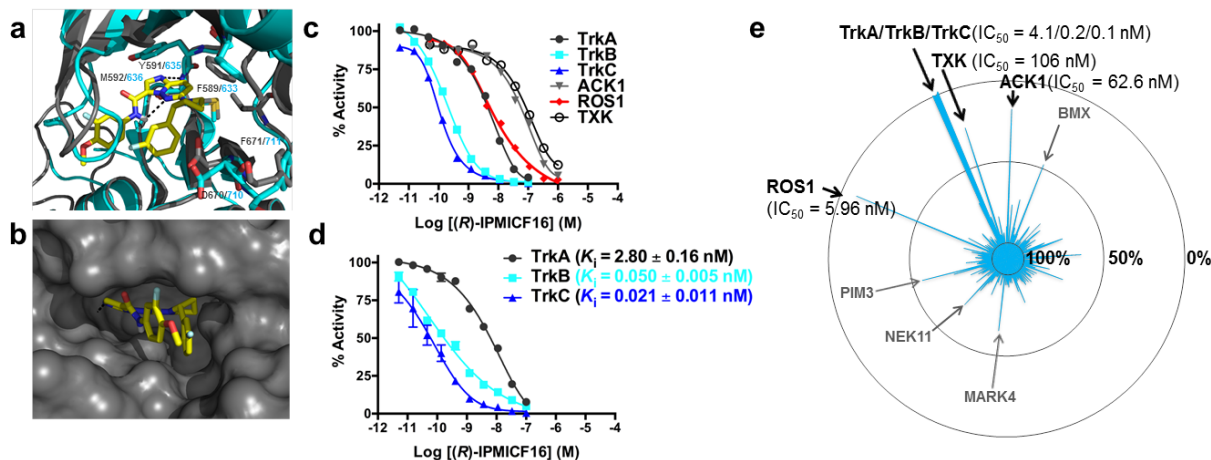


Figure 5.1. Binding mode, potency/affinity and kinome selectivity profiling of (R)-IPMICF16. (a) View of the predicted type-I binding mode of (R)-IPMICF16 with TrkA (grey ribbons, PDB: 4PMT) overlaid onto the X-ray crystal structure of TrkB (DFG-in conformation, cyan ribbons, PDB: 4AT3). (b) Surface rendering of (R)-IPMICF16 bound to the ATP binding site of TrkA illustrating the overlap between the 2-fluorophenylpyrrolidine moiety and the ribose pocket. (c) Dose-response curve for inhibitor (R)-IPMICF16 versus TrkA, TrkB, TrkC, ACK1, ROS1 and TXK (1 μM ATP, $n = 1$). (d) Dose-response curve for inhibitor (R)-IPMICF16 versus TrkA, TrkB, TrkC, ([ATP] = $K_{\text{m ATP}}$, $n = 3$, error bars represent standard deviation from the mean). (e) Comprehensive kinase selectivity profile of (R)-IPMICF16 against 369 kinases (Kinases are ordered alphabetically and data represented as radar chart with 100.0%, 50.0% and 0 % activity relative to control (200 nM, $n = 2$) ($[\gamma\text{-}^{33}\text{P}]\text{ATP}$ -based enzymatic assay performed by Reaction Biology).

We applied those principles in our selection process for radiotracer development from a recently reported library of 6-(2-(3-fluorophenyl)pyrrolidin-1-yl)imidazo[1,2-*b*]pyridazine pan-Trk inhibitors.³⁶ The validation of [^{11}C]-(*R*)-IPMICF16 as a potential clinical radiotracer emerged from

the preclinical validation of a series of racemic radiolabeled derivatives with picomolar potencies for TrkB/C which included [^{11}C]-(\pm)-IPMICF16 (**Figure S5.1a**, **Figure S5.2**, **Supporting Information**). A concomitant comparative advanced preclinical evaluation of the radiolabeled pan-Trk inhibitor [^{11}C]GW441756 (**Figure S5.1a**, **Supporting Information**)³⁷ is provided. Following preclinical validation in rodents and non-human primates (*vide infra*), radiotracer [^{11}C]-(\pm)-IPMICF16 was selected for structural refinement and the enantioselective synthesis of the putatively fitting *R*-enantiomer was undertaken (**Figure S5.1b**, **Supporting Information**, **Figure 5.1a,b**).^{36, 38}

The non-radioactive inhibitor (*R*)-IPMICF16 displays half-maximal inhibitory concentrations (IC_{50}s) of 4.0, 0.2 and 0.1 nM for human TrkA, TrkB and TrkC, respectively, in [γ - ^{33}P]ATP-based enzymatic assays (**Figure 5.1c**). Inhibitory measurements at K_m ATP and conversion using Cheng-Prusoff analysis³⁹ for competitive inhibition gave inhibitory constants (K_i) values of 2.80 ± 0.16 nM, 0.050 ± 0.005 nM and 0.021 ± 0.011 nM for TrkA, TrkB and TrkC respectively ($n = 3$, s.d.) ($\sim 200,000$ - $500,000$ -fold over K_m ATP for Trk)⁴⁰. (*R*)-IPMICF16 therefore exhibits notable intra-Trk isoform selectivities of 56-fold for TrkB and 133-fold for TrkC with regard to TrkA. In order to evaluate the broader selectivity profile of our lead, comprehensive kinome screening on a panel of 369 human kinases was conducted at 0.2 μM cut-off (Reaction Biology Corp., full wild type kinase panel). This assay revealed that (*R*)-IPMICF16 exhibits $>1000/2000$ -fold TrkB/C selectivity for 99% of targets tested, with only four kinases (BMX, TXK, ACK1 and ROS1) at or above their IC_{50} values for the tested concentration (**Figure 5.1e**, **Supplementary Information Section 6**). Aside from BMX, which was inhibited approximately at IC_{50} with (*R*)-IPMICF16 0.2 μM , individual dose response curves were generated for TXK, ACK1 and ROS1 revealing IC_{50}s of 106 nM, 62.6 nM and 5.96 nM respectively (**Figure 5.1c,e**). (*R*)-IPMICF16 exhibits ~ 30 - and 60-fold selectivity for TrkB and TrkC respectively versus ROS1 – the closest off-target identified. As anticipated, (*S*)-IPMICF16 displayed still acceptable TrkB/C

activities albeit in the nanomolar rather than the picomolar range (**Figure S5.3, Supporting Information**).^{36, 38}

Overall, for the purpose of this study, the radiosynthesis of [¹¹C]-(*R*)-IPMICF16 was implemented at four distinct production sites including a Good Manufacturing Practice (GMP)-compliant automated synthesis for first-in-human PET imaging. For human PET studies, [¹¹C]-(*R*)-IPMICF16 was prepared from (*R*)-**5.14** using [¹¹C]CH₃I in the presence of K₂CO₃ with radiochemical yields (RCYs) of 13.0 ± 2.0 % (s.d., decay-corrected RCYs at end-of-synthesis based upon [¹¹C]CO₂, *n* = 3, > 99% radiochemical purity), and specific activity of 118 GBq/μmol (**Figure S5.1b, Supporting Information**). Throughout the translational imaging study, the radiosynthesis of [¹¹C]-(*R*)-IPMICF16 was highly reproducible, robust and flexible to protocol adaptation (*n* > 40). In all cases, from preclinical to clinical PET, the identity of all radiotracers including [¹¹C]-(*R*)-IPMICF16, was confirmed by non-radioactive standard co-injection using high-performance liquid chromatography (HPLC) (**Supplementary Information Section 7**).

5.3.2 In vivo PET imaging of [¹¹C]-(*R*)-IPMICF16 in the rodent brain demonstrates rapid and specific TrkB/C binding. Initial PET imaging experiments with [¹¹C]-(*±*)-IPMICF16 in Sprague Dawley rats as part of the racemic series screening confirmed this scaffold as a lead based on overall brain penetration, brain-to-blood ratio and stability (**Figure S5.4a-c, Supporting Information**). The radioactivity uptake of [¹¹C]-(*R*)-IPMICF16 in the FVB mouse brain (wildtype mice) was rapid and peak brain uptake (maximum SUV) of 1.33 ± 0.19 (s.d.) was reached within 1 min following intravenous injection (i.v.) (SUV, standardized uptake value - normalization for injected dose and body weight) as illustrated by the corresponding whole-brain time-activity curve (TAC) (**Figure 5.2a,g**). The radiotracer was found extensively distributed within the CNS in accordance with reported TrkB expression (**Figure 5.2d,e,i**).⁴¹ Peak brain radioactivity was followed by moderate washout throughout the remainder of the 60 min scan (0.40 ± 0.02 SUV at 60 min post injection, s.d., $\Delta_{\text{SUVpeak-60min}} = - 69\%$). Biodistribution imaging

studies highlighted extensive liver uptake suggesting hepatobiliary clearance as the primary route of excretion (Figure 5.2h).

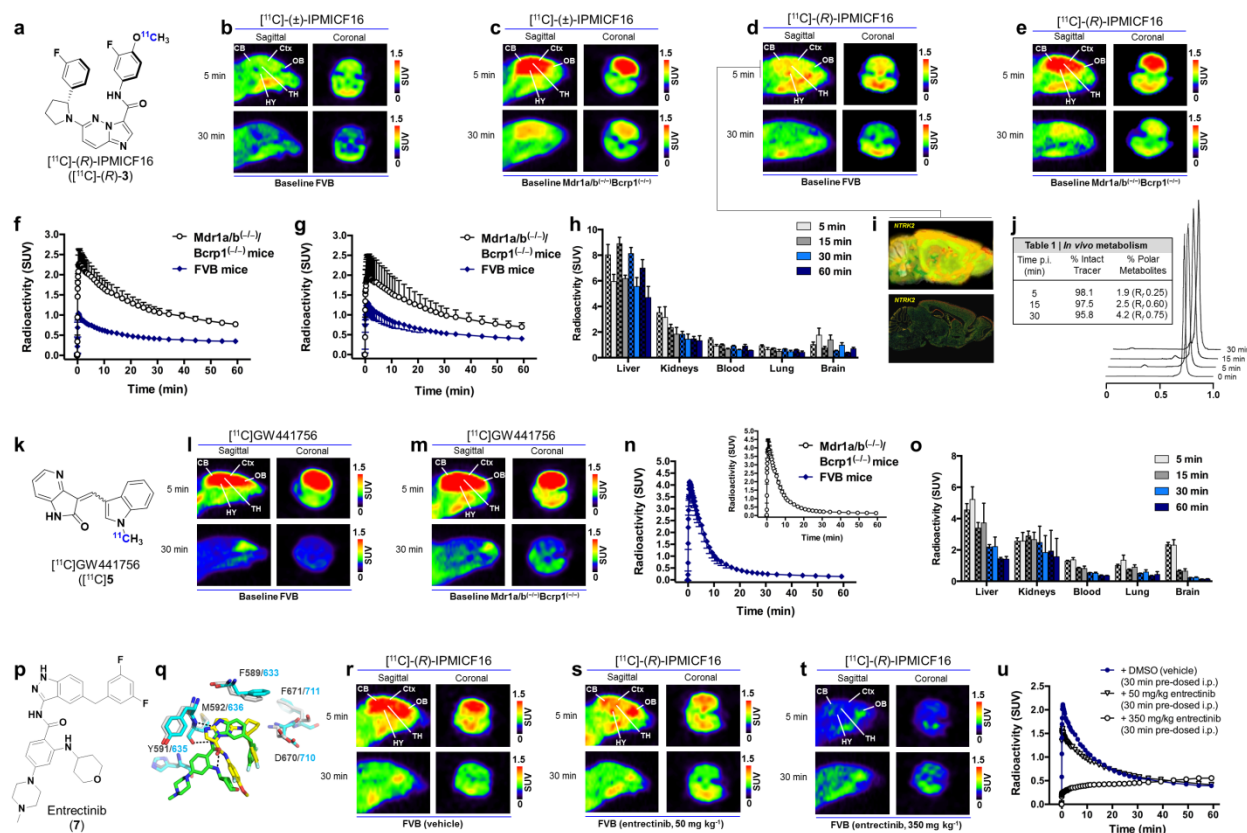


Figure 5.2. Preclinical *in vivo* PET imaging of [^{11}C](\pm)-IPMICF16, [^{11}C](*R*)-IPMICF16 and [^{11}C]GW441756 in FVB and *Mdr1a/b*^{-/-}*Bcrp1*^{-/-} mice, [^{11}C](*R*)-IPMICF16 *in vivo* stability and blocking studies. CB, cerebellum; Ctx, cortex; HY, hypothalamus; OB, olfactory bulb; TH, thalamus. Expressed as mean \pm SD. (a) Chemical structure of [^{11}C](*R*)-IPMICF16. (b) Representative brain images of [^{11}C](\pm)-IPMICF16 in FVB mice. (c) Representative brain images of [^{11}C](\pm)-IPMICF16 in *Mdr1a/b*^{-/-}*Bcrp1*^{-/-} mice. (d) Representative brain images of [^{11}C](*R*)-IPMICF16 in FVB mice. (e) Representative brain images of [^{11}C](*R*)-IPMICF16 in *Mdr1a/b*^{-/-}*Bcrp1*^{-/-} mice. (f) TACs for [^{11}C](\pm)-IPMICF16 brain uptake at baseline ($n = 3/\text{group}$). (g) TACs for [^{11}C](*R*)-IPMICF16 brain uptake at baseline ($n = 3/\text{group}$). (h) Selected biodistribution data presenting the accumulation of [^{11}C](*R*)-IPMICF16 in liver, kidneys, blood (heart), lung in comparison to brain over the duration the scans ($n = 3$; checkered colors = FVB mice; full colors = *Mdr1a/b*^{-/-}*Bcrp1*^{-/-} mice). (i) *NTRK2* transcripts analyzed by *in situ* hybridization in the Allen Brain Atlas project. Images are taken from the Allen Brain Atlas (<http://mouse.brain-map.org>). Image credit: Allen Institute for Brain Science. (j) *In vivo* [^{11}C](*R*)-IPMICF16 stability and metabolite composition at 5, 15 and 30 min post injection in FVB mouse ($n = 1$) with corresponding radio-TLC. (k) Chemical structure of [^{11}C]GW441756. (l) Representative brain images of [^{11}C]GW441756 in FVB mice. (m) Representative brain images of [^{11}C]GW441756 in *Mdr1a/b*^{-/-}*Bcrp1*^{-/-} mice. (n) TACs for [^{11}C]GW441756 brain exposition at baseline ($n = 3/\text{group}$). (o) Selected biodistribution data presenting the accumulation of [^{11}C]GW441756 in liver, kidneys, blood (heart), lung in comparison to brain over the duration the scans ($n = 3$; checkered colors = FVB mice; full colors = *Mdr1a/b*^{-/-}*Bcrp1*^{-/-} mice). (p) Chemical structure of Entrectinib (7). (q) Protein structure of NTRK2 with residues F589/G33, F671/G11, M592/G36, Y591/R33, and D670/G10 highlighted. (r) Brain PET images of [^{11}C](*R*)-IPMICF16 in FVB (vehicle). (s) Brain PET images of [^{11}C](*R*)-IPMICF16 in FVB (entrectinib, 50 mg kg⁻¹). (t) Brain PET images of [^{11}C](*R*)-IPMICF16 in FVB (entrectinib, 350 mg kg⁻¹). (u) TACs for [^{11}C](*R*)-IPMICF16 brain uptake in FVB mice treated with DMSO (vehicle) (30 min pre-dosed i.p.), 50 mg/kg entrectinib (30 min pre-dosed i.p.), or 350 mg/kg entrectinib (30 min pre-dosed i.p.).

mice). (p) Chemical structure of entrectinib. (q) Predicted binding mode of entrectinib (green sticks) overlaid onto the binding of (R)-IPMICF16 (yellow sticks) (TrkA; grey, PDB: 4PMT and TrkB; cyan, PDB: 4AT3). (r) Representative brain images of [¹¹C]-(R)-IPMICF16 in FVB mice following pretreatment with vehicle (DMSO, 100 μL, 30 min pre-dosed i.p.). (s) Representative brain images of [¹¹C]-(R)-IPMICF16 in FVB mice following pretreatment with 50 mg/kg entrectinib (DMSO solution, 100 μL, 30 min pre-dosed i.p.). (t) Representative brain images of [¹¹C]-(R)-IPMICF16 in FVB mice following pretreatment with 350 mg/kg entrectinib (DMSO solution, 100 μL, 30 min pre-dosed i.p.). (u) TACs for [¹¹C]-(R)-IPMICF16 brain uptake with entrectinib pretreatment in comparison to vehicle (*n* = 1/group).

Despite similar overall brain kinetics profile, with [¹¹C]-(±)-IPMICF16 lower maximum SUV (1.04 ± 0.12 at 0.5 min, s.d.) were reached as compared to the enantiopure radiotracer (**Figure 5.2b,c,f**). These results demonstrate that [¹¹C]-(R)-IPMICF16 readily diffuses through the blood-brain barrier (BBB) and persists moderately in the rodent brain while suggesting faster elimination of the racemate. Comparative analysis with [¹¹C]GW441756, the only available pan-Trk radiotracer lead previously reported was performed (**Figure 5.2k**). *In vivo* PET of [¹¹C]GW441756 in FVB mice revealed substantial and rapid brain penetration (maximum SUV of 4.14 ± 0.55 at 1 min, s.d.) which was followed by prompt and extensive washout (0.14 ± 0.02 SUV at 60 min post injection, s.d., $\Delta_{\text{SUVpeak-60min}} = -97\%$, **Figure 5.2l-n**) on par with previously reported data in rats.³⁷ Renal clearance was more prominent with [¹¹C]GW441756 compared to [¹¹C]-(R)-IPMICF16 (**Figure 5.2o**). With the expectation that Trk CNS binding should be associated with tracer retention in the brain to allow for eventual quantification, the kinetics of [¹¹C]GW441756, in contrast to [¹¹C]-(R)-IPMICF16, likely indicate limited target engagement in rodents due to rapid subsequent washout, despite extensive initial permeation of the BBB. This observation can be rationalized in part by the significantly higher potency of [¹¹C]-(R)-IPMICF16 compared to [¹¹C]GW441756 (34-46-fold potency difference for TrkB/C). Metabolite analysis revealed [¹¹C]-(R)-IPMICF16 to be particularly robust *in vivo*, with > 95% intact tracer 30 min post injection in mouse blood plasma (**Figure 5.2j**). In order to investigate potential efflux, baseline scans were then conducted in *Mdr1a/b*^(-/-)*Bcrp1*^(-/-) knockout mice with both [¹¹C]-(±)-IPMICF16 and [¹¹C]-(R)-IPMICF16 (as well as [¹¹C]-(±)-**5.4** – data presented in **Figure S5.4** and

Figure S5.2d-f, Supporting Information). Increased whole-brain uptake was observed for all tracers (**Figure 5.2b-g**) indicating that primary ABC transporter components P-glycoprotein (P-gp –*Mdr1a/b*) and breast cancer resistance protein (BCRP –*Bcrp1*) at the BBB play a role in elimination of the tracer from the brain in mice. In the case of IPMICF16 tracers (racemic and *R*), this effect was most pronounced with the racemate compared to the *R*-enantiomer with $\text{SUV}_{0-60\text{min}}(\text{FVB})/\text{SUV}_{0-60\text{min}}(\text{Mdr1a/b}^{(-/-)}\text{Bcrp1}^{(-/-)})$ ratios of 0.56 for [^{11}C]-(*R*)-IPMICF16 compared to 0.39 for [^{11}C]-(\pm)-IPMICF16 (**Figure 5.2f,g**). This result was however paralleled by opposite variations in blood radioactivity which may in part explain inter-tracer variations (**Figure 5.2h, Figure S5.5, Supporting Information**). Whole brain TACs displayed kinetics consistent with results obtained in FVB mice. Calcein-AM cellular assay in P-gp and BCRP overexpressing Madin-Darby Canine Kidney (MDCKII) cells and Lineweaver-Burk plot analysis confirmed (*R*)-IPMICF16 as a P-gp/BCRP substrate with moderate affinity (EC_{50} of $2.9 \pm 1.3 \mu\text{M}$ and $2.23 \pm 1.1 \mu\text{M}$ respectively, s.d., **Figure S5.6, Supporting Information**). Interestingly, while no difference was observed in the brain distribution of [^{11}C]GW441756 under microdosing PET imaging conditions between FVB and *Mdr1a/b}^{(-/-)}\text{Bcrp1}^{(-/-)}* mice groups (**Figure 5.2i-n**), the calcein-AM assay outlined P-gp interaction of GW441756 at higher doses (EC_{50} of $79.2 \pm 8.3 \mu\text{M}$, s.d.) (**Figure S6e, Supporting Information**). In contrast to (*R*)-IPMICF16, this disparity is consistent with the possibility that GW441756 acts as a weak P-gp inhibitor rather than a substrate.

Supported by recent next-generation sequencing (NGS) efforts, oncogenic Trk fusions have been described in over twenty tumor types, reinforcing the view that Trk chimeric proteins are low-frequency but recurrent oncogenic drivers in human cancer². Yet, concerns over neurotoxicity arising from sustained CNS Trk blockade upon treatment for peripheral conditions have been described^{15-16, 42-43} Current clinical trial efforts include genomically-driven phase II trials for *NTRK* fusion-positive patient subpopulations based on promising phase I results with

entrectinib (**Figure 5.2p**, **Figure S5.1a** and **Table S5.1, Supporting Information**).⁴⁴⁻⁴⁵ In order to provide unambiguous evidence for TrkB/C specific binding, we conducted Trk receptor heterologous blocking through pharmacological challenge *in vivo* using this inhibitor. [¹¹C]-(R)-IPMICF16 brain uptake following entrectinib administration (30 min intraperitoneal pre dosing) was investigated, simultaneously providing confirmation of brain penetration and target engagement of a currently advanced pan-Trk inhibitor clinical lead using a non-invasive technique (**Figure 5.2q**). Pretreatment doses were selected under and above a threshold of 240 mg/kg which was previously shown to achieve 0.43 brain-to-plasma ratio in mice with sustained treatment regimen (240 mg/kg/day in continuous 2 weeks administration).²⁵ We observed dose-dependent whole brain radioactivity reduction (SUV_{0-60min}) of -7% and -40% with 50 mg/kg and 350 mg/kg pretreated mice (single doses) compared to vehicle-treated control respectively (**Figure 5.2r-u**). At the time of maximum SUV (1 min post injection) in the vehicle-treated animals, brain concentration was reduced in animals treated with entrectinib at pharmacological doses (50 and 350 mg/kg respectively) by 29% and 88% respectively. This is consistent with a rapid brain penetration and target binding followed by a tracer washout. As expected, trends in brain-to-blood K_p ratios during dynamic scanning did not differ from SUV measurements as entrectinib pretreatment did not affect blood radioactivity upon [¹¹C]-(R)-IPMICF16 injection (as measured at 50 mg/kg). Data from a Calcein-AM cellular assay with MDCKII cells included herein also demonstrate that entrectinib is not a prominent substrate for P-gp or BCRP (**Figure S5.6f-h, Supporting Information**). At this point, [¹¹C]-(R)-IPMICF16 emerged as a unique lead on the basis of favorable pharmacology and imaging properties in FVB mice. In spite of its efflux liability at microdoses described in *Mdr1a/b*^(-/-)*Bcrp1*^(-/-) mice, the choice of [¹¹C]-(R)-IPMICF16 was supported by documented inter-species variation in intracerebral disposition of actively effluxed PET tracers between rodents and higher species which was in line with our concurrently collected data in non-human primates (*vide infra*).^{33, 46-47}

5.3.3 [¹¹C]-(R)-IPMICF16 accumulates in the non-human primate brain in accordance to TrkB/C expression. [¹¹C]-(R)-IPMICF16 brain uptake was higher in non-human primates compared to rodents and displayed distinctively slow brain kinetics characterized by steady radioactivity increase without washout from brain tissue for the entire duration of the 60 min scan (**Figure 5.3a, Figure S5.7e, Supporting Information**). Based on volumetric region-of-interest (ROI) analysis, [¹¹C]-(R)-IPMICF16 uptake was shown to be heterogeneously distributed, ubiquitous across gray matter regions and most pronounced in the thalamus (~0.8 SUV at 60 min post injection) while white matter displayed comparatively low accumulation (~0.3 SUV at 60 min post injection) matching known TrkB/C receptor distribution (thalamus ≥ cerebellum ≥ cortex >>> white matter) (**Figure 5.3a, Figure S5.7e, Supporting Information**). Binding kinetics of [¹¹C]-(R)-IPMICF16 were different from [¹¹C]-(±)-IPMICF16, exhibiting higher gray matter uptake compared to the racemic tracer 60 min post injection (**Figure 5.3b, Figure S5.7d,e, Supporting Information**). [¹¹C]-(R)-IPMICF16 also presented significantly higher test-retest reproducibility of SUVs compared to [¹¹C]-(±)-IPMICF16. Brain pharmacokinetics of [¹¹C]GW441756 contrasted with [¹¹C]-(R)-IPMICF16, reaching maximum SUV of 2.41 SUV in cerebellum at 4 min post injection (2.17 SUV in thalamus at 2.5 min) followed by sustained washout (**Figure 5.3c and Figure S5.7f, Supporting Information**). Whole brain washout in primates was however reduced compared to mice (0.62 SUV at 60 min post injection, $\Delta_{\text{SUV}_{\text{peak-60min}}} = -65\%$). [¹¹C]GW441756 and [¹¹C]-(R)-IPMICF16 showed identical brain concentration 60 min post injection despite opposite kinetic trends. Based on known CNS TrkB/C full length levels, regional gray-to-white matter SUV ratios ($\text{SUV}_{\text{gray matter}}/\text{SUV}_{\text{white matter}}$) were used as an estimate for specific binding and tracer prioritization. As illustrated in **Figure 5.3d**, specific signal approximations using summed SUV ratios for 30–60 min post injection were markedly higher for [¹¹C]-(R)-IPMICF16 compared to [¹¹C]-(±)-IPMICF16 and [¹¹C]GW441756 in all gray matter regions with representative average values of 2.3 and 2.1 in the thalamus and cerebellum

respectively (similar trends were observed in 0-60 min summed data, **Figure S5.8, Supporting Information**). Despite [^{11}C]GW441756 displaying higher uptake than [^{11}C]-(*R*)-IPMICF16, the use of this tracer is impeded by lower specific binding, inferior target selectivity and intrinsic contamination with an inseparable [^{11}C]-(*E*)-GW441756 inactive photoisomer,³⁷ which constitute major hurdles to clinical translation. Taken together, the results obtained with [^{11}C]-(*R*)-IPMICF16 in primates are in contrast to the efflux kinetic profile in rodents and are indicative of a moderate and continuous brain uptake as well as favorable TrkB/C specific signal properties in the primate brain.

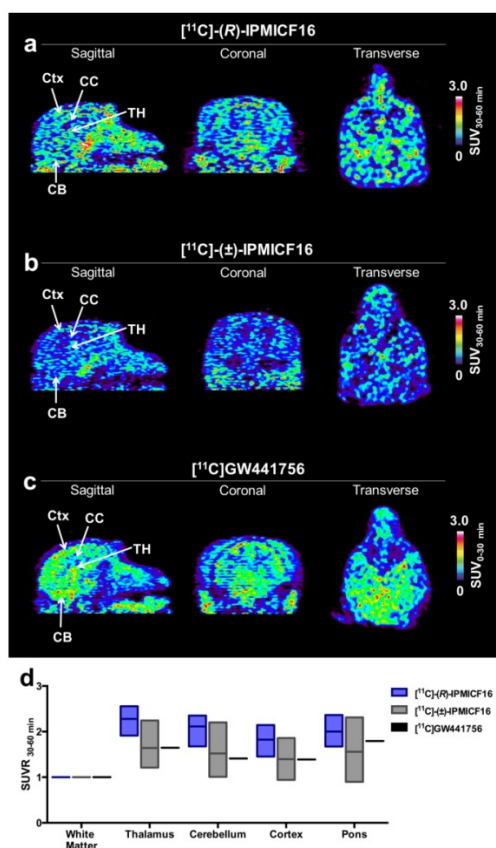


Figure 5.3. *In vivo* PET imaging of [^{11}C]-(*R*)-IPMICF16, [^{11}C]-(\pm)-IPMICF16 and [^{11}C]GW441756 in the rhesus monkey brain. CB, cerebellum; CC, corpus callosum; Ctx, cortex; TH, thalamus. (a) Representative *in vivo* PET images of [^{11}C]-(*R*)-IPMICF16. (b) Representative *in vivo* PET images of [^{11}C]-(\pm)-IPMICF16. (c) Representative *in vivo* PET images of [^{11}C]GW441756. (d) Comparative regional SUVR ratio (SUVR, summed 30-60 min) for [^{11}C]-(*R*)-IPMICF16 ($n = 3$), [^{11}C]-(\pm)-IPMICF16 ($n = 3$) and [^{11}C]GW441756 ($n = 1$). [^{11}C]-(*R*)-IPMICF16 displays higher gray-to-white matter SUVR compared to [^{11}C]-(\pm)-IPMICF16 and [^{11}C]GW441756.

5.3.4 [^{11}C]-(*R*)-IPMICF16 binds *TrkB/C* in human post-mortem brain tissue and parallels decreased *TrkB* hippocampal density in AD brain tissue *in vitro*. To further assess the binding specificity and selectivity of our lead radiotracer in brain tissue as well as to provide proof-of-principle evidence of its potential use in the context of neurodegenerative diseases, *in vitro* autoradiography experiments using post-mortem tissue from human healthy control (HC) and aged-matched AD patient groups were conducted. Binding properties of [^{11}C]-(*R*)-IPMICF16 were measured in four brain regions (20 μM cryosections) including the hippocampus which has been shown to undergo drastic *TrkB* full length reduction in AD brains¹³⁻¹⁴ as well as unaffected regions with regards to *TrkB* expression (e.g. parietal cortex and cerebellum).⁴⁸

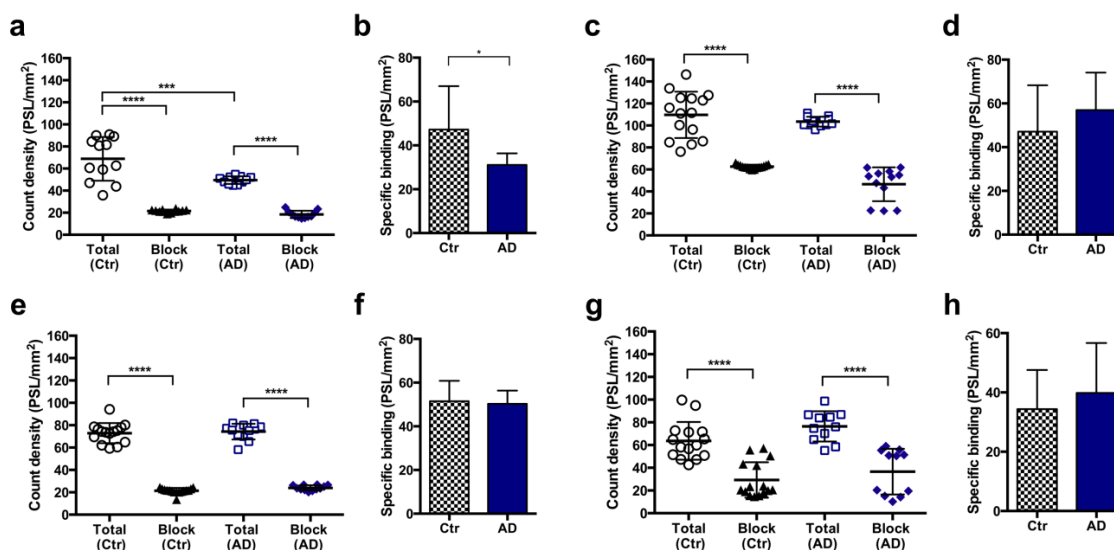


Figure 5.4. Regional quantification for the *in vitro* human brain tissue autoradiography experiments with [^{11}C]-(*R*)-IPMICF16. Quantification for the hippocampus ($n = 11-12$) (a,b), inferior parietal cortex ($n = 12-15$) (c,d), prefrontal cortex ($n = 12-15$) (e,f) and cerebellum ($n = 11-15$) (g,h) for baseline ([^{11}C]-(*R*)-IPMICF16) and blocking ([^{11}C]-(*R*)-IPMICF16 + GW441756, 10 μM) of healthy control (black) and AD (blue) human brain cryosections. PSL/mm² = photo-stimulated luminescence events per square millimetre. Specific binding_{Ctrl/AD} = Total_{Ctrl/AD} - Block_{Ctrl/AD}. Expressed as mean \pm SD. *** $P \leq 0.001$, **** $P \leq 0.0001$.

In an initial series of baseline experiments using HC human brains ($n = 12-15$), [^{11}C]-(*R*)-IPMICF16 displayed extensive, yet heterogeneous total binding in all regions mirroring the near-

ubiquitous expression of TrkB/C in neurons of the mammalian brain as characterized using [¹²⁵I]BDNF, [¹²⁵I]NT-3 and [¹²⁵I]NT-4/5 and mRNA hybridization (**Figure 5.4** and **Figure S5.9, Supporting Information**).⁴¹ In order to evaluate the extent of specific binding (impact of brain lipids and proteins non-specific binding) and TrkB/C selectivity (impact of off-target receptor-mediated interactions), competition blocking experiments using the chemically distinct selective pan-Trk type I inhibitor GW441756 (10 μM) were conducted in HC brains. Heterologous blocking was prominent in all analyzed ROIs ($P \leq 0.0001$) with the most pronounced effects observed in the prefrontal cortex ($\Delta \sim -71\%$, $n = 15$) and hippocampus ($\Delta \sim -69\%$, $n = 12$), while significant albeit less pronounced blocking was observed in the inferior parietal cortex ($\Delta \sim -43\%$, $n = 15$) and cerebellum ($\Delta \sim -54\%$, $n = 15$), revealing high specific and TrkB/C-selective binding of [¹¹C]-(R)-IPMDCF16 throughout the brain (**Figure 5.4**). Total or specific/selective binding inter-individual variability did not correlate with gender, age or post-mortem delay in HC samples. Having demonstrated excellent TrkB/C-binding in human healthy brains, measurements of total and specific/selective binding of [¹¹C]-(R)-IPMDCF16 in post-mortem tissue from AD patients in the corresponding ROIs ($n = 11-12$) were performed. Total tracer binding and specific/selective-TrkB/C binding were found to be significantly reduced in the hippocampus of AD brains compared to HC ($\Delta \sim -35\%$, $P \leq 0.001$) as reported using IHC and ISH techniques.¹³⁻¹⁴ With the exception of this effect, non-specific/non-selective levels upon blocking with GW441756 in AD brains were similar to the observations from HC brains suggesting strong TrkB/C interaction in the AD group as well ($P \leq 0.0001$). No additional noticeable differences between AD and HC groups in total tracer binding or specific/selective binding were observed in the other regions analyzed. Again, inter-individual binding differences within the AD brain samples could not be ascribed to differences in gender, age or post-mortem delay.

5.3.5 Imaging TrkB/C in the human brain using [^{11}C]-(*R*)-IPM1CF16. These encouraging preclinical data prompted the evaluation of [^{11}C]-(*R*)-IPM1CF16 as a radiotracer for use in humans *in vivo*. First-in-human brain uptake measurements of [^{11}C]-(*R*)-IPM1CF16 were performed in one healthy male volunteer (41 years of age). Radiotracer brain uptake was prompt with maximum SUV reached in all analyzed ROIs at 25 sec post injection (including white matter) (1.5 SUV in the thalamus) followed by rapid stabilization and steady retention with negligible decrease during the 60 min scan.

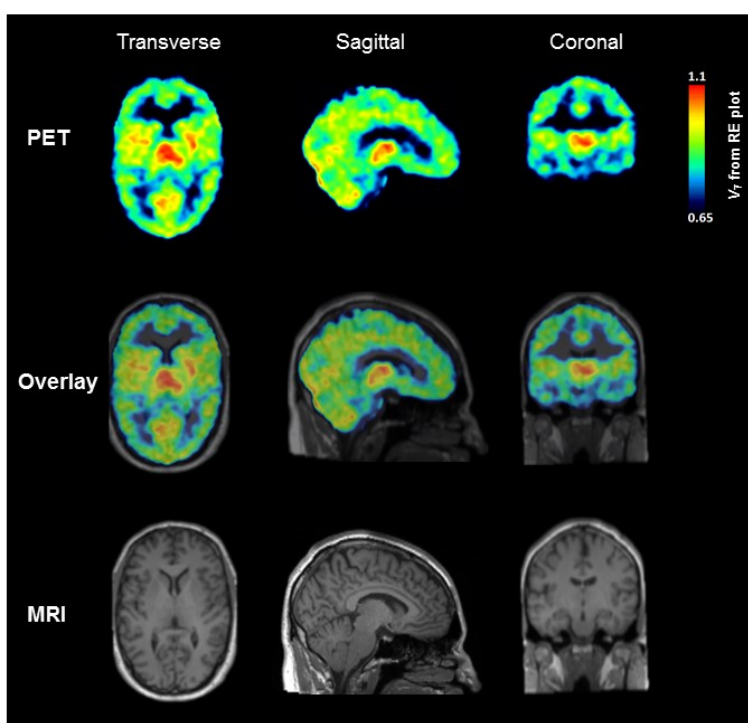


Figure 5.5. *In vivo* PET imaging of [^{11}C]-(*R*)-IPM1CF16 in the human brain. Top row: V_T images (RE plot) of the human subject illustrating the distribution of TrkB/C. The highest values are observed in the thalamus, followed by cerebellum and cortical gray matter, with low values in white matter. Middle row: fusion with the subject MR for anatomic localization. Bottom row: T1 MP-RAGE MR image of the subject.

The uptake was heterogeneous but prevalent within the gray matter regions with the highest uptake seen in the thalamus (0.7 SUV) and lowest in white matter (0.4 SUV) with overall distribution aligning with non-human primate results and known TrkB/C expression (thalamus \geq cerebellum \geq cortex \gg white matter) (Figure S5.10a, Supporting Information). Uptake in

gray matter regions was superior to white matter at all time points. The mean plasma-to-blood ratio was 1.04 and the unbound fraction in the plasma ($F_{u,p}$) was $87 \pm 5\%$ (s.d., based on 3 measurements made 6, 18, and 20 min post injection) (Figure S5.11, Supporting Information). Figure S5.10b (Supporting Information) summarizes the data of the kinetic analysis. Since volume of distribution (V_T) derived from relative equilibrium-based graphical plot (RE plot) images showed a more robust result compared to the Logan plot, these images are used to visualize V_T distribution in Figure 5.5. There were no adverse events or clinically detectable pharmacologic effects associated with the injection of [^{11}C]-(*R*)-IPMICF16.

5.4 Discussion

The development of the first lead radiotracer for non-invasive PET imaging of TrkB/C receptors in the living brain is described. Human PET imaging with [^{11}C]-(*R*)-IPMICF16 was translated from preclinical research and demonstrated moderate brain uptake in agreement with regional TrkB/C distribution and favorable gray-to-white matter ratios. It was shown that obstacles commonly associated with the development of orthosteric probes for intracellular *in vivo* neuroimaging of protein kinases such as i) the combination of favorable physicochemical properties for rapid membrane diffusion (see result section), ii) the achievement of adequate affinity in light of high intracellular ATP concentration, as well as iii) the realization of sufficient target selectivity within the human protein kinome which presents highly conserved ATP/inhibitor-binding site can be overcome by thorough SAR screening. Our biochemical examination showed that (*R*)-IPMICF16 displays intrinsic affinity in the low picomolar range for TrkB/C. Moreover, we demonstrated that (*R*)-IPMICF16 displays exceptional kinome selectivity in comprehensive screenings (including notably TrkA) well beyond the 30-100-fold threshold considered necessary for CNS radiotracers.^{28, 33} Importantly, unwanted interaction with ROS1, the only target for which (*R*)-IPMICF16 shows less than 100-fold selectivity identified to date, is not an impediment foreseen due to the lack of detectable *ROS1* levels in normal human brain

tissue.⁴⁹ Based on available data, (*R*)-IPMICF16 displays both the highest affinity for TrkB/C and the best kinome selectivity of all pan-Trk inhibitors characterized to date and therefore constitutes a prime lead for radiotracer development.

A central objective of the present report is to provide the most comprehensive overview of the development of [¹¹C]-(*R*)-IPMICF16 from radiotracer design to human use. At its core, the work presented here was enabled by the efficient enantioselective synthesis of the required non-radioactive standard and non-precursor as well as by the reliable radiosynthesis of [¹¹C]-(*R*)-IPMICF16. In particular, we showed that [¹¹C]-(*R*)-IPMICF16 can be obtained in high specific activity, excellent radiochemical purity as well as sufficient isolated RCYs both in manual radiosyntheses as well as in fully GMP-compliant automated radiosyntheses for use in clinical studies. In addition, with extensive metabolism often emerging as a detrimental factor precluding radiotracer development, we investigated the stability of [¹¹C]-(*R*)-IPMICF16 *in vivo*. Only < 5% of emerging polar metabolites were detected during *in vivo* radio-TLC metabolism studies. No lipophilic metabolites that could pass the BBB were observed. Our report also highlights the importance of multi-tracer/multi-species translational studies in the context of PET radiotracer development.

To provide additional evidence of TrkB/C specificity and selectivity of [¹¹C]-(*R*)-IPMICF16 in brain tissue, we determined radiotracer binding properties in autoradiography experiments using healthy human brain tissue. In a first set of data collected using HC tissue, we showed extensive specific and selective binding, using the selective pan-Trk inhibitor GW441756 as a second structurally distinct heterologous pharmacological competitor. Anomalies in neurotrophin/Trk receptor systems have been described in various CNS diseases and conditions and are best characterised in the context of AD. For instance, genome association analysis has suggested a possible role for polymorphism of the genes for both *BDNF* and *NTRK2* (TrkB) as risk factors in AD,⁵⁰ although this remains a subject of debate.⁵¹ Direct

evidence of involvement of the BDNF/TrkB system in AD comes from studies indicating that TrkB full length levels are profoundly decreased in the hippocampus of patients with AD,¹³ although apparently not in the parietal cortex.⁴⁸ Moreover, progressive loss of TrkB signal (as well as of the TrkA/C variants) in basal forebrain cholinergic nuclei is well correlated with the clinical progression of the disease.¹¹ Treatment with agonists of the BDNF/TrkB system in transgenic mice models of AD results in an increase of dendritic spines in the hippocampus and cortex, an inhibition of neuronal apoptosis and neurodegeneration, and improves spatial memory performance.⁵²⁻⁵⁴ We therefore used AD as a proof-of-concept for the application of [¹¹C]-(*R*)-IPM1CF16 as quantitative radiotracer, and determined a [¹¹C]-(*R*)-IPM1CF16 specific binding profile in AD brains as a parallel study to our HC experiments. Considering known trends previously measured using IHC, we show that hippocampal [¹¹C]-(*R*)-IPM1CF16 binding is significantly decreased in AD versus HC. Those results indicate the potential use for Trk PET radiotracers in the study and diagnosis of neurodegenerative diseases.

5.5 Conclusion

In conclusion, our study provides a novel molecular imaging probe for the non-invasive study of neuronal signal transduction at the interface of neurology and oncology which is as of yet unexplored. Importantly, the data described herein delineates, to the best of our knowledge, the first use of a small molecule kinase inhibitor radiotracer as an *in vivo* tool to assess endogenous kinase densities using PET neuroimaging in human. Collectively, our preclinical and clinical data demonstrate that [¹¹C]-(*R*)-IPM1CF16 represents a promising neuroimaging lead tracer for TrkB/C. The data presented here also establish a profound basis to lead towards future efforts in the functional study of kinases *in vitro* and *in vivo* in the context of drug development and neurodegenerative diseases.

ACKNOWLEDGEMENTS

We thank Dr. Esther Schirrmacher for reading the manuscript and providing useful comments. We are thankful to Angelina Morales-Izquierdo, Karine Gilbert and Alexandra Furtos for the mass spectrometry and SFC analyses. We are also grateful to Dave Clendening and Blake Lazurko from the Edmonton PET Centre and Gassan Massarweh and Dean Jolly from the Montreal Neurological Institute for radionuclide production. We thank Michel Simard for the X-ray crystallographic service. We are also grateful to Frank Wuest for access to radiochemistry laboratory for the small animal PET imaging work. This work was financially supported by Canada Foundation for Innovation (CFI) project no. 203639 to R.S, Cancer Research Society and C⁷ Council to RS, Natural Science and Engineering Research Council of Canada (NSERC) to RS and Weston Brain Institute to RS and US Department of Energy / National Institute of Biomedical Imaging and Bioengineering (DE-SC0012484) to PJHS.

COMPETING FINANCIAL INTERESTS

The authors declare no competing financial interests.

5.6 Material and methods

Chemical Syntheses. The general procedures for chemistry are provided in *SI Appendix* (Supplementary Information Section 3). The detailed chemical syntheses and characterization of all new compounds, including the synthetic sequence leading to *N*-(3-fluoro-4-methoxyphenyl)-6-((*R*)-2-(3-fluorophenyl)pyrrolidin-1-yl)imidazo[1,2-*b*]pyridazine-3-carboxamide ((*R*)-IPMICF16) and the phenolic precursor *N*-(3-fluoro-4-hydroxyphenyl)-6-((*R*)-2-(3-fluorophenyl)pyrrolidin-1-yl)imidazo[1,2-*b*]pyridazine-3-carboxamide as well as ^1H and ^{13}C spectra of new compounds and chiral SFC analysis are provided in *SI Appendix* (**Figure S5.1** and **Supplementary Section 3-5** and **8**).

***In Vitro* Biological Evaluations.** The potencies of (*R*)-IPMICF16 and (*S*)-IPMICF16 and the K_i values and selectivity profile (369 kinases) for (*R*)-IPMICF16 were obtained through [γ - ^{33}P]ATP-based enzymatic assays (Reaction Biology Corporation, Malvern, PA). Complete description of the assays can be found in the *SI Appendix* (**Supplementary Information Section 6**).

Docking analyses. Molecular docking simulations of (*R*)-IPMICF16 were performed using the X-ray co-crystal structure of the TrkB-cpdn5 complex (PDB code: 4AT3), the TrkA-N4-(4-morpholinophenyl)-N6-(pyridin-3-ylmethyl)pyrido-[3,2-*d*]pyrimidine-4,6-diamine complex (PDB code: 4PMT) using the FITTED 3.5 program (FORECASTER platform). Docking structures and figures were prepared using Pymol.

P-gp/BCRP Assays and Lineweaver-Burk plot analysis. *Cell Culture.* Native MDCKII cells or stably transfected with human P-gp or wild-type BCRP (482A) were seeded at a density of 156.250 cells/cm² using Dulbecco's modified Eagle's medium (DMEM) with 10% FCS, 4.0 mM L-Glutamine, 100 U/ml Penicillin, 100 $\mu\text{g}/\text{ml}$ Streptomycin and 100 $\mu\text{g}/\text{ml}$ Kanamycin (Biochrom, Munich, Germany) and split after reaching cell confluency to 70-80%. Cell passages from 7-25 have been used throughout the experiments. *Calcein-AM Uptake-Assay.* The assay for quantifying P-gp efflux activity was performed as described previously.⁵⁵ Briefly, human P-gp overexpressing MDCKII cells were washed two times with Krebs-Ringer Buffer (142 mM NaCl, 3 mM KCl, 1.5 mM $\text{K}_2\text{HPO}_4 \cdot 3 \text{H}_2\text{O}$, 10 mM HEPES, 4 mM D-Glucose, 1.2 mM MgCl_2 , 1.4 mM CaCl_2 , pH 7.4) and preincubated with 100 μl of double-concentrated modulator for 15 min that was followed by addition of 100 μl 4°C cold 2 μM Calcein-AM (Sigma-Aldrich, Taufkirchen, Germany) solution for 30 min. Plates were incubated at 37°C at 200 rpm. Control cells were exposed to Calcein-AM in absence of a transport modulator. Subsequently, MDCKII cells were

washed with ice-cold Krebs-Ringer Buffer to stop transporter activity and intracellular fluorescence was released after incubation with 0.1% Triton X for 20 min at 37°C. The amount of intracellular fluorescence was recorded using a fluorescence plate reader (Tecan Infinite F200 Pro, $\lambda_{(\text{excitation})} = 485 \text{ nm}$ and $\lambda_{(\text{emission})} = 520 \text{ nm}$). Background fluorescence was subtracted from each signal and intracellularly accumulated fluorescence was related to control cells. EC_{50} values were calculated via non-linear regression using the 4-parameter logistic equation with variable Hill-slope (GraphPad Prism[®] version 6.01) to generate dose-response curves. *Lineweaver-Burk Plot*. First, Michaelis-Menten Kinetics were calculated from efflux experiments measuring extracellular fluorescence every 90 sec on a Tecan Infinite F200 Pro. The kinetics were determined by assigning the linear gradient of the efflux curve (RFU (relative fluorescent unit) per time) as velocity ($v = \text{RFU}/\text{time}$) against the respective Calcein-AM concentration ($[S] = 1, 2 \text{ and } 3 \mu\text{M}$) according to the following equation:

$$\frac{v_{\max} * [S]}{K_m + [S]} = v$$

where v represents the efflux velocity, v_{\max} the maximum reaction velocity, $[S]$ the Calcein-substrate concentration and K_m the Michaelis-Menten constant. A Lineweaver-Burk-Plot was obtained by plotting $1/v$ as the ordinate against $1/[S]$ as the abscissa to estimate the type of inhibitory mode. *BODIPY-Prazosin Uptake-Assay*. BCRP efflux activity was analysed in native and human Bcrp MDCKII cells employing a flow cytometer (FACSCalibur[™] flow cytometer, Becton–Dickinson). In general, the net uptake of the BCRP-specific fluorescent substrate BODIPY-Prazosin into MDCKII cells in presence or absence of BCRP modulators or non-modulators was determined.⁵⁶ MDCKII cells were grown as monolayer, trypsinised and the density adjusted to 2.5×10^7 cells/ml in DMEM/Ham's F12 1:1. Hence, cells were washed twice with 37°C pre-warmed medium and increasing concentrations of test compound added to a volume of 600 μl cell suspension. Cells were incubated for 15 min at 37°C and 300 μl BODIPY-Prazosin in DMEM/Ham's F12 1:1 (2 μM) was added to a final concentration of 0.5 μM and incubated for 30 min at 37°C, 700 rpm (Thermoshaker Incubator, Thriller[®], Peqlab). Subsequently, the incubation was stopped with ice-cold medium and suspensions were centrifuged at $200 \times g$ for 5 min and washed with 4°C PBS (2% FCS). Finally, intracellular BODIPY-Prazosin fluorescence was measured using a FACSCalibur[™] flow cytometer equipped with a 488 nm argon laser and a 530/30 band-pass filter. By gating on forward and sideward scatter, MDCKII cells were selected and dead cells excluded likewise using propidium iodide staining (1.0 $\mu\text{g}/\text{ml}$). Twenty thousand cells were sorted in one run. Data were analysed with

CellQuest™ Pro (Franklin Lakes, NJ, USA). The increase in intracellular fluorescence (MF, median fluorescence) caused by a test compound was referred to control fluorescence levels (100%) and given as percentage of control.

Radiochemical Syntheses. The general procedures for radiochemistry for all 4 production sites are provided in *SI Appendix (Supplementary Information Section 7)*. The complete descriptions of the radiochemical syntheses for preclinical studies (three sites: manual synthesis at the Edmonton PET Center (University of Alberta), automated synthesis at the McConnell Brain Imaging Center (McGill University) and automated synthesis at the University of Michigan PET Center (University of Michigan)) and first-in-human study (one site: Ludwig-Maximilians-University of Munich) are provided in *SI Appendix (Supplementary Information Section 7)*. The manual and automated radiosyntheses of [¹¹C]-(\pm)-IPMICF16 and [¹¹C]-(*R*)-IPMICF16 proceeded from the desmethyl phenolic precursors and the manual and automated radiosyntheses of [¹¹C]-(\pm)-IPMICF22 proceeded from the corresponding primary amide as described in *SI Appendix*. The manual radiosyntheses of [¹⁸F]-(\pm)-IPMICF6, [¹⁸F]-(\pm)-IPMICF10 and [¹¹C]GW441756 were performed as previously reported^{36,38}.

Rodent PET Imaging Studies. *Animals.* All animal studies were carried out according to the guidelines of the Canadian Council on Animal Care (CCAC) and approved by the Cross Cancer Institute Animal-Care Committee (AC14214). *In vivo* studies were done using female Sprague Dawley rats (body weight: 320-420 g, University of Alberta, Edmonton, AB, Canada, 6-12 months of age), normal female FVB mice (body weight: 24-30 g, Charles-River Laboratories, Quebec, Canada, 3-9 months of age) and female *Mdr1a/b*^(-/-)*Bcrp1*^(-/-) mice (body weight: 24-30 g, Taconic, Hudson, NY, USA, 3-9 months of age). *Imaging procedure and analysis.* PET imaging scans of [¹⁸F]-(\pm)-IPMICF6, [¹⁸F]-(\pm)-IPMICF10, [¹¹C]-(\pm)-IPMICF16, [¹¹C]-(\pm)-IPMICF22, [¹¹C]-(*R*)-IPMICF16 and [¹¹C]GW441756 were performed on an INVEON® PET scanner (Siemens Preclinical Solutions, Knoxville, TN, U.S.A.). PET imaging experiments followed the same procedure for all 6 radiotracers: Prior to radiotracer injection, rodents were anesthetized through inhalation of isoflurane in 40% oxygen/ 60% nitrogen (gas flow 1 L/min), and body temperature was kept constant at 37 °C. Mice or rats were placed in a prone position into the center of the field of view. A transmission scan for attenuation correction was only acquired for rat experiments, not for mice. Mice were injected with 10-50 MBq of ¹¹C-labeled radiotracer in 100-150 μ L of isotonic saline solution (0.9% w/v of NaCl) through a tail vein catheter. Rats were injected with 15-72 MBq of ¹¹C-labeled or 11-21 MBq of ¹⁸F-labeled radiotracer in 200-600 μ L of saline solution (0.9% w/v of NaCl). Data acquisition was performed over 60 min in 3D list mode.

The dynamic list mode data were sorted into sinograms with 54 time frames (10 × 2, 8 × 5, 6 × 10, 6 × 20, 8 × 60, 10 × 120, 6 × 300 s). The frames were reconstructed using maximum a posteriori (MAP) as reconstruction mode. No correction for partial volume effects was applied. The image files were processed using the ROVER v2.0.51 software (ABX GmbH, Radeberg, Germany). Masks defining 3D regions of interest (ROI) were set, and the ROIs were defined by 50% thresholding. Mean standardized uptake values [$SUV_{\text{mean}} = (\text{activity/mL tissue})/(\text{injected activity/body weight}), \text{mL/g}$] were calculated for each ROI, and time–activity curves (TAC) were generated. All semi-quantified PET data are presented as means ± SD.

Metabolic Stability Study *in Vivo*. One normal FVB mouse was anesthetized through inhalation of isoflurane in 40% oxygen/60% nitrogen (gas flow 1 L/min) prior to intravenous injection of 117 MBq [^{11}C]-(*R*)-IPMICF16 via the tail vein. Venous blood samples were collected at 5, 15 and 30 min post injection through the tail vein catheter and further processed as follows: Blood cells were separated by centrifugation (13,000 rpm × 5 min). The supernatant was removed, and proteins were precipitated by addition of 2 volume parts of methanol (2 vol of MeOH/1 vol of sample). Another centrifugation step (13,000 rpm × 5 min) was performed to separate plasma as supernatant from the precipitated proteins. The clear plasma supernatants were analyzed by radio-TLC to determine the fraction of intact radiotracer (10%MeOH/CH₂Cl₂ $R_f = 0.8$).

Non-Human primates PET Imaging Studies. *Animals.* All primate imaging studies were performed in accordance with the standards set by the University Committee on Use and Care of Animals (UCUCA) at the University of Michigan. Imaging was done using a mature female rhesus monkey (*Macaca mulatta*) (body weight = 6.1 kg with negligible variation throughout the duration of the study, 15 years of age). ***Imaging procedure and analysis.*** PET imaging of [^{11}C]-(\pm)-IPMICF6, [^{11}C]-(\pm)-IPMICF10, [^{11}C]-(\pm)-IPMICF16, [^{11}C]-(\pm)-IPMICF22, [^{11}C]-(*R*)-IPMICF16 and [^{11}C]GW441756 was done using the Concorde Microsystems MicroPET P4 tomograph. PET imaging experiments followed the same procedure for all 6 radiotracers analyzed. The animal was anesthetized (isoflurane) and intubated, a venous catheter was inserted into one hindlimb and the animal positioned on the bed of the MicroPET gantry. A head-holder was used to prevent motion artifacts. Isoflurane anesthesia was continued throughout the study. Following a transmission scan, the animal was injected *i.v.* with the radiotracer (96-167 MBq) as a bolus over 1 min, and the brain imaged for 90 min (5 × 1 min frames – 2 × 2.5 min frames – 2 × 5 min frames – 7 × 10 min frames) for ^{18}F radiotracers or 60 min (5 × 1 min frames – 2 × 2.5 min frames – 2 × 5 min frames – 4 × 10 min frames) for ^{11}C radiotracers. Emission data were

corrected for attenuation and scatter, and reconstructed using the 3D maximum a priori method (3D MAP algorithm). Using a summed image of the entire data set, regions of interest (ROIs) were drawn manually on multiple planes to obtain volumetric ROIs for the whole brain, thalamus, cortex, pons, cerebellum and subcortical white matter. The volumetric ROIs were then applied to the full dynamic data sets to obtain the regional tissue time-radioactivity data. All semiquantified PET data are presented as means \pm SD when applicable.

Human Tissue Autoradiography. Frozen brain samples from age-matched healthy controls and AD-positive brains (diagnosis confirmed by neuropathological reports; CERAD criterion) were obtained from the Douglas-Bell Canada Brain Bank (Douglas Mental Health University Institute, Montreal, Canada). Utilization of these samples was approved by both the Douglas Institute's research ethics board and the Brain Bank's scientific review committee. Samples were excluded in cases of psychiatric conditions, epilepsy, non-AD dementia, brain neoplasms, and traumatic brain injuries. In total, brain tissue from 29 subjects was analyzed (16 healthy controls and 13 AD: 23 samples from the hippocampus (HP) (12 controls, 11 AD), 27 samples from the prefrontal cortex (PFC) (15 controls, 12 AD), 27 samples from the inferior parietal cortex (IPC) (15 controls, 12 AD) and 26 samples from the cerebellum (CB) (15 controls, 11 AD) (see Table S3). Using a freezing sliding microtome (Leica CM3050S) at -15°C , each block of tissue was cut into serial $20\mu\text{m}$ -thick sections, which were then thaw-mounted on coated microscope slides. Baseline and blocking experiments were performed on adjacent sections. The optimal conditions for the *in vitro* autoradiography binding techniques such as incubation time, washing procedure, and time of exposure onto the phosphor imaging plate were obtained after preliminary experiments (data not shown). On the day of synthesis, sections were warmed to room temperature, air-dried, and then preincubated in a 0.1 M phosphate-buffered saline solution (pH 7.4) for 20 min. Tissue was then air-dried once more and incubated with 48.2 MBq/L of [^{11}C]-(*R*)-IPMDCF16 (107 GBq/ μmol) alone (baseline) or [^{11}C]-(*R*)-IPMDCF16 + GW441756 10 μM (blocking) in the same buffer solution at room temperature for 60 min. After incubation, slides were dipped three times in buffer and one time in water in distilled water (4°C) and dried under a stream of cool air. The sections were then exposed on a radioluminographic imaging plate (Fujifilm BAS-MS2025) for 3 h (Supplementary Fig. S6). The drawn ROIs obtained from histological staining of adjacent sections as previously described were then transposed to the corresponding autoradiography images. Activity in photostimulated luminescence unit per mm^2 was calculated for each ROI using Image Gauge 4.0 (Fujifilm). Grey and white matter binding were averaged. Group differences in binding were then investigated

using a one-way ANOVA and specific binding was analyzed using an unpaired two-tailed Student t test for each ROI.

PET/MR Imaging Study in Human Subject. *Imaging procedure.* Dynamic PET data were acquired on a Siemens Biograph 64 True Point PET/CT scanner (Siemens Medical Solutions, Erlangen, Germany) at the Department of Nuclear Medicine, University of Munich (LMU) with an injection of 567 MBq of [^{11}C]-(*R*)-IPM1CF16. Reconstruction included standard corrections for attenuation (low dose CT), scatter, decay and random counts. Dynamic PET data were recorded in list mode over 60 min and reconstructed using a 3D ordered subsets expectation maximization (OSEM) algorithm with 4 iterations and 8 subsets, followed by a Gaussian filter with five millimeters FWHM. A second reconstruction was executed with the Siemens TrueX algorithm (Siemens Medical Solutions, Erlangen, Germany) which employs a model of the system point spread function of the tomographic device to provide better resolution recovery and reduced partial volume effects and therefore improved delineation and quantification of vessels, using 4 iterations, 16 subsets and no filter. Both dynamic studies were realized in a $256 \times 256 \times 109$ matrix with zoom 2 (voxel size of $1.336 \times 1.336 \times 2.027$) in 30 time frames (12×10 , 4×30 , 2×60 , 2×120 , 10×300 s). A correction of patient motion between time frames was performed using the PMOD Fusion tool (v3.4, PMOD Technologies, Zurich, Switzerland). *Blood sampling and image derived input function.* Manual blood samples were taken every 35 seconds until 3 min p.i. followed by additional manual blood samples 4, 5, 10, 19, 21, 31, 56 min p.i.. For determination of plasma-to-blood ratio and binding to plasma proteins analysis three blood samples were taken at 6, 18, and 20 min p.i.. Plasma was separated from cells with a centrifugation speed of $3000 \times g$ for 3 min. For determination of tracer fraction in plasma bound to proteins for each time point one probe was diluted with ice cold acetonitrile (1:4) followed by centrifugation (speed of $16000 \times g$, 4 degree Celsius for 3 min). Whole blood, whole plasma, supernatant (free tracer in plasma), and tracer bound to proteins was measured with a gamma-counter (Packard Cobra Quantum). The final arterial plasma input for pharmacokinetic modeling was generated by rescaling the image derived input function (IDIF) obtained from images with TrueX reconstruction based on manual blood samples.⁵⁷⁻⁵⁸ The IDIF VOI was delineated as proposed by Mourik *et al.*: starting at three planes below the Circle of Willis the four hottest voxels per slice within eleven consecutive planes. This yields a total volume of 159 mm^3 . *Image analyses.* Anatomical brain regions were defined in the OSEM3D reconstructions with PMOD Neuro tool (v3.4 PMOD Technologies, Zurich, Switzerland) based on the Hammers maximum probability atlas (Hammers N30R83)⁵⁹. Mean SUV values for 0-10, 10-30, 30-60 min p.i.

averaged images, and the parameter distribution volume V_T was derived with Logan and relative equilibrium-based⁶⁰ (RE) graphical plot and the corrected IDIF as input function. Parametric images were generated using the cerebral voxels identified by the overlay on the subjects MRI. For this anatomical comparison a T1 MP-RAGE MR image of the subject with isotropic voxels recorded on a 3 Tesla scanner (Magnetom Trio, Siemens, Erlangen) equipped with a 32-channel head coil was used.

5.7 Supporting Information of Article 8

Shedding Light on Trk Neurotrophin Receptors with PET Neuroimaging

Vadim Bernard-Gauthier^{a,1}, Justin J. Bailey^a, Andrew V. Mossine^b, Simon Lindner^c, Lena Vomacka^c, Arturo Aliaga^d, Xia Shao^b, Carole A. Quesada^b, Phillip Sherman^b, Anne Mahringer^e, Alexey Kostikov^f, Marilyn Grand'Maison^g, Pedro Rosa-Neto^d, Jean-Paul Soucy^h, Alexander Thiel^{f,i}, David R. Kaplan^j, Gert Fricker^e, Björn Wängler^k, Peter Bartenstein^c, Ralf Schirmmayer^{a,1,2}, Peter J. H. Scott^{b,1,2}

^aDepartment of Oncology, Division of Oncological Imaging, University of Alberta, Edmonton, AB, T6G 2R3, Canada.

^bDivision of Nuclear Medicine, Department of Radiology, The University of Michigan Medical School, Ann Arbor, MI, 48109, United States.

^cDepartment of Nuclear Medicine, Ludwig-Maximilians-University of Munich, Marchioninstr. 15, Munich, 81377, Germany.

^dTranslational Neuroimaging Laboratory, McGill Centre for Studies in Aging, Douglas Mental Health University Institute, 6875 Boulevard LaSalle, Montreal, QC, H4H 1R3, Canada.

^eInstitute of Pharmacy and Molecular Biotechnology, University of Heidelberg, Heidelberg 69120, Germany.

^fMcConnell Brain Imaging Centre, Montreal Neurological Institute, McGill University, 3801 University Street, Montreal, QC, H3A 2B4, Canada.

^gBiospective Inc., 6100 Avenue Royalmount, Montreal, QC H4P 2R2, Canada.

^hDepartment of Neurology and Neurosurgery, Montreal Neurological Institute, McGill University, 3801 University Street, Montreal, QC, H3A 2B4, Canada.

ⁱJewish General Hospital, Lady Davis Institute, Montreal, QC, HT3 1E2, Canada.

^jProgram in Neurosciences and Mental Health, Hospital for Sick Children, Toronto, ON, M5G 0A4, Canada.

^kMolecular Imaging and Radiochemistry, Department of Clinical Radiology and Nuclear Medicine, Medical Faculty Mannheim of Heidelberg University, Theodor-Kutzer-Ufer 1-3, Mannheim 68167, Germany.

^lThe Interdepartmental Program in Medicinal Chemistry, University of Michigan, Ann Arbor, MI 48109, United States.

¹Corresponding authors:

Prof. R. Schirrmacher. E-mail: schirрма@ualberta.ca. Phone: 780-248-1829.

Vadim Bernard-Gauthier. E-mail: bernardg@ualberta.ca. Phone: 780-248-5660.

²P.J.H.S. and R.S. contributed equally to this work.

CONTENTS OF SUPPORTING INFORMATION

1. SUPPLEMENTARY TABLES (**Tables S5.1-S5.3**)
2. SUPPLEMENTARY FIGURES (**Figures S5.1-S5.12**)
3. CHEMISTRY
4. CHIRAL SFC/MS ANALYSES OF INTERMEDIATES (\pm)-**5.12**, (*R*)-**5.12** AND (*S*)-**5.12**
5. CRYSTALLOGRAPHIC DATA FOR COMPOUND (*R_s*,*R*)-**9** (**Figures S5.13**)
6. BIOLOGICAL EVALUATION (**Tables S5.4**)
7. RADIOCHEMISTRY (**Figures S5.14-S5.28**)
8. NMR SPECTRA

1. SUPPLEMENTARY TABLES

Table S5.1. Characteristics of TrkA/B/C inhibitors in recent and current clinical trials for cancer treatment (updated August 2016, <https://clinicaltrials.gov/>)

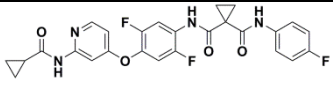
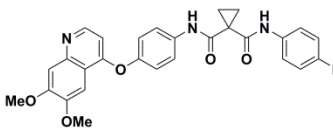
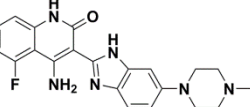
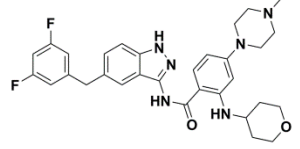
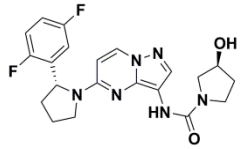
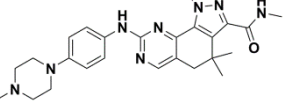
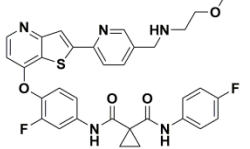
| Compound ID | Structure | Current stage (overview) | Kinase targets | Clinical trial ID/Sponsor |
|---|---|---|---|---|
| Altiratinib (DCC-2701, DCC-270, DP-5164) |  | Phase 1 in patients with locally advanced tumors and metastatic solid tumors including TRK genomic alterations | <i>Multi-targeted</i> ; including: TrkA/B/C , MET, TIE2 and VEGFR | NCT02228811 (recruiting) /Deciphera Pharmaceuticals LLC |
| Cabozantinib (XL-184, BMS-907351) |  | Multiple ongoing Phase 2 trials including in patients with RET fusion-positive advanced non-small cell lung cancer and those with other genotypes: <i>ROS1</i> or <i>NTRK</i> Fusions or increased MET or AXL activity | <i>Multi-targeted</i> ; including: MET, RET, VEGFR, KIT, CSF-1R, FLT3, TIE2 TrkA/B/C , AXL | N/A, Approved 2016 for kidney cancer treatment; NCT01639508 (recruiting) / Memorial Sloan Kettering Cancer Center |
| Dovitinib (TKI-258, CHIR-258) |  | Multiple ongoing trials including Phase 2 in patients with tumor pathway activations including mutations or translocations of Trk | <i>Multi-targeted</i> ; including: KIT, FLT3, FGFR, VEGFR, TrkA/B/C | NCT01831726 (completed 2016) / Novartis Pharmaceuticals |
| DS-6051b | (structure undisclosed) | Phase 1 first-in-human in patients with advanced solid tumors; Phase 1 Study in Japanese subjects with advanced solid malignant tumors with <i>NTRK</i> and <i>ROS1</i> fusions | <i>Selective ROS1</i> , TrkA/B/C | NCT02279433 (recruiting) / Daiichi Sankyo Co., Ltd.; NCT02675491 (recruiting) / Daiichi Sankyo Co., Ltd. |
| Entrectinib (RXDX-101) |  | Phase 2 in patients with locally advanced or metastatic solid tumors with rearrangement including for <i>NTRK1/2/3</i> (STARTRK-2); Phase 1/1b in pediatric patients with relapsed refractory solid tumors/primary CNS tumors/neuroblastoma/non-neuroblastoma | <i>Multi-targeted</i> ; ROS1, ALK, TrkA/B/C | NCT02568267 (recruiting) / Ignyta, Inc.; NCT02650401 (recruiting) / Ignyta, Inc.; NCT02097810 (recruiting) / Ignyta, Inc. |
| LOXO-101 |  | Phase 1 in patients with advanced adult solid tumors with <i>NTRK1/2/3</i> genetic alterations; Pediatric Solid or Primary Central Nervous System Tumors (SCOUT); Phase 2 in patients with <i>NTRK</i> fusion-positive tumors (NAVIGATE) | <i>Selective TrkA/B/C</i> | NCT02576431 (recruiting) / Loxo Oncology, Inc.; NCT02122913 (recruiting) / Loxo Oncology, Inc.; NCT02637687 (recruiting) / Loxo Oncology, Inc.; |
| Miliciclib (PHA-848125AC) |  | Phase 2 in patients with malignant thymoma; Phase 2 in patients with unresectable thymic carcinoma | <i>Multi-targeted</i> ; including: CDK, TrkA | NCT01301391 (recruiting) / Tiziana Life Sciences, PLC; NCT01011439 (ongoing) / Tiziana Life Sciences, PLC |
| Sitravatinib (MGCD516) |  | Phase 1 in patient with advanced cancer including with genetic alteration of <i>NTRK1/2/3</i> | <i>Multi-targeted</i> ; including: MET, AXL, MER, VEGFR, PDGFR, DDR2, Eph, TrkA/B/C | NCT02219711 (recruiting) / Mirati Therapeutics Inc. |
| PLX7486 | (structure undisclosed) | Phase 1 in patients with advanced solid tumors as a single agent and with gemcitabine plus nab-paclitaxel | <i>Multi-targeted</i> ; including: CSF-1R, TrkA/B/C | NCT01804530 (recruiting) / Plexixon |

Table S5.2. SAR and *in vitro* enzymatic activities and physicochemical data for imidazo[1,2-*b*]pyridazines Trk inhibitors³⁶

| Cpd | R | clogP | IC ₅₀ (nM) ^a | | | TrkA/TrkB; TrkA/TrkC selectivities |
|-------------------------------------|---|-------|------------------------------------|-------|-------|--|
| | | | TrkA | TrkB | TrkC | |
| 5.4 ((±)-IPMICF22) | | 1.51 | 7.66 | 0.565 | 0.374 | 13.6; 20.5 |
| 5.1 ((±)-IPMICF6) | | 2.08 | 1.91 | 0.076 | 0.076 | 25.1; 25.1 |
| 5.3 ((±)-IPMICF16) | | 3.17 | 1.94 | 0.080 | 0.095 | 24.3; 20.4 |
| 5.2 ((±)-IPMICF10) | | 3.61 | 2.10 | 0.099 | 0.127 | 21.2; 16.5 |

^a [γ -³³P]ATP-based enzymatic assay performed by Reaction Biology (From Ref. 36).

Table S5.3. Demographic characteristics and autoradiography data for brain tissue from healthy controls and Alzheimer's disease patients

| Patient | Healthy control (HC) or Alzheimer's disease (AD) | Gender | Age | Post-Mortem delay (PMD, hours) | Tissue dissections for autoradiography | | | |
|---------|--|--------|-----|--------------------------------|--|------------------|------------------|-----------------|
| | | | | | HP ¹ | PFC ² | IPC ³ | CB ⁴ |
| 1 | HC | M | 60 | 7.25 | X | X | X | X |
| 2 | HC | F | 74 | 11.00 | X | X | X | X |
| 3 | HC | M | 71 | 76.00 | X | X | N/A** | X |
| 4 | HC | M | 70 | 32.75 | N/A | N/A | X | X |
| 5 | HC | F | 90 | 13-37 | N/A | X | X | X |
| 6 | HC | F | 81 | 29.00 | X | X | X | X |
| 7 | HC | F | 77 | 31.00 | X | X | X | N/A |
| 8 | HC | M | 91 | 6.75 | N/A | X | X | X |
| 9 | HC | M | 69 | 12.00 | N/A | X | X | X |
| 10 | HC | M | 79 | 14.75 | X | X | X | X |
| 11 | HC | M | 59 | 17.75 | X | X | X | X |
| 12 | HC | M | 61 | 8.75 | X | X | X | X |
| 13 | HC | F | 95 | 23.75 | X | X | X | X |
| 14 | HC | M | 85 | 26.75 | X | X | X | X |
| 15 | HC | M | 88 | 8.00 | X | X | X | X |
| 16 | HC | F | 51 | 26.25 | X | X | X | X |
| 17 | AD | M | 67 | 96.00 | X | X | X | X |
| 18 | AD | M | 92 | 13.25 | X | X | N/A | X |
| 19 | AD | M | 66 | 8.50 | N/A | X | X | X |
| 20 | AD | M | 67 | 10.50 | X | X | X | X |
| 21 | AD | F | 77 | 11.25 | X | X | X | X |
| 22 | AD | M | 76 | 24.00 | N/A | X | X | X |
| 23 | AD | F | 74 | 18.00 | X | X | X | N/A |
| 24 | AD | M | 73 | 26.25 | X | X | X | X |
| 25 | AD | M | 63 | 21.00 | X | N/A | X | X |
| 26 | AD | F | 88 | 24.50 | X | X | X | N/A |
| 27 | AD | M | 79 | 19.25 | X | X | X | X |
| 28 | AD | M | 79 | 12.75 | X | X | X | X |
| 29 | AD | M | 79 | 24.75 | X | X | X | X |

¹Hippocampus; ²Prefrontal cortex; ³Inferior parietal cortex; ⁴Cerebellum; *Dissection used for autoradiography experiments; ** Dissection excluded from autoradiography experiments due to unavailability or deterioration of tissue during autoradiography manipulations.

2. SUPPLEMENTARY FIGURES

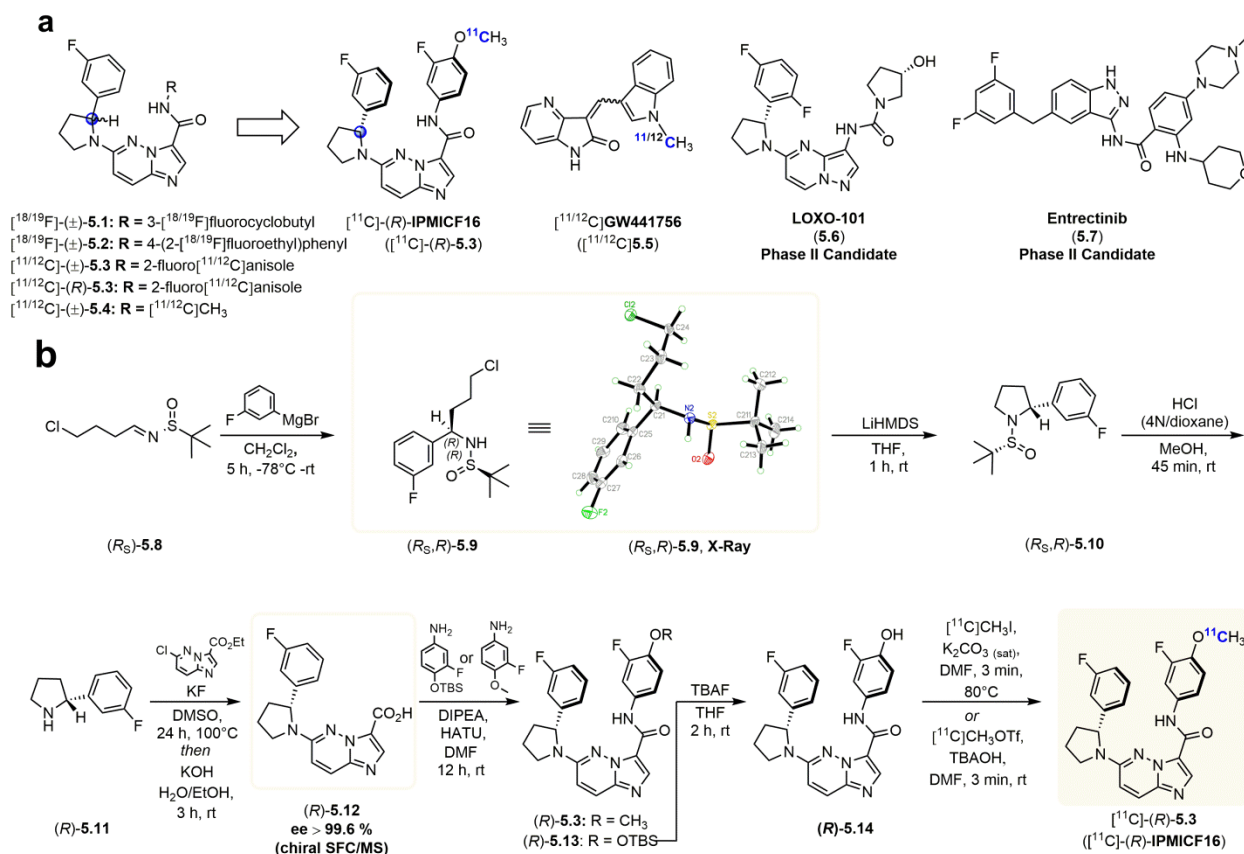


Figure S5.1. Trk tyrosine kinase inhibitor radiotracers, selected clinical Trk inhibitors and synthesis of $[^{11}\text{C}]-(R)\text{-IPMICF16}$. The key (R) -2-(3-fluorophenyl)pyrrolidine ($(R)\text{-}5.11$) intermediate required for securing $(R)\text{-IPMICF16}$ was synthesized via a Ellman sulfonamide route in place of the previously described enantioselective lithiation as the key step due to the limited availability of (-)-sparteine required using the latter technique.⁶¹ Diastereoselective Grignard addition to γ -chloro N -sulfinyl aldimine $(R_S)\text{-}5.8$ ⁶² delivered the diastereomer $(R_S,R)\text{-}5.9$ in 72% yield as the unique addition product (structure confirmed by X-ray crystallography, Fig 1b). Base-promoted ring closure followed by sulfinyl group cleavage cleanly afforded pyrrolidine $(R)\text{-}5.11$ on gram scale providing an efficient and mild alternative to the known and less scalable $sec\text{-BuLi}$ /lithiation sequence. With $(R)\text{-}5.11$ in hand, the carboxylic acid $(R)\text{-}5.12$ (ee > 99.6%; chiral SFC/MS, **Supplementary Information Section 4**) was obtained and derivatized with the required anilines for the synthesis of the non-radioactive standard and nor-precursor $(R)\text{-}5.14$. **(a)** Chemical structures of pan-Trk selective type-I PET radiotracers and inhibitors including $[^{11}\text{C}]-(R)\text{-IPMICF16}$ and $[^{11}\text{C}]$ GW441756 and Trk kinase inhibitor under clinical evaluation for the treatment of solid tumors. **(b)** Synthesis of $(R)\text{-IPMICF16}$ and radiosynthesis of $[^{11}\text{C}]-(R)\text{-IPMICF16}$ based on an *Ellman's sulfonamide-chiral pyrrolidine* approach. DMF, *N,N*-dimethylformamide; LiHMDS, lithium bis(trimethylsilyl)amide; DIPEA, *N,N*-diisopropylethylamine; HATU, 1-[bis(dimethylamino)methylene]-1*H*-1,2,3-triazolo[4,5-*b*]pyridinium 3-oxid hexafluorophosphate; TBAF, tetrabutylammonium fluoride; TBAOH, tetrabutylammonium hydroxide; THF, tetrahydrofuran.

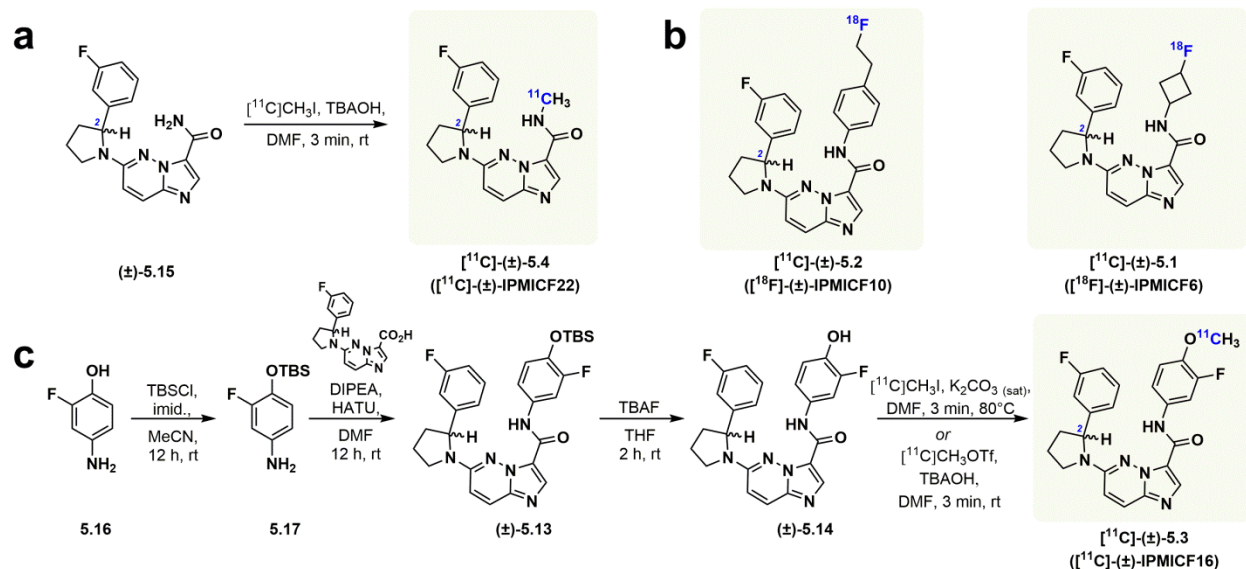


Figure S5.2. The racemic series. The decision to convert inhibitors **5.1-5.4** into radiotracers ensues from favorable CNS drug-like and radiotracer-like attributes evidenced by multiparameter optimization (MPO) scores (CNS MPO ~ 4.4-5.8 and CNS PET MPO ~ 3.3-5.3) and one-step radiolabeling amenability with either carbon-11 or fluorine-18. *Chemical and radiochemical syntheses.* Precursors for $[^{18}\text{F}](\pm)\text{-5.1}$, $[^{18}\text{F}](\pm)\text{-2}$ and $[^{11}\text{C}](\pm)\text{-5.4}$ were obtained as previously described (as well as for GW441756).³⁶⁻³⁷ (a) Radiosynthesis of $[^{11}\text{C}](\pm)\text{-IPMICF22}$. (b) Chemical structure of $[^{18}\text{F}](\pm)\text{-IPMICF10}$ and $[^{18}\text{F}](\pm)\text{-IPMICF6}$. (c) Precursor synthesis and radiosynthesis of $[^{11}\text{C}](\pm)\text{-IPMICF16}$. DMF, *N,N*-dimethylformamide; HATU, 1-[bis(dimethylamino)methylene]-1*H*-1,2,3-triazolo[4,5-*b*]pyridinium 3-oxid hexafluorophosphate; TBAF, tetrabutylammonium fluoride; TBAOH, tetrabutylammonium hydroxide; TBSCl, *tert*-butyldimethylsilyl chloride; THF, tetrahydrofuran.

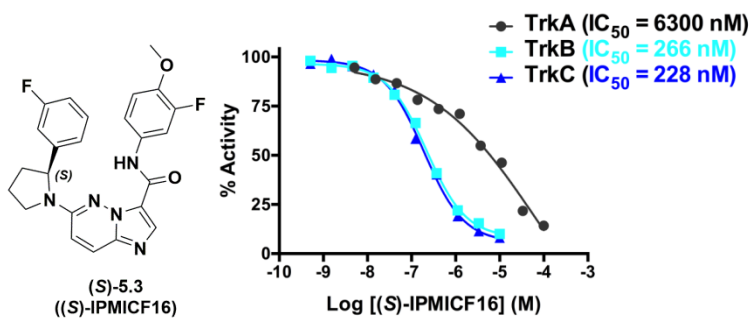


Figure S5.3. Structure (left) and dose-response curve (right) for inhibitor (S)-IPMICF16 ($n = 1$) versus TrkA, TrkB and TrkC ($[\gamma\text{-}^{33}\text{P}]\text{ATP}$ -based enzymatic assay performed by Reaction Biology).

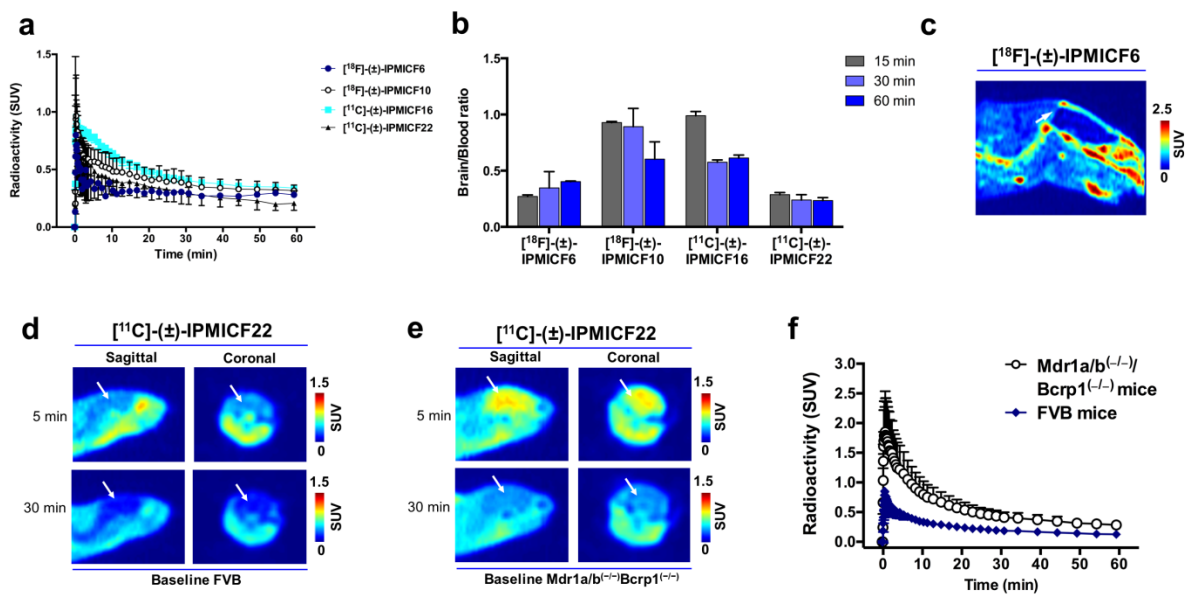


Figure S5.4. Preclinical rodents *in vivo* PET imaging data for representative IPMICF radiotracers. (a) TACs showing tracer uptakes (whole brain) for $[^{18}\text{F}]-(\pm)\text{-IPMICF6}$, $[^{18}\text{F}]-(\pm)\text{-IPMICF10}$, $[^{11}\text{C}]-(\pm)\text{-IPMICF16}$ and $[^{11}\text{C}]-(\pm)\text{-IPMICF22}$ in Sprague Dawley rats ($n = 2$ per radiotracer, expressed as mean \pm SD). (b) Radiotracers brain/blood (heart) ratios at 15 min, 30 min and 60 min post injection in Sprague Dawley rats. Expressed as mean \pm SD. (c) Representative PET image of $[^{18}\text{F}]-(\pm)\text{-IPMICF6}$ in Sprague Dawley rat showing extensive bone uptake characteristic of ^{18}F -defluorination. (d) Representative brain images of $[^{11}\text{C}]-(\pm)\text{-IPMICF22}$ in FVB mice. (e) Representative brain images of $[^{11}\text{C}]-(\pm)\text{-IPMICF22}$ in $\text{Mdr1a/b}^{(-/-)}\text{Bcrp1}^{(-/-)}$ mice. (f) TACs for $[^{11}\text{C}]-(\pm)\text{-IPMICF22}$ brain uptake at baseline ($n = 3/\text{group}$, expressed as mean \pm SD). Although $[^{18}\text{F}]-(\pm)\text{-IPMICF10}$ offered similar imaging properties as $[^{11}\text{C}]-(\pm)\text{-IPMICF16}$ in rats, it was demonstrated to be unsuitable for *in vivo* use in higher species based on nonhuman primate imaging data due to extensive defluorination (**Supplementary Figure 7b**).

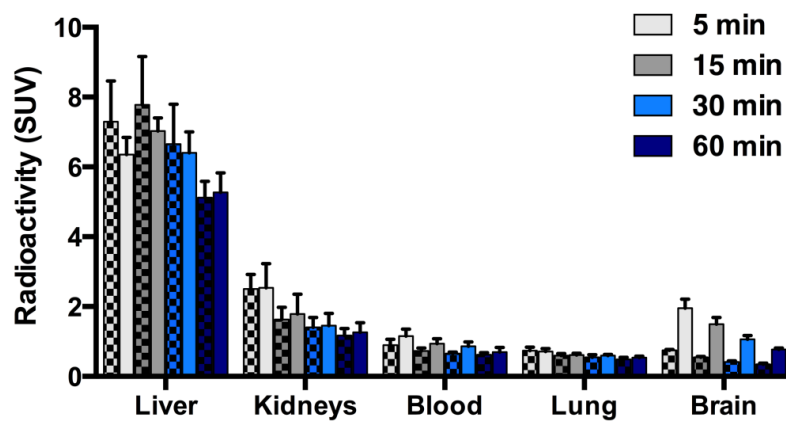


Figure S5.5. [^{11}C]-(+)-IPMICF16 biodistribution in mice. Selected biodistribution data presenting the accumulation of [^{11}C]-(+)-IPMICF16 in liver, kidneys, blood (heart), lung in comparison to brain over the duration the scans ($n = 3$; checkered colors = FVB mice; full colors = $\text{Mdr1a/b}^{(-/-)}\text{Bcrp1}^{(-/-)}$ mice). Expressed as mean \pm SD.

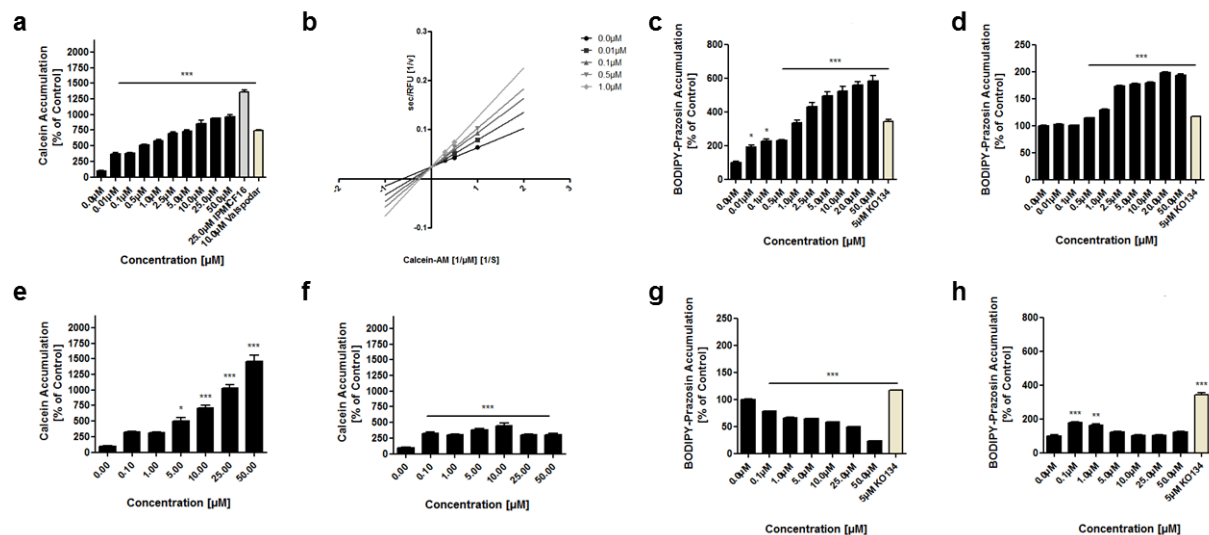


Figure S5.6. Calcein-AM and BODIPY-Prazosin cellular assays and Lineweaver Burk plot to study interactions with P-gp and BCRP. Calcein-AM assays were conducted in human P-gp overexpressing Madin-Darby Canine Kidney (MDCKII) cells. BODIPY-Prazosin assays were conducted in native and human BCRP overexpressing MDCKII cells. In all cases, intracellular fluorescence in the absence of test compounds was set as 100%. Valspodar and KO134 were used as positive control for P-gp and BCRP assays respectively. (a) Results obtained from Calcein-AM assay for P-gp with (R)-IPMICF16 ($EC_{50} = 2.9 \pm 1.3 \mu\text{M}$ for P-gp). (b) Lineweaver Burk plot determined with (\pm)-IPMICF16 showing competitive inhibition of fluorescent Calcein and hence, transport of the former by P-gp. (c) Results obtained from BODIPY-Prazosin assay for BCRP with (R)-IPMICF16 ($EC_{50} = 2.23 \pm 1.1\mu\text{M}$ in overexpressing cells). (d) Results obtained from BODIPY-Prazosin assay for BCRP with (R)-IPMICF16 in native MDCKII cells. (e) Results obtained from Calcein-AM assay for P-gp with GW441756 ($EC_{50} = 79.2 \mu\text{M}$ for P-gp). (f) Results obtained from Calcein-AM assay for P-gp with Entrectinib. (g) Results obtained from BODIPY-Prazosin assay for BCRP with Entrectinib (in native cells). (h) Results obtained from BODIPY-Prazosin assay for BCRP with Entrectinib (in overexpressing cells).

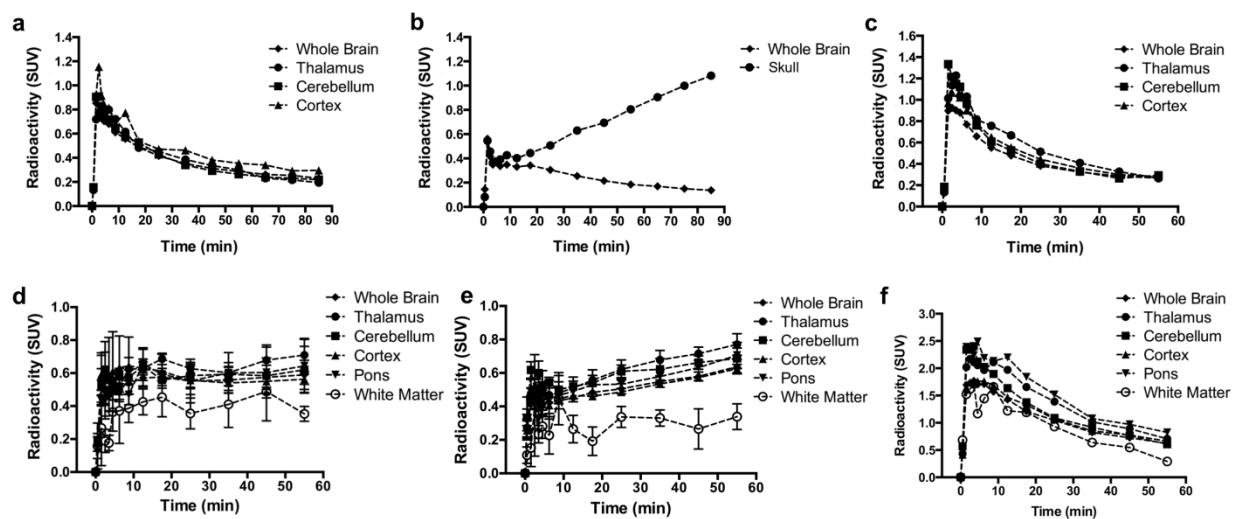


Figure S5.7. Rhesus monkey regional brain TACs from radiotracers screening. TACs showing tracers binding and regional distribution in baseline conditions in the NHP brain for (a) $[^{18}\text{F}](\pm)$ -IPMICF6 ($[^{18}\text{F}](\pm)$ -5.1, 0–90 min, $n = 1$). (b) $[^{18}\text{F}](\pm)$ -IPMICF10 ($[^{18}\text{F}](\pm)$ -5.2, 0–90 min, $n = 1$); skull uptake is indicative of ^{18}F -defluorination. (c) $[^{11}\text{C}](\pm)$ -IPMICF22 ($[^{11}\text{C}](\pm)$ -5.4, 0–60 min, $n = 1$). (d) $[^{11}\text{C}](\pm)$ -IPMICF16 ($[^{11}\text{C}](\pm)$ -5.3, 0–60 min, $n = 3$, expressed as mean \pm SD). (e) $[^{11}\text{C}](R)$ -IPMICF16 ($[^{11}\text{C}](R)$ -5.3, 0–60 min, $n = 3$, expressed as mean \pm SD). (f) $[^{11}\text{C}]$ GW441756 ($[^{11}\text{C}]$ 5.5, 0–60 min, $n = 1$). The SUV scale is adjusted to uptake.

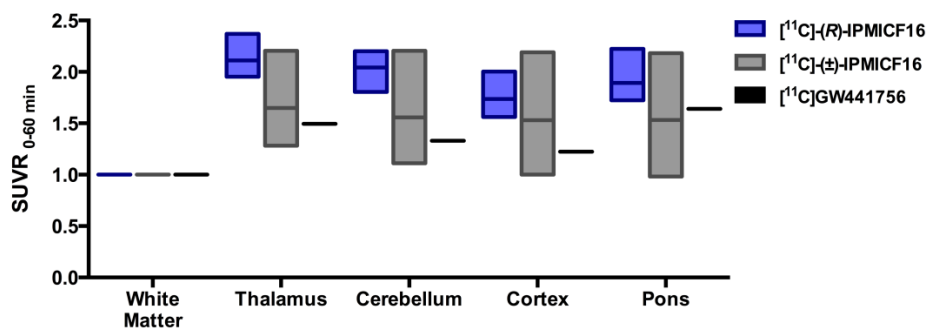


Figure S5.8. Comparative regional SUV ratio (SUVR, summed 0-60 min) for [¹¹C]-(*R*)-IPMIF16, [¹¹C]-(\pm)-IPMIF16 and [¹¹C]GW441756.

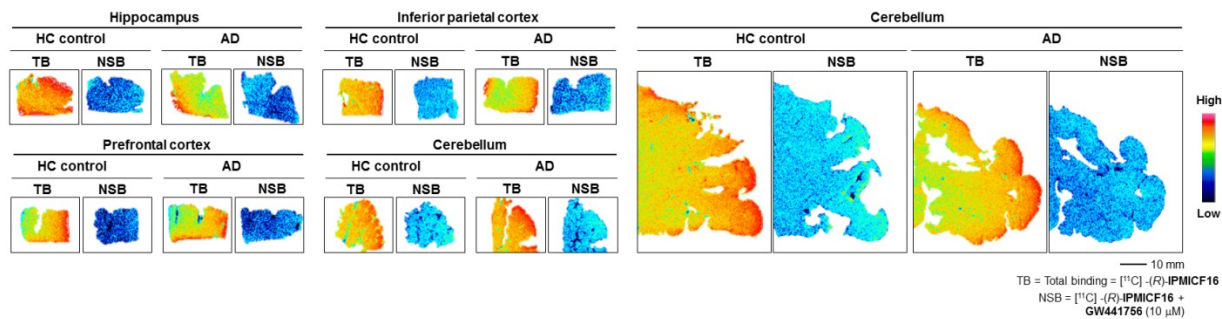


Figure S5.9. $[^{11}\text{C}]-(R)\text{-IPMIF16}$ binding is highly specific and TrkB/C-selective in the human brain *in vitro*. Representative *in vitro* autoradiograms. Sections of human brains showing the binding of $[^{11}\text{C}]-(R)\text{-IPMIF16}$ and competition experiments with GW441756 (10 μM) (successive sections between baseline and blocking). HC = healthy control, AD = Alzheimer disease. TB = total binding ($[^{11}\text{C}]-(R)\text{-IPMIF16}$), NSB = non-specific binding ($[^{11}\text{C}]-(R)\text{-IPMIF16} + \text{GW441756, 10 } \mu\text{M}$).

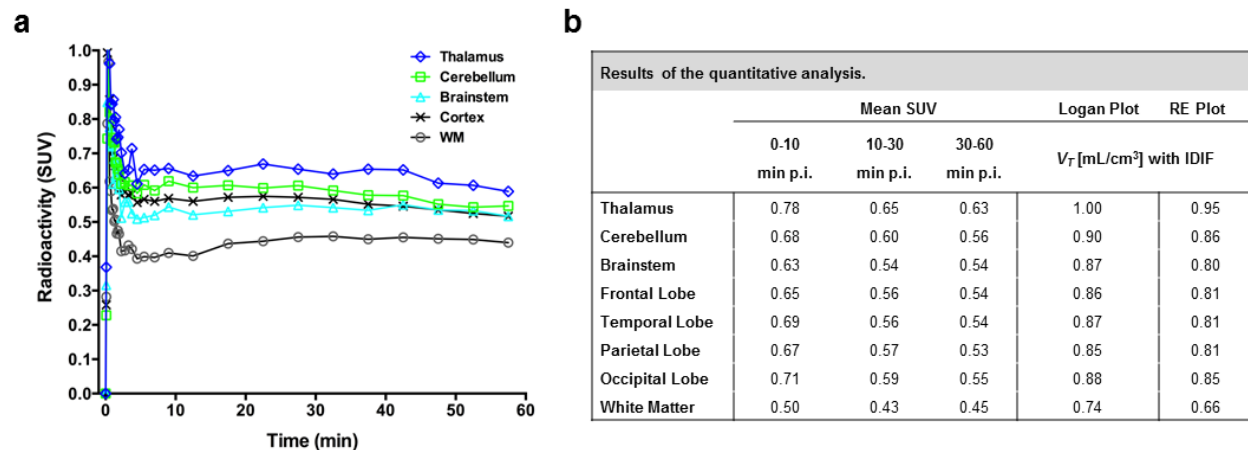


Figure S5.10. Analysis of [¹¹C]-(*R*)-IPMIF16 in the human brain. (a) Time activity curves of the human [¹¹C]-(*R*)-IPMIF16 study 0-60 min p.i.. For illustrative purposes the SUV scale was truncated at 1.0. All gray matter regions show a rapid stabilization starting at around 5 min p.i.. Activity retention in thalamus is considerably higher compared to the other gray matter regions, whereas white matter shows a significantly lower retention. (b) Results of the quantitative analysis. The first 3 rows provide the average SUV data 0-10 min p.i., 10-30 min p.i. and 30-60 min, indicating largely stable values after 10 min p.i.. The thalamus shows consistently the highest values, whereas the other gray matter values appear to be similar (with the cerebellum being slightly higher compared to cortex) and the white matter is markedly lower. This relation is also observed in the V_T values derived by Logan and the RE plot.

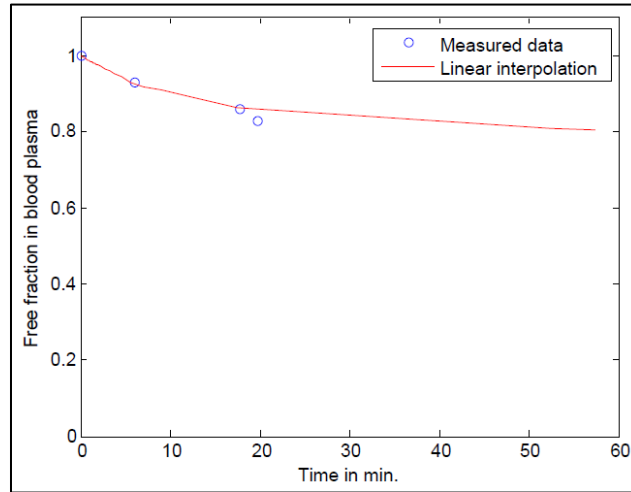


Figure S5.11. Unbound fraction in the plasma ($F_{u,p}$) based on 3 measurements made 6, 18, and 20 min post injection.

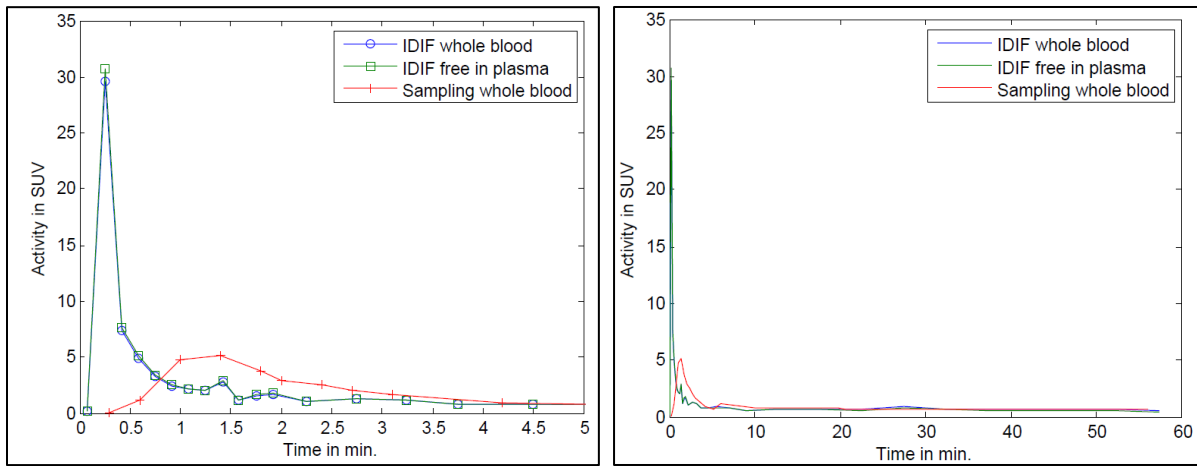


Figure S5.12. Image derived input function (IDIF) of whole blood (blue) obtained from images with TrueX reconstruction and rescaling based on a bi-exponential fit to manual blood sample data (red) between 5 and 60 min. p.i., and unbound plasma IDIF (green).

3. CHEMISTRY

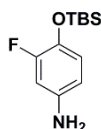
3.1 General Procedures.

All moisture sensitive reactions were carried out in oven-dried flasks under nitrogen atmosphere with dry solvents. Reagents and solvents were purchased at the highest commercial quality from Fisher, Sigma-Aldrich, Alfa-Aesar, Synthonix or Oakwood Products and were used without further purification unless specified otherwise. Compounds used for blocking PET studies, GW441756 hydrochloride and entrectinib, were purchased from Aldrich (G3420) and Cedarlane (HY-1267) respectively. Organic solutions were concentrated under reduced pressure on a Heidolph rotary evaporator. In general, reactions were magnetically stirred and monitored by TLC performed on pre-coated glass-backed TLC plates (Analtech, 250 microns) and chromatographic purification of products was accomplished using flash chromatography on Alfa-Aesar silica gel (230-450 mesh). TLC visualization was performed by fluorescence quenching, KMnO_4 or ninhydrin. ^1H NMR and ^{13}C NMR spectra were recorded on a Agilent/Varian DD2 MR two channel 400 MHz spectrometer, a Agilent/Varian VNMRS two-channel 500 MHz spectrometer or a Agilent/Varian Inova four-channel 500 MHz spectrometer in CDCl_3 or d_6 -DMSO and peak positions are given in parts per million using TMS as internal standard. Peaks are reported as: s = singlet, d = doublet, t = triplet, q = quartet, p = quintet, m = multiplet, b = broad; coupling constant(s) in Hz; integration. High Resolution Mass Spectra (HRMS) analysis was obtained from the Mass Spectrometry Facility of the Chemistry Department of the University of Alberta (Agilent Technologies 6220 oaTOF) or from the Regional Center for Mass Spectrometry of The Chemistry Department of the Université de Montréal (LC-MSD-TOF Agilent). Compounds tested for biological evaluation were >95% pure (HPLC/MS). The chiral SFC/MS analysis was performed at the Regional Mass Spectrometry Center of the department of chemistry of the Université de Montréal. Crystallographic analysis was performed by the X-Ray Diffraction Laboratory of the department of chemistry of the Université de Montréal.

The syntheses of (\pm)-**5.15**, (\pm)-**5.4** ((\pm)-IPMICF22), (\pm)-**5.2** ((\pm)-IPMICF10), (\pm)-**5.1** ((\pm)-IPMICF6), (\pm)-**5.3** ((\pm)-IPMICF16) and (\pm)-**5.12** (**Figure S5.2**) have been reported in the literature.³⁶ The synthetic sequences leading to the radiolabeling precursors (\pm)-**5.14** and (*R*)-**5.14** as well as the compounds (*R*)-**3**/*(S)*-**3** ((*R*)-IPMICF16/*(S)*-IPMICF16) are described here. The synthesis of compound (*R_S*)-**8** has been described in the literature.⁶² The absolute stereochemistry of (*R_S*,*R*)-**5.9** was confirmed by X-ray crystallography analysis. Compounds (*R*)-**5.12**, (*R*)-**5.13**, (*R*)-**5.14** and (*R*)-**5.3** were synthesized in accordance with the methods

described for the corresponding racemic compounds. All R_f /NMR/MS data obtained for those compounds were in full agreement with the corresponding known racemates. The synthesis of (*S*)-**3** ((*S*)-IPMICF16) was carried out following the procedure described for (*R*)-**5.3** ((*R*)-IPMICF16) with (*S_S*)-**8** as starting material. The synthesis of compound (*S_S*)-**5.8** has been described in the literature³. All R_f /NMR/MS data obtained for compounds (*S_S*,*S*)-**5.9** and (*S_S*,*S*)-**5.10** were in full agreement with the corresponding (*R_S*,*R*)-enantiomers. The enantiopurities of the pyrrolidine C2 centers in both the (*R*)- and (*S*)-synthetic sequences were further confirmed at the stage of the key intermediates (*R*)-**5.12** and (*S*)-**5.12** using chiral SFC/MS analysis (ee > 99.6%).

3.2 Chemical Synthesis



4-((*tert*-Butyldimethylsilyloxy)-3-fluoroaniline (**5.17**):

tert-Butyldimethylsilyl chloride (791 mg, 5.25 mmol, 1.05 equiv) was added to a solution of 4-amino-2-fluorophenol (636 mg, 5.0 mmol, 1.0 equiv) and imidazole (851 mg, 12.5 mmol, 2.5 equiv) in anhydrous acetonitrile (25 mL) at 23°C. The reaction mixture was stirred at this temperature for 12 h and then diluted with water (50 mL) and ethyl acetate (50 mL). The organic layer was separated and extracted with ethyl acetate (3 X 50 mL). The organic layers were combined, washed with brine (50 mL) and dried over anhydrous sodium sulfate, filtered and concentrated under reduced pressure. The crude product was purified by flash column chromatography (25→50% ethyl acetate in hexane) to afford 712 mg of the title compound (59%).

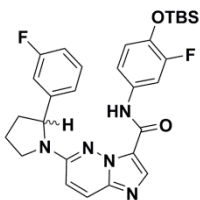
Physical State: red oil.

R_f: 0.57 (1:1 hexanes/EtOAc, UV light).

HRMS (ESI+): *m/z* calc. for C₁₂H₂₁FNOSi (M + H)⁺: 242.1371, found 242.1368.

¹H NMR (400 MHz, CHLOROFORM-*d*): δ = 6.71 (dd, J = 8.6, 9.3 Hz, 1H), 6.42 (dd, J = 2.8, 12.1 Hz, 1H), 6.31 (ddd, J = 1.3, 2.8, 8.5 Hz, 1H), 3.61 - 3.30 (m, 2H), 1.04 - 0.94 (m, 9H), 0.15 (d, J = 1.0 Hz, 6H).

¹³C NMR (101 MHz, CHLOROFORM-*d*): δ = 154.35 (d, J = 242.8 Hz, 1C), 141.10 (d, J = 9.1 Hz, 1C), 135.32 (d, J = 12.6 Hz, 1C), 122.65 (br d, J = 3.1 Hz, 1C), 110.71 (d, J = 3.1 Hz, 1C), 103.90 (br d, J = 22.2 Hz, 1C), 25.63, 18.24, -4.83 (br d, J = 1.7 Hz, 1C).



N-(4-((*tert*-Butyldimethylsilyl)oxy)-3-fluorophenyl)-6-(2-(3-fluorophenyl)pyrrolidin-1-yl)imidazo[1,2-*b*]pyridazine-3-carboxamide ((±)-**5.13**):

N,N-Diisopropylethylamine (0.12 mL, 0.69 mmol, 2.5 equiv) was added to a solution of 6-(2-(3-fluorophenyl)pyrrolidin-1-yl)imidazo[1,2-*b*]pyridazine-3-carboxylic acid ((±)-**5.12**, 90 mg, 0.28 mmol, 1.0 equiv) in *N,N*-dimethylformamide (3 mL). HATU (107 mg, 0.28 mmol, 1.0 equiv) was then added in one portion and the reaction mixture was stirred at 23°C for 5 min. A solution of 4-((*tert*-butyldimethylsilyl)oxy)-3-fluoroaniline (**5.17**) 81 mg, 0.34 mmol, 1.2 equiv) in *N,N*-dimethylformamide (1 mL) was added dropwise and the reaction mixture was stirred at 23°C for 12 h. The reaction mixture was diluted with ethyl acetate (50 mL), washed with water (25 mL) and brine (25 mL), dried over anhydrous sodium sulfate, filtered and concentrated under reduced pressure. The crude product was purified by flash column chromatography (1→5% methanol in dichloromethane) to afford 96 mg of the title compound (62%).

Physical State: white solid.

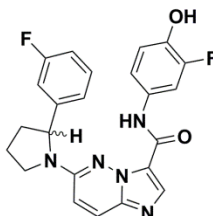
R_f: 0.13 (1:99 MeOH/CH₂Cl₂, UV light).

HRMS (ESI⁺): *m/z* calc. for C₂₉H₃₄F₂N₅O₂Si (M + H)⁺: 550.2444, found 550.2458.

¹H NMR (498 MHz, CHLOROFORM-*d*): δ = 10.46 (br s, 1H), 8.29 (s, 1H), 7.72 (br d, J = 9.9 Hz, 1H), 7.51 (br s, 1H), 7.34 - 7.29 (m, 1H), 7.05 - 6.95 (m, 3H), 6.93 - 6.86 (m, 2H), 6.60 - 6.53 (m, 1H), 5.11 (br d, J = 7.9 Hz, 1H), 4.03 - 3.95 (m, 1H), 3.84 - 3.76 (m, 1H), 2.63 - 2.54 (m, 1H), 2.23 - 2.10 (m, 3H), 1.04 (s, 9H), 0.23 (s, 6H).

¹³C NMR (125 MHz, CHLOROFORM-*d*): δ = 163.23 (d, J = 247.5 Hz, 1C), 156.98, 153.77 (br d, J = 244.1 Hz, 1C), 152.09, 145.12 - 144.87 (m, 1C), 144.80 - 144.60 (m, 1C), 139.78 (d, J =

12.6 Hz, 1C), 137.98, 132.03 (br s, 1C), 130.73 (br d, $J = 8.3$ Hz, 1C), 127.15, 122.13, 121.12 (br d, $J = 2.6$ Hz, 1C), 116.09 (br s, 1C), 115.88 - 115.72 (m, 1C), 114.64 (br d, $J = 21.4$ Hz, 1C), 112.57 (br d, $J = 22.2$ Hz, 1C), 110.92 (br s, 1C), 109.44 (br s, 1C), 62.08, 48.66, 35.87, 25.61, 22.77, 18.32, -4.72.



N-(3-Fluoro-4-hydroxyphenyl)-6-(2-(3-fluorophenyl)pyrrolidin-1-yl)imidazo[1,2-*b*]pyridazine-3-carboxamide ((±)-**5.14**):

Tetrabutylammonium fluoride (1.0 M in tetrahydrofuran, 0.23 mL, 0.23 mmol, 1.5 equiv) was added dropwise to a solution of *N*-(4-((*tert*-butyldimethylsilyloxy)-3-fluorophenyl)-6-(2-(3-fluorophenyl)pyrrolidin-1-yl)imidazo[1,2-*b*]pyridazine-3-carboxamide ((±)-**5.7**, 85 mg, 0.15 mmol, 1.0 equiv) in tetrahydrofuran (5 mL) at 23°C. After 2 h, the reaction mixture was quenched with water (25 mL) and diluted with ethyl acetate (50 mL). The organic layer was separated and the aqueous layer was washed with ethyl acetate (3 X 50 mL). The organic layers were combined, washed with brine (50 mL) and dried over anhydrous sodium sulfate, filtered and concentrated under reduced pressure. The crude product was purified by flash column chromatography (1→10% methanol in dichloromethane) to afford 65 mg of the title compound (91%).

Physical State: tan solid.

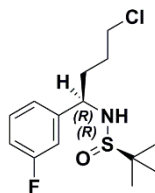
R_f: 0.45 (1:9 MeOH/CH₂Cl₂, UV light).

HRMS (ESI+): *m/z* calc. for C₂₃H₂₀F₂N₅O₂ (M + H)⁺: 436.1580, found 436.1596.

¹H NMR (400 MHz, DMSO-*d*₆): δ = 7.98 (s, 1H), 7.77 (d, $J = 9.9$ Hz, 1H), 7.42 (br dd, $J = 1.9, 12.9$ Hz, 1H), 7.27 - 7.16 (m, 1H), 7.01 (d, $J = 7.8$ Hz, 1H), 6.96 (td, $J = 1.9, 10.0$ Hz, 1H), 6.92 - 6.83 (m, 3H), 6.80 (d, $J = 10.0$ Hz, 1H), 5.19 (dd, $J = 1.5, 8.0$ Hz, 1H), 4.01 - 3.90 (m, 1H), 3.76 - 3.65 (m, 1H), 2.07 - 1.88 (m, 3H), 1.59 - 1.48 (m, 1H).

¹³C NMR (101 MHz, DMSO-*d*₆): δ = 162.97 (d, $J = 245.0$ Hz, 1C), 156.77, 152.64, 150.91 (d, $J = 240.0$ Hz, 1C), 145.85 (d, $J = 6.2$ Hz, 1C), 141.68 (d, $J = 12.5$ Hz, 1C), 136.64, 130.59 (d, $J = 8.3$ Hz, 1C), 129.90 (d, $J = 9.1$ Hz, 1C), 126.63, 124.69, 122.07, 121.68 (d, $J = 2.7$ Hz, 1C),

117.85 (d, $J = 3.3$ Hz, 1C), 117.03 (br s, 1C), 113.88 (d, $J = 21.4$ Hz, 1C), 112.76, 112.50 (br d, $J = 8.3$ Hz, 1C), 109.65, 61.79, 48.64, 35.55, 22.56.



(R)-N-((*R*)-4-Chloro-1-(3-fluorophenyl)butyl)-2-methylpropane-2-sulfonamide ((*R_S*,*R*)- (**5.9**):

To a solution of (*R_S*)-**5.8** (900 mg, 4.29 mmol, 1.0 equiv) in CH₂Cl₂ (22 mL) at -78 °C under nitrogen was added 3-fluorophenylmagnesium bromide (5.15 mL of 1.0 M THF solution, 5.15 mmol, 1.2 equiv). The reaction mixture was stirred at -78 °C for 4 h, brought to room temperature and quenched with saturated NH₄Cl (25 mL). The organic layer was washed with saturated NaHCO₃ (25 mL), brine (25 mL), dried over anhydrous sodium sulfate, filtered and concentrated under reduced pressure. The crude product was purified by flash column chromatography (20→100% ethyl acetate in hexane) to afford 942 mg of the title compound (72%). For X-ray crystallography analysis, the title compound was recrystallized from EtOAc/hexanes yielding white needles.

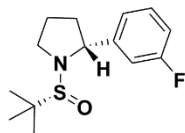
Physical State: White solid.

R_f: 0.17 (1:4 EtOAc/hexanes, UV light/KMnO₄).

HRMS (ESI⁺): m/z calc. for C₁₄H₂₂ClFNOS (M + H)⁺: 306.1089, found 306.1084.

¹H NMR (498 MHz, CHLOROFORM-*d*) $\delta = 7.32$ (dt, $J = 5.9, 7.9$ Hz, 1H), 7.11 (d, $J = 7.7$ Hz, 1H), 7.04 (td, $J = 2.1, 9.7$ Hz, 1H), 7.01 - 6.97 (m, 1H), 4.40 - 4.34 (m, 1H), 3.49 (t, $J = 6.5$ Hz, 2H), 3.45 (d, $J = 3.9$ Hz, 1H), 2.19 - 2.09 (m, 1H), 1.95 - 1.85 (m, 1H), 1.82 - 1.71 (m, 1H), 1.67 - 1.57 (m, 1H), 1.23 (s, 9H).

¹³C NMR (125 MHz, CHLOROFORM-*d*) $\delta = 162.99$ (d, $J = 247.0$ Hz, 1C), 144.56 (d, $J = 6.7$ Hz, 1C), 130.41 (br d, $J = 8.3$ Hz, 1C), 122.88 (br d, $J = 2.8$ Hz, 1C), 115.03 (d, $J = 21.2$ Hz, 1C), 113.88 (d, $J = 21.9$ Hz, 1C), 58.14, 55.93, 44.53, 33.87, 28.69, 22.61.



(R)-1-((R)-tert-Butylsulfinyl)-2-(3-fluorophenyl)pyrrolidine ((R_S,R)- (5.10):

To a solution of (R_S,R)-**5.9** (3.25 g, 11.9 mmol, 1.0 equiv) in THF (50 mL) at 23°C was added LiHMDS (17.9 mL of 1.0 M THF solution, 17.9 mmol, 1.5 equiv). The reaction mixture was stirred at 23°C for 1 h and quenched with NH₄Cl (25 mL) and extracted ethyl acetate (3 X 50 mL). The organic layers were combined, washed with brine (50 mL) and dried over anhydrous sodium sulfate, filtered and concentrated under reduced pressure. The crude product was purified by flash column chromatography (20→40% ethyl acetate in hexane) to afford 2.29 g of the title compound (71%).

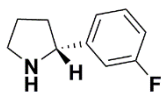
Physical State: white solid.

R_f: 0.38 (2:3 EtOAc/hexanes, UV light).

HRMS (ESI+): *m/z* calc. for C₁₄H₂₂FNOS (M + H)⁺: 270.1328, found 270.1322.

¹H NMR (498 MHz, CHLOROFORM-*d*) δ = 7.27 (dt, *J* = 6.0, 7.9 Hz, 1H), 7.03 (td, *J* = 0.7, 7.7 Hz, 1H), 6.96 (td, *J* = 2.1, 10.0 Hz, 1H), 6.93 - 6.87 (m, 1H), 5.07 (dd, *J* = 2.8, 8.2 Hz, 1H), 3.68 - 3.61 (m, 1H), 3.60 - 3.53 (m, 1H), 2.21 - 2.12 (m, 1H), 1.94 - 1.86 (m, 1H), 1.85 - 1.78 (m, 1H), 1.77 - 1.71 (m, 1H), 1.06 (s, 9H).

¹³C NMR (125 MHz, CHLOROFORM-*d*) δ = 162.92 (d, *J* = 245.9 Hz, 1C), 147.56 (d, *J* = 6.5 Hz, 1C), 129.94 (d, *J* = 8.3 Hz, 1C), 122.12 (br d, *J* = 2.8 Hz, 1C), 113.51 (br d, *J* = 5.9 Hz, 1C), 113.34 (br d, *J* = 6.7 Hz, 1C), 57.49, 56.83, 55.23, 36.53, 24.23, 23.02.



(R)-2-(3-fluorophenyl)pyrrolidine ((R)- (5.11):

To a solution of (R)-**5.10** (660 mg, 2.45 mmol, 1.0 equiv) in MeOH (10 mL) was added HCl (2.0 mL, 4.0 M solution in dioxane). The reaction mixture was stirred 45 min at 23°C and then concentrated to dryness. The crude residue was dissolved in water (10 mL) and neutralized to

pH ~ 12 using a 6 N NaOH solution. The aqueous phase was extracted with ethyl acetate (5 X 10 mL). The organic layers were combined, washed with brine (50 mL) and dried over anhydrous sodium sulfate, filtered and concentrated under reduced pressure to afford 400 mg of the crude title compound (99%, crude) which was used directly in the following step without further purification.

4. CHIRAL SFC/MS ANALYSES OF INTERMEDIATES (\pm)-12, (*R*)-12 AND (*S*)-12

Data form this subsection can be found in **Annex 4**.

5. CRYSTALLOGRAPHIC DATA FOR COMPOUND (*R_S*,*R*)-9

Data form this subsection can be found in **Annex 4**.

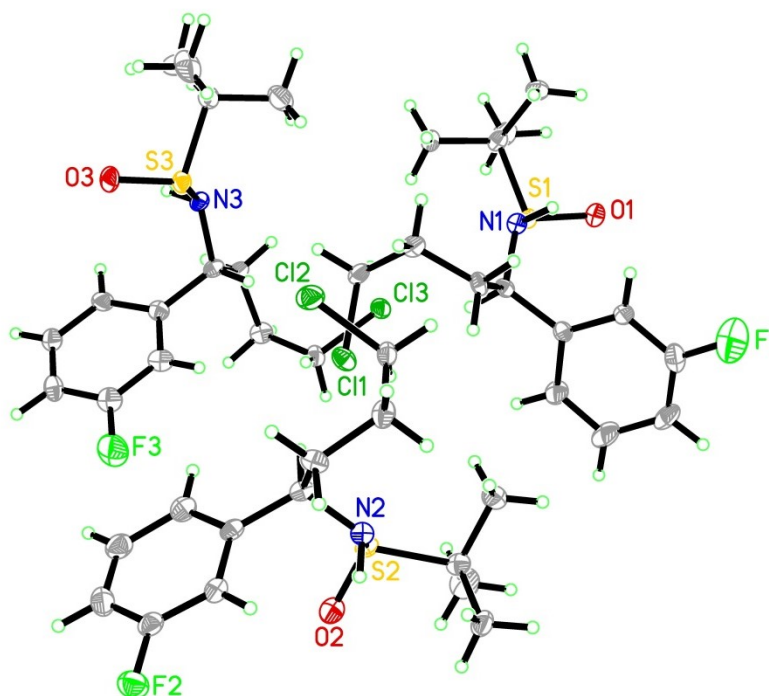


Figure S5.13. ORTEP view of the $C_{14}H_{21}ClFNO_5$ compound with the numbering scheme adopted ((R_S-R) -5.9).

6. BIOLOGICAL EVALUATION

6.1 [γ -³³P]ATP-Based Enzymatic Assay⁶³

Compound (*R*)-IPMICF16 was initially tested in a [γ -³³P]ATP based enzymatic assay by Reaction Biology Corporation (Malvern, PA). Briefly, the compound was tested for 10-concentrations IC₅₀ curves with 3-fold serial dilution starting at 0.1 μ M (when required, additional dilutions were made). The reactions were performed with 1 μ M ATP and profiled against 3 tyrosine kinases (tropomyosin receptor kinase A (TrkA), tropomyosin receptor kinase B (TrkB), tropomyosin receptor kinase C (TrkC)) in singlicate with staurosporine as a control. Following selectivity profiling, (*vide infra*), additional measurements were carried out to investigate for off-Trk kinase activity. Compound (*R*)-IPMICF16 was tested for 10-concentration IC₅₀ curve with 3-fold serial dilution starting at 1.0 μ M for inhibitory activity against ACK1, ROS1 and TXK as described for TrkA, TrkB and TrkC (1 μ M ATP). Compound (*R*)-IPMICF16 was also assessed for 10-concentrations IC₅₀ curves with 3-fold serial dilution starting at 0.1 μ M at [ATP] = $K_{m \text{ ATP}}$ for K_i determination (against TrkA, TrkB and TrkC) in triplicate with staurosporine as a control. Values for K_i were derived from the Cheng Prusoff equation: $K_i = IC_{50}/(1+([S]/K_{m \text{ ATP}})) = IC_{50}/2$ for [S] = $K_{m \text{ ATP}}$. Compound (*S*)-IPMICF16 was tested for 10-concentrations IC₅₀ curves with 3-fold serial dilution starting at 100 μ M. The reactions were performed with 1 μ M ATP and profiled against 3 tyrosine kinases (tropomyosin receptor kinase A (TrkA), tropomyosin receptor kinase B (TrkB), tropomyosin receptor kinase C (TrkC)) in singlicate with staurosporine as a control.

6.2 Selectivity Profiling.

Compounds (*R*)-IPMICF16 was subsequently investigated for general kinase selectivity (tested against 369 wild type kinase at Reaction Biology Corporation) using “HotSpot” assay platform. Briefly, kinase/substrate pairs along with required cofactors were prepared in reaction buffer. The selected compounds were delivered into the reaction. [γ -³³P]ATP (10 μ M) was delivered into the reaction mixture to initiate the reactions, and the reactions continued for 120 min at room temperature, followed by spotting of the reactions onto P81 ion exchange filter paper (Whatman). Unbound phosphate was removed by extensive washing of filters in 0.75% phosphoric acid. After subtraction of background derived from control reactions containing inactive enzyme, kinase activity data were expressed as the percent remaining kinase activity in test samples compared to vehicle (DMSO) reactions (at 0.2 μ M of (*R*)-IPMICF16).

Table S5.4. Selectivity of (*R*)-IPMICF16 tested on a panel of 369 protein kinases at Reaction Biology Corporation (expressed as the percentage of kinase activity measured at 0.2 μ M of (*R*)-IPMICF16 compared to a 100% DMSO control.

| Kinases | % Enzyme Activity (relative to DMSO controls) | | IC50 (M) Control Cmpd | Control Cmpd ID |
|-------------|---|--------|-----------------------|-----------------|
| | (<i>R</i>)-IPMICF16 | | | |
| | Data 1 | Data 2 | | |
| ABL1 | 92.49 | 87.63 | 2.45E-08 | Staurosporine |
| ABL2/ARG | 97.20 | 94.97 | 1.25E-08 | Staurosporine |
| ACK1 | 17.74 | 17.18 | 3.29E-08 | Staurosporine |
| AKT1 | 99.18 | 98.56 | 5.20E-09 | Staurosporine |
| AKT2 | 100.54 | 97.41 | 2.27E-08 | Staurosporine |
| AKT3 | 106.43 | 106.37 | 3.52E-09 | Staurosporine |
| ALK | 77.12 | 75.90 | 1.44E-09 | Staurosporine |
| ALK1/ACVRL1 | 98.31 | 98.14 | 2.06E-08 | LDN193189 |
| ALK2/ACVR1 | 100.31 | 96.94 | 2.29E-08 | LDN193189 |
| ALK3/BMPR1A | 109.67 | 106.67 | 3.23E-08 | LDN193189 |
| ALK4/ACVR1B | 103.74 | 103.21 | 2.32E-07 | LDN193189 |
| ALK5/TGFR1 | 105.15 | 105.00 | 2.58E-07 | LDN193189 |
| ALK6/BMPR1B | 97.13 | 96.97 | 8.78E-09 | LDN193189 |
| ARAF | 72.95 | 72.36 | 1.90E-08 | GW5074 |
| ARK5/NUAK1 | 98.77 | 97.39 | 1.59E-09 | Staurosporine |
| ASK1/MAP3K5 | 91.06 | 89.31 | 1.08E-08 | Staurosporine |
| Aurora A | 110.17 | 108.96 | 1.67E-09 | Staurosporine |
| Aurora B | 95.60 | 94.87 | 4.33E-09 | Staurosporine |
| Aurora C | 94.86 | 93.44 | 1.45E-09 | Staurosporine |
| AXL | 96.89 | 95.44 | 7.20E-09 | Staurosporine |
| BLK | 95.91 | 93.96 | 1.33E-09 | Staurosporine |
| BMPR2 | 98.83 | 96.19 | 7.48E-07 | Staurosporine |
| BMX/ETK | 47.62 | 47.43 | 3.36E-09 | Staurosporine |
| BRAF | 93.59 | 93.10 | 2.58E-08 | GW5074 |
| BRK | 93.77 | 93.05 | 1.61E-07 | Staurosporine |
| BRSK1 | 96.40 | 95.80 | 5.12E-10 | Staurosporine |
| BRSK2 | 103.65 | 100.53 | 1.60E-09 | Staurosporine |
| BTK | 102.07 | 101.27 | 1.92E-08 | Staurosporine |
| CAMK1a | 99.54 | 99.40 | 2.23E-09 | Staurosporine |
| CAMK1b | 113.77 | 110.28 | 4.56E-09 | Staurosporine |
| CAMK1d | 102.52 | 102.29 | 2.83E-10 | Staurosporine |
| CAMK1g | 98.56 | 97.51 | 4.22E-09 | Staurosporine |
| CAMK2a | 96.53 | 95.89 | 4.72E-11 | Staurosporine |
| CAMK2b | 101.31 | 100.63 | 7.51E-11 | Staurosporine |
| CAMK2d | 100.54 | 99.92 | 4.45E-11 | Staurosporine |
| CAMK2g | 98.28 | 98.06 | 4.53E-10 | Staurosporine |
| CAMK4 | 85.81 | 85.72 | 9.21E-08 | Staurosporine |
| CAMKK1 | 88.84 | 88.12 | 6.51E-08 | Staurosporine |
| CAMKK2 | 97.70 | 95.99 | 2.36E-08 | Staurosporine |
| CDC7/DBF4 | 105.84 | 102.06 | 1.39E-08 | Staurosporine |

| Table S5.4 (Continued) | | | | |
|---------------------------------|--------|--------|-----------------|----------------------|
| CDK1/cyclin A | 100.91 | 100.67 | 2.30E-09 | Staurosporine |
| CDK1/cyclin B | 97.08 | 95.78 | 2.79E-09 | Staurosporine |
| CDK1/cyclin E | 104.50 | 102.78 | 2.69E-09 | Staurosporine |
| CDK14/cyclin Y (PFTK1) | 104.98 | 103.52 | 8.95E-08 | Staurosporine |
| CDK16/cyclin Y (PCTAIRE) | 105.43 | 104.77 | 2.65E-08 | Staurosporine |
| CDK17/cyclin Y (PCTK2) | 80.23 | 79.83 | 6.31E-09 | Staurosporine |
| CDK18/cyclin Y (PCTK3) | 106.62 | 105.59 | 2.12E-08 | Staurosporine |
| CDK19/cyclin C | 95.03 | 92.14 | 2.53E-11 | Staurosporine |
| CDK2/cyclin A | 93.75 | 93.74 | 7.51E-10 | Staurosporine |
| CDK2/Cyclin A1 | 109.13 | 105.94 | 1.33E-09 | Staurosporine |
| CDK2/cyclin E | 87.92 | 87.46 | 1.45E-09 | Staurosporine |
| CDK2/cyclin O | 83.81 | 82.18 | 1.37E-09 | Staurosporine |
| CDK3/cyclin E | 101.70 | 101.15 | 2.56E-09 | Staurosporine |
| CDK4/cyclin D1 | 92.26 | 91.88 | 1.40E-08 | Staurosporine |
| CDK4/cyclin D3 | 93.43 | 92.91 | 3.35E-08 | Staurosporine |
| CDK5/p25 | 96.08 | 95.32 | 2.40E-09 | Staurosporine |
| CDK5/p35 | 99.38 | 98.13 | 1.24E-09 | Staurosporine |
| CDK6/cyclin D1 | 97.74 | 97.34 | 3.98E-09 | Staurosporine |
| CDK6/cyclin D3 | 91.33 | 86.35 | 2.35E-08 | Staurosporine |
| CDK7/cyclin H | 98.61 | 95.45 | 5.22E-08 | Staurosporine |
| CDK9/cyclin K | 103.12 | 100.61 | 1.49E-08 | Staurosporine |
| CDK9/cyclin T1 | 103.64 | 103.46 | 5.72E-09 | Staurosporine |
| CDK9/cyclin T2 | 92.97 | 92.59 | 4.08E-09 | Staurosporine |
| CHK1 | 113.49 | 106.84 | 1.51E-10 | Staurosporine |
| CHK2 | 98.94 | 97.89 | 5.41E-09 | Staurosporine |
| CK1a1 | 96.46 | 95.77 | 5.89E-06 | Staurosporine |
| CK1a1L | 112.32 | 110.09 | 2.91E-06 | Staurosporine |
| CK1d | 113.47 | 113.17 | 1.91E-07 | D4476 |
| CK1epsilon | 99.61 | 99.21 | 3.67E-07 | D4476 |
| CK1g1 | 84.96 | 84.41 | 7.26E-06 | Staurosporine |
| CK1g2 | 87.94 | 87.06 | 9.56E-07 | Staurosporine |
| CK1g3 | 97.96 | 96.51 | 1.99E-06 | Staurosporine |
| CK2a | 77.31 | 69.61 | 2.86E-07 | GW5074 |
| CK2a2 | 84.62 | 84.18 | 5.48E-07 | Staurosporine |
| c-Kit | 95.88 | 95.49 | 3.97E-08 | Staurosporine |
| CLK1 | 107.74 | 107.55 | 8.40E-09 | Staurosporine |
| CLK2 | 101.41 | 98.60 | 3.86E-09 | Staurosporine |
| CLK3 | 103.28 | 102.52 | 1.38E-06 | Staurosporine |
| CLK4 | 106.90 | 104.20 | 4.34E-08 | Staurosporine |
| c-MER | 97.16 | 93.84 | 5.68E-09 | Staurosporine |
| c-MET | 96.22 | 95.06 | 1.29E-07 | Staurosporine |
| COT1/MAP3K8 | 89.10 | 88.85 | 6.22E-06 | Ro-31-8220 |
| CSK | 98.52 | 98.09 | 1.08E-08 | Staurosporine |
| c-Src | 92.44 | 91.83 | 2.09E-09 | Staurosporine |
| CTK/MATK | 95.49 | 94.47 | 2.65E-07 | Staurosporine |
| DAPK1 | 98.51 | 98.26 | 2.02E-08 | Staurosporine |

| Table S5.4 (Continued) | | | | |
|-------------------------------|--------|--------|-----------------|----------------------|
| DAPK2 | 95.87 | 95.29 | 5.66E-09 | Staurosporine |
| DCAMKL1 | 104.08 | 103.70 | 1.30E-07 | Staurosporine |
| DCAMKL2 | 100.65 | 99.83 | 3.62E-08 | Staurosporine |
| DDR1 | 64.57 | 63.39 | 2.43E-09 | Staurosporine |
| DDR2 | 101.12 | 100.68 | 1.72E-09 | Staurosporine |
| DLK/MAP3K12 | 84.64 | 81.27 | 9.81E-08 | Staurosporine |
| DMPK | 102.38 | 101.78 | 9.09E-08 | Staurosporine |
| DMPK2 | 105.87 | 103.75 | 7.78E-10 | Staurosporine |
| DRAK1/STK17A | 102.24 | 100.67 | 3.31E-08 | Staurosporine |
| DYRK1/DYRK1A | 100.29 | 99.31 | 2.57E-09 | Staurosporine |
| DYRK1B | 93.85 | 92.52 | 5.81E-10 | Staurosporine |
| DYRK2 | 98.89 | 97.43 | 2.28E-07 | Staurosporine |
| DYRK3 | 94.58 | 90.66 | 4.08E-08 | Staurosporine |
| DYRK4 | 91.20 | 89.61 | 4.55E-06 | GW5074 |
| EGFR | 92.06 | 91.53 | 1.28E-07 | Staurosporine |
| EPHA1 | 97.32 | 94.84 | 1.55E-07 | Staurosporine |
| EPHA2 | 98.10 | 97.66 | 4.20E-08 | Staurosporine |
| EPHA3 | 93.95 | 93.24 | 2.13E-08 | Staurosporine |
| EPHA4 | 100.24 | 99.38 | 1.21E-08 | Staurosporine |
| EPHA5 | 103.49 | 101.29 | 1.68E-08 | Staurosporine |
| EPHA6 | 83.77 | 81.90 | 1.62E-08 | Staurosporine |
| EPHA7 | 94.37 | 94.34 | 3.16E-08 | Staurosporine |
| EPHA8 | 97.80 | 97.22 | 1.32E-07 | Staurosporine |
| EPHB1 | 102.92 | 101.98 | 3.09E-08 | Staurosporine |
| EPHB2 | 91.99 | 91.15 | 5.39E-08 | Staurosporine |
| EPHB3 | 97.81 | 96.62 | 9.81E-07 | Staurosporine |
| EPHB4 | 94.33 | 91.47 | 1.59E-07 | Staurosporine |
| ERBB2/HER2 | 73.44 | 72.91 | 6.95E-08 | Staurosporine |
| ERBB4/HER4 | 101.14 | 101.06 | 2.85E-07 | Staurosporine |
| ERK1 | 98.09 | 97.38 | 2.06E-05 | Staurosporine |
| ERK2/MAPK1 | 103.99 | 98.66 | 1.63E-05 | Staurosporine |
| ERK5/MAPK7 | 99.25 | 95.33 | 1.07E-05 | Staurosporine |
| ERK7/MAPK15 | 105.92 | 104.49 | 8.16E-09 | Staurosporine |
| ERN1/IRE1 | 89.84 | 89.20 | 8.20E-08 | Staurosporine |
| ERN2/IRE2 | 97.65 | 96.17 | 3.17E-08 | Staurosporine |
| FAK/PTK2 | 95.68 | 95.13 | 1.14E-08 | Staurosporine |
| FER | 98.03 | 97.98 | 2.46E-10 | Staurosporine |
| FES/FPS | 91.07 | 90.06 | 8.56E-10 | Staurosporine |
| FGFR1 | 102.48 | 102.08 | 5.75E-09 | Staurosporine |
| FGFR2 | 103.72 | 101.43 | 2.41E-09 | Staurosporine |
| FGFR3 | 95.94 | 95.36 | 1.17E-08 | Staurosporine |
| FGFR4 | 99.30 | 97.79 | 7.03E-08 | Staurosporine |
| FGR | 92.98 | 91.09 | 5.12E-10 | Staurosporine |
| FLT1/VEGFR1 | 96.30 | 94.41 | 1.16E-08 | Staurosporine |
| FLT3 | 90.88 | 90.51 | 1.49E-09 | Staurosporine |
| FLT4/VEGFR3 | 97.90 | 96.78 | 3.11E-09 | Staurosporine |
| FMS | 100.47 | 100.21 | 1.63E-09 | Staurosporine |

| Table S5.4 (Continued) | | | | |
|-------------------------------|--------|--------|-----------------|----------------------|
| FRK/PTK5 | 106.17 | 105.23 | 1.17E-08 | Staurosporine |
| FYN | 94.90 | 94.35 | 2.12E-09 | Staurosporine |
| GCK/MAP4K2 | 97.81 | 96.43 | 8.79E-10 | Staurosporine |
| GLK/MAP4K3 | 89.30 | 89.24 | 8.64E-11 | Staurosporine |
| GRK1 | 100.77 | 99.78 | 4.84E-08 | Staurosporine |
| GRK2 | 101.70 | 100.03 | 7.09E-07 | Staurosporine |
| GRK3 | 97.82 | 96.79 | 6.89E-07 | Staurosporine |
| GRK4 | 90.73 | 90.48 | 5.48E-08 | Staurosporine |
| GRK5 | 105.37 | 105.09 | 4.35E-08 | Staurosporine |
| GRK6 | 100.93 | 100.78 | 2.65E-08 | Staurosporine |
| GRK7 | 92.36 | 91.30 | 3.87E-09 | Staurosporine |
| GSK3a | 107.61 | 101.25 | 3.04E-09 | Staurosporine |
| GSK3b | 97.23 | 95.08 | 7.79E-09 | Staurosporine |
| Haspin | 93.02 | 90.17 | 3.42E-08 | Staurosporine |
| HCK | 91.83 | 88.50 | 2.00E-09 | Staurosporine |
| HGK/MAP4K4 | 105.56 | 105.25 | 3.56E-10 | Staurosporine |
| HIPK1 | 93.81 | 92.13 | 3.80E-07 | Ro-31-8220 |
| HIPK2 | 99.22 | 98.96 | 4.79E-07 | Staurosporine |
| HIPK3 | 106.18 | 103.47 | 3.73E-07 | Staurosporine |
| HIPK4 | 96.15 | 95.83 | 4.89E-07 | Staurosporine |
| HPK1/MAP4K1 | 99.64 | 98.58 | 5.00E-08 | Ro-31-8220 |
| IGF1R | 95.65 | 95.44 | 2.66E-08 | Staurosporine |
| IKKa/CHUK | 101.70 | 97.34 | 1.47E-07 | Staurosporine |
| IKKb/IKBKB | 102.19 | 101.34 | 2.93E-07 | Staurosporine |
| IKKe/IKBKE | 98.43 | 96.18 | 2.82E-10 | Staurosporine |
| IR | 95.79 | 93.98 | 1.06E-08 | Staurosporine |
| IRAK1 | 104.00 | 102.05 | 2.52E-08 | Staurosporine |
| IRAK4 | 103.98 | 97.88 | 4.53E-09 | Staurosporine |
| IRR/INSRR | 81.09 | 80.54 | 4.69E-09 | Staurosporine |
| ITK | 101.53 | 101.33 | 1.07E-08 | Staurosporine |
| JAK1 | 98.65 | 96.40 | 5.76E-10 | Staurosporine |
| JAK2 | 88.98 | 88.37 | 2.26E-10 | Staurosporine |
| JAK3 | 102.06 | 99.85 | 1.10E-10 | Staurosporine |
| JNK1 | 98.21 | 98.09 | 5.03E-07 | Staurosporine |
| JNK2 | 97.80 | 97.29 | 1.95E-06 | Staurosporine |
| JNK3 | 99.36 | 98.26 | 1.04E-07 | JNKi VIII |
| KDR/VEGFR2 | 100.74 | 100.16 | 1.22E-08 | Staurosporine |
| KHS/MAP4K5 | 102.67 | 101.38 | 1.50E-10 | Staurosporine |
| KSR1 | 98.70 | 97.94 | 4.19E-06 | Staurosporine |
| KSR2 | 96.53 | 92.93 | 6.33E-06 | Staurosporine |
| LATS1 | 100.26 | 99.23 | 1.36E-08 | Staurosporine |
| LATS2 | 99.05 | 96.93 | 5.61E-09 | Staurosporine |
| LCK | 97.01 | 96.53 | 1.95E-09 | Staurosporine |
| LCK2/ICK | 96.73 | 93.63 | 3.80E-08 | Staurosporine |
| LIMK1 | 104.48 | 103.89 | 1.82E-09 | Staurosporine |
| LIMK2 | 97.41 | 96.19 | 9.50E-08 | Staurosporine |
| LKB1 | 106.09 | 105.48 | 5.22E-08 | Staurosporine |

| Table S5.4 (Continued) | | | | |
|-------------------------------|--------|--------|-----------------|----------------------|
| LOK/STK10 | 93.55 | 91.35 | 1.82E-08 | Staurosporine |
| LRRK2 | 99.12 | 98.84 | 5.26E-09 | Staurosporine |
| LYN | 94.93 | 93.21 | 6.69E-10 | Staurosporine |
| LYN B | 97.73 | 95.68 | 2.15E-09 | Staurosporine |
| MAK | 100.71 | 99.96 | 1.75E-08 | Staurosporine |
| MAPKAPK2 | 101.34 | 101.25 | 1.27E-07 | Staurosporine |
| MAPKAPK3 | 96.03 | 92.03 | 4.29E-06 | Staurosporine |
| MAPKAPK5/PRAK | 101.35 | 101.14 | 2.06E-07 | Staurosporine |
| MARK1 | 99.38 | 99.23 | 2.22E-10 | Staurosporine |
| MARK2/PAR-1Ba | 100.47 | 97.73 | 1.41E-10 | Staurosporine |
| MARK3 | 96.88 | 96.40 | 4.06E-10 | Staurosporine |
| MARK4 | 65.45 | 65.17 | 7.88E-11 | Staurosporine |
| MEK1 | 104.06 | 103.28 | 3.07E-08 | Staurosporine |
| MEK2 | 99.03 | 97.44 | 6.38E-08 | Staurosporine |
| MEK3 | 101.35 | 100.68 | 1.04E-08 | Staurosporine |
| MEK5 | 115.35 | 115.24 | 5.86E-08 | Staurosporine |
| MEKK1 | 108.80 | 107.43 | 6.81E-07 | Staurosporine |
| MEKK2 | 95.47 | 94.60 | 3.26E-08 | Staurosporine |
| MEKK3 | 94.02 | 92.80 | 3.91E-08 | Staurosporine |
| MEKK6 | 104.14 | 102.46 | 6.09E-07 | Staurosporine |
| MELK | 121.18 | 119.03 | 2.58E-10 | Staurosporine |
| MINK/MINK1 | 100.05 | 99.11 | 3.76E-10 | Staurosporine |
| MKK4 | 108.63 | 106.74 | 2.61E-06 | Staurosporine |
| MKK6 | 108.66 | 105.84 | 5.83E-09 | Staurosporine |
| MKK7 | 108.68 | 108.31 | 1.78E-06 | Staurosporine |
| MLCK/MYLK | 96.06 | 93.05 | 4.39E-08 | Staurosporine |
| MLCK2/MYLK2 | 104.53 | 103.95 | 1.39E-08 | Staurosporine |
| MLK1/MAP3K9 | 98.16 | 97.24 | 6.34E-10 | Staurosporine |
| MLK2/MAP3K10 | 88.21 | 83.94 | 2.73E-09 | Staurosporine |
| MLK3/MAP3K11 | 110.40 | 106.43 | 6.06E-09 | Staurosporine |
| MLK4 | 102.37 | 102.11 | 1.49E-06 | Staurosporine |
| MNK1 | 109.01 | 107.61 | 4.47E-08 | Staurosporine |
| MNK2 | 99.54 | 95.63 | 1.63E-08 | Staurosporine |
| MRCKa/CDC42BPA | 109.55 | 104.88 | 3.70E-09 | Staurosporine |
| MRCKb/CDC42BPB | 98.79 | 98.38 | 2.64E-09 | Staurosporine |
| MSK1/RPS6KA5 | 101.38 | 93.92 | 6.35E-10 | Staurosporine |
| MSK2/RPS6KA4 | 103.34 | 102.22 | 3.95E-09 | Staurosporine |
| MSSK1/STK23 | 98.77 | 97.16 | 2.45E-06 | Staurosporine |
| MST1/STK4 | 101.36 | 100.36 | 1.38E-09 | Staurosporine |
| MST2/STK3 | 93.44 | 92.19 | 4.82E-09 | Staurosporine |
| MST3/STK24 | 97.44 | 92.93 | 7.24E-09 | Staurosporine |
| MST4 | 96.62 | 96.22 | 3.95E-09 | Staurosporine |
| MUSK | 93.09 | 89.23 | 1.02E-07 | Staurosporine |
| MYLK3 | 105.78 | 105.35 | 1.85E-07 | Staurosporine |
| MYLK4 | 91.54 | 90.18 | 3.54E-08 | Staurosporine |
| MYO3A | 88.54 | 80.71 | 1.14E-08 | Staurosporine |
| MYO3b | 106.15 | 105.96 | 8.10E-09 | Staurosporine |

| Table S5.4 (Continued) | | | | |
|-------------------------------|--------|--------|----------|---------------|
| NEK1 | 89.17 | 88.36 | 9.89E-09 | Staurosporine |
| NEK11 | 71.92 | 71.39 | 4.44E-07 | Staurosporine |
| NEK2 | 104.84 | 104.61 | 3.88E-07 | Staurosporine |
| NEK3 | 109.42 | 107.61 | 3.39E-05 | Staurosporine |
| NEK4 | 102.88 | 100.36 | 1.87E-07 | Staurosporine |
| NEK5 | 98.81 | 96.50 | 7.35E-08 | Staurosporine |
| NEK6 | 103.43 | 100.80 | 2.49E-05 | PKR Inhibitor |
| NEK7 | 100.26 | 88.58 | 4.97E-06 | PKR Inhibitor |
| NEK8 | 103.66 | 102.26 | 3.23E-08 | Staurosporine |
| NEK9 | 111.21 | 108.64 | 1.30E-07 | Staurosporine |
| NIM1 | 98.16 | 95.48 | 1.51E-07 | Staurosporine |
| NLK | 87.27 | 85.98 | 4.77E-08 | Staurosporine |
| OSR1/OXSR1 | 101.95 | 101.49 | 8.99E-08 | Staurosporine |
| P38a/MAPK14 | 103.75 | 102.05 | 1.84E-08 | SB202190 |
| P38b/MAPK11 | 99.14 | 98.24 | 3.01E-08 | SB202190 |
| P38d/MAPK13 | 97.63 | 97.16 | 8.48E-08 | Staurosporine |
| P38g | 104.82 | 104.72 | 8.43E-08 | Staurosporine |
| p70S6K/RPS6KB1 | 99.30 | 98.57 | 5.20E-10 | Staurosporine |
| p70S6Kb/RPS6KB2 | 92.36 | 92.21 | 7.47E-10 | Staurosporine |
| PAK1 | 95.88 | 92.91 | 2.16E-10 | Staurosporine |
| PAK2 | 97.46 | 96.55 | 1.74E-09 | Staurosporine |
| PAK3 | 92.21 | 88.66 | 2.44E-10 | Staurosporine |
| PAK4 | 95.87 | 95.61 | 2.48E-08 | Staurosporine |
| PAK5 | 99.27 | 97.18 | 3.90E-09 | Staurosporine |
| PAK6 | 104.64 | 102.29 | 6.13E-08 | Staurosporine |
| PASK | 86.85 | 85.05 | 6.62E-09 | Staurosporine |
| PBK/TOPK | 102.34 | 102.17 | 5.43E-08 | Staurosporine |
| PDGFRa | 99.80 | 99.17 | 9.56E-10 | Staurosporine |
| PDGFRb | 94.54 | 93.53 | 2.23E-09 | Staurosporine |
| PDK1/PDPK1 | 96.60 | 95.68 | 4.91E-10 | Staurosporine |
| PEAK1 | 99.75 | 99.43 | 2.69E-09 | Staurosporine |
| PHKg1 | 93.49 | 93.16 | 1.83E-09 | Staurosporine |
| PHKg2 | 101.38 | 99.50 | 4.53E-10 | Staurosporine |
| PIM1 | 76.46 | 76.09 | 2.63E-09 | Staurosporine |
| PIM2 | 98.84 | 97.71 | 1.36E-08 | Staurosporine |
| PIM3 | 57.10 | 55.53 | 8.60E-11 | Staurosporine |
| PKA | 103.34 | 101.72 | 7.98E-10 | Staurosporine |
| PKAcb | 99.69 | 98.65 | 1.55E-09 | Staurosporine |
| PKAcg | 99.04 | 98.47 | 7.97E-09 | Staurosporine |
| PKCa | 93.41 | 92.39 | 3.57E-10 | Staurosporine |
| PKCb1 | 92.19 | 91.06 | 4.48E-09 | Staurosporine |
| PKCb2 | 102.49 | 100.86 | 2.23E-09 | Staurosporine |
| PKCd | 93.72 | 91.74 | 1.75E-10 | Staurosporine |
| PKCepsilon | 99.11 | 98.71 | 1.39E-10 | Staurosporine |
| PKCeta | 86.23 | 83.50 | 3.13E-10 | Staurosporine |
| PKCg | 105.76 | 104.61 | 1.18E-09 | Staurosporine |
| PKCiota | 101.11 | 99.50 | 1.04E-08 | Staurosporine |

| Table S5.4 (Continued) | | | | |
|-------------------------------|--------|--------|-----------------|----------------------|
| PKCmu/PRKD1 | 94.74 | 94.52 | 9.21E-10 | Staurosporine |
| PKCnu/PRKD3 | 109.48 | 103.63 | 1.60E-09 | Staurosporine |
| PKCtheta | 98.57 | 92.35 | 3.04E-09 | Staurosporine |
| PKCzeta | 104.04 | 103.06 | 6.03E-08 | Staurosporine |
| PKD2/PRKD2 | 95.18 | 93.74 | 5.91E-10 | Staurosporine |
| PKG1a | 90.76 | 90.71 | 9.93E-10 | Staurosporine |
| PKG1b | 101.59 | 101.12 | 2.38E-09 | Staurosporine |
| PKG2/PRKG2 | 97.72 | 92.24 | 5.45E-09 | Staurosporine |
| PKN1/PRK1 | 114.70 | 111.33 | 3.12E-09 | Staurosporine |
| PKN2/PRK2 | 95.31 | 94.93 | 6.57E-09 | Staurosporine |
| PKN3/PRK3 | 92.25 | 91.98 | 7.75E-09 | Staurosporine |
| PLK1 | 99.44 | 96.26 | 1.36E-07 | Staurosporine |
| PLK2 | 98.97 | 98.38 | 2.37E-07 | Staurosporine |
| PLK3 | 96.01 | 95.04 | 1.70E-07 | Staurosporine |
| PLK4/SAK | 91.11 | 85.26 | 1.21E-08 | Staurosporine |
| PRKX | 100.57 | 100.40 | 6.05E-10 | Staurosporine |
| PYK2 | 102.45 | 101.16 | 6.58E-09 | Staurosporine |
| RAF1 | 83.23 | 82.49 | 9.96E-09 | GW5074 |
| RET | 101.35 | 100.05 | 1.30E-09 | Staurosporine |
| RIPK2 | 96.72 | 91.73 | 4.12E-07 | Staurosporine |
| RIPK3 | 105.03 | 104.88 | 1.40E-06 | GW5074 |
| RIPK4 | 103.97 | 98.07 | 5.12E-07 | Staurosporine |
| RIPK5 | 102.82 | 101.89 | 2.84E-08 | Staurosporine |
| ROCK1 | 98.43 | 96.65 | 5.38E-10 | Staurosporine |
| ROCK2 | 98.91 | 96.92 | 3.42E-10 | Staurosporine |
| RON/MST1R | 97.07 | 95.75 | 2.21E-07 | Staurosporine |
| ROS/ROS1 | 9.81 | 9.33 | 1.18E-10 | Staurosporine |
| RSK1 | 95.05 | 94.11 | 1.28E-10 | Staurosporine |
| RSK2 | 103.42 | 102.98 | 1.09E-10 | Staurosporine |
| RSK3 | 98.01 | 97.80 | 1.67E-10 | Staurosporine |
| RSK4 | 107.04 | 106.81 | 6.54E-11 | Staurosporine |
| SBK1 | 103.99 | 101.13 | 8.40E-08 | Staurosporine |
| SGK1 | 83.64 | 83.13 | 6.51E-09 | Staurosporine |
| SGK2 | 100.38 | 96.62 | 1.34E-08 | Staurosporine |
| SGK3/SGKL | 97.92 | 97.68 | 6.80E-08 | Staurosporine |
| SIK1 | 99.10 | 96.79 | 4.43E-10 | Staurosporine |
| SIK2 | 95.22 | 94.03 | 3.43E-10 | Staurosporine |
| SIK3 | 100.60 | 100.02 | 1.35E-09 | Staurosporine |
| SLK/STK2 | 102.40 | 100.36 | 1.34E-08 | Staurosporine |
| SNARK/NUAK2 | 100.73 | 97.91 | 1.54E-09 | Staurosporine |
| SNRK | 95.46 | 95.15 | 1.86E-08 | Staurosporine |
| SRMS | 102.79 | 102.27 | 9.14E-06 | Staurosporine |
| SRPK1 | 99.94 | 99.51 | 1.47E-08 | Staurosporine |
| SRPK2 | 106.02 | 105.29 | 1.19E-07 | Staurosporine |
| SSTK/TSSK6 | 102.67 | 101.99 | 1.70E-07 | Staurosporine |
| STK16 | 104.08 | 102.22 | 2.45E-07 | Staurosporine |
| STK21/CIT | 95.80 | 95.52 | 1.15E-06 | Staurosporine |

| Table S5.4. (Continued) | | | | |
|--------------------------------|--------|--------|-----------------|------------------------|
| STK22D/TSSK1 | 98.24 | 97.69 | 3.99E-11 | Staurosporine |
| STK25/YSK1 | 97.65 | 94.06 | 2.67E-09 | Staurosporine |
| STK32B/YANK2 | 90.32 | 89.14 | 3.23E-08 | Staurosporine |
| STK32C/YANK3 | 88.65 | 88.39 | 1.42E-07 | Staurosporine |
| STK33 | 104.94 | 104.13 | 3.66E-08 | Staurosporine |
| STK38/NDR1 | 101.20 | 101.10 | 8.09E-10 | Staurosporine |
| STK38L/NDR2 | 100.86 | 96.99 | 1.04E-09 | Staurosporine |
| STK39/STLK3 | 95.70 | 91.90 | 8.75E-09 | Staurosporine |
| SYK | 99.72 | 99.00 | 1.10E-09 | Staurosporine |
| TAK1 | 95.56 | 94.69 | 5.43E-08 | Staurosporine |
| TAOK1 | 101.70 | 100.95 | 5.57E-10 | Staurosporine |
| TAOK2/TAO1 | 94.26 | 92.09 | 3.95E-09 | Staurosporine |
| TAOK3/JIK | 102.20 | 100.21 | 1.89E-09 | Staurosporine |
| TBK1 | 103.76 | 103.55 | 1.81E-09 | Staurosporine |
| TEC | 101.12 | 99.46 | 5.94E-08 | Staurosporine |
| TESK1 | 100.79 | 100.28 | 2.62E-07 | Staurosporine |
| TESK2 | 96.37 | 95.72 | 1.40E-05 | Staurosporine |
| TGFBR2 | 106.25 | 99.30 | 1.28E-07 | LDN193189 |
| TIE2/TEK | 97.45 | 97.09 | 3.28E-08 | Staurosporine |
| TLK1 | 99.36 | 97.40 | 2.40E-08 | Staurosporine |
| TLK2 | 103.07 | 99.62 | 3.94E-09 | Staurosporine |
| TNIK | 73.81 | 69.83 | 1.61E-10 | Staurosporine |
| TNK1 | 72.16 | 71.97 | 5.18E-10 | Staurosporine |
| TRKA | -0.25 | -0.58 | 1.51E-09 | Staurosporine |
| TRKB | 0.80 | 0.75 | 6.33E-11 | Staurosporine |
| TRKC | -1.64 | -1.78 | 1.43E-10 | Staurosporine |
| TSSK2 | 94.63 | 90.26 | 5.46E-09 | Staurosporine |
| TSSK3/STK22C | 84.09 | 81.09 | 6.17E-09 | Staurosporine |
| TTBK1 | 92.77 | 90.48 | 8.88E-05 | SB202190 |
| TTBK2 | 112.04 | 109.72 | 7.58E-06 | SB202190 |
| TXK | 26.24 | 24.23 | 1.38E-08 | Staurosporine |
| TYK1/LTK | 77.53 | 76.97 | 1.75E-08 | Staurosporine |
| TYK2 | 98.34 | 96.33 | 3.35E-10 | Staurosporine |
| TYRO3/SKY | 95.02 | 93.93 | 2.43E-09 | Staurosporine |
| ULK1 | 103.91 | 101.93 | 5.87E-09 | Staurosporine |
| ULK2 | 95.54 | 94.56 | 2.66E-09 | Staurosporine |
| ULK3 | 105.88 | 103.63 | 5.12E-09 | Staurosporine |
| VRK1 | 84.11 | 82.99 | 6.11E-07 | Ro-31-8220 |
| VRK2 | 96.22 | 95.83 | 2.97E-05 | Ro-31-8220 |
| WEE1 | 110.92 | 110.74 | 9.75E-08 | Wee-1 Inhibitor |
| WNK1 | 100.37 | 94.51 | 1.35E-05 | Staurosporine |
| WNK2 | 97.17 | 95.30 | 1.04E-06 | Staurosporine |
| WNK3 | 94.95 | 92.76 | 2.42E-06 | Wee-1 Inhibitor |
| YES/YES1 | 104.02 | 102.15 | 1.59E-09 | Staurosporine |
| YSK4/MAP3K19 | 109.29 | 103.89 | 1.22E-08 | Staurosporine |
| ZAK/MLTK | 104.99 | 104.78 | 1.64E-06 | GW5074 |
| ZAP70 | 101.91 | 100.62 | 7.34E-09 | Staurosporine |

| | | | | |
|-------------------------------|--------|--------|-----------------|----------------------|
| Table S5.4 (Continued) | | | | |
| ZIPK/DAPK3 | 105.80 | 105.27 | 3.29E-09 | Staurosporine |

7. RADIOCHEMISTRY

7.1 Radiotracers and Sites

For *in vivo* rodent preclinical PET imaging baseline and blocking experiments (Sprague Dawley rats, FVB mice, *Mdr1a/b*^(-/-) *Bcrp1*^(-/-) mice), radiotracers [¹¹C]-(\pm)-IPMICF16, [¹¹C]-(*R*)-IPMICF16, [¹¹C]-(\pm)-IPMICF22, [¹¹C]GW441756, [¹⁸F]-(\pm)-IPMICF6 and [¹⁸F]-(\pm)-IPMICF10 were produced at the Edmonton PET Center Site. For *in vitro* autoradiography experiments, the radiotracer [¹¹C]-(*R*)-IPMICF16 was produced at the cyclotron laboratory of the McConnell Brain Imaging Center Site (Montreal Neurological Institute, McGill University). For *in vivo* non-human primate preclinical PET imaging baseline experiments (rhesus monkey), radiotracers [¹¹C]-(\pm)-IPMICF16, [¹¹C]-(*R*)-IPMICF16, [¹¹C]-(\pm)-IPMICF22, [¹¹C]GW441756, [¹⁸F]-(\pm)-IPMICF6 and [¹⁸F]-(\pm)-IPMICF10 were produced at the University of Michigan PET Center site. For *in vivo* clinical first-in-human PET imaging experiment, the radiotracer [¹¹C]-(*R*)-IPMICF16 was produced at Munich site.

7.2 Edmonton PET Center Site

7.2.1 *General Considerations.* [¹¹C]CH₃I was produced on a TracerLab FX Mel-unit from GE-Healthcare. [¹¹C]CO₂ was produced via the ¹⁴N(p, α)¹¹C nuclear reaction on a TR 19/9 cyclotron from ACSU (Advanced Cyclotron Systems Incorporation) by proton bombardment of a nitrogen/oxygen (99/1%) target gas mixture and trapped on a molecular sieve/Shimalite®-nickel catalyst-unit, which was first flushed with hydrogen and then heated up to 425 °C at 2-3 psi to convert it into [¹¹C]CH₄. The [¹¹C]CH₄ was absorbed on a carbospher-trap at -80 °C. The trap was purged with helium to remove the remaining hydrogen. Next, the [¹¹C]CH₄ was released at 60 °C. Unconverted CO₂ and moisture was removed by a NaOH/P₂O₅ trap. The [¹¹C]CH₃I was produced by the reaction of [¹¹C]CH₄ with gaseous I₂ at 725°C. The unconverted [¹¹C]CH₄ was recycled back for reaction with iodine. Gaseous [¹¹C]CH₃I was then directly bubbled into the reaction mixture containing the required precursor. Semi-preparative, radio-preparative HPLC purifications and quality control analyses were performed using a Phenomenex LUNA® C18 column (100 Å, 250 × 10 mm, 10 μm) using a Gilson 322 Pump module fitted with a 171 Diode Array and a radio detector. HPLC grade acetonitrile was purchased from Aldrich. C18 Light Sep-Paks were purchased from Waters Corporation and were preconditioned with 10 mL of ethanol followed by 10 mL of sterile water prior to use. The manual radiosyntheses of [¹¹C]-(\pm)-

IPMICF16 ($[^{11}\text{C}]-(\pm)\text{-5.3}$), $[^{11}\text{C}]-(R)\text{-IPMICF16}$ ($[^{11}\text{C}]-(R)\text{-5.3}$) and $[^{11}\text{C}]-(\pm)\text{-IPMICF22}$ ($[^{11}\text{C}]-(\pm)\text{-5.4}$) were performed and optimized in the radiochemistry laboratory of the Edmonton PET Center Site and are described below. The manual radiosyntheses of $[^{11}\text{C}]\text{GW441756}$ ($[^{11}\text{C}]\text{5}$), $[^{18}\text{F}]-(\pm)\text{-IPMICF6}$ ($[^{18}\text{F}]-(\pm)\text{-5.1}$) and $[^{18}\text{F}]-(\pm)\text{-IPMICF10}$ ($[^{18}\text{F}]-(\pm)\text{-5.2}$) were performed as previously described.^{1,5}

7.2.2 Radiosyntheses of $[^{11}\text{C}]-(\pm)\text{-IPMICF16}$ and $[^{11}\text{C}]-(R)\text{-IPMICF16}$. To a 1 mL conical vial containing 1.0-1.5 mg of phenolic precursor **5.14** (or $(R)\text{-5.14}$) was added 500 μL DMF and 10 μL K_2CO_3 sat. aqueous solution. $[^{11}\text{C}]\text{CH}_3\text{I}$ was bubbled through the reaction mixture for 1-3 min trapping $\sim 3.5\text{-}4.0$ GBq (96-108 mCi) in the reaction vessel. A 200 μL aliquot was taken and placed into a vial preheated to 80°C for 3 min. The reaction was quenched with 0.5 mL HPLC eluent and a fraction transferred for purification (~ 1 GBq). The diluted reaction mixture was purified by semi-preparative HPLC (mobile phase: 25% water/75% acetonitrile (v/v) isocratic; flow rate: 3.0 mL/min). The peaks at 9.26 and 9.76 min corresponding to $[^{11}\text{C}]-(\pm)\text{-IPMICF16}$ (or $[^{11}\text{C}]-(R)\text{-IPMICF16}$) were collected (**Figure S5.14**), combined and diluted with 15 mL H_2O and the solution was transferred through a preconditioned C18 Light Sep-Pak. The radiotracer was eluted dropwise with EtOH. Drops 6-12 were combined and the volume was reduced to 10-15 μL under a stream of N_2 while heating at 80°C yielding pure $[^{11}\text{C}]-(\pm)\text{-IPMICF16}$ (or $[^{11}\text{C}]-(R)\text{-IPMICF16}$) (35.7 ± 9.7 % nondecay-corrected radiochemical yield at end-of-synthesis based upon activity injected on HPLC, $n = 18$, radiochemical purity $> 99\%$, $S_A \sim 35$ GBq/ μmol , **Figure S5.15**). The radiotracer was re-dissolved in 150 μL 0.9% saline for delivery of the injectable formulation for *in vivo* analyses. Quality control was assessed by analytical HPLC (mobile phase: 25% water/75% acetonitrile (v/v) isocratic; flow rate: 3.0 mL/min, ($t_{r [^{11}\text{C}]-(R)\text{-IPMICF16}} = 9.7$ min)

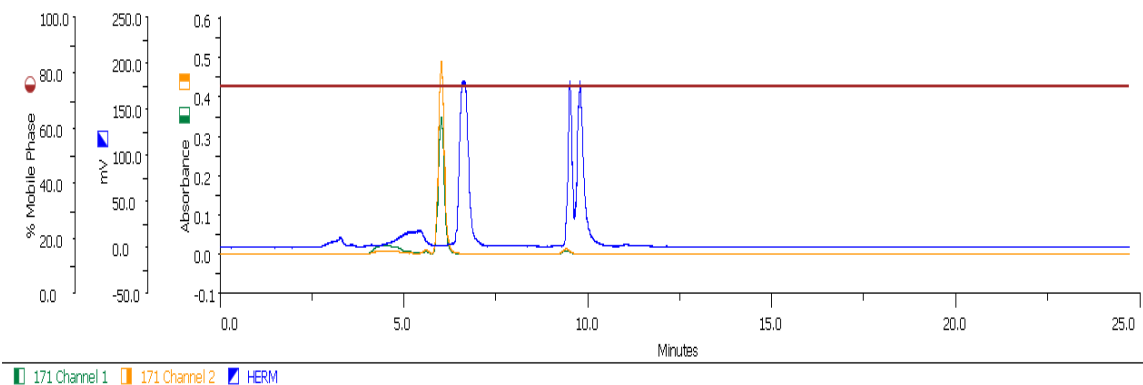


Figure S5.14. Representative semi-preparative HPLC chromatograms for the radiosynthesis $[^{11}\text{C}]-(R)\text{-IPMICF16}$ (UV yellow, Rad blue).

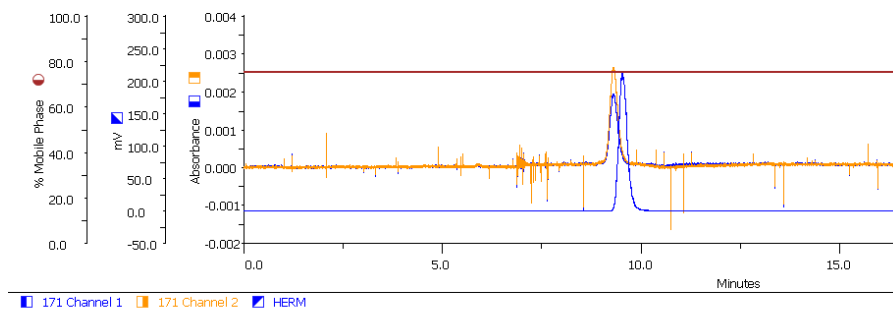


Figure S5.15. Representative HPLC-QC chromatograms of the collected [^{11}C]-(*R*)-IPMICF16 co-injected with the non-radioactive standard IPMICF16 (**5.3**) (UV yellow, Rad blue).

7.2.3 Radiosynthesis of [^{11}C]-(\pm)-IPMICF22. To a 1 mL conical vial containing 2.0 mg of desmethyl precursor (\pm)-**5.15** was added 400 μL of DMF and 10 μL of TBAOH (1.0 M in MeOH). [^{11}C]CH₃I was bubbled through the reaction mixture for 1-3 min trapping ~ 3.2 -4.0 GBq (87-108 mCi) in the reaction vessel. The reaction was quenched with 0.6 mL μL 50/50 H₂O/MeCN and a fraction transferred for purification (~ 0.6 GBq). The diluted reaction mixture was purified by semi-preparative HPLC (mobile phase: 45% water/55% acetonitrile (v/v) isocratic; flow rate: 3.0 mL/min). The peaks at 8.8 and 9.0 min corresponding to [^{11}C]-(\pm)-IPMICF22 were collected (**Figure S5.16**), combined and diluted with 15 mL H₂O and the solution was transferred through a preconditioned C18 Light Sep-Pak. The radiotracer was eluted dropwise with EtOH (first 2 drops discarded). Drops 3-14 were pooled and the volume was reduced to 10-30 μL under a stream of N₂ while heating at 80°C yielding pure [^{11}C]-(\pm)-IPMICF22 (25.4 \pm 4.2 % nondecay-corrected radiochemical yield at end-of-synthesis based upon activity injected on HPLC, $n = 9$, radiochemical purity > 99%, $S_A \sim 35$ GBq/ μmol , (**Figure S5.17**). The radiotracer was re-dissolved in 150 μL 0.9% saline for delivery of the injectable formulation for *in vivo* analyses. Quality control was assessed by analytical HPLC (mobile phase: 45% water/55% acetonitrile (v/v) isocratic; flow rate: 3.0 mL/min, ($t_{r[\text{11C}]-(\pm)\text{-IPMICF22}} = 9.0$ min)

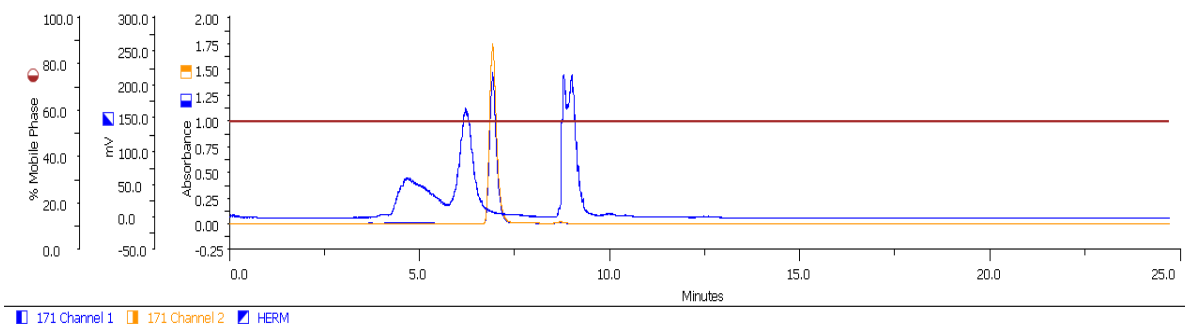


Figure S5.16. Representative semi-preparative HPLC chromatograms for the radiosynthesis [^{11}C]-(+)-IPMICF22 (UV yellow, Rad blue).

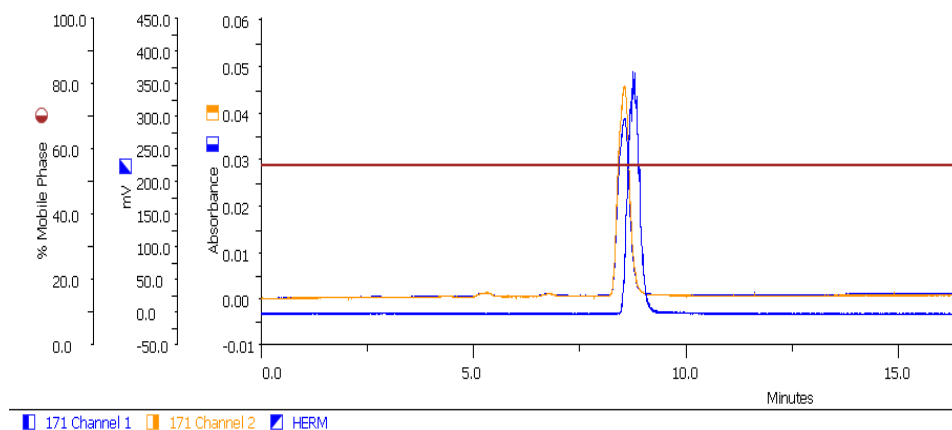


Figure S5.17. Representative HPLC-QC chromatograms of the collected [^{11}C]-(+)-IPMICF16 co-injected with the non-radioactive standard IPMICF22 (**5.4**) (UV yellow, Rad blue).

7.3 University of Michigan PET Center Site

7.3.1 General Considerations. The production of fluorine-18 labeled radiotracers ([^{18}F]-(+)-IPMICF6 and [^{18}F]-(+)-IPMICF10) was carried out using a TRACERLAB FXfn automated radiochemistry synthesis module (General Electric, GE). [^{18}F]Fluoride was produced via the $^{18}\text{O}(p,n)^{18}\text{F}$ nuclear reaction using a GE PET Trace cyclotron (40 μA beam for 30 min generated 48-52 GBq (1300-1400 mCi) of [^{18}F]fluoride). The [^{18}F]fluoride was delivered to the synthesis module (in a 1.5 mL bolus of [^{18}O]water) and trapped on a QMA-light Sep-Pak to remove [^{18}O]water. [^{18}F]Fluoride was then eluted into the reaction vessel using aqueous potassium carbonate (3.5 mg in 0.5 mL of water). A solution of Kryptofix 2.2.2 (15 mg in 1 mL of acetonitrile) was then added to the reaction vessel and the [^{18}F]fluoride was dried by evaporating the water-acetonitrile azeotrope. Evaporation was achieved by heating the reaction vessel to 80 $^{\circ}\text{C}$ and drawing full vacuum for 6 min. After this time, the reaction vessel was

cooled to 60 °C and subjected to both an argon stream and vacuum draw simultaneously for another 6 min.

The production of carbon-11 labeled radiotracers ($[^{11}\text{C}]-(\pm)\text{-IPMICF16}$, $[^{11}\text{C}]-(R)\text{-IPMICF16}$, $[^{11}\text{C}]-(\pm)\text{-IPMICF22}$ and $[^{11}\text{C}]\text{GW441756}$) was carried out using a TRACERLAB FXc-pro automated radiochemistry synthesis module (General Electric, GE). Carbon-11 was produced via the $^{14}\text{N}(p,\alpha)^{11}\text{C}$ nuclear reaction using a GEMS PET Trace cyclotron equipped with a carbon-11 target. Carbon-11 was delivered from the cyclotron target (40 μA , 30 min beam provided ~ 3 Ci of carbon-11 as $[^{11}\text{C}]\text{CO}_2$) via a 1/16" Teflon delivery line by nitrogen pressure directly to a column packed with 0.3 g of molecular sieve and 0.2 g of Shimalite–Nickle where it was trapped at room temperature. The column was then sealed under hydrogen gas and heated to 350°C for 20 seconds to reduce the $[^{11}\text{C}]\text{CO}_2$ to $[^{11}\text{C}]\text{CH}_4$. The $[^{11}\text{C}]\text{CH}_4$ was passed through a column of phosphorous pentoxide desiccant and trapped on a column of carbosphere cooled to -75°C (with liquid nitrogen). Gaseous $[^{11}\text{C}]\text{CH}_4$ was released by heating the carbosphere column to 80°C. Once released the methane entered a circulation loop, which includes a gas pump, a column of iodine at 100°C, the Tracerlab standard iodine reactor tube at 720°C, two adjacent columns of Ascarite II and a column of Porapak Q at room temperature. The gaseous mixture was circulated for 5 min while $[^{11}\text{C}]\text{CH}_3\text{I}$ accumulated on the Porapak column. The $[^{11}\text{C}]\text{CH}_3\text{I}$ ($\sim 0.5\text{-}0.9$ Ci) was then released from the Porapak column and delivered to the reaction mixture containing the required precursor. Alternatively, the $[^{11}\text{C}]\text{CH}_3\text{I}$ converted to $[^{11}\text{C}]\text{CH}_3\text{OTf}$ by passing it through a silver triflate Graphpac column pre-heated to 190°C. The resulting $[^{11}\text{C}]\text{CH}_3\text{OTf}$ was released into the reaction mixture containing the required precursor. Semi-preparative, radio-preparative HPLC purifications were performed using a Phenomenex LUNA® C18 column (100 Å, 250 × 10 mm, 10 μm). Quality control HPLC analyses were performed using Phenomenex Luna C8 (4.6 × 150 mm, 3 μm). Unless otherwise stated, reagents and solvents were commercially available and used without further purification: Sodium Chloride, 0.9% USP and Sterile Water for Injection, USP were purchased from Hospira; ethanol was purchased from American Regent; HPLC grade acetonitrile was purchased from Fisher Scientific. C18 Light Sep-Paks and Porapak Q were purchased from Waters Corporation. Sep-Paks were preconditioned with 10 mL of ethanol followed by 10 mL of sterile water prior to use.

7.3.2 Radiosyntheses of $[^{18}\text{F}]-(\pm)\text{-IPMICF6}$. A solution of tosylate precursor (2.5 mg) in anhydrous DMF (300 μL) was added to $[^{18}\text{F}]\text{fluoride}$ dried as described above, and the solution was heated at 120°C with stirring for 10 min. The reaction mixture was cooled to 50 °C,

quenched with 600 μL 50/50 $\text{H}_2\text{O}/\text{MeCN}$ and loaded onto HPLC (mobile phase: 40% water/60% acetonitrile (v/v) isocratic; flow rate: 3.0 mL/min). The peak between 14.3-16.2 min corresponding to $[^{18}\text{F}]-(\pm)\text{-IPMICF6}$ (Figure S5.18) was collected and diluted with 15 mL H_2O and the solution was transferred through a preconditioned C18 1cc Vac Sep Pak. The radiotracer was eluted with 500 μL EtOH and then the ethanolic product was passed through a sterile filter and into the product vial. The C18 cartridge was then washed with 4.5 mL buffered saline, which was also passed through the sterile filter and collected in the product vial. Pure $[^{18}\text{F}]-(\pm)\text{-IPMICF6}$ was obtained in 4.4 % nondecay-corrected radiochemical yield at end-of-synthesis based upon dry $[^{18}\text{F}]\text{fluoride}$, $n = 1$, radiochemical purity > 99%, $S_A \sim 250 \text{ GBq}/\mu\text{mol}$. Quality control mobile phase: 40% water/60% acetonitrile (v/v) isocratic; flow rate: 1.0 mL/min (Figure S5.19).

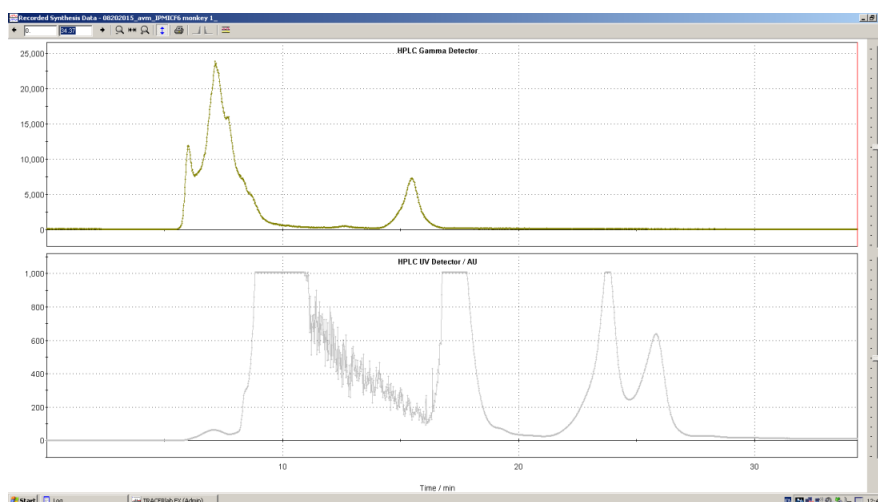


Figure S5.18. Representative semi-preparative HPLC chromatograms for the radiosynthesis $[^{18}\text{F}]-(\pm)\text{-IPMICF6}$ (Rad above, UV below).

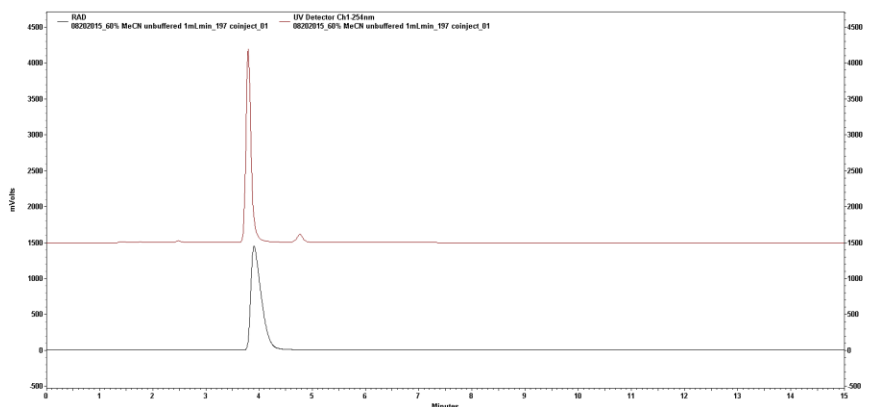


Figure S5.19. Representative HPLC-QC chromatograms of the collected $[^{18}\text{F}]-(\pm)\text{-IPMICF6}$ co-injected with the non-radioactive standard IPMICF6 (5.1) (UV above, Rad below).

7.3.3 Radiosyntheses of [^{18}F]-(\pm)-IPMICF10. A solution of tosylate precursor (2.5 mg) in anhydrous DMF (300 μL) was added to [^{18}F]fluoride dried as described above, and the solution was heated at 100°C with stirring for 20 min. The reaction mixture was cooled to 50 °C, quenched with 600 μL MeCN and loaded onto HPLC (mobile phase: 30% water/70% acetonitrile (v/v) isocratic; flow rate: 3.0 mL/ min). The peak between 10.2-11.2 min corresponding to [^{18}F]-(\pm)-IPMICF10 (**Figure S5.20**) was collected and diluted with 30 mL H₂O and the solution was transferred through a preconditioned C18 1cc Vac Sep Pak. The radiotracer was eluted with 500 μL EtOH and then the ethanolic product was passed through a sterile filter and into the product vial. The C18 cartridge was then washed with 4.5 mL buffered saline, which was also passed through the sterile filter and collected in the product vial. Pure [^{18}F]-(\pm)-IPMICF10 was obtained in 1.5 % nondecay-corrected radiochemical yield at end-of-synthesis based upon dry [^{18}F]fluoride, $n = 1$, radiochemical purity > 99%, $S_A \sim 101 \text{ GBq}/\mu\text{mol}$. Quality control mobile phase: 40% water/60% acetonitrile (v/v) isocratic; flow rate: 1.0 mL/ min (**Figure S5.21**).

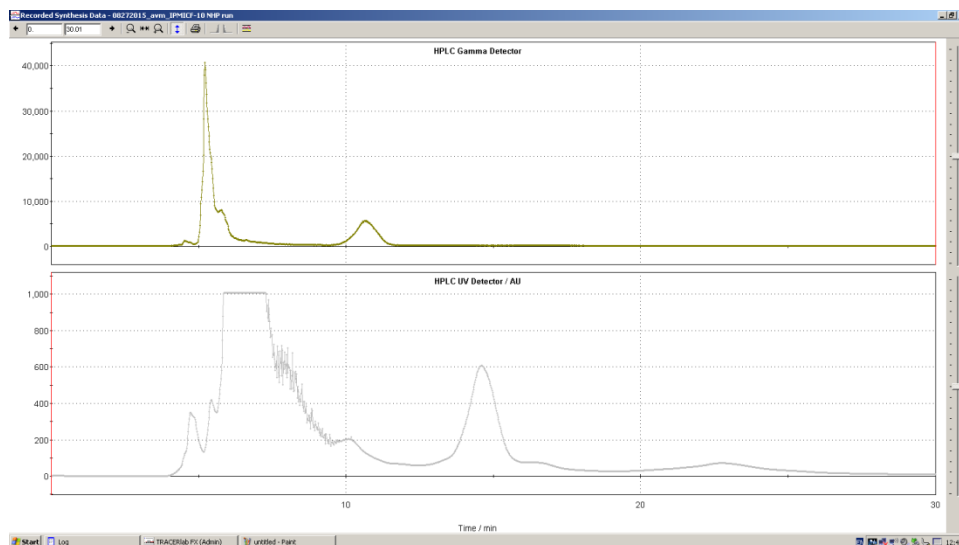


Figure S5.20. Representative semi-preparative HPLC chromatograms for the radiosynthesis [^{18}F]-(\pm)-IPMICF10 (Rad above, UV below).

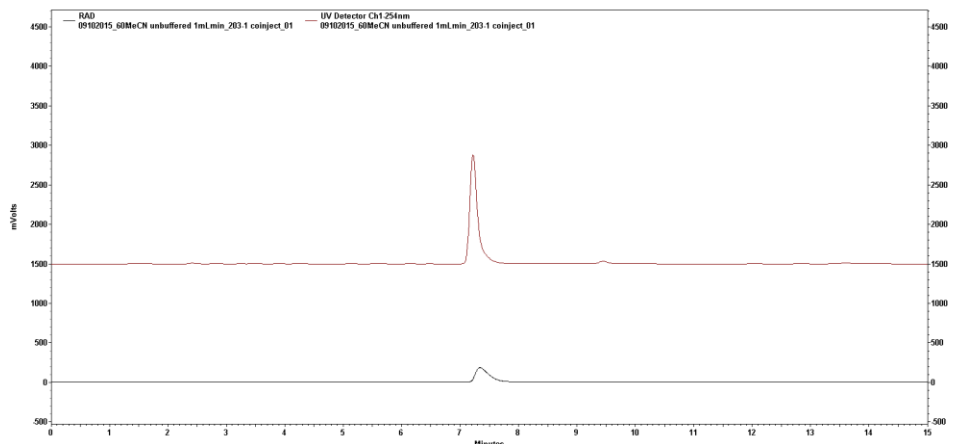


Figure S5.21. Representative HPLC-QC chromatograms of the collected [^{18}F]-(\pm)-IPMICF10 co-injected with the non-radioactive standard IPMICF10 (**5.2**) (UV above, Rad below).

7.3.4 Radiosyntheses of [^{11}C]-(\pm)-IPMICF16 and [^{11}C]-(*R*)-IPMICF16. [^{11}C]CH₃OTf was bubbled through a reaction solution containing 1.25 mg precursor (\pm)-**5.14** (or (*R*)-**5.14**), 2 μL 1.0 M methanolic TBAOH and 200 μL DMF at room temperature for 3 min at 15 mL min with Ar carrier gas. The reaction was quenched with 600 μL 25/75 H₂O/MeCN and loaded onto HPLC (mobile phase: 25% water/75% acetonitrile (v/v) isocratic; flow rate: 3.0 mL/ min). The peak between 9.4-10.2 min corresponding to [^{11}C]-(\pm)-IPMICF16 (or [^{11}C]-(*R*)-IPMICF16, **Figure S5.22**) was collected and diluted with 50 mL H₂O and the solution was transferred through a preconditioned C18 1cc Vac Sep Pak. The radiotracer was eluted with 500 μL EtOH and then the ethanolic product was passed through a sterile filter and into the product vial. The C18 cartridge was then washed with 4.5 mL buffered saline, which was also passed through the sterile filter and collected in the product vial. Pure [^{11}C]-(\pm)-IPMICF16 (or [^{11}C]-(*R*)-IPMICF16) was obtained in 13.3 % nondecay-corrected radiochemical yield at end-of-synthesis based upon [^{11}C]CH₃I, $n = 3$ per radiotracer, radiochemical purity > 99%, $S_A \sim 348 \text{ GBq}/\mu\text{mol}$. Quality control mobile phase: 25% water/75% acetonitrile (v/v) isocratic; flow rate: 1.0 mL/ min (**Figure S5.23**).

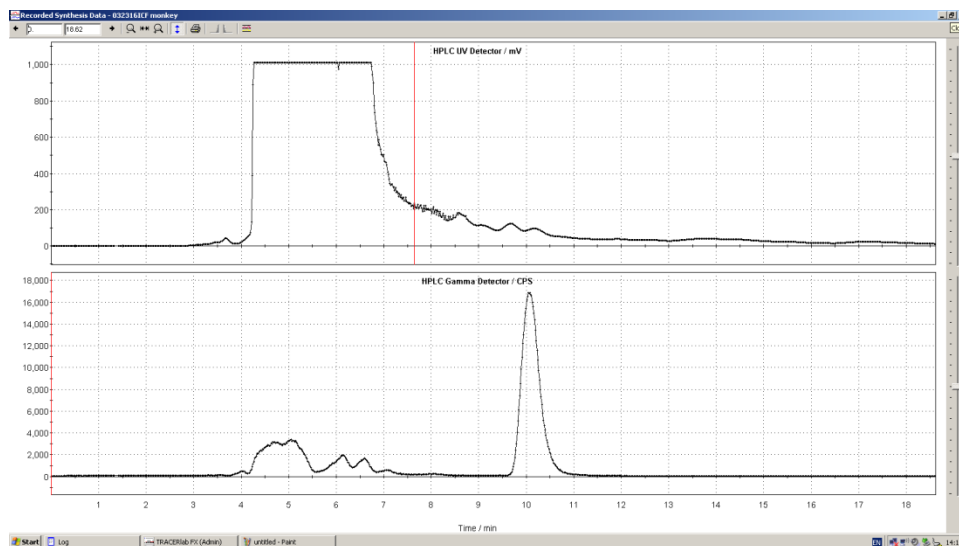


Figure S5.22. Representative semi-preparative HPLC chromatogram for the radiosynthesis [^{11}C]-(*R*)-IPMICF16 (UV above, Rad below).

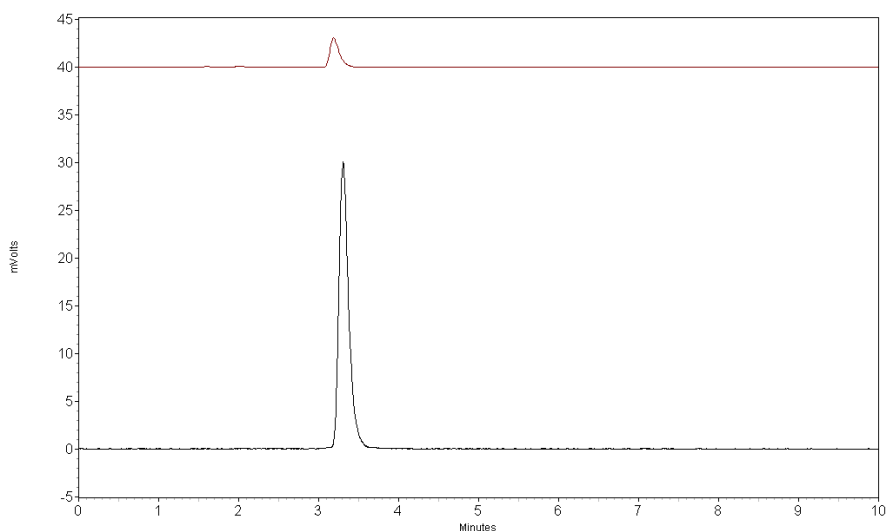


Figure S5.23. Representative HPLC-QC chromatograms of the collected [^{11}C]-(*R*)-IPMICF16 co-injected with the non-radioactive standard IPMICF16 (**5.3**) (UV above, Rad below).

7.3.5 Radiosynthesis of [^{11}C]-(\pm)-IPMICF22. [^{11}C]CH₃I was bubbled through a reaction solution containing 1.0 mg precursor (\pm)-**5.15**, 5 μL 1.0 M methanolic TBAOH and 100 μL DMF at room temperature for 3 min at 15 mL min with Ar carrier gas. The reaction was quenched with 600 μL 50/50 H₂O/MeCN and loaded onto HPLC (mobile phase: 50% water/50% acetonitrile (v/v) isocratic; flow rate: 3.0 mL/ min). The peak between 9.1-9.55 min corresponding to [^{11}C]-(\pm)-IPMICF22 (**Figure S5.24**) was collected and diluted with 50 mL H₂O and the solution was

transferred through a preconditioned C18 1cc Vac Sep Pak. The radiotracer was eluted with 500 μL EtOH and then the ethanolic product was passed through a sterile filter and into the product vial. The C18 cartridge was then washed with 4.5 mL buffered saline, which was also passed through the sterile filter and collected in the product vial. Pure [^{11}C]-(\pm)-IPMICF22 was obtained in 1.8 % nondecay-corrected radiochemical yield at end-of-synthesis based upon [^{11}C]CH $_3\text{I}$, $n = 1$, radiochemical purity > 99%, $S_A \sim 204 \text{ GBq}/\mu\text{mol}$. Quality control mobile phase: 50% water/50% acetonitrile (v/v) isocratic; flow rate: 1.0 mL/ min (**Figure S5.25**).

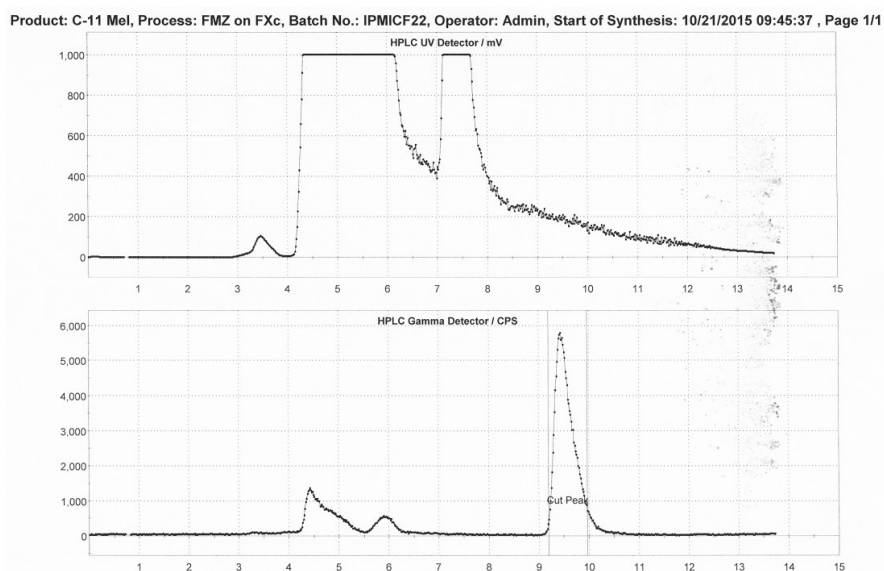


Figure S5.24. Representative semi-preparative HPLC chromatograms for the radiosynthesis [^{11}C]-(\pm)-IPMICF22 (UV above, Rad below).

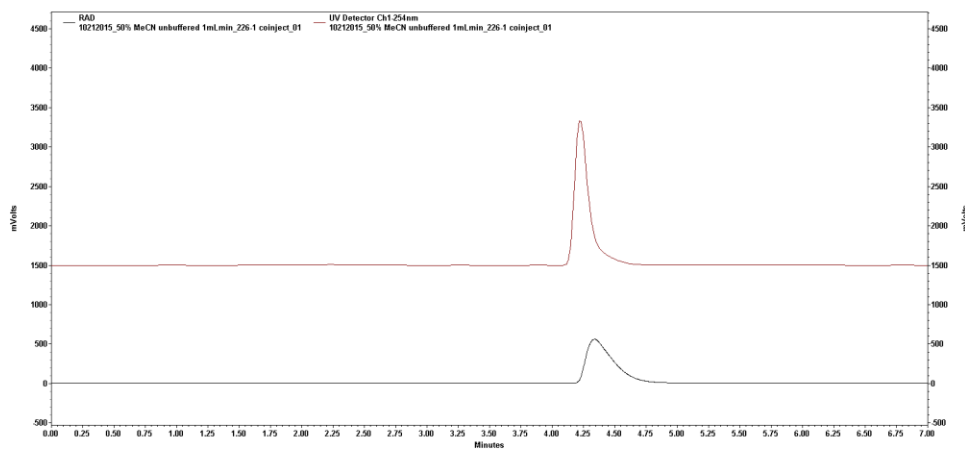


Figure S5.25. Representative HPLC-QC chromatograms of the collected [^{11}C]-(\pm)-IPMICF22 co-injected with the non-radioactive standard IPMICF22 (**5.4**) (UV above, Rad below).

7.3.6 Radiosyntheses of [^{11}C]GW441756. [^{11}C]CH $_3\text{I}$ was bubbled through a reaction solution containing 1.1 mg of desmethyl precursor, 100 μL DMSO at room temperature for 3 min at 15 mL min with Ar carrier gas. The reaction mixture was allowed to react for 2 min, then sparged with He for 3 min at 15 mL/min to evaporate excess [^{11}C]-methyl iodide. The reaction was then quenched with 600 μL 50/50 H $_2\text{O}$ /MeCN and loaded onto HPLC (mobile phase: 50% water/50% acetonitrile (v/v) isocratic; flow rate: 3.0 mL/ min). The peaks from 6.6-7.0 and 8.6-9.4 min corresponding to (Z)-[^{11}C]GW441756 and (E)-[^{11}C]GW441756 respectively (**Figure S5.26**) were collected and diluted with 50 mL H $_2\text{O}$ and the solution was transferred through a preconditioned C18 1cc Vac Sep Pak. The radiotracer was eluted with 500 μL EtOH and then the ethanolic product was passed through a sterile filter and into the product vial. The C18 cartridge was then washed with 4.5 mL buffered saline, which was also passed through the sterile filter and collected in the product vial. Pure [^{11}C]GW441756 (mixed *E/Z* ~ 3:2) was obtained in 4.9 % nondecay-corrected radiochemical yield at end-of-synthesis based upon [^{11}C]CH $_3\text{I}$, $n = 1$, radiochemical purity > 99%, $S_A \sim 189$ GBq/ μmol . Quality control mobile phase: 50% water/50% acetonitrile (v/v) isocratic; flow rate: 1.0 mL/ min (**Figure S5.27**).

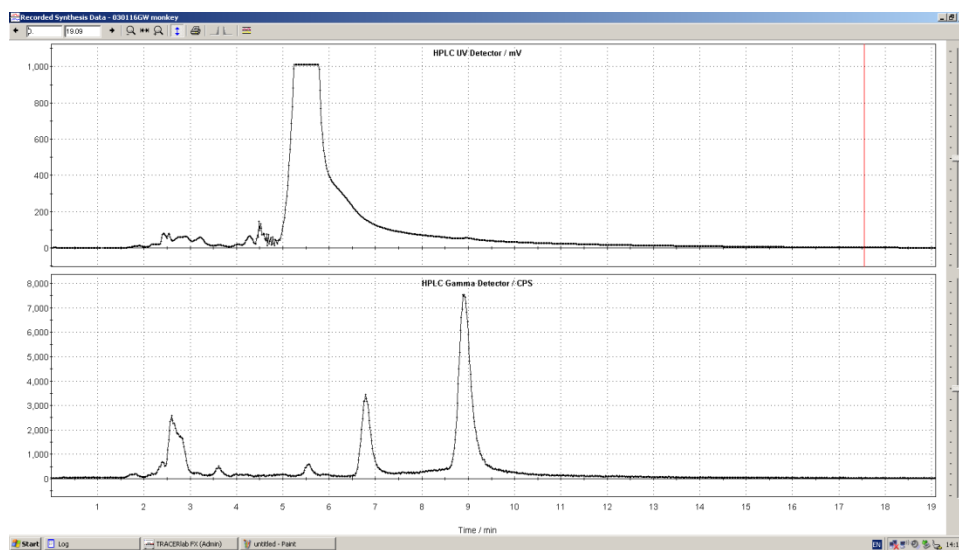


Figure S5.26. Representative semi-preparative HPLC chromatograms for the radiosynthesis [^{11}C]GW441756 (UV above, Rad below).

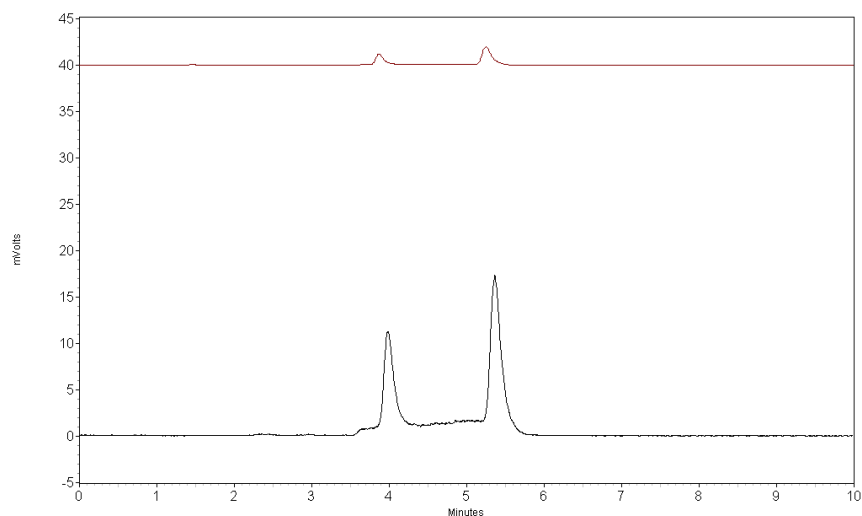


Figure S5.27. Representative HPLC-QC chromatograms of the collected [^{11}C]GW441756 co-injected with the non-radioactive standard GW441756 (**5.5**) (UV above, Rad below).

7.4 McConnell Brain Imaging Center Site

7.4.1 General Considerations. Carbon-11 was produced in a chemical form of [^{11}C]CO₂ and converted into [^{11}C]CH₃I using Synthra automated module by the so-called dry chemistry previously described ([^{11}C]CO₂-[^{11}C]CH₄-[^{11}C]CH₃I). Semi-preparative, radio-preparative HPLC purifications were performed using a Phenomenex LUNA® C18 column (100 Å, 250 × 10 mm, 10 μm) and quality control analysis was performed on an Agilent 1200 system (Agilent Technologies, Santa Clara, CA, USA; running on Agilent ChemStation software) equipped with a Raytest Gabi Star radioactivity detector (Raytest Isotopenmessgeräte GmbH, Straubenhardt, Germany) using a Phenomenex Partisil ODS-3 (250 × 4.6 mm, 5 μm) column.

7.4.2 Radiosyntheses of [^{11}C]-(*R*)-IPMICF16. The radiotracer was synthesized manually by bubbling the resulting [^{11}C]CH₃I 5.6-8.9 GBq (150-240 mCi) into a vial containing a solution of the precursor (*R*)-**5.14** (1.7 mg in 0.3 mL DMF) and K₂CO₃ (10 μL of concentrated aqueous solution). The crude mixture was then diluted with HPLC eluent (1.5 mL, 75% MeCN/25% H₂O) and immediately injected onto HPLC (mobile phase: 25% water/75% acetonitrile (v/v) isocratic; flow rate: 3.0 mL/min). The peak at 10.5 min corresponding to [^{11}C]-(*R*)-IPMICF16 was collected. An aliquot of the pure [^{11}C]-(*R*)-IPMICF16 (13.0 ± 3.0 % nondecay-corrected radiochemical yield at end-of-synthesis based upon [^{11}C]CH₃I, *n* = 3, radiochemical purity > 98%, *S_A* ~ 107 GBq/μmol, **Figure S5.28**) was diluted with 10 mL H₂O and the solution was

transferred through a preconditioned C18 Plus Sep-Pak. The radiotracer was eluted dropwise with EtOH and used directly in the autoradiography experiments. Quality control was assessed by analytical HPLC (mobile phase: 30% water/70% acetonitrile (v/v) isocratic; flow rate: 1.0 mL/min, ($t_{r[^{11}\text{C}]-(R)\text{-IPMICF16}} = 9.0$ min)

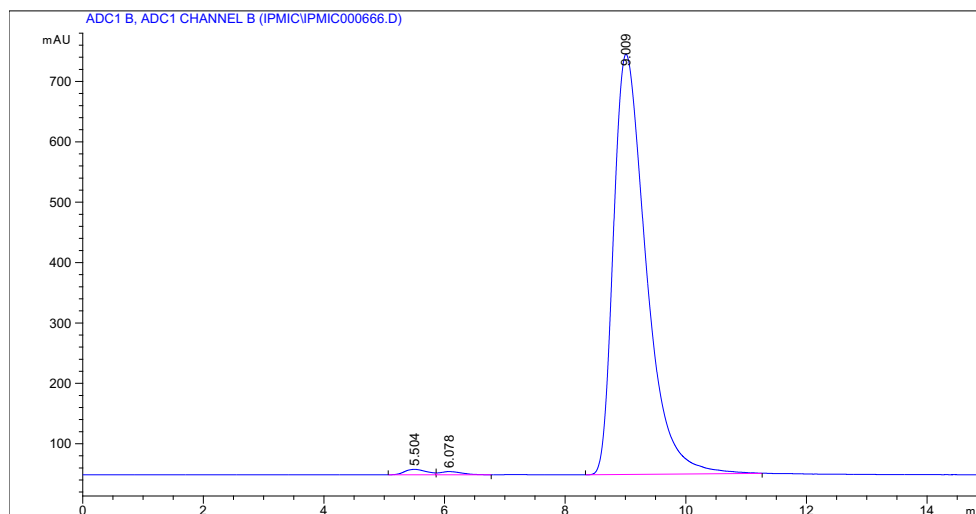


Figure S5.28. Representative HPLC-QC chromatogram of the collected [^{11}C]-(*R*)-IPMICF16 used for in vitro autoradiography experiments.

7.5 Munich Site

7.5.1 General Considerations.

[¹¹C]CO₂ was produced via the ¹⁴N(p,α)¹¹C reaction by proton irradiation of a N₂/1% O₂ target of a GE PETtrace cyclotron and converted into [¹¹C]CH₃I by reduction with H₂/Ni and iodination with I₂ using a GE FX C Pro automated module.

7.5.2 Radiosyntheses of [¹¹C]-(R)-IPMICF16.

[¹¹C]CH₃I was bubbled into a solution of the precursor (R)-**5.14** (1.7 mg in 0.3 mL DMF) and K₂CO₃ (10 μL of a saturated aq. solution) at -20°C. The crude mixture was heated to 80°C for 3 min, diluted with HPLC eluent (1.5 mL,) and purified via semipreparative HPLC (Phenomenex LUNA C18 column, 100 Å, 250 × 10 mm, 10 μm, 75% MeCN/25% H₂O (v/v) isocratic; flow rate: 3 mL/min). The pure [¹¹C]-(R)-IPMICF16 was diluted with 10 mL H₂O, trapped on a preconditioned C18 cartridge (Waters SepPak C18 light), washed with water (3 mL) and then eluted with EtOH (1 mL) followed by sterile filtration and formulation with PBS. [¹¹C]-(R)-IPMICF16 was obtained in 13 ± 2 % decay-corrected radiochemical yield at end-of-synthesis based upon [¹¹C]CO₂, *n* = 3, radiochemical purity > 99%, S_A = 118 GBq/μmol.

Quality control for human PET scan ([¹¹C]-(R)-IPMICF16):

| | |
|---------------------|--|
| Appearance | Clear, colorless solution, free of particles |
| Identity | 5.27 min (standard 5.23 min) |
| RCP | >99% |
| Residual solvents | 2.3% EtOH |
| pH | 7.226 |
| Half life | 0.341 h (+1.15%) |
| Radionuclide purity | 511 keV |
| Endotoxins | <0.4 EU/mL |

8. NMR SPECTRA

Data form this subsection can be found in **Annex 4**.

5.8 References

1. Chao, M. V., Neurotrophins and their receptors: a convergence point for many signalling pathways. *Nat Rev Neurosci* **2003**, 4 (4), 299-309.
2. Chao, M. V., Neurotrophin Receptors - a Window into Neuronal Differentiation. *Neuron* **1992**, 9 (4), 583-593.
3. Deinhardt K, C. M., Trk Receptors. *Handb Exp Pharmacol.* **2014**, 220, 103-119.
4. Oyesiku, N. M.; Evans, C. O.; Houston, S.; Darrell, R. S.; Smith, J. S.; Fulop, Z. L.; Dixon, C. E.; Stein, D. G., Regional changes in the expression of neurotrophic factors and their receptors following acute traumatic brain injury in the adult rat brain. *Brain Research* **1999**, 833 (2), 161-172.
5. Ray, M. T.; Weickert, C. S.; Webster, M. J., Decreased BDNF and TrkB mRNA expression in multiple cortical areas of patients with schizophrenia and mood disorders. *Transl Psychiat* **2014**, 4.
6. Reinhart, V.; Bove, S. E.; Volfson, D.; Lewis, D. A.; Kleiman, R. J.; Lanz, T. A., Evaluation of TrkB and BDNF transcripts in prefrontal cortex, hippocampus, and striatum from subjects with schizophrenia, bipolar disorder, and major depressive disorder. *Neurobiol Dis* **2015**, 77, 220-7.
7. Deng, V.; Matagne, V.; Banine, F.; Frerking, M.; Ohliger, P.; Budden, S.; Pevsner, J.; Dissen, G. A.; Sherman, L. S.; Ojeda, S. R., FXDY1 is an MeCP2 target gene overexpressed in the brains of Rett syndrome patients and Mecp2-null mice. *Hum Mol Genet* **2007**, 16 (6), 640-650.
8. Gines, S.; Bosch, M.; Marco, S.; Gavalda, N.; Diaz-Hernandez, M.; Lucas, J. J.; Canals, J. M.; Alberch, J., Reduced expression of the TrkB receptor in Huntington's disease mouse models and in human brain. *European Journal of Neuroscience* **2006**, 23 (3), 649-658.
9. Fumagalli, F.; Racagni, G.; Riva, M. A., Shedding light into the role of BDNF in the pharmacotherapy of Parkinson's disease. *Pharmacogenomics J* **2006**, 6 (2), 95-104.
10. Nagahara, A. H.; Tuszynski, M. H., Potential therapeutic uses of BDNF in neurological and psychiatric disorders. *Nature Reviews Drug Discovery* **2011**, 10 (3), 209-219.
11. Ginsberg, S. D.; Che, S. L.; Wu, J.; Counts, S. E.; Mufson, E. J., Down regulation of trk but not p75(NTR) gene expression in single cholinergic basal forebrain neurons mark the progression of Alzheimer's disease. *Journal of Neurochemistry* **2006**, 97 (2), 475-487.

12. Ferrer, I.; Marin, C.; Rey, M. J.; Ribalta, T.; Goutan, E.; Blanco, R.; Tolosa, E.; Marti, E., BDNF and full-length and truncated TrkB expression in Alzheimer disease. Implications in therapeutic strategies. *J Neuropath Exp Neur* **1999**, *58* (7), 729-739.
13. Allen, S. J.; Wilcock, G. K.; Dawbarn, D., Profound and selective loss of catalytic TrkB immunoreactivity in Alzheimer's disease. *Biochem Bioph Res Co* **1999**, *264* (3), 648-651.
14. Zhang, F.; Kang, Z. L.; Li, W.; Xiao, Z. C.; Zhou, X. F., Roles of brain-derived neurotrophic factor/tropomyosin-related kinase B (BDNF/TrkB) signalling in Alzheimer's disease. *J Clin Neurosci* **2012**, *19* (7), 946-949.
15. Vaishnavi, A.; Le, A. T.; Doebele, R. C., TRKING Down an Old Oncogene in a New Era of Targeted Therapy. *Cancer Discovery* **2015**, *5* (1), 25-34.
16. McCarthy, C.; Walker, E., Tropomyosin receptor kinase inhibitors: a patent update 2009-2013. *Expert Opinion on Therapeutic Patents* **2014**, *24* (7), 731-744.
17. Martin-Zanca, D.; Hughes, S. H.; Barbacid, M., A human oncogene formed by the fusion of truncated tropomyosin and protein tyrosine kinase sequences. *Nature* **1986**, *319* (6056), 743-8.
18. Kaplan, D. R.; Hempstead, B. L.; Martinzanca, D.; Chao, M. V.; Parada, L. F., The Trk Protooncogene Product - a Signal Transducing Receptor for Nerve Growth-Factor. *Science* **1991**, *252* (5005), 554-558.
19. Klein, R.; Jing, S. Q.; Nanduri, V.; O'Rourke, E.; Barbacid, M., The Trk Protooncogene Encodes a Receptor for Nerve Growth-Factor. *Cell* **1991**, *65* (1), 189-197.
20. Mufson, E. J.; Li, J. M.; Sobreviela, T.; Kordower, J. H., Decreased trkA gene expression within basal forebrain neurons in Alzheimer's disease. *Neuroreport* **1996**, *8* (1), 25-29.
21. Weickert, C. S.; Ligons, D. L.; Romanczyk, T.; Ungaro, G.; Hyde, T. M.; Herman, M. M.; Weinberger, D. R.; Kleinman, J. E., Reductions in neurotrophin receptor mRNAs in the prefrontal cortex of patients with schizophrenia. *Mol Psychiatr* **2005**, *10* (7), 637-650.
22. Romanczyk, T. B.; Weickert, C. S.; Webster, M. J.; Herman, M. M.; Akil, M.; Kleinman, J. E., Alterations in trkB mRNA in the human prefrontal cortex throughout the lifespan. *European Journal of Neuroscience* **2002**, *15* (2), 269-280.
23. Beltaifa, S.; Webster, M. J.; Ligons, D. L.; Fatula, R. J.; Herman, M. M.; Kleinman, J. E.; Weickert, C. S., Discordant changes in cortical TrkC mRNA and protein during the human lifespan. *European Journal of Neuroscience* **2005**, *21* (9), 2433-2444.
24. Webster, M. J.; Herman, M. M.; Kleinman, J. E.; Shannon Weickert, C., BDNF and trkB mRNA expression in the hippocampus and temporal cortex during the human lifespan. *Gene Expr Patterns* **2006**, *6* (8), 941-51.

25. Menichincheri, M.; Ardini, E.; Magnaghi, P.; Avanzi, N.; Banfi, P.; Bossi, R.; Buffa, L.; Canevari, G.; Ceriani, L.; Colombo, M.; Corti, L.; Donati, D.; Fasolini, M.; Felder, E.; Fiorelli, C.; Fiorentini, F.; Galvani, A.; Isacchi, A.; Borgia, A. L.; Marchionni, C.; Nesi, M.; Orrenius, C.; Panzeri, A.; Pesenti, E.; Rusconi, L.; Saccardo, M. B.; Vanotti, E.; Perrone, E.; Orsini, P., Discovery of Entrectinib: A New 3-Aminoindazole As a Potent Anaplastic Lymphoma Kinase (ALK), c-ros Oncogene 1 Kinase (ROS1), and Pan-Tropomyosin Receptor Kinases (Pan-TRKs) inhibitor. *J Med Chem* **2016**, *59* (7), 3392-408.
26. Ardini, E.; Menichincheri, M.; Banfi, P.; Bosotti, R.; De Ponti, C.; Pulci, R.; Ballinari, D.; Ciomei, M.; Texido, G.; Degrassi, A.; Avanzi, N.; Amboldi, N.; Saccardo, M. B.; Casero, D.; Orsini, P.; Bandiera, T.; Mologni, L.; Anderson, D.; Wei, G.; Harris, J.; Vernier, J. M.; Li, G.; Felder, E.; Donati, D.; Isacchi, A.; Pesenti, E.; Magnaghi, P.; Galvani, A., Entrectinib, a Pan-TRK, ROS1, and ALK Inhibitor with Activity in Multiple Molecularly Defined Cancer Indications. *Mol Cancer Ther* **2016**, *15* (4), 628-39.
27. Van de Bittner, G. C.; Ricq, E. L.; Hooker, J. M., A Philosophy for CNS Radiotracer Design. *Accounts Chem Res* **2014**, *47* (10), 3127-3134.
28. Zhang, L.; Villalobos, A.; Beck, E. M.; Bocan, T.; Chappie, T. A.; Chen, L.; Grimwood, S.; Heck, S. D.; Helal, C. J.; Hou, X.; Humphrey, J. M.; Lu, J.; Skaddan, M. B.; McCarthy, T. J.; Verhoest, P. R.; Wager, T. T.; Zasadny, K., Design and selection parameters to accelerate the discovery of novel central nervous system positron emission tomography (PET) ligands and their application in the development of a novel phosphodiesterase 2A PET ligand. *J Med Chem* **2013**, *56* (11), 4568-79.
29. Holland, J. P.; Cumming, P.; Vasdev, N., PET radiopharmaceuticals for probing enzymes in the brain. *Am J Nucl Med Mol Imaging* **2013**, *3* (3), 194-216.
30. Wey, H. Y.; Gilbert, T. M.; Zurcher, N. R.; She, A.; Bhanot, A.; Taillon, B. D.; Schroeder, F. A.; Wang, C. G.; Haggarty, S. J.; Hooker, J. M., Insights into neuroepigenetics through human histone deacetylase PET imaging. *Sci Transl Med* **2016**, *8* (351).
31. Frisen, J.; Verge, V. M. K.; Fried, K.; Risling, M.; Persson, H.; Trotter, J.; Hokfelt, T.; Lindholm, D., Characterization of Glial Trkb Receptors - Differential Response to Injury in the Central and Peripheral Nervous Systems. *P Natl Acad Sci USA* **1993**, *90* (11), 4971-4975.
32. Rose, C. R.; Blum, R.; Pichler, B.; Lepier, A.; Kafitz, K. W.; Konnerth, A., Truncated TrkB-T1 mediates neurotrophin-evoked calcium signalling in glia cells. *Nature* **2003**, *426* (6962), 74-78.
33. Pike, V. W., PET radiotracers: crossing the blood-brain barrier and surviving metabolism. *Trends Pharmacol Sci* **2009**, *30* (8), 431-40.

34. Rankovic, Z., CNS Drug Design: Balancing Physicochemical Properties for Optimal Brain Exposure. *Journal of Medicinal Chemistry* **2015**, *58* (6), 2584-2608.
35. Wager, T. T.; Hou, X. J.; Verhoest, P. R.; Villalobos, A., Moving beyond Rules: The Development of a Central Nervous System Multiparameter Optimization (CNS MPO) Approach To Enable Alignment of Druglike Properties. *Acs Chemical Neuroscience* **2010**, *1* (6), 435-449.
36. Bernard-Gauthier, V.; Bailey, J. J.; Aliaga, A.; Kostikov, A.; Rosa-Neto, P.; Wuest, M.; Brodeur, G. M.; Bedell, B. J.; Wuest, F.; Schirmacher, R., Development of subnanomolar radiofluorinated (2-pyrrolidin-1-yl)imidazo[1,2-b]pyridazine pan-Trk inhibitors as candidate PET imaging probes. *Medchemcomm* **2015**, *6* (12), 2184-2193.
37. Bernard-Gauthier, V.; Aliaga, A.; Aliaga, A.; Boudjemeline, M.; Hopewell, R.; Kostikov, A.; Rosa-Neto, P.; Thiel, A.; Schirmacher, R., Syntheses and Evaluation of Carbon-11-and Fluorine-18-Radiolabeled pan-Tropomyosin Receptor Kinase (Trk) Inhibitors: Exploration of the 4-Aza-2-oxindole Scaffold as Trk PET Imaging Agents. *Acs Chemical Neuroscience* **2015**, *6* (2), 260-276.
38. Choi, H. S.; Rucker, P. V.; Wang, Z. C.; Fan, Y.; Albaugh, P.; Chopiuk, G.; Gessier, F.; Sun, F. X.; Adrian, F.; Liu, G. X.; Hood, T.; Li, N. X.; Jia, Y.; Che, J. W.; McCormack, S.; Li, A.; Li, J.; Steffy, A.; Culazzo, A.; Tompkins, C.; Phung, V.; Kreuzsch, A.; Lu, M.; Hu, B.; Chaudhary, A.; Prashad, M.; Tuntland, T.; Liu, B.; Harris, J.; Seidel, H. M.; Loren, J.; Molteni, V., (R)-2-Phenylpyrrolidine Substituted Imidazopyridazines: A New Class of Potent and Selective Pan-IRK Inhibitors. *Acs Medicinal Chemistry Letters* **2015**, *6* (5), 562-567.
39. Cheng Y, P. W., Relationship between the inhibition constant (K₁) and the concentration of inhibitor which causes 50 per cent inhibition (I₅₀) of an enzymatic reaction. *Biochem Pharmacol.* **1973**, *22* (23), 3099-3108.
40. Knight, Z. A.; Shokat, K. M., Features of selective kinase inhibitors. *Chem Biol* **2005**, *12* (6), 621-637.
41. Altar, C. A.; Siuciak, J. A.; Wright, P.; Ip, N. Y.; Lindsay, R. M.; Wiegand, S. J., In-Situ Hybridization of Trkb and Trkc Receptor Messenger-Rna in Rat Forebrain and Association with High-Affinity Binding of [I-125] Bdnf, [I-125] Nt-4/5 and [I-125] Nt-3. *European Journal of Neuroscience* **1994**, *6* (9), 1389-1405.
42. Weiss, G. J.; Hidalgo, M.; Borad, M. J.; Laheru, D.; Tibes, R.; Ramanathan, R. K.; Blydorn, L.; Jameson, G.; Jimeno, A.; Isaacs, J. D.; Scaburri, A.; Pacciarini, M. A.; Fiorentini, F.; Ciomei, M.; Von Hoff, D. D., Phase I study of the safety, tolerability and pharmacokinetics of PHA-848125AC, a dual tropomyosin receptor kinase A and cyclin-dependent kinase inhibitor, in patients with advanced solid malignancies. *Invest New Drug* **2012**, *30* (6), 2334-2343.

43. Skerratt, S. E.; Andrews, M.; Bagal, S. K.; Bilsland, J.; Brown, D.; Bungay, P. J.; Cole, S.; Gibson, K. R.; Jones, R.; Morao, I.; Nedderman, A.; Omoto, K.; Robinson, C.; Ryckmans, T.; Skinner, K.; Stupple, P.; Waldron, G., The Discovery of a Potent, Selective, and Peripherally Restricted Pan-Trk Inhibitor (PF-06273340) for the Treatment of Pain. *Journal of Medicinal Chemistry* **2016**, *59* (22), 10084-10099.
44. Doebele, R. C.; Davis, L. E.; Vaishnavi, A.; Le, A. T.; Estrada-Bernal, A.; Keysar, S.; Jimeno, A.; Varella-Garcia, M.; Aisner, D. L.; Li, Y. L.; Stephens, J.; Morosini, D.; Tuch, B. B.; Fernandes, M.; Nanda, N.; Low, J. A., An Oncogenic NTRK Fusion in a Patient with Soft-Tissue Sarcoma with Response to the Tropomyosin-Related Kinase Inhibitor LOXO-101. *Cancer Discovery* **2015**, *5* (10), 1049-1057.
45. Farago, A. F.; Le, L. P.; Zheng, Z.; Muzikansky, A.; Drilon, A.; Patel, M.; Bauer, T. M.; Liu, S. V.; Ou, S. H.; Jackman, D.; Costa, D. B.; Multani, P. S.; Li, G. G.; Hornby, Z.; Chow-Maneval, E.; Luo, D.; Lim, J. E.; Iafrate, A. J.; Shaw, A. T., Durable Clinical Response to Entrectinib in NTRK1-Rearranged Non-Small Cell Lung Cancer. *J Thorac Oncol* **2015**, *10* (12), 1670-4.
46. Syvanen, S.; Lindhe, O.; Palner, M.; Kornum, B. R.; Rahman, O.; Langstrom, B.; Knudsen, G. M.; Hammarlund-Udenaes, M., Species Differences in Blood-Brain Barrier Transport of Three Positron Emission Tomography Radioligands with Emphasis on P-Glycoprotein Transport. *Drug Metab Dispos* **2009**, *37* (3), 635-643.
47. Deo, A. K.; Theil, F. P.; Nicolas, J. M., Confounding Parameters in Preclinical Assessment of Blood-Brain Barrier Permeation: An Overview With Emphasis on Species Differences and Effect of Disease States. *Mol Pharmaceut* **2013**, *10* (5), 1581-1595.
48. Savaskan, E.; Muller-Spahn, F.; Olivieri, G.; Bruttel, S.; Otten, U.; Rosenberg, C.; Hulette, C.; Hock, C., Alterations in trk A, trk B and trk C receptor immunoreactivities in parietal cortex and cerebellum in Alzheimer's disease. *Eur Neurol* **2000**, *44* (3), 172-80.
49. Birchmeier, C.; Sharma, S.; Wigler, M., Expression and rearrangement of the ROS1 gene in human glioblastoma cells. *Proc Natl Acad Sci U S A* **1987**, *84* (24), 9270-4.
50. Cozza, A.; Melissari, E.; Iacopetti, P.; Mariotti, V.; Tedde, A.; Nacmias, B.; Conte, A.; Sorbi, S.; Pellegrini, S., SNPs in neurotrophin system genes and Alzheimer's disease in an Italian population. *J Alzheimers Dis* **2008**, *15* (1), 61-70.
51. Vepsalainen, S.; Castren, E.; Helisalmi, S.; Iivonen, S.; Mannermaa, A.; Lehtovirta, M.; Hanninen, T.; Soininen, H.; Hiltunen, M., Genetic analysis of BDNF and TrkB gene polymorphisms in Alzheimer's disease. *J Neurol* **2005**, *252* (4), 423-428.

52. Castello, N. A.; Nguyen, M. H.; Tran, J. D.; Cheng, D.; Green, K. N.; LaFerla, F. M., 7,8-Dihydroxyflavone, a Small Molecule TrkB Agonist, Improves Spatial Memory and Increases Thin Spine Density in a Mouse Model of Alzheimer Disease-Like Neuronal Loss. *Plos One* **2014**, *9* (3).
53. Li, N.; Liu, G. T., The novel squamosamide derivative FLZ enhances BDNF/TrkB/CREB signaling and inhibits neuronal apoptosis in APP/PS1 mice. *Acta Pharmacol Sin* **2010**, *31* (3), 265-272.
54. Massa, S. M.; Yang, T.; Xie, Y. M.; Shi, J.; Bilgen, M.; Joyce, J. N.; Nehama, D.; Rajadas, J.; Longo, F. M., Small molecule BDNF mimetics activate TrkB signaling and prevent neuronal degeneration in rodents. *Journal of Clinical Investigation* **2010**, *120* (5), 1774-1785.
55. Bauer, B.; Miller, D. S.; Fricker, G., Compound profiling for p-glycoprotein at the blood-brain barrier using a microplate screening system. *Pharmaceut Res* **2003**, *20* (8), 1170-1176.
56. Mahringer, A.; Delzer, J.; Fricker, G., A fluorescence-based in vitro assay for drug interactions with breast cancer resistance protein (BCRP, ABCG2). *Eur J Pharm Biopharm* **2009**, *72* (3), 605-13.
57. Mourik, J. E. M.; Lubberink, M.; Klumpers, U. M. H.; Comans, E. F.; Lammertsma, A. A.; Boellaard, R., Partial volume corrected image derived input functions for dynamic PET brain studies: Methodology and validation for [C-11] flumazenil. *Neuroimage* **2008**, *39* (3), 1041-1050.
58. Mourik, J. E. M.; Lubberink, M.; Schuitemaker, A.; Tolboom, N.; van Berckel, B. N. M.; Lammertsma, A. A.; Boellaard, R., Image-derived input functions for PET brain studies. *Eur J Nucl Med Mol I* **2009**, *36* (3), 463-471.
59. Hammers, A.; Allom, R.; Koeppe, M. J.; Free, S. L.; Myers, R.; Lemieux, L.; Mitchell, T. N.; Brooks, D. J.; Duncan, J. S., Three-dimensional maximum probability atlas of the human brain, with particular reference to the temporal lobe. *Hum Brain Mapp* **2003**, *19* (4), 224-47.
60. Zhou, Y.; Ye, W.; Basic, J. R.; Crabb, A. H.; Hilton, J.; Wong, D. F., A consistent and efficient graphical analysis method to improve the quantification of reversible tracer binding in radioligand receptor dynamic PET studies. *Neuroimage* **2009**, *44* (3), 661-70.
61. J. Haas, S. W. A., Y. Jiang and G. Zhang, WO/2010/048314 A1; International application No. PCT/US2009/061519. **2010**, April 29.
62. Reddy, L. R.; Prashad, M., Asymmetric synthesis of 2-substituted pyrrolidines by addition of Grignard reagents to gamma-chlorinated N-tert-butanefulfinyl imine. *Chem Commun* **2010**, *46* (2), 222-224.

63. Anastassiadis, T.; Deacon, S. W.; Devarajan, K.; Ma, H.; Peterson, J. R., Comprehensive assay of kinase catalytic activity reveals features of kinase inhibitor selectivity. *Nat Biotechnol* **2011**, 29 (11), 1039-45.

Article 9

A version of this chapter is in preparation for submission to: Bioorganic & Medicinal Chemistry Letters.

Bernard-Gauthier, V.; Vesnaver, M.; Mahringer, A.; Fricker, G. & Schirmacher, R. Development of [¹⁸F]QMICF as a Potential Radiotracer for Tropomyosin Receptor Kinases Oncological PET Imaging.

Author contributions: **V.B.G.** managed the study, designed all experiments, conducted all chemical syntheses, performed radiochemistry, interpreted all data and wrote the paper; M.V. contributed to the synthesis of (±)-**6.6** and enantiomers thereof under the supervision of **V.B.G.**; A.M. performed and analysed P-gp cellular assays; G.F. contributed new reagents and analytic tools; R.S. supervised research and corrected manuscript; the manuscript was approved by all co-authors.

Development of [¹⁸F]QMICF as a Potential Radiotracer for Tropomyosin Receptor Kinases Oncological PET Imaging

Vadim Bernard-Gauthier^{a,1}, Matthew Vesnaver^b, Anne Mahringer^c, Gert Fricker^c, Ralf Schirmmayer^{a,1}

^aDepartment of Oncology, Division of Oncological Imaging, University of Alberta, Edmonton, AB, T6G 2R3, Canada.

^bMcConnell Brain Imaging Centre, Montreal Neurological Institute, McGill University, 3801 University Street, Montreal, QC, H3A 2B4, Canada.

^cInstitute of Pharmacy and Molecular Biotechnology, University of Heidelberg, Heidelberg 69120, Germany.

6.1 Abstract

Diverse *NTRK1/2/3* fusions have recently been characterized as low incidence oncogenic alterations across various tumor histologies. Tyrosine kinase inhibitors (TKIs) of the tropomyosin receptor kinase family TrkA/B/C (encoded by *NTRK1/2/3*) are showing promises in the clinic for the treatment of cancer patients which diseases harbor *NTRK* tumor drivers. We describe herein the development and radiosynthesis of [¹⁸F]QMICF ([¹⁸F]-(*R*)-**6.9**), a quinazoline-based type-II pan-Trk radiotracer with nanomolar potencies for TrkA/B/C and relevant TrkA fusions including TrkA-TPM3. Starting from a racemic FLT3 (fms like tyrosine kinase 3) inhibitor lead with off-target TrkA activity ((±)-**6.6**), we developed and synthesized the fluorinated derivative (*R*)-**6.9** which primarily acts as a pan-Trk inhibitor and displays favorable selectivity profile on a diverse set of kinases including FLT3. Purposely designed to be labeled in one step, the tracer [¹⁸F]QMICF was synthesized from the corresponding mesylate precursor. The results presented herein support the further exploration of [¹⁸F]QMICF for imaging of Trk fusions *in vivo*.

6.2 Introduction

Constitutively activated and aberrantly expressed kinase fusion proteins resulting from chromosomal rearrangement are frequent oncogenic drivers in human cancer.¹⁻² Over thirty years ago, *trk* was one of the first oncogenic fusion characterized in human.³ The *trk* oncogene was identified from a colon carcinoma and later shown to originate from the juxtaposition of the transmembrane and kinase domains of the proto-oncogene *NTRK1* with a non-muscle tropomyosin gene partner (*TPM3*).³⁻⁴ The signalling and pro-survival roles of the proto-oncoprotein TrkA/B/C family of receptor tyrosine kinases (encoded by *NTRK1/2/3* respectively) and their respective neurotrophic factor cognate ligands (nerve growth factor (NGF), brain-derived neurotrophic factor (BDNF) and neurotrophin-3 (NT-3)) have been characterized extensively in developmental neurobiology.⁵ In spite of the early characterisation of *trk*, the clinical relevance of Trk receptors in human cancer and especially *NTRK* fusions has only become evident recently.⁶⁻⁸ The unbiased identification of gene rearrangements in this context has been facilitated by next-generation sequencing (NGS) highlighting a role for *NTRK* fusions in several tumor types. Current clinical trial efforts for Trk-based therapy involve over a dozen antineoplastic inhibitors (**Figure 6.1A**) with most trials relying on genomic characterization for patients selection within a “basket trial” design, embodying the paradigmatic shift towards precision medicine in clinical oncology.⁹ Patients selection in those trials largely relies on tumor biopsy followed by fluorescence *in situ* hybridization (FISH) or NGS.⁶ Important challenges with unfolding genomically-driven trial for drugs targeting low-incidence drivers such as multiple *NTRK* fusions relate to the fact that such markers may be both diverse and not routinely screened, making their identification and the enrollment of prospective patients complex using available techniques. In addition, problems may arise due to the inability to collect tissue samples and the difficulty to assess heterogeneous tumor tissue or metastatic conditions

adequately based on punctual biopsy or due to the invasiveness of serial biopsies to follow disease progression.

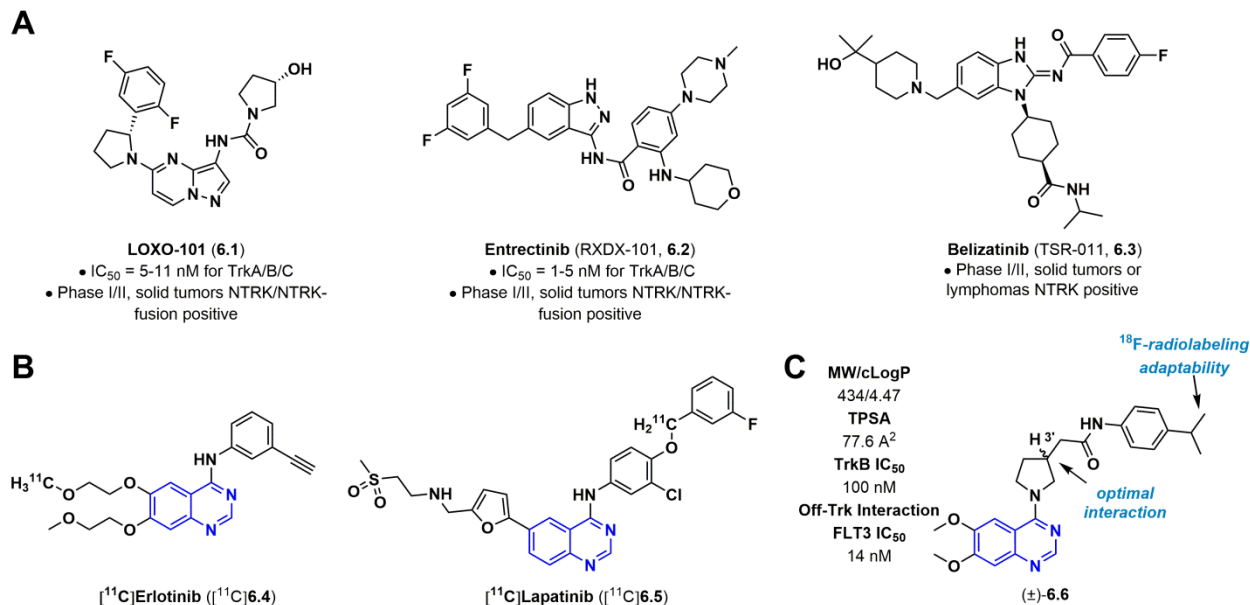


Figure 6.1. Chemical structures and characteristics of (A) pan-Trk anticancer inhibitors under clinical investigation, (B) quinazoline-based EGFR/HER2 radiolabeled inhibitors validated in clinical investigations and (C) the TrkB/FLT3 radiotracer lead (±)-6.6.

In a clinical trial context, a potential avenue to address such challenges resides in the use of positron emission tomography (PET) with targeted radiotracers, enabling *in vivo* visualization and target quantification of define molecular markers non-invasively and dynamically throughout the body including primary tumors and metastatic sites.¹⁰ Recently, radiolabeled tyrosine kinase inhibitor (TKIs) have been developed to image tumor in preclinical and clinical studies for a number of targets including EGFR (epidermal growth factor receptor), HER2 (human epidermal growth factor receptor 2) and VEGFRs (vascular endothelial growth factor receptors) among others.¹¹⁻¹² Of particular interest, tumor uptake of [¹¹C]erlotinib, whose carbon-12 isotopologue is approved for the treatment of advanced or metastatic non-small cell lung cancer (NSCLC), has been used to identify patients with EGFR activating mutations who

are most likely to respond to erlotinib therapy (**Figure 6.1B**).¹³⁻¹⁵ To date, all PET TKIs evaluated in human for tumor imaging have been quinazoline-based radiotracers (**Figure 6.1B**).¹⁶⁻¹⁷ Furthermore, 8 out of 28 approved small molecule kinase inhibitors bear quinolone/quinazoline hinge binder motifs, which highlights the importance and suitability of this fragment in kinase inhibitor development in general.¹⁸ In view of those facts, we sought to develop a quinazoline-based pan-Trk radiotracer with the final goal of providing a molecular imaging probe for patient selection within genomically-driven trials for Trk inhibitors. A primary objective was to obtain a radiotracer labeled with fluorine-18 ($t_{1/2} = 109$ min; 97% β^+ ; $E_{\max}(\beta^+) = 0.64$ MeV) due to the more suitable nuclear properties compared to carbon-11 ($t_{1/2} = 20.3$ min; >99% β^+ ; $E_{\max}(\beta^+) = 0.96$ MeV). In the light of the limitations associated with the multi-step radiosynthesis of our previous Trk tracer lead,¹⁹ the PET tracer in this study should be obtained in one radiosynthetic step to facilitate clinical translational efforts.

6.3 Results and discussion

6.3.1 Compound optimization and in silico study. As a starting point, we selected the racemic dual FLT3/TrkA inhibitor (\pm)-**6.6** having suitable properties for membrane permeation and TrkA pharmacology (**Figure 6.1C**).²⁰ Owing to the high expression levels of FLT3 throughout the immune system and in bone marrow, the prospect of a tracer which primarily interacts with this target (IC_{50} FLT3 = 14 nM) over Trk (IC_{50} TrkA = 100 nM) was initially considered problematic. It was however anticipated that the described FLT3 and TrkA (and likely pan-Trk) activities could represent intrinsic interactions of the distinct enantiomers from the racemic lead.

In order to assess this hypothesis, the individual enantiomers (*S*)-**6.6** and (*R*)-**6.6** were synthesized from the commercially available (*S*)- and (*R*)-(1-boc-pyrrolidin-3-yl)-acetic acids as previously described for the racemate.²⁰ Docking studies conducted in parallel suggested that

the quinazoline lead acts as conventional type-II inhibitor with a N_1 -quinazoline-hinge interaction and the 4-isopropylphenyl moiety occupying the allosteric pocket (**Figure 6.2A-C**). The *in silico* assessment also provided indications that (*R*)-**6** was primarily responsible for the Trk activity observed with (\pm)-**6** due to more optimal interaction with both the hinge and the DFG motif. To the contrary of (*S*)-**6**, binding of (*R*)-**6** to the DFG triad occurs via the oxygen of the carbonyl with NH backbone from Asp710 (TrkB) and paralog residues in TrkA/C. This interaction releases the amide proton of the inhibitor in the favorable orientation for additional direct or water-mediated interaction with Lys588 and Glu604 (TrkB) – as previously shown with all co-crystallized amide- and urea-bearing type-II pan-Trk inhibitors.²¹⁻²³

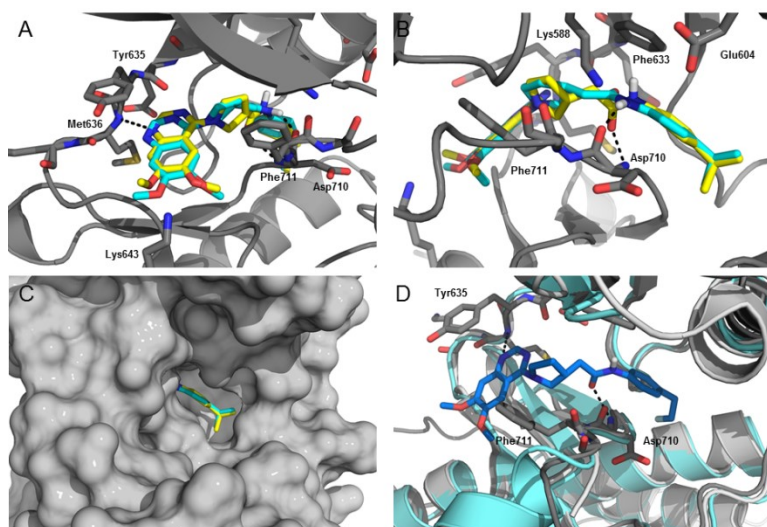
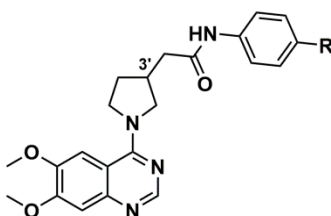


Figure 6.2. Comparison of the predicted binding poses for (*R*)-**6.6** (yellow) and (*S*)-**6.6** (cyan) bound to TrkB in the DFG-out conformation (PDB code: 4AT5) at (A) the hinge and at (B) the DFG motif and allosteric site. (C) Surface model of the overlap of (*R*)-**6.6** and (*S*)-**6.6** in the allosteric site (TrkB surface depicted in gray for clarity). (D) Predicted binding pose of (*R*)-**6.9** (pale blue) bound to TrkB (gray cartoon and sticks, PDB code: 4AT5) with TrkC (cyan, PDB code: 3V5Q) and TrkA (pale gray, PDB code: 4PMM) overlapped in the DFG-out conformation. The glycine rich loops were removed for simplicity. View from the allosteric site.

Stereochemistry at carbon-3' of the pyrrolidine ring for (*S*)-**6.6** appears to force the DFG-inhibitor interaction to occur through the amide proton of the inhibitor with the carbonyl from the

backbone of Asp710, constraining the oxygen of the carbonyl of (S)-**6.6** inward in the vicinity of the gatekeeper Phe633. In addition, a weaker hydrogen bond seems likely for (S)-**6.6** compared to (R)-**6.6** due to a shift of the quinazoline core away from Met636 to accommodate the placement of the pyrrolidine ring towards the allosteric pocket with this enantiomer.

Table 6.1. In Vitro enzymatic activities and physico-chemical Data for Compounds (S)-**6.6**, (R)-**6.6** and (R)-**6.9**



| Cpd | 3' | R ₁ | clogP | TPSA (Å ²) | IC ₅₀ (nM) ^a | | | | | | | |
|------------|-----|-----------------------------------|-------|------------------------|------------------------------------|----------------|-----------|----------|------|----------------------|-------------------------|------|
| | | | | | TrkA | TrkA-TFG | TrkA-TPM3 | TrkA-TPR | TrkB | TrkC | FLT3 | |
| 6.6 | (S) | <i>i</i> -Pr | 4.47 | 76.58 | 5570 | - ^c | - | - | - | 694 | 673 | - |
| 6.6 | (R) | <i>i</i> -Pr | 4.47 | 76.58 | 66.2 | - | - | - | - | 7.36 | 9.75 | - |
| 6.9 | (R) | CH ₂ CH ₂ F | 3.76 | 76.58 | 650 ± 34 ^b | 353 | 162 | 105 | - | 118 ± 7 ^b | 85.2 ± 8.7 ^b | 4410 |

^a[γ-³³P]ATP-based enzymatic assay performed by Reaction Biology. ^bTriplicates. ^cNot determined.

6.3.2 Biological evaluation. The predicted preferential binding of (R)-**6.6** over the S-enantiomer was confirmed by [γ-³³P]ATP-based enzymatic assays. Accordingly, we found a >70-fold potency preference of (R)-**6** for human TrkA/B/C compared to (S)-**6.6** (IC₅₀s of 66.2 nM, 7.36 nM and 9.75 nM for TrkA, TrkB and TrkC respectively - (R)-**6.6**) (Table 6.1). Satisfyingly, we observed that inhibitor (R)-**6.6** displayed a reverse activity profile with respect to Trk/FLT3 compared to the racemic lead, only partially inhibiting the latter target at 1.0 μM (Table 6.2). This observation suggests that the S-enantiomer may be responsible for low nanomolar FLT3 interaction as observed with the racemate. Our screening also showed favorable selectivity on a panel of kinases including tyrosine kinases (TK) as well as other diverse targets from different branches of the human kinome. Outside of FLT3, only CSF-1R (colony-stimulating factor-1

receptor) was found being inhibited at about IC₅₀ value at 1.0 μM (>10-fold selectivity for TrkA and >100-fold for TrkB/C versus all other off-target tested).

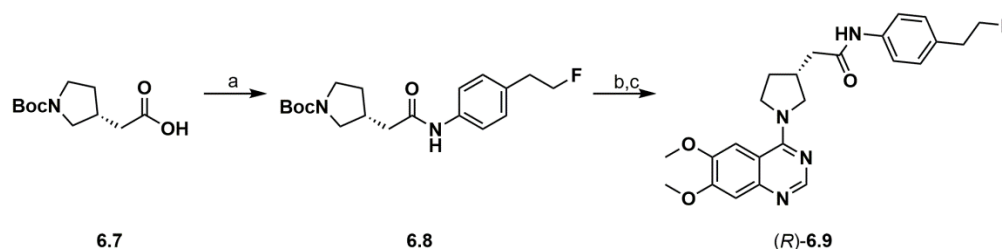
Table 6.2. Kinase Profiling of (R)-6.6 and (R)-6.9

| Kinase Target | Inhibitory activity of (R)-6.6 (% remaining at 1.0 μM ± SD) ^a | Inhibitory activity of (R)-6.9 (% remaining at 1.0 μM ± SD) ^a |
|---------------|--|--|
| CSF-1R | 41.17 ± 0.06 | 65.26 ± 0.41 |
| VEGFR-2 | 98.63 ± 2.07 | 99.72 ± 0.96 |
| ITK | 106.30 ± 0.25 | 107.79 ± 0.41 |
| FLT3 | 26.40 ± 1.17 | 80.84 ± 1.46 |
| ERK1/MAPK3 | 86.54 ± 0.56 | 101.48 ± 0.47 |
| ABL1 | 93.09 ± 0.62 | 98.84 ± 0.23 |
| c-Src | 91.72 ± 0.24 | 98.09 ± 0.17 |
| EGFR | 107.38 ± 0.33 | 100.61 ± 0.90 |
| c-MET | 100.82 ± 0.47 | 88.42 ± 3.16 |
| P38a/MAPK14 | 103.07 ± 1.93 | 114.72 ± 0.12 |
| ALK | 90.26 ± 0.45 | 99.19 ± 0.85 |
| ERBB2/HER2 | 109.06 ± 0.11 | 100.93 ± 0.48 |
| JNK1 | 94.44 ± 0.76 | 98.35 ± 0.07 |
| PDHK1 | 109.57 ± 1.91 | 96.08 ± 0.73 |
| PDGFRa | 71.63 ± 0.03 | 52.97 ± 3.83 |
| JAK1 | 105.13 ± 4.33 | 102.73 ± 1.05 |
| SYK | 99.12 ± 0.50 | 109.09 ± 0.80 |
| RET | 72.30 ± 0.27 | 91.10 ± 0.31 |
| BRAF | 69.71 ± 0.66 | 92.23 ± 0.27 |
| c-KIT | 72.46 ± 0.01 | 90.09 ± 0.25 |
| TrkA | 2.95 ± 0.46 ^b | 3.37 ± 0.65 |
| TrkB | 0.44 ± 0.29 ^b | 0.56 ± 0.18 |
| TrkC | 0.39 ± 0.52 ^b | 0.58 ± 0.40 |

^a [γ -³³P]ATP-based enzymatic assay performed by Reaction Biology. Values relative to DMSO controls; duplicate experiments. ^b Derived from dose-response curves at 1.11X10⁻⁰⁷ M (triplicates).

6.3.3 Development of (R)-[¹⁸F]6.9. The allosteric pocket fragment of (R)-6.6 was selected for structural modification and fluorine incorporation. In spite of an expected decrease in potency due to less optimal overlap with the allosteric pocket, we opted for a 4-(2-fluoroethyl)phenyl motif as a close analog to the 4-isopropylphenyl in (R)-6.6 compared to 4-(2-fluoro-1-methyl-

ethyl)phenyl in order to prevent pronounced elimination of the envisioned sulfonic ester radiolabeling precursor (as well as the $^{19}\text{F}/^{18}\text{F}$ -fluorinated compounds) (Figure 6.2D, Scheme 6.1). The fluorinated reference standard (*R*)-**6.9** was synthesized in three steps and 40% overall chemical yield starting from the HBTU-mediated coupling reaction of (*R*)-(1-boc-pyrrolidin-3-yl)-acetic acid with 4-(2-fluoroethyl)aniline (Scheme 6.1).



Scheme 6.1. Synthesis of (*R*)-2-(1-(6,7-dimethoxyquinazolin-4-yl)pyrrolidin-3-yl)-*N*-(4-(2-fluoroethyl)phenyl)acetamide (*R*)-**6.9**. Reagents and conditions: (a) 4-(2-Fluoroethyl)aniline, HBTU, DIPEA, DMF, rt, 16 h (98%); (b) TFA, CH_2Cl_2 , rt, 2 h; (c) 4-chloro-6,7-dimethoxyquinazoline, K_2CO_3 , DMF, 70°C , 16 h (41%, 2 steps).

We determined the potency of (*R*)-**6.9** to be similarly to the non-fluorinated inhibitors. Overall, (*R*)-**6.9** retained excellent nanomolar potencies and selectivity towards human TrkA/B/C despite ~10-fold reduction compared to (*R*)-**6.6** (Table 6.1, Table 6.2). The pan-Trk inhibitory profile of (*R*)-**6.9** was the same as our previous fluorinated GW2580 tracer.¹⁹ Importantly, the inhibitor showed improved potency for TrkA-TFG (TFG: Trk-fused gene, IC_{50} = 353 nM), TrkA-TPM3 (IC_{50} = 162 nM) and TrkA-TPR (TPR: translocated promoter region, IC_{50} = 105 nM) coiled-coil domain-containing fusion proteins compared to unaltered TrkA (Table 6.1). Inhibitor (*R*)-**6.9** exhibited an IC_{50} for FLT3 of 4410 nM and hence, 10- to 50-fold selectivity for TrkA-TFG, TrkA-TPM3, TrkA-TPR, TrkB and TrkC. A major challenge with the use of radiolabeled kinase inhibitor for PET imaging is the propensity of this class of compounds to be recognized by adenosine triphosphate-binding cassette (ABC) transporters such as P-glycoprotein which are largely expressed at the blood-brain-barrier, in excretory organs as well as in various tumor cells.²⁴ Efflux by P-gp limits intracellular target binding and potentially leads to non-linear

pharmacokinetics as described in the case of [^{11}C]erlotinib.²⁵ Yet, using Calcein-AM uptake assay, we determined that (*R*)-**6.9** displayed only marginal interaction with P-gp at concentration up to 10 μM in P-gp overexpressing MDCKII cells (**Figure 6.3**) which is expected to translate favorably *in vivo*.

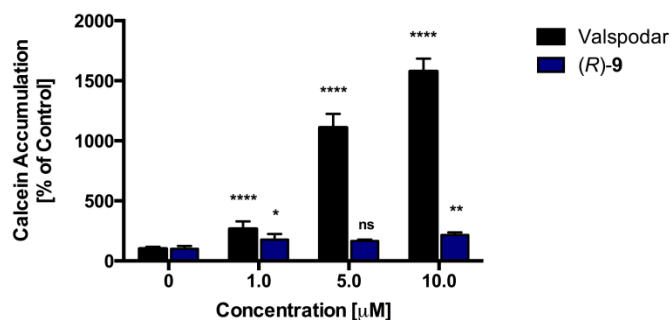
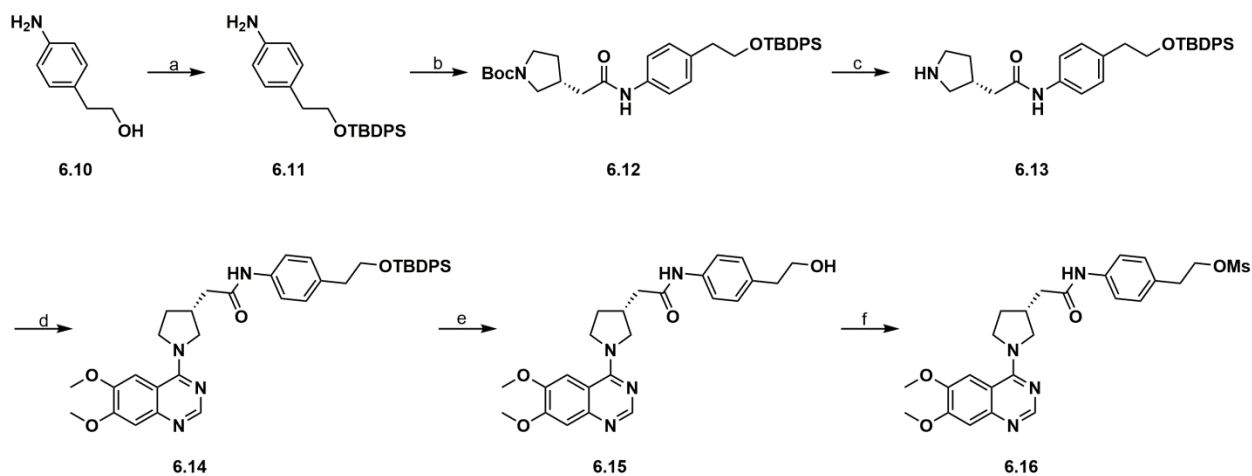


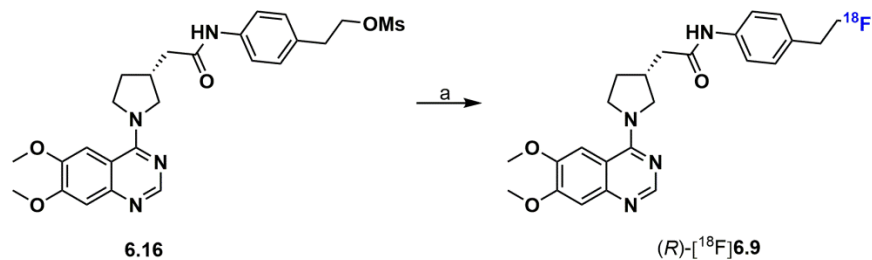
Figure 6.3. Results from Calcein-AM uptake assay demonstrate low interaction of (*R*)-**6.9** with P-gp in the range of 1-10 μM (the intracellular fluorescence in the absence of test compounds was set as 100% and 1 μM Calcein-AM was used in MDCKII cells. Valspodar was used as a positive control).

The synthesis of the mesylate precursor **6.16** was carried out in 6 steps from 4-aminophenethyl alcohol as illustrated in **Scheme 6.2**. Hydroxyl protection followed by amide bond formation cleanly afforded the enantiopure diprotected pyrrolidine intermediate **6.12**. Following amine deprotection, the free pyrrolidine **6.13** was reacted with 4-chloro-6,7-dimethoxyquinazoline to give the advanced quinazoline intermediate **6.14**. Tetrabutylammonium fluoride-mediated silyl ether cleavage afforded the hydroxyl-bearing quinazoline **6.15** which was readily converted into **6.16** using methanesulfonyl chloride (MsCl) using conventional conditions. Unexpectedly, the choice of the mesylate leaving group was made after several unsuccessful attempts to introduce a 4-toluenesulfonyl leaving group using 4-toluenesulfonyl chloride (TsCl) under various reaction conditions. The precursor **6.16** was obtained in 36% overall yield from commercially available aniline **6.10**. The radiosynthesis of (*R*)-[^{18}F]**6.9** (herein referred as [^{18}F]-(*R*)-QMICF) is showed in **Scheme 6.3**. The titled radiotracer was obtained in

one step and 18% radiochemical yield (RCY, radio-TLC) from the corresponding mesylate precursor.



Scheme 6.2. Synthesis of the mesylate precursor **6.16**. Reagents and conditions: (a) TBDPSCI, imid., DMF, rt, 16 h (80%); (*R*)-(1-Boc-pyrrolidin-3-yl)-acetic acid, HBTU, DIPEA, DMF, rt, 16 h (78%); (c) TFA, CH₂Cl₂, rt, 2 h (99%); (d) 4-chloro-6,7-dimethoxyquinazoline, K₂CO₃, DMF, 70°C, 16 h (76%); (e) TBAF, THF, rt, 4 h (92%); (f) MsCl, Et₃N, CH₂Cl₂, rt, 10 min (83%).



Scheme 6.3. Radiosynthesis of (*R*)-[¹⁸F]**6.9** ([¹⁸F]-(*R*)-QMICF). Reagents and conditions: (a) Kryptofix-222/K⁺/[¹⁸F]F⁻, MeCN, 80°C, 20 min (18%).

6.4 Conclusion

In summary, starting from a racemic FLT3 inhibitor lead with off-target TrkA activity, we have developed a fluorinated derivative ((*R*)-**6.9**) which primarily inhibits TrkA/B/C as well as clinically relevant TrkA fusion protein targets and displays favorable selectivity profile on a diverse set of kinases which include FLT3. The efficient synthesis of the non-radioactive standard of (*R*)-**6.9** and the one-step radiosynthesis of the corresponding quinazoline-based

^{18}F -labeled radiotracer is provided. The tracer [^{18}F]-(*R*)-QMICF is currently being evaluated for tumor imaging in TrkA-TPM3-overexpressing colon carcinoma KM12²⁶ mice tumor xenograft but the biological data presented herein supports the view that [^{18}F]-(*R*)-QMICF may be equally relevant towards multiple neoplasms with diverse *NTKR* fusions. Results from the *in vivo* assessment of [^{18}F]-(*R*)-QMICF as a tool tracer for the quantification of Trk status in cancer will be reported in due course.

Acknowledgements

We thank Marilyn Grand'Maison and Dr. Esther Schirmacher for reading the manuscript and providing useful comments. We are grateful to Dave Clendening and Blake Lazurko from the Edmonton PET Centre for radionuclide production. We are also grateful to Frank Wuest for access to radiochemistry laboratory. This work was financially supported by Canada Foundation for Innovation (CFI) project no. 203639 to R.S, Cancer Research Society and C⁷ Council to RS, Natural Science and Engineering Research Council of Canada (NSERC) to RS.

6.5 Supporting Information of Article 9

**Development of [¹⁸F]QMICF as a Potential Radiotracer for Tropomyosin
Receptor Kinases Oncological PET Imaging**

*Vadim Bernard-Gauthier^{a,1}, Matthew Vesnaver^b, Anne Mahringer^c, Gert Fricker^c, Ralf
Schirmmayer^{a,1}*

^aDepartment of Oncology, Division of Oncological Imaging, University of Alberta, Edmonton, AB, T6G 2R3, Canada. ^bMcConnell Brain Imaging Centre, Montreal Neurological Institute, McGill University, 3801 University Street, Montreal, QC, H3A 2B4, Canada. ^cInstitute of Pharmacy and Molecular Biotechnology, University of Heidelberg, Heidelberg 69120, Germany.

¹Corresponding authors

CONTENTS OF SUPPORTING INFORMATION

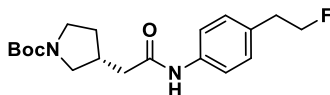
1. CHEMISTRY
2. BIOLOGICAL EVALUATION (**Figure S6.1**)
3. DOCKING STUDIES
4. RADIOCHEMISTRY
5. NMR SPECTRA

1. CHEMISTRY

1.1 General Procedure

All moisture sensitive reactions were carried out in oven-dried flasks under nitrogen atmosphere with dry solvents. Compounds (*R*)-(1-Boc-pyrrolidin-3-yl)-acetic acid and (*S*)-(1-Boc-pyrrolidin-3-yl)-acetic were purchased from Aldrich (CDS015569 and CDS009494). Other reagents and solvents were purchased at the highest commercial quality from Fisher, Sigma-Aldrich or Alfa-Aesar and were used without further purification unless specified otherwise. Organic solutions were concentrated under reduced pressure on a Heidolph rotary evaporator. In general, reactions were magnetically stirred and monitored by TLC performed on pre-coated glass-backed TLC plates (Analtech, 250 microns) and chromatographic purification of products was accomplished using flash chromatography on Alfa-Aesar silica gel (230-450 mesh). TLC visualization was performed by fluorescence quenching, KMnO_4 or ninhydrin. ^1H NMR and ^{13}C NMR spectra were recorded on a Agilent/Varian DD2 MR two channel 400 MHz spectrometer spectrometer, a Agilent/Varian VNMRS two-channel 500 MHz spectrometer or a Agilent/Varian Inova four-channel 500 MHz spectrometer in CDCl_3 or d_6 -DMSO and peak positions are given in parts per million using TMS as internal standard. Peaks are reported as: s = singlet, d = doublet, t = triplet, q = quartet, p = quintet, m = multiplet, b = broad; coupling constant(s) in Hz; integration. High Resolution Mass Spectra (HRMS) analysis was obtained from the Mass Spectrometry Facility of the Chemistry Department of the University of Alberta (Agilent Technologies 6220 oaTOF) or from the Regional Center for Mass Spectrometry of The Chemistry Department of the Université de Montréal (LC-MSD-TOF Agilent). The purities of the final compounds for biological evaluation were greater than 95% as determined from reverse-phase HPLC (254 nm). Compounds (*S*)-**6.6** and (*R*)-**6.6** were synthesized from (*R*)-(1-Boc-pyrrolidin-3-yl)-acetic acid and (*S*)-(1-Boc-pyrrolidin-3-yl)-acetic according to the known method used for the synthesis of the corresponding racemate.¹ All NMR/MS data obtained for those compounds were in full agreement with the corresponding known racemate. Computational physicochemical properties. CLogP and TPSA values were obtained with the program Pallas 3.0 for Windows (CompuDrug; San Francisco, CA).

1.2 Chemical Synthesis of Novel Compounds



tert-Butyl (*R*)-3-(2-((4-(2-fluoroethyl)phenyl)amino)-2-oxoethyl)pyrrolidine-1-carboxylate (**6.8**):

N,N-Diisopropylethylamine (0.23 mL, 1.32 mmol, 3.0 equiv) was added to a solution of (*R*)-(1-Boc-pyrrolidin-3-yl)-acetic (100 mg, 0.44 mmol, 1.0 equiv) in *N,N*-dimethylformamide (4.0 mL). HBTU (188 mg, 0.57 mmol, 1.3 equiv) was then added in one portion and the reaction mixture was stirred at 23°C for 5 min. A solution of 4-(2-fluoroethyl)aniline (79 mg, 0.57 mmol, 1.3 equiv) in *N,N*-dimethylformamide (1.0 mL) was added dropwise and the reaction mixture was stirred at 23°C for 16 h. The reaction mixture was diluted with ethyl acetate (50 mL), washed with water (25 mL) and brine (25 mL), dried over anhydrous sodium sulfate, filtered and concentrated under reduced pressure. The crude product was purified by flash column chromatography (40% EtOAc in hexanes) to afford 151 mg of the title compound (98%).

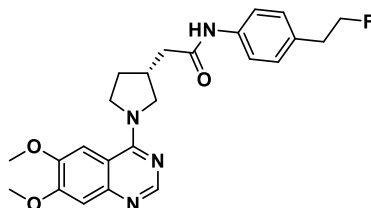
Physical State: pale yellow oil.

R_f: 0.12 (3:2 hexanes/EtOAc, UV light).

HRMS (ESI⁺): *m/z* calc. for C₁₉H₂₈FN₂O₃ (M + H)⁺: 351.2078, found 351.2079.

¹H NMR (400 MHz, CHLOROFORM-*d*) δ = 8.13 (d, *J* = 29.6 Hz, 1H), 7.45 (br s, 2H), 7.14 (br d, *J* = 2.9 Hz, 2H), 4.57 (td, *J* = 6.5, 47.1 Hz, 2H), 3.64 - 3.53 (m, 1H), 3.47 - 3.37 (m, 1H), 3.34 - 3.21 (m, 1H), 3.01 - 2.87 (m, 3H), 2.73 - 2.59 (m, 1H), 2.47 - 2.28 (m, 2H), 2.14 - 2.03 (m, 1H), 1.65 - 1.50 (m, 1H), 1.49 - 1.29 (m, 9H).

¹³C NMR (101MHz, CHLOROFORM-*d*) δ = 169.86, 154.66, 136.65, 132.98 (br s, 1C), 129.37, 120.24 (br s, 1C), 84.04 (d, *J* = 169.0 Hz, 1C), 79.34, 51.28 (br s, 1C, conformer 1), 50.93 (br s, 1C, conformer 2), 45.57 (br s, 1C, conformer 1), 45.02 (conformer 2), 40.47, 36.29 (d, *J* = 20.3 Hz, 1C), 35.62 (br s, 1C, conformer 1), 35.07 - 34.85 (br s, 1C, conformer 2), 31.48 (br s, 1C, conformer 1), 30.74 (conformer 2), 28.53.



(R)-2-(1-(6,7-dimethoxyquinazolin-4-yl)pyrrolidin-3-yl)-N-(4-(2-fluoroethyl)phenyl)acetamide(6.9):

To a solution of *tert*-butyl (*R*)-3-(2-((4-(2-fluoroethyl)phenyl)amino)-2-oxoethyl)pyrrolidine-1-carboxylate (175 mg, 0.50 mmol, 1.0 equiv) in CH₂Cl₂ (4.0 mL) was added TFA (2.0 mL) dropwise. After 2 h at 23°C, the reaction mixture was diluted with ethyl acetate (50 mL) and carefully washed with aqueous saturated NaHCO₃ (2 X 25 mL) and brine (25 mL). The organic layer was then dried over anhydrous sodium sulfate, filtered and concentrated under reduced pressure. The crude amine (130 mg, 104%) was used in the next step without further purification. The crude amine (130 mg) was dissolved in DMF (5.0 mL) and 4-chloro-6,7-dimethoxyquinazoline (180 mg, 0.80 mmol, 1.6 equiv) and K₂CO₃ (216 mg, 1.25 mmol, 2.5 equiv) were successively added. The reaction mixture was stirred at 70°C for 16 h. The reaction mixture was diluted with ethyl acetate (100 mL), washed with water (25 mL) and brine (2 X 25 mL), filtered and concentrated under reduced pressure. The crude product was purified by flash column chromatography (2→10% MeOH in CH₂Cl₂) to afford 90 mg of the title compound (41%, 2 steps).

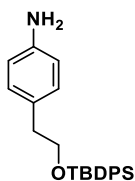
Physical State: white solid.

R_f: 0.40 (1:9 MeOH/CH₂Cl₂, UV light).

HRMS (ESI+): *m/z* calc. for C₂₄H₂₈FN₄O₃ (M + H)⁺: 439.214, found 439.2135.

¹H NMR (498 MHz, CHLOROFORM-*d*) δ = 8.47 (s, 1H), 8.11 (br s, 1H), 7.49 (d, *J* = 8.4 Hz, 2H), 7.39 (s, 1H), 7.18 (d, *J* = 8.3 Hz, 2H), 7.14 (s, 1H), 4.60 (td, *J* = 6.5, 47.1 Hz, 2H), 4.10 (dd, *J* = 6.9, 10.9 Hz, 1H), 4.03 - 3.95 (m, 2H), 3.95 (s, 3H), 3.93 (s, 3H), 3.71 (dd, *J* = 7.4, 10.6 Hz, 1H), 2.97 (td, *J* = 6.4, 23.6 Hz, 2H), 2.92 - 2.85 (m, 1H), 2.60 - 2.48 (m, 2H), 2.32 (br dt, *J* = 6.2, 11.8 Hz, 1H), 1.80 (br qd, *J* = 8.1, 12.2 Hz, 1H).

¹³C NMR (125 MHz, CHLOROFORM-*d*) δ = 169.48, 159.12, 153.82, 148.43, 147.35, 136.47, 133.31, 133.27, 129.52, 120.16, 110.11, 107.07, 104.53, 84.00 (d, *J* = 169.0 Hz, 1C), 56.07, 56.01, 55.50, 50.04, 40.40, 36.32 (d, *J* = 20.4 Hz, 1C), 35.43, 31.59.

4-(2-((*tert*-Butyldiphenylsilyl)oxy)ethyl)aniline (6.11):

tert-Butyl(chloro)diphenylsilane (1.32, 4.8 mmol, 1.0 equiv) was added to a solution of 4-aminophenethyl alcohol (660 mg, 4.8 mmol, 1.0 equiv) and imidazole (654 mg, 9.6 mmol, 2.0 equiv) in anhydrous *N,N*-dimethylformamide (25 mL) at 23°C. The reaction mixture was stirred at this temperature for 16 h and then diluted with water (50 mL) and ethyl acetate (50 mL). The organic layer was separated and the aqueous phase was extracted with ethyl acetate (3 X 50 mL). The organic layers were combined, washed with brine (50 mL) and dried over anhydrous sodium sulfate, filtered and concentrated under reduced pressure. The crude product was purified by flash column chromatography (30% ethyl acetate in hexane) to afford 1.44 g of the title compound (80%).

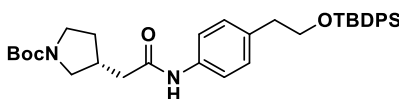
Physical State: yellow oil.

R_f: 0.48 (7:3 hexanes/EtOAc, UV light).

HRMS (ESI+): *m/z* calc. for C₂₄H₃₀NOSi (M + H)⁺: 376.2091, found 376.2091.

¹H NMR (498 MHz, CHLOROFORM-*d*) δ = 7.70 - 7.65 (m, 4H), 7.49 - 7.38 (m, 6H), 6.99 (d, *J* = 8.3 Hz, 2H), 6.64 (d, *J* = 8.3 Hz, 2H), 3.85 (t, *J* = 7.1 Hz, 2H), 3.57 (br s, 2H), 2.82 (t, *J* = 7.1 Hz, 2H), 1.10 (s, 9H).

¹³C NMR (125 MHz, CHLOROFORM-*d*) δ = 144.56, 135.64, 134.00, 130.10, 129.58, 129.12, 127.62, 115.13, 65.62, 38.52, 26.92, 19.22.



tert-Butyl (*R*)-3-(2-((4-(2-((*tert*-butyldiphenylsilyl)oxy)ethyl)phenyl)amino)-2-oxoethyl)pyrrolidine-1-carboxylate (6.12):

N,N-Diisopropylethylamine (0.68 mL, 3.93 mmol, 3.0 equiv) was added to a solution of (*R*)-(1-Boc-pyrrolidin-3-yl)-acetic (300 mg, 1.21 mmol, 1.0 equiv) in *N,N*-dimethylformamide (9.0 mL). HBTU (375 mg, 1.70 mmol, 1.3 equiv) was then added in one portion and the reaction mixture was stirred at 23°C for 5 min. A solution of 4-(2-((*tert*-Butyldiphenylsilyl)oxy)ethyl)aniline (639 mg, 1.70 mmol, 1.3 equiv) in *N,N*-dimethylformamide (1.0 mL) was added dropwise and the reaction mixture was stirred at 23°C for 16 h. The reaction mixture was diluted with ethyl acetate (100 mL), washed with water (50 mL) and brine (50 mL), dried over anhydrous sodium sulfate, filtered and concentrated under reduced pressure. The crude product was purified by flash column chromatography (50% EtOAc in hexanes) to afford 601 mg of the title compound (78%).

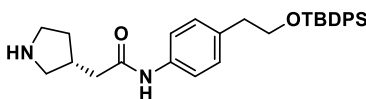
Physical State: colorless gum.

R_f: 0.43 (1:1 hexanes/EtOAc, UV light).

HRMS (ESI+): *m/z* calc. for C₃₅H₄₆N₂NaO₄Si (M + Na)⁺: 609.3119, found 609.3116.

¹H NMR (498 MHz, CHLOROFORM-*d*) δ = 7.63 - 7.58 (m, 4H), 7.45 - 7.34 (m, 8H), 7.18 (s, 1H), 7.12 (d, *J* = 8.4 Hz, 2H), 3.83 (t, *J* = 6.9 Hz, 2H), 3.65 (dd, *J* = 7.2, 10.8 Hz, 1H), 3.52 - 3.45 (m, 1H), 3.38 - 3.31 (m, 1H), 3.03 (br dd, *J* = 7.7, 10.8 Hz, 1H), 2.83 (t, *J* = 6.8 Hz, 2H), 2.73 (br tt, *J* = 7.4, 15.0 Hz, 1H), 2.50 - 2.37 (m, 2H), 2.19 - 2.10 (m, 1H), 1.67 - 1.60 (m, 1H), 1.48 (s, 9H), 1.04 (s, 9H).

¹³C NMR (125 MHz, CHLOROFORM-*d*) δ = 169.63, 155.01, 135.76, 135.56, 135.47, 133.77, 129.75, 129.56, 127.60, 119.74, 79.25, 65.06, 51.31, 45.24, 40.82, 38.67, 31.29, 31.20, 28.55, 26.83, 19.16.



(R)-N-(4-(2-((*tert*-butyldiphenylsilyl)oxy)ethyl)phenyl)-2-(pyrrolidin-3-yl)acetamide (6.13):

To a solution of (*tert*-Butyl (*R*)-3-(2-((4-(2-((*tert*-butyldiphenylsilyl)oxy)ethyl)phenyl)amino)-2-oxoethyl)pyrrolidine-1-carboxylate (550 mg, 0.94 mmol, 1.0 equiv) in CH₂Cl₂ (10.0 mL) was added TFA (2.0 mL) dropwise. After 2 h at 23°C, the reaction mixture was concentrated and carefully diluted in water (20 mL). The pH was adjusted to pH~7 and the aqueous phase was extracted with ethyl acetate (3 X 50 mL). The organic phases were combined and washed with brine (50 mL), dried over anhydrous sodium sulfate, filtered and concentrated under reduced pressure. The crude product (450 mg, 99%) was used without further purification in the next step.

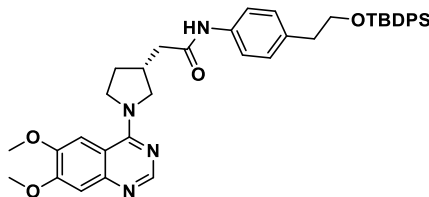
Physical State: pale yellow solid.

R_f: baseline (1:1 hexanes/EtOAc, UV light).

HRMS (ESI+): *m/z* calc. for C₃₀H₃₉N₂O₂Si (M + H)⁺: 487.2775, found 487.2781.

¹H NMR (498 MHz, CHLOROFORM-*d*) δ = 8.59 (s, 1H), 7.61 (dd, *J* = 1.4, 6.6 Hz, 4H), 7.46 (d, *J* = 8.4 Hz, 2H), 7.44 - 7.34 (m, 6H), 7.09 (d, *J* = 8.4 Hz, 2H), 3.82 (t, *J* = 6.9 Hz, 2H), 3.40 - 3.33 (m, 1H), 3.32 - 3.21 (m, 2H), 3.17 (br dd, *J* = 4.5, 11.4 Hz, 1H), 2.97 - 2.89 (m, 1H), 2.81 (t, *J* = 6.9 Hz, 2H), 2.59 (dd, *J* = 10.0, 14.5 Hz, 1H), 2.48 (dd, *J* = 5.7, 14.5 Hz, 1H), 2.25 - 2.16 (m, 1H), 1.78 (dt, *J* = 6.7, 13.2 Hz, 1H), 1.04 (s, 9H).

^{13}C NMR (125 MHz, CHLOROFORM-*d*) δ = 169.01, 135.94, 135.54, 135.41, 134.81, 133.77, 129.57, 127.61, 119.83, 65.09, 49.49 (br s, 1C), 44.22, 39.61, 38.69, 35.16, 30.12, 26.84, 19.16.



(*R*)-*N*-(4-(2-((*tert*-Butyldiphenylsilyl)oxy)ethyl)phenyl)-2-(1-(6,7-dimethoxyquinazolin-4-yl)pyrrolidin-3-yl)acetamide (6.14):

4-Chloro-6,7-dimethoxyquinazoline (335 mg, 1.49 mmol, 1.6 equiv) and K_2CO_3 (322 mg, 2.33 mmol, 2.5 equiv) were successively added to a solution of (*R*)-*N*-(4-(2-((*tert*-butyldiphenylsilyl)oxy)ethyl)phenyl)-2-(pyrrolidin-3-yl)acetamide (450 mg, 0.93 mmol, 1.0 equiv) in DMF (10.0 mL). The reaction mixture was stirred at 70°C for 16 h. The reaction mixture was diluted with ethyl acetate (100 mL), washed with water (25 mL) and brine (3 X 25 mL), filtered and concentrated under reduced pressure. The crude product was purified by flash column chromatography (5→10% MeOH in CH_2Cl_2) to afford 477 mg of the title compound (76%).

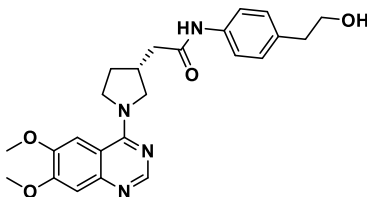
Physical State: white solid.

R_f: 0.15 (5:95 MeOH/ CH_2Cl_2 , UV light).

HRMS (ESI+): *m/z* calc. for $\text{C}_{40}\text{H}_{47}\text{N}_4\text{O}_4\text{Si}$ ($\text{M} + \text{H}^+$): 675.3361, found 675.3360.

^1H NMR (498 MHz, CHLOROFORM-*d*) δ = 8.51 (s, 1H), 7.66 - 7.56 (m, 4H), 7.51 (s, 1H), 7.45 - 7.40 (m, 5H), 7.39 - 7.34 (m, 4H), 7.19 (s, 1H), 7.13 (d, J = 8.4 Hz, 2H), 4.14 (dd, J = 6.9, 10.8 Hz, 1H), 4.07 - 4.00 (m, 2H), 4.00 (s, 3H), 3.96 (s, 3H), 3.83 (t, J = 6.8 Hz, 2H), 3.75 (dd, J = 7.7, 10.8 Hz, 1H), 2.95 - 2.87 (m, 1H), 2.83 (t, J = 6.8 Hz, 2H), 2.61 - 2.49 (m, 2H), 2.36 (br dt, J = 6.2, 11.6 Hz, 1H), 1.83 (br d, J = 3.8 Hz, 1H), 1.04 (s, 9H)

^{13}C NMR (125 MHz, CHLOROFORM-*d*) δ = 169.14, 159.25 (br s, 1C), 153.83, 147.37, 135.77, 135.50, 135.55, 133.76, 129.78, 129.56, 127.60, 119.75, 110.20, 107.32, 104.54, 65.04, 56.11, 56.05, 55.55, 50.10, 40.50, 38.67, 35.43, 31.65, 26.83, 19.16.



(R)-2-(1-(6,7-Dimethoxyquinazolin-4-yl)pyrrolidin-3-yl)-N-(4-(2-hydroxyethyl)phenyl)acetamide(6.15):

Tetrabutylammonium fluoride (1.0 M in tetrahydrofuran, 0.66 mL, 0.66 mmol, 1.05 equiv) was added dropwise to a solution of (R)-N-(4-(2-((*tert*-Butyldiphenylsilyl)oxy)ethyl)phenyl)-2-(1-(6,7-dimethoxyquinazolin-4-yl)pyrrolidin-3-yl)acetamide (425 mg, 0.63 mmol, 1.0 equiv) in tetrahydrofuran (7.0 mL) at 23°C. After 4 h, the reaction mixture was quenched with water (25 mL) and diluted with ethyl acetate (100 mL). The phases were separated and the organic layer was washed with water (2 X 25 mL). The combined organic layers were dried over anhydrous sodium sulfate, filtered and concentrated under reduced pressure. The crude product was purified by flash column chromatography (5→10% methanol in dichloromethane) to afford 252 mg of the title compound (92%).

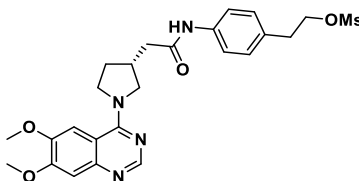
Physical State: white solid.

R_f: 0.15 (1:9 MeOH/CH₂Cl₂, UV light).

HRMS (ESI+): *m/z* calc. for C₂₄H₂₉N₄O₄ (M + H)⁺: 437.2183, found 437.2188.

¹H NMR (498 MHz, DMSO-*d*₆) δ = 9.90 (s, 1H), 8.30 (s, 1H), 7.49 (d, *J* = 4.4 Hz, 2H), 7.46 (s, 1H), 7.11 (d, *J* = 8.5 Hz, 2H), 7.09 (s, 1H), 4.58 (br t, *J* = 4.3 Hz, 1H), 4.00 (dd, *J* = 6.9, 10.8 Hz, 1H), 3.97 - 3.89 (m, 2H), 3.87 (s, 3H), 3.83 (s, 3H), 3.60 (dd, *J* = 7.8, 10.9 Hz, 1H), 3.54 (dt, *J* = 4.5, 6.7 Hz, 2H), 2.70 - 2.62 (m, 3H), 2.51 - 2.47 (m, 2H), 2.15 (br d, *J* = 5.4 Hz, 1H), 1.75 - 1.66 (m, 1H).

¹³C NMR (125 MHz, DMSO-*d*₆) δ = 170.23, 158.70, 153.78, 153.19, 148.62, 147.25, 137.52, 134.69, 129.43, 119.53, 109.88, 107.41, 105.30, 62.73, 56.05, 56.01, 55.69, 49.99, 39.87, 38.93, 35.53, 31.41.

(R)-4-(2-(1-(6,7-dimethoxyquinazolin-4-yl)pyrrolidin-3-yl)acetamido)phenethyl methanesulfonate(6.16):

Triethylamine (14 μL, 0.104 mmol, 1.5 equiv) and methanesulfonyl chloride (7.0 μL, 0.083 mmol, 1.2 equiv) were successively added to a solution of (R)-2-(1-(6,7-Dimethoxyquinazolin-4-

yl)pyrrolidin-3-yl)-*N*-(4-(2-hydroxyethyl)phenyl)acetamide (30 mg, 0.069 mmol, 1.0 equiv) in CH₂Cl₂ (3.0 mL) at 23°C. After 10 min, the reaction mixture was quenched with water (25 mL) and diluted with CH₂Cl₂ (25 mL). The phases were separated and the aqueous layer was extracted with CH₂Cl₂ (2 X 25 mL). The combined organic layers were washed with brine (25 mL), dried over anhydrous sodium sulfate, filtered and concentrated under reduced pressure. The crude product was purified by flash column chromatography (5→10% methanol in dichloromethane) to afford 30 mg of the title compound (83%).

Physical State: off-white solid.

R_f: 0.23 (1:9 MeOH/CH₂Cl₂, UV light).

HRMS (ESI⁺): *m/z* calc. for C₂₅H₃₀N₄O₆S (M + H)⁺: 515.1959, found 515.1971.

¹H NMR (400 MHz, CHLOROFORM-*d*) δ = 8.78 (br s, 1H), 8.32 (s, 1H), 7.63 (d, *J* = 8.3 Hz, 2H), 7.50 (s, 1H), 7.22 - 7.12 (m, 3H), 4.39 (t, *J* = 6.8 Hz, 2H), 4.25 - 4.17 (m, 1H), 4.12 (br dd, *J* = 6.9, 11.3 Hz, 1H), 3.97 (s, 3H), 3.96 (s, 3H), 3.94 - 3.87 (m, 2H), 3.04 - 2.99 (m, 2H), 2.89 (s, 3H), 2.76 - 2.65 (m, 2H), 2.36 - 2.27 (m, 1H), 1.97 - 1.86 (m, 1H), 1.68 - 1.57 (m, 1H).

¹³C NMR (126MHz, CHLOROFORM-*d*) δ = 169.63, 159.10, 153.89, 147.41, 136.95, 132.21, 129.52, 120.14, 110.03 (br s, 1C), 106.92 (br s, 1C), 104.61, 70.17, 56.13, 56.09, 55.56, 50.17, 37.41, 35.45, 35.05, 31.57.

2. BIOLOGICAL EVALUATION

2.1 [γ -³³P]ATP-Based Enzymatic Assay.

Compound (*R*)-**6.6**, (*S*)-**6.6** and (*R*)-**6.9** were tested in a [γ -³³P]ATP based enzymatic assay by Reaction Biology Corporation (Malvern, PA). Briefly, the compound was tested in a 10-concentration IC₅₀ curve with 3-fold serial dilution starting at 10 μ M. The reactions were performed with 1 μ M ATP and initially profiled against 3 tyrosine kinases (tropomyosin receptor kinase A (TrkA), tropomyosin receptor kinase B (TrkB), tropomyosin receptor kinase C (TrkC)). IC₅₀ values less than 5.08E-10 M or higher than 1.00E-05 is estimated based on the best curve fitting available ($n = 1$) for (*R*)-**6.6**, (*S*)-**6.6** and $n = 1$ for (*R*)-**6.9**. Inhibitor (*R*)-**6.9** was also assessed against TrkA fusion kinases (TrkA-TGF, TrkA-TPM3 and TrkA-TPR). Compounds (*R*)-**6.6** and (*R*)-**6.9** were also tested for inhibitory activity at 1.0 μ M on a panel of 20 selected kinases (SYK, PDK1/PDHK1, PDGFR α , P38 α /MAPK14, KDR/VEGFR2, JNK1, JAK1, ITK, FMS, ERK1, ERBB2/HER2, EGFR, c-SRC, c-MET, c-KIT, BRAF, ALK, ABL1, FLT3 and RET) under similar conditions ($n = 2$).

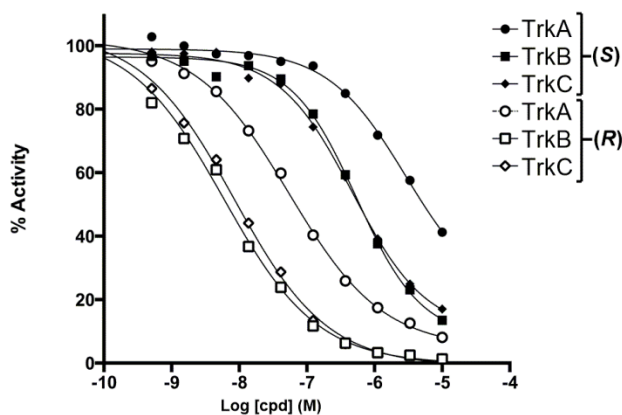


Figure S6.1. Dose-response curves for inhibitors (*R*)-**6.6**, (*S*)-**6.6** against TrkA, TrkB and TrkC.

2.2 Calcein-AM assay.

Cell Culture. Native MDCKII cells or stably transfected with human P-gp or wild-type BCRP (482A) were seeded at a density of 156.250 cells/cm² using Dulbecco's modified Eagle's medium (DMEM) with 10% FCS, 4.0 mM L-Glutamine, 100 U/ml Penicillin, 100 µg/ml Streptomycin and 100 µg/ml Kanamycin (Biochrom, Munich, Germany) and split after reaching cell confluency to 70-80%. Cell passages from 7-25 have been used throughout the experiments. *Calcein-AM Uptake-Assay.* The assay for quantifying P-gp efflux activity was performed as described previously.²⁷ Briefly, human P-gp overexpressing MDCKII cells were washed two times with Krebs-Ringer Buffer (142 mM NaCl, 3 mM KCl, 1.5 mM K₂HPO₄*3 H₂O, 10 mM HEPES, 4 mM D-Glucose, 1.2 mM MgCl₂, 1.4 mM CaCl₂, pH 7.4) and preincubated with 100 µl of double-concentrated modulator for 15 min that was followed by addition of 100 µl 4°C cold 2 µM Calcein-AM (Sigma-Aldrich, Taufkirchen, Germany) solution for 30 min. Plates were incubated at 37°C at 200 rpm. Control cells were exposed to Calcein-AM in absence of a transport modulator. Subsequently, MDCKII cells were washed with ice-cold Krebs-Ringer Buffer to stop transporter activity and intracellular fluorescence was released after incubation with 0.1% Triton X for 20 min at 37°C. The amount of intracellular fluorescence was recorded using a fluorescence plate reader (Tecan Infinite F200 Pro, $\lambda_{(\text{excitation})} = 485 \text{ nm}$ and $\lambda_{(\text{emission})} = 520 \text{ nm}$). Background fluorescence was subtracted from each signal and intracellularly accumulated fluorescence was related to control cells. EC₅₀ values were calculated via non-linear regression using the 4-parameter logistic equation with variable Hill-slope (GraphPad Prism[®] version 6.01) to generate dose-response curves.

3. DOCKING STUDIES

Molecular docking simulations of (*R*)-**6.6**, (*S*)-**6.6** and (*R*) **6.9** were performed using the X-ray co-crystal structure of TrkB-GW2580 complex (PDB code: 4AT5) and TrkC complex (PDB code: 3V5Q) using FITTED 3.5 program (FORECASTER platform).²⁸⁻²⁹ Docking structures and figures were prepared using Pymol.

4. RADIOCHEMISTRY

The manual radiosyntheses of (*R*)-[¹⁸F]**6.9** ([¹⁸F]-(*R*)-QMICF) was performed at medical isotope and cyclotron facility of the University of Alberta (Edmonton PET Center, ACSI 19/9 MeV cyclotron). No-carrier-added (n.c.a) aqueous [¹⁸F]Fluoride was produced by a ¹⁸O(p,n)¹⁸F nuclear reaction on an enriched [¹⁸O]water target. No-carrier-added (n.c.a) aqueous [¹⁸F]fluoride was passed through a Sep-Pak Light QMA cartridge (Waters) (typically 1-2 GBq in 2.0 mL water). The cartridge was dried by airflow, and the ¹⁸F activity was eluted with 1.0 mL of a Kryptofix 2.2.2/K₂CO₃ solution (from a 10.0 mL stock solution of 22.6 mg of Kryptofix 222 and 4.2 mg of K₂CO₃ in acetonitrile/water (95/5)) to a 10.0 mL conical vial. The solvent was removed at 100°C under atmospheric pressure and a stream of nitrogen gas. The residue was azeotropically dried with a total of 6.0 mL of anhydrous acetonitrile at 100°C to afford the dried K2.2.2/K[¹⁸F]F complex residue which was dissolved in anhydrous acetonitrile. A 20 µL aliquot of this K2.2.2/K[¹⁸F]F solution was added to a solution of the mesylate precursor **6.16** (2.0 mg) in DMF (200 µL) and heated at 80°C for 20 min. The reaction mixture was cooled to room temperature and diluted with 600 µL of a mixture of MeCN/H₂O (1:1) and analyzed by radio-TLC (R_f 0.4 10% MeOH/CH₂Cl₂, 18% RCY).

5. NMR SPECTRA

Data from this subsection can be found in **Annex 5**.

6.6 References

1. Stransky, N.; Cerami, E.; Schalm, S.; Kim, J. L.; Lengauer, C., The landscape of kinase fusions in cancer. *Nat Commun* **2014**, *5*.
2. Mertens, F.; Johansson, B.; Fioretos, T.; Mitelman, F., The emerging complexity of gene fusions in cancer. *Nature Reviews Cancer* **2015**, *15* (6), 371-381.
3. Pulciani, S.; Santos, E.; Lauver, A. V.; Long, L. K.; Aaronson, S. A.; Barbacid, M., Oncogenes in Solid Human-Tumors. *Nature* **1982**, *300* (5892), 539-542.
4. Martin-Zanca, D.; Hughes, S. H.; Barbacid, M., A human oncogene formed by the fusion of truncated tropomyosin and protein tyrosine kinase sequences. *Nature* **1986**, *319* (6056), 743-8.
5. Deinhardt K, C. M., Trk Receptors. *Handb Exp Pharmacol.* **2014**, *220*, 103-119.
6. Vaishnavi, A.; Le, A. T.; Doebele, R. C., TRKking Down an Old Oncogene in a New Era of Targeted Therapy. *Cancer Discovery* **2015**, *5* (1), 25-34.
7. Doebele, R. C.; Davis, L. E.; Vaishnavi, A.; Le, A. T.; Estrada-Bernal, A.; Keysar, S.; Jimeno, A.; Varella-Garcia, M.; Aisner, D. L.; Li, Y. L.; Stephens, J.; Morosini, D.; Tuch, B. B.; Fernandes, M.; Nanda, N.; Low, J. A., An Oncogenic NTRK Fusion in a Patient with Soft-Tissue Sarcoma with Response to the Tropomyosin-Related Kinase Inhibitor LOXO-101. *Cancer Discovery* **2015**, *5* (10), 1049-1057.
8. Farago, A. F.; Le, L. P.; Zheng, Z.; Muzikansky, A.; Drilon, A.; Patel, M.; Bauer, T. M.; Liu, S. V.; Ou, S. H.; Jackman, D.; Costa, D. B.; Multani, P. S.; Li, G. G.; Hornby, Z.; Chow-Maneval, E.; Luo, D.; Lim, J. E.; Iafrate, A. J.; Shaw, A. T., Durable Clinical Response to Entrectinib in NTRK1-Rearranged Non-Small Cell Lung Cancer. *J Thorac Oncol* **2015**, *10* (12), 1670-4.
9. Redig, A. J.; Janne, P. A., Basket Trials and the Evolution of Clinical Trial Design in an Era of Genomic Medicine. *J Clin Oncol* **2015**, *33* (9), 975-+.
10. Farwell, M. D.; Pryma, D. A.; Mankoff, D. A., PET/CT Imaging in Cancer: Current Applications and Future Directions. *Cancer* **2014**, *120* (22), 3433-3445.
11. Slobbe, P.; Poot, A. J.; Windhorst, A. D.; van Dongen, G. A., PET imaging with small-molecule tyrosine kinase inhibitors: TKI-PET. *Drug Discov Today* **2012**, *17* (21-22), 1175-87.
12. Bernard-Gauthier, V.; Bailey, J. J.; Berke, S.; Schirmacher, R., Recent Advances in the Development and Application of Radiolabeled Kinase Inhibitors for PET Imaging. *Molecules* **2015**, *20* (12), 22000-22027.

13. Memon, A. A.; Jakobsen, S.; Dagnaes-Hansen, F.; Sorensen, B. S.; Keiding, S.; Nexø, E., Positron emission tomography (PET) imaging with [¹¹C]-labeled erlotinib: a micro-PET study on mice with lung tumor xenografts. *Cancer Res* **2009**, *69* (3), 873-8.
14. Bahce, I.; Smit, E. F.; Lubberink, M.; van der Veldt, A. A. M.; Yaqub, M.; Windhorst, A. D.; Schuit, R. C.; Thunnissen, E.; Heideman, D. A. M.; Postmus, P. E.; Lammertsma, A. A.; Hendrikse, N. H., Development of [¹¹C]erlotinib Positron Emission Tomography for In Vivo Evaluation of EGF Receptor Mutational Status. *Clinical Cancer Research* **2013**, *19* (1), 183-193.
15. Yaqub, M.; Bahce, I.; Voorhoeve, C.; Sehuit, R. C.; Windhorst, A. D.; Hoekstra, O. S.; Boellaard, R.; Hendrikse, N. H.; Smit, E. F.; Lammertsma, A. A., Quantitative and Simplified Analysis of C-11-Erlotinib Studies. *Journal of Nuclear Medicine* **2016**, *57* (6), 861-866.
16. Meng, X.; Loo, B. W.; Ma, L.; Murphy, J. D.; Sun, X. D.; Yu, J. M., Molecular Imaging with C-11-PD153035 PET/CT Predicts Survival in Non-Small Cell Lung Cancer Treated with EGFR-TKI: A Pilot Study. *Journal of Nuclear Medicine* **2011**, *52* (10), 1573-1579.
17. Saleem, A.; Searle, G. E.; Kenny, L. M.; Huiban, M.; Kozlowski, K.; Waldman, A. D.; Woodley, L.; Palmieri, C.; Lowdell, C.; Kaneko, T.; Murphy, P. S.; Lau, M. R.; Aboagye, E. O.; Coombes, R. C., Lapatinib access into normal brain and brain metastases in patients with Her-2 overexpressing breast cancer. *Ejnmri Res* **2015**, *5*.
18. Wu, P.; Nielsen, T. E.; Clausen, M. H., Small-molecule kinase inhibitors: an analysis of FDA-approved drugs. *Drug Discovery Today* **2016**, *21* (1), 5-10.
19. Bernard-Gauthier, V.; Schirmacher, R., 5-(4-((4-[¹⁸F]fluorobenzyl)oxy)-3-methoxybenzyl)pyrimidine-2,4-diamine: A selective dual inhibitor for potential PET imaging of Trk/CSF-1R. *Bioorg Med Chem Lett* **2014**, *24* (20), 4784-4790.
20. Johnson, J., Alkylquinoline and alkylquinazoline kinase modulators. US2006281772. **2006**.
21. Albaugh, P.; Fan, Y.; Mi, Y.; Sun, F.; Adrian, F.; Li, N.; Jia, Y.; Sarkisova, Y.; Kreuzsch, A.; Hood, T.; Lu, M.; Liu, G.; Huang, S.; Liu, Z.; Loren, J.; Tuntland, T.; Karanewsky, D. S.; Seidel, H. M.; Molteni, V., Discovery of GNF-5837, a Selective TRK Inhibitor with Efficacy in Rodent Cancer Tumor Models. *ACS Med Chem Lett* **2012**, *3* (2), 140-5.
22. Skerratt, S. E.; Andrews, M.; Bagal, S. K.; Bilsland, J.; Brown, D.; Bungay, P. J.; Cole, S.; Gibson, K. R.; Jones, R.; Morao, I.; Nedderman, A.; Omoto, K.; Robinson, C.; Ryckmans, T.; Skinner, K.; Stuppel, P.; Waldron, G., The Discovery of a Potent, Selective, and Peripherally Restricted Pan-Trk Inhibitor (PF-06273340) for the Treatment of Pain. *Journal of Medicinal Chemistry* **2016**, *59* (22), 10084-10099.

23. Bertrand, T.; Kothe, M.; Liu, J.; Dupuy, A.; Rak, A.; Berne, P. F.; Davis, S.; Gladysheva, T.; Valtre, C.; Crenne, J. Y.; Mathieu, M., The crystal structures of TrkA and TrkB suggest key regions for achieving selective inhibition. *J Mol Biol* **2012**, *423* (3), 439-53.
24. Ozvegy-Laczka, C.; Cserepes, J.; Elkind, N. B.; Sarkadi, B., Tyrosine kinase inhibitor resistance in cancer: role of ABC multidrug transporters. *Drug Resist Update* **2005**, *8* (1-2), 15-26.
25. Traxl, A.; Wanek, T.; Mairinger, S.; Stanek, J.; Filip, T.; Sauberer, M.; Muller, M.; Kuntner, C.; Langer, O., Breast Cancer Resistance Protein and P-Glycoprotein Influence In Vivo Disposition of ¹¹C-Erlotinib. *J Nucl Med* **2015**, *56* (12), 1930-6.
26. Medico, E.; Russo, M.; Picco, G.; Cancelliere, C.; Valtorta, E.; Corti, G.; Buscarino, M.; Isella, C.; Lamba, S.; Martinoglio, B.; Veronese, S.; Siena, S.; Sartore-Bianchi, A.; Beccuti, M.; Mottolese, M.; Linnebacher, M.; Cordero, F.; Di Nicolantonio, F.; Bardelli, A., The molecular landscape of colorectal cancer cell lines unveils clinically actionable kinase targets. *Nat Commun* **2015**, *6*, 7002.
27. Bauer, B.; Miller, D. S.; Fricker, G., Compound profiling for p-glycoprotein at the blood-brain barrier using a microplate screening system. *Pharmaceut Res* **2003**, *20* (8), 1170-1176.
28. Englebienne, P.; Moitessier, N., Docking ligands into flexible and solvated macromolecules. 5. Force-field-based prediction of binding affinities of ligands to proteins. *J Chem Inf Model* **2009**, *49* (11), 2564-71.
29. Therrien, E.; Englebienne, P.; Arrowsmith, A. G.; Mendoza-Sanchez, R.; Corbeil, C. R.; Weill, N.; Campagna-Slater, V.; Moitessier, N., Integrating Medicinal Chemistry, Organic/Combinatorial Chemistry, and Computational Chemistry for the Discovery of Selective Estrogen Receptor Modulators with FORECASTER, a Novel Platform for Drug Discovery. *Journal of Chemical Information and Modeling* **2012**, *52* (1), 210-224.

Current and future work, conclusion and perspective

Data presented in this chapter are part of a manuscript in preparation for submission to: Journal of Nuclear Medicine. (Article 10)

Bernard-Gauthier, V.; Mossine, A.V.; Aliaga, A.; Shao, X.; Quesada, C.A.; Sherman, P.; Mahringer, A.; Kostikov, A.; Fricker, G.; Rosa-Neto, P.; Scott P.J.H.; Schirmacher, R. Preclinical evaluation of [¹⁸F]-(*R*)-IPMICF17: a PET radiotracer for the tropomyosin receptor kinases TrkA/B/C.

Only selected data from experiments conducted by **V.B.G.** are included in this Chapter.

7.1 Current and future work

The iterative optimisation of the (2-pyrrolidin-1-yl)imidazo[1,2-*b*]pyridazine (IPMICF) series (**Chapter 4 – 5**), including completed and undergoing work will be briefly presented in the first section of this chapter. The subsequent sections (**7.1.2 – 7.1.6**) present future proposed work to refine and optimize the different radiotracer series presented in the thesis as well as other relevant projected work based on recent progress in the field of Trk inhibitors development. Section **7.2** will discuss significance and present a general conclusion.

7.1.1 Development of [¹⁸F]-(*R*)-IPMICF17. Although our first generation radiotracer [¹¹C]-(*R*)-IPMICF16 holds substantial promises for *in vivo* use as shown in **Chapter 5**, the development of a suitable fluorine-18-labeled derivative from this series would be advantageous – so far not achieved with [¹⁸F]-(\pm)-IPMICF6 or [¹⁸F]-(\pm)-IPMICF10. Moreover, we expect that the P-gp/BCRP liabilities of [¹¹C]-(*R*)-IPMICF16 observed in rodents may add additional variables during upcoming target engagement screening of Trk inhibitors. This may be especially true for compounds (including self-block) which also display interactions with efflux transporters, as pharmacological treatment with such compounds can potentiate brain uptake or give rise to blood concentration fluctuations leading to paradoxical increases in radiotracer brain uptake and changes in kinetics.¹ In this context, careful screening with P-gp/BCRP cellular assays and blood plasma normalization may be required.² Identifying a radiotracer from this series which does not interact or interacts minimally with efflux transporters would therefore allow for more straightforward *in vivo* analyses in rodents and would also be beneficial for clinical use. Such a tracer would also clarify whether or not the overall uptake of [¹¹C]-(*R*)-IPMICF16 in the primate brain (human and non-human) is primarily dictated by active efflux transport (as in rodent), or if in higher species, parameters such as target density (B_{max}) or passive permeability account for the observed uptake. Yet, it is important to note that, the absence of a gold-standard radiotracer for comparison, not only for Trk but for CNS kinases in general, currently precludes the

determination of what constitutes an acceptable brain uptake in this context. At the moment, the only other radiolabeled kinase inhibitor shown to engage its target *in vivo* is the glycogen synthase kinase-3 (GSK3) tracer [^{11}C]PF-367.³ Notably, in a preclinical non-human primate study, this tracer displayed brain uptake comparable to [^{11}C]-(*R*)-IPMICF16 while not being susceptible to P-gp efflux.

Nevertheless, in order to clarify those questions and explore further the IPMICF series, our optimization of [^{11}C]-(*R*)-IPMICF16 combined the thorough re-evaluation of our IPMICF library (**Chapter 4**) using P-gp Calcein-AM cellular assay with a SAR exploration of the adjacent 2-phenylpyrrolidine (**Figure 7.1**). With regard to the 2-phenylpyrrolidine fragment, we were interested in briefly exploring the role of fluorination towards potency.⁴⁻⁵

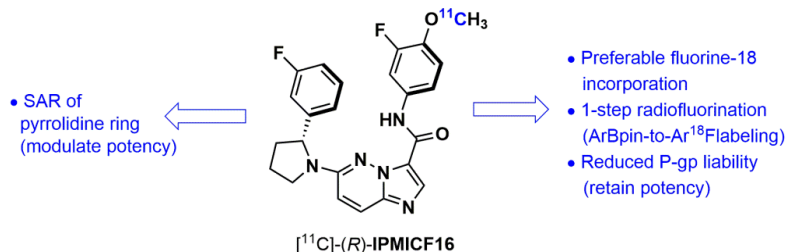
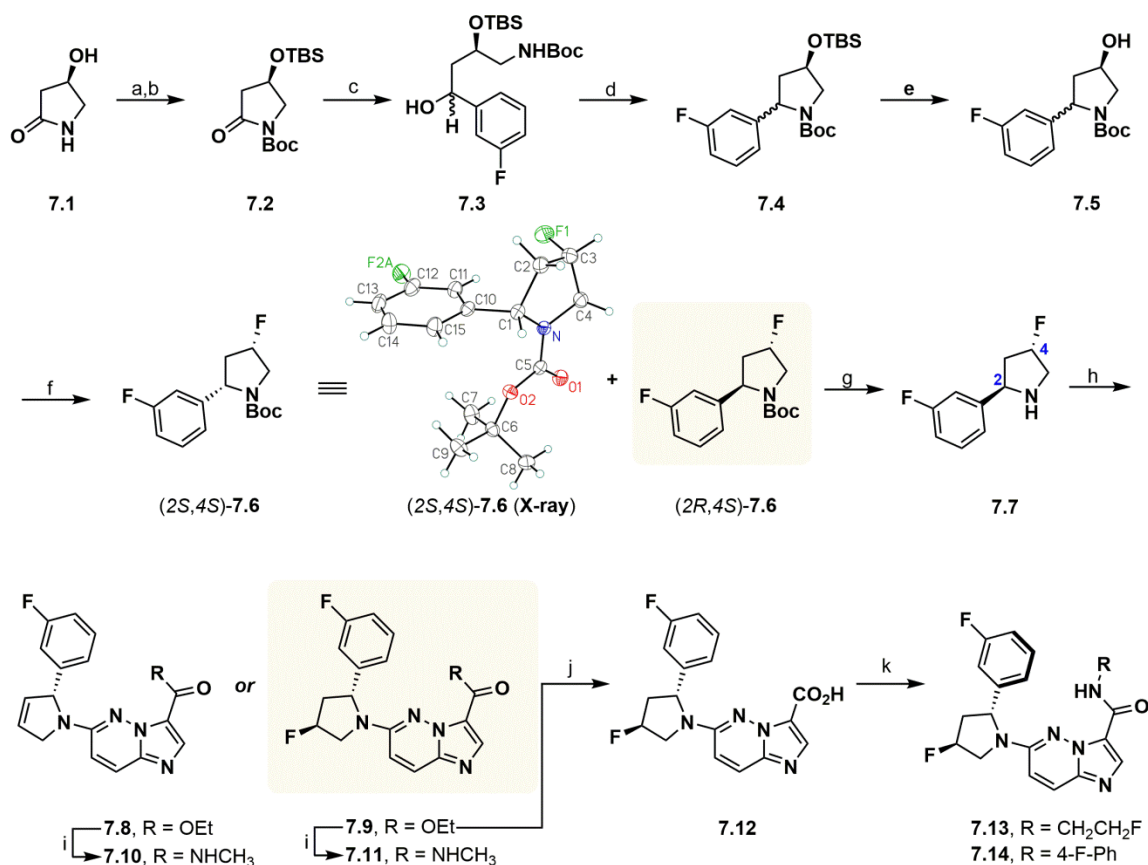


Figure 7.1. [^{11}C]-(*R*)-IPMICF16: first round of lead optimization.

Building on the (2*R*,4*S*)-4-fluoro-2-(3-fluorophenyl)pyrrolidine-containing inhibitor **4.8** (**Chapter 4**) initially used to develop our IPMICF series, we aimed to define the role of selective pyrrolidine and phenyl fluorine substitutions on Trk potency. As alluded in **Chapter 4**, the use of the chiral fluorinated pyrrolidine found in **4.8** was envisioned early in the project, but was ultimately considered counter-productive due to the amount of material needed for SAR derivatization and the expected low overall yield from the synthesis of this specific pyrrolidine intermediate. Commercially available racemic 2-(3-fluorophenyl)pyrrolidine was chosen until the enantioselective synthesis described in **Chapter 5** was established. For the second-generation exploration presented here, the synthesis of pyrrolidine **7.7** was undertaken. The synthesis was

adapted from previous literature⁶ and began with the successive protection of the hydroxyl and amide groups of (*R*)-(+)-4-hydroxy-2-pyrrolidinone with TBS and Boc respectively (**Scheme 7.1**). Grignard reaction using 3-fluorophenyl magnesium bromide was then performed followed by reduction with NaBH₄ providing the linear hydroxyl intermediate **7.3** in 59% yield (from **7.2**). Reaction with methanesulfonyl chloride (MsCl) induced intramolecular cyclization affording pyrrolidine **7.4** as a diastereomeric mixture.

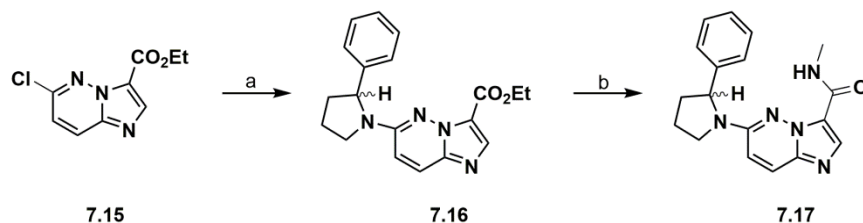


Scheme 7.1. Synthesis of novel imidazo[1,2-*b*]pyridazine inhibitors. Reagents and conditions: (a) TBSCl, imidazole, DMF, rt, 3 h; (b) Boc₂O, MeCN, Et₃N, DMAP, (83%, 2 steps); (c) 3-Fluorophenyl magnesium bromide, THF, 0°C, 2 h, then MeOH, NaBH₄, 0°C, 1 h (59%, 2 steps); (d) MsCl, CH₂Cl₂, Et₃N, -60°C, 1 h; (e) TBAF, THF, rt, 2 h (51%, 2 steps); (f) DAST, CH₂Cl₂, -78°C - rt, 16 h (78%); (g) TFA, CH₂Cl₂, rt, 2 h (93%, crude); (h) 6-chloroimidazo[1,2-*b*]pyridazine-3-carboxylate, KF, DMSO, 120°C, 12 h (70%) or 6-chloroimidazo[1,2-*b*]pyridazine-3-carboxylate, KF, DMSO, 100°C, 12 h (47%); (i) MeNH₂, rt (29-90%); (j) LiOH, THF/EtOH/H₂O, rt, 3 h (65%); (k) amine, HATU, DIPEA, DMF, rt, 16 h (52% for **7.13**, 94% for **7.14**).

Although the separation of the diastereomers could be performed anywhere from this intermediate using gel column chromatography, the best separation was achieved once the fluorine was installed at the pyrrolidine C₄. Hence the silyl ether protecting group was removed using conventional TBAF conditions on the diastereomers mixture to provide the 4-hydroxypyrrolidine intermediate **7.4** in 51% after two steps. Deoxyfluorination of alcohol **7.4** was performed efficiently using diethylaminosulfur trifluoride (DAST) and followed by separation which afforded pure (2*S*,4*S*)- and (2*R*,4*S*)-diastereomers (up to gram-scale separation, 78% overall, 26:74 (2*S*,4*S*)-**7.6**/(2*R*,4*S*)-**7.6**). Absolute stereochemistry of the isolated diastereomers was confirmed by X-ray crystallographic analysis of (2*S*,4*S*)-**7.6** (**Scheme 7.1**). Subsequent Boc deprotection followed by reaction with 6-chloroimidazo[1,2-*b*]pyridazine-3-carboxylate afforded diastereomerically pure **7.9** which was reacted with methylamine solution to yield amide **7.11**. Although efficient, the synthesis of (2*R*,4*S*)-**7.7** required 8 steps and led to < 20% overall yield from enantiopure pyrrolidinone **7.1** (300\$/g). In comparison, the Ellman sulfinamide route developed in **Chapter 5** for the synthesis of (*R*)-2-(3-fluorophenyl)pyrrolidine ((*R*)-**5.11**) proceeded in 5 steps and > 30% overall yield using commodity chemicals (e.g. methyl 4-chlorobutyrate starting material, 0.81\$/g). In spite of the advantage provided with regard to potency with the C-4 fluorine substitution (*vide infra*), the latter route and the corresponding pyrrolidine are likely to be more attractive if further extensive SAR screening of the amide moiety IPMICF scaffold is required.

In the course of the optimization of the synthesis of **7.9**, we also observed under certain conditions the formation of a derivative distinct from **7.9**, later ascribed as the dehydrofluorination product **7.8**. Expectedly, it was noted that the formation of **7.8** was largely favored and in some instances exclusively obtained in good yields when the reaction was performed > 100°C, or in the presence of > 5 equivalents of KF, or again in the presence of K₂CO₃ instead of KF at high temperatures. Instead of discarding **7.8**, we completed the

synthesis of the amide **7.10** for biological evaluation. In order to complement our brief screening of the 2-phenylpyrrolidine fragment, we synthesized the methylamide **7.17** which lacks the 3-fluorophenyl substitution (**Scheme 7.2**).



Scheme 7.2. Synthesis of non-fluorinated inhibitor **7.17**. Reagents and conditions: (a) 2-Phenylpyrrolidine, KF, DMSO, 110°C, 16 h (94%); (b) MeNH₂, rt, 16 h (62 %).

Compounds **7.10**, **7.11**, **7.17** were then evaluated against TrkB and compared with the monofluorinated derivative **4.12** (**Table 7.1**). We observed the extent of fluorination at the 3-phenyl and the 4-pyrrolidine positions of the phenylpyrrolidine group to have a remarkable influence on TrkB potency. Although compounds **7.17** and **4.12** are racemic derivatives, the knowledge that the *S*-isomer likely exhibits about 1000-fold lower potency compared to the *R*-enantiomer enables suitable comparison of the IC₅₀s values obtained (see **Chapter 5**). In particular, our results show a remarkable gain in terms of potency moving from **7.17** to **4.12** (~10-fold) (**Table 7.1**). Although the (*R*)-2-(3-fluorophenyl)pyrrolidine motif has emerged from patent literature in recent years as a prominent type I Trk inhibitor pharmacophore (see **Chapter 1**),⁷ to the best of our knowledge no systematic explanation has been provided clarifying the reasons of this specific fluoroaryl arrangement. The degree of improvement moving from **7.17** to **4.12** likely indicates the involvement of a specific fluorine-backbone interaction. Based on the inspection of Trk crystallographic data, the origin of this effect appears to be an orthogonal multipolar C-F⋯C=O interaction between the fluorine substituent positioned deep inside the binding pocket with the carbonyl backbone of the TrkB Asn698 residue (or Asn655/685 in TrkA/C). This possibility is further supported by the observation of a corresponding short

distance 3.3 Å C-F...C=O contact in the crystal structure of a (*R*)-2-(3-fluorophenyl)pyrrolidine-bearing inhibitor with TrkA from Novartis – element which was however not emphasized in the corresponding Novartis publication (see PDB: 4YNE).^{5,8}

Table 7.1. SAR and *In Vitro* Enzymatic Activities and Physicochemical Data for Novel Imidazo[1,2-*b*]pyridazines Trk Inhibitors

| Cpd | Structure | IC ₅₀ (nM) ^a | | |
|-------------------------------|-----------|------------------------------------|---------------|---------------|
| | | TrkA | TrkB | TrkC |
| 7.17 | | ^b | 4.20 | ^b |
| (4.12) | | 7.66 | 0.565 | 0.374 |
| 7.10 | | ^b | 0.324 | ^b |
| 7.11 | | ^b | 0.051 | ^b |
| (4.23) | | 5.00 | 0.584 | 0.408 |
| 7.13 | | 1.68 ± 0.13 ^e | 0.048 ± 0.003 | 0.134 ± 0.009 |
| 7.14 | | 4.21 | 0.150 | 0.310 |
| 7.20 (<i>R</i>)-IPMICF17 | | ^b | 0.198 | ^b |

^a[γ-³³P]ATP-based enzymatic assay performed by Reaction Biology. ^bNot measured.

We also observe about 4-5-fold further improvement with the additional fluorination in 7.11 compared to 4.12. An optimized hydrophobic shape complementarity imparted by the slightly larger fluorine substituent compared to hydrogen may explain this effect.⁹ Inhibitor 7.10

which bears a slightly more compact pyrrolidine ring exhibited an IC_{50} of 324 pM for TrkB, falling in the same range as **4.12**. Our screening, even cursory, underscores the importance of fluorine-for-hydrogen replacement in SAR and offers a rational basis to modulate the potency of future radiotracers from the IPMICF series using minimal structural alterations. Consistent with the literature precedents, it may also be expected that those structural changes would in turn favor passive diffusion and limit efflux susceptibility. Pfizer for example has recently provided a robust meta-analysis showing that the strategic substitution of hydrogen with fluorine atoms leads to reduced probability of P-gp efflux and enhanced probability for passive permeability in a 0-to-5 fluorine replacement range.¹⁰ This study also introduces the concept of fluorine-corrected molecular weight (MW_{FC}) as a more relevant descriptor for drug design compared to MW *per se* which is relevant here – providing systematic demonstration that the additional MW imparted by fluorine incorporation is largely balanced by favorable effects regarding other key physico-chemical parameters.

In parallel, to identify an optimized derivative of IPMICF16, we sought to determine to which extent the amide moiety and in some instance, the aryl substituent patterns of the amide groups specifically influenced the P-gp mediated efflux within our IPMICF series. The screening of the amide fragment was chosen for this task in order to maximize our chances to identify a suitable compound given the flexibility of the amide substitution with regard to potency. A complete re-evaluation of the IPMICF series presented in **Chapter 4** was therefore undertaken using P-gp Calcein-AM cellular assay. All tested derivatives from alkyl-, benzyl- and phenylamide scaffolds displayed important interaction with P-gp leading to single digit micromolar EC_{50} s or stronger susceptibilities except for one. Remarkably, the seemingly simple replacement of the 3-fluoro-4-methoxyphenyl moiety found in IPMICF16 for a 4-fluorophenyl fragment led to a drastic abrogation of the efflux liability (*data not presented*, communication with Dr. A. Marhinger). The compound identified, **4.23** (the racemic counterpart of **7.20**, see

Table 7.1 – coined IPMICF17), displayed a cellular $EC_{50} \gg 50 \mu\text{M}$ (the highest concentration tested) for P-gp compared to $1.3 \mu\text{M}$ in the case of (\pm)-IPMIC16. Although the specific reasons for such a drastic shift between such similar compounds cannot be established with certainty, it may relate to factors such as TPSA reduction and rotatable bond (RB) count reduction.¹¹ The unexpected identification of this analog offers a near-ideal scenario to probe the specific role of P-gp regarding brain disposition while it also offers a platform to explore the feasibility of recent radiofluorination techniques, such as the copper-mediated boronic ester approach.¹²⁻¹⁴

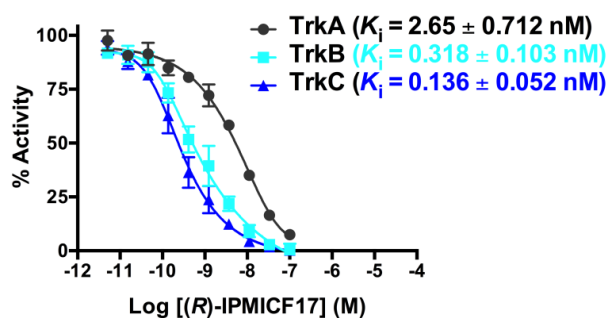
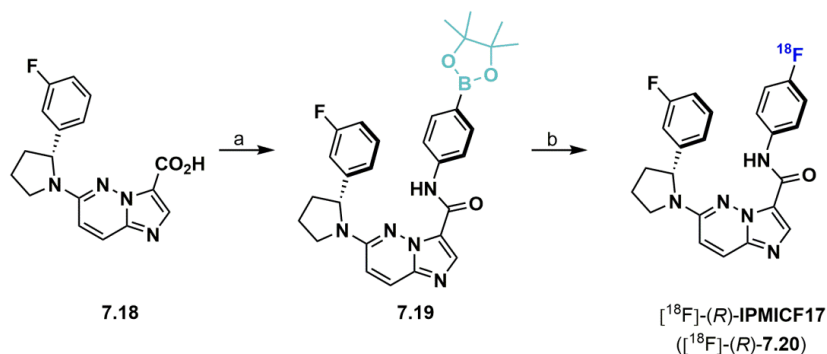


Figure 7.2. Dose-response curve for inhibitor (*R*)-IPMICF17 versus TrkA, TrkB, TrkC, ($[\text{ATP}] = K_{\text{m ATP}}$, $n = 3$, error bars represent standard deviation from the mean). ($[\gamma\text{-}^{33}\text{P}]\text{ATP}$ -based enzymatic assay performed by Reaction Biology). K_i is the inhibitory constant and K_m is Michaelis–Menten constant for ATP.

Having both clarified the pyrrolidine SAR and identified an optimized amide substituent, we next completed the synthesis of the corresponding 4-fluorophenyl-containing inhibitors **7.14** and **7.20**. Inhibitor **7.14** was obtained following the hydrolysis of the ester **7.9** in the presence of LiOH and HATU-mediated coupling using 4-fluoroaniline (61%, 2 steps, **Scheme 7.1**). The enantiopure inhibitor **7.20** was synthesized as described for the corresponding racemic derivative using (*R*)-2-(3-fluorophenyl)pyrrolidine (see **Chapter 4** and **5**). For comparison, the compound **7.13** was also prepared and evaluated. TrkB inhibition assays revealed an IC_{50} of 198 pM for **7.20** and a relatively negligible potency benefit for trifluorinated **7.14** ($IC_{50} = 150 \text{ pM}$ for TrkB). The assay also confirmed the exquisite potency of **7.13** ($IC_{50} = 48 \text{ pM}$ for TrkB). Those results prompted us to select the inhibitor **7.20** for radiotracer translation. Although **7.13**

displayed a marginal potency advantage compared **7.20**, it was abandoned based on its substantiated tendency to undergo dehydrofluorination under ^{18}F -radiolabeling-like conditions (high temperature, basic milieu, polar aprotic solvent). Complete human Trk family kinases profiling and K_i values determination demonstrated excellent TrkB/C affinity in line with (*R*)-IPMICF16 (6-fold difference for TrkB/C; K_i of 2.65 ± 0.72 nM, 0.318 ± 0.103 nM and 0.136 ± 0.052 nM for TrkA, TrkB and TrkC respectively, $n = 3$, s.d.) (**Figure 7.2**).



Scheme 7.3. Synthesis of boronic ester precursor **7.19** and radiosynthesis of $[^{18}\text{F}]$ -(*R*)-IPMICF17. Reagents and conditions: (a) 4-Aminophenylboronic acid pinacol ester, HBTU, DIPEA, DMF, rt, 16 h (75%); (b) Kryptofix-222/ $\text{K}^+/[^{18}\text{F}]\text{F}^-$, MeCN:DMF (1:10), $[\text{Cu}(\text{OTf})_2(\text{pyr})_4]$ (0.27 equiv), 110°C , 20 min (~30% RCY).

In order to prepare $[^{18}\text{F}]$ -(*R*)-**7.20** ($[^{18}\text{F}]$ -(*R*)-IPMICF17), the pinacolborane precursor **7.19** was first synthesized (**Scheme 7.3**). We then undertook the radiosynthesis of $[^{18}\text{F}]$ -(*R*)-IPMICF17 screening conditions initially described by Tredwell and colleagues.¹² Satisfyingly, $[^{18}\text{F}]$ -(*R*)-IPMICF17 could be obtained in 30% RCY (assessed by radio-TLC) using 0.27 equivalent of $[\text{Cu}(\text{OTf})_2(\text{pyr})_4]$. This result offered confidence in feasibility of this approach. It is worth mentioning that the radiolabeling of $[^{18}\text{F}]$ -(*R*)-IPMICF17 using conventional means would have required a three steps sequence from 1,4-dinitrobenzene making this route likely unsuitable for automation and routine production. Differently, we adapted our one-step copper-mediated radiofluorination of **7.19** using a low base protocol¹³⁻¹⁴ which enabled large scale fully automated productions of $[^{18}\text{F}]$ -(*R*)-IPMICF17 (2% RCY, non-decay-corrected at end-of-synthesis based upon 13-16 GBq of $[^{18}\text{F}]\text{F}^-/\text{H}_2\text{O}$, > 99% radiochemical purity, 17 GBq/ μmol).

Our novel low-Pgp efflux TrkB/C radiotracer is currently undergoing extensive preclinical PET imaging in non-human primate (Prof. P. Scott group, University of Michigan) and autoradiography assessment in human tissue (Montreal Neurological Institute, by myself in collaboration with Prof. P. Rosa-Neto). Assuming comparable or improved preclinical profile for [^{18}F]-(*R*)-IPMICF17 compared to [^{11}C]-(*R*)-IPMICF16, first-in-human should be expected in the course of the current year. Below, we described further potential modifications of the radiotracers series described in this thesis as well as future work regarding tracer design and validation.

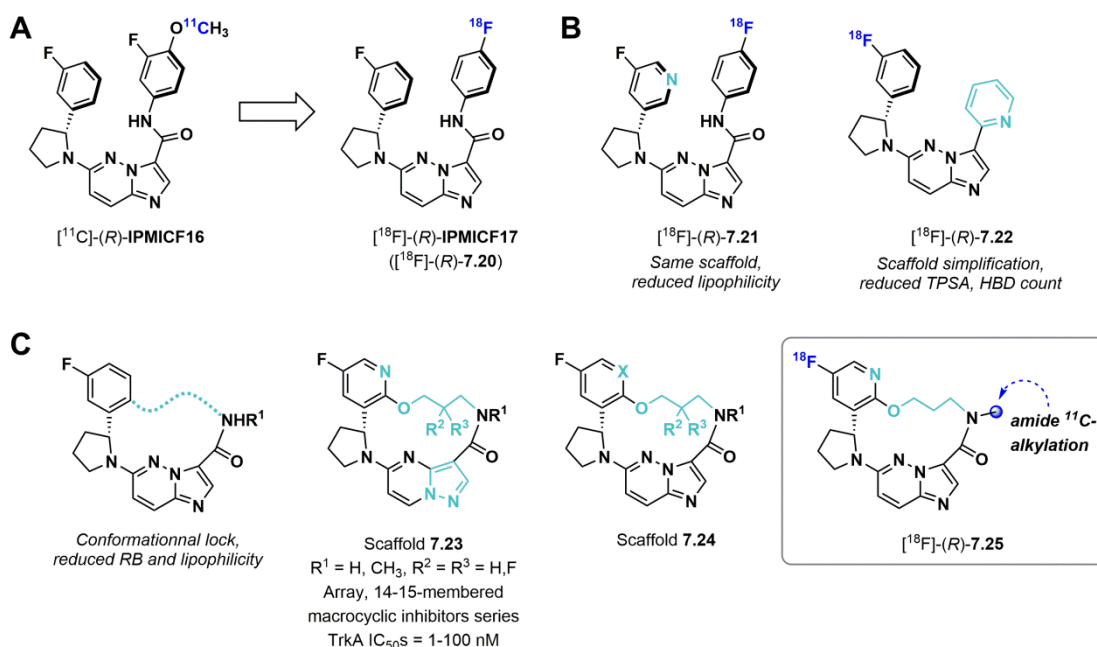


Figure 7.3. Structural optimization of the IPMICF series. (A) First and second-generation IPMICF radiotracers. (B) Putative structural modification for optimization. (C) Macrocyclic IPMICF radiotracers and scaffolds.

7.1.2 Proposed SAR for optimizing brain penetration of the IPMICF series. Apart from the ongoing work with the development and validation of [^{18}F]-(*R*)-IPMICF17, we can envision various scenarios leading to further optimized third-generation IPMICF tracers. In order to probe the influence of lipophilicity on specific binding and P-gp recognition, one interesting avenue

may be to explore variations in nitrogen-based hinge binder bicyclic heterocycles or the incorporation of a fluoropyridine replacement as found in [^{18}F]-(*R*)-**7.21** (**Figure 7.3B**).⁷ Until now, our work has focussed exclusively on imidazo[1,2-*b*]pyridazine-3-amide derivatives. The study of derivatives lacking the amide group in order to reduced hydrogen bond donor (HBD) count could turn out favorable regarding membrane passive permeability (**Figure 7.3B**).^{7-8, 15} Alternatively, further balance of brain penetration, efflux and potency may be achievable via macrocyclization using low nanomolar potency scaffolds recently patented by Array as a starting point (**Figure 7.3C**).^{11, 16-17} Modeling simulations of representative 14-membered macrocyclic derivatives suggest excellent overlap, consistent with a strong reinforcement of the bioactive binding conformation from nonmacrocyclic derivatives (**Figure 7.4**). A similar brain permeation-driven macrocyclization strategy has been used in the development of the dual ALK/ROS1 inhibitor lorlatinib from the linear and brain-restricted crizotinib.¹⁸⁻¹⁹

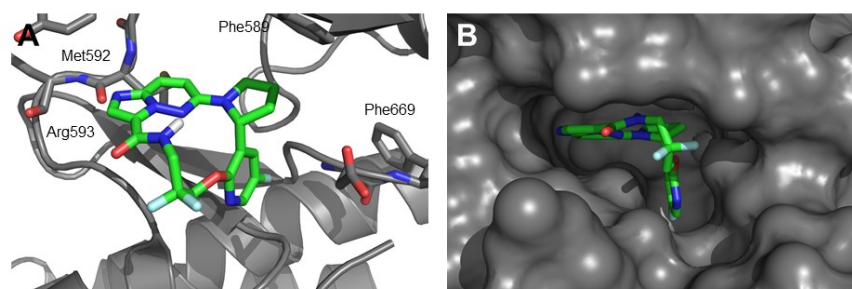


Figure 7.4. Predicted binding poses for representative macrocyclic Trk inhibitor lead bound to TrkA in DFG-in conformation (PDB 4PMT). (A) Docking of the inhibitor to the ATP binding site of TrkA (the glycine rich loop was removed for simplicity). (B) Surface model of the inhibitor docked to TrkA (PDB 4PMT).

7.1.3 Progress in the GW2580 series. Beyond the IPMICF series, we described in **Chapter 2** our efforts in the development of a 2,4-diaminopyrimidine-based dual CSF-1R/Trk-targeted radiotracers. We showed that the lead tracer from this screening could be obtained following a multi-step radiochemical synthesis starting from 4-formyl-*N,N,N*-trimethylanilinium triflate (**7.26**, **Figure 7.5**). This approach was highly challenging from a practical standpoint which prevented routine production and preclinical evaluation of the tracer. The recent development in our group

of a two-step one-pot sequence, starting from the pinacolborane tetra-Boc-protected precursor **7.28** using the copper-mediated radiofluorination approach in lieu of our previous four-step sequence, is expected to enable the complete preclinical validation of [^{18}F]**7.27** in the near future (work undertaken by Damion Choi and myself). Depending on the *in vivo* profile of [^{18}F]**7.27** in rodent and non-human primate, further derivatizations or applications, especially for tumor imaging, may be envisioned (*vide infra*).

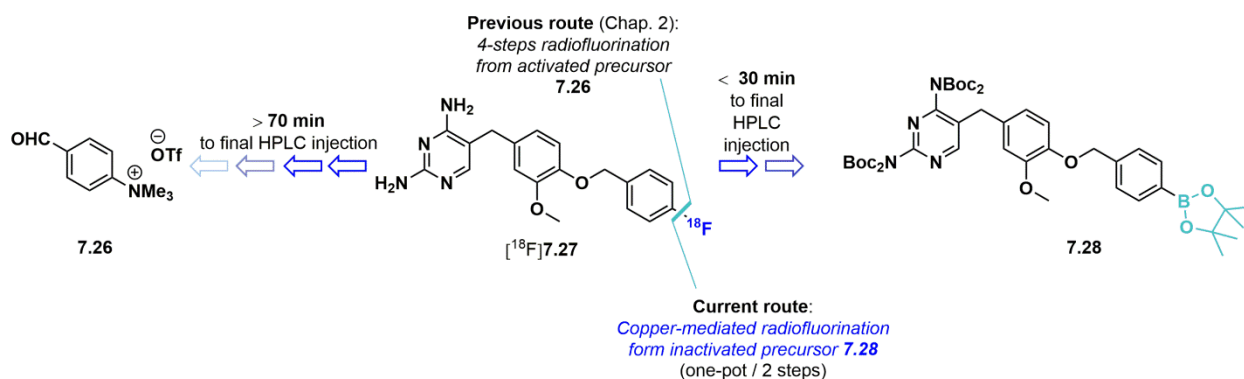


Figure 7.5. Novel radiosynthesis of [^{18}F]**7.27**.

7.1.4 Proposed work to improve the GW441756 series. We identified [^{11}C]GW441756 as the first brain penetrant pan-Trk radiotracer and showed that representative tracers from this series enabled selective imaging of TrkB/C in rodent brains and human neuroblastoma tumors.²⁰ Non-human primate PET imaging demonstrated extensive brain penetration but ambiguous pharmacokinetics with respect to specific binding *in vivo* (**Chapter 5**). The main drawback of [^{11}C]GW441756 remains its propensity to undergo rapid photoisomerization as described in details in **Chapter 3 (Figure 7.6A)**. It is unclear how the non-specific binding from the inactive (*E*)-isomer influences the PET imaging results. Achieving a non-isomerizable conformationally restricted [^{11}C]GW441756 analog should be the primary focus of a second-generation investigation based on this scaffold. For example, this could be achieved through the synthesis of a fused tricyclic oxindole core or by the incorporation of indazole moiety to disrupt the

isomerization process (**Figure 7.6B**). An interesting alternative to achieve this goal could be the synthesis of a cyclopropane-linked spiro radiotracer such as [^{11}C]7.32. A similar strategy has recently been successfully exploited in the discovery and optimization of an orally active anticancer polo-like kinase 4 (PLK4) inhibitors (**Figure 7.6C**).²¹⁻²³ Docking studies support the view that the 1*S*,2*R* enantiomer should provide effective binding to Trk (**Figure 7.7**).

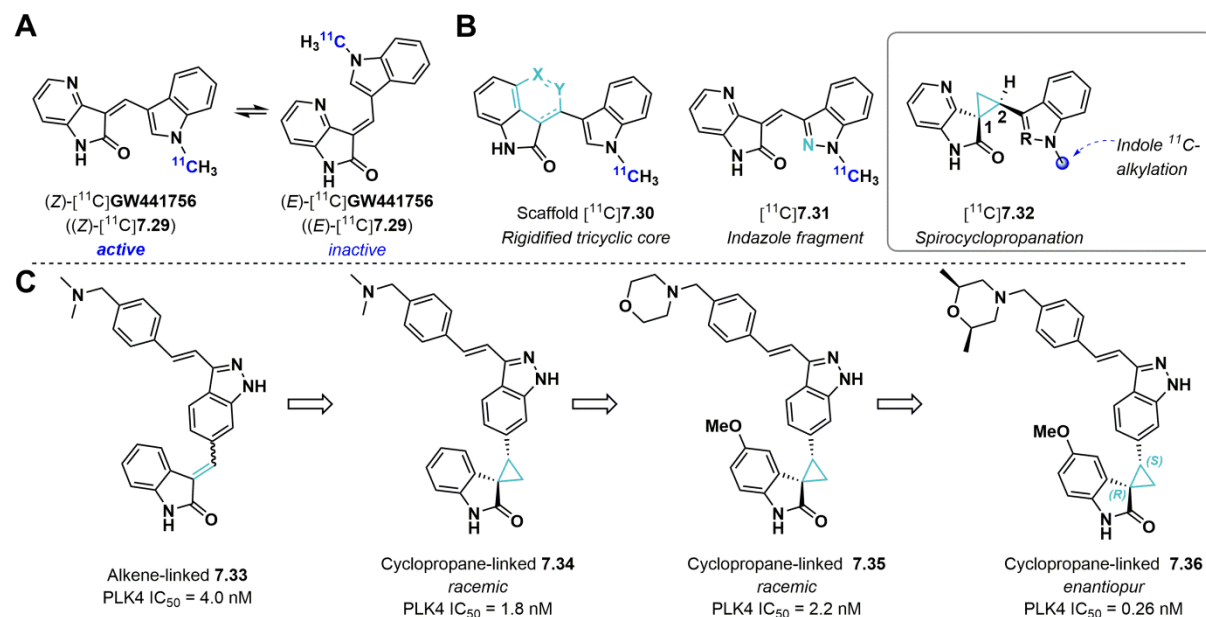


Figure 7.6. Conformational stabilisation via bioisosteric modifications of GW441756. (A) Photoisomerization of [^{11}C]GW441756. (B) Potential structural modification to address the photoisomerization liability. (C) Representative SAR examples from PLK4 cyclopropane-linked inhibitors series.

7.1.5 Proposed work with other scaffolds. Outside of the series already explored in this thesis, inhibitors from other Trk inhibitor chemical classes should be explored as PET tracers. For example, to accelerate the development of new Trk radiotracers, we have obtained recently gram amounts of PF-06273340 and miliclib from Pfizer and Nerviano respectively (**Chapter 1**, compounds **1.35** and **1.44**) in order to prepare a ^{18}F -fluorodeoxy derivative of PF-06273340 and [^{11}C]miliclib (isotopologue). Other scaffolds, especially recent JM domain-interacting allosteric TrkA-selective inhibitors should also be pursued as radiotracers.

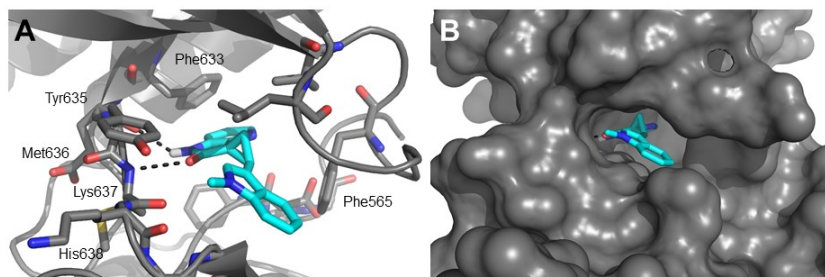


Figure 7.7. Predicted binding poses for compound **7.32** bound to TrkA in DFG-in conformation (PDB 4AT3). (A) Docking of the inhibitor to the ATP binding site of TrkA. (B) Surface model of the inhibitor docked to TrkA.

7.1.6 Current and proposed *in vitro/in vivo* experiments. In term of *in vivo* imaging experiments, one of the principal limitations relative to providing the most extensive evidence of specific binding in the study of our most advance leads has been the impossibility to perform preblock or chase studies in non-human primates. At the current stage, those experimental restrictions are largely due to the lack of approved Trk inhibitors (ideally also BBB permeable) or other suitable tool inhibitors with prominent Trk activity and established safety profile. Further PET experiments should focus on screening compounds suitable for competition experiments *in vivo* in rodent and, depending on ethics considerations, in primate preferably. The use of a non-P-gp substrate radiotracer such as [^{18}F]-(*R*)-IPMIF17 should accelerate screening of clinically relevant Trk inhibitors and allow extensive CNS target engagement studies. In addition, future *in vivo* work should assess the efficacy of the Trk tracer library described here for peripheral tumor imaging in mice. For this purpose, we have recently acquired TrkA-dependant KM12 cells to be used in xenograft tumor model imaging experiments.^{8, 24-25} While the lack of viable TrkA/B/C null mice has prevented the assessment of radiotracer target binding in rodent under micro-dosing conditions, alternative approaches to assess specific brain uptake and biodistribution of Trk tracers in animals, which display variable Trk expression, are currently under consideration. Two of the most relevant experimental paradigms in this context involve the use of a heterozygous TrkB knockout (TrkB^{+/-})²⁶ mice model or MeCP2-deficient mice which have been

shown to display increased TrkB expression (2.5-fold increase compared to wild-type).²⁷ With full length TrkB known to undergo important expression changes from early postnatal days to old age in mammals, the conduct of longitudinal studies in mice, or ideally rats to enable regional brain uptake analysis, should offer an interesting and simple alternative to genetically engineered mice model.²⁸⁻³⁰ The use of a tritiated IPMICF tracer, in all logic [*methyl*-³H₃]-(*R*)-IPMICF16, should facilitate detailed comprehensive *in vitro* screening of pre-characterized human tumor samples and *post mortem* brain tissue from specific diseases to explore the application landscape of Trk radiotracers beyond neuroblastoma and Alzheimer disease (AD) and define key parameters such as tissue B_{\max} in various therapeutically relevant context. Finally, the completion of the first-in-human with [¹¹C]-(*R*)-IPMICF16 should facilitate further use in human. In particular, brain imaging studies in AD patients or tumor imaging studies with cancer patients enrolled in anti-Trk clinical trials should be pursued.

7.2 Conclusion and significance

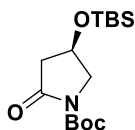
Changes in expression and dysfunctional signaling of TrkA/B/C receptors are found in multiple neurological diseases and cancers. As a consequence, drug-like small molecules which modulate Trk activity, especially pan-Trk tyrosine kinase inhibitors (TKI) and neurotrophin mimics, are being heavily pursued as novel therapeutics. However, the specific understanding of spatiotemporal changes in TrkA/B/C expression and distribution, which occur in healthy and disease conditions, has been falling behind those recent and rapid clinical progresses due to the lack of approach to assess Trk status non-invasively in living subjects. In this context, the present thesis describes the rationale design and discovery of a first-in-class library of Trk-targeted TKI PET radiotracers and their use in the context of oncological and neurological research. We demonstrate that structurally diverse Trk radiotracers with exceptional levels of kinome selectivity, both from type I and type II inhibitor classes can be obtained following diverse radiochemical approaches. It is shown that the tracers developed can in some

instances be used to selectively annotate TrkB expression in clinically relevant poor prognosis human neuroblastoma samples or define the spatial distribution of Trk receptors in the mammalian brain from mice to human. By utilizing rigorous multiparameter optimization, we furthermore illustrate that radiolabeled Trk TKIs can be tailored to yield brain penetrant probes which display suitable *in vivo* imaging properties for clinical translation. Stemmed from multi-species analyses, our findings delineate the first lead for TrkB/C imaging in human but concurrently constitute, to the best of our knowledge, the first demonstration that CNS kinase targets can be tackled *in vivo* non-invasively using PET in general. While none of the currently used neuroimaging clinical PET tracers target proteins from the human kinome – despite the central relevance of kinases both in terms of fundamental biology, drug development and medical research – the work presented here provides a strong indication that CNS kinase PET imaging in human is achievable. Importantly, this approach may be generalizable to the development of novel diagnostic tools aimed at distinct kinase targets relevant to neurodegenerative diseases and neurooncologic malignancies outside Trk. Notably, the carbon-12 isotopologue of the most advanced radiotracer described here, (*R*)-IPMICF16, stands as both the most potent and most selective TrkB/C inhibitor characterized to date. A further immediate corollary from the development of a Trk radiotracer for CNS imaging based on a TKI scaffold, which is of relevance for anti-neoplastic targeted drug design, is the possibility to use such a probe to define the brain disposition of relevant anti-cancer Trk pharmacological inhibitors. A demonstration of this application is provided with pretreatment imaging experiments in mice using the phase II inhibitor entrectinib. Additionally, we offer a unique demonstration of the potential of Trk radiotracers for receptor quantification and visualization in AD providing the groundwork for further clinical evaluation. Overall, the work delineated here describes a novel class of radiopharmaceuticals with applications at the interface of oncological diagnostic imaging, drug development and neuroimaging.

7.3 Material and methods

General. All moisture sensitive reactions were carried out in oven-dried flasks under nitrogen atmosphere with dry solvents. Reagents and solvents were purchased at the highest commercial quality from Fisher, Sigma-Aldrich, Alfa-Aesar, Synthonix or Oakwood Products and were used without further purification unless specified otherwise. Organic solutions were concentrated under reduced pressure on a Heidolph rotary evaporator. In general, reactions were magnetically stirred and monitored by TLC performed on pre-coated glass-backed TLC plates (Analtech, 250 microns) and chromatographic purification of products was accomplished using flash chromatography on Alfa-Aesar silica gel (230-450 mesh). TLC visualization was performed by fluorescence quenching, KMnO_4 or ninhydrin. ^1H NMR and ^{13}C NMR spectra were recorded on a Agilent/Varian DD2 MR two channel 400 MHz spectrometer, a Agilent/Varian VNMRS two-channel 500 MHz spectrometer or a Agilent/Varian Inova four-channel 500 MHz spectrometer or 700 MHz Four-Channel dual receiver VNMRS & ProTune in CDCl_3 or d_6 -DMSO and peak positions are given in parts per million using TMS as internal standard. Peaks are reported as: s = singlet, d = doublet, t = triplet, q = quartet, p = quintet, m = multiplet, b = broad; coupling constant(s) in Hz; integration. High Resolution Mass Spectra (HRMS) analysis was obtained from the Mass Spectrometry Facility of the Chemistry Department of the University of Alberta (Agilent Technologies 6220 oaTOF) or from the Regional Center for Mass Spectrometry of The Chemistry Department of the Université de Montréal (LC-MSD-TOF Agilent). Compounds tested for biological evaluation were >95% pure (HPLC/MS). Crystallographic analysis was performed by the X-Ray Diffraction Laboratory of the department of chemistry of the University of Alberta. Compound (*R*)-**7.20** was synthesized as for the racemate (see **Chapter 4**). NMR spectrum and crystallographic data analysis can be found in **Annex 6**.

Chemical Synthesis

tert-Butyl (R)-4-((tert-butyldimethylsilyl)oxy)-2-oxopyrrolidine-1-carboxylate (7.2):

This compound was synthesized from (R)-(+)-4-hydroxy-2-pyrrolidinone according to Albaugh *et al.*⁶ (83%, 2 steps).

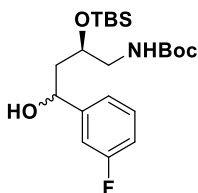
Physical State: white solid.

R_f: 0.85 (EtOAc, KMnO₄).

HRMS (ESI⁺): *m/z* calc. for C₁₅H₂₉NO₄Si (M + H)⁺: 315.1866, found 315.1861.

¹H NMR (400 MHz, CHLOROFORM-*d*) δ = 4.38 (dt, *J* = 3.2, 6.0 Hz, 1H), 3.86 (dd, *J* = 5.6, 11.4 Hz, 1H), 3.61 (ddd, *J* = 0.8, 2.9, 11.4 Hz, 1H), 2.70 (dd, *J* = 6.3, 17.3 Hz, 1H), 2.45 (ddd, *J* = 0.8, 3.5, 17.3 Hz, 1H), 1.53 (s, 9H), 0.87 (s, 9H).

¹³C NMR (101 MHz, CHLOROFORM-*d*) δ = 172.00, 150.04, 82.96, 63.86, 55.41, 43.14, 28.02, 25.65, 17.95, -4.81, -4.88.

tert-Butyl ((2R)-2-((tert-butyldimethylsilyl)oxy)-4-(3-fluorophenyl)-4-hydroxybutyl)carbamate (7.3):

This compound was synthesized from (tert-butyl (R)-4-((tert-butyldimethylsilyl)oxy)-2-oxopyrrolidine-1-carboxylate according to Albaugh *et al.*⁶ (59%, 2 steps).

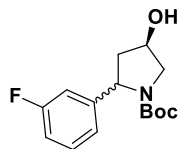
Physical State: colorless oil.

R_f: 0.40 (4:1 hexanes/EtOAc, UV light)

HRMS (ESI⁺): *m/z* calc. for C₂₁H₃₇FNO₄Si (M + H)⁺: 414.247, found 414.2467.

¹H NMR (498 MHz, CHLOROFORM-*d*) δ = 7.32 - 7.26 (m, 1H), 7.13 - 7.07 (m, 2H), 6.98 - 6.90 (m, 1H), 4.94 - 4.86 (m, 1H), 4.08 (td, *J* = 5.1, 10.3 Hz, 1H), 3.46 - 3.26 (m, 2H), 3.25 - 3.16 (m, 1H), 1.89 - 1.80 (m, 2H), 1.45 (s, 9H), 0.96 - 0.91 (m, 9H), 0.16 - 0.08 (m, 6H).

¹³C NMR (125 MHz, CHLOROFORM-*d*) δ = 162.97 (d, J = 245.7 Hz, 1C), 156.30 (br s, 1C, diastereomer 1), 156.21 (br s, 1C, diastereomer 2), 147.77 (br s, 1C, diastereomer 1), 147.72 (br s, 1C, diastereomer 2), 129.85 (br s, 1C, diastereomer 1), 129.78 (br s, 1C, diastereomer 2), 121.13 (br s, 1C, diastereomer 1), 121.11 (diastereomer 2), 114.09 (br s, 1C, diastereomer 1), 113.92 (br s, 1C, diastereomer 2), 112.65 (diastereomer 1), 112.47 (diastereomer 2), 79.54 (br s, 1C), 71.04 (br s, 1C, diastereomer 1), 70.44 (br s, 1C, diastereomer 2), 70.14 (diastereomer 1), 70.00 (br s, 1C, diastereomer 2), 45.91 (br s, 1C, diastereomer 1), 45.58 (br s, 1C, diastereomer 2), 43.44 (diastereomer 1), 43.34 (diastereomer 2), 28.38, 25.81, 18.02 (diastereomer 1), 17.98 (diastereomer 2), -4.50 (diastereomer 1), -4.73 (diastereomer 2). (In some instance, relevant fluorine-carbon coupling could not be distinguished from diastereomer mixtures. Diastereomer signals were arbitrarily assigned).



tert-Butyl (*R*)-2-(3-fluorophenyl)-4-hydroxypyrrolidine-1-carboxylate (**7.5**):

This compound was synthesized from *tert*-butyl ((2*R*)-2-((*tert*-butyldimethylsilyl)oxy)-4-(3-fluorophenyl)-4-hydroxybutyl)carbamate according to Albaugh *et al.*⁶ (51%, 2 steps).

Physical State: white solid.

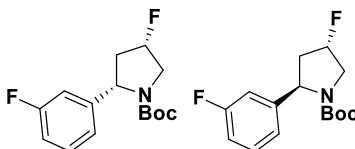
R_f: 0.20, 0.25 (1:1 hexanes/EtOAc, UV light)

HRMS (ESI⁺): m/z calc. for C₁₅H₂₀FNNaO₃ (M + Na)⁺: 304.1319, found 304.1314.

¹H NMR (400 MHz, CHLOROFORM-*d*) δ = 7.30 - 7.22 (m, 1H), 7.10 - 6.84 (m, 1H), 5.02 - 4.91 (m, 0.5H), 4.88 (br s, 1H), 4.52 - 4.43 (m, 1H), 3.88 (dd, J = 5.8, 11.6 Hz, 1H), 3.73 (br d, J = 2.6 Hz, 1H), 3.55 (dd, J = 3.7, 11.9 Hz, 1H), 2.61 (ddd, J = 5.6, 8.6, 13.8 Hz, 1H), 2.44 - 2.33 (m, 0.5H), 2.03 - 1.93 (m, 1H), 1.54 - 1.19 (m, 9H).

¹³C NMR (101 MHz, CHLOROFORM-*d*) δ = 163.27 (br d, J = 245.1 Hz, 1C), 154.91 - 154.43 (m, 1C), 147.42 (br s, 1C), 130.11 - 129.63 (m, 1C), 121.47 - 121.10 (m, 1C), 113.61 (br d, J = 21.4 Hz, 1C), 113.16 - 112.20 (m, 1C), 80.00 (br s, 1C, diastereomer 1), 79.92 (br s, 1C, diastereomer 2), 70.65 (br s, 1C, diastereomer 1), 69.93 (br s, 1C, diastereomer 2), 60.00 (br s, 1C), 55.91 (br s, 1C, diastereomer 1), 55.55 (br s, 1C, diastereomer 2), 44.95 (br s, 1C, diastereomer 1), 43.90 (br s, 1C, diastereomer 2), 28.36 (br s, 1C). (In some instance, relevant

fluorine-carbon coupling could not be distinguished from diastereomer mixtures. Diastereomer signals were arbitrarily assigned).



tert-Butyl (2*S*,4*S*)-4-fluoro-2-(3-fluorophenyl)pyrrolidine-1-carboxylate (2*S*,4*S*-7.6) and *tert*-butyl (2*R*,4*S*)-4-fluoro-2-(3-fluorophenyl)pyrrolidine-1-carboxylate (2*R*,4*S*-7.6):

Those compounds were synthesized from *tert*-butyl (*R*)-2-(3-fluorophenyl)-4-hydroxypyrrolidine-1-carboxylate according to Albaugh *et al.*⁶ (78% overall, 26:74 2*S*,4*S*-7.6/2*R*,4*S*-7.6). Compound (2*S*,4*S*-7.6) was recrystallized from hexanes/EtOAc.

Physical State: white solids.

R_f: 0.56 (2*S*,4*S*-7.6), 0.72 (2*R*,4*S*-7.6) (1:1 hexanes/EtOAc, UV light)

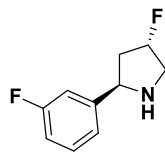
HRMS (ESI+): *m/z* calc. for C₁₅H₁₉F₂NNaO₂ (M + Na)⁺: 306.1276, found 306.1277.

¹H NMR (2*S*,4*S*-7.6) (400 MHz, CHLOROFORM-*d*) δ = 7.24 (dt, *J* = 5.9, 7.9 Hz, 1H), 7.02 (d, *J* = 7.8 Hz, 1H), 6.96 (td, *J* = 2.1, 10.1 Hz, 1H), 6.92 - 6.85 (m, 1H), 5.22 (tt, *J* = 1.5, 4.7, 53.6 Hz, 1H), 4.97 (br d, *J* = 8.8 Hz, 1H), 3.92 (dd, *J* = 13.3, 24.6 Hz, 1H), 3.80 (ddd, *J* = 4.5, 13.3, 32.1 Hz, 1H), 2.56 (dddd, *J* = 4.8, 9.7, 14.6, 37.8 Hz, 1H), 2.28 (qdd, *J* = 1.9, 14.6, 20.0 Hz, 1H), 1.52 - 1.13 (m, 9H).

¹³C NMR (2*S*,4*S*-7.6) (101 MHz, CHLOROFORM-*d*) δ = 163.17 (br d, *J* = 245.5 Hz, 1C), 154.26 (br s, 1C), 146.62 (br s, 1C), 129.73 (br d, *J* = 8.0 Hz, 1C), 121.54 (br s, 1C), 113.64 (br d, *J* = 21.2 Hz, 1C), 112.99 (br d, *J* = 22.2 Hz, 1C), 92.20 (br d, *J* = 182.0 Hz, 1C), 80.24, 59.88 (br s, 1C), 54.08 (br d, *J* = 24.1 Hz, 1C), 41.11 (br d, *J* = 20.2 Hz, 1C), 28.35 (br s, 1C).

¹H NMR (2*R*,4*S*-7.6) (400 MHz, CHLOROFORM-*d*) δ = 7.30 - 7.22 (m, 1H), 6.97 (d, *J* = 7.3 Hz, 3H), 5.18 (td, *J* = 3.4, 52.6 Hz, 1H), 4.99 - 4.85 (m, 1H), 4.06 (dd, *J* = 14.1, 23.2 Hz, 1H), 3.69 (ddd, *J* = 3.3, 13.4, 36.6 Hz, 1H), 2.73 - 2.60 (m, 1H), 1.96 (dddd, *J* = 4.0, 9.5, 13.7, 39.6 Hz, 1H), 1.58 - 0.94 (m, 9H).

¹³C NMR (2*R*,4*S*-7.6) (101 MHz, CHLOROFORM-*d*) δ = 163.30 (br d, *J* = 246.0 Hz, 1C), 154.54, 146.93 (br s, 1C), 130.09 (br d, *J* = 8.2 Hz, 1C), 121.21 (br s, 1C), 113.87 (br d, *J* = 21.4 Hz, 1C), 112.52 (br d, *J* = 21.8 Hz, 1C), 91.32 (br d, *J* = 178.3 Hz, 1C), 80.17, 59.78 (br s, 1C), 54.15 (br d, *J* = 23.0 Hz, 1C), 43.29 (br d, *J* = 16.7 Hz, 1C), 28.25 (br s, 1C).

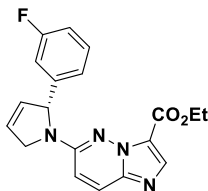


(2R,4S)-4-Fluoro-2-(3-fluorophenyl)pyrrolidine (7.7):

This compound was synthesized from *tert*-butyl (2R,4S)-4-fluoro-2-(3-fluorophenyl)pyrrolidine-1-carboxylate according to Albaugh *et al.*⁶ (93%, crude).

Physical State: pale orange oil.

R_f: baseline (1:1 hexanes/EtOAc, UV light)



Ethyl (R)-6-(2-(3-fluorophenyl)-2,5-dihydro-1H-pyrrol-1-yl)imidazo[1,2-b]pyridazine-3-carboxylate (7.8):

To a solution of ethyl 6-chloroimidazo[1,2-*b*]pyridazine-3-carboxylate (226 mg, 1.0 mmol) in DMSO (5.0 mL) was added KF (581 mg, 10 mmol). This reaction mixture was heated at 100°C and (2R,4S)-4-fluoro-2-(3-fluorophenyl)pyrrolidine (220 mg, 1.2 mmol) was added. After stirring the reaction mixture at 120°C for 12 h, the heterogeneous mixture was cooled at room temperature, poured into water and extracted with EtOAc (3 X 50 mL). The combined organic layers were washed with brine, dried over Na₂SO₄ and concentrated in *vacuo*. The crude residue was purified by flash chromatography (30→0% hexane in ethyl acetate) to afford 246 mg of the title compound (70%).

Physical State: pale yellow oil.

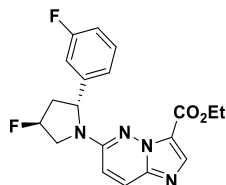
R_f: 0.32 (10:1 89 MeOH/Et₃N/CH₂Cl₂, UV light).

HRMS (ESI⁺): *m/z* calc. for C₁₉H₁₈FN₂O₂ (M + H)⁺: 353.1408, found 353.1401.

¹H NMR (400 MHz, CHLOROFORM-*d*) δ = 8.11 (s, 1H), 7.63 (d, *J* = 9.8 Hz, 1H), 7.33 - 7.22 (m, 1H), 7.16 (br d, *J* = 7.7 Hz, 1H), 7.08 (br d, *J* = 9.5 Hz, 1H), 6.93 (dt, *J* = 2.0, 8.3 Hz, 1H), 6.54

(d, $J = 9.8$ Hz, 1H), 6.08 - 6.02 (m, 1H), 5.92 - 5.83 (m, 1H), 5.68 (br s, 1H), 4.69 - 4.53 (m, 2H), 4.41 (q, $J = 7.1$ Hz, 2H), 1.41 (t, $J = 7.1$ Hz, 3H).

^{13}C NMR (101 MHz, CHLOROFORM-*d*) $\delta = 163.14$ (d, $J = 246.9$ Hz, 1C), 159.10, 152.25, 143.68 (d, $J = 6.2$ Hz, 1C), 138.85, 138.91 - 138.80 (m, 1C), 130.89, 130.37 (br s, 1C), 126.00 (br s, 1C), 125.04 (br s, 1C), 122.39 (br d, $J = 3.7$ Hz, 1C), 119.57, 114.80 (d, $J = 21.1$ Hz, 1C), 113.76, 111.36 (br s, 1C), 68.52 (br s, 1C), 60.29, 55.37, 14.46.



Ethyl 6-((2R,4S)-4-fluoro-2-(3-fluorophenyl)pyrrolidin-1-yl)imidazo[1,2-b]pyridazine-3-carboxylate (7.9):

To a solution of ethyl 6-chloroimidazo[1,2-*b*]pyridazine-3-carboxylate (226 mg, 1.0 mmol) in DMSO (5.0 mL) was added KF (291 mg, 5 mmol). This reaction mixture was heated at 100°C and (2R,4S)-4-fluoro-2-(3-fluorophenyl)pyrrolidine (315 mg, 1.7 mmol) was added. After stirring the reaction mixture at this temperature for 12 h, the heterogeneous mixture was cooled at room temperature, poured into water and extracted with EtOAc (3 X 50 mL). The combined organic layers were washed with brine, dried over Na₂SO₄ and concentrated in *vacuo*. The crude residue was purified by flash chromatography (30→0% hexane in ethyl acetate) to afford 174 mg of the title compound (47%).

Physical State: pale yellow oil.

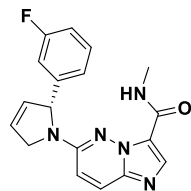
R_f: 0.10 (EtOAc, UV light)

HRMS (ESI+): *m/z* calc. for C₁₉H₁₉F₂N₄O₂ (M + H)⁺: 373.1471, found 373.1465.

^1H NMR (498 MHz, CHLOROFORM-*d*) $\delta = 8.17$ (s, 1H), 7.68 (d, $J = 9.9$ Hz, 1H), 7.34 (dt, $J = 5.8, 8.0$ Hz, 1H), 7.11 (d, $J = 7.8$ Hz, 1H), 7.05 - 6.97 (m, 1H), 6.53 (d, $J = 9.9$ Hz, 1H), 5.50 - 5.33 (m, 1H), 5.15 (dd, $J = 7.2, 9.0$ Hz, 1H), 4.55 - 4.47 (m, 1H), 4.44 (q, $J = 7.1$ Hz, 2H), 4.12 (ddd, $J = 3.2, 13.5, 37.1$ Hz, 1H), 2.97 - 2.87 (m, 1H), 2.26 - 2.10 (m, 1H), 1.44 (t, $J = 7.1$ Hz, 3H).

^{13}C NMR (126 MHz, CHLOROFORM-*d*) $\delta = 163.43$ (d, $J = 247.7$ Hz, 1C), 158.96, 153.27, 144.93 (d, $J = 6.4$ Hz, 1C), 131.09 (br s, 1C), 131.03, 125.63, 124.87, 121.27 (br d, $J = 2.8$ Hz,

1C), 119.68, 115.00 (br d, $J = 21.4$ Hz, 1C), 112.72 (br d, $J = 22.2$ Hz, 1C), 111.93, 91.17 (br d, $J = 177.8$ Hz, 1C), 60.89, 60.53, 56.06 - 55.73 (m, 1C), 44.04 (d, $J = 21.4$ Hz, 1C), 14.50.



(R)-6-(2-(3-Fluorophenyl)-2,5-dihydro-1H-pyrrol-1-yl)-N-methylimidazo[1,2-*b*]pyridazine-3-carboxamide (7.10):

Ethyl (R)-6-(2-(3-fluorophenyl)-2,5-dihydro-1H-pyrrol-1-yl)imidazo[1,2-*b*]pyridazine-3-carboxylate (20 mg, 0.06 mmol) was dissolved in a methylamine solution (33 wt. % in absolute ethanol, 2 mL). The reaction mixture was stirred at room temperature for 16 h then concentrated and dried in *vacuo*. The crude product was purified by flash column chromatography (5→10% methanol in dichloromethane) to afford 18 mg of the title compound (90%).

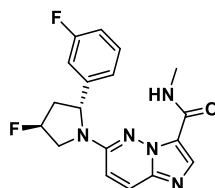
Physical State: white solid.

R_f: 0.30 (1:9 MeOH/CH₂Cl₂, UV light).

HRMS (ESI+): m/z calc. for C₁₈H₁₇FN₅O (M + H)⁺: 338.1412, found 338.1415.

¹H NMR (498 MHz, CHLOROFORM-*d*) $\delta = 8.27 - 7.99$ (m, 2H), 7.82 (br d, $J = 9.8$ Hz, 1H), 7.36 (dt, $J = 5.8, 7.8$ Hz, 1H), 7.09 (d, $J = 7.7$ Hz, 1H), 7.02 - 6.95 (m, 2H), 6.69 (br d, $J = 8.9$ Hz, 1H), 6.09 - 6.02 (m, 1H), 5.98 - 5.92 (m, 1H), 5.72 (br d, $J = 2.7$ Hz, 1H), 4.71 - 4.62 (m, 1H), 4.59 - 4.50 (m, 1H), 2.95 (br d, $J = 3.8$ Hz, 3H).

¹³C NMR (125 MHz, CHLOROFORM-*d*) $\delta = 163.38$ (br d, $J = 248.0$ Hz, 1C), 159.75, 151.28, 143.48 (br d, $J = 6.2$ Hz, 1C), 137.04, 131.68, 130.92 (d, $J = 8.3$ Hz, 1C), 127.32, 126.58, 123.92, 122.71, 121.06 (br s, 1C), 114.99 (br d, $J = 20.9$ Hz, 1C), 112.54 (br d, $J = 21.9$ Hz, 1C), 110.05, 68.95, 55.59, 25.67.



6-((2R,4S)-4-Fluoro-2-(3-fluorophenyl)pyrrolidin-1-yl)-N-methylimidazo[1,2-b]pyridazine-3-carboxamide (7.11):

Ethyl 6-((2R,4S)-4-fluoro-2-(3-fluorophenyl)pyrrolidin-1-yl)imidazo[1,2-b]pyridazine-3-carboxylate (225 mg, 0.60 mmol) was dissolved in a methylamine solution (33 wt. % in absolute ethanol, 7 mL). The reaction mixture was stirred at room temperature for 2 h then concentrated and dried in *vacuo*. The crude product was purified by flash column chromatography (5→10% methanol in dichloromethane) to afford 62 mg of the title compound (29%).

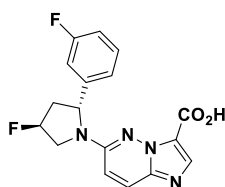
Physical State: white solid.

R_f: 0.50 (1:9 MeOH/CH₂Cl₂, UV light).

HRMS (ESI+): *m/z* calc. for C₁₈H₁₈F₂N₅O (M + H)⁺: 358.1474, found 358.1475.

¹H NMR (498 MHz, CHLOROFORM-*d*) δ = 8.22 (s, 1H), 8.00 - 7.89 (m, 1H), 7.81 (d, *J* = 9.9 Hz, 1H), 7.37 (dt, *J* = 5.8, 7.9 Hz, 1H), 7.08 (d, *J* = 7.7 Hz, 1H), 7.04 - 6.95 (m, 2H), 6.69 (d, *J* = 9.9 Hz, 1H), 5.44 (td, *J* = 2.4, 52.4 Hz, 1H), 5.23 (dd, *J* = 6.9, 9.8 Hz, 1H), 4.24 - 4.09 (m, 2H), 2.99 - 2.85 (m, 4H), 2.15 (dddd, *J* = 3.6, 9.7, 13.8, 40.5 Hz, 1H).

¹³C NMR (126 MHz, CHLOROFORM-*d*) δ = 163.43 (d, *J* = 248.0 Hz, 1C), 159.66, 152.09, 144.39 (d, *J* = 6.4 Hz, 1C), 137.72 (br s, 1C), 137.63, 131.20 (br d, *J* = 8.2 Hz, 1C), 127.38, 122.77, 120.45 (br d, *J* = 2.8 Hz, 1C), 114.95 (br d, *J* = 21.4 Hz, 1C), 111.90 (br d, *J* = 22.2 Hz, 1C), 110.46, 90.88 (br d, *J* = 178.9 Hz, 1C), 60.89, 56.45 (d, *J* = 23.5 Hz, 1C), 43.60 (d, *J* = 20.9 Hz, 1C), 25.70.



6-((2R,4S)-4-Fluoro-2-(3-fluorophenyl)pyrrolidin-1-yl)imidazo[1,2-b]pyridazine-3-carboxylic acid (7.12):

To a solution of ethyl 6-((2R,4S)-4-fluoro-2-(3-fluorophenyl)pyrrolidin-1-yl)imidazo[1,2-b]pyridazine-3-carboxylate (1.0 g, 2.69 mmol) in THF (6 mL), ethanol (3 mL) and water (1.5 mL) was added LiOH (322 mg, 13.4 mmol). The reaction mixture was stirred at room temperature for 3 h and evaporated to dryness. The residue was diluted with water (25 mL) and the pH was adjusted to 5-6 using concentrated hydrochloric acid. The aqueous phase was extracted with

CH₂Cl₂ (2 X 50 mL) and EtOAc (2 X 50 mL). The combined organic layers were washed with brine, dried over Na₂SO₄ and concentrated in *vacuo* to afford 600 mg the title compound (65 %)

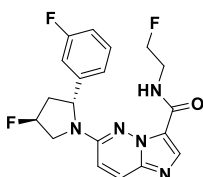
Physical State: off-white solid.

R_f: 0.40 (1:9 MeOH/CH₂Cl₂, UV light).

HRMS (ESI⁺): *m/z* calc. for C₁₇H₁₄F₂N₄O₂ (M + H)⁺: 345.1158, found 345.1148.

¹H NMR (500MHz, DMSO-*d*₆) δ = 7.99 (s, 1H), 7.88 (d, *J* = 9.9 Hz, 1H), 7.37 - 7.30 (m, 1H), 7.30 - 7.20 (m, 2H), 7.07 - 6.96 (m, 1H), 6.80 (br d, *J* = 9.5 Hz, 1H), 5.48 (d, *J* = 53.1 Hz, 1H), 5.20 (br t, *J* = 8.2 Hz, 1H), 4.23 - 4.00 (m, 2H), 2.88 - 2.72 (m, 1H), 2.25 - 2.08 (m, 1H).

¹³C NMR (126MHz, DMSO-*d*₆) δ = 162.29 (d, *J* = 243.6 Hz, 1C), 159.25, 152.55, 145.84 (d, *J* = 6.7 Hz, 1C), 138.68, 138.27, 130.93 - 130.36 (m, 1C), 130.56 (d, *J* = 8.2 Hz, 1C), 126.06, 122.33 (br s, 1C), 119.18, 114.03 (br d, *J* = 21.1 Hz, 1C), 113.39 (d, *J* = 21.7 Hz, 1C), 112.39 (br s, 1C), 92.10 (d, *J* = 174.0 Hz, 1C), 59.74, 55.49 (br d, *J* = 21.7 Hz, 1C), 42.55 (br d, *J* = 20.9 Hz, 1C).



6-((2R,4S)-4-fluoro-2-(3-fluorophenyl)pyrrolidin-1-yl)-N-(2-fluoroethyl)imidazo[1,2-b]pyridazine-3-carboxamide (7.13):

DIPEA (26 μL, 0.15 mmol) was added to a solution of 6-((2R,4S)-4-fluoro-2-(3-fluorophenyl)pyrrolidin-1-yl)imidazo[1,2-b]pyridazine-3-carboxylic acid (20 mg, 0.058 mmol) in DMF (1 mL). HATU (22 mg, 0.058) and a solution of 2-fluoroethylamine hydrochloride (7 mg, 0.069 mmol) in DMF (0.5 mL) were successively added dropwise. The reaction mixture was stirred at room temperature for 16 h. After completion, the reaction mixture was diluted with EtOAc (50 mL), washed with water (25 mL) and brine (25 mL). The organic phase was dried over Na₂SO₄ and concentrated in *vacuo*. The crude product was purified by flash column chromatography (0→1% methanol in dichloromethane) to afford 12 mg of the title compound (52%).

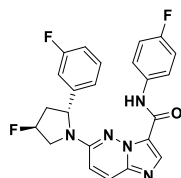
Physical State: white solid.

R_f: 0.50 (1:9 MeOH/ CH₂Cl₂, UV light).

HRMS (ESI⁺): *m/z* calc. for C₁₉H₁₉F₃N₅O (M + H)⁺: 390.1536, found 390.154.

¹H NMR (498 MHz, CHLOROFORM-*d*) δ = 8.83 (br s, 1H), 8.26 (s, 1H), 7.75 (d, J = 9.9 Hz, 1H), 7.36 (dt, J = 5.8, 7.9 Hz, 1H), 7.08 (d, J = 7.8 Hz, 1H), 7.03 - 6.97 (m, 2H), 6.58 (d, J = 9.9 Hz, 1H), 5.44 (td, J = 3.4, 52.1 Hz, 1H), 5.20 (dd, J = 7.1, 9.3 Hz, 1H), 4.74 - 4.55 (m, 2H), 4.28 - 4.06 (m, 2H), 3.98 (s, 1H), 3.67 (br d, J = 1.6 Hz, 1H), 3.01 - 2.87 (m, 1H), 2.17 (dddd, J = 3.7, 9.3, 13.5, 40.1 Hz, 1H).

¹³C NMR (125 MHz, CHLOROFORM-*d*) δ = 163.38 (d, J = 248.0 Hz, 1C), 159.17, 152.19, 144.42 (d, J = 6.5 Hz, 1C), 137.63, 136.71, 131.17 (br d, J = 8.3 Hz, 1C), 127.08, 122.32 (br s, 1C), 120.75 (br d, J = 2.6 Hz, 1C), 115.03 (br d, J = 21.2 Hz, 1C), 112.17 (br d, J = 22.2 Hz, 1C), 110.74, 90.88 (br d, J = 178.3 Hz, 1C), 83.32 (d, J = 165.9 Hz, 1C), 60.76, 56.04 (br d, J = 23.2 Hz, 1C), 43.80 (d, J = 21.2 Hz, 1C), 39.12 (d, J = 19.4 Hz, 1C).



6-((2R,4S)-4-Fluoro-2-(3-fluorophenyl)pyrrolidin-1-yl)-N-(4-fluorophenyl)imidazo[1,2-b]pyridazine-3-carboxamide (7.14):

DIPEA (26 μ L, 0.15 mmol) was added to a solution of 6-((2R,4S)-4-fluoro-2-(3-fluorophenyl)pyrrolidin-1-yl)imidazo[1,2-b]pyridazine-3-carboxylic acid (20 mg, 0.058 mmol) in DMF (1 mL). HATU (22 mg, 0.058) and a solution of 4-fluoroaniline (8 mg, 0.069 mmol) in DMF (0.5 mL) were successively added dropwise. The reaction mixture was stirred at room temperature for 16 h. After completion, the reaction mixture was diluted with EtOAc (50 mL), washed with water (25 mL) and brine (25 mL). The organic phase was dried over Na₂SO₄ and concentrated in *vacuo*. The crude product was purified by flash column chromatography (0→1% methanol in dichloromethane) to afford 24 mg of the title compound (94%).

Physical State: white solid.

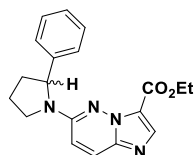
R_f: 0.17 (1:1:98 MeOH/Et₃N/CH₂Cl₂, UV light).

HRMS (ESI+): m/z calc. for C₂₃H₁₉F₃N₅O (M + H)⁺: 438.1536, found 438.1537.

¹H NMR (498 MHz, CHLOROFORM-*d*) δ = 10.36 (br s, 1H), 8.35 (s, 1H), 7.77 (d, J = 9.9 Hz, 1H), 7.61 - 7.55 (m, 2H), 7.32 - 7.28 (m, 1H), 7.15 - 7.09 (m, 2H), 7.04 (d, J = 7.7 Hz, 1H), 6.99 (ddt, J = 0.9, 2.6, 8.4 Hz, 1H), 6.95 (td, J = 2.1, 9.4 Hz, 1H), 6.59 (d, J = 9.8 Hz, 1H), 5.51 (td, J

= 3.9, 52.0 Hz, 1H), 5.24 (dd, $J = 7.2, 9.0$ Hz, 1H), 4.38 - 4.29 (m, 1H), 4.28 - 4.16 (m, 1H), 3.05 - 2.93 (m, 1H), 2.23 (dddd, $J = 3.7, 9.1, 14.2, 39.6$ Hz, 1H).

^{13}C NMR (176MHz, CHLOROFORM- d) $\delta = 179.06, 163.42$ (d, $J = 248.3$ Hz, 1C), 159.53 (d, $J = 243.9$ Hz, 1C), 157.03, 152.33, 143.93 (d, $J = 6.6$ Hz, 1C), 138.53, 133.69, 131.26 (br d, $J = 8.1$ Hz, 1C), 127.34, 122.58 (br d, $J = 7.3$ Hz, 1C), 122.46, 120.82 (br d, $J = 2.9$ Hz, 1C), 115.75 (br d, $J = 22.4$ Hz, 1C), 115.21 (d, $J = 20.9$ Hz, 1C), 112.12 (br d, $J = 22.4$ Hz, 1C), 110.70, 90.71 (br d, $J = 179.0$ Hz, 1C), 60.91, 55.95 (d, $J = 23.5$ Hz, 1C), 43.76 (d, $J = 21.3$ Hz, 1C).



Ethyl 6-(2-phenylpyrrolidin-1-yl)imidazo[1,2-*b*]pyridazine-3-carboxylate (7.16):

To a solution of ethyl 6-chloroimidazo[1,2-*b*]pyridazine-3-carboxylate (226 mg, 1.0 mmol) in DMSO (5.0 mL) was added KF (174 mg, 3 mmol). This reaction mixture was heated at 110°C and 2-phenylpyrrolidine (147 mg, 1 mmol) was added. After stirring the reaction mixture at this temperature for 12 h, a second portion of 2-phenylpyrrolidine (147 mg, 1 mmol) was added and the reaction was left at the same temperature for 6 h. The heterogeneous mixture was then cooled at room temperature, poured into water and extracted with CH_2Cl_2 (3 X 50 mL). The combined organic layers were washed with brine, dried over Na_2SO_4 and concentrated in *vacuo*. The crude residue was purified by flash chromatography (10% methanol in dichloromethane) to afford 315 mg of the title compound (94%).

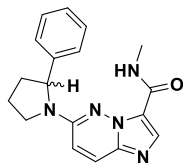
Physical State: off-white solid.

R_f : 0.24 (1:99 MeOH/ CH_2Cl_2 , UV light).

HRMS (ESI+): m/z calc. for $\text{C}_{19}\text{H}_{21}\text{N}_4\text{O}_2$ ($\text{M} + \text{H}$) $^+$: 337.1659, found 337.1657.

^1H NMR (498 MHz, CHLOROFORM- d) $\delta = 8.13$ (s, 1H), 7.56 (d, $J = 9.8$ Hz, 1H), 7.36 - 7.31 (m, 2H), 7.29 - 7.22 (m, 3H), 6.48 (d, $J = 9.9$ Hz, 1H), 5.03 - 4.96 (m, 1H), 4.42 (q, $J = 7.1$ Hz, 2H), 4.05 - 3.98 (m, 1H), 3.90 - 3.82 (m, 1H), 2.55 - 2.46 (m, 1H), 2.12 - 2.01 (m, 3H), 1.43 (t, $J = 7.1$ Hz, 3H).

^{13}C NMR (125 MHz, CHLOROFORM- d) $\delta = 159.35, 153.07, 143.07, 139.41, 136.21, 128.83, 128.39, 127.57, 127.32, 125.69, 125.56, 62.41, 60.26, 48.56, 36.28, 22.79, 14.46$.



N-Methyl-6-(2-phenylpyrrolidin-1-yl)imidazo[1,2-*b*]pyridazine-3-carboxamide (7.17):

Ethyl 6-(2-phenylpyrrolidin-1-yl)imidazo[1,2-*b*]pyridazine-3-carboxylate (160 mg, 0.60 mmol) was dissolved in a methylamine solution (33 wt. % in absolute ethanol, 5 mL). The reaction mixture was stirred at room temperature for 2 h then concentrated and dried in *vacuo* to afford 95 mg of the title compound (62%).

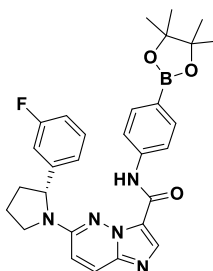
Physical State: off-white solid.

R_f: 0.10 (1:99 MeOH/CH₂Cl₂, UV light).

HRMS (ESI+): *m/z* calc. for C₁₈H₂₀N₅O (M + H)⁺: 322.1662, found 322.1663.

¹H NMR (700 MHz, CHLOROFORM-*d*) δ = 8.12 (s, 2H), 7.67 (br d, *J* = 9.7 Hz, 1H), 7.34 - 7.29 (m, 2H), 7.25 - 7.22 (m, 1H), 7.18 - 7.15 (m, 2H), 6.61 (br s, 1H), 5.08 - 5.00 (m, 1H), 3.91 - 3.85 (m, 1H), 3.66 (dt, *J* = 7.2, 9.2 Hz, 1H), 2.96 - 2.65 (m, 3H), 2.54 - 2.45 (m, 1H), 2.17 - 2.05 (m, 2H), 2.02 (tdd, *J* = 3.1, 6.1, 12.5 Hz, 1H).

¹³C NMR (176MHz, CHLOROFORM-*d*) δ = 159.86, 151.76, 142.36, 137.58 (br s, 1C), 136.83, 128.90, 127.32, 126.75, 125.17, 122.50 (br s, 1C), 110.42 (br s, 1C), 62.55, 48.71 (br s, 1C), 35.81, 25.51, 22.98.



(*R*)-6-(2-(3-Fluorophenyl)pyrrolidin-1-yl)-*N*-(4-(4,4,5,5-tetramethyl-1,3,2-dioxaborolan-2-yl)phenyl)imidazo[1,2-*b*]pyridazine-3-carboxamide (7.19):

DIPEA (43 μL, 0.25 mmol) was added to a solution of 6-((2*R*,4*S*)-4-fluoro-2-(3-fluorophenyl)pyrrolidin-1-yl)imidazo[1,2-*b*]pyridazine-3-carboxylic acid (33 mg, 0.10 mmol) in DMF (3 mL). HBTU (38 mg, 0.10 mmol) was then added in one portion and the reaction mixture

was stirred at 23°C for 5 min. A solution of 4-aminophenylboronic acid pinacol ester (22 mg, 0.10 mmol) in DMF (1 mL) was added dropwise and the reaction mixture was stirred at 23°C for 16 h. The reaction mixture was diluted with ethyl acetate (50 mL), washed with water (25 mL) and brine (25 mL), dried over anhydrous sodium sulfate, filtered and concentrated under reduced pressure. The crude product was purified by flash column chromatography (1→5% methanol in dichloromethane) to afford 40 mg of the title compound (62%).

Physical State: white solid.

R_f: 0.13 (5:95 MeOH/CH₂Cl₂, UV light).

HRMS (ESI+): *m/z* calc. for C₂₉H₃₁[¹⁰B]FN₅O₃ (M + H)⁺: 527.2613, found 527.2615.

¹H NMR (400 MHz, CHLOROFORM-*d*) δ = 10.70 (br s, 1H), 8.31 (s, 1H), 7.82 (d, *J* = 8.4 Hz, 2H), 7.70 (d, *J* = 9.8 Hz, 1H), 7.61 (br d, *J* = 7.4 Hz, 2H), 7.32 (dt, *J* = 5.9, 8.0 Hz, 1H), 7.03 - 6.94 (m, 2H), 6.91 (br d, *J* = 9.5 Hz, 1H), 6.53 (br d, *J* = 9.8 Hz, 1H), 5.09 (br d, *J* = 8.1 Hz, 1H), 4.00 (br d, *J* = 6.2 Hz, 1H), 3.86 - 3.76 (m, 1H), 2.57 (br s, 1H), 2.20 - 2.08 (m, 3H), 1.36 (s, 12H).

¹³C NMR (126 MHz, CHLOROFORM-*d*) δ = 163.26 (d, *J* = 247.7 Hz, 1C), 157.14, 152.12, 144.77 (br d, *J* = 5.9 Hz, 1C), 140.73, 138.23, 138.08, 135.89, 130.78 (br d, *J* = 8.0 Hz, 1C), 127.18, 122.54, 121.19 (d, *J* = 2.6 Hz, 1C), 119.22, 114.70 (d, *J* = 21.1 Hz, 1C), 112.60 (d, *J* = 22.2 Hz, 1C), 111.01, 83.74, 62.09, 48.70, 35.93, 24.92, 22.71.

Docking analyses. Molecular docking simulations were performed using PDB files 4AT3, and 4PMT using the FITTED 3.5 program (FORECASTER platform). Docking structures and figures were prepared using Pymol (see previous chapters).

In Vitro Biological Evaluations. The potencies of **7.17**, **7.10**, **7.11**, **7.13**, **7.14** and **7.20** were obtained through [γ -³³P]ATP-based enzymatic assays (Reaction Biology Corporation, Malvern, PA) as previously described (see previous chapters).

Radiochemistry. The manual radiosynthesis of [¹⁸F]-(R)-IPMICF17 ([¹⁸F]-(R)-**7.20**) was performed at medical isotope and cyclotron facility of the University of Alberta (Edmonton PET Center, ACSI 19/9 MeV cyclotron). No-carrier-added (n.c.a) aqueous [¹⁸F]Fluoride was produced by a ¹⁸O(p,n)¹⁸F nuclear reaction on an enriched [¹⁸O]water target. No-carrier-added

(n.c.a) aqueous [^{18}F]fluoride was passed through a Sep-Pak Light QMA cartridge (Waters) (typically 1-2 GBq in 2.0 mL water). The cartridge was dried by airflow, and the ^{18}F activity was eluted with 1.0 mL of a Kryptofix 2.2.2/ K_2CO_3 solution (from a 10.0 mL stock solution of 22.6 mg of Kryptofix 222 and 4.2 mg of K_2CO_3 in acetonitrile/water (95/5)) to a 10.0 mL conical vial. The solvent was removed at 100°C under atmospheric pressure and a stream of nitrogen gas. The residue was azeotropically dried with a total of 6.0 mL of anhydrous acetonitrile at 100°C to afford the dried $\text{K}2.2.2/\text{K}[^{18}\text{F}]\text{F}$ complex residue which was dissolved in anhydrous acetonitrile. A 20 μL aliquot of this $\text{K}2.2.2/\text{K}[^{18}\text{F}]\text{F}$ solution was added to a solution of the Bpin precursor **7.19** (10.5 mg) and $[\text{Cu}(\text{OTf})_2(\text{pyr})_4]$ (3.6 mg) in DMF (200 μL) and heated at 110°C for 20 min. The reaction mixture was cooled to room temperature and diluted with 600 μL of a mixture of MeCN/ H_2O (1:1) and analyzed by radio-TLC (R_f 0.66 10% MeOH/ CH_2Cl_2 , 30% RCY).

$[^{18}\text{F}]$ -(R)-IPMICF17 was also produced at the PET radiochemistry facility of the McConnell Brain Imaging Center Site (Montreal Neurological Institute, McGill University). *HPLC Methods*. Semi preparative, radio-preparative high performance liquid chromatography (HPLC) purification was performed using a Phenomenex LUNA $^{\text{®}}$ C18 column (100 \AA , 250 \times 10 mm, 10 μm). Method A: elution at 4.0 ml min^{-1} with a mixture of MeCN (A) and 20 mM NaH_2PO_4 (B) isocratic at 60% A and 40% B ($t_{r [^{18}\text{F}] \text{IPMICF17}} = 15$ min). Quality control analysis was performed on an Agilent 1200 system (Agilent Technologies, Santa Clara, CA, USA; running on Agilent ChemStation software) equipped with a Raytest Gabi Star radioactivity detector (Raytest Isotopenmessgeräte GmbH, Straubenhardt, Germany) using a Phenomenex Partisil ODS-3 (250 \times 4.6 mm, 5 μm) column. Method B: elution at 1.0 ml min^{-1} with a mixture of MeCN (A) and 0.1% aqueous TFA (B) isocratic at 60% A and 40% B ($t_{r [^{18}\text{F}] \text{IPMICF17}} = 10.3$ min). *Radiosynthesis of $[^{18}\text{F}]$ -(R)-IPMICF17*. No-carrier-added (n.c.a) aqueous [^{18}F]fluoride was produced by a $^{18}\text{O}(\text{p},\text{n})^{18}\text{F}$ nuclear reaction on an enriched [^{18}O]water target of the cyclotron (IBA Cyclon 18/9 MeV cyclotron). The azeotropic drying of $^{18}\text{F}^-$, radiolabeling and purification were carried out using semi-automated radiosynthesis module Scintomics GRP (Germany) equipped with a preparative HPLC (Knauer) with radioactivity and UV detector and a home-made manifold setup. $[^{18}\text{F}]\text{F}/\text{H}_2\text{O}$ (310 – 440 mCi) was passed through a Sep-Pak Light QMA cartridge (Waters) as an aqueous solution in ^{18}O -enriched water and the ^{18}F activity was eluted with 500 μL of a potassium triflate solution (KOTf, 10 mg/mL) premixed with 3 μL of potassium carbonate (K_2CO_3 0.125M) into a conical Wheaton vial (5 mL). Acetonitrile (1 mL) was added and the solvents were azeotropically removed at 100°C in vacuum, first under stream of air and then in closed system. Following azeotropic drying, the reaction vial was heated to 110°C and charged with Bpin precursor **7.19**

(2.5 mg in 0.4 mL DMF). After 5 minutes of preincubation in order to solubilize inorganic salts, $[\text{Cu}(\text{OTf})_2(\text{pyr})_4]$ (13.5 mg in 0.4 mL DMF) was added and the mixture was allowed to react for 20 min at 110°C. The crude mixture was then diluted with HPLC eluent (1.5 mL, 60% MeCN 40% 20mM NaH_2PO_4) and injected onto HPLC through a Nylon filter to remove copper precipitates. The radiochemically pure $[\text{}^{18}\text{F}]$ -(R)-IPMICF17 was obtained in 1.8 ± 0.2 % RCY (EOS, non-decay corrected isolated yield from $^{18}\text{F}^-/\text{H}_2\text{O}$; non-optimized), > 99% radiochemical purity and effective specific activity of 450 ± 79 Ci/mmol due to the presence of the protodeboronation product. Collected from HPLC $[\text{}^{18}\text{F}]$ -(R)-IPMICF17 was diluted with 20 mL H_2O and passed through a preconditioned (10 mL EtOH followed by 10 mL water) Sep-Pak tC18 Plus cartridge and then eluted with 2 mL EtOH and used directly in the autoradiography experiments. Quality control, of the isolated $[\text{}^{18}\text{F}]$ -(R)-IPMICF17 was performed using HPLC method B.

7.4 References

1. Traxl, A.; Wanek, T.; Mairinger, S.; Stanek, J.; Filip, T.; Sauberer, M.; Muller, M.; Kuntner, C.; Langer, O., Breast Cancer Resistance Protein and P-Glycoprotein Influence In Vivo Disposition of C-11-Erlotinib. *Journal of Nuclear Medicine* **2015**, *56* (12), 1930-1936.
2. Syvanen, S.; Lindhe, O.; Palner, M.; Kornum, B. R.; Rahman, O.; Langstrom, B.; Knudsen, G. M.; Hammarlund-Udenaes, M., Species Differences in Blood-Brain Barrier Transport of Three Positron Emission Tomography Radioligands with Emphasis on P-Glycoprotein Transport. *Drug Metab Dispos* **2009**, *37* (3), 635-643.
3. Liang, S.; Chen, J. S.; Normandin, M.; Collier, T.; Perlis, R.; Holson, E.; Haggarty, S.; El Fakhri, G.; Kurumbail, R.; Vasdev, N., Discovery of [C-11]PF-367 for neuroimaging of glycogen synthase kinase 3. *Journal of Nuclear Medicine* **2015**, *56* (3).
4. Muller, K.; Faeh, C.; Diederich, F., Fluorine in pharmaceuticals: Looking beyond intuition. *Science* **2007**, *317* (5846), 1881-1886.
5. Pollock, J.; Borkin, D.; Lund, G.; Purohit, T.; Dyguda-Kazimierowicz, E.; Grembecka, J.; Cierpicki, T., Rational Design of Orthogonal Multipolar Interactions with Fluorine in Protein-Ligand Complexes. *J Med Chem* **2015**, *58* (18), 7465-74.
6. Albaugh PA, C. G., Fan Y, Flatt BT, Loren J, Molteni V, et al., Imidazo [1, 2] pyridazin compounds and compositions as trk inhibitors. . *WO2012034091 A1* **2012**.
7. McCarthy, C.; Walker, E., Tropomyosin receptor kinase inhibitors: a patent update 2009-2013. *Expert Opinion on Therapeutic Patents* **2014**, *24* (7), 731-744.
8. Choi, H. S.; Rucker, P. V.; Wang, Z. C.; Fan, Y.; Albaugh, P.; Chopiuk, G.; Gessier, F.; Sun, F. X.; Adrian, F.; Liu, G. X.; Hood, T.; Li, N. X.; Jia, Y.; Che, J. W.; McCormack, S.; Li, A.; Li, J.; Steffy, A.; Culazzo, A.; Tompkins, C.; Phung, V.; Kreuzsch, A.; Lu, M.; Hu, B.; Chaudhary, A.; Prashad, M.; Tuntland, T.; Liu, B.; Harris, J.; Seidel, H. M.; Loren, J.; Molteni, V., (R)-2-

Phenylpyrrolidine Substituted Imidazopyridazines: A New Class of Potent and Selective Pan-IRK Inhibitors. *Acs Medicinal Chemistry Letters* **2015**, 6 (5), 562-567.

9. Bissantz, C.; Kuhn, B.; Stahl, M., A medicinal chemist's guide to molecular interactions. *J Med Chem* **2010**, 53 (14), 5061-84.

10. Pettersson, M.; Hou, X. J.; Kuhn, M.; Wager, T. T.; Kauffman, G. W.; Verhoest, P. R., Quantitative Assessment of the Impact of Fluorine Substitution on P-Glycoprotein (P-gp) Mediated Efflux, Permeability, Lipophilicity, and Metabolic Stability. *Journal of Medicinal Chemistry* **2016**, 59 (11), 5284-5296.

11. Rankovic, Z., CNS Drug Design: Balancing Physicochemical Properties for Optimal Brain Exposure. *Journal of Medicinal Chemistry* **2015**, 58 (6), 2584-2608.

12. Tredwell, M.; Preshlock, S. M.; Taylor, N. J.; Gruber, S.; Huiban, M.; Passchier, J.; Mercier, J.; Genicot, C.; Gouverneur, V., A general copper-mediated nucleophilic ¹⁸F fluorination of arenes. *Angew Chem Int Ed Engl* **2014**, 53 (30), 7751-5.

13. Zlatopolskiy, B. D.; Zischler, J.; Krapf, P.; Zarrad, F.; Urusova, E. A.; Kordys, E.; Endepols, H.; Neumaier, B., Copper-mediated aromatic radiofluorination revisited: efficient production of PET tracers on a preparative scale. *Chemistry* **2015**, 21 (15), 5972-9.

14. Mossine, A. V.; Brooks, A. F.; Makaravage, K. J.; Miller, J. M.; Ichiishi, N.; Sanford, M. S.; Scott, P. J., Synthesis of [¹⁸F]Arenes via the Copper-Mediated [¹⁸F]Fluorination of Boronic Acids. *Org Lett* **2015**, 17 (23), 5780-3.

15. Di, L.; Rong, H. J.; Feng, B., Demystifying Brain Penetration in Central Nervous System Drug Discovery. *Journal of Medicinal Chemistry* **2013**, 56 (1), 2-12.

16. Andrews SW, C. K., Haas J,; al., e., Preparation of macrocyclic compounds as trk kinase inhibitors. *WO2011146336* **2011**.

17. Marsault, E.; Peterson, M. L., Macrocycles are great cycles: applications, opportunities, and challenges of synthetic macrocycles in drug discovery. *J Med Chem* **2011**, *54* (7), 1961-2004.
18. Johnson, T. W.; Richardson, P. F.; Bailey, S.; Brooun, A.; Burke, B. J.; Collins, M. R.; Cui, J. J.; Deal, J. G.; Deng, Y. L.; Dinh, D.; Engstrom, L. D.; He, M.; Hoffman, J.; Hoffman, R. L.; Huang, Q.; Kania, R. S.; Kath, J. C.; Lam, H.; Lam, J. L.; Le, P. T.; Lingardo, L.; Liu, W.; McTigue, M.; Palmer, C. L.; Sach, N. W.; Smeal, T.; Smith, G. L.; Stewart, A. E.; Timofeevski, S.; Zhu, H.; Zhu, J.; Zou, H. Y.; Edwards, M. P., Discovery of (10R)-7-amino-12-fluoro-2,10,16-trimethyl-15-oxo-10,15,16,17-tetrahydro-2H-8,4-(m etheno)pyrazolo[4,3-h][2,5,11]-benzoxadiazacyclotetradecine-3-carbonitrile (PF-06463922), a macrocyclic inhibitor of anaplastic lymphoma kinase (ALK) and c-ros oncogene 1 (ROS1) with preclinical brain exposure and broad-spectrum potency against ALK-resistant mutations. *J Med Chem* **2014**, *57* (11), 4720-44.
19. Heffron, T. P., Small Molecule Kinase Inhibitors for the Treatment of Brain Cancer. *J Med Chem* **2016**, *59* (22), 10030-10066.
20. Bernard-Gauthier, V.; Aliaga, A.; Aliaga, A.; Boudjemeline, M.; Hopewell, R.; Kostikov, A.; Rosa-Neto, P.; Thiel, A.; Schirmacher, R., Syntheses and Evaluation of Carbon-11-and Fluorine-18-Radiolabeled pan-Tropomyosin Receptor Kinase (Trk) Inhibitors: Exploration of the 4-Aza-2-oxindole Scaffold as Trk PET Imaging Agents. *Acs Chemical Neuroscience* **2015**, *6* (2), 260-276.
21. Laufer, R.; Forrest, B.; Li, S. W.; Liu, Y.; Sampson, P.; Edwards, L.; Lang, Y. H.; Awrey, D. E.; Mao, G. D.; Plotnikova, O.; Leung, G.; Hodgson, R.; Beletskaya, I.; Mason, J. M.; Luo, X. Y.; Wei, X.; Yao, Y.; Feher, M.; Ban, F. Q.; Kiarash, R.; Green, E.; Mak, T. W.; Pan, G. H.; Pauls, H. W., The Discovery of PLK4 Inhibitors: (E)-3-((1H-Indazol-6-yl)methylene)indolin-2-ones as Novel Antiproliferative Agents. *Journal of Medicinal Chemistry* **2013**, *56* (15), 6069-6087.

22. Sampson, P. B.; Liu, Y.; Patel, N. K.; Feher, M.; Forrest, B.; Li, S. W.; Edwards, L.; Laufer, R.; Lang, Y.; Ban, F.; Awrey, D. E.; Mao, G.; Plotnikova, O.; Leung, G.; Hodgson, R.; Mason, J. M.; Wei, X.; Kiarash, R.; Green, E.; Qiu, W.; Chirgadze, N. Y.; Mak, T. W.; Pan, G.; Pauls, H. W., The discovery of Polo-like kinase 4 inhibitors: design and optimization of spiro[cyclopropane-1,3'[3H]indol]-2'(1'H).ones as orally bioavailable antitumor agents. *J Med Chem* **2015**, *58* (1), 130-46.
23. Sampson, P. B.; Liu, Y.; Forrest, B.; Cumming, G.; Li, S. W.; Patel, N. K.; Edwards, L.; Laufer, R.; Feher, M.; Ban, F.; Awrey, D. E.; Mao, G.; Plotnikova, O.; Hodgson, R.; Beletskaya, I.; Mason, J. M.; Luo, X.; Nadeem, V.; Wei, X.; Kiarash, R.; Madeira, B.; Huang, P.; Mak, T. W.; Pan, G.; Pauls, H. W., The discovery of Polo-like kinase 4 inhibitors: identification of (1R,2S)-2-(3-((E)-4-(((cis)-2,6-dimethylmorpholino)methyl)styryl)-1H-indazol-6-yl)-5'-methoxyspiro[cyclopropane-1,3'-indolin]-2'-one (CFI-400945) as a potent, orally active antitumor agent. *J Med Chem* **2015**, *58* (1), 147-69.
24. Menichincheri, M.; Ardini, E.; Magnaghi, P.; Avanzi, N.; Banfi, P.; Bossi, R.; Buffa, L.; Canevari, G.; Ceriani, L.; Colombo, M.; Corti, L.; Donati, D.; Fasolini, M.; Felder, E.; Fiorelli, C.; Fiorentini, F.; Galvani, A.; Isacchi, A.; Borgia, A. L.; Marchionni, C.; Nesi, M.; Orrenius, C.; Panzeri, A.; Pesenti, E.; Rusconi, L.; Saccardo, M. B.; Vanotti, E.; Perrone, E.; Orsini, P., Discovery of Entrectinib: A New 3-Aminoindazole As a Potent Anaplastic Lymphoma Kinase (ALK), c-ros Oncogene 1 Kinase (ROS1), and Pan-Tropomyosin Receptor Kinases (Pan-TRKs) inhibitor. *J Med Chem* **2016**, *59* (7), 3392-408.
25. Ardini, E.; Menichincheri, M.; Banfi, P.; Bosotti, R.; De Ponti, C.; Pulci, R.; Ballinari, D.; Ciomei, M.; Texido, G.; Degrassi, A.; Avanzi, N.; Amboldi, N.; Saccardo, M. B.; Casero, D.; Orsini, P.; Bandiera, T.; Mologni, L.; Anderson, D.; Wei, G.; Harris, J.; Vernier, J. M.; Li, G.; Felder, E.; Donati, D.; Isacchi, A.; Pesenti, E.; Magnaghi, P.; Galvani, A., Entrectinib, a Pan-TRK, ROS1, and ALK Inhibitor with Activity in Multiple Molecularly Defined Cancer Indications. *Mol Cancer Ther* **2016**, *15* (4), 628-39.

26. Devi, L.; Ohno, M., TrkB reduction exacerbates Alzheimer's disease-like signaling aberrations and memory deficits without affecting beta-amyloidosis in 5XFAD mice. *Transl Psychiatry* **2015**, *5*, e562.
27. Abuhatzira, L.; Makedonski, K.; Kaufman, Y.; Razin, A.; Shemer, R., MeCP2 deficiency in the brain decreases BDNF levels by REST/CoREST-mediated repression and increases TRKB production. *Epigenetics* **2007**, *2* (4), 214-22.
28. Webster, M. J.; Herman, M. M.; Kleinman, J. E.; Shannon Weickert, C., BDNF and trkB mRNA expression in the hippocampus and temporal cortex during the human lifespan. *Gene Expr Patterns* **2006**, *6* (8), 941-51.
29. Silhol, M.; Bonnichon, V.; Rage, F.; Tapia-Arancibia, L., Age-related changes in brain-derived neurotrophic factor and tyrosine kinase receptor isoforms in the hippocampus and hypothalamus in male rats. *Neuroscience* **2005**, *132* (3), 613-624.
30. Romanczyk, T. B.; Weickert, C. S.; Webster, M. J.; Herman, M. M.; Akil, M.; Kleinman, J. E., Alterations in trkB mRNA in the human prefrontal cortex throughout the lifespan. *European Journal of Neuroscience* **2002**, *15* (2), 269-280.

Complete Bibliography

A

A controlled trial of recombinant methionyl human BDNF in ALS: The BDNF Study Group (Phase III). *Neurology* **1999**, 52 (7), 1427-33.

Abraham, D.; Zins, K.; Sioud, M.; Lucas, T.; Schafer, R.; Stanley, E. R.; Aharinejad, S., Stromal cell-derived CSF-1 blockade prolongs xenograft survival of CSF-1-negative neuroblastoma. *International Journal of Cancer* **2010**, 126 (6), 1339-1352.

Abuhatzira, L.; Makedonski, K.; Kaufman, Y.; Razin, A.; Shemer, R., MeCP2 deficiency in the brain decreases BDNF levels by REST/CoREST-mediated repression and increases TRKB production. *Epigenetics* **2007**, 2 (4), 214-22.

Achim, C. L.; Katyal, S.; Wiley, C. A.; Shiratori, M.; Wang, G.; Oshika, E.; Petersen, B. E.; Li, J. M.; Michalopoulos, G. K., Expression of HGF and cMet in the developing and adult brain. *Dev Brain Res* **1997**, 102 (2), 299-303.

Alam, I. S.; Arshad, M. A.; Nguyen, Q. D.; Aboagye, E. O., Radiopharmaceuticals as probes to characterize tumour tissue. *Eur J Nucl Med Mol Imaging* **2015**, 42 (4), 537-61.

Albaugh PA, C. G., Fan Y, Flatt BT, Loren J, Molteni V, et al., Imidazo [1, 2] pyridazin compounds and compositions as trk inhibitors. . *WO2012034091 A1* **2012**.

Albaugh, P.; Fan, Y.; Mi, Y.; Sun, F.; Adrian, F.; Li, N.; Jia, Y.; Sarkisova, Y.; Kreusch, A.; Hood, T.; Lu, M.; Liu, G.; Huang, S.; Liu, Z.; Loren, J.; Tuntland, T.; Karanewsky, D. S.; Seidel, H. M.; Molteni, V., Discovery of GNF-5837, a Selective TRK Inhibitor with Efficacy in Rodent Cancer Tumor Models. *ACS Med. Chem. Lett.* **2012**, 3 (2), 140-145.

Albaugh, P.; Fan, Y.; Mi, Y.; Sun, F.; Adrian, F.; Li, N.; Jia, Y.; Sarkisova, Y.; Kreusch, A.; Hood, T.; Lu, M.; Liu, G.; Huang, S.; Liu, Z.; Loren, J.; Tuntland, T.; Karanewsky, D. S.; Seidel, H. M.; Molteni, V., Discovery of GNF-5837, a Selective TRK Inhibitor with Efficacy in Rodent Cancer Tumor Models. *ACS Med Chem Lett* **2012**, 3 (2), 140-5.

Aliaga, A.; Rousseau, J. A.; Cadorette, J.; Croteau, E.; van Lier, J. E.; Lecomte, R.; Benard, F., A small animal positron emission tomography study of the effect of chemotherapy and hormonal therapy on the uptake of 2-deoxy-2-[F-18]fluoro-D-glucose in murine models of breast cancer. *Mol Imaging Biol* **2007**, 9 (3), 144-150.

Allen, S. J.; Wilcock, G. K.; Dawbarn, D., Profound and selective loss of catalytic TrkB immunoreactivity in Alzheimer's disease. *Biochem Bioph Res Co* **1999**, 264 (3), 648-651.

Aller, S. G.; Yu, J.; Ward, A.; Weng, Y.; Chittaboina, S.; Zhuo, R.; Harrell, P. M.; Trinh, Y. T.; Zhang, Q.; Urbatsch, I. L.; Chang, G., Structure of P-glycoprotein reveals a molecular basis for poly-specific drug binding. *Science* **2009**, 323 (5922), 1718-22.

Alonso, M.; Medina, J. H.; Pozzo-Miller, L., ERK1/2 activation is necessary for BDNF to increase dendritic spine density in hippocampal CA1 pyramidal neurons. *Learn Memory* **2004**, 11 (2), 172-178.

Altar, C. A.; Burton, L. E.; Bennett, G. L.; Dugich-Djordjevic, M., Recombinant human nerve growth factor is biologically active and labels novel high-affinity binding sites in rat brain. *Proc Natl Acad Sci U S A* **1991**, 88 (1), 281-5.

Altar, C. A.; Criden, M. R.; Lindsay, R. M.; DiStefano, P. S., Characterization and topography of high-affinity ¹²⁵I-neurotrophin-3 binding to mammalian brain. *J Neurosci* **1993**, *13* (2), 733-43.

Altar, C. A.; Dugich-Djordjevic, M.; Armanini, M.; Bakhit, C., Medial-to-lateral gradient of neostriatal NGF receptors: relationship to cholinergic neurons and NGF-like immunoreactivity. *J Neurosci* **1991**, *11* (3), 828-36.

Altar, C. A.; Siuciak, J. A.; Wright, P.; Ip, N. Y.; Lindsay, R. M.; Wiegand, S. J., In-Situ Hybridization of Trkb and Trkc Receptor Messenger-Rna in Rat Forebrain and Association with High-Affinity Binding of [¹²⁵I] Bdnf, [¹²⁵I] Nt-4/5 and [¹²⁵I] Nt-3. *European Journal of Neuroscience* **1994**, *6* (9), 1389-1405.

Ametamey, S. M.; Honer, M.; Schubiger, P. A., Molecular imaging with PET. *Chem Rev* **2008**, *108* (5), 1501-16.

Anastassiadis, T.; Deacon, S. W.; Devarajan, K.; Ma, H.; Peterson, J. R., Comprehensive assay of kinase catalytic activity reveals features of kinase inhibitor selectivity. *Nat Biotechnol* **2011**, *29* (11), 1039-45.

Anderson, K. D.; Alderson, R. F.; Altar, C. A.; DiStefano, P. S.; Corcoran, T. L.; Lindsay, R. M.; Wiegand, S. J., Differential distribution of exogenous BDNF, NGF, and NT-3 in the brain corresponds to the relative abundance and distribution of high-affinity and low-affinity neurotrophin receptors. *J Comp Neurol* **1995**, *357* (2), 296-317.

Andrews SW, C. K., Haas J.; al., e., Preparation of macrocyclic compounds as trk kinase inhibitors. WO2011146336 **2011**.

Andrews, S. W.; Blake, J. F.; Brandhuber, B. J.; Kercher, T.; Winski, S. L. N-(monocyclic aryl),N'-pyrazolyl-urea, thiourea, guanidine and cyanoguanidine compounds as trka kinase inhibitors. WO2014078325 A1, 2014.

Andrews, S. W.; Condroski, K. R.; Haas, J.; Jiang, Y.; Kolakowski, G. R.; Seo, J.; Yang, H. W.; Zhao, Q. Macrocyclic compounds as inhibitors of trk kinase. WO2011146336 A1, 2011.

Apfel, S. C.; Schwartz, S.; Adornato, B. T.; Freeman, R.; Biton, V.; Rendell, M.; Vinik, A.; Giuliani, M.; Stevens, J. C.; Barbano, R.; Dyck, P. J., Efficacy and safety of recombinant human nerve growth factor in patients with diabetic polyneuropathy: A randomized controlled trial. rhNGF Clinical Investigator Group. *JAMA* **2000**, *284* (17), 2215-21.

Ardini, E.; Bosotti, R.; Borgia, A. L.; De Ponti, C.; Somaschini, A.; Cammarota, R.; Amboldi, N.; Radrizzani, L.; Milani, A.; Magnaghi, P.; Ballinari, D.; Casero, D.; Gasparri, F.; Banfi, P.; Avanzi, N.; Saccardo, M. B.; Alzani, R.; Bandiera, T.; Felder, E.; Donati, D.; Pesenti, E.; Sartore-Bianchi, A.; Gambacorta, M.; Pierotti, M. A.; Siena, S.; Veronese, S.; Galvani, A.; Isacchi, A., The TPM3-NTRK1 rearrangement is a recurring event in colorectal carcinoma and is associated with tumor sensitivity to TRKA kinase inhibition. *Mol Oncol* **2014**, *8* (8), 1495-507.

Ardini, E.; Menichincheri, M.; Banfi, P.; Bosotti, R.; De Ponti, C.; Pulci, R.; Ballinari, D.; Ciomei, M.; Texido, G.; Degrassi, A.; Avanzi, N.; Amboldi, N.; Saccardo, M. B.; Casero, D.; Orsini, P.; Bandiera, T.; Mologni, L.; Anderson, D.; Wei, G.; Harris, J.; Vernier, J.-M.; Li, G.; Felder, E.; Donati, D.; Isacchi, A.; Pesenti, E.; Magnaghi, P.; Galvani, A., Entrectinib, a Pan-TRK, ROS1 and ALK Inhibitor with Activity in Multiple Molecularly Defined Cancer Indications. *Mol. Cancer Ther.* **2016**, *15* (4), 628-629.

Ardini, E.; Menichincheri, M.; Banfi, P.; Bosotti, R.; De Ponti, C.; Pulci, R.; Ballinari, D.; Ciomei, M.; Texido, G.; Degrassi, A.; Avanzi, N.; Amboldi, N.; Saccardo, M. B.; Casero, D.; Orsini, P.; Bandiera, T.; Mologni, L.; Anderson, D.; Wei, G.; Harris, J.; Vernier, J. M.; Li, G.; Felder, E.; Donati, D.; Isacchi, A.; Pesenti, E.; Magnaghi, P.; Galvani, A., Entrectinib, a Pan-TRK, ROS1, and ALK Inhibitor with Activity in Multiple Molecularly Defined Cancer Indications. *Mol Cancer Ther* **2016**, *15* (4), 628-39.

Arevalo, J. C.; Conde, B.; Hempstead, B. I.; Chao, M. V.; Martin-Zanca, D.; Perez, P., A novel mutation within the extracellular domain of TrkA causes constitutive receptor activation. *Oncogene* **2001**, *20* (10), 1229-34.

Arevalo, J. C.; Conde, B.; Hempstead, B. L.; Chao, M. V.; Martin-Zanca, D.; Perez, P., TrkA immunoglobulin-like ligand binding domains inhibit spontaneous activation of the receptor. *Mol Cell Biol* **2000**, *20* (16), 5908-16.

Arkenau, H.-T.; Sachdev, J. C.; Mita, M. M.; Dziadziuszko, R.; Lin, C.-C.; Yang, J. C.; Infante, J. R.; Anthony, S. P.; Voskoboynik, M.; Su, W.-C.; Castro, J. D.; Natale, R. B.; Zhang, Z.-Y.; Hughes, L.; Bobilev, D.; Weiss, G. J., Phase (Ph) 1/2a study of TSR-011, a potent inhibitor of ALK and TRK, in advanced solid tumors including crizotinib-resistant ALK positive non-small cell lung cancer. *J. Clin. Oncol.* **2015**, *33*, suppl; abstr 8063.

B

Bahce, I.; Smit, E. F.; Lubberink, M.; van der Veldt, A. A. M.; Yaqub, M.; Windhorst, A. D.; Schuit, R. C.; Thunnissen, E.; Heideman, D. A. M.; Postmus, P. E.; Lammertsma, A. A.; Hendrikse, N. H., Development of [C-11]erlotinib Positron Emission Tomography for In Vivo Evaluation of EGF Receptor Mutational Status. *Clinical Cancer Research* **2013**, *19* (1), 183-193.

Bailey, J. J. S., R.; Farrell, K.; Bernard-Gauthier, V. , Tropomyosin receptor kinase inhibitors: an updated patent review 2010-2016 Part 1. . *Expert Opin. Ther. Patents.* **2017**, *Accepted*.

Bailey, J. J. S., R.; Farrell, K.; Bernard-Gauthier, V. , Tropomyosin receptor kinase inhibitors: an updated patent review 2010-2016 Part 2. . *Expert Opin. Ther. Patents.* **2017**, *Accepted*.

Banfield, M. J.; Naylor, R. L.; Robertson, A. G.; Allen, S. J.; Dawbarn, D.; Brady, R. L., Specificity in Trk receptor:neurotrophin interactions: the crystal structure of TrkB-d5 in complex with neurotrophin-4/5. *Structure* **2001**, *9* (12), 1191-9.

Barde, Y. A.; Edgar, D.; Thoenen, H., Purification of a new neurotrophic factor from mammalian brain. *EMBO J* **1982**, *1* (5), 549-53.

Barker, P. A., High affinity not in the vicinity? *Neuron* **2007**, *53* (1), 1-4.

Bauer, B.; Miller, D. S.; Fricker, G., Compound profiling for p-glycoprotein at the blood-brain barrier using a microplate screening system. *Pharmaceut Res* **2003**, *20* (8), 1170-1176.

Baydyuk, M.; Nguyen, M. T.; Xu, B., Chronic deprivation of TrkB signaling leads to selective late-onset nigrostriatal dopaminergic degeneration. *Exp Neurol* **2011**, *228* (1), 118-25.

Beglova, N.; Maliartchouk, S.; Ekiel, I.; Zaccaro, M. C.; Saragovi, H. U.; Gehring, K., Design and solution structure of functional peptide mimetics of nerve growth factor. *J Med Chem* **2000**, *43* (19), 3530-40.

Beltaifa, S.; Webster, M. J.; Ligons, D. L.; Fatula, R. J.; Herman, M. M.; Kleinman, J. E.; Weickert, C. S., Discordant changes in cortical TrkC mRNA and protein during the human lifespan. *European Journal of Neuroscience* **2005**, *21* (9), 2433-2444.

Berkemeier, L. R.; Winslow, J. W.; Kaplan, D. R.; Nikolics, K.; Goeddel, D. V.; Rosenthal, A., Neurotrophin-5: a novel neurotrophic factor that activates trk and trkB. *Neuron* **1991**, *7* (5), 857-66.

Bernard-Gauthier, V.; Aliaga, A.; Aliaga, A.; Boudjemeline, M.; Hopewell, R.; Kostikov, A.; Rosa-Neto, P.; Thiel, A.; Schirmacher, R., Syntheses and Evaluation of Carbon-11-and Fluorine-18-Radiolabeled pan-Tropomyosin Receptor Kinase (Trk) Inhibitors: Exploration of the 4-Aza-2-oxindole Scaffold as Trk PET Imaging Agents. *Acs Chemical Neuroscience* **2015**, *6* (2), 260-276.

Bernard-Gauthier, V.; Bailey, J. J.; Aliaga, A.; Kostikov, A.; Rosa-Neto, P.; Wuest, M.; Brodeur, G. M.; Bedell, B. J.; Wuest, F.; Schirmacher, R., Development of subnanomolar radiofluorinated (2-pyrrolidin-1-yl)imidazo[1,2-b]pyridazine pan-Trk inhibitors as candidate PET imaging probes. *Medchemcomm* **2015**, *6* (12), 2184-2193.

Bernard-Gauthier, V.; Bailey, J. J.; Berke, S.; Schirmacher, R., Recent Advances in the Development and Application of Radiolabeled Kinase Inhibitors for PET Imaging. *Molecules* **2015**, *20* (12), 22000-22027.

Bernard-Gauthier, V.; Boudjemeline, M.; Rosa-Neto, P.; Thiel, A.; Schirmacher, R., Towards tropomyosin-related kinase B (TrkB) receptor ligands for brain imaging with PET: radiosynthesis and evaluation of 2-(4-[(¹⁸F]fluorophenyl)-7,8-dihydroxy-4H-chromen-4-one and 2-(4-[(N-methyl-(¹¹C)-dimethylamino)phenyl]-7,8-dihydroxy-4H-chromen-4-one. *Bioorg Med Chem* **2013**, *21* (24), 7816-29.

Bernard-Gauthier, V.; Schirmacher, R., 5-(4-((4-[¹⁸F]fluorobenzyl)oxy)-3-methoxybenzyl)pyrimidine-2,4-diamine: A selective dual inhibitor for potential PET imaging of Trk/CSF-1R. *Bioorg Med Chem Lett* **2014**, *24* (20), 4784-4790.

Bernard-Gauthier, V.; Schirmacher, R., Evaluation of WO2015042088 A1 - a novel urea-based scaffold for TrkA inhibition. *Expert Opin Ther Pat* **2016**, *26* (2), 291-5.

Bertrand, T.; Kothe, M.; Liu, J.; Dupuy, A.; Rak, A.; Berne, P. F.; Davis, S.; Gladysheva, T.; Valtre, C.; Crenne, J. Y.; Mathieu, M., The crystal structures of TrkA and TrkB suggest key regions for achieving selective inhibition. *J Mol Biol* **2012**, *423* (3), 439-53.

Bertrand, T.; Kothe, M.; Liu, J.; Dupuy, A.; Rak, A.; Berne, P. F.; Davis, S.; Gladysheva, T.; Valtre, C.; Crenne, J. Y.; Mathieu, M., The Crystal Structures of TrkA and TrkB Suggest Key Regions for Achieving Selective Inhibition. *Journal of Molecular Biology* **2012**, *423* (3), 439-453.

Beuthien-Baumann, B.; Hamacher, K.; Oberdorfer, F.; Steinbach, J., Preparation of fluorine-18 labelled sugars and derivatives and their application as tracer for positron-emission-tomography. *Carbohydr Res* **2000**, *327* (1-2), 107-18.

Bibel, M.; Hoppe, E.; Barde, Y. A., Biochemical and functional interactions between the neurotrophin receptors trk and p75NTR. *EMBO J* **1999**, *18* (3), 616-22.

Binder, D. K.; Routbort, M. J.; Ryan, T. E.; Yancopoulos, G. D.; McNamara, J. O., Selective inhibition of kindling development by intraventricular administration of TrkB receptor body. *J Neurosci* **1999**, *19* (4), 1424-36.

Birchmeier, C.; Sharma, S.; Wigler, M., Expression and rearrangement of the ROS1 gene in human glioblastoma cells. *Proc Natl Acad Sci U S A* **1987**, *84* (24), 9270-4.

Bissantz, C.; Kuhn, B.; Stahl, M., A medicinal chemist's guide to molecular interactions. *J Med Chem* **2010**, *53* (14), 5061-84.

Block, D., Coenen, H.H., Stöcklin, G. , The n.c.a. nucleophilic 18F-fluorination of 1,N-disubstituted alkanes as fluoralkylation agents. . *J. Labelled Compd. Radiopharm* **1987**, *24*, 1029-1042.

Bothwell, M. A.; Shooter, E. M., Dissociation equilibrium constant of beta nerve growth factor. *J Biol Chem* **1977**, *252* (23), 8532-6.

Brahimi, F.; Malakhov, A.; Lee, H. B.; Pattarawarapan, M.; Ivanisevic, L.; Burgess, K.; Saragovi, H. U., A peptidomimetic of NT-3 acts as a TrkC antagonist. *Peptides* **2009**, *30* (10), 1833-9.

Bramson, H. N.; Corona, J.; Davis, S. T.; Dickerson, S. H.; Edelstein, M.; Frye, S. V.; Gampe, R. T.; Harris, P. A.; Hassell, A.; Holmes, W. D.; Hunter, R. N.; Lackey, K. E.; Lovejoy, B.; Luzzio, M. J.; Montana, V.; Rocque, W. J.; Rusnak, D.; Shewchuk, L.; Veal, J. M.; Walker, D. H.; Kuyper, L. F., Oxindole-based inhibitors of cyclin-dependent kinase 2 (CDK2): Design, synthesis, enzymatic activities, and X-ray crystallographic analysis. *Journal of Medicinal Chemistry* **2001**, *44* (25), 4339-4358.

Brandhuber, B. J.; Jiang, Y.; Kolakowski, G. R.; Winski, S. L. Pyrazolyl urea, thiourea, guanidine and cyanoguanidine compounds as trka kinase inhibitors. WO2014078417 A1, 2014.

Brodeur, G. M.; Minturn, J. E.; Ho, R.; Simpson, A. M.; Iyer, R.; Varela, C. R.; Light, J. E.; Kolla, V.; Evans, A. E., Trk receptor expression and inhibition in neuroblastomas. *Clin Cancer Res* **2009**, *15* (10), 3244-50.

Burriss, H. A.; Brose, M. S.; Shaw, A. T.; Bauer, T. M.; Farago, A. F.; Doebele, R. C.; Smith, S.; Fernandes, M.; Cruickshank, S.; Low, J. A., A first-in-human study of LOXO-101, a highly selective inhibitor of the tropomyosin receptor kinase (TRK) family. . *J. Clin. Oncol.* **2015**, *33*, suppl TPS2624.

C

Caldeira, M. V.; Melo, C. V.; Pereira, D. B.; Carvalho, R.; Correia, S. S.; Backos, D. S.; Carvalho, A. L.; Esteban, J. A.; Duarte, C. B., Brain-derived neurotrophic factor regulates the expression and synaptic delivery of alpha-amino-3-hydroxy-5-methyl-4-isoxazole propionic acid receptor subunits in hippocampal neurons. *J Biol Chem* **2007**, *282* (17), 12619-28.

Campagna-Slater, V.; Pottel, J.; Therrien, E.; Cantin, L. D.; Moitessier, N., Development of a Computational Tool to Rival Experts in the Prediction of Sites of Metabolism of Xenobiotics by P450s. *Journal of Chemical Information and Modeling* **2012**, *52* (9), 2471-2483.

Cantacuzene, D.; Kirk, K. L.; McCulloh, D. H.; Creveling, C. R., Effect of fluorine substitution on the agonist specificity of norepinephrine. *Science* **1979**, *204* (4398), 1217-9.

Cardinale, J. E., J.; Humpert, S.; Coenen, H. H. , Iodonium ylides for one-step, no-carrier-added radiofluorination of electron rich arenes, exemplified with 4-([18F]fluorophenoxy)-phenylmethyl)-piperidine NET and SERT ligands. *RSC Adv.* **2014**, *4*, 17293-17299.

- Cardinale, J.; Ermert, J.; Humpert, S.; Coenen, H. H., Iodonium ylides for one-step, no-carrier-added radiofluorination of electron rich arenes, exemplified with 4-([F-18] fluorophenoxy)-phenylmethyl) piperidine NET and SERT ligands. *Rsc Adv* **2014**, *4* (33), 17293-17299.
- Castello, N. A.; Nguyen, M. H.; Tran, J. D.; Cheng, D.; Green, K. N.; LaFerla, F. M., 7,8-Dihydroxyflavone, a Small Molecule TrkB Agonist, Improves Spatial Memory and Increases Thin Spine Density in a Mouse Model of Alzheimer Disease-Like Neuronal Loss. *Plos One* **2014**, *9* (3).
- Cattaneo, A., Immunosympathectomy as the first phenotypic knockout with antibodies. *P Natl Acad Sci USA* **2013**, *110* (13), 4877-4885.
- Cattaneo, A.; Calissano, P., Nerve Growth Factor and Alzheimer's Disease: New Facts for an Old Hypothesis. *Molecular Neurobiology* **2012**, *46* (3), 588-604.
- Cazorla, M.; Jouvenceau, A.; Rose, C.; Guilloux, J. P.; Pilon, C.; Dranovsky, A.; Premont, J., Cyclotraxin-B, the first highly potent and selective TrkB inhibitor, has anxiolytic properties in mice. *PLoS One* **2010**, *5* (3), e9777.
- Cazorla, M.; Premont, J.; Mann, A.; Girard, N.; Kellendonk, C.; Rognan, D., Identification of a low-molecular weight TrkB antagonist with anxiolytic and antidepressant activity in mice. *J Clin Invest* **2011**, *121* (5), 1846-57.
- Cazorla, M.; Premont, J.; Mann, A.; Girard, N.; Kellendonk, C.; Rognan, D., Identification of a low-molecular weight TrkB antagonist with anxiolytic and antidepressant activity in mice. *Journal of Clinical Investigation* **2011**, *121* (5), 1846-1857.
- Chao, M. V., Neurotrophin Receptors - a Window into Neuronal Differentiation. *Neuron* **1992**, *9* (4), 583-593.
- Chao, M. V., Neurotrophins and their receptors: a convergence point for many signalling pathways. *Nat Rev Neurosci* **2003**, *4* (4), 299-309.
- Chao, M. V.; Hempstead, B. L., p75 and Trk: a two-receptor system. *Trends Neurosci* **1995**, *18* (7), 321-6.
- Chen, W. G.; Chang, Q.; Lin, Y.; Meissner, A.; West, A. E.; Griffith, E. C.; Jaenisch, R.; Greenberg, M. E., Derepression of BDNF transcription involves calcium-dependent phosphorylation of MeCP2. *Science* **2003**, *302* (5646), 885-9.
- Cheng Y, P. W., Relationship between the inhibition constant (K1) and the concentration of inhibitor which causes 50 per cent inhibition (I50) of an enzymatic reaction. *Biochem Pharmacol.* **1973**, *22* (23), 3099-3108.
- Chitu, V.; Stanley, E. R., Colony-stimulating factor-1 in immunity and inflammation. *Curr Opin Immunol* **2006**, *18* (1), 39-48.
- Choi, H. S.; Rucker, P. V.; Wang, Z. C.; Fan, Y.; Albaugh, P.; Chopiuk, G.; Gessier, F.; Sun, F. X.; Adrian, F.; Liu, G. X.; Hood, T.; Li, N. X.; Jia, Y.; Che, J. W.; McCormack, S.; Li, A.; Li, J.; Steffy, A.; Culazzo, A.; Tompkins, C.; Phung, V.; Kreuzsch, A.; Lu, M.; Hu, B.; Chaudhary, A.; Prashad, M.; Tuntland, T.; Liu, B.; Harris, J.; Seidel, H. M.; Loren, J.; Molteni, V., (R)-2-Phenylpyrrolidine Substituted Imidazopyridazines: A New Class of Potent and Selective Pan-IRK Inhibitors. *Acs Medicinal Chemistry Letters* **2015**, *6* (5), 562-567.

Choi, H.-S.; Rucker, P. V.; Wang, Z.; Fan, Y.; Albaugh, P.; Chopiuk, G.; Gessier, F.; Sun, F.; Adrian, F.; Liu, G.; Hood, T.; Li, N.; Jia, Y.; Che, J.; McCormack, S.; Li, A.; Li, J.; Steffy, A.; Culazzo, A.; Tompkins, C.; Phung, V.; Kreuzsch, A.; Lu, M.; Hu, B.; Chaudhary, A.; Prashad, M.; Tuntland, T.; Liu, B.; Harris, J.; Seidel, H. M.; Loren, J.; Molteni, V., (R)-2-Phenylpyrrolidine Substituted Imidazopyridazines: A New Class of Potent and Selective Pan-TRK Inhibitors. *ACS Med. Chem. Lett.* **2015**, *6* (5), 562-567.

Coffey, E. T., Nuclear and cytosolic JNK signalling in neurons. *Nature Reviews Neuroscience* **2014**, *15* (5), 285-299.

Cohen, S., Purification of a Nerve-Growth Promoting Protein from the Mouse Salivary Gland and Its Neuro-Cytotoxic Antiserum. *Proc Natl Acad Sci U S A* **1960**, *46* (3), 302-11.

Cohen, S.; Levi-Montalcini, R., A Nerve Growth-Stimulating Factor Isolated from Snake Venom. *Proc Natl Acad Sci U S A* **1956**, *42* (9), 571-4.

Cohen, S.; Levi-Montalcini, R.; Hamburger, V., A Nerve Growth-Stimulating Factor Isolated from Sarcom as 37 and 180. *Proc Natl Acad Sci U S A* **1954**, *40* (10), 1014-8.

Cole, E. L.; Shao, X.; Sherman, P.; Quesada, C.; Fawaz, M. V.; Desmond, T. J.; Scott, P. J., Synthesis and evaluation of [(11)C]PyrATP-1, a novel radiotracer for PET imaging of glycogen synthase kinase-3beta (GSK-3beta). *Nucl Med Biol* **2014**, *41* (6), 507-12.

Conover, J. C.; Yancopoulos, G. D., Neurotrophin regulation of the developing nervous system: analyses of knockout mice. *Rev Neurosci* **1997**, *8* (1), 13-27.

Constandil, L.; Goich, M.; Hernandez, A.; Bourgeois, L.; Cazorla, M.; Hamon, M.; Villanueva, L.; Pelissier, T., Cyclotraxin-B, a new TrkB antagonist, and glial blockade by propentofylline, equally prevent and reverse cold allodynia induced by BDNF or partial infraorbital nerve constriction in mice. *J Pain* **2012**, *13* (6), 579-89.

Conway, J. G.; McDonald, B.; Parham, J.; Keith, B.; Rusnak, D. W.; Shaw, E.; Jansen, M.; Lin, P.; Payne, A.; Crosby, R. M.; Johnson, J. H.; Frick, L.; Lin, M. H.; Depee, S.; Tadepalli, S.; Votta, B.; James, I.; Fuller, K.; Chambers, T. J.; Kull, F. C.; Chamberlain, S. D.; Hutchins, J. T., Inhibition of colony-stimulating-factor-1 signaling in vivo with the orally bioavailable cFMS kinase inhibitor GW2580. *Proc Natl Acad Sci U S A* **2005**, *102* (44), 16078-83.

Cooper, J. D.; Salehi, A.; Delcroix, J. D.; Howe, C. L.; Belichenko, P. V.; Chua-Couzens, J.; Kilbridge, J. F.; Carlson, E. J.; Epstein, C. J.; Mobley, W. C., Failed retrograde transport of NGF in a mouse model of Down's syndrome: reversal of cholinergic neurodegenerative phenotypes following NGF infusion. *Proc Natl Acad Sci U S A* **2001**, *98* (18), 10439-44.

Corbeil, C. R.; Englebienne, P.; Yannopoulos, C. G.; Chan, L.; Das, S. K.; Bilimoria, D.; L'Heureux, L.; Moitessier, N., Docking ligands into flexible and solvated macromolecules. 2. Development and application of fitted 1.5 to the virtual screening of potential HCV polymerase inhibitors. *J Chem Inf Model* **2008**, *48* (4), 902-9.

Cordon-Cardo, C.; O'Brien, J. P.; Casals, D.; Rittman-Grauer, L.; Biedler, J. L.; Melamed, M. R.; Bertino, J. R., Multidrug-resistance gene (P-glycoprotein) is expressed by endothelial cells at blood-brain barrier sites. *Proc Natl Acad Sci U S A* **1989**, *86* (2), 695-8.

Coulier, F.; Kumar, R.; Ernst, M.; Klein, R.; Martin-Zanca, D.; Barbacid, M., Human trk oncogenes activated by point mutation, in-frame deletion, and duplication of the tyrosine kinase domain. *Mol Cell Biol* **1990**, *10* (8), 4202-10.

Coulier, F.; Martinzanca, D.; Ernst, M.; Barbacid, M., Mechanism of Activation of the Human Trk Oncogene. *Molecular and Cellular Biology* **1989**, *9* (1), 15-23.

Counts, S. E.; Nadeem, M.; Wu, J.; Ginsberg, S. D.; Saragovi, H. U.; Mufson, E. J., Reduction of cortical TrkA but not p75(NTR) protein in early-stage Alzheimer's disease. *Ann Neurol* **2004**, *56* (4), 520-531.

Cozza, A.; Melissari, E.; Iacopetti, P.; Mariotti, V.; Tedde, A.; Nacmias, B.; Conte, A.; Sorbi, S.; Pellegrini, S., SNPs in neurotrophin system genes and Alzheimer's disease in an Italian population. *J Alzheimers Dis* **2008**, *15* (1), 61-70.

Croucher, J. L.; Iyer, R.; Li, N. X.; Molteni, V.; Loren, J.; Gordon, W. P.; Tuntland, T.; Liu, B.; Brodeur, G. M., TrkB inhibition by GNF-4256 slows growth and enhances chemotherapeutic efficacy in neuroblastoma xenografts. *Cancer Chemoth Pharm* **2015**, *75* (1), 131-141.

D

Dahlin, J. L.; Nissink, J. W.; Strasser, J. M.; Francis, S.; Higgins, L.; Zhou, H.; Zhang, Z.; Walters, M. A., PAINS in the assay: chemical mechanisms of assay interference and promiscuous enzymatic inhibition observed during a sulfhydryl-scavenging HTS. *J Med Chem* **2015**, *58* (5), 2091-113.

Davis, M. I.; Hunt, J. P.; Herrgard, S.; Ciceri, P.; Wodicka, L. M.; Pallares, G.; Hocker, M.; Treiber, D. K.; Zarrinkar, P. P., Comprehensive analysis of kinase inhibitor selectivity. *Nat Biotechnol* **2011**, *29* (11), 1046-51.

De Braud, F.; Niger, M.; Damian, S.; Bardazza, B.; Martinetti, A.; Pelosi, G.; Marrapese, G.; Palmeri, L.; Cerea, G.; Valtorta, E.; Veronese, S.; Sartore-Bianchi, A.; Ardini, E.; Isachi, A.; Martignoni, M.; Galvani, A.; Luo, D.; Yeh, L.; Senderowicz, A.; Siena, S., Alka-372-001: first-in-human, phase I study of entrectinib—an oral pan-trk, ROS1, and ALK inhibitor—in patients with advanced solid tumors with relevant molecular alterations. *J. Clin. Oncol.* **2015**, *33*, suppl; abstr 2517.

Dechant, G.; Barde, Y. A., The neurotrophin receptor p75(NTR): novel functions and implications for diseases of the nervous system. *Nature Neuroscience* **2002**, *5* (11), 1131-1136.

Deinhardt K, C. M., Trk Receptors. *Handb Exp Pharmacol.* **2014**, *220*, 103-119.

Deng, V.; Matagne, V.; Banine, F.; Frerking, M.; Ohliger, P.; Budden, S.; Pevsner, J.; Dissen, G. A.; Sherman, L. S.; Ojeda, S. R., FXD1 is an MeCP2 target gene overexpressed in the brains of Rett syndrome patients and Mecp2-null mice. *Hum Mol Genet* **2007**, *16* (6), 640-650.

Deo, A. K.; Theil, F. P.; Nicolas, J. M., Confounding Parameters in Preclinical Assessment of Blood-Brain Barrier Permeation: An Overview With Emphasis on Species Differences and Effect of Disease States. *Mol Pharmaceut* **2013**, *10* (5), 1581-1595.

Devi, L.; Ohno, M., TrkB reduction exacerbates Alzheimer's disease-like signaling aberrations and memory deficits without affecting beta-amyloidosis in 5XFAD mice. *Transl Psychiatry* **2015**, *5*, e562.

Di, L.; Rong, H. J.; Feng, B., Demystifying Brain Penetration in Central Nervous System Drug Discovery. *Journal of Medicinal Chemistry* **2013**, *56* (1), 2-12.

Dobrucki, L. W.; Sinusas, A. J., PET and SPECT in cardiovascular molecular imaging. *Nat Rev Cardiol* **2010**, *7* (1), 38-47.

Doebele, R. C.; Davis, L. E.; Vaishnavi, A.; Le, A. T.; Estrada-Bernal, A.; Keysar, S.; Jimeno, A.; Varella-Garcia, M.; Aisner, D. L.; Li, Y. L.; Stephens, J.; Morosini, D.; Tuch, B. B.; Fernandes, M.; Nanda, N.; Low, J. A., An Oncogenic NTRK Fusion in a Patient with Soft-Tissue Sarcoma with Response to the Tropomyosin-Related Kinase Inhibitor LOXO-101. *Cancer Discovery* **2015**, *5* (10), 1049-1057.

Doebele, R. C.; Davis, L. E.; Vaishnavi, A.; Le, A. T.; Estrada-Bernal, A.; Keysar, S.; Jimeno, A.; Varella-Garcia, M.; Aisner, D. L.; Li, Y.; Stephens, P. J.; Morosini, D.; Tuch, B. B.; Fernandes, M.; Nanda, N.; Low, J. A., An Oncogenic NTRK Fusion in a Patient with Soft-Tissue Sarcoma with Response to the Tropomyosin-Related Kinase Inhibitor LOXO-101. *Cancer Discov.* **2015**, *5* (10), 1049-1057.

Doi, H., Pd-mediated rapid cross-couplings using [(11) C]methyl iodide: groundbreaking labeling methods in (11) C radiochemistry. *J Labelled Comp Radiopharm* **2015**, *58* (3), 73-85.

Dolle, F., Fluorine-18-labelled fluoropyridines: advances in radiopharmaceutical design. *Curr Pharm Des* **2005**, *11* (25), 3221-35.

Donohue, S. R.; Halldin, C.; Schou, M.; Hong, J.; Phebus, L.; Chernet, E.; Hitchcock, S. A.; Gardinier, K. M.; Ruley, K. M.; Krushinski, J. H.; Schaus, J.; Pike, V. W., Radiolabeling of a high potency cannabinoid subtype-1 receptor ligand, N-(4-fluoro-benzyl)-4-(3-(piperidin-1-yl)-indole-1-sulfonyl)benzamide (PipISB), with carbon-11 or fluorine-18. *J Labelled Compd Rad* **2008**, *51* (3-4), 146-152.

Dorsey, S. G.; Renn, C. L.; Carim-Todd, L.; Barrick, C. A.; Bambrick, L.; Krueger, B. K.; Ward, C. W.; Tessarollo, L., In vivo restoration of physiological levels of truncated TrkB.T1 receptor rescues neuronal cell death in a trisomic mouse model. *Neuron* **2006**, *51* (1), 21-8.

Downward, J.; Parker, P.; Waterfield, M. D., Autophosphorylation Sites on the Epidermal Growth-Factor Receptor. *Nature* **1984**, *311* (5985), 483-485.

Drilon, A.; Li, G.; Dogan, S.; Gounder, M.; Shen, R.; Arcila, M.; Wang, L.; Hyman, D. M.; Hechtman, J.; Wei, G.; Cam, N. R.; Christiansen, J.; Luo, D.; Maneval, E. C.; Bauer, T.; Patel, M.; Liu, S. V.; Ou, S. H. I.; Farago, A.; Shaw, A.; Shoemaker, R. F.; Lim, J.; Hornby, Z.; Multani, P.; Ladanyi, M.; Berger, M.; Katabi, N.; Ghossein, R.; Ho, A. L., What hides behind the MASC: clinical response and acquired resistance to entrectinib after ETV6-NTRK3 identification in a mammary analogue secretory carcinoma (MASC). *Ann. Oncol.* **2016**, *27* (5), 920-926.

Du, X.; Hill, R. A., 7,8-Dihydroxyflavone as a pro-neurotrophic treatment for neurodevelopmental disorders. *Neurochem Int* **2015**, *89*, 170-80.

E

Ehrenkaufer, R. E.; Potocki, J. F.; Jewett, D. M., Simple synthesis of F-18-labeled 2-fluoro-2-deoxy-D-glucose: concise communication. *J Nucl Med* **1984**, *25* (3), 333-7.

Eide, F. F.; Vining, E. R.; Eide, B. L.; Zang, K. L.; Wang, X. Y.; Reichardt, L. F., Naturally occurring truncated trkB receptors have dominant inhibitory effects on brain-derived neurotrophic factor signaling. *Journal of Neuroscience* **1996**, *16* (10), 3123-3129.

Englebienne, P.; Moitessier, N., Docking ligands into flexible and solvated macromolecules. 5. Force-field-based prediction of binding affinities of ligands to proteins. *J Chem Inf Model* **2009**, *49* (11), 2564-71.

Eriksdotter Jonhagen, M.; Nordberg, A.; Amberla, K.; Backman, L.; Ebendal, T.; Meyerson, B.; Olson, L.; Seiger; Shigeta, M.; Theodorsson, E.; Viitanen, M.; Winblad, B.; Wahlund, L. O., Intracerebroventricular infusion of nerve growth factor in three patients with Alzheimer's disease. *Dement Geriatr Cogn Disord* **1998**, 9 (5), 246-57.

Esposito, D.; Patel, P.; Stephens, R. M.; Perez, P.; Chao, M. V.; Kaplan, D. R.; Hempstead, B. L., The cytoplasmic and transmembrane domains of the p75 and Trk a receptors regulate high affinity binding to nerve growth factor. *Journal of Biological Chemistry* **2001**, 276 (35), 32687-32695.

Euhus, D. M.; Timmons, C. F.; Tomlinson, G. E., ETV6-NTRK3—Trk-ing the primary event in human secretory breast cancer. *Cancer Cell* **2002**, 2 (5), 347-348.

Eumann, C. N. N.; Hooker, J. M.; Ritter, T., Concerted nucleophilic aromatic substitution with F-19(-) and F-18(-). *Nature* **2016**, 534 (7607), 369-373.

Evans, A. E.; Kisselbach, K. D.; Liu, X.; Eggert, A.; Ikegaki, N.; Camoratto, A. M.; Dionne, C.; Brodeur, G. M., Effect of CEP-751 (KT-6587) on neuroblastoma xenografts expressing TrkB. *Med Pediatr Oncol* **2001**, 36 (1), 181-184.

Evans, A. E.; Kisselbach, K. D.; Liu, X.; Eggert, A.; Ikegaki, N.; Camoratto, A. M.; Dionne, C.; Brodeur, G. M., Effect of CEP-751 (KT-6587) on neuroblastoma xenografts expressing TrkB. *Med. Pediatr. Oncol.* **2001**, 36 (1), 181-184.

Evans, A. E.; Kisselbach, K. D.; Yamashiro, D. J.; Ikegaki, N.; Camoratto, A. M.; Dionne, C. A.; Brodeur, G. M., Antitumor Activity of CEP-751 (KT-6587) on Human Neuroblastoma and Medulloblastoma Xenografts. *Clin. Cancer Res.* **1999**, 5 (11), 3594-3602.

F

Farago, A. F.; Le, L. P.; Zheng, Z.; Muzikansky, A.; Drilon, A.; Patel, M.; Bauer, T. M.; Liu, S. V.; Ou, S. H.; Jackman, D.; Costa, D. B.; Multani, P. S.; Li, G. G.; Hornby, Z.; Chow-Maneval, E.; Luo, D.; Lim, J. E.; Iafrate, A. J.; Shaw, A. T., Durable Clinical Response to Entrectinib in NTRK1-Rearranged Non-Small Cell Lung Cancer. *J Thorac Oncol* **2015**, 10 (12), 1670-4.

Farago, A. F.; Le, L. P.; Zheng, Z.; Muzikansky, A.; Drilon, A.; Patel, M.; Bauer, T. M.; Liu, S. V.; Ou, S.-H. I.; Jackman, D.; Costa, D. B.; Multani, P. S.; Li, G. G.; Hornby, Z.; Chow-Maneval, E.; Luo, D.; Lim, J. E.; Iafrate, A. J.; Shaw, A. T., Durable Clinical Response to Entrectinib in NTRK1-Rearranged Non-Small Cell Lung Cancer. *J. Thorac. Oncol.* **2015**, 10 (12), 1670-1674.

Farwell, M. D.; Pryma, D. A.; Mankoff, D. A., PET/CT Imaging in Cancer: Current Applications and Future Directions. *Cancer* **2014**, 120 (22), 3433-3445.

Fenner, B. M., Truncated TrkB: Beyond a dominant negative receptor. *Cytokine Growth F R* **2012**, 23 (1-2), 15-24.

Ferrer, I.; Marin, C.; Rey, M. J.; Ribalta, T.; Goutan, E.; Blanco, R.; Tolosa, E.; Marti, E., BDNF and full-length and truncated TrkB expression in Alzheimer disease. Implications in therapeutic strategies. *J Neuropath Exp Neur* **1999**, 58 (7), 729-739.

Franck, D.; Kniess, T.; Steinbach, J.; Zitzmann-Kolbe, S.; Friebe, M.; Dinkelborg, L. M.; Graham, K., Investigations into the synthesis, radiofluorination and conjugation of a new [F-18]fluorocyclobutyl prosthetic group and its in vitro stability using a tyrosine model system.

Bioorgan Med Chem **2013**, *21* (3), 643-652.

Frisen, J.; Verge, V. M. K.; Fried, K.; Risling, M.; Persson, H.; Trotter, J.; Hokfelt, T.; Lindholm, D., Characterization of Glial TrkB Receptors - Differential Response to Injury in the Central and Peripheral Nervous Systems. *P Natl Acad Sci USA* **1993**, *90* (11), 4971-4975.

Fumagalli, F.; Racagni, G.; Riva, M. A., Shedding light into the role of BDNF in the pharmacotherapy of Parkinson's disease. *Pharmacogenomics J* **2006**, *6* (2), 95-104.

Furuya, N.; Momose, T.; Katsuno, K.; Fushimi, N.; Muranaka, H.; Handa, C.; Ozawa, T.; Kinoshita, T., The juxtamembrane region of TrkA kinase is critical for inhibitor selectivity. *Bioorg Med Chem Lett* **2017**.

G

Gajiwala, K. S.; Wu, J. C.; Christensen, J.; Deshmukh, G. D.; Diehl, W.; DiNitto, J. P.; English, J. M.; Greig, M. J.; He, Y. A.; Jacques, S. L.; Lunney, E. A.; McTigue, M.; Molina, D.; Quenzer, T.; Wells, P. A.; Yu, X.; Zhang, Y.; Zou, A. H.; Emmett, M. R.; Marshall, A. G.; Zhang, H. M.; Demetri, G. D., KIT kinase mutants show unique mechanisms of drug resistance to imatinib and sunitinib in gastrointestinal stromal tumor patients. *P Natl Acad Sci USA* **2009**, *106* (5), 1542-1547.

Galan, J. F.; Brown, J.; Wildin, J. L.; Liu, Z.; Liu, D.; Moyna, G.; Pophristic, V., Intramolecular hydrogen bonding in ortho-substituted arylamide oligomers: a computational and experimental study of ortho-fluoro- and ortho-chloro-N-methylbenzamides. *J Phys Chem B* **2009**, *113* (38), 12809-15.

Gao, M.; Wang, M.; Zheng, Q. H., Synthesis of carbon-11-labeled isonicotinamides as new potential PET agents for imaging of GSK-3 enzyme in Alzheimer's disease. *Bioorg Med Chem Lett* **2017**, *27* (4), 740-743.

Garcia-Suarez, O.; Perez-Pinera, P.; Laura, R.; Germana, A.; Esteban, I.; Cabo, R.; Silos-Santiago, I.; Cobo, J. L.; Vega, J. A., TrkB is necessary for the normal development of the lung. *Resp Physiol Neurobi* **2009**, *167* (3), 281-291.

Garg, S.; Thopate, S. R.; Minton, R. C.; Black, K. W.; Lynch, A. J.; Garg, P. K., 3-Amino-4-(2-((4-[¹⁸F]fluorobenzyl)methylamino)methylphenylsulfanyl)benzotrile, an F-18 fluorobenzyl analogue of DASB: synthesis, in vitro binding, and in vivo biodistribution studies. *Bioconjug Chem* **2007**, *18* (5), 1612-8.

Garuti, L.; Roberti, M.; Bottegoni, G., Non-ATP Competitive Protein Kinase Inhibitors. *Curr. Med. Chem.* **2010**, *17* (25), 2804-2821.

Gauthier, L. R.; Charrin, B. C.; Borrell-Pages, M.; Dompierre, J. P.; Rangone, H.; Cordelieres, F. P.; De Mey, J.; MacDonald, M. E.; Lessmann, V.; Humbert, S.; Saudou, F., Huntingtin controls neurotrophic support and survival of neurons by enhancing BDNF vesicular transport along microtubules. *Cell* **2004**, *118* (1), 127-38.

Geiger, T. R.; Peeper, D. S., The neurotrophic receptor TrkB in anoikis resistance and metastasis: A prespective. *Cancer Research* **2005**, *65* (16), 7033-7036.

George, D. J.; Dionne, C. A.; Jani, J.; Angeles, T.; Murakata, C.; Lamb, J.; Isaacs, J. T., Sustained in vivo regression of Dunning H rat prostate cancers treated with combinations of androgen ablation and Trk tyrosine kinase inhibitors, CEP-751 (KT-6587) or CEP-701 (KT-

5555). *Cancer Res* **1999**, 59 (10), 2395-401.

Ghilardi, J. R.; Freeman, K. T.; Jimenez-Andrade, J. M.; Mantyh, W. G.; Bloom, A. P.; Kuskowski, M. A.; Mantyh, P. W., Administration of a tropomyosin receptor kinase inhibitor attenuates sarcoma-induced nerve sprouting, neuroma formation and bone cancer pain. *Mol Pain* **2010**, 6.

Gilissen, C.; Bormans, G.; de Groot, T.; Verbruggen, A., Synthesis of N-(2-[F-18]fluoroethyl)-N'-methylthiourea: a hydrogen peroxide scavenger. *J Labelled Compd Rad* **1998**, 41 (6), 491-502.

Gines, S.; Bosch, M.; Marco, S.; Gavalda, N.; Diaz-Hernandez, M.; Lucas, J. J.; Canals, J. M.; Alberch, J., Reduced expression of the TrkB receptor in Huntington's disease mouse models and in human brain. *European Journal of Neuroscience* **2006**, 23 (3), 649-658.

Ginsberg, S. D.; Che, S. L.; Wu, J.; Counts, S. E.; Mufson, E. J., Down regulation of trk but not p75(NTR) gene expression in single cholinergic basal forebrain neurons mark the progression of Alzheimer's disease. *Journal of Neurochemistry* **2006**, 97 (2), 475-487.

Glaser, M.; Arstad, E.; Gaeta, A.; Nairne, J.; Trigg, W.; Robins, E. G., Copper-mediated reduction of 2-[18F]fluoroethyl azide to 2-[18F]fluoroethylamine. *J Labelled Compd Rad* **2012**, 55 (9), 326-331.

Gomes, J. R.; Costa, J. T.; Melo, C. V.; Felizzi, F.; Monteiro, P.; Pinto, M. J.; Inacio, A. R.; Wieloch, T.; Almeida, R. D.; Graos, M.; Duarte, C. B., Excitotoxicity downregulates TrkB.FL signaling and upregulates the neuroprotective truncated TrkB receptors in cultured hippocampal and striatal neurons. *J Neurosci* **2012**, 32 (13), 4610-22.

Gong, Y.; Cao, P.; Yu, H. J.; Jiang, T., Crystal structure of the neurotrophin-3 and p75NTR symmetrical complex. *Nature* **2008**, 454 (7205), 789-93.

Green, A.; Li, Y.; Stachel, S. TrkA kinase inhibitors, compositions and methods thereof. WO2012125667, 2012.

Greenfield, N. J.; Swapna, G. V.; Huang, Y.; Palm, T.; Graboski, S.; Montelione, G. T.; Hitchcock-DeGregori, S. E., The structure of the carboxyl terminus of striated alpha-tropomyosin in solution reveals an unusual parallel arrangement of interacting alpha-helices. *Biochemistry* **2003**, 42 (3), 614-9.

Griesbach, G. S.; Hovda, D. A.; Gomez-Pinilla, F., Exercise-induced improvement in cognitive performance after traumatic brain injury in rats is dependent on BDNF activation. *Brain Research* **2009**, 1288, 105-115.

Gupta, V. K.; You, Y. Y.; Gupta, V. B.; Klistorner, A.; Graham, S. L., TrkB Receptor Signalling: Implications in Neurodegenerative, Psychiatric and Proliferative Disorders. *Int J Mol Sci* **2013**, 14 (5), 10122-10142.

H

Hamacher, K.; Coenen, H. H.; Stocklin, G., Efficient stereospecific synthesis of no-carrier-added 2-[18F]-fluoro-2-deoxy-D-glucose using aminopolyether supported nucleophilic substitution. *J Nucl Med* **1986**, 27 (2), 235-8.

Hammers, A.; Allom, R.; Koepp, M. J.; Free, S. L.; Myers, R.; Lemieux, L.; Mitchell, T. N.; Brooks, D. J.; Duncan, J. S., Three-dimensional maximum probability atlas of the human brain, with particular reference to the temporal lobe. *Hum Brain Mapp* **2003**, *19* (4), 224-47.

Haque, N. S.; Hlavin, M. L.; Fawcett, J. W.; Dunnett, S. B., The neurotrophin NT4/5, but not NT3, enhances the efficacy of nigral grafts in a rat model of Parkinson's disease. *Brain Res* **1996**, *712* (1), 45-52.

Hari, Sanjay B.; Merritt, Ethan A.; Maly, Dustin J., Sequence Determinants of a Specific Inactive Protein Kinase Conformation. *Chem. Biol.* **2013**, *20* (6), 806-815.

Hartmann, J. T.; Haap, M.; Kopp, H. G.; Lipp, H. P., Tyrosine kinase inhibitors - a review on pharmacology, metabolism and side effects. *Curr Drug Metab* **2009**, *10* (5), 470-81.

He, X. P.; Kotloski, R.; Nef, S.; Luikart, B. W.; Parada, L. F.; McNamara, J. O., Conditional deletion of TrkB but not BDNF prevents epileptogenesis in the kindling model. *Neuron* **2004**, *43* (1), 31-42.

Heffron, T. P., Small Molecule Kinase Inhibitors for the Treatment of Brain Cancer. *J Med Chem* **2016**, *59* (22), 10030-10066.

Heffron, T. P., Small Molecule Kinase Inhibitors for the Treatment of Brain Cancer. *J. Med. Chem.* **2016**.

Hefti, F. F.; Rosenthal, A.; Walicke, P. A.; Wyatt, S.; Vergara, G.; Shelton, D. L.; Davies, A. M., Novel class of pain drugs based on antagonism of NGF. *Trends Pharmacol Sci* **2006**, *27* (2), 85-91.

Hempstead, B. L.; Martin-Zanca, D.; Kaplan, D. R.; Parada, L. F.; Chao, M. V., High-affinity NGF binding requires coexpression of the trk proto-oncogene and the low-affinity NGF receptor. *Nature* **1991**, *350* (6320), 678-83.

Hetman, M.; Cavanaugh, J. E.; Kimelman, D.; Xia, Z., Role of glycogen synthase kinase-3beta in neuronal apoptosis induced by trophic withdrawal. *J Neurosci* **2000**, *20* (7), 2567-74.

Hicks, J. W.; VanBrocklin, H. F.; Wilson, A. A.; Houle, S.; Vasdev, N., Radiolabeled small molecule protein kinase inhibitors for imaging with PET or SPECT. *Molecules* **2010**, *15* (11), 8260-78.

Hisaoka, M.; Sheng, W. Q.; Tanaka, A.; Hashimoto, H., Gene expression of TrkC (NTRK3) in human soft tissue tumours. *Journal of Pathology* **2002**, *197* (5), 661-667.

Hitchcock, S. A., Structural modifications that alter the P-glycoprotein efflux properties of compounds. *J Med Chem* **2012**, *55* (11), 4877-95.

Hohn, A.; Leibrock, J.; Bailey, K.; Barde, Y. A., Identification and characterization of a novel member of the nerve growth factor/brain-derived neurotrophic factor family. *Nature* **1990**, *344* (6264), 339-41.

Holland, J. P.; Cumming, P.; Vasdev, N., PET radiopharmaceuticals for probing enzymes in the brain. *Am J Nucl Med Mol Imaging* **2013**, *3* (3), 194-216.

Holtzman, D. M.; Kilbridge, J.; Li, Y. W.; Cunningham, E. T.; Lenn, N. J.; Clary, D. O.; Reichardt, L. F.; Mobley, W. C., Trka Expression in the Cns - Evidence for the Existence of Several Novel Ngf-Responsive Cns Neurons. *Journal of Neuroscience* **1995**, *15* (2), 1567-1576.

Hong, D. S.; Brose, M. S.; Doebele, R. C.; Shaw, A. T.; Dowlati, A.; Bauer, T. M.; Farago, A. F.; Estrada-Bernal, A.; Lee, A. T.; Cox, M. C.; Nanda, N.; Low, J. A.; Burris, H. A., Abstract PR13: Clinical safety and activity from a phase 1 study of LOXO-101, a selective TRKA/B/C inhibitor, in solid-tumor patients with NTRK gene fusions. *Mol. Cancer Ther.* **2015**, *14* (12 Supplement 2), PR13-PR13.

Hong, S.; Kim, J.; Seo, J. H.; Jung, K. H.; Hong, S. S.; Hong, S., Design, Synthesis, and Evaluation of 3,5-Disubstituted 7-Azaindoles as Trk Inhibitors with Anticancer and Antiangiogenic Activities. *Journal of Medicinal Chemistry* **2012**, *55* (11), 5337-5349.

Huang, E. J.; Reichardt, L. F., Neurotrophins: roles in neuronal development and function. *Annu Rev Neurosci* **2001**, *24*, 677-736.

Huang, E. J.; Reichardt, L. F., Trk receptors: roles in neuronal signal transduction. *Annu Rev Biochem* **2003**, *72*, 609-42.

Huang, Y. Z.; Hernandez, F. J.; Gu, B.; Stockdale, K. R.; Nanapaneni, K.; Scheetz, T. E.; Behlke, M. A.; Peek, A. S.; Bair, T.; Giangrande, P. H.; McNamara, J. O., 2nd, RNA aptamer-based functional ligands of the neurotrophin receptor, TrkB. *Mol Pharmacol* **2012**, *82* (4), 623-35.

Hugenberg, V.; Riemann, B.; Hermann, S.; Schober, O.; Schafers, M.; Szardenings, K.; Lebedev, A.; Gangadharmath, U.; Kolb, H.; Walsh, J.; Zhang, W.; Kopka, K.; Wagner, S., Inverse 1,2,3-triazole-1-yl-ethyl substituted hydroxamates as highly potent matrix metalloproteinase inhibitors: (radio)synthesis, in vitro and first in vivo evaluation. *J Med Chem* **2013**, *56* (17), 6858-70.

Huse, M.; Kuriyan, J., The Conformational Plasticity of Protein Kinases. *Cell* **2002**, *109* (3), 275-282.

Hwang, D. R.; Simpson, N. R.; Montoya, J.; Man, J. J.; Laruelle, M., An improved one-pot procedure for the preparation of [¹¹C-carbonyl]-WAY100635. *Nucl Med Biol* **1999**, *26* (7), 815-9.

I

Ide, H.; Seligson, D. B.; Memarzadeh, S.; Xin, L.; Horvath, S.; Dubey, P.; Flick, M. B.; Kacinski, B. M.; Palotie, A.; Witte, O. N., Expression of colony-stimulating factor 1 receptor during prostate development and prostate cancer progression. *Proc Natl Acad Sci U S A* **2002**, *99* (22), 14404-9.

Indo, Y.; Tsuruta, M.; Hayashida, Y.; Karim, M. A.; Ohta, K.; Kawano, T.; Mitsubuchi, H.; Tonoki, H.; Awaya, Y.; Matsuda, I., Mutations in the TRKA/NGF receptor gene in patients with congenital insensitivity to pain with anhidrosis. *Nat Genet* **1996**, *13* (4), 485-8.

Ingraham, C. A.; Cox, M. E.; Ward, D. C.; Fults, D. W.; Maness, P. F., C-Src and Other Proto-Oncogenes Implicated in Neuronal Differentiation. *Mol Chem Neuropathol* **1989**, *10* (1), 1-14.

Iversen, L. L., Rita Levi-Montalcini: Neuroscientist par excellence. *P Natl Acad Sci USA* **2013**, *110* (13), 4862-4863.

Iwahara, T.; Fujimoto, J.; Wen, D. Z.; Cupples, R.; Bucay, N.; Arakawa, T.; Mori, S.; Ratzkin, B.; Yamamoto, T., Molecular characterization of ALK, a receptor tyrosine kinase expressed specifically in the nervous system. *Oncogene* **1997**, *14* (4), 439-449.

Iwata, R.; Ido, T.; Takahashi, T.; Nakanishi, H.; Iida, S., Optimization of [¹¹C]HCN production and no-carrier-added [¹¹C]amino acid synthesis. *Int J Rad Appl Instrum A* **1987**, *38* (2), 97-102.

Iyer, R.; Evans, A. E.; Qi, X.; Ho, R.; Minturn, J. E.; Zhao, H.; Balamuth, N.; Maris, J. M.; Brodeur, G. M., Lestaurtinib Enhances the Antitumor Efficacy of Chemotherapy in Murine Xenograft Models of Neuroblastoma. *Clin. Cancer Res.* **2010**, *16* (5), 1478-1485.

Iyer, R.; Wehrmann, L.; Golden, R. L.; Naraparaju, K.; Croucher, J. L.; MacFarland, S. P.; Guan, P.; Kolla, V.; Wei, G.; Cam, N.; Li, G.; Hornby, Z.; Brodeur, G. M., Entrectinib is a potent inhibitor of Trk-driven neuroblastomas in a xenograft mouse model. *Cancer Lett.* **2016**, *372* (2), 179-186.

J

J. Haas, S. W. A., Y. Jiang and G. Zhang, WO/2010/048314 A1; International application No. PCT/US2009/061519. **2010**, April 29.

Jacobson, O.; Mishani, E., [¹¹C]-dimethylamine as a labeling agent for PET biomarkers. *Appl Radiat Isot* **2008**, *66* (2), 188-93.

Jang, S. W.; Liu, X.; Chan, C. B.; France, S. A.; Sayeed, I.; Tang, W.; Lin, X.; Xiao, G.; Andero, R.; Chang, Q.; Ressler, K. J.; Ye, K., Deoxygedunin, a natural product with potent neurotrophic activity in mice. *PLoS One* **2010**, *5* (7), e11528.

Jang, S. W.; Liu, X.; Chan, C. B.; Weinshenker, D.; Hall, R. A.; Xiao, G.; Ye, K., Amitriptyline is a TrkA and TrkB receptor agonist that promotes TrkA/TrkB heterodimerization and has potent neurotrophic activity. *Chem Biol* **2009**, *16* (6), 644-56.

Jang, S. W.; Liu, X.; Pradoldej, S.; Tosini, G.; Chang, Q.; Iuvone, P. M.; Ye, K., N-acetylserotonin activates TrkB receptor in a circadian rhythm. *Proc Natl Acad Sci U S A* **2010**, *107* (8), 3876-81.

Jang, S. W.; Liu, X.; Yepes, M.; Shepherd, K. R.; Miller, G. W.; Liu, Y.; Wilson, W. D.; Xiao, G.; Bianchi, B.; Sun, Y. E.; Ye, K., A selective TrkB agonist with potent neurotrophic activities by 7,8-dihydroxyflavone. *Proc Natl Acad Sci U S A* **2010**, *107* (6), 2687-92.

Jewett, D. M., A simple synthesis of [¹¹C]methyl triflate. *Int J Rad Appl Instrum A* **1992**, *43* (11), 1383-5.

Jia, Y.; Yun, C. H.; Park, E.; Ercan, D.; Manuia, M.; Juarez, J.; Xu, C.; Rhee, K.; Chen, T.; Zhang, H.; Palakurthi, S.; Jang, J.; Lelais, G.; DiDonato, M.; Bursulaya, B.; Michellys, P. Y.; Epple, R.; Marsilje, T. H.; McNeill, M.; Lu, W.; Harris, J.; Bender, S.; Wong, K. K.; Janne, P. A.; Eck, M. J., Overcoming EGFR(T790M) and EGFR(C797S) resistance with mutant-selective allosteric inhibitors. *Nature* **2016**, *534* (7605), 129-32.

Johnson, T. W.; Richardson, P. F.; Bailey, S.; Brooun, A.; Burke, B. J.; Collins, M. R.; Cui, J. J.; Deal, J. G.; Deng, Y. L.; Dinh, D.; Engstrom, L. D.; He, M.; Hoffman, J.; Hoffman, R. L.; Huang, Q.; Kania, R. S.; Kath, J. C.; Lam, H.; Lam, J. L.; Le, P. T.; Lingardo, L.; Liu, W.; McTigue, M.; Palmer, C. L.; Sach, N. W.; Smeal, T.; Smith, G. L.; Stewart, A. E.; Timofeevski, S.; Zhu, H.; Zhu, J.; Zou, H. Y.; Edwards, M. P., Discovery of (10R)-7-amino-12-fluoro-2,10,16-trimethyl-15-oxo-10,15,16,17-tetrahydro-2H-8,4-(m etheno)pyrazolo[4,3-h][2,5,11]-benzoxadiazacyclotetradecine-3-carbonitrile (PF-06463922), a macrocyclic inhibitor of anaplastic lymphoma kinase (ALK) and c-ros oncogene 1 (ROS1) with preclinical brain exposure and broad-spectrum potency against ALK-resistant mutations. *J Med Chem* **2014**, *57* (11), 4720-44.

Johnson., J., Alkylquinoline and alkylquinazoline kinase modulators. US2006281772. **2006**.

Jones, K. R.; Reichardt, L. F., Molecular-Cloning of a Human Gene That Is a Member of the Nerve Growth-Factor Family. *P Natl Acad Sci USA* **1990**, *87* (20), 8060-8064.

Jovanovic, J. N.; Czernik, A. J.; Fienberg, A. A.; Greengard, P.; Sihra, T. S., Synapsins as mediators of BDNF-enhanced neurotransmitter release. *Nature Neuroscience* **2000**, *3* (4), 323-329.

K

Kaplan, D. R.; Hempstead, B. L.; Martinzanca, D.; Chao, M. V.; Parada, L. F., The Trk Protooncogene Product - a Signal Transducing Receptor for Nerve Growth-Factor. *Science* **1991**, *252* (5005), 554-558.

Kaplan, D. R.; Hempstead, B. L.; Martin-Zanca, D.; Chao, M. V.; Parada, L. F., The trk proto-oncogene product: a signal transducing receptor for nerve growth factor. *Science* **1991**, *252* (5005), 554-8.

Kaplan, D. R.; Martin-Zanca, D.; Parada, L. F., Tyrosine phosphorylation and tyrosine kinase activity of the trk proto-oncogene product induced by NGF. *Nature* **1991**, *350* (6314), 158-60.

Karaman, M. W.; Herrgard, S.; Treiber, D. K.; Gallant, P.; Atteridge, C. E.; Campbell, B. T.; Chan, K. W.; Ciceri, P.; Davis, M. I.; Edeen, P. T.; Faraoni, R.; Floyd, M.; Hunt, J. P.; Lockhart, D. J.; Milanov, Z. V.; Morrison, M. J.; Pallares, G.; Patel, H. K.; Pritchard, S.; Wodicka, L. M.; Zarrinkar, P. P., A quantitative analysis of kinase inhibitor selectivity. *Nat Biotechnol* **2008**, *26* (1), 127-32.

Khotskaya, Y. B.; Holla, V. R.; Farago, A. F.; Mills Shaw, K. R.; Meric-Bernstam, F.; Hong, D. S., Targeting TRK family proteins in cancer. *Pharmacol Ther* **2017**.

Kim, M. S.; Lee, W. S.; Jeong, J.; Kim, S. J.; Jin, W., Induction of metastatic potential by TrkB via activation of IL6/JAK2/STAT3 and PI3K/AKT signaling in breast cancer. *Oncotarget* **2015**, *6* (37), 40158-71.

Kim, S. H.; Tokarski, J. S.; Leavitt, K. J.; Fink, B. E.; Salvati, M. E.; Moquin, R.; Obermeier, M. T.; Trainor, G. L.; Vite, G. G.; Stadnick, L. K.; Lippy, J. S.; You, D.; Lorenzi, M. V.; Chen, P., Identification of 2-amino-5-(thioaryl)thiazoles as inhibitors of nerve growth factor receptor TrkA. *Bioorg Med Chem Lett* **2008**, *18* (2), 634-9.

Klein, R.; Conway, D.; Parada, L. F.; Barbacid, M., The Trkb Tyrosine Protein-Kinase Gene Codes for a 2nd Neurogenic Receptor That Lacks the Catalytic Kinase Domain. *Cell* **1990**, *61* (4), 647-656.

Klein, R.; Jing, S. Q.; Nanduri, V.; O'Rourke, E.; Barbacid, M., The Trk Protooncogene Encodes a Receptor for Nerve Growth-Factor. *Cell* **1991**, *65* (1), 189-197.

Klein, R.; Lamballe, F.; Bryant, S.; Barbacid, M., The Trkb Tyrosine Protein-Kinase Is a Receptor for Neurotrophin-4. *Neuron* **1992**, *8* (5), 947-956.

Klein, R.; Nanduri, V.; Jing, S. Q.; Lamballe, F.; Tapley, P.; Bryant, S.; Cordoncardo, C.; Jones, K. R.; Reichardt, L. F.; Barbacid, M., The Trkb Tyrosine Protein-Kinase Is a Receptor for Brain-Derived Neurotrophic Factor and Neurotrophin-3. *Cell* **1991**, *66* (2), 395-403.

Klein, R.; Parada, L. F.; Coulier, F.; Barbacid, M., Trkb, a Novel Tyrosine Protein-Kinase Receptor Expressed during Mouse Neural Development. *Embo Journal* **1989**, *8* (12), 3701-3709.

Klein, R.; Silos-Santiago, I.; Smeyne, R. J.; Lira, S. A.; Brambilla, R.; Bryant, S.; Zhang, L.; Snider, W. D.; Barbacid, M., Disruption of the neurotrophin-3 receptor gene *trkC* eliminates the muscle afferents and results in abnormal movements. *Nature* **1994**, 368 (6468), 249-51.

Klein, R.; Smeyne, R. J.; Wurst, W.; Long, L. K.; Auerbach, B. A.; Joyner, A. L.; Barbacid, M., Targeted disruption of the *trkB* neurotrophin receptor gene results in nervous system lesions and neonatal death. *Cell* **1993**, 75 (1), 113-22.

Knight, Z. A.; Shokat, K. M., Features of selective kinase inhibitors. *Chem Biol* **2005**, 12 (6), 621-637.

Ko, E.; Kamkaew, A.; Burgess, K., Small Molecule Ligands For Active Targeting Of *TrkC*-expressing Tumor Cells. *ACS Med Chem Lett* **2012**, 3 (12), 1008-1012.

Kopka, K.; Faust, A.; Keul, P.; Wagner, S.; Breyholz, H. J.; Holtke, C.; Schober, O.; Schafers, M.; Levkau, B., 5-Pyrrolidinylsulfanyl isatins as a potential tool for the molecular imaging of caspases in apoptosis. *Journal of Medicinal Chemistry* **2006**, 49 (23), 6704-6715.

Kumar, V.; Zhang, M. X.; Swank, M. W.; Kunz, J.; Wu, G. Y., Regulation of dendritic morphogenesis by Ras-PI3K-Akt-mTOR and Ras-MAPK signaling pathways. *J Neurosci* **2005**, 25 (49), 11288-99.

Kumata, K.; Yui, J.; Xie, L.; Zhang, Y.; Nengaki, N.; Fujinaga, M.; Yamasaki, T.; Shimoda, Y.; Zhang, M. R., Radiosynthesis and preliminary PET evaluation of glycogen synthase kinase 3 β (GSK-3 β) inhibitors containing [(11)C]methylsulfanyl, [(11)C]methylsulfinyl or [(11)C]methylsulfonyl groups. *Bioorg Med Chem Lett* **2015**, 25 (16), 3230-3.

L

Lagadec, C.; Meignan, S.; Adriaenssens, E.; Foveau, B.; Vanhecke, E.; Romon, R.; Toillon, R. A.; Oxombre, B.; Hondermarck, H.; Le Bourhis, X., *TrkA* overexpression enhances growth and metastasis of breast cancer cells. *Oncogene* **2009**, 28 (18), 1960-70.

Lamballe, F.; Klein, R.; Barbacid, M., *Trkc*, a New Member of the *Trk* Family of Tyrosine Protein-Kinases, Is a Receptor for Neurotrophin-3. *Cell* **1991**, 66 (5), 967-979.

Langstrom, B.; Antoni, G.; Gullberg, P.; Halldin, C.; Malmberg, P.; Nagren, K.; Rimland, A.; Svard, H., Synthesis of L- and D-[methyl-11C]methionine. *J Nucl Med* **1987**, 28 (6), 1037-40.

Laufer, R.; Forrest, B.; Li, S. W.; Liu, Y.; Sampson, P.; Edwards, L.; Lang, Y. H.; Awrey, D. E.; Mao, G. D.; Plotnikova, O.; Leung, G.; Hodgson, R.; Beletskaya, I.; Mason, J. M.; Luo, X. Y.; Wei, X.; Yao, Y.; Feher, M.; Ban, F. Q.; Kiarash, R.; Green, E.; Mak, T. W.; Pan, G. H.; Pauls, H. W., The Discovery of PLK4 Inhibitors: (E)-3-((1H-Indazol-6-yl)methylene)indolin-2-ones as Novel Antiproliferative Agents. *Journal of Medicinal Chemistry* **2013**, 56 (15), 6069-6087.

Laurent, D.; Eric, A.; Ikram El, Y.-B.; Xuefen Le, B.; Victor, N.; Hubert, H., Nerve Growth Factor Receptors and Signaling in Breast Cancer. *Curr. Cancer Drug Targets* **2004**, 4 (6), 463-470.

Lawn, S.; Krishna, N.; Pisklakova, A.; Qu, X.; Fenstermacher, D. A.; Fournier, M.; Vrionis, F. D.; Tran, N.; Chan, J. A.; Kenchappa, R. S.; Forsyth, P. A., Neurotrophin signaling via *TrkB* and *TrkC* receptors promotes the growth of brain tumor-initiating cells. *J Biol Chem* **2015**, 290 (6), 3814-24.

- Lee, E.; Hooker, J. M.; Ritter, T., Nickel-Mediated Oxidative Fluorination for PET with Aqueous [F-18] Fluoride. *J Am Chem Soc* **2012**, *134* (42), 17456-17458.
- Lee, E.; Kamlet, A. S.; Powers, D. C.; Neumann, C. N.; Boursalian, G. B.; Furuya, T.; Choi, D. C.; Hooker, J. M.; Ritter, T., A fluoride-derived electrophilic late-stage fluorination reagent for PET imaging. *Science* **2011**, *334* (6056), 639-42.
- Leibrock, J.; Lottspeich, F.; Hohn, A.; Hofer, M.; Hengerer, B.; Masiakowski, P.; Thoenen, H.; Barde, Y. A., Molecular cloning and expression of brain-derived neurotrophic factor. *Nature* **1989**, *341* (6238), 149-52.
- Lemaire, C.; Libert, L.; Plenevaux, A.; Aerts, J.; Franci, X.; Luxen, A., Fast and reliable method for the preparation of ortho- and para-[F-18]fluorobenzyl halide derivatives: Key intermediates for the preparation of no-carrier-added PET aromatic radiopharmaceuticals. *J Fluorine Chem* **2012**, *138*, 48-55.
- LeSauteur, L.; Wei, L.; Gibbs, B. F.; Saragovi, H. U., Small peptide mimics of nerve growth factor bind TrkA receptors and affect biological responses. *J Biol Chem* **1995**, *270* (12), 6564-9.
- Lever, S. Z.; Fan, K. H.; Lever, J. R., Tactics for preclinical validation of receptor-binding radiotracers. *Nucl Med Biol* **2017**, *44*, 4-30.
- Levi-Montalcini, R.; Booker, B., Destruction of the Sympathetic Ganglia in Mammals by an Antiserum to a Nerve-Growth Protein. *Proc Natl Acad Sci U S A* **1960**, *46* (3), 384-91.
- Levi-Montalcini, R.; Booker, B., Excessive Growth of the Sympathetic Ganglia Evoked by a Protein Isolated from Mouse Salivary Glands. *Proc Natl Acad Sci U S A* **1960**, *46* (3), 373-84.
- Levi-Montalcini, R.; Cohen, S., In Vitro and in Vivo Effects of a Nerve Growth-Stimulating Agent Isolated from Snake Venom. *Proc Natl Acad Sci U S A* **1956**, *42* (9), 695-9.
- Levin, C. S., Primer on molecular imaging technology. *Eur J Nucl Med Mol Imaging* **2005**, *32* Suppl 2, S325-45.
- Levitzki, A., Tyrosine kinase inhibitors: views of selectivity, sensitivity, and clinical performance. *Annu Rev Pharmacol Toxicol* **2013**, *53*, 161-85.
- Lewis, C. E.; Pollard, J. W., Distinct role of macrophages in different tumor microenvironments. *Cancer Research* **2006**, *66* (2), 605-612.
- Lewis, R. T.; Bode, C. M.; Choquette, D. M.; Potashman, M.; Romero, K.; Stellwagen, J. C.; Teffera, Y.; Moore, E.; Whittington, D. A.; Chen, H.; Epstein, L. F.; Emkey, R.; Andrews, P. S.; Yu, V. L.; Saffran, D. C.; Xu, M.; Drew, A.; Merkel, P.; Szilvassy, S.; Brake, R. L., The Discovery and Optimization of a Novel Class of Potent, Selective, and Orally Bioavailable Anaplastic Lymphoma Kinase (ALK) Inhibitors with Potential Utility for the Treatment of Cancer. *J. Med. Chem.* **2012**, *55* (14), 6523-6540.
- Li, L.; Shao, X.; Cole, E. L.; Ohnmacht, S. A.; Ferrari, V.; Hong, Y. T.; Williamson, D. J.; Fryer, T. D.; Quesada, C. A.; Sherman, P.; Riss, P. J.; Scott, P. J.; Aigbirhio, F. I., Synthesis and Initial in Vivo Studies with [(11)C]SB-216763: The First Radiolabeled Brain Penetrative Inhibitor of GSK-3. *ACS Med Chem Lett* **2015**, *6* (5), 548-52.
- Li, N.; Liu, G. T., The novel squamosamide derivative FLZ enhances BDNF/TrkB/CREB signaling and inhibits neuronal apoptosis in APP/PS1 mice. *Acta Pharmacol Sin* **2010**, *31*

(3), 265-272.

Liang, S. H.; Vasdev, N., Total Radiosynthesis: Thinking outside "the box". *Aust J Chem* **2015**, *68* (9), 1319-1328.

Liang, S.; Chen, J. S.; Normandin, M.; Collier, T.; Perlis, R.; Holson, E.; Haggarty, S.; El Fakhri, G.; Kurumbail, R.; Vasdev, N., Discovery of [C-11]PF-367 for neuroimaging of glycogen synthase kinase 3. *Journal of Nuclear Medicine* **2015**, *56* (3).

Link, J. M.; Krohn, K. A.; Clark, J. C., Production of [11C]CH3I by single pass reaction of [11C]CH4 with I2. *Nucl Med Biol* **1997**, *24* (1), 93-7.

Lippa, B.; Morris, J.; Corbett, M.; Kwan, T. A.; Noe, M. C.; Snow, S. L.; Gant, T. G.; Mangiaracina, M.; Coffey, H. A.; Foster, B.; Knauth, E. A.; Wessel, M. D., Discovery of novel isothiazole inhibitors of the TrkA kinase: Structure-activity relationship, computer modeling, optimization, and identification of highly potent antagonists. *Bioorg Med Chem Lett* **2006**, *16* (13), 3444-3448.

Liu, C.; Chan, C. B.; Ye, K., 7,8-dihydroxyflavone, a small molecular TrkB agonist, is useful for treating various BDNF-implicated human disorders. *Transl Neurodegener* **2016**, *5*, 2.

Liu, J. J.; Dermatakis, A.; Lukacs, C.; Konzelmann, F.; Chen, Y.; Kammlott, U.; Depinto, W.; Yang, H.; Yin, X. F.; Chen, Y. S.; Schutt, A.; Simcox, M. E.; Luk, K. C., 3,5,6-trisubstituted naphthostyrils as CDK2 inhibitors. *Bioorg Med Chem Lett* **2003**, *13* (15), 2465-2468.

Liu, X.; Chan, C. B.; Jang, S. W.; Pradoldej, S.; Huang, J.; He, K.; Phun, L. H.; France, S.; Xiao, G.; Jia, Y.; Luo, H. R.; Ye, K., A synthetic 7,8-dihydroxyflavone derivative promotes neurogenesis and exhibits potent antidepressant effect. *J Med Chem* **2010**, *53* (23), 8274-86.

Liu, X.; Chan, C. B.; Qi, Q.; Xiao, G.; Luo, H. R.; He, X.; Ye, K., Optimization of a small tropomyosin-related kinase B (TrkB) agonist 7,8-dihydroxyflavone active in mouse models of depression. *J Med Chem* **2012**, *55* (19), 8524-37.

Liu, Y.; Gray, N. S., Rational design of inhibitors that bind to inactive kinase conformations. *Nat Chem Biol* **2006**, *2* (7), 358-64.

Longo, F. M.; Massa, S. M., Small-molecule modulation of neurotrophin receptors: a strategy for the treatment of neurological disease. *Nat Rev Drug Discov* **2013**, *12* (7), 507-25.

M

Mahringer, A.; Delzer, J.; Fricker, G., A fluorescence-based in vitro assay for drug interactions with breast cancer resistance protein (BCRP, ABCG2). *Eur J Pharm Biopharm* **2009**, *72* (3), 605-13.

Maliartchouk, S.; Feng, Y.; Ivanisevic, L.; Debeir, T.; Cuello, A. C.; Burgess, K.; Saragovi, H. U., A designed peptidomimetic agonistic ligand of TrkA nerve growth factor receptors. *Mol Pharmacol* **2000**, *57* (2), 385-91.

Manach, C.; Williamson, G.; Morand, C.; Scalbert, A.; Remesy, C., Bioavailability and bioefficacy of polyphenols in humans. I. Review of 97 bioavailability studies. *Am J Clin Nutr* **2005**, *81* (1 Suppl), 230S-242S.

Manning, G.; Whyte, D. B.; Martinez, R.; Hunter, T.; Sudarsanam, S., The protein kinase complement of the human genome. *Science* **2002**, *298* (5600), 1912-34.

Mantyh, P. W.; Koltzenburg, M.; Mendell, L. M.; Tive, L.; Shelton, D. L., Antagonism of Nerve Growth Factor-TrkA Signaling and the Relief of Pain. *Anesthesiology* **2011**, *115* (1), 189-204.

Marik, J.; Bohorquez, S. M.; Williams, S. P.; van Bruggen, N., New imaging paradigms in drug development: the PET imaging approach. *Drug Discov Today Technol* **2011**, *8* (2-4), e63-9.

Marsault, E.; Peterson, M. L., Macrocycles are great cycles: applications, opportunities, and challenges of synthetic macrocycles in drug discovery. *J Med Chem* **2011**, *54* (7), 1961-2004.

Marshall, J. L.; Kindler, H.; Deeken, J.; Bhargava, P.; Vogelzang, N. J.; Rizvi, N.; Luhtala, T.; Boylan, S.; Dordal, M.; Robertson, P.; Hawkins, M. J.; Ratain, M. J., Phase I trial of orally administered CEP-701, a novel neurotrophin receptor-linked tyrosine kinase inhibitor. *Invest New Drugs* **2005**, *23* (1), 31-7.

Martignoni, M.; Groothuis, G. M. M.; de Kanter, R., Species differences between mouse, rat, dog, monkey and human CYP-mediated drug metabolism, inhibition and induction. *Expert Opin Drug Met* **2006**, *2* (6), 875-894.

Martinowich, K.; Manji, H.; Lu, B., New insights into BDNF function in depression and anxiety. *Nat Neurosci* **2007**, *10* (9), 1089-93.

Martins-de-Souza, D.; Carvalho, P. C.; Schmitt, A.; Junqueira, M.; Nogueira, F. C.; Turck, C. W.; Domont, G. B., Deciphering the human brain proteome: characterization of the anterior temporal lobe and corpus callosum as part of the Chromosome 15-centric Human Proteome Project. *J Proteome Res* **2014**, *13* (1), 147-57.

Martinzanca, D.; Barbacid, M.; Parada, L. F., Expression of the Trk Protooncogene Is Restricted to the Sensory Cranial and Spinal Ganglia of Neural Crest Origin in Mouse Development. *Gene Dev* **1990**, *4* (5), 683-694.

Martin-Zanca, D.; Hughes, S. H.; Barbacid, M., A human oncogene formed by the fusion of truncated tropomyosin and protein tyrosine kinase sequences. *Nature* **1986**, *319* (6056), 743-8.

Mashhoon, N.; DeMaggio, A. J.; Tereshko, V.; Bergmeier, S. C.; Egli, R.; Hoekstra, M. F.; Kuret, J., Crystal structure of a conformation-selective casein kinase-1 inhibitor. *Journal of Biological Chemistry* **2000**, *275* (26), 20052-20060.

Massa, S. M.; Yang, T.; Xie, Y. M.; Shi, J.; Bilgen, M.; Joyce, J. N.; Nehama, D.; Rajadas, J.; Longo, F. M., Small molecule BDNF mimetics activate TrkB signaling and prevent neuronal degeneration in rodents. *Journal of Clinical Investigation* **2010**, *120* (5), 1774-1785.

Massa, S. M.; Yang, T.; Xie, Y.; Shi, J.; Bilgen, M.; Joyce, J. N.; Nehama, D.; Rajadas, J.; Longo, F. M., Small molecule BDNF mimetics activate TrkB signaling and prevent neuronal degeneration in rodents. *J Clin Invest* **2010**, *120* (5), 1774-85.

Massaweh, G.; Schirmacher, E.; la Fougere, C.; Kovacevic, M.; Wangler, C.; Jolly, D.; Gravel, P.; Reader, A. J.; Thiel, A.; Schirmacher, R., Improved work-up procedure for the production of [(18)F]flumazenil and first results of its use with a high-resolution research tomograph in human stroke. *Nucl Med Biol* **2009**, *36* (7), 721-7.

Matsumoto, K.; Wada, R. K.; Yamashiro, J. M.; Kaplan, D. R.; Thiele, C. J., Expression of brain-derived neurotrophic factor and p145TrkB affects survival, differentiation, and invasiveness of human neuroblastoma cells. *Cancer Res* **1995**, *55* (8), 1798-806.

Matthews, P. M.; Rabiner, E. A.; Passchier, J.; Gunn, R. N., Positron emission tomography molecular imaging for drug development. *Br J Clin Pharmacol* **2012**, *73* (2), 175-86.

McArthur, J. C.; Yiannoutsos, C.; Simpson, D. M.; Adornato, B. T.; Singer, E. J.; Hollander, H.; Marra, C.; Rubin, M.; Cohen, B. A.; Tucker, T.; Navia, B. A.; Schifitto, G.; Katzenstein, D.; Rask, C.; Zaborski, L.; Smith, M. E.; Shriver, S.; Millar, L.; Clifford, D. B.; Karalnik, I. J., A phase II trial of nerve growth factor for sensory neuropathy associated with HIV infection. AIDS Clinical Trials Group Team 291. *Neurology* **2000**, *54* (5), 1080-8.

McCarthy, C.; Walker, E., Tropomyosin receptor kinase inhibitors: a patent update 2009 – 2013. *Expert Opin. Ther. Pat.* **2014**, *24* (7), 731-744.

McCarthy, C.; Walker, E., Tropomyosin receptor kinase inhibitors: a patent update 2009-2013. *Expert Opinion on Therapeutic Patents* **2014**, *24* (7), 731-744.

McDonald, N. Q.; Lapatto, R.; Murray-Rust, J.; Gunning, J.; Wlodawer, A.; Blundell, T. L., New protein fold revealed by a 2.3-Å resolution crystal structure of nerve growth factor. *Nature* **1991**, *354* (6352), 411-4.

McKelvey, L.; Shorten, G. D.; O'Keeffe, G. W., Nerve growth factor-mediated regulation of pain signalling and proposed new intervention strategies in clinical pain management. *J. Neurochem.* **2013**, *124* (3), 276-289.

McMahon, S. B.; Bennett, D. L.; Priestley, J. V.; Shelton, D. L., The biological effects of endogenous nerve growth factor on adult sensory neurons revealed by a trkA-IgG fusion molecule. *Nat Med* **1995**, *1* (8), 774-80.

McNamee, K. E.; Burleigh, A.; Gompels, L. L.; Feldmann, M.; Allen, S. J.; Williams, R. O.; Dawbarn, D.; Vincent, T. L.; Inglis, J. J., Treatment of murine osteoarthritis with TrkAd5 reveals a pivotal role for nerve growth factor in non-inflammatory joint pain. *Pain* **2010**, *149* (2), 386-92.

Meakin, S. O.; Shooter, E. M., Molecular Investigations on the High-Affinity Nerve Growth-Factor Receptor. *Neuron* **1991**, *6* (1), 153-163.

Medico, E.; Russo, M.; Picco, G.; Cancelliere, C.; Valtorta, E.; Corti, G.; Buscarino, M.; Isella, C.; Lamba, S.; Martinoglio, B.; Veronese, S.; Siena, S.; Sartore-Bianchi, A.; Beccuti, M.; Mottolise, M.; Linnebacher, M.; Cordero, F.; Di Nicolantonio, F.; Bardelli, A., The molecular landscape of colorectal cancer cell lines unveils clinically actionable kinase targets. *Nat Commun* **2015**, *6*, 7002.

Medves, S.; Demoulin, J. B., Tyrosine kinase gene fusions in cancer: translating mechanisms into targeted therapies. *J Cell Mol Med* **2012**, *16* (2), 237-48.

Memon, A. A.; Jakobsen, S.; Dagnaes-Hansen, F.; Sorensen, B. S.; Keiding, S.; Nexø, E., Positron emission tomography (PET) imaging with [¹¹C]-labeled erlotinib: a micro-PET study on mice with lung tumor xenografts. *Cancer Res* **2009**, *69* (3), 873-8.

Memon, A. A.; Weber, B.; Winterdahl, M.; Jakobsen, S.; Meldgaard, P.; Madsen, H. H. T.; Keiding, S.; Nexø, E.; Sorensen, B. S., PET imaging of patients with non-small cell lung cancer employing an EGF receptor targeting drug as tracer. *Brit J Cancer* **2011**, *105* (12), 1850-1855.

Meng, X.; Loo, B. W., Jr.; Ma, L.; Murphy, J. D.; Sun, X.; Yu, J., Molecular imaging with ¹¹C-PD153035 PET/CT predicts survival in non-small cell lung cancer treated with EGFR-TKI: a pilot study. *J Nucl Med* **2011**, *52* (10), 1573-9.

Meng, X.; Loo, B. W.; Ma, L.; Murphy, J. D.; Sun, X. D.; Yu, J. M., Molecular Imaging with C-11-PD153035 PET/CT Predicts Survival in Non-Small Cell Lung Cancer Treated with EGFR-TKI: A Pilot Study. *Journal of Nuclear Medicine* **2011**, *52* (10), 1573-1579.

Menichincheri, M.; Ardini, E.; Magnaghi, P.; Avanzi, N.; Banfi, P.; Bossi, R.; Buffa, L.; Canevari, G.; Ceriani, L.; Colombo, M.; Corti, L.; Donati, D.; Fasolini, M.; Felder, E.; Fiorelli, C.; Fiorentini, F.; Galvani, A.; Isacchi, A.; Borgia, A. L.; Marchionni, C.; Nesi, M.; Orrenius, C.; Panzeri, A.; Pesenti, E.; Rusconi, L.; Saccardo, M. B.; Vanotti, E.; Perrone, E.; Orsini, P., Discovery of Entrectinib: A New 3-Aminoindazole As a Potent Anaplastic Lymphoma Kinase (ALK), c-ros Oncogene 1 Kinase (ROS1), and Pan-Tropomyosin Receptor Kinases (Pan-TRKs) inhibitor. *J. Med. Chem.* **2016**, *59* (7), 3392-3408.

Menichincheri, M.; Ardini, E.; Magnaghi, P.; Avanzi, N.; Banfi, P.; Bossi, R.; Buffa, L.; Canevari, G.; Ceriani, L.; Colombo, M.; Corti, L.; Donati, D.; Fasolini, M.; Felder, E.; Fiorelli, C.; Fiorentini, F.; Galvani, A.; Isacchi, A.; Borgia, A. L.; Marchionni, C.; Nesi, M.; Orrenius, C.; Panzeri, A.; Pesenti, E.; Rusconi, L.; Saccardo, M. B.; Vanotti, E.; Perrone, E.; Orsini, P., Discovery of Entrectinib: A New 3-Aminoindazole As a Potent Anaplastic Lymphoma Kinase (ALK), c-ros Oncogene 1 Kinase (ROS1), and Pan-Tropomyosin Receptor Kinases (Pan-TRKs) inhibitor. *J Med Chem* **2016**, *59* (7), 3392-408.

Merlio, J. P.; Ernfors, P.; Jaber, M.; Persson, H., Molecular cloning of rat trkC and distribution of cells expressing messenger RNAs for members of the trk family in the rat central nervous system. *Neuroscience* **1992**, *51* (3), 513-32.

Mertens, F.; Johansson, B.; Fioretos, T.; Mitelman, F., The emerging complexity of gene fusions in cancer. *Nature Reviews Cancer* **2015**, *15* (6), 371-381.

Middlemas, D. S.; Lindberg, R. A.; Hunter, T., Trkb, a Neural Receptor Protein-Tyrosine Kinase - Evidence for a Full-Length and 2 Truncated Receptors. *Molecular and Cellular Biology* **1991**, *11* (1), 143-153.

Miller, P. W.; Long, N. J.; Vilar, R.; Gee, A. D., Synthesis of ¹¹C, ¹⁸F, ¹⁵O, and ¹³N radiolabels for positron emission tomography. *Angew Chem Int Ed Engl* **2008**, *47* (47), 8998-9033.

Minturn, J. E.; Evans, A. E.; Villablanca, J. G.; Yanik, G. A.; Park, J. R.; Shusterman, S.; Groshen, S.; Hellriegel, E. T.; Bensen-Kennedy, D.; Matthay, K. K.; Brodeur, G. M.; Maris, J. M., Phase I trial of lestaurtinib for children with refractory neuroblastoma: a new approaches to neuroblastoma therapy consortium study. *Cancer Chemother. Pharmacol.* **2011**, *68* (4), 1057-1065.

Miranda, C.; Greco, A.; Miele, C.; Pierotti, M. A.; Van Obberghen, E., IRS-1 and IRS-2 are recruited by TrkA receptor and oncogenic TRK-T1. *J Cell Physiol* **2001**, *186* (1), 35-46.

Mohammadi, M.; McMahon, G.; Sun, L.; Tang, C.; Hirth, P.; Yeh, B. K.; Hubbard, S. R.; Schlessinger, J., Structures of the tyrosine kinase domain of fibroblast growth factor receptor in complex with inhibitors. *Science* **1997**, *276* (5314), 955-960.

Mologni, L.; Rostagno, R.; Brussolo, S.; Knowles, P. P.; Kjaer, S.; Murray-Rust, J.; Rosso, E.; Zambon, A.; Scapozza, L.; McDonald, N. Q.; Lucchini, V.; Gambacorti-Passerini, C., Synthesis, structure-activity relationship and crystallographic studies of 3-substituted indolin-2-one RET inhibitors. *Bioorgan Med Chem* **2010**, *18* (4), 1482-1496.

Moon, B. S.; Kil, H. S.; Park, J. H.; Kim, J. S.; Park, J.; Chi, D. Y.; Lee, B. C.; Kim, S. E., Facile aromatic radiofluorination of [¹⁸F]flumazenil from diaryliodonium salts with evaluation of their stability and selectivity. *Org Biomol Chem* **2011**, *9* (24), 8346-55.

Morrison, K. B.; Tognon, C. E.; Garnett, M. J.; Deal, C.; Sorensen, P. H. B., ETV6-NTRK3 transformation requires insulin-like growth factor 1 receptor signaling and is associated with constitutive IRS-1 tyrosine phosphorylation. *Oncogene* **2002**, *21* (37), 5684-5695.

Mossine, A. V.; Brooks, A. F.; Makaravage, K. J.; Miller, J. M.; Ichiishi, N.; Sanford, M. S.; Scott, P. J., Synthesis of [¹⁸F]Arenes via the Copper-Mediated [¹⁸F]Fluorination of Boronic Acids. *Org Lett* **2015**, *17* (23), 5780-3.

Mourik, J. E. M.; Lubberink, M.; Klumpers, U. M. H.; Comans, E. F.; Lammertsma, A. A.; Boellaard, R., Partial volume corrected image derived input functions for dynamic PET brain studies: Methodology and validation for [¹¹C]-flumazenil. *Neuroimage* **2008**, *39* (3), 1041-1050.

Mourik, J. E. M.; Lubberink, M.; Schuitemaker, A.; Tolboom, N.; van Berckel, B. N. M.; Lammertsma, A. A.; Boellaard, R., Image-derived input functions for PET brain studies. *Eur J Nucl Med Mol I* **2009**, *36* (3), 463-471.

Mufson, E. J.; Counts, S. E.; Fahnestock, M.; Ginsberg, S. D., Cholinergic molecular substrates of mild cognitive impairment in the elderly. *Curr Alzheimer Res* **2007**, *4* (4), 340-350.

Mufson, E. J.; Li, J. M.; Sobreviela, T.; Kordower, J. H., Decreased trkA gene expression within basal forebrain neurons in Alzheimer's disease. *Neuroreport* **1996**, *8* (1), 25-29.

Muller, K.; Faeh, C.; Diederich, F., Fluorine in pharmaceuticals: Looking beyond intuition. *Science* **2007**, *317* (5846), 1881-1886.

Muller, S.; Chaikuad, A.; Gray, N. S.; Knapp, S., The ins and outs of selective kinase inhibitor development. *Nat Chem Biol* **2015**, *11* (11), 818-21.

Muragaki, Y.; Timothy, N.; Leight, S.; Hempstead, B. L.; Chao, M. V.; Trojanowski, J. Q.; Lee, V. M., Expression of trk receptors in the developing and adult human central and peripheral nervous system. *J Comp Neurol* **1995**, *356* (3), 387-97.

Murdoch, C.; Giannoudis, A.; Lewis, C. E., Mechanisms regulating the recruitment of macrophages into hypoxic areas of tumors and other ischemic tissues. *Blood* **2004**, *104* (8), 2224-34.

N

Nagahara, A. H.; Tuszynski, M. H., Potential therapeutic uses of BDNF in neurological and psychiatric disorders. *Nature Reviews Drug Discovery* **2011**, *10* (3), 209-219.

Nagasubramanian, R.; Wei, J.; Gordon, P.; Rastatter, J. C.; Cox, M. C.; Pappo, A., Infantile Fibrosarcoma With NTRK3-ETV6 Fusion Successfully Treated With the Tropomyosin-Related Kinase Inhibitor LOXO-101. *Pediatr. Blood Cancer* **2016**, *63* (8), 1468-1470.

Nakagawara , A.; Arima-Nakagawara , M.; Scavarda , N. J.; Azar , C. G.; Cantor , A. B.; Brodeur , G. M., Association between High Levels of Expression of the TRK Gene and Favorable Outcome in Human Neuroblastoma. *N. Engl. J. Med.* **1993**, 328 (12), 847-854.

Nakagawara, A., Trk receptor tyrosine kinases: A bridge between cancer and neural development. *Cancer Letters* **2001**, 169 (2), 107-114.

Nakagawara, A.; Azar, C. G.; Scavarda, N. J.; Brodeur, G. M., Expression and function of TRK-B and BDNF in human neuroblastomas. *Mol Cell Biol* **1994**, 14 (1), 759-67.

Nakagawara, A.; Azar, C. G.; Scavarda, N. J.; Brodeur, G. M., Expression and Function of Trk-B and Bdnf in Human Neuroblastomas. *Molecular and Cellular Biology* **1994**, 14 (1), 759-767.

Narayanan, R.; Yepuru, M.; Coss, C. C.; Wu, Z.; Bauler, M. N.; Barrett, C. M.; Mohler, M. L.; Wang, Y.; Kim, J.; Snyder, L. M.; He, Y.; Levy, N.; Miller, D. D.; Dalton, J. T., Discovery and preclinical characterization of novel small molecule TRK and ROS1 tyrosine kinase inhibitors for the treatment of cancer and inflammation. *PLoS One* **2013**, 8 (12), e83380.

Neelamegam, R.; Hellenbrand, T.; Schroeder, F. A.; Wang, C.; Hooker, J. M., Imaging evaluation of 5HT2C agonists, [(11)C]WAY-163909 and [(11)C]vabicaserin, formed by Pictet-Spengler cyclization. *J Med Chem* **2014**, 57 (4), 1488-94.

Nishijima, K.; Kuge, Y.; Seki, K.; Ohkura, K.; Motoki, N.; Nagatsu, K.; Tanaka, A.; Tsukamoto, E.; Tamaki, N., A simplified and improved synthesis of [11C]phosgene with iron and iron (III) oxide. *Nucl Med Biol* **2002**, 29 (3), 345-50.

Nishio, T., Sunohara, N.; Furukawa, S. , Neutrophin switching in spinal motoneurons of amyotrophic lateral sclerosis. *neuroreports* **1998**, 9, 1661-1665.

O

O'Brien, Z.; Moghaddam, M. F., Small molecule kinase inhibitors approved by the FDA from 2000 to 2011: a systematic review of preclinical ADME data. *Expert Opin Drug Met* **2013**, 9 (12), 1597-1612.

Okamura, K.; Harada, T.; Wang, S.; Ijichi, K.; Furuyama, K.; Koga, T.; Okamoto, T.; Takayama, K.; Yano, T.; Nakanishi, Y., Expression of TrkB and BDNF is associated with poor prognosis in non-small cell lung cancer. *Lung Cancer* **2012**, 78 (1), 100-6.

Osman, S.; Lundkvist, C.; Pike, V. W.; Halldin, C.; McCarron, J. A.; Swahn, C. G.; Ginovart, N.; Luthra, S. K.; Bench, C. J.; Grasby, P. M.; Wikstrom, H.; Barf, T.; Cliffe, I. A.; Fletcher, A.; Farde, L., Characterization of the radioactive metabolites of the 5-HT1A receptor radioligand, [O-methyl-11C]WAY-100635, in monkey and human plasma by HPLC: comparison of the behaviour of an identified radioactive metabolite with parent radioligand in monkey using PET. *Nucl Med Biol* **1996**, 23 (5), 627-34.

Otvos, L., Jr.; Wade, J. D., Current challenges in peptide-based drug discovery. *Front Chem* **2014**, 2, 62.

Otzen, T.; Wempe, E. G.; Kunz, B.; Bartels, R.; Lehwark-Yvetot, G.; Hansel, W.; Schaper, K. J.; Seydel, J. K., Folate-synthesizing enzyme system as target for development of inhibitors and inhibitor combinations against *Candida albicans*-synthesis and biological activity of new 2,4-diaminopyrimidines and 4'-substituted 4-aminodiphenyl sulfones. *J Med Chem* **2004**, 47 (1), 240-53.

Oyesiku, N. M.; Evans, C. O.; Houston, S.; Darrell, R. S.; Smith, J. S.; Fulop, Z. L.; Dixon, C. E.; Stein, D. G., Regional changes in the expression of neurotrophic factors and their receptors following acute traumatic brain injury in the adult rat brain. *Brain Research* **1999**, *833* (2), 161-172.

Ozvegy-Laczka, C.; Cserepes, J.; Elkind, N. B.; Sarkadi, B., Tyrosine kinase inhibitor resistance in cancer: role of ABC multidrug transporters. *Drug Resist Update* **2005**, *8* (1-2), 15-26.

P

P. A. Albaugh, G. C., Y. Fan, B. T. Flatt, J. Loren, V. Molteni and J. M. Smith, WO/2012/034091 A1; International application No. PCT/US2011/051108. **2011**, *September 9*.

P. K. Sasmal, S. A., A. Tehim, V. Pradkar, P. Dattatreya and N. J. Mavinahalli, WO/2013/088256 A1; International application No. PCT/IB2012/003013. **2013**, *June 20*.

Parent, M.; Bedard, M. A.; Aliaga, A.; Soucy, J. P.; St-Pierre, E. L.; Cyr, M.; Kostikov, A.; Schirmmacher, E.; Massarweh, G.; Rosa-Neto, P., PET imaging of cholinergic deficits in rats using [¹⁸F]fluoroethoxybenzovesamicol ([¹⁸F]FEOBV). *Neuroimage* **2012**, *62* (1), 555-561.

Park, H.; Poo, M. M., Neurotrophin regulation of neural circuit development and function. *Nature Reviews Neuroscience* **2013**, *14* (1), 7-23.

Passiglia, F.; Caparica, R.; Giovannetti, E.; Giallombardo, M.; Listi, A.; Diana, P.; Cirrincione, G.; Caglevic, C.; Raez, L. E.; Russo, A.; Rolfo, C., The potential of neurotrophic tyrosine kinase (NTRK) inhibitors for treating lung cancer. *Expert Opin Investig Drugs* **2016**, *25* (4), 385-92.

Patel, M. R.; Bauer, T. M.; Liu, S. V.; Drilon, A. E.; Wheler, J. J.; Shaw, A. T.; Farago, A. F.; Ou, S.-H. I.; Luo, D.; Yeh, L.; Hornby, Z.; Senderowicz, A. M.; Lim, J., STARTRK-1: Phase 1/2a study of entrectinib, an oral Pan-Trk, ROS1, and ALK inhibitor, in patients with advanced solid tumors with relevant molecular alterations. *J. Clin. Oncol.* **2015**, *33*, suppl; abstr 2596.

Paterson, L. M.; Kornum, B. R.; Nutt, D. J.; Pike, V. W.; Knudsen, G. M., 5-HT radioligands for human brain imaging with PET and SPECT. *Med Res Rev* **2013**, *33* (1), 54-111.

Pattarawarapan, M.; Burgess, K., Molecular basis of neurotrophin-receptor interactions. *J Med Chem* **2003**, *46* (25), 5277-91.

Pattarawarapan, M.; Zaccaro, M. C.; Saragovi, U. H.; Burgess, K., New templates for syntheses of ring-fused, C-10 beta-turn peptidomimetics leading to the first reported small-molecule mimic of neurotrophin-3. *Journal of Medicinal Chemistry* **2002**, *45* (20), 4387-4390.

Peng, X.; Greene, L. A.; Kaplan, D. R.; Stephens, R. M., Deletion of a conserved juxtamembrane sequence in Trk abolishes NGF-promoted neuritogenesis. *Neuron* **1995**, *15* (2), 395-406.

Perreault, M.; Feng, G.; Will, S.; Gareski, T.; Kubasiak, D.; Marquette, K.; Vugmeyster, Y.; Unger, T. J.; Jones, J.; Qadri, A.; Hahm, S.; Sun, Y.; Rohde, C. M.; Zwijnenberg, R.; Paulsen, J.; Gimeno, R. E., Activation of TrkB with TAM-163 Results in Opposite Effects on Body Weight in Rodents and Non-Human Primates. *PLoS One* **2013**, *8* (5), e62616.

Petrulli, J. R.; Sullivan, J. M.; Zheng, M. Q.; Bennett, D. C.; Charest, J.; Huang, Y.; Morris, E. D.; Contessa, J. N., Quantitative analysis of [¹¹C]-erlotinib PET demonstrates specific binding for activating mutations of the EGFR kinase domain. *Neoplasia* **2013**, *15* (12), 1347-53.

Pettersson, M.; Hou, X. J.; Kuhn, M.; Wager, T. T.; Kauffman, G. W.; Verhoest, P. R., Quantitative Assessment of the Impact of Fluorine Substitution on P-Glycoprotein (P-gp) Mediated Efflux, Permeability, Lipophilicity, and Metabolic Stability. *Journal of Medicinal Chemistry* **2016**, *59* (11), 5284-5296.

Petty, B. G.; Cornblath, D. R.; Adornato, B. T.; Chaudhry, V.; Flexner, C.; Wachsman, M.; Sinicropi, D.; Burton, L. E.; Peroutka, S. J., The effect of systemically administered recombinant human nerve growth factor in healthy human subjects. *Ann Neurol* **1994**, *36* (2), 244-6.

Pez, D.; Leal, I.; Zuccotto, F.; Boussard, C.; Brun, R.; Croft, S. L.; Yardley, V.; Perez, L. M. R.; Pacanowska, D. G.; Gilbert, I. H., 2,4-diaminopyrimidines as inhibitors of leishmanial and trypanosomal dihydrofolate reductase. *Bioorgan Med Chem* **2003**, *11* (22), 4693-4711.

Piel, M.; Vernaleken, I.; Rosch, F., Positron emission tomography in CNS drug discovery and drug monitoring. *J Med Chem* **2014**, *57* (22), 9232-58.

Pike, V. W. A., F. I. , Reactions of cyclotron-produced [¹⁸F]fluoride with diaryliodonium salts—a novel single-step route to no-carrier-added [¹⁸F]fluoroarenes *J. Chem. Soc. Chem. Commun.* **1995**, *21*, 2215.

Pike, V. W., PET radiotracers: crossing the blood-brain barrier and surviving metabolism. *Trends Pharmacol Sci* **2009**, *30* (8), 431-40.

Pillai, A., Brain-derived neurotrophic factor/TrkB signaling in the pathogenesis and novel pharmacotherapy of schizophrenia. *Neurosignals* **2008**, *16* (2-3), 183-193.

Pixley, F. J.; Stanley, E. R., CSF-1 regulation of the wandering macrophage: complexity in action. *Trends Cell Biol* **2004**, *14* (11), 628-38.

Poduslo, J. F.; Curran, G. L., Permeability at the blood-brain and blood-nerve barriers of the neurotrophic factors: NGF, CNTF, NT-3, BDNF. *Brain Res Mol Brain Res* **1996**, *36* (2), 280-6.

Politis, M.; Piccini, P., Positron emission tomography imaging in neurological disorders. *J Neurol* **2012**, *259* (9), 1769-80.

Pollock, J.; Borkin, D.; Lund, G.; Purohit, T.; Dyguda-Kazimierowicz, E.; Grembecka, J.; Cierpicki, T., Rational Design of Orthogonal Multipolar Interactions with Fluorine in Protein-Ligand Complexes. *J Med Chem* **2015**, *58* (18), 7465-74.

Prakash, C. R.; Theivendren, P.; Raja, S. , Indolin-2-ones in clinical trials as potential kinase inhibitors: a review. *Pharmacology & Pharmacy* **2012**, *3*, 62-71.

Preshlock, S.; Tredwell, M.; Gouverneur, V., (¹⁸F)-Labeling of Arenes and Heteroarenes for Applications in Positron Emission Tomography. *Chem Rev* **2016**, *116* (2), 719-66.

Pulciani, S.; Santos, E.; Lauver, A. V.; Long, L. K.; Aaronson, S. A.; Barbacid, M., Oncogenes in Solid Human-Tumors. *Nature* **1982**, *300* (5892), 539-542.

Purser, S.; Moore, P. R.; Swallow, S.; Gouverneur, V., Fluorine in medicinal chemistry. *Chem Soc Rev* **2008**, *37* (2), 320-30.

Pyonteck, S. M.; Gadea, B. B.; Wang, H. W.; Gocheva, V.; Hunter, K. E.; Tang, L. H.; Joyce, J. A., Deficiency of the macrophage growth factor CSF-1 disrupts pancreatic neuroendocrine tumor development. *Oncogene* **2012**, *31* (11), 1459-1467.

Q

Qaim, S. M., Cyclotron production of medical radionuclides. In *Handbook of Nuclear Chemistry, 2nd ed.*; Vertes, A., Nagy, S., Klencsar, Z., Lovas, R. G., Rösch, F., Eds.; Springer: Dordrecht, The Netherlands **2011**, 1903-1933.

Qian, M. D.; Zhang, J.; Tan, X. Y.; Wood, A.; Gill, D.; Cho, S., Novel agonist monoclonal antibodies activate TrkB receptors and demonstrate potent neurotrophic activities. *J Neurosci* **2006**, *26* (37), 9394-403.

R

Raab, S.; Plate, K. H., Different networks, common growth factors: shared growth factors and receptors of the vascular and the nervous system. *Acta Neuropathol* **2007**, *113* (6), 607-626.

Radziejewski, C.; Robinson, R. C.; DiStefano, P. S.; Taylor, J. W., Dimeric structure and conformational stability of brain-derived neurotrophic factor and neurotrophin-3. *Biochemistry* **1992**, *31* (18), 4431-6.

Ragsdale, C.; Woodgett, J., Neurobiology. trking neurotrophic receptors. *Nature* **1991**, *350* (6320), 660-1.

Rankovic, Z., CNS Drug Design: Balancing Physicochemical Properties for Optimal Brain Exposure. *Journal of Medicinal Chemistry* **2015**, *58* (6), 2584-2608.

Ranzi, V.; Meakin, S. O.; Miranda, C.; Mondellini, P.; Pierotti, M. A.; Greco, A., The signaling adapters fibroblast growth factor receptor substrate 2 and 3 are activated by the thyroid TRK oncoproteins. *Endocrinology* **2003**, *144* (3), 922-8.

Ray, M. T.; Weickert, C. S.; Webster, M. J., Decreased BDNF and TrkB mRNA expression in multiple cortical areas of patients with schizophrenia and mood disorders. *Transl Psychiat* **2014**, *4*.

Reddy, L. R.; Prashad, M., Asymmetric synthesis of 2-substituted pyrrolidines by addition of Grignard reagents to gamma-chlorinated N-tert-butanefulfinyl imine. *Chem Commun* **2010**, *46* (2), 222-224.

Redig, A. J.; Janne, P. A., Basket Trials and the Evolution of Clinical Trial Design in an Era of Genomic Medicine. *J Clin Oncol* **2015**, *33* (9), 975-+.

Reichardt, L. F., Neurotrophin-regulated signalling pathways. *Philos Trans R Soc Lond B Biol Sci* **2006**, *361* (1473), 1545-64.

Reinhart, V.; Bove, S. E.; Volfson, D.; Lewis, D. A.; Kleiman, R. J.; Lanz, T. A., Evaluation of TrkB and BDNF transcripts in prefrontal cortex, hippocampus, and striatum from subjects with schizophrenia, bipolar disorder, and major depressive disorder. *Neurobiol Dis* **2015**, *77*, 220-7.

- Ren, H.; Wey, H. Y.; Strebl, M.; Neelamegam, R.; Ritter, T.; Hooker, J. M., Synthesis and Imaging Validation of [F-18]MDL100907 Enabled by Ni-Mediated Fluorination. *Acs Chemical Neuroscience* **2014**, *5* (7), 611-615.
- Reuther, G. W.; Lambert, Q. T.; Caligiuri, M. A.; Der, C. J., Identification and Characterization of an Activating TrkA Deletion Mutation in Acute Myeloid Leukemia. *Mol. Cell. Biol.* **2000**, *20* (23), 8655-8666.
- Rex, C. S.; Lin, C. Y.; Kramar, E. A.; Chen, L. Y.; Gall, C. M.; Lynch, G., Brain-derived neurotrophic factor promotes long-term potentiation-related cytoskeletal changes in adult hippocampus. *J Neurosci* **2007**, *27* (11), 3017-29.
- Ricci, A.; Felici, L.; Mariotta, S.; Mannino, F.; Schmid, G.; Terzano, C.; Cardillo, G.; Amenta, F.; Bronzetti, E., Neurotrophin and neurotrophin receptor protein expression in the human lung. *Am J Resp Cell Mol* **2004**, *30* (1), 12-19.
- Riccio, A.; Pierchala, B. A.; Ciarallo, C. L.; Ginty, D. D., An NGF-TrkA-mediated retrograde signal to transcription factor CREB in sympathetic neurons. *Science* **1997**, *277* (5329), 1097-100.
- Robinson, R. C.; Radziejewski, C.; Spraggon, G.; Greenwald, J.; Kostura, M. R.; Burtnick, L. D.; Stuart, D. I.; Choe, S.; Jones, E. Y., The structures of the neurotrophin 4 homodimer and the brain-derived neurotrophic factor/neurotrophin 4 heterodimer reveal a common Trk-binding site. *Protein Sci* **1999**, *8* (12), 2589-97.
- Robinson, R. C.; Radziejewski, C.; Stuart, D. I.; Jones, E. Y., Structure of the brain-derived neurotrophic factor/neurotrophin 3 heterodimer. *Biochemistry* **1995**, *34* (13), 4139-46.
- Roccatò, E.; Miranda, C.; Ranzi, V.; Gishizki, M.; Pierotti, M. A.; Greco, A., Biological activity of the thyroid TRK-T3 oncogene requires signalling through Shc. *Br J Cancer* **2002**, *87* (6), 645-53.
- Romanczyk, T. B.; Weickert, C. S.; Webster, M. J.; Herman, M. M.; Akil, M.; Kleinman, J. E., Alterations in trkB mRNA in the human prefrontal cortex throughout the lifespan. *European Journal of Neuroscience* **2002**, *15* (2), 269-280.
- Rose, C. R.; Blum, R.; Pichler, B.; Lepier, A.; Kafitz, K. W.; Konnerth, A., Truncated TrkB-T1 mediates neurotrophin-evoked calcium signalling in glia cells. *Nature* **2003**, *426* (6962), 74-78.
- Rotstein, B. H.; Liang, S. H.; Holland, J. P.; Collier, T. L.; Hooker, J. M.; Wilson, A. A.; Vasdev, N., ¹¹C fixation: a renaissance in PET radiochemistry. *Chem Commun (Camb)* **2013**, *49* (50), 5621-9.
- Rotstein, B. H.; Liang, S. H.; Placzek, M. S.; Hooker, J. M.; Gee, A. D.; Dolle, F.; Wilson, A. A.; Vasdev, N., (11)C[double bond, length as m-dash]O bonds made easily for positron emission tomography radiopharmaceuticals. *Chem Soc Rev* **2016**, *45* (17), 4708-26.
- Rotstein, B. H.; Stephenson, N. A.; Vasdev, N.; Liang, S. H., Spirocyclic hypervalent iodine(III)-mediated radiofluorination of non-activated and hindered aromatics. *Nat Commun* **2014**, *5*.
- Rubin, B. P.; Chen, C.-J.; Morgan, T. W.; Xiao, S.; Grier, H. E.; Kozakewich, H. P.; Perez-Atayde, A. R.; Fletcher, J. A., Congenital Mesoblastic Nephroma t(12;15) Is Associated with ETV6-NTRK3 Gene Fusion: Cytogenetic and Molecular Relationship to Congenital (Infantile) Fibrosarcoma. *The American Journal of Pathology* **1998**, *153* (5), 1451-1458.

Rudin, M.; Weissleder, R., Molecular imaging in drug discovery and development. *Nature Reviews Drug Discovery* **2003**, *2* (2), 123-131.

Russo, M.; Misale, S.; Wei, G.; Siravegna, G.; Crisafulli, G.; Lazzari, L.; Corti, G.; Rospo, G.; Novara, L.; Mussolin, B.; Bartolini, A.; Cam, N.; Patel, R.; Yan, S.; Shoemaker, R.; Wild, R.; Di Nicolantonio, F.; Bianchi, A. S.; Li, G.; Siena, S.; Bardelli, A., Acquired Resistance to the TRK Inhibitor Entrectinib in Colorectal Cancer. *Cancer Discov.* **2016**, *6* (1), 36-44.

S

S. Allen, S. S. A., K. R. Condroski, J.; Haas, L. Huang, L.; Jiang, T. Kercher and J. Seo, WO/2011/006074 A1; International application No. PCT/US2010/041538. **2011**, *January 11*.

S. W. Andrews, J. H., Y. Jiang and G. Zhang, G. , WO/2010/033941; International application No. PCT/US2009/057726;. **2010**, (March 25).

S. W. Andrews, K. R. C., J. Haas, Y. Jiang, G. R. Kolakowski, J. Seo, H. Yang and Q. Zhao, WO/2011/146336 A1; International Application No. PCT/IB2012/003012. **2013**, *June 20*.

Saleem, A.; Searle, G. E.; Kenny, L. M.; Huiban, M.; Kozlowski, K.; Waldman, A. D.; Woodley, L.; Palmieri, C.; Lowdell, C.; Kaneko, T.; Murphy, P. S.; Lau, M. R.; Aboagye, E. O.; Coombes, R. C., Lapatinib access into normal brain and brain metastases in patients with Her-2 overexpressing breast cancer. *Ejnmami Res* **2015**, *5*.

Sampson, P. B.; Liu, Y.; Forrest, B.; Cumming, G.; Li, S. W.; Patel, N. K.; Edwards, L.; Laufer, R.; Feher, M.; Ban, F.; Awrey, D. E.; Mao, G.; Plotnikova, O.; Hodgson, R.; Beletskaya, I.; Mason, J. M.; Luo, X.; Nadeem, V.; Wei, X.; Kiarash, R.; Madeira, B.; Huang, P.; Mak, T. W.; Pan, G.; Pauls, H. W., The discovery of Polo-like kinase 4 inhibitors: identification of (1R,2S)-2-(3-((E)-4-(((cis)-2,6-dimethylmorpholino)methyl)styryl)-1H-indazol-6-yl)-5'-methoxyspiro[cyclopropane-1,3'-indolin]-2'-one (CFI-400945) as a potent, orally active antitumor agent. *J Med Chem* **2015**, *58* (1), 147-69.

Sampson, P. B.; Liu, Y.; Patel, N. K.; Feher, M.; Forrest, B.; Li, S. W.; Edwards, L.; Laufer, R.; Lang, Y.; Ban, F.; Awrey, D. E.; Mao, G.; Plotnikova, O.; Leung, G.; Hodgson, R.; Mason, J. M.; Wei, X.; Kiarash, R.; Green, E.; Qiu, W.; Chirgadze, N. Y.; Mak, T. W.; Pan, G.; Pauls, H. W., The discovery of Polo-like kinase 4 inhibitors: design and optimization of spiro[cyclopropane-1,3'[3H]indol]-2'(1'H).ones as orally bioavailable antitumor agents. *J Med Chem* **2015**, *58* (1), 130-46.

Sanchez-Ortiz, E.; Yui, D. S.; Song, D. L.; Li, Y.; Rubenstein, J. L.; Reichardt, L. F.; Parada, L. F., TrkA Gene Ablation in Basal Forebrain Results in Dysfunction of the Cholinergic Circuitry. *Journal of Neuroscience* **2012**, *32* (12), 4065-4079.

Santos, R.; Ursu, O.; Gaulton, A.; Bento, A. P.; Donadi, R. S.; Bologa, C. G.; Karlsson, A.; Al-Lazikani, B.; Hersey, A.; Oprea, T. I.; Overington, J. P., A comprehensive map of molecular drug targets. *Nat Rev Drug Discov* **2017**, *16* (1), 19-34.

Sarkisyan, K. S.; Yampolsky, I. V.; Solntsev, K. M.; Lukyanov, S. A.; Lukyanov, K. A.; Mishin, A. S., Tryptophan-based chromophore in fluorescent proteins can be anionic. *Sci Rep-Uk* **2012**, *2*.

Sartore-Bianchi, A.; Ardini, E.; Bosotti, R.; Amatu, A.; Valtorta, E.; Somaschini, A.; Radrizzani, L.; Palmeri, L.; Banfi, P.; Bonazzina, E.; Misale, S.; Marrapese, G.; Leone, A.; Alzani, R.; Luo, D.; Hornby, Z.; Lim, J.; Veronese, S.; Vanzulli, A.; Bardelli, A.; Martignoni, M.; Davite, C.; Galvani, A.; Isacchi, A.; Siena, S., Sensitivity to Entrectinib Associated With a Novel LMNA-NTRK1 Gene Fusion in Metastatic Colorectal Cancer. *J. Natl. Cancer Inst.* **2016**, *108* (1).

Savaskan, E.; Muller-Spahn, F.; Olivieri, G.; Bruttel, S.; Otten, U.; Rosenberg, C.; Hulette, C.; Hock, C., Alterations in trk A, trk B and trk C receptor immunoreactivities in parietal cortex and cerebellum in Alzheimer's disease. *Eur Neurol* **2000**, *44* (3), 172-80.

Scarpi, D.; Cirelli, D.; Matrone, C.; Castronovo, G.; Rosini, P.; Occhiato, E. G.; Romano, F.; Bartali, L.; Clemente, A. M.; Bottegoni, G.; Cavalli, A.; De Chiara, G.; Bonini, P.; Calissano, P.; Palamara, A. T.; Garaci, E.; Torcia, M. G.; Guarna, A.; Cozzolino, F., Low molecular weight, non-peptidic agonists of TrkA receptor with NGF-mimetic activity. *Cell Death Dis* **2012**, *3*, e339.

Schifitto, G.; Yiannoutsos, C.; Simpson, D. M.; Adornato, B. T.; Singer, E. J.; Hollander, H.; Marra, C. M.; Rubin, M.; Cohen, B. A.; Tucker, T.; Koranik, I. J.; Katzenstein, D.; Haidich, B.; Smith, M. E.; Shriver, S.; Millar, L.; Clifford, D. B.; McArthur, J. C.; Team, A. C. T. G., Long-term treatment with recombinant nerve growth factor for HIV-associated sensory neuropathy. *Neurology* **2001**, *57* (7), 1313-6.

Schneider, H. J., Hydrogen bonds with fluorine. Studies in solution, in gas phase and by computations, conflicting conclusions from crystallographic analyses. *Chemical Science* **2012**, *3* (5), 1381-1394.

Schneider, R.; Schweiger, M., A novel modular mosaic of cell adhesion motifs in the extracellular domains of the neurogenic trk and trkB tyrosine kinase receptors. *Oncogene* **1991**, *6* (10), 1807-11.

Schramm, A.; Schulte, J. H.; Astrahantseff, K.; Apostolov, O.; Limpt, V. v.; Sieverts, H.; Kuhfittig-Kulle, S.; Pfeiffer, P.; Versteeg, R.; Eggert, A., Biological effects of TrkA and TrkB receptor signaling in neuroblastoma. *Cancer Lett.* **2005**, *228* (1-2), 143-153.

Schramm, A.; Schulte, J. H.; Astrahantseff, K.; Apostolov, O.; Limpt, V.; Sieverts, H.; Kuhfittig-Kulle, S.; Pfeiffer, P.; Versteeg, R.; Eggert, A., Biological effects of TrkA and TrkB receptor signaling in neuroblastoma. *Cancer Lett* **2005**, *228* (1-2), 143-53.

Schratt, G. M.; Nigh, E. A.; Chen, W. G.; Hu, L.; Greenberg, M. E., BDNF regulates the translation of a select group of mRNAs by a mammalian target of rapamycin-phosphatidylinositol 3-kinase-dependent pathway during neuronal development. *J Neurosci* **2004**, *24* (33), 7366-77.

Scwab, G. M.; Fujioka, S.; Schmidt, C.; Li, Z.; Frederick, W. A.; Yang, W.; Yokoi, K.; Evans, D. B.; Abbruzzese, J. L.; Hess, K. R.; Zhang, W.; Fidler, I. J.; Chiao, P. J., Overexpression of tropomyosin-related kinase B in metastatic human pancreatic cancer cells. *Clin Cancer Res* **2005**, *11* (2 Pt 1), 440-9.

Scott, S. A.; Mufson, E. J.; Weingartner, J. A.; Skau, K. A.; Crutcher, K. A., Nerve Growth-Factor in Alzheimers-Disease - Increased Levels Throughout the Brain Coupled with Declines in Nucleus Basalis. *Journal of Neuroscience* **1995**, *15* (9), 6213-6221.

Shabbir, M.; Stuart, R., Lestaurtinib, a multitargeted tyrosinase kinase inhibitor: from bench to bedside. *Expert Opinion on Investigational Drugs* **2010**, *19* (3), 427-436.

Sharma, K.; Schmitt, S.; Bergner, C. G.; Tyanova, S.; Kannaiyan, N.; Manrique-Hoyos, N.; Kongi, K.; Cantuti, L.; Hanisch, U. K.; Philips, M. A.; Rossner, M. J.; Mann, M.; Simons, M., Cell type- and brain region-resolved mouse brain proteome. *Nat Neurosci* **2015**, *18* (12), 1819-31.

Shewchuk, L. M. H., A. M.; Holmes, W. D. , U.S. Pat. Appl. US 2.004.002.145 **2004**.

Shia, C. S.; Tsai, S. Y.; Kuo, S. C.; Hou, Y. C.; Chao, P. D., Metabolism and pharmacokinetics of 3,3',4',7-tetrahydroxyflavone (fisetin), 5-hydroxyflavone, and 7-hydroxyflavone and antihemolysis effects of fisetin and its serum metabolites. *J Agric Food Chem* **2009**, *57* (1), 83-9.

Shibayama, E.; Koizumi, H., Cellular localization of the Trk neurotrophin receptor family in human non-neuronal tissues. *Am J Pathol* **1996**, *148* (6), 1807-18.

Silhol, M.; Bonnichon, V.; Rage, F.; Tapia-Arancibia, L., Age-related changes in brain-derived neurotrophic factor and tyrosine kinase receptor isoforms in the hippocampus and hypothalamus in male rats. *Neuroscience* **2005**, *132* (3), 613-624.

Skerratt, S. E.; Andrews, M.; Bagal, S. K.; Bilsland, J.; Brown, D.; Bungay, P. J.; Cole, S.; Gibson, K. R.; Jones, R.; Morao, I.; Nedderman, A.; Omoto, K.; Robinson, C.; Ryckmans, T.; Skinner, K.; Stupple, P.; Waldron, G., The Discovery of a Potent, Selective, and Peripherally Restricted Pan-Trk Inhibitor (PF-06273340) for the Treatment of Pain. *Journal of Medicinal Chemistry* **2016**, *59* (22), 10084-10099.

Slobbe, P.; Poot, A. J.; Windhorst, A. D.; van Dongen, G. A., PET imaging with small-molecule tyrosine kinase inhibitors: TKI-PET. *Drug Discov Today* **2012**, *17* (21-22), 1175-87.

Smeyne, R. J.; Klein, R.; Schnapp, A.; Long, L. K.; Bryant, S.; Lewin, A.; Lira, S. A.; Barbacid, M., Severe sensory and sympathetic neuropathies in mice carrying a disrupted Trk/NGF receptor gene. *Nature* **1994**, *368* (6468), 246-9.

Snider, W. D., Functions of the Neurotrophins during Nervous-System Development - What the Knockouts Are Teaching Us. *Cell* **1994**, *77* (5), 627-638.

Stachel, S. J.; Sanders, J. M.; Henze, D. A.; Rudd, M. T.; Su, H. P.; Li, Y. W.; Nanda, K. K.; Egbertson, M. S.; Manley, P. J.; Jones, K. L. G.; Brnardic, E. J.; Green, A.; Grobler, J. A.; Hanney, B.; Leitl, M.; Lai, M. T.; Munshi, V.; Murphy, D.; Rickert, K.; Riley, D.; Krasowska-Zoladek, A.; Daley, C.; Zuck, P.; Kane, S. A.; Bilodeau, M. T., Maximizing Diversity from a Kinase Screen: Identification of Novel and Selective pan-Trk Inhibitors for Chronic Pain. *Journal of Medicinal Chemistry* **2014**, *57* (13), 5800-5816.

Stachel, S. J.; Sanders, J. M.; Henze, D. A.; Rudd, M. T.; Su, H.-P.; Li, Y.; Nanda, K. K.; Egbertson, M. S.; Manley, P. J.; Jones, K. L. G.; Brnardic, E. J.; Green, A.; Grobler, J. A.; Hanney, B.; Leitl, M.; Lai, M.-T.; Munshi, V.; Murphy, D.; Rickert, K.; Riley, D.; Krasowska-Zoladek, A.; Daley, C.; Zuck, P.; Kane, S. A.; Bilodeau, M. T., Maximizing Diversity from a Kinase Screen: Identification of Novel and Selective pan-Trk Inhibitors for Chronic Pain. *J. Med. Chem.* **2014**, *57* (13), 5800-5816.

Stenhagen, I. S.; Kirjavainen, A. K.; Forsback, S. J.; Jorgensen, C. G.; Robins, E. G.; Luthra, S. K.; Solin, O.; Gouverneur, V., [18F]fluorination of an arylboronic ester using [18F]selectfluor bis(triflate): application to 6-[18F]fluoro-L-DOPA. *Chem Commun (Camb)* **2013**, *49* (14), 1386-8.

Stephenson, N. A.; Holland, J. P.; Kassenbrock, A.; Yokell, D. L.; Livni, E.; Liang, S. H.; Vasdev, N., Iodonium ylide-mediated radiofluorination of 18F-FPEB and validation for human use. *J Nucl Med* **2015**, *56* (3), 489-92.

Stransky, N.; Cerami, E.; Schalm, S.; Kim, J. L.; Lengauer, C., The landscape of kinase fusions in cancer. *Nat Commun* **2014**, *5*.

Su, H. P.; Rickert, K.; Burlein, C.; Narayan, K.; Bukhtiyarova, M.; Hurzy, D. M.; Stump, C. A.; Zhang, X.; Reid, J.; Krasowska-Zoladek, A.; Tummala, S.; Shipman, J. M.; Kornienko, M.; Lemaire, P. A.; Krosky, D.; Heller, A.; Achab, A.; Chamberlin, C.; Saradjian, P.; Sauvagnat, B.; Yang, X.; Ziebell, M. R.; Nickbarg, E.; Sanders, J. M.; Bilodeau, M. T.; Carroll, S. S.; Lumb, K. J.; Soisson, S. M.; Henze, D. A.; Cooke, A. J., Structural characterization of nonactive site, TrkA-selective kinase inhibitors. *Proc Natl Acad Sci U S A* **2017**, *114* (3), E297-E306.

Sun, L.; Tran, N.; Tang, F.; App, H.; Hirth, P.; McMahon, G.; Tang, C., Synthesis and biological evaluations of 3-substituted indolin-2-ones: A novel class of tyrosine kinase inhibitors that exhibit selectivity toward particular receptor tyrosine kinases. *Journal of Medicinal Chemistry* **1998**, *41* (14), 2588-2603.

Syvanen, S.; Lindhe, O.; Palner, M.; Kornum, B. R.; Rahman, O.; Langstrom, B.; Knudsen, G. M.; Hammarlund-Udenaes, M., Species Differences in Blood-Brain Barrier Transport of Three Positron Emission Tomography Radioligands with Emphasis on P-Glycoprotein Transport. *Drug Metab Dispos* **2009**, *37* (3), 635-643.

T

Tacconelli, A.; Farina, A. R.; Cappabianca, L.; DeSantis, G.; Tessitore, A.; Vetuschi, A.; Sferra, R.; Rucci, N.; Argenti, B.; Screpanti, I.; Gulino, A.; Mackay, A. R., TrkA alternative splicing: A regulated tumor-promoting switch in human neuroblastoma. *Cancer Cell* **2004**, *6* (4), 347-360.

Takei, N.; Inamura, N.; Kawamura, M.; Namba, H.; Hara, K.; Yonezawa, K.; Nawa, H., Brain-derived neurotrophic factor induces mammalian target of rapamycin-dependent local activation of translation machinery and protein synthesis in neuronal dendrites. *J Neurosci* **2004**, *24* (44), 9760-9.

Teare, H.; Robins, E. G.; Kirjavainen, A.; Forsback, S.; Sandford, G.; Solin, O.; Luthra, S. K.; Gouverneur, V., Radiosynthesis and evaluation of [18F]Selectfluor bis(triflate). *Angew Chem Int Ed Engl* **2010**, *49* (38), 6821-4.

Tessarollo, L.; Tsoulfas, P.; Martinzanca, D.; Gilbert, D. J.; Jenkins, N. A.; Copeland, N. G.; Parada, L. F., Trkc, a Receptor for Neurotrophin-3, Is Widely Expressed in the Developing Nervous-System and in Nonneuronal Tissues. *Development* **1993**, *118* (2), 463-475.

Therrien, E.; Englebienne, P.; Arrowsmith, A. G.; Mendoza-Sanchez, R.; Corbeil, C. R.; Weill, N.; Campagna-Slater, V.; Moitessier, N., Integrating Medicinal Chemistry, Organic/Combinatorial Chemistry, and Computational Chemistry for the Discovery of Selective Estrogen Receptor Modulators with FORECASTER, a Novel Platform for Drug Discovery. *Journal of Chemical Information and Modeling* **2012**, *52* (1), 210-224.

Thiele, C. J.; Li, Z.; McKee, A. E., On Trk--the TrkB signal transduction pathway is an increasingly important target in cancer biology. *Clin Cancer Res* **2009**, *15* (19), 5962-7.

Thoenen, H.; Sendtner, M., Neurotrophins: from enthusiastic expectations through sobering experiences to rational therapeutic approaches. *Nat Neurosci* **2002**, *5 Suppl*, 1046-50.

Todd, D.; Gowers, I.; Dowler, S. J.; Wall, M. D.; McAllister, G.; Fischer, D. F.; Dijkstra, S.; Fratantoni, S. A.; van de Bospoort, R.; Veenman-Koepke, J.; Flynn, G.; Arjomand, J.; Dominguez, C.; Munoz-Sanjuan, I.; Wityak, J.; Bard, J. A., A monoclonal antibody TrkB receptor agonist as a potential therapeutic for Huntington's disease. *PLoS One* **2014**, *9* (2), e87923.

Travaglia, A.; Pietropaolo, A.; Di Martino, R.; Nicoletti, V. G.; La Mendola, D.; Calissano, P.; Rizzarelli, E., A small linear peptide encompassing the NGF N-terminus partly mimics the biological activities of the entire neurotrophin in PC12 cells. *ACS Chem Neurosci* **2015**, *6* (8), 1379-92.

Traxl, A.; Wanek, T.; Mairinger, S.; Stanek, J.; Filip, T.; Sauberer, M.; Muller, M.; Kuntner, C.; Langer, O., Breast Cancer Resistance Protein and P-Glycoprotein Influence In Vivo Disposition of ¹¹C-Erlotinib. *J Nucl Med* **2015**, *56* (12), 1930-6.

Traxl, A.; Wanek, T.; Mairinger, S.; Stanek, J.; Filip, T.; Sauberer, M.; Muller, M.; Kuntner, C.; Langer, O., Breast Cancer Resistance Protein and P-Glycoprotein Influence In Vivo Disposition of C-11-Erlotinib. *Journal of Nuclear Medicine* **2015**, *56* (12), 1930-1936.

Tredwell, M.; Preshlock, S. M.; Taylor, N. J.; Gruber, S.; Huiban, M.; Passchier, J.; Mercier, J.; Genicot, C.; Gouverneur, V., A general copper-mediated nucleophilic ¹⁸F fluorination of arenes. *Angew Chem Int Ed Engl* **2014**, *53* (30), 7751-5.

Tsao, D.; Thomsen, H. K.; Chou, J.; Stratton, J.; Hagen, M.; Loo, C.; Garcia, C.; Sloane, D. L.; Rosenthal, A.; Lin, J. C., TrkB agonists ameliorate obesity and associated metabolic conditions in mice. *Endocrinology* **2008**, *149* (3), 1038-48.

U

Ultsch, M. H.; Wiesmann, C.; Simmons, L. C.; Henrich, J.; Yang, M.; Reilly, D.; Bass, S. H.; de Vos, A. M., Crystal structures of the neurotrophin-binding domain of TrkA, TrkB and TrkC. *J Mol Biol* **1999**, *290* (1), 149-59.

Urfer, R.; Tsoulfas, P.; O'Connell, L.; Shelton, D. L.; Parada, L. F.; Presta, L. G., An immunoglobulin-like domain determines the specificity of neurotrophin receptors. *EMBO J* **1995**, *14* (12), 2795-805.

V

Vaishnavi, A.; Capelletti, M.; Le, A. T.; Kako, S.; Butaney, M.; Ercan, D.; Mahale, S.; Davies, K. D.; Aisner, D. L.; Pilling, A. B.; Berge, E. M.; Kim, J.; Sasaki, H.; Park, S.-i.; Kryukov, G.; Garraway, L. A.; Hammerman, P. S.; Haas, J.; Andrews, S. W.; Lipson, D.; Stephens, P. J.; Miller, V. A.; Varella-Garcia, M.; Janne, P. A.; Doebele, R. C., Oncogenic and drug-sensitive NTRK1 rearrangements in lung cancer. *Nat. Med.* **2013**, *19* (11), 1469-1472.

Vaishnavi, A.; Le, A. T.; Doebele, R. C., TRKking Down an Old Oncogene in a New Era of Targeted Therapy. *Cancer Discovery* **2015**, *5* (1), 25-34.

Van de Bittner, G. C.; Ricq, E. L.; Hooker, J. M., A Philosophy for CNS Radiotracer Design. *Accounts Chem Res* **2014**, *47* (10), 3127-3134.

van Dongen, G. A.; Poot, A. J.; Vugts, D. J., PET imaging with radiolabeled antibodies and tyrosine kinase inhibitors: immuno-PET and TKI-PET. *Tumour Biol* **2012**, *33* (3), 607-15.

Vepsalainen, S.; Castren, E.; Helisalmi, S.; Iivonen, S.; Mannermaa, A.; Lehtovirta, M.; Hanninen, T.; Soininen, H.; Hiltunen, M., Genetic analysis of BDNF and TrkB gene polymorphisms in Alzheimer's disease. *J Neurol* **2005**, *252* (4), 423-428.

Vidaurre, O. G.; Gascon, S.; Deogracias, R.; Sobrado, M.; Cuadrado, E.; Montaner, J.; Rodriguez-Pena, A.; Diaz-Guerra, M., Imbalance of neurotrophin receptor isoforms TrkB-FL/TrkB-T1 induces neuronal death in excitotoxicity. *Cell Death Dis* **2012**, *3*, e256.

W

Wager, T. T.; Hou, X. J.; Verhoest, P. R.; Villalobos, A., Moving beyond Rules: The Development of a Central Nervous System Multiparameter Optimization (CNS MPO) Approach To Enable Alignment of Druglike Properties. *ACS Chemical Neuroscience* **2010**, *1* (6), 435-449.

Wager, T. T.; Hou, X.; Verhoest, P. R.; Villalobos, A., Central Nervous System Multiparameter Optimization Desirability: Application in Drug Discovery. *ACS Chem Neurosci* **2016**, *7* (6), 767-75.

Wang, B.; Qin, L.; Neumann, K. D.; Uppaluri, S.; Cerny, R. L.; DiMagno, S. G., Improved arene fluorination methodology for I(III) salts. *Org Lett* **2010**, *12* (15), 3352-5.

Wang, T.; Lamb, M. L.; Block, M. H.; Davies, A. M.; Han, Y.; Hoffmann, E.; Ioannidis, S.; Josey, J. A.; Liu, Z.-Y.; Lyne, P. D.; MacIntyre, T.; Mohr, P. J.; Omer, C. A.; Sjögren, T.; Thress, K.; Wang, B.; Wang, H.; Yu, D.; Zhang, H.-J., Discovery of Disubstituted Imidazo[4,5-b]pyridines and Purines as Potent TrkA Inhibitors. *ACS Med. Chem. Lett.* **2012**, *3* (9), 705-709.

Wang, T.; Yu, D.; Lamb, M. L., Trk kinase inhibitors as new treatments for cancer and pain. *Expert Opin Ther Pat* **2009**, *19* (3), 305-19.

Wang, T.; Yu, D.; Lamb, M. L., Trk kinase inhibitors as new treatments for cancer and pain. *Expert Opin. Ther. Pat.* **2009**, *19* (3), 305-319.

Watson, F. L.; Porcionatto, M. A.; Bhattacharyya, A.; Stiles, C. D.; Segal, R. A., TrkA glycosylation regulates receptor localization and activity. *J Neurobiol* **1999**, *39* (2), 323-36.

Watson, J. J.; Allen, S. J.; Dawbarn, D., Targeting Nerve Growth Factor in Pain. *Biodrugs* **2008**, *22* (6), 349-359.

Webster, M. J.; Herman, M. M.; Kleinman, J. E.; Shannon Weickert, C., BDNF and trkB mRNA expression in the hippocampus and temporal cortex during the human lifespan. *Gene Expr Patterns* **2006**, *6* (8), 941-51.

Weeraratna, A. T.; Dalrymple, S. L.; Lamb, J. C.; Denmeade, S. R.; Miknyoczki, S.; Dionne, C. A.; Isaacs, J. T., Pan-trk Inhibition Decreases Metastasis and Enhances Host Survival in Experimental Models as a Result of Its Selective Induction of Apoptosis of Prostate Cancer Cells. *Clin. Cancer Res.* **2001**, *7* (8), 2237-2245.

Wehrman, T.; He, X.; Raab, B.; Dukipatti, A.; Blau, H.; Garcia, K. C., Structural and mechanistic insights into nerve growth factor interactions with the TrkA and p75 receptors. *Neuron* **2007**, *53* (1), 25-38.

Weickert, C. S.; Ligons, D. L.; Romanczyk, T.; Ungaro, G.; Hyde, T. M.; Herman, M. M.; Weinberger, D. R.; Kleinman, J. E., Reductions in neurotrophin receptor mRNAs in the prefrontal cortex of patients with schizophrenia. *Mol Psychiatr* **2005**, *10* (7), 637-650.

Weiss, G. J.; Hidalgo, M.; Borad, M. J.; Laheru, D.; Tibes, R.; Ramanathan, R. K.; Blaydorn, L.; Jameson, G.; Jimeno, A.; Isaacs, J. D.; Scaburri, A.; Pacciarini, M. A.; Fiorentini, F.; Ciomei, M.; Von Hoff, D. D., Phase I study of the safety, tolerability and pharmacokinetics of PHA-848125AC, a dual tropomyosin receptor kinase A and cyclin-dependent kinase inhibitor, in patients with advanced solid malignancies. *Invest. New Drugs* **20122**, 30 (6), 2334-2343.

Weiss, G. J.; Hidalgo, M.; Borad, M. J.; Laheru, D.; Tibes, R.; Ramanathan, R. K.; Blaydorn, L.; Jameson, G.; Jimeno, A.; Isaacs, J. D.; Scaburri, A.; Pacciarini, M. A.; Fiorentini, F.; Ciomei, M.; Von Hoff, D. D., Phase I study of the safety, tolerability and pharmacokinetics of PHA-848125AC, a dual tropomyosin receptor kinase A and cyclin-dependent kinase inhibitor, in patients with advanced solid malignancies. *Invest. New Drugs* **2012**, 30 (6), 2334-2343.

Weiss, G. J.; Hidalgo, M.; Borad, M. J.; Laheru, D.; Tibes, R.; Ramanathan, R. K.; Blaydorn, L.; Jameson, G.; Jimeno, A.; Isaacs, J. D.; Scaburri, A.; Pacciarini, M. A.; Fiorentini, F.; Ciomei, M.; Von Hoff, D. D., Phase I study of the safety, tolerability and pharmacokinetics of PHA-848125AC, a dual tropomyosin receptor kinase A and cyclin-dependent kinase inhibitor, in patients with advanced solid malignancies. *Invest New Drug* **2012**, 30 (6), 2334-2343.

Wellmer, A.; Misra, V. P.; Sharief, M. K.; Kopelman, P. G.; Anand, P., A double-blind placebo-controlled clinical trial of recombinant human brain-derived neurotrophic factor (rhBDNF) in diabetic polyneuropathy. *J Peripher Nerv Syst* **2001**, 6 (4), 204-10.

Wey, H. Y.; Gilbert, T. M.; Zurcher, N. R.; She, A.; Bhanot, A.; Taillon, B. D.; Schroeder, F. A.; Wang, C. G.; Haggarty, S. J.; Hooker, J. M., Insights into neuroepigenetics through human histone deacetylase PET imaging. *Sci Transl Med* **2016**, 8 (351).

Wiesmann, C.; Ultsch, M. H.; Bass, S. H.; de Vos, A. M., Crystal structure of nerve growth factor in complex with the ligand-binding domain of the TrkA receptor. *Nature* **1999**, 401 (6749), 184-8.

Wilkinson, G. R., Drug therapy - Drug metabolism and variability among patients in drug response. *New Engl J Med* **2005**, 352 (21), 2211-2221.

Wood, E. R.; Kuyper, L.; Petrov, K. G.; Hunter, R. N.; Harris, P. A.; Lackey, K., Discovery and in vitro evaluation of potent TrkA kinase inhibitors: oxindole and aza-oxindoles. *Bioorg Med Chem Lett* **2004**, 14 (4), 953-957.

Wu, G.; Diaz, A. K.; Paugh, B. S.; Rankin, S. L.; Ju, B.; Li, Y.; Zhu, X.; Qu, C.; Chen, X.; Zhang, J.; Easton, J.; Edmonson, M.; Ma, X.; Lu, C.; Nagahawatte, P.; Hedlund, E.; Rusch, M.; Pounds, S.; Lin, T.; Onar-Thomas, A.; Huether, R.; Kriwacki, R.; Parker, M.; Gupta, P.; Becksfort, J.; Wei, L.; Mulder, H. L.; Boggs, K.; Vadodaria, B.; Yergeau, D.; Russell, J. C.; Ochoa, K.; Fulton, R. S.; Fulton, L. L.; Jones, C.; Boop, F. A.; Broniscer, A.; Wetmore, C.; Gajjar, A.; Ding, L.; Mardis, E. R.; Wilson, R. K.; Taylor, M. R.; Downing, J. R.; Ellison, D. W.; Zhang, J.; Baker, S. J.; St. Jude Children's Research Hospital-Washington University Pediatric Cancer Genome, P., The genomic landscape of diffuse intrinsic pontine glioma and pediatric non-brainstem high-grade glioma. *Nat Genet* **2014**, 46 (5), 444-50.

Wu, P.; Clausen, M. H.; Nielsen, T. E., Allosteric small-molecule kinase inhibitors. *Pharmacol. Ther.* **2015**, 156, 59-68.

Wu, P.; Nielsen, T. E.; Clausen, M. H., Small-molecule kinase inhibitors: an analysis of FDA-approved drugs. *Drug Discovery Today* **2016**, 21 (1), 5-10.

Wuest, F.; Berndt, M.; Kniess, T., Carbon-11 labeling chemistry based upon [11C]methyl iodide. *Ernst Schering Res Found Workshop* **2007**, (62), 183-213.

X

Xiao, J.; Hughes, R. A.; Lim, J. Y.; Wong, A. W.; Ivanusic, J. J.; Ferner, A. H.; Kilpatrick, T. J.; Murray, S. S., A small peptide mimetic of brain-derived neurotrophic factor promotes peripheral myelination. *J Neurochem* **2013**, 125 (3), 386-98.

Y

Y. Fan, J. L., V. Molteni, P. A. Albaugh, G. Chopiuk, J. M. Smith and B. T. Flatt, US/2012/0065184 A1; International application No. PCT/US2012/026377. **2012**, August 30.

Yaqub, M.; Bahce, I.; Voorhoeve, C.; Sehuit, R. C.; Windhorst, A. D.; Hoekstra, O. S.; Boellaard, R.; Hendrikse, N. H.; Smit, E. F.; Lammertsma, A. A., Quantitative and Simplified Analysis of C-11-Erlotinib Studies. *Journal of Nuclear Medicine* **2016**, 57 (6), 861-866.

Ye, Y.; Schimler, S. D.; Hanley, P. S.; Sanford, M. S., Cu(OTf)₂-mediated fluorination of aryltrifluoroborates with potassium fluoride. *J Am Chem Soc* **2013**, 135 (44), 16292-5.

Yeh, I.; Tee, M. K.; Botton, T.; Hunter Shain, A.; Sparatta, A. J.; Gagnon, A.; Vemula, S. S.; Garrido, M. C.; Nakamaru, K.; Isoyama, T.; McCalmont, T. H.; LeBoit, P. E.; Bastian, B. C., NTRK3 kinase fusions in Spitz tumours. *The Journal of Pathology* **2016**, doi: 10.1002/path.4775.

Yis, U.; Mademan, I.; Kavukcu, S.; Baets, J., A novel NTRK1 mutation in a patient with congenital insensitivity to pain with anhidrosis. *Acta Neurol Belg* **2015**, 115 (3), 509-11.

Yu, Y.; Zhang, S.; Wang, X.; Yang, Z.; Ou, G., Overexpression of TrkB promotes the progression of colon cancer. *APMIS* **2010**, 118 (3), 188-95.

Z

Zaretski, J.; Boehm, K. M.; Swamidass, S. J., Improved Prediction of CYP-Mediated Metabolism with Chemical Fingerprints. *J Chem Inf Model* **2015**, 55 (5), 972-82.

Zeliadt, N., Rita Levi-Montalcini: NGF, the prototypical growth factor. *P Natl Acad Sci USA* **2013**, 110 (13), 4873-4876.

Zhang, A. J.; Khare, S.; Gokulan, K.; Linthicum, D. S.; Burgess, K., Dimeric beta-turn peptidomimetics as ligands for the neurotrophin receptor TrkC. *Bioorg Med Chem Lett* **2001**, 11 (2), 207-10.

Zhang, F.; Kang, Z. L.; Li, W.; Xiao, Z. C.; Zhou, X. F., Roles of brain-derived neurotrophic factor/tropomyosin-related kinase B (BDNF/TrkB) signalling in Alzheimer's disease. *J Clin Neurosci* **2012**, 19 (7), 946-949.

Zhang, J.; Yang, P. L.; Gray, N. S., Targeting cancer with small molecule kinase inhibitors. *Nat Rev Cancer* **2009**, 9 (1), 28-39.

Zhang, L.; Villalobos, A.; Beck, E. M.; Bocan, T.; Chappie, T. A.; Chen, L.; Grimwood, S.; Heck, S. D.; Helal, C. J.; Hou, X.; Humphrey, J. M.; Lu, J.; Skaddan, M. B.; McCarthy, T. J.; Verhoest, P. R.; Wager, T. T.; Zasadny, K., Design and selection parameters to accelerate the discovery of novel central nervous system positron emission tomography (PET) ligands and their application in the development of a novel phosphodiesterase 2A PET ligand. *J Med Chem* **2013**, *56* (11), 4568-79.

Zhou, Y.; Ye, W.; Brasic, J. R.; Crabb, A. H.; Hilton, J.; Wong, D. F., A consistent and efficient graphical analysis method to improve the quantification of reversible tracer binding in radioligand receptor dynamic PET studies. *Neuroimage* **2009**, *44* (3), 661-70.

Zhu, Z.; Kleeff, J.; Kaye, H.; Wang, L.; Korc, M.; Buchler, M. W.; Friess, H., Nerve growth factor and enhancement of proliferation, invasion, and tumorigenicity of pancreatic cancer cells. *Mol Carcinog* **2002**, *35* (3), 138-47.

Zischler, J.; Kolks, N.; Modemann, D.; Neumaier, B.; Zlatopolskiy, B. D., Alcohol-Enhanced Cu-Mediated Radiofluorination. *Chemistry* **2016**.

Zlatopolskiy, B. D.; Zischler, J.; Krapf, P.; Zarrad, F.; Urusova, E. A.; Kordys, E.; Endepols, H.; Neumaier, B., Copper-mediated aromatic radiofluorination revisited: efficient production of PET tracers on a preparative scale. *Chemistry* **2015**, *21* (15), 5972-9.

Zoghbi, S. S.; Shetty, H. U.; Ichise, M.; Fujita, M.; Imaizumi, M.; Liow, J. S.; Shah, J.; Musachio, J. L.; Pike, V. W.; Innis, R. B., PET imaging of the dopamine transporter with ¹⁸F-FECNT: a polar radiometabolite confounds brain radioligand measurements. *J Nucl Med* **2006**, *47* (3), 520-7.

Zou, H. B.; Zhang, L.; Ouyang, J. F.; Giulianotti, M. A.; Yu, Y. P., Synthesis and biological evaluation of 2-indolinone derivatives as potential antitumor agents. *Eur J Med Chem* **2011**, *46* (12), 5970-5977.

Zuccato, C.; Marullo, M.; Conforti, P.; MacDonald, M. E.; Tartari, M.; Cattaneo, E., Systematic assessment of BDNF and its receptor levels in human cortices affected by Huntington's disease. *Brain Pathol* **2008**, *18* (2), 225-238.

Zuccotto, F.; Ardini, E.; Casale, E.; Angiolini, M., Through the "Gatekeeper Door": Exploiting the Active Kinase Conformation. *J. Med. Chem.* **2010**, *53* (7), 2681-2694.

Additional Experimental Data (Crystallographic Data for Compounds 2.25 and (E)-2.29 from Supporting Information Section 7 - Chapter 2)

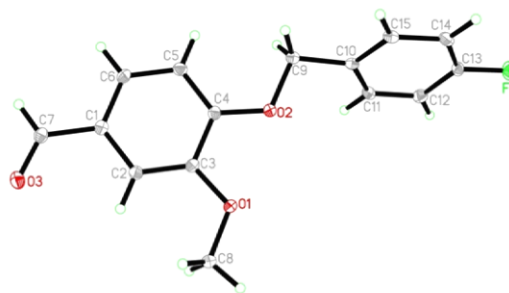
*The data from this Annex have been published in Supporting Information of: Bernard-Gauthier, V. & Schirmacher, R. 5-(4-((4-[¹⁸F]fluorobenzyl)oxy)-3-methoxybenzyl)pyrimidine-2,4-diamine: A Selective Dual Inhibitor for Potential PET Imaging of Trk/CSF-1R. *Bioorg. Med. Chem. Lett.* **2014**, *24*, 4784-4790.*

CRYSTAL AND MOLECULAR STRUCTURE OF
C₁₅ H₁₃ F O₃ COMPOUND (INSN17)

Equipe Schirrmacher

Montreal Neurological Institute and Hospital

3801 University Street, Montreal, Quebec, Canada H3A 2B4



Structure solved and refined in the laboratory of X-ray diffraction
Université de Montréal by Michel Simard.

Table 1. Crystal data and structure refinement for C15 H13 F O3.

| | |
|-----------------------------------|--|
| Identification code | INSN17 |
| Empirical formula | C15 H13 F O3 |
| Formula weight | 260.25 |
| Temperature | 100K |
| Wavelength | 1.54178 Å |
| Crystal system | Triclinic |
| Space group | P-1 |
| Unit cell dimensions | a = 8.3577(8) Å α = 87.894(3)° b = 8.5150(8) Å β = 83.575(3)° c = 8.8676(8) Å γ = 84.611(3)° |
| Volume | 624.11(10) Å ³ |
| Z | 2 |
| Density (calculated) | 1.385 g/cm ³ |
| Absorption coefficient | 0.887 mm ⁻¹ |
| F(000) | 272 |
| Crystal size | 0.22 x 0.20 x 0.16 mm |
| Theta range for data collection | 5.021 to 71.716° |
| Index ranges | -10 ≤ h ≤ 10, -10 ≤ k ≤ 10, -10 ≤ l ≤ 10 |
| Reflections collected | 25462 |
| Independent reflections | 2361 [R _{int} = 0.020] |
| Absorption correction | Semi-empirical from equivalents |
| Max. and min. transmission | 0.7535 and 0.6735 |
| Refinement method | Full-matrix least-squares on F ² |
| Data / restraints / parameters | 2361 / 0 / 173 |
| Goodness-of-fit on F ² | 1.060 |
| Final R indices [I > 2σ(I)] | R ₁ = 0.0320, wR ₂ = 0.0873 |

R indices (all data)

$$R_1 = 0.0322, wR_2 = 0.0874$$

Largest diff. peak and hole

$$0.222 \text{ and } -0.204 \text{ e/\AA}^3$$

Table 2. Atomic coordinates ($\times 10^4$) and equivalent isotropic displacement parameters ($\text{\AA}^2 \times 10^3$) for C15 H13 F O3.

U_{eq} is defined as one third of the trace of the orthogonalized U_{ij} tensor.

| | x | y | z | U_{eq} |
|-------|----------|---------|---------|----------|
| C(1) | -2143(1) | 6134(1) | 1429(1) | 20(1) |
| C(2) | -766(1) | 6985(1) | 1222(1) | 19(1) |
| C(3) | 692(1) | 6310(1) | 1620(1) | 18(1) |
| C(4) | 794(1) | 4761(1) | 2275(1) | 19(1) |
| C(5) | -575(1) | 3936(1) | 2490(1) | 21(1) |
| C(6) | -2038(1) | 4619(1) | 2057(1) | 21(1) |
| C(7) | -3677(1) | 6854(1) | 957(1) | 22(1) |
| C(8) | 2045(1) | 8568(1) | 779(1) | 25(1) |
| C(9) | 2445(1) | 2610(1) | 3249(1) | 22(1) |
| C(10) | 4117(1) | 2260(1) | 3710(1) | 20(1) |
| C(11) | 4581(1) | 3050(1) | 4917(1) | 21(1) |
| C(12) | 6078(1) | 2672(1) | 5436(1) | 23(1) |
| C(13) | 7080(1) | 1465(1) | 4737(1) | 23(1) |
| C(14) | 6679(1) | 669(1) | 3530(1) | 24(1) |
| C(15) | 5183(1) | 1082(1) | 3009(1) | 22(1) |
| O(1) | 2113(1) | 6996(1) | 1410(1) | 21(1) |
| O(2) | 2289(1) | 4200(1) | 2625(1) | 21(1) |
| O(3) | -3874(1) | 8189(1) | 429(1) | 27(1) |
| F(1) | 8533(1) | 1052(1) | 5263(1) | 33(1) |

Table 3. Hydrogen coordinates ($\times 10^4$) and isotropic displacement parameters ($\text{\AA}^2 \times 10^3$) for C15 H13 F O3.

| | x | y | z | U_{eq} |
|-------|-------|------|------|----------|
| H(2) | -846 | 8030 | 806 | 23 |
| H(5) | -511 | 2903 | 2934 | 25 |
| H(6) | -2968 | 4045 | 2193 | 25 |
| H(7) | -4577 | 6239 | 1071 | 27 |
| H(8A) | 1638 | 8579 | -216 | 37 |
| H(8B) | 3130 | 8934 | 663 | 37 |
| H(8C) | 1320 | 9267 | 1457 | 37 |
| H(9A) | 2253 | 1854 | 2481 | 27 |
| H(9B) | 1634 | 2503 | 4141 | 27 |
| H(11) | 3861 | 3860 | 5391 | 25 |
| H(12) | 6404 | 3223 | 6246 | 28 |
| H(14) | 7406 | -141 | 3064 | 29 |
| H(15) | 4886 | 557 | 2170 | 26 |

Table 4. Anisotropic parameters ($\text{\AA}^2 \times 10^3$) for C15 H13 F O3.

The anisotropic displacement factor exponent takes the form:

$$-2 \pi^2 [h^2 a^{*2} U_{11} + \dots + 2 h k a^* b^* U_{12}]$$

| | U11 | U22 | U33 | U23 | U13 | U12 |
|-------|-------|-------|-------|-------|-------|-------|
| C(1) | 18(1) | 23(1) | 17(1) | -3(1) | -1(1) | -1(1) |
| C(2) | 21(1) | 18(1) | 19(1) | -1(1) | -2(1) | -2(1) |
| C(3) | 18(1) | 20(1) | 18(1) | -2(1) | -2(1) | -4(1) |
| C(4) | 18(1) | 21(1) | 18(1) | -2(1) | -2(1) | -1(1) |
| C(5) | 21(1) | 19(1) | 22(1) | 1(1) | 0(1) | -2(1) |
| C(6) | 17(1) | 24(1) | 22(1) | -2(1) | 1(1) | -5(1) |
| C(7) | 19(1) | 26(1) | 22(1) | -3(1) | -1(1) | -2(1) |
| C(8) | 22(1) | 20(1) | 33(1) | 5(1) | -6(1) | -6(1) |
| C(9) | 22(1) | 18(1) | 28(1) | 3(1) | -4(1) | -4(1) |
| C(10) | 21(1) | 16(1) | 21(1) | 4(1) | -2(1) | -3(1) |
| C(11) | 23(1) | 17(1) | 22(1) | 1(1) | 0(1) | -1(1) |
| C(12) | 26(1) | 23(1) | 21(1) | 2(1) | -4(1) | -5(1) |
| C(13) | 18(1) | 24(1) | 26(1) | 9(1) | -4(1) | -1(1) |
| C(14) | 24(1) | 18(1) | 27(1) | 3(1) | 4(1) | 2(1) |
| C(15) | 26(1) | 18(1) | 21(1) | 1(1) | -2(1) | -4(1) |
| O(1) | 18(1) | 19(1) | 28(1) | 3(1) | -6(1) | -5(1) |
| O(2) | 18(1) | 18(1) | 28(1) | 3(1) | -5(1) | -2(1) |
| O(3) | 23(1) | 27(1) | 30(1) | 1(1) | -6(1) | 2(1) |
| F(1) | 22(1) | 38(1) | 39(1) | 8(1) | -9(1) | 2(1) |

Table 5. Bond lengths [Å] and angles [°] for C15 H13 F O3

| | |
|----------------|-------------------|
| C(1)-C(6) | C(3)-C(2)-C(1) |
| 1.3854(14) | 120.33(9) |
| C(1)-C(2) | O(1)-C(3)-C(2) |
| 1.4077(14) | 125.30(9) |
| C(1)-C(7) | O(1)-C(3)-C(4) |
| 1.4656(14) | 115.12(9) |
| C(2)-C(3) | C(2)-C(3)-C(4) |
| 1.3748(14) | 119.57(9) |
| C(3)-O(1) | O(2)-C(4)-C(5) |
| 1.3634(12) | 125.22(9) |
| C(3)-C(4) | O(2)-C(4)-C(3) |
| 1.4208(14) | 115.05(8) |
| C(4)-O(2) | C(5)-C(4)-C(3) |
| 1.3596(12) | 119.72(9) |
| C(4)-C(5) | C(4)-C(5)-C(6) |
| 1.3898(14) | 120.21(9) |
| C(5)-C(6) | C(1)-C(6)-C(5) |
| 1.3918(15) | 120.15(9) |
| C(7)-O(3) | O(3)-C(7)-C(1) |
| 1.2170(13) | 124.23(9) |
| C(8)-O(1) | O(2)-C(9)-C(10) |
| 1.4302(12) | 108.79(8) |
| C(9)-O(2) | C(15)-C(10)-C(11) |
| 1.4431(12) | 119.28(10) |
| C(9)-C(10) | C(15)-C(10)-C(9) |
| 1.5003(14) | 120.78(9) |
| C(10)-C(15) | C(11)-C(10)-C(9) |
| 1.3925(14) | 119.82(9) |
| C(10)-C(11) | C(12)-C(11)-C(10) |
| 1.3938(14) | 121.06(9) |
| C(11)-C(12) | C(13)-C(12)-C(11) |
| 1.3869(15) | 117.76(10) |
| C(12)-C(13) | F(1)-C(13)-C(14) |
| 1.3819(16) | 118.54(9) |
| C(13)-F(1) | F(1)-C(13)-C(12) |
| 1.3605(12) | 118.39(10) |
| C(13)-C(14) | C(14)-C(13)-C(12) |
| 1.3758(16) | 123.07(10) |
| C(14)-C(15) | C(13)-C(14)-C(15) |
| 1.3912(15) | 118.31(9) |
| | C(14)-C(15)-C(10) |
| C(6)-C(1)-C(2) | 120.48(9) |
| 120.00(9) | C(3)-O(1)-C(8) |
| C(6)-C(1)-C(7) | 116.48(8) |
| 120.40(9) | C(4)-O(2)-C(9) |
| C(2)-C(1)-C(7) | 116.43(7) |
| 119.59(9) | |

Table 6. Torsion angles [°] for C15 H13 F O3.

—

| | |
|-------------------------|--------------|
| C(6)-C(1)-C(2)-C(3) | 1.00 (15) |
| C(7)-C(1)-C(2)-C(3) | -178.21 (8) |
| C(1)-C(2)-C(3)-O(1) | 177.03 (9) |
| C(1)-C(2)-C(3)-C(4) | -1.48 (14) |
| O(1)-C(3)-C(4)-O(2) | 1.22 (12) |
| C(2)-C(3)-C(4)-O(2) | 179.88 (8) |
| O(1)-C(3)-C(4)-C(5) | -177.88 (8) |
| C(2)-C(3)-C(4)-C(5) | 0.78 (14) |
| O(2)-C(4)-C(5)-C(6) | -178.58 (9) |
| C(3)-C(4)-C(5)-C(6) | 0.42 (15) |
| C(2)-C(1)-C(6)-C(5) | 0.22 (15) |
| C(7)-C(1)-C(6)-C(5) | 179.42 (9) |
| C(4)-C(5)-C(6)-C(1) | -0.92 (15) |
| C(6)-C(1)-C(7)-O(3) | 178.28 (9) |
| C(2)-C(1)-C(7)-O(3) | -2.52 (15) |
| O(2)-C(9)-C(10)-C(15) | -116.50 (10) |
| O(2)-C(9)-C(10)-C(11) | 67.54 (11) |
| | |
| C(15)-C(10)-C(11)-C(12) | -0.59 (14) |
| C(9)-C(10)-C(11)-C(12) | 175.44 (9) |
| C(10)-C(11)-C(12)-C(13) | -1.25 (15) |
| C(11)-C(12)-C(13)-F(1) | -178.24 (8) |
| C(11)-C(12)-C(13)-C(14) | 2.20 (15) |
| F(1)-C(13)-C(14)-C(15) | 179.21 (8) |
| C(12)-C(13)-C(14)-C(15) | -1.22 (15) |
| C(13)-C(14)-C(15)-C(10) | -0.72 (15) |
| C(11)-C(10)-C(15)-C(14) | 1.60 (14) |
| C(9)-C(10)-C(15)-C(14) | -174.39 (9) |
| C(2)-C(3)-O(1)-C(8) | 2.56 (14) |
| C(4)-C(3)-O(1)-C(8) | -178.87 (8) |
| C(5)-C(4)-O(2)-C(9) | 0.91 (14) |
| C(3)-C(4)-O(2)-C(9) | -178.13 (8) |
| C(10)-C(9)-O(2)-C(4) | -174.22 (8) |

REFERENCES

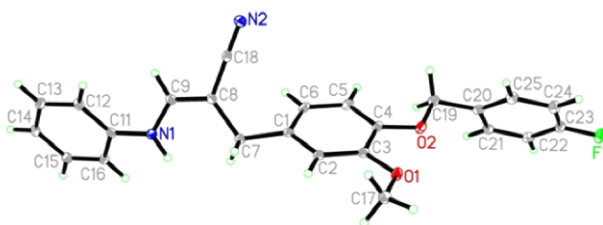
- APEX2 (2013), Bruker AXS Inc., Madison, WI 53719-1173.
- SAINT (2013) V8.34A, Bruker AXS Inc., Madison, WI 53719-1173.
- Sheldrick, G. M. (2012). SADABS-2012/1, Bruker AXS Inc., Madison, WI 53719-1173.
- Sheldrick, G.M. (2008). Acta Cryst. A64, 112-122.
- Spek, A.L. (2009). Acta Cryst. D65, 148.
- Maris, T. (2004). UdmX, University of Montréal, Montréal, QC, Canada.
- XP (1998) Version 5.1, Bruker AXS Inc., Madison, WI 53719-1173.
- XPREP (2013); X-ray data Preparation and Reciprocal space Exploration Program. Bruker AXS Inc., Madison, WI

CRYSTAL AND MOLECULAR STRUCTURE OF
C₂₄ H₂₁ F N₂ O₂ COMPOUND (INSN16)

Equipe Schirrmacher

Montreal Neurological Institute and Hospital

3801 University Street, Montreal, Quebec, Canada H3A 2B4



Structure solved and refined in the laboratory of X-ray
diffraction Université de Montréal by Michel Simard.

Table 1. Crystal data and structure refinement for C₂₄ H₂₁ F N₂ O₂.

| | |
|-----------------------------------|--|
| Identification code | INSN16 |
| Empirical formula | C ₂₄ H ₂₁ F N ₂ O ₂ |
| Formula weight | 388.43 |
| Temperature | 100K |
| Wavelength | 1.54178 Å |
| Crystal system | Monoclinic |
| Space group | P2 ₁ /c |
| Unit cell dimensions | a = 14.1102(2) Å $\alpha = 90^\circ$ b = 12.8934(2) Å $\beta = 103.5036(7)^\circ$ c = 10.7758(2) Å $\gamma = 90^\circ$ |
| Volume | 1906.23(5) Å ³ |
| Z | 4 |
| Density (calculated) | 1.353 g/cm ³ |
| Absorption coefficient | 0.760 mm ⁻¹ |
| F(000) | 816 |
| Crystal size | 0.13 x 0.10 x 0.06 mm |
| Theta range for data collection | 3.221 to 71.726° |
| Index ranges | -17 ≤ h ≤ 17, -15 ≤ k ≤ 15, -13 ≤ l ≤ 13 |
| Reflections collected | 52711 |
| Independent reflections | 3678 [R _{int} = 0.023] |
| Absorption correction | Semi-empirical from equivalents |
| Max. and min. transmission | 0.7535 and 0.6910 |
| Refinement method | Full-matrix least-squares on F ² |
| Data / restraints / parameters | 3678 / 0 / 267 |
| Goodness-of-fit on F ² | 1.022 |
| Final R indices [I > 2σ(I)] | R ₁ = 0.0356, wR ₂ = 0.0915 |

R indices (all data)

$R_1 = 0.0364$, $wR_2 = 0.0922$

Largest diff. peak and hole

0.318 and $-0.198 \text{ e}/\text{\AA}^3$

Table 2. Atomic coordinates ($\times 10^4$) and equivalent isotropic displacement parameters ($\text{\AA}^2 \times 10^3$) for C24 H21 F N2 O2.

U_{eq} is defined as one third of the trace of the orthogonalized U_{ij} tensor.

| | x | y | z | U_{eq} |
|-------|---------|---------|----------|----------|
| C(1) | 6378(1) | 6687(1) | 4141(1) | 20(1) |
| C(2) | 7358(1) | 6948(1) | 4662(1) | 19(1) |
| C(3) | 7826(1) | 6625(1) | 5878(1) | 18(1) |
| C(4) | 7317(1) | 6030(1) | 6604(1) | 18(1) |
| C(5) | 6360(1) | 5752(1) | 6075(1) | 21(1) |
| C(6) | 5893(1) | 6086(1) | 4854(1) | 21(1) |
| C(7) | 5884(1) | 7122(1) | 2846(1) | 28(1) |
| C(8) | 5194(1) | 6401(1) | 1955(1) | 18(1) |
| C(9) | 4379(1) | 6709(1) | 1092(1) | 18(1) |
| C(11) | 3133(1) | 7947(1) | 73(1) | 18(1) |
| C(12) | 2861(1) | 7448(1) | -1107(1) | 21(1) |
| C(13) | 1989(1) | 7725(1) | -1950(1) | 23(1) |
| C(14) | 1406(1) | 8499(1) | -1635(1) | 21(1) |
| C(15) | 1698(1) | 9009(1) | -473(1) | 21(1) |
| C(16) | 2556(1) | 8738(1) | 377(1) | 20(1) |
| C(17) | 9351(1) | 7308(1) | 5678(1) | 25(1) |
| C(18) | 5412(1) | 5324(1) | 1956(1) | 18(1) |
| C(19) | 7320(1) | 5133(1) | 8536(1) | 21(1) |
| C(20) | 7928(1) | 5050(1) | 9874(1) | 20(1) |
| C(21) | 7607(1) | 5505(1) | 10873(1) | 21(1) |
| C(22) | 8163(1) | 5451(1) | 12117(1) | 23(1) |
| C(23) | 9045(1) | 4941(1) | 12331(1) | 22(1) |
| C(24) | 9392(1) | 4473(1) | 11375(1) | 24(1) |
| C(25) | 8820(1) | 4528(1) | 10140(1) | 23(1) |
| N(1) | 3993(1) | 7673(1) | 978(1) | 20(1) |
| N(2) | 5572(1) | 4445(1) | 1981(1) | 22(1) |
| O(1) | 8773(1) | 6845(1) | 6456(1) | 22(1) |
| O(2) | 7824(1) | 5787(1) | 7819(1) | 21(1) |
| F(1) | 9596(1) | 4898(1) | 13545(1) | 30(1) |

Table 3. Hydrogen coordinates ($\times 10^4$) and isotropic displacement parameters ($\text{\AA}^2 \times 10^3$) for C24 H21 F N2 O2.

| | x | y | z | U_{eq} |
|--------|-----------|-----------|-----------|----------|
| H(2) | 7703 | 7351 | 4174 | 22 |
| H(5) | 6018 | 5331 | 6548 | 25 |
| H(6) | 5233 | 5898 | 4510 | 25 |
| H(7A) | 6396 | 7345 | 2413 | 33 |
| H(7B) | 5516 | 7749 | 2980 | 33 |
| H(9) | 4049 | 6198 | 515 | 21 |
| H(12) | 3265 | 6925 | -1332 | 25 |
| H(13) | 1794 | 7380 | -2748 | 27 |
| H(14) | 810 | 8680 | -2210 | 26 |
| H(15) | 1305 | 9549 | -261 | 25 |
| H(16) | 2751 | 9091 | 1170 | 24 |
| H(17A) | 9311 | 6885 | 4912 | 37 |
| H(17B) | 10031 | 7349 | 6160 | 37 |
| H(17C) | 9107 | 8007 | 5428 | 37 |
| H(19A) | 7216 | 4436 | 8141 | 26 |
| H(19B) | 6675 | 5435 | 8541 | 26 |
| H(21) | 6999 | 5858 | 10701 | 25 |
| H(22) | 7942 | 5756 | 12801 | 28 |
| H(24) | 10002 | 4125 | 11555 | 29 |
| H(25) | 9039 | 4206 | 9464 | 28 |
| H(1) | 4227 (11) | 8141 (13) | 1598 (15) | 31 (4) |

Table 4. Anisotropic parameters ($\text{\AA}^2 \times 10^3$) for C24 H21 F N2 O2.

The anisotropic displacement factor exponent takes the form:

$$-2 \pi^2 [h^2 a^{*2} U_{11} + \dots + 2 h k a^* b^* U_{12}]$$

| | U11 | U22 | U33 | U23 | U13 | U12 |
|-------|-------|-------|-------|-------|-------|-------|
| C(1) | 20(1) | 14(1) | 22(1) | -4(1) | -1(1) | 2(1) |
| C(2) | 20(1) | 14(1) | 21(1) | -2(1) | 4(1) | 0(1) |
| C(3) | 15(1) | 16(1) | 21(1) | -5(1) | 3(1) | 0(1) |
| C(4) | 20(1) | 19(1) | 16(1) | -5(1) | 4(1) | 1(1) |
| C(5) | 19(1) | 24(1) | 21(1) | -6(1) | 7(1) | -4(1) |
| C(6) | 16(1) | 22(1) | 24(1) | -8(1) | 1(1) | -1(1) |
| C(7) | 28(1) | 16(1) | 32(1) | 4(1) | -8(1) | -2(1) |
| C(8) | 18(1) | 16(1) | 19(1) | 2(1) | 3(1) | 0(1) |
| C(9) | 19(1) | 17(1) | 18(1) | 1(1) | 5(1) | 0(1) |
| C(11) | 18(1) | 17(1) | 19(1) | 5(1) | 3(1) | -2(1) |
| C(12) | 22(1) | 18(1) | 23(1) | 2(1) | 6(1) | 5(1) |
| C(13) | 24(1) | 24(1) | 18(1) | -2(1) | 2(1) | 2(1) |
| C(14) | 18(1) | 24(1) | 20(1) | 4(1) | 1(1) | 4(1) |
| C(15) | 21(1) | 19(1) | 22(1) | 2(1) | 7(1) | 3(1) |
| C(16) | 22(1) | 19(1) | 19(1) | 0(1) | 4(1) | -1(1) |
| C(17) | 18(1) | 27(1) | 28(1) | 3(1) | 5(1) | -4(1) |
| C(18) | 14(1) | 23(1) | 16(1) | 2(1) | 2(1) | -1(1) |
| C(19) | 20(1) | 24(1) | 21(1) | -1(1) | 6(1) | -5(1) |
| C(20) | 21(1) | 18(1) | 21(1) | 0(1) | 7(1) | -6(1) |
| C(21) | 21(1) | 19(1) | 24(1) | 1(1) | 8(1) | -2(1) |
| C(22) | 28(1) | 22(1) | 21(1) | -2(1) | 11(1) | -4(1) |
| C(23) | 24(1) | 24(1) | 17(1) | 3(1) | 4(1) | -8(1) |
| C(24) | 20(1) | 27(1) | 26(1) | 2(1) | 7(1) | -1(1) |
| C(25) | 23(1) | 26(1) | 22(1) | -3(1) | 9(1) | -1(1) |
| N(1) | 19(1) | 16(1) | 21(1) | -1(1) | -1(1) | 1(1) |
| N(2) | 23(1) | 19(1) | 24(1) | 1(1) | 4(1) | 2(1) |
| O(1) | 15(1) | 27(1) | 22(1) | 2(1) | 1(1) | -4(1) |
| O(2) | 20(1) | 27(1) | 16(1) | -1(1) | 3(1) | -6(1) |
| F(1) | 28(1) | 42(1) | 17(1) | 3(1) | 2(1) | -6(1) |

Table 5. Bond lengths [Å] and angles [°] for C24 H21 F N2 O2

| | | | |
|---------------|-------------|----------------------|-------------|
| C (1)-C (6) | 1.3807 (17) | C (21)-C (22) | 1.3882 (17) |
| C (1)-C (2) | 1.4055 (16) | C (22)-C (23) | 1.3782 (18) |
| C (1)-C (7) | 1.5149 (17) | C (23)-F (1) | 1.3583 (14) |
| C (2)-C (3) | 1.3875 (16) | C (23)-C (24) | 1.3794 (18) |
| C (3)-O (1) | 1.3654 (13) | C (24)-C (25) | 1.3877 (18) |
| C (3)-C (4) | 1.4073 (16) | C (6)-C (1)-C (2) | 118.78 (11) |
| C (4)-O (2) | 1.3732 (14) | C (6)-C (1)-C (7) | 122.64 (11) |
| C (4)-C (5) | 1.3854 (16) | C (2)-C (1)-C (7) | 118.51 (11) |
| C (5)-C (6) | 1.3942 (17) | C (3)-C (2)-C (1) | 120.86 (11) |
| C (7)-C (8) | 1.5152 (16) | O (1)-C (3)-C (2) | 124.65 (10) |
| C (8)-C (9) | 1.3585 (16) | O (1)-C (3)-C (4) | 115.60 (10) |
| C (8)-C (18) | 1.4229 (16) | C (2)-C (3)-C (4) | 119.75 (10) |
| C (9)-N (1) | 1.3501 (15) | O (2)-C (4)-C (5) | 125.05 (10) |
| C (11)-C (16) | 1.3904 (16) | O (2)-C (4)-C (3) | 115.77 (10) |
| C (11)-C (12) | 1.3969 (16) | C (5)-C (4)-C (3) | 119.17 (10) |
| C (11)-N (1) | 1.4132 (15) | C (4)-C (5)-C (6) | 120.62 (11) |
| C (12)-C (13) | 1.3938 (17) | C (1)-C (6)-C (5) | 120.79 (11) |
| C (13)-C (14) | 1.3860 (17) | C (1)-C (7)-C (8) | 116.48 (10) |
| C (14)-C (15) | 1.3894 (17) | C (9)-C (8)-C (18) | 115.74 (10) |
| C (15)-C (16) | 1.3818 (17) | C (9)-C (8)-C (7) | 124.77 (10) |
| C (17)-O (1) | 1.4297 (14) | C (18)-C (8)-C (7) | 119.43 (10) |
| C (18)-N (2) | 1.1547 (16) | N (1)-C (9)-C (8) | 126.17 (11) |
| C (19)-O (2) | 1.4384 (14) | C (16)-C (11)-C (12) | 120.05 (11) |
| C (19)-C (20) | 1.4996 (16) | C (16)-C (11)-N (1) | 118.50 (10) |
| C (20)-C (21) | 1.3914 (16) | C (12)-C (11)-N (1) | 121.45 (10) |
| C (20)-C (25) | 1.3965 (17) | | |

C (13) -C (12) -C (11)
119.25 (11)
C (14) -C (13) -C (12)
120.59 (11)
C (13) -C (14) -C (15)
119.57 (11)
C (16) -C (15) -C (14)
120.50 (11)
C (15) -C (16) -C (11)
120.00 (11)
N (2) -C (18) -C (8)
178.00 (12)
O (2) -C (19) -C (20)
108.30 (9)
C (21) -C (20) -C (25)
119.00 (11)
C (21) -C (20) -C (19)
119.81 (11)
C (25) -C (20) -C (19)
121.19 (10)
C (22) -C (21) -C (20)
120.95 (11)

C (23) -C (22) -C (21)
117.99 (11)
F (1) -C (23) -C (22)
118.19 (11)
F (1) -C (23) -C (24)
118.58 (11)
C (22) -C (23) -C (24)
123.24 (11)
C (23) -C (24) -C (25)
117.78 (11)
C (24) -C (25) -C (20)
121.04 (11)
C (9) -N (1) -C (11)
123.82 (10)
C (3) -O (1) -C (17)
116.78 (9)
C (4) -O (2) -C (19)
115.65 (9)

Table 6. Torsion angles [°] for C24 H21 F N2 O2.

| | | | |
|-----------------------------|---|-----------------------------|---|
| | | C (14)-C (15)-C (16)-C (11) | - |
| | | 0.09 (17) | |
| C (6)-C (1)-C (2)-C (3) | - | C (12)-C (11)-C (16)-C (15) | |
| 1.10 (16) | | 1.86 (17) | |
| C (7)-C (1)-C (2)-C (3) | | N (1)-C (11)-C (16)-C (15) | - |
| 175.85 (10) | | 178.49 (10) | |
| C (1)-C (2)-C (3)-O (1) | - | O (2)-C (19)-C (20)-C (21) | |
| 179.95 (10) | | 111.57 (11) | |
| C (1)-C (2)-C (3)-C (4) | - | O (2)-C (19)-C (20)-C (25) | - |
| 0.08 (16) | | 67.92 (14) | |
| O (1)-C (3)-C (4)-O (2) | | C (25)-C (20)-C (21)-C (22) | |
| 2.85 (14) | | 0.36 (17) | |
| C (2)-C (3)-C (4)-O (2) | - | C (19)-C (20)-C (21)-C (22) | - |
| 177.03 (10) | | 179.14 (10) | |
| O (1)-C (3)-C (4)-C (5) | - | C (20)-C (21)-C (22)-C (23) | |
| 178.45 (10) | | 0.56 (17) | |
| C (2)-C (3)-C (4)-C (5) | | C (21)-C (22)-C (23)-F (1) | |
| 1.67 (16) | | 179.18 (10) | |
| O (2)-C (4)-C (5)-C (6) | | C (21)-C (22)-C (23)-C (24) | - |
| 176.48 (10) | | 0.92 (18) | |
| C (3)-C (4)-C (5)-C (6) | - | F (1)-C (23)-C (24)-C (25) | - |
| 2.09 (17) | | 179.79 (10) | |
| C (2)-C (1)-C (6)-C (5) | | C (22)-C (23)-C (24)-C (25) | |
| 0.69 (17) | | 0.30 (18) | |
| C (7)-C (1)-C (6)-C (5) | - | C (23)-C (24)-C (25)-C (20) | |
| 176.13 (11) | | 0.67 (18) | |
| C (4)-C (5)-C (6)-C (1) | | C (21)-C (20)-C (25)-C (24) | - |
| 0.92 (17) | | 1.00 (17) | |
| C (6)-C (1)-C (7)-C (8) | - | C (19)-C (20)-C (25)-C (24) | |
| 41.91 (17) | | 178.49 (11) | |
| C (2)-C (1)-C (7)-C (8) | | C (8)-C (9)-N (1)-C (11) | - |
| 141.26 (11) | | 178.97 (11) | |
| C (1)-C (7)-C (8)-C (9) | | C (16)-C (11)-N (1)-C (9) | |
| 147.30 (12) | | 150.06 (11) | |
| C (1)-C (7)-C (8)-C (18) | - | C (12)-C (11)-N (1)-C (9) | - |
| 35.57 (17) | | 30.30 (17) | |
| C (18)-C (8)-C (9)-N (1) | | C (2)-C (3)-O (1)-C (17) | - |
| 175.15 (11) | | 9.45 (16) | |
| C (7)-C (8)-C (9)-N (1) | - | C (4)-C (3)-O (1)-C (17) | |
| 7.62 (19) | | 170.67 (10) | |
| C (16)-C (11)-C (12)-C (13) | - | C (5)-C (4)-O (2)-C (19) | |
| 2.37 (17) | | 4.50 (16) | |
| N (1)-C (11)-C (12)-C (13) | | C (3)-C (4)-O (2)-C (19) | - |
| 178.00 (10) | | 176.89 (10) | |
| C (11)-C (12)-C (13)-C (14) | | C (20)-C (19)-O (2)-C (4) | - |
| 1.13 (18) | | 173.58 (9) | |
| C (12)-C (13)-C (14)-C (15) | | | |
| 0.62 (18) | | | |
| C (13)-C (14)-C (15)-C (16) | - | | |
| 1.15 (18) | | | |

Table 7. Bond lengths [Å] and angles [°] related to the hydrogen bonding for C24 H21 F N2 O2.

| D-H | ..A | d(D-H) | d(H..A) | d(D..A) | <DHA |
|-----------|--------|------------|------------|-------------|------------|
| N(1)-H(1) | N(2)#1 | 0.904 (17) | 2.247 (17) | 3.1312 (14) | 165.9 (14) |

Symmetry transformations used to generate equivalent atoms:

#1 -x+1, y+1/2, -z+1/2

REFERENCES

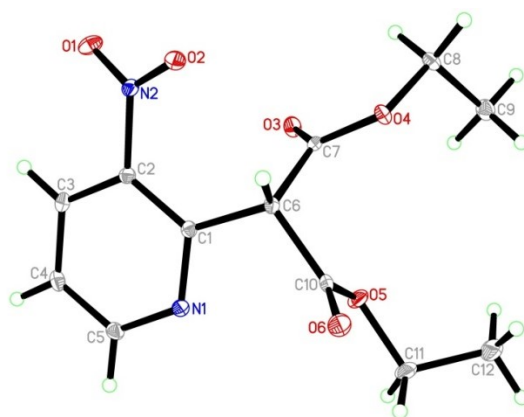
- APEX2 (2013), Bruker AXS Inc., Madison, WI 53719-1173.
- SAINT (2013) V8.34A, Bruker AXS Inc., Madison, WI 53719-1173.
- Sheldrick, G. M. (2012). SADABS-2012/1, Bruker AXS Inc., Madison, WI 53719-1173.
- Sheldrick, G.M. (2008). Acta Cryst. A64, 112-122.
- Spek, A.L. (2009). Acta Cryst. D65, 148.
- Maris, T. (2004). UdmX, University of Montréal, Montréal, QC, Canada.
- XP (1998) Version 5.1, Bruker AXS Inc., Madison, WI 53719-1173.
- XPREP (2013); X-ray data Preparation and Reciprocal space Exploration Program. Bruker AXS Inc., Madison, WI 53719-1173

Annex 2

Additional Experimental Data (Crystallographic Data for Compounds 3.12 and (Z)-3.9 from Supporting Information Section 3 - Chapter 3)

*The data from this Annex have been published in Supporting Information of: **Bernard-Gauthier, V.**; Aliaga, A.; Aliaga, A.; Boudjemeline, M.; Hopewell, R.; Kostikov, A.; Rosa-Neto, P.; Thiel, A.; Schirmacher, R. Syntheses and Evaluation of Carbon-11- and Fluorine-18-Radiolabeled pan-Tropomyosin Receptor Kinases (Trk) Inhibitors: Exploration of the 4-aza-2-Oxindole Scaffold as Trk PET Imaging Agents *ACS Chem. Neurosci.* **2015**, 6, 260-267.*

CRYSTAL AND MOLECULAR STRUCTURE OF
C₁₂ H₁₄ N₂ O₆ COMPOUND (INSN15)



Structure solved and refined in the laboratory of X-ray diffraction
Université de Montréal by Michel Simard.

Table 1. Crystal data and structure refinement for C12 H14 N2 O6.

| Identification code | INSN15 |
|-----------------------------------|---|
| Empirical formula | C12 H14 N2 O6 |
| Formula weight | 282.25 |
| Temperature | 100K |
| Wavelength | 1.54178 Å |
| Crystal system | Monoclinic |
| Space group | C2/c |
| Unit cell dimensions | a = 19.8614(6) Å $\alpha = 90^\circ$ b = 7.8836(2) Å $\beta = 95.6344(12)^\circ$ c = 16.6615(5) Å $\gamma = 90^\circ$ |
| Volume | 2596.24(13) Å ³ |
| Z | 8 |
| Density (calculated) | 1.444 g/cm ³ |
| Absorption coefficient | 1.004 mm ⁻¹ |
| F(000) | 1184 |
| Crystal size | 0.16 x 0.12 x 0.06 mm |
| Theta range for data collection | 4.474 to 71.717° |
| Index ranges | -24 ≤ h ≤ 22, -9 ≤ k ≤ 9, -20 ≤ l ≤ 20 |
| Reflections collected | 70890 |
| Independent reflections | 2522 [R _{int} = 0.045] |
| Absorption correction | Semi-empirical from equivalents |
| Max. and min. transmission | 0.7535 and 0.6865 |
| Refinement method | Full-matrix least-squares on F ² |
| Data / restraints / parameters | 2522 / 0 / 183 |
| Goodness-of-fit on F ² | 1.046 |
| Final R indices [I > 2σ(I)] | R ₁ = 0.0337, wR ₂ = 0.0860 |

R indices (all data)

$$R_1 = 0.0343, wR_2 = 0.0866$$

Largest diff. peak and hole

$$0.453 \text{ and } -0.240 \text{ e/\AA}^3$$

Table 2. Atomic coordinates ($\times 10^4$) and equivalent isotropic displacement parameters ($\text{\AA}^2 \times 10^3$) for C12 H14 N2 O6.

U_{eq} is defined as one third of the trace of the orthogonalized U_{ij} tensor.

| | x | y | z | U_{eq} |
|-------|----------|----------|----------|----------|
| C(1) | 4488 (1) | 4433 (1) | 6553 (1) | 12 (1) |
| C(2) | 5083 (1) | 4216 (1) | 6174 (1) | 13 (1) |
| C(3) | 5442 (1) | 5600 (2) | 5935 (1) | 16 (1) |
| C(4) | 5213 (1) | 7199 (2) | 6106 (1) | 17 (1) |
| C(5) | 4643 (1) | 7328 (2) | 6519 (1) | 17 (1) |
| C(6) | 4030 (1) | 3007 (1) | 6780 (1) | 13 (1) |
| C(7) | 3775 (1) | 1903 (1) | 6059 (1) | 13 (1) |
| C(8) | 3145 (1) | -618 (2) | 5720 (1) | 19 (1) |
| C(9) | 2430 (1) | -73 (2) | 5459 (1) | 21 (1) |
| C(10) | 3429 (1) | 3747 (1) | 7167 (1) | 15 (1) |
| C(11) | 2351 (1) | 5091 (2) | 6867 (1) | 26 (1) |
| C(12) | 1761 (1) | 3927 (2) | 6774 (1) | 31 (1) |
| N(1) | 4282 (1) | 5992 (1) | 6725 (1) | 15 (1) |
| N(2) | 5354 (1) | 2529 (1) | 6022 (1) | 15 (1) |
| O(1) | 5744 (1) | 2394 (1) | 5502 (1) | 24 (1) |
| O(2) | 5185 (1) | 1332 (1) | 6435 (1) | 20 (1) |
| O(3) | 3844 (1) | 2210 (1) | 5367 (1) | 19 (1) |
| O(4) | 3461 (1) | 549 (1) | 6328 (1) | 16 (1) |
| O(5) | 2948 (1) | 4259 (1) | 6603 (1) | 21 (1) |
| O(6) | 3402 (1) | 3810 (1) | 7884 (1) | 23 (1) |

Table 3. Hydrogen coordinates ($\times 10^4$) and isotropic displacement parameters ($\text{\AA}^2 \times 10^3$) for C12 H14 N2 O6.

| | x | y | z | U_{eq} |
|--------|------|-------|------|----------|
| H(3) | 5836 | 5454 | 5661 | 19 |
| H(4) | 5439 | 8185 | 5944 | 21 |
| H(5) | 4501 | 8427 | 6664 | 21 |
| H(6) | 4293 | 2271 | 7188 | 15 |
| H(8A) | 3143 | -1779 | 5946 | 23 |
| H(8B) | 3411 | -638 | 5247 | 23 |
| H(9A) | 2216 | -905 | 5079 | 31 |
| H(9B) | 2436 | 1039 | 5196 | 31 |
| H(9C) | 2174 | 3 | 5931 | 31 |
| H(11A) | 2248 | 6127 | 6541 | 31 |
| H(11B) | 2442 | 5433 | 7439 | 31 |
| H(12A) | 1697 | 3511 | 6218 | 46 |
| H(12B) | 1355 | 4536 | 6900 | 46 |
| H(12C) | 1843 | 2966 | 7144 | 46 |

Table 4. Anisotropic parameters ($\text{\AA}^2 \times 10^3$) for C12 H14 N2 O6.

The anisotropic displacement factor exponent takes the form:

$$-2 \pi^2 [h^2 a^{*2} U_{11} + \dots + 2 h k a^* b^* U_{12}]$$

| | U11 | U22 | U33 | U23 | U13 | U12 |
|-------|-------|-------|-------|--------|-------|-------|
| C(1) | 11(1) | 14(1) | 12(1) | 0(1) | -1(1) | 0(1) |
| C(2) | 12(1) | 14(1) | 13(1) | -1(1) | -1(1) | 2(1) |
| C(3) | 11(1) | 20(1) | 15(1) | 1(1) | 0(1) | -1(1) |
| C(4) | 15(1) | 16(1) | 20(1) | 4(1) | -2(1) | -4(1) |
| C(5) | 16(1) | 12(1) | 22(1) | 0(1) | -2(1) | 1(1) |
| C(6) | 11(1) | 13(1) | 14(1) | 0(1) | 1(1) | -1(1) |
| C(7) | 9(1) | 12(1) | 17(1) | -1(1) | 2(1) | 1(1) |
| C(8) | 20(1) | 13(1) | 24(1) | -6(1) | 1(1) | -4(1) |
| C(9) | 20(1) | 22(1) | 21(1) | -2(1) | 0(1) | -4(1) |
| C(10) | 13(1) | 14(1) | 19(1) | -4(1) | 4(1) | -6(1) |
| C(11) | 15(1) | 29(1) | 35(1) | -12(1) | 4(1) | 5(1) |
| C(12) | 17(1) | 34(1) | 42(1) | -10(1) | 5(1) | 1(1) |
| N(1) | 13(1) | 14(1) | 18(1) | -1(1) | 1(1) | 1(1) |
| N(2) | 12(1) | 16(1) | 17(1) | -3(1) | 0(1) | 1(1) |
| O(1) | 23(1) | 28(1) | 22(1) | -4(1) | 10(1) | 6(1) |
| O(2) | 19(1) | 14(1) | 29(1) | 2(1) | 4(1) | 1(1) |
| O(3) | 20(1) | 21(1) | 15(1) | -2(1) | 4(1) | -5(1) |
| O(4) | 17(1) | 13(1) | 18(1) | -1(1) | 1(1) | -4(1) |
| O(5) | 12(1) | 28(1) | 22(1) | -8(1) | 1(1) | 4(1) |
| O(6) | 26(1) | 27(1) | 17(1) | -4(1) | 8(1) | -4(1) |

Table 5. Bond lengths [Å] and angles [°] for C12 H14 N2 O6

| | |
|-------------------|---------------------|
| C (1)-N (1) | C (3)-C (2)-C (1) |
| 1.3366 (15) | 120.91 (10) |
| C (1)-C (2) | C (3)-C (2)-N (2) |
| 1.4023 (16) | 117.16 (10) |
| C (1)-C (6) | C (1)-C (2)-N (2) |
| 1.5182 (15) | 121.93 (10) |
| C (2)-C (3) | C (4)-C (3)-C (2) |
| 1.3844 (16) | 118.11 (10) |
| C (2)-N (2) | C (3)-C (4)-C (5) |
| 1.4661 (14) | 118.17 (11) |
| C (3)-C (4) | N (1)-C (5)-C (4) |
| 1.3793 (17) | 123.79 (11) |
| C (4)-C (5) | C (1)-C (6)-C (10) |
| 1.3837 (17) | 109.59 (9) |
| C (5)-N (1) | C (1)-C (6)-C (7) |
| 1.3386 (15) | 112.66 (9) |
| C (6)-C (10) | C (10)-C (6)-C (7) |
| 1.5271 (15) | 109.71 (9) |
| C (6)-C (7) | O (3)-C (7)-O (4) |
| 1.5290 (15) | 125.77 (10) |
| C (7)-O (3) | O (3)-C (7)-C (6) |
| 1.1996 (14) | 125.53 (10) |
| C (7)-O (4) | O (4)-C (7)-C (6) |
| 1.3365 (13) | 108.70 (9) |
| C (8)-O (4) | O (4)-C (8)-C (9) |
| 1.4633 (14) | 110.39 (10) |
| C (8)-C (9) | O (6)-C (10)-O (5) |
| 1.5064 (17) | 126.13 (11) |
| C (10)-O (6) | O (6)-C (10)-C (6) |
| 1.2012 (15) | 123.20 (11) |
| C (10)-O (5) | O (5)-C (10)-C (6) |
| 1.3345 (15) | 110.65 (9) |
| C (11)-O (5) | O (5)-C (11)-C (12) |
| 1.4610 (14) | 110.30 (11) |
| C (11)-C (12) | C (1)-N (1)-C (5) |
| 1.4838 (19) | 118.92 (10) |
| N (2)-O (1) | O (1)-N (2)-O (2) |
| 1.2217 (13) | 123.74 (10) |
| N (2)-O (2) | O (1)-N (2)-C (2) |
| 1.2343 (13) | 118.13 (10) |
| | O (2)-N (2)-C (2) |
| N (1)-C (1)-C (2) | 118.12 (9) |
| 119.96 (10) | C (7)-O (4)-C (8) |
| N (1)-C (1)-C (6) | 116.92 (9) |
| 115.01 (10) | C (10)-O (5)-C (11) |
| C (2)-C (1)-C (6) | 117.98 (10) |
| 125.02 (10) | |

Table 6. Torsion angles [°] for C12 H14 N2 O6.

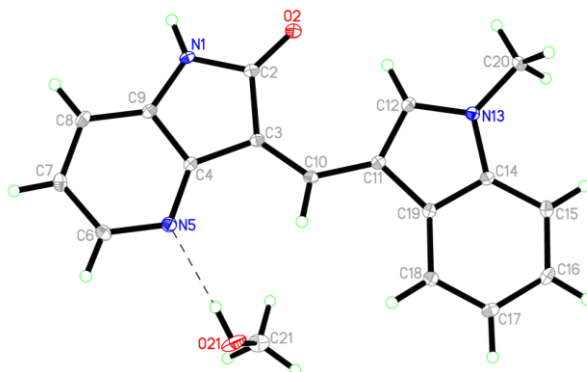
—

| | |
|------------------------|-------------|
| N(1)-C(1)-C(2)-C(3) | -3.56(16) |
| C(6)-C(1)-C(2)-C(3) | 175.14(10) |
| N(1)-C(1)-C(2)-N(2) | 175.85(10) |
| C(6)-C(1)-C(2)-N(2) | -5.46(17) |
| C(1)-C(2)-C(3)-C(4) | 2.31(16) |
| N(2)-C(2)-C(3)-C(4) | -177.13(10) |
| C(2)-C(3)-C(4)-C(5) | 1.13(16) |
| C(3)-C(4)-C(5)-N(1) | -3.65(18) |
| N(1)-C(1)-C(6)-C(10) | -0.30(13) |
| C(2)-C(1)-C(6)-C(10) | -179.05(10) |
| N(1)-C(1)-C(6)-C(7) | 122.14(10) |
| C(2)-C(1)-C(6)-C(7) | -56.62(14) |
| C(1)-C(6)-C(7)-O(3) | -9.30(16) |
| C(10)-C(6)-C(7)-O(3) | 113.07(12) |
| C(1)-C(6)-C(7)-O(4) | 171.07(9) |
| C(10)-C(6)-C(7)-O(4) | -66.56(11) |
| C(1)-C(6)-C(10)-O(6) | -98.76(13) |
| | |
| C(7)-C(6)-C(10)-O(6) | 137.06(11) |
| C(1)-C(6)-C(10)-O(5) | 82.61(11) |
| C(7)-C(6)-C(10)-O(5) | -41.57(12) |
| C(2)-C(1)-N(1)-C(5) | 1.17(16) |
| C(6)-C(1)-N(1)-C(5) | -177.65(10) |
| C(4)-C(5)-N(1)-C(1) | 2.46(17) |
| C(3)-C(2)-N(2)-O(1) | -21.33(14) |
| C(1)-C(2)-N(2)-O(1) | 159.24(10) |
| C(3)-C(2)-N(2)-O(2) | 157.51(10) |
| C(1)-C(2)-N(2)-O(2) | -21.92(15) |
| O(3)-C(7)-O(4)-C(8) | -3.10(16) |
| C(6)-C(7)-O(4)-C(8) | 176.52(9) |
| C(9)-C(8)-O(4)-C(7) | -88.32(12) |
| O(6)-C(10)-O(5)-C(11) | 4.83(18) |
| C(6)-C(10)-O(5)-C(11) | -176.59(10) |
| C(12)-C(11)-O(5)-C(10) | -105.81(13) |

REFERENCES

- APEX2 (2013), Bruker AXS Inc., Madison, WI 53719-1173.
- SAINT (2013) V8.34A, Bruker AXS Inc., Madison, WI 53719-1173.
- Sheldrick, G. M. (2012). SADABS-2012/1, Bruker AXS Inc., Madison, WI 53719-1173.
- Sheldrick, G.M. (2008). Acta Cryst. A64, 112-122.
- Spek, A.L. (2009). Acta Cryst. D65, 148.
- Maris, T. (2004). UdmX, University of Montréal, Montréal, QC, Canada.
- XP (1998) Version 5.1, Bruker AXS Inc., Madison, WI 53719-1173.
- XPREP (2013); X-ray data Preparation and Reciprocal space Exploration Program. Bruker AXS Inc., Madison, WI 53719-1173.

CRYSTAL AND MOLECULAR STRUCTURE OF
C₁₈ H₁₇ N₃ O₂ COMPOUND (INSN14)



Structure solved and refined in the laboratory of X-ray diffraction
Université de Montréal by Michel Simard.

Table 1. Crystal data and structure refinement for C18 H17 N3 O2.

| | |
|-----------------------------------|--|
| Identification code | INSN14 |
| Empirical formula | C18 H17 N3 O2 |
| Formula weight | 307.34 |
| Temperature | 100K |
| Wavelength | 1.54178 Å |
| Crystal system | Monoclinic |
| Space group | P2 ₁ |
| Unit cell dimensions | a = 8.6286(5) Å $\alpha = 90^\circ$ b = 6.1649(4) Å $\beta = 99.9863(19)^\circ$ c = 14.2037(9) Å $\gamma = 90^\circ$ |
| Volume | 744.11(8) Å ³ |
| Z | 2 |
| Density (calculated) | 1.372 g/cm ³ |
| Absorption coefficient | 0.741 mm ⁻¹ |
| F(000) | 324 |
| Crystal size | 0.18 x 0.16 x 0.05 mm |
| Theta range for data collection | 3.159 to 71.540° |
| Index ranges | -10 ≤ h ≤ 10, -7 ≤ k ≤ 7, -17 ≤ l ≤ 17 |
| Reflections collected | 30266 |
| Independent reflections | 2851 [R _{int} = 0.036] |
| Absorption correction | Semi-empirical from equivalents |
| Max. and min. transmission | 0.7535 and 0.6788 |
| Refinement method | Full-matrix least-squares on F ² |
| Data / restraints / parameters | 2851 / 1 / 218 |
| Goodness-of-fit on F ² | 1.076 |
| Final R indices [I > 2σ(I)] | R ₁ = 0.0269, wR ₂ = 0.0706 |

| | |
|------------------------------------|---|
| R indices (all data) | $R_1 = 0.0270, wR_2 = 0.0706$ |
| Absolute structure parameter | 0.08(4) |
| Largest diff. peak and hole | 0.198 and -0.150 e/Å³ |

Table 2. Atomic coordinates ($\times 10^4$) and equivalent isotropic displacement parameters ($\text{\AA}^2 \times 10^3$) for C18 H17 N3 O2.

U_{eq} is defined as one third of the trace of the orthogonalized U_{ij} tensor.

| | x | y | z | U_{eq} |
|-------|----------|----------|---------|----------|
| C(2) | -808(2) | 2667(3) | 2495(1) | 15(1) |
| C(3) | 851(2) | 2457(3) | 2344(1) | 14(1) |
| C(4) | 880(2) | 506(3) | 1767(1) | 14(1) |
| C(6) | 1772(2) | -2219(3) | 918(1) | 18(1) |
| C(7) | 307(2) | -3215(3) | 749(1) | 18(1) |
| C(8) | -955(2) | -2300(3) | 1101(1) | 18(1) |
| C(9) | -651(2) | -389(3) | 1605(1) | 15(1) |
| C(10) | 2123(2) | 3733(3) | 2660(1) | 14(1) |
| C(11) | 2309(2) | 5685(3) | 3207(1) | 14(1) |
| C(12) | 1218(2) | 6864(3) | 3609(1) | 15(1) |
| C(14) | 3456(2) | 8764(3) | 3921(1) | 14(1) |
| C(15) | 4580(2) | 10365(3) | 4221(1) | 17(1) |
| C(16) | 6063(2) | 10036(3) | 3995(1) | 19(1) |
| C(17) | 6405(2) | 8165(3) | 3505(1) | 18(1) |
| C(18) | 5280(2) | 6587(3) | 3214(1) | 16(1) |
| C(19) | 3766(2) | 6895(3) | 3416(1) | 14(1) |
| C(20) | 1134(2) | 10217(3) | 4590(1) | 18(1) |
| N(1) | -1618(2) | 929(3) | 2040(1) | 17(1) |
| N(5) | 2082(2) | -368(2) | 1426(1) | 16(1) |
| N(13) | 1889(2) | 8679(2) | 4034(1) | 14(1) |
| O(2) | -1414(1) | 4056(2) | 2935(1) | 22(1) |
| C(21) | 4901(2) | 2878(4) | 792(2) | 31(1) |
| O(21) | 5123(2) | 1077(3) | 1404(1) | 31(1) |

Table 3. Hydrogen coordinates ($\times 10^4$) and isotropic displacement parameters ($\text{\AA}^2 \times 10^3$) for C18 H17 N3 O2.

| | x | y | z | U_{eq} |
|--------|------------|----------|-----------|----------|
| H(6) | 2604 | -2877 | 662 | 21 |
| H(7) | 165 | -4525 | 393 | 21 |
| H(8) | -1967 | -2955 | 999 | 22 |
| H(10) | 3070 | 3225 | 2481 | 17 |
| H(12) | 151 | 6456 | 3588 | 18 |
| H(15) | 4341 | 11612 | 4561 | 20 |
| H(16) | 6861 | 11093 | 4174 | 23 |
| H(17) | 7437 | 7975 | 3370 | 21 |
| H(18) | 5531 | 5329 | 2885 | 19 |
| H(20A) | 1538 | 10005 | 5272 | 28 |
| H(20B) | -6 | 9979 | 4465 | 28 |
| H(20C) | 1362 | 11700 | 4407 | 28 |
| H(1) | -2640 (30) | 830 (40) | 1969 (16) | 24 (6) |
| H(21A) | 4815 | 2392 | 128 | 46 |
| H(21B) | 5798 | 3866 | 949 | 46 |
| H(21C) | 3933 | 3635 | 872 | 46 |
| H(21) | 4160 (30) | 640 (50) | 1468 (18) | 38 (7) |

Table 4. Anisotropic parameters ($\text{\AA}^2 \times 10^3$) for C18 H17 N3 O2.

The anisotropic displacement factor exponent takes the form:

$$-2 \pi^2 [h^2 a^{*2} U_{11} + \dots + 2 h k a^* b^* U_{12}]$$

| | U11 | U22 | U33 | U23 | U13 | U12 |
|-------|-------|-------|-------|-------|-------|-------|
| C(2) | 13(1) | 17(1) | 17(1) | 2(1) | 4(1) | 0(1) |
| C(3) | 14(1) | 15(1) | 14(1) | 2(1) | 3(1) | 0(1) |
| C(4) | 13(1) | 14(1) | 13(1) | 2(1) | 1(1) | -1(1) |
| C(6) | 19(1) | 17(1) | 17(1) | 1(1) | 3(1) | 4(1) |
| C(7) | 23(1) | 14(1) | 15(1) | 0(1) | 0(1) | 0(1) |
| C(8) | 17(1) | 19(1) | 17(1) | 1(1) | -1(1) | -5(1) |
| C(9) | 14(1) | 15(1) | 15(1) | 3(1) | 2(1) | -1(1) |
| C(10) | 12(1) | 16(1) | 14(1) | 2(1) | 2(1) | 3(1) |
| C(11) | 13(1) | 14(1) | 13(1) | 2(1) | 2(1) | -1(1) |
| C(12) | 15(1) | 16(1) | 14(1) | 1(1) | 2(1) | -2(1) |
| C(14) | 13(1) | 14(1) | 13(1) | 2(1) | 1(1) | 1(1) |
| C(15) | 19(1) | 15(1) | 15(1) | -1(1) | 0(1) | 0(1) |
| C(16) | 16(1) | 18(1) | 21(1) | 1(1) | -2(1) | -4(1) |
| C(17) | 12(1) | 21(1) | 20(1) | 3(1) | 2(1) | 1(1) |
| C(18) | 16(1) | 16(1) | 15(1) | 1(1) | 2(1) | 2(1) |
| C(19) | 15(1) | 13(1) | 13(1) | 2(1) | 0(1) | 0(1) |
| C(20) | 19(1) | 19(1) | 19(1) | -4(1) | 6(1) | 2(1) |
| N(1) | 10(1) | 19(1) | 23(1) | -3(1) | 4(1) | -3(1) |
| N(5) | 15(1) | 16(1) | 16(1) | 0(1) | 2(1) | 1(1) |
| N(13) | 14(1) | 14(1) | 15(1) | -1(1) | 3(1) | 0(1) |
| O(2) | 16(1) | 22(1) | 29(1) | -6(1) | 8(1) | -1(1) |
| C(21) | 26(1) | 36(1) | 31(1) | 4(1) | 6(1) | 2(1) |
| O(21) | 12(1) | 36(1) | 45(1) | 12(1) | 2(1) | -3(1) |

Table 5. Bond lengths [Å] and angles [°] for C18 H17 N3 O2

| | | | |
|----------------|------------|-------------------|------------|
| C(2)-O(2) | 1.229(2) | O(2)-C(2)-C(3) | 129.62(16) |
| C(2)-N(1) | 1.378(2) | N(1)-C(2)-C(3) | 106.63(15) |
| C(2)-C(3) | 1.490(2) | C(10)-C(3)-C(4) | 124.76(15) |
| C(3)-C(10) | 1.362(2) | C(10)-C(3)-C(2) | 129.96(16) |
| C(3)-C(4) | 1.458(2) | C(4)-C(3)-C(2) | 105.28(14) |
| C(4)-N(5) | 1.332(2) | N(5)-C(4)-C(9) | 123.19(16) |
| C(4)-C(9) | 1.414(2) | N(5)-C(4)-C(3) | 128.94(15) |
| C(6)-N(5) | 1.352(2) | C(9)-C(4)-C(3) | 107.88(14) |
| C(6)-C(7) | 1.388(3) | N(5)-C(6)-C(7) | 123.75(16) |
| C(7)-C(8) | 1.394(3) | C(6)-C(7)-C(8) | 120.26(17) |
| C(8)-C(9) | 1.380(3) | C(9)-C(8)-C(7) | 116.20(16) |
| C(9)-N(1) | 1.384(2) | C(8)-C(9)-N(1) | 131.13(16) |
| C(10)-C(11) | 1.427(2) | C(8)-C(9)-C(4) | 120.39(16) |
| C(11)-C(12) | 1.388(3) | N(1)-C(9)-C(4) | 108.46(15) |
| C(11)-C(19) | 1.448(2) | C(3)-C(10)-C(11) | 132.42(15) |
| C(12)-N(13) | 1.353(2) | C(12)-C(11)-C(10) | 130.25(16) |
| C(14)-N(13) | 1.390(2) | C(12)-C(11)-C(19) | 105.83(15) |
| C(14)-C(15) | 1.397(2) | C(10)-C(11)-C(19) | 123.87(15) |
| C(14)-C(19) | 1.407(2) | N(13)-C(12)-C(11) | 110.40(15) |
| C(15)-C(16) | 1.387(2) | N(13)-C(14)-C(15) | 128.95(16) |
| C(16)-C(17) | 1.404(3) | N(13)-C(14)-C(19) | 107.62(14) |
| C(17)-C(18) | 1.386(2) | C(15)-C(14)-C(19) | 123.43(16) |
| C(18)-C(19) | 1.398(2) | C(16)-C(15)-C(14) | 116.44(16) |
| C(20)-N(13) | 1.458(2) | C(15)-C(16)-C(17) | 121.06(17) |
| C(21)-O(21) | 1.402(3) | C(18)-C(17)-C(16) | 121.87(16) |
| O(2)-C(2)-N(1) | 123.74(16) | C(17)-C(18)-C(19) | 118.33(16) |

C (18) -C (19) -C (14)
118.84 (15)
C (18) -C (19) -C (11)
134.22 (16)
C (14) -C (19) -C (11)
106.93 (15)
C (2) -N (1) -C (9)
111.75 (14)
C (4) -N (5) -C (6)
116.17 (15)

C (12) -N (13) -C (14)
109.21 (14)
C (12) -N (13) -C (20)
125.64 (15)
C (14) -N (13) -C (20)
124.98 (14)

Table 6. Torsion angles [°] for C18 H17 N3 O2.

| | | | |
|-------------------------|---------|-------------------------|---------|
| | | N(13)-C(14)-C(19)-C(11) | |
| O(2)-C(2)-C(3)-C(10) | 0.6(3) | 1.20(17) | |
| N(1)-C(2)-C(3)-C(10) | - | C(15)-C(14)-C(19)-C(11) | - |
| 178.79(17) | | 178.07(15) | |
| O(2)-C(2)-C(3)-C(4) | - | C(12)-C(11)-C(19)-C(18) | - |
| 179.90(17) | | 179.97(18) | |
| N(1)-C(2)-C(3)-C(4) | | C(10)-C(11)-C(19)-C(18) | -2.3(3) |
| 0.68(18) | | C(12)-C(11)-C(19)-C(14) | - |
| C(10)-C(3)-C(4)-N(5) | -1.7(3) | 0.95(18) | |
| C(2)-C(3)-C(4)-N(5) | | C(10)-C(11)-C(19)-C(14) | |
| 178.78(17) | | 176.76(15) | |
| C(10)-C(3)-C(4)-C(9) | | O(2)-C(2)-N(1)-C(9) | - |
| 178.57(15) | | 179.63(16) | |
| C(2)-C(3)-C(4)-C(9) | - | C(3)-C(2)-N(1)-C(9) | - |
| 0.94(17) | | 0.17(19) | |
| N(5)-C(6)-C(7)-C(8) | 0.7(3) | C(8)-C(9)-N(1)-C(2) | |
| C(6)-C(7)-C(8)-C(9) | 0.5(2) | 178.11(17) | |
| C(7)-C(8)-C(9)-N(1) | | C(4)-C(9)-N(1)-C(2) | - |
| 179.69(17) | | 0.44(19) | |
| C(7)-C(8)-C(9)-C(4) | -1.9(2) | C(9)-C(4)-N(5)-C(6) | -1.2(2) |
| N(5)-C(4)-C(9)-C(8) | 2.4(2) | C(3)-C(4)-N(5)-C(6) | |
| C(3)-C(4)-C(9)-C(8) | - | 179.14(16) | |
| 177.87(14) | | C(7)-C(6)-N(5)-C(4) | -0.3(2) |
| N(5)-C(4)-C(9)-N(1) | - | C(11)-C(12)-N(13)-C(14) | |
| 178.87(16) | | 0.42(18) | |
| C(3)-C(4)-C(9)-N(1) | | C(11)-C(12)-N(13)-C(20) | - |
| 0.86(18) | | 175.06(15) | |
| C(4)-C(3)-C(10)-C(11) | | C(15)-C(14)-N(13)-C(12) | |
| 178.80(16) | | 178.19(17) | |
| C(2)-C(3)-C(10)-C(11) | -1.8(3) | C(19)-C(14)-N(13)-C(12) | - |
| C(3)-C(10)-C(11)-C(12) | 1.7(3) | 1.02(17) | |
| C(3)-C(10)-C(11)-C(19) | - | C(15)-C(14)-N(13)-C(20) | -6.3(3) |
| 175.42(17) | | C(19)-C(14)-N(13)-C(20) | |
| C(10)-C(11)-C(12)-N(13) | - | 174.50(15) | |
| 177.17(16) | | | |
| C(19)-C(11)-C(12)-N(13) | | | |
| 0.34(18) | | | |
| N(13)-C(14)-C(15)-C(16) | - | | |
| 179.06(16) | | | |
| C(19)-C(14)-C(15)-C(16) | 0.0(2) | | |
| C(14)-C(15)-C(16)-C(17) | -1.1(3) | | |
| C(15)-C(16)-C(17)-C(18) | 1.0(3) | | |
| | | | |
| C(16)-C(17)-C(18)-C(19) | 0.2(2) | | |
| C(17)-C(18)-C(19)-C(14) | -1.2(2) | | |
| C(17)-C(18)-C(19)-C(11) | | | |
| 177.71(17) | | | |
| N(13)-C(14)-C(19)-C(18) | - | | |
| 179.60(14) | | | |
| C(15)-C(14)-C(19)-C(18) | 1.1(2) | | |

Table 7. Bond lengths [\AA] and angles [$^\circ$] related to the hydrogen bonding for C18 H17 N3 O2.

| D-H | ..A | d(D-H) | d(H..A) | d(D..A) | <DHA |
|-------------|---------|---------|---------|----------|--------|
| N(1)-H(1) | O(21)#1 | 0.87(3) | 1.96(3) | 2.802(2) | 161(2) |
| O(21)-H(21) | N(5) | 0.89(3) | 1.89(3) | 2.777(2) | 172(2) |

Symmetry transformations used to generate equivalent atoms:

#1 $x-1, y, z$

REFERENCES

- Flack, H. D. & Bernardinelli, G. (2000). *J. Appl. Cryst.* 33, 1143-1148.
- Parsons, S. & Flack, H. D. (2004). *Acta Cryst.* A60, s61.
- APEX2 (2013), Bruker AXS Inc., Madison, WI 53719-1173.
- SAINT (2013) V8.34A, Bruker AXS Inc., Madison, WI 53719-1173.
- Sheldrick, G. M. (2012). SADABS-2012/1, Bruker AXS Inc., Madison, WI 53719-1173.
- Sheldrick, G.M. (2008). *Acta Cryst.* A64, 112-122.
- Spek, A.L. (2009). *Acta Cryst.* D65, 148.
- Maris, T. (2004). UdmX, University of Montréal, Montréal, QC, Canada.
- XP (1998) Version 5.1, Bruker AXS Inc., Madison, WI 53719-1173.
- XPREP (2013); X-ray data Preparation and Reciprocal space Exploration Program. Bruker AXS Inc., Madison, WI 53719-1173.

Additional Experimental Data (NMR Spectrum and Crystallographic Data for Compound 4.22 from Supporting Information Section 5 and 6 - Chapter 4)

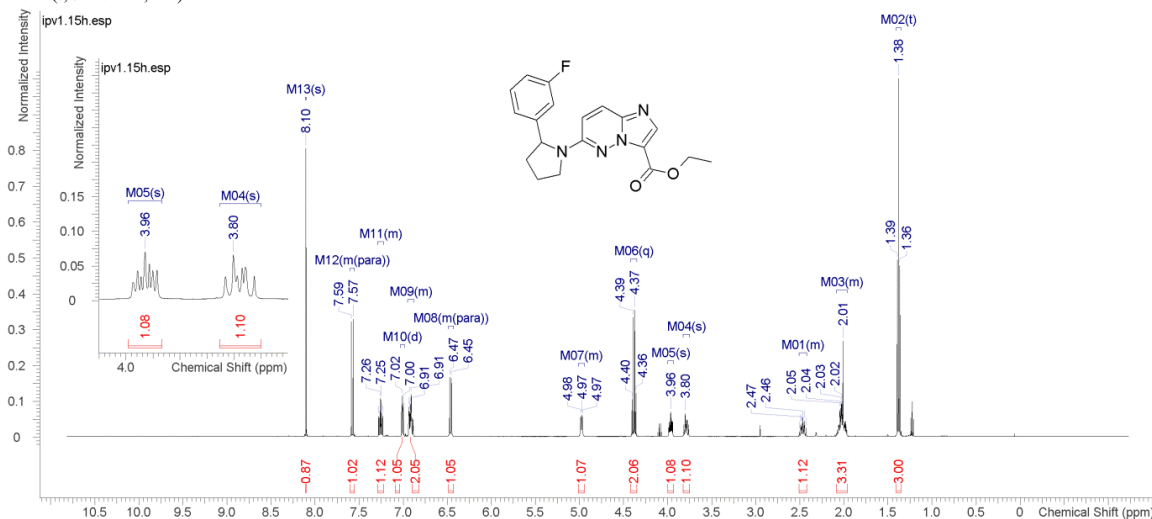
*The data from this Annex have been published in Supporting Information of: **Bernard-Gauthier, V.**; Bailey, J. J.; Aliaga, A.; Kostikov, A.; Rosa-Neto, P.; Wuest, M.; Brodeur, G. M.; Bedell, B. J.; Wuest, F.; Schirmacher, R. Development of Subnanomolar Radiofluorinated (2-Pyrrolidin-1-yl)imidazo[1,2-*b*]pyridazine pan-Trk Inhibitors as Candidate PET Imaging Probes. *MedChemComm*, **2015**, **6**, 2184-2193.*

¹H NMR and ¹³C NMR for compound 4.10

IPV 1.15X 498.118 MHz H1 1D in cdcl3 (ref. to CDCl3 @ 7.26 ppm), temp 26.4 C -> actual temp = 27.0 C, autotx probe

| Multiplets | Integrals Sum | 19.91 | Number of Nuclei | 19 H's | |
|------------------------|---------------|--|------------------|------------------------|--|
| Acquisition Time (sec) | 4.9997 | Comment IPV 1.15X 498.118 MHz H1 1D in cdcl3 (ref. to CDCl3 @ 7.26 ppm), temp 26.4 C -> actual temp = 27.0 C, autotx probe | | | |
| Date | Jan 7 2015 | Date Stamp | Jan 7 2015 | File Name | G:\2015.01\2015.01.07.i5_IPV_1.15X_H1_1D.fid\fid |
| Frequency (MHz) | 498.1178 | Nucleus | 1H | Number of Transients | 16 |
| Original Points Count | 30001 | Pulse Sequence | s2pul | Receiver Gain | 32.00 |
| Points Count | 32768 | Spectrum Offset (Hz) | 2388.2478 | Spectrum Type | standard |
| Solvent | CHLOROFORM-d | Sweep Width (Hz) | 6000.42 | Temperature (degree C) | 26.400 |

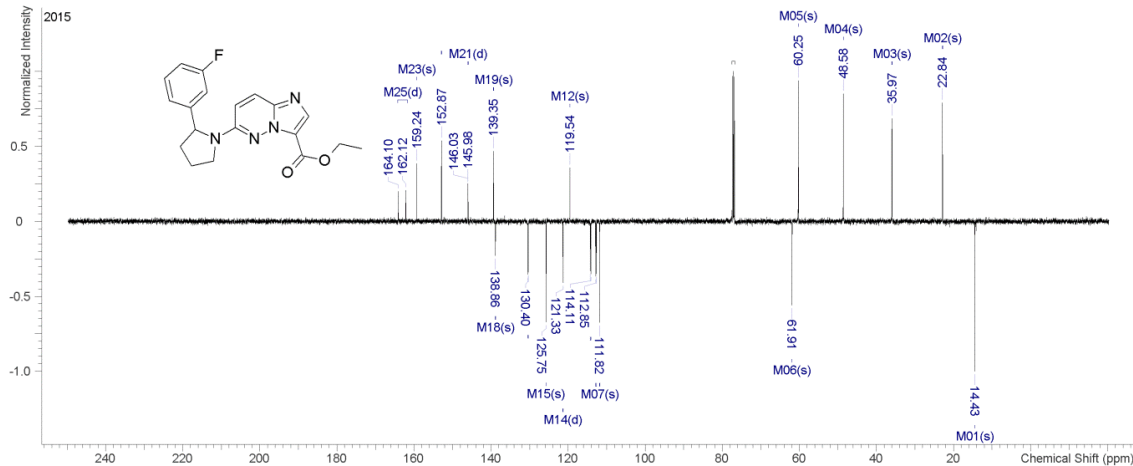
¹H NMR (498MHz, CHLOROFORM-d) δ = 8.10 (s, 1H), 7.60 - 7.55 (m, J =9.9 Hz, 1H), 7.29 - 7.22 (m, 1H), 7.01 (d, J =7.5 Hz, 1H), 6.95 - 6.88 (m, 2H), 6.49 - 6.43 (m, J =9.9 Hz, 1H), 5.01 - 4.94 (m, 1H), 4.38 (q, J =7.1 Hz, 2H), 3.96 (s, 1H), 3.80 (s, 1H), 2.51 - 2.42 (m, 1H), 2.08 - 1.96 (m, 3H), 1.38 (t, J =7.1 Hz, 3H)



IPV 1.15X 125.266 MHz C13[H1] APT_ad in cdcl3 (ref. to CDCl3 @ 77.06 ppm), temp 26.4 C -> actual temp = 27.0 C, autotx probe C & CH2 same, CH & CH3 opposite side of solvent signal

| Multiplets | Integrals Sum | 0.00 | Number of Nuclei | 19 C's | |
|------------------------|---------------|---|------------------|----------------------|---|
| Acquisition Time (sec) | 1.9958 | Comment IPV 1.15X 125.266 MHz C13[H1] APT_ad in cdcl3 (ref. to CDCl3 @ 77.06 ppm), temp 26.4 C -> actual temp = 27.0 C, autotx probe C & CH2 same, CH & CH3 opposite side of solvent signal | | | |
| Date | Jan 7 2015 | Date Stamp | Jan 7 2015 | File Name | C:\Users\admin\Documents\NMR jan2015\2015.01\2015.01.07.i5_IPV_1.15X_C13_APT_ad.fid\fid |
| Frequency (MHz) | 125.2656 | Nucleus | 13C | Number of Transients | 104 |
| Original Points Count | 67510 | Points Count | 131072 | Pulse Sequence | APT_ad |
| Receiver Gain | 30.00 | SW(cyclical) (Hz) | 33826.64 | Solvent | cdcl3 |
| Spectrum Offset (Hz) | 14370.3086 | Spectrum Type | APT | Sweep Width (Hz) | 33826.38 |
| Temperature (degree C) | 26.400 | | | | |

¹³C NMR (125MHz, cdcl₃) δ = 163.11 (d, J =247.0 Hz, 1C), 159.24, 152.87, 146.01 (d, J =6.5 Hz, 1C), 139.35, 138.86, 130.37 (br d, J =8.0 Hz, 1C), 125.75, 121.32 (d, J =2.6 Hz, 1C), 119.54, 114.19 (br d, J =2.1 Hz, 1C), 112.76 (br d, J =22.2 Hz, 1C), 111.82, 61.91, 60.25, 48.58, 35.97, 22.84, 14.43

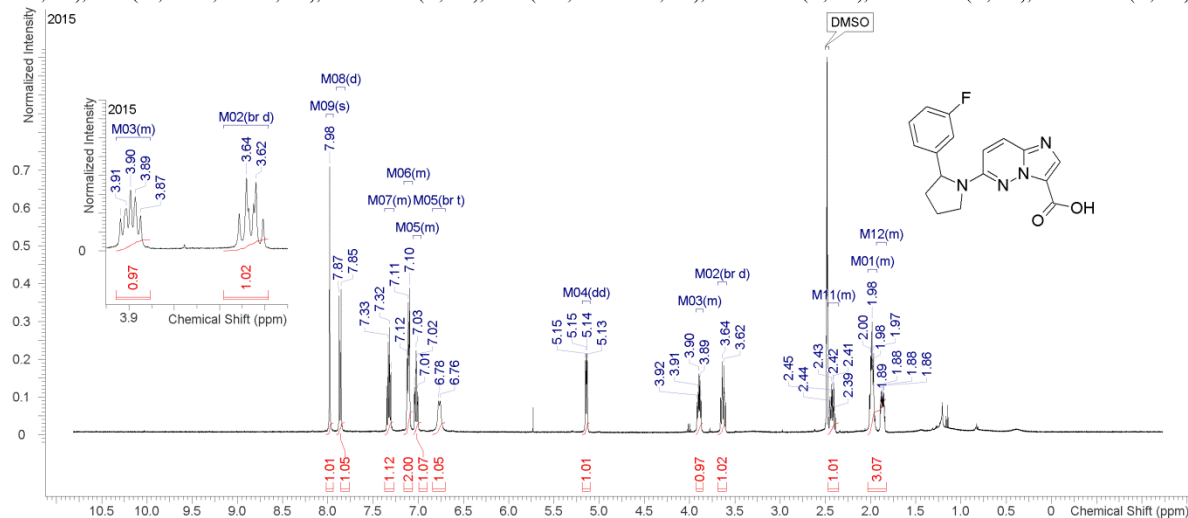


¹H NMR and ¹³C NMR for compound 4.9

IPV 1.16 498.120 MHz H1 1D in dmsol (ref. to DMSO @ 2.49 ppm), temp 26.4 C -> actual temp = 27.0 C, autotxdb probe

| Multiplets Integrals Sum 14.38 | | Number of Nuclei 14 H's | |
|--------------------------------|---|-------------------------|--|
| Acquisition Time (sec) | 4.9997 | Comment | IPV 1.16 498.120 MHz H1 1D in dmsol (ref. to DMSO @ 2.49 ppm), temp 26.4 C -> actual temp = 27.0 C, autotxdb probe |
| Date | Jan 16 2015 | Date Stamp | Jan 16 2015 |
| File Name | C:\Users\admin\Documents\NMR\jan2015\2015.01.16.15_IPV_1.16_H1_1D.fid | Frequency (MHz) | 498.1202 |
| Nucleus | ¹ H | Number of Transients | 16 |
| Pulse Sequence | s2pul | Receiver Gain | 32.00 |
| Spectrum Offset (Hz) | 2388.2527 | Spectrum Type | standard |
| | | Original Points Count | 30001 |
| | | SW(cyclical) (Hz) | 6000.60 |
| | | Solvent | dmsol |
| | | Sweep Width (Hz) | 6000.42 |
| | | Temperature (degree C) | 26.400 |

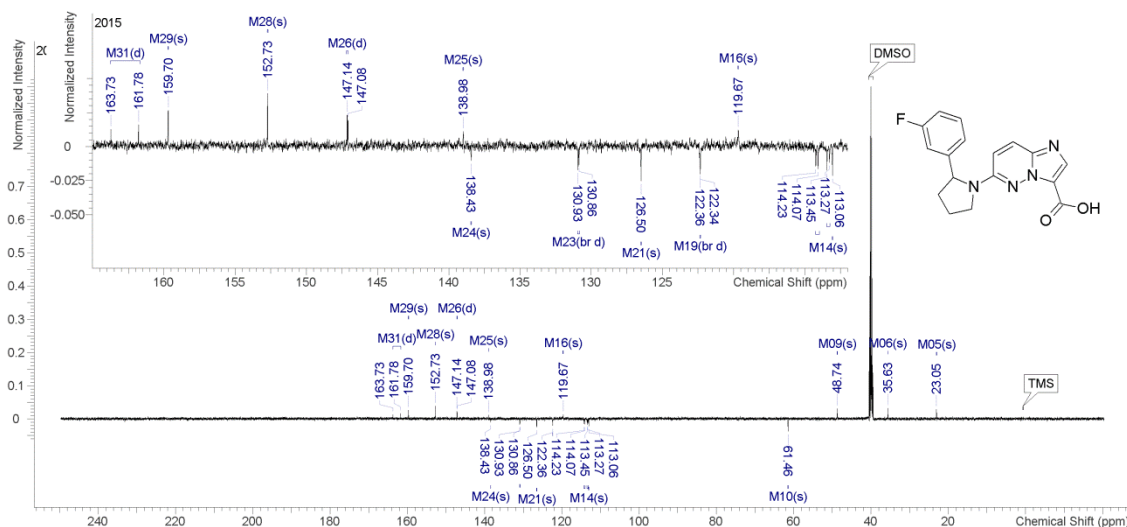
¹H NMR (498MHz, dmsol) δ = 7.98 (s, 1H), 7.86 (d, J =9.9 Hz, 1H), 7.37 - 7.27 (m, 1H), 7.16 - 7.06 (m, 2H), 7.06 - 6.97 (m, 1H), 7.02 (br t, J =8.4 Hz, 1H), 5.14 (dd, J =2.8, 8.1 Hz, 1H), 3.93 - 3.85 (m, 1H), 3.63 (br d, J =10.4 Hz, 1H), 2.47 - 2.35 (m, 1H), 2.03 - 1.93 (m, 2H), 1.93 - 1.83 (m, 1H)



IPV 1.16 125.266 MHz C13[H1] APT_ad in dmsol (ref. to DMSO @ 39.5 ppm), temp 26.4 C -> actual temp = 27.0 C, autotxdb probe C & CH2 same, CH & CH3 opposite side of solvent signal

| Multiplets Integrals Sum 0.00 | | Number of Nuclei 17 C's | |
|-------------------------------|--|-------------------------|--|
| Acquisition Time (sec) | 1.9958 | Comment | IPV 1.16 125.266 MHz C13[H1] APT_ad in dmsol (ref. to DMSO @ 39.5 ppm), temp 26.4 C -> actual temp = 27.0 C, autotxdb probe C & CH2 same, CH & CH3 opposite side of solvent signal |
| Date | Jan 16 2015 | Date Stamp | Jan 16 2015 |
| File Name | F:\Schirma\2015.01\2015.01.16.15_IPV_1.16_C13_APT_ad.fid | Frequency (MHz) | 125.2662 |
| Nucleus | ¹³ C | Number of Transients | 512 |
| Original Points Count | 67510 | Points Count | 131072 |
| Pulse Sequence | APT_ad | Receiver Gain | 30.00 |
| SW(cyclical) (Hz) | 33826.64 | Solvent | DMSO-d6 |
| Spectrum Offset (Hz) | 14370.3350 | Spectrum Type | APT |
| Temperature (degree C) | 26.400 | Sweep Width (Hz) | 33826.38 |

¹³C NMR (125MHz, DMSO-d₆) δ = 162.75 (d, J =243.6 Hz, 1C), 159.70, 152.73, 147.11 (d, J =6.5 Hz, 1C), 138.98, 138.43, 130.89 (br d, J =8.5 Hz, 1C), 126.50, 122.35 (br d, J =2.1 Hz, 1C), 119.67, 114.15 (d, J =20.9 Hz, 1C), 113.36 (br d, J =21.9 Hz, 1C), 113.06, 61.46, 48.74, 35.63, 23.05

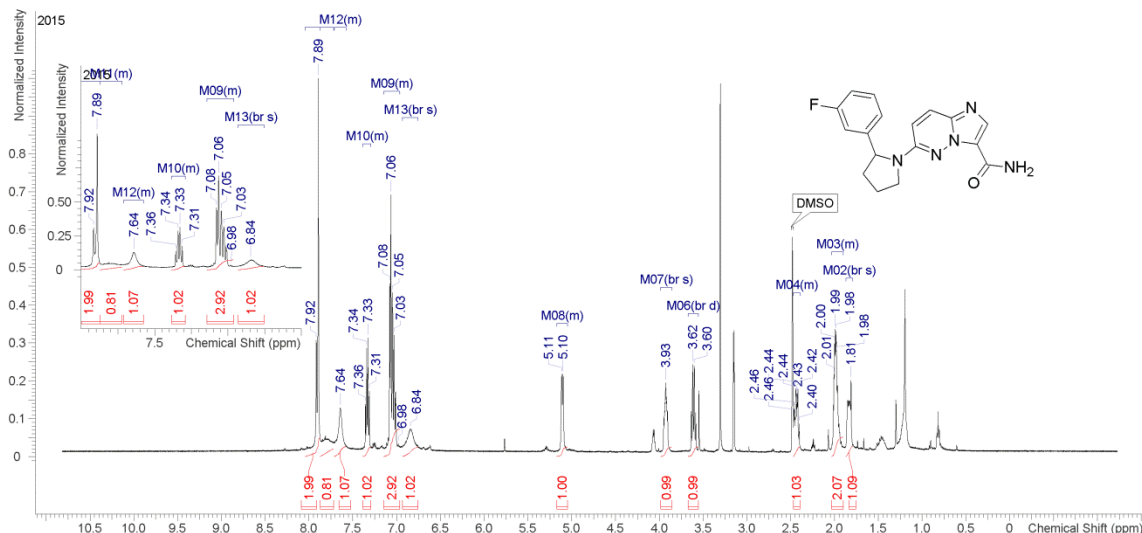


¹H NMR and ¹³C NMR for compound 4.11

IPV 1.45 498.120 MHz H1 1D in dms0 (ref. to DMSO @ 2.49 ppm), temp 26.4 C -> actual temp = 27.0 C, autotdb probe

| Multiplets Integrals Sum 16.00 | | Number of Nuclei 16 H's | |
|--------------------------------|---|-------------------------|--|
| Acquisition Time (sec) | 4.9997 | Comment | IPV 1.45 498.120 MHz H1 1D in dms0 (ref. to DMSO @ 2.49 ppm), temp 26.4 C -> actual temp = 27.0 C, autotdb probe |
| Date | Feb 17 2015 | Date Stamp | Feb 17 2015 |
| File Name | F:\Schirma\2015.02\2015.02.17.15_IPV_1.45_H1_1D.fid | File Name | F:\Schirma\2015.02\2015.02.17.15_IPV_1.45_H1_1D.fid |
| Frequency (MHz) | 498.1202 | Nucleus | 1H |
| Number of Transients | 16 | Original Points Count | 30001 |
| Points Count | 65536 | Pulse Sequence | s2pul |
| Receiver Gain | 32.00 | SW(cyclical) (Hz) | 6000.60 |
| Solvent | DMSO-d6 | Spectrum Offset (Hz) | 2388.2983 |
| Spectrum Type | standard | Sweep Width (Hz) | 6000.51 |
| Temperature (degree C) | 26.400 | | |

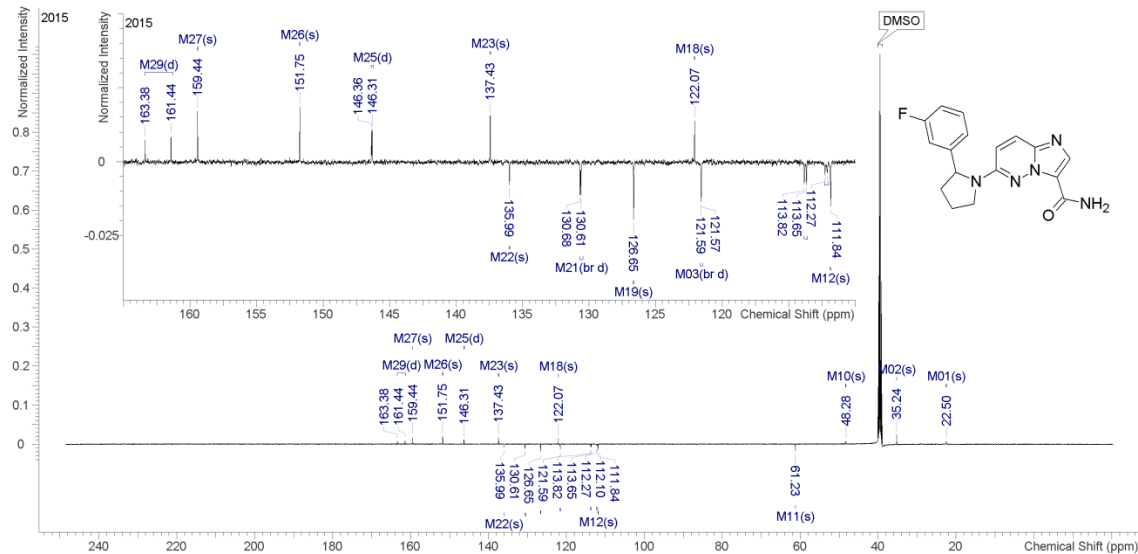
¹H NMR (498MHz, DMSO-d₆) δ = 8.04 - 7.87 (m, 2H), 7.87 - 7.72 (m, 1H), 7.71 - 7.58 (m, 1H), 7.39 - 7.29 (m, 1H), 7.14 - 6.96 (m, 3H), 6.84 (br s, 1H), 5.17 - 5.05 (m, 1H), 3.93 (br s, 1H), 3.61 (br d, J=9.6 Hz, 1H), 2.47 - 2.40 (m, 1H), 2.04 - 1.90 (m, 2H), 1.81 (br s, 1H)



Jamie_Bailey, IPV1_45x 125.691 MHz C13[H1] APT_ad in dms0 (ref. to DMSO @ 39.5 ppm), temp 27.7 C -> actual temp = 27.0 C, coldlud probe C & CH2 same, CH & CH3 opposite side of solvent signal

| Multiplets Integrals Sum 0.00 | | Number of Nuclei 17 C's | |
|-------------------------------|---|-------------------------|--|
| Acquisition Time (sec) | 2.0000 | Comment | Jamie_Bailey, IPV1_45x 125.691 MHz C13[H1] APT_ad in dms0 (ref. to DMSO @ 39.5 ppm), temp 27.7 C -> actual temp = 27.0 C, coldlud probe C & CH2 same, CH & CH3 opposite side of solvent signal |
| Date | Apr 28 2015 | Date Stamp | Apr 28 2015 |
| File Name | F:\Schirma\2015.04\2015.04.28.u5_IPV1_45x_loc8_13.47_C13_APT_ad.fid | File Name | F:\Schirma\2015.04\2015.04.28.u5_IPV1_45x_loc8_13.47_C13_APT_ad.fid |
| Frequency (MHz) | 125.6908 | Nucleus | 13C |
| Original Points Count | 67568 | Number of Transients | 308 |
| Points Count | 131072 | Pulse Sequence | APT_ad |
| Receiver Gain | 30.00 | SW(cyclical) (Hz) | 14348.9590 |
| Solvent | DMSO-d6 | Spectrum Offset (Hz) | 33783.53 |
| Spectrum Type | APT | Sweep Width (Hz) | 27.600 |
| Temperature (degree C) | 27.600 | | |

¹³C NMR (126MHz, DMSO-d₆) δ = 162.41 (d, J=244.1 Hz, 1C), 159.44, 151.75, 146.33 (d, J=6.4 Hz, 1C), 137.43, 135.99, 130.64 (br d, J=8.2 Hz, 1C), 126.65, 122.07, 121.58 (br d, J=2.1 Hz, 1C), 113.74 (br d, J=20.9 Hz, 1C), 112.18 (br d, J=21.4 Hz, 1C), 111.84, 61.23, 48.28, 35.24, 22.50



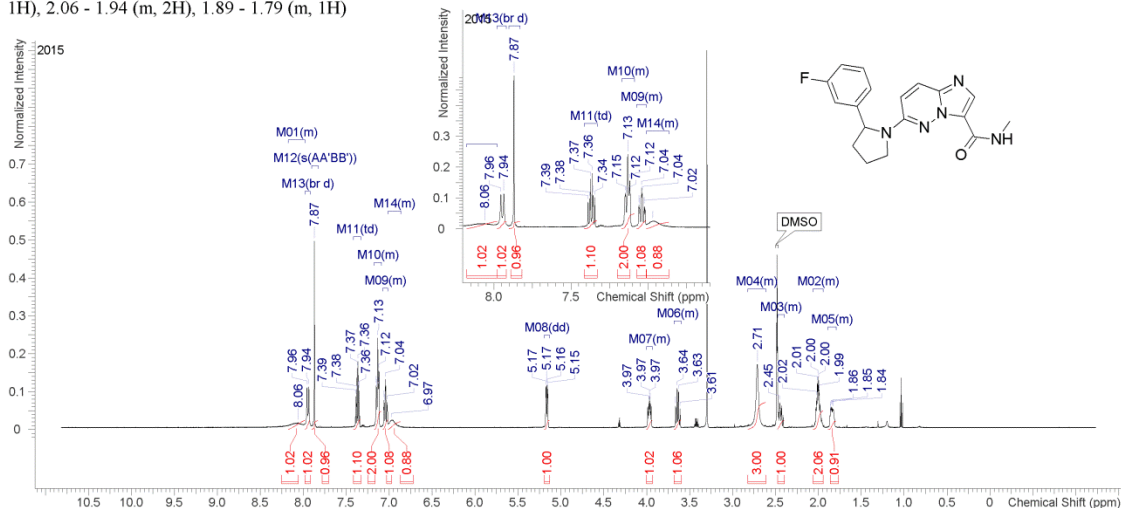
¹H NMR and ¹³C NMR for compound 4.12

IPV 1.44 498.120 MHz H1 1D in dmsol (ref. to DMSO @ 2.49 ppm), temp 26.4 C -> actual temp = 27.0 C, autotx probe

Multiplets Integrals Sum 18.13 Number of Nuclei 18 H's

| Acquisition Time (sec) | 4.9997 | Comment | IPV 1.44 498.120 MHz H1 1D in dmsol (ref. to DMSO @ 2.49 ppm), temp 26.4 C -> actual temp = 27.0 C, autotx probe | | |
|------------------------|-------------|----------------------|--|-----------------------|---|
| Date | Feb 17 2015 | Date Stamp | Feb 17 2015 | File Name | F:\Schirma\2015.02\2015.02.17.15_IPV_1.44_H1_1D.fid.tif |
| Frequency (MHz) | 498.1202 | Nucleus | 1H | Number of Transients | 16 |
| Points Count | 65536 | Pulse Sequence | s2pul | Receiver Gain | 32.00 |
| Solvent | DMSO-d6 | Spectrum Offset (Hz) | 2388.2983 | Spectrum Type | standard |
| Temperature (degree C) | 26.400 | | | Original Points Count | 30001 |
| | | | | SW(cyclical) (Hz) | 6000.60 |
| | | | | Sweep Width (Hz) | 6000.51 |

¹H NMR (498MHz, DMSO-d₆) δ = 8.18 - 7.98 (m, 1H), 7.95 (br d, J=9.9 Hz, 1H), 7.87 (s, 1H), 7.37 (dt, J=6.1, 8.0 Hz, 1H), 7.17 - 7.09 (m, 2H), 7.07 - 7.01 (m, 1H), 7.01 - 6.86 (m, 1H), 5.16 (dd, J=2.7, 8.3 Hz, 1H), 4.00 - 3.93 (m, 1H), 3.68 - 3.60 (m, 1H), 2.82 - 2.61 (m, 3H), 2.47 - 2.39 (m, 1H), 2.06 - 1.94 (m, 2H), 1.89 - 1.79 (m, 1H)

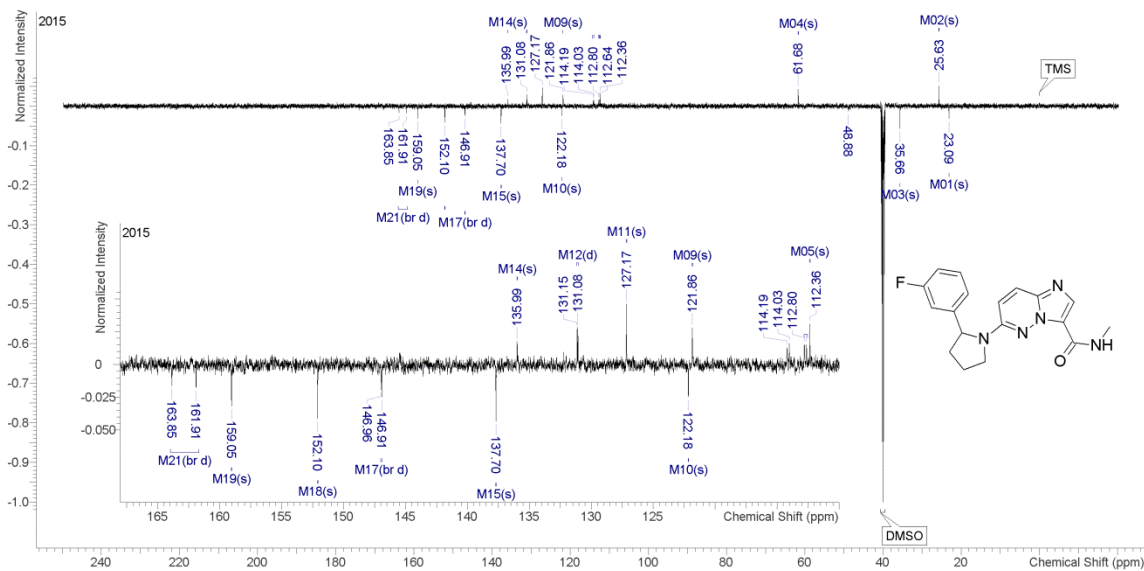


IPV 1.44 125.266 MHz C13[H1] APT_ad in dmsol (ref. to DMSO @ 39.5 ppm), temp 26.4 C -> actual temp = 27.0 C, autotx probe C & CH2 same, CH & CH3 opposite side of solvent signal

Multiplets Integrals Sum 0.00 Number of Nuclei 17 C's

| Acquisition Time (sec) | 1.9958 | Comment | IPV 1.44 125.266 MHz C13[H1] APT_ad in dmsol (ref. to DMSO @ 39.5 ppm), temp 26.4 C -> actual temp = 27.0 C, autotx probe C & CH2 same, CH & CH3 opposite side of solvent signal | | |
|------------------------|-------------|-------------------|--|----------------------|--|
| Date | Feb 17 2015 | Date Stamp | Feb 17 2015 | File Name | F:\Schirma\2015.02\2015.02.17.15_IPV_1.44_C13_APT_ad.fid.tif |
| Frequency (MHz) | 125.2662 | Nucleus | 13C | Number of Transients | 176 |
| Original Points Count | 67510 | Points Count | 131072 | Pulse Sequence | APT_ad |
| Receiver Gain | 30.00 | SW(cyclical) (Hz) | 33826.64 | Solvent | DMSO-d6 |
| Spectrum Offset (Hz) | 14370.3350 | Spectrum Type | APT | Sweep Width (Hz) | 33826.38 |
| Temperature (degree C) | 26.400 | | | | |

¹³C NMR (125MHz, DMSO-d₆) δ = 162.88 (br d, J=243.9 Hz, 1C), 159.05, 152.10, 146.94 (br d, J=6.2 Hz, 1C), 137.70, 135.99, 131.12 (d, J=8.0 Hz, 1C), 127.17, 122.18, 121.86, 114.11 (br d, J=20.6 Hz, 1C), 112.72 (br d, J=20.1 Hz, 1C), 112.36, 61.68, 35.66, 25.63, 23.09

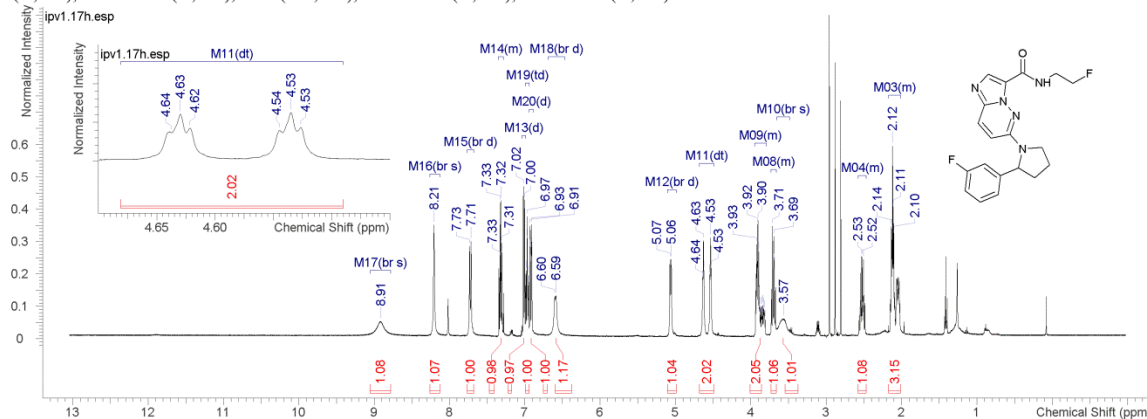


¹H NMR and ¹³C NMR for compound 4.13

IPV 1.17 498.118 MHz H1 1D in cdcl3 (ref. to CDCl3 @ 7.26 ppm), temp 26.4 C -> actual temp = 27.0 C, autotxb probe

| Multiplets Integrals Sum 19.68 | | Number of Nuclei 19 H's | |
|--------------------------------|--------------|-------------------------|--|
| Acquisition Time (sec) | 4.9935 | Comment | IPV 1.17 498.118 MHz H1 1D in cdcl3 (ref. to CDCl3 @ 7.26 ppm), temp 26.4 C -> actual temp = 27.0 C, autotxb probe |
| Date | Jan 16 2015 | Date Stamp | Jan 16 2015 |
| Frequency (MHz) | 498.1184 | Nucleus | 1H |
| Points Count | 65536 | Pulse Sequence | s2pul |
| Solvent | CHLOROFORM-d | Spectrum Offset (Hz) | 3005.9861 |
| Temperature (degree C) | 26.400 | Spectrum Type | standard |
| | | Number of Transients | 16 |
| | | Original Points Count | 34868 |
| | | Receiver Gain | 32.00 |
| | | SW(cyclical) (Hz) | 6982.63 |
| | | Sweep Width (Hz) | 6982.52 |

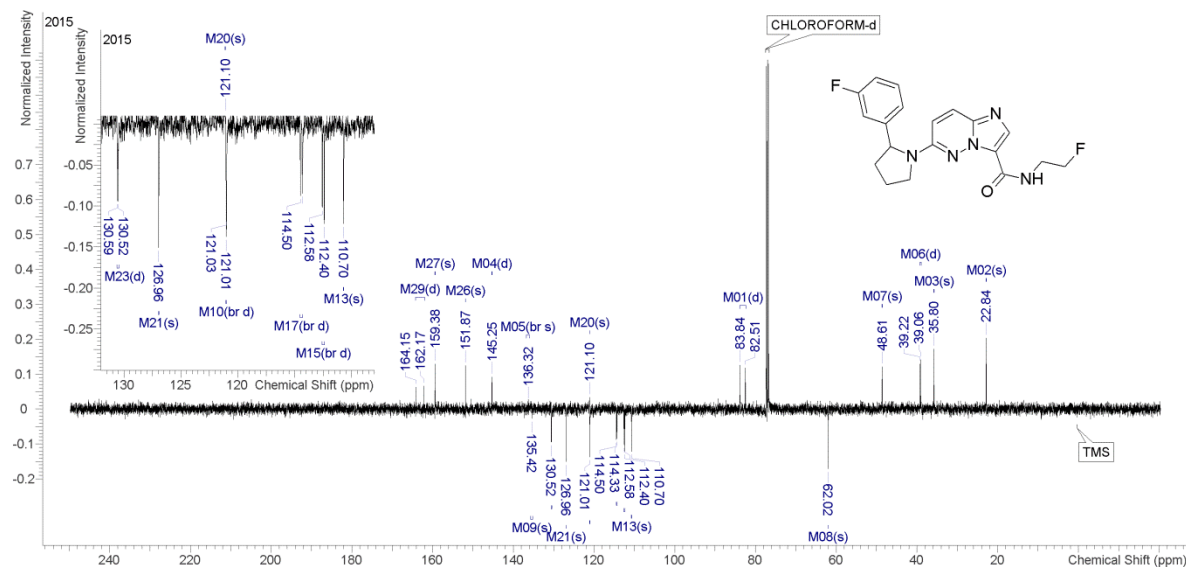
¹H NMR (498MHz, CHLOROFORM-d) δ = 8.91 (br s, 1H), 8.21 (br s, 1H), 7.72 (br d, J =9.8 Hz, 1H), 7.35 - 7.29 (m, 1H), 7.01 (d, J =7.8 Hz, 1H), 6.97 (dt, J =1.9, 8.4 Hz, 1H), 6.92 (d, J =9.7 Hz, 1H), 6.59 (br d, J =7.6 Hz, 1H), 5.07 (br d, J =8.0 Hz, 1H), 4.58 (td, J =4.1, 47.3 Hz, 2H), 3.95 - 3.80 (m, 2H), 3.73 - 3.66 (m, 1H), 3.57 (br s, 1H), 2.57 - 2.47 (m, 1H), 2.17 - 2.01 (m, 3H)



IPV 1.17 125.266 MHz C13[H1] APT_ad in cdcl3 (ref. to CDCl3 @ 77.06 ppm), temp 26.4 C -> actual temp = 27.0 C, autotxb probe C & CH2 same, CH & CH3 opposite side of solvent signal

| Multiplets Integrals Sum 0.00 | | Number of Nuclei 19 C's | |
|-------------------------------|-------------|-------------------------|---|
| Acquisition Time (sec) | 1.9958 | Comment | IPV 1.17 125.266 MHz C13[H1] APT_ad in cdcl3 (ref. to CDCl3 @ 77.06 ppm), temp 26.4 C -> actual temp = 27.0 C, autotxb probe C & CH2 same, CH & CH3 opposite side of solvent signal |
| Date | Jan 16 2015 | Date Stamp | Jan 16 2015 |
| Frequency (MHz) | 125.2656 | Nucleus | 13C |
| Original Points Count | 67510 | Points Count | 131072 |
| Receiver Gain | 30.00 | SW(cyclical) (Hz) | 33826.64 |
| Spectrum Offset (Hz) | 14370.3086 | Spectrum Type | APT |
| Temperature (degree C) | 26.400 | Solvent | CHLOROFORM-d |
| | | Number of Transients | 204 |
| | | Pulse Sequence | APT_ad |
| | | Sweep Width (Hz) | 33826.38 |

¹³C NMR (125MHz, CHLOROFORM-d) δ = 163.16 (d, J =247.2 Hz, 1C), 159.38, 151.87, 145.27 (d, J =6.2 Hz, 1C), 136.32 (br s, 1C), 135.42, 130.55 (d, J =8.3 Hz, 1C), 126.96, 121.10, 121.02 (br d, J =2.8 Hz, 1C), 114.41 (br d, J =21.2 Hz, 1C), 112.49 (br d, J =21.9 Hz, 1C), 110.70, 83.17 (d, J =166.2 Hz, 1C), 62.02, 48.61, 39.14 (d, J =19.4 Hz, 1C), 35.80, 22.84

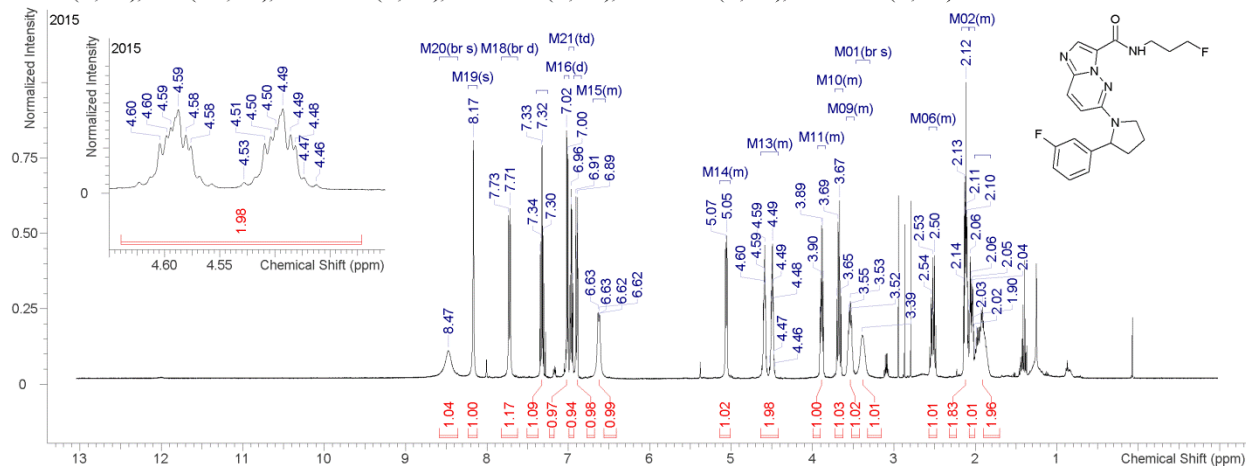


¹H NMR and ¹³C NMR for compound 4.14

IPV 1.18 498.118 MHz H1 1D in cdcl3 (ref. to CDCl3 @ 7.26 ppm), temp 26.4 C -> actual temp = 27.0 C, autotdb probe

| Multiplets Integrals Sum 21.05 | | Number of Nuclei 23 H's | |
|--------------------------------|---|-------------------------|--|
| Acquisition Time (sec) | 4.9935 | Comment | IPV 1.18 498.118 MHz H1 1D in cdcl3 (ref. to CDCl3 @ 7.26 ppm), temp 26.4 C -> actual temp = 27.0 C, autotdb probe |
| Date | Jan 16 2015 | Date Stamp | Jan 16 2015 |
| File Name | G:\2015.01\2015.01.16.i5_IPV_1.18_H1_1D.fid | File Name | G:\2015.01\2015.01.16.i5_IPV_1.18_H1_1D.fid |
| Frequency (MHz) | 498.1184 | Nucleus | 1H |
| Original Points Count | 65536 | Number of Transients | 16 |
| Points Count | 65536 | Receiver Gain | 32.00 |
| Solvent | cdcl3 | SW(cyclical) (Hz) | 6982.63 |
| Temperature (degree C) | 26.400 | Spectrum Offset (Hz) | 3005.9861 |
| | | Spectrum Type | standard |
| | | Sweep Width (Hz) | 6982.52 |

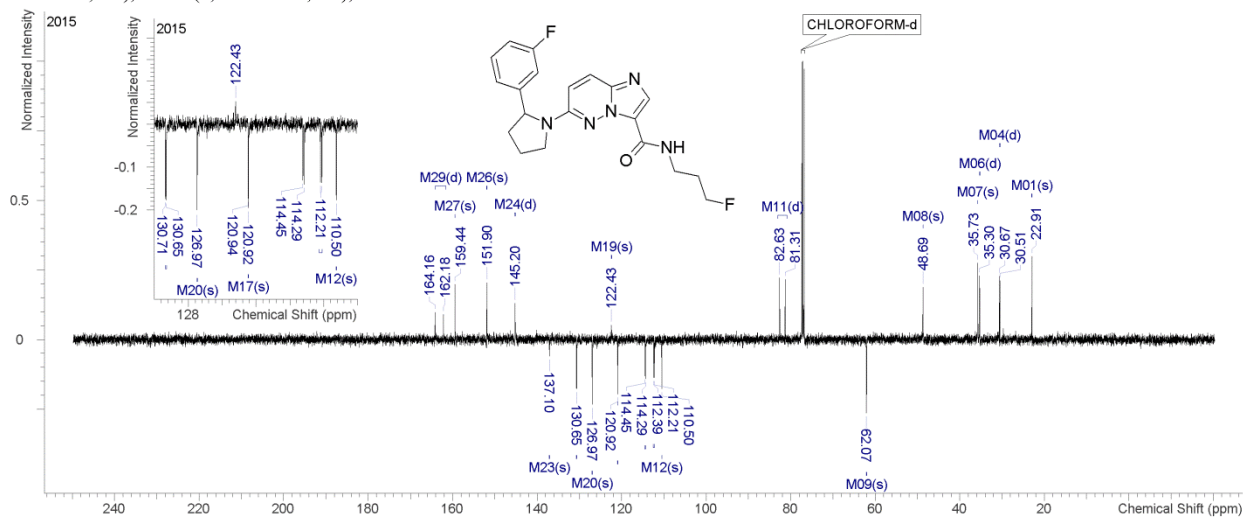
¹H NMR (498MHz, cdcl₃) δ = 8.47 (br s, 1H), 8.17 (s, 1H), 7.72 (br d, J=9.8 Hz, 1H), 7.33 (dt, J=5.8, 7.9 Hz, 1H), 7.01 (d, J=7.7 Hz, 1H), 6.96 (dt, J=2.1, 8.4 Hz, 1H), 6.93 - 6.84 (m, 3H), 6.70 - 6.55 (m, 1H), 5.14 - 5.01 (m, 1H), 4.64 - 4.42 (m, 2H), 3.94 - 3.85 (m, 1H), 3.72 - 3.63 (m, 1H), 3.59 - 3.49 (m, 1H), 3.39 (br s, 1H), 2.57 - 2.48 (m, 1H), 2.16 - 2.08 (m, 2H), 2.07 - 2.01 (m, 1H), 2.01 - 1.81 (m, 2H)



IPV 1.18 125.266 MHz C13[H1] APT_ad in cdcl3 (ref. to CDCl3 @ 77.06 ppm), temp 26.4 C -> actual temp = 27.0 C, autotdb probe C & CH2 same, CH & CH3 opposite side of solvent signal

| Multiplets Integrals Sum 0.00 | | Number of Nuclei 20 C's | |
|-------------------------------|---|-------------------------|--|
| Acquisition Time (sec) | 1.9958 | | |
| Comment | IPV 1.18 125.266 MHz C13[H1] APT_ad in cdcl3 (ref. to CDCl3 @ 77.06 ppm), temp 26.4 C -> actual temp = 27.0 C, autotdb probe C & CH2 same, CH & CH3 opposite side of solvent signal | | |
| Date | Jan 16 2015 | Date Stamp | Jan 16 2015 |
| File Name | C:\Users\admin\Documents\NMR jan2015\2015.01\2015.01.16.i5_IPV_1.18_C13_APT_ad.fid | File Name | C:\Users\admin\Documents\NMR jan2015\2015.01\2015.01.16.i5_IPV_1.18_C13_APT_ad.fid |
| Frequency (MHz) | 125.2656 | Nucleus | 13C |
| Original Points Count | 67510 | Points Count | 131072 |
| Receiver Gain | 30.00 | SW(cyclical) (Hz) | 33826.64 |
| Spectrum Offset (Hz) | 14370.3086 | Spectrum Type | APT |
| Temperature (degree C) | 26.400 | Sweep Width (Hz) | 33826.38 |

¹³C NMR (125MHz, cdcl₃) δ = 163.17 (d, J=247.2 Hz, 1C), 159.44, 151.90, 145.23 (d, J=6.2 Hz, 1C), 137.10, 130.68 (br d, J=8.0 Hz, 1C), 126.97, 122.43, 120.94, 120.92, 114.37 (d, J=21.2 Hz, 1C), 112.30 (d, J=22.2 Hz, 1C), 110.50, 81.97 (d, J=164.4 Hz, 1C), 62.07, 48.69, 35.73, 35.28 (d, J=5.2 Hz, 1C), 30.59 (d, J=19.4 Hz, 1C), 22.91

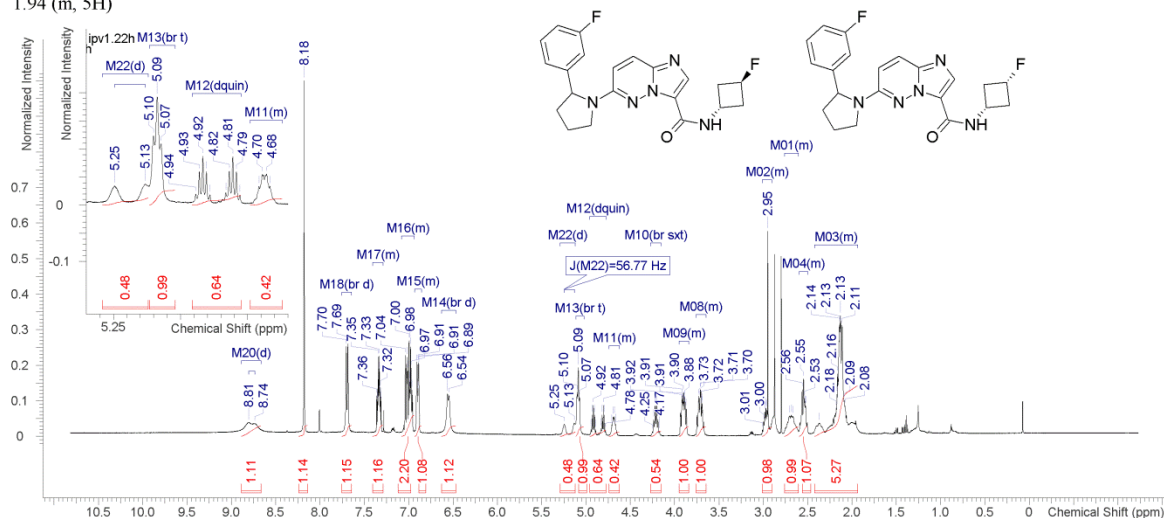


¹H NMR and ¹³C NMR for compound 4.16

IPV 1.22 498.118 MHz H1 1D in cdcl3 (ref. to CDC13 @ 7.26 ppm), temp 26.4 C -> actual temp = 27.0 C, autoxdb probe

| Multiplets Integrals Sum 22.32 | | Number of Nuclei 23 H's | |
|--------------------------------|---|-------------------------|--|
| Acquisition Time (sec) | 4.9997 | Comment | IPV 1.22 498.118 MHz H1 1D in cdcl3 (ref. to CDC13 @ 7.26 ppm), temp 26.4 C -> actual temp = 27.0 C, autoxdb probe |
| Date | Jan 16 2015 | Date Stamp | Jan 16 2015 |
| File Name | G:\2015.01\2015.01.16.i5_IPV_1.22_H1_1D.fid | File Name | G:\2015.01\2015.01.16.i5_IPV_1.22_H1_1D.fid |
| Frequency (MHz) | 498.1178 | Nucleus | 1H |
| Original Points Count | 30001 | Number of Transients | 16 |
| Points Count | 32768 | Receiver Gain | 32.00 |
| Solvent | CHLOROFORM-d | Spectrum Offset (Hz) | 2388.2478 |
| Temperature (degree C) | 26.400 | Spectrum Type | standard |
| | | SW(cyclical) (Hz) | 6000.60 |
| | | Sweep Width (Hz) | 6000.42 |

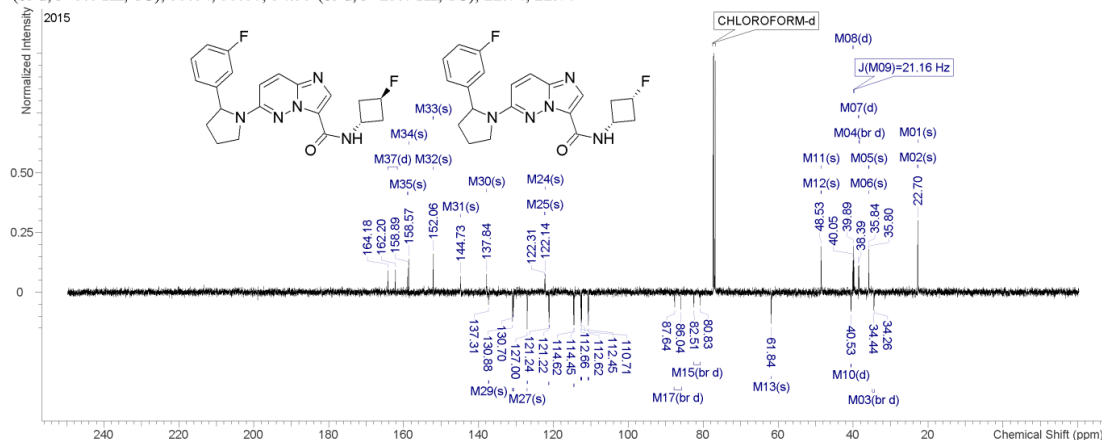
¹H NMR (498MHz, CHLOROFORM-d) δ = 8.77 (d, J =34.6 Hz, 1H), 8.18 (s, 1H), 7.69 (br d, J =9.9 Hz, 1H), 7.41 - 7.29 (m, 1H), 7.08 - 6.94 (m, 2H), 6.93 - 6.85 (m, 1H), 6.55 (br d, J =8.6 Hz, 1H), 5.19 (d, J =56.8 Hz, 1H), 5.09 (br t, J =7.0 Hz, 1H), 4.86 (quind, J =6.6, 55.7 Hz, 1H), 4.74 - 4.62 (m, 1H), 4.21 (br sxt, J =7.8 Hz, 1H), 3.95 - 3.84 (m, 1H), 3.76 - 3.65 (m, 1H), 3.01 - 2.90 (m, 1H), 2.76 - 2.60 (m, 1H), 2.59 - 2.50 (m, 1H), 2.42 - 1.94 (m, 5H)



IPV 1.22 125.266 MHz C13[H1] APT_ad in cdcl3 (ref. to CDC13 @ 77.06 ppm), temp 26.4 C -> actual temp = 27.0 C, autoxdb probe C & CH2 same, CH & CH3 opposite side of solvent signal

| Multiplets Integrals Sum 0.00 | | Number of Nuclei 37 C's | |
|-------------------------------|--|-------------------------|---|
| Acquisition Time (sec) | 1.9958 | Comment | IPV 1.22 125.266 MHz C13[H1] APT_ad in cdcl3 (ref. to CDC13 @ 77.06 ppm), temp 26.4 C -> actual temp = 27.0 C, autoxdb probe C & CH2 same, CH & CH3 opposite side of solvent signal |
| Date | Jan 16 2015 | Date Stamp | Jan 16 2015 |
| File Name | C:\Users\admin\Documents\NMR\jan2015\2015.01\2015.01.16.i5_IPV_1.22_C13_APT_ad.fid | File Name | C:\Users\admin\Documents\NMR\jan2015\2015.01\2015.01.16.i5_IPV_1.22_C13_APT_ad.fid |
| Frequency (MHz) | 125.2656 | Nucleus | 13C |
| Original Points Count | 67510 | Points Count | 131072 |
| Receiver Gain | 32.00 | SW(cyclical) (Hz) | 33826.64 |
| Solvent | cdcl3 | Spectrum Offset (Hz) | APT |
| Temperature (degree C) | 26.400 | Spectrum Type | APT |
| | | Number of Transients | 220 |
| | | Pulse Sequence | APT_ad |
| | | Sweep Width (Hz) | 33826.38 |

¹³C NMR (125MHz, cdcl₃) δ = 163.19 (d, J =247.8 Hz, 1C), 158.89, 158.57, 152.09, 152.06, 144.73, 137.84, 137.31, 130.81 (d, J =8.3 Hz, 1C), 130.71 - 130.64 (m, 1C), 130.67 (br d, J =8.0 Hz, 1C), 127.03, 127.00, 122.31, 122.14, 121.23 (br d, J =2.6 Hz, 1C), 121.10 (br d, J =2.6 Hz, 1C), 114.54 (br d, J =21.2 Hz, 1C), 112.62 (d, J =4.9 Hz, 1C), 112.47 (br d, J =4.9 Hz, 1C), 110.71, 110.62, 86.84 (br d, J =200.3 Hz, 1C), 81.67 (br d, J =210.6 Hz, 1C), 61.84, 48.53, 48.46, 40.57 (d, J =8.3 Hz, 1C), 39.97 (d, J =20.1 Hz, 1C), 39.83 (d, J =21.2 Hz, 1C), 38.55 (d, J =3.4 Hz, 1C), 38.37 (br d, J =3.6 Hz, 1C), 35.84, 35.80, 34.35 (br d, J =23.0 Hz, 1C), 22.74, 22.70

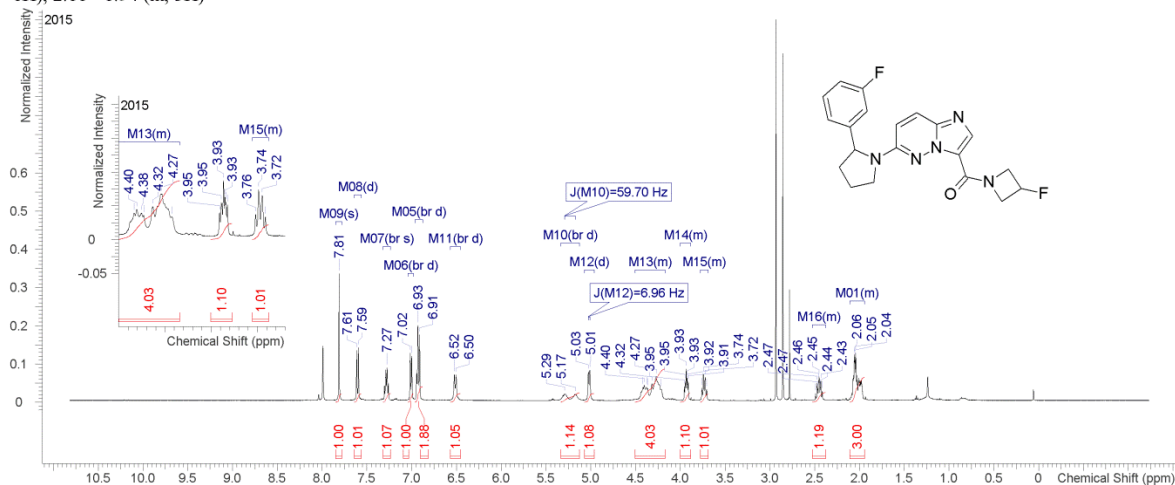


¹H NMR and ¹³C NMR for compound 4.17

IPV 1.19 498.118 MHz H1 1D in cdcl3 (ref. to CDCI3 @ 7.26 ppm), temp 26.4 C -> actual temp = 27.0 C, autoxgb probe

| Multiplets | Integrals Sum | 19.58 | Number of Nuclei | 19 H's | |
|------------------------|---|----------------------|--|------------------------|----------|
| Acquisition Time (sec) | 4.9997 | Comment | IPV 1.19 498.118 MHz H1 1D in cdcl3 (ref. to CDCI3 @ 7.26 ppm), temp 26.4 C -> actual temp = 27.0 C, autoxgb probe | | |
| Date | Jan 16 2015 | Date Stamp | Jan 16 2015 | | |
| File Name | C:\Users\admin\Documents\NMR\jan2015\2015.01\2015.01.16.i5_IPV_1.19_H1_1D.fid | | | Frequency (MHz) | 498.1178 |
| Nucleus | 1H | Number of Transients | 16 | Original Points Count | 30001 |
| Pulse Sequence | s2pul | Receiver Gain | 32.00 | SW(cyclical) (Hz) | 6000.60 |
| Spectrum Offset (Hz) | 2388.2478 | Spectrum Type | standard | Sweep Width (Hz) | 6000.42 |
| | | | | Solvent | cdcl3 |
| | | | | Temperature (degree C) | 26.400 |

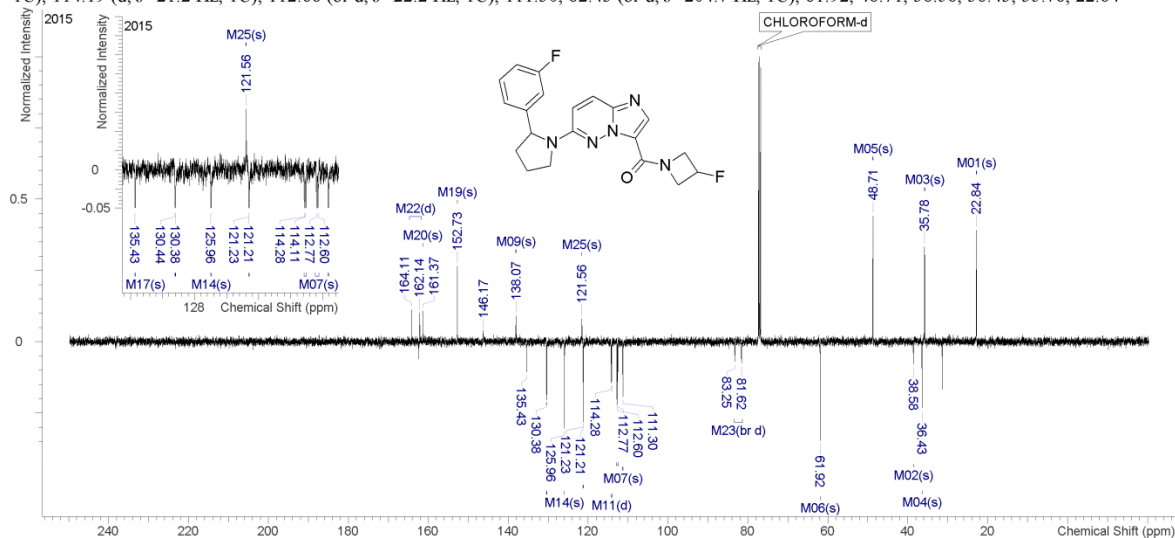
¹H NMR (498MHz, cdcl₃) δ = 7.81 (s, 1H), 7.60 (d, J=9.9 Hz, 1H), 7.27 (br s, 1H), 7.01 (br d, J=7.7 Hz, 1H), 6.92 (br d, J=9.0 Hz, 2H), 6.51 (br d, J=9.9 Hz, 1H), 5.23 (br d, J=59.7 Hz, 1H), 5.02 (d, J=7.0 Hz, 1H), 4.50 - 4.17 (m, 4H), 4.00 - 3.89 (m, 1H), 3.78 - 3.69 (m, 1H), 2.53 - 2.38 (m, 1H), 2.11 - 1.94 (m, 3H)



IPV 1.19 125.266 MHz C13[H1] APT_ad in cdcl3 (ref. to CDCI3 @ 77.06 ppm), temp 26.4 C -> actual temp = 27.0 C, autoxgb probe C & CH2 same, CH & CH3 opposite side of solvent signal

| Multiplets | Integrals Sum | 0.00 | Number of Nuclei | 20 C's | |
|------------------------|--|----------------------|---|-----------------------|----------|
| Acquisition Time (sec) | 1.9958 | Comment | IPV 1.19 125.266 MHz C13[H1] APT_ad in cdcl3 (ref. to CDCI3 @ 77.06 ppm), temp 26.4 C -> actual temp = 27.0 C, autoxgb probe C & CH2 same, CH & CH3 opposite side of solvent signal | | |
| Date | Jan 16 2015 | Date Stamp | Jan 16 2015 | | |
| File Name | C:\Users\admin\Documents\NMR\jan2015\2015.01\2015.01.16.i5_IPV_1.19_C13_APT_ad.fid | | | Frequency (MHz) | 125.2656 |
| Nucleus | 13C | Number of Transients | 188 | Original Points Count | 67510 |
| Points Count | 131072 | Pulse Sequence | APT_ad | | |
| Receiver Gain | 30.00 | SW(cyclical) (Hz) | 33826.64 | | |
| Spectrum Offset (Hz) | 14370.3086 | Spectrum Type | APT | | |
| Temperature (degree C) | 26.400 | Sweep Width (Hz) | 33826.38 | | |

¹³C NMR (125MHz, cdcl₃) δ = 163.12 (d, J=247.0 Hz, 1C), 161.37, 152.73, 138.07, 135.43, 130.44, 130.38, 125.96, 121.56, 121.22 (d, J=2.6 Hz, 1C), 114.19 (d, J=21.2 Hz, 1C), 112.68 (br d, J=22.2 Hz, 1C), 111.30, 82.43 (br d, J=204.7 Hz, 1C), 61.92, 48.71, 38.58, 36.43, 35.78, 22.84

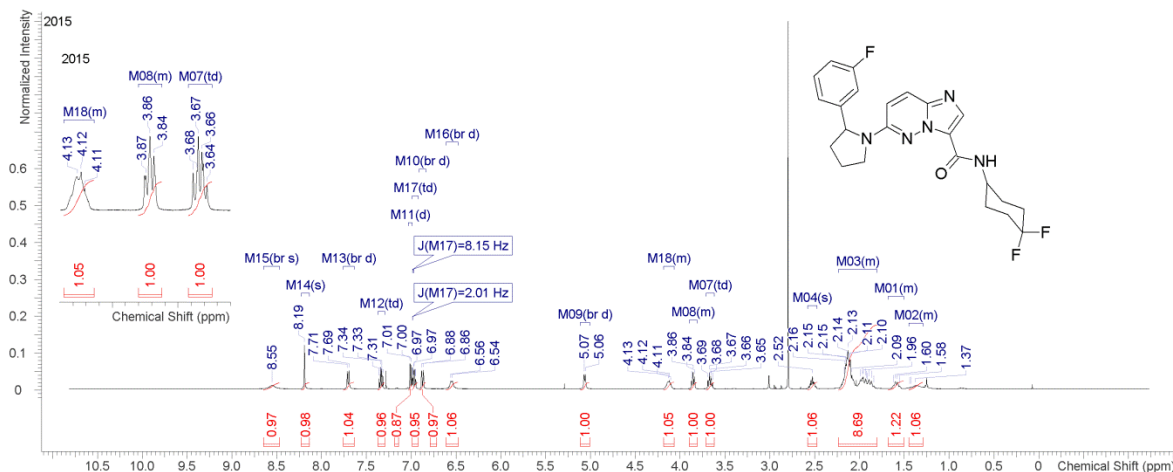


¹H NMR and ¹³C NMR for compound 4.18

IPV 1.28XX 498.118 MHz H1 1D in cdcl3 (ref. to CDCI3 @ 7.26 ppm), temp 26.4 C -> actual temp = 27.0 C, autotdx probe

| Multiplets | Integrals Sum | 23.89 | Number of Nuclei | 25 H's | |
|------------------------|---|----------------------|--|------------------------|----------|
| Acquisition Time (sec) | 4.9997 | Comment | IPV 1.28XX 498.118 MHz H1 1D in cdcl3 (ref. to CDCI3 @ 7.26 ppm), temp 26.4 C -> actual temp = 27.0 C, autotdx probe | | |
| Date | Jan 27 2015 | Date Stamp | Jan 27 2015 | | |
| File Name | C:\Users\admin\Documents\NMR\jan2015\2015.01\2015.01.27.15_IPV_1.28XX_H1_1D.fid\fid | | | Frequency (MHz) | 498.1178 |
| Nucleus | 1H | Number of Transients | 16 | Original Points Count | 30001 |
| Pulse Sequence | s2pul | Receiver Gain | 32.00 | SW(cyclical) (Hz) | 6000.60 |
| Spectrum Offset (Hz) | 2388.2478 | Spectrum Type | standard | Sweep Width (Hz) | 6000.42 |
| | | | | Solvent | cdcl3 |
| | | | | Temperature (degree C) | 26.400 |

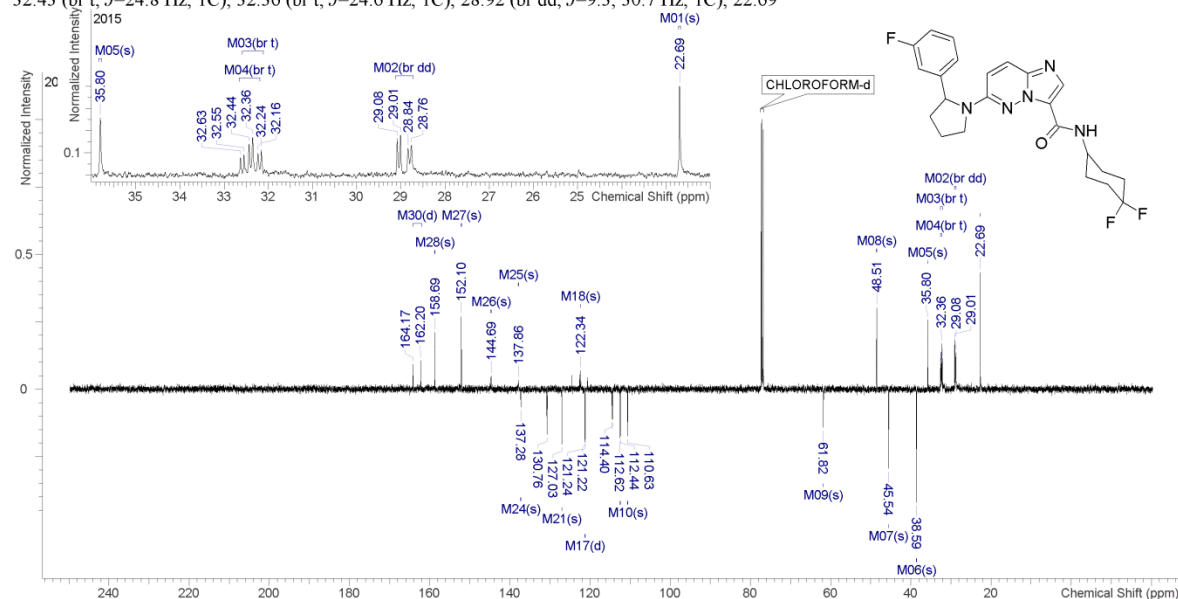
¹H NMR (498MHz, cdcl₃) δ = 8.55 (br s, 1H), 8.19 (s, 1H), 7.70 (br d, J=9.9 Hz, 1H), 7.34 (dt, J=5.9, 7.9 Hz, 1H), 7.01 (d, J=7.7 Hz, 1H), 6.97 (dt, J=2.0, 8.2 Hz, 1H), 6.87 (br d, J=9.5 Hz, 1H), 6.55 (br d, J=8.6 Hz, 1H), 5.06 (br d, J=7.7 Hz, 1H), 4.18 - 4.07 (m, 1H), 3.90 - 3.81 (m, 1H), 3.67 (dt, J=7.1, 9.6 Hz, 1H), 2.52 (s, 1H), 2.23 - 1.81 (m, 9H), 1.68 - 1.51 (m, 2H), 1.45 - 1.29 (m, 1H)



IPV 1.28XX 125.266 MHz C13[H1] APT_ad in cdcl3 (ref. to CDCI3 @ 77.06 ppm), temp 26.4 C -> actual temp = 27.0 C, autotdx probe C & CH2 same, CH & CH3 opposite side of solvent signal

| Multiplets | Integrals Sum | 0.00 | Number of Nuclei | 22 C's | |
|------------------------|--|----------------------|---|------------------------|------------|
| Acquisition Time (sec) | 1.9958 | Comment | IPV 1.28XX 125.266 MHz C13[H1] APT_ad in cdcl3 (ref. to CDCI3 @ 77.06 ppm), temp 26.4 C -> actual temp = 27.0 C, autotdx probe C & CH2 same, CH & CH3 opposite side of solvent signal | | |
| Date | Jan 27 2015 | Date Stamp | Jan 27 2015 | | |
| File Name | F:\Schirma\2015.01\2015.01.27.15_IPV_1.28XX_C13_APT_ad.fid\fid | | | Frequency (MHz) | 125.2656 |
| Nucleus | 13C | Number of Transients | 220 | Original Points Count | 67510 |
| Points Count | 131072 | Pulse Sequence | APT_ad | Receiver Gain | 30.00 |
| SW(cyclical) (Hz) | 33826.64 | Solvent | CHLOROFORM-d | Spectrum Offset (Hz) | 14370.3086 |
| Spectrum Type | APT | Sweep Width (Hz) | 33826.38 | Temperature (degree C) | 26.400 |

¹³C NMR (125MHz, CHLOROFORM-d) δ = 163.19 (d, J=247.5 Hz, 1C), 158.69, 152.10, 144.69, 137.86, 137.28, 130.73 (br d, J=8.3 Hz, 1C), 127.03, 122.34, 121.23 (d, J=2.8 Hz, 1C), 114.49 (br d, J=21.2 Hz, 1C), 112.53 (br d, J=22.2 Hz, 1C), 110.63, 61.82, 48.51, 45.54, 38.59, 35.80, 32.43 (br t, J=24.8 Hz, 1C), 32.36 (br t, J=24.6 Hz, 1C), 28.92 (br dd, J=9.3, 30.7 Hz, 1C), 22.69

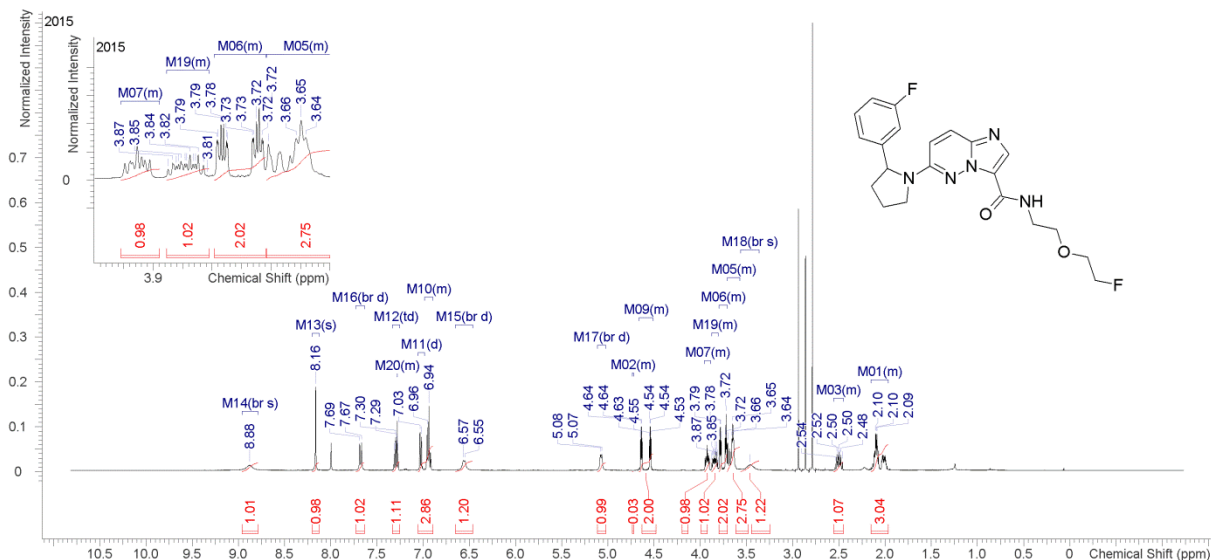


¹H NMR and ¹³C NMR for compound 4.19

IPV 1.23 498.118 MHz H1 1D in cdcl3 (ref. to CDCl3 @ 7.26 ppm), temp 26.4 C -> actual temp = 27.0 C, autotdx probe

| Multiplets Integrals Sum 23.29 | | Number of Nuclei 25 H's | | | | | |
|--------------------------------|---|-------------------------|--|-----------------------|---------|------------------------|--------|
| Acquisition Time (sec) | 4.9997 | Comment | IPV 1.23 498.118 MHz H1 1D in cdcl3 (ref. to CDCl3 @ 7.26 ppm), temp 26.4 C -> actual temp = 27.0 C, autotdx probe | | | | |
| Date | Jan 20 2015 | Date Stamp | Jan 20 2015 | | | | |
| File Name | C:\Users\admin\Documents\NMR jan2015\2015.01\2015.01.20.i5_IPV_1.23_H1_1D.fid | | Frequency (MHz) | 498.1178 | | | |
| Nucleus | 1H | Number of Transients | 16 | Original Points Count | 30001 | Points Count | 32768 |
| Pulse Sequence | s2pul | Receiver Gain | 32.00 | SW(cyclical) (Hz) | 6000.60 | Solvent | cdcl3 |
| Spectrum Offset (Hz) | 2388.2478 | Spectrum Type | standard | Sweep Width (Hz) | 6000.42 | Temperature (degree C) | 26.400 |

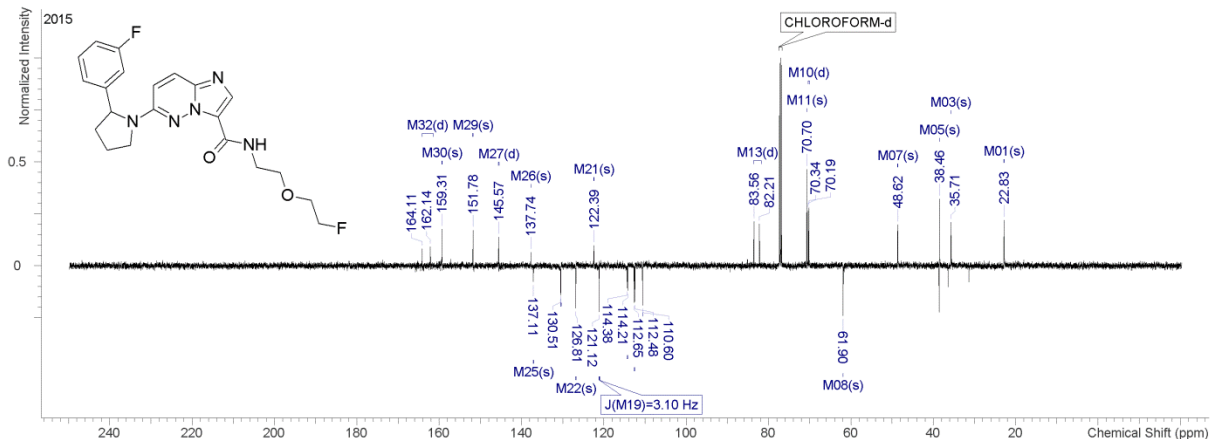
¹H NMR (498MHz, cdcl₃) δ = 8.88 (br s, 1H), 8.16 (s, 1H), 7.68 (br d, *J*=9.9 Hz, 1H), 7.28 - 7.28 (m, 1H), 7.29 (dt, *J*=5.9, 8.1 Hz, 1H), 7.03 (d, *J*=7.7 Hz, 1H), 6.99 - 6.89 (m, 2H), 6.56 (br d, *J*=8.4 Hz, 1H), 5.07 (br d, *J*=7.3 Hz, 1H), 4.74 - 4.72 (m, 1H), 4.66 - 4.51 (m, 2H), 3.95 - 3.89 (m, 1H), 3.88 - 3.81 (m, 1H), 3.80 - 3.71 (m, 2H), 3.71 - 3.57 (m, 3H), 3.46 (br s, 1H), 2.56 - 2.45 (m, 1H), 2.15 - 1.96 (m, 3H)



IPV 1.23 125.266 MHz C13[H1] APT_ad in cdcl3 (ref. to CDCl3 @ 77.06 ppm), temp 26.4 C -> actual temp = 27.0 C, autotdx probe C & CH2 same, CH & CH3 opposite side of solvent signal

| Multiplets Integrals Sum 0.00 | | Number of Nuclei 21 C's | | |
|-------------------------------|--|-------------------------|---|----------|
| Acquisition Time (sec) | 1.9958 | Comment | IPV 1.23 125.266 MHz C13[H1] APT_ad in cdcl3 (ref. to CDCl3 @ 77.06 ppm), temp 26.4 C -> actual temp = 27.0 C, autotdx probe C & CH2 same, CH & CH3 opposite side of solvent signal | |
| Date | Jan 20 2015 | Date Stamp | Jan 20 2015 | |
| File Name | C:\Users\admin\Documents\NMR jan2015\2015.01\2015.01.20.i5_IPV_1.23_C13_APT_ad.fid | | Frequency (MHz) | 125.2656 |
| Nucleus | 13C | Number of Transients | 192 | |
| Original Points Count | 67510 | Points Count | 131072 | |
| Receiver Gain | 30.00 | SW(cyclical) (Hz) | 33826.64 | |
| Spectrum Offset (Hz) | 14370.3086 | Spectrum Type | APT | |
| Temperature (degree C) | 26.400 | Sweep Width (Hz) | 33826.38 | |

¹³C NMR (125MHz, cdcl₃) δ = 163.12 (d, *J*=247.0 Hz, 1C), 159.31, 151.78, 145.54 (d, *J*=6.5 Hz, 1C), 137.74, 137.11, 130.48 (br d, *J*=8.0 Hz, 1C), 126.81, 122.39, 121.09 (d, *J*=3.1 Hz, 1C), 114.30 (br d, *J*=21.2 Hz, 1C), 112.56 (br d, *J*=22.2 Hz, 1C), 110.60, 82.89 (d, *J*=169.8 Hz, 1C), 70.70, 70.26 (d, *J*=19.6 Hz, 1C), 61.90, 48.62, 38.46, 35.71, 22.83

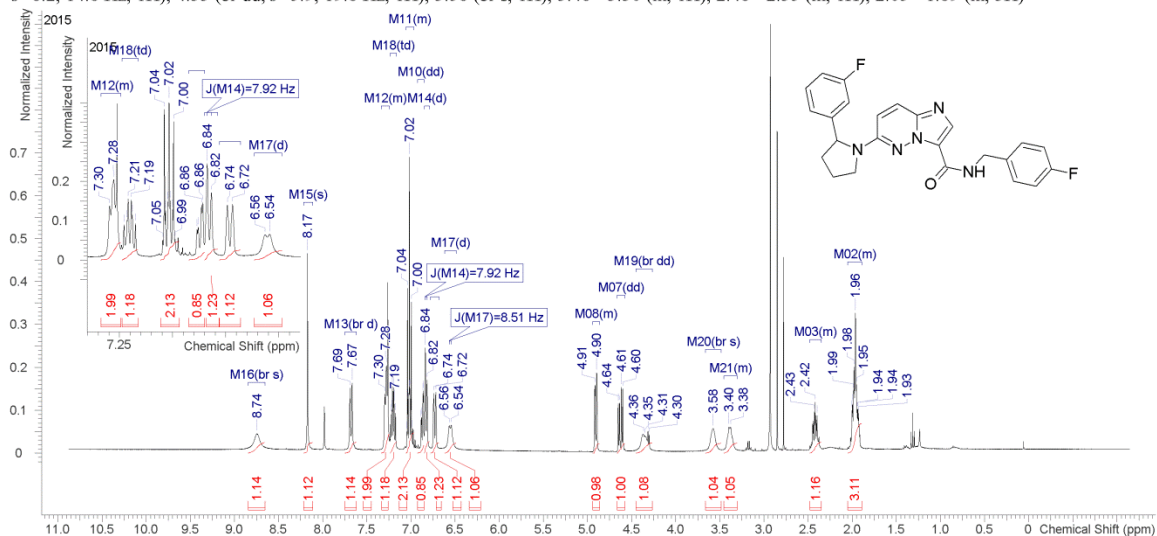


¹H NMR and ¹³C NMR for compound 4.20

IPV 1.31 399.984 MHz H1 1D in cdcl3 (ref. to CDC13 @ 7.26 ppm), temp 25.9 C -> actual temp = 27.0 C, onenmr probe

| Multiplets | Integrals Sum | 22.38 | Number of Nuclei | 21 H's | |
|------------------------|--|----------------------|---|------------------------|----------|
| Acquisition Time (sec) | 4.9999 | Comment | IPV 1.31 399.984 MHz H1 1D in cdcl3 (ref. to CDC13 @ 7.26 ppm), temp 25.9 C -> actual temp = 27.0 C, onenmr probe | | |
| Date | Jan 23 2015 | Date Stamp | Jan 23 2015 | | |
| File Name | C:\Users\admin\Documents\NMR jan2015\2015.01\2015.01.23.mr4_IPV_1.31_H1_1D.fid\fid | | | Frequency (MHz) | 399.9845 |
| Nucleus | 1H | Number of Transients | 16 | Original Points Count | 24038 |
| Pulse Sequence | s2pul | Receiver Gain | 24.00 | SW(cyclical) (Hz) | 4807.69 |
| Spectrum Offset (Hz) | 1947.6067 | Spectrum Type | standard | Sweep Width (Hz) | 4807.55 |
| | | | | Solvent | cdcl3 |
| | | | | Temperature (degree C) | 25.900 |

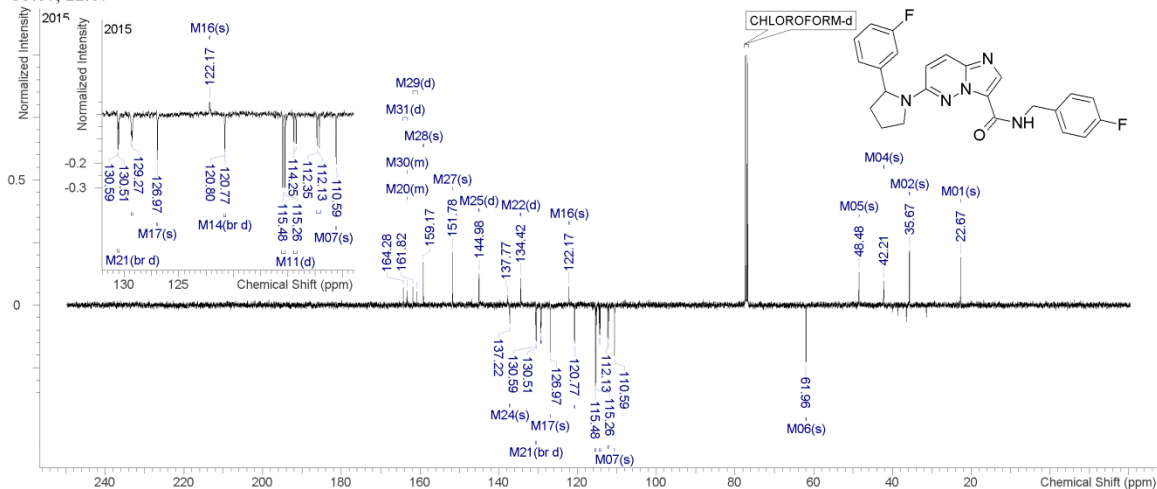
¹H NMR (400MHz, cdcl₃) δ = 8.74 (br s, 1H), 8.17 (s, 1H), 7.68 (br d, J=9.8 Hz, 1H), 7.34 - 7.24 (m, 2H), 7.20 (dt, J=5.9, 7.8 Hz, 1H), 7.06 - 6.97 (m, 2H), 6.87 (dd, J=2.3, 8.4 Hz, 1H), 6.83 (d, J=7.9 Hz, 1H), 6.73 (br d, J=9.7 Hz, 1H), 6.55 (d, J=8.5 Hz, 1H), 4.94 - 4.86 (m, 1H), 4.62 (dd, J=6.2, 14.8 Hz, 1H), 4.33 (br dd, J=5.9, 19.8 Hz, 1H), 3.58 (br s, 1H), 3.46 - 3.30 (m, 1H), 2.48 - 2.35 (m, 1H), 2.05 - 1.89 (m, 3H)



IPV 1.31 100.587 MHz C13[H1] APT_ad in cdcl3 (ref. to CDC13 @ 77.06 ppm), temp 25.9 C -> actual temp = 27.0 C, onenmr probe C & CH2 same, CH & CH3 opposite side of solvent signal

| Multiplets | Integrals Sum | 0.00 | Number of Nuclei | 23 C's | |
|------------------------|---|-------------------|--|----------------------|----------|
| Acquisition Time (sec) | 2.0000 | Comment | IPV 1.31 100.587 MHz C13[H1] APT_ad in cdcl3 (ref. to CDC13 @ 77.06 ppm), temp 25.9 C -> actual temp = 27.0 C, onenmr probe C & CH2 same, CH & CH3 opposite side of solvent signal | | |
| Date | Jan 23 2015 | Date Stamp | Jan 23 2015 | | |
| File Name | C:\Users\admin\Documents\NMR jan2015\2015.01\2015.01.23.mr4_IPV_1.31_C13_APT_ad.fid\fid | | | | |
| Frequency (MHz) | 100.5872 | Nucleus | 13C | Number of Transients | 476 |
| Original Points Count | 54348 | Points Count | 65536 | Pulse Sequence | APT_ad |
| Receiver Gain | 30.00 | SW(cyclical) (Hz) | 27173.91 | Solvent | cdcl3 |
| Spectrum Offset (Hz) | 11531.6846 | Spectrum Type | APT | Sweep Width (Hz) | 27173.50 |
| Temperature (degree C) | 25.900 | | | | |

¹³C NMR (101MHz, cdcl₃) δ = 163.31 - 163.28 (m, 1C), 163.31 - 163.28 (m, 1C), 163.80 (d, J=97.0 Hz, 1C), 161.35 (d, J=95.0 Hz, 1C), 159.17, 151.78, 145.01 (d, J=6.2 Hz, 1C), 137.22, 134.43 (d, J=3.3 Hz, 1C), 130.55 (br d, J=8.3 Hz, 1C), 129.31 (br d, J=8.3 Hz, 1C), 126.97, 122.17, 120.78 (br d, J=2.5 Hz, 1C), 115.37 (br d, J=21.6 Hz, 1C), 114.36 (d, J=21.1 Hz, 1C), 112.24 (br d, J=22.0 Hz, 1C), 110.59, 61.96, 48.48, 42.21, 35.67, 22.67

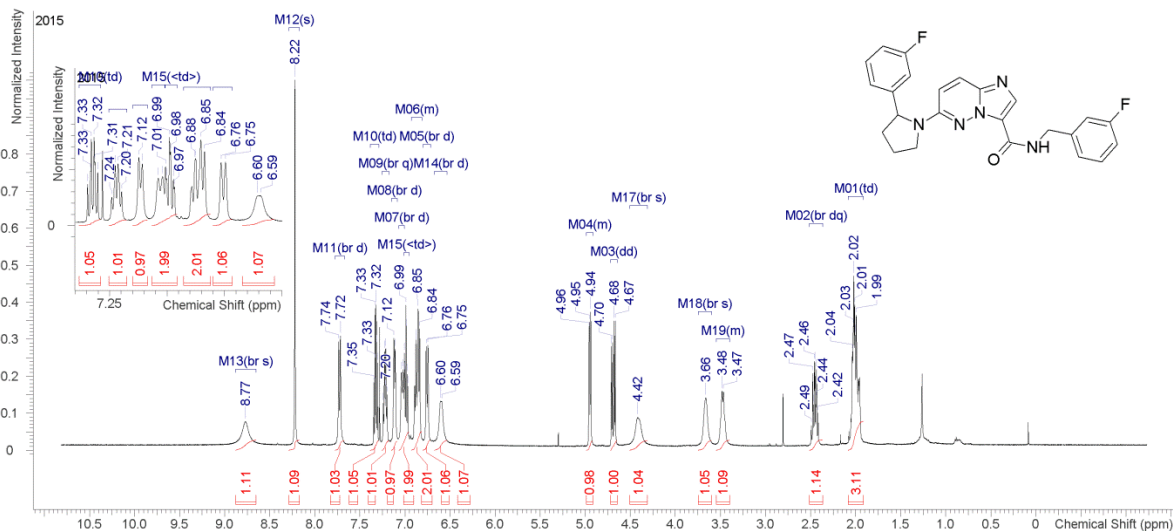


¹H NMR and ¹³C NMR for compound 4.21

IPV 1.29XX 498.118 MHz H1 1D in cdcl3 (ref. to CDCl3 @ 7.26 ppm), temp 26.4 C -> actual temp = 27.0 C, autotdx probe

| Multiplets Integrals Sum 21.81 | | Number of Nuclei 21 H's | |
|--------------------------------|---|-------------------------|--|
| Acquisition Time (sec) | 4.9997 | Comment | IPV 1.29XX 498.118 MHz H1 1D in cdcl3 (ref. to CDCl3 @ 7.26 ppm), temp 26.4 C -> actual temp = 27.0 C, autotdx probe |
| Date | Jan 27 2015 | Date Stamp | Jan 27 2015 |
| File Name | C:\Users\admin\Documents\NMR jan2015\2015.01\2015.01.27.15_IPV_1.29XX_H1_1D.fid | Frequency (MHz) | 498.1178 |
| Nucleus | 1H | Number of Transients | 16 |
| Pulse Sequence | s2pul | Receiver Gain | 32.00 |
| Spectrum Offset (Hz) | 2388.2478 | Spectrum Type | standard |
| | | Original Points Count | 30001 |
| | | Points Count | 32768 |
| | | SW(cyclical) (Hz) | 6000.60 |
| | | Solvent | cdcl3 |
| | | Sweep Width (Hz) | 6000.42 |
| | | Temperature (degree C) | 26.400 |

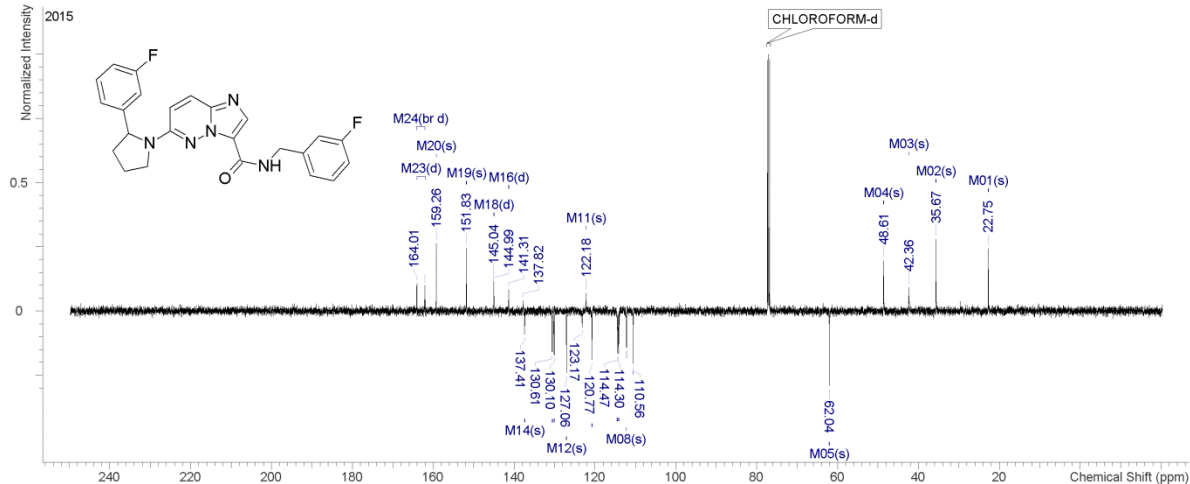
¹H NMR (498MHz, cdcl₃) δ = 8.77 (br s, 1H), 8.22 (s, 1H), 7.73 (br d, *J*=9.7 Hz, 1H), 7.32 (dt, *J*=6.1, 7.8 Hz, 1H), 7.22 (br q, *J*=7.7 Hz, 1H), 7.12 (br d, *J*=7.5 Hz, 1H), 7.03 (br d, *J*=9.5 Hz, 1H), 6.99 (dt, *J*=2.2, 8.4 Hz, 1H), 6.93 - 6.81 (m, 2H), 6.75 (br d, *J*=9.5 Hz, 1H), 6.60 (br d, *J*=6.6 Hz, 1H), 4.99 - 4.92 (m, 1H), 4.69 (dd, *J*=6.2, 15.2 Hz, 1H), 4.42 (br s, 1H), 3.66 (br s, 1H), 3.54 - 3.40 (m, 1H), 2.45 (br qd, *J*=8.5, 11.8 Hz, 1H), 2.02 (dt, *J*=4.8, 7.9 Hz, 3H)



IPV 1.29XX 125.266 MHz C13[H1] APT_ad in cdcl3 (ref. to CDCl3 @ 77.06 ppm), temp 26.4 C -> actual temp = 27.0 C, autotdx probe C & CH2 same, CH & CH3 opposite side of solvent signal

| Multiplets Integrals Sum 0.00 | | Number of Nuclei 22 C's | |
|-------------------------------|--|-------------------------|---|
| Acquisition Time (sec) | 1.9958 | Comment | IPV 1.29XX 125.266 MHz C13[H1] APT_ad in cdcl3 (ref. to CDCl3 @ 77.06 ppm), temp 26.4 C -> actual temp = 27.0 C, autotdx probe C & CH2 same, CH & CH3 opposite side of solvent signal |
| Date | Jan 27 2015 | Date Stamp | Jan 27 2015 |
| File Name | C:\Users\admin\Documents\NMR jan2015\2015.01\2015.01.27.15_IPV_1.29XX_C13_APT_ad.fid | Frequency (MHz) | 125.2656 |
| Nucleus | 13C | Number of Transients | 172 |
| Pulse Sequence | APT_ad | Points Count | 131072 |
| Receiver Gain | 32.00 | SW(cyclical) (Hz) | 33826.64 |
| Spectrum Offset (Hz) | 14370.3086 | Solvent | cdcl3 |
| Temperature (degree C) | 26.400 | Spectrum Type | APT |
| | | Sweep Width (Hz) | 33826.38 |

¹³C NMR (125MHz, cdcl₃) δ = 163.09 (br d, *J*=247.2 Hz, 1C), 163.03 (d, *J*=246.2 Hz, 1C), 159.26, 151.83, 145.02 (d, *J*=6.2 Hz, 1C), 141.34 (d, *J*=6.7 Hz, 1C), 137.41, 130.57 (br d, *J*=8.3 Hz, 1C), 130.13 (d, *J*=8.3 Hz, 1C), 127.06, 122.18, 120.77, 114.30 (d, *J*=21.2 Hz, 1C), 114.13 (br d, *J*=20.9 Hz, 1C), 112.32, 112.14, 110.56, 62.04, 48.61, 42.36, 35.67, 22.75

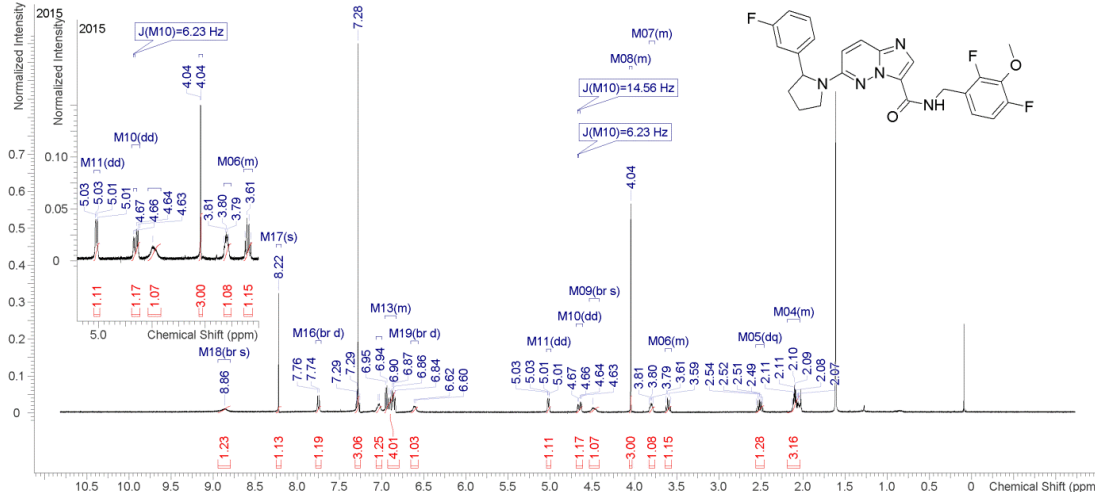


¹H NMR and ¹³C NMR for compound 4.22

IPV 1.34 HPLC pure fraction 20.3 min - 22.0 min 498.118 MHz H1 1D in cdcl3 (ref. to CDCl3 @ 7.26 ppm), temp 26.4 C -> actual temp = 27.0 C, autobx probe

| Multiplets Integrals Sum 25.93 | | Number of Nuclei 24 H's | |
|---|----------------------------------|---|--------------------------------|
| Acquisition Time (sec) 4.9997 | | | |
| Comment IPV 1.34 HPLC pure fraction 20.3 min - 22.0 min 498.118 MHz H1 1D in cdcl3 (ref. to CDCl3 @ 7.26 ppm), temp 26.4 C -> actual temp = 27.0 C, autobx probe | | | |
| Date Apr 14 2015 | Date Stamp Apr 14 2015 | File Name F:\Schirrna\2015.04\2015.04.14.i5_IPV_1.34_20.3-22.0_H1_1D.fid | Number of Transients 16 |
| Frequency (MHz) 498.1178 | Nucleus 1H | Pulse Sequence s2pul | Solvent CHLOROFORM-d |
| Original Points Count 30001 | Points Count 65536 | Sweep Width (Hz) 6000.60 | Spectrum Type standard |
| Receiver Gain 32.00 | SW(cyclical) (Hz) 6000.60 | Sweep Width (Hz) 6000.51 | |
| Spectrum Offset (Hz) 2388.2935 | | | |
| Temperature (degree C) 26.400 | | | |

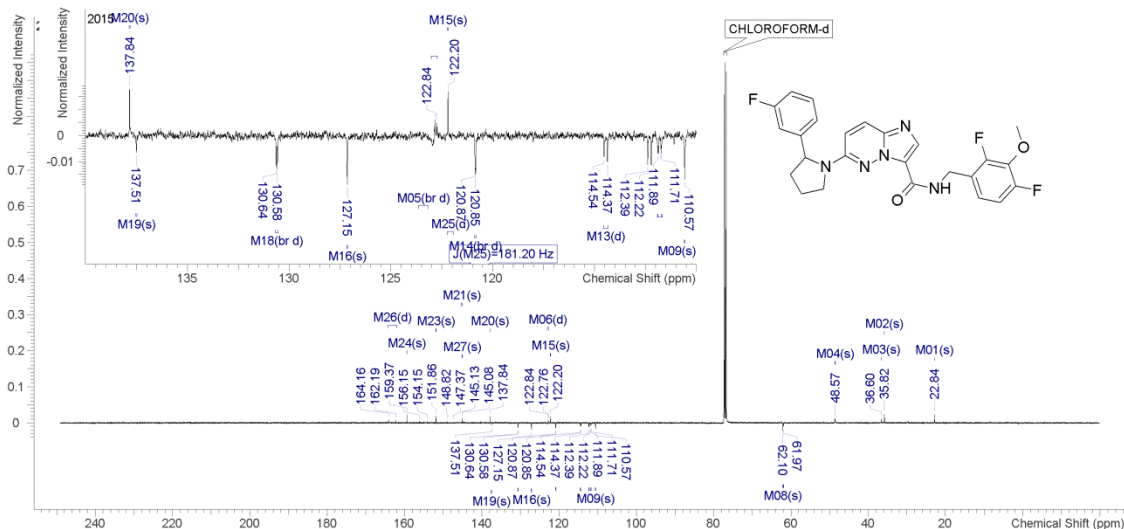
¹H NMR (498MHz, CHLOROFORM-d) δ = 8.86 (br s, 1H), 8.22 (s, 1H), 7.75 (br d, $J=9.6$ Hz, 1H), 7.32 - 7.25 (m, 3H), 7.03 (br d, $J=6.3$ Hz, 1H), 6.96 - 6.83 (m, 4H), 6.61 (br d, $J=9.4$ Hz, 1H), 5.02 (dd, $J=1.7, 8.7$ Hz, 1H), 4.66 (dd, $J=6.2, 14.6$ Hz, 1H), 4.49 (br s, 1H), 4.06 - 4.03 (m, 3H), 3.83 - 3.76 (m, 1H), 3.64 - 3.56 (m, 1H), 2.51 (qd, $J=8.7, 11.9$ Hz, 1H), 2.19 - 2.04 (m, 3H)



Jamie_Bailey_IPV_1_34 125.690 MHz C13[H1] APT_ad in cdcl3 (ref. to CDCl3 @ 77.06 ppm), temp 27.7 C -> actual temp = 27.0 C, colddual probe C & CH2 same, CH & CH3 opposite side of solvent signal

| Multiplets Integrals Sum 0.00 | | Number of Nuclei 25 C's | |
|--|----------------------------------|--|--|
| Acquisition Time (sec) 2.0000 | | | |
| Comment Jamie_Bailey_IPV_1_34 125.690 MHz C13[H1] APT_ad in cdcl3 (ref. to CDCl3 @ 77.06 ppm), temp 27.7 C -> actual temp = 27.0 C, colddual probe C & CH2 same, CH & CH3 opposite side of solvent signal | | | |
| Date May 13 2015 | Date Stamp May 13 2015 | File Name F:\Schirrna\2015.05\2015.05.13.u5_IPV_1.34_loc12_12.20_C13_APT_ad.fid | Frequency (MHz) 125.6902 |
| Nucleus 13C | Number of Transients 648 | Original Points Count 67568 | Receiver Gain 30.00 |
| Points Count 131072 | Pulse Sequence APT_ad | Solvent CHLOROFORM-d | Spectrum Offset (Hz) 14411.0176 |
| SW(cyclical) (Hz) 33783.79 | Sweep Width (Hz) 33783.53 | Temperature (degree C) 27.600 | |

¹³C NMR (126MHz, CHLOROFORM-d) δ = 163.17 (d, $J=247.4$ Hz, 1C), 159.37, 155.15 (br d, $J=252.1$ Hz, 1C), 151.86, 148.25 (d, $J=181.2$ Hz, 1C), 145.13, 145.08, 137.84, 137.51, 130.61 (br d, $J=8.2$ Hz, 1C), 127.15, 122.80 (d, $J=10.1$ Hz, 1C), 122.20, 120.86 (br d, $J=2.3$ Hz, 1C), 114.45 (d, $J=21.1$ Hz, 1C), 112.30 (d, $J=21.9$ Hz, 1C), 111.82 (br d, $J=19.3$ Hz, 1C), 111.79 (br d, $J=19.3$ Hz, 1C), 110.57, 62.10, 62.02 - 61.92 (m, 1C), 48.57, 36.60, 35.82, 22.84

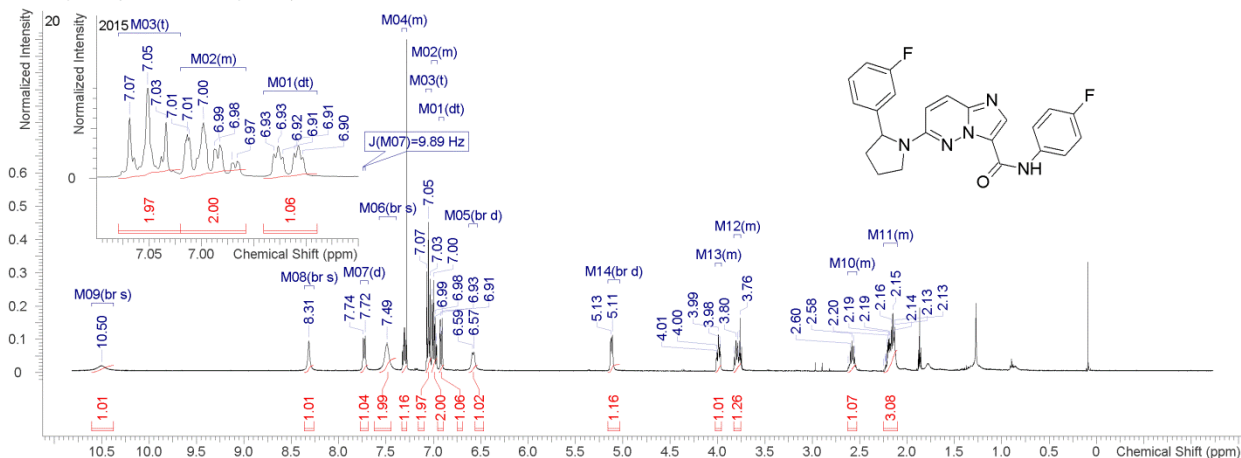


¹H NMR and ¹³C NMR for compound 4.23

IPV 1.33 498.118 MHz H1 1D in cdcl3 (ref. to CDCl3 @ 7.26 ppm), temp 26.4 C -> actual temp = 27.0 C, autoxdb probe

| Multiplets Integrals Sum 19.83 | | Number of Nuclei 19 H's | | | | | |
|--------------------------------|---|-------------------------|--|-----------------------|---------|------------------------|--------|
| Acquisition Time (sec) | 4.9997 | Comment | IPV 1.33 498.118 MHz H1 1D in cdcl3 (ref. to CDCl3 @ 7.26 ppm), temp 26.4 C -> actual temp = 27.0 C, autoxdb probe | | | | |
| Date | Jan 23 2015 | Date Stamp | Jan 23 2015 | | | | |
| File Name | C:\Users\admin\Documents\NMR\jan2015\2015.01\2015.01.23.i5_IPV_1.33_H1_1D.fid\fid | | Frequency (MHz) | 498.1178 | | | |
| Nucleus | 1H | Number of Transients | 16 | Original Points Count | 30001 | Points Count | 32768 |
| Pulse Sequence | s2pul | Receiver Gain | 32.00 | SW(cyclical) (Hz) | 6000.60 | Solvent | cdcl3 |
| Spectrum Offset (Hz) | 2388.2478 | Spectrum Type | standard | Sweep Width (Hz) | 6000.42 | Temperature (degree C) | 26.400 |

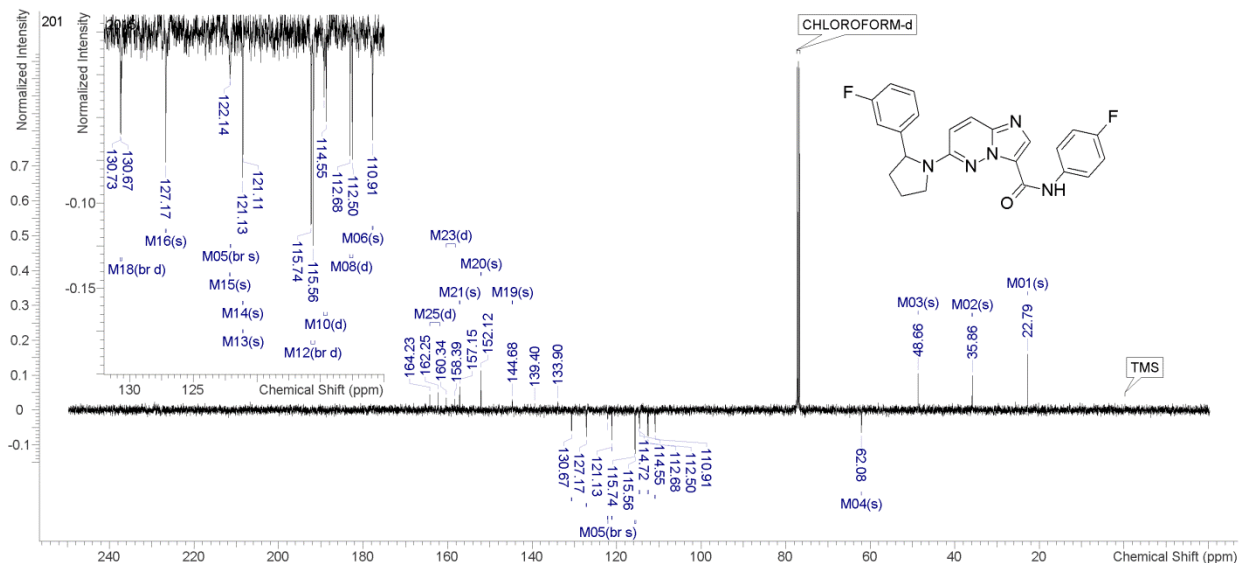
¹H NMR (498MHz, cdcl₃) δ = 10.50 (br s, 1H), 8.31 (br s, 1H), 7.73 (d, J=9.9 Hz, 1H), 7.49 (br s, 2H), 7.33 - 7.28 (m, 1H), 7.05 (t, J=8.7 Hz, 2H), 7.02 - 6.96 (m, 2H), 6.92 (td, J=2.0, 9.5 Hz, 1H), 6.58 (br d, J=8.1 Hz, 1H), 5.12 (br d, J=8.1 Hz, 1H), 4.02 - 3.96 (m, 1H), 3.83 - 3.76 (m, 1H), 2.62 - 2.53 (m, 1H), 2.25 - 2.10 (m, 3H)



IPV 1.33 125.266 MHz C13[H1] APT_ad in cdcl3 (ref. to CDCl3 @ 77.06 ppm), temp 26.4 C -> actual temp = 27.0 C, autoxdb probe C & CH2 same, CH & CH3 opposite side of solvent signal

| Multiplets Integrals Sum 0.00 | | Number of Nuclei 19 C's | | |
|-------------------------------|--|-------------------------|---|----------|
| Acquisition Time (sec) | 1.9958 | Comment | IPV 1.33 125.266 MHz C13[H1] APT_ad in cdcl3 (ref. to CDCl3 @ 77.06 ppm), temp 26.4 C -> actual temp = 27.0 C, autoxdb probe C & CH2 same, CH & CH3 opposite side of solvent signal | |
| Date | Jan 23 2015 | Date Stamp | Jan 23 2015 | |
| File Name | F:\Schirma\2015.01\2015.01.23.i5_IPV_1.33_C13_APT_ad.fid\fid | | Frequency (MHz) | 125.2656 |
| Nucleus | 13C | Number of Transients | 276 | |
| Original Points Count | 67510 | Points Count | 131072 | |
| Receiver Gain | 30.00 | SW(cyclical) (Hz) | 33826.64 | |
| Pulse Sequence | APT_ad | Solvent | CHLOROFORM-d | |
| Spectrum Offset (Hz) | 14370.3086 | Spectrum Type | APT | |
| Temperature (degree C) | 26.400 | Sweep Width (Hz) | 33826.38 | |

¹³C NMR (125MHz, CHLOROFORM-d) δ = 163.24 (d, J=247.8 Hz, 1C), 159.37 (d, J=243.4 Hz, 1C), 157.15, 152.12, 144.68, 130.70 (br d, J=8.3 Hz, 1C), 127.17, 122.14, 122.10 (br s, 1C), 121.13, 121.11, 115.65 (br d, J=22.7 Hz, 1C), 114.64 (d, J=21.4 Hz, 1C), 112.59 (d, J=22.2 Hz, 1C), 110.91, 62.08, 48.66, 35.86, 22.79

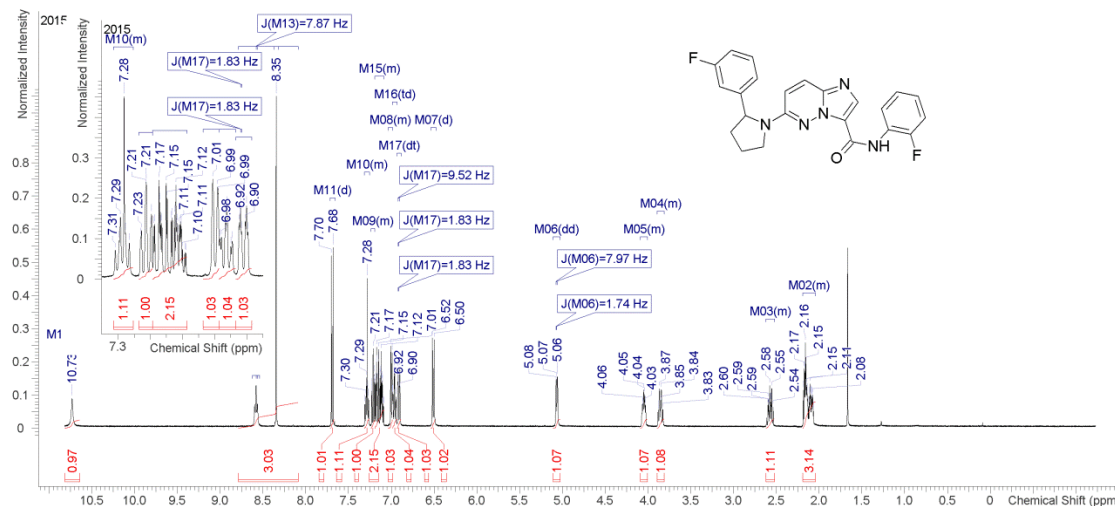


¹H NMR and ¹³C NMR for compound 4.25

IPV 1.37 498.118 MHz H1 1D in cdcl3 (ref. to CDCl3 @ 7.26 ppm), temp 26.4 C -> actual temp = 27.0 C, autotxnb probe

| Multiplets | Integrals | Sum | 20.87 | Number of Nuclei | 21 H's |
|------------------------|--------------|----------------------|---|----------------------|---|
| Acquisition Time (sec) | 4.9997 | Comment | IPV 1.37 498.118 MHz H1 1D in cdcl3 (ref. to CDCl3 @ 7.26 ppm), temp 26.4 C -> actual temp = 27.0 C, autotxnb probe | | |
| Date | May 6 2015 | Date Stamp | May 6 2015 | File Name | F:\Schirra\2015.05\2015.05.06.i5_IPV_1.37_H1_1D.fid.fid |
| Frequency (MHz) | 498.1178 | Nucleus | 1H | Number of Transients | 16 |
| Original Points Count | 30001 | Spectrum Offset (Hz) | 2388.2935 | Receiver Gain | 32.00 |
| Points Count | 65536 | Pulse Sequence | s2pul | SW(cyclical) (Hz) | 6000.60 |
| Solvent | CHLOROFORM-d | Spectrum Type | standard | Sweep Width (Hz) | 6000.51 |
| Temperature (degree C) | 26.400 | | | | |

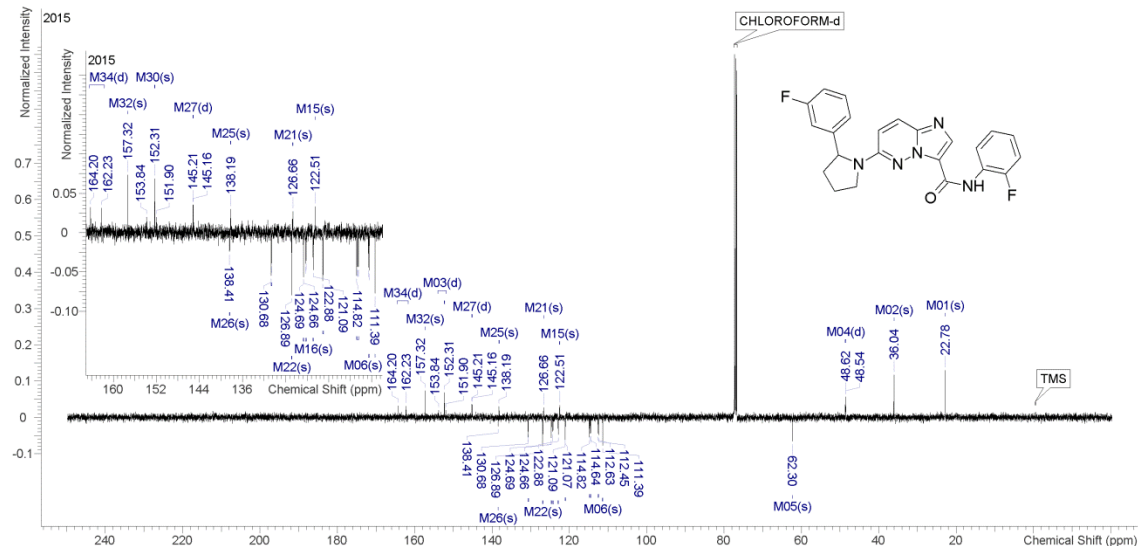
¹H NMR (498MHz, CHLOROFORM-d) δ = 10.73 (br s, 1H), 8.58 (t, J=7.9 Hz, 1H), 8.35 (s, 1H), 8.79 - 8.09 (m, 1H), 7.69 (d, J=9.9 Hz, 1H), 7.31 - 7.25 (m, 1H), 7.24 - 7.19 (m, 1H), 7.19 - 7.09 (m, 3H), 7.04 - 6.99 (m, 1H), 6.96 (dt, J=2.3, 8.4 Hz, 1H), 6.91 (td, J=1.8, 9.5 Hz, 1H), 6.51 (d, J=9.9 Hz, 1H), 5.07 (dd, J=1.7, 8.0 Hz, 1H), 4.09 - 4.01 (m, 1H), 3.89 - 3.81 (m, 1H), 2.62 - 2.52 (m, 1H), 2.19 - 2.04 (m, 3H)



IPV 1.37 125.266 MHz C13[H1] APT_ad in cdcl3 (ref. to CDCl3 @ 77.06 ppm), temp 26.4 C -> actual temp = 27.0 C, autotxnb probe C & CH2 same, CH & CH3 opposite side of solvent signal

| Multiplets | Integrals | Sum | 0.00 | Number of Nuclei | 23 C's |
|------------------------|--------------|----------------------|--|----------------------|--|
| Acquisition Time (sec) | 1.9958 | Comment | IPV 1.37 125.266 MHz C13[H1] APT_ad in cdcl3 (ref. to CDCl3 @ 77.06 ppm), temp 26.4 C -> actual temp = 27.0 C, autotxnb probe C & CH2 same, CH & CH3 opposite side of solvent signal | | |
| Date | May 6 2015 | Date Stamp | May 6 2015 | File Name | F:\Schirra\2015.05\2015.05.06.i5_IPV_1.37_C13_APT_ad.fid.fid |
| Frequency (MHz) | 125.2656 | Nucleus | 13C | Number of Transients | 444 |
| Original Points Count | 67510 | Spectrum Offset (Hz) | 14370.3086 | Receiver Gain | 30.00 |
| Points Count | 131072 | Pulse Sequence | APT_ad | SW(cyclical) (Hz) | 33826.64 |
| Solvent | CHLOROFORM-d | Spectrum Type | APT | Sweep Width (Hz) | 33826.38 |
| Temperature (degree C) | 26.400 | | | | |

¹³C NMR (125MHz, CHLOROFORM-d) δ = 163.22 (d, J=247.8 Hz, 1C), 157.32, 152.31, 152.87 (d, J=242.8 Hz, 1C), 145.19 (d, J=5.9 Hz, 1C), 138.41, 138.19, 130.65 (br d, J=8.5 Hz, 1C), 126.89, 126.66, 124.67 (d, J=3.1 Hz, 1C), 124.24 (br d, J=8.0 Hz, 1C), 122.88, 122.51, 121.08 (d, J=3.1 Hz, 1C), 114.74 (d, J=19.1 Hz, 1C), 114.55 (d, J=21.2 Hz, 1C), 112.54 (br d, J=22.2 Hz, 1C), 111.39, 62.30, 48.58 (d, J=9.8 Hz, 1C), 36.04, 22.78

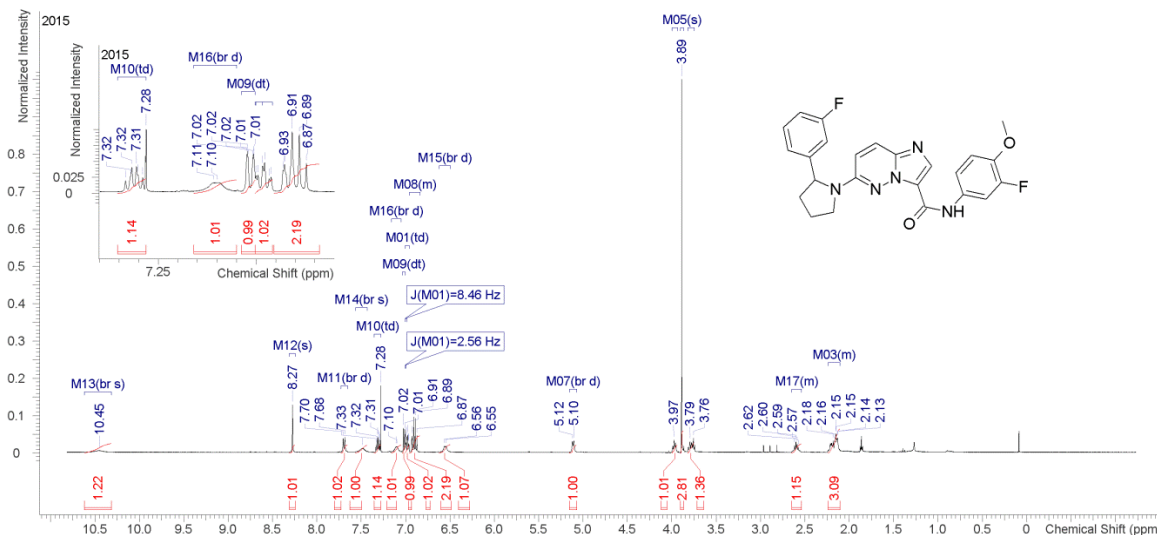


¹H NMR and ¹³C NMR for compound 4.26

IPV 1.32 498.118 MHz H1 1D in cdcl3 (ref. to CDCl3 @ 7.26 ppm), temp 26.4 C -> actual temp = 27.0 C, autoxdb probe

| Multiplets | Integrals | Sum | 22.09 | Number of Nuclei | 22 H's |
|------------------------|---|----------------------|--|------------------------|----------|
| Acquisition Time (sec) | 4.9997 | Comment | IPV 1.32 498.118 MHz H1 1D in cdcl3 (ref. to CDCl3 @ 7.26 ppm), temp 26.4 C -> actual temp = 27.0 C, autoxdb probe | | |
| Date | Jan 23 2015 | Date Stamp | Jan 23 2015 | | |
| File Name | C:\Users\admin\Documents\NMR\jan2015\2015.01\2015.01.23.15_IPV_1.32_H1_1D.fid.fid | | | Frequency (MHz) | 498.1178 |
| Nucleus | 1H | Number of Transients | 16 | Original Points Count | 30001 |
| Pulse Sequence | s2pul | Receiver Gain | 32.00 | SW(cyclical) (Hz) | 6000.60 |
| Spectrum Offset (Hz) | 2388.2478 | Spectrum Type | standard | Sweep Width (Hz) | 6000.42 |
| | | | | Solvent | cdcl3 |
| | | | | Temperature (degree C) | 26.400 |

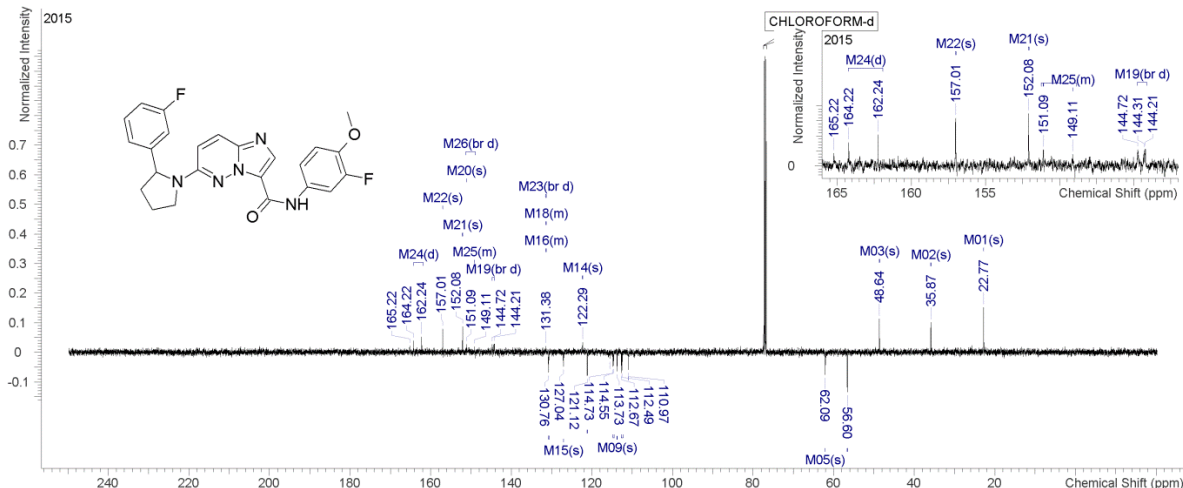
¹H NMR (498MHz, cdcl₃) δ = 10.45 (br s, 1H), 8.27 (s, 1H), 7.69 (br d, J=9.9 Hz, 1H), 7.48 (br s, 1H), 7.31 (dt, J=6.0, 7.9 Hz, 1H), 7.10 (br d, J=4.4 Hz, 1H), 7.01 (td, J=0.7, 7.7 Hz, 1H), 6.98 (dt, J=2.6, 8.5 Hz, 2H), 6.95 - 6.84 (m, 2H), 6.55 (br d, J=8.2 Hz, 1H), 5.11 (br d, J=7.9 Hz, 1H), 3.97 (br s, 1H), 3.89 (s, 3H), 3.78 (br d, J=19.4 Hz, 1H), 2.65 - 2.54 (m, 1H), 2.24 - 2.11 (m, 3H)



IPV 1.32 125.266 MHz C13[H1] APT_ad in cdcl3 (ref. to CDCl3 @ 77.06 ppm), temp 26.4 C -> actual temp = 27.0 C, autoxdb probe C & CH2 same, CH & CH3 opposite side of solvent signal

| Multiplets | Integrals | Sum | 0.00 | Number of Nuclei | 23 C's |
|------------------------|--|-------------------|---|----------------------|----------|
| Acquisition Time (sec) | 1.9958 | Comment | IPV 1.32 125.266 MHz C13[H1] APT_ad in cdcl3 (ref. to CDCl3 @ 77.06 ppm), temp 26.4 C -> actual temp = 27.0 C, autoxdb probe C & CH2 same, CH & CH3 opposite side of solvent signal | | |
| Date | Jan 23 2015 | Date Stamp | Jan 23 2015 | | |
| File Name | C:\Users\admin\Documents\NMR\jan2015\2015.01\2015.01.23.15_IPV_1.32_C13_APT_ad.fid.fid | | | | |
| Frequency (MHz) | 125.2656 | Nucleus | 13C | Number of Transients | 508 |
| Original Points Count | 67510 | Points Count | 131072 | Pulse Sequence | APT_ad |
| Receiver Gain | 30.00 | SW(cyclical) (Hz) | 33826.64 | Solvent | cdcl3 |
| Spectrum Offset (Hz) | 14370.3086 | Spectrum Type | APT | Sweep Width (Hz) | 33826.38 |
| Temperature (degree C) | 26.400 | | | | |

¹³C NMR (125MHz, cdcl₃) δ = 163.23 (d, J=247.8 Hz, 1C), 157.01, 152.08, 151.09, 149.10 - 149.10 (m, 1C), 150.10 (br d, J=247.8 Hz, 1C), 144.47 (br d, J=63.7 Hz, 1C), 131.41 (br d, J=7.5 Hz, 1C), 131.37 - 131.29 (m, 1C), 131.37 - 131.29 (m, 1C), 130.73 (br d, J=8.5 Hz, 1C), 127.04, 122.29, 121.13 (br d, J=2.6 Hz, 1C), 114.64 (br d, J=21.4 Hz, 1C), 113.73, 112.58 (br d, J=21.9 Hz, 1C), 110.97, 62.09, 56.60, 48.64, 35.87, 22.77

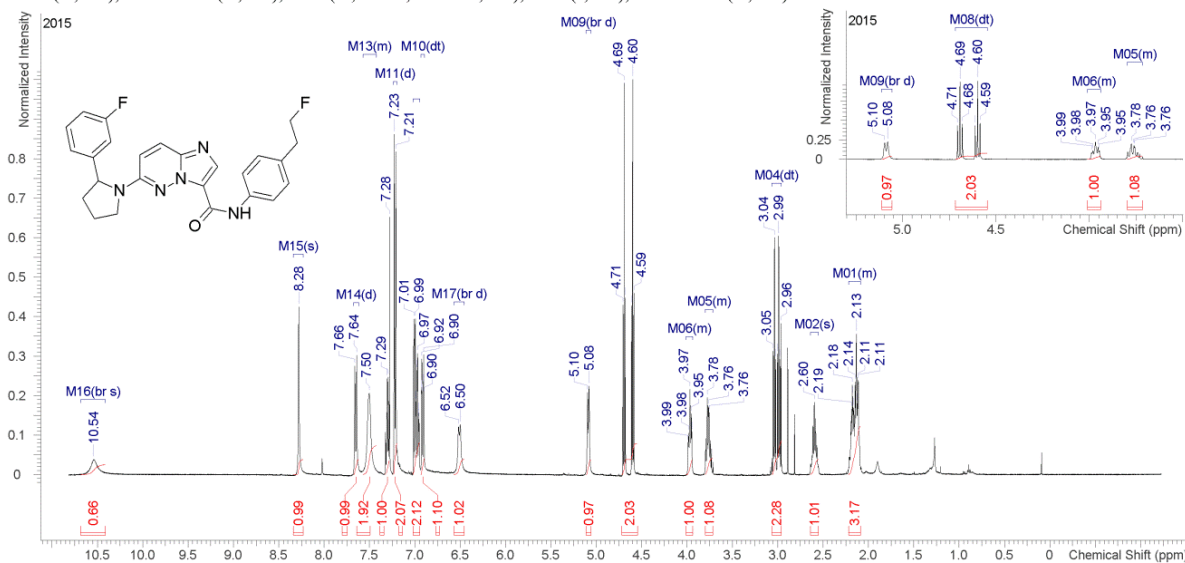


¹H NMR and ¹³C NMR for compound 4.27

IPV 1.26 498.118 MHz H1 1D in cdcl3 (ref. to CDCl3 @ 7.26 ppm), temp 26.4 C -> actual temp = 27.0 C, autotx probe

| Multiplets Integrals Sum 23.41 | | Number of Nuclei 23 H's | |
|--------------------------------|---|-------------------------|---|
| Acquisition Time (sec) | 4.9997 | Comment | IPV 1.26 498.118 MHz H1 1D in cdcl3 (ref. to CDCl3 @ 7.26 ppm), temp 26.4 C -> actual temp = 27.0 C, autotx probe |
| Date | Jan 23 2015 | Date Stamp | Jan 23 2015 |
| File Name | C:\Users\admin\Documents\NMR\jan2015\2015.01\2015.01.23.i5_IPV_1.26_H1_1D.fid | Frequency (MHz) | 498.1178 |
| Nucleus | ¹ H | Number of Transients | 16 |
| Pulse Sequence | s2pul | Original Points Count | 30001 |
| Spectrum Offset (Hz) | 2388.2478 | Receiver Gain | 32.00 |
| | | SW(cyclical) (Hz) | 6000.60 |
| | | Sweep Width (Hz) | 6000.42 |
| | | Points Count | 32768 |
| | | Solvent | cdcl3 |
| | | Temperature (degree C) | 26.400 |

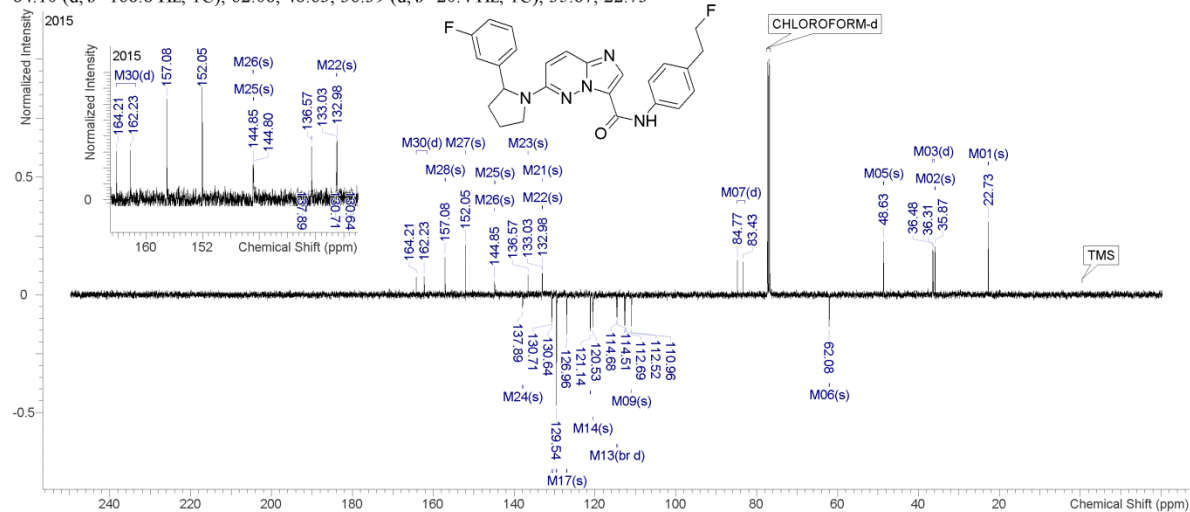
¹H NMR (498MHz, cdcl₃) δ = 10.54 (br s, 1H), 8.28 (s, 1H), 7.65 (d, J=9.9 Hz, 1H), 7.57 - 7.42 (m, 2H), 7.33 - 7.28 (m, 1H), 7.22 (d, J=8.2 Hz, 2H), 7.02 - 6.95 (m, 2H), 6.91 (td, J=1.9, 9.6 Hz, 1H), 6.51 (br d, J=9.2 Hz, 1H), 5.09 (br d, J=8.1 Hz, 1H), 4.65 (td, J=6.4, 47.1 Hz, 2H), 4.01 - 3.94 (m, 1H), 3.80 - 3.71 (m, 1H), 3.01 (td, J=6.4, 23.4 Hz, 2H), 2.60 (s, 1H), 2.22 - 2.09 (m, 3H)



IPV 1.26 125.266 MHz C13[H1] APT_ad in cdcl3 (ref. to CDCl3 @ 77.06 ppm), temp 26.4 C -> actual temp = 27.0 C, autotx probe C & CH2 same, CH & CH3 opposite side of solvent signal

| Multiplets Integrals Sum 0.00 | | Number of Nuclei 23 C's | |
|-------------------------------|--|-------------------------|--|
| Acquisition Time (sec) | 1.9958 | Comment | IPV 1.26 125.266 MHz C13[H1] APT_ad in cdcl3 (ref. to CDCl3 @ 77.06 ppm), temp 26.4 C -> actual temp = 27.0 C, autotx probe C & CH2 same, CH & CH3 opposite side of solvent signal |
| Date | Jan 23 2015 | Date Stamp | Jan 23 2015 |
| File Name | F:\Schirra\2015.01\2015.01.23.i5_IPV_1.26_C13_APT_ad.fid | Frequency (MHz) | 125.2656 |
| Nucleus | ¹³ C | Number of Transients | 244 |
| Pulse Sequence | APT_ad | Original Points Count | 67510 |
| Points Count | 131072 | Receiver Gain | 30.00 |
| SW(cyclical) (Hz) | 33826.64 | Spectrum Offset (Hz) | 14370.3086 |
| Solvent | CHLOROFORM-d | Temperature (degree C) | 26.400 |
| Sweep Width (Hz) | 33826.38 | | |

¹³C NMR (125MHz, CHLOROFORM-d) δ = 163.22 (d, J=247.5 Hz, 1C), 157.08, 152.05, 144.85, 144.80, 137.89, 136.57, 133.03, 132.98, 130.67 (br d, J=8.3 Hz, 1C), 129.54, 126.96, 121.15 (br d, J=2.6 Hz, 1C), 120.53, 114.60 (br d, J=21.2 Hz, 1C), 112.60 (br d, J=21.9 Hz, 1C), 110.96, 84.10 (d, J=168.8 Hz, 1C), 62.08, 48.63, 36.39 (d, J=20.4 Hz, 1C), 35.87, 22.73

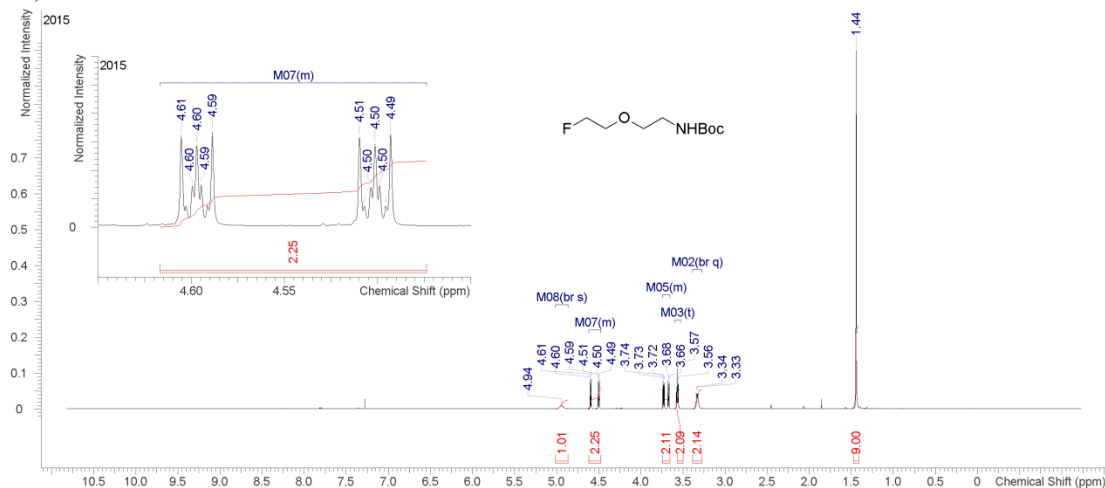


¹H NMR and ¹³C NMR for compound 4.29

JB-RAN-03 498.118 MHz H1 1D in cdcl3 (ref. to CDCl3 @ 7.26 ppm), temp 26.4 C -> actual temp = 27.0 C, autoxtdb probe

| Multiplets | Integrals Sum | Number of Nuclei | 18 H's |
|------------------------|--|------------------------|--|
| Acquisition Time (sec) | 4.9997 | Comment | JB-RAN-03 498.118 MHz H1 1D in cdcl3 (ref. to CDCl3 @ 7.26 ppm), temp 26.4 C -> actual temp = 27.0 C, autoxtdb probe |
| Date | Jan 12 2015 | Date Stamp | Jan 12 2015 |
| File Name | C:\Users\admin\Documents\NMR jan2015\2015.01\2015.01.12.i5_JB-RAN-03_H1_1D.fid\fid | | |
| Nucleus | 1H | Number of Transients | 16 |
| Pulse Sequence | s2pul | Receiver Gain | 32.00 |
| Spectrum Offset (Hz) | 2388.2478 | Spectrum Type | standard |
| | | Original Points Count | 30001 |
| | | SW(cyclical) (Hz) | 6000.60 |
| | | Sweep Width (Hz) | 6000.42 |
| | | Frequency (MHz) | 498.1178 |
| | | Points Count | 32768 |
| | | Solvent | cdcl3 |
| | | Temperature (degree C) | 26.400 |

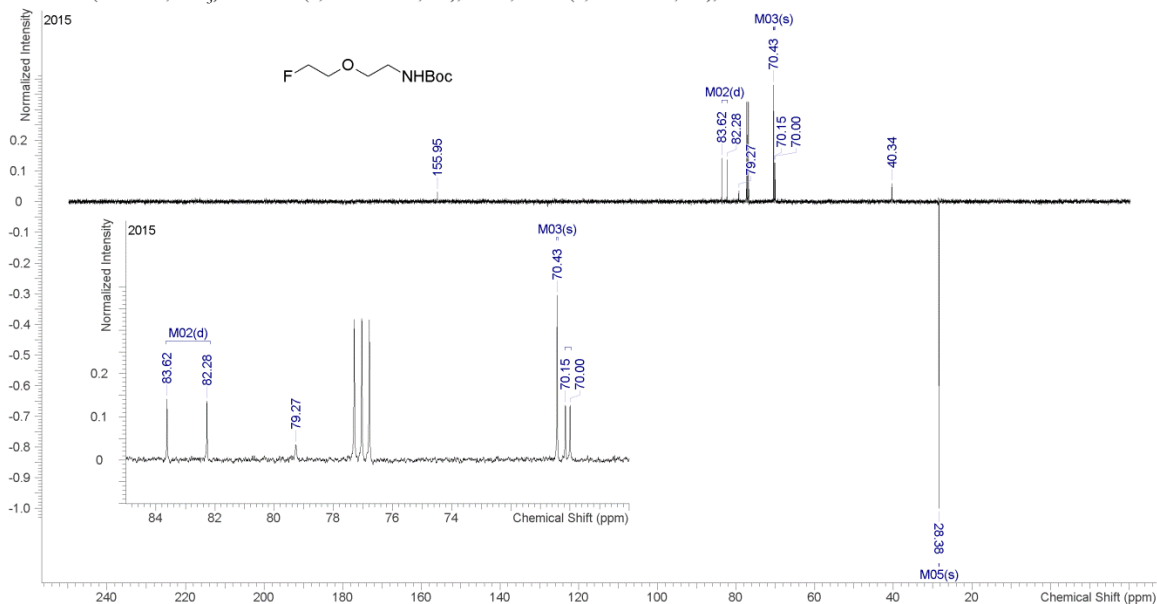
¹H NMR (498MHz, cdcl₃) δ = 4.94 (br s, 1H), 4.62 - 4.47 (m, 2H), 3.75 - 3.65 (m, 2H), 3.57 (t, *J*=5.2 Hz, 2H), 3.33 (br q, *J*=5.1 Hz, 2H), 1.44 (s, 9H)



JB-RAN-03 125.266 MHz C13[H1] APT_ad in cdcl3 (ref. to CDCl3 @ 77.06 ppm), temp 26.4 C -> actual temp = 27.0 C, autoxtdb probe C & CH2 same, CH & CH3 opposite side of solvent signal

| Multiplets | Integrals Sum | Number of Nuclei | 4 C's |
|------------------------|---|----------------------|---|
| Acquisition Time (sec) | 1.9958 | Comment | JB-RAN-03 125.266 MHz C13[H1] APT_ad in cdcl3 (ref. to CDCl3 @ 77.06 ppm), temp 26.4 C -> actual temp = 27.0 C, autoxtdb probe C & CH2 same, CH & CH3 opposite side of solvent signal |
| Date | Jan 12 2015 | Date Stamp | Jan 12 2015 |
| File Name | C:\Users\admin\Documents\NMR jan2015\2015.01\2015.01.12.i5_JB-RAN-03_C13_APT_ad.fid\fid | | |
| Frequency (MHz) | 125.2656 | Nucleus | 13C |
| Original Points Count | 67510 | Points Count | 131072 |
| Receiver Gain | 30.00 | SW(cyclical) (Hz) | 33826.64 |
| Spectrum Offset (Hz) | 14370.3086 | Spectrum Type | APT |
| Temperature (degree C) | 26.400 | Sweep Width (Hz) | 33826.38 |
| | | Number of Transients | 92 |
| | | Pulse Sequence | APT_ad |
| | | Solvent | cdcl3 |

¹³C NMR (125MHz, cdcl₃) δ = 82.95 (d, *J*=169.0 Hz, 1C), 70.43, 70.08 (d, *J*=19.6 Hz, 1C), 28.38

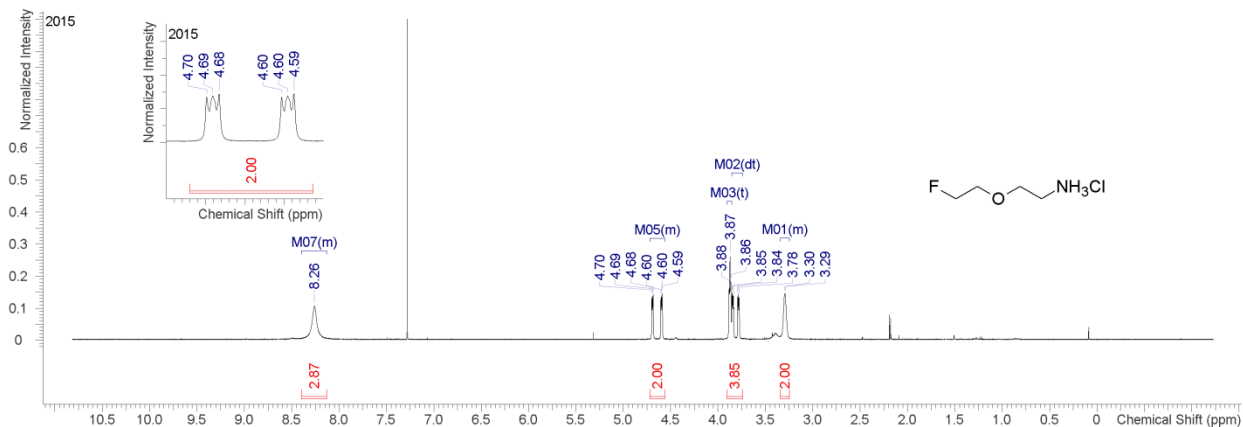


¹H NMR and ¹³C NMR for compound 4.30

JB-RAN-04 498.118 MHz H1 1D in cdcl3 (ref. to CDCI3 @ 7.26 ppm), temp 26.4 C -> actual temp = 27.0 C, autotdx probe

| Multiplets | Integrals | Sum | 10.72 | Number of Nuclei | 11 H's |
|------------------------|-------------|----------------------|---|----------------------|--|
| Acquisition Time (sec) | 4.9997 | Comment | JB-RAN-04 498.118 MHz H1 1D in cdcl3 (ref. to CDCI3 @ 7.26 ppm), temp 26.4 C -> actual temp = 27.0 C, autotdx probe | | |
| Date | Jan 12 2015 | Date Stamp | Jan 12 2015 | File Name | G:\2015.01\2015.01.12.i5_JB-RAN-04_H1_1D.fid\fid |
| Frequency (MHz) | 498.1178 | Nucleus | 1H | Number of Transients | 16 |
| Points Count | 32768 | Pulse Sequence | s2pul | Receiver Gain | 32.00 |
| Solvent | cdcl3 | Spectrum Offset (Hz) | 2388.2478 | Spectrum Type | standard |
| Temperature (degree C) | 26.400 | | | SW(cyclical) (Hz) | 6000.60 |
| | | | | Sweep Width (Hz) | 6000.42 |

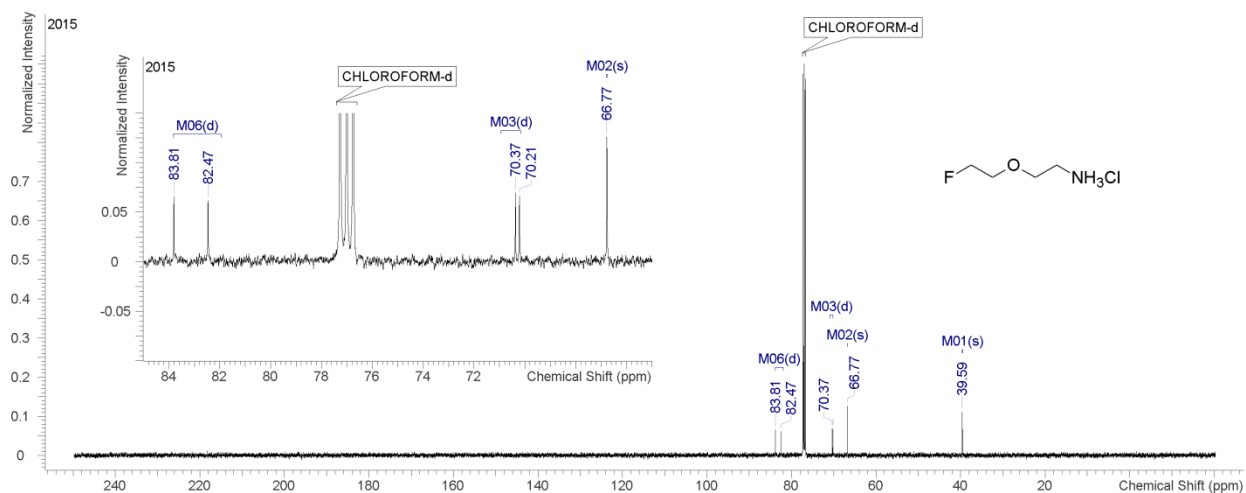
¹H NMR (498MHz, cdcl₃) δ = 8.40 - 8.13 (m, 3H), 4.72 - 4.56 (m, 2H), 3.87 (t, J=4.8 Hz, 2H), 3.81 (td, J=3.8, 30.0 Hz, 2H), 3.34 - 3.24 (m, 2H)



JB-RAN-04 125.266 MHz C13[H1] APT_ad in cdcl3 (ref. to CDCI3 @ 77.06 ppm), temp 26.4 C -> actual temp = 27.0 C, autotdx probe C & CH2 same, CH & CH3 opposite side of solvent signal

| Multiplets | Integrals | Sum | 0.00 | Number of Nuclei | 4 C's |
|------------------------|-------------|-------------------|--|----------------------|---|
| Acquisition Time (sec) | 1.9958 | Comment | JB-RAN-04 125.266 MHz C13[H1] APT_ad in cdcl3 (ref. to CDCI3 @ 77.06 ppm), temp 26.4 C -> actual temp = 27.0 C, autotdx probe C & CH2 same, CH & CH3 opposite side of solvent signal | | |
| Date | Jan 12 2015 | Date Stamp | Jan 12 2015 | File Name | C:\Users\admin\Documents\NMR jan2015\2015.01.12.i5_JB-RAN-04_C13_APT_ad.fid\fid |
| Frequency (MHz) | 125.2656 | Nucleus | 13C | Number of Transients | 1040 |
| Original Points Count | 67510 | Points Count | 131072 | Pulse Sequence | APT_ad |
| Receiver Gain | 30.00 | SW(cyclical) (Hz) | 33826.64 | Solvent | cdcl3 |
| Spectrum Offset (Hz) | 14370.3086 | Spectrum Type | APT | Sweep Width (Hz) | 33826.38 |
| Temperature (degree C) | 26.400 | | | | |

¹³C NMR (125MHz, cdcl₃) δ = 83.14 (d, J=168.0 Hz, 1C), 70.29 (d, J=19.4 Hz, 1C), 66.77, 39.59

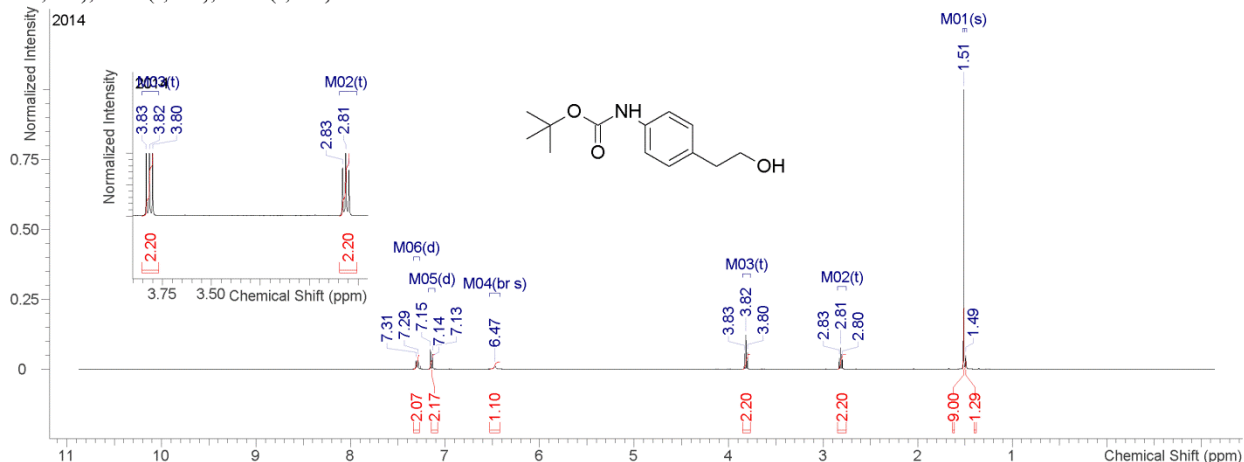


¹H NMR and ¹³C NMR for compound 4.32

IPV 1.2 399.984 MHz H1 1D in cdcl3 (ref. to CDCl3 @ 7.26 ppm), temp 25.9 C -> actual temp = 27.0 C, onenmr probe

| Multiplets | Integrals | Sum | 20.04 | Number of Nuclei | 19 H's |
|---|-------------|--------------------------|-------------|-----------------------------|---|
| Acquisition Time (sec) 4.9999 | | | | | |
| Comment IPV 1.2 399.984 MHz H1 1D in cdcl3 (ref. to CDCl3 @ 7.26 ppm), temp 25.9 C -> actual temp = 27.0 C, onenmr probe | | | | | |
| Date | Oct 23 2014 | Date Stamp | Oct 23 2014 | File Name | F:\2014.10\2014.10.23.mr4_IPV-1_2_H1_1D.fid\fid |
| Frequency (MHz) | 399.9845 | Nucleus | 1H | Number of Transients | 16 |
| Original Points Count | 24038 | Points Count | 32768 | Pulse Sequence | s2pul |
| Receiver Gain | 38.00 | SW(cyclical) (Hz) | 4807.69 | Solvent | cdcl3 |
| Spectrum Offset (Hz) | 1947.6067 | Spectrum Type | standard | Sweep Width (Hz) | 4807.55 |
| Temperature (degree C) | 25.900 | | | | |

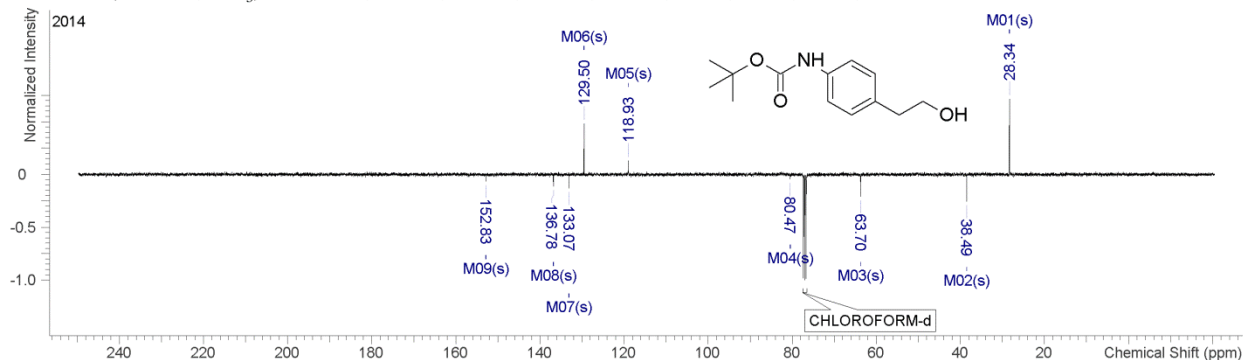
¹H NMR (400MHz, cdcl₃) δ = 7.30 (d, J=8.4 Hz, 2H), 7.15 (d, J=7.4 Hz, 2H), 6.47 (br s, 1H), 3.82 (t, J=6.6 Hz, 2H), 2.81 (t, J=6.6 Hz, 2H), 1.51 (s, 9H), 1.49 (s, 1H)



IPV 1.2 100.587 MHz C13[H1] APT_ad in cdcl3 (ref. to CDCl3 @ 77.06 ppm), temp 25.9 C -> actual temp = 27.0 C, onenmr probe C & CH2 same, CH & CH3 opposite side of solvent signal

| Multiplets | Integrals | Sum | 0.00 | Number of Nuclei | 9 C's |
|--|-------------|-------------------------|-------------|-------------------------------|--|
| Acquisition Time (sec) 2.5000 | | | | | |
| Comment IPV 1.2 100.587 MHz C13[H1] APT_ad in cdcl3 (ref. to CDCl3 @ 77.06 ppm), temp 25.9 C -> actual temp = 27.0 C, onenmr probe C & CH2 same, CH & CH3 opposite side of solvent signal | | | | | |
| Date | Oct 23 2014 | Date Stamp | Oct 23 2014 | File Name | F:\2014.10\2014.10.23.mr4_IPV-1_2_C13_APT_ad.fid\fid |
| Frequency (MHz) | 100.5872 | Nucleus | 13C | Number of Transients | 264 |
| Original Points Count | 67935 | Pulse Sequence | APT_ad | Receiver Gain | 38.00 |
| Points Count | 131072 | Solvent | cdcl3 | Spectrum Offset (Hz) | 11531.7881 |
| SW(cyclical) (Hz) | 27173.91 | Sweep Width (Hz) | 27173.71 | Temperature (degree C) | 25.900 |
| Spectrum Type | APT | | | | |

¹³C NMR (101MHz, cdcl₃) δ = 152.83, 136.78, 133.07, 129.50, 118.93, 80.47, 63.70, 38.49, 28.34

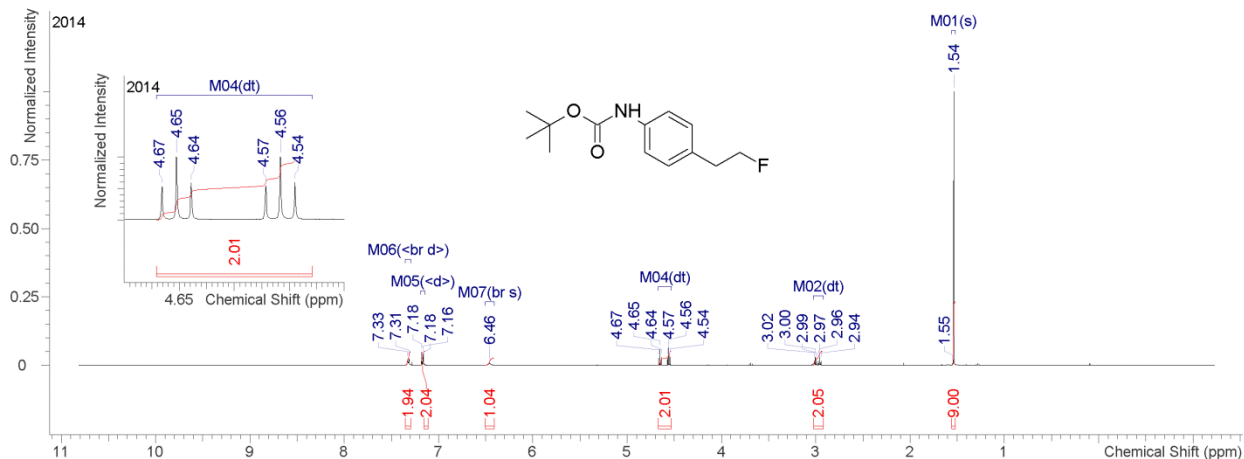


¹H NMR and ¹³C NMR for compound 4.33

IPV 1.3 498.118 MHz H1 1D in cdcl3 (ref. to CDCl3 @ 7.26 ppm), temp 26.4 C -> actual temp = 27.0 C, autoxdb probe

| | | | |
|---------------------------------|---|--------------------------|-------------|
| Multiplets Integrals Sum | 18.07 | Number of Nuclei | 18 H's |
| Acquisition Time (sec) | 4.9997 | | |
| Comment | IPV 1.3 498.118 MHz H1 1D in cdcl3 (ref. to CDCl3 @ 7.26 ppm), temp 26.4 C -> actual temp = 27.0 C, autoxdb probe | | |
| Date | Oct 28 2014 | Date Stamp | Oct 28 2014 |
| File Name | F:\2014.10\2014.10.28.i5_IPV-1_3_H1_1D.fid\fid | | |
| Frequency (MHz) | 498.1178 | Nucleus | 1H |
| Original Points Count | 30001 | Points Count | 32768 |
| Receiver Gain | 32.00 | SW(cyclical) (Hz) | 6000.60 |
| Spectrum Offset (Hz) | 2388.2478 | Spectrum Type | standard |
| Temperature (degree C) | 26.400 | Sweep Width (Hz) | 6000.42 |

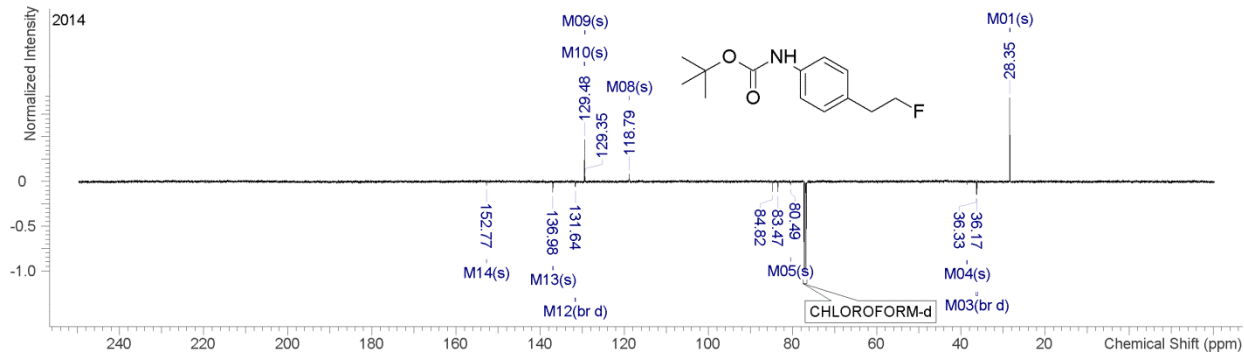
¹H NMR (498MHz, cdcl₃) δ = 7.32 (br d, J=8.2 Hz, 2H), 7.17 (d, J=7.9 Hz, 2H), 6.46 (br s, 1H), 4.60 (td, J=6.6, 47.1 Hz, 2H), 2.98 (td, J=6.6, 22.9 Hz, 2H), 1.54 (s, 9H)



IPV 1.3 125.266 MHz C13[H1] APT_ad in cdcl3 (ref. to CDCl3 @ 77.06 ppm), temp 26.4 C -> actual temp = 27.0 C, autoxdb probe C & CH2 same, CH & CH3 opposite side of solvent signal

| | | | |
|---------------------------------|--|-------------------------------|-------------|
| Multiplets Integrals Sum | 0.00 | Number of Nuclei | 11 C's |
| Acquisition Time (sec) | 2.4948 | | |
| Comment | IPV 1.3 125.266 MHz C13[H1] APT_ad in cdcl3 (ref. to CDCl3 @ 77.06 ppm), temp 26.4 C -> actual temp = 27.0 C, autoxdb probe C & CH2 same, CH & CH3 opposite side of solvent signal | | |
| Date | Oct 28 2014 | Date Stamp | Oct 28 2014 |
| File Name | F:\2014.10\2014.10.28.i5_IPV-1_3_C13_APT_ad.fid\fid | | |
| Nucleus | 13C | Number of Transients | 376 |
| Points Count | 131072 | Pulse Sequence | APT_ad |
| SW(cyclical) (Hz) | 33826.64 | Solvent | cdcl3 |
| Spectrum Type | APT | Sweep Width (Hz) | 33826.38 |
| | | Frequency (MHz) | 125.2656 |
| | | Original Points Count | 84369 |
| | | Receiver Gain | 38.00 |
| | | Spectrum Offset (Hz) | 14370.3086 |
| | | Temperature (degree C) | 26.400 |

¹³C NMR (125MHz, cdcl₃) δ = 152.77, 136.98, 131.67 (br d, J=6.7 Hz, 1C), 129.48, 129.35, 118.79, 84.15 (br d, J=169.0 Hz, 1C), 80.49, 38.54, 36.25 (br d, J=20.4 Hz, 1C), 28.35

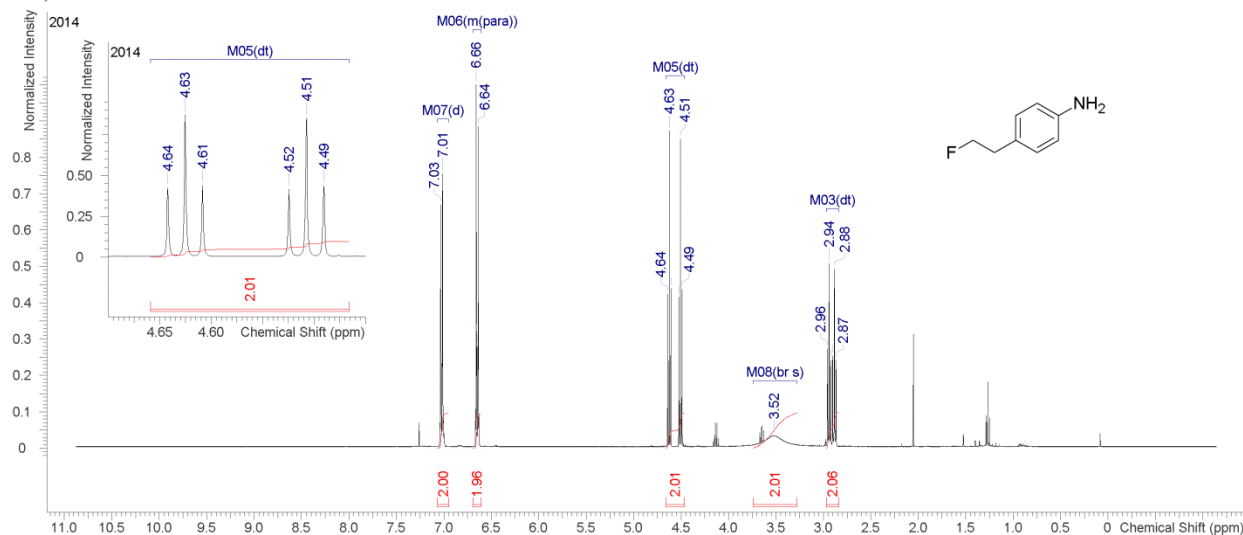


¹H NMR and ¹³C NMR for compound 4.34

IPV 1.4 399.984 MHz H1 1D in cdcl3 (ref. to CDCl3 @ 7.26 ppm), temp 25.9 C -> actual temp = 27.0 C, onenmr probe

| Multiplets | Integrals | Sum | 10.04 | Number of Nuclei | 10 H's | | |
|------------------------|--|----------------------|--|-----------------------|-----------------|------------------------|--------|
| Acquisition Time (sec) | 4.9999 | Comment | IPV 1.4 399.984 MHz H1 1D in cdcl3 (ref. to CDCl3 @ 7.26 ppm), temp 25.9 C -> actual temp = 27.0 C, onenmr probe | | | | |
| Date | Oct 30 2014 | Date Stamp | Oct 30 2014 | | | | |
| File Name | C:\Users\admin\Documents\Master NMR\2014.10\2014.10.30.mr4_IPV-1_4_H1_1D.fid.fid | | | | Frequency (MHz) | 399.9845 | |
| Nucleus | 1H | Number of Transients | 16 | Original Points Count | 24038 | Points Count | 32768 |
| Pulse Sequence | s2pul | Receiver Gain | 24.00 | SW(cyclical) (Hz) | 4807.69 | Solvent | cdcl3 |
| Spectrum Offset (Hz) | 1947.6067 | Spectrum Type | standard | Sweep Width (Hz) | 4807.55 | Temperature (degree C) | 25.900 |

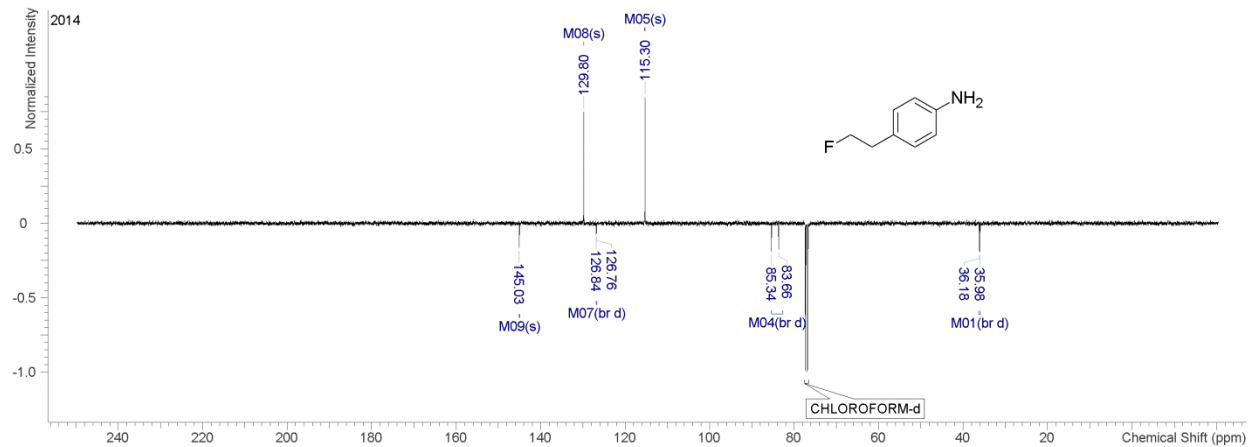
¹H NMR (400MHz, cdcl₃) δ = 7.02 (d, J=8.2 Hz, 2H), 6.70 - 6.61 (m, 2H), 4.57 (td, J=6.6, 47.2 Hz, 2H), 3.52 (br s, 2H), 2.91 (td, J=6.8, 22.2 Hz, 2H)



IPV 1.4 100.587 MHz C13[H1] APT_ad in cdcl3 (ref. to CDCl3 @ 77.06 ppm), temp 25.9 C -> actual temp = 27.0 C, onenmr probe C & CH2 same, CH & CH3 opposite side of solvent signal

| Multiplets | Integrals | Sum | 0.00 | Number of Nuclei | 6 C's | | |
|------------------------|---|----------------------|---|-----------------------|-----------------|------------------------|--------|
| Acquisition Time (sec) | 2.5000 | Comment | IPV 1.4 100.587 MHz C13[H1] APT_ad in cdcl3 (ref. to CDCl3 @ 77.06 ppm), temp 25.9 C -> actual temp = 27.0 C, onenmr probe C & CH2 same, CH & CH3 opposite side of solvent signal | | | | |
| Date | Oct 30 2014 | Date Stamp | Oct 30 2014 | | | | |
| File Name | C:\Users\admin\Documents\Master NMR\2014.10\2014.10.30.mr4_IPV-1_4_C13_APT_ad.fid.fid | | | | Frequency (MHz) | 100.5872 | |
| Nucleus | 13C | Number of Transients | 272 | Original Points Count | 67935 | Points Count | 131072 |
| Pulse Sequence | APT_ad | Receiver Gain | 38.00 | SW(cyclical) (Hz) | 27173.91 | Solvent | cdcl3 |
| Spectrum Offset (Hz) | 11531.7881 | Spectrum Type | APT | Sweep Width (Hz) | 27173.71 | Temperature (degree C) | 25.900 |

¹³C NMR (101MHz, cdcl₃) δ = 145.03, 129.80, 126.80 (br d, J=7.3 Hz, 1C), 115.30, 84.50 (br d, J=169.0 Hz, 1C), 36.08 (br d, J=20.1 Hz, 1C)

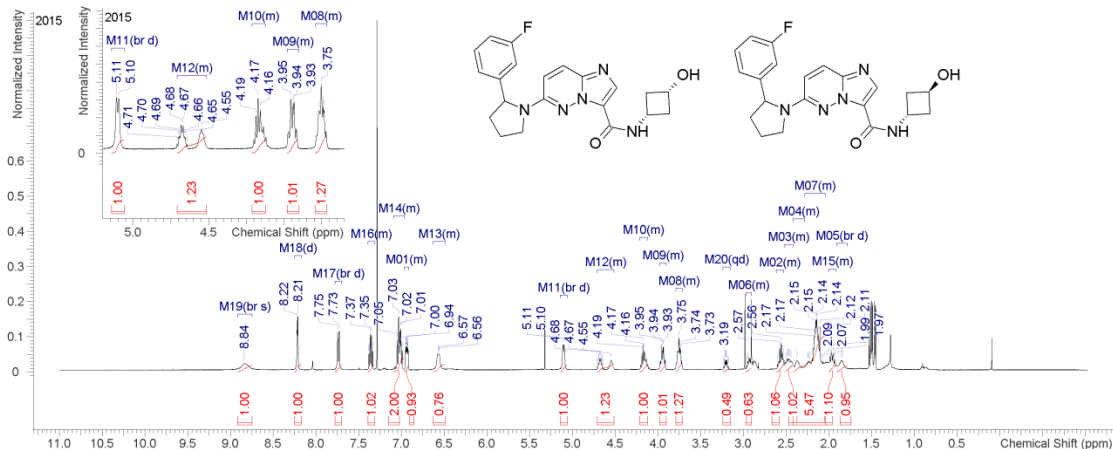


¹H NMR and ¹³C NMR for compound 4.35

Jamie_Bailey, IPVI_58 499.806 MHz H1 PRESAT in cdcl3 (ref. to CDC13 @ 7.26 ppm), temp 27.7 C -> actual temp = 27.0 C, coldlual probe

| Multiplets Integrals Sum 23.96 | | Number of Nuclei 23 H's | |
|--------------------------------|--|-------------------------|------------|
| Acquisition Time (sec) | 5.0000 | | |
| Comment | Jamie_Bailey, IPVI_58 499.806 MHz H1 PRESAT in cdcl3 (ref. to CDC13 @ 7.26 ppm), temp 27.7 C -> actual temp = 27.0 C, coldlual probe | | |
| Date | Apr 1 2015 | Date Stamp | Apr 1 2015 |
| Frequency (MHz) | 499.8064 | Nucleus | 1H |
| Original Points Count | 30048 | Points Count | 32768 |
| Receiver Gain | 50.00 | SW(cyclical) (Hz) | 6009.62 |
| Spectrum Offset (Hz) | 2493.3027 | Spectrum Type | standard |
| Temperature (degree C) | 27.700 | Sweep Width (Hz) | 6009.43 |

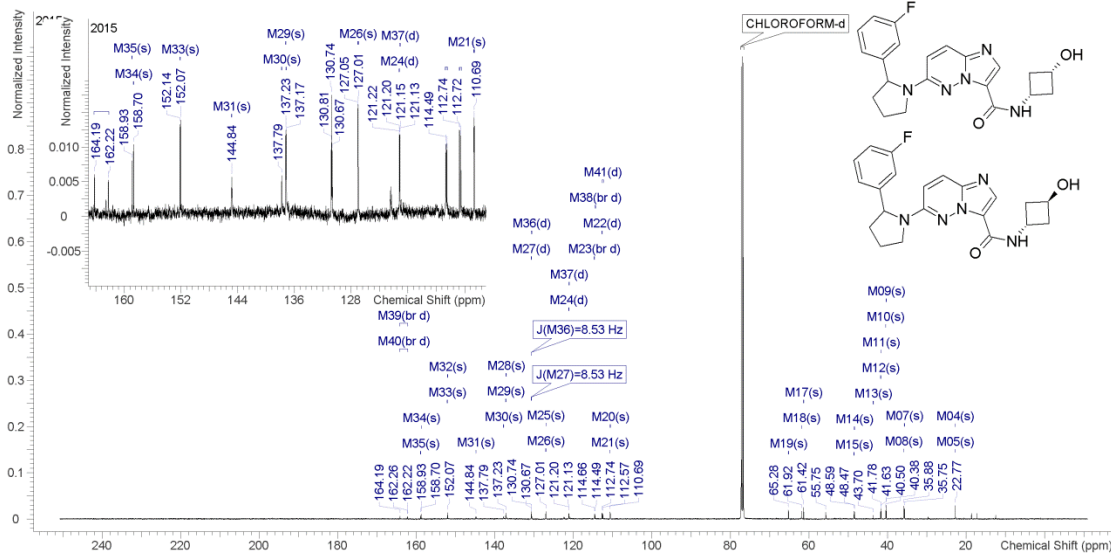
¹H NMR (500MHz, CHLOROFORM-d) δ = 8.84 (br s, 1H), 8.22 (d, $J=3.7$ Hz, 1H), 7.74 (br d, $J=9.9$ Hz, 1H), 7.39 - 7.32 (m, 1H), 7.09 - 6.97 (m, 2H), 6.97 - 6.91 (m, 1H), 6.63 - 6.49 (m, 1H), 5.10 (br d, $J=7.3$ Hz, 1H), 4.71 - 4.52 (m, 1H), 4.21 - 4.12 (m, 1H), 3.98 - 3.90 (m, 1H), 3.79 - 3.72 (m, 1H), 3.20 (dq, $J=4.2, 7.5$ Hz, 1H), 2.97 - 2.91 (m, 1H), 2.61 - 2.53 (m, 1H), 2.52 - 2.42 (m, 1H), 2.42 - 2.28 (m, 1H), 2.28 - 2.04 (m, 3H), 2.00 - 1.91 (m, 1H), 1.85 (br d, $J=9.2$ Hz, 1H)



Jamie_Bailey, IPVI_58 125.691 MHz C13[H1] 1D in cdcl3 (ref. to CDC13 @ 77.06 ppm), temp 27.7 C -> actual temp = 27.0 C, coldlual probe

| Multiplets Integrals Sum 0.00 | | Number of Nuclei 36 C's | |
|-------------------------------|--|-------------------------|------------|
| Acquisition Time (sec) | 2.5000 | | |
| Comment | Jamie_Bailey, IPVI_58 125.691 MHz C13[H1] 1D in cdcl3 (ref. to CDC13 @ 77.06 ppm), temp 27.7 C -> actual temp = 27.0 C, coldlual probe | | |
| Date | Apr 1 2015 | Date Stamp | Apr 1 2015 |
| Frequency (MHz) | 125.6909 | Nucleus | 13C |
| Original Points Count | 82237 | Points Count | 131072 |
| Receiver Gain | 30.00 | SW(cyclical) (Hz) | 32894.74 |
| Spectrum Offset (Hz) | 15081.4736 | Spectrum Type | standard |
| Temperature (degree C) | 27.700 | Sweep Width (Hz) | 32894.49 |

¹³C NMR (126MHz, CHLOROFORM-d) δ = 163.24 (br d, $J=247.5$ Hz, 1C), 163.21 (br d, $J=247.5$ Hz, 1C), 158.93, 158.70, 152.14, 152.07, 144.84, 137.79, 137.23, 137.17, 130.76 (d, $J=8.5$ Hz, 1C), 130.71 (d, $J=8.5$ Hz, 1C), 127.05, 127.01, 121.21 (d, $J=2.8$ Hz, 1C), 121.14 (d, $J=2.8$ Hz, 1C), 114.67 (br d, $J=3.3$ Hz, 1C), 114.50 (br d, $J=3.5$ Hz, 1C), 112.73 (d, $J=3.3$ Hz, 1C), 112.55 (d, $J=3.8$ Hz, 1C), 110.69, 110.65, 65.28, 61.92, 61.42, 48.59, 48.47, 43.70, 41.78, 41.63, 40.50, 40.38, 35.88, 35.75, 22.77, 22.76

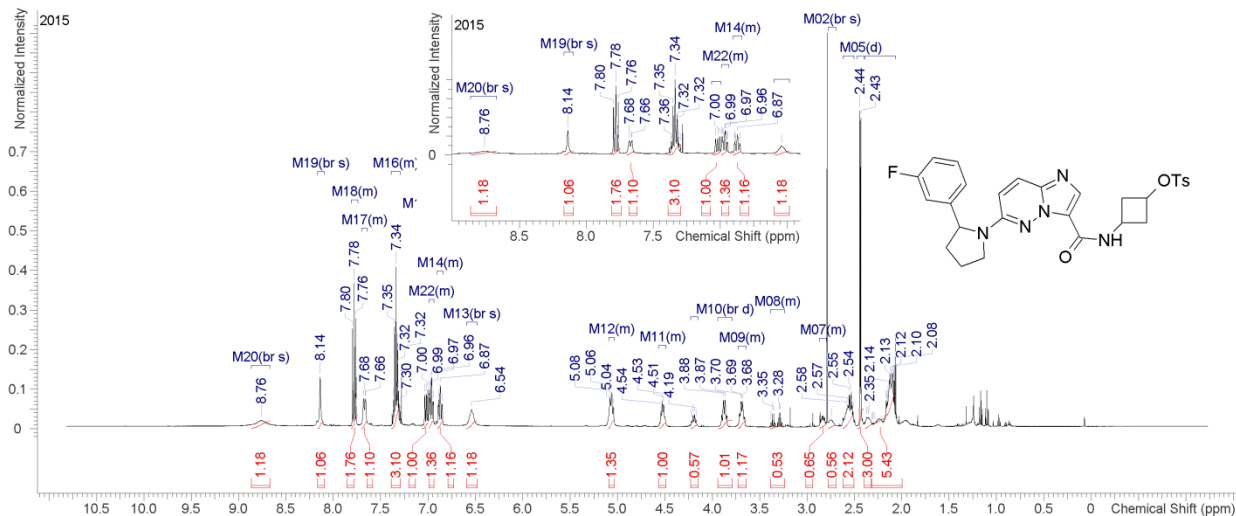


¹H NMR and ¹³C NMR for compound 4.36

498.118 MHz H1 1D in cdcl3 (ref. to CDCl3 @ 7.26 ppm), temp 26.4 C -> actual temp = 27.0 C, autoxdb probe

| Multiplets | Integrals | Sum | 30.30 | Number of Nuclei | 30 H's |
|------------------------|--------------|----------------------|---|-----------------------|--|
| Acquisition Time (sec) | 4.9997 | Comment | 498.118 MHz H1 1D in cdcl3 (ref. to CDCl3 @ 7.26 ppm), temp 26.4 C -> actual temp = 27.0 C, autoxdb probe | | |
| Date | Apr 8 2015 | Date Stamp | Apr 8 2015 | File Name | F:\Schirma\2015.04\2015.04.08.i5_IPV_1.60X_H1_1D.fid\fid |
| Frequency (MHz) | 498.1178 | Nucleus | 1H | Number of Transients | 16 |
| Points Count | 65536 | Pulse Sequence | s2pul | Receiver Gain | 32.00 |
| Solvent | CHLOROFORM-d | Spectrum Offset (Hz) | 2388.2935 | Spectrum Type | standard |
| Temperature (degree C) | 26.400 | | | Original Points Count | 30001 |
| | | | | SW(cyclical) (Hz) | 6000.60 |
| | | | | Sweep Width (Hz) | 6000.51 |

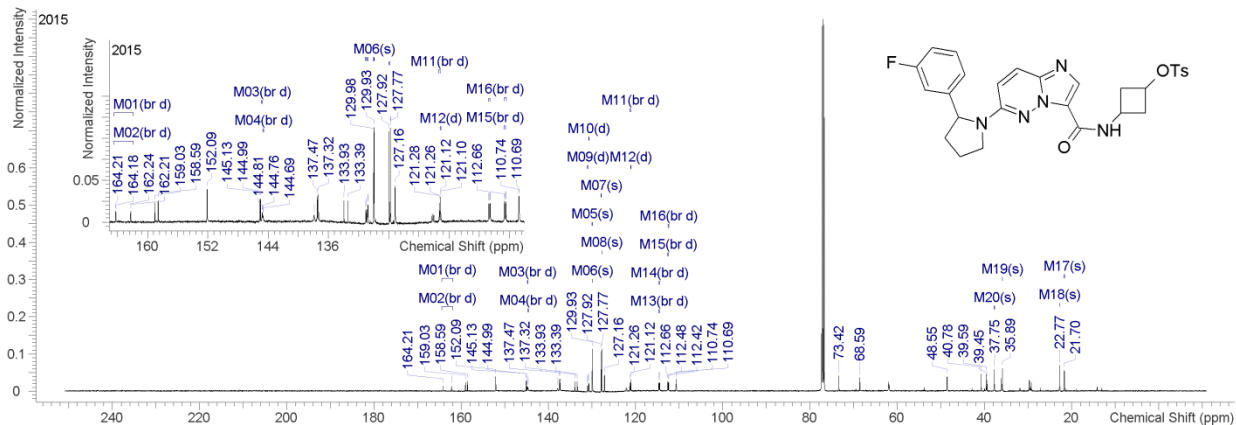
¹H NMR (498MHz, CHLOROFORM-d) δ = 8.76 (br s, 1H), 8.14 (br s, 1H), 7.81 - 7.74 (m, 2H), 7.70 - 7.64 (m, 1H), 7.39 - 7.29 (m, 3H), 7.07 - 7.00 (m, 1H), 6.99 - 6.94 (m, 1H), 6.90 - 6.84 (m, 1H), 6.54 (br s, 1H), 5.09 - 5.04 (m, 1H), 4.56 - 4.49 (m, 1H), 4.23 - 4.15 (m, 1H), 3.87 (br d, $J=8.6$ Hz, 1H), 3.73 - 3.64 (m, 1H), 3.39 - 3.24 (m, 1H), 2.87 - 2.79 (m, 1H), 2.74 (br s, 1H), 2.62 - 2.50 (m, 2H), 2.44 (d, $J=4.7$ Hz, 3H), 2.39 - 2.07 (m, 5H)



Jamie_Bailey_IPV1_60A 125.691 MHz C13[H1] 1D in cdcl3 (ref. to CDCl3 @ 77.06 ppm), temp 27.7 C -> actual temp = 27.0 C, coldludal probe

| Multiplets | Integrals | Sum | 0.00 | Number of Nuclei | 20 C's |
|------------------------|------------|------------------|---|------------------------|---|
| Acquisition Time (sec) | 2.5000 | Comment | Jamie_Bailey_IPV1_60A 125.691 MHz C13[H1] 1D in cdcl3 (ref. to CDCl3 @ 77.06 ppm), temp 27.7 C -> actual temp = 27.0 C, coldludal probe | | |
| Date | Apr 1 2015 | Date Stamp | Apr 1 2015 | File Name | F:\Schirma\2015.04\2015.04.1.u5_IPV1_60A_loc12_15.52_C13_1D.fid\fid |
| Frequency (MHz) | 125.6909 | Nucleus | 13C | Number of Transients | 576 |
| Points Count | 131072 | Pulse Sequence | s2pul | Receiver Gain | 30.00 |
| SW(cyclical) (Hz) | 32894.74 | Solvent | CHLOROFORM-d | Spectrum Offset (Hz) | 15081.4736 |
| Spectrum Type | standard | Sweep Width (Hz) | 32894.49 | Temperature (degree C) | 27.700 |

¹³C NMR (126MHz, CHLOROFORM-d) δ = 163.20 (br d, $J=247.5$ Hz, 1C), 163.23 (br d, $J=247.5$ Hz, 1C), 144.78 (br d, $J=6.0$ Hz, 1C), 144.66 (br d, $J=6.0$ Hz, 1C), 131.01 (d, $J=8.0$ Hz, 1C), 130.76 (d, $J=8.0$ Hz, 1C), 129.98, 129.93, 127.92, 127.77, 121.27 (br d, $J=2.5$ Hz, 1C), 121.11 (d, $J=2.5$ Hz, 1C), 114.64 (br d, $J=21.3$ Hz, 1C), 114.60 (br d, $J=21.1$ Hz, 1C), 112.57 (br d, $J=22.1$ Hz, 1C), 112.51 (br d, $J=22.1$ Hz, 1C), 37.75, 35.89, 22.77, 21.69

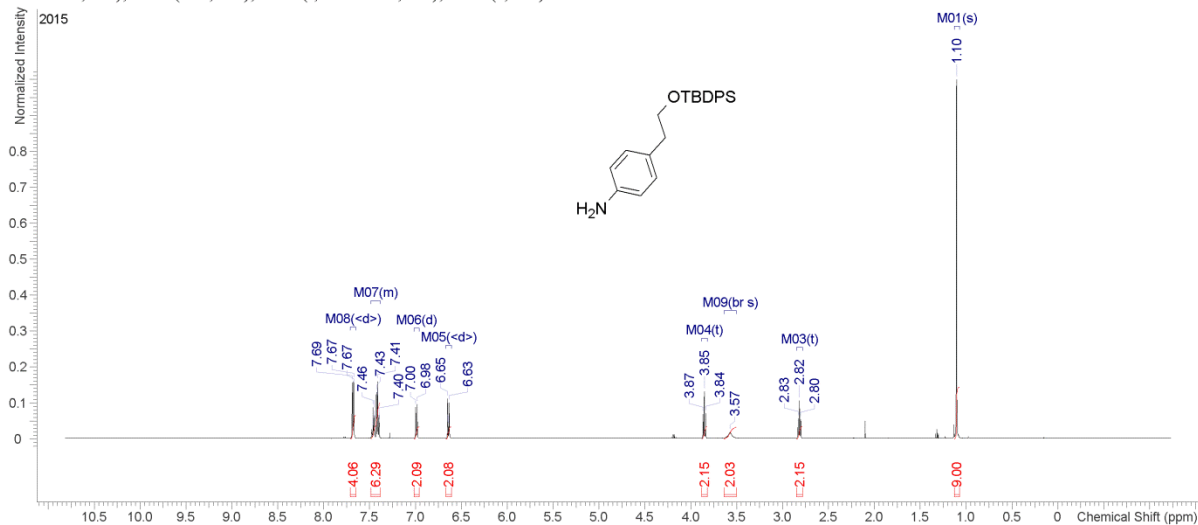


¹H NMR and ¹³C NMR for compound 4.38

MV 1.10 498.118 MHz H1 1D in cdcl3 (ref. to CDCl3 @ 7.26 ppm), temp 26.4 C -> actual temp = 27.0 C, autotdx probe

| Multiplets Integrals Sum 29.85 | | Number of Nuclei 29 H's | |
|--------------------------------|--------------|-------------------------|---|
| Acquisition Time (sec) | 4.9997 | Comment | MV 1.10 498.118 MHz H1 1D in cdcl3 (ref. to CDCl3 @ 7.26 ppm), temp 26.4 C -> actual temp = 27.0 C, autotdx probe |
| Date | Mar 6 2015 | Date Stamp | Mar 6 2015 |
| Frequency (MHz) | 498.1178 | Nucleus | 1H |
| Points Count | 65536 | Pulse Sequence | s2pul |
| Solvent | CHLOROFORM-d | Spectrum Offset (Hz) | 2388.2935 |
| Temperature (degree C) | 26.400 | Receiver Gain | 32.00 |
| | | Spectrum Type | standard |
| | | Original Points Count | 30001 |
| | | SW(cyclical) (Hz) | 6000.60 |
| | | Sweep Width (Hz) | 6000.51 |

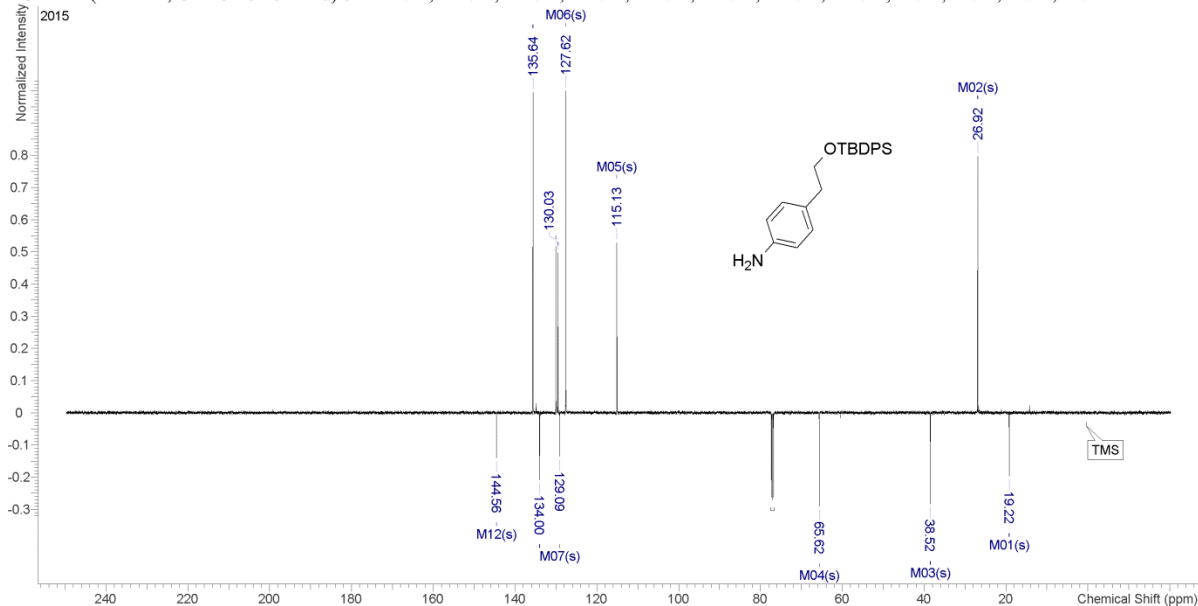
¹H NMR (498MHz, CHLOROFORM-d) δ = 7.68 (d, J =7.0 Hz, 4H), 7.49 - 7.38 (m, 6H), 6.99 (d, J =8.3 Hz, 2H), 6.64 (d, J =7.8 Hz, 2H), 3.85 (t, J =7.1 Hz, 2H), 3.57 (br s, 2H), 2.82 (t, J =7.1 Hz, 2H), 1.10 (s, 9H)



MV 1.10 125.266 MHz C13[H1] APT_ad in cdcl3 (ref. to CDCl3 @ 77.06 ppm), temp 26.4 C -> actual temp = 27.0 C, autotdx probe C & CH2 same, CH & CH3 opposite side of solvent signal

| Multipliers Integrals Sum 0.00 | | Number of Nuclei 12 C's | |
|--------------------------------|------------|-------------------------|--|
| Acquisition Time (sec) | 1.9958 | Comment | MV 1.10 125.266 MHz C13[H1] APT_ad in cdcl3 (ref. to CDCl3 @ 77.06 ppm), temp 26.4 C -> actual temp = 27.0 C, autotdx probe C & CH2 same, CH & CH3 opposite side of solvent signal |
| Date | Mar 6 2015 | Date Stamp | Mar 6 2015 |
| Frequency (MHz) | 125.2656 | Nucleus | 13C |
| Original Points Count | 67510 | Points Count | 131072 |
| Receiver Gain | 30.00 | SW(cyclical) (Hz) | 33826.64 |
| Spectrum Offset (Hz) | 14370.3086 | Spectrum Type | APT |
| Temperature (degree C) | 26.400 | Sweep Width (Hz) | 33826.38 |
| | | Number of Transients | 124 |
| | | Pulse Sequence | APT_ad |
| | | Solvent | CHLOROFORM-d |

¹³C NMR (125MHz, CHLOROFORM-d) δ = 144.56, 135.64, 134.00, 130.03, 129.54, 129.09, 127.62, 115.13, 65.62, 38.52, 26.92, 19.22

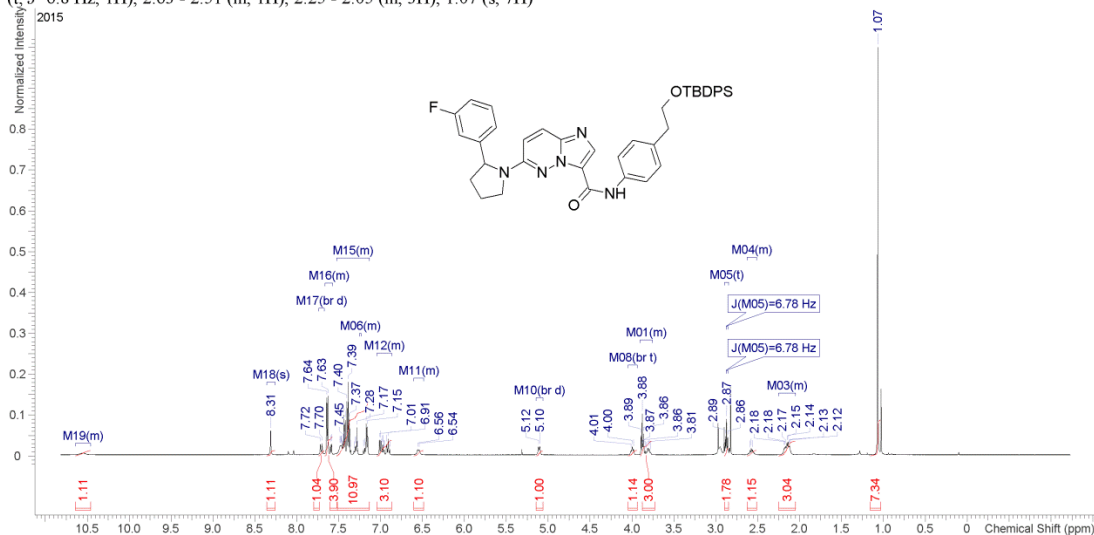


¹H NMR and ¹³C NMR for compound 4.39

IPV 1.59 498.118 MHz H1 1D in cdcl3 (ref. to CDCl3 @ 7.26 ppm), temp 26.4 C -> actual temp = 27.0 C, autotxdb probe

| Multiplets Integrals Sum 40.77 | | Number of Nuclei 39 H's | |
|--------------------------------|--------------|-------------------------|---|
| Acquisition Time (sec) | 4.9997 | Comment | IPV 1.59 498.118 MHz H1 1D in cdcl3 (ref. to CDCl3 @ 7.26 ppm), temp 26.4 C -> actual temp = 27.0 C, autotxdb probe |
| Date | Apr 1 2015 | Date Stamp | Apr 1 2015 |
| Frequency (MHz) | 498.1178 | Nucleus | 1H |
| Points Count | 65536 | Pulse Sequence | s2pul |
| Solvent | CHLOROFORM-d | Spectrum Offset (Hz) | 2388.2935 |
| Temperature (degree C) | 26.400 | Receiver Gain | 32.00 |
| | | Spectrum Type | standard |
| | | Original Points Count | 30001 |
| | | SW(cyclical) (Hz) | 6000.60 |
| | | Sweep Width (Hz) | 6000.51 |

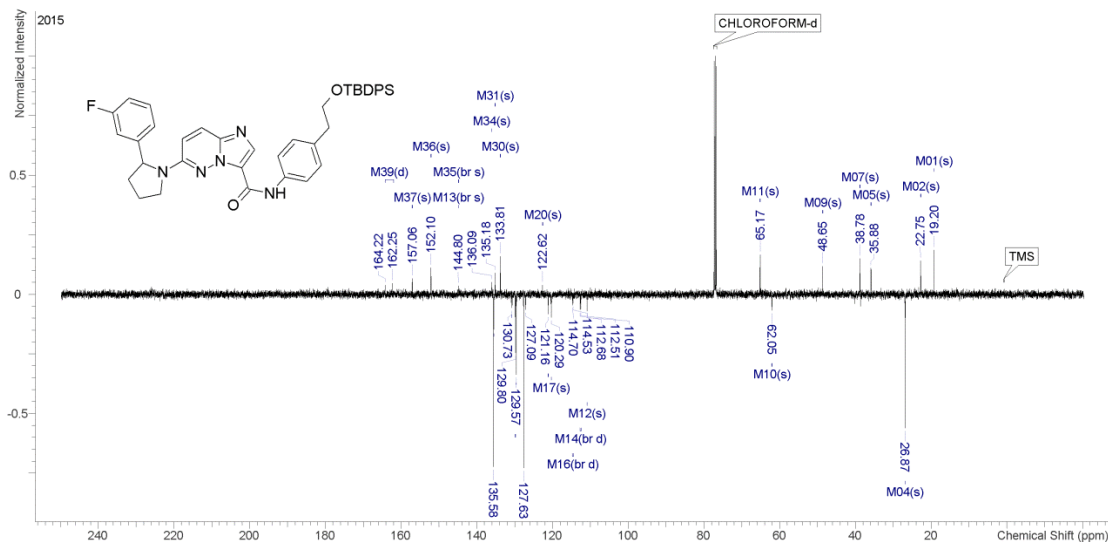
¹H NMR (498MHz, CHLOROFORM-d) δ = 10.64 - 10.46 (m, 1H), 8.31 (s, 1H), 7.71 (br d, J =10.0 Hz, 1H), 7.66 - 7.57 (m, 4H), 7.25 - 7.23 (m, 1H), 7.53 - 7.13 (m, 10H), 7.04 - 6.87 (m, 3H), 6.60 - 6.49 (m, 1H), 5.11 (br d, J =7.6 Hz, 1H), 4.00 (br t, J =7.0 Hz, 1H), 3.90 - 3.76 (m, 3H), 2.87 (t, J =6.8 Hz, 1H), 2.63 - 2.51 (m, 1H), 2.25 - 2.05 (m, 3H), 1.07 (s, 7H)



IPV 1.59 125.266 MHz C13[H1] APT_ad in cdcl3 (ref. to CDCl3 @ 77.06 ppm), temp 26.4 C -> actual temp = 27.0 C, autotxdb probe C & CH2 same, CH & CH3 opposite side of solvent signal

| Multiplets Integrals Sum 0.00 | | Number of Nuclei 30 C's | |
|-------------------------------|--------------|-------------------------|--|
| Acquisition Time (sec) | 1.9958 | Comment | IPV 1.59 125.266 MHz C13[H1] APT_ad in cdcl3 (ref. to CDCl3 @ 77.06 ppm), temp 26.4 C -> actual temp = 27.0 C, autotxdb probe C & CH2 same, CH & CH3 opposite side of solvent signal |
| Date | Apr 1 2015 | Date Stamp | Apr 1 2015 |
| Frequency (MHz) | 125.2656 | Nucleus | 13C |
| Original Points Count | 67510 | Points Count | 131072 |
| Receiver Gain | 30.00 | SW(cyclical) (Hz) | 33826.64 |
| Solvent | CHLOROFORM-d | Spectrum Offset (Hz) | 14370.3066 |
| Temperature (degree C) | 26.400 | Spectrum Type | APT |
| | | Sweep Width (Hz) | 33826.38 |

¹³C NMR (125MHz, CHLOROFORM-d) δ = 163.24 (d, J =247.5 Hz, 1C), 157.06, 152.10, 144.84 (br s, 1C), 144.80 (br s, 1C), 136.09, 135.58, 135.51, 135.18, 133.81, 130.73, 129.80, 129.57, 127.63, 127.09, 122.62, 121.16, 120.29, 114.62 (br d, J =21.2 Hz, 1C), 112.60 (br d, J =22.2 Hz, 1C), 110.90, 65.17, 62.05, 48.65, 38.78, 35.88, 26.87, 26.80, 22.75, 19.20

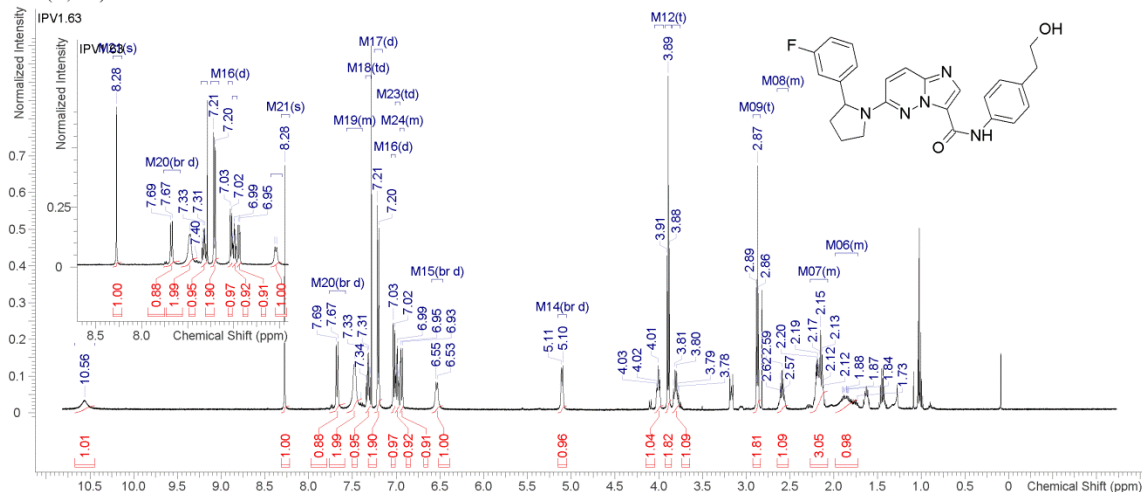


¹H NMR and ¹³C NMR for compound 4.40

IPV 1.63 498.118 MHz H1 1D in cdcl3 (ref. to CDCl3 @ 7.26 ppm), temp 26.4 C -> actual temp = 27.0 C, autotdb probe

| Multiplets | Integrals Sum | 23.38 | Number of Nuclei | 26 H's |
|------------------------|---------------|--|------------------|---|
| Acquisition Time (sec) | 4.9997 | Comment IPV 1.63 498.118 MHz H1 1D in cdcl3 (ref. to CDCl3 @ 7.26 ppm), temp 26.4 C -> actual temp = 27.0 C, autotdb probe | | |
| Date | Apr 8 2015 | Date Stamp | Apr 8 2015 | File Name F:\Schirra\2015.04\2015.04.08.i5_IPV_1.63_H1_1D.fid\fid |
| Frequency (MHz) | 498.1178 | Nucleus | 1H | Number of Transients 16 |
| Points Count | 65536 | Pulse Sequence | s2pul | Receiver Gain 32.00 |
| Solvent | CHLOROFORM-d | Spectrum Offset (Hz) | 2388.2935 | Spectrum Type standard |
| Temperature (degree C) | 26.400 | | | Sweep Width (Hz) 6000.51 |

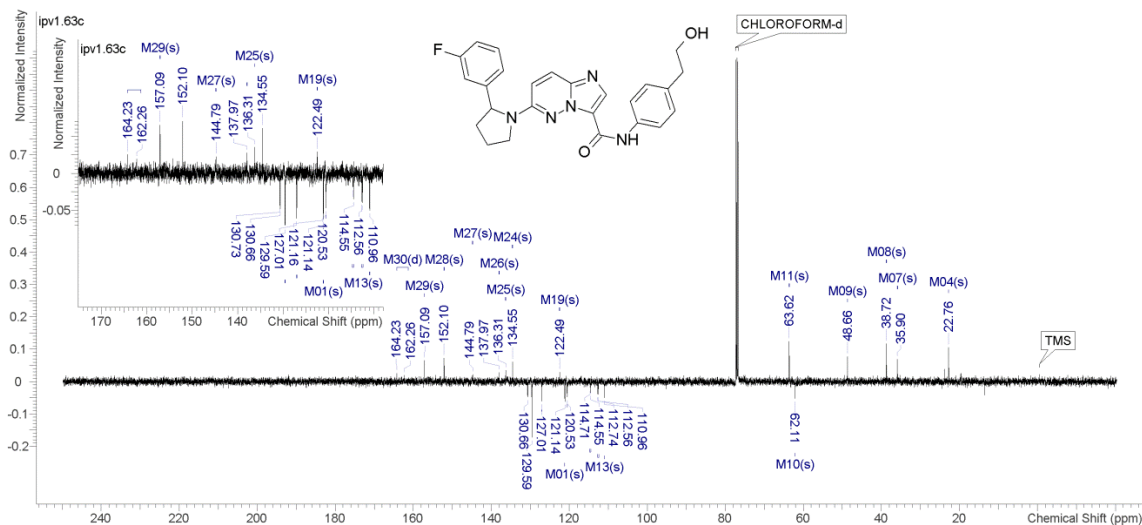
¹H NMR (498MHz, CHLOROFORM-d) δ = 10.56 (br s, 3H), 8.28 (s, 1H), 7.68 (br d, J =9.7 Hz, 1H), 7.57 - 7.39 (m, 2H), 7.32 (dt, J =6.0, 7.8 Hz, 1H), 7.21 (d, J =8.4 Hz, 2H), 7.03 (d, J =7.7 Hz, 1H), 6.99 (dt, J =2.2, 8.4 Hz, 1H), 6.96 - 6.91 (m, 1H), 6.54 (br d, J =9.4 Hz, 1H), 5.11 (br d, J =7.8 Hz, 1H), 4.05 - 3.95 (m, 1H), 3.89 (t, J =6.5 Hz, 2H), 3.84 - 3.75 (m, 1H), 2.87 (t, J =6.5 Hz, 2H), 2.65 - 2.52 (m, 1H), 2.27 - 2.07 (m, 3H), 1.98 - 1.73 (m, 1H)



IPV 1.63 125.266 MHz C13[H1] APT_ad in cdcl3 (ref. to CDCl3 @ 77.06 ppm), temp 26.4 C -> actual temp = 27.0 C, autotdb probe C & CH2 same, CH & CH3 opposite side of solvent signal

| Multiplets | Integrals Sum | 0.00 | Number of Nuclei | 23 C's |
|------------------------|---------------|---|------------------|--|
| Acquisition Time (sec) | 1.9958 | Comment IPV 1.63 125.266 MHz C13[H1] APT_ad in cdcl3 (ref. to CDCl3 @ 77.06 ppm), temp 26.4 C -> actual temp = 27.0 C, autotdb probe C & CH2 same, CH & CH3 opposite side of solvent signal | | |
| Date | Apr 8 2015 | Date Stamp | Apr 8 2015 | File Name F:\Schirra\2015.04\2015.04.08.i5_IPV_1.63_C13_APT_ad.fid\fid |
| Frequency (MHz) | 125.2656 | Nucleus | 13C | Number of Transients 280 |
| Original Points Count | 67510 | Points Count | 131072 | Pulse Sequence APT_ad |
| Receiver Gain | 30.00 | SW(cyclical) (Hz) | 33826.64 | Solvent CHLOROFORM-d |
| Spectrum Offset (Hz) | 14370.3086 | Spectrum Type | APT | Sweep Width (Hz) 33826.38 |
| Temperature (degree C) | 26.400 | | | |

¹³C NMR (125MHz, CHLOROFORM-d) δ = 163.25 (d, J =247.5 Hz, 1C), 157.09, 152.10, 144.79, 137.97, 136.31, 134.55, 130.70 (d, J =8.0 Hz, 1C), 129.59, 127.01, 122.49, 121.16, 121.14, 120.53, 114.63 (d, J =20.6 Hz, 1C), 112.65 (br d, J =21.9 Hz, 1C), 110.96, 63.62, 62.11, 48.66, 38.72, 35.90, 22.76

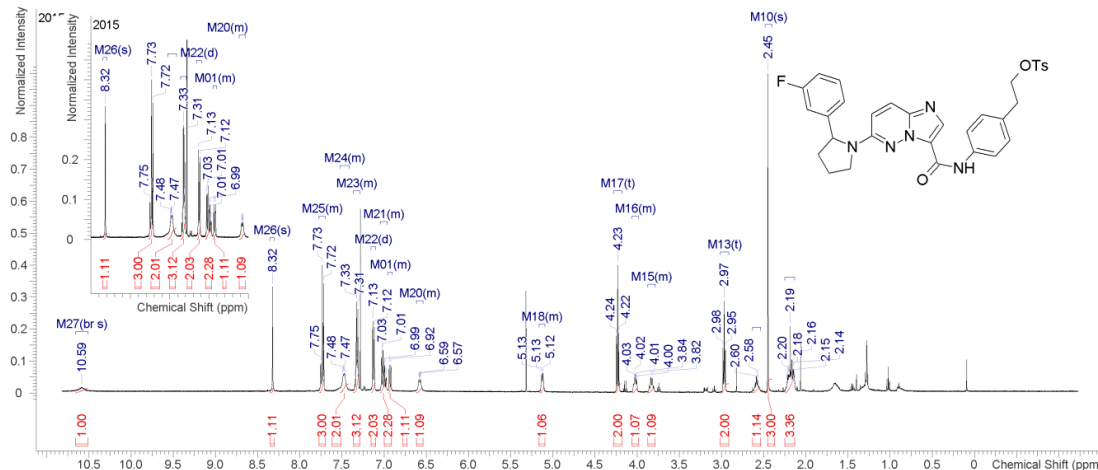


¹H NMR and ¹³C NMR for compound 4.41

IPV 1.64 498.118 MHz H1 1D in cdc13 (ref. to CDC13 @ 7.26 ppm), temp 26.4 C -> actual temp = 27.0 C, autoxbr probe

| Multiplets Integrals Sum 31.48 | | Number of Nuclei 30 H's | |
|--------------------------------|--------------|------------------------------|--|
| Acquisition Time (sec) | 4.9997 | Comment | IPV 1.64 498.118 MHz H1 1D in cdc13 (ref. to CDC13 @ 7.26 ppm), temp 26.4 C -> actual temp = 27.0 C, autoxbr probe |
| Date | Apr 14 2015 | Date Stamp | Apr 14 2015 |
| Frequency (MHz) | 498.1178 | Nucleus | 1H |
| Points Count | 65536 | Pulse Sequence | s2pul |
| Solvent | CHLOROFORM-d | Spectrum Offset (Hz) | 2388.2935 |
| Temperature (degree C) | 26.400 | Spectrum Type | standard |
| | | File Name | F:\Schirma\2015.04\2015.04.14.i5_IPV_1.64_H1_1D.fid.fid |
| | | Number of Transients | 16 |
| | | Receiver Gain | 32.00 |
| | | Original Points Count | 30001 |
| | | SW(cyclical) (Hz) | 6000.60 |
| | | Sweep Width (Hz) | 6000.51 |

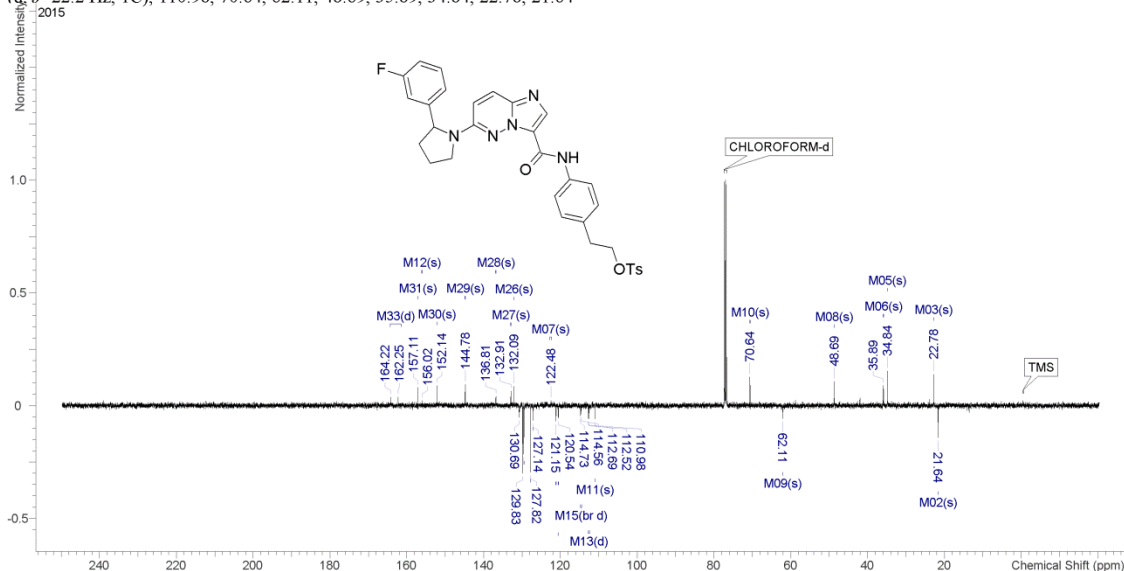
¹H NMR (498MHz, CHLOROFORM-d) δ = 10.59 (br s, 1H), 8.32 (s, 1H), 7.77 - 7.70 (m, 3H), 7.53 - 7.41 (m, 2H), 7.36 - 7.29 (m, 3H), 7.13 (d, J =8.3 Hz, 2H), 7.05 - 6.96 (m, 2H), 6.95 - 6.90 (m, 1H), 6.61 - 6.54 (m, 1H), 5.16 - 5.09 (m, 1H), 4.23 (t, J =7.0 Hz, 2H), 4.06 - 3.99 (m, 1H), 3.87 - 3.79 (m, 1H), 2.97 (t, J =6.9 Hz, 2H), 2.63 - 2.53 (m, 1H), 2.45 (s, 3H), 2.25 - 2.13 (m, 3H)



IPV 1.64x 125.266 MHz C13[H1] APT_ad in cdc13 (ref. to CDC13 @ 77.06 ppm), temp 26.4 C -> actual temp = 27.0 C, autoxbr probe C & CH2 same, CH & CH3 opposite side of solvent signal

| Multiplets Integrals Sum 0.00 | | Number of Nuclei 27 C's | |
|-------------------------------|-------------|-----------------------------|--|
| Acquisition Time (sec) | 1.9958 | Comment | IPV 1.64x 125.266 MHz C13[H1] APT_ad in cdc13 (ref. to CDC13 @ 77.06 ppm), temp 26.4 C -> actual temp = 27.0 C, autoxbr probe C & CH2 same, CH & CH3 opposite side of solvent signal |
| Date | May 29 2015 | Date Stamp | May 29 2015 |
| Frequency (MHz) | 125.2656 | Nucleus | 13C |
| Original Points Count | 67510 | Points Count | 131072 |
| Receiver Gain | 30.00 | SW(cyclical) (Hz) | 33826.64 |
| Spectrum Offset (Hz) | 14370.3086 | Spectrum Type | APT |
| Temperature (degree C) | 26.400 | Sweep Width (Hz) | 33826.38 |
| | | File Name | F:\Schirma\2015.05\2015.05.29.i5_IPV_1.64x_C13_APT_ad.fid.fid |
| | | Number of Transients | 256 |
| | | Pulse Sequence | APT_ad |
| | | Solvent | CHLOROFORM-d |

¹³C NMR (125MHz, CHLOROFORM-d) δ = 163.23 (d, J =247.8 Hz, 1C), 157.11, 156.02, 152.14, 144.78, 136.81, 132.91, 130.73 (br d, J =8.3 Hz, 1C), 129.83, 129.52, 127.82, 127.14, 122.48, 121.16 (br d, J =2.8 Hz, 1C), 120.57 (br s, 1C), 120.54, 114.64 (br d, J =20.9 Hz, 1C), 112.60 (d, J =22.2 Hz, 1C), 110.98, 70.64, 62.11, 48.69, 35.89, 34.84, 22.78, 21.64



STRUCTURE REPORT

XCL Code: UNI1504 **Date:** 22 May 2015

Compound: *N*-(2,4-difluoro-3-methoxybenzyl)-6-{2-(3-fluorophenyl)pyrrolidin-1-yl}imidazo[1,2-*b*]pyridazine-3-carboxamide•1.4H₂O

Formula: C₂₅H_{23.8}F₃N₅O_{3.4} (C₂₅H₂₂F₃N₅O₂•1.4H₂O)

Clients: Prof. R. Schirmacher, Department of Oncology

Crystallographer: R. McDonald

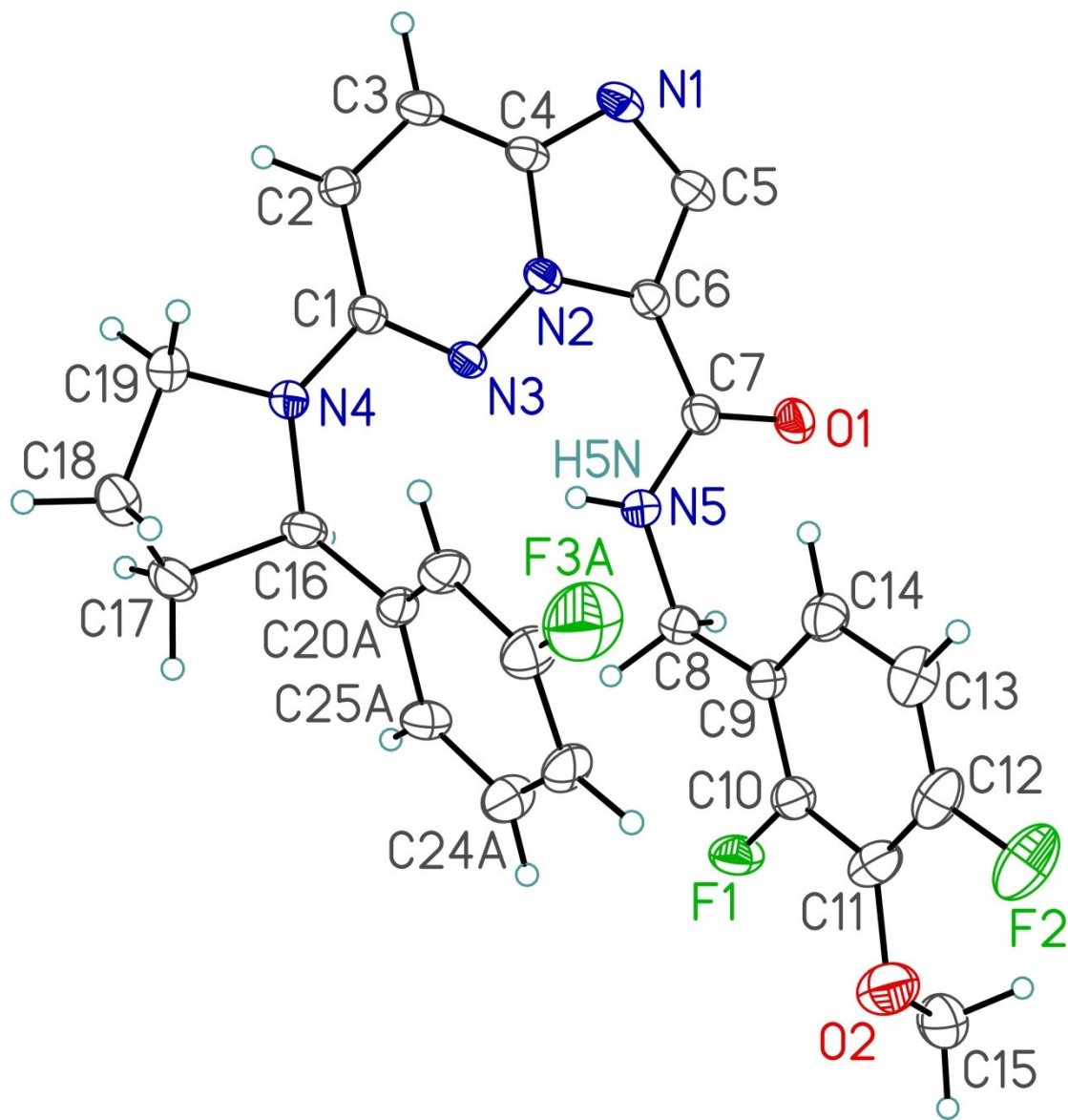


Figure 1. Perspective view of the *N*-(2,4-difluoro-3-methoxybenzyl)-6-{2-(3-fluorophenyl)pyrrolidin-1-yl}imidazo[1,2-*b*]pyridazine-3-carboxamide molecule showing the atom labelling scheme. Non-hydrogen atoms are represented by Gaussian ellipsoids at the 30% probability level. Hydrogen atoms are shown with arbitrarily small thermal parameters.

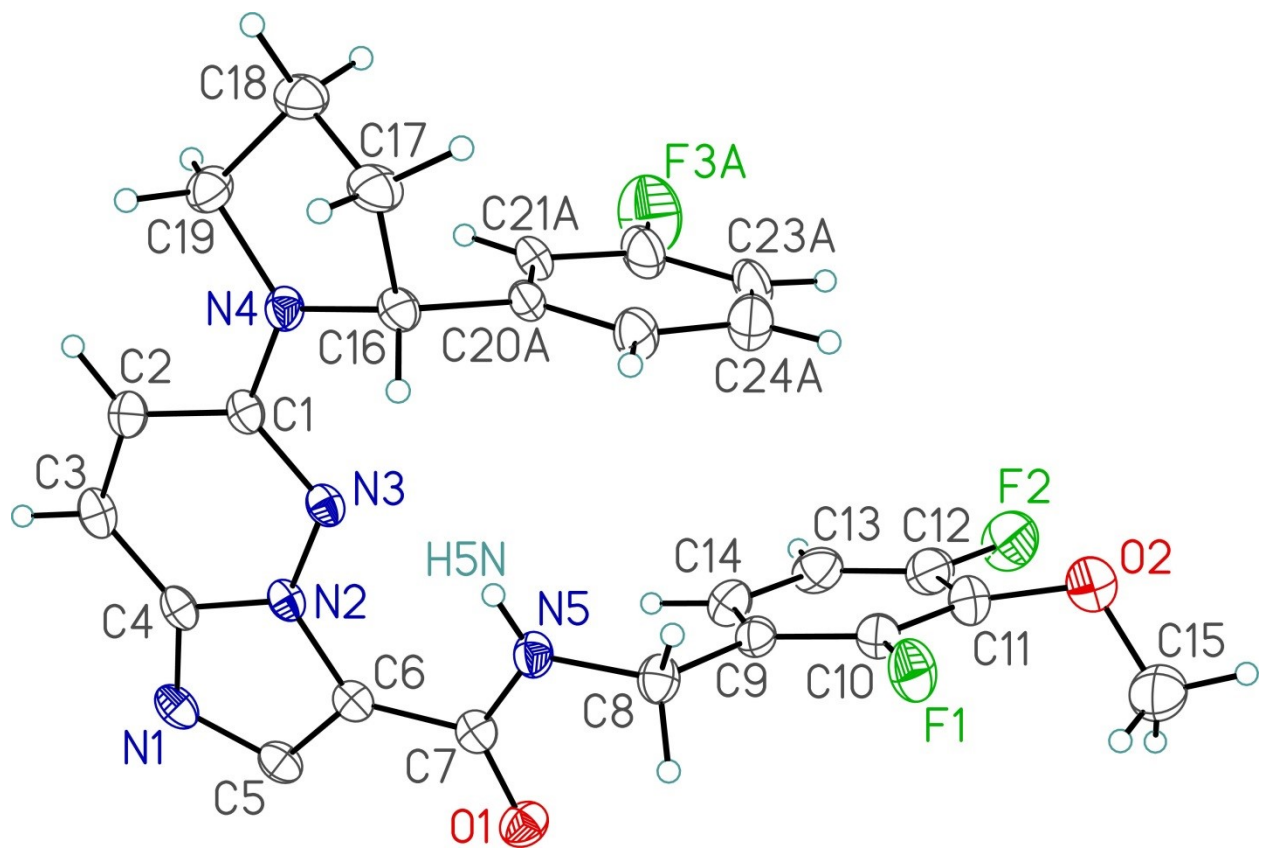


Figure 2. Alternate view of the molecule.

List of Tables

- Table 1.** Crystallographic Experimental Details
- Table 2.** Atomic Coordinates and Equivalent Isotropic Displacement Parameters
- Table 3.** Selected Interatomic Distances
- Table 4.** Selected Interatomic Angles
- Table 5.** Hydrogen-Bonded Interactions
- Table 6.** Torsional Angles
- Table 7.** Anisotropic Displacement Parameters
- Table 8.** Derived Atomic Coordinates and Displacement Parameters for Hydrogen Atoms

Table 1. Crystallographic Experimental Details*A. Crystal Data*

| | |
|--|--|
| formula | C ₂₅ H _{23.8} F ₃ N ₅ O _{3.4} |
| formula weight | 505.69 |
| crystal dimensions (mm) | 0.29 × 0.24 × 0.02 |
| crystal system | monoclinic |
| space group | <i>P</i> 2 ₁ / <i>c</i> (No. 14) |
| unit cell parameters ^a | |
| <i>a</i> (Å) | 13.8619 (3) |
| <i>b</i> (Å) | 10.1495 (2) |
| <i>c</i> (Å) | 17.3464 (4) |
| β (deg) | 104.9414 (13) |
| <i>V</i> (Å ³) | 2357.98 (9) |
| <i>Z</i> | 4 |
| ρ _{calcd} (g cm ⁻³) | 1.424 |
| μ (mm ⁻¹) | 0.959 |

B. Data Collection and Refinement Conditions

| | |
|--|---|
| diffractometer | Bruker D8/APEX II CCD ^b |
| radiation (λ [Å]) | Cu Kα (1.54178) (microfocus source) |
| temperature (°C) | -100 |
| scan type | ω and φ scans (1.0°) (5 s exposures) |
| data collection 2θ limit (deg) | 145.48 |
| total data collected | 14514 (-14 ≤ <i>h</i> ≤ 16, -12 ≤ <i>k</i> ≤ 12, -21 ≤ <i>l</i> ≤ 21) |
| independent reflections | 4601 (<i>R</i> _{int} = 0.0576) |
| number of observed reflections (<i>NO</i>) | 3236 [<i>F</i> _o ² ≥ 2σ(<i>F</i> _o ²)] |

| | |
|---|--|
| structure solution method | direct methods/dual space (<i>SHELXD</i> ^c) |
| refinement method | full-matrix least-squares on F^2 (<i>SHELXL-2014</i> ^d) |
| absorption correction method | Gaussian integration (face-indexed) |
| range of transmission factors | 1.0000–0.6593 |
| data/restraints/parameters | 4601 / 12 ^e / 402 |
| goodness-of-fit (S) ^f [all data] | 1.054 |
| final R indices ^g | |
| $R_1 [F_o^2 \geq 2\sigma(F_o^2)]$ | 0.0726 |
| wR_2 [all data] | 0.2321 |
| largest difference peak and hole | 0.928 and $-0.357 \text{ e } \text{\AA}^{-3}$ |

^aObtained from least-squares refinement of 5514 reflections with $6.60^\circ < 2\theta < 145.20^\circ$.

^bPrograms for diffractometer operation, data collection, data reduction and absorption correction were those supplied by Bruker.

(continued)

Table 1. Crystallographic Experimental Details (continued)

^cSchneider, T. R.; Sheldrick, G. M. *Acta Crystallogr.* **2002**, *D58*, 1772-1779.

^dSheldrick, G. M. *Acta Crystallogr.* **2015**, *C71*, 3–8.

^e(a) The C16–C20A and C16–C20B distances were constrained to be equal (within 0.03 Å) during refinement. (b) The carbon atoms of the minor (40%) conformer of the disordered 3-fluorophenyl group were refined as an idealized regular hexagon, with C–C bond distances of 1.390 Å and C–C–C bond angles of 120.0°. (c) The O–H and H···H distances within the disordered solvent water molecules were constrained to be 0.840(3) Å and 1.370(3) Å during refinement. (c) The H1SB···N1(at 1–x, \bar{y} , 1–z) distance was constrained to be 2.22(2) Å during refinement. (e) The H1SD···N1(at 1–x, \bar{y} , 1–z) distance was constrained to be 1.97(2) Å during refinement.

$fS = [\sum w(F_o^2 - F_c^2)^2 / (n - p)]^{1/2}$ (n = number of data; p = number of parameters varied; $w = [\sigma^2(F_o^2) + (0.1241P)^2 + 1.7884P]^{-1}$ where $P = [\text{Max}(F_o^2, 0) + 2F_c^2]/3$).

$gR_1 = \sum ||F_o| - |F_c|| / \sum |F_o|$; $wR_2 = [\sum w(F_o^2 - F_c^2)^2 / \sum w(F_o^4)]^{1/2}$.

Table 2. Atomic Coordinates and Equivalent Isotropic Displacement Parameters

(a) atoms of *N*-(2,4-difluoro-3-methoxybenzyl)-6-{2-(3-fluorophenyl)pyrrolidin-1-yl}imidazo[1,2-*b*]pyridazine-3-carboxamide

| Atom | <i>x</i> | <i>y</i> | <i>z</i> | $U_{\text{eq}}, \text{\AA}^2$ |
|-------------------|-------------|------------|--------------|-------------------------------|
| F1 | 0.29978(16) | 0.4603(2) | 0.05861(12) | 0.0561(6)* |
| F2 | 0.05424(19) | 0.1307(3) | 0.01556(16) | 0.0846(9)* |
| F3A ^a | -0.0203(4) | 0.3952(6) | 0.2866(3) | 0.1031(18)* |
| F3B ^b | 0.0855(6) | 0.5225(13) | 0.1295(4) | 0.153(5)* |
| O1 | 0.47929(19) | 0.1999(2) | 0.30617(13) | 0.0460(6)* |
| O2 | 0.1364(2) | 0.3422(3) | -0.04391(17) | 0.0733(9)* |
| N1 | 0.50741(19) | 0.2115(2) | 0.55712(16) | 0.0394(6)* |
| N2 | 0.41956(18) | 0.3635(2) | 0.47520(13) | 0.0300(5)* |
| N3 | 0.35888(18) | 0.4688(2) | 0.44806(14) | 0.0308(5)* |
| N4 | 0.26532(19) | 0.6351(2) | 0.47788(14) | 0.0338(6)* |
| N5 | 0.3869(2) | 0.3850(3) | 0.30329(15) | 0.0375(6)* |
| C1 | 0.3284(2) | 0.5324(3) | 0.50423(16) | 0.0307(6)* |
| C2 | 0.3590(2) | 0.4991(3) | 0.58702(17) | 0.0357(6)* |
| C3 | 0.4208(2) | 0.3947(3) | 0.61077(18) | 0.0370(7)* |
| C4 | 0.4515(2) | 0.3211(3) | 0.55273(17) | 0.0329(6)* |
| C5 | 0.5105(2) | 0.1855(3) | 0.48105(19) | 0.0378(7)* |
| C6 | 0.4569(2) | 0.2773(3) | 0.42802(18) | 0.0340(6)* |
| C7 | 0.4415(2) | 0.2850(3) | 0.34104(18) | 0.0355(6)* |
| C8 | 0.3713(3) | 0.4071(3) | 0.21827(17) | 0.0396(7)* |
| C9 | 0.2846(2) | 0.3297(3) | 0.16709(17) | 0.0358(7)* |
| C10 | 0.2534(3) | 0.3601(3) | 0.08689(19) | 0.0424(7)* |
| C11 | 0.1749(3) | 0.2973(4) | 0.0338(2) | 0.0538(9)* |
| C12 | 0.1301(3) | 0.1949(4) | 0.0657(2) | 0.0572(10)* |
| C13 | 0.1572(3) | 0.1618(4) | 0.1439(2) | 0.0534(9)* |
| C14 | 0.2361(3) | 0.2298(3) | 0.1952(2) | 0.0454(8)* |
| C15 | 0.1970(4) | 0.3200(4) | -0.0949(3) | 0.0697(12)* |
| C16 | 0.2482(2) | 0.6875(3) | 0.39732(17) | 0.0378(7)* |
| C17 | 0.2103(3) | 0.8272(3) | 0.4074(2) | 0.0481(8)* |
| C18 | 0.1524(3) | 0.8091(3) | 0.4702(2) | 0.0471(8)* |
| C19 | 0.2204(3) | 0.7165(3) | 0.53000(19) | 0.0432(8)* |
| C20A ^a | 0.1767(7) | 0.6164(11) | 0.3288(5) | 0.0392(19)* |
| C21A ^a | 0.1084(6) | 0.5319(8) | 0.3415(4) | 0.0421(17)* |
| C22A ^a | 0.0476(5) | 0.4782(7) | 0.2770(5) | 0.0538(16)* |
| C23A ^a | 0.0500(6) | 0.5044(8) | 0.1989(5) | 0.0491(17)* |
| C24A ^a | 0.1185(6) | 0.5977(7) | 0.1880(4) | 0.0573(18)* |
| C25A ^a | 0.1841(6) | 0.6549(7) | 0.2520(4) | 0.0442(15)* |

| | | | | |
|-------------------|-----------|-----------|-----------|-----------|
| C20B ^b | 0.1701(7) | 0.5890(9) | 0.3431(5) | 0.064(9)* |
| C21B ^b | 0.1614(6) | 0.5934(8) | 0.2615(5) | 0.051(2)* |

Table 2. Atomic Coordinates and Displacement Parameters (continued)

| Atom | x | y | z | $U_{eq}, \text{\AA}^2$ |
|-------------------|-----------|------------|-----------|------------------------|
| C22B ^b | 0.0933(6) | 0.5121(10) | 0.2102(4) | 0.070(5)* |
| C23B ^b | 0.0340(5) | 0.4263(9) | 0.2404(5) | 0.071(3)* |
| C24B ^b | 0.0427(5) | 0.4219(7) | 0.3220(5) | 0.066(3)* |
| C25B ^b | 0.1108(7) | 0.5032(9) | 0.3734(4) | 0.045(3)* |
| H5N | 0.367(3) | 0.439(4) | 0.331(2) | 0.052(11) |

(b) solvent water atoms

| Atom | x | y | z | $U_{eq}, \text{\AA}^2$ |
|---------------------|-----------|------------|-----------|------------------------|
| O1SA ^a | 0.3735(4) | -0.0600(5) | 0.2970(3) | 0.0588(13) |
| H1SA ^{a,c} | 0.413(4) | 0.003(4) | 0.297(5) | 0.088 |
| H1SB ^{a,c} | 0.403(4) | -0.119(3) | 0.329(2) | 0.088 |
| O1SB ^b | 0.3829(5) | -0.0348(7) | 0.3282(4) | 0.0464(15) |
| H1SC ^{b,c} | 0.421(5) | 0.025(6) | 0.320(5) | 0.070 |
| H1SD ^{b,c} | 0.414(5) | -0.081(5) | 0.367(3) | 0.070 |
| O2SB ^b | 0.3413(6) | 0.7538(9) | 0.2265(5) | 0.077(2) |
| H2SA ^{b,c} | 0.356(6) | 0.824(5) | 0.252(5) | 0.115 |
| H2SB ^{b,c} | 0.394(3) | 0.717(8) | 0.222(6) | 0.115 |

Anisotropically-refined atoms are marked with an asterisk (*). The form of the anisotropic displacement parameter is: $\exp[-2\pi^2(h^2a^{*2}U_{11} + k^2b^{*2}U_{22} + l^2c^{*2}U_{33} + 2klb^{*c^*}U_{23} + 2hla^{*c^*}U_{13} + 2hka^{*b^*}U_{12})]$.

^aRefined with an occupancy factor of 0.6. ^bRefined with an occupancy factor of 0.4. ^cRefined with an isotropic displacement parameter 150% of that of the attached oxygen atom.

Table 3. Selected Interatomic Distances (Å)

| Atom1 | Atom2 | Distance | Atom1 | Atom2 | Distance |
|-------|-------|-----------|-------|-------|-----------------------|
| F1 | C10 | 1.361(4) | C9 | C10 | 1.381(4) |
| F2 | C12 | 1.347(4) | C9 | C14 | 1.374(4) |
| F3A | C22A | 1.305(9) | C10 | C11 | 1.386(5) |
| F3B | C22B | 1.380(10) | C11 | C12 | 1.396(6) |
| O1 | C7 | 1.245(4) | C12 | C13 | 1.353(5) |
| O2 | C11 | 1.393(4) | C13 | C14 | 1.402(5) |
| O2 | C15 | 1.388(5) | C16 | C17 | 1.538(4) |
| N1 | C4 | 1.346(4) | C16 | C20A | 1.520(7) ^a |
| N1 | C5 | 1.357(4) | C16 | C20B | 1.591(6) ^a |
| N2 | N3 | 1.366(3) | C17 | C18 | 1.521(5) |
| N2 | C4 | 1.372(3) | C18 | C19 | 1.532(5) |
| N2 | C6 | 1.386(4) | C20A | C21A | 1.337(13) |
| N3 | C1 | 1.326(4) | C20A | C25A | 1.416(12) |
| N4 | C1 | 1.362(4) | C21A | C22A | 1.331(10) |
| N4 | C16 | 1.456(4) | C22A | C23A | 1.389(11) |
| N4 | C19 | 1.475(4) | C23A | C24A | 1.387(10) |
| N5 | C7 | 1.333(4) | C24A | C25A | 1.370(10) |
| N5 | C8 | 1.452(4) | C20B | C21B | 1.390 ^a |
| C1 | C2 | 1.429(4) | C20B | C25B | 1.390 ^a |
| C2 | C3 | 1.358(4) | C21B | C22B | 1.390 ^a |
| C3 | C4 | 1.405(4) | C22B | C23B | 1.390 ^a |
| C5 | C6 | 1.384(4) | C23B | C24B | 1.390 ^a |
| C6 | C7 | 1.470(4) | C24B | C25B | 1.390 ^a |
| C8 | C9 | 1.516(4) | | | |

^aDistances restrained during refinement. See footnote e of Table 1 for details.

Table 4. Selected Interatomic Angles (deg)

| Atom1 | Atom2 | Atom3 | Angle | Atom1 | Atom2 | Atom3 | Angle |
|-------|-------|-------|----------|-------|-------|-------|-----------------------|
| C11 | O2 | C15 | 114.9(3) | C10 | C11 | C12 | 115.6(3) |
| C4 | N1 | C5 | 105.5(2) | F2 | C12 | C11 | 117.2(4) |
| N3 | N2 | C4 | 126.7(2) | F2 | C12 | C13 | 119.7(4) |
| N3 | N2 | C6 | 125.5(2) | C11 | C12 | C13 | 123.0(3) |
| C4 | N2 | C6 | 107.8(2) | C12 | C13 | C14 | 119.0(4) |
| N2 | N3 | C1 | 114.4(2) | C9 | C14 | C13 | 120.7(3) |
| C1 | N4 | C16 | 122.2(2) | N4 | C16 | C17 | 101.7(2) |
| C1 | N4 | C19 | 124.0(2) | N4 | C16 | C20A | 119.3(6) ^a |
| C16 | N4 | C19 | 113.2(2) | N4 | C16 | C20B | 104.8(4) ^a |
| C7 | N5 | C8 | 122.2(3) | C17 | C16 | C20A | 110.7(5) ^a |
| N3 | C1 | N4 | 115.2(2) | C17 | C16 | C20B | 116.5(5) ^a |
| N3 | C1 | C2 | 123.7(3) | C16 | C17 | C18 | 103.2(3) |
| N4 | C1 | C2 | 121.1(3) | C17 | C18 | C19 | 102.3(3) |
| C1 | C2 | C3 | 119.3(3) | N4 | C19 | C18 | 102.2(2) |
| C2 | C3 | C4 | 118.8(3) | C16 | C20A | C21A | 121.5(9) ^a |
| N1 | C4 | N2 | 110.5(3) | C16 | C20A | C25A | 114.4(9) ^a |
| N1 | C4 | C3 | 132.5(3) | C21A | C20A | C25A | 123.9(6) |
| N2 | C4 | C3 | 117.0(3) | C20A | C21A | C22A | 116.5(7) |
| N1 | C5 | C6 | 111.7(3) | F3A | C22A | C21A | 118.6(7) |
| N2 | C6 | C5 | 104.5(3) | F3A | C22A | C23A | 116.6(7) |
| N2 | C6 | C7 | 126.5(3) | C21A | C22A | C23A | 124.9(7) |
| C5 | C6 | C7 | 129.0(3) | C22A | C23A | C24A | 116.9(7) |
| O1 | C7 | N5 | 123.1(3) | C23A | C24A | C25A | 120.9(6) |
| O1 | C7 | C6 | 119.6(3) | C20A | C25A | C24A | 116.8(7) |
| N5 | C7 | C6 | 117.3(3) | C16 | C20B | C21B | 116.7(5) ^a |
| N5 | C8 | C9 | 113.8(3) | C16 | C20B | C25B | 123.3(5) ^a |
| C8 | C9 | C10 | 118.0(3) | C21B | C20B | C25B | 120.0 ^a |
| C8 | C9 | C14 | 124.1(3) | C20B | C21B | C22B | 120.0 ^a |
| C10 | C9 | C14 | 117.9(3) | F3B | C22B | C21B | 117.9(8) ^a |
| F1 | C10 | C9 | 118.4(3) | F3B | C22B | C23B | 122.1(8) ^a |
| F1 | C10 | C11 | 117.9(3) | C21B | C22B | C23B | 120.0 ^a |
| C9 | C10 | C11 | 123.7(3) | C22B | C23B | C24B | 120.0 ^a |
| O2 | C11 | C10 | 122.1(4) | C23B | C24B | C25B | 120.0 ^a |
| O2 | C11 | C12 | 121.9(4) | C20B | C25B | C24B | 120.0 ^a |

^aAngle includes distance(s) restrained during refinement. See footnote e of Table 1 for details.

Table 5. Hydrogen-Bonded Interactions

| D—H \cdots A | D—H (Å) | H \cdots A (Å) | D \cdots A (Å) | \angle D—H \cdots A (deg) |
|--------------------------------------|------------|---------------------|---------------------|----------------------------------|
| N5—H5N \cdots N3 | 0.82(4) | 2.09(4) | 2.772(4) | 141(4) |
| O1SA—H1SA \cdots O1 | 0.840(3) | 2.19(2) | 3.002(6) | 163(7) |
| O1SA—H1SB \cdots N1 ^a | 0.841(3) | 2.256(16) | 3.056(6) | 159(4) |
| O1SB—H1SC \cdots O1 | 0.840(3) | 1.99(3) | 2.805(7) | 163(8) |
| O1SB—H1SD \cdots N1 ^a | 0.841(3) | 1.985(14) | 2.816(7) | 169(7) |
| O2SB—H2SA \cdots O1SB ^b | 0.840(3) | 1.92(2) | 2.743(11) | 168(10) |
| O2SB—H2SB \cdots O1 ^c | 0.840(3) | 1.95(4) | 2.745(9) | 157(10) |

^aAt $1-x, \bar{y}, 1-z$.

^bAt $x, 1+y, z$.

^cAt $1-x, 1/2+y, 1/2-z$.

Table 6. Torsional Angles (deg)

| Atom1 | Atom2 | Atom3 | Atom4 | Angle | Atom1 | Atom2 | Atom3 | Atom4 | Angle |
|-------|-------|-------|-------|------------------------|-------|-------|-------|-------|------------------------|
| C15 | O2 | C11 | C10 | 72.8(5) | N2 | C6 | C7 | O1 | -179.6(3) |
| C15 | O2 | C11 | C12 | -114.1(5) | N2 | C6 | C7 | N5 | 0.5(5) |
| C5 | N1 | C4 | N2 | 0.2(3) | C5 | C6 | C7 | O1 | 0.5(5) |
| C5 | N1 | C4 | C3 | 179.2(3) | C5 | C6 | C7 | N5 | -179.3(3) |
| C4 | N1 | C5 | C6 | -0.2(3) | N5 | C8 | C9 | C10 | 169.5(3) |
| C4 | N2 | N3 | C1 | -1.1(4) | N5 | C8 | C9 | C14 | -11.6(4) |
| C6 | N2 | N3 | C1 | 176.4(3) | C8 | C9 | C10 | F1 | -2.0(4) |
| N3 | N2 | C4 | N1 | 177.7(2) | C8 | C9 | C10 | C11 | -179.7(3) |
| N3 | N2 | C4 | C3 | -1.5(4) | C14 | C9 | C10 | F1 | 179.0(3) |
| C6 | N2 | C4 | N1 | -0.1(3) | C14 | C9 | C10 | C11 | 1.3(5) |
| C6 | N2 | C4 | C3 | -179.3(3) | C8 | C9 | C14 | C13 | -179.3(3) |
| N3 | N2 | C6 | C5 | -177.9(2) | C10 | C9 | C14 | C13 | -0.4(5) |
| N3 | N2 | C6 | C7 | 2.3(4) | F1 | C10 | C11 | O2 | -6.8(5) |
| C4 | N2 | C6 | C5 | 0.0(3) | F1 | C10 | C11 | C12 | 179.8(3) |
| C4 | N2 | C6 | C7 | -179.8(3) | C9 | C10 | C11 | O2 | 170.9(3) |
| N2 | N3 | C1 | N4 | -178.1(2) | C9 | C10 | C11 | C12 | -2.6(5) |
| N2 | N3 | C1 | C2 | 2.7(4) | O2 | C11 | C12 | F2 | 7.3(6) |
| C16 | N4 | C1 | N3 | -11.5(4) | O2 | C11 | C12 | C13 | -170.4(4) |
| C16 | N4 | C1 | C2 | 167.7(3) | C10 | C11 | C12 | F2 | -179.2(3) |
| C19 | N4 | C1 | N3 | 178.2(3) | C10 | C11 | C12 | C13 | 3.1(6) |
| C19 | N4 | C1 | C2 | -2.5(4) | F2 | C12 | C13 | C14 | -179.9(3) |
| C1 | N4 | C16 | C17 | -158.1(3) | C11 | C12 | C13 | C14 | -2.3(6) |
| C1 | N4 | C16 | C20A | 79.9(5) ^a | C12 | C13 | C14 | C9 | 0.8(6) |
| C1 | N4 | C16 | C20B | 80.2(5) ^a | N4 | C16 | C17 | C18 | -33.8(3) |
| C19 | N4 | C16 | C17 | 13.1(3) | C20A | C16 | C17 | C18 | 94.0(6) ^a |
| C19 | N4 | C16 | C20A | -108.9(5) ^a | C20B | C16 | C17 | C18 | 79.5(5) ^a |
| C19 | N4 | C16 | C20B | -108.6(5) ^a | N4 | C16 | C20A | C21A | 19.5(10) ^a |
| C1 | N4 | C19 | C18 | -176.4(3) | N4 | C16 | C20A | C25A | -165.0(5) ^a |
| C16 | N4 | C19 | C18 | 12.5(4) | C17 | C16 | C20A | C21A | -97.9(9) ^a |
| C8 | N5 | C7 | O1 | -3.4(5) | C17 | C16 | C20A | C25A | 77.5(7) ^a |
| C8 | N5 | C7 | C6 | 176.5(3) | N4 | C16 | C20B | C21B | -162.6(4) ^a |
| C7 | N5 | C8 | C9 | 85.7(4) | N4 | C16 | C20B | C25B | 18.7(6) ^a |
| N3 | C1 | C2 | C3 | -1.8(4) | C17 | C16 | C20B | C21B | 85.9(6) ^a |
| N4 | C1 | C2 | C3 | 179.0(3) | C17 | C16 | C20B | C25B | -92.8(6) ^a |
| C1 | C2 | C3 | C4 | -1.0(4) | C16 | C17 | C18 | C19 | 42.0(3) |
| C2 | C3 | C4 | N1 | -176.5(3) | C17 | C18 | C19 | N4 | -33.1(3) |
| C2 | C3 | C4 | N2 | 2.5(4) | C16 | C20A | C21A | C22A | 178.0(8) ^a |
| N1 | C5 | C6 | N2 | 0.1(3) | C25A | C20A | C21A | C22A | 3.0(12) |
| N1 | C5 | C6 | C7 | 180.0(3) | C16 | C20A | C25A | C24A | -177.4(7) ^a |

| | | | | |
|------|------|------|------|-----------|
| C21A | C20A | C25A | C24A | -2.1(12) |
| C20A | C21A | C22A | F3A | -179.9(8) |

Table 6. Torsional Angles (continued)

| Atom1 | Atom2 | Atom3 | Atom4 | Angle | Atom1 | Atom2 | Atom3 | Atom4 | Angle |
|-------|-------|-------|-------|------------------------|-------|-------|-------|-------|------------------------|
| C20A | C21A | C22A | C23A | -0.5(12) | C21B | C20B | C25B | C24B | 0.0 ^a |
| F3A | C22A | C23A | C24A | 176.7(7) | C20B | C21B | C22B | F3B | 178.4(8) ^a |
| C21A | C22A | C23A | C24A | -2.8(12) | C20B | C21B | C22B | C23B | 0.0 ^a |
| C22A | C23A | C24A | C25A | 3.7(11) | F3B | C22B | C23B | C24B | -178.3(9) ^a |
| C23A | C24A | C25A | C20A | -1.4(11) | C21B | C22B | C23B | C24B | 0.0 ^a |
| C16 | C20B | C21B | C22B | -178.7(8) ^a | C22B | C23B | C24B | C25B | 0.0 ^a |
| C25B | C20B | C21B | C22B | 0.0 ^a | C23B | C24B | C25B | C20B | 0.0 ^a |
| C16 | C20B | C25B | C24B | 178.7(9) ^a | | | | | |

^aAngle includes distance(s) restrained during refinement. See footnote e of Table 1 for details.

Table 7. Anisotropic Displacement Parameters (U_{ij} , Å²)

| Atom | U_{11} | U_{22} | U_{33} | U_{23} | U_{13} | U_{12} |
|------|------------|------------|------------|-------------|------------|-------------|
| F1 | 0.0632(14) | 0.0569(12) | 0.0442(11) | 0.0170(9) | 0.0067(9) | -0.0047(10) |
| F2 | 0.0550(16) | 0.119(2) | 0.0765(17) | -0.0365(16) | 0.0115(12) | -0.0316(15) |
| F3A | 0.097(4) | 0.101(4) | 0.101(4) | -0.005(3) | 0.007(3) | -0.040(3) |
| F3B | 0.088(5) | 0.313(14) | 0.035(3) | -0.064(5) | -0.026(3) | 0.099(7) |
| O1 | 0.0567(15) | 0.0370(11) | 0.0475(13) | 0.0001(10) | 0.0190(11) | 0.0073(10) |
| O2 | 0.070(2) | 0.092(2) | 0.0543(17) | -0.0022(15) | 0.0086(14) | 0.0196(17) |
| N1 | 0.0335(14) | 0.0349(13) | 0.0450(15) | 0.0107(11) | 0.0014(11) | 0.0003(10) |
| N2 | 0.0299(13) | 0.0251(11) | 0.0315(12) | 0.0042(9) | 0.0016(9) | -0.0020(9) |
| N3 | 0.0317(13) | 0.0249(11) | 0.0321(12) | 0.0032(9) | 0.0018(9) | -0.0001(9) |
| N4 | 0.0398(15) | 0.0296(12) | 0.0293(12) | 0.0002(9) | 0.0041(10) | 0.0019(10) |
| N5 | 0.0449(16) | 0.0343(13) | 0.0307(13) | 0.0006(10) | 0.0053(11) | 0.0038(11) |
| C1 | 0.0310(15) | 0.0259(12) | 0.0319(14) | 0.0008(10) | 0.0021(11) | -0.0052(10) |
| C2 | 0.0412(17) | 0.0332(14) | 0.0316(15) | 0.0002(11) | 0.0072(12) | -0.0050(12) |
| C3 | 0.0397(18) | 0.0348(15) | 0.0321(14) | 0.0098(11) | 0.0011(12) | -0.0086(12) |
| C4 | 0.0299(15) | 0.0313(13) | 0.0329(15) | 0.0074(11) | 0.0000(11) | -0.0049(11) |
| C5 | 0.0333(17) | 0.0326(15) | 0.0449(17) | 0.0075(12) | 0.0055(13) | 0.0009(12) |
| C6 | 0.0324(16) | 0.0298(14) | 0.0379(16) | 0.0017(11) | 0.0056(12) | -0.0010(11) |
| C7 | 0.0363(17) | 0.0309(14) | 0.0379(16) | 0.0000(11) | 0.0068(12) | -0.0021(12) |
| C8 | 0.0480(19) | 0.0358(15) | 0.0340(15) | 0.0031(12) | 0.0091(13) | -0.0011(13) |
| C9 | 0.0401(18) | 0.0337(14) | 0.0335(15) | -0.0008(11) | 0.0096(12) | 0.0048(12) |
| C10 | 0.0436(19) | 0.0441(17) | 0.0393(17) | 0.0001(13) | 0.0101(13) | 0.0036(14) |
| C11 | 0.048(2) | 0.071(2) | 0.0382(18) | -0.0054(16) | 0.0033(15) | 0.0031(18) |
| C12 | 0.041(2) | 0.074(3) | 0.055(2) | -0.0229(19) | 0.0094(16) | -0.0089(18) |
| C13 | 0.045(2) | 0.060(2) | 0.059(2) | -0.0116(17) | 0.0220(17) | -0.0129(17) |
| C14 | 0.050(2) | 0.0471(18) | 0.0419(17) | -0.0018(14) | 0.0169(15) | -0.0041(15) |
| C15 | 0.084(3) | 0.060(2) | 0.066(3) | -0.003(2) | 0.021(2) | 0.018(2) |
| C16 | 0.0384(17) | 0.0407(16) | 0.0327(15) | 0.0079(12) | 0.0059(12) | 0.0086(13) |
| C17 | 0.051(2) | 0.0408(17) | 0.051(2) | 0.0117(14) | 0.0112(16) | 0.0149(15) |
| C18 | 0.047(2) | 0.0382(16) | 0.056(2) | 0.0007(14) | 0.0123(15) | 0.0087(14) |
| C19 | 0.054(2) | 0.0374(16) | 0.0391(17) | -0.0011(13) | 0.0139(14) | 0.0069(14) |
| C20A | 0.037(5) | 0.043(3) | 0.030(4) | -0.005(4) | -0.004(3) | 0.013(3) |
| C21A | 0.030(3) | 0.055(4) | 0.035(4) | -0.002(3) | -0.004(3) | 0.004(3) |
| C22A | 0.042(4) | 0.062(4) | 0.048(4) | -0.006(3) | -0.004(3) | -0.006(3) |
| C23A | 0.036(5) | 0.058(4) | 0.042(4) | -0.012(3) | -0.012(3) | 0.000(3) |
| C24A | 0.065(5) | 0.064(4) | 0.040(3) | -0.002(3) | 0.007(3) | 0.005(3) |
| C25A | 0.050(4) | 0.046(4) | 0.036(3) | 0.011(3) | 0.009(2) | 0.001(3) |
| C20B | 0.055(12) | 0.111(19) | 0.016(5) | -0.006(7) | -0.009(6) | 0.060(12) |
| C21B | 0.042(6) | 0.072(8) | 0.037(6) | 0.008(5) | 0.008(4) | 0.020(5) |

| | | | | | | |
|------|----------|-----------|----------|-----------|-----------|----------|
| C22B | 0.030(8) | 0.121(13) | 0.044(7) | -0.044(7) | -0.019(6) | 0.019(8) |
| C23B | 0.036(7) | 0.102(11) | 0.066(8) | -0.025(8) | -0.003(5) | 0.005(6) |

Table 7. Anisotropic Displacement Parameters (continued)

| Atom | U_{11} | U_{22} | U_{33} | U_{23} | U_{13} | U_{12} |
|------|----------|----------|----------|-----------|-----------|-----------|
| C24B | 0.039(6) | 0.060(6) | 0.081(8) | -0.032(6) | -0.020(5) | -0.005(5) |
| C25B | 0.043(6) | 0.043(5) | 0.043(6) | -0.005(5) | -0.002(5) | 0.009(4) |

The form of the anisotropic displacement parameter is:

$$\exp[-2\pi^2(h^2a^2U_{11} + k^2b^2U_{22} + l^2c^2U_{33} + 2klb^*c^*U_{23} + 2hla^*c^*U_{13} + 2hka^*b^*U_{12})]$$

Table 8. Derived Atomic Coordinates and Displacement Parameters for Hydrogen Atoms

| Atom | <i>x</i> | <i>y</i> | <i>z</i> | <i>U</i> _{eq} , Å ² |
|-------------------|----------|----------|----------|---|
| H2 | 0.3364 | 0.5495 | 0.6251 | 0.043 |
| H3 | 0.4428 | 0.3719 | 0.6656 | 0.044 |
| H8A | 0.4330 | 0.3828 | 0.2029 | 0.047 |
| H8B | 0.3593 | 0.5022 | 0.2071 | 0.047 |
| H13 | 0.1233 | 0.0935 | 0.1637 | 0.064 |
| H14 | 0.2564 | 0.2065 | 0.2501 | 0.055 |
| H15A | 0.1644 | 0.3545 | -0.1480 | 0.084 |
| H15B | 0.2612 | 0.3647 | -0.0743 | 0.084 |
| H15C | 0.2084 | 0.2251 | -0.0985 | 0.084 |
| H16 | 0.3142 | 0.6953 | 0.3844 | 0.045 |
| H17A | 0.2665 | 0.8894 | 0.4260 | 0.058 |
| H17B | 0.1663 | 0.8601 | 0.3567 | 0.058 |
| H18A | 0.0863 | 0.7686 | 0.4471 | 0.057 |
| H18B | 0.1431 | 0.8941 | 0.4954 | 0.057 |
| H19A | 0.2721 | 0.7662 | 0.5693 | 0.052 |
| H19B | 0.1816 | 0.6619 | 0.5586 | 0.052 |
| H21A ^a | 0.1035 | 0.5113 | 0.3938 | 0.051 |
| H23A ^a | 0.0068 | 0.4605 | 0.1550 | 0.059 |
| H24A ^a | 0.1198 | 0.6222 | 0.1355 | 0.069 |
| H25A ^a | 0.2323 | 0.7174 | 0.2453 | 0.053 |
| H21B ^b | 0.2019 | 0.6521 | 0.2408 | 0.061 |
| H23B ^b | -0.0126 | 0.3708 | 0.2053 | 0.085 |
| H24B ^b | 0.0022 | 0.3632 | 0.3427 | 0.080 |
| H25B ^b | 0.1168 | 0.5001 | 0.4292 | 0.054 |

^aIncluded with an occupancy factor of 0.6. ^bIncluded with an occupancy factor of 0.4.

Additional Experimental Data (Chiral SFC/MS Analyses of Intermediates (\pm)-5.12, (*R*)-5.12 and (*S*)-5.12, Crystallographic Data for Compound (*R_S-R*)-5.9. and NMR Spectrum from Supporting Information Section 4, 5 and 8 - Chapter 5)

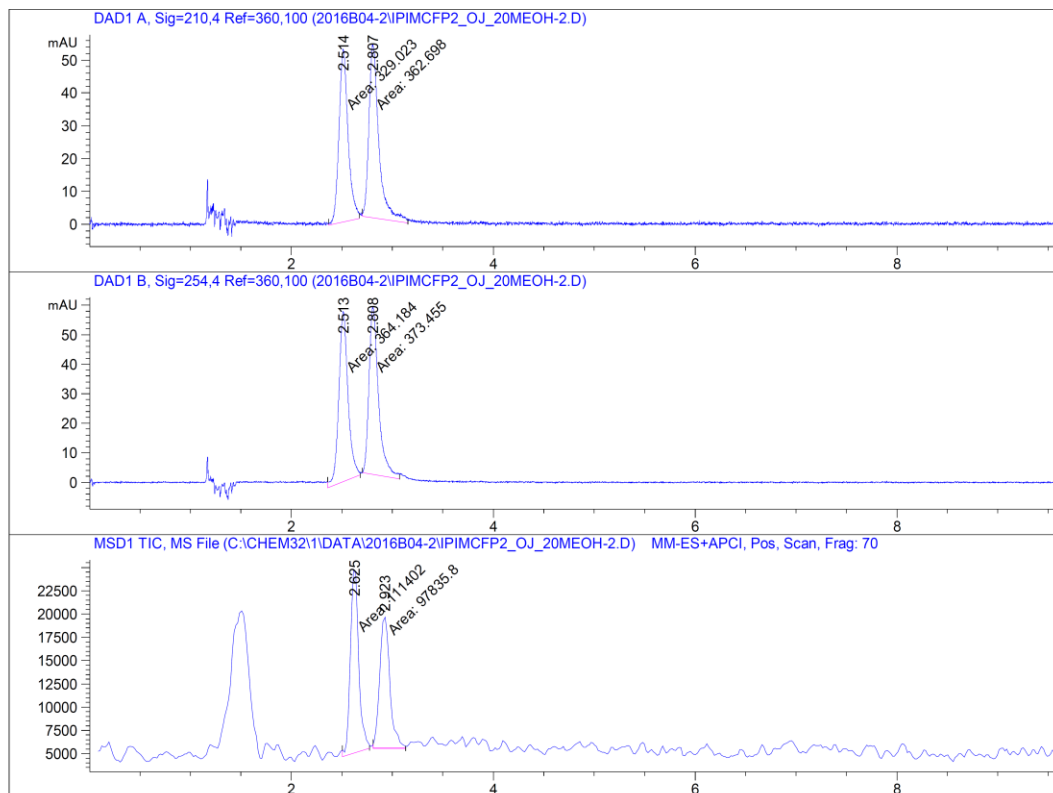
*The data from this Annex are included in Supporting Information of: Bernard-Gauthier, V.; Bailey, J.J.; Mossine, A.V.; Lindner, S.; Vomacka, L.; Aliaga, A.; Shao, X.; Quesada, C.A.; Sherman, P.; Mahringer, A.; Kostikov, A.; Grand'Maison, M.; Rosa-Neto, P.; Soucy, J.-P.; Thiel, A.; Kaplan, D.R.; Fricker, G.; Wängler, B.; Bartenstein, P.; Schirmacher, R.; Scott P.J.H. Shedding Light on Selective Neurotrophin Receptors *in vivo*: a First-in-Class Radioligand Candidate for Trk PET Neuroimaging. Submitted to *Proceedings of the National Academy of Sciences of the United States of America*, PNAS.*

The analysis was conducted on compounds (\pm)-5.12, (*S*)-5.12, (*R*)-5.12. The compounds (\pm)-5.12, (*S*)-5.12, (*R*)-5.12 are referred herein as (\pm)-IPMICFP2, (*S*)-IPMICFP2 and (*R*)-IPMICFP2.

Data File C:\CHEM32\1\DATA\2016B04-2\IPMICFP2_OJ_20MEOH-2.D

Sample Name: IPMICFP2

| | |
|----------------------------------|-------------------------------|
| Sample ID : IPMICFP2 | Operator : Karine |
| Location : Vial 41 | BPR Press : 150 bar |
| Solvent : 1 (MeOH), start @ ???% | Column : OJ-H (1) |
| Col Temp : 30deg C 30deg C | Inj Vol : 15uL into 20uL loop |



=====
 Area Percent Report
 =====

Sorted By : Signal
 Multiplier : 1.0000
 Dilution : 1.0000
 Use Multiplier & Dilution Factor with ISTDs

Data File C:\CHEM32\1\DATA\2016B04-2\IPIMCFP2_OJ_20MEOH-2.D
Sample Name: IPIMCFP2

Signal 1: DAD1 A, Sig=210,4 Ref=360,100

| Peak # | RetTime [min] | Type | Width [min] | Area [mAU*s] | Height [mAU] | Area % |
|----------|---------------|------|-------------|--------------|--------------|---------|
| 1 | 2.514 | MM | 0.1048 | 329.02277 | 52.31275 | 47.5659 |
| 2 | 2.807 | MM | 0.1142 | 362.69772 | 52.92664 | 52.4341 |
| Totals : | | | | 691.72049 | 105.23939 | |

Signal 2: DAD1 B, Sig=254,4 Ref=360,100

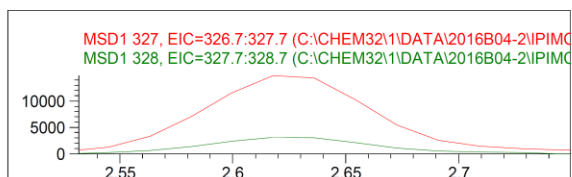
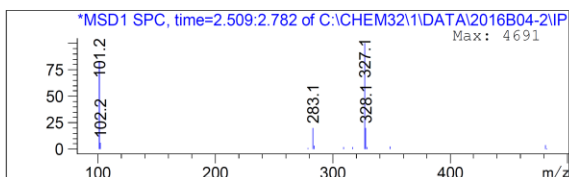
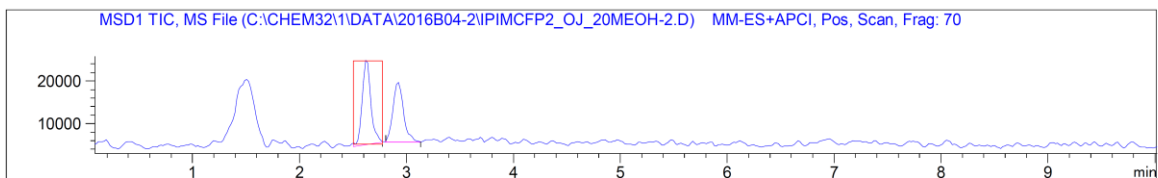
| Peak # | RetTime [min] | Type | Width [min] | Area [mAU*s] | Height [mAU] | Area % |
|----------|---------------|------|-------------|--------------|--------------|---------|
| 1 | 2.513 | MM | 0.1050 | 364.18365 | 57.78342 | 49.3715 |
| 2 | 2.808 | MM | 0.1099 | 373.45532 | 56.64462 | 50.6285 |
| Totals : | | | | 737.63898 | 114.42804 | |

Signal 3: MSD1 TIC, MS File

| Peak # | RetTime [min] | Type | Width [min] | Area | Height | Area % |
|----------|---------------|------|-------------|-----------|-----------|---------|
| 1 | 2.625 | MM | 0.0914 | 1.11402e5 | 2.03156e4 | 53.2419 |
| 2 | 2.923 | MM | 0.1145 | 9.78358e4 | 1.42457e4 | 46.7581 |
| Totals : | | | | 2.09238e5 | 3.45613e4 | |

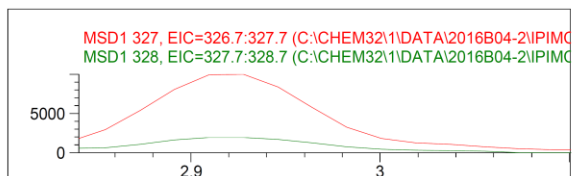
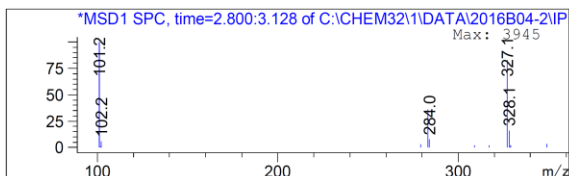
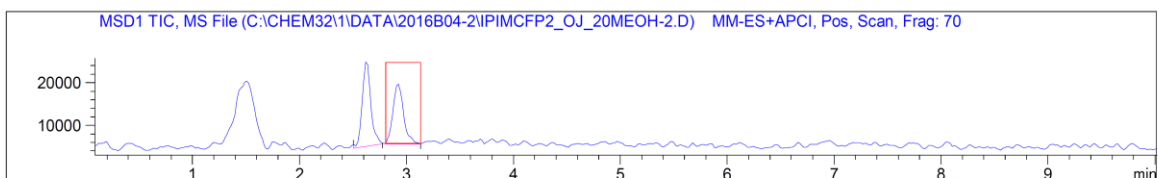
=====

Data File C:\CHEM32\1\DATA\2016B04-2\IPIMCFP2_OJ_20MEOH-2.D
Sample Name: IPIMCFP2



Peak #1 at 2.625 min (2.504 to 2.777 min)
-> The analysis found only one component, indicating a pure peak. <-

Component 1: Peak at Scan 140.4. Top ions are 327 328



Peak #2 at 2.923 min (2.808 to 3.133 min)
-> The analysis found only one component, indicating a pure peak. <-

Component 1: Peak at Scan 156.6. Top ions are 327 328

*** End of Report ***

Sample Name: R-IPIMCFP2

Sample ID : R-IPIMCFP2

Location : Vial 42

Solvent : 1 (MeOH), start @ ???%

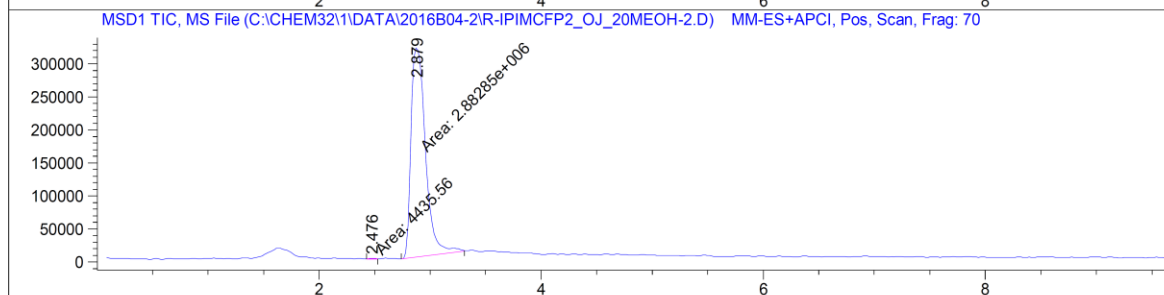
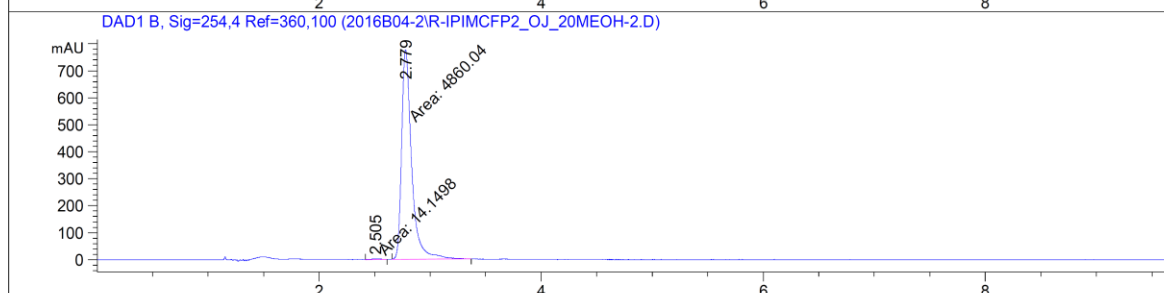
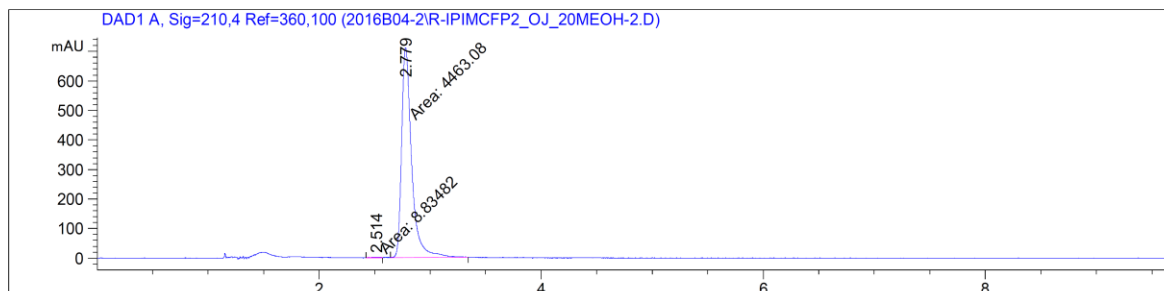
Col Temp : 30deg C 30deg C

Operator : Karine

BPR Press : 150 bar

Column : OJ-H (1)

Inj Vol : 15uL into 20uL loop



=====
Area Percent Report
=====

Sorted By : Signal
Multiplier : 1.0000
Dilution : 1.0000
Use Multiplier & Dilution Factor with ISTDs

Data File C:\CHEM32\1\DATA\2016B04-2\R-IPIMCFP2_OJ_20MEOH-2.D
Sample Name: R-IPIMCFP2

Signal 1: DAD1 A, Sig=210,4 Ref=360,100

| Peak # | RetTime [min] | Type | Width [min] | Area [mAU*s] | Height [mAU] | Area % |
|----------|---------------|------|-------------|--------------|--------------|---------|
| 1 | 2.514 | MM | 0.0810 | 8.83482 | 1.81851 | 0.1976 |
| 2 | 2.779 | MM | 0.1045 | 4463.08008 | 712.12042 | 99.8024 |
| Totals : | | | | 4471.91490 | 713.93893 | |

Signal 2: DAD1 B, Sig=254,4 Ref=360,100

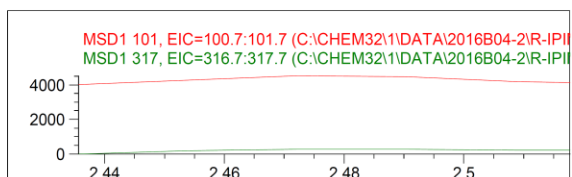
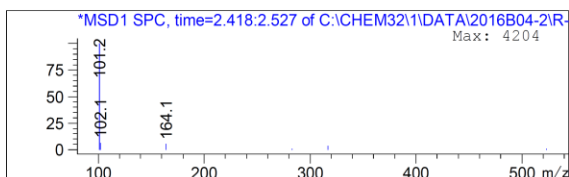
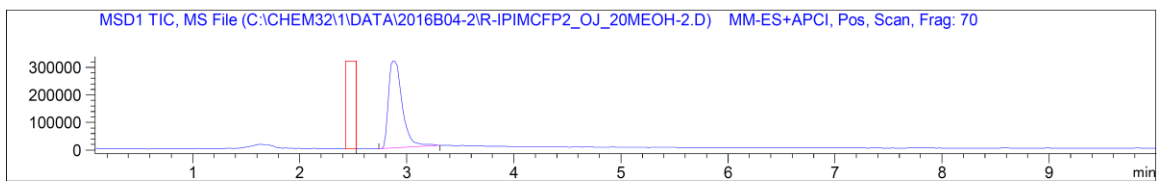
| Peak # | RetTime [min] | Type | Width [min] | Area [mAU*s] | Height [mAU] | Area % |
|----------|---------------|------|-------------|--------------|--------------|---------|
| 1 | 2.505 | MM | 0.0973 | 14.14984 | 2.42276 | 0.2903 |
| 2 | 2.779 | MM | 0.1044 | 4860.04199 | 775.69159 | 99.7097 |
| Totals : | | | | 4874.19183 | 778.11435 | |

Signal 3: MSD1 TIC, MS File

| Peak # | RetTime [min] | Type | Width [min] | Area | Height | Area % |
|----------|---------------|------|-------------|------------|-----------|---------|
| 1 | 2.476 | MM | 0.0742 | 4435.55908 | 996.02661 | 0.1536 |
| 2 | 2.879 | MM | 0.1510 | 2.88285e6 | 3.18215e5 | 99.8464 |
| Totals : | | | | 2.88728e6 | 3.19211e5 | |

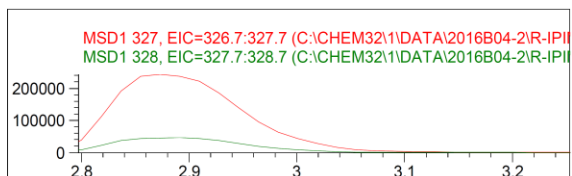
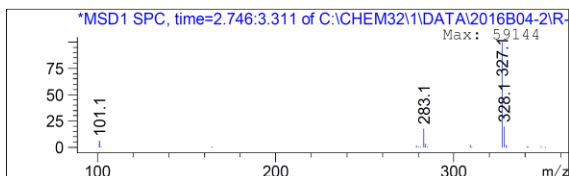
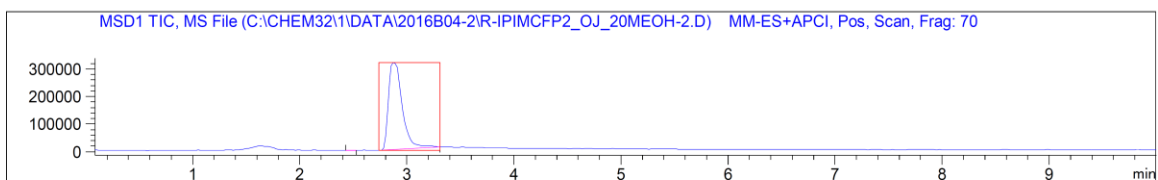
=====

Data File C:\CHEM32\1\DATA\2016B04-2\R-IPIMCFP2_OJ_20MEOH-2.D
Sample Name: R-IPIMCFP2



Peak #1 at 2.476 min (2.425 to 2.528 min)
-> The analysis found only one component, indicating a pure peak. <-

Component 1: Peak at Scan 132.3. Top ions are 101 317



Peak #2 at 2.879 min (2.740 to 3.311 min)
-> The analysis found only one component, indicating a pure peak. <-

Component 1: Peak at Scan 154.3. Top ions are 327 328

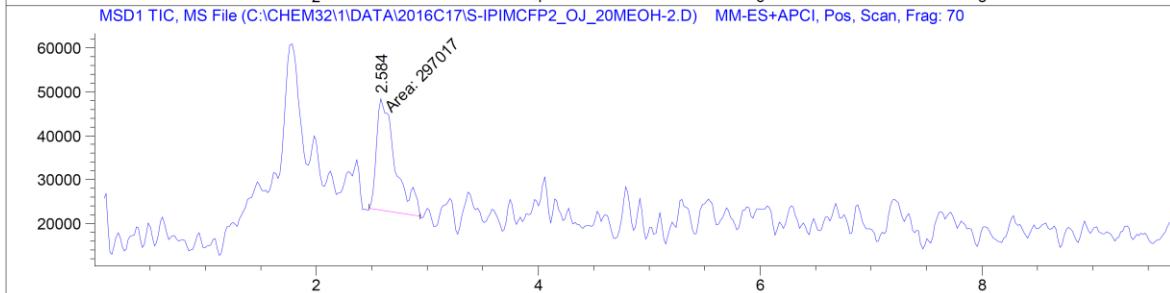
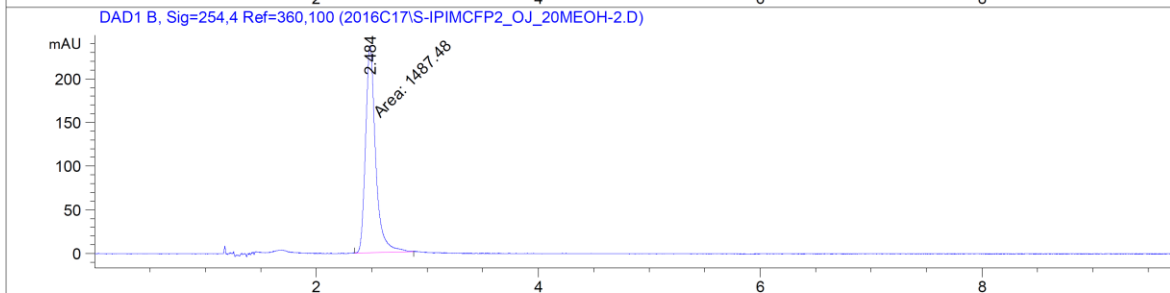
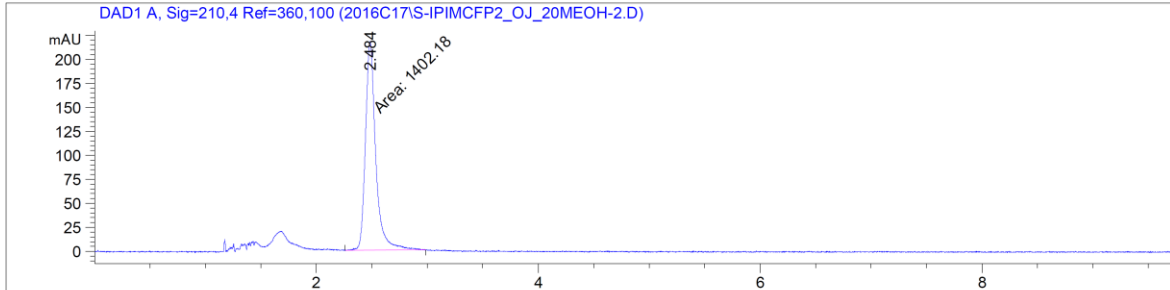
*** End of Report ***

Data File C:\CHEM32\1\DATA\2016C17\S-IPIMCFP2_OJ_20MEOH-2.D

Sample Name: S-IPIMCFP2

Sample ID : S-IPIMCFP2
Location : Vial 22
Solvent : 1 (MeOH), start @ ???%
Col Temp : 30deg C 30deg C

Operator : Karine
BPR Press : 150 bar
Column : OJ-H (1)
Inj Vol : 15uL into 20uL loop



=====
Area Percent Report
=====

Sorted By : Signal
Multiplier : 1.0000
Dilution : 1.0000
Use Multiplier & Dilution Factor with ISTDs

Data File C:\CHEM32\1\DATA\2016C17\S-IPIMCFP2_OJ_20MEOH-2.D
Sample Name: S-IPIMCFP2

Signal 1: DAD1 A, Sig=210,4 Ref=360,100

| Peak # | RetTime [min] | Type | Width [min] | Area [mAU*s] | Height [mAU] | Area % |
|----------|---------------|------|-------------|--------------|--------------|----------|
| 1 | 2.484 | MM | 0.1073 | 1402.17969 | 217.83234 | 100.0000 |
| Totals : | | | | 1402.17969 | 217.83234 | |

Signal 2: DAD1 B, Sig=254,4 Ref=360,100

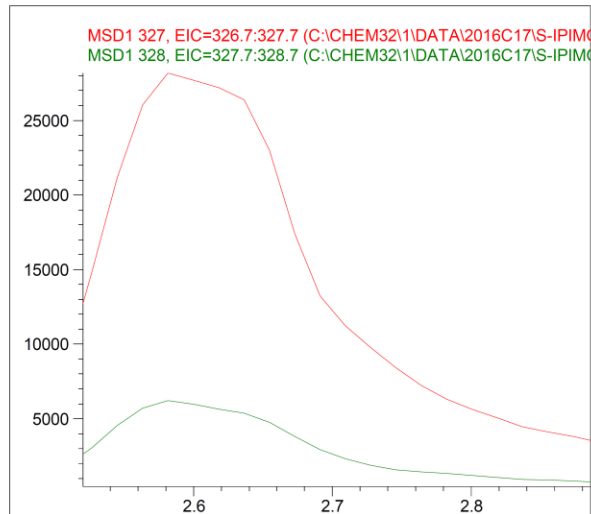
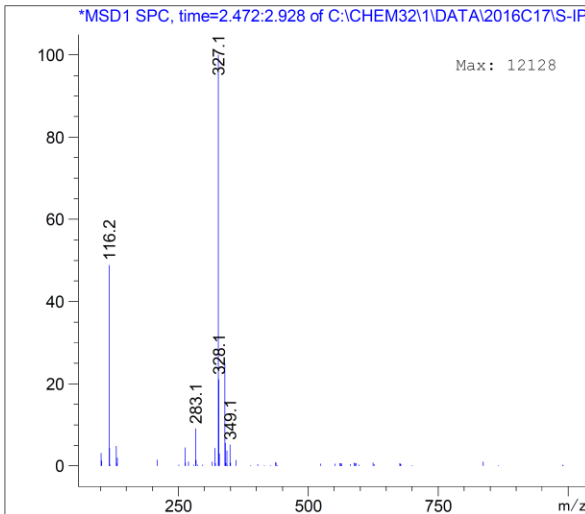
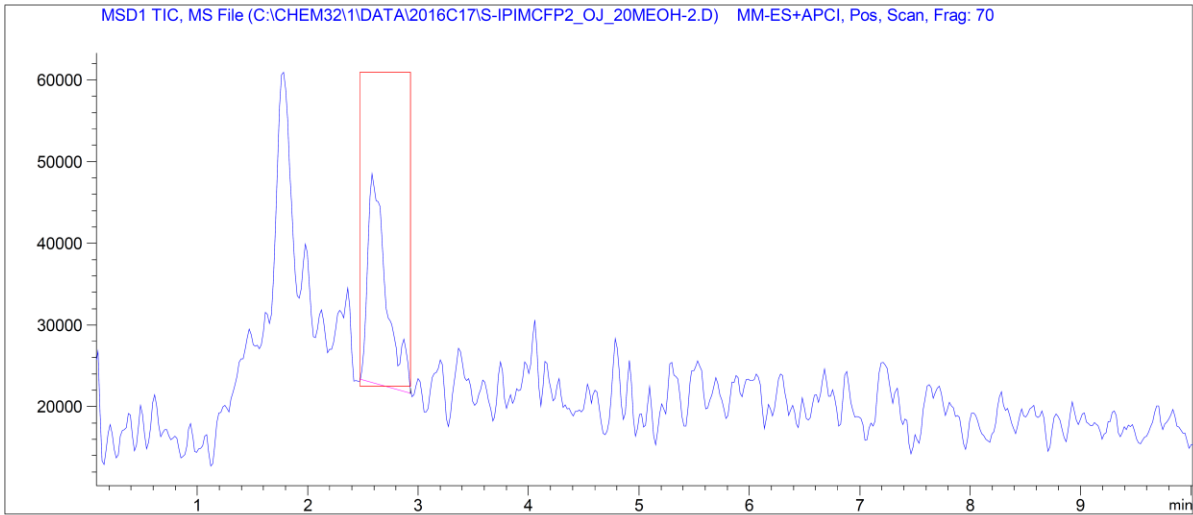
| Peak # | RetTime [min] | Type | Width [min] | Area [mAU*s] | Height [mAU] | Area % |
|----------|---------------|------|-------------|--------------|--------------|----------|
| 1 | 2.484 | MM | 0.1048 | 1487.48401 | 236.67047 | 100.0000 |
| Totals : | | | | 1487.48401 | 236.67047 | |

Signal 3: MSD1 TIC, MS File

| Peak # | RetTime [min] | Type | Width [min] | Area | Height | Area % |
|----------|---------------|------|-------------|-----------|-----------|----------|
| 1 | 2.584 | MM | 0.1928 | 2.97017e5 | 2.56792e4 | 100.0000 |
| Totals : | | | | 2.97017e5 | 2.56792e4 | |

=====

Data File C:\CHEM32\1\DATA\2016C17\S-IPIMCFP2_OJ_20MEOH-2.D
Sample Name: S-IPIMCFP2



Peak #1 at 2.584 min (2.475 to 2.932 min)
-> The analysis found only one component, indicating a pure peak. <-

Component 1: Peak at Scan 138.2. Top ions are 327 328

*** End of Report ***

Table 1. Crystal data and structure refinement for (*R_S*-*R*)-5.9.

| | |
|---|---|
| Identification code | (<i>R_S</i> - <i>R</i>)-11 |
| Empirical formula | C ₁₄ H ₂₁ ClFNOS |
| Formula weight | 305.83 |
| Temperature/K | 100 |
| Crystal system | trigonal |
| Space group | P3 ₂ |
| a/Å | 18.5172(8) |
| b/Å | 18.5172(8) |
| c/Å | 12.0526(6) |
| α/° | 90 |
| β/° | 90 |
| γ/° | 120 |
| Volume/Å ³ | 3579.0(4) |
| Z | 9 |
| ρ _{calc} /g/cm ³ | 1.277 |
| μ/mm ⁻¹ | 3.384 |
| F(000) | 1458.0 |
| Crystal size/mm ³ | 0.24 × 0.16 × 0.04 |
| Radiation | CuKα (λ = 1.54178) |
| 2θ range for data collection/° | 5.51 to 143.958 |
| Index ranges | -22 ≤ h ≤ 22, -22 ≤ k ≤ 22, -14 ≤ l ≤ 14 |
| Reflections collected | 98583 |
| Independent reflections | 9363 [R _{int} = 0.0377, R _{sigma} = 0.0160] |
| Data/restraints/parameters | 9363/1/527 |
| Goodness-of-fit on F ² | 1.090 |
| Final R indexes [I >= 2σ (I)] | R1 = 0.0615, wR2 = 0.1424 |
| Final R indexes [all data] | R1 = 0.0615, wR2 = 0.1425 |
| Largest diff. peak/hole / e Å ⁻³ | 1.94/-0.40 |
| Flack parameter | -0.002(4) |

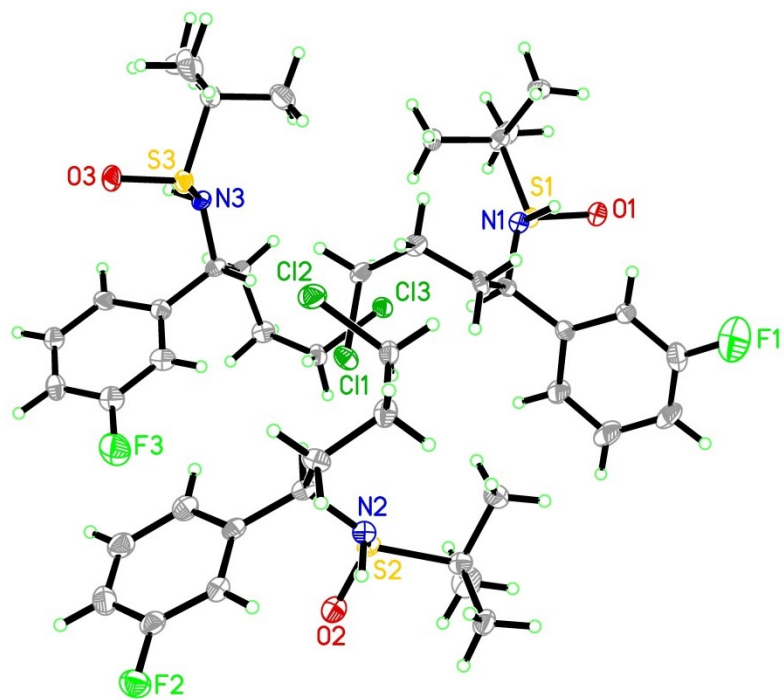


Figure 1. ORTEP view of the $C_{14}H_{21}ClFNOS$ compound with the numbering scheme adopted ((R_S - R)-**5.9**).

Table 2. Fractional Atomic Coordinates ($\times 10^4$) and Equivalent Isotropic Displacement Parameters ($\text{\AA}^2 \times 10^3$) for (*R_S*-*R*)-**5.9**. U_{eq} is defined as 1/3 of the trace of the orthogonalised U_{ij} tensor.

| Atom | x | y | z | U(eq) |
|------|------------|------------|------------|----------|
| Cl1 | 6326.4(10) | 6746.7(11) | 6394.5(14) | 49.2(3) |
| S1 | 6816.0(9) | 4339.3(8) | 4012.8(10) | 35.8(3) |
| F1 | 4170(7) | 1842(7) | 6697(12) | 144(4) |
| O1 | 6422(3) | 3417(3) | 3797(3) | 42.6(9) |
| N1 | 6794(3) | 4539(3) | 5356(4) | 36.5(9) |
| C11 | 6131(4) | 4694(4) | 5702(5) | 37.1(10) |
| C12 | 6320(4) | 5051(4) | 6881(4) | 39.9(11) |
| C13 | 7132(4) | 5888(4) | 6979(5) | 45.5(12) |
| C14 | 7193(4) | 6586(4) | 6247(6) | 44.6(13) |
| C15 | 5269(4) | 3926(4) | 5668(5) | 40.9(11) |
| C16 | 5102(4) | 3183(4) | 6181(6) | 48.9(14) |
| C17 | 4298(6) | 2512(5) | 6128(7) | 57.8(17) |
| C18 | 3657(5) | 2548(5) | 5602(7) | 58.0(17) |
| C19 | 3810(5) | 3317(6) | 5150(9) | 70(2) |
| C110 | 4609(5) | 3975(5) | 5146(6) | 53.8(16) |
| C111 | 7947(4) | 4766(4) | 3844(5) | 40.0(12) |
| C112 | 8367(4) | 5680(4) | 4150(6) | 45.4(12) |
| C113 | 8243(4) | 4269(4) | 4568(6) | 48.3(13) |
| C114 | 8046(5) | 4647(5) | 2600(5) | 53.0(16) |
| Cl2 | 7103.9(11) | 7098.0(12) | 9574.3(15) | 56.4(4) |
| S2 | 4146.9(8) | 6399.8(9) | 7518.5(10) | 39.8(3) |
| F2 | 4192(3) | 8989(3) | 10678(4) | 60.9(10) |
| O2 | 3652(3) | 6821(3) | 7266(4) | 49.7(10) |
| N2 | 4367(3) | 6447(3) | 8872(4) | 40.1(10) |
| C21 | 5171(3) | 7168(4) | 9178(5) | 38.5(11) |
| C22 | 5409(4) | 6992(4) | 10323(5) | 42.9(12) |
| C23 | 5505(4) | 6210(4) | 10359(5) | 47.6(13) |
| C24 | 6085(4) | 6187(4) | 9492(6) | 44.2(13) |
| C25 | 5164(4) | 7986(4) | 9202(5) | 41.9(12) |
| C26 | 4653(4) | 8111(4) | 9946(5) | 44.4(12) |
| C27 | 4677(4) | 8866(4) | 9932(6) | 47.4(14) |
| C28 | 5160(5) | 9499(5) | 9222(7) | 55.2(15) |
| C29 | 5632(5) | 9377(5) | 8483(7) | 57.0(16) |
| C210 | 5652(5) | 8620(5) | 8474(7) | 56.0(16) |
| C211 | 3404(4) | 5263(4) | 7403(5) | 42.8(12) |
| C212 | 3924(5) | 4836(5) | 7604(7) | 54.0(15) |
| C213 | 2696(4) | 4980(4) | 8252(6) | 52.2(14) |

| | | | | |
|------|------------|-----------|------------|----------|
| C214 | 3084(6) | 5153(6) | 6225(6) | 63.7(19) |
| CI3 | 6747.2(10) | 6317.5(9) | 3052.8(14) | 47.1(3) |
| S3 | 9347.0(9) | 8895.8(9) | 5948.7(12) | 41.4(3) |
| F3 | 6730(4) | 9686(4) | 6217(5) | 81.2(15) |
| O3 | 9802(3) | 9800(3) | 6265(4) | 51.5(11) |
| N3 | 9125(3) | 8753(3) | 4605(4) | 42.2(10) |
| C31 | 8265(3) | 8556(4) | 4326(5) | 39.8(11) |
| C32 | 8141(3) | 8296(4) | 3092(5) | 42.7(12) |
| C33 | 7258(4) | 7981(4) | 2658(5) | 45.2(13) |
| C34 | 6582(4) | 7193(4) | 3207(6) | 45.5(13) |
| C35 | 8111(4) | 9272(4) | 4555(5) | 44.1(12) |
| C36 | 7482(4) | 9168(5) | 5278(5) | 49.3(13) |
| C37 | 7347(5) | 9808(5) | 5519(6) | 54.1(16) |
| C38 | 7848(5) | 10597(4) | 5083(6) | 51.5(14) |
| C39 | 8479(4) | 10717(4) | 4357(6) | 51.4(14) |
| C310 | 8617(4) | 10071(4) | 4091(6) | 50.0(14) |
| C311 | 10144(5) | 8569(4) | 5942(6) | 51.3(14) |
| C312 | 9699(6) | 7644(5) | 5740(8) | 65.0(19) |
| C313 | 10812(5) | 9044(6) | 5102(8) | 65.9(19) |
| C314 | 10479(7) | 8764(6) | 7154(8) | 71(2) |

Table 3. Anisotropic Displacement Parameters ($\text{\AA}^2 \times 10^3$) for (R_S-R) -5.9. The Anisotropic displacement factor exponent takes the form: $-2\pi^2[h^2a^{*2}U_{11}+2hka^*b^*U_{12}+\dots]$.

| Atom | U_{11} | U_{22} | U_{33} | U_{23} | U_{13} | U_{12} |
|------|----------|----------|----------|----------|----------|----------|
| Cl1 | 58.8(8) | 51.1(8) | 45.8(7) | 6.3(6) | 4.0(6) | 33.6(7) |
| S1 | 39.4(6) | 37.1(6) | 29.4(5) | -0.5(4) | 1.9(5) | 18.0(5) |
| F1 | 121(7) | 93(6) | 201(12) | 34(7) | 18(7) | 41(5) |
| O1 | 46(2) | 41(2) | 35.3(19) | -3.1(15) | 3.8(16) | 17.6(18) |
| N1 | 41(2) | 38(2) | 28.3(19) | -1.4(16) | 3.4(16) | 18.2(18) |
| C11 | 42(3) | 40(3) | 35(2) | 4(2) | 3(2) | 24(2) |
| C12 | 50(3) | 37(3) | 34(2) | 7(2) | 7(2) | 24(2) |
| C13 | 43(3) | 53(3) | 42(3) | -6(2) | 4(2) | 25(3) |
| C14 | 36(3) | 45(3) | 48(3) | -1(2) | 5(2) | 17(2) |
| C15 | 44(3) | 40(3) | 43(3) | -5(2) | 2(2) | 23(2) |
| C16 | 43(3) | 46(3) | 62(4) | 9(3) | 11(3) | 25(3) |
| C17 | 68(4) | 42(3) | 61(4) | 5(3) | 18(3) | 25(3) |
| C18 | 43(3) | 57(4) | 58(3) | -16(3) | 0(3) | 14(3) |
| C19 | 43(4) | 66(5) | 82(5) | -6(4) | -23(4) | 13(4) |
| C110 | 49(3) | 51(4) | 56(4) | -4(3) | -15(3) | 21(3) |
| C111 | 34(2) | 42(3) | 38(3) | -3(2) | 7(2) | 14(2) |
| C112 | 43(3) | 41(3) | 49(3) | 2(2) | 1(3) | 18(2) |
| C113 | 42(3) | 50(3) | 55(3) | -2(3) | 6(3) | 25(3) |
| C114 | 48(3) | 66(4) | 36(3) | -8(3) | 9(2) | 22(3) |
| Cl2 | 48.1(8) | 62.5(9) | 60.4(10) | -12.7(7) | -5.2(7) | 29.0(7) |
| S2 | 35.4(6) | 45.1(7) | 36.7(6) | 0.2(5) | -1.6(5) | 18.5(6) |
| F2 | 62(2) | 62(2) | 66(2) | 4(2) | 10(2) | 36(2) |
| O2 | 49(2) | 50(2) | 45(2) | 4.2(19) | -5.4(18) | 21(2) |
| N2 | 42(2) | 45(2) | 34(2) | 2.7(19) | -0.3(18) | 22(2) |
| C21 | 37(3) | 45(3) | 32(2) | 0(2) | 0(2) | 19(2) |
| C22 | 50(3) | 54(3) | 32(2) | -7(2) | -2(2) | 32(3) |
| C23 | 51(3) | 45(3) | 42(3) | -3(2) | -8(2) | 21(3) |
| C24 | 42(3) | 35(3) | 52(3) | -4(2) | -4(2) | 16(2) |
| C25 | 35(3) | 47(3) | 40(3) | 0(2) | -6(2) | 17(2) |
| C26 | 42(3) | 44(3) | 41(3) | 2(2) | -3(2) | 17(2) |
| C27 | 41(3) | 48(3) | 50(3) | 3(3) | -7(2) | 19(3) |
| C28 | 56(4) | 44(3) | 60(4) | -3(3) | -8(3) | 22(3) |
| C29 | 47(3) | 51(4) | 66(4) | 14(3) | 5(3) | 19(3) |
| C210 | 45(3) | 53(4) | 60(4) | 6(3) | 8(3) | 17(3) |
| C211 | 41(3) | 45(3) | 39(3) | -7(2) | -7(2) | 19(2) |
| C212 | 57(4) | 51(3) | 59(4) | -1(3) | 1(3) | 31(3) |
| C213 | 46(3) | 43(3) | 59(4) | -7(3) | 1(3) | 16(3) |
| C214 | 67(4) | 65(5) | 50(4) | -15(3) | -16(3) | 26(4) |

| | | | | | | |
|------|---------|---------|---------|-----------|----------|---------|
| CI3 | 47.6(7) | 44.6(7) | 51.7(7) | -0.1(6) | -8.4(6) | 25.1(6) |
| S3 | 44.9(6) | 38.2(6) | 40.3(6) | -1.7(5) | -6.0(5) | 20.1(6) |
| F3 | 87(4) | 81(3) | 80(3) | -10(3) | 22(3) | 45(3) |
| O3 | 54(2) | 43(2) | 53(3) | -12.4(19) | -8(2) | 21(2) |
| N3 | 40(2) | 41(2) | 43(2) | -9.2(19) | -7.1(18) | 18(2) |
| C31 | 36(2) | 46(3) | 35(2) | -2(2) | -3.7(19) | 19(2) |
| C32 | 38(3) | 46(3) | 39(3) | 0(2) | 2(2) | 17(2) |
| C33 | 50(3) | 53(3) | 32(2) | -1(2) | -7(2) | 25(3) |
| C34 | 50(3) | 37(3) | 51(3) | -1(2) | -14(3) | 23(3) |
| C35 | 46(3) | 46(3) | 42(3) | -2(2) | -5(2) | 24(3) |
| C36 | 52(3) | 59(4) | 38(3) | -1(2) | -1(2) | 29(3) |
| C37 | 56(4) | 64(4) | 43(3) | -5(3) | -3(3) | 30(3) |
| C38 | 62(4) | 42(3) | 50(3) | -11(3) | -7(3) | 26(3) |
| C39 | 50(3) | 46(3) | 57(3) | 2(3) | -2(3) | 23(3) |
| C310 | 45(3) | 50(3) | 57(3) | 9(3) | 2(3) | 25(3) |
| C311 | 51(3) | 42(3) | 61(4) | 2(3) | -13(3) | 24(3) |
| C312 | 71(5) | 58(4) | 79(5) | -7(4) | -13(4) | 42(4) |
| C313 | 46(3) | 79(5) | 73(5) | 2(4) | 4(3) | 32(4) |
| C314 | 97(6) | 61(4) | 63(4) | -1(3) | -30(4) | 45(4) |

Table 4. Bond Lengths for (*R_S*-*R*)-5.9.

| Atom | Atom | Length/Å | Atom | Atom | Length/Å |
|------|------|-----------|------|------|-----------|
| Cl1 | C14 | 1.780(7) | C25 | C26 | 1.405(9) |
| S1 | O1 | 1.506(4) | C25 | C210 | 1.379(10) |
| S1 | N1 | 1.665(4) | C26 | C27 | 1.377(10) |
| S1 | C111 | 1.844(6) | C27 | C28 | 1.363(11) |
| F1 | C17 | 1.331(13) | C28 | C29 | 1.344(13) |
| N1 | C11 | 1.455(7) | C29 | C210 | 1.420(12) |
| C11 | C12 | 1.532(8) | C211 | C212 | 1.539(9) |
| C11 | C15 | 1.518(8) | C211 | C213 | 1.534(9) |
| C12 | C13 | 1.532(9) | C211 | C214 | 1.513(9) |
| C13 | C14 | 1.522(10) | Cl3 | C34 | 1.803(7) |
| C15 | C16 | 1.394(9) | S3 | O3 | 1.499(5) |
| C15 | C110 | 1.417(10) | S3 | N3 | 1.660(5) |
| C16 | C17 | 1.383(11) | S3 | C311 | 1.853(8) |
| C17 | C18 | 1.377(13) | F3 | C37 | 1.345(10) |
| C18 | C19 | 1.415(15) | N3 | C31 | 1.484(7) |
| C19 | C110 | 1.368(11) | C31 | C32 | 1.544(8) |
| C111 | C112 | 1.513(9) | C31 | C35 | 1.516(9) |
| C111 | C113 | 1.553(9) | C32 | C33 | 1.528(8) |
| C111 | C114 | 1.540(8) | C33 | C34 | 1.518(9) |
| Cl2 | C24 | 1.798(7) | C35 | C36 | 1.388(9) |
| S2 | O2 | 1.502(5) | C35 | C310 | 1.411(9) |
| S2 | N2 | 1.674(5) | C36 | C37 | 1.359(11) |
| S2 | C211 | 1.856(7) | C37 | C38 | 1.384(12) |
| F2 | C27 | 1.367(9) | C38 | C39 | 1.386(11) |
| N2 | C21 | 1.464(8) | C39 | C310 | 1.380(10) |
| C21 | C22 | 1.533(8) | C311 | C312 | 1.505(11) |
| C21 | C25 | 1.522(9) | C311 | C313 | 1.498(11) |
| C22 | C23 | 1.544(9) | C311 | C314 | 1.557(11) |
| C23 | C24 | 1.515(10) | | | |

Table 5. Bond Angles for (*R_S-R*)-5.9.

| Atom | Atom | Atom | Angle/° | Atom | Atom | Atom | Angle/° |
|------|------|------|-----------|------|------|------|----------|
| O1 | S1 | N1 | 111.6(2) | C27 | C26 | C25 | 118.5(6) |
| O1 | S1 | C111 | 105.6(3) | F2 | C27 | C26 | 118.1(6) |
| N1 | S1 | C111 | 99.2(3) | C28 | C27 | F2 | 118.2(7) |
| C11 | N1 | S1 | 116.0(4) | C28 | C27 | C26 | 123.7(7) |
| N1 | C11 | C12 | 108.6(5) | C29 | C28 | C27 | 118.3(7) |
| N1 | C11 | C15 | 113.8(5) | C28 | C29 | C210 | 120.7(7) |
| C15 | C11 | C12 | 109.6(5) | C25 | C210 | C29 | 120.4(7) |
| C11 | C12 | C13 | 113.9(5) | C212 | C211 | S2 | 105.8(5) |
| C14 | C13 | C12 | 115.6(5) | C213 | C211 | S2 | 111.1(4) |
| C13 | C14 | Cl | 113.2(4) | C213 | C211 | C212 | 111.5(6) |
| C16 | C15 | C11 | 121.5(6) | C214 | C211 | S2 | 103.9(5) |
| C16 | C15 | C110 | 119.2(6) | C214 | C211 | C212 | 112.5(6) |
| C110 | C15 | C11 | 119.3(6) | C214 | C211 | C213 | 111.6(6) |
| C17 | C16 | C15 | 118.3(7) | O3 | S3 | N3 | 112.5(3) |
| F1 | C17 | C16 | 115.1(10) | O3 | S3 | C311 | 105.7(3) |
| F1 | C17 | C18 | 121.7(9) | N3 | S3 | C311 | 96.8(3) |
| C18 | C17 | C16 | 123.0(7) | C31 | N3 | S3 | 114.2(4) |
| C17 | C18 | C19 | 118.9(7) | N3 | C31 | C32 | 105.6(4) |
| C110 | C19 | C18 | 118.7(8) | N3 | C31 | C35 | 113.1(5) |
| C19 | C110 | C15 | 121.7(8) | C35 | C31 | C32 | 112.6(5) |
| C112 | C111 | S1 | 106.9(4) | C33 | C32 | C31 | 114.4(5) |
| C112 | C111 | C113 | 112.9(5) | C34 | C33 | C32 | 115.3(5) |
| C112 | C111 | C114 | 111.5(5) | C33 | C34 | Cl3 | 113.0(5) |
| C113 | C111 | S1 | 110.3(4) | C36 | C35 | C31 | 120.3(6) |
| C114 | C111 | S1 | 103.7(4) | C36 | C35 | C310 | 117.8(6) |
| C114 | C111 | C113 | 111.1(6) | C310 | C35 | C31 | 121.9(6) |
| O2 | S2 | N2 | 111.5(3) | C37 | C36 | C35 | 121.3(7) |
| O2 | S2 | C211 | 106.0(3) | F3 | C37 | C36 | 119.9(7) |
| N2 | S2 | C211 | 98.9(3) | F3 | C37 | C38 | 118.6(7) |
| C21 | N2 | S2 | 113.8(4) | C36 | C37 | C38 | 121.4(7) |
| N2 | C21 | C22 | 107.6(5) | C37 | C38 | C39 | 118.3(6) |
| N2 | C21 | C25 | 113.7(5) | C310 | C39 | C38 | 120.9(6) |
| C25 | C21 | C22 | 109.9(5) | C39 | C310 | C35 | 120.2(6) |
| C21 | C22 | C23 | 113.9(5) | C312 | C311 | S3 | 107.5(5) |
| C24 | C23 | C22 | 115.0(6) | C312 | C311 | C314 | 110.1(6) |
| C23 | C24 | Cl2 | 111.2(5) | C313 | C311 | S3 | 111.8(5) |
| C26 | C25 | C21 | 121.2(5) | C313 | C311 | C312 | 112.4(7) |
| C210 | C25 | C21 | 120.5(6) | C313 | C311 | C314 | 112.4(7) |
| C210 | C25 | C26 | 118.3(7) | C314 | C311 | S3 | 102.1(6) |

Table 6. Hydrogen Bonds for (*R_S*-*R*)-5.9.

| D | H | A | d(D-H)/Å | d(H-A)/Å | d(D-A)/Å | D-H-A/° |
|----|----|-----------------|----------|----------|----------|---------|
| N1 | H1 | O1 ¹ | 0.91 | 2.11 | 2.923(6) | 148.8 |
| N2 | H2 | O2 ² | 0.91 | 2.08 | 2.980(7) | 169.9 |
| N3 | H3 | O3 ³ | 0.91 | 2.07 | 2.962(8) | 167.2 |

¹1+Y-X,1-X,1/3+Z; ²+Y-X,1-X,1/3+Z; ³2-Y,1+X-Y,-1/3+Z

Table 7. Torsion Angles for (*R_S*-*R*)-5.9

| A | B | C | D | Angle/° | A | B | C | D | Angle/° |
|------|-----|------|------|-----------|------|-----|------|------|-----------|
| S1 | N1 | C11 | C12 | -167.6(4) | C21 | C25 | C26 | C27 | 179.8(6) |
| S1 | N1 | C11 | C15 | 70.0(6) | C21 | C25 | C210 | C29 | 178.8(7) |
| F1 | C17 | C18 | C19 | 170.9(11) | C22 | C21 | C25 | C26 | -57.9(7) |
| O1 | S1 | N1 | C11 | -99.2(5) | C22 | C21 | C25 | C210 | 123.3(6) |
| O1 | S1 | C111 | C112 | -175.4(4) | C22 | C23 | C24 | Cl2 | 55.9(6) |
| O1 | S1 | C111 | C113 | -52.3(5) | C25 | C21 | C22 | C23 | -175.2(5) |
| O1 | S1 | C111 | C114 | 66.7(5) | C25 | C26 | C27 | F2 | -178.4(5) |
| N1 | S1 | C111 | C112 | -59.7(5) | C25 | C26 | C27 | C28 | 1.0(10) |
| N1 | S1 | C111 | C113 | 63.4(5) | C26 | C25 | C210 | C29 | -0.1(11) |
| N1 | S1 | C111 | C114 | -177.7(5) | C26 | C27 | C28 | C29 | 1.0(11) |
| N1 | C11 | C12 | C13 | 62.0(6) | C27 | C28 | C29 | C210 | -2.6(12) |
| N1 | C11 | C15 | C16 | 51.5(7) | C28 | C29 | C210 | C25 | 2.1(13) |
| N1 | C11 | C15 | C110 | -131.4(6) | C210 | C25 | C26 | C27 | -1.4(9) |
| C11 | C12 | C13 | C14 | 57.6(7) | C211 | S2 | N2 | C21 | 156.4(4) |
| C11 | C15 | C16 | C17 | 179.1(6) | S3 | N3 | C31 | C32 | -170.2(4) |
| C11 | C15 | C110 | C19 | -176.0(8) | S3 | N3 | C31 | C35 | 66.2(6) |
| C12 | C11 | C15 | C16 | -70.3(7) | F3 | C37 | C38 | C39 | -179.5(7) |
| C12 | C11 | C15 | C110 | 106.7(6) | O3 | S3 | N3 | C31 | -97.5(5) |
| C12 | C13 | C14 | Cl1 | 52.5(7) | O3 | S3 | C311 | C312 | 174.5(5) |
| C15 | C11 | C12 | C13 | -173.0(5) | O3 | S3 | C311 | C313 | -61.8(6) |
| C15 | C16 | C17 | F1 | -175.7(9) | O3 | S3 | C311 | C314 | 58.6(6) |
| C15 | C16 | C17 | C18 | -0.6(11) | N3 | S3 | C311 | C312 | -69.9(6) |
| C16 | C15 | C110 | C19 | 1.1(12) | N3 | S3 | C311 | C313 | 53.9(6) |
| C16 | C17 | C18 | C19 | -3.9(12) | N3 | S3 | C311 | C314 | 174.3(5) |
| C17 | C18 | C19 | C110 | 6.9(14) | N3 | C31 | C32 | C33 | 174.2(5) |
| C18 | C19 | C110 | C15 | -5.6(14) | N3 | C31 | C35 | C36 | -121.6(6) |
| C110 | C15 | C16 | C17 | 2.0(10) | N3 | C31 | C35 | C310 | 55.4(7) |
| C111 | S1 | N1 | C11 | 149.9(4) | C31 | C32 | C33 | C34 | -62.9(8) |
| S2 | N2 | C21 | C22 | -162.8(4) | C31 | C35 | C36 | C37 | 178.2(6) |
| S2 | N2 | C21 | C25 | 75.1(6) | C31 | C35 | C310 | C39 | -177.3(6) |
| F2 | C27 | C28 | C29 | -179.5(7) | C32 | C31 | C35 | C36 | 118.8(6) |
| O2 | S2 | N2 | C21 | -92.4(5) | C32 | C31 | C35 | C310 | -64.3(7) |
| O2 | S2 | C211 | C212 | 177.2(4) | C32 | C33 | C34 | Cl3 | -59.9(6) |
| O2 | S2 | C211 | C213 | -61.7(5) | C35 | C31 | C32 | C33 | -61.9(7) |
| O2 | S2 | C211 | C214 | 58.5(6) | C35 | C36 | C37 | F3 | 179.6(7) |
| N2 | S2 | C211 | C212 | -67.3(5) | C35 | C36 | C37 | C38 | -2.2(11) |
| N2 | S2 | C211 | C213 | 53.9(5) | C36 | C35 | C310 | C39 | -0.2(10) |
| N2 | S2 | C211 | C214 | 174.1(5) | C36 | C37 | C38 | C39 | 2.2(11) |
| N2 | C21 | C22 | C23 | 60.5(7) | C37 | C38 | C39 | C310 | -1.3(11) |

| | | | | | | | | | |
|-----|-----|-----|------|-----------|------|-----|------|-----|----------|
| N2 | C21 | C25 | C26 | 62.8(7) | C38 | C39 | C310 | C35 | 0.3(11) |
| N2 | C21 | C25 | C210 | -116.0(7) | C310 | C35 | C36 | C37 | 1.1(10) |
| C21 | C22 | C23 | C24 | 52.7(8) | C311 | S3 | N3 | C31 | 152.4(4) |

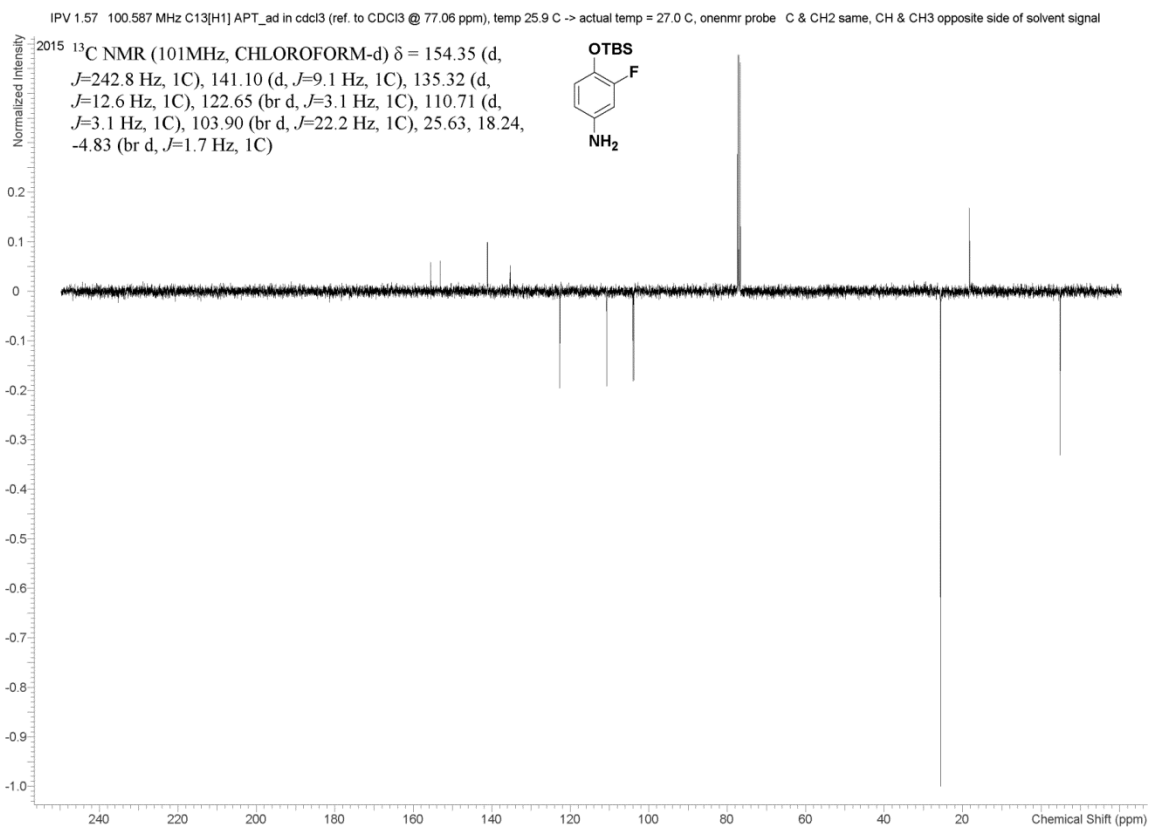
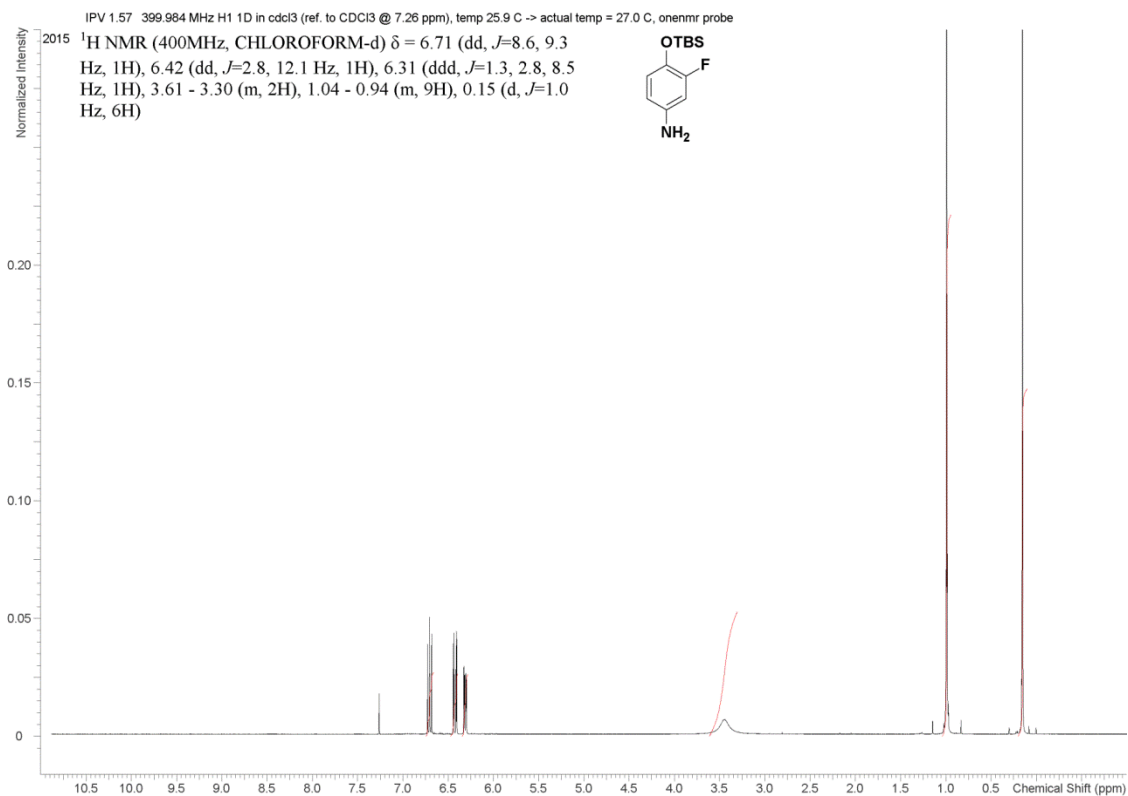
Table 8. Hydrogen Atom Coordinates ($\text{\AA}\times 10^4$) and Isotropic Displacement Parameters ($\text{\AA}^2\times 10^3$) for (R_S - R)-5.9

| Atom | x | y | z | U(eq) |
|------|------|-------|-------|-------|
| H1 | 6732 | 4083 | 5726 | 44 |
| H11 | 6134 | 5123 | 5196 | 44 |
| H12A | 6351 | 4643 | 7380 | 48 |
| H12B | 5852 | 5124 | 7136 | 48 |
| H13A | 7200 | 6074 | 7762 | 55 |
| H13B | 7603 | 5799 | 6797 | 55 |
| H14A | 7233 | 6453 | 5462 | 53 |
| H14B | 7710 | 7110 | 6434 | 53 |
| H16 | 5529 | 3139 | 6557 | 59 |
| H18 | 3121 | 2065 | 5543 | 70 |
| H19 | 3366 | 3376 | 4855 | 85 |
| H110 | 4724 | 4478 | 4785 | 65 |
| H11A | 8936 | 5969 | 3855 | 68 |
| H11B | 8384 | 5737 | 4959 | 68 |
| H11C | 8052 | 5926 | 3833 | 68 |
| H11D | 8189 | 4368 | 5355 | 72 |
| H11E | 8828 | 4454 | 4401 | 72 |
| H11F | 7900 | 3673 | 4407 | 72 |
| H11G | 7793 | 4050 | 2436 | 79 |
| H11H | 8640 | 4930 | 2409 | 79 |
| H11I | 7768 | 4883 | 2162 | 79 |
| H2 | 3990 | 6353 | 9419 | 48 |
| H21 | 5599 | 7220 | 8629 | 46 |
| H22A | 4977 | 6921 | 10865 | 51 |
| H22B | 5942 | 7482 | 10556 | 51 |
| H23A | 5713 | 6175 | 11102 | 57 |
| H23B | 4947 | 5711 | 10264 | 57 |
| H24A | 5849 | 6153 | 8745 | 53 |
| H24B | 6132 | 5682 | 9604 | 53 |
| H26 | 4300 | 7684 | 10449 | 53 |
| H28 | 5164 | 10014 | 9249 | 66 |
| H29 | 5957 | 9801 | 7961 | 68 |
| H210 | 6003 | 8550 | 7964 | 67 |
| H21A | 4130 | 4938 | 8370 | 81 |
| H21B | 4398 | 5065 | 7090 | 81 |
| H21C | 3575 | 4235 | 7480 | 81 |
| H21D | 2932 | 5195 | 8987 | 78 |
| H21E | 2376 | 4369 | 8275 | 78 |

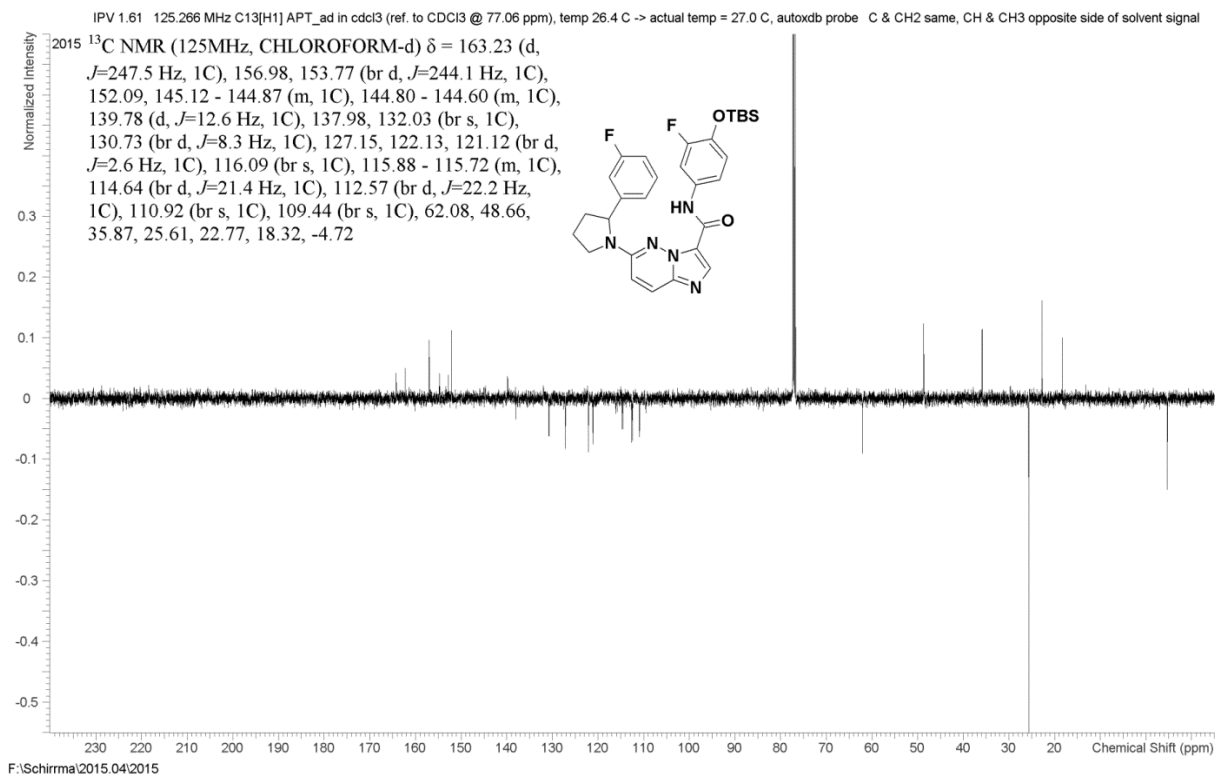
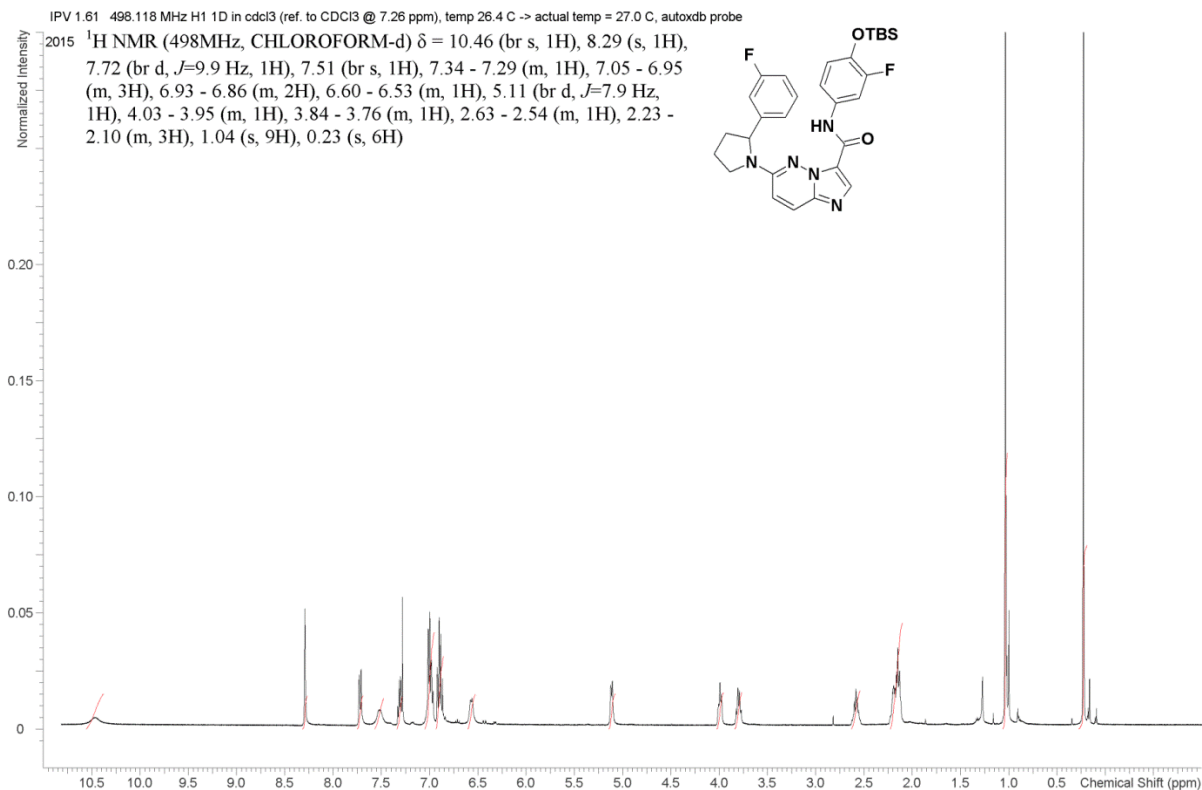
| | | | | |
|------|-------|-------|------|-----|
| H21F | 2328 | 5195 | 8036 | 78 |
| H21G | 2771 | 5448 | 6132 | 96 |
| H21H | 2717 | 4559 | 6072 | 96 |
| H21I | 3555 | 5382 | 5708 | 96 |
| H3 | 9492 | 9191 | 4182 | 51 |
| H31 | 7865 | 8065 | 4779 | 48 |
| H32A | 8534 | 8781 | 2640 | 51 |
| H32B | 8284 | 7852 | 2988 | 51 |
| H33A | 7118 | 8427 | 2757 | 54 |
| H33B | 7251 | 7876 | 1851 | 54 |
| H34A | 6036 | 7048 | 2880 | 55 |
| H34B | 6562 | 7303 | 4007 | 55 |
| H36 | 7140 | 8639 | 5612 | 59 |
| H38 | 7760 | 11045 | 5276 | 62 |
| H39 | 8821 | 11251 | 4037 | 62 |
| H310 | 9053 | 10164 | 3595 | 60 |
| H31A | 9214 | 7368 | 6233 | 98 |
| H31B | 10079 | 7431 | 5889 | 98 |
| H31C | 9513 | 7529 | 4966 | 98 |
| H31D | 10580 | 8879 | 4354 | 99 |
| H31E | 11265 | 8921 | 5200 | 99 |
| H31F | 11030 | 9643 | 5201 | 99 |
| H31G | 10757 | 9367 | 7282 | 107 |
| H31H | 10877 | 8569 | 7269 | 107 |
| H31I | 10013 | 8479 | 7674 | 107 |

Experimental: Single crystals of C₁₄H₂₁ClFNOS [(*R*_S-*R*)-**5.9**]. The crystal was kept at 100 K during data collection. Using Olex2, the structure was solved with the SIR2004 structure solution program using Direct Methods and refined with the XH refinement package using CGLS minimisation.

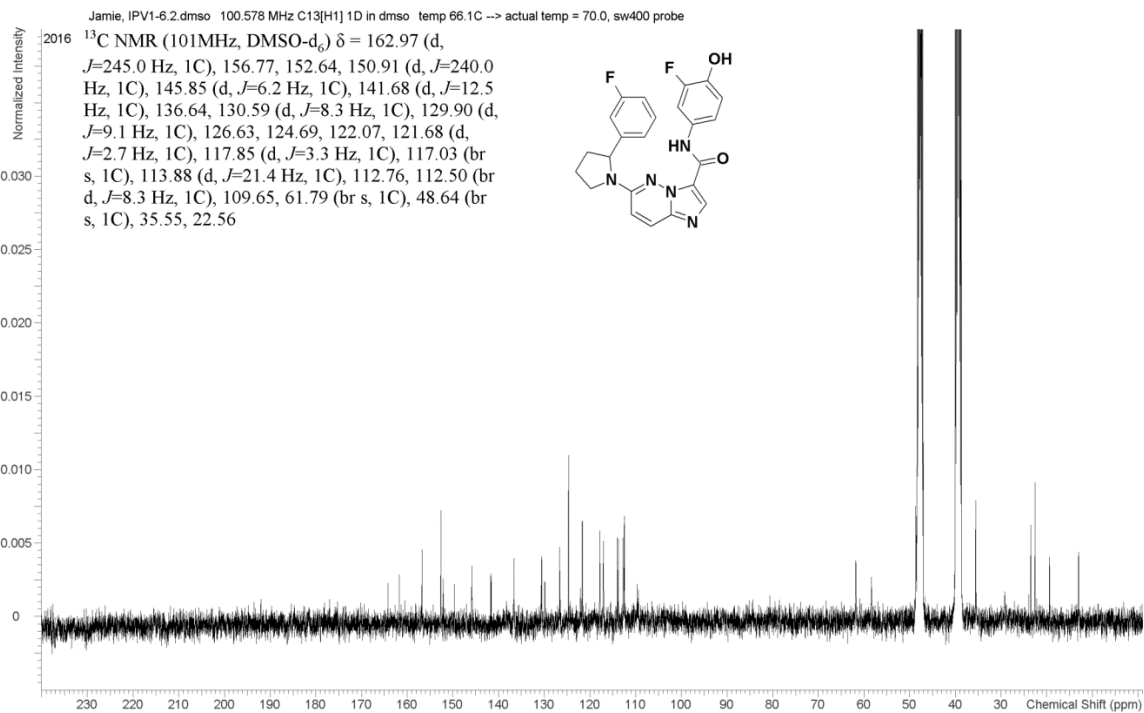
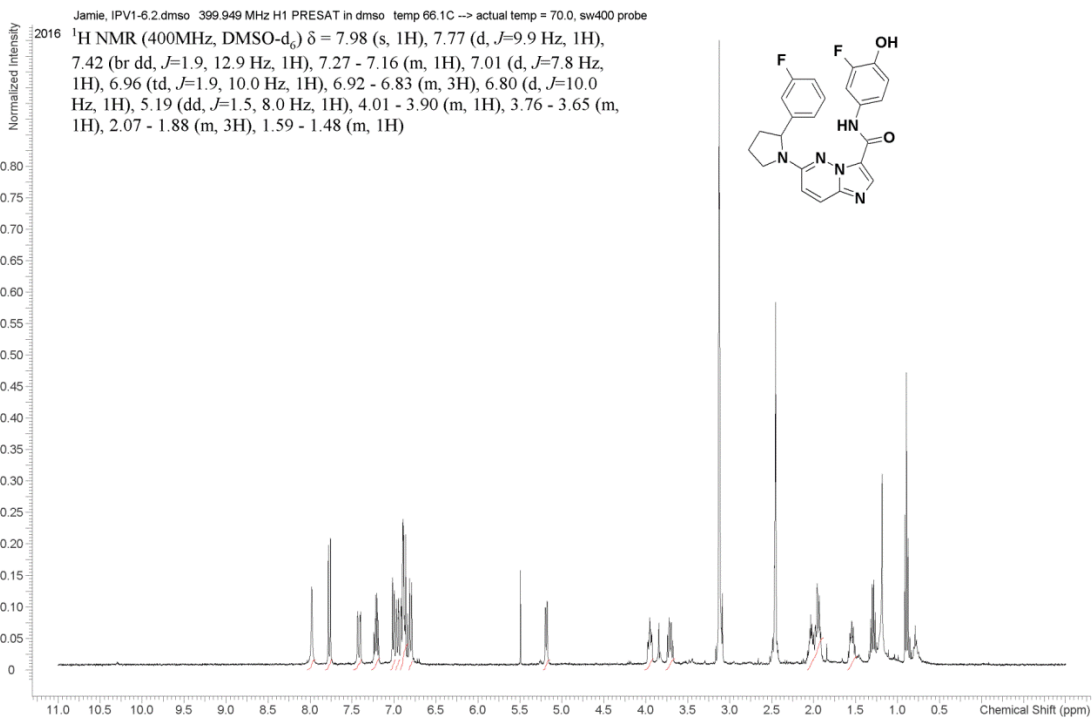
^1H NMR and ^{13}C NMR for compound 5.17



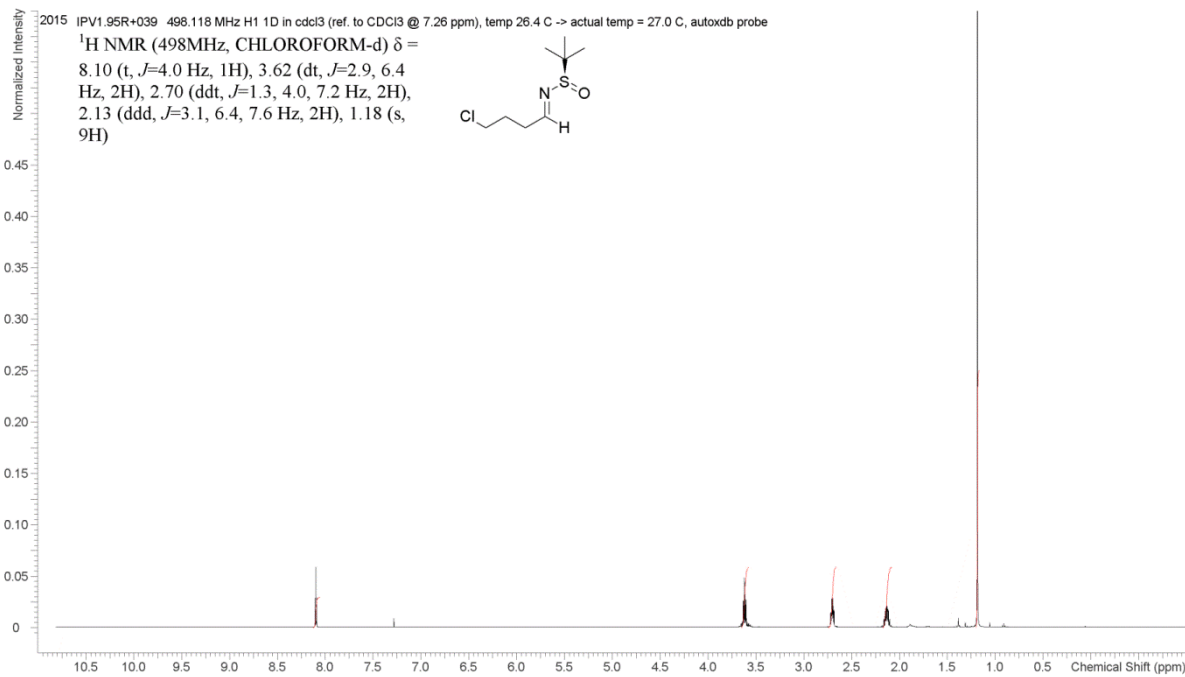
¹H NMR and ¹³C NMR for compound 5.13



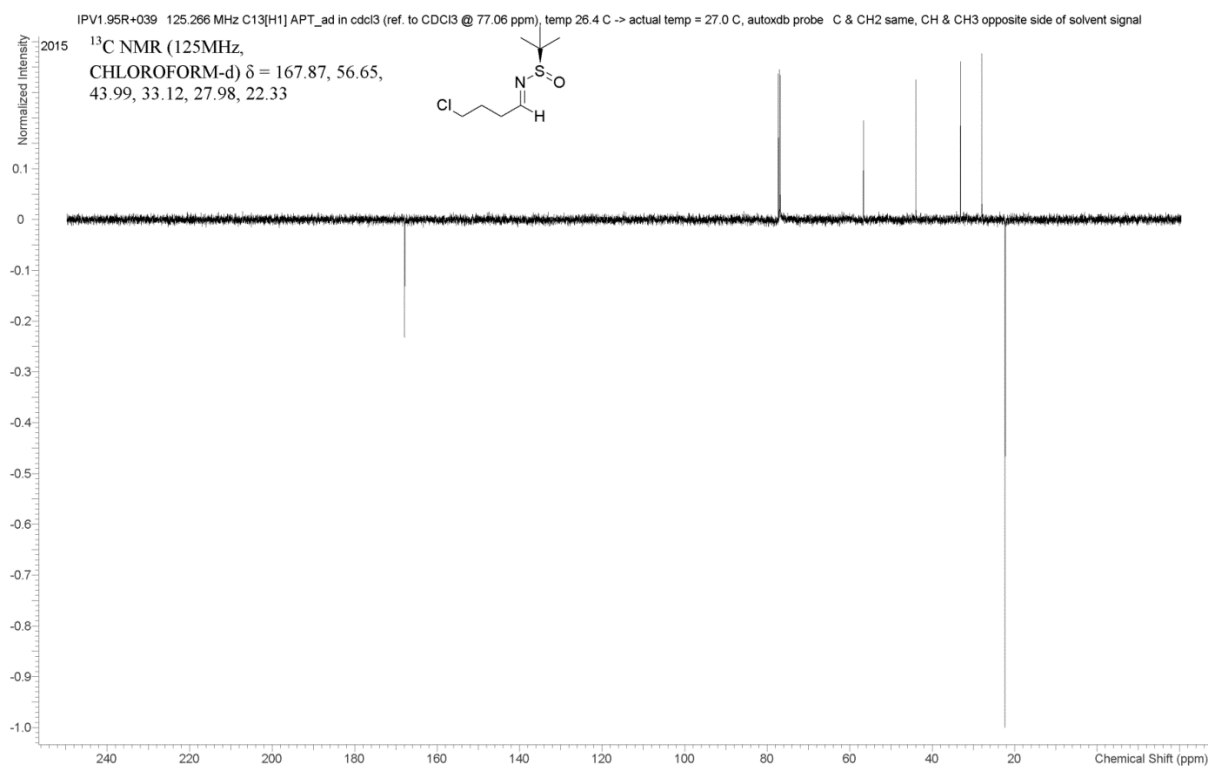
¹H NMR and ¹³C NMR for compound 5.14



^1H NMR and ^{13}C NMR for compound (R_S)-5.8

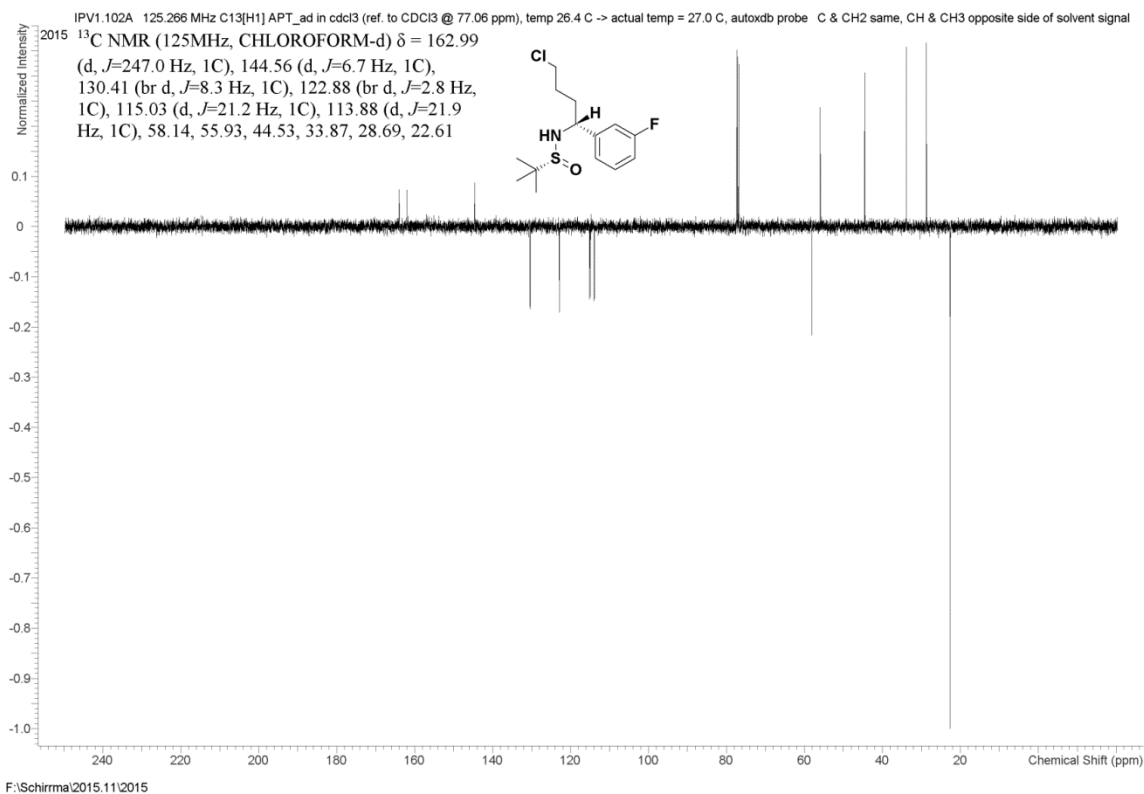
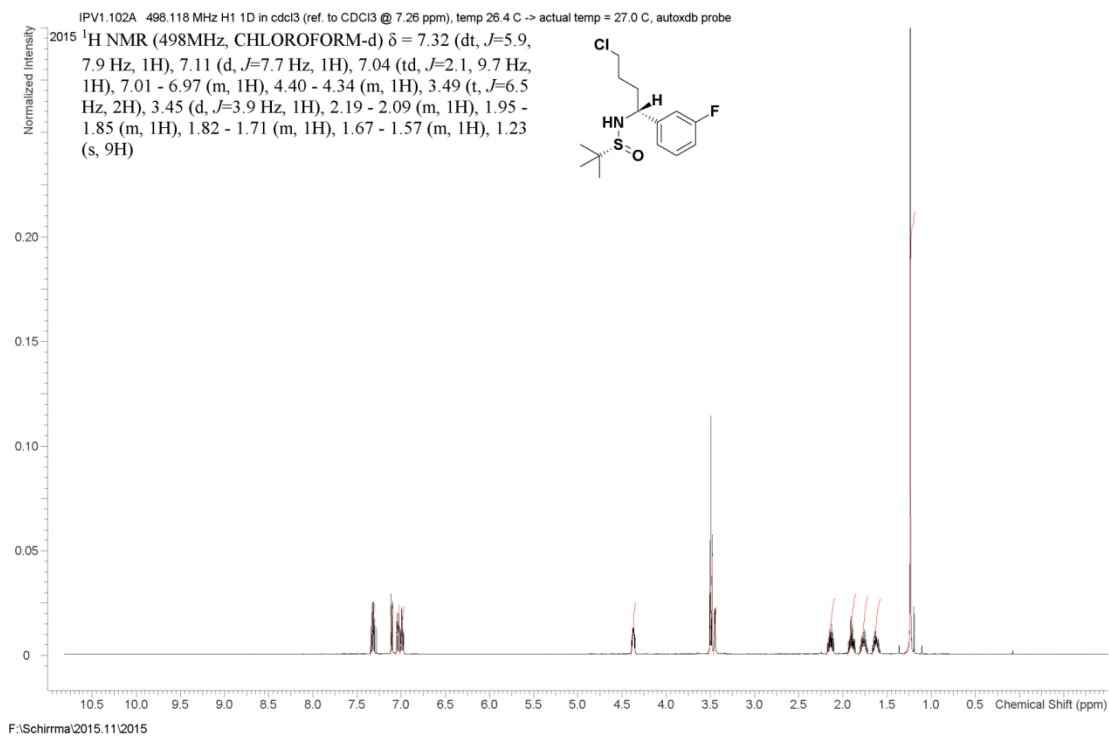


F:\Schirma\2015.11\2015

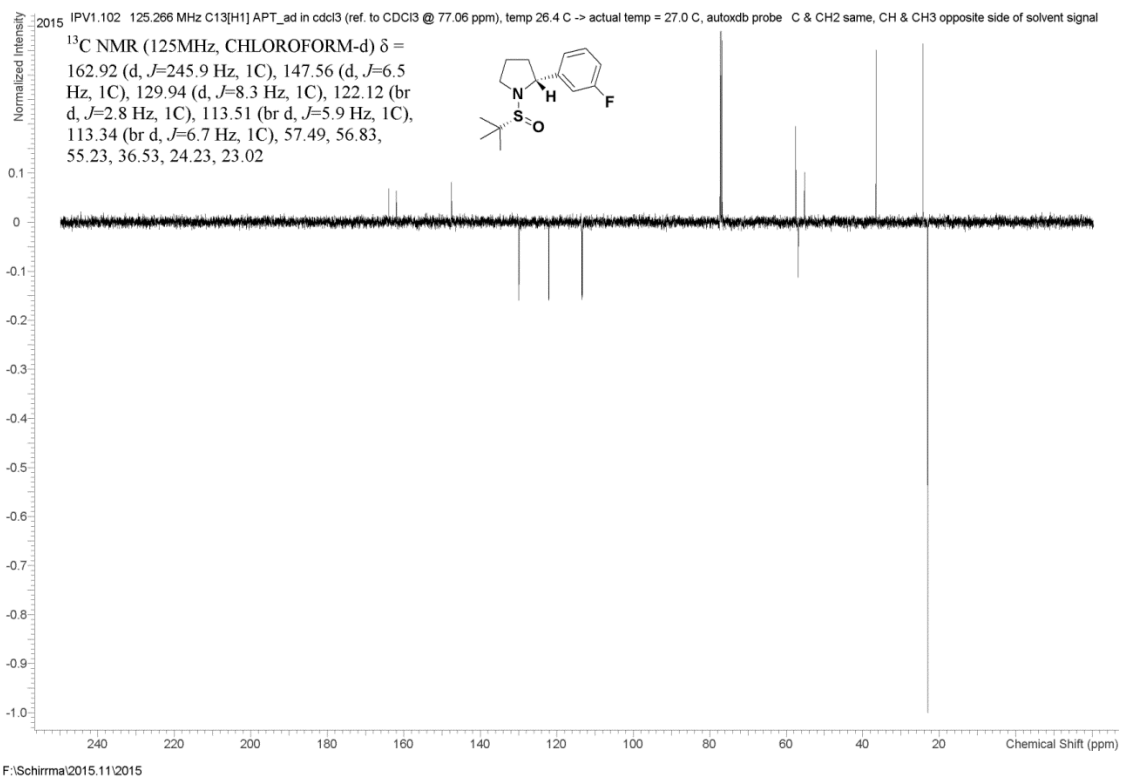
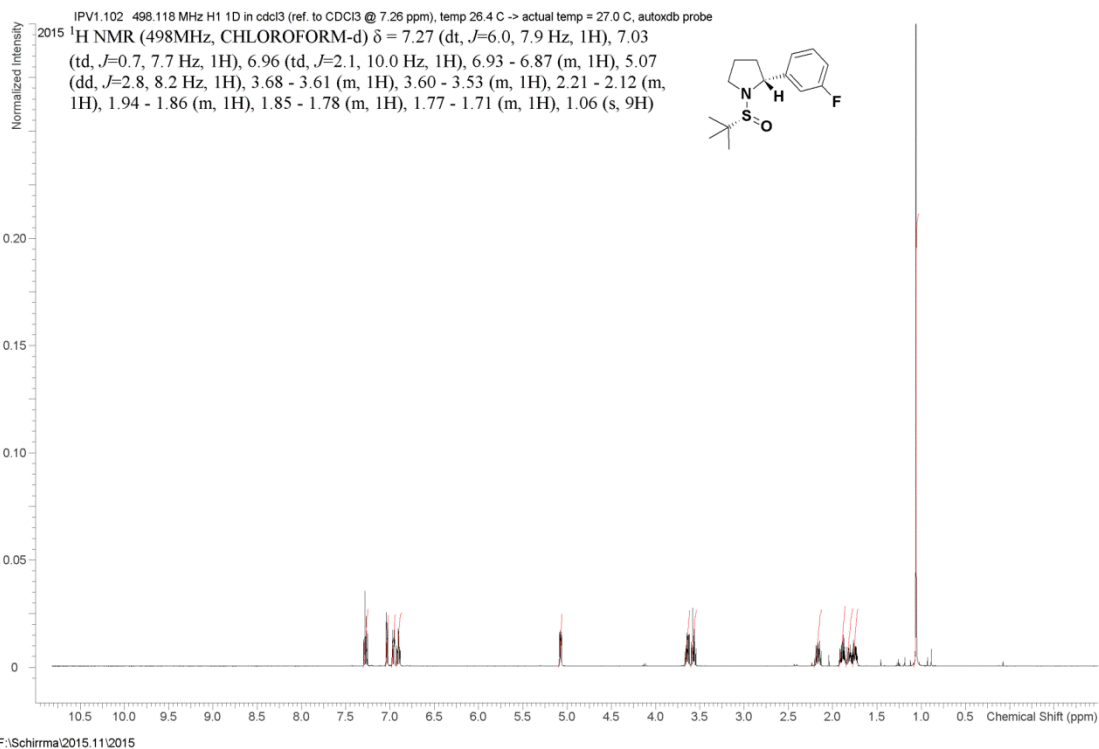


F:\Schirma\2015.11\2015

^1H NMR and ^{13}C NMR for compound (*R,S*)-**5.9**



^1H NMR and ^{13}C NMR for compound (*R*_S-*R*)-5.10

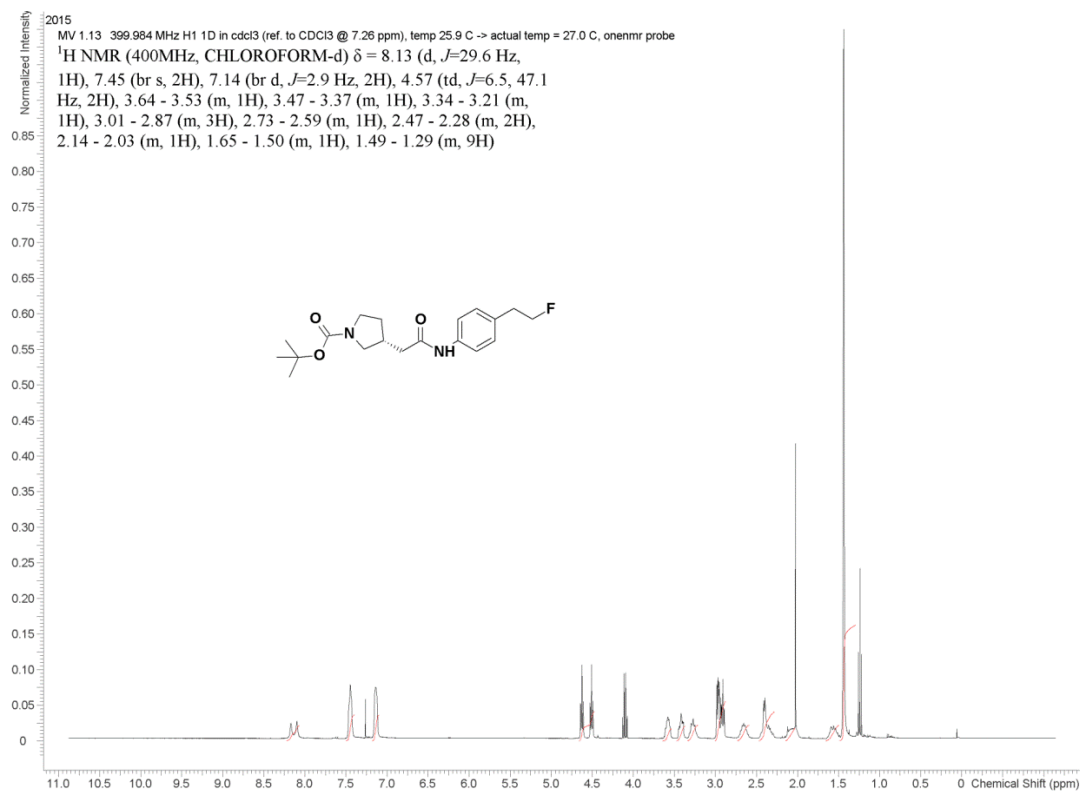


Annex 5

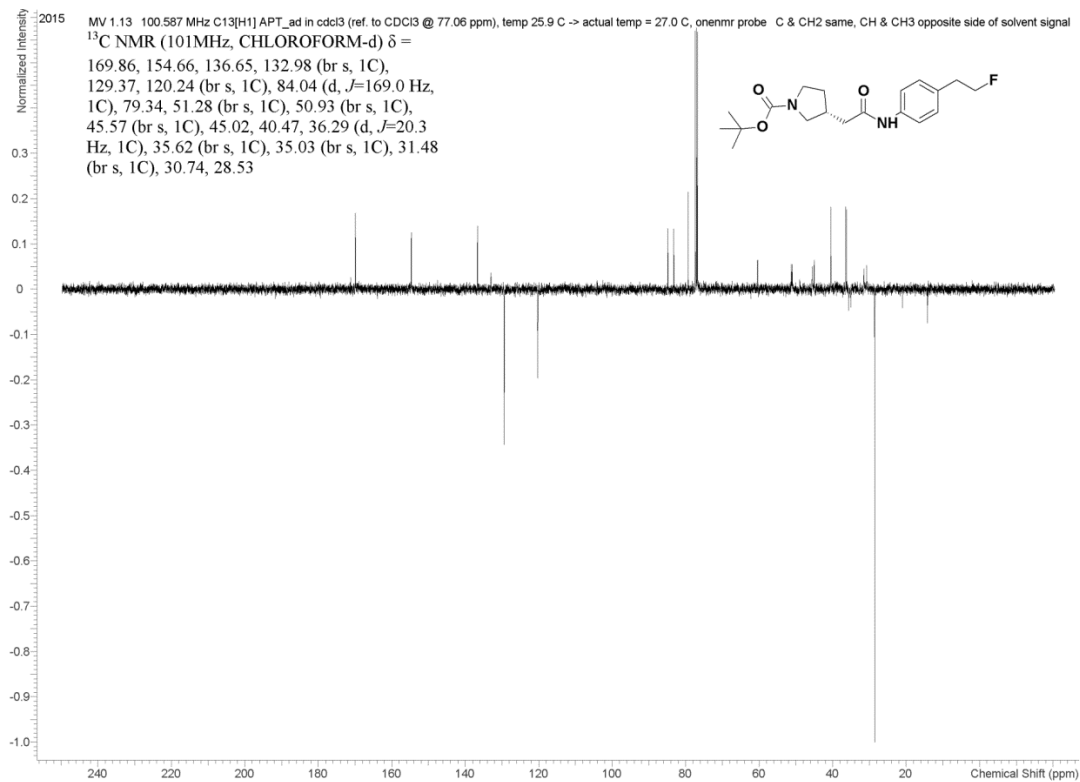
Additional Experimental Data (NMR Spectrum from Supporting Information Section 5 - Chapter 6)

*The data from this Annex are included in Supporting Information of: **Bernard-Gauthier, V.**; Vesnaver, M.; Mahringer, A.; Fricker, G. & Schirmacher, R. Development of [¹⁸F]QMICF as a Potential Radiotracer for Tropomyosin Receptor Kinases Oncological PET Imaging. In preparation for *Bioorganic & Medicinal Chemistry Letters*.*

¹H NMR and ¹³C NMR for compound 6.8

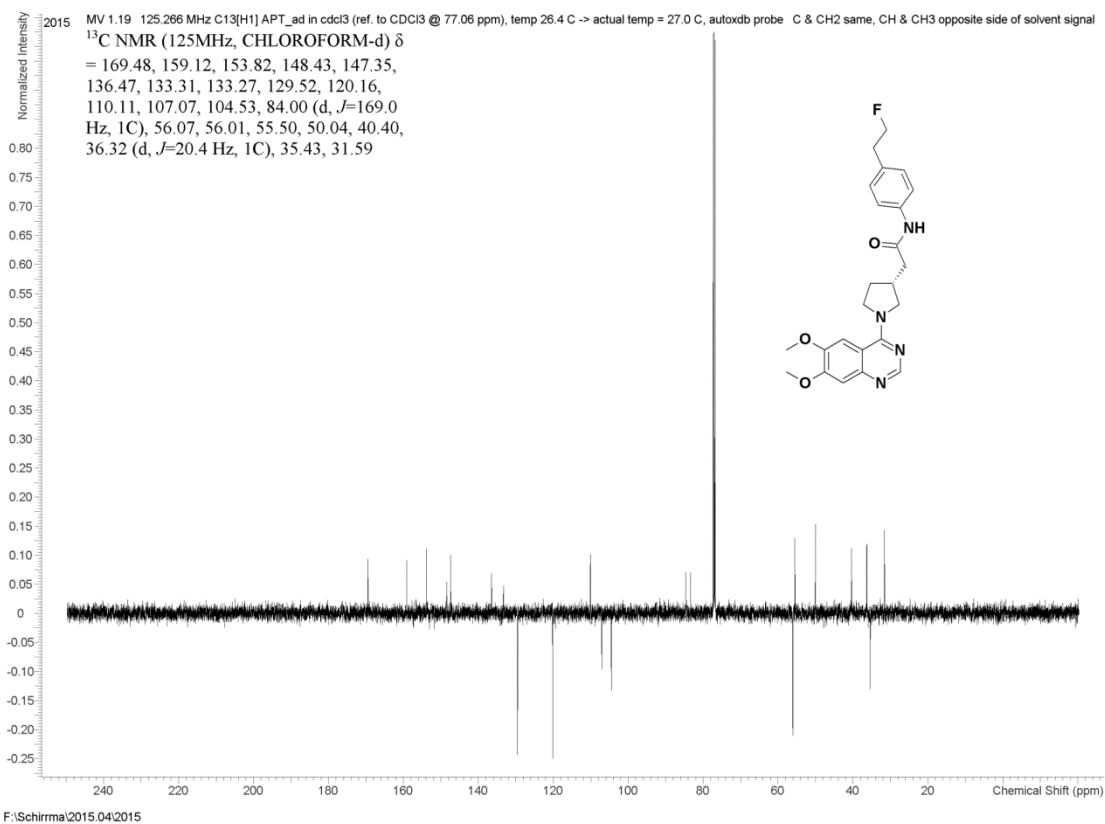
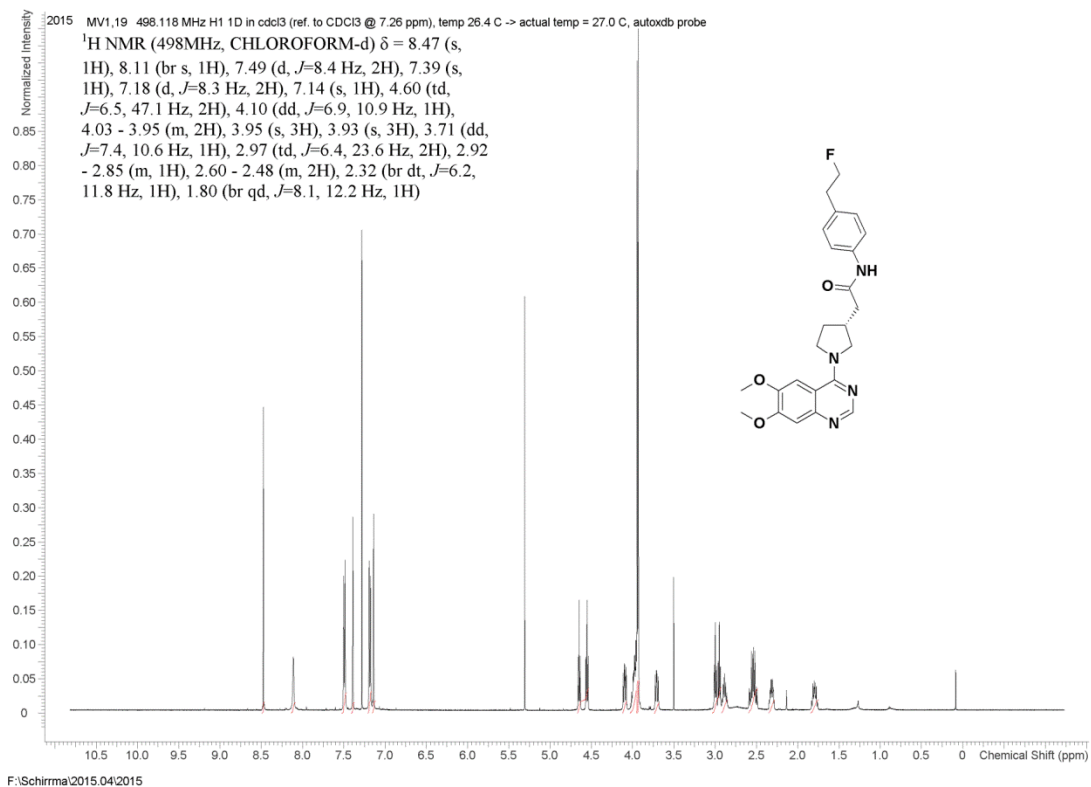


F:\Schirma\2015.03\2015

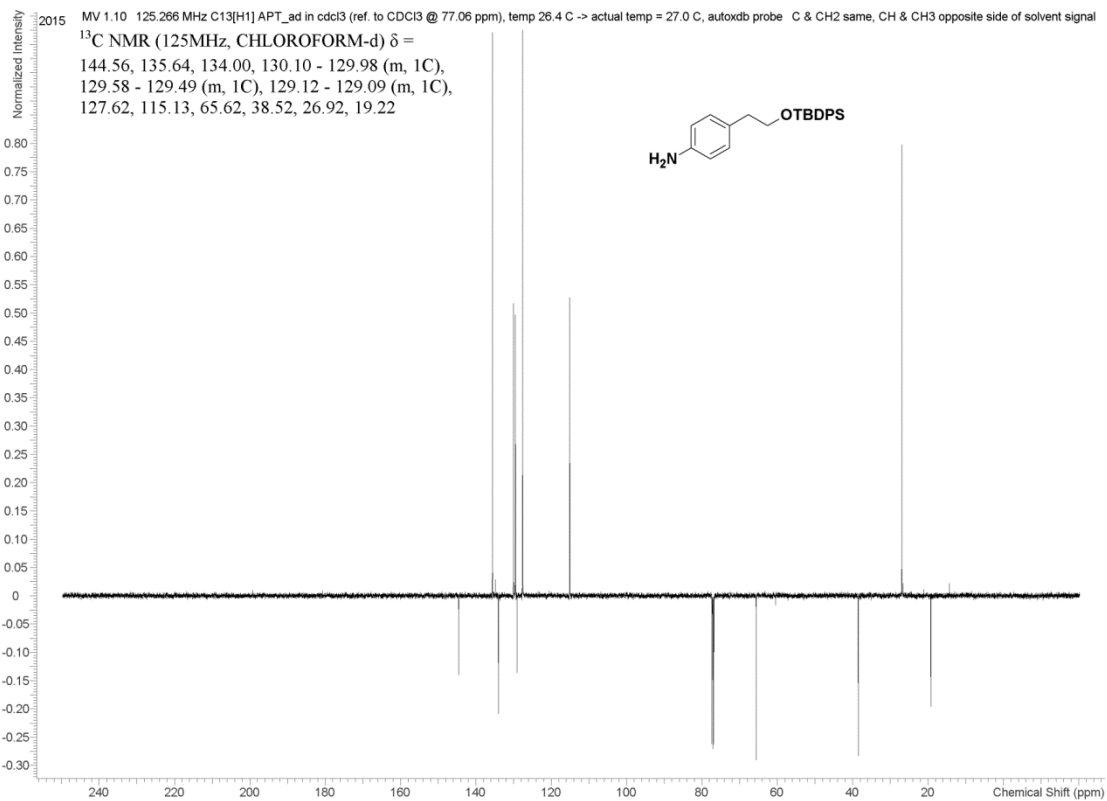
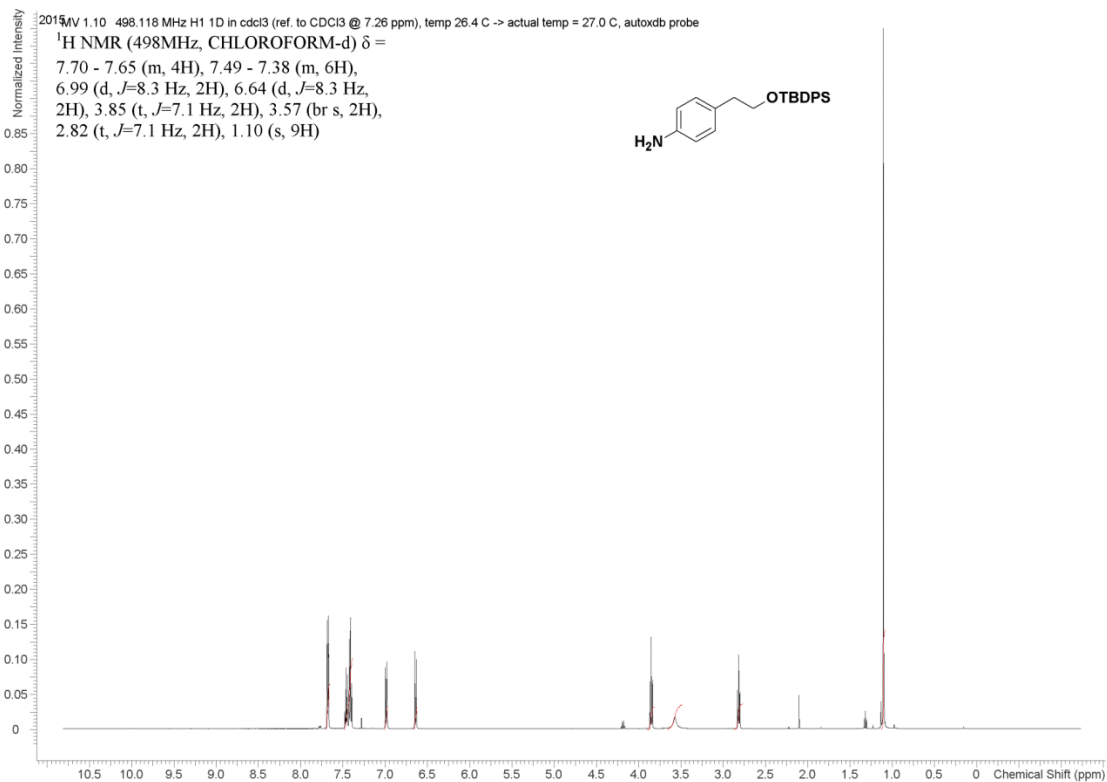


F:\Schirma\2015.03\2015

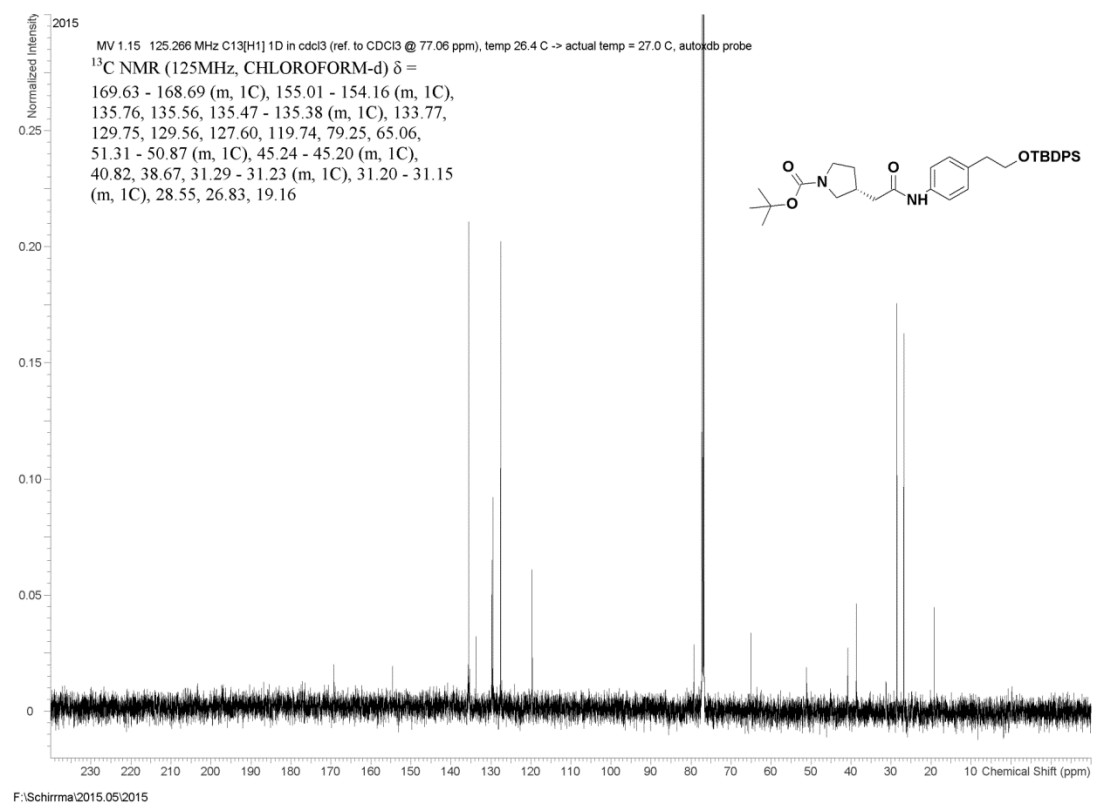
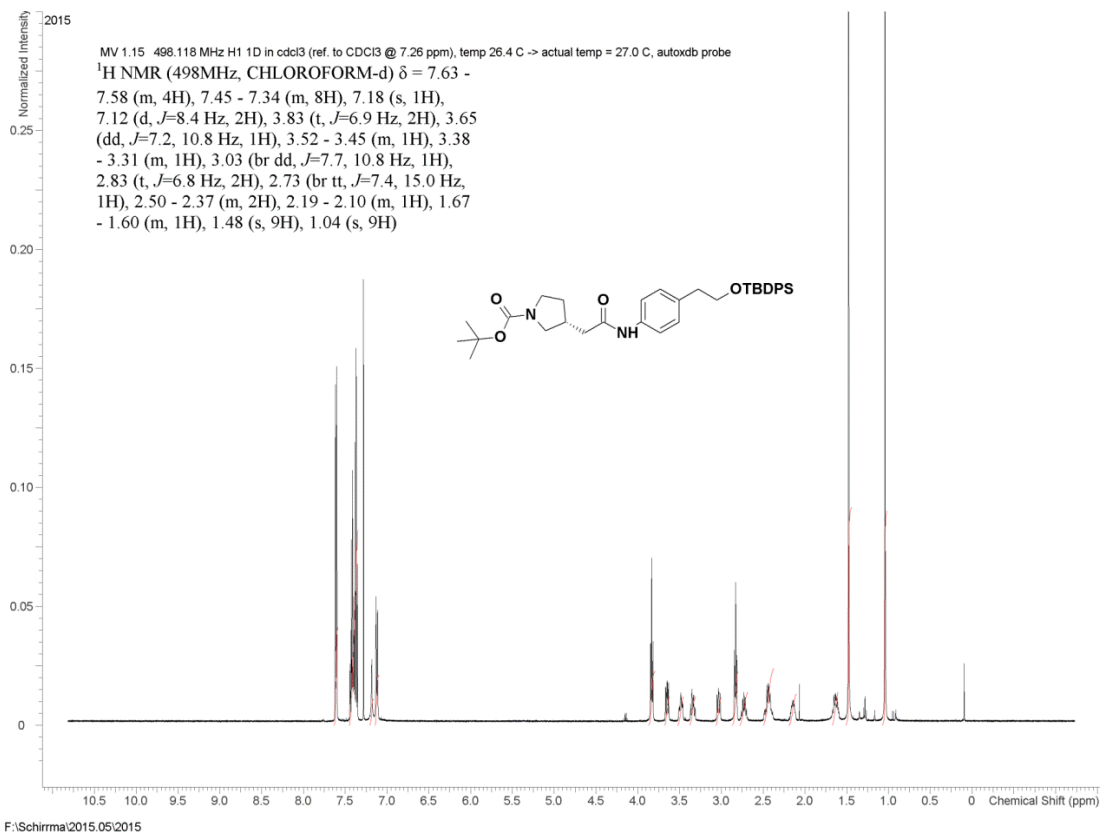
¹H NMR and ¹³C NMR for compound 6.9



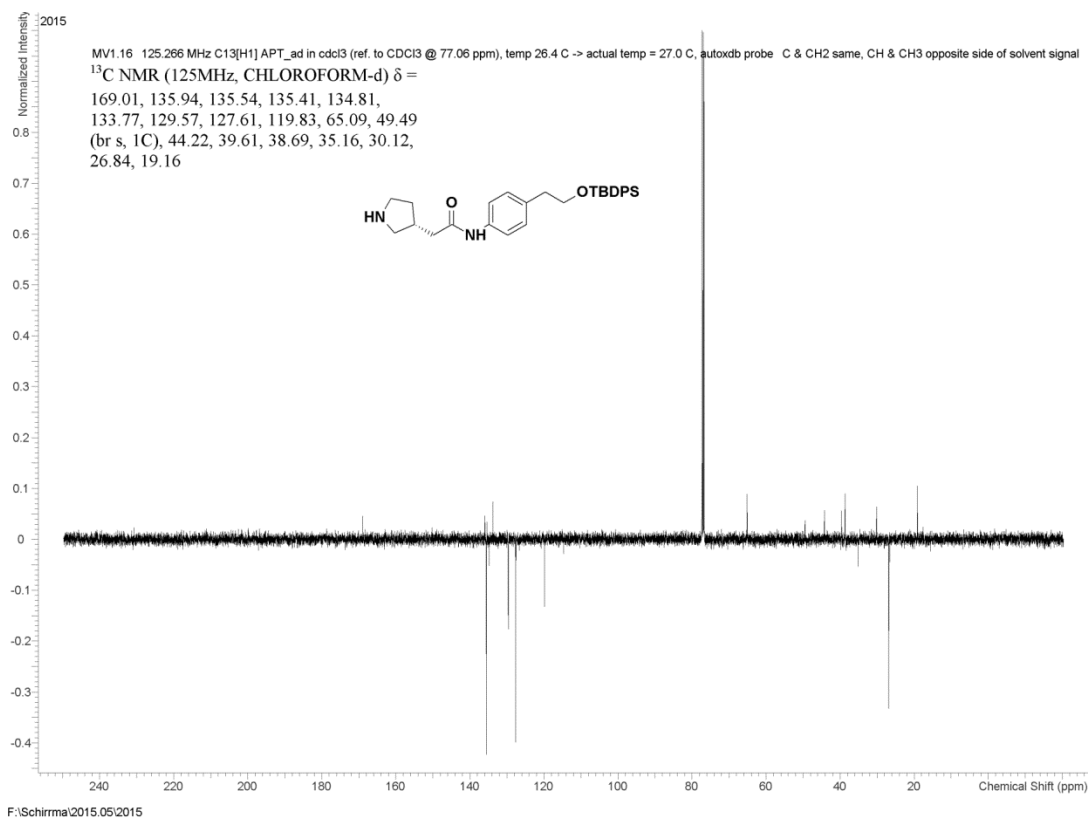
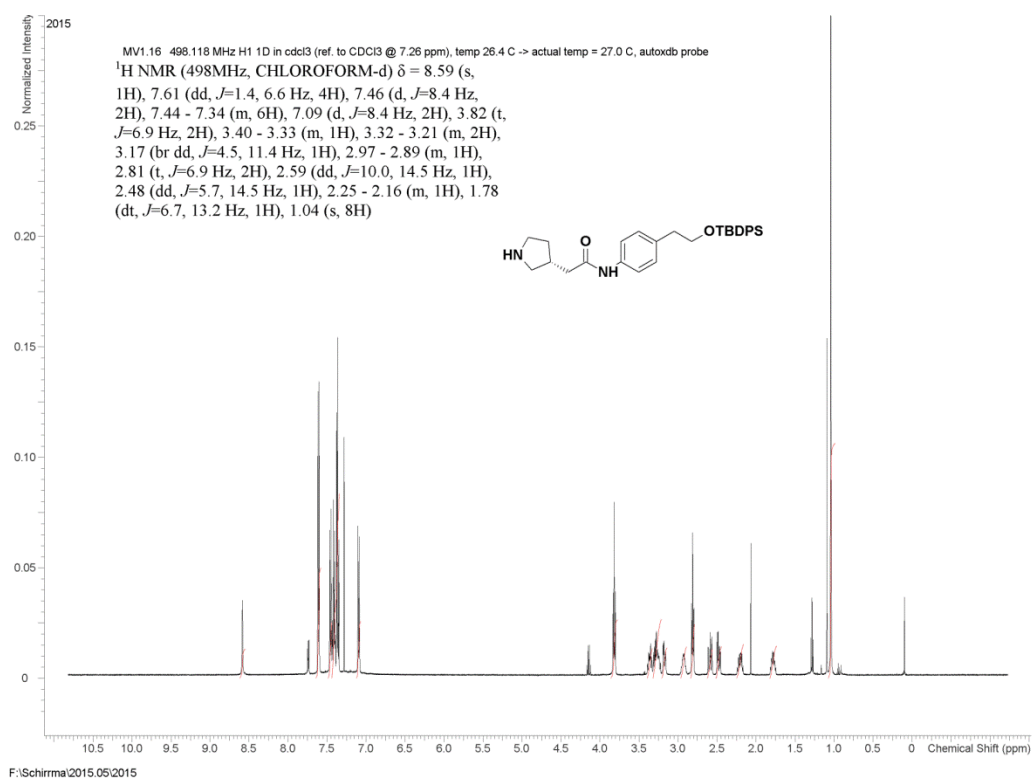
¹H NMR and ¹³C NMR for compound 6.11



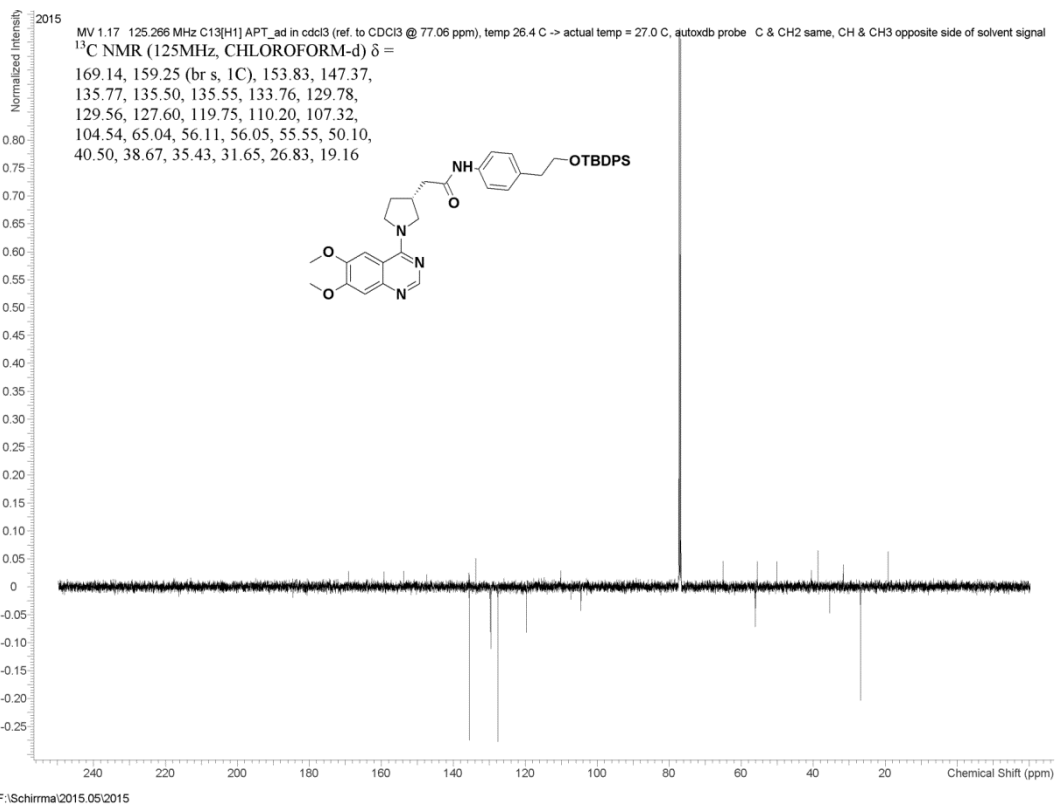
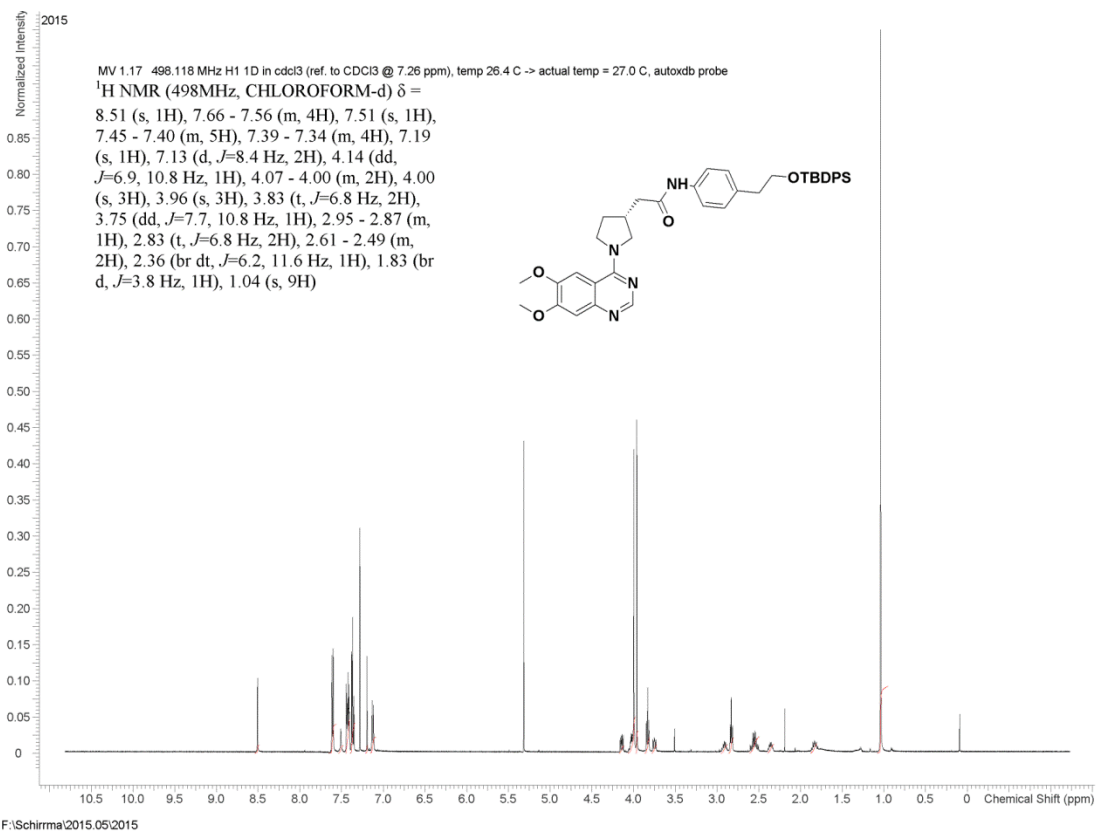
¹H NMR and ¹³C NMR for compound 6.12



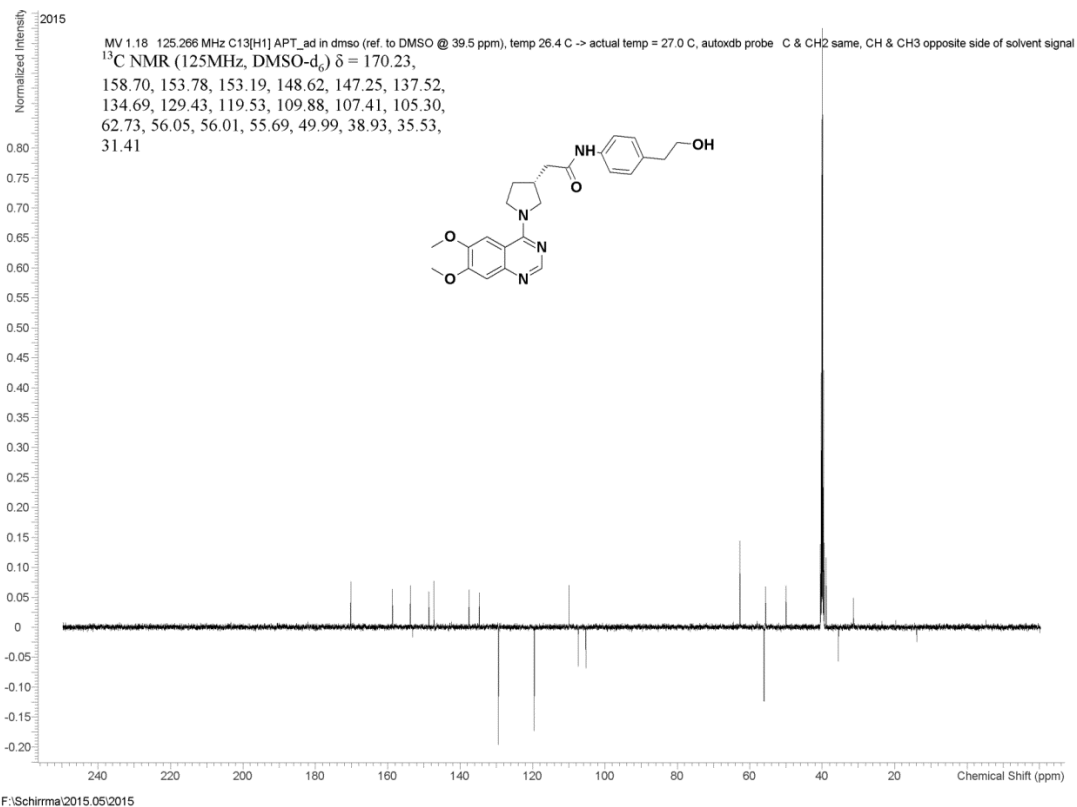
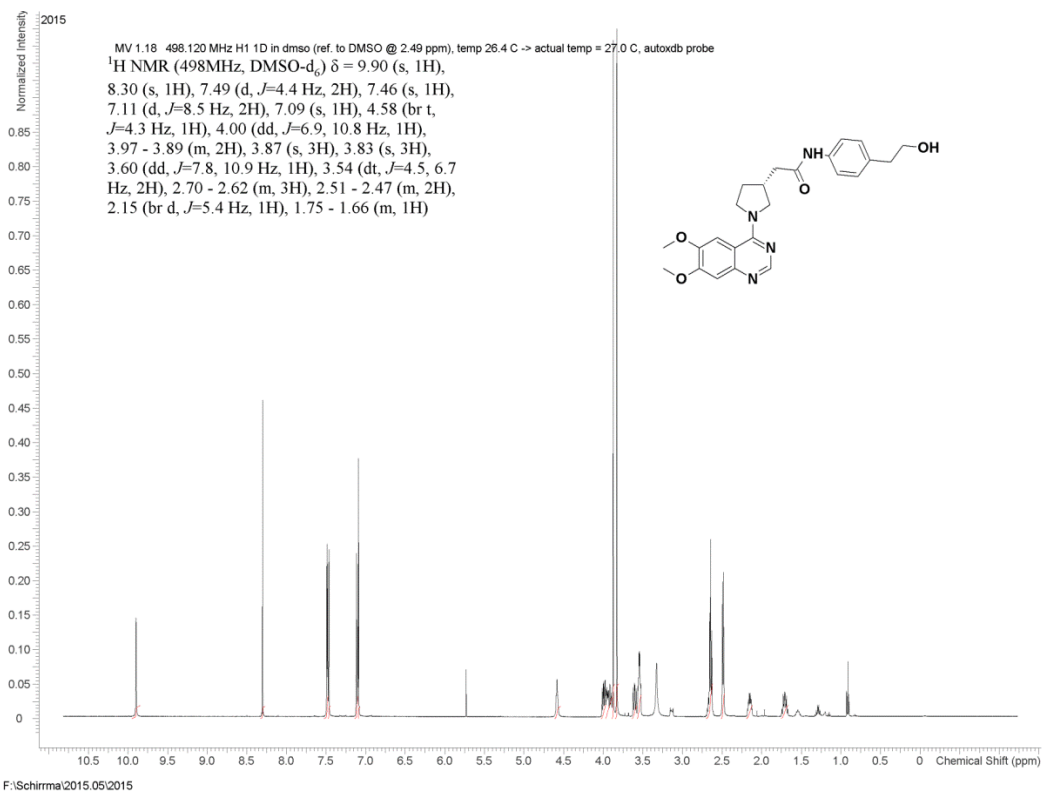
^1H NMR and ^{13}C NMR for compound 6.13



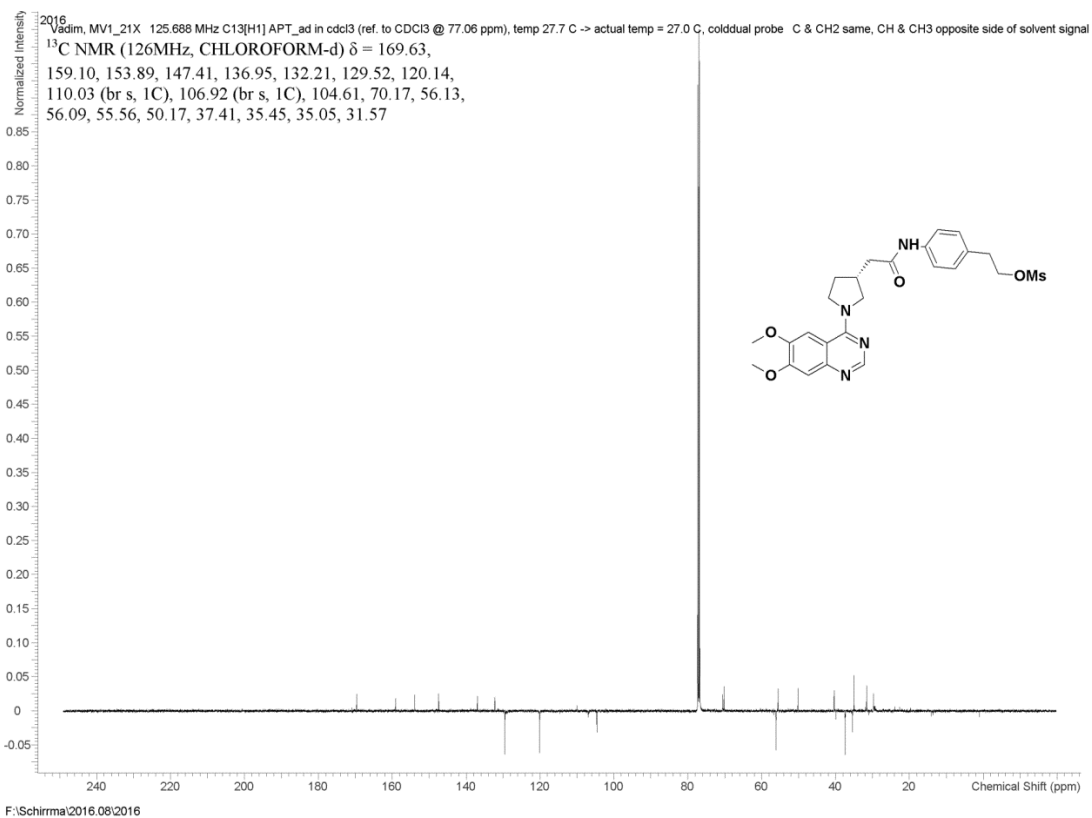
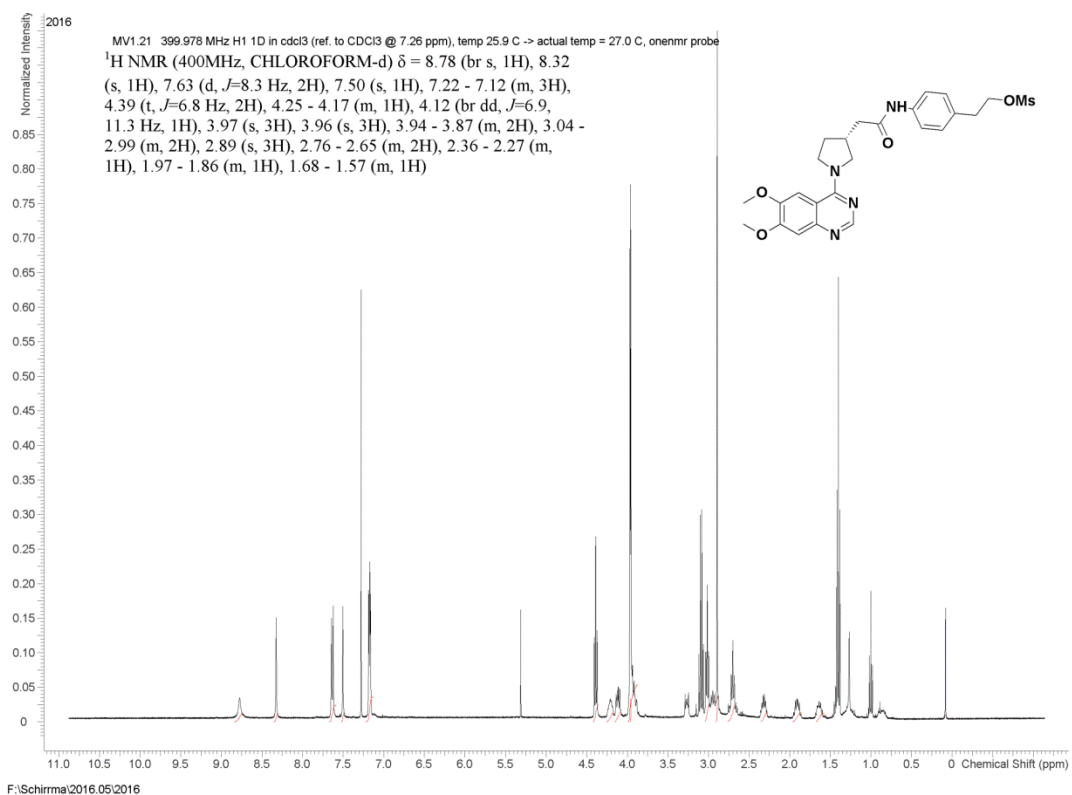
¹H NMR and ¹³C NMR for compound 6.14



¹H NMR and ¹³C NMR for compound 6.15



^1H NMR and ^{13}C NMR for compound **6.16**



Additional Experimental Data (NMR Spectrum and Crystallographic Data for Compound (2S,4S)-7.6 - Chapter 7)

STRUCTURE REPORT

XCL Code: UNI1405 **Date:** 12 December 2014

Compound: *t*-Butyl (2*S*,4*S*)-4-fluoro-2-(3-fluorophenyl)pyrrolidine-1-carboxylate

Formula: C₁₅H₁₉F₂NO₂

Client: Prof. R. Schirmacher, Department of Oncology

Crystallographer: R. McDonald

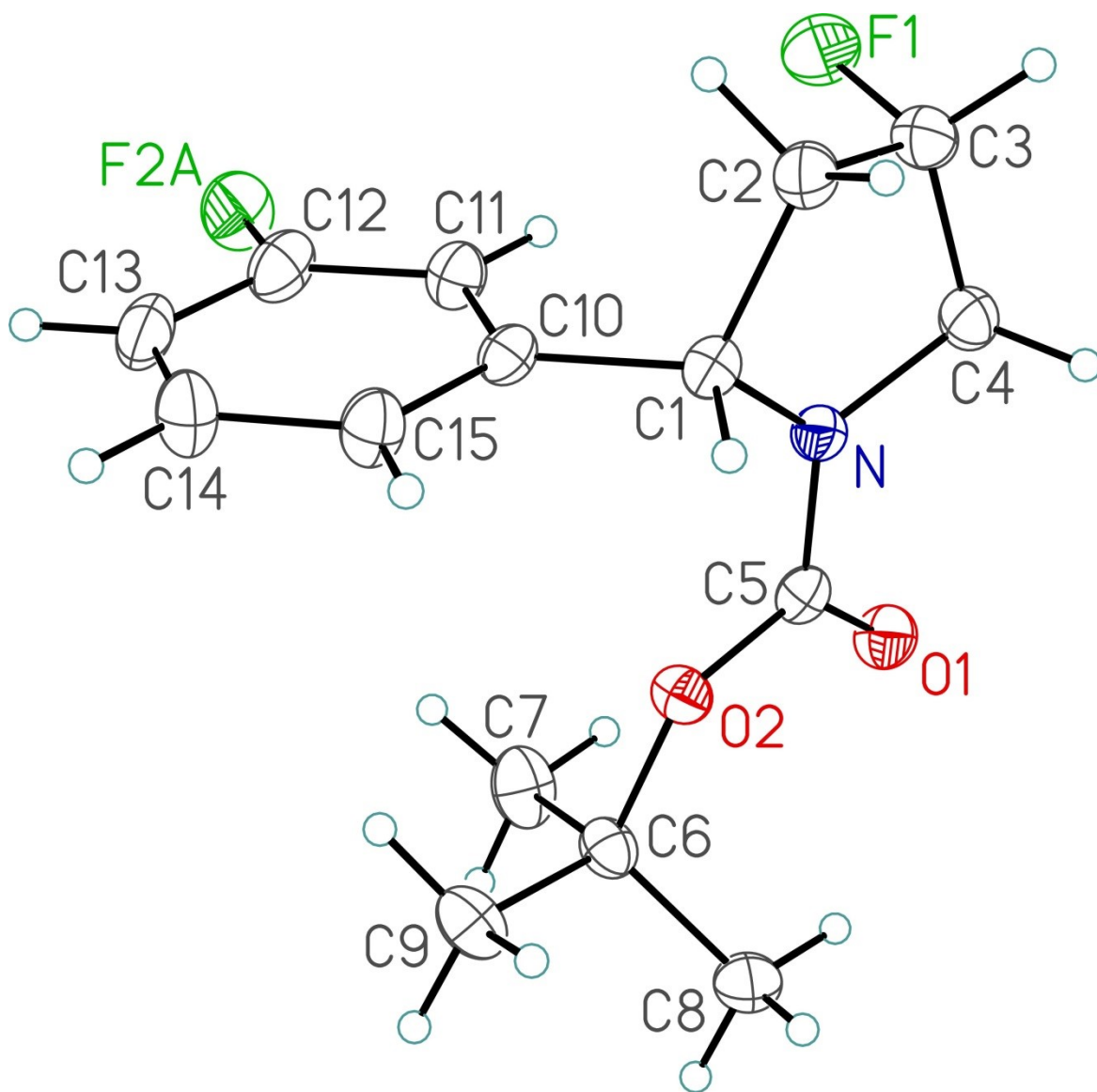


Figure 1. Perspective view of the *t*-butyl (2*S*,4*S*)-4-fluoro-2-(3-fluorophenyl)pyrrolidine-1-carboxylate molecule showing the atom labelling scheme. Non-hydrogen atoms are represented by Gaussian ellipsoids at the 30% probability level. Hydrogen atoms are shown with arbitrarily small thermal parameters.

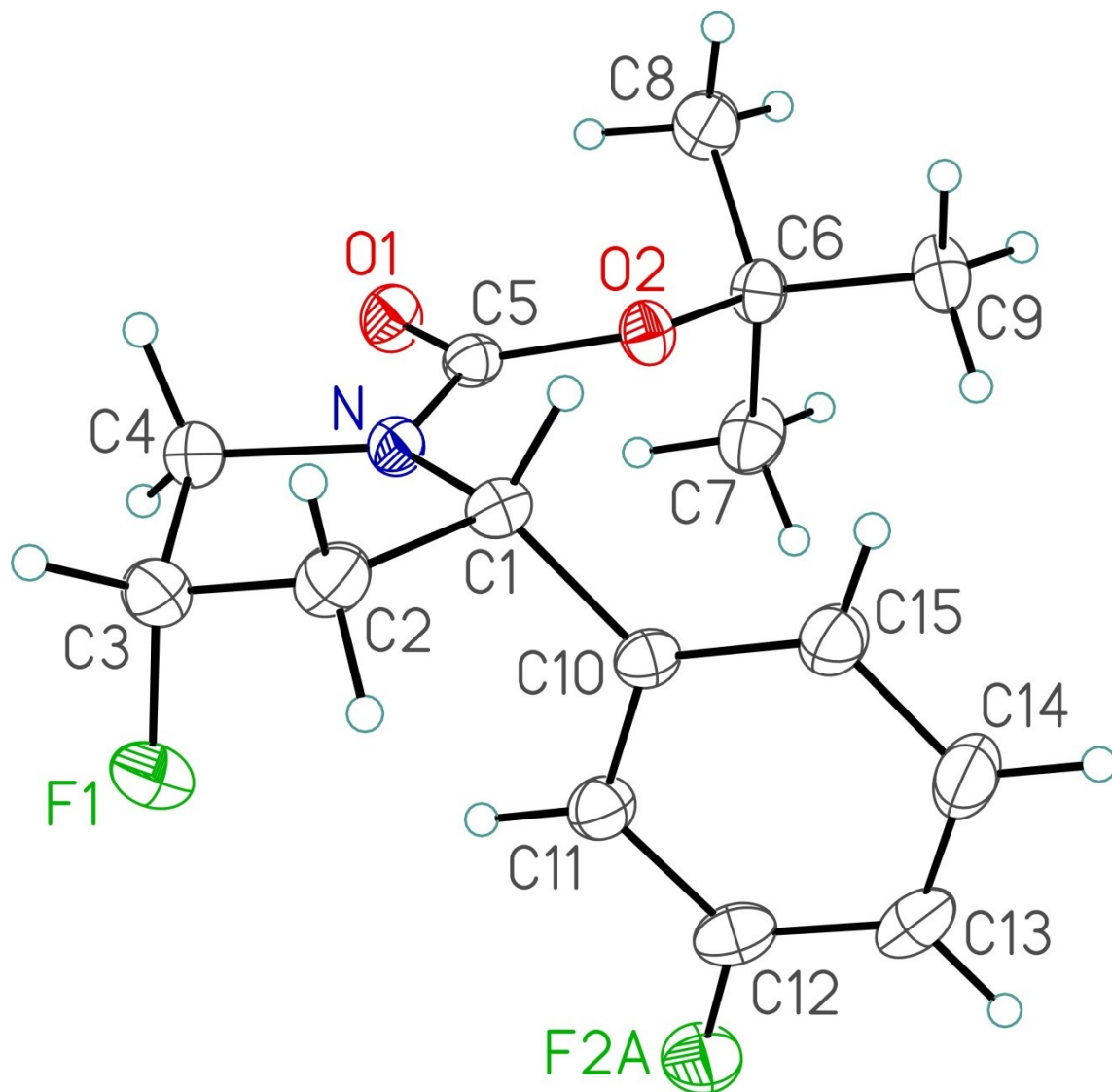


Figure 2. Alternate view of the molecule.

List of Tables

Table 1. Crystallographic Experimental Details

Table 2. Atomic Coordinates and Equivalent Isotropic Displacement Parameters

Table 3. Selected Interatomic Distances

Table 4. Selected Interatomic Angles

Table 5. Torsional Angles

Table 6. Anisotropic Displacement Parameters

Table 7. Derived Atomic Coordinates and Displacement Parameters for Hydrogen Atoms

Table 1. Crystallographic Experimental Details*A. Crystal Data*

| | |
|---|--|
| formula | C ₁₅ H ₁₉ F ₂ NO ₂ |
| formula weight | 283.31 |
| crystal dimensions (mm) | 0.45 × 0.08 × 0.06 |
| crystal system | orthorhombic |
| space group | <i>P</i> 2 ₁ 2 ₁ 2 ₁ (No. 19) |
| unit cell parameters ^a | |
| <i>a</i> (Å) | 6.1009 (2) |
| <i>b</i> (Å) | 12.8503 (3) |
| <i>c</i> (Å) | 18.4701 (5) |
| <i>V</i> (Å ³) | 1448.03 (7) |
| <i>Z</i> | 4 |
| ρ_{calcd} (g cm ⁻³) | 1.300 |
| μ (mm ⁻¹) | 0.867 |

B. Data Collection and Refinement Conditions

| | |
|--|---|
| diffractometer | Bruker D8/APEX II CCD ^b |
| radiation (λ [Å]) | Cu K α (1.54178) (microfocus source) |
| temperature (°C) | -100 |
| scan type | ω and ϕ scans (1.0°) (5 s exposures) |
| data collection 2θ limit (deg) | 145.82 |
| total data collected | 9912 ($-7 \leq h \leq 7$, $-15 \leq k \leq 15$, $-22 \leq l \leq 21$) |
| independent reflections | 2868 ($R_{\text{int}} = 0.0573$) |
| number of observed reflections (<i>NO</i>) | 2557 [$F_o^2 \geq 2\sigma(F_o^2)$] |
| structure solution method | direct methods/dual space (<i>SHELXD</i> ^c) |

| | |
|---|--|
| refinement method | full-matrix least-squares on F^2 (SHELXL-2013 ^d) |
| absorption correction method | Gaussian integration (face-indexed) |
| range of transmission factors | 1.0000–0.6356 |
| data/restraints/parameters | 2868 / 0 / 190 |
| Flack absolute structure parameter ^e | -0.18(11) |
| goodness-of-fit (S) ^f [all data] | 1.000 |
| final R indices ^g | |
| R_1 [$F_o^2 \geq 2\sigma(F_o^2)$] | 0.0455 |
| wR_2 [all data] | 0.1282 |
| largest difference peak and hole | 0.285 and -0.241 e Å ⁻³ |

^aObtained from least-squares refinement of 9547 reflections with $8.38^\circ < 2\theta < 142.30^\circ$.

^bPrograms for diffractometer operation, data collection, data reduction and absorption correction were those supplied by Bruker.

(continued)

Table 1. Crystallographic Experimental Details (continued)

^cSchneider, T. R.; Sheldrick, G. M. *Acta Crystallogr.* **2002**, *D58*, 1772-1779.

^dSheldrick, G. M. *Acta Crystallogr.* **2008**, *A64*, 112–122.

^eFlack, H. D. *Acta Crystallogr.* **1983**, *A39*, 876–881; Flack, H. D.; Bernardinelli, G. *Acta Crystallogr.* **1999**, *A55*, 908–915; Flack, H. D.; Bernardinelli, G. *J. Appl. Cryst.* **2000**, *33*, 1143–1148. The Flack parameter will refine to a value near zero if the structure is in the correct configuration and will refine to a value near one for the inverted configuration. The low anomalous scattering power of the atoms in this structure (none heavier than oxygen) implies that the data alone cannot be used for absolute structure assignment. The absolute structure of the compound is established from the known stereochemistry of the precursor compounds.

$$fS = [\sum w(F_o^2 - F_c^2)^2 / (n - p)]^{1/2} \quad (n = \text{number of data}; p = \text{number of parameters varied}; w = [\sigma^2(F_o^2) + (0.0897P)^2]^{-1} \text{ where } P = [\text{Max}(F_o^2, 0) + 2F_c^2]/3).$$

$$gR_1 = \sum ||F_o| - |F_c|| / \sum |F_o|; wR_2 = [\sum w(F_o^2 - F_c^2)^2 / \sum w(F_o^4)]^{1/2}.$$

Table 2. Atomic Coordinates and Equivalent Isotropic Displacement Parameters

| Atom | x | y | z | U_{eq} , Å ² |
|------------------|------------|--------------|-------------|---------------------------|
| F1 | -0.1074(4) | -0.02534(14) | 0.61218(11) | 0.0664(6)* |
| F2A ^a | 0.0102(6) | -0.2797(2) | 0.42013(17) | 0.0601(8)* |
| F2B ^b | 0.6648(12) | -0.1558(5) | 0.3480(5) | 0.088(2)* |
| O1 | -0.2181(3) | 0.18873(15) | 0.41240(11) | 0.0423(4)* |
| O2 | 0.1228(3) | 0.13726(14) | 0.37546(9) | 0.0332(4)* |
| N | 0.0240(4) | 0.11276(15) | 0.48946(11) | 0.0330(5)* |
| C1 | 0.2375(4) | 0.06515(18) | 0.50433(13) | 0.0331(5)* |
| C2 | 0.2360(5) | 0.0540(2) | 0.58761(15) | 0.0447(6)* |
| C3 | 0.0048(6) | 0.0712(2) | 0.61204(15) | 0.0457(7)* |
| C4 | -0.0987(5) | 0.1387(2) | 0.55491(14) | 0.0399(6)* |
| C5 | -0.0391(4) | 0.14949(18) | 0.42382(14) | 0.0312(5)* |
| C6 | 0.0820(4) | 0.1444(2) | 0.29745(13) | 0.0354(5)* |
| C7 | -0.0770(5) | 0.0602(3) | 0.27514(19) | 0.0537(8)* |
| C8 | 0.0036(6) | 0.2526(2) | 0.27664(16) | 0.0492(7)* |
| C9 | 0.3094(5) | 0.1245(3) | 0.26621(16) | 0.0484(7)* |
| C10 | 0.2729(4) | -0.03690(17) | 0.46364(13) | 0.0325(5)* |
| C11 | 0.1160(5) | -0.1148(2) | 0.46332(16) | 0.0408(6)* |
| C12 | 0.1590(5) | -0.2066(2) | 0.42675(17) | 0.0474(7)* |
| C13 | 0.3522(6) | -0.2225(2) | 0.39037(18) | 0.0505(8)* |
| C14 | 0.5049(6) | -0.1446(3) | 0.39134(19) | 0.0563(8)* |
| C15 | 0.4681(5) | -0.0518(2) | 0.42745(17) | 0.0450(6)* |

Anisotropically-refined atoms are marked with an asterisk (*). The form of the anisotropic displacement parameter is: $\exp[-2\pi^2(h^2a^{*2}U_{11} + k^2b^{*2}U_{22} + l^2c^{*2}U_{33} + 2klb^{*c^*}U_{23} + 2hla^{*c^*}U_{13} + 2hka^{*b^*}U_{12})]$. ^aRefined with an occupancy factor of 0.65. ^bRefined with an occupancy factor of 0.35.

Table 3. Selected Interatomic Distances (Å)

| Atom1 | Atom2 | Distance | Atom1 | Atom2 | Distance |
|-------|-------|----------|-------|-------|----------|
| F1 | C3 | 1.418(3) | C2 | C3 | 1.498(5) |
| F2A | C12 | 1.312(4) | C3 | C4 | 1.505(4) |
| F2B | C14 | 1.270(7) | C6 | C7 | 1.511(4) |
| O1 | C5 | 1.221(3) | C6 | C8 | 1.520(4) |
| O2 | C5 | 1.341(3) | C6 | C9 | 1.525(4) |
| O2 | C6 | 1.465(3) | C10 | C11 | 1.385(4) |
| N | C1 | 1.465(3) | C10 | C15 | 1.379(4) |
| N | C4 | 1.460(3) | C11 | C12 | 1.384(4) |
| N | C5 | 1.357(3) | C12 | C13 | 1.372(5) |
| C1 | C2 | 1.545(4) | C13 | C14 | 1.368(5) |
| C1 | C10 | 1.527(3) | C14 | C15 | 1.385(4) |

Table 4. Selected Interatomic Angles (deg)

| Atom1 | Atom2 | Atom3 | Angle | Atom1 | Atom2 | Atom3 | Angle |
|-------|-------|-------|------------|-------|-------|-------|----------|
| C5 | O2 | C6 | 121.49(18) | O2 | C6 | C9 | 101.9(2) |
| C1 | N | C4 | 113.3(2) | C7 | C6 | C8 | 112.6(3) |
| C1 | N | C5 | 124.4(2) | C7 | C6 | C9 | 111.1(2) |
| C4 | N | C5 | 121.0(2) | C8 | C6 | C9 | 110.1(3) |
| N | C1 | C2 | 102.7(2) | C1 | C10 | C11 | 121.7(2) |
| N | C1 | C10 | 113.1(2) | C1 | C10 | C15 | 118.7(2) |
| C2 | C1 | C10 | 114.3(2) | C11 | C10 | C15 | 119.6(2) |
| C1 | C2 | C3 | 106.9(2) | C10 | C11 | C12 | 119.2(3) |
| F1 | C3 | C2 | 109.0(2) | F2A | C12 | C11 | 121.6(3) |
| F1 | C3 | C4 | 107.6(3) | F2A | C12 | C13 | 116.2(3) |
| C2 | C3 | C4 | 105.6(2) | C11 | C12 | C13 | 121.9(3) |
| N | C4 | C3 | 103.5(2) | C12 | C13 | C14 | 118.0(3) |
| O1 | C5 | O2 | 126.3(2) | F2B | C14 | C13 | 115.6(4) |
| O1 | C5 | N | 123.5(2) | F2B | C14 | C15 | 121.7(4) |
| O2 | C5 | N | 110.2(2) | C13 | C14 | C15 | 121.8(3) |
| O2 | C6 | C7 | 109.4(2) | C10 | C15 | C14 | 119.5(3) |
| O2 | C6 | C8 | 111.1(2) | | | | |

Table 5. Torsional Angles (deg)

| Atom1 | Atom2 | Atom3 | Atom4 | Angle | Atom1 | Atom2 | Atom3 | Atom4 | Angle |
|-------|-------|-------|-------|-----------|-------|-------|-------|-------|-----------|
| C6 | O2 | C5 | O1 | -17.0(4) | C2 | C1 | C10 | C11 | 68.6(3) |
| C6 | O2 | C5 | N | 163.8(2) | C2 | C1 | C10 | C15 | -110.3(3) |
| C5 | O2 | C6 | C7 | -61.7(3) | C1 | C2 | C3 | F1 | 89.4(3) |
| C5 | O2 | C6 | C8 | 63.2(3) | C1 | C2 | C3 | C4 | -26.0(3) |
| C5 | O2 | C6 | C9 | -179.5(2) | F1 | C3 | C4 | N | -88.7(3) |
| C4 | N | C1 | C2 | 4.4(3) | C2 | C3 | C4 | N | 27.7(3) |
| C4 | N | C1 | C10 | 128.1(2) | C1 | C10 | C11 | C12 | -178.7(2) |
| C5 | N | C1 | C2 | 171.5(2) | C15 | C10 | C11 | C12 | 0.2(4) |
| C5 | N | C1 | C10 | -64.8(3) | C1 | C10 | C15 | C14 | 178.8(3) |
| C1 | N | C4 | C3 | -20.2(3) | C11 | C10 | C15 | C14 | -0.1(4) |
| C5 | N | C4 | C3 | 172.2(2) | C10 | C11 | C12 | F2A | -174.8(3) |
| C1 | N | C5 | O1 | 179.8(2) | C10 | C11 | C12 | C13 | -0.4(4) |
| C1 | N | C5 | O2 | -1.0(3) | F2A | C12 | C13 | C14 | 175.1(3) |
| C4 | N | C5 | O1 | -14.0(4) | C11 | C12 | C13 | C14 | 0.4(5) |
| C4 | N | C5 | O2 | 165.2(2) | C12 | C13 | C14 | F2B | -169.3(6) |
| N | C1 | C2 | C3 | 13.5(3) | C12 | C13 | C14 | C15 | -0.2(5) |
| C10 | C1 | C2 | C3 | -109.4(2) | F2B | C14 | C15 | C10 | 168.5(6) |
| N | C1 | C10 | C11 | -48.5(3) | C13 | C14 | C15 | C10 | 0.1(5) |
| N | C1 | C10 | C15 | 132.6(2) | | | | | |

Table 6. Anisotropic Displacement Parameters (U_{ij} , Å²)

| Atom | U_{11} | U_{22} | U_{33} | U_{23} | U_{13} | U_{12} |
|------|------------|------------|------------|-------------|-------------|-------------|
| F1 | 0.0910(16) | 0.0449(9) | 0.0634(12) | 0.0092(9) | 0.0194(12) | -0.0125(10) |
| F2A | 0.0697(19) | 0.0431(13) | 0.0676(18) | -0.0100(12) | 0.0072(16) | -0.0199(14) |
| F2B | 0.063(4) | 0.080(4) | 0.121(6) | -0.046(4) | 0.047(4) | 0.002(3) |
| O1 | 0.0324(9) | 0.0458(10) | 0.0488(10) | 0.0047(9) | 0.0017(8) | 0.0110(8) |
| O2 | 0.0274(8) | 0.0409(9) | 0.0312(8) | 0.0016(7) | -0.0001(7) | 0.0024(7) |
| N | 0.0337(10) | 0.0318(9) | 0.0336(10) | 0.0029(8) | 0.0042(8) | 0.0051(8) |
| C1 | 0.0331(12) | 0.0290(10) | 0.0372(12) | -0.0009(9) | -0.0031(10) | 0.0011(9) |
| C2 | 0.0574(18) | 0.0398(12) | 0.0370(12) | -0.0020(11) | -0.0068(12) | 0.0095(13) |
| C3 | 0.0581(18) | 0.0406(13) | 0.0383(13) | 0.0009(11) | 0.0052(13) | -0.0040(14) |
| C4 | 0.0397(13) | 0.0383(12) | 0.0416(14) | -0.0005(11) | 0.0085(11) | 0.0017(11) |
| C5 | 0.0278(10) | 0.0270(9) | 0.0388(12) | 0.0009(9) | -0.0008(9) | 0.0008(9) |
| C6 | 0.0347(12) | 0.0421(12) | 0.0296(11) | -0.0032(10) | -0.0021(9) | 0.0023(11) |
| C7 | 0.0444(17) | 0.0588(17) | 0.0580(18) | -0.0195(15) | -0.0038(13) | -0.0053(14) |
| C8 | 0.0622(18) | 0.0488(16) | 0.0366(14) | 0.0079(11) | -0.0012(14) | 0.0101(14) |
| C9 | 0.0407(14) | 0.0623(18) | 0.0420(14) | -0.0048(13) | 0.0086(11) | -0.0017(13) |
| C10 | 0.0301(11) | 0.0300(11) | 0.0375(12) | 0.0016(9) | -0.0050(10) | 0.0036(9) |
| C11 | 0.0391(13) | 0.0348(12) | 0.0484(14) | -0.0026(11) | 0.0005(12) | -0.0005(10) |
| C12 | 0.0535(18) | 0.0323(12) | 0.0563(17) | -0.0043(12) | -0.0118(13) | -0.0029(12) |
| C13 | 0.064(2) | 0.0351(13) | 0.0522(16) | -0.0082(12) | -0.0092(14) | 0.0147(13) |
| C14 | 0.0533(18) | 0.0540(16) | 0.0614(19) | -0.0101(15) | 0.0101(15) | 0.0141(16) |
| C15 | 0.0390(14) | 0.0393(13) | 0.0568(16) | -0.0043(12) | 0.0052(12) | 0.0018(11) |

The form of the anisotropic displacement parameter is:

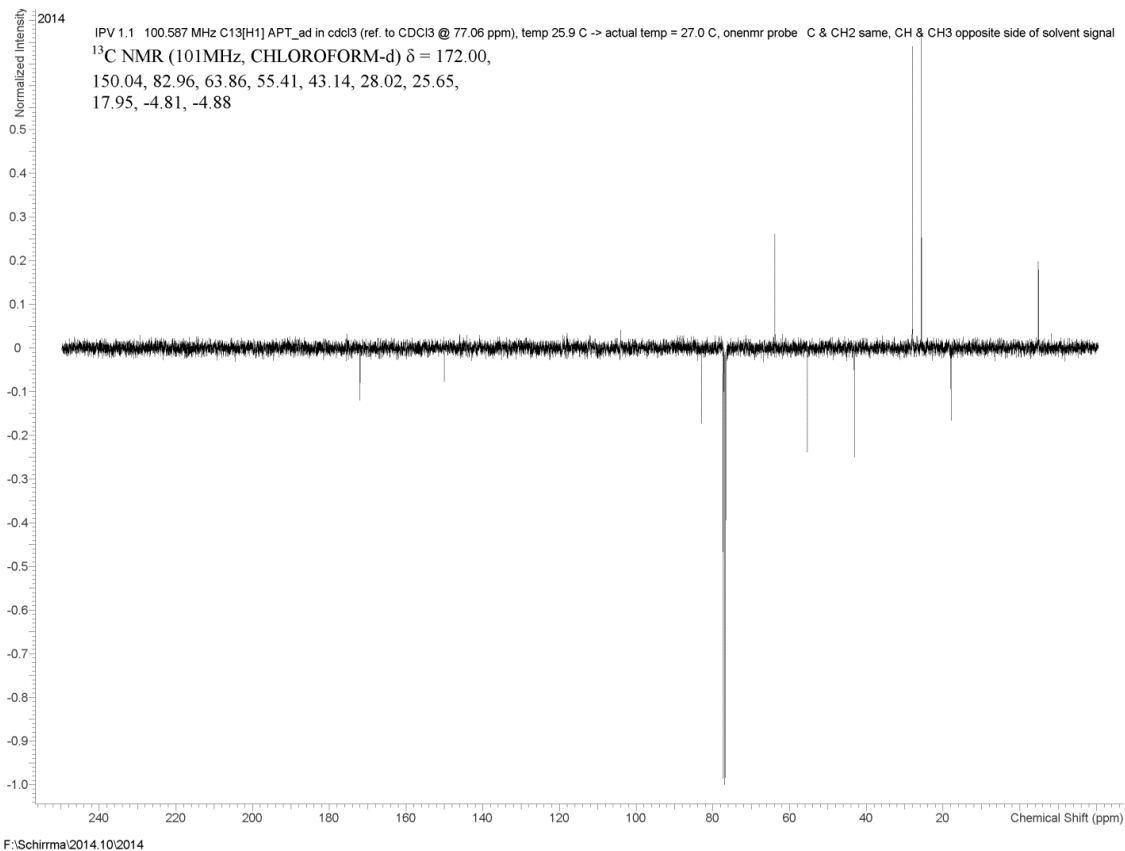
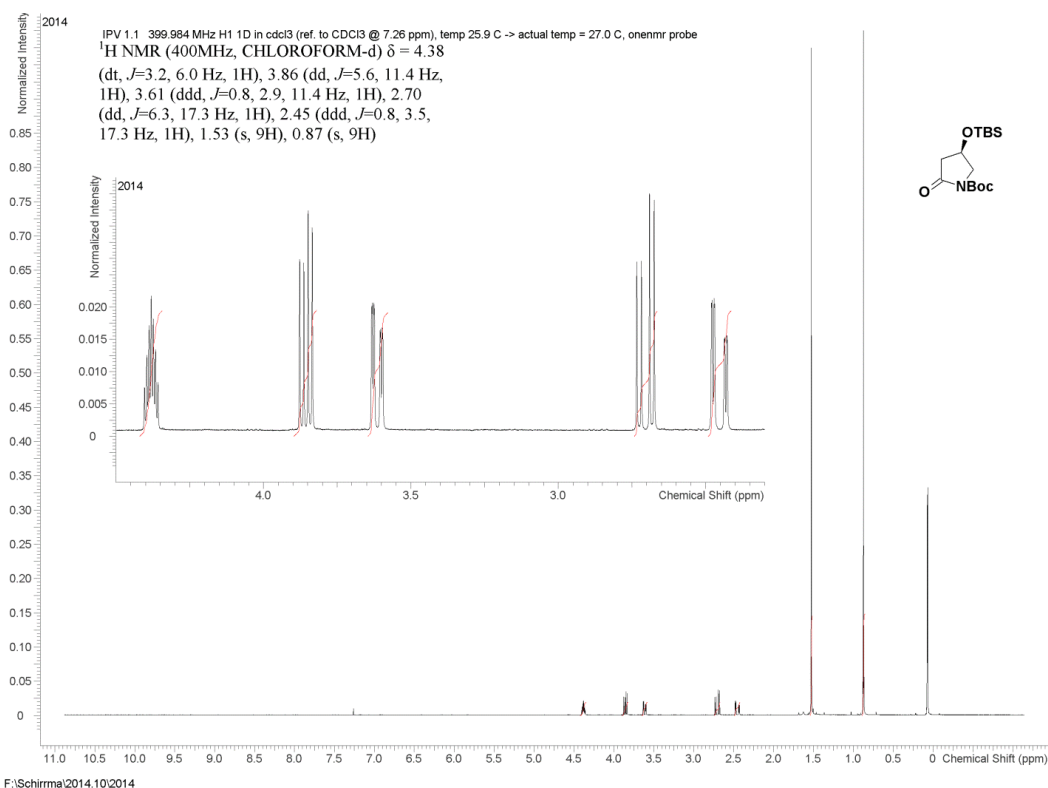
$$\exp[-2\pi^2(h^2a^2U_{11} + k^2b^2U_{22} + l^2c^2U_{33} + 2klb^*c^*U_{23} + 2hla^*c^*U_{13} + 2hka^*b^*U_{12})]$$

Table 7. Derived Atomic Coordinates and Displacement Parameters for Hydrogen Atoms

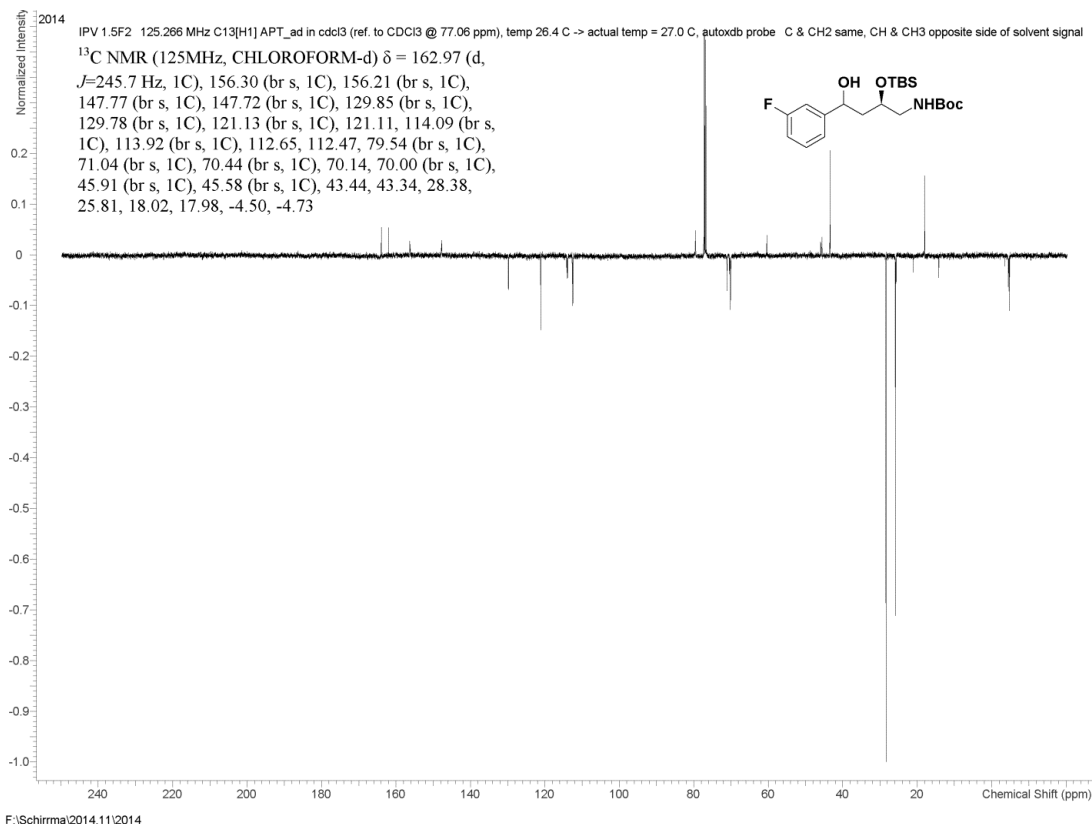
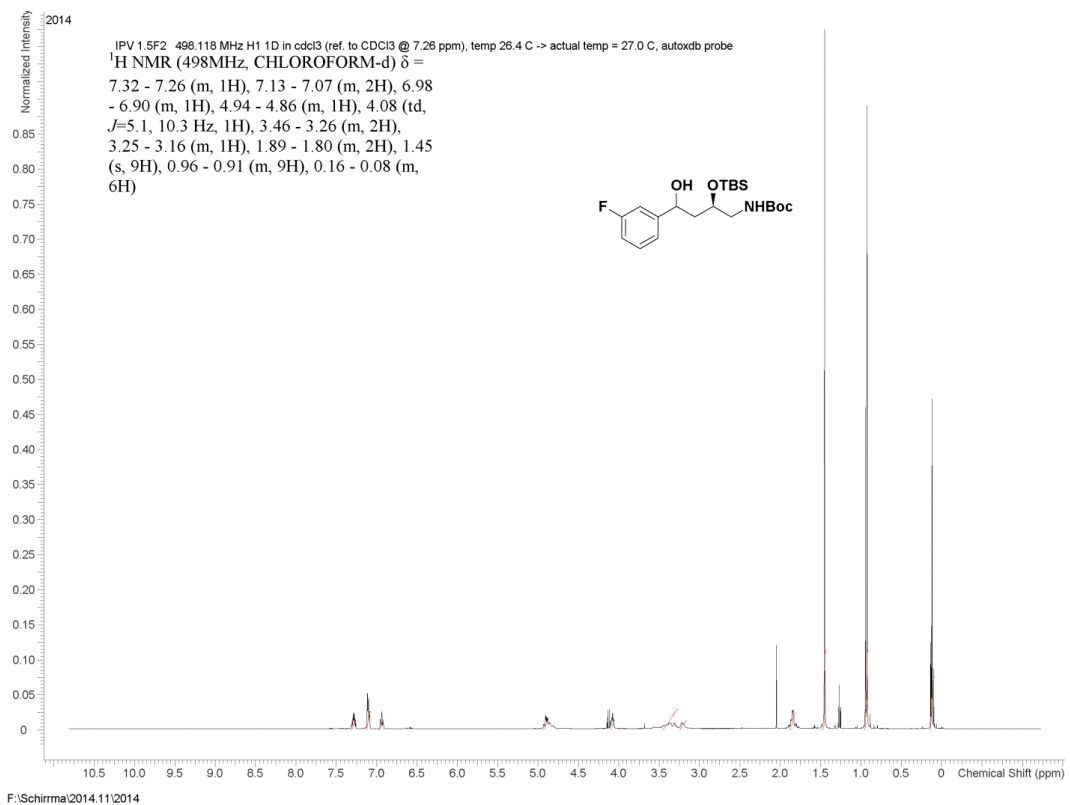
| Atom | <i>x</i> | <i>y</i> | <i>z</i> | $U_{\text{eq}}, \text{\AA}^2$ |
|-------------------|----------|----------|----------|-------------------------------|
| H1 | 0.3555 | 0.1152 | 0.4903 | 0.040 |
| H2A | 0.2863 | -0.0164 | 0.6018 | 0.054 |
| H2B | 0.3348 | 0.1061 | 0.6099 | 0.054 |
| H3 | -0.0004 | 0.1052 | 0.6607 | 0.055 |
| H4A | -0.2562 | 0.1222 | 0.5491 | 0.048 |
| H4B | -0.0830 | 0.2134 | 0.5670 | 0.048 |
| H7A | -0.1044 | 0.0649 | 0.2230 | 0.064 |
| H7B | -0.0144 | -0.0081 | 0.2865 | 0.064 |
| H7C | -0.2152 | 0.0691 | 0.3014 | 0.064 |
| H8A | -0.0225 | 0.2554 | 0.2243 | 0.059 |
| H8B | -0.1329 | 0.2684 | 0.3024 | 0.059 |
| H8C | 0.1156 | 0.3039 | 0.2898 | 0.059 |
| H9A | 0.3027 | 0.1274 | 0.2132 | 0.058 |
| H9B | 0.4113 | 0.1777 | 0.2839 | 0.058 |
| H9C | 0.3606 | 0.0556 | 0.2814 | 0.058 |
| H11 | -0.0193 | -0.1054 | 0.4879 | 0.049 |
| H12B ^a | 0.0516 | -0.2601 | 0.4268 | 0.057 |
| H13 | 0.3791 | -0.2858 | 0.3653 | 0.061 |
| H14A ^b | 0.6398 | -0.1545 | 0.3666 | 0.068 |
| H15 | 0.5765 | 0.0013 | 0.4273 | 0.054 |

^aIncluded with an occupancy factor of 0.35. ^bIncluded with an occupancy factor of 0.65.

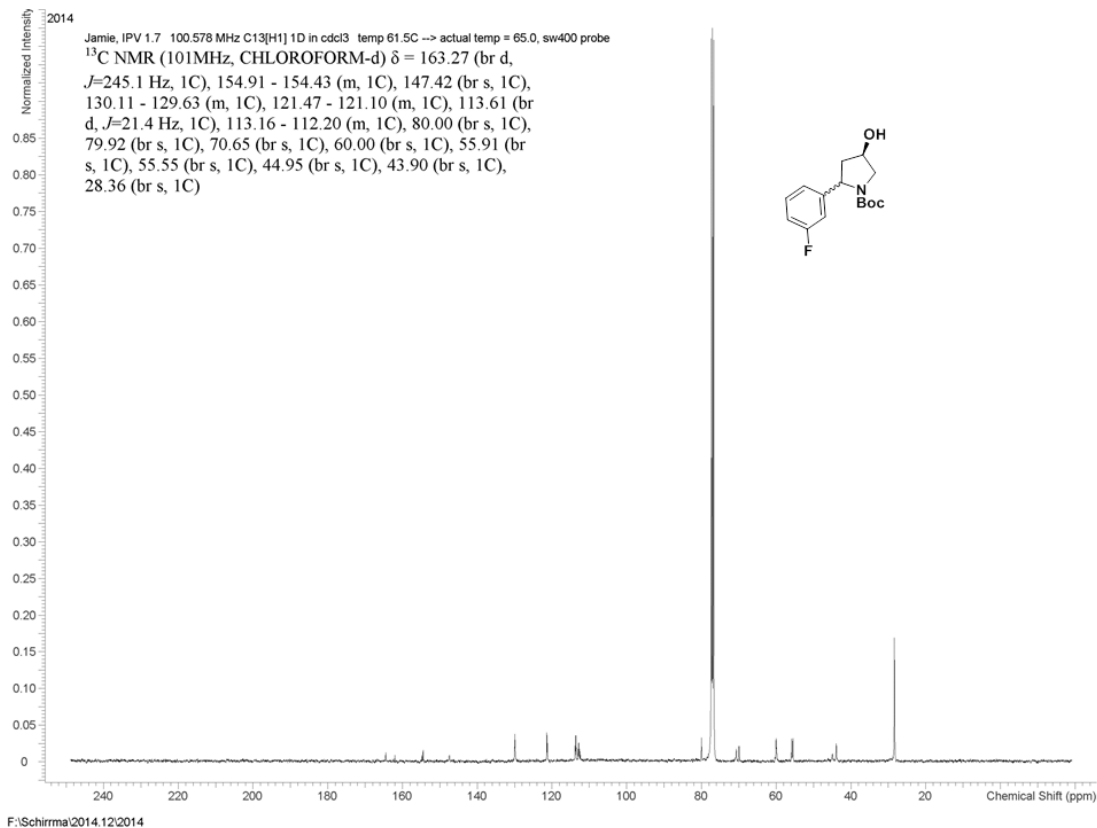
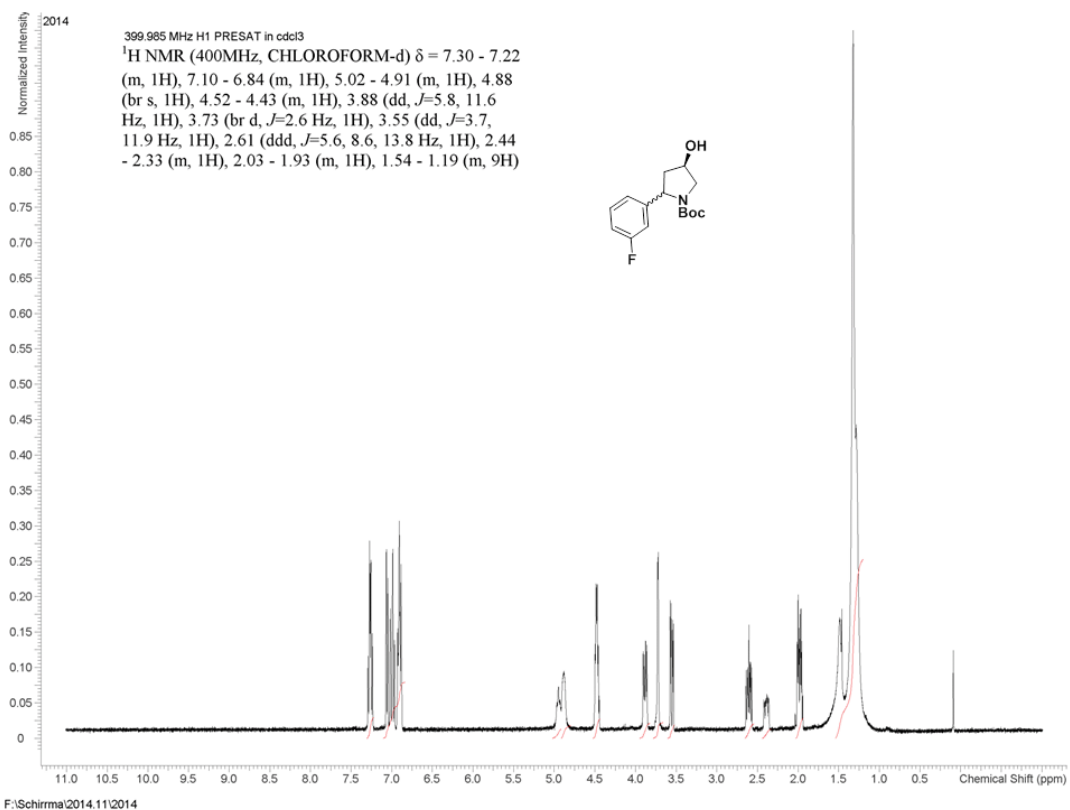
¹H NMR and ¹³C NMR for compound 7.2



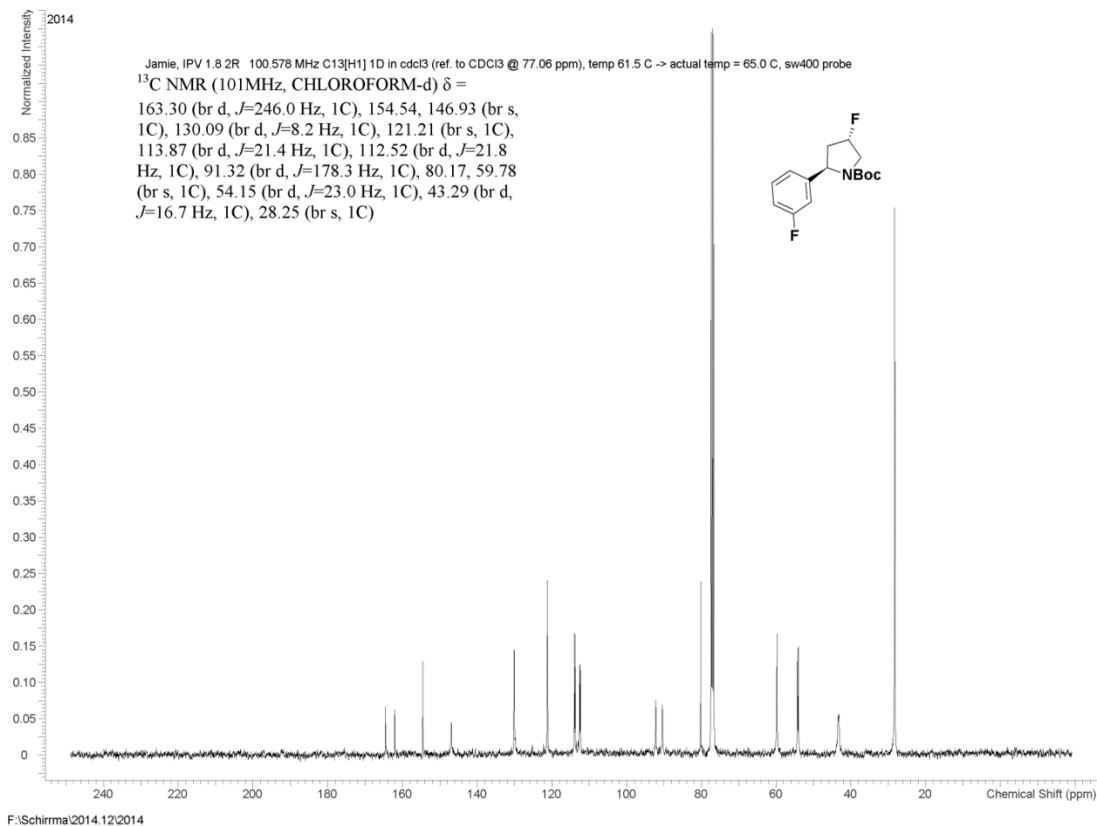
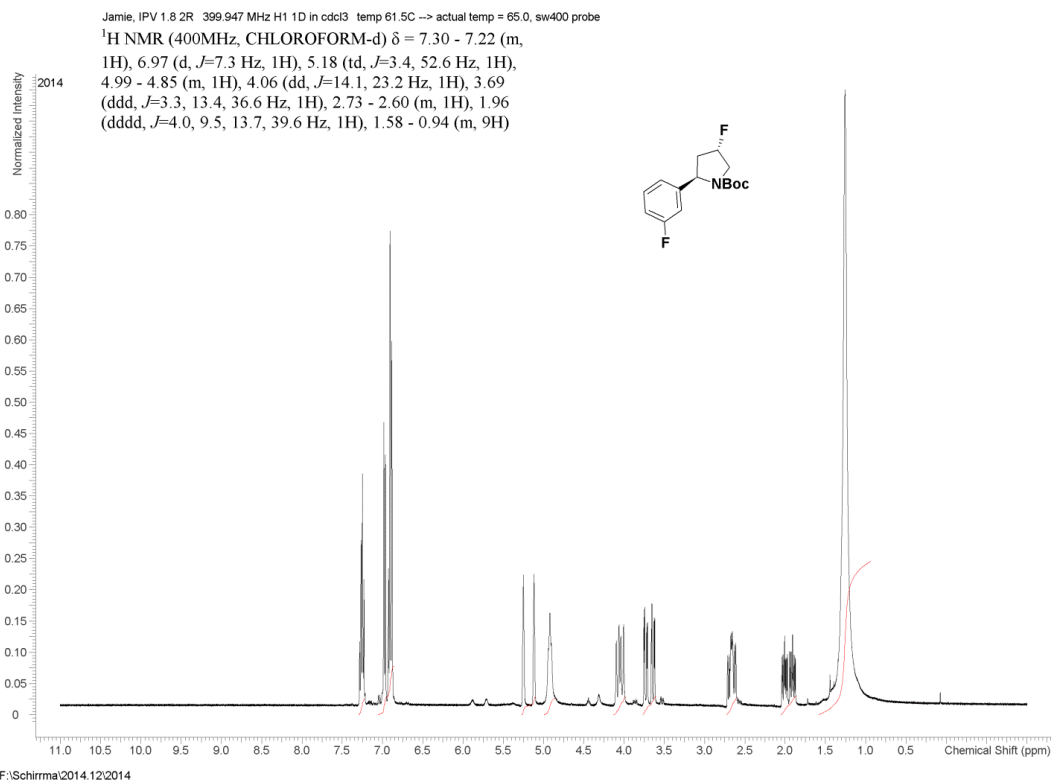
¹H NMR and ¹³C NMR for compound 7.3



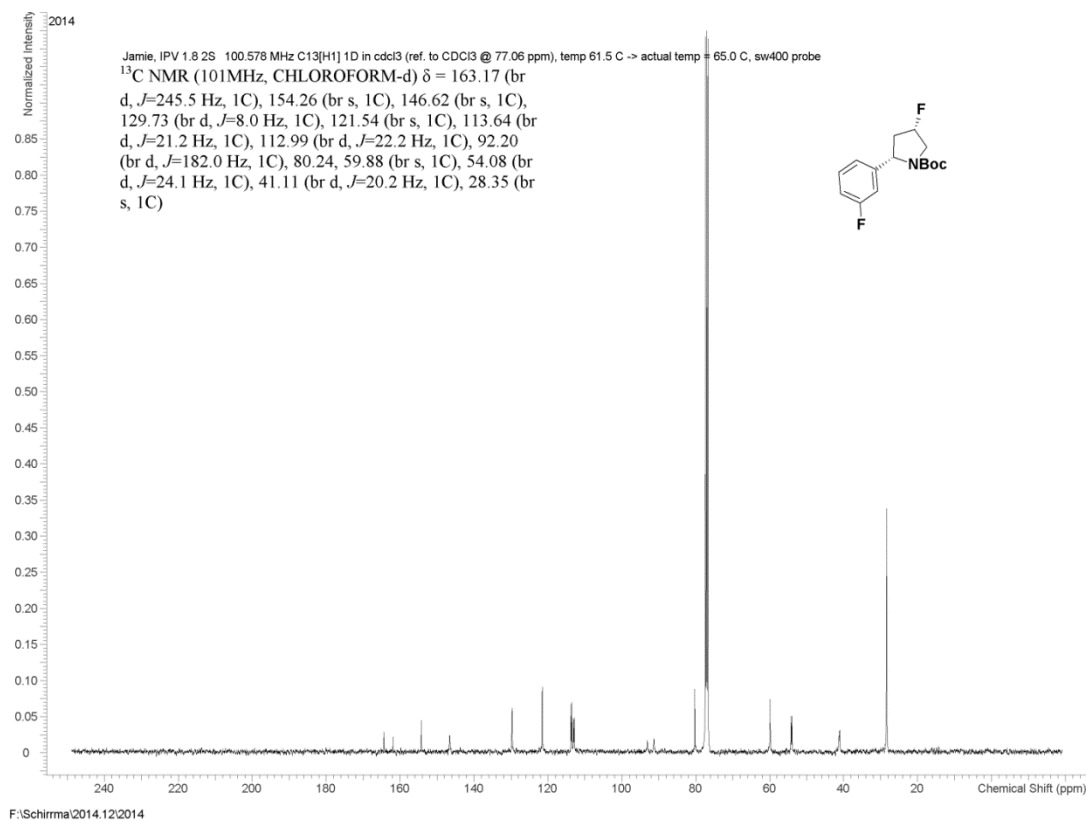
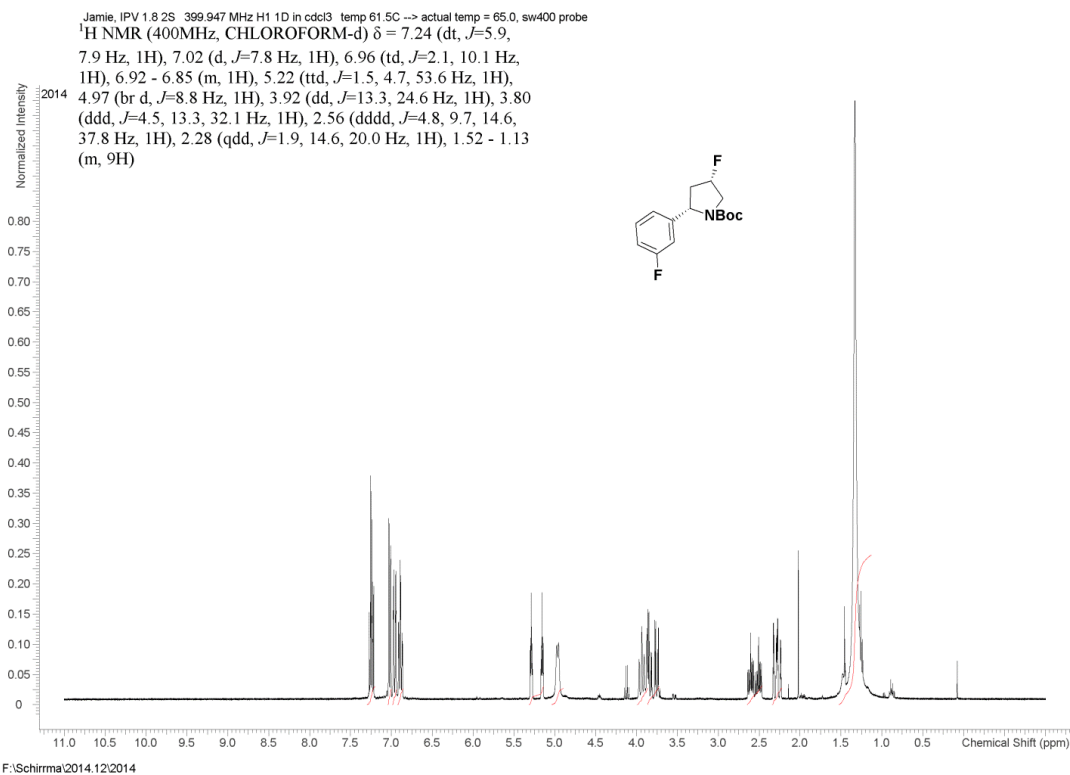
¹H NMR and ¹³C NMR for compound 7.5



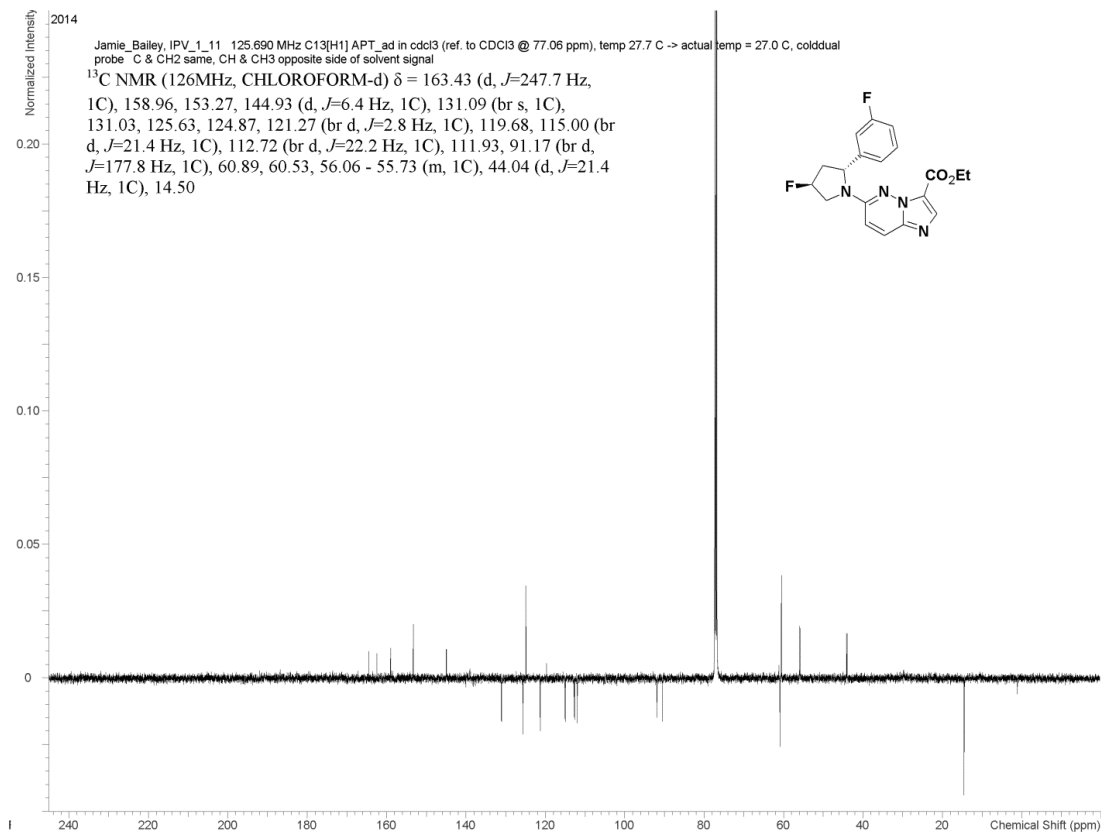
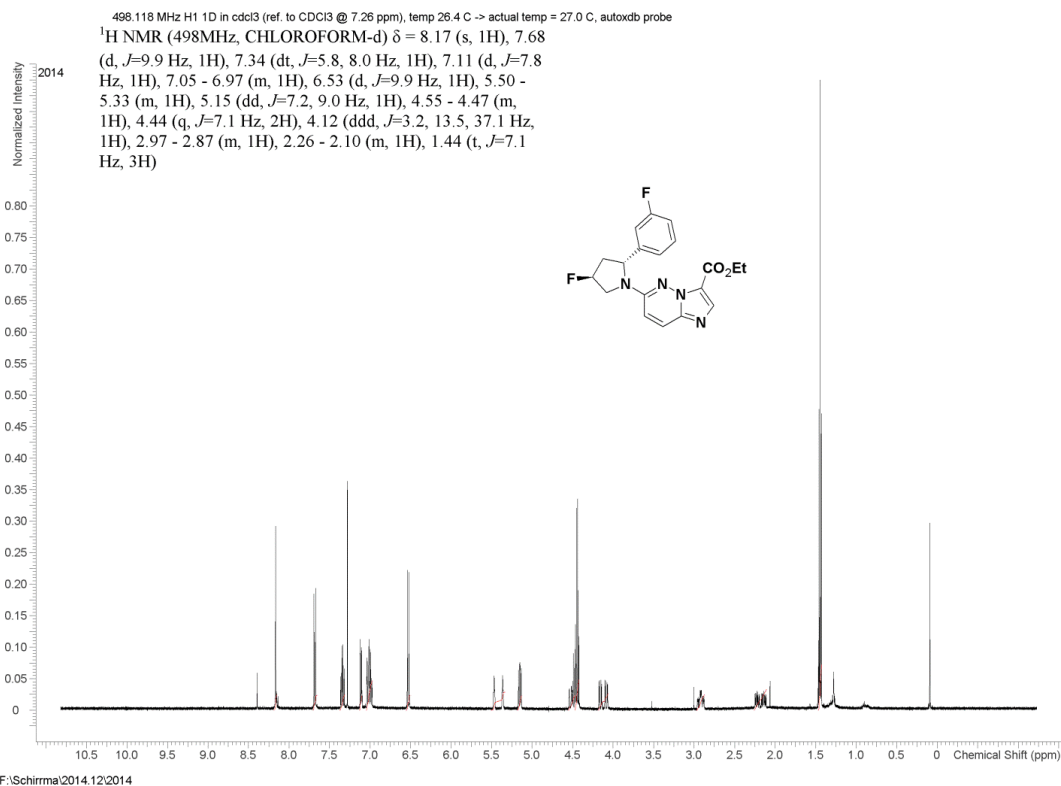
^1H NMR and ^{13}C NMR for compound (2*R*,4*S*)-7.6



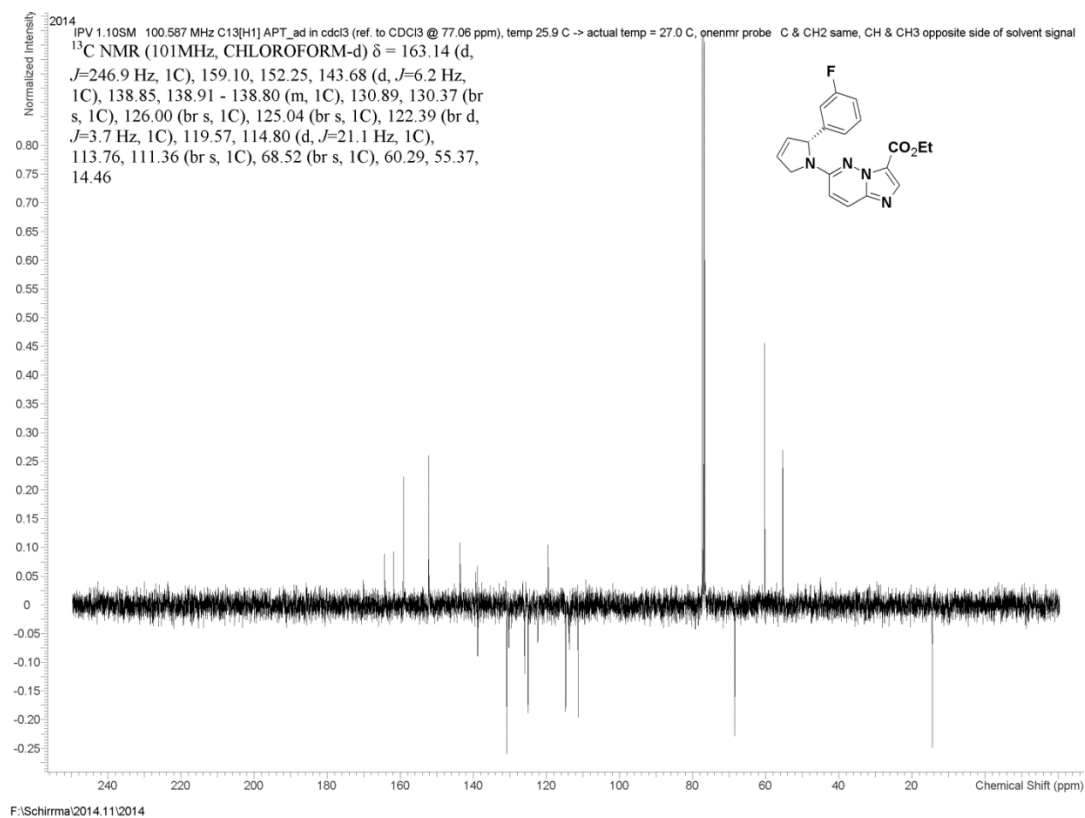
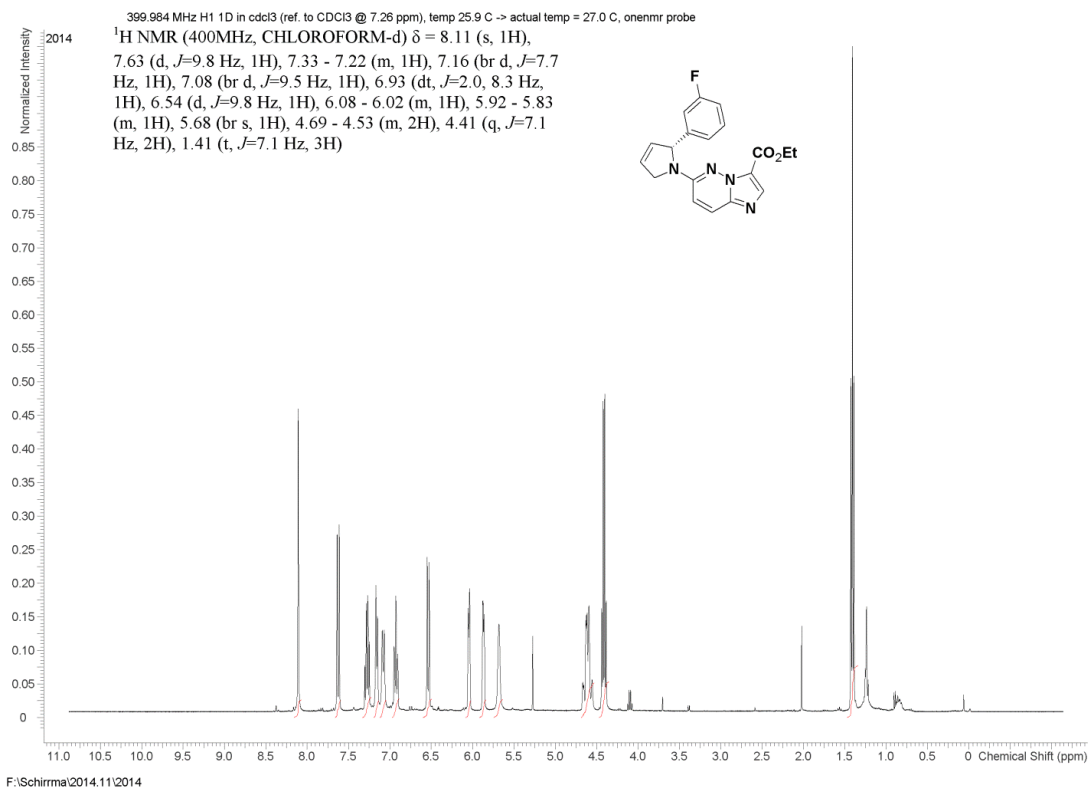
¹H NMR and ¹³C NMR for compound (2*S*,4*S*)-7.6



¹H NMR and ¹³C NMR for compound 7.9



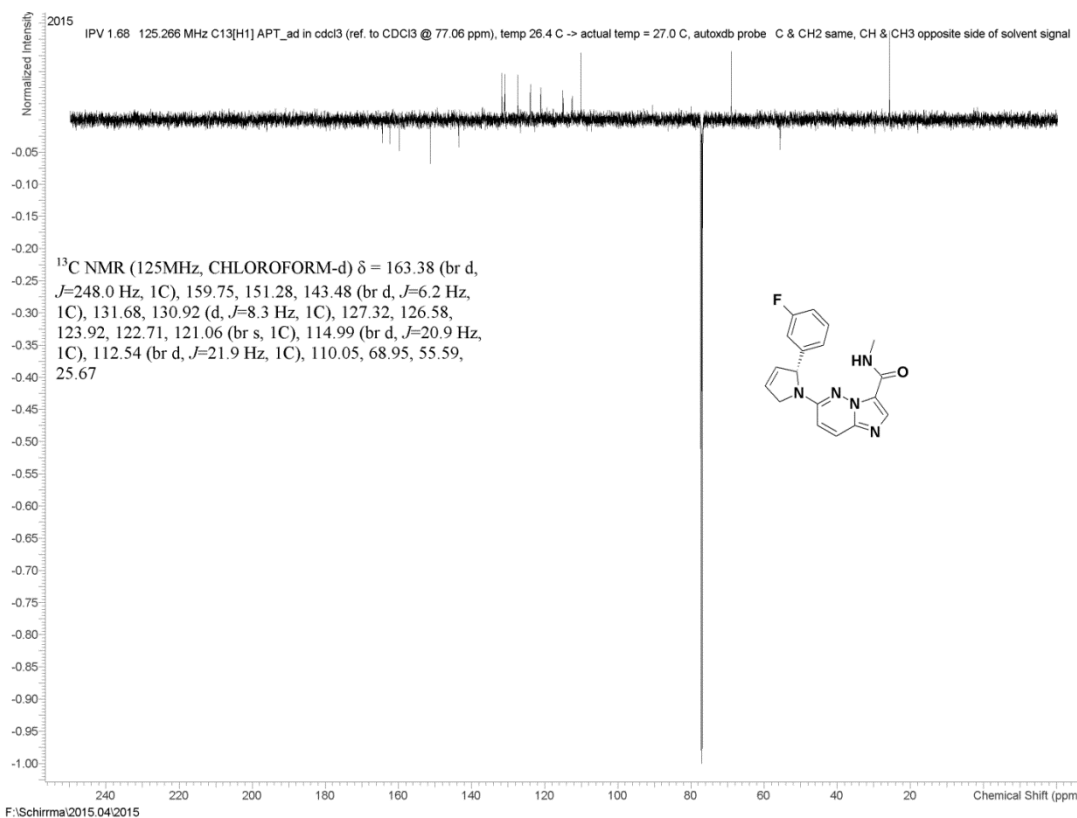
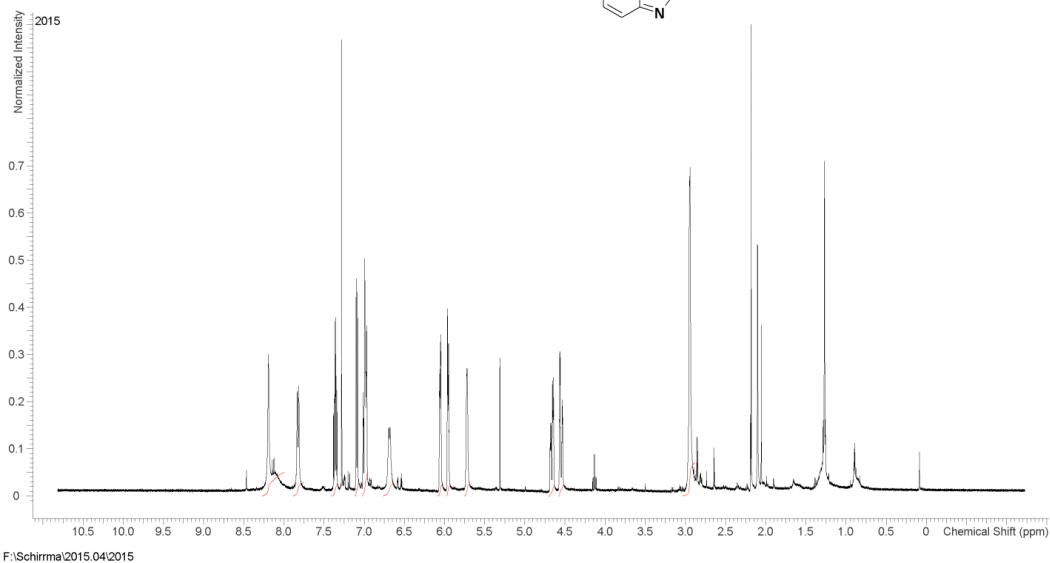
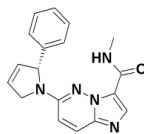
¹H NMR and ¹³C NMR for compound 7.8



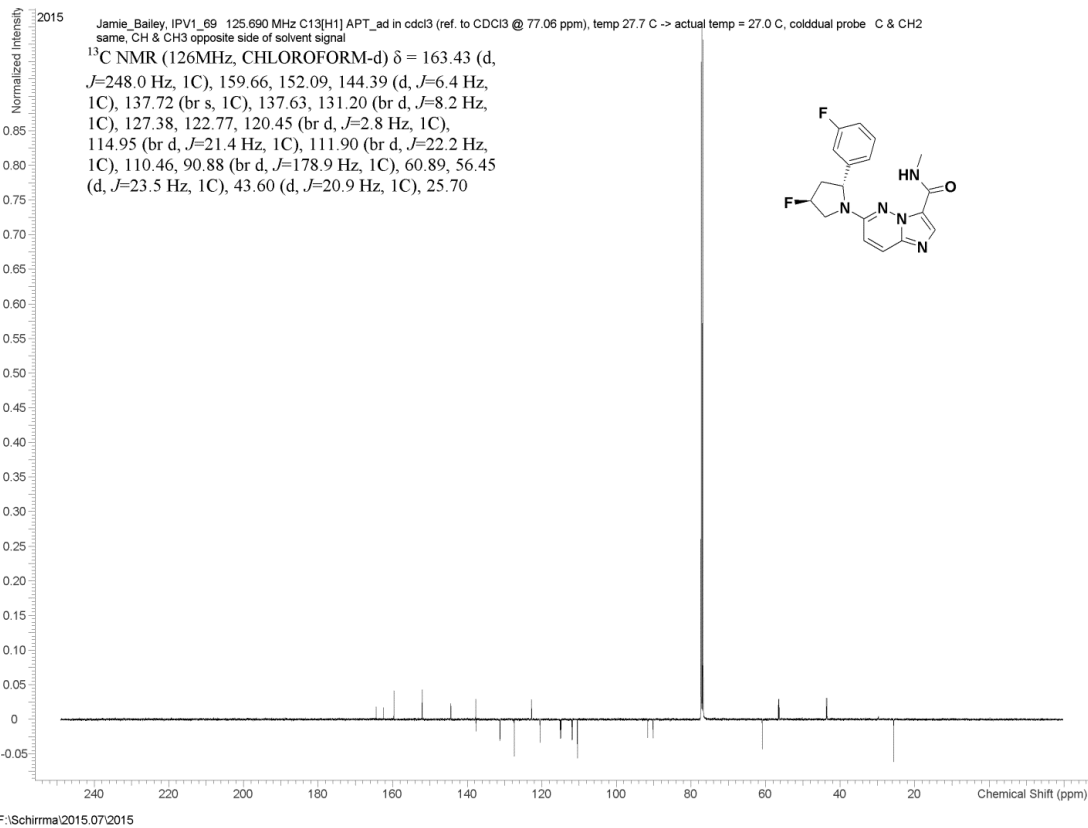
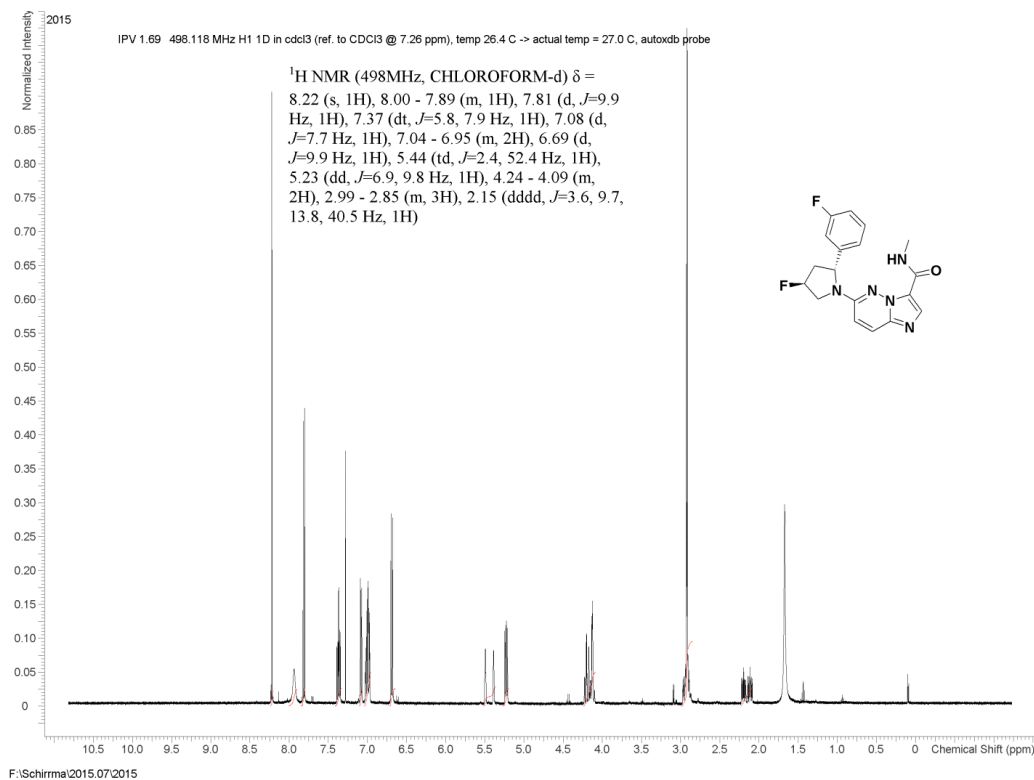
¹H NMR and ¹³C NMR for compound 7.10

IPV 1.68 498.118 MHz H1 1D in cdcl3 (ref. to CDCl3 @ 7.26 ppm), temp 26.4 C -> actual temp = 27.0 C, autotx probe

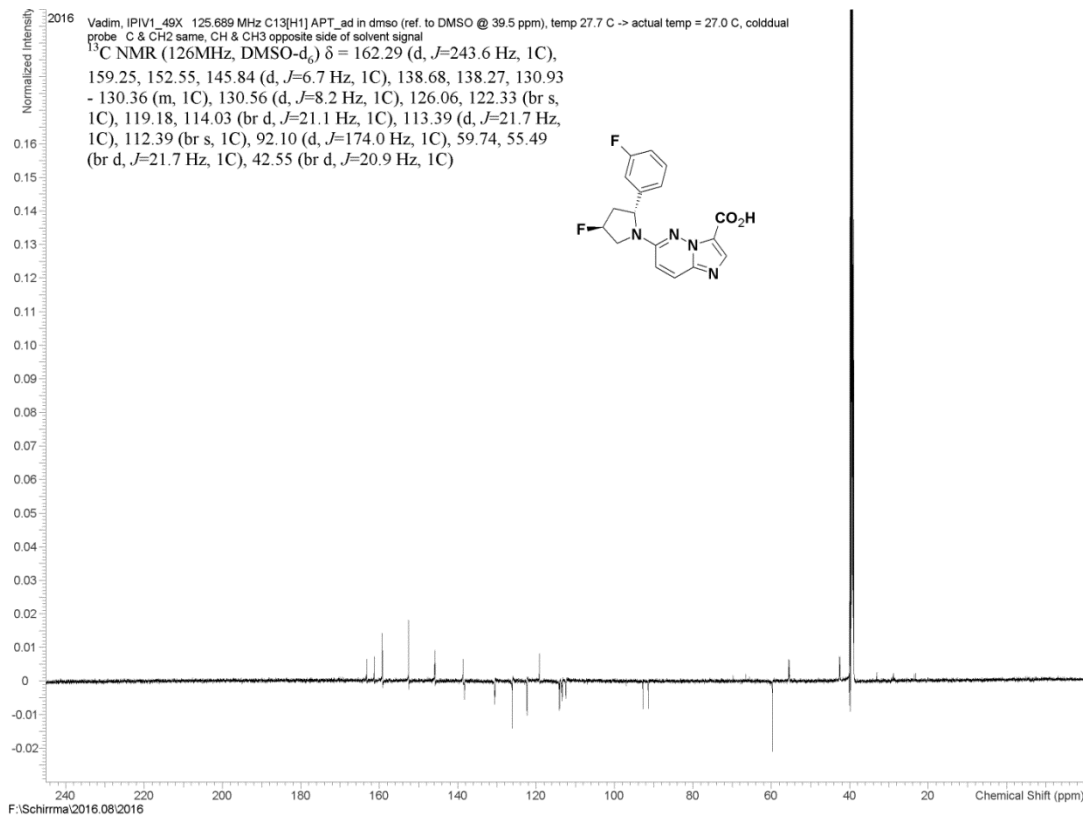
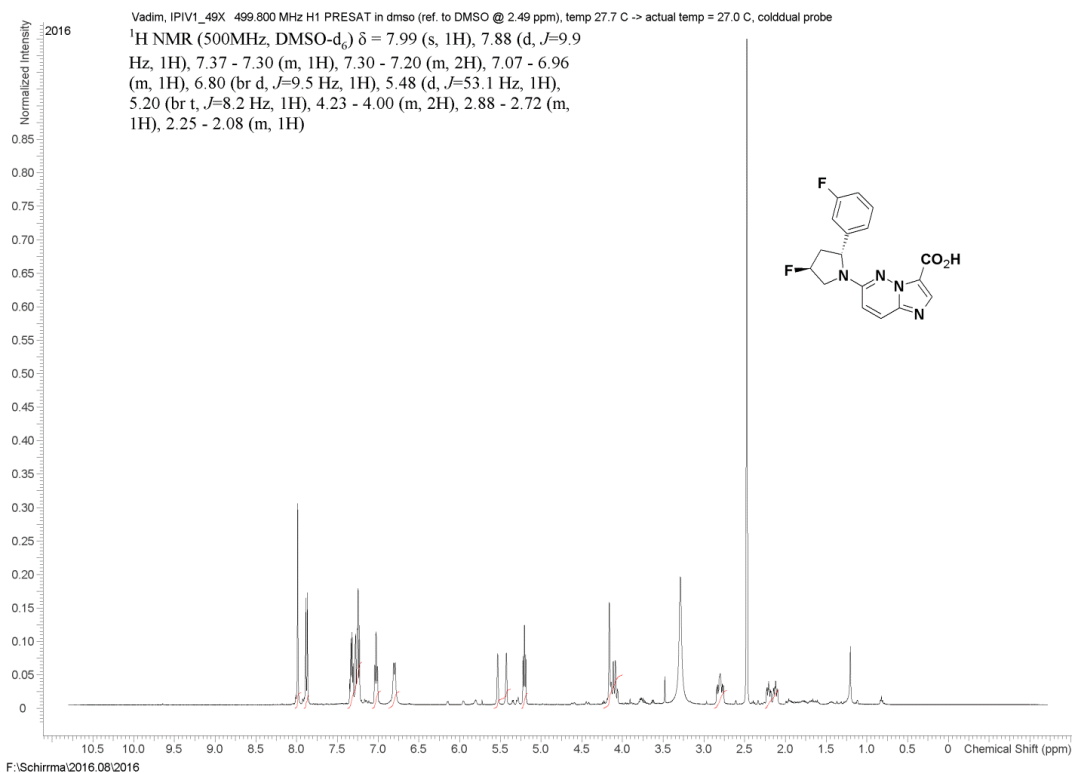
¹H NMR (498MHz, CHLOROFORM-d) δ = 8.27 - 7.99 (m, 2H), 7.82 (br d, $J=9.8$ Hz, 1H), 7.36 (dt, $J=5.8, 7.8$ Hz, 1H), 7.09 (d, $J=7.7$ Hz, 1H), 7.02 - 6.95 (m, 2H), 6.69 (br d, $J=8.9$ Hz, 1H), 6.09 - 6.02 (m, 1H), 5.98 - 5.92 (m, 1H), 5.72 (br d, $J=2.7$ Hz, 1H), 4.71 - 4.62 (m, 1H), 4.59 - 4.50 (m, 1H), 2.95 (br d, $J=3.8$ Hz, 3H)



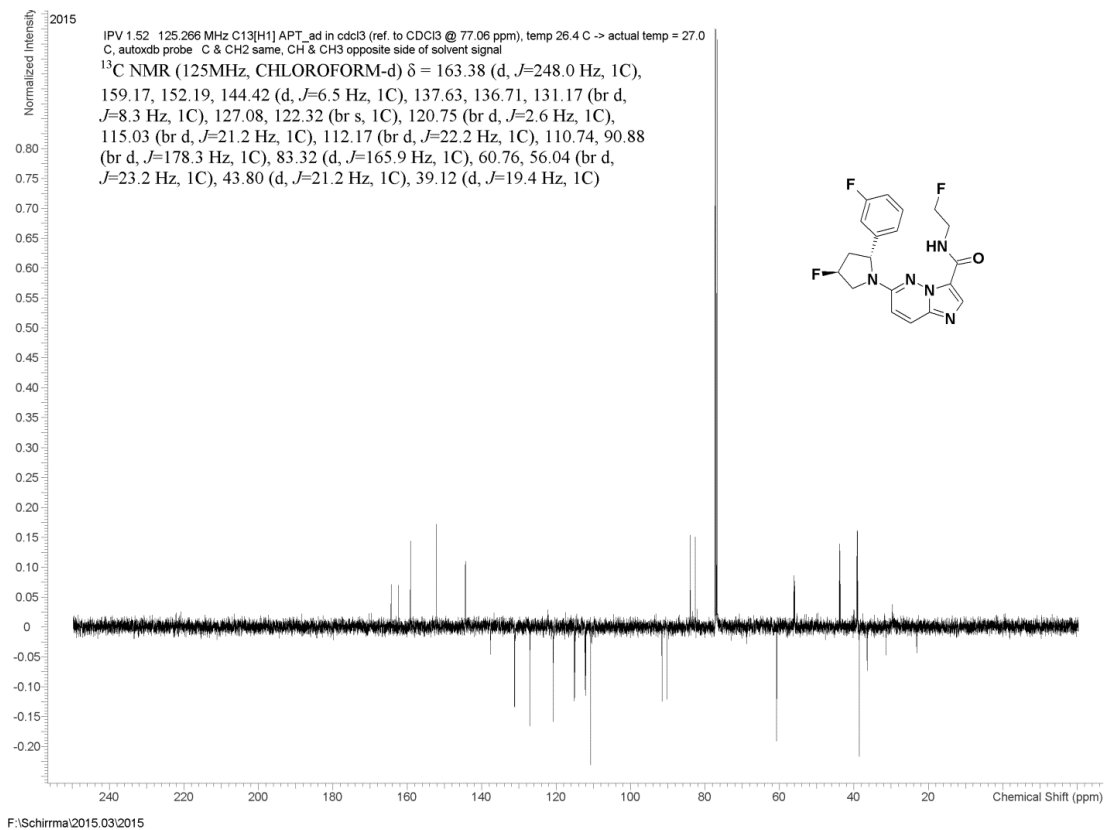
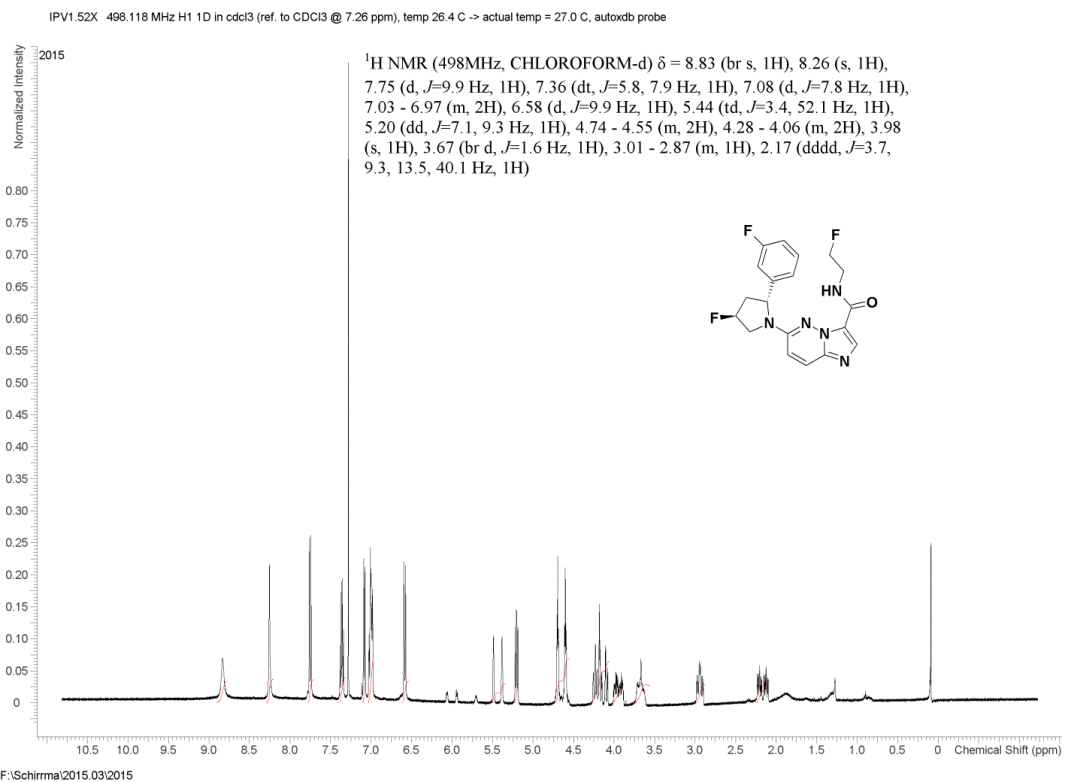
¹H NMR and ¹³C NMR for compound 7.11



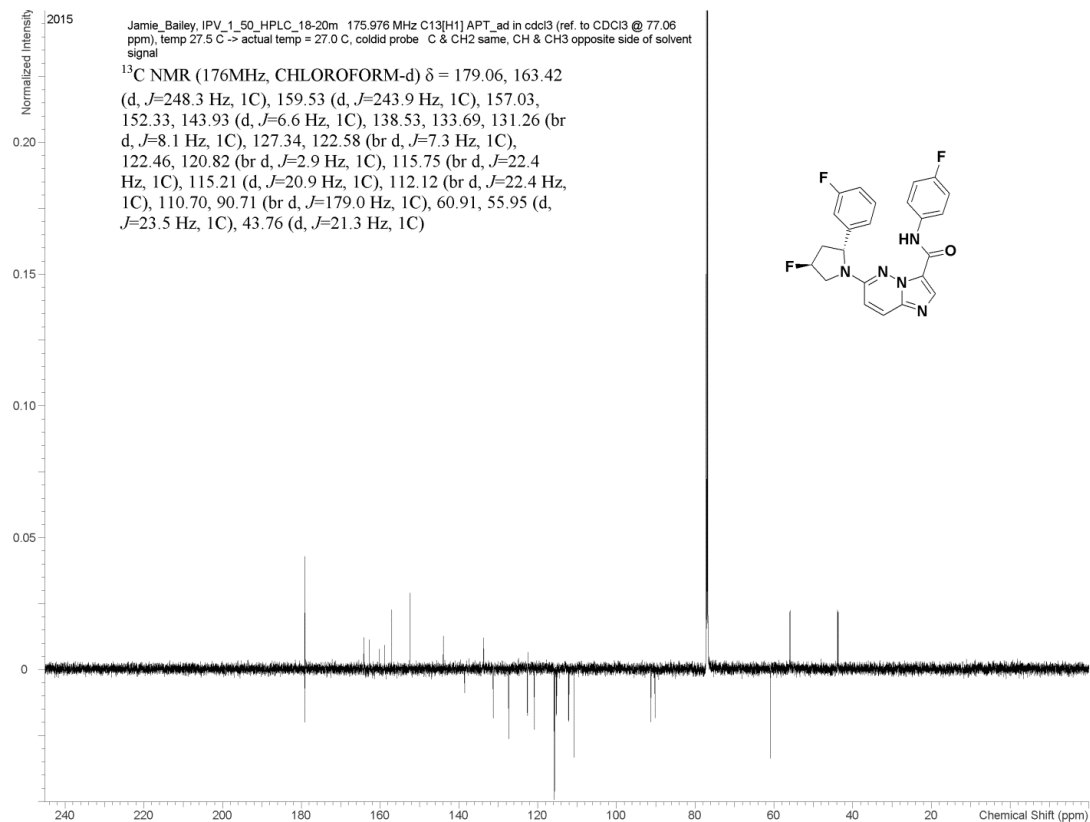
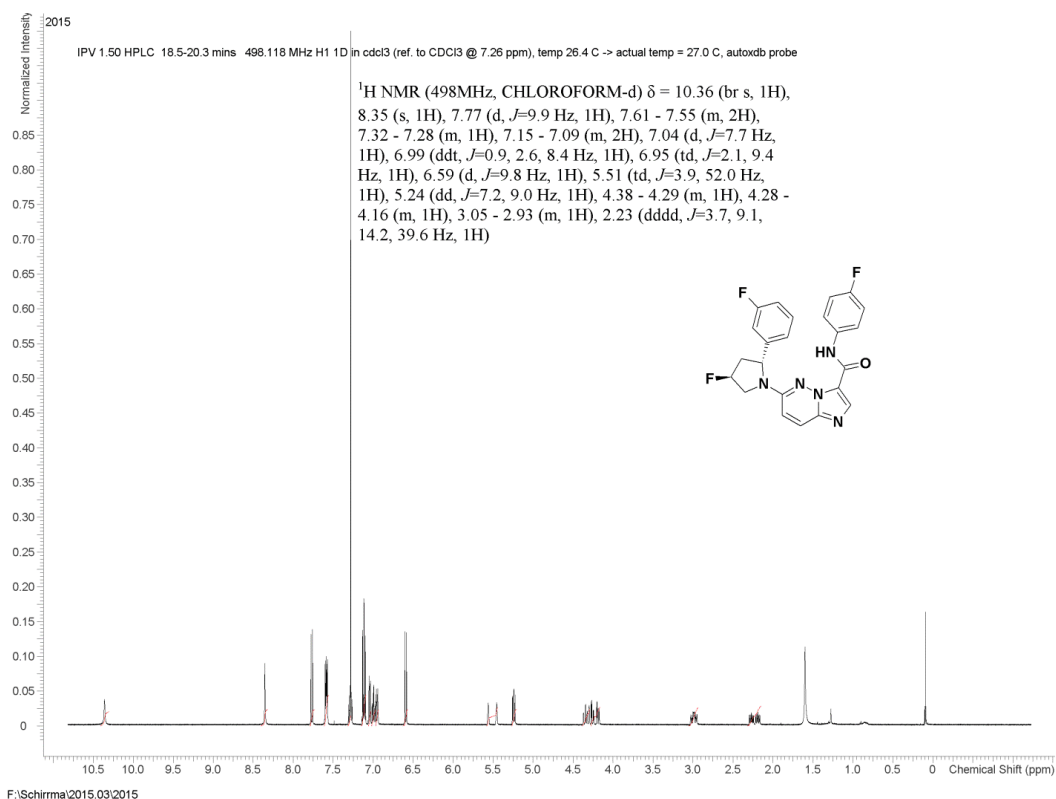
¹H NMR and ¹³C NMR for compound 7.12



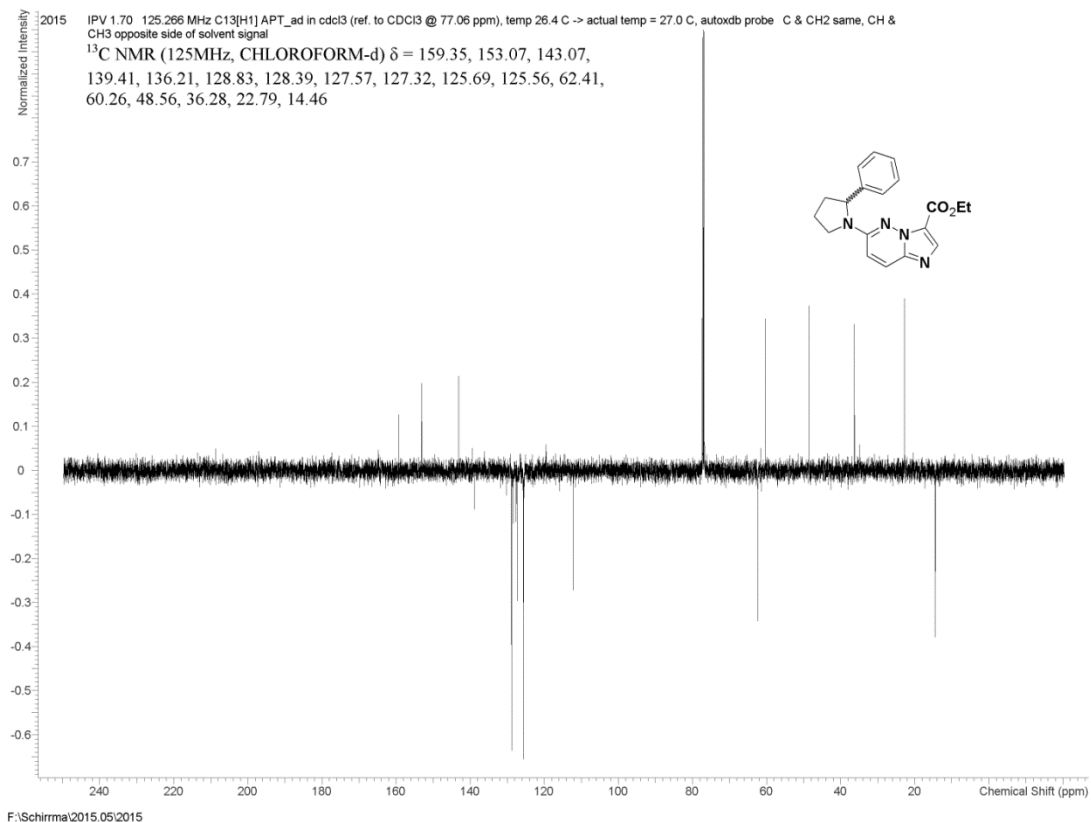
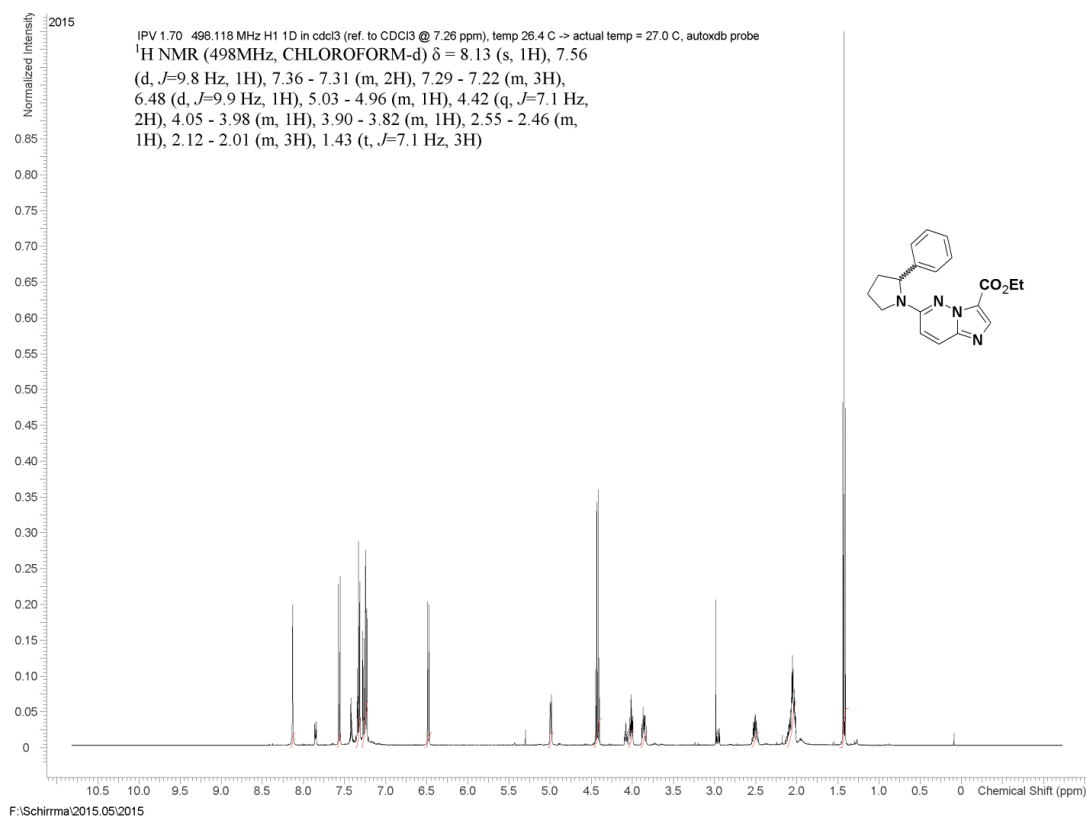
¹H NMR and ¹³C NMR for compound 7.13



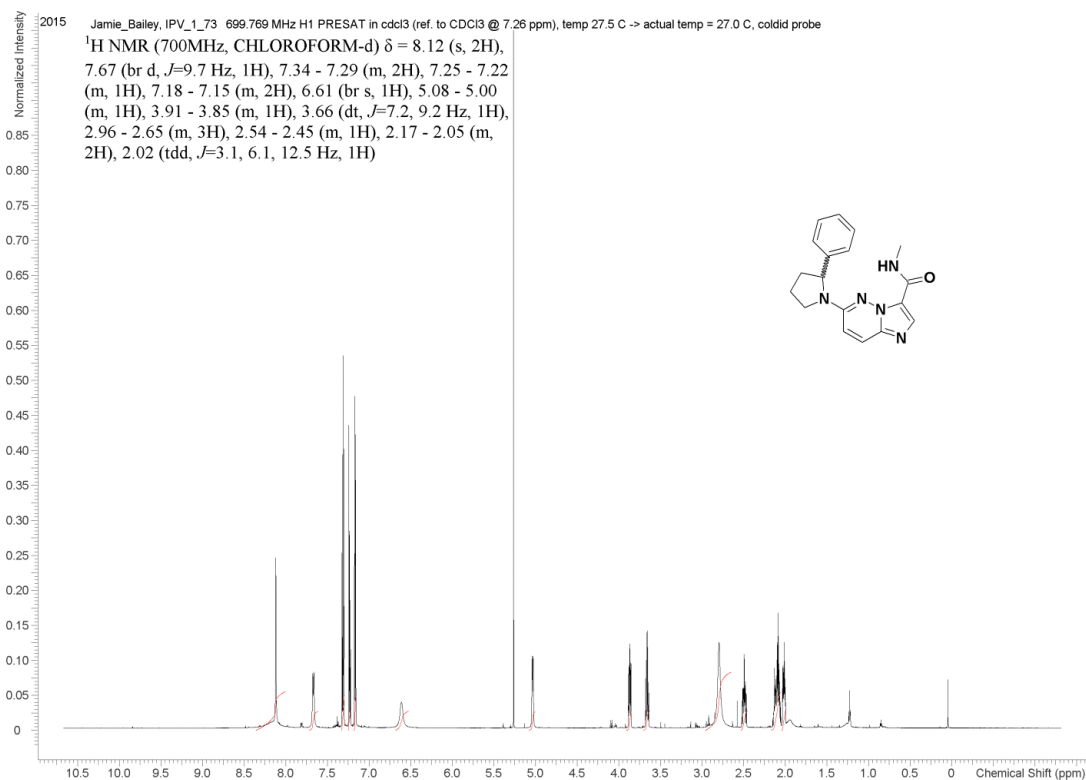
¹H NMR and ¹³C NMR for compound 7.14



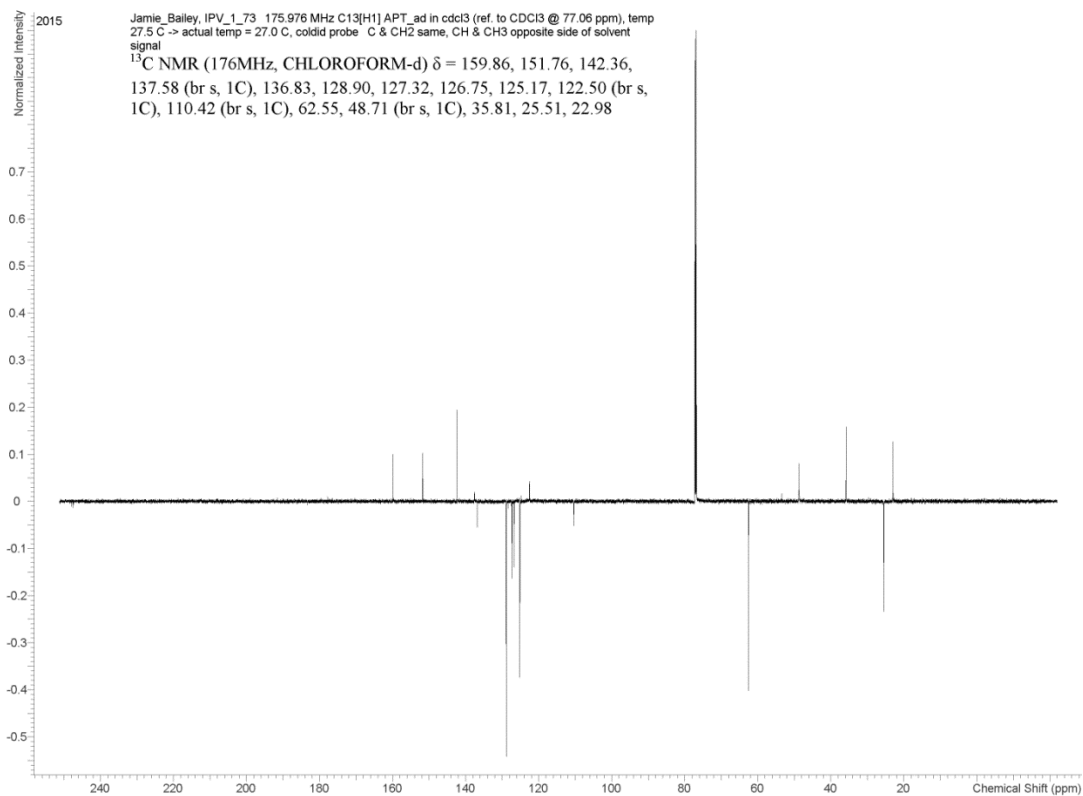
^1H NMR and ^{13}C NMR for compound 7.16



¹H NMR and ¹³C NMR for compound 7.17



F:\Schirma\2015.05\2015



F:\Schirma\2015.05\2015

^1H NMR and ^{13}C NMR for compound 7.19

